LITHOLOGY AND PROVENANCE OF LATE EOCENE – OLIGOCENE SEDIMENTS IN EASTERN TARANAKI BASIN MARGIN AND IMPLICATIONS FOR PALEOGEOGRAPHY

A thesis
submitted in partial fulfilment
of the requirements for the degree of
Master of Science in Earth and Ocean Sciences
at the
University of Waikato

by

Bradley Scott Hopcroft

University of Waikato
2009

THE UNIVERSITY OF WAIKATO
Te Whare Wānanga o Waikato

DEPOSIT OF MASTERS THESIS , DOCTORAL OR MPHIL THESIS IN THE UNIVERSITY OF WAIKATO LIBRARY

Author: Bradley Scott Hopcroft

Title of thesis: Lithology and provenance of Late Eocene - Oligocene sediments in eastern Taranaki Basin margin and implications for paleogeography

Degree: Master of Science Year of submission: 2009

An application to embargo has been made: Yes (No) *(circle as required)*

Termination date of the embargo:

Declaration

I hereby deposit a print and digital copy of my thesis with the University of Waikato Library. I confirm that any changes required by the examiners have been carried out to the satisfaction of my primary supervisor and that the content of the digital copy corresponds exactly to the content of the print copy in its entirety.

This thesis is my own work and, to the best of my knowledge and belief, it contains:

- no material previously published or written by another person, except where this is appropriately cited through full and accurate referencing.
- no material which to a substantial extent has been accepted for the qualification of any other degree or diploma of a university or other institution of higher learning.

I have either used no substantial portions of third party copyright material, including charts, diagrams, graphs, photographs or maps in my thesis, or I have obtained permission for such material to be made accessible worldwide via the internet.

Conditions of use

From the date of deposit of this thesis or the cessation of any approved access restrictions, the conditions of use are as follows:

1. This thesis may be consulted for the purposes of private study or research provided that appropriate acknowledgement is made of its use;

2. The digital copy is made available via the Internet by the University of Waikato Library in downloadable, read-only format with unrestricted access, in the interests of open access to research information, provided that the thesis is not subject to an embargo. Should an embargo be in place, the digital copy will only be made available as set out above once the embargo has been lifted.

3. In accordance with Section 56 of the Copyright Act 1994, the University of Waikato Library may make a copy of this thesis for supply to the collection of another prescribed library on request from that library.

Signed: _____ Date: 16/02/09

I have seen and discussed the content of this form
The Chief Supervisor: Professor Peter J.J. Kamp Signature: P.J. Kamp

Instructions for use of this form:
This completed and signed form should be bound into the copy of the thesis intended for the University of Waikato Library.

ABSTRACT

The latest Eocene and Oligocene was a time of marked paleoenvironmental change in Taranaki Basin, involving a transition from the accumulation of coal measures and inner shelf deposits to the development of upper bathyal environments. Up until the end of the Early Oligocene (Lower Whaingaroan Stage) Taranaki Basin had an extensional tectonic setting. Marine transgression culminated in the accumulation of condensed facies of the Matapo Sandstone Member of the lower part of the Ngatoro Group. During the Late Oligocene (Upper Whaingaroan Stage) Taranaki Basin's tectonic setting changed to one of crustal shortening with basement overthrusting westward into the basin on Taranaki Fault. The major part of the Ngatoro Group in thickness, including the Tariki Sandstone Member, Otaraoa Formation, Tikorangi Formation and Taimana Formation, accumulated in response to this change in tectonic setting.

Various methods of stratigraphic and sedimentological characterisation have been undertaken to evaluate the stratigraphy of the Ngatoro Group. Wireline log records have been calibrated through particle sizing and carbonate digestion of well cuttings. A suite of wireline motifs have been defined for formations and members of the Ngatoro Group. The integration with other lithological and paleoenvironmental data sources has helped to better define the Late Eocene – Oligocene stratigraphy and sedimentary facies for eastern Taranaki Basin margin.

U-Pb geochronology by laser ablation inductively coupled plasma-mass spectrometry (LA-ICP-MS) has been used to determine detrital ages for over 350 zircons from 13 samples of Late Eocene – Oligocene sandstone samples in eastern Taranaki Basin and correlative onshore North Island units. The spread of ages (1554 – 102 Ma) and the proportion of ages in particular age bands integrated with modal petrography data have aided provenance evaluation. A range of source rocks contributed to the Late Eocene – Oligocene sedimentary units analysed, mainly the Waipapa Terrane (Early Permian to Late Jurassic) as shown by $^{206}Pb/^{238}U$ zircon ages and the abundance of fine-grained sedimentary rock fragments observed in samples. The Median Batholith (i.e. Darran/Median Suite

and Separation Point Suite) is also identified as a significant source, indicated by Early Triassic to Early Jurassic and Early Cretaceous $^{206}Pb/^{238}U$ zircon ages and an abundance of quartz in samples. Other minor sources identified include Murihiku and Caples Terranes, Rakaia Sub-terrane and possibly the Karamea Batholith. The Tariki Sandstone and the Hauturu Sandstone have the same source, with the main $^{206}Pb/^{238}U$ zircon ages of aggregated samples (124 – 116 Ma and 121 Ma, respectively) consistent with a Separation Point Suite/Median Batholith (124 – 116 Ma) source. Derivation of sediments from a landmass that existed to the east and southeast of the Wellington area has been inferred for the Late Eocene – Oligocene units, with subsequent migration of sediments northward into Taranaki Basin and the Waikato Region (i.e. Te Kuiti Group depocentre) via longshore drift.

New provenance data have been used to revise understanding about the development of eastern Taranaki Basin margin through the Late Eocene to earliest Miocene. Three new paleogeography maps are presented for the Runangan (Late Eocene), Lower Whaingaroan (Early Oligocene) and Upper Whaingaroan (early-mid-Oligocene). New paleogeography interpretations illustrate a dramatic change in the basin development between Matapo Sandstone (Lower Whaingaroan) and Tariki Sandstone (Upper Whaingaroan) deposition, consistent with an Upper Whaingaroan age for the start of reverse movement on Taranaki Fault.

ACKNOWLEDGEMENTS

Many people have helped, supported and ultimately contributed to the final completion of this thesis. The biggest thanks however goes to Professor Peter Kamp for his help and general supervision for the entire project. Also, the wealth of knowledge he contributed and applied to various lab work, data analysis and thesis editing was greatly appreciated. I am very grateful that this project turned out the way it did and I appreciate the good will and enthusiasm Peter showed to me. Also a big thanks to Dr Rochelle Hansen who helped particularly in the interpretation of wireline logs and thesis editing.

Thanks go to the many friendly faces around the Department who helped me in the course of this project including: Dr Ganqing Xu for help with mineral separation and the recovery of zircons; Dr Roger Briggs for help with petrography; Jacinta Parenzee and Annette Rodgers for help with the preparation of samples; Steve Cameron for running the ICP-MS, and Dr Steve Hood for always being there to bounce ideas. Also a special thanks go to Ms Rebecca Richards for sharing her expertise in the practical aspect of U-Pb geochronology and data analysis.

Thanks to my family and friends for being there for the ups and downs. A big thanks to Reg Brown for his much appreciated support and mentoring over many years, the everlasting supply of food, and exciting holiday experiences we have shared together. Thanks to Dr Judy Macdonald for her worldly advice, and for providing employment and a plentiful supply of coffee during my university studies. Thanks are also expressed to Tracey for her support and companionship throughout the MSc years.

I would wish to acknowledge GNS Science, Lower Hutt, and thank Dr Peter King for providing access to well log data and well cutting samples, and for helping supervise aspects of this research project. A big thanks also goes to the organisations that provided funding: University of Waikato, AusIMM, George Mason Charitable Trust and the Broad Memorial Fund.

TABLE OF CONTENTS

LIST OF FIGURES

LIST OF TABLES

CHAPTER ONE
INTRODUCTION

1.1 OVERVIEW

The character of the Late Eocene – Oligocene succession in Taranaki Basin's eastern margin reflects a change from a passive or mildly extensional phase of development to an active phase, characterised by fault and fold-related deformation associated with the formation of the Australian-Pacific plate boundary zone through New Zealand. Determining the exact timing of this change in basin style and associated sedimentation is important because it has implications for the types of structures that might be oil-bearing, and hence for concepts around exploration plays. Determination of the basin's paleogeography is an outcome of better understanding about the Late Eocene – Oligocene sedimentary succession in eastern parts of the basin.

Late Eocene – Oligocene units in Taranaki Basin are entirely in the subsurface and hence there have been few detailed investigations of them. In terms of sediment provenance, the conclusion of earlier investigations is that the Kapuni and Moa Groups (i.e. McKee Formation and Turi Formation) and sandstone units within the Ngatoro Group (i.e. Otaraoa Formation, Tikorangi Formation, Taimana Formation) were derived from granitic terrane (Smale & Morton 1987; Smale 1996). This study presents a reassessment of the provenance of these units using U-Pb geochronology of zircon grains separated from them, integrated with sediment petrography. The study aims to identify the specific source rocks of selected Late Eocene – Oligocene units in eastern Taranaki Basin and to improve information and understanding about the paleogeographic setting of the eastern parts of the Basin. Along with subsurface Taranaki Basin samples, several correlative units in the Te Kuiti Group east of Taranaki Fault have also been included in this analysis.

1.2 RESEARCH OBJECTIVES

This study has the following research objectives:

1. To undertake an assessment of Late Eocene – Oligocene subsurface stratigraphic units in the eastern parts of Taranaki Basin using geophysical well logs to better define their facies and lithostratigraphy.
2. To undertake re-assessment of the provenance of the Late Eocene – Oligocene sediments along the eastern margin of the basin using zircon U-Pb geochronology integrated with petrography.
3. To develop a paleogeographic synthesis of the evolution of the eastern margin of Taranaki Basin.
4. To test a hypothesis that the lower and upper parts of the Ngatoro Group, which have different stratigraphic and sedimentologic characteristics, reflecting their accumulation under different tectonic conditions (extension versus shortening).

1.3 METHODS

Geophysical well log data have been obtained from Crown Minerals, Ministry of Economic Development (MED) open file petroleum technical database. Using major log types, a suite of distinct wireline motifs have been defined for the subsurface Late Eocene – Oligocene formations/members in selected exploration holes along the eastern basin margin. With the integration of other lithological and paleoenvironmental data sources (grain size and carbonate content wireline log calibration, well completion reports and biostratigraphy), the lithostratigraphy and depositional facies have been defined, forming the basis for interpretation of the related depositional paleoenvironments.

From sampled well cuttings and outcrop samples for correlative units onshore, the light mineral, heavy mineral and zircon fractions have been separated. The light and heavy mineral fractions have been analysed petrographically via modal analysis, revealing the mineral constituent ratios and allowing preliminary provenance interpretations to be made. Detrital zircons have been U-Pb dated using laser ablation inductively coupled plasma-mass spectrometry (LA-ICP-MS). Age data prepared as simple histogram and probability density functions have

identified the various age peaks. When compared with the U-Pb zircon age characteristics and petrography of New Zealand basement, specific basement sources for Late Eocene – Oligocene units have been inferred.

The new provenance data for Late Eocene – Oligocene subsurface and onshore units, integrated with depositional facies data and existing paleogeographic maps (King & Thrasher 1996, Tripathi 2009) have enabled new paleogeography maps to be drawn for the Late Eocene – Oligocene interval along the eastern margin of the basin.

1.4 THESIS STRUCTURE AND FORMAT

The results of this study are presented in thesis chapters. A brief description of each chapter is given in the next section.

Chapter 2: Geological Setting

Chapter 2 discusses the geological and structural setting of the basin and its broad Cretaceous – Cenozoic evolution. It also provides an overview of the underlying basement geology and an introduction to the Late Eocene – Oligocene sedimentary units in the basin and of correlative units onshore. The chapter also discusses published ideas on the Paleogene evolution of the Taranaki Fault Zone.

Chapter 3: Geophysical Well Log Interpretation

Chapter 3 provides an overview of the major log types used in geophysical well log interpretation and their application to facies identification. This chapter also describes a suite of wireline motifs defined for Late Eocene – Oligocene eastern Taranaki Basin margin units and discusses the data sources used and integrated in determination of the depositional paleoenvironments. Based on this information, defined wireline motifs are interpreted in terms of the existing lithostratigraphy, depositional facies and environments.

Chapter 4: Sedimentary Petrography

Chapter 4 includes modal petrography of the light and heavy mineral fractions in the Late Eocene – Oligocene subsurface and onshore units. This chapter also presents modal abundance of mineral and lithic components in quartz/feldspar/lithics (QFL) ternary diagrams as indicators of provenance and source rock types. It also includes descriptions of the results of grain size and carbonate content on calibration of the wireline logs.

Chapter 5: U-Pb Geochronology

Chapter 5 outlines the LA-ICP-MS U-Pb zircon dating technique used in this study and the associated data quality considerations and issues. It then presents and discusses data quality and sample characteristics for individual samples. This chapter also presents $^{206}Pb/^{238}U$ age probability density plots prepared for each sample, concluding by outlining how these plots may be used in the interpretation of sediment provenance.

Chapter 6: Provenance and Paleogeography

Chapter 6 provides an overview of the U-Pb zircon age characteristics and lithology of New Zealand basement. The provenance of Late Eocene – Oligocene units is inferred from comparison of the U-Pb age and petrographic characteristics of samples with the U-Pb ages of zircons and the petrographic characteristics of New Zealand basement terranes. The paleogeography of the eastern margin of Taranaki Basin is discussed for five key intervals during accumulation of the Late Eocene to earliest Miocene successions. This chapter also discusses the Paleogene evolution of Taranaki Fault zone, specifically the evidence for the timing of the start of shortening across the fault zone from the basin's stratigraphy.

Chapter 7: Summary and Conclusions

Chapter 7 provides a summary of the major outcomes of this study. No new data, interpretations or ideas are introduced in this chapter.

Appendices included at the end of this thesis contain details about samples, wireline motif subdivisions in selected wells, and various laboratory data.

CHAPTER TWO
GEOLOGICAL SETTING

2.1 INTRODUCTION

Taranaki Basin has evolved since the mid-Cretaceous break-up of New Zealand from eastern Gondwanaland. It formed initially as an intra-continental rift transform during the Late Cretaceous to Paleocene while seafloor spreading was occurring in the Tasman Sea (83 – 57 Ma). During the Eocene – Early Oligocene the basin's developed was akin to passive development with a mild phase of extension superimposed. The Neogene development of the basin has been characterised by active margin deformation and associated sedimentation (King & Thrasher 1996).

This chapter presents a literature review of the geological and structural setting of Taranaki Basin, as well as its broad Cretaceous – Cenozoic evolution particularly of its eastern margin. The Late Eocene to earliest Miocene subsurface stratigraphy of the eastern margin is also discussed, including age equivalent units in the Waikato region (Te Kuiti Group), Taumarunui region (Taumarunui quartz sandstone) and in the Otaihanga area (Otaihanga Outlier). Of particular interest in this study is the dramatic change in eastern margin basin dynamics that occurred between the Eocene (passive margin) and Miocene (active convergent margin) phases, mainly involving shortening across the Taranaki Fault Zone associated with development of the Australian – Pacific convergent plate boundary through New Zealand. Lastly, alternative existing Late Eocene – Early Miocene Taranaki Fault displacement models are discussed.

2.2 GEOLOGICAL AND STRUCTURAL SETTING

Taranaki Basin is predominantly an offshore basin covering an area of around 100,000 km^2, located along the western margin of North Island, New Zealand (Fig. 2.1.A). The eastern margin of the basin has traditionally been delineated by the Patea-Tongaporutu-Herangi basement high, which lies immediately east of the subsurface Taranaki Fault (King & Thrasher 1996). On its western side, Taranaki Basin passes beyond the present day shelf-slope margin and the boundary is

arbitrarily defined by latitude 171˚E (King & Thrasher 1996). At present, Taranaki Basin lies in a back-arc position behind the Taupo Volcanic Zone (TVZ) and Hikurangi Margin subduction zone (Fig. 2.1.A).

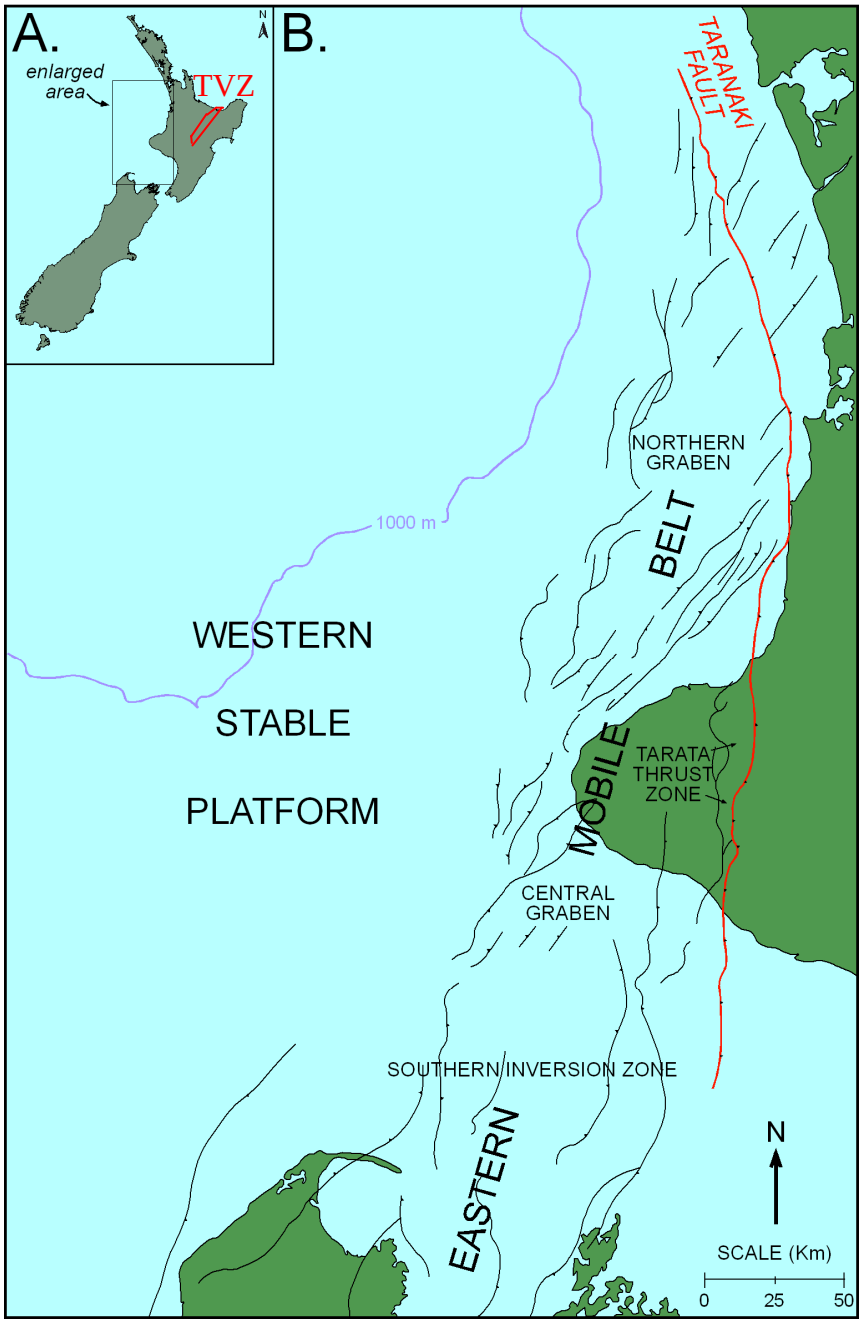

Figure 2.1. A. Taranaki Basin location map. **B.** Map of enlarged Taranaki Basin area, illustrating structural provinces of the basin. Note location and length (~400 km) of Taranaki Fault (red). Modified from King and Thrasher (1996) and Crown Minerals (2007).

Taranaki Basin is floored entirely by continental crust with a complex subsurface morphology. King and Thrasher (1996) structurally defined a broad subdivision of the basin into the Western Stable Platform (WSP), a relatively featureless section of seafloor, encompassing the western region of the basin, and the Eastern Mobile Belt (EMB), a structurally complex eastern region of the basin (Fig. 2.1.B). The EMB includes four main structural parts: North Taranaki Graben (Northern Graben), South Taranaki Graben (Central Graben), Tarata Thrust Zone, and Southern Inversion Zone (Fig. 2.1.B). Pliocene-Pleistocene faults have a predominant north or northeast strike. The north-south striking Taranaki Fault, which moved mainly during the Late Oligocene and Miocene is identified as one of the major structural features of the basin (Fig. 2.1.B). At present, Taranaki Fault is ~400 km in length and passes northward from Wanganui Basin through Taranaki Peninsula and towards the Northland Basin (King & Thrasher 1996). This fault currently dips eastward (25 – 40º), overthrusting Murihiku Terrane basement westward into Taranaki Basin, uplifting the basement surface by about 6 km relative to the basement surface beneath the basin succession (King & Thrasher 1996). The western margin of the overthrust block underlies the Herangi Range in the north and forms the subsurface Patea-Tongaporutu High in the south.

2.3 CRETACEOUS - CENOZOIC EVOLUTION OF TARANAKI BASIN

Five main phases of basin development have been proposed by King and Thrasher (1996). Each phase represents different tectonic environments, the later ones associated with the development of the modern Australian-Pacific plate boundary zone, and each is associated with a particular part of the sedimentary fill of the basin (King & Thrasher 1996). Figure 2.2 shows the legend for paleogeography maps presented in this section.

The first phase occurred from the mid – Late Cretaceous through to the Paleocene. Following the Early Cretaceous fragmentation of eastern Gondwanaland, Tasman Sea spreading separated the New Zealand subcontinent from Antarctica and Australia. The oblique Late Cretaceous rifting evident in Taranaki Basin would not normally be expected during the spreading phase of continental margin development, and therefore it has been explained by Thrasher (1990) as a

manifestation of propagation of a major mid-ocean ridge transform into neighbouring continental crust, perhaps exploiting a pre-existing terrane boundary. Figure 2.3 illustrates the Latest Cretaceous paleogeographic setting of the basin (from King & Thrasher 1996). The extension associated with this phase caused the formation of a series of relatively small (10 – 50 km wide and 50 – 150 km long) Sub-basins and half-grabens (i.e. Mania and Pakawau Sub-basins), controlled by north and northeast striking normal faults. Late Cretaceous strata were deposited in these sub-basins during their formation (King & Thrasher 1996).

The second phase of basin development occurred during the Paleocene to Early Oligocene as Taranaki Basin evolved as a type of passive margin, characterised by regional subsidence (King & Thrasher 1996). Figure 2.4 illustrates the Late Eocene paleogeography. A large northwest facing (northwest deepening) marine embayment formed, bounded by land to the south and east (Fig. 2.4). From the Early Paleogene, as regional subsidence and marine inundation continued, this embayment expanded with resulting southward and eastward onlap and marine transgression (King & Thrasher 1996). Late Eocene – Early Oligocene strata (e.g. Turi Formation and the Matapo Sandstone Member) were subsequently deposited with southward depositional onlap.

The third phase of Taranaki Basin development occurred during the mid-Oligocene to Early Miocene and involved culmination of the passive margin phase and development of an active-convergent margin basin setting, associated with Australian-Pacific plate boundary development through New Zealand (King & Thrasher 1996). Tripathi and Kamp (2008) report that by 29 Ma the first reverse movement across the Taranaki Fault Zone had occurred. This consequently caused large paleogeographic changes along the eastern margin of the basin, with the Taranaki Fault forming a prominent eastern margin to the basin. A north trending foredeep trough formed adjacent to Taranaki Fault (Fig. 2.5), caused by overthrusting on Taranaki fault and fold/fault deformation on the Taranaki Fault Zone to the west (King & Thrasher 1996). It is this change in paleogeography (Eocene embayment to Oligocene foredeep) controlled dominantly by the evolving Taranaki Fault Zone that is of particular interest in this study. From the Middle Oligocene, renewed and rapid subsidence caused bathyal environments to develop in the foredeep. Throughout the later part (Late

Oligocene) of this interval, mainly calcareous mudstone and limestone accumulated in the foredeep (e.g. Otaraoa Formation, Tikorangi Formation and Taimana Formation). By the Late Oligocene a continental slope existed along the eastern margin of the basin, with its upper end pinned to the top of the basement overthrust.

The fourth phase of basin development occurred during the Miocene and is referred to as the convergent margin phase of Taranaki Basin, which reflects the formation of the Australian-Pacific plate boundary zone through New Zealand. Carbonate sedimentation during the Oligocene gave way to terrigenous sedimentation (Wai-iti Group) at the Waitakean-Otaian stage boundary (King & Thrasher 1996). This change marks the end of the marine transgressive megacycle and the start of a regressive sedimentary megacycle and northwestward progradation of a shelf-slope sedimentary wedge that has continued to the present day. Figure 2.6 from King and Thrasher (1996) illustrates the Late Miocene palaeography of the basin. It shows the start of northwestward progradation of the modern shelf-slope system that buried the trace of the Taranaki Fault. The Tarata Thrust Zone continued to be active into the Late Miocene, and this interval also included substantial inversion in the southern parts of the basin.

The last (fifth) phase of development occurred during the Plio-Pleistocene, when deformation behind the active magmatic arc (Taupo Volcanic Zone) caused extension forming the Northern and Central Grabens. This period is characterised by very high sediment input into the basin causing the continental shelf-slope system to substantially widen (Fig. 2.7; Hansen & Kamp 2006).

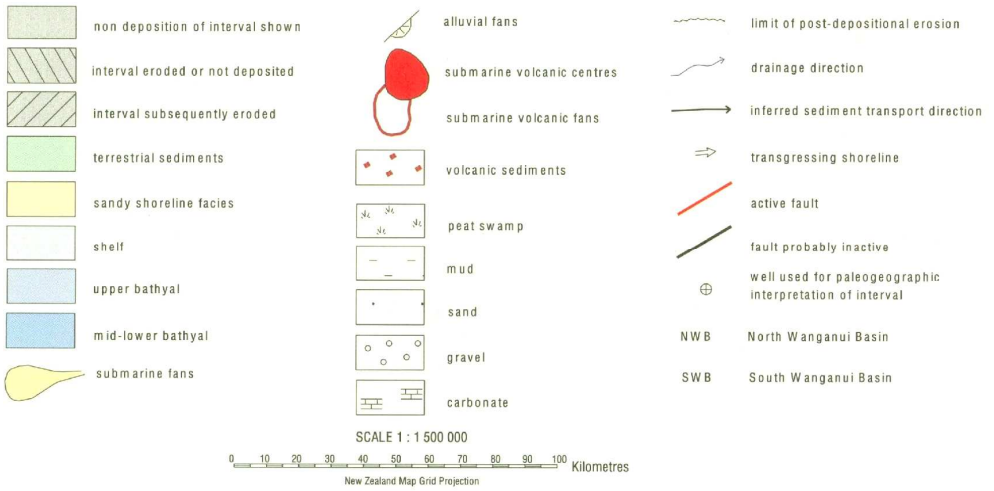

Figure 2.2. Legend for figures 2.3 – 2.7, illustrating paleobathymetry, paleodepositional environments, lateral scale and other paleogeographic map features. From King and Thrasher (1996).

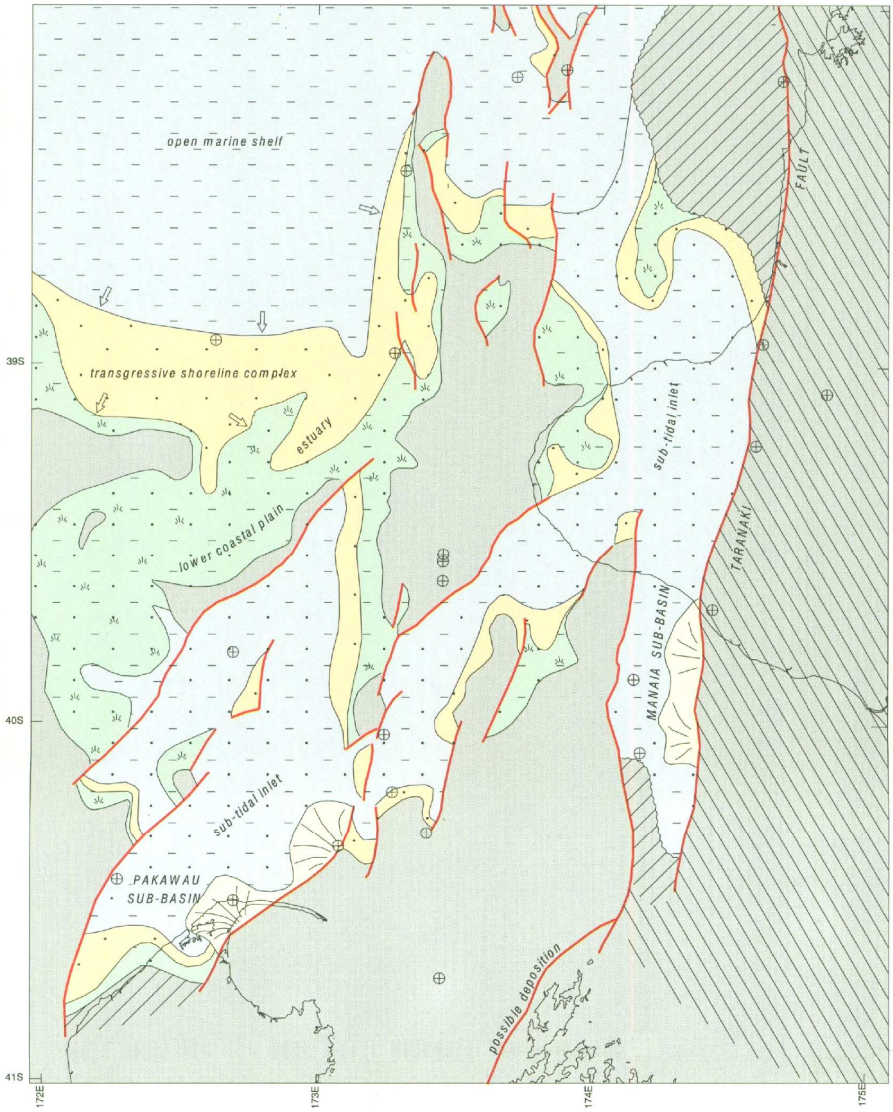

Figure 2.3. Paleogeographic map of Taranaki Basin for the latest Cretaceous Period (~65 Ma). Note the depositional extent in eastern and southern Taranaki Basin, limited to fault controlled sub-basins. From King and Thrasher (1996, Map 13).

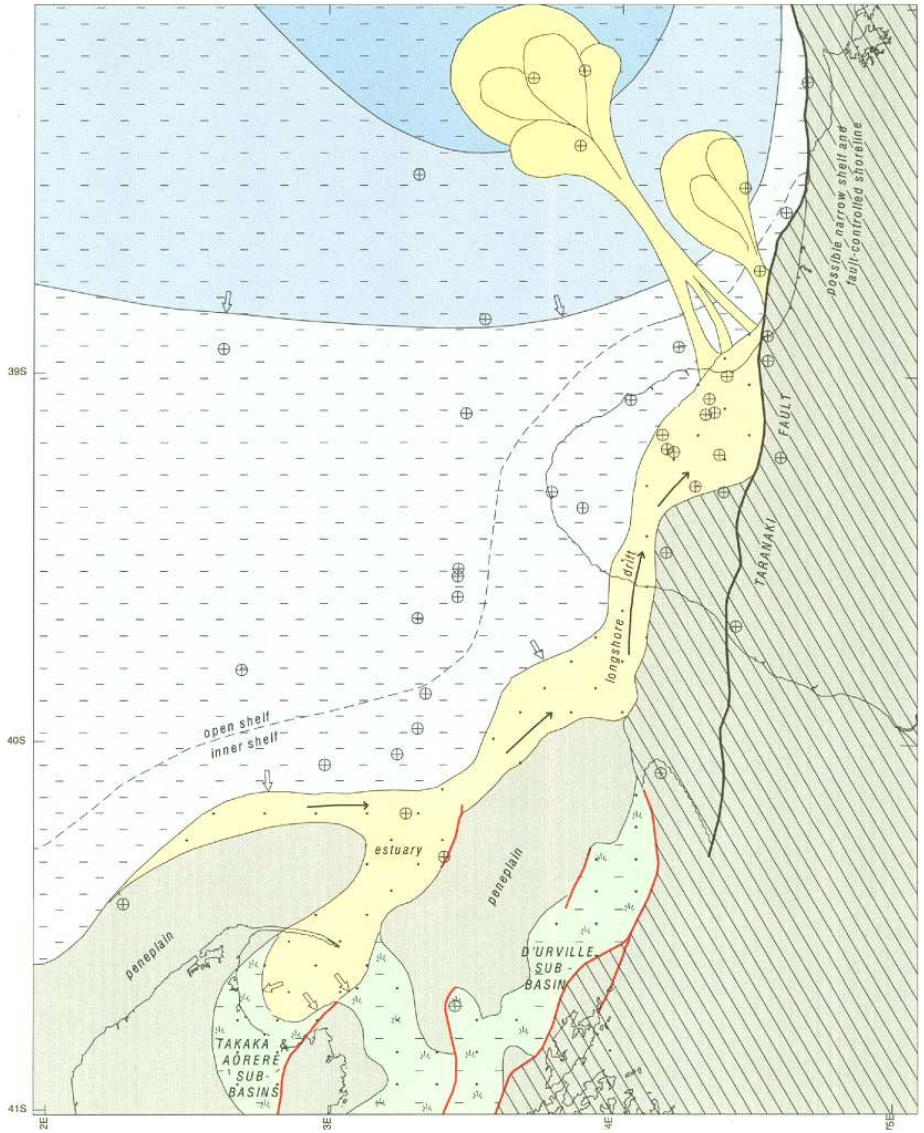

Figure 2.4. Paleogeographic map of Taranaki Basin for the Late Eocene (~36 Ma). Note the presence of a northwestward deepening basin. From King and Thrasher (1996, Map 17).

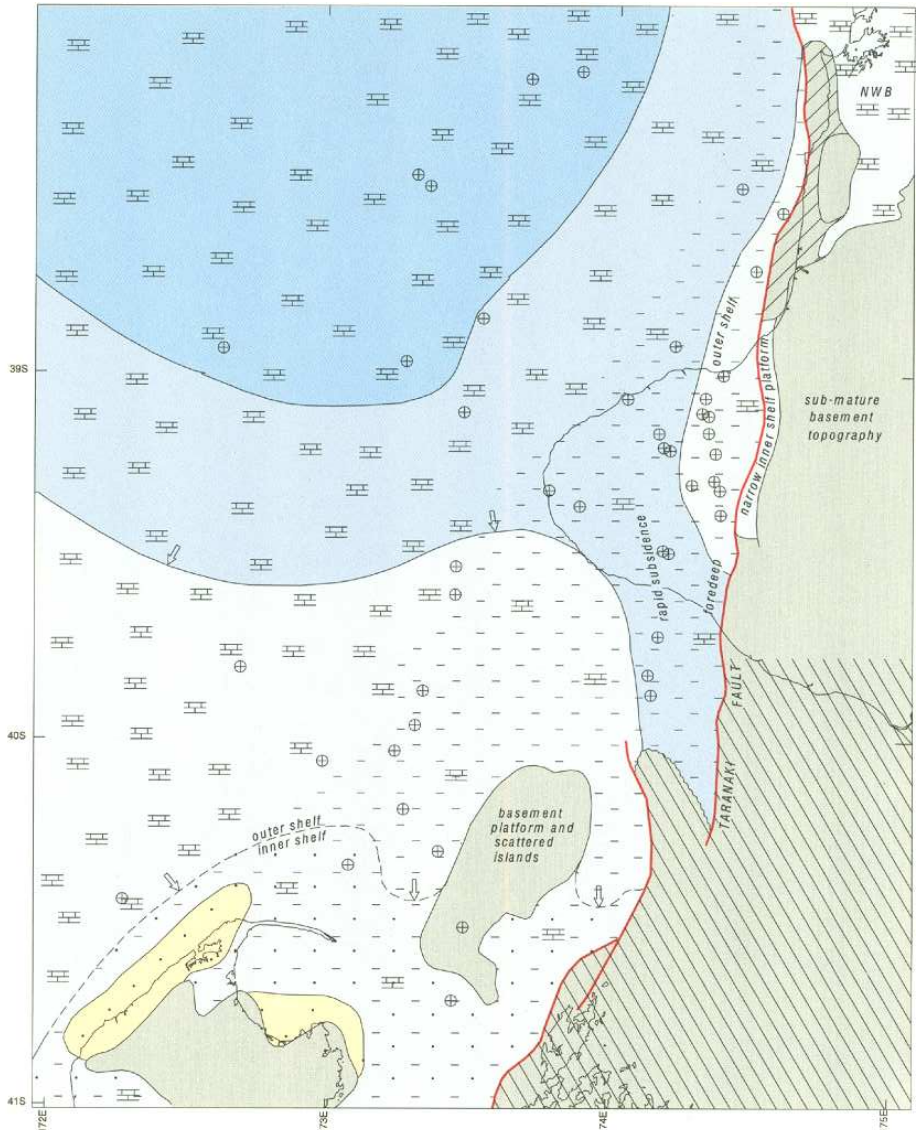

Figure 2.5. Paleogeographic map of Taranaki Basin for the Oligocene Period (~28 Ma). Note development of a foredeep trough adjacent to Taranaki Fault. From King and Thrasher (1996, Map 18).

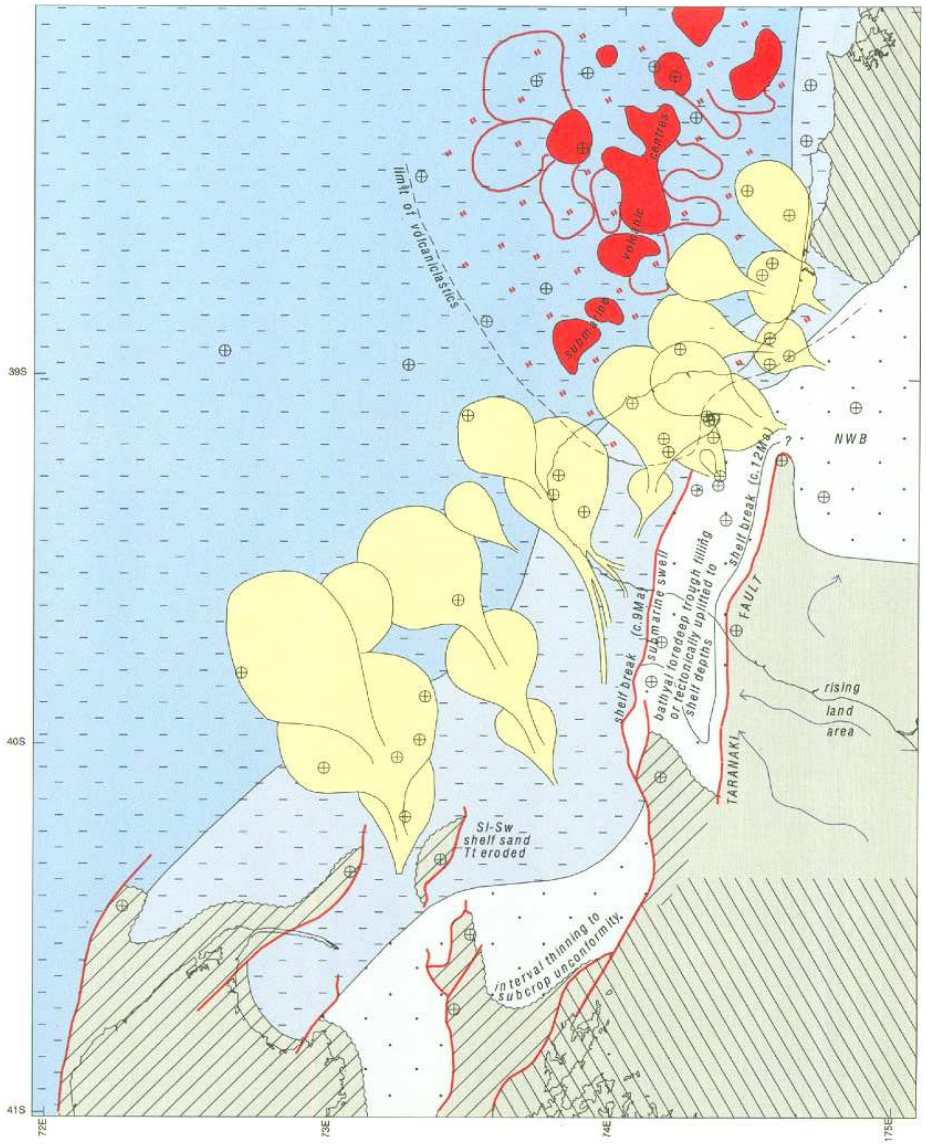

Figure 2.6. Paleogeographic map of Taranaki Basin for the Late Miocene Period (~8 Ma). Note the high sediment influx into the basin and masking of the Taranaki Fault. From King and Thrasher (1996, Map 21).

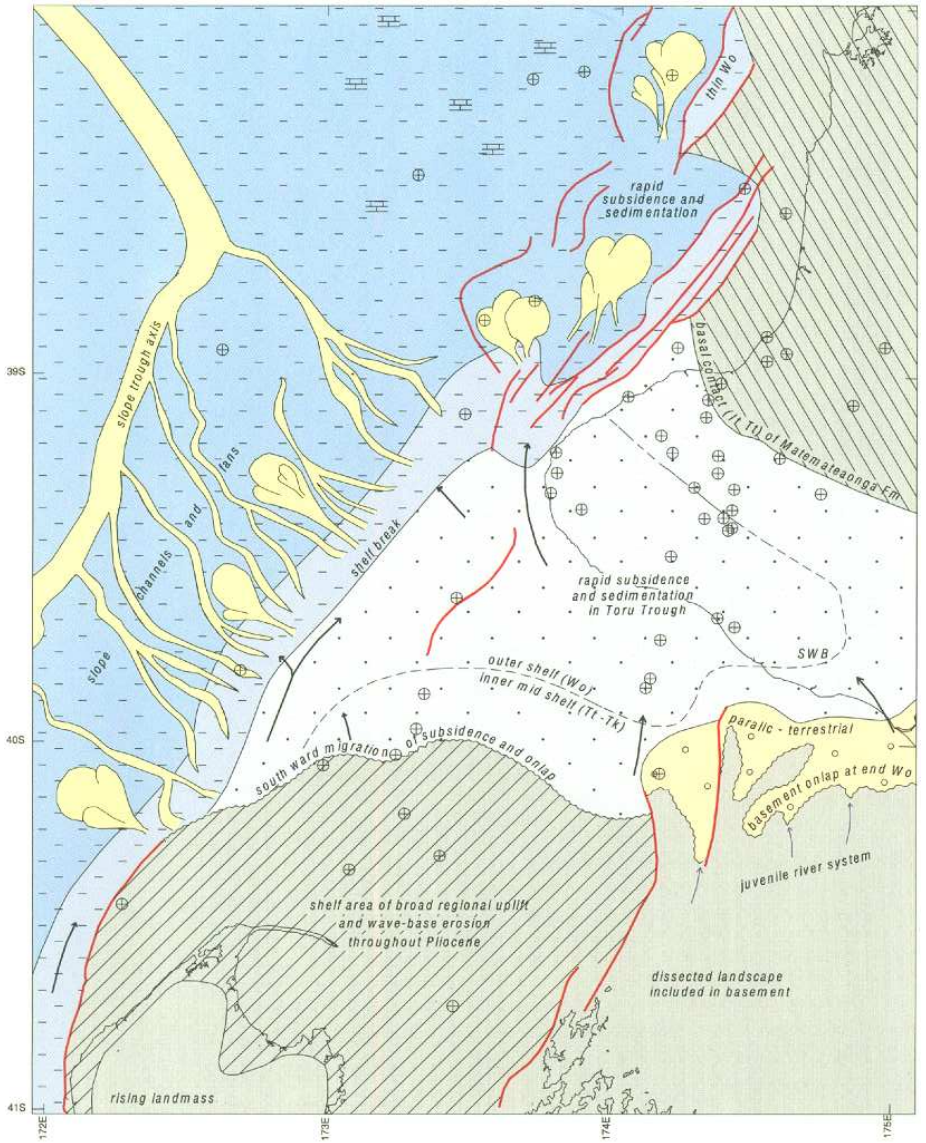

Figure 2.7. Paleogeographic map of Taranaki Basin for the Early Pliocene Period (~5 Ma). Note the northwestward progradation of the shelf and subsidence-deposition in the south Taranaki Peninsula area. From King and Thrasher (1996, Map 22).

2.4 BASEMENT GEOLOGY

New Zealand basement has Cambrian to Early Cretaceous ages and is of sedimentary, volcanic and plutonic heritage, with some units exhibiting a metamorphic overprint (Mortimer 2004). The distribution of the basement terranes and their ages are now well understood for onshore parts of New Zealand, with many workers contributing to the interpretation and classification of terranes over the last few decades. Figure 2.8 displays the distribution of the terranes and associated ages. The basement rocks underlying the Late Cretaceous – Cenozoic sedimentary sequences of the Taranaki Peninsula area have been assigned to the Murihiku and Brook Street Terranes and to the Median Batholith. It is possible that these terranes and others farther afield from the basin (particularly south of Taranaki Basin) acted as source rocks for the Late Eocene – Oligocene successions observed in the study area. In King and Thrasher (1996) and Smale (1996), Separation Point Batholith (Median Batholith) and Karamea Batholith are interpreted as the dominant source of terrigenous sediments for the Oligocene Ngatoro Group. Brief descriptions of the Murihiku Terrane, Median Batholith and Karamea Batholith (and related batholiths) are given below.

2.4.1 Murihiku Terrane

The distribution of the Murihiku terrane throughout New Zealand is shown in Fig. 2.8. It crops out in Southland and as the Kawhia Syncline in central-western North Island. In western North Island, Murihiku basement rocks (Murihiku Supergroup) mark the eastern boundary of Taranaki Basin forming the hanging wall of Taranaki Fault (King & Thrasher 1996). The eastern limit is marked by the north-south striking Waipa Fault. Murihiku rocks in the western North Island area are mainly volcaniclastic sandstone and siltstone of Late Triassic to Late Jurassic age (Briggs et al. 2004).

2.4.2 Median Batholith

The Median Batholith is a term used to define plutons that have intruded the contact between the Takaka Terrane and the Brook Street Terrane (Mortimer 2004). Figure 2.8 displays the distribution of the Median Batholith through New

Zealand, especially in Fiordland, northwest Nelson and extending to the north offshore of western North Island. Median Batholith is a composite cordilleran batholith, comprising dozens of 1-10 km size gabbroic-granitic I-type plutons with Late Devonian (Riwaka Complex) to Early Cretaceous (Separation Point Suite) ages (Muir et al. 1996; Mortimer 2004).

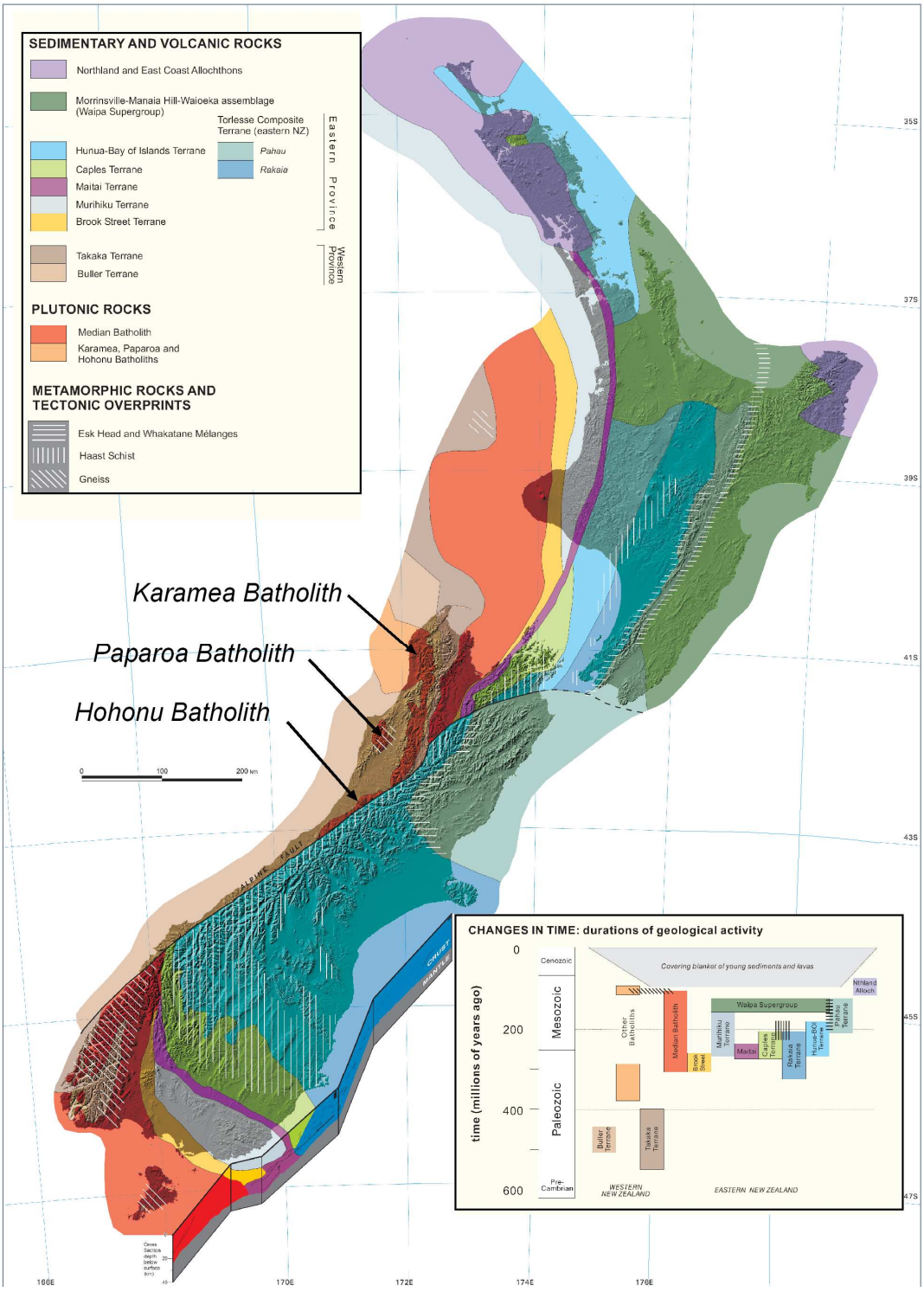

Figure 2.8. The distribution of terranes (basement rocks) through New Zealand with corresponding ages. Modified from Mortimer and Smith Lyttle (2001).

2.4.3 Karamea, Paparoa and Hohonu Batholiths

The Karamea, Paparoa and Hohonu Batholiths occur in northwestern South Island lying within the Buller Terrane (metamorphosed siliciclastic basement) (Fig. 2.8). The Karamea, Paparoa and Hohonu batholiths are all granite dominated (Mortimer 2004). The Karamea Batholith has middle to Late Devonian (~375 Ma) U-Pb zircon ages (Muir et al. 1996), the Windy Point Granite of the Paparoa Batholith has mostly Carboniferous U-Pb zircon ages (~328 Ma) (Muir et al. 1994) and the Hohonu Batholith has middle to Late Devonian (Summit Granite) to Late Cretaceous (French Creek Granite) ages (Waight et al. 1997).

2.5 TARANAKI BASIN SUBSURFACE STRATIGRAPHY

Many workers have analysed Taranaki Basin's stratigraphy, however in the most comprehensive synthesis appeared in the monograph by King and Thrasher (1996). Taranaki Basin has a Cretaceous – Cenozoic sedimentary fill that is mainly subsurface, with much of the information base sourced from geophysical well logs from about 350 exploration wells drilled during the last 50 years (Crown Minerals 2007), and over 20,000 km of seismic reflection profile data (King & Thrasher 1996). Figure 2.9 displays the Cretaceous – Cenozoic stratigraphic framework of Taranaki Basin. The lithostratigraphy and distribution of subsurface units are related to the tectonic development of Taranaki Basin, with the five stages of basin development described in Section 2.3 shown on the figure. At the broadest level the Cretaceous – Cenozoic sedimentary record is considered a major depositional cycle, with a transgressive phase during the Late Cretaceous to Early Miocene, followed by a regressive phase that is ongoing to the present day. In this study the Late Eocene – Oligocene sedimentary succession in the Taranaki Peninsula area is of particular interest, spanning the change from passive margin development with renewed extension to active margin (convergence) development. The Late Eocene – Oligocene succession is described in more detail in the following section, together with brief description of the underlying (Eocene Kapuni Group) and overlying (Miocene Wai-iti Group) strata. For more detailed lithostratigraphic descriptions the readers are referred to King and Thrasher (1996).

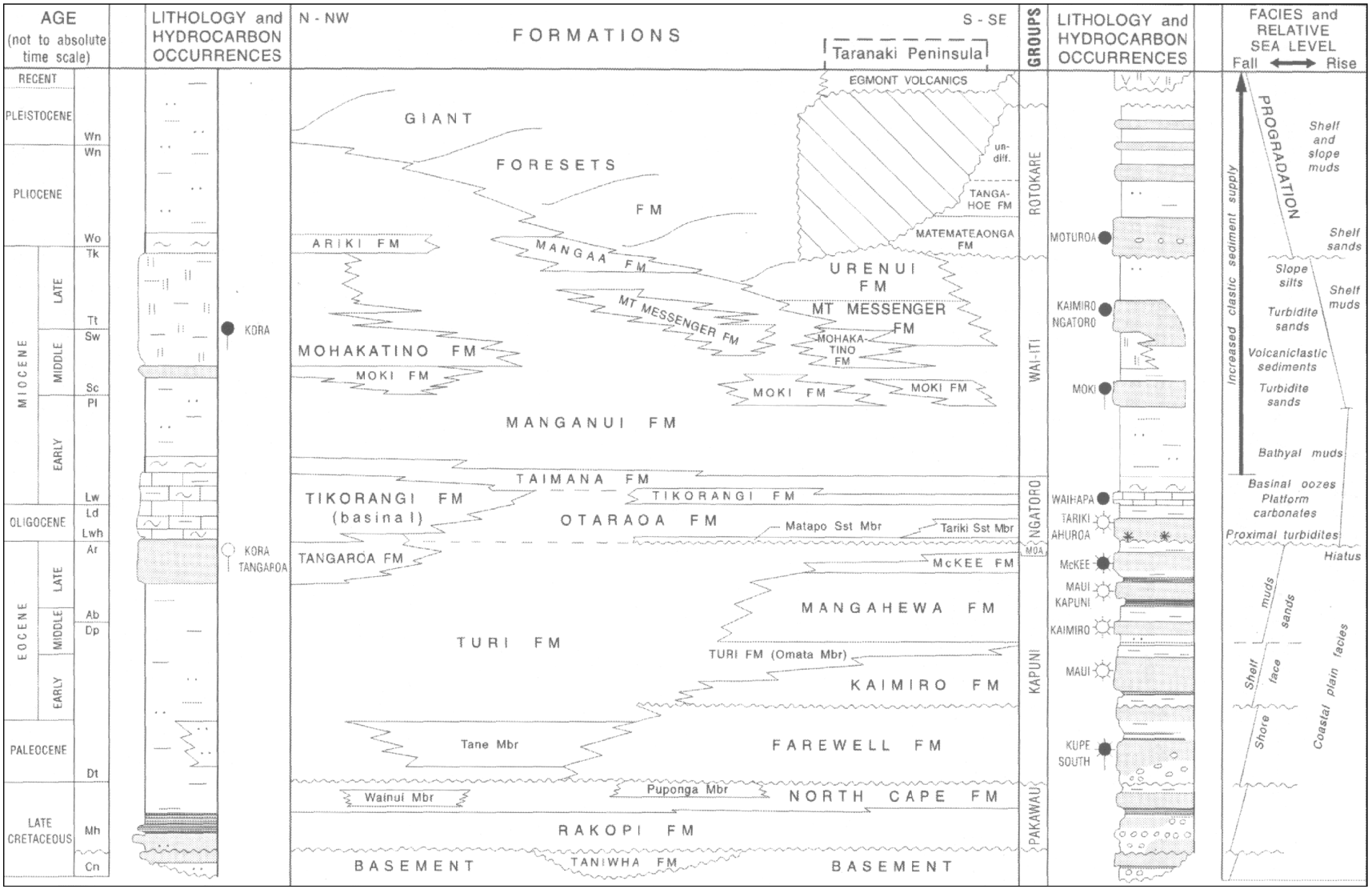

Figure 2.9. Cretaceous-Cenozoic framework for Taranaki Basin. Note, figure is not to scale. From King and Thrasher (1996, Fig. 4.1).

2.5.1 Kapuni Group

The Kapuni Group represents terrestrial and intercalated marginal marine strata of Paleocene to Eocene age. In this study Mangahewa and McKee Formation are observed to underlie Moa and Ngatoro Group strata. The Mangahewa Formation is a terrestrial dominated formation, consisting of coal measures, interbedded sandstone, siltstone and mudstone. It is at its thickest in the Taranaki Peninsula area representing all terrestrial and marginal marine lithofacies of middle to Late Eocene age (excluding McKee Formation) (Fig. 2.9). The McKee Formation is a quartzose, fine to coarse grained carbonaceous unit, with an interpreted inner shelf to coastal depositional setting, probably a transgressive shoreface or barrier bar complex (Palmer 1985; King & Thrasher 1996). The McKee Formation is restricted to the Taranaki Peninsula area and has a Runangan (Late Eocene) age (Fig. 2.9; King & Thrasher 1996).

2.5.2 Moa Group

The Moa Group represents an entirely marine succession of Paleocene to latest Eocene age. Figure 2.9 shows the age and lateral distribution of the Moa Group, with the group distributed mostly in the west and northwest of Taranaki Basin.

2.5.2.1 Turi Formation

The Turi Formation is mainly a non calcareous, carbonaceous, marine mudstone with minor sandstone interbeds, trace lithics, pyrite and glauconite (King & Thrasher 1996). The deposition of Turi Formation marks a change from non-marine and marine depositional environments with southward depositional onlap, reflecting the basin-wide and ongoing marine transgression. Although the Turi Formation is recorded in the west and northwest in Taranaki Basin to have Early Paleogene ages (Fig. 2.9), in the Taranaki Peninsula area, Turi Formation is of Late Eocene and possibly earliest Oligocene age. The Turi Formation was deposited in an Eocene embayment, with the thickest accumulation in the northeast of the basin (over 800 m intersected in Turi-1), reflecting north to northwest deepening (King & Thrasher 1996). The variation in Turi Formation thickness through the basin possibly supports erosion at the marine/non-marine

interface, also accounting for the complete absence of McKee Formation and Turi formation in some areas (Carter et al. 1987a).

2.5.3 Ngatoro Group

The Ngatoro Group represents generally calcareous rocks of Oligocene – earliest Miocene age in Taranaki Basin, reflecting deposition in a moderately starved basin setting, although considerable volumes of sediment still accumulated. The Ngatoro Group succession is thickest in a foredeep trough along the eastern margin of the basin, particularly in the central Taranaki Peninsula area (King & Thrasher 1996).

2.5.3.1 Otaraoa Formation

Matapo Sandstone Member

Matapo Sandstone is a very condensed unit, typically 5 to 20 m thick, located at the base of Otaraoa Formation. It is typically a fine to coarse grained, partly to highly calcareous, highly glauconitic sandstone of Lower Whaingaroan age (King & Thrasher 1996). The accumulation of Matapo Sandstone represents submergence of the basin in the Taranaki Peninsula area to outer shelf depths (King & Thrasher 1996). Matapo Sandstone represents southward migration of facies as part of what appears to be a normal marine transgression.

Otaraoa Formation

Otaraoa Formation represents a sequence of calcareous siltstone and sandstone. The Otaraoa *intra* Member is a term used to define Otaraoa Formation that occurs between the base of the formation and the Tariki Sandstone Member (King & Thrasher 1996). Otaraoa Formation is thicker than 100 m everywhere in the eastern margin of the basin and is at its thickest in the central Taranaki Peninsula area where it exceeds 1000 m, with progressive thinning to the south and west.

Tariki Sandstone Member

The Tariki Sandstone Member of de Bock et al. (1990) is comprised mainly of stacked clean sandstone interbedded with calcareous mudstone. In de Bock et al. (1990), this sequence is interpreted as a series of stacked turbidites with an Upper Whaingaroan age. This member is only observed along the eastern margin of the basin in the Taranaki Peninsula area (Fig. 2.9), accumulating within the rapidly subsiding Oligocene foredeep trough at bathyal depths. The packets of turbidites within the Tariki Sandstone reflect different stages of accumulation of a submarine fan. The sediment forming the member was clearly derived from the direction of the Patea-Tongaporutu High although the sediment may have been worked along a shoreline from a more distant source before being captured by shelf channels and redeposited down a slope. Although Tariki Sandstone may lie in close stratigraphic proximity to the Matapo Sandstone, these units accumulated in completely different environments.

2.5.3.2 Tikorangi Formation

The Tikorangi Formation is a limestone interval that occurs in various parts of eastern Taranaki Basin. The formation is of lower Waitakian age and was deposited on a west-facing slope (Hood et al. 2003). Tikorangi Formation is mainly comprised of crypto to finely crystalline grainstone, alternating with interbeds of packstone, wackestone, sandy limestone, calcareous siltstone and marl (King & Thrasher 1996). To the west of Taranaki Peninsula, age equivalent foraminiferal carbonate (marly) sediments were deposited at bathyal depths (King & Thrasher 1996).

2.5.3.3 Taimana Formation

The Taimana Formation is comprised of a calcareous mudstone between Tikorangi Formation and the terrigenous Wai-iti Group. The Taimana Formation has a similar lithology to the Otaraoa Formation and in places where Tikorangi Formation is absent, Otaraoa Formation and Taimana Formation are often indistinguishable (King & Thrasher 1996). Taimana Formation is mainly a calcareous siltstone interval with fine sandstone interbeds. In the eastern margin

of the basin, Taimana Formation has a lower Waitakian to upper Waitakian-Otaian age. In the west of the basin (distal area), Taimana Formation gets as young as Altonian to Clifdenian (King & Thrasher 1996).

2.5.4 Wai-iti Group

The Wai-iti Group incorporates most of the Miocene succession in Taranaki Basin, dominantly a regressive, terrigenous succession. In this study, the basin floor mudstone and siltstone of Manganui Formation overlie calcareous sediments of the Ngatoro Group. The thick (2000 – 3000 m) Miocene Wai-iti Group succession observed along the eastern margin of the basin progressively thins to the west and northwest. Following the initial filling of the Oligocene foredeep, northwestward progradation of a shelf-slope margin occurred. (King & Thrasher 1996; Hansen & Kamp 2006).

2.6 ONSHORE NORTH ISLAND AGE EQUIVALENT UNITS

The Late Eocene – Oligocene units in Taranaki Basin described above are correlatives of the Te Kuiti Group exposed in the Waikato area to the east of the Herangi High. Some of the sandstones units in the Te Kuiti Group and other North Island correlatives have also been examined (petrographically, Chapter 4) in this study and U-Pb geochronology undertaken upon zircons (Chapter 5) from them to help constrain Late Eocene – Oligocene paleogeographic interpretations (Chapter 6). For sampling locations and information about onshore North Island correlative units see Appendix I.

2.6.1 Te Kuiti Group lithostratigraphy, age and paleoenvironments

The Te Kuiti Group represents a succession dominated by calcareous sandstone, siltstone and limestone that outcrop discontinuously to the east (upthrown side) of Taranaki Fault, in central-western North Island. This mixed carbonate-siliciclastic succession is equivalent to Moa Group and the Ngatoro Group in Taranaki Basin. The marine onlap evident in Taranaki Basin also affected the Te Kuiti Group basin with a well known transition from terrestrial coal measures (Waikato Coal Measures) through to shelfal and upper slope limestone, marl and terrigenous

lithologies. Figure 2.10 displays a revised lithostratigraphy and chronostratigraphy for the Te Kuiti Group (Tripathi & Kamp 2008). The model presented in Figure 2.10 illustrates the stratigraphic evolution of the Te Kuiti Group in relation to the various stages of movement on the Taranaki Fault, and is discussed in more detail in Section 2.5. At the broadest level, the Te Kuiti Group is subdivided into two subgroups, the basal Okoko Subgroup and overlying Castle Craig Subgroup. A prominent unconformity marks the change from the dominantly mixed carbonate-siliciclastic sediments of the Okoko Subgroup to the carbonate dominated sediments of the Castle Craig Subgroup (Tripathi & Kamp 2008).

The Glen Massey Formation is comprised of three members, a lower flaggy limestone (Elgood Limestone Member), overlying calcareous siltstone (Dunphail Siltstone Member) and calcareous sandstone (Ahirau Sandstone Member) (Kear & Schofield 1959; White & Waterhouse 1993). The Ahirau Sandstone Member has been sampled and analysed in this study. Glen Massey Formation as observed in outcrop has a Lower Whaingaroan (Early Oligocene) age and was deposited in inner to outer shelf environments (Tripathi 2009). The Aotea Formation is subdivided into five members, a basal carbonate facies (Waimai Limestone Member), a fine to medium sandstone with varying amounts of carbonate (Hauturu Sandstone Member, which is sampled in this study), a massive to crudely bedded fine muddy sandstone (Kihi Sandstone Member), and a calcareous sandstone with thin siltstone interbeds (Mangiti Sandstone Member) that grades upward into a massive siltstone (Patikirau Siltstone Member) (Tripathi 2009). Aotea Formation sediments have an Upper Whaingaroan to Duntroonian age and were deposited in shelf to upper bathyal water depths (Kear & Schofield 1959; Tripathi 2009).

2.6.2 Pungapunga Formation (Taumarunui quartz sandstone)

The Pungapunga Formation was used by Cartwright (2003) to define Te Kuiti Group rocks observed in the central-eastern parts of the King Country, where they overlie basement (Waipapa Terrane). Because the quartzitic sandstone at the base of the Pungapunga Formation was sampled from the Taumarunui area, it is informally referred to in this thesis as Taumarunui quartz sandstone member. This sandstone unit ranges from poorly to well sorted and is a medium to coarse sandstone which becomes glauconitic and calcareous in its upper parts

(Cartwright 2003). Taumarunui quartz sandstone sediments likely have a Lower Whaingaroan age, and were deposited in a coastal plain or fluvial environment (Cartwright 2003).

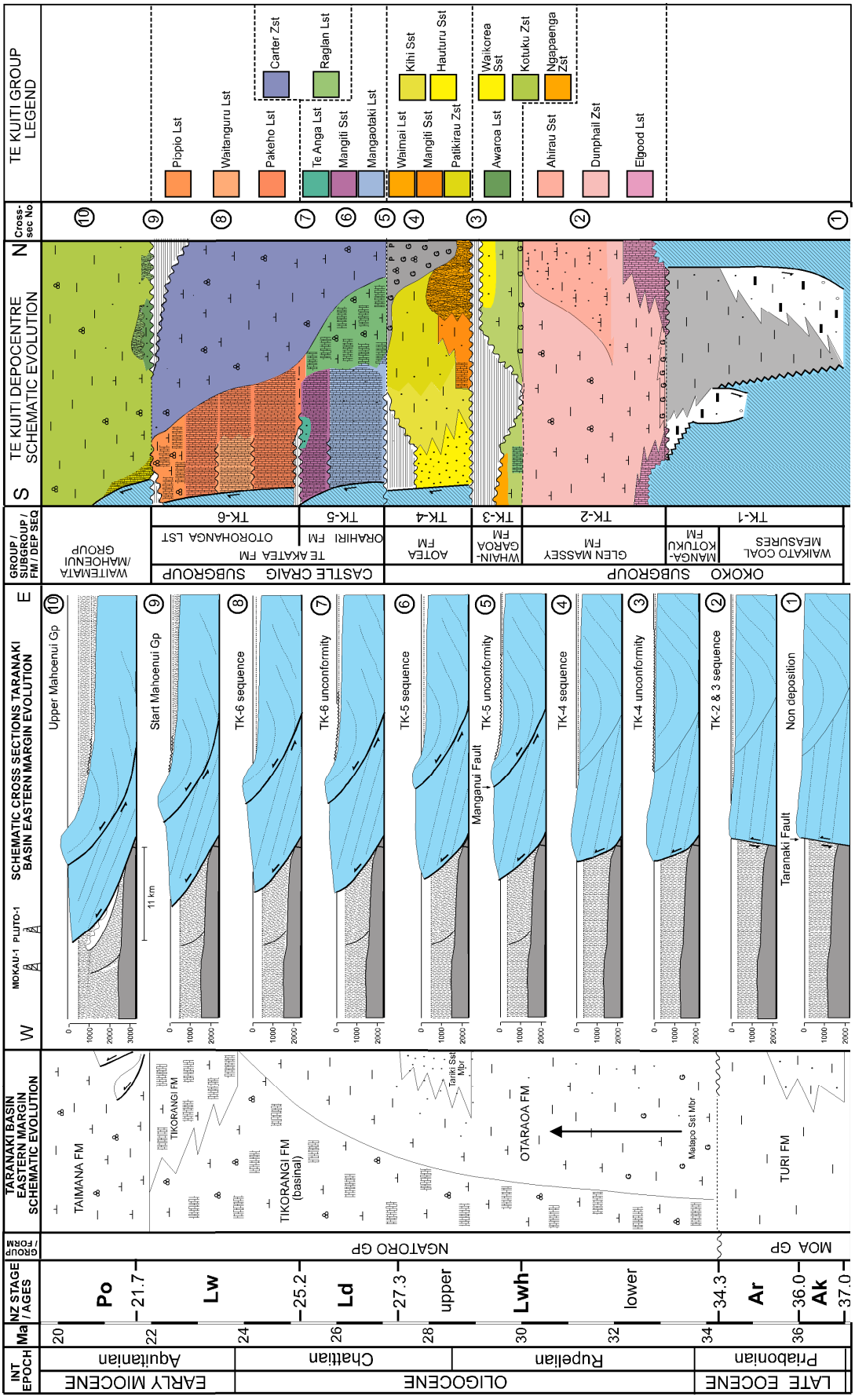

Figure 2.10. Late Eocene – Early Miocene displacement model for Taranaki Fault Zone with comparative chronostratigraphic panels for the Te Kuiti Group and Taranaki Basin. From Tripathi and Kamp (2008).

2.6.3 Otaihanga Outlier

The Late Eocene – Oligocene aged Otaihanga Outlier are the oldest cover rock succession exposed in Wanganui Basin, and occurs northeast of Wellington, near Paraparaumu, were they are exposed as a small outlier against basement (King & Thrasher 1996, after Grant-Taylor & Williams 1977). This small outcrop area represents a remnant of what was once probably more extensive Oligocene cover. A quartz sandstone sample obtained from the base of the succession is referred to as the Otaihanga Outlier in this thesis. This quartz sandstone crops out in a quarry as a 8 m-thick, bed with limonite stained grit (King & Thrasher 1996). The quartz sandstone is overlain by a glauconitic muddy sandstone up to 60 m thick, that is thought to have a Whaingaroan age (early to Late Oligocene). The quartz sandstone may be Late Eocene or Early Oligocene in age. The depositional environment of the quartz sandstone is not clear as it may have accumulated in a fluvial or marginal marine depositional environment (King & Thrasher 1996, after Grant-Taylor & Williams 1977). In King and Thrasher (1996) this facies is regarded as a possible lateral equivalent of the McKee Formation, with the overlying glauconitic muddy sandstone being of possible Lower Whaingaroan age and a correlative of the Matapo Sandstone Member in Taranaki Basin.

2.7 PALEOGENE TARANAKI FAULT DISPLACEMENT

As mentioned in Section 2.3, Taranaki Basin evolved during the late Paleogene in different tectonic regimes. During the Late Eocene and Early Oligocene there was crustal extensional regime with possible normal displacement on Taranaki Fault and related faults in the southern part of the basin. This represented the northern end of a zone of continental extension in southern New Zealand that was co-linear with sea floor spreading in the Emerald Basin (e.g. Kamp 1986; King 2000). From about 29 Ma, according to Tripathi and Kamp (2008), Taranaki Fault started to accommodate crustal shortening, which led, mainly during the Early Miocene (Otaian), to overthrusting of Murihiku Terrane basement into the eastern margin of the basin. Stagpoole and Nicol (2008) have an earlier timing for the start of shortening across Taranaki Basin in the peninsula area, which they place at about 40 Ma (Middle Eocene).

Tripathi and Kamp (2008) base their evidence for a mid-Oligocene initiation of reverse displacement on Taranaki Fault is based on interpretation of the lithostratigraphy and sequence stratigraphy of the Late Eocene – Oligocene Te Kuiti Group succession that crops out in the Waikato and King Country regions, and they have drawn a useful series of cross-sections to scale to show how the displacement on Taranaki Fault changed from normal to reverse (Fig. 2.10). Comparative chronostratigraphic panels, one for Taranaki Basin succession and the other for the Te Kuiti Group succession are also displayed in Figure 2.10, showing how accumulation of particular formations and members relate to the timing and magniture of displacement. In this model, reverse displacement across the Taranaki Fault Zone started at c. 29 Ma (Upper Whaingaroan), but there was minimal actual horizontal displacement at that early stage. This was followed by episodic cycles of uplift and subsidence of the hanging wall during the Oligocene associated with 1 to a few km of horizontal displacement across the Taranaki Fault Zone (Tripathi & Kamp 2008). The majority of horizontal displacement (overthrusting) is considered to have occurred during the Otaian (Early Miocene). Tripathi and Kamp's 2008 model usefully shows correlation of Taranaki Basin units with those of the Te Kuiti Group (Fig. 2.10). New geological data presented in this thesis for the eastern margin of Taranaki Basin tests this model.

CHAPTER THREE
GEOPHYSICAL WELL LOG INTERPRETATION

3.1 INTRODUCTION

Geophysical well logs (or more commonly wireline logs) are a continuous recording of sophisticated geophysical parameters about the character and composition of formations measured and plotted against depth along a borehole (Rider 1986). Wireline logs are important interpretive datasets, used for studying subsurface rocks and for enabling subsurface correlations between well sections. In particular, wireline logging is used in petroleum geology to analyse and define subsurface stratigraphy, as an alternative to cutting core samples, which is very expensive, and as an important means of evaluating well cutting samples (Kearey & Brooks 1991). The geophysical data obtained from wireline logs can be interpreted in terms of geological parameters, and, combined with calibration against well cuttings, wireline log interpretation can result in precise definition of formation characteristics such as thickness, lithology, porosity, permeability and stratal dip (Asquith 1982; Rider 1986; Kearey & Brooks 1991).

Because of the entirely subsurface nature of the Late Eocene – Oligocene units in Taranaki Basin, most of the available lithostratigraphic information is gained through interpretation of geophysical data. This chapter outlines and discusses the identification and interpretation of geophysical well-log patterns through the Late Eocene – Oligocene section of selected wells along Taranaki Basin's eastern margin, particularly around Taranaki Peninsula. Using geophysical wireline log characteristics calibrated against geological descriptions from well completion reports and samples obtained from well cuttings, a suite of wireline motifs has been described. Integration of wireline log data with other lithological and paleoenvironmental data sources has formed the basis for interpretation of depositional paleoenvironments for the Late Eocene and Oligocene sediments in Taranaki basin. Understanding the distribution and occurrence of Late Eocene – Oligocene sandstones through the eastern margin of the basin using these geophysical well logs has also been an important issue for U-Pb geochronology

and provenance interpretations to assist understanding about the paleogeographic development of the basin (Chapters 5 & 6).

3.2 WELL LOG TYPES

An extensive suite of physical and geophysical parameters can potentially be measured during well logging, including measurement of spontaneous phenomena and induced reactions. In some cases up to 100 geophysical parameters can be measured simultaneously during logging. Many of these parameters are of interest to geoscientists for geological interpretations, while other parameters are also of interest to engineers and drilling operators. For geological interpretation however there are a select few log types routinely used in conjunction with each other for comparison and interpretation of geological information. These include gamma-ray (GR) log, calliper (CALI) log, resistivity (RES) logs, sonic velocity (DT) log and spontaneous potential (SP) log, as summarised in Table 3.1 and discussed in more detail in the following section.

Table 3.1 Main log types, properties measured, and geological uses. From Cant (1992).

Log	Property Measured	Units	Geological uses
Gamma-ray	Formations natural radioactivity, related to decaying K, Th and U	API	Lithology proxy (shaliness), correlation, curve shape analysis
Caliper	Diameter of bore hole	Centimetres	Evaluation of hole conditions and reliability of other logs
Resistivity	Formations resistive properties to an applied current	Ohm-metre	Fluid analysis and suggesting porosity
Sonic	Velocity of a compressional sound wave	Microseconds/metre	Identification of porous zones and tightly cemented zones
Spontaneous potential	Natural electrical potential (compared to drilling mud)	Millivolts	Lithology (in some cases), correlation, curve shape analysis, identification of porous zones

3.2.1 Gamma-ray log

The GR log provides a record of the natural radioactivity (gamma emissions), induced by the decay of uranium, thorium and potassium in a formation. Most rocks show some degree of natural radioactivity but shales have by far the strongest emission of radioactivity because the naturally occurring isotopes bond more effectively to fine grained sediments, particularly clay minerals (Rider 1986; Cant 1992). Although the GR log is not directly a function of grain size, the ability of this log type to identify fine grained or shale rich formations (high GR) allows it to be used to distinguish between 'dirty' lithologies such as shale and cleaner (clay-free) lithologies such as sandstone and limestone (Fig. 3.1; Cant 1992). Hence the GR log is often used as a proxy for grain size or as a shaliness indicator, where an increase or decrease in a GR response reflects a decrease (increase in clay content) or increase (decrease in clay content) in grain size respectively. While the relationship between GR value and shale volume/grain size is complicated, in detrital sediments the GR log provides a reliable first indicator of lithology and grain size trends stratigraphically, which should be confirmed by other logs (Cant 1992). The GR log is the principal log used in this study to define wireline motifs, interpret lithology and to correlate units between wells/holes.

3.2.2 Calliper log

The CALI log provides a vertical recording of well bore hole diameter with depth, showing a formations mechanical response to drilling (Rider 1986). Hole size and shape changes while drilling due to erosion by the circulating drilling mud and from mud infiltration or caking. If a measured hole is the same size as the drill bit (on-gauge), this suggests the formation is coherent and hard. Holes smaller than the drill bit (over-gauge) are typical of permeable beds such as sandstone, where the infiltration of drilling mud causes caking on the borehole walls decreasing borehole diameter (Fig. 3.1; Rider 1986). Holes with much larger calliper measurements than the drill bit occur where part of the formation has been 'washed out' or eroded by the drilling mud. This is typical of unconsolidated material and shales (Fig. 3.1). Calliper logs are an important indicator of the

reliability of other logs, as caving or 'washouts' can create zones of poor data quality on other logs, particularly GR logs (Rider 1986; Cant 1992).

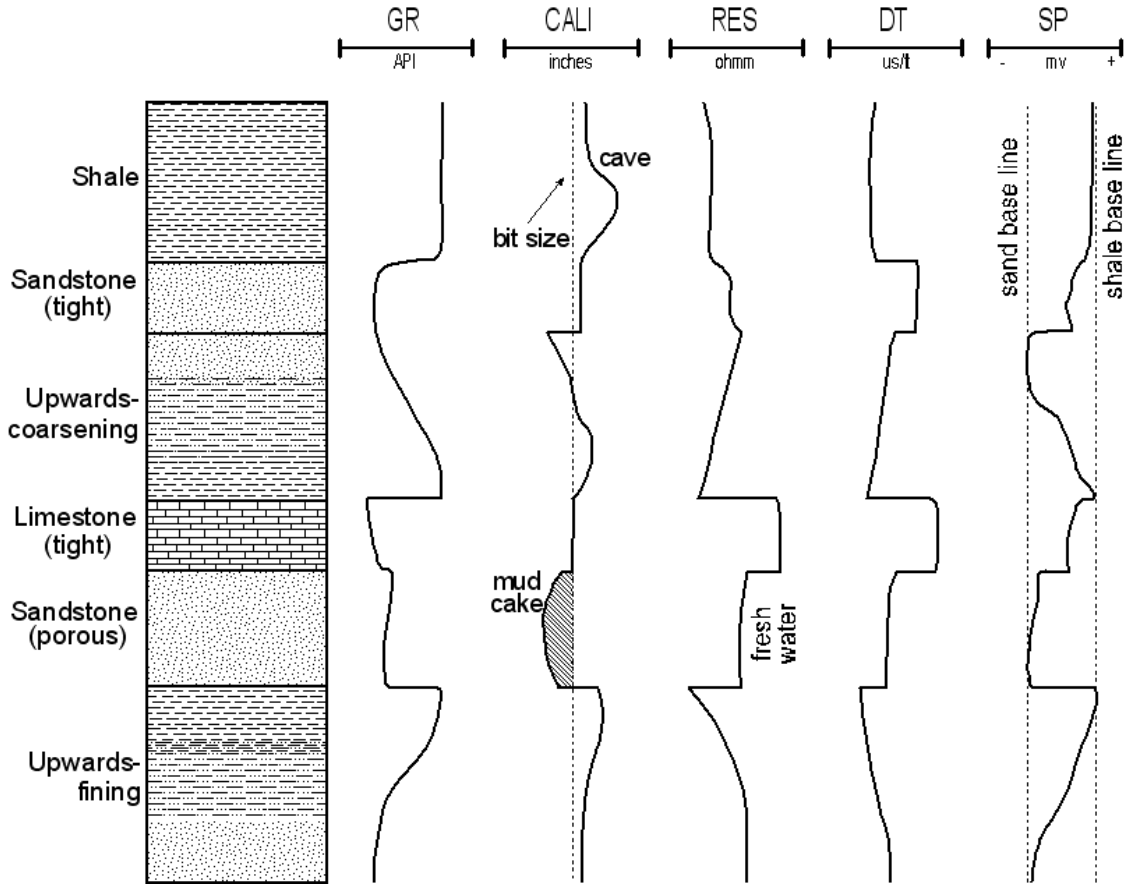

Figure 3.1. Some typical responses of major log types to changes in basic lithology. Adapted from Rider (1986).

3.2.3 Resistivity log

Resistivity logs (RES) are a type of electrical log, providing a measurement of a formation's resistivity to an applied electrical current (Doveton 1994). Different resistivity tools allow measurements at different bed resolution, from anywhere between the vicinity of the borehole wall, to deep (1 – 3m) within the uninvaded (not infiltrated by drilling mud) formation. Micro-resistivity tools are depth limited, targeting the immediate vicinity of the borehole, providing bedding characteristic resolution (Rider 1986). Shallow (laterlog) investigating tools target the resistivity of the invaded (infiltrated by drilling mud) zone, providing coarser resolution, the right scale for bed-boundary indications (Rider 1986). The deeper (induction) investigating tools target the resistivity of the uninvaded formation, with coarser resolution than laterlog measurements. Although the induction logs

give poor bedding resolution, the ‘averaging’ of the bedding effects makes this log a good gross formation character indicator (Rider 1986). The major resistivity log types encountered in this study include the deep laterolog (LLD), shallow laterolog (LLS), deep induction log (ILD) and micro-spherically focused log (MSFL). These resistivity log types are used in conjunction with each other.

Resistivity logs are used for evaluating fluids within formations and in the petroleum industry are primarily used for the determination of hydrocarbon versus water bearing zones (Asquith 1982). Resistivity logs however also have the ability to indicate porosity and to a lesser extent indicate lithology. As hydrocarbons, freshwater and most grains and minerals making up the matrix of a rock are non-conductive, resistive properties are almost entirely a function of porewater salinity and the cation exchange capacity of clay minerals. Thus as clay content decreases or grain size increases, resistivity could be expected to decrease, causing resistivity logs to typically mirror (oppose) GR trends, as illustrated in Fig. 3.1. Deep induction logs may provide a good lithology indicator, with increasing resistivity suggesting decreasing clay content (Rider 1986).

3.2.4 Sonic log

The DT log provides a measurement of the transit time of a compressional sound wave through a formation (Rider 1986). An interval two-way travel time (twt) is primarily dependent on lithology, matrix material and porosity. Sonic logs cannot be used directly as an indication of lithology as common rock types do not show diagnostic velocities. However, faster velocities are recorded in ‘higher velocity’ materials such as tightly cemented sandstone and carbonate, while medium velocities are typically associated with sand and shale and lower velocities are typical of shale (Fig. 3.1; Cant 1992; Rider 1992; Doveton 1994). Rider (1986) indicates that formation velocities for particular horizons are very typical between wells within a given area, suggesting sonic logs may be useful in regional correlation. The most common use of sonic logs however is in the calibration of seismic lines and the calculation of a formation’s porosity, possible if lithology or the transit time for a formation’s matrix is known (Rider 1986).

3.2.5 Spontaneous potential log

The SP log provides a measure of natural electrical potentials that occur in boreholes, often termed the battery effect, where the differences in electrochemical factors between drilling mud (usually fresh water) and a formations porewater (usually saline water) produce electrical currents, causing a deflection observed on SP logs (Sheriff 1989; Doveton 1994). Primarily this log is used to identify impermeable zones such as shale versus permeable zones such as sand (Asquith 1982). The SP log is not considered a good lithology indicator, although shale typically possesses a relatively featureless and positively deflected SP curve, while permeable zones such as sands typically show a negatively deflected SP curve (Fig. 3.1). In a sequence of sand and shale, a 'shale line' is commonly drawn through the anomaly maxima and a 'sand line' through the anomaly minima, allowing sand to shale ratios to be calculated (Fig. 3.1; Asquith 1982; Rider 1986; Doveton 1994). Although SP log bed resolution is poor, sharp deflections in SP log can be interpreted as permeable bed boundaries, making shale to sand boundary identification one of the fundamental uses of this logging tool (Kearey & Brooks 1991).

3.3 DATA ACQUISITION AND RESOLUTION

Using the Crown Minerals Group, Ministry of Economic Development (MED) open file petroleum technical database, a suite of LAS format (basic log distribution format) geophysical wireline log exploration well data were obtained for fifteen wells/holes along the eastern margin of Taranaki Basin, from Turi-1 in the north to Toko-1 in the south (Fig. 3.2). The fifteen wells that were used in analysis had complete Late Eocene – Oligocene sections and were selected on the basis of their close proximity to Taranaki Peninsula and Taranaki Fault.

Wireline logs can supply very fine resolution data, with major log parameters measured at 0.005 – 0.015 m intervals. The data available for each bore hole consisted of up to 100 log types plotted against depth and all information regarding hole drilling. Using geophysical log software WellCAD^{TM}, LAS log data were viewed, particular logs of interest (GR, CALI, RES, DT & SP) were displayed and certain target depths were then selected and edited for analysis. The availability of major log types through the fifteen wells analysed are summarised

in Table 3.2. For most wells, the majority of the log types of interest (GR, CALI, DT, SP) were available in complete sections spanning the Late Eocene – Oligocene interval. However, as noted in Table 3.2, a complete set of resistivity logs was often not available.

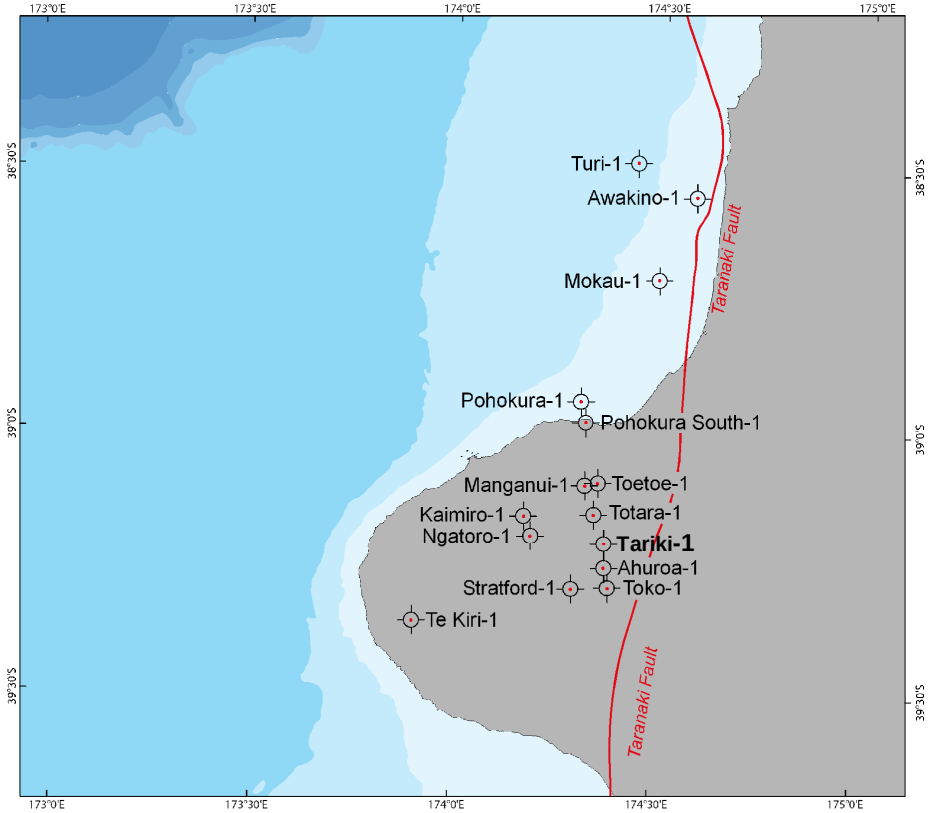

Figure 3.2. Map illustrating the location of the fifteen wells selected for wireline motif characterisation and interpretation. Note Taranaki Fault in red.

Table 3.2 The availability of major log types for selected wells used in analysis. Complete and incomplete logs for the Late Eocene – Oligocene are represented by blue checks or green checks, respectively.

					Resistivity			
Hole	**GR**	**CALI**	**DT**	**SP**	**LLD**	**LLS**	**MSFL**	**ILD**
Ahuroa-1	✓	✓	✓	✓	✓	✓	✓	
Awakino-1	✓	✓	✓	✓	✓	✓	✓	
Kaimiro-1	✓	✓	✓	✓	✓	✓	✓	✓
Manganui-1	✓	✓	✓	✓	✓	✓	✓	✓
Mokau-1	✓	✓	✓	✓	✓	✓	✓	
Ngatoro-1	✓	✓	✓	✓	✓	✓	✓	
Pohokura-1	✓	✓	✓	✓	✓	✓		
Pohokura South-1	✓	✓	✓	✓	✓	✓		
Stratford-1	✓	✓	✓	✓				✓
Tariki-1	✓	✓	✓	✓	✓	✓	✓	✓
Te Kiri-1	✓	✓	✓	✓			✓	✓
Toetoe-1	✓	✓	✓	✓	✓	✓	✓	✓
Toko-1	✓	✓	✓	✓	✓	✓		
Totara-1	✓	✓	✓	✓	✓	✓	✓	✓
Turi-1	✓	✓	✓	✓	✓	✓		

3.4 WIRELINE FACIES IDENTIFICATION

The definition and interpretation of subsurface facies using wireline log data alone is relatively imprecise and generalised, especially without the use of cores, such as in this study, which would otherwise allow traditional facies analysis (Cant 1992). A common approach to subsurface facies analysis is to use the shape of well-log curves (geometric appearance) to interpret depositional facies, where distinctive log shapes, trends and shifts may reflect subtle or abrupt changes in lithology, suggesting differing depositional environments or facies changes. Characterisation and classification may be made from a number of factors including log trend (decreasing upwards, increasing upwards, stable and irregular), curve characteristics (smooth or serrated) and lower and upper contact nature (abrupt or gradational) (Fig. 3.3; Rider 1986). The relationship between different log types may also be used to help interpret the data, for example, viewing GR and DT logs together is a method used to reveal vertical log patterns, as these two logs commonly mirror (oppose) each other (Cant 1992). Figure 3.4 illustrates the

common vertical log patterns used in classification on a gamma-ray log, with cylindrical, funnel shaped, bell shaped, symmetrical and irregular patterns evident. The scale of these well-log curve patterns may vary significantly, from a few metres to several hundred metres.

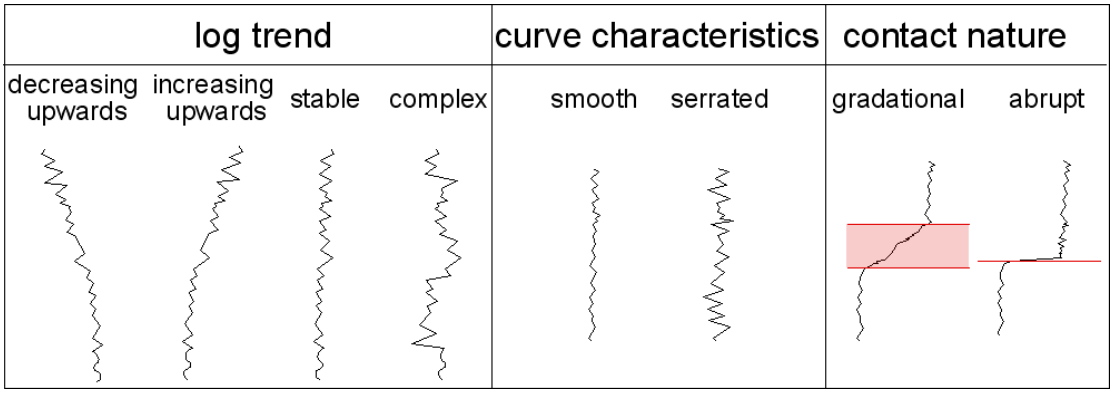

Figure 3.3. Terms used for wireline log characterisation and classification, including log trends, curve characteristics and contact nature.

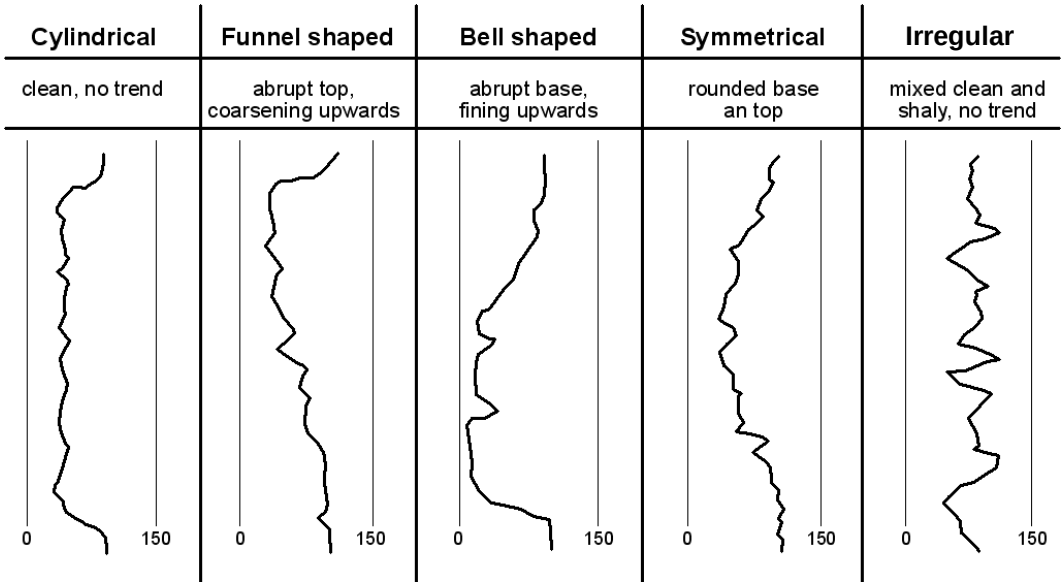

Figure 3.4. The most common idealised GR log curve shapes. From Cant (1992).

3.5 WIRELINE MOTIF CLASSIFICATION

For each of fifteen wells in this study, a suite of distinctive wireline motifs were defined for Late Eocene – Oligocene units using the log types discussed previously. For complete wireline motif subdivisions in selected wells see Appendix II. Wireline facies have been interpreted from these wireline motifs combined with lithology and compositional data from well completion reports, biostratigraphy reports, and the determination of grain size and carbonate content from well cutting samples. This method of lithological discrimination is not ideal

in contrast to outcrop geological investigation, but is necessary considering the completely subsurface occurrence of these the formations and general lack of core material.

3.5.1 Moa Group

3.5.1.1 Turi Formation

The Turi Formation is a homogenous mud-dominated interval intersected over much of Taranaki Basin. This is reflected in the relatively featureless wireline signal of the main log types through this interval. King and Thrasher (1996) report that any base-line shifts and breaks evident on wireline logs are indicative of fluctuating sediment supply or changes in relative base level rather then changes in lithology. However, close examination of the Turi Formation in the fifteen wells *has* revealed subtle changes in wireline facies, possibly reflecting slight changes in lithology and/or composition. Three wireline motifs have been identified through the Turi Formation, characterised primarily by the geometric appearance (overall shape of logs) of the main log types (RES, DT and SP logs), but dominantly the GR log.

Motif Tu1

Motif Tu1 represents sections of Turi Formation that display a relatively smooth (low amplitude log variations) and stable (relatively linear), medium to high value GR log with corresponding smooth and stable RES, DT and SP logs. Motif Tu1 typically displays a concave cylindrical log curve shape when comparing GR and sonic logs together. Figure 3.5 illustrates the typical Tu1 wireline motif characteristics in Pohokura-1. The relatively 'featureless' RES, DT and SP logs and medium to high value GR log suggests that this motif supports very homogenous and fine-grained lithology. A slight upwards-increasing GR log trend is typical of this motif. Before passing upwards into the overlying Otaraoa Formation a slight upwards-decreasing GR log trend is common (Fig. 3.5). Tu1 is the dominant wireline motif observed within Turi Formation.

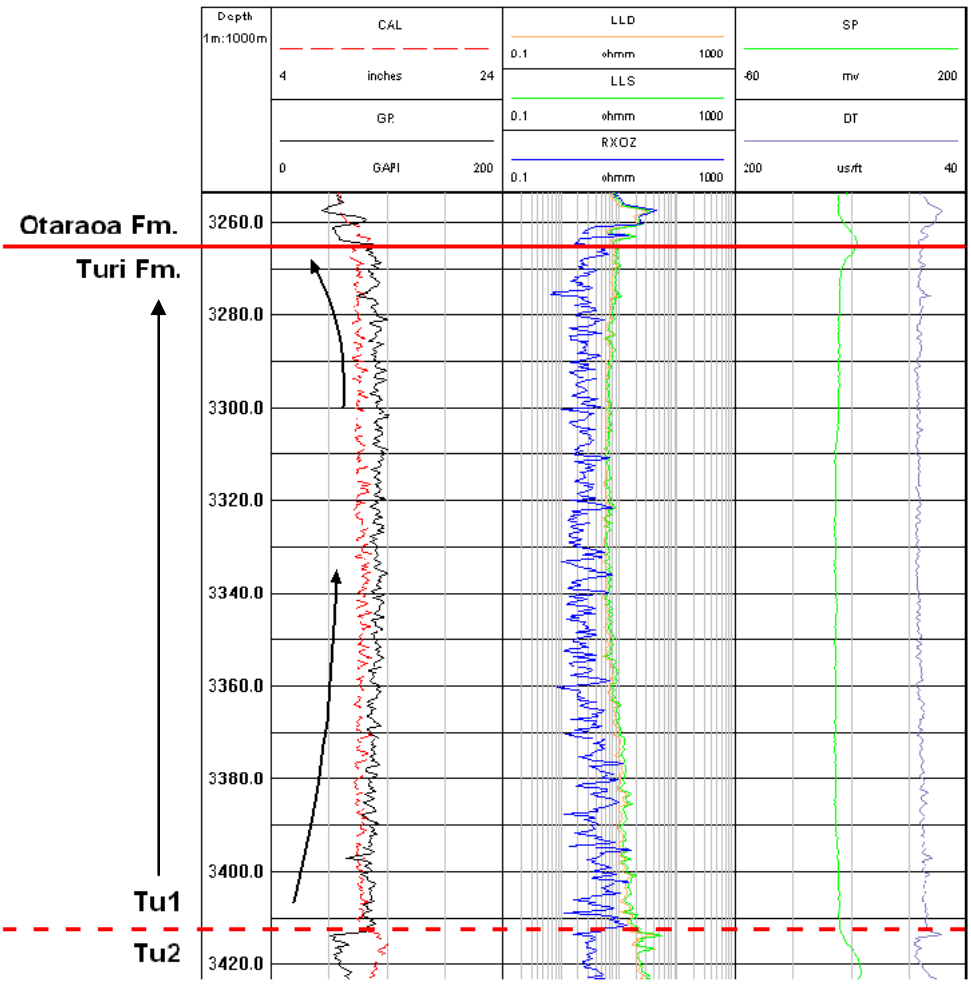

Figure 3.5. Motif Tu1, Pohokura-1. Note lower 10 m of Otaraoa Formation and upper 10 m of Tu2 shown for comparison.

Motif Tu2

Motif Tu2 represents sections of Turi Formation that display a relatively smooth to serrated, medium to low value GR log, with corresponding smooth to serrated, medium to high value RES and DT logs. Figure 3.6 illustrates the typical Tu2 wireline motif characteristics in Kaimiro-1. The medium to low GR values apparent in Tu2 suggest a sandier facies in contrast to the finer grained Tu1, and as observed in Kaimiro-1, Tu2 displays an upwards-increasing GR log trend, suggesting a fining in lithology towards the overlying Tu1 motif (Fig. 3.6). Of the 15 wells analysed, Tu2 is only observed in Kaimiro-1 and Pohokura-1.

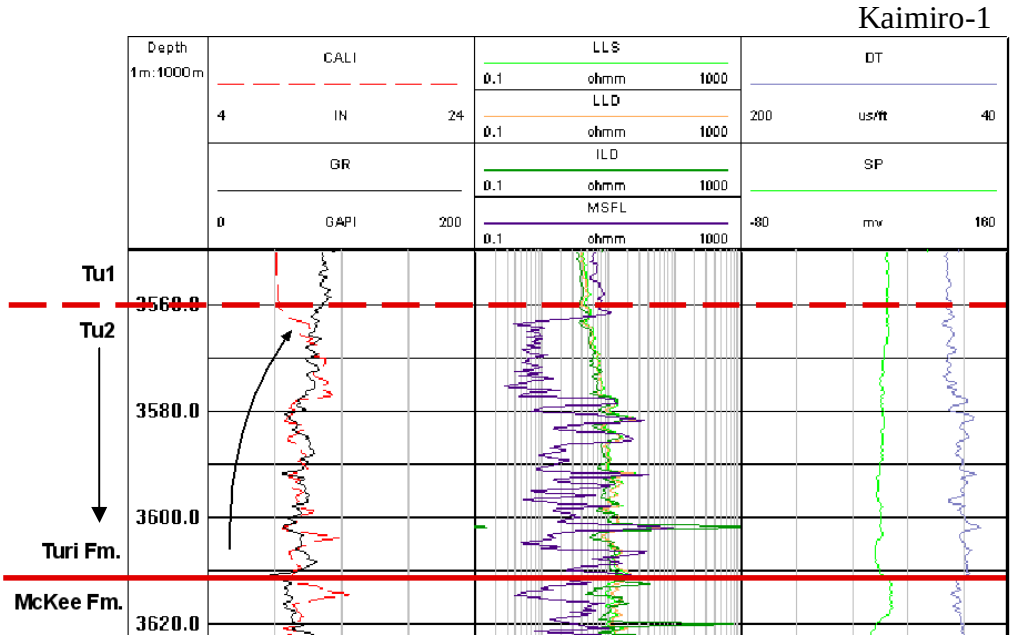

Figure 3.6. Motif Tu2, Kaimiro-1. Note lower 10 m of McKee Formation and upper 10 m of Tu1 shown for comparison.

Motif Tu3

Motif Tu3 represents sections of Turi Formation that display a relatively serrated, medium to low value GR log, with a correspondingly smooth to serrated DT log and a very negatively deflected, very serrated SP log signal. Figure 3.7 illustrates the Tu3 wireline motif characteristics in Turi-1. Above a casing change evident at 3357 m, the calliper log signal is very chaotic, suggesting a large semi-caved or washed out zone (Fig. 3.7). Because GR logs can be severely affected by washed out zones, the GT log has not been used in this interpretation. The fluctuating SP log suggests interbedding and the upwards-increasing DT log trend suggests an upwards-coarsening in lithology towards the overlying Otaraoa Formation. Out of the 15 analysed wells, Tu3 is only observed in Turi-1.

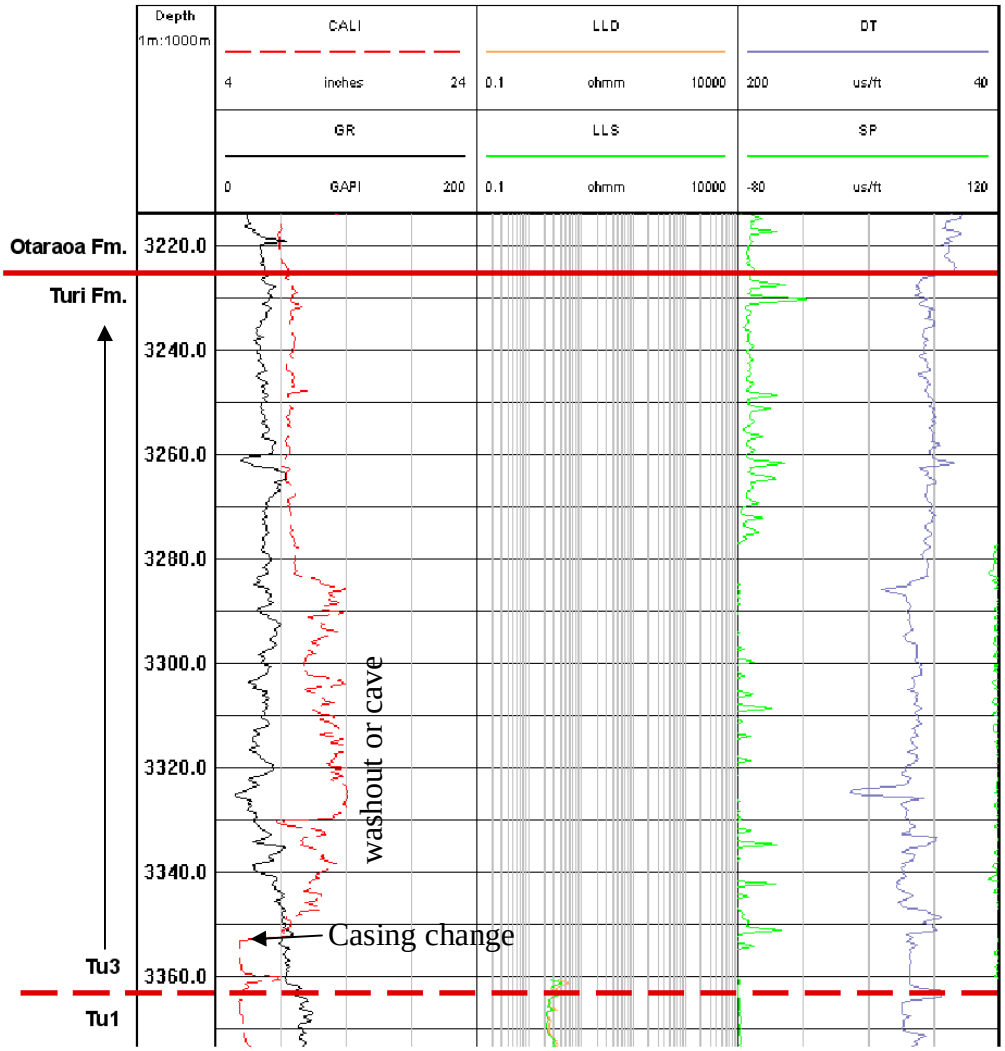

Figure 3.7. Motif Tu3, Turi-1. Note lower 10 m of Otaraoa Formation and upper 10 m of Tu1 shown for comparison.

3.5.2 Ngatoro Group

3.5.2.1 Otaraoa Formation

Matapo Sandstone Member

The thin (~5 m) and condensed nature of the Matapo Sandstone Member makes wireline log analysis difficult. Typically this unit is picked on wireline logs by a moderate positive shift in RES log passing upward from the underlying Turi Formation (Gordon et al. 1993). The characteristic log pattern for Matapo Sandstone is given by a shift from a relatively high GR value to a relatively low GR value across a very small (~2 m) distance. Corresponding (mirrored) responses occur in RES and DT logs, reflecting lithological and/or compositional changes.

In this study, two distinct wireline motifs have mainly been defined for Matapo Sandstone. These two wireline motifs have been characterised by the geometric appearance of the GR log, but also RES, DT and SP logs.

Motif Ma1

Motif Ma1 represents sections of Matapo Sandstone that display a relatively smooth to serrated, medium to low value GR log with a corresponding smooth to serrated, medium to high value RES and DT log. Figure 3.8 illustrates the typical Ma1 wireline motif characteristics in Tariki-1, where the relatively low GR value of Ma1 can be seen in contrast to the underlying Ma2 motif. In Tariki-1, Ma1 displays an upwards-increasing GR log trend mirrored by upwards-decreasing RES and DT logs. This trend is quite typical of Ma1, suggesting an upward-fining in lithology or decreasing carbonate content into the overlying Otaraoa Formation. Ma1 is the dominant wireline motif identified in Matapo Sandstone, commonly occurring above Ma2.

Motif Ma2

Motif Ma2 represents sections of Matapo Sandstone that display a relatively smooth to serrated, medium to high value GR log with correspondingly smooth to serrated, medium to high value RES and DT log. Figure 3.8 illustrates the typical Ma2 wireline motif characteristics in Tariki-1, where the relatively high GR value of Ma2 contrasts markedly to the overlying Ma1 motif. In Tariki-1, Ma2 displays a sharply upwards-decreasing GR log trend from a high GR value. Maximum values for both the RES and DT logs also occur within this motif. These log responses are quite typical of Ma2 indicating a coarsening in lithology or an increasing carbonate content upwards into the overlying Ma1 motif. Ma2 normally occurs in association with, and below, Ma1.

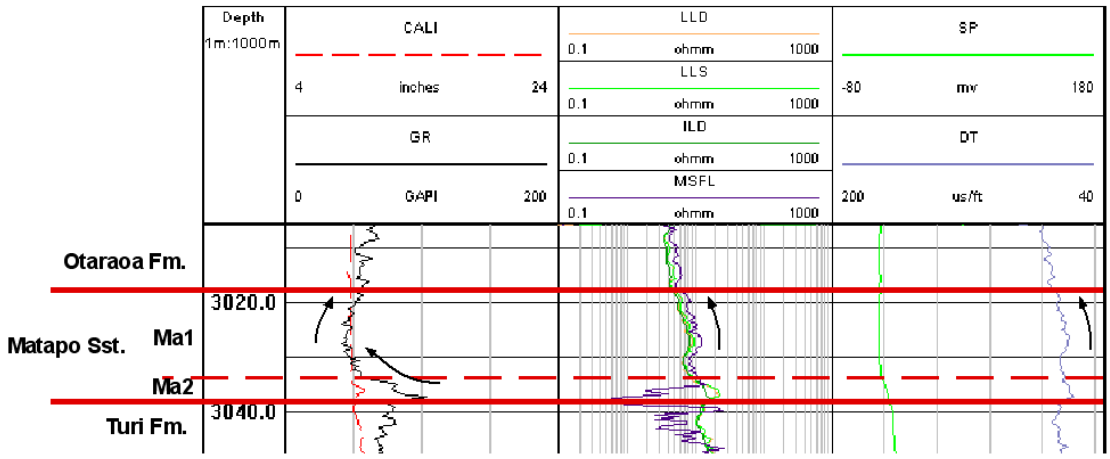

Figure 3.8. Motifs Ma1 and Ma2, Tariki-1. Note lower 10 m of Otaraoa Formation and upper 10 m of Turi Formation shown for comparison.

Otaraoa Formation

The Otaraoa Formation is a calcareous mud dominated interval and occurs over much of Taranaki Basin. The wireline signature for Otaraoa Formation is typically quite bland, reflecting a homogenous muddy lithology. The lower half of Otaraoa Formation typically shows an upwards-increasing GR log (upwards-decreasing DT log) trend from its base. The upper half typically displays an upwards-decreasing GR log (upwards-increasing DT log) trend. The upper contact with the overlying Tikorangi Formation is often quite gradational, but can be abrupt.

Three distinct wireline motifs within the Otaraoa Formation have been defined on closer examination of the well logs. Each of these three motifs likely reflect slight changes in lithology and/or composition.

Motif Ot1

Motif Ot1 represents sections of Otaraoa Formation that display a relatively smooth and stable, medium to high value, relatively cylindrical shaped GR log with corresponding smooth and stable, relatively cylindrical RES, DT and SP logs. Figure 3.9 illustrates the typical Ot1 wireline motif characteristics in Manganui-1, in which the GR, RES, DT and SP logs suggest that this motif is very homogenous and relatively fine-grained throughout the interval. In Manganui-1, an upwards-increasing GR log base shift is evident for the lower half of Ot1, suggesting a fining in lithology and/or a decrease in carbonate content upwards. An upwards-decreasing GR log base shift is also evident for the top half

of Ot1, culminating in a sharp upper contact with Tikorangi Formation. This indicates a coarsening in lithology and/or an increase in carbonate content upwards towards the carbonate dominated Tikorangi Formation (Fig. 3.9). Motif Ot1 is the dominant motif observed in Otaraoa Formation.

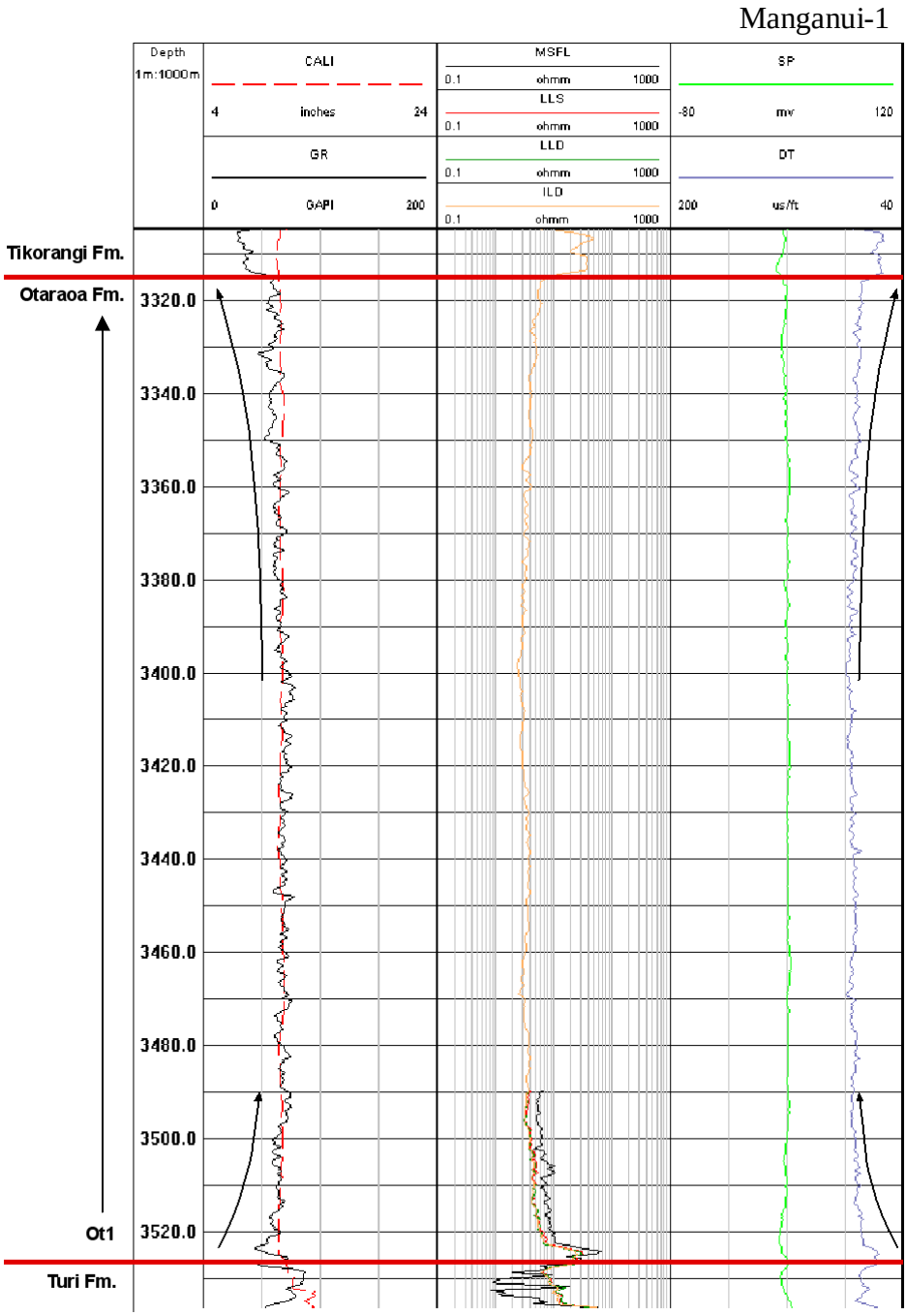

Figure 3.9. Motif Ot1, Manganui-1. Note lower 10 m of Tikorangi Formation and upper 8 m of Turi Formation shown for comparison.

Motif Ot2

Motif Ot2 represents sections of Otaraoa Formation that display a smooth to serrated, symmetrical, medium to low value GR log, with correspondingly smooth to serrated, medium to very high value RES log and smooth to serrated, medium to high value Dt log. Figure 3.10 illustrates the typical Ot2 wireline motif characteristics in Mokau-1. This log character suggests a carbonate-dominated zone in contrast to the over and underlying section. The GR, RES and DT logs display a gradational upper contact between Ot2 and the overlying and 'bland' Ot1 motif (Fig. 3.10). Ot2 is identified in basal Otaraoa Formation in Mokau-1 and Awakino-1.

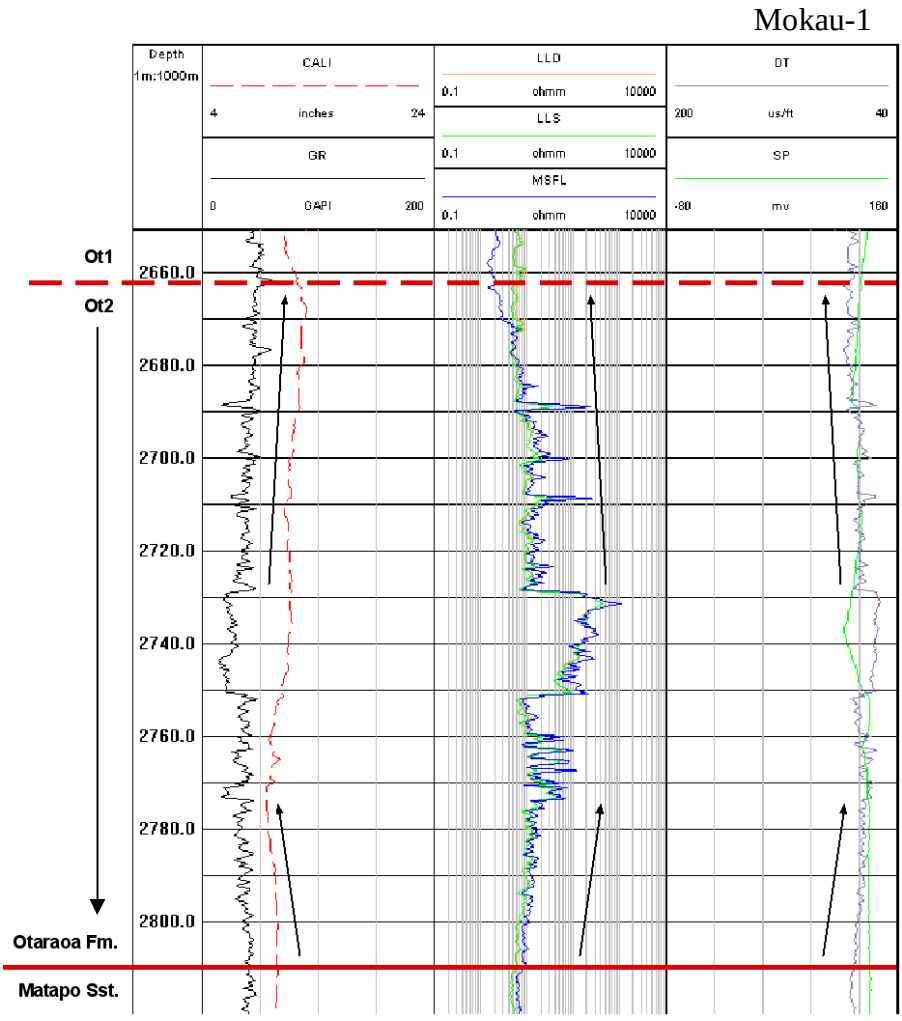

Figure 3.10. Motif Ot2, Mokau-1. Note lower 10 m of Ot1 and upper 10 m of Matapo Sandstone shown for comparison.

Motif Ot3

Motif Ot3 represents sections of Otaraoa Formation that display a relatively smooth to moderately serrated, medium to low value GR log with corresponding smooth to serrated, medium to high value DT log and a tightly serrated SP log. Figure 3.11 displays Ot3 in Turi-1. In Turi-1, from the base of the Ot3 motif, an upwards-increasing GR log trend is followed by an upwards-decreasing GR log trend, suggesting an initial upwards-coarsening in lithology followed by a fining in lithology, respectively (Fig. 3.11). Motif Ot3 is only observed in Turi-1 and in the upper 220 m (out of 669 m) of Ahuroa-1.

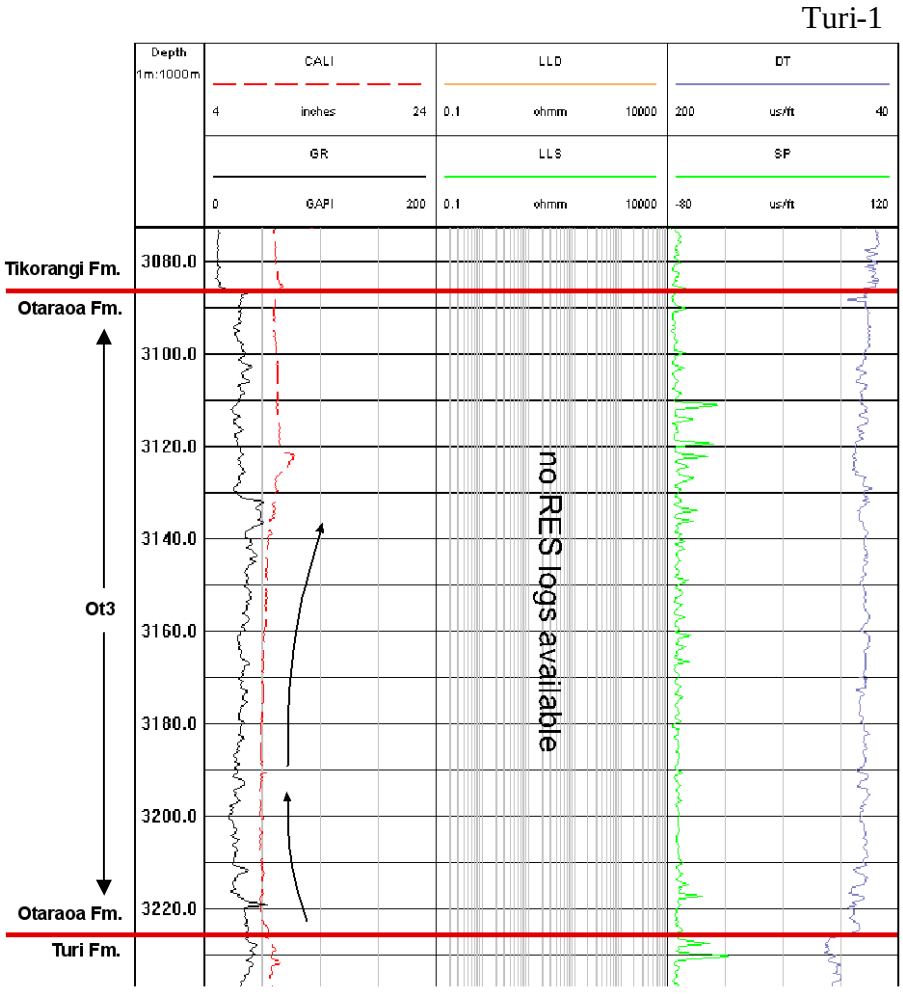

Figure 3.11. Motif Ot3, Turi-1. Note the lower 10 m of Tikorangi Formation and upper 10 m of Turi Formation shown for comparison.

Tariki Sandstone Member

Tariki Sandstone is comprised mostly of interbedded sandstone, siltstone and mudstone lithologies (de Bock et al. 1990). In general Tariki Sandstone is recognised on wireline logs by a distinct 'blocky' profile, reflecting amalgamated sandstone intervals, separated by serrated intervals reflecting the more thinly interbedded facies (Higgs et al. 2004).

For the fifteen wells analysed in this study, three distinct wireline motifs have been defined for Tariki Sandstone (after de Bock et al. 1990). These three wireline motifs have been characterised by the geometric appearance of the GR log, while the RES, DT and SP logs are also useful in interpreting zones with significantly different lithologies.

Motif Ta1

Motif Ta1 represents sections of Tariki Sandstone that display a relatively smooth to serrated, relatively low value, blocky and cylindrical shaped GR log, with a negatively deflected SP log and serrated, medium to high value RES and DT logs. Figure 3.12 illustrates the typical Ta1 wireline motif in Toko-1, where the characteristic blocky GR log shape reflects the thick amalgamated sandstone packages that make up Ta1. Sharp lower and upper contacts to Ta2 are evident in all log types (Fig. 3.12).

Motif Ta2

Motif Ta2 represents sections of Tariki Sandstone that display a relatively smooth and featureless, medium to high value GR log with correspondingly smooth, relatively low value RES and DT logs. This wireline response suggests a relatively homogenous and fine-grained succession. Figure 3.12 illustrates the typical Ta2 wireline motif characteristics in Toko-1, where the relatively high GR value of Ta2 is observed in sharp contrast to the over and underlying Ta1 motif. Of the fifteen analysed wells in this study, Ta2 is only seen in Toko-1 and Ahuroa-1.

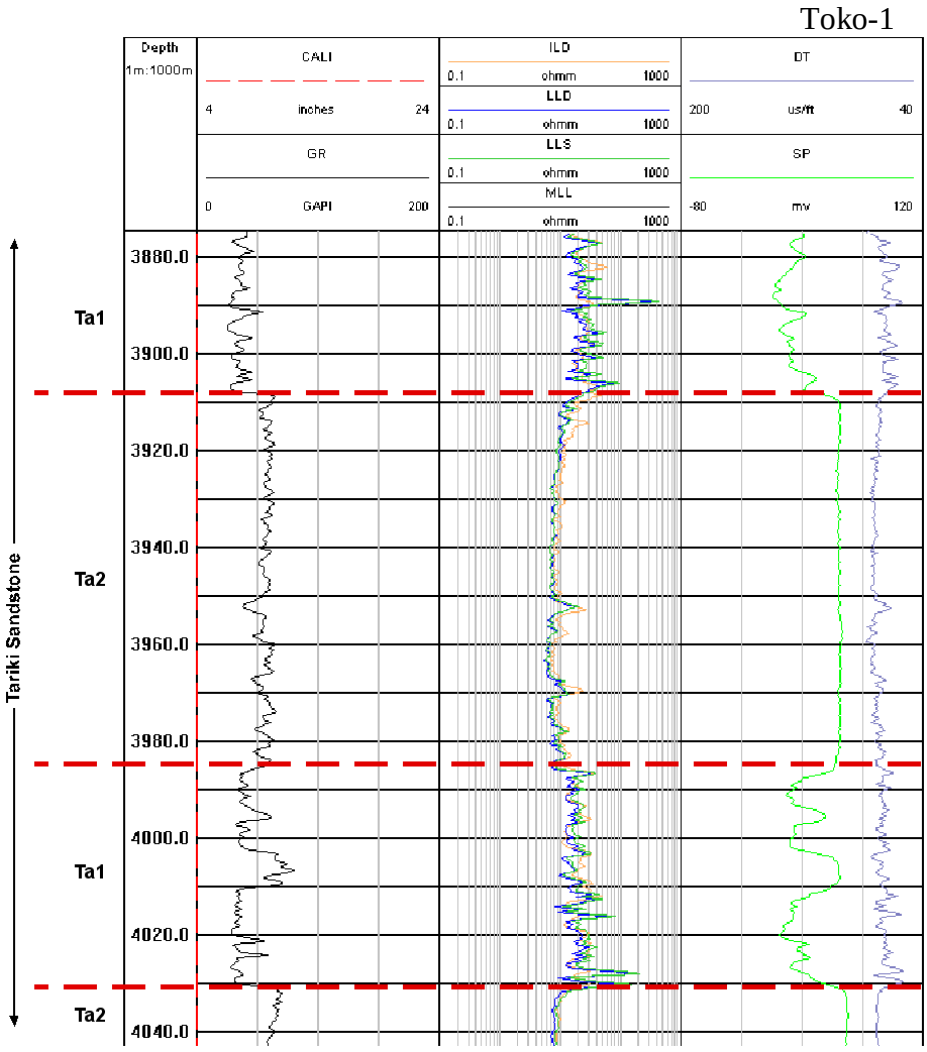

Figure 3.12. Motifs Ta1 and Ta2, Toko-1.

Motif Ta3

Motif Ta3 represents sections of Tariki Sandstone that display a tightly serrated, often irregularly shaped, low to high value GR log and serrated, low to high value RES and DT logs. This wireline signal suggests a more interbedded (sandstone-siltstone-mudstone) nature in contrast to Ta1 and Ta2. Figure 3.13 illustrates the typical Ta3 wireline motif characteristics in Totara-1. Here the very serrated (or interbedded) nature of the GR, RES and DT logs is clearly observed in contrast to the under and overlying Otaraoa Formation. An irregular but symmetrical log pattern is also evident when comparing GR-RES or GR-DT logs (Fig. 3.13). Ta3 is observed in Ahuroa-1, Toetoe-1, Tariki-1 and Totara-1.

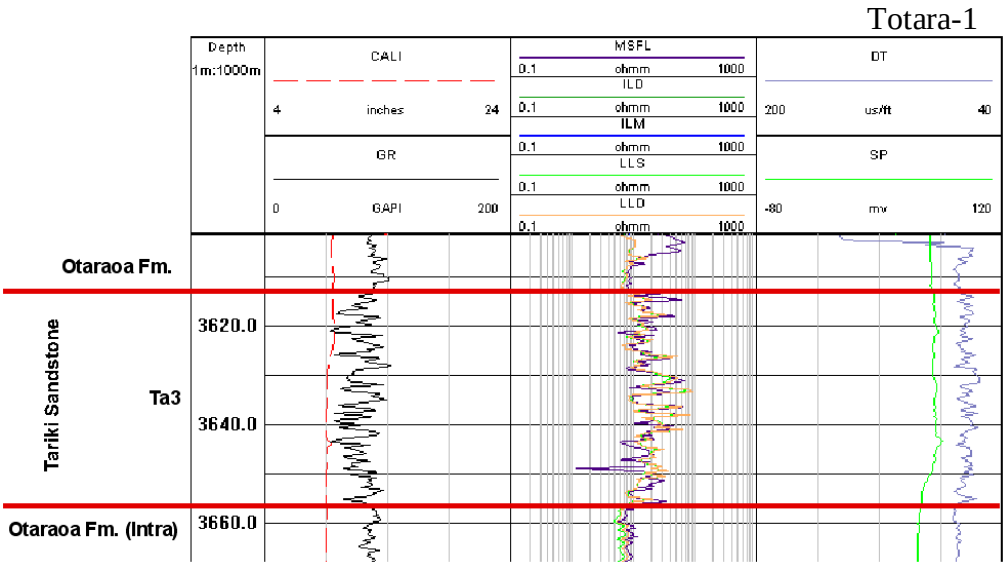

Figure 3.13. Motif Ta3, Totara-1. Note lower 10 m of Otaraoa Formation and upper 10 m of Otaraoa Formation's Intra Member are shown for comparison.

3.5.2.2 Tikorangi Formation

Tikorangi Formation is a very highly calcareous, mainly fine to coarse-grained unit with a distinctive wireline log signature. The lower contact of this formation is marked by the gradational to abrupt increase of both GR and DT values in comparison to the more argillaceous Otaraoa Formation. The upper boundary of this formation is usually quite abrupt, marked by a gradational to abrupt shift in DT and GR log value passing upwards into the overlying Taimana formation.

For the fifteen wells in this study, three distinct wireline motifs have been identified within the Tikorangi Formation. These three wireline motifs have been defined using the geometric appearance of major log types (RES, DT and SP logs), although are dominantly characterised by the GR log.

Motif Tk1

Motif Tk1 represents sections of Tikorangi Formation that display a very smooth, featureless and stable, cylindrical-shaped, low value GR log, and a relatively smooth, relatively high value DT log. This wireline signal suggests a relatively homogenous, very clean and coarse-grained unit and/or a very high carbonate content. Figure 3.14 illustrates the typical Tk1 wireline motif characteristics in Mokau-1. In Mokau-1 the distinct cylindrical log curve shape is apparent in GR-

DT log comparison (Fig. 3.14). The sharp lower and upper contacts are also clearly illustrated in Mokau-1, with an abrupt change upwards from the very calcareous Otaraoa Formation, and again between the Tikorangi Formation and Taimana Formation contact. Motif Tk1 is only seen in Turi-1 and Mokau-1.

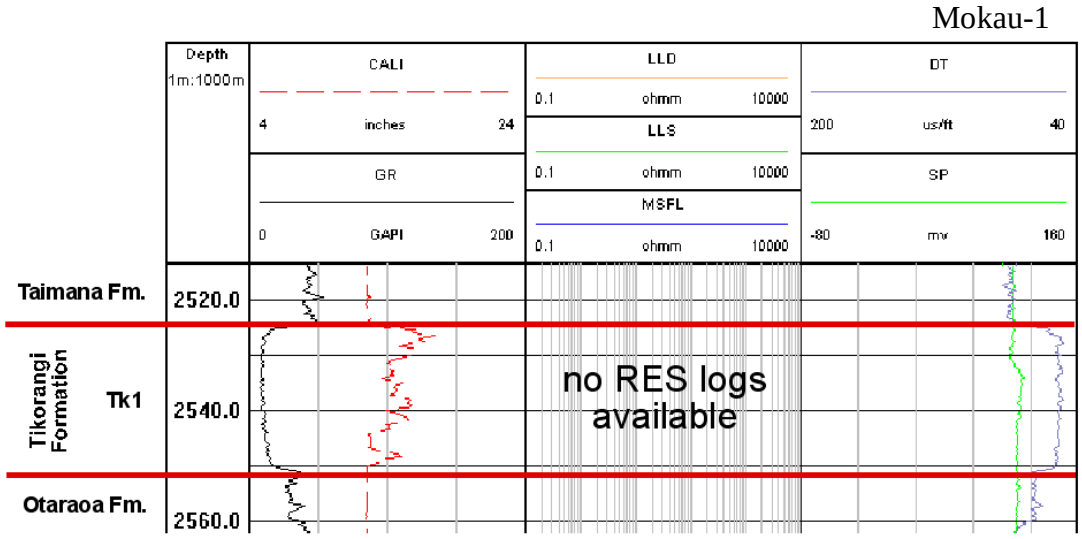

Figure 3.14. Motif Tk1, Mokau-1. Note the lower 10 m of Taimana Formation and upper 10 m of Otaraoa Formation are shown for comparison.

Motif Tk2

Motif Tk2 represents sections of Tikorangi Formation that display a moderately serrated, medium to low value GR log together with a tightly serrated to moderately serrated, medium to high value RES and DT logs. Combined, this wireline signal suggests an interbedded mudstone and sandstone interval with high carbonate content. Figure 3.15 illustrates an example of the typical Tk2 wireline motif in Toko-1, where the moderately serrated GR, RES and DT log curve shapes are clearly observed. In Toko-1, Tk2 displays an upwards-decreasing GR log trend together with upwards-increasing RES and DT log trends (Fig. 3.15). The contact between the underlying Otaraoa Formation and the overlying Tk2 motif of the Tikorangi Formation is subtle (Fig. 3.15), very different to the sharp contact observed between Tk1 and Otaraoa Formation (Fig. 3.14). Tk2 is the dominant motif observed in the Tikorangi Formation over the 15 wells.

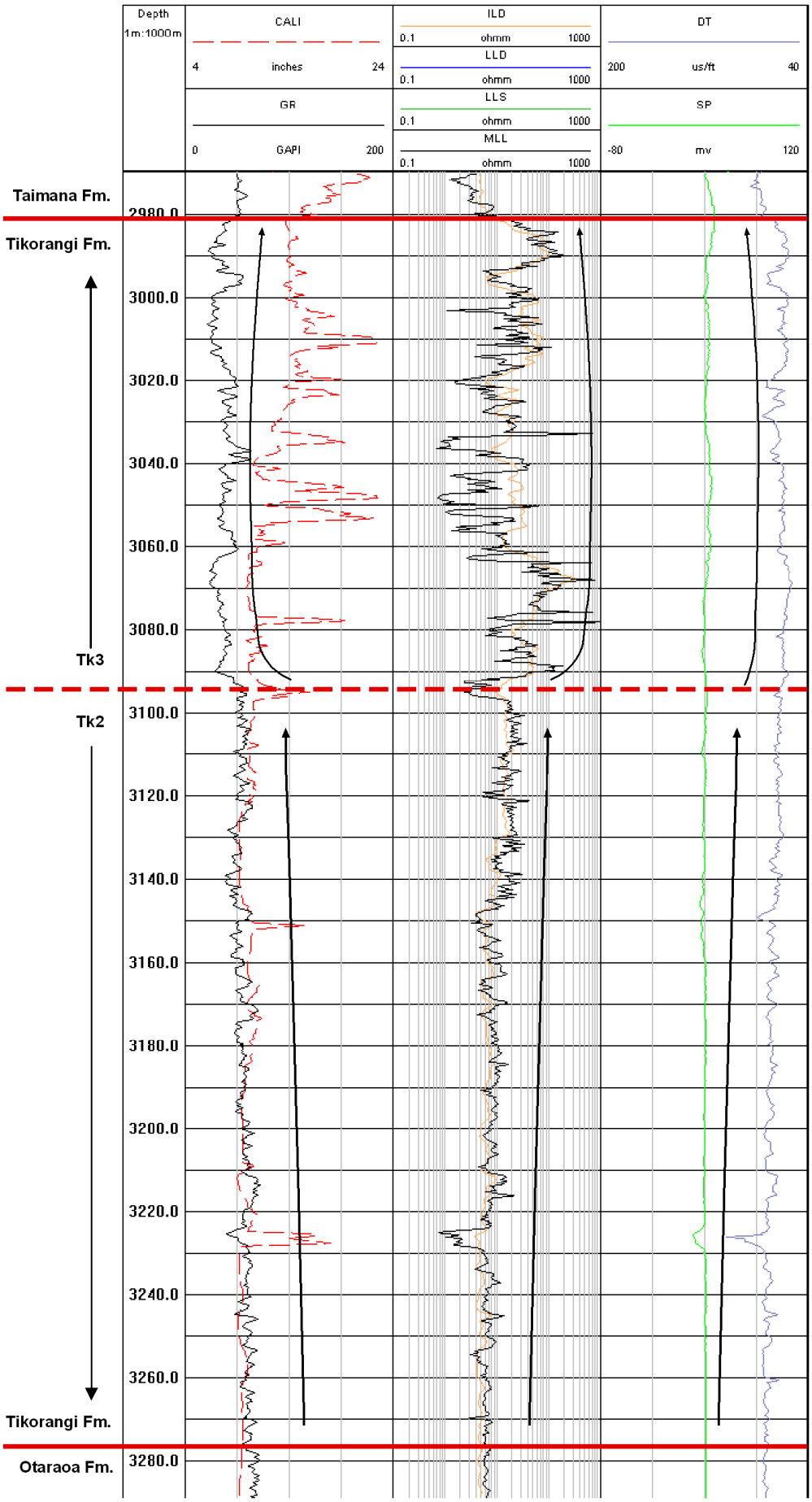

Figure 3.15. Motifs Tk2 and Tk3, Toko-1. Note lower 10 m of Taimana Formation and upper 10 m of Otaraoa Formation are shown for comparison.

Motif Tk3

Motif Tk3 represents sections of Tikorangi Formation that display a poorly to moderately serrated, blocky, relatively low value GR log (lower than Tk2) together with a very serrated RES log and relatively high value DT log (higher than Tk2). Figure 3.15 illustrates Tk3 wireline motif characteristics in Toko-1. The decrease in GR log, increasingly serrate RES log and increase in DT log value can be seen passing up from the underlying Tk2 motif, this trend is then reversed up towards the overlying Taimana Formation (Fig. 3.15). This wireline signal suggests higher carbonate content and a coarser-grained interval in contrast to Tk2. Of the wells in this study Tk3 is only observed in Toko-1.

3.5.2.3 Taimana Formation

Taimana formation is a fairly homogenous, highly calcareous mud dominated interval, similar to that of Otaraoa Formation (King & Thrasher 1996). The lower boundary of Taimana Formation coincides with the peak of a sometimes abrupt change (increasing DT and decreasing GR log values) between the underlying Tikorangi Formation (Section 3.5.2.2) and the Taimana Formation (Young & Carter 1989). The upper boundary of Taimana Formation is recognised by a fairly abrupt deflection in GR between the underlying Taimana Formation and the overlying clastic dominated Wai-iti Group. Detailed examination of Taimana Formation has resulted in the recognition of two distinct wireline motifs.

Motif Tm1

Motif Tm1 represents sections of Taimana Formation that display a relatively smooth to slightly serrated, medium to high value GR log with correspondingly smooth to slightly serrated RES and DT logs. This log signal suggests a fairly homogenous lithology although some interbedding is apparent. Figure 3.16 illustrates the typical Tm1 wireline facies characteristics in Pohokura-1. Here an increase in GR log value and corresponding decrease in RES and DT log values are observed passing upwards into the Taimana Formation from the underlying Tikorangi Formation, reflecting decreasing carbonate content, typical of Taimana Formation in general. Another typical characteristic of Tm1 is a gradational GR log increase passing up from Tm1 up into the clastic-rich Wai-iti Group (Fig. 3.16). Tm1 is the dominant motif observed in the Taimana Formation.

Motif Tm2

Motif Tm2 represents sections of Taimana Formation that are similar to Tm1 but display a very serrated, variably low to high value GR log and relatively smooth to slightly serrated RES and DT logs. This log signal indicates a more interbedded unit in contrast to Tm1, with thick (~3 m) mudstone intercalated with sandstone. Figure 3.17 shows a ~130 m (of a total 190 m) Tm2 section in Kaimiro-1, illustrating typical Tm2 motif characteristics. Here the highly serrated Tm2 motif is observed to overlie the significantly less serrate Tm1 motif (Fig. 3.17). Tm1 is only observed in Kaimiro-1 in this study.

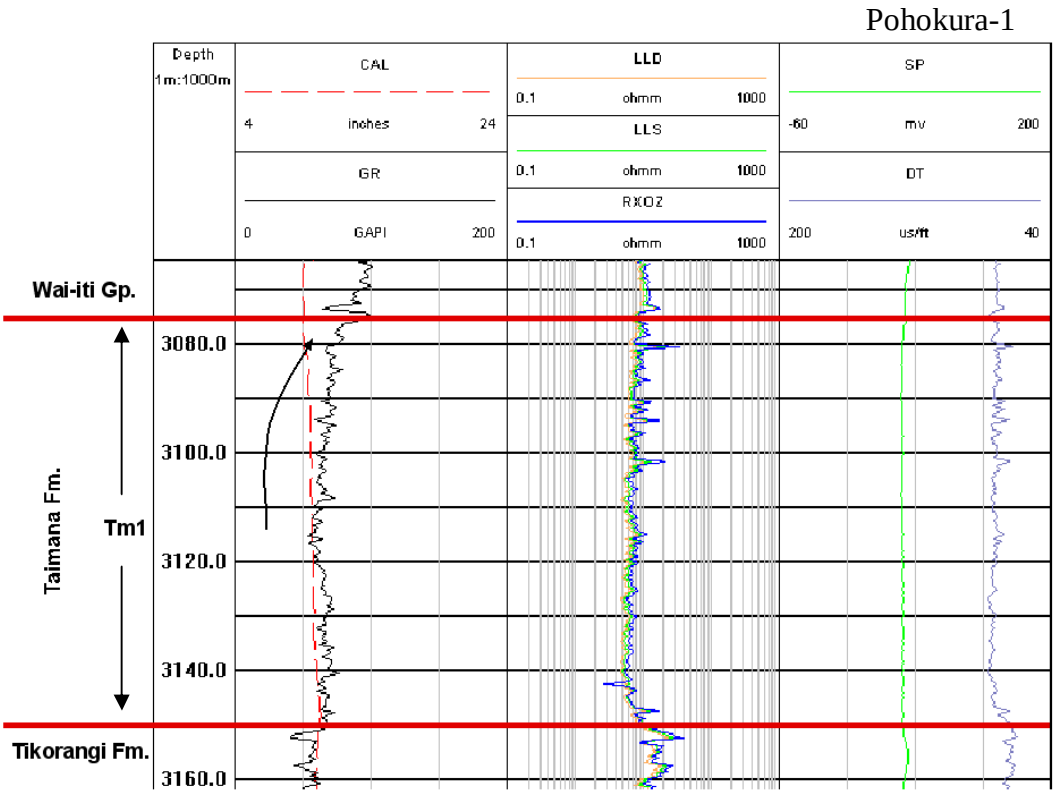

Figure 3.16. Motif Tm1, Pohokura-1. Note lower 10 m of the Wai-iti Group and upper 10 m of Tikorangi Formation shown for comparison.

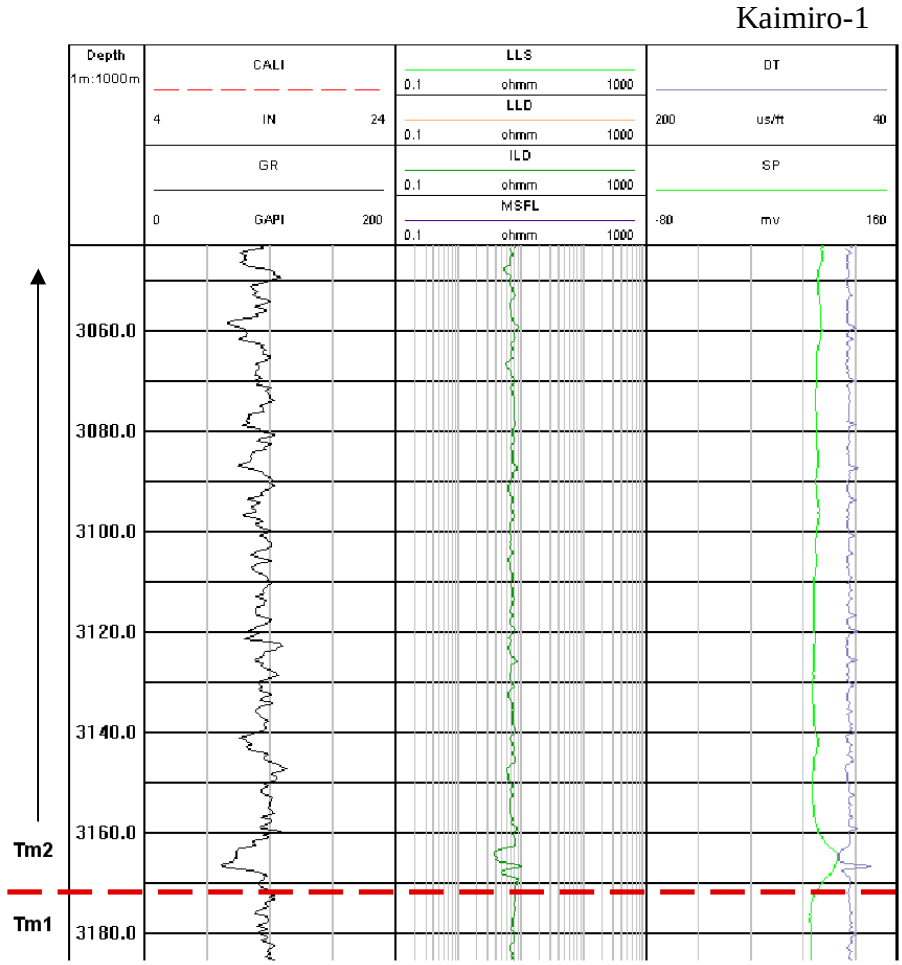

Figure 3.17. Motif Tm2 in Kaimiro-1. Note only ~130 m (out of ~190 m) of Tm2 shown, and upper 10 m of Tm1 shown for comparison

3.6 INTERPRETATION OF PALEO-DEPOSITIONAL ENVIRONMENTS

The interpretation of depositional paleoenvironments from subsurface units should not only include wireline log characteristics or log shape, but the integration of many data sets, including recovered samples (core, side wall core, well cuttings) and environmental information from fauna (paleoecology) (Rider 1986). Open file well completion reports available through Crown Minerals Group, Ministry of Economic Development (MED) petroleum technical database provide an integration of drilling/stratigraphic data, including lithological descriptions of units, mud log reports, core and sidewall core descriptions, and biostratigraphic data. The following section discusses data sources used and integrated to interpret depositional facies for the Late Eocene – Oligocene wireline motifs outlined in Section 3.5.

3.6.1 Wireline logs

The shape of well logs has been long used as a method of interpreting depositional paleoenvironments (Cant 1992). As mentioned in Section 3.2.1, because the GR log may be used as an indicator of clay (shale) content, geometric log shapes may indicate depositional facies. However, complications may arise as log shapes do not diagnostically indicate a particular facies. For example the bell shaped GR-DT log shape in Fig. 3.4, indicating an upwards-fining sequence, may be interpreted as an alluvial/fluvial channel, but may also indicate a transgressive sand sequence. Similarly, the funnel shaped GR log may be indicative of deltaic progradation or deeper marine shelf progradation (Rider 1986). This problem illustrates how a more definite and accurate facies classification is only possible with the integration of other sedimentological data sources (Rider 1986). Interpretation of the lithology of each of the units here has been made through comparison of the major log types (GR, CALI, RES, DT and SP), observing the relationship between each and noting anomalous log readings or where log types do not corroborate each other, which may be a result of caving. The interpreted lithology is compared where possible with other sedimentological data sources such as core/well cutting descriptions, in order to build as robust an interpretation as possible.

3.6.2 Drilling derived data – mud logs (well cuttings and core)

The mud log is a geologist's recording of the drilling of a well, integrating any lithological data derived from drilling mud and captured well cuttings. Well cuttings are small chips broken off the formation as the drill advances, which are then brought to the surface via circulating drilling mud (after lag time). Well cuttings are often forgotten about, but they are actually very important, being the only continuous sample of formation lithology up a borehole (Rider 1986). By the time well cuttings reach the surface however, they are typically quite mixed and heterogeneous due to the sometimes large drill-to-capture lag times, mixing of chips in the drilling mud column and contamination from up-hole caving (Rider 1986). Lithology on mud logs is usually expressed as a percentage of chip types, commonly recorded as sand, mudstone (shale) and limestone proportions. The mud log can be thought to provide a gross lithological record, which may be later compared with lithology inferred from major log types (Rider 1986). Cores provide direct physical sampling of a targeted interval, the only record of 'real' subsurface lithology. Cores are very expensive to obtain (generally reserved for reservoirs) but are very valuable, providing a continuous cylindrical sample of a formation, and lithology can be assessed directly from cores with no interpretation necessary (Rider 1986).

3.6.3 Well cuttings calibration

Carbonate percentage (Section 4.4.1) and grain size (Section 4.4.2) data have been obtained from sampled well cuttings, targeting specific wireline motifs for the purpose of wireline log calibration. For sampled wells, formation/member and depths see Appendix III. Table 3.3 summarises these data showing wells sampled, formations targeted and particular wireline motifs, targeted depths, average grain size results, and carbonate percentage results for each sample analysed. For carbonate digestion and grain size data see Appendix III. As mentioned in section 3.6.2, well cuttings may not always be representative of a formation's true depths. Well cuttings retrieved in this study were also mixed with some proportion of drilling mud. This is a problem when formation characteristics resemble that of the drilling mud, making it hard to distinguish between the two sources. Because of this the validity of grain size data is questioned, possibly being misrepresented

by an unknown proportion of drilling mud. This is also true to some degree with calculated carbonate percentage as some unknown proportion of (non-calcareous) drilling mud is processed together with the sampled interval. Although this is a problem, the calculated carbonate percentages illustrated in Table 3.3 broadly complement those suggested by wireline log character. In this study, because of the potential problems of drilling mud contamination, grain size data have not been used directly in wireline log calibration, and the carbonate percentages have only been used as a broad indication of carbonate content.

Table 3.3. Summary of grain size and carbonate content wireline log calibration data, with associated sampled well and targeted formation/member, depth and motif.

Well	Formation/Member	Depth (m)	Wireline motif	Average grain size (mm)	Wentworth size class	Carbonate content (%)
Awakino-1	Taimana Formation	1881 - 1884	Tm1	0.042	Coarse silt	60
Kaimiro-1	Taimana Formation	3004 - 3007	Tm2	0.091	Very fine sand	12
Kaimiro-1	Taimana Formation	3145 - 3148	Tm2	0.031	Coarse silt	9
Toko-1	Taimana Formation	2863 - 2866	Tm1	0.04	Coarse silt	15
Toko-1	Taimana Formation	2914 - 2917	Tm1	0.022	Medium silt	17
Mokau-1	Otaraoa Formation	2740 - 2750	Ot2	0.013	Fine silt	61
Mokau-1	Otaraoa Formation	2700 - 2710	Ot2	0.017	Medium silt	59
Tariki-1	Otaraoa Formation	2346 - 2349	Ot1	0.025	Medium silt	44
Tariki-1	Otaraoa Formation	2583 - 2586	Ot1	0.126	Fine sand	27
Toetoe-1	Otaraoa Formation (*intra* Member)	2115 - 2118	Ot1	0.021	Medium silt	51
Toetoe-1	Otaraoa Formation (*intra* Member)	2094 - 2097	Ot2	0.037	Coarse silt	44
Ahuroa-1	Otaraoa Formation (Matapo Sandstone Member)	3213 - 3216	Ma2	0.024	Medium silt	57
Ahuroa-1	Otaraoa Formation (Matapo Sandstone Member)	3222 - 3225	Ma2	0.059	Coarse silt	38
Tariki-1	Otaraoa Formation (Matapo Sandstone Member)	3024 - 3027	Ma1	0.018	Medium silt	62
Pohokura-1	Turi Formation	3312	Tu1	0.247	Fine sand	11
Pohokura-1	Turi Formation	3390	Tu1	0.024	Medium silt	9

3.6.4 Biostratigraphy and paleoenvironmental assessment

Foraminifera (forams) are widely used to place a relative age on sedimentary sequences based on the presence/absence of stratigraphically significant taxa. The stratigraphic extent of particular (mainly planktic) forams define particular New Zealand biostratigraphic stages, and routinely form the basis for determination of biostratigraphic age and correlation within and between basins. Forams are also used widely in paleoenvironmental assessment, as many benthic forams are facies-bound and restricted to particular sedimentary environments. When depositional environments change, forams typically migrate with the facies (e.g. Hayward et al. 1999 for a Taranaki Basin example).

In this study, existing foraminiferal data have been used to make paleoenvironmental assessments of the Late Eocene – Oligocene sedimentary succession in Taranaki Basin. The foraminiferal information has been derived chiefly from petroleum well completion reports lodged in the MED petroleum Report Library. Matching particular taxa to specific water depths is however problematic, as depth is only one environmental parameter affecting the distribution of forams (Hayward et al. 1999). Erosion, transport and reworking are processes that can confound paleoenvironmental assessments from forams. In some cases older taxa may be eroded and reworked into younger sediments. Both benthic and planktic forams can also be transported to different environments causing faunal mixing (Hayward et al. 1999). Transport and reworking may also be on quite large scales including reworking and deposition down slope and through mass movement events (slumps, turbidites) causing redistribution of shallow water fauna to sometimes bathyal depths (e.g. Tariki Sandstone Member). The resulting analysis of faunal populations may be a broad paleowater depth range.

3.7 WIRELINE MOTIFS, LITHOSTRATIGRAPHY AND ENVIRONMENTAL INTERPRETATIONS OF LATE EOCENE – OLIGOCENE UNITS IN TARANAKI BASIN

The lithological characteristics, facies and depositional environments of Late Eocene – Oligocene units in Taranaki Basin, interpreted on the basis of wireline log characteristics, lithological data from well completion reports, well cuttings

calibration data and paleoecological data are discussed in this section. A summary of the wireline motifs defined in Section 3.5, associated lithologies and depositional environments are given in Table 3.4.

3.7.1 Turi Formation

Lithostratigraphy

The Tu1 wireline motif represents an interbedded mudstone and siltstone interval with minor sandstone. Typically, this interval is highly-to-partly carbonaceous, slightly-to-very calcareous in part, micaceous, with lithic fragments, trace pyrite and fine glauconite. Motif Tu1 displays a characteristic upwards-fining lithology, from a more clayey siltstone lithology to a silty claystone lithology (Webster & Rainy 1987; Carter & Rainy 1988; Murray 2001). The lithology of Tu2 and Tu3 wireline motifs are similar to that of Tu1, but coarser grained, dominated by interbedded fine-grained sandstone, claystone and siltstone (Murray 2000). Tu2 underlies Tu1 in Pohokura-1 and Kaimiro-1 supporting an upward fining in lithology, possibly due to onlap (marine transgression). The presence of Tu3 in the upper section of Turi Formation in Turi-1 indicates a slight upward-coarsening before the transition into the overlying Otaraoa Formation.

Time and spatial distribution

Turi Formation has a Bortonian (Middle Eocene) to Upper Whaingaroan (Late Oligocene) age. Although Turi Formation is fairly widespread through much of Taranaki Basin, in many of the fifteen study wells in the central Taranaki Peninsula area (e.g. Ahuroa-1, Manganui-1, Ngatoro-1, Stratford-1, Tariki-1, Toetoe-1 and Totara-1) Turi Formation is fairly thin (<30 m) and is completely absent in the south-east (Toko-1) (Fig. 3.18). In central Taranaki Peninsula Turi Formation is at its thickest in the west and north (Fig. 3.18). The westernmost well (Te Kiri-1) intersects approximately ~131 m of Turi Formation, and the northernmost five wells (Turi-1, Awakino-1, Mokau-1, Pohokura-1 and Pohokura South-1) intersect >120 m each, with 867 m in the northernmost of these (Turi-1). Motif Tu1 has a similar thickness distribution pattern to that of Turi Formation as

a whole, while Tu2 is limited to the central-northern Taranaki Peninsula area and Tu3 is only present in Turi-1 (Fig. 3.18).

Table. 3.4 Wireline motifs, associated wireline characteristics, dominant lithology and inferred depositional environments for Late Eocene-Oligocene units, eastern margin, Taranaki Basin

		Wireline motif	Wireline characteristics	Dominant lithology	Inferred depositional environment
Turi Formation	Tu1		• relatively smooth and cylindrical GR log, medium-high API values • slight upwards-increasing GR log trend • featureless RES, DT and SP logs	mudstone and siltstone with minor sandstone	inner shelf (0-15m)
	Tu2	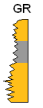	• smooth to serrated GR log, medium-low API values • smooth to serrated, medium to high value RES and DT logs	sandstone with interbedded mudstone and siltstone.	inner shelf (0-15m)
	Tu3		• serrated SP log • low API values • smooth to serrated, medium to high value DT log	sandy mudstone and siltstone with sandstone interbeds	inner shelf (0-15m)
Otaraoa Formation	*Matapo Sandstone* Ma1	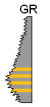	• smooth to serrated GR log, medium-low API values • smooth to serrated, medium-high value RES and DT logs • upper half displays upwards-increasing GR log	calcareous interbedded mudstone, siltstone and sandstone	outer shelf-upper bathyal (100-1000 m)
	Matapo Sandstone Ma2		• smooth to serrated GR log, medium-high API values • smooth to serrated, medium-high value RES and DT logs • typically very large positive GR deflection	very calcareous mudstone, siltstone and sandstone. glauconitic	outer shelf (100-200 m)
	Otaraoa Formation Ot1	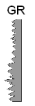	• relatively smooth GR log, medium-high API values • relatively smooth, medium-high value RES and DT logs • typically lower half displays an upwards-increasing GR log & upper half an upwards-decreasing GR log	calcareous claystone, siltstone with minor fine sand interbeds	outer shelf-upper bathyal (100-1000 m)
	Otaraoa Formation Ot2		• smooth to serrated, symetrical GR log • medium to very high value RES and DT logs • gradational lower and upper contacts	muddy limestone with calcareous mudstone interbeds	outer shelf-upper bathyal (100-1000 m)
	Otaraoa Formation Ot3		• tightly serrated SP log • smooth to moderately serrated GR log	calcareous claystone, siltstone with minor fine sandstone interbeds	outer shelf-upper bathyal (100-1000 m)
	Tariki Sandstone Ta1		• smooth to serrated, blocky GR log, low API values • negatively defelcted SP log • serrated, medium to high value RES and DT logs	fine-coarse gained sandstone	outer shelf-upper bathyal (100-600 m)
	Tariki Sandstone Ta2	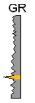	• relatively smooth and featureless, GR log, high API values • rare thin (~2m) low GR value peaks • relatively smooth, low value RES and DT logs	mudstone with minor sandstone interbeds	outer shelf-upper bathyal (100-600 m)
	Tariki Sandstone Ta3		• serrated to very serrated GR log, high-low fluctuating API values • serrated, low-high value RES and DT logs	thinnly interbedded mudstone and sandstone	outer shelf-upper bathyal (100-600 m)
					turbidite sequence
Tikorangi Formation	Tk1		• smooth, cylindrical GR log, low API values • relatively smooth, high value RES and DT logs • sharp lower and upper contacts	bioclast dominated limestone	redeposited slope (~200 m)
	Tk2		• moderately serrated GR log, medium-low API values • serrated, medium to high value RES and DT logs • gradational lower contact	muddy, silty and sandy bioclast dominate limestone	redeposited outer shelf-upper bathyal (100-1000 m)
	Tk3		• poorely to moderately serrated, blocky GR log, low API values • very serrated RES log, • high value and blocky DT log	bioclast dominated grainstone and packstone, limestone	redeposited outer shelf-upper bathyal (100-1000 m)
Taimana Formation	Tm1	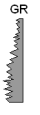	• smooth to slightly serrated GR log, medium-high API values • smooth to slightly serrated medium-high value RES and DT logs • typically displays an upwards-increasing GR log	calcareous mudstone with minor sandstone	slope to bathyal (200-1000 m)
	Tm2		• very serrated GR log, variably low-high API values • smooth to slightly serrated, medium value RES and DT logs	calcareous mudstone with sandstone stringers	slope to bathyal (200-1000 m)

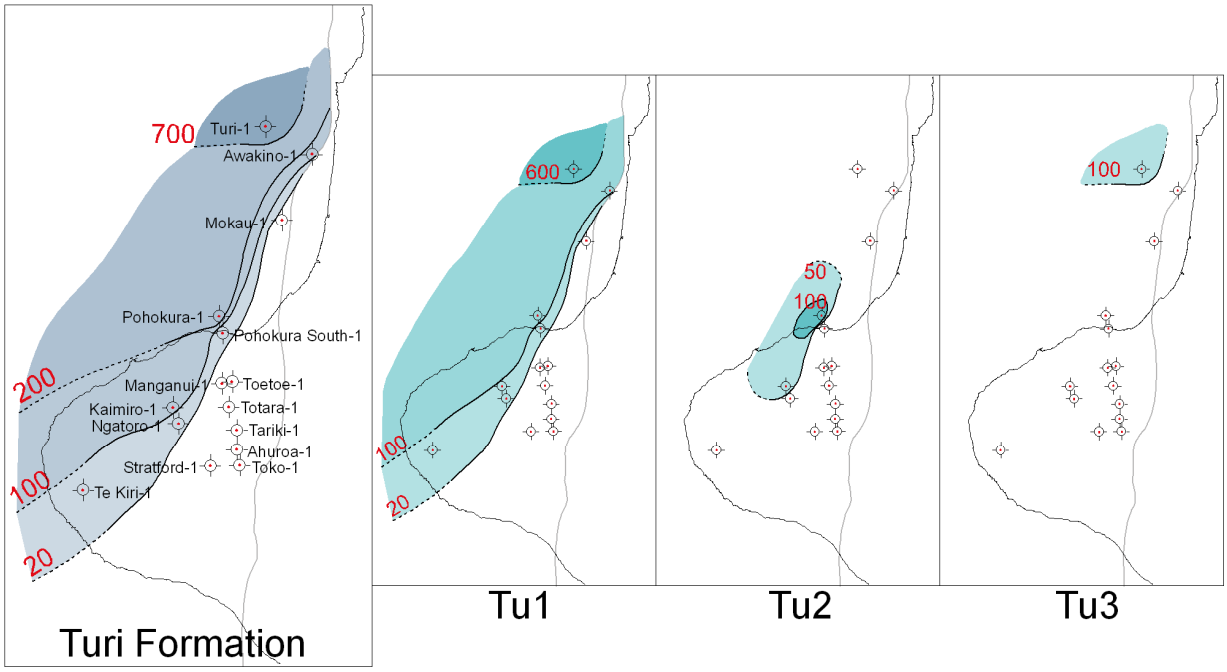

Figure 3.18. Thickness (m) distribution of the Turi Formation, and associated motifs (Tu1, Tu2 and Tu3). Taranaki Fault location marked in grey.

Paleoenvironmental data and depositional facies

Foraminiferal studies of Turi Formation indicate an inner shelf (0 – 30 m water depth) depositional environment under neritic water mass conditions (Carter 1983; Lock 1983; de Bock et al. 1985; Webster & Rainy 1987; Carter & Rainy 1988; STOS 1988; Murray 2001). In Taranaki Peninsula, the Turi Formation represents the initiation of highstand deposition, the later part of an Eocene regional transgressive phase (Carter & Rainy 1988; King & Thrasher 1996). This is illustrated by the transition from underlying sand dominated, coastal plain/marginal marine facies of the Mangahewa and McKee Formations, through to the overlying shallow marine inner shelf setting of Turi Formation.

3.7.2 Matapo Sandstone

Lithostratigraphy

The Ma1 wireline motif consists mostly of interbedded siltstone, mudstone and sandstone, intercalated with fine-to-course grained, moderately sorted silty sandstone. Ma1 is typically moderately to very calcareous, glauconitic, and in parts pyritic (Palmer 1985; Carter et al. 1987b). The lithology of Ma1 typically

shows an upward-fining trend, with the upper part of this motif resembling and gradationally passing into calcareous mud dominated Ot1 motif (Carter & Rainy 1988). The lithology of Ma2 is typically finer grained than Ma1, consisting of a highly calcareous sandy mudstone, with abundant glauconite (Webster & Rainey 1987; STOS 1988).

Time and spatial distribution

The Matapo Sandstone has a Runangan (Late Eocene) to Lower Whaingaroan age for the fifteen well sections investigated here. Thickness is fairly uniform, between 5 to 15 m for most wells, and up to 56 m in Ngatoto-1. It is absent in Manganui-1, Stratford-1 and Turi-1 (Fig. 3.19). Ma1 and Ma2 have similar thickness distribution patterns, being thickest in the Ngatoro-1 and Mokau-1 areas (Fig. 3.19).

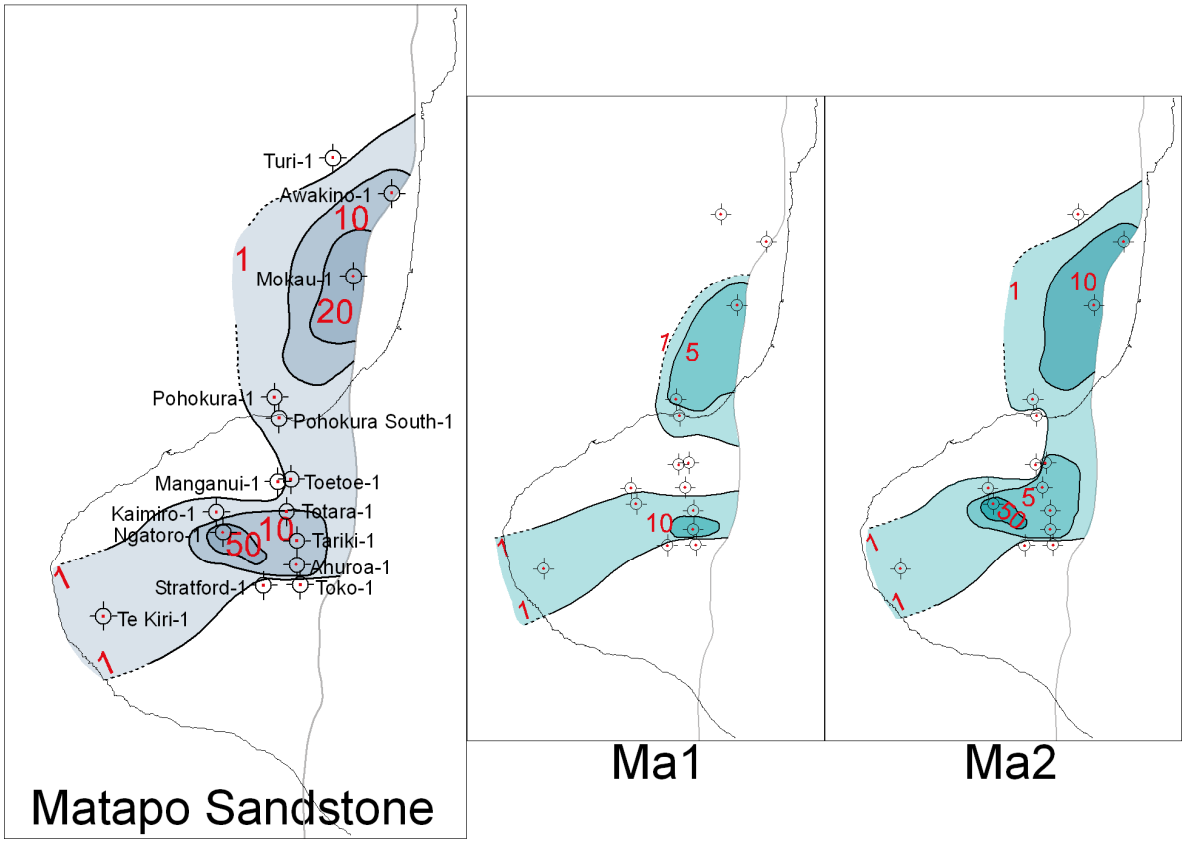

Figure 3.19. Thickness (m) distribution of the Matapo Sandstone Member, and associated motifs (Ma1, and Ma2). Taranaki Fault location marked in grey.

Paleoenvironmental data and depositional facies

In many of the well sections examined in this study, microfauna were not analysed from Matapo Sandstone samples with the exception of McKee-1 (northern Taranaki Peninsula), where forams indicate an outer shelf (100 – 200 m) environment, and Kaimiro-1, where fauna sampled from Ma1 indicate outer shelf to upper bathyal water depths (100 – 400 m) (Carter 1983). The basal, highly calcareous Ma2 motif (e.g. Table 3.3) represents a condensed sedimentary section with significant glauconite content. Glauconite (detrital or authigenic) is composed of around 5% potassium by weight, and the ^{40}K radioactive isotope of potassium naturally emits gamma radiation as it decays. Because of this, the presence of glauconite may induce its own gamma ray value of 75 – 90 API (Rider 1986). The strong gamma ray peaks observed in Ma2 may be caused by this phenomenon. Furthermore, glauconite formation is associated with outer shelf settings (McRae 1972).

During Matapo Sandstone deposition, water depth was increasing, with a decrease in terrigenous sediment input to the shelf. The accumulation of glauconite is strongly dependent upon very low to minimal terrigenous sedimentation. The overlying Ma1 motif and its sharp transition into moderately calcareous Otaraoa Formation suggests a marked increase in water depth and an increase in sediment flux to the basin.

3.7.3 Otaraoa Formation

Lithostratigraphy

The Ot1 wireline motif represents an interbedded claystone and siltstone interval, with minor argillaceous very fine to fine grained sandstone intervals. Ot1 is typically moderately to very calcareous (e.g. Table 3.3), with trace mica, pyrite and carbonaceous flakes (Carter 1983; Webster & Rainey 1987; Carter & Rainy 1988). Although Ot1 is typically a thick interval (up to 500 m in Tariki-1), lithologically it appears to be relatively homogenous. As mentioned previously (Section 3.5.2.1), Ot1 commonly shows an upward increasing GR log trend from the Matapo Sandstone, with a corresponding upward decreasing DT log trend. These trends reflect upwards-decreasing carbonate content within Otaraoa. Towards the top of Otaraoa Formation this trend reverses, with an upwards-

decreasing GR log trend and upwards-increasing DT log trend indicating increasing carbonate content into the overlying Tikorangi Formation (Carter et al. 1987b). Ot3 lithology is similar to that of Ot1 but coarser. In Ahuroa-1, Ot3 indicates a significant proportion of limestone interbeds with minor very fine to fine sandstone intervals (Carter et al. 1987a). Ot2 represents a fine grained carbonate sequence with calcareous mudstone interbeds (de Bock et al. 1985; STOS 1988). In Awakino-1 and Mokau-1, Ot1 passes gradationally upward into Ot2.

Time and spatial distribution

The Otaraoa Formation is assigned an Upper Whaingaroan to mid Waitakian age. Otaraoa Formation therefore represents a substantial portion of the middle to Late Oligocene succession in Taranaki Basin. It is thickest (typically >100 m) along the eastern margin of Taranaki Basin, adjacent to the Taranaki Fault (Fig. 3.20), and has a maximum thickness of over 1000 m in the southern-central Taranaki Peninsula area (e.g. Waihapa Field) (King & Thrasher 1996). Otaraoa Formation grades laterally into condensed carbonate of the Tikorangi Formation, particularly in its upper parts (King & Thrasher 1996). The carbonate dominated Ot2 wireline motif is only observed in the lower section of Otaraoa Formation in the northern wells, Awakino-1 and Mokau-1 (Fig. 3.20). Motif Ot2 is an earlier occurrence of a Tikorangi Formation-like interval within Otaraoa Formation. Motif Ot1 has a similar thickness distribution pattern to that of Otaraoa Formation because it is the main wireline facies and Ot3 is only observed in vicinity of Ahuroa-1 (Fig. 3.20).

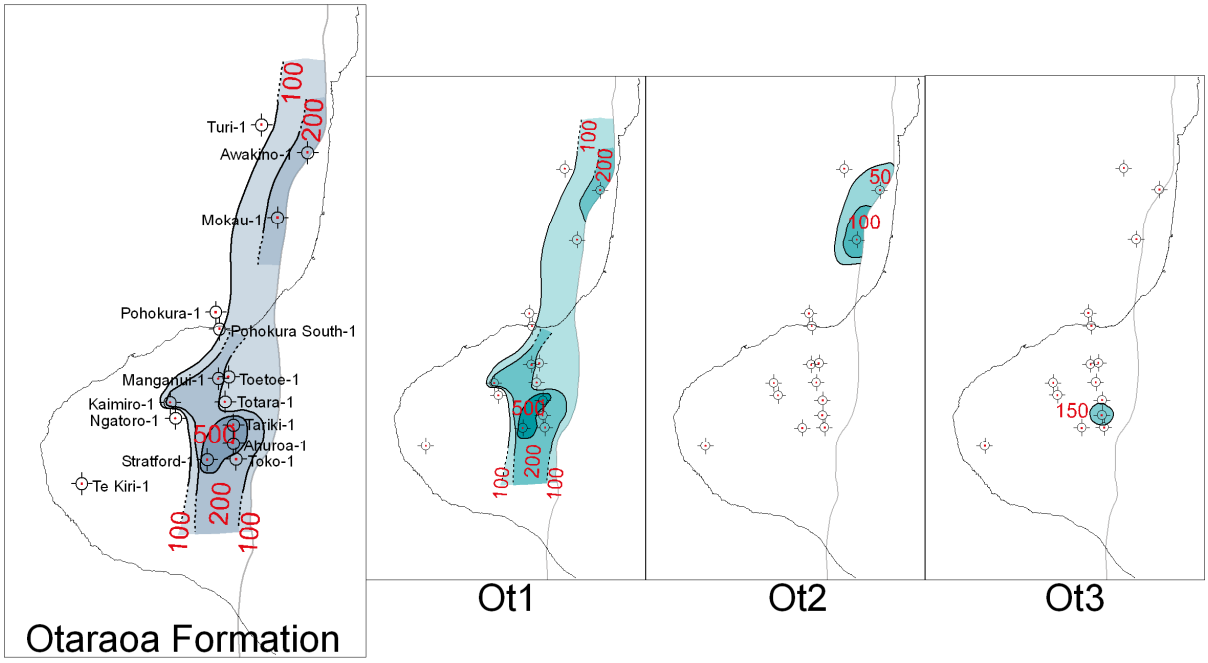

Figure 3.20. Thickness (m) distribution of the Otaraoa Formation, and associated motifs (Ot1, Ot2 and Ot3). Taranaki Fault location marked in grey.

Paleoenvironmental data and depositional facies

Foraminiferal assemblages within Otaraoa Formation indicate an upper to mid-bathyal depositional environment around 400 – 600 m of water depth (King & Thrasher 1996; H. Morgans pers comm. 2008). Deposition of the Otaraoa Formation occurred in response to the development of a foredeep along the eastern margin of central parts of Taranaki Basin. The deposits are chiefly calcareous mudstone (Ot1 facies), with limestones facies (Ot2 and Ot3) at times. The foredeep sediments may have been sourced from two directions, one involving progradation from the south, which is suggested in some south-north oriented seismic reflection lines, and the other direction being from the east. The Murihiku Terrane basement forming the upthrown side of Taranaki Fault supported the Patea-Tongaporutu-Herangi High, upon which shallow marine carbonate sediment was generated (Hood et al. 2003). The limestone facies in Otaraoa Formation (Ot2 & Ot3) represent progradation of relatively coarse inner-shelf carbonate sediments across a narrow shelf and down a west-facing continental slope, the top of which was pinned to the tip of the Murihiku Terrane basement being thrust into Taranaki Basin from the Upper Whaingaroan onwards (Tripathi & Kamp 2008). The Ot2 and Ot3 facies have considerable fine grained

carbonate within them, reflecting the distal parts of the redepositied carbonates sourced from the basement high to the east of Taranaki Fault. Also, the slope deposits have been foreshortened by subsequent (especially Otaian) thrust movement on Taranaki Fault such that the Otaraoa Formation as observed in the well sections in the Peninsula area are now closer to the original shelf carbonate source. The Ot1 facies can be interpreted as fine grained calcareous mudstone having an origin as hemipelagic sedimentation, as well as redeposited slope sediments.

3.7.4 Tariki Sandstone

Lithostratigraphy

The Ta1 wireline motif represents fine to medium and occasionally coarse grained, moderately to poorly sorted, calcareous to slightly calcareous sandstone, with abundant quartz, and occasional pyrite and coal fragments (Adams et al. 1980; Carter et al. 1987b). This motif has a distinctly different lithology to Ta2 wireline motif, which is dominated by argillaceous, bioturbated mudstone with minor thinly interbedded sandstone (Higgs et al. 2004). The Ta3 wireline motif is composed of thinly interbedded sandstone and siltstone, with minor mudstone, chert and coal fragments (Carter & Rainy 1988).

Time and spatial distribution

The Tariki Sandstone is observed to have a strictly Upper Whaingaroan age and is only observed in central Taranaki Peninsula wells adjacent to Taranaki Fault (Fig. 3.21). In the fifteen wells studied, Tariki Sandstone shows large thickness variations, with a maximum thickness of 321 m in Toko-1. A progressive northward thinning of this unit is evident, with 248 m in Ahuroa-1, and less than 200 m in Tariki-1, Totara-1 and Toetoe-1 (Fig. 3.21). Motif Ta1 is thickest in Ahuroa-1 and Tariki-1, with a northward thinning evident (Fig. 3.21). Ta2 is thickest in Toko-1 and shows a similar northward thinning (Fig. 3.21). Ta3 is thickest in Toetoe-1, and shows southward thinning to Ahuroa-1 and Tariki-1 (Fig. 3.21).

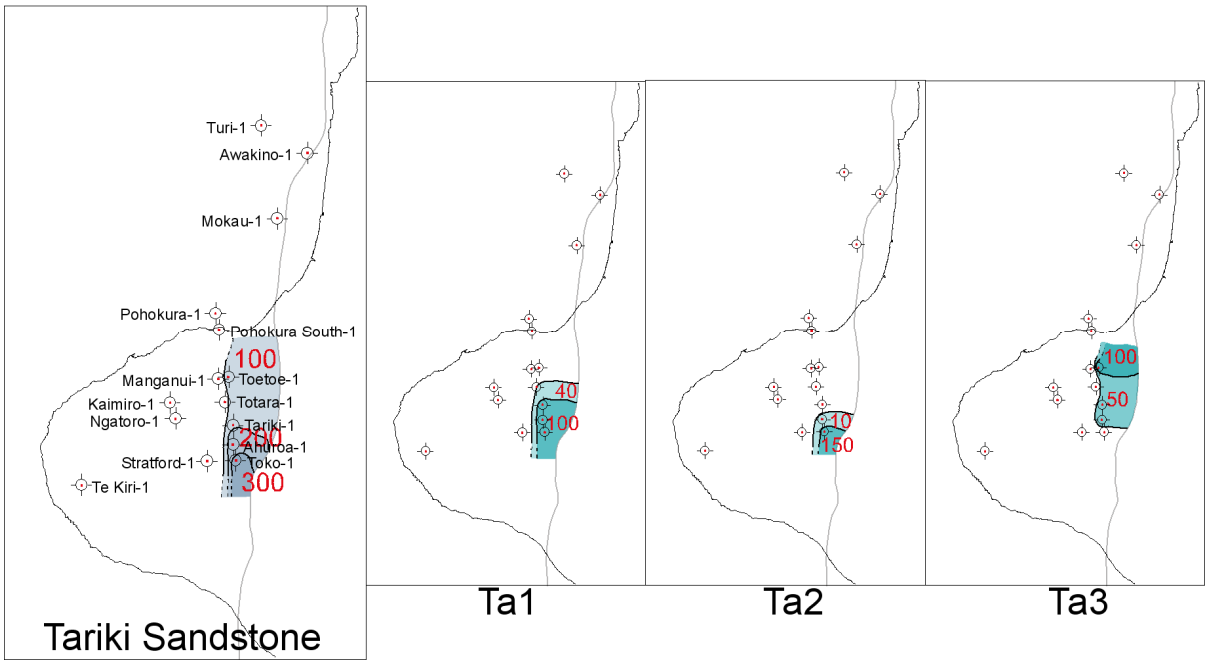

Figure 3.21. Thickness (m) distribution of the Tariki Sandstone Member, and associated motifs (Ta1, Ta2 and Ta3). Taranaki Fault location marked in grey.

Paleoenvironmental data and depositional facies

Tariki Sandstone contains mixed shallow and deep-water foraminiferal assemblages (de Bock et al. 1990). In the central Taranaki Peninsula area (Ahuroa-Tariki fields) taxa suggest an uppermost to upper bathyal (200 – 600 m) depositional environment, while to the south (Toko-1 and Waiahpa-1), outer shelf to uppermost bathyal (100 – 400 m) paleo-water depths are interpreted (Higgs et al. 2004, after Morgans & Waghorn 1999). Tariki Sandstone is interpreted to represent a series of upper bathyal (i.e. upper slope) turbidites, submarine channel, crevasse splay and levee deposits that accumulated in a north-south trending foredeep trough along the eastern margin of Taranaki Basin (de Bock et al. 1990; King & Thrasher 1996). The thick, clean to upward thinning sandstone (Ta1) dominant in Ahuroa-1 and Tariki-1 are interpreted as stacked channel sandy debris flow deposits forming a slope to basin floor fan. The thin sandstone interbedded within siltstone beds (Ta2) are interpreted as distal lobe and overbank deposits. The Ta3 facies are interpreted as distal turbidites (de Bock et al. 1990; Higgs et al. 2004). The appearance of Tariki Sandstone within Otaraoa Formation reflects the upper bathyal conditions that had developed along the eastern margin of the basin during the Upper Whaingaroan, and the formation of a trough between the Taranaki Fault and the Tariki Fault Zone, being a fold-fault thrust

zone outboard of Taranaki Fault. It is possible that the terrigenous sediments forming the sandstone facies of Tariki Sandstone were transported from a shoreline (where the textural maturity developed) attached to the Patea-Tongaporutu High and across a narrow shelf before being fed down the slope and into the trough.

3.7.5 Tikorangi Formation

Lithostratigraphy

The Tk1 wireline motif represents redeposited bioclast dominated limestone beds (SBPT 1975, STOS 1988). Wireline log records suggest that this interval has a very high carbonate content (Hood et al. 2003). The sharp upper and lower contacts with Taimana Formation and Otaraoa Formation, respectively (evident in GR and DT logs), reflect this relatively pure limestone interval (Fig. 3.14). The Tk2 wireline motif represents an interbedded, argillaceous, muddy, silty to fine sand sized limestone dominated interval. This interval is typically well sorted, composed dominantly of echinoderm and bivalve fragments with minor quartz, pyrite, glauconite and volcanic rock fragments (Adams et al. 1980; Carter et al. 1987a; Murray 2000, Hood et al. 2003). This interval typically shows an upward coarsening (cleaning upward) and upward increasing carbonate content from the underlying very calcareous mud dominated Otaraoa Formation. The Tk3 wireline motif is similar to that of Tk2 however is coarser grained, with grainstone and packstone composed of very fine to coarse sand grains (Adams et al. 1980). In Toko-1 this interval displays a upward coarsening trend, showing a gradation from the underlying silt to fine sand dominated Tk2 motif, to the bioclast dominated grainstone and packstone of Tk3 (Adams et al. 1980).

Time and spatial distribution

Tikorangi Formation has a Waitakian age for the fifteen wells in this study and it occurs in the same depocentre as Tariki Sandstone; that is, along the eastern margin of Taranaki Basin and adjacent to Taranaki Fault (Fig. 3.22). Tikorangi Formation progressively thins to the north (25 m in Turi-1) from its thickest occurrence in Toko-1 (296 m) (Fig. 3.22). To the west, Tikorangi Formation thins

rapidly, with a 51 m sequence observed in Stratford-1 and no record in the three westernmost wells (Ngatoro-1, Kaimiro-1 and Te Kiri-1) (Fig. 3.22). Tk1 has a similar thickness distribution to that of Tikorangi Formation (Fig. 3.22). Tk1 is only observed in the northern wells (Mokau1 and Turi-1) and Tk3 is only observed in Toko-1 (Fig. 3.22).

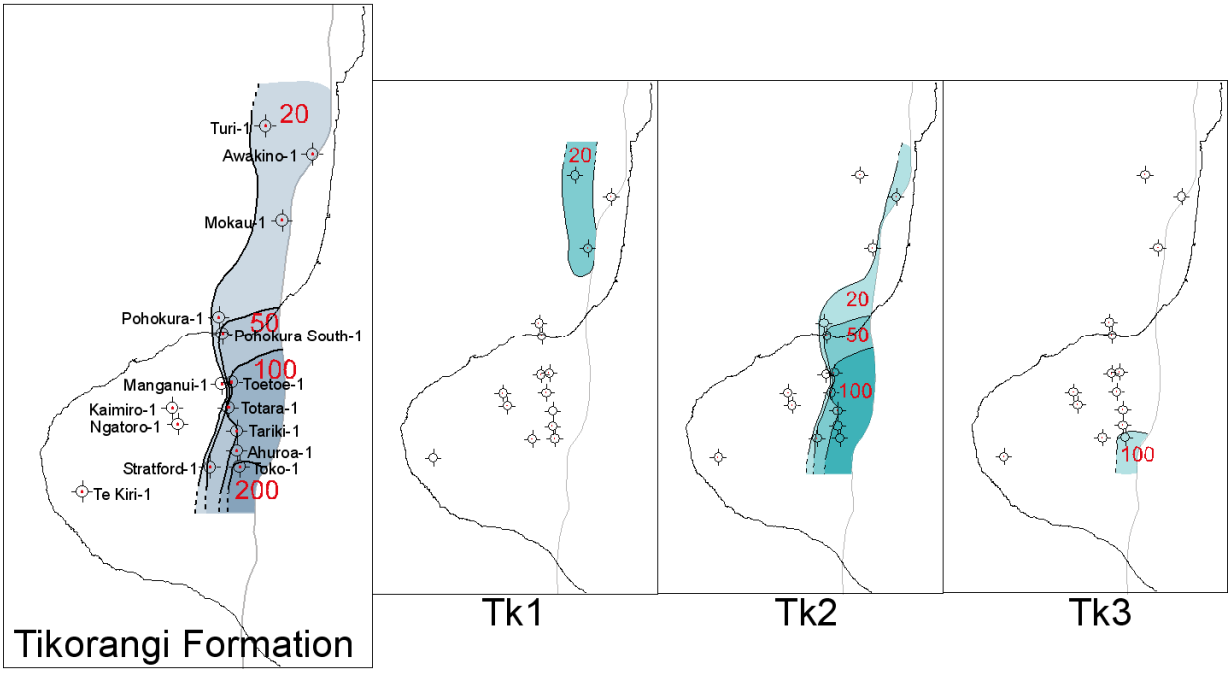

Figure 3.22. Thickness (m) distribution of the Tikorangi Formation, and associated motifs (Tk1, Tk2 and Tk3). Taranaki Fault location marked in grey.

Paleoenvironmental data and depositional facies

Planktonic foraminiferal assemblages and diverse benthonic fauna suggest deposition in outer shelf and upper bathyal water depths for Tikorangi Formation (Adams et al. 1980; Lock 1983; STOS 1988; King & Thrasher 1996). However much of the shelfal taxa may be redeposited and hence an upper bathyal depositional setting is preferred. Along the central-eastern margin of the basin, around Taranaki Peninsula, Tikorangi Formation was probably deposited on a moderate westward dipping continental slope with its upper part pinned to a westward advancing basement thrust block. The carbonate-dominated nature of Tikorangi Formation reflects the production of inner shelf carbonate around the Patea-Tongaporutu-Herangi High.

3.7.6 Taimana Formation

Lithostratigraphy

The Tm1 wireline motif represents a similar lithology to the mud dominated and calcareous Otaraoa Formation. Where Tikorangi Formation is absent these two formations are often undifferentiated (King & Thrasher 1996). Motif Tm1 is typically a moderately calcareous mudstone interval (e.g. Table 3.3), with trace amounts of fine sandstone, glauconite and pyrite. This interval shows a highly calcareous base, with an upward decreasing carbonate content into the overlying Wai-iti Group (Murray 2000; Murray 2001). The lithology of Tm2 is similar to that of Tm1, however it displays sandstone stringers, interbedded within Tm1's calcareous mudstone (Carter 1983).

Time and spatial distribution

The Taimana Formation has an upper Waitakian to Otaian age (King & Thrasher 1996). Taimana Formation is thickest adjacent to Taranaki Fault and shows westward thinning (Fig. 3.23). Tm2 has a similar thickness distribution to Taimana Formation, being at its thickest in Manganui-1 (>200 m). Tm1 is only observed in Kaimiro-1 (Fig. 3.23).

Paleoenvironmental data and depositional facies

The faunal assemblage from Taimana Formation indicates bathyal depositional environments (200 – 1000 m water depth) (Adams et al. 1980; Carter 1983). The composition of Taimana Formation indicates that a terrigenous mud source was re-established at the beginning of the Miocene. The sharp contact often observed on wireline logs between Taimana Formation and the overlying Wai-iti Group reflects a sudden change to more terrigenous mudstone, reflecting the wider distribution of material derived from the developing plate boundary through New Zealand.

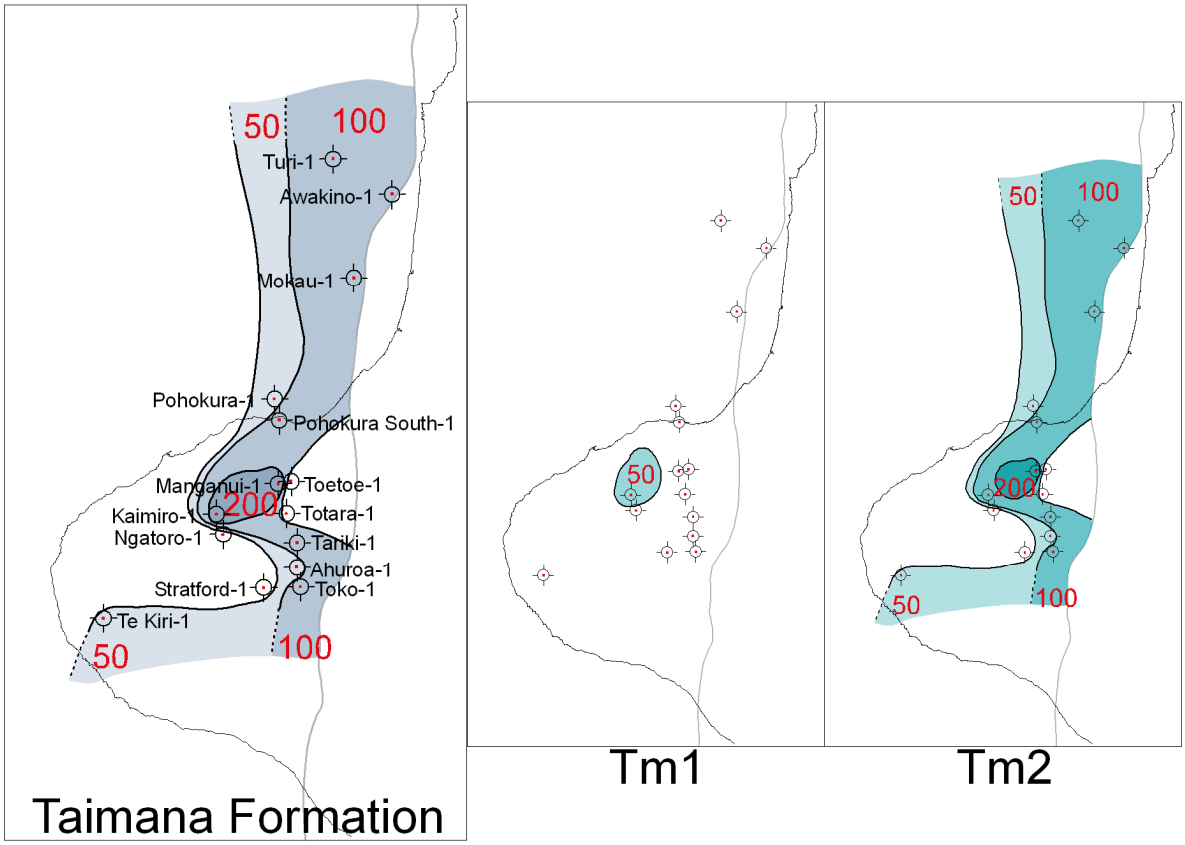

Figure 3.23. Thickness (m) distribution of the Taimana Formation, and associated motifs (Tm1 and Tm2). Taranaki Fault location marked in grey.

3.8 CONCLUSIONS

The interpretation of various geological parameters from wireline log records illustrates the importance of wireline logging for examining subsurface stratigraphy. When log data are integrated with other lithological data sources (drilling derived data, recovered samples and published literature) and paleoenvironmental data sources (biostratigraphy and paleoecological data from foraminifera) a concise understanding of the physical subsurface geological characteristics, the depositional age of units and the depositional paleoenvironments of units can be obtained. Because of the entirely subsurface nature of the Late Eocene – Oligocene succession in Taranaki Basin, wireline log analysis has been employed as a tool to view the subsurface stratigraphy. Using the geometric appearance of major log types (GR, CALI, RES, DT and SP) a suite of wireline motifs have been defined for the Late Eocene – Oligocene section in 15 wells in the Taranaki Peninsula area of eastern margin Taranaki Basin. With

the integration of lithological data and paleoenvironmental data sources, the lithostratigraphy, time and spatial distribution and depositional paleoenvironments of the various wireline motifs have been subsequently interpreted, illustrating the progressive change in depositional paleoenvironments through the Late Eocene to the Early Miocene. The Turi Formation accumulated in an inner shelf depositional setting during the Runangan (Late Eocene), followed by condensed outer shelf facies in the Matapo Sandstone. This reflects regular southward-directed onlap within Taranaki Basin. Upper bathyal conditions suddenly developed during the Upper Whaingaroan with accumulation of the Otaraoa Formation. Tariki sandstone is a terrigenous fan deposit within Otaraoa Formation and its formation emphasises the development of a west-facing slope along the eastern margin of the basin, as well as a shoreline along the western side of the Patea-Tongaporutu High where the textural maturity of the sandstone developed (from alongshore drift). The Tikorangi Limestone facies have a similar origin and distribution to the Tariki Sandstone, except that the facies are comprised of carbonate. The carbonate was sourced from productive shoreline areas on the western side of the Patea-Tongaporutu-Herangi High, transported across the narrow shelf and redeposited onto the slope. The Taimana Formation is chiefly a calcareous mudstone and reflects the accumulation of hemipelagic deposits in bathyal conditions. The lithostratigraphic and paleoenvironmental data discussed in this chapter helps constrain paleogeographic interpretations presented later in this thesis (Chapter 6).

CHAPTER FOUR
SEDIMENTARY PETROGRAPHY

4.1 INTRODUCTION

Petrographic analyses of sedimentary rock samples provide insights into the mineral constituents and their origins. Petrographic descriptions and the identification and classification of mineralogical content is useful for the comparison of samples, determination of the depositional environments of the host rocks and provenance analysis (Carozzi 1993). This chapter outlines the samples obtained in this study and the methodology used for various types of labratory analyses. Wireline log calibration (Section 3.6.3) is also outlined with respect to determination of the carbonate content and grain size character of well cutting samples. This chapter primarily establishes the composition and characteristics of the constituents of Eocene – Oligocene sandstone units sampled in this investigation. Using the modal mineral proportions and the characteristics of samples, preliminary interpretations are drawn in this chapter about sediment provenance.

4.2 SAMPLES

Twenty nine samples were obtained in this study for different analytical purposes (see Appendix I), including petrographic analysis, wireline log calibration and for U-Pb geochronology (Chapter 5). Table 4.1 summarises the 22 subsurface well cutting samples obtained from Late Eocene – Oligocene units in the eastern margin of Taranaki Basin (see Appendix I). Sandstones sampled were analysed petrographically and used for the purpose of U-Pb geochronology. The more argillaceous samples were used for wireline log calibration, where carbonate content and grain size have been determined (see Appendix III). Table 4.2 summarises the 7 onshore sandstone samples analysed in this study, including 5 Te Kuiti Group samples from the Waikato Region, a quartz sandstone from Taumarunui and an Otaihanga quartz sandstone sample, all obtained from outcrop (see Appendix I for details about onshore samples). Although these onshore samples are not Taranaki Basin units, they are of similar age to those sandstones.

A sampling location map for North Island age equivalent units is included in Appendix I.

Table 4.1. Subsurface sample summary, with sampled well, formation/member, depths and sample purpose. Note most samples are used for the purpose of wireline log calibration.

Well	Formation/Member	Depth (m)	Sample purpose
Awakino-1	Taimana Formation	1881 - 1884	Wireline log calibration
Toko-1	Taimana Formation	2863 - 2866	Wireline log calibration
Toko-1	Taimana Formation	2914 - 2917	Wireline log calibration
Kaimiro-1	Taimana Formation	3004 - 3007	Wireline log calibration
Kaimiro-1	Taimana Formation	3145 - 3148	Wireline log calibration
Tariki-1	Otaraoa Formation	2346 - 2349	Wireline log calibration
Tariki-1	Otaraoa Formation	2583 - 2586	Wireline log calibration
Mokau-1	Otaraoa Formation	2700 - 2710	Wireline log calibration
Mokau-1	Otaraoa Formation	2740 - 2750	Wireline log calibration
Tariki-1	Otaraoa Formation (Tariki Sandstone Member)	2810 - 2860	Petrography and U-Pb geochronology
Tariki-1	Otaraoa Formation (Tariki Sandstone Member)	2870 - 2920	Petrography and U-Pb geochronology
Tariki-1	Otaraoa Formation (Tariki Sandstone Member)	2940 - 2990	Petrography and U-Pb geochronology
Toetoe-1	Otaraoa Formation (*intra* Member)	2094 - 2097	Wireline log calibration
Toetoe-1	Otaraoa Formation (*intra* Member)	2115 - 2118	Wireline log calibration
Tariki-1	Otaraoa Formation (Matapo Sandstone Member)	3024 - 3027	Wireline log calibration
Ahuroa-1	Otaraoa Formation (Matapo Sandstone Member)	3213 - 3216	Wireline log calibration
Ahuroa-1	Otaraoa Formation (Matapo Sandstone Member)	3222 - 3225	Wireline log calibration
Ngatoro-1	Otaraoa Formation (Matapo Sandstone Member)	3550 - 3600	Petrography and U-Pb geochronology
Pohokura-1	Turi Formation	3312	Wireline log calibration
Pohokura-1	Turi Formation	3390	Wireline log calibration
Pohokura-1	Turi Formation	3420 - 3470	Petrography and U-Pb geochronology
Kaimiro-1	McKee Formation	3784 - 3740	Petrography and U-Pb geochronology

Table 4.2. Onshore sample summary, with sample area, formation/member and sample purpose.

Sample area	Formation/ member	Sample purpose
Port Waikato	Glen Massey Formation (Ahirau Sandstone Member)	Petrography and U-Pb geochronology
Aotea Harbour	Glen Massey Formation (Ahirau Sandstone Member)	Petrography and U-Pb geochronology
Awamarino	Glen Massey Formation (Ahirau Sandstone Member)	Petrography and U-Pb geochronology
Hautapu Hill	Aotea Formation (Hauturu Sandstone Member)	Petrography and U-Pb geochronology
Kihi Road	Aotea Formation (Hauturu Sandstone Member)	Petrography and U-Pb geochronology
Taumarunui	Taumarunui quartz sandstone	Petrography and U-Pb geochronology
Otaihanga	Otaihanga Outlier	Petrography and U-Pb geochronology

4.3 METHODS

4.3.1 Carbonate fraction analysis

Well cuttings samples were initially gently crushed to disseminate aggregated grains. For sample information see Appendix III. Carbonate content was determined by standard carbonate digestion procedure. Using dilute hydrochloric acid, the carbonate content was dissolved from samples in a beaker. This solution was then filtered and washed through filter paper. After drying, the residual left on the filter paper represented the clastic portion of the sample. Simple pre/post sample weight calculations give the carbonate content as a proportion (or percentage).

4.3.2 Grain size analysis

Well cuttings samples for grain size analysis were initially gently crushed to disseminate aggregated grains. For sample information see Appendix III. These samples were then oven heated (dried), followed by addition of dilute hydrogen peroxide, which further disseminated the grains. Samples were then analysed, using a Malvern-Mastersizer S instrument to determine the grain size distributions.

4.3.3 Mineral separation

Heavy and light minerals were separated for samples by standard mineral separation procedures. One kilogram sandstone samples from outcrop and well cuttings were initially crushed using a jaw crusher and Bico disc mill in Waikato University's rock crushing facility. Samples were then separated based on grain density using a Gemini Table. The heavier mineral fraction recovered was then put through a heavy liquid (Sodium Polytungstate 2.85 gm/cc) to separate light from heavy minerals. The light mineral fraction and the heavy magnetic mineral fraction were retained for petrographic analysis (Section 4.3.4). Zircon grains were hand separated from the heavy mineral fraction (Section 5.2).

4.3.4 Grain mounts

Grain mounts were made from the light fraction and the heavy magnetic mineral fractions respectively (Appendix IV provides sample information). Due to the high carbonate content of samples analysed, carbonate digestion was performed on grains before slide mounting. A thin cover of grains was then applied to epoxy resin covered microscope slides. Upon drying, grain mounts were ground to a thickness of approximately 0.03 mm. Modal analysis was undertaken on the grain mounts using a petrographic microscope. For each grain mount 300 points were counted.

4.4 RESULTS

4.4.1 Carbonate content and calibration of wireline logs

Because well cutting samples retrieved in this study had intermixed drilling mud/fluid, an unknown proportion of (non-calcareous) drilling mud was unavoidably processed along with the sampled formation. This causes an underestimate of the total carbonate content of the sample. As mentioned in Section 3.6.2, well cuttings may not always be representative of formation depths due to the mixing and contamination of cuttings. In most cases well cuttings are representative of several metres of depth. Table 3.3 includes carbonate content determinations for 16 samples. For sample information and carbonate digestion data see Appendix III. Although there is no direct comparison of calculated values

to a standard, the values calculated in this study were somewhat expected and seemed to complement carbonate content suggested by wireline log signals and well completion report descriptions.

4.4.2 Grain size and calibration of wireline logs

As mentioned in Section 3.6.3, the spread of depths within particular well cutting samples and the presence of drilling mud also proved a problem in grain size determination and the calibration of wireline logs. Because the formation characteristics (very fine grained lithologies) resemble that of the drilling mud, it is hard to distinguish between the two. The resulting grain size distributions measured for each sample included any drilling mud fraction, likely causing an underestimate of the mean grain size for a sample. Table 3.3 includes the mean grain size determinations for 16 samples. For sample information and grain size data see Appendix III. The majority of the mean grain sizes over the Oligocene interval are of fine to coarse silt (0.013 – 0.059 mm) (Wentworth size classes). The coarsest determined mean grain size is fine sand (0.247 mm)

4.4.3 Modal petrography of Late Eocene – Oligocene units

Modal composition data were obtained for the light mineral fraction as well as the heavy magnetic mineral fraction for ten subsurface and onshore detrital grain mounts. For sample information and modal petrography data see Appendix IV. The purpose was to identify the main siliciclastic mineral constituents. The relative proportions of these constituents were determined by point counting of the detrital mounts. The proportions and the presence of components are used to interpret the provenance of the sediments.

McKee Formation

Light mineral fraction

The light mineral components of the McKee Formation are summarised in Figure 4.1. Sedimentary rock fragments (45%) and angular quartz grains (34%) are the primary components. Sedimentary rock fragments are typically quite weathered,

fine grained and composed of silt-sized grains. This is shown in Fig. 4.1 where a typical fine sand size sedimentary rock fragment is shown with opaque minerals (possibly ilmenite). Minor plagioclase feldspar (9%), volcanic rock fragments (7%), opaque minerals (limonite and magnetite; 2%), orthoclase feldspar (0.5%), microcline feldspar (0.5%), amphibole and glauconite also occur in small quantities (Fig. 4.1).

Heavy magnetic mineral fraction

The magnetic heavy mineral fraction in McKee Formation is dominated by sedimentary and undifferentiated rock fragments (sedimentary and/or volcanic), with abundant limonite and glauconite-filled foraminifera. The large proportion of rock fragments recovered in the magnetic mineral fraction of the McKee Formation indicates the inclusion of significant amounts of magnetic minerals in the rock fragments.

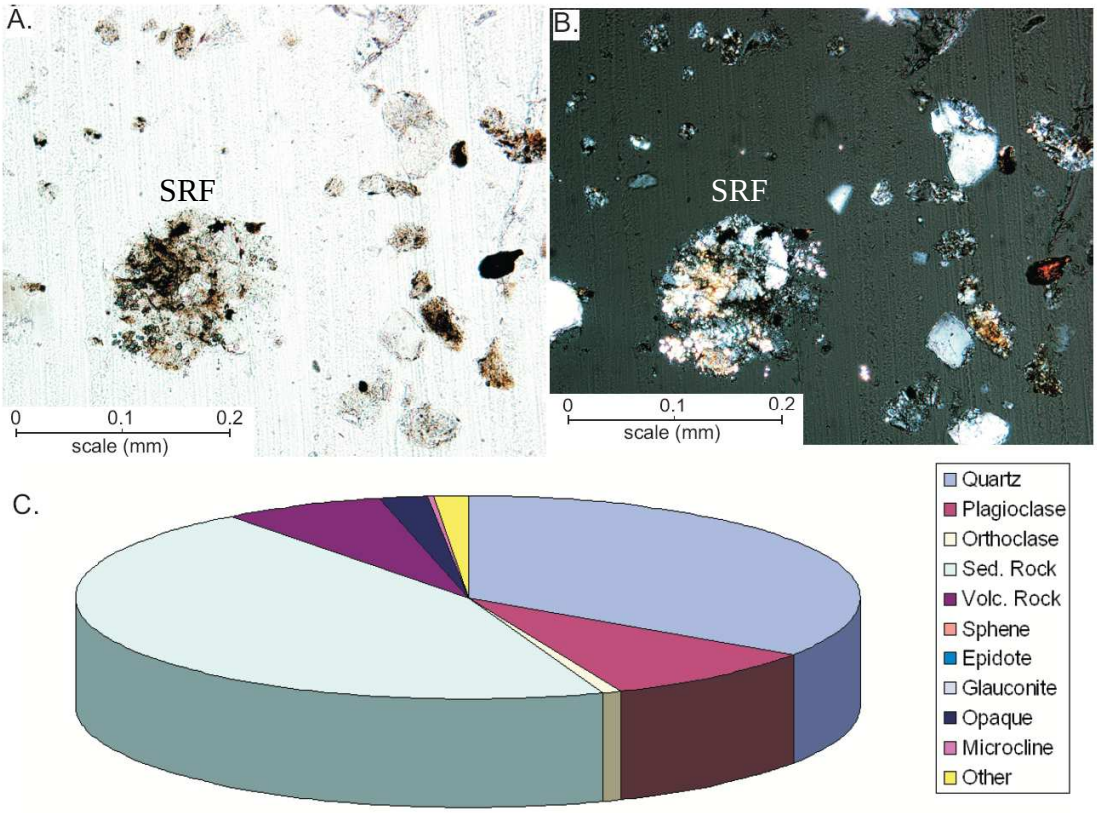

Figure 4.1. A. Photomicrograph identifying a sedimentary rock fragment in the light mineral fraction of the McKee Formation, x200, under plane polarised light and **B.** with x-nicols. **C.** Component percentages from petrographic modal analysis.

Turi Formation

Light mineral fraction

Similar to the McKee Formation, the Turi Formation is primarily composed of sedimentary rock fragments (52%) and quartz grains (30%). Figure 4.2 summarises the siliciclast content of the Turi Formation and illustrates a typical sedimentary rock fragment, which appears similar to those observed in the McKee Formation (Fig. 4.1). Minor plagioclase feldspar (10%), orthoclase feldspar (4%), volcanic rock fragments (4%) and trace amounts of glauconite are also observed (Fig. 4.2). Grains are typically angular and the sample is poorly sorted.

Heavy magnetic mineral fraction

Undifferentiated rock fragments (sedimentary and/or volcanic) and limonite dominate Turi Formation's magnetic heavy mineral fraction. Abundant opaque minerals and minor glauconite were also observed. The large proportion of rock fragments recovered in the magnetic mineral fraction suggests the presence of significant amounts of magnetic minerals in the rock fragments.

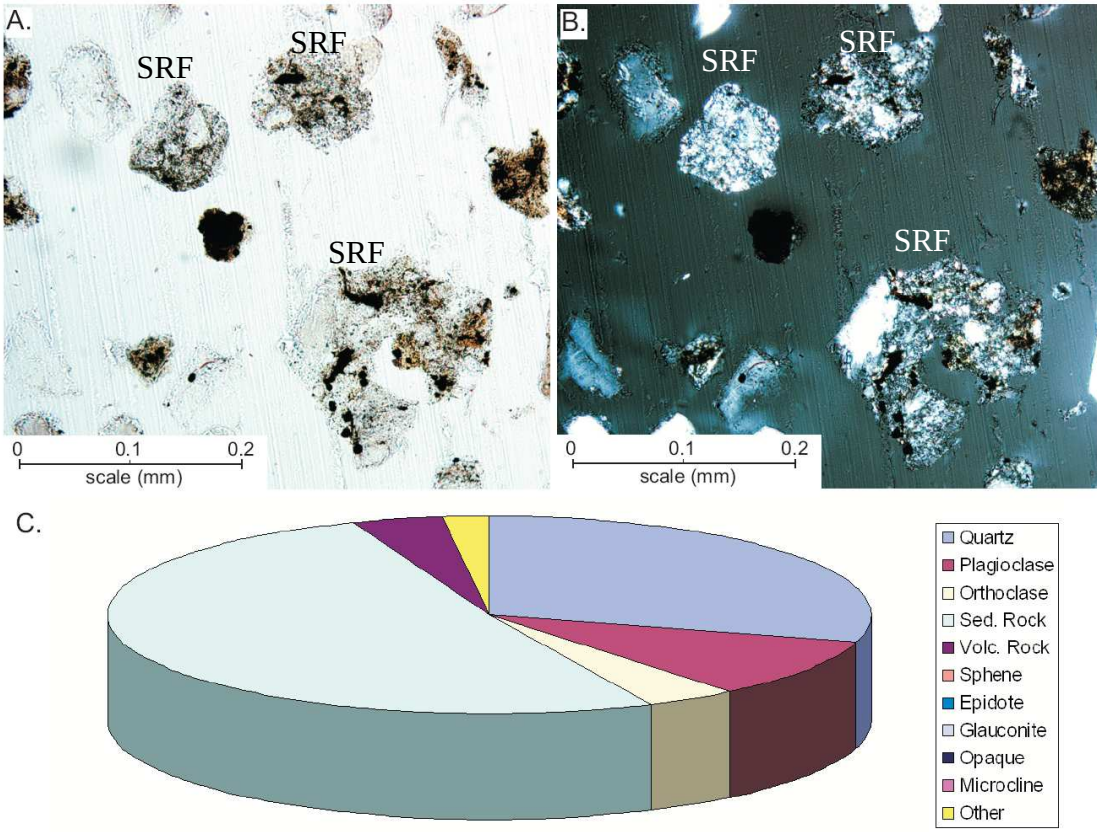

Figure 4.2. A. Photomicrograph identifying sedimentary rock fragments in the light mineral fraction of the Turi Formation, x200, under plane polarised light and **B.** with x-nicols. **C.** Component percentages from petrographic modal analysis.

Matapo Sandstone

Light mineral fraction

The Matapo Sandstone Member is composed mostly of rock fragments (89%), 80% being sedimentary rock fragments and 9% volcanic rock fragments. The sedimentary rock fragments are composed of very fine-grained lithics, less weathered than those observed in the McKee Formation and Turi Formation (Fig. 4.3). Minor quartz (5%), and trace amounts of plagioclase feldspar (3%), orthoclase (2%), glauconite, biotite and opaque minerals (limonite or magnetite) are also observed (Fig 4.3). Matapo Sandstone Member is finer grained than other subsurface samples analysed.

Heavy magnetic mineral fraction

Matapo Sandstone's magnetic heavy mineral fraction is also dominated by sedimentary rock fragments (~85%) with trace glauconite, opaque minerals and limonite being the other components. The abundance of sedimentary rock fragments in the heavy magnetic mineral fraction is due to the content of magnetic minerals.

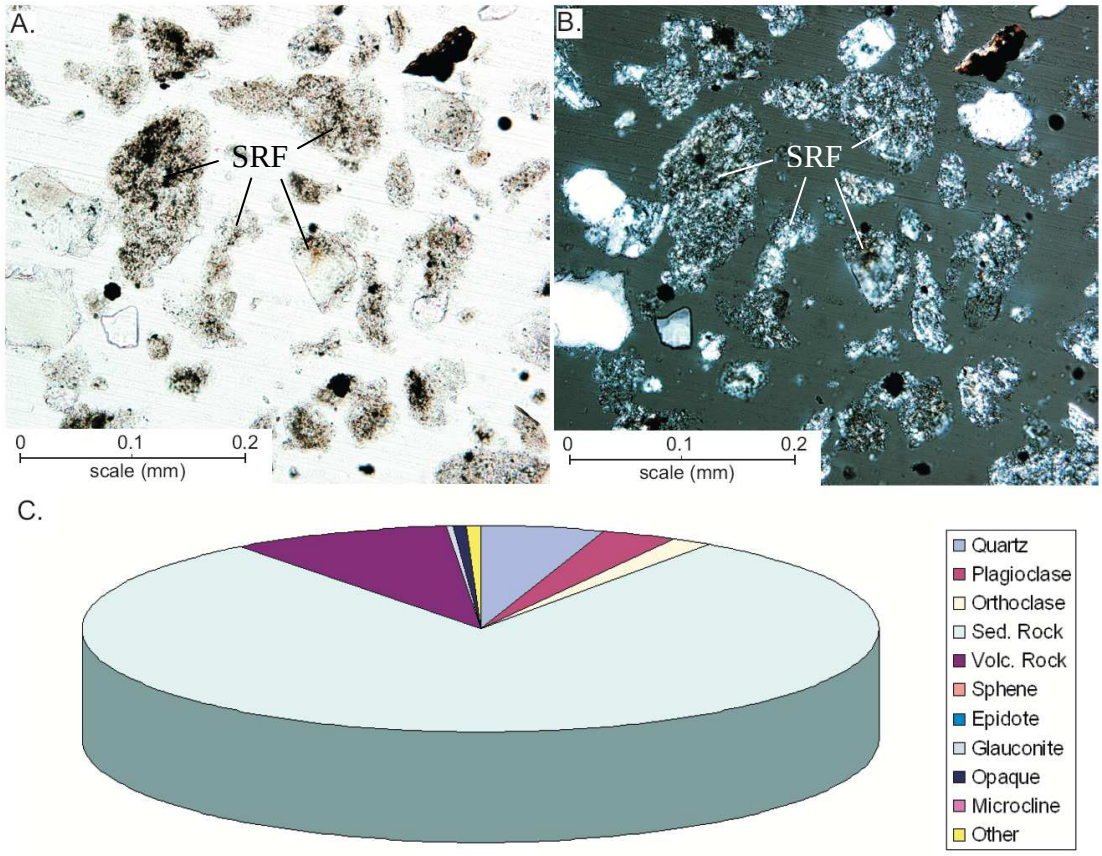

Figure 4.3. A. Photomicrograph displaying the abundance of sedimentary rock fragments in the light mineral fraction of the Matapo Sandstone, x200, under plane polarised light and **B.** with x-nicols. **C.** Component percentages from petrographic modal analysis.

Taumarunui quartz sandstone

Light mineral fraction

The siliciclast content of this sample is illustrated in Fig. 4.4 and is primarily composed of quartz (56%) and sedimentary rock fragments (22%). The sedimentary rock fragments are typically very fine grained and sub-rounded (Fig. 4.4). Abundant plagioclase feldspar (13%), minor volcanic rock fragments (6%), trace amounts of orthoclase feldspar (3%) and opaque minerals (limonite or magnetite) are also observed (Fig. 4.4).

Heavy magnetic mineral fraction

The heavy magnetic fraction of the Taumarunui quartz sandstone is dominated by limonite, with abundant opaque minerals and trace sedimentary and volcanic rock fragments, amphibole and epidote.

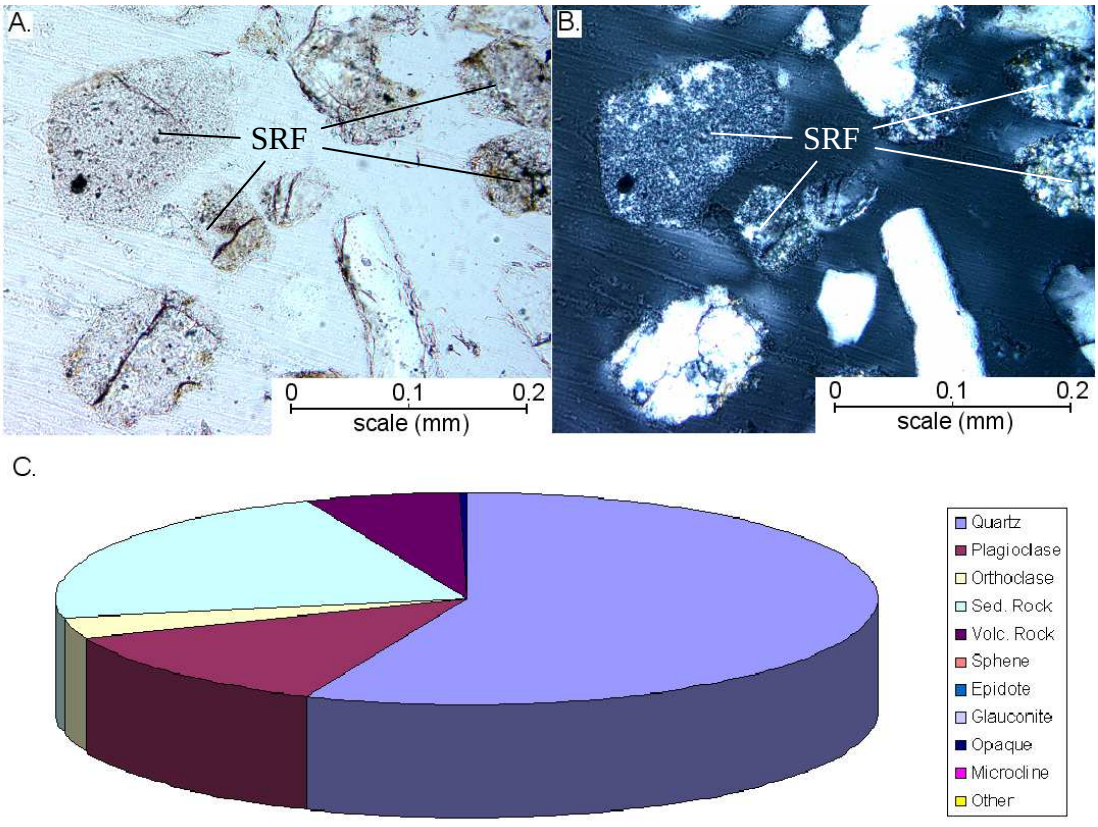

Figure 4.4. A. Photomicrograph identifying sedimentary rock fragments in the light mineral fraction of the Taumarunui quartz sandstone, x200, under plane polarised light and **B.** with x-nicols. **C.** Component percentages from petrographic modal analysis.

Ahirau Sandstone

Light mineral fraction

Two Ahirau Sandstone samples were analysed petrographically. The average siliciclastic composition of Ahirau Sandstone is shown in Fig. 4.5. Angular quartz (55%) is the primary component of Ahirau Sandstone. Abundant sedimentary rock fragments (18%), with minor plagioclase feldspar (6%), glauconite (6%), and trace volcanic rock fragments (4%), orthoclase feldspar (4%), sphene, epidote and biotite are also observed. Figure 4.5 shows a typical sedimentary rock fragment observed in Ahirau Sandstone alongside a large (0.2 mm) orthoclase feldspar grain.

Heavy magnetic mineral fraction

Ahirau Sandstone's heavy magnetic mineral fraction is dominated by opaque minerals with abundant amphibole and glauconite grains. Minor limonite, sedimentary and volcanic rock fragments and sphene are also observed.

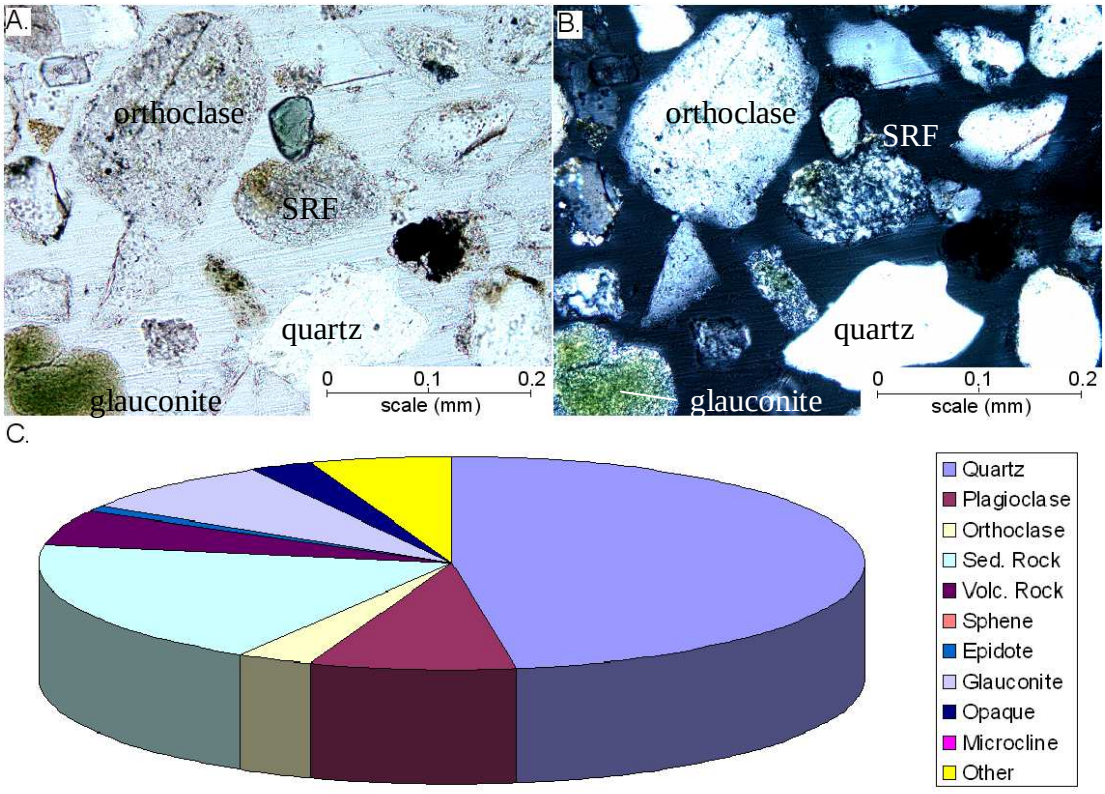

Figure 4.5. A. Photomicrograph identifying a sedimentary rock fragment, orthoclase, quartz and glauconite in the light mineral fraction of the Ahirau Sandstone, x200, under plane polarised light and **B.** with x-nicols. **C.** Average component percentages from petrographic modal analysis.

Tariki Sandstone

Light mineral fraction

Two Tariki Sandstone samples from different depths in Tariki-1 were analysed petrographically, and both have similar constituents. The average siliciclastic composition of Tariki Sandstone is summarised in Fig. 4.6. Quartz (51%), plagioclase feldspar (21%) and sedimentary rock fragments (21%) are the dominant components, with trace amounts of orthoclase feldspar (4%), volcanic rock fragments (4%), glauconite and limonite. Figure 4.6 shows a medium sand size sedimentary rock fragment from the Tariki Sandstone, which is composed of very fine-grained material, similar to that observed the McKee Formation, Turi Formation and Matapo Sandstone. Some of the rock fragments resemble granitic rock fragments, composed dominantly of quartz, feldspar and opaque minerals.

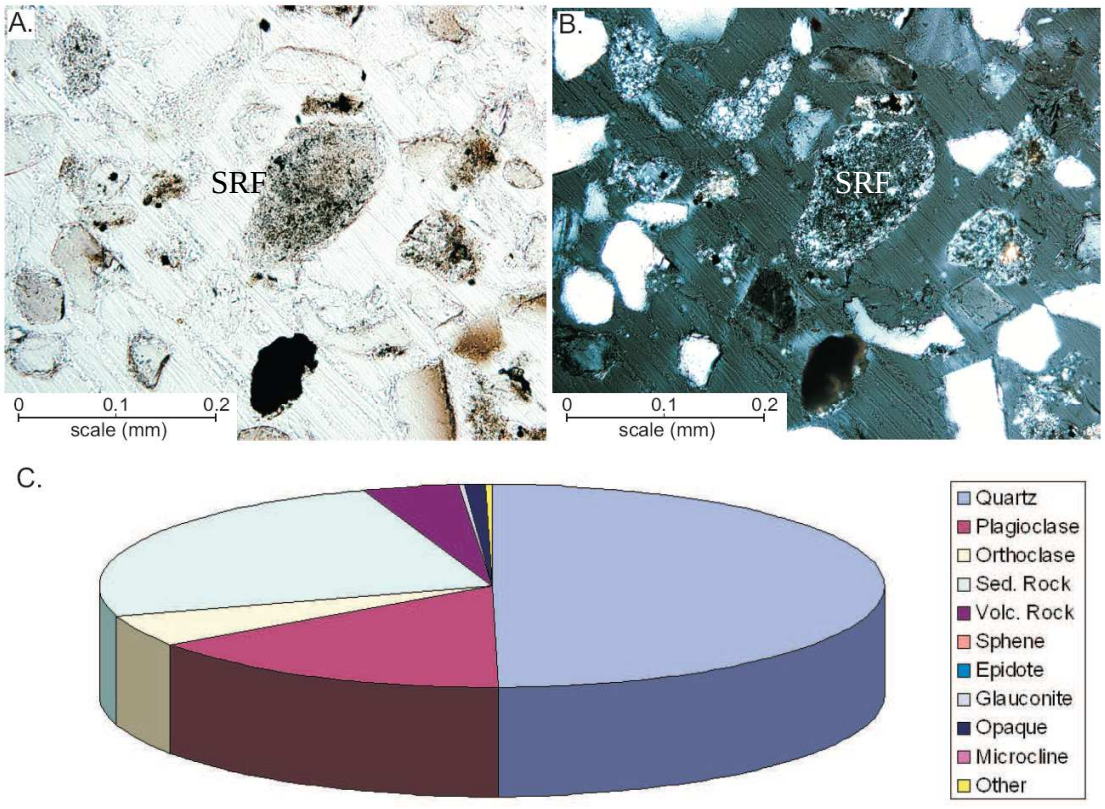

Figure 4.6. A. Photomicrograph identifying a sedimentary rock fragment in the light mineral fraction of the Tariki Sandstone, x200, under plane polarised light and **B.** with x-nicols. **C.** Average component percentages from petrographic modal analysis.

Heavy magnetic mineral fraction

Tariki Sandstone's magnetic heavy mineral fraction is dominated by sedimentary rock fragments, undifferentiated sedimentary/volcanic rock fragments, opaque minerals and limonite. Trace glauconite, sphene and epidote are also observed. The abundance of sedimentary rock fragments in the magnetic heavy mineral fraction suggests rock fragments have magnetic minerals within them.

Hauturu Sandstone

Light mineral fraction

Two Hauturu Sandstone samples were analysed petrographically, and both had similar constituents. The average composition of Hauturu Sandstone is shown in Figure 4.7, with the primary component being quartz (65%), consisting mostly of angular crystals. Abundant plagioclase feldspar (14%) and sedimentary rock fragments (10%), with minor orthoclase feldspar (6%) and trace amounts of glauconite (3%), volcanic rock fragments (2%), microcline feldspar and amphibole occur in both samples. Figure 4.7 shows a typical sedimentary rock fragment observed in Hauturu Sandstone. Rock fragments are typically quite fresh, with a few being moderately weathered.

Heavy magnetic mineral fraction

Hauturu Sandstone's magnetic heavy mineral fraction is dominated by opaque minerals and glauconite. Minor limonite and trace sedimentary and volcanic rock fragments, amphibole and sphene are also observed.

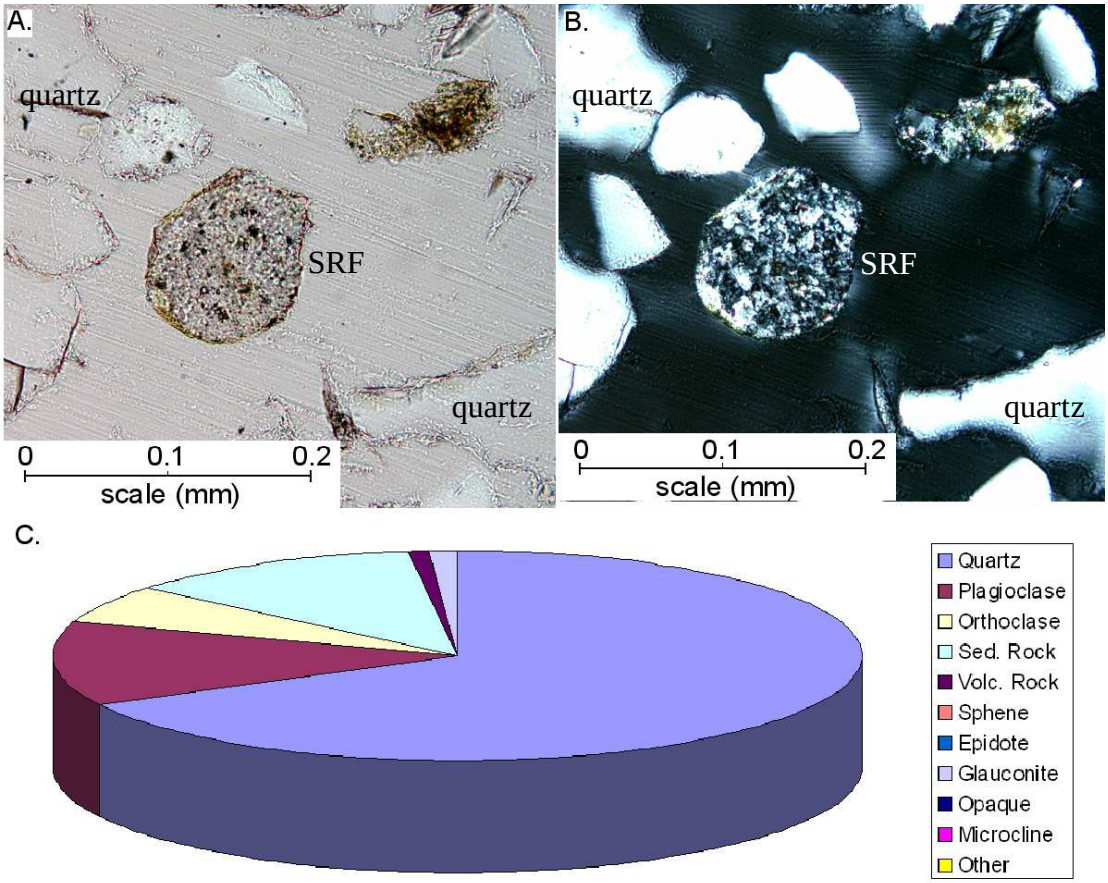

Figure 4.7. A. Photomicrograph identifying a rounded sedimentary rock fragment and quartz in the light mineral fraction of the Hauturu Sandstone, x200, under plane polarised light and **B.** with x-nicols. **C.** Average component percentages from petrographic modal analysis.

4.5 MODAL PETROGRAPHY

The relative proportions of different types of terrigenous grains in sedimentary rocks can be used as a guide to interpret the nature of the associated source rocks (Dickinson & Suczek 1979; Dickinson et al. 1983). A common approach is to plot modal data on tectonic classification schemes, thereby establishing the nature of the tectonic setting of the possible source area(s) (Dickinson et al. 1983). Figure 4.8 is a QFL (quartz, feldspar and lithics) ternary plot showing the relationship between sandstone composition and tectonic setting or provenance type. Dickinson & Suczek (1979) have classified all provenance types into three general groups: continental blocks, magmatic arcs, and recycled orogens. Continental block provenances have sediment derived either from stable shields and platforms, or from uplifted (faulted) basement blocks (Dickinson & Suczek 1979; Dickinson et al. 1983). Within magmatic arcs, sediment sources can be from within island arcs, or active continental margins (Dickinson & Suczek

1979). Within recycled orogens, sediment sources are from uplifted sedimentary strata and volcanic rocks in subduction zones, along collision orogens or within foreland fold-thrust belts (Dickinson & Suczek 1979; Dickinson et al. 1983). These three broad provenance categories are further subdivided into specific variants via specific plate settings.

Figure 4.9 shows the modal data obtained in this study plotted on a QFL ternary diagram. For QFL data see Appendix IV. The intention is to identify the provenance type for the sandstone samples. Most samples cluster in the recycled orogen provenance category, with two samples plotting in the magmatic arc category. There is a clear trend between the quartz and lithics poles, with little change in the total feldspar component between samples. This is also shown in Fig. 4.10 where there is an obvious linear relationship between quartz and lithic abundance, indicating that the feldspar component has not varied much stratigraphically between samples (that is, over time). Although there are limited data points plotted, an age to QFL quartz percentage relationship is apparent. The oldest three samples on this plot (McKee Formation, Turi Formation and Matapo Sandstone Member) have the lowest QFL quartz content and the youngest rock samples (Hauturu Sandstone) have the highest QFL quartz content (Fig. 4.10). The increasing quartz content with decreasing age could indicate an increase in the importance of a granitic provenance of Late Eocene – Oligocene Taranaki Basin sediments over time.

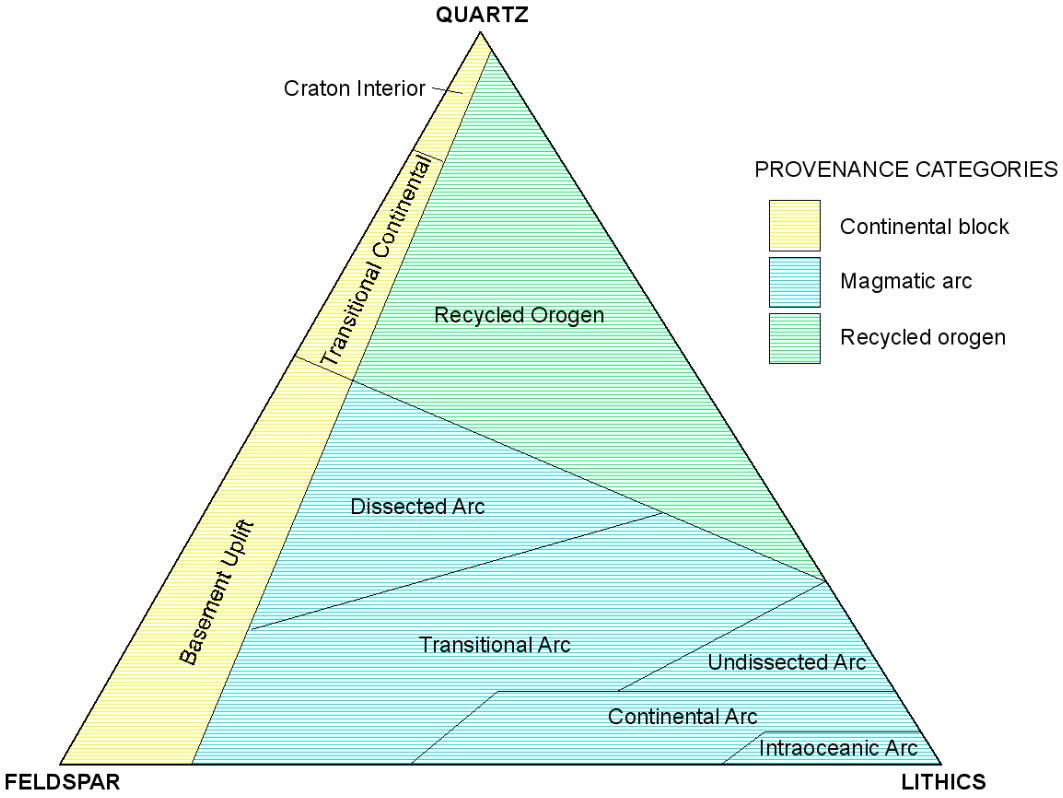

Figure 4.8. QFL plot showing broad provenance categories after Dickinson and Suczek (1979) and provenance fields after Dickinson and Suczek (1979), Dickenson et al. (1983) and Marsaglia and Ingersoll (1992).

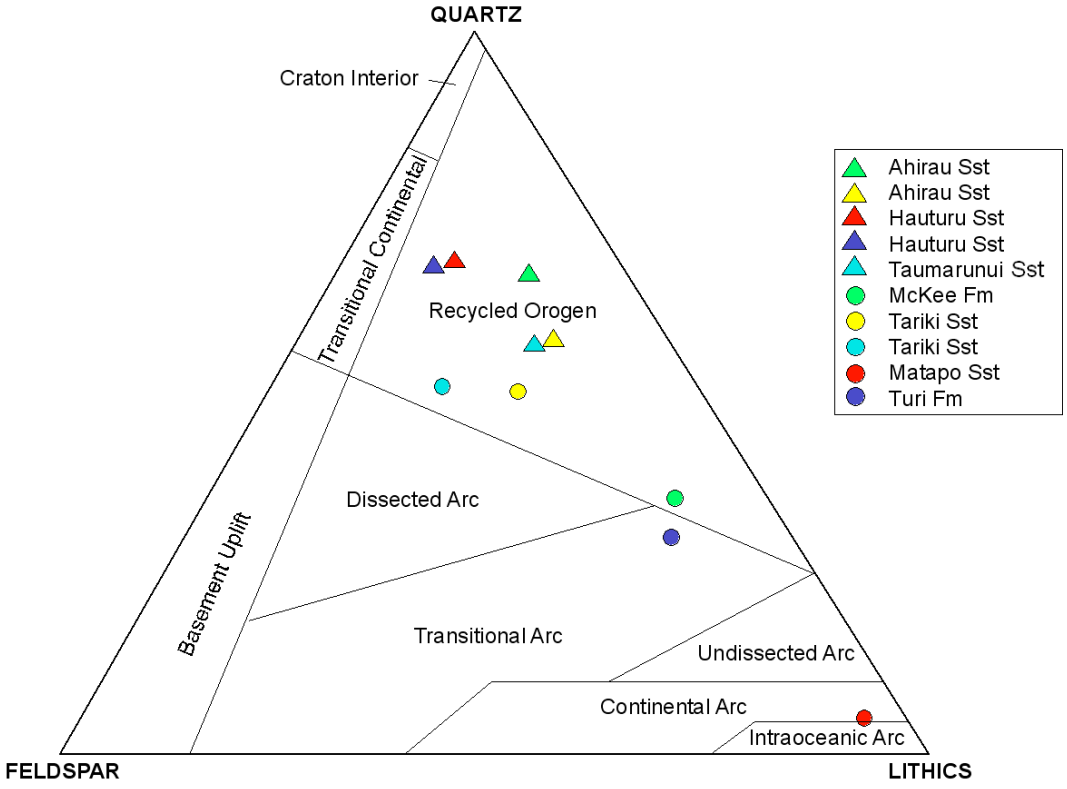

Figure 4.9. QFL plot showing provenance fields after Dickinson and Suczek (1979), Dickenson et al. (1983) and Marsaglia and Ingersoll (1992), with plotted Late Eocene – Oligocene sandstone samples.

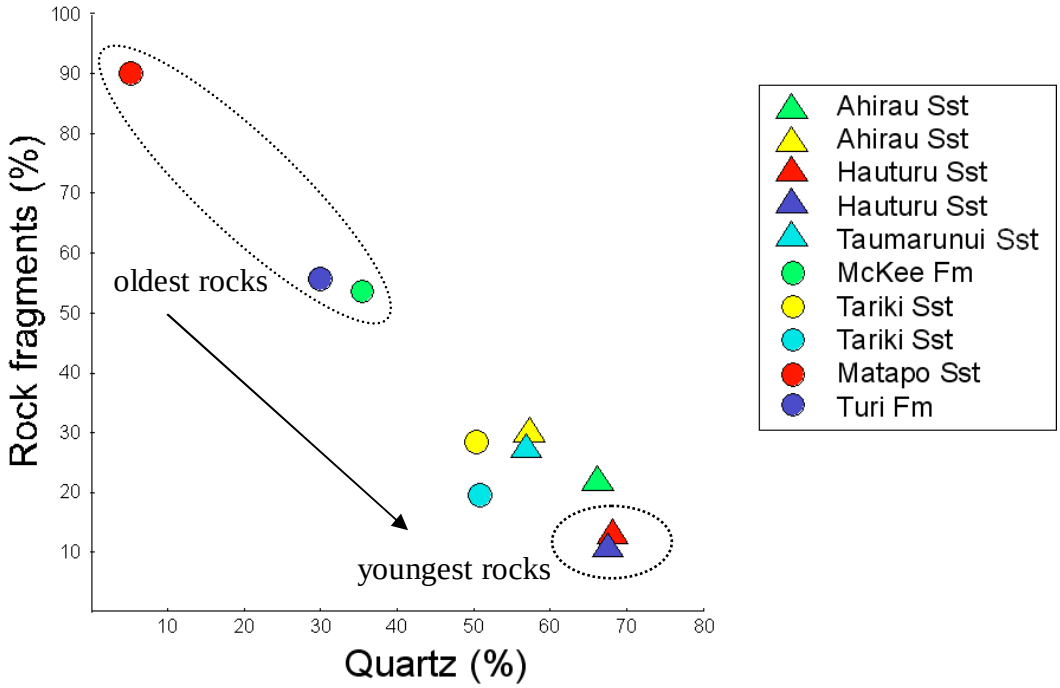

Figure 4.10. Plot showing linear relationship between QFL quartz and rock fragment percentages, for Late Eocene – Oligocene sandstone samples. Note increasing quartz content with decreasing age trend.

4.6 PROVENANCE INTERPRETATION OF THE LATE EOCENE – OLIGOCENE UNITS

The modal abundance of mineral and lithic components and QFL ternary diagrams may be used as indicators of provenance type and source rock types for the sandstone samples. Smale (1992) discusses three potential source areas known for Cretaceous – Oligocene sedimentary sequences in Taranaki Basin, including Murihiku Terrane along the eastern margin of the basin, Torlesse Terrane farther to the east, basement in the northwest Nelson area to the south, and basement in eastern Nelson and western Marlborough in the southwest (Fig. 2.8).

Through the Cenozoic, movement on the Taranaki Fault has caused deformation and uplift along the eastern margin of Taranaki Basin. The resulting uplift of Murihiku Terrane, which includes the Patea-Tongaporutu High, is the closest and 'obvious' source for both Late Eocene – Oligocene subsurface Taranaki Basin and onshore strata. Although some components may be sourced from Murihiku Terrane, an origin from other Mesozoic or Paleozoic terranes is likely. Modal petrographic data for Murihiku Terrane is given in Briggs et al. (2004). Feldspar is the most common mineral constituent, averaging between 27 – 44%, of which

plagioclase is most common (22 – 32%), orthoclase less common (5 – 12%) with rare microcline. Quartz is much less abundant with a 12% modal average, ranging from 18% (Late Triassic rocks) – 7% (Late Jurassic rocks) in. Rock fragments are the most abundant of all components ranging from 0 – 80% with a modal average of 46%, of which, dominantly andesitic volcanic rock fragments are the most common type (Briggs et al. 2004). By comparing sample constituent data obtained in this study to that of Murihiku Terrane, the aim of the following subsection is to hypothesise that the Murihiku Terrane may not be the dominant source of the Late Eocene – Oligocene sediments in Taranaki Basin.

4.6.1 McKee and Turi Formations

The similarities in mineral proportions and grain types between McKee Formation and Turi Formation suggest a common source. This is shown in Figure 4.9, with very similar positions on the plot close to the lithic pole (along the recycled orogen and magmatic arc provenance boundary). Because the dominant component of these units is fine-grained sedimentary rock fragments, a sedimentary rock provenance is likely, possibly a greywacke source. Smale and Morton (1987) and King and Thrasher (1996) however have suggested a Karamea Granite and Pikikiruna Schist (north-west Nelson) source for the grains within these stratigraphic units. The ~30% modal quartz component observed within McKee Formation and Turi Formation sandstone is much higher than that of Murihiku Terrane, supporting a source from other Mesozoic terranes (eg. Waihapa, Torlesse and Caples Terrane) or from the Paleozoic Greenland Group, although some granitoid provenance is not precluded. The poorly sorted and angular nature of grains observed in these units, suggest they are texturally immature sandstone.

4.6.2 Matapo Sandstone

The position of Matapo Sandstone samples plotted on Figure 4.9 suggests a magmatic arc provenance. However, sedimentary rock fragments are the dominant component observed which does not fit with volcaniclastic sand that might be expected from an undissected arc (Dickinson et al. 1983). The abundance of fine-grained sedimentary rock fragments suggests a dominant fine-grained sedimentary

basement source for Matapo Sandstone. King and Thrasher (1996) and Smale (1996), suggest a granitic provenance as the dominant source of clastics for the Ngatoro Group, with Separation Point Batholith and Karamea Batholith inferred as specific source rocks. Low-grade metamorphic material is recorded in Matapo Sandstone in Okoki-1 (King & Thrasher, 1996).

4.6.3 Taumarunui quartz sandstone

Because the Taumarunui quartz sandstone is dominated by quartz and sedimentary rock fragments with few if any volcanic rock fragments, derivation from a quartz rich basement source area is likely. The fine-grained sedimentary rock fragments also suggests a fine-grained sedimentary provenance, possibly a greywacke source. The Taumarunui quartz sandstone is more quartzose than the McKee Formation and Turi Formation samples analysed, and plots close to the quartz pole (recycled orogen), similar to the composition of Ahirau Sandstone and Tariki Sandstone (Fig. 4.9).

4.6.4 Ahirau Sandstone

The presence of large orthoclase feldspar grains, minor volcanic rock fragments and the very abundant amphibole component observed in the magnetic heavy mineral fraction suggests a dominant igneous provenance for Ahirau Sandstone, possibly a Murihiku basement source. However, the (~55%) quartz component of Ahirau Sandstone is much higher than for Murihiku basement as reported by Briggs et al. (2004), suggesting more than one source area and including derivation from a quartz rich basement source area. Ahirau Sandstone has an equivalent provenance field (recycled orogen) to the Taumarunui quartz sandstone, Tariki Sandstone and Hauturu Sandstone (Fig. 4.9).

4.6.5 Tariki Sandstone

The abundant fine-grained sedimentary rock fragment component of Tariki Sandstone suggests a fine-grained sedimentary provenance, possibly a greywacke source. The high (~51%) quartz component of Tariki Sandstone is also much higher than for Murihiku Terrane, suggesting an additional source involving a

quartz rich basement. This is supported by the presence of trace granitic rock fragments in Tariki Sandstone samples. King and Thrasher (1996) reported volcanic rock fragments in Tariki Sandstone and inferred them to have been derived from Brook Street Volcanics (Brook Street Terrane) or Tasman Intrusives (Median Tectonic Zone).

4.6.6 Hauturu Sandstone

Hauturu Sandstone is markedly quartzose (~65%) and much higher so than that of Murihiku Basement. This is consistent with derivation from a quartz rich basement such as a granitoid belt or quartz rich basement such as Torlesse Terrane or parts of Caples Terrane (e.g. Momis Sandstone, Turnbull 1979).

4.7 CONCLUSIONS

Twenty nine Late Eocene – Oligocene onshore and subsurface samples have been used for the purpose of wireline log calibration and petrographic analysis. The carbonate content and grain size of targeted facies for Taranaki Basin samples has successfully aided wireline log interpretation (Chapter 3). The results of petrographic description and modal analysis for sandstone samples are given in this chapter. QFL ternary diagrams have been plotted for the light mineral fraction, revealing the broad provenance categories for each of the analysed samples, which are interpreted to be mostly of recycled orogen provenance. Mineral constituent data have also been used to interpret source rock types, with comparisons made with the composition of Murihiku Terrane, an obvious and nearby potential source unit. In most cases the high quartz content observed in samples discounts Murihiku Basement as a dominant source, suggesting derivation from granitic or other quartz rich basement. Although the mineralogical characteristics and modal analysis of samples may indicate the type of source rock, it cannot uniquely identify specific basement units.

The following chapter (Chapter 5) reports U-Pb geochronology results for zircon grains from the same samples for which the mineralogy has been determined. This has been undertaken in an attempt to more specifically establish the provenance of the Late Eocene – Oligocene siliciclastic component of sediments in Taranaki Basin.

CHAPTER FIVE
U-Pb GEOCHRONOLOGY

5.1 INTRODUCTION

U-Pb dating involves measurement of the relative abundance of uranium to lead in uranium-bearing minerals, particularly zircon. There are two radioactive decay chains, one involving the decay of ^{238}U to ^{206}Pb, and the other ^{235}U to ^{207}Pb. Ages can be derived independently using both of these chains by measuring the $^{206}Pb/^{238}U$ and $^{207}Pb/^{235}U$ ratios. Zircon is one of the most common accessory minerals in igneous, sedimentary and metamorphic rocks. It is very resistant to physical abrasion and weathering, naturally contains high levels of uranium and the atomic structure of zircon is effective at retaining radiogenic lead. These factors allow precise U-Pb ages to be calculated (Catanzaro 1968; Cawood et al. 1999). With significant development in the technology of laser ablation and inductively coupled plasma-mass spectrometry (ICP-MS) instrumentation over the last few decades, and capability of this technology to rapidly generate single grain ages, U-Pb zircon dating has proved to be a precise and increasingly attractive dating technique (Campbell et al. 2005).

In this study the U-Pb ages of more than 350 detrital zircon grains were determined from 13 clastic sedimentary rocks with Eocene – Oligocene stratigraphic ages (Appendix VII). The U-Pb ages are used to assist in establishing the provenance of the source rock of the Eocene – Oligocene sandstone units sampled in Taranaki Basin as well as the Te Kuiti Group. The U-Pb ages in this study were obtained using a laser ablation inductively coupled plasma-mass spectrometry (LA-ICP-MS) technique adapted from Jackson et al. (2004). Zircon age measurements are a powerful tool for detrital sedimentary provenance investigations, basin analysis and stratigraphic correlations (Košler et al. 2002; Vermeesch 2004). Patterns of zircon ages obtained for the samples processed in this study have provided valuable incites into the zircon-bearing source rocks and the contemporary paleogeography (e.g. transport directions) (Cawood et al. 1999; Košler et al. 2002).

5.2 METHODS

Zircon grains were separated from sandstones by the common mineral separation procedures (see Section 3.3.3). About 1 kg sandstone samples were crushed and processed through heavy liquids to separate the heavy mineral fraction, which was further processed using a Frantz magnetic separator to produce a zircon rich fraction. From this fraction a representative zircon population was handpicked under a microscope.

A typological classification proposed by Pupin (1980) (see Appendix V) that identifies and defines different zircon morphologies (the arrangement of crystal faces) was used to separate the main zircon types and subtypes in particular samples. Colour was also used to sort zircon grains within samples into groups. Clear crystal appearance under reflected light suggests relatively young zircon age or low uranium and thorium content whereas coloured crystals (yellow, pink, amber) tend to suggest older ages or higher uranium and thorium contents (Catanzaro 1968, Garver & Kamp 2002). Including colour and morphology as criteria for identifying crystals for U-Pb dating is useful as a means of ensuring that the full range of zircon crystals in a sample are analysed.

With sub-populations sorted, crystals are mounted on thin-section slides using adhesive tape and a 25mm 10 x 10 grid. All samples were then loaded into the laser ablation microprobe sample cell together with appropriate standards to be analysed using a methodology adapted from Jackson et al. (2004). For LA-ICP-MS operating conditions see Appendix V. Using the focused laser of the microprobe, targeted crystals were ablated for 60 seconds using spot sizes of 30 μm. Ablated material is carried into an ICP-MS for isotopic quantification via a helium carrier gas (Appendix V). Uranium and lead signal intensity data from each crystal were measured for 60 seconds while ablation occurred. Each sample analysis includes several analyses of the standard zircons GJ-1 and Temora-1, which are used to calibrate the analytical data and as an independent check on data accuracy. Raw ICP-MS data were exported and reduced using GLITTER software allowing isotope signal range to be selected from which relevant isotope ratios can be calculated and displayed. For data acquisition parameters see Appendix V. These data were then exported to Isoplot 3.00 (a geochronological

toolkit for Microsoft Excel) where concordia plots, age calculations and age probability density plots could be created for population analysis.

5.3 U-Pb AGES

5.3.1 Data quality

5.3.1.1 Signal selection

For each crystal, raw ICP-MS data were imported into GLITTER software, a data reduction program that shows ^{206}Pb, ^{207}Pb, ^{208}Pb, ^{232}Th, ^{238}U, ^{29}Si, ^{87}Sr, ^{89}Y, ^{91}Zr and ^{177}Hf isotope concentration signals over time, or crystal depth. A signal output that shows constant and stable isotope concentrations over time is ideal indicating homogenous ablation, however, over the course of ablation, isotope concentration signals often appear to vary suggesting non-homogeneity or an outside influence. In many cases analytical error can cause the appearance of non-homogeneity where error may arise from ICP-MS sensitivity, measurement error, or the addition of foreign material into the system which is then measured along with a sample. However, the most likely cause of variable isotope concentration is variation in laser power. During probing, laser power seems to always vary, in some cases with momentary reductions of up to 30% or momentary power peaks. This causes changes in the amount of ablated material and isotope concentration. Other signal variations may reflect the non-homogeneity of crystals caused by lead loss, common lead gain, crystal surface contamination, or inherited older cores (zoning) (Jackson et al. 2004).

Because zircon crystals are very robust minerals, existing crystals may be incorporated into, and 'survive', a younger igneous melt. During this process the accretion or overgrowth of new material occurs around an older zircon core, resulting in zoning. During analysis this zoning is often evident from the bi-modal nature, or 'terraced' appearance of signal intensity. With zoned crystals one can calculate core or rim ages using the different parts of signal. This highlights the importance of identifying crystal zonation so that different parts of the signal can be analysed. Figure 5.1.A shows the ^{206}Pb signal intensity for sample 10 (Matapo Sandstone). Signal 1 involves the lower of two terraces with Signal 2 selected from the later (deeper into crystal) section of signal. These two signal sections analysed independently on a concordia plot show significantly different age

determinations with signal selection 1 and 2 possessing $^{206}Pb/^{238}U$ ages of 280±17 Ma and 783±18 Ma, respectively (Fig. 5.1.B). This sample represents a zoned zircon crystal with an older Neoproterozoic core and a Permian outer rim (Fig. 5.1.C). The presence of zoned crystals gives insights to the complex geological histories that crystals can possess.

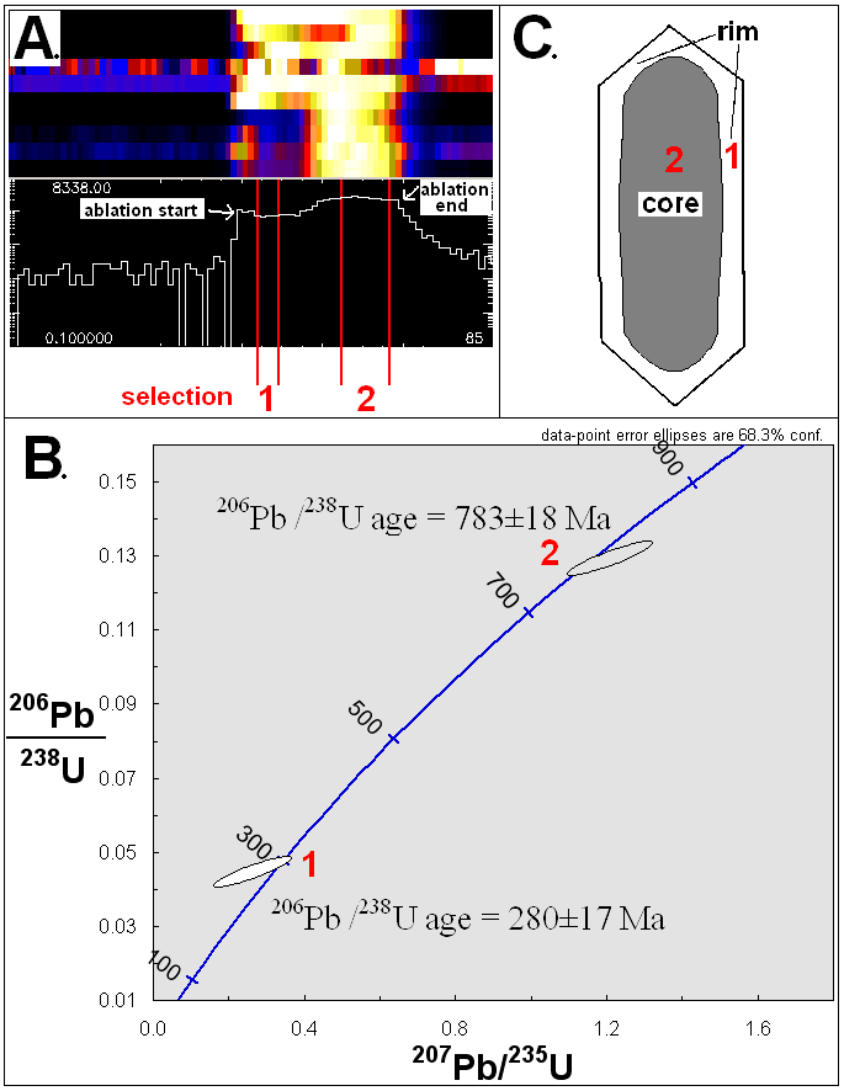

Figure. 5.1 A. ^{206}Pb signal intensity for sample 10 (Matapo Sandstone), with corresponding signal selections 1 and 2. **B**. Concordia plot with selections 1 and 2 plotted, and corresponding ^{206}Pb age determinations. **C**. Schematic illustrating zoned nature of sampled crystal. The older crystal core and younger rim corresponding to signal selection 2 and 1, respectively.

Before signal data is exported to GLITTER software it is very important to visually examine the data as a function of time during laser ablation. For each mass sweep, the data were examined carefully identifying possible signal portions to be used in analysis and age calculation. For each sample the most concordant section of signal was identified and exported to GLITTER. In most cases the most stable section of signal typically lay 5 – 10 seconds after ablation started. Signal selection images are provided in Appendix VI.

5.3.1.2 Concordance

Unlike other radiometric dating techniques that use a single decay series for age calculation, uranium-lead dating uses two decay chains (^{238}U-^{206}Pb and ^{235}U-^{207}Pb) and independent ages may be calculated for each ratio. If crystals have not lost any parent or daughter material (i.e. there is a closed system) ages derived from each of the $^{206}Pb/^{238}U$ and $^{207}Pb/^{235}U$ ratios should be the same, or concordant. Most zircons crystals however are to some degree discordant, indicating that there has been a degree of open system behaviour. This is most commonly due to bulk radiogenic lead loss, but there can also be loss of ^{207}Pb relative to ^{206}Pb (Catanzaro 1968). Catanzaro (1968) suggests that results are probably discordant if the $^{206}Pb/^{238}U$ and $^{207}Pb/^{235}U$ derived ages differ by more than 5%. Similarly, Scott and Palin (2008) disregard data that have more than 10% discordance.

Metamictisation is a process in which minerals lose their internal atomic structure due to radiation damage. The increasing crystal porosity caused by metamictisation can lead to an increase in lead loss. Increasing U-Pb discordance and increasing colouration of crystals are features of metamictisation of zircon (e.g. Dickin 2005). Ideally, concordant or near-concordant crystals should be considered for geological interpretation of U-Pb ages, while discordant crystals should be disregarded in terms of having geologically meaningful U-Pb ages. This makes the examination of crystal concordance a very important issue before age interpretation.

Plotting ages on concordia plots aids interpretation of crystal age concordance. Figure 5.2.A is a concordia plot for sample 5 (Hauturu Sandstone) illustrating $^{206}Pb/^{238}U$ vs $^{207}Pb/^{235}U$ ages and the associated error ellipses. For this sample,

one very discordant crystal is observed (white ellipse), lying far to the right off the concordia line (blue). This suggests some form of analysis error, contamination or significant Pb-loss event. This one discordant crystal has been removed from further analysis with the remaining 34 crystals plotted (with associated error ellipses in white) illustrated in Fig. 5.2.B. These ellipses are observed to lie in close proximity to the concordia line (blue), suggesting crystal concordance, and that the crystals are from a 'closed system' with respect to U-Pb age.

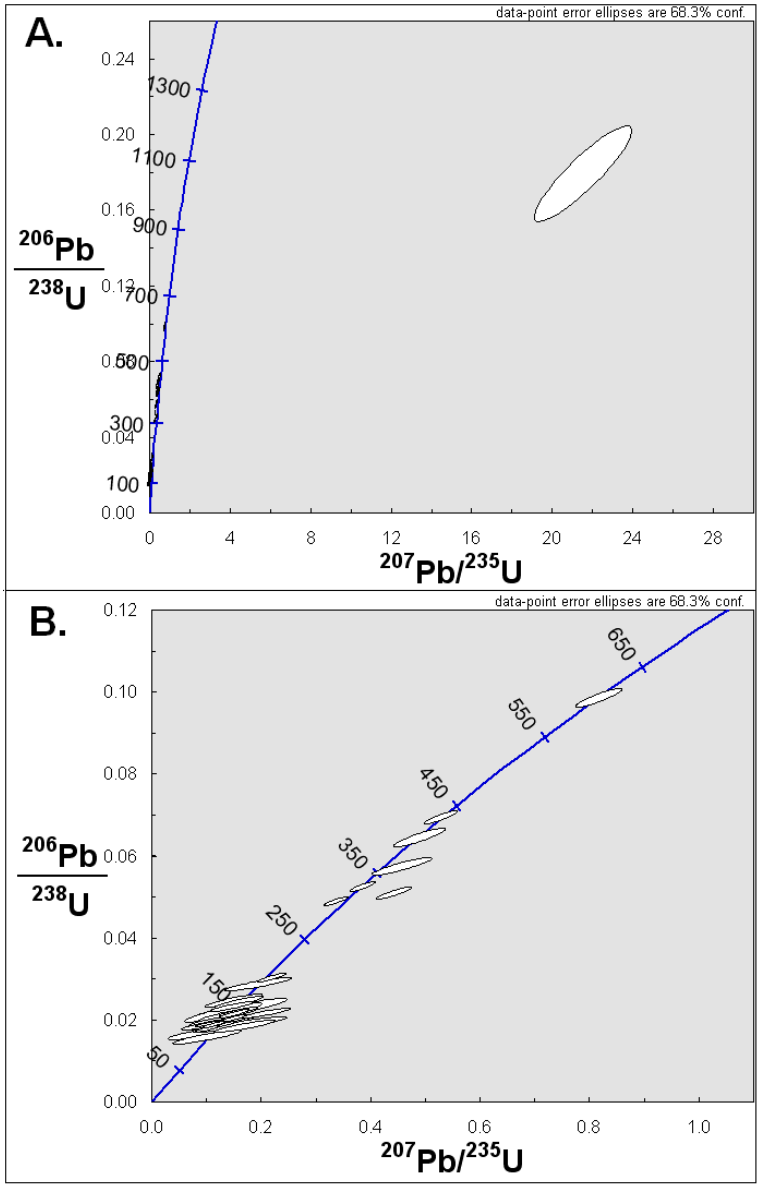

Figure. 5.2 U-Pb concordia plot of single (1σ error ellipses) zircon analysis from sample 5 (Hauturu Sandstone). **A.** Raw analysis with one very discordant ellipse present **B.** Residual 34 concordant/near-concordant crystals after single discordant crystal removed.

Concordia plots have been prepared for each sample population. In most samples many crystals appeared to have concordant ages, lying in close proximity to the concordia line. However, in some samples more discordant crystals were observed. A lot of these 'apparent' discordant ages may be associated with error from ^{207}Pb measurements. In relatively young crystals (<1000 Ma) ^{207}Pb is present in such small amounts that the use of the $^{207}Pb/^{235}U$ decay chain becomes ineffective (Black et al. 2004). This causes inaccurate $^{207}Pb/^{235}U$ ages to be calculated with corresponding high errors, therefore causing apparent discordance. Because of this, in some cases near-concordant crystals were not removed for interpretation (Fig. 5.2) and age probability distribution plots (Section 5.3.3) were constructed using $^{206}Pb/^{238}U$ ages alone.

5.3.1.3 Zircon Standards

During sample analysis three standards were used to evaluate data quality and to help calibrate the U-Pb ages. By comparing the quality of concurrent analyses of standard and sample zircon it is possible to identify the components of imprecision that have arisen from the analytical procedure and those that reflect heterogeneity of the unknown crystals (Black et al. 2004). The standards used in this procedure were Nist-610, GJ-1 zircon and Temora-2 zircon:

Nist-610 standard

The Nist-610 standard is a glass reference material ablated in the sample cell before and after sample analysis for standardisation. This allows isotope ratios from Nist-610 obtained during different sample analyses to be compared, highlighting any drift in ICP-MS sensitivity or calibration from sample to sample.

GJ-1 Zircon

The GJ-1 standard is employed as an external standard and is the main standard for GLITTER software, calibrating elemental fractionation. GJ-1 is probed multiple times before and after sample analyses, as well as several times during analysis. This standard zircon is well dated, well behaved and shows no zoning. Jackson et al. (2004) provides a $^{207}Pb/^{206}Pb$ age for this crystal of 608.5 ± 0.4 Ma.

Temora-2 Zircon

The Temora-2 zircon is used as an independent external standard probed several times during sample analyses to check ICP-MS accuracy and precision. Black et al. (2004) gives Temora-2 a $^{206}Pb/^{238}U$ age of 416.8 ± 1.3 Ma.

The effectiveness of these standards in reinforcing data quality is seen in Fig. 5.3, where a concordia plot for sample 5 (Hauturu Sandstone) shows the distribution of a sample population (white) with GJ-1 zircons (red) and Temora-2 zircons (blue). Most GJ-1 error ellipses can be seen to cluster around the concordia line between 550 – 650 Ma centred on 600 Ma. Temora-2 error ellipses show similar character lying centred on 400 Ma. Waikato analyses give weighted mean $^{206}Pb/^{238}U$ ages of 602±12 Ma and 416±28 Ma for GJ-1 and Temora-2 standard zircons respectively, very similar to the standard reference ages given above. The larger associated errors reflect ICP-MS analyses versus TIMS analyses for the standards.

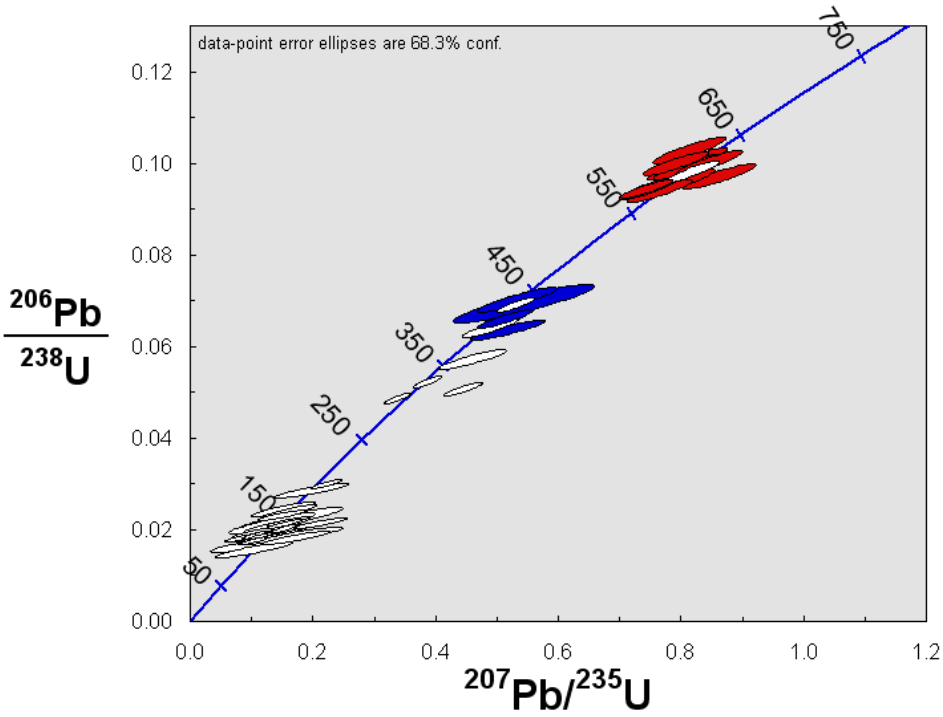

Figure. 5.3 U-Pb concordia plot of single zircon analysis from sample 5 (Hauturu Sandstone), showing sample population (white), GJ-1 standard zircon (red) and Temora-2 standard zircon 1σ error ellipses.

5.3.2 Sample analysis

The following section discusses data quality for each sample with respect to concordia plots. Sample characteristics is also discussed, including the presence of different zircon morphologies, zircon colour and population $^{206}Pb/^{238}U$ age patterns. A full set of $^{207}Pb/^{235}U$ and $^{206}Pb/^{238}U$ GLITTER software isotope ratios and age estimate data are provided in Appendix VII.

Sample 8 (McKee Formation)

Twenty nine zircon grains were analysed in this sample with 27 concordant/near-concordant ages used in its interpretation. Figure 5.4 is a concordia plot showing individual crystal error ellipses with 1σ uncertainty. Most crystals appear to be concordant with a dominant cluster around 200 Ma and a minor cluster around 450 Ma. Figure 5.5 shows individual $^{206}Pb/^{238}U$ ages plotted with respect to crystal morphology and crystal colour identified for the entire sample. $^{206}Pb/^{238}U$ ages range from 149.3 to 1554.2 Ma with a dominant age cluster around 170 Ma. Although there is a large age range, the oldest two (932.3 and 1554.2 Ma) crystals may be thought of as rare outliers, as 89% of ages fall below 500 Ma and 40% below 200 Ma. Pupin (1980) morphologies identified include P1, S5, S15 and S10 subtypes. However, there was no apparent relationship between morphology and age. Analysed crystals were dominantly clear, however four coloured crystals (pale amber, amber and pink) yielded the oldest $^{206}Pb/^{238}U$ ages (Fig. 5.5).

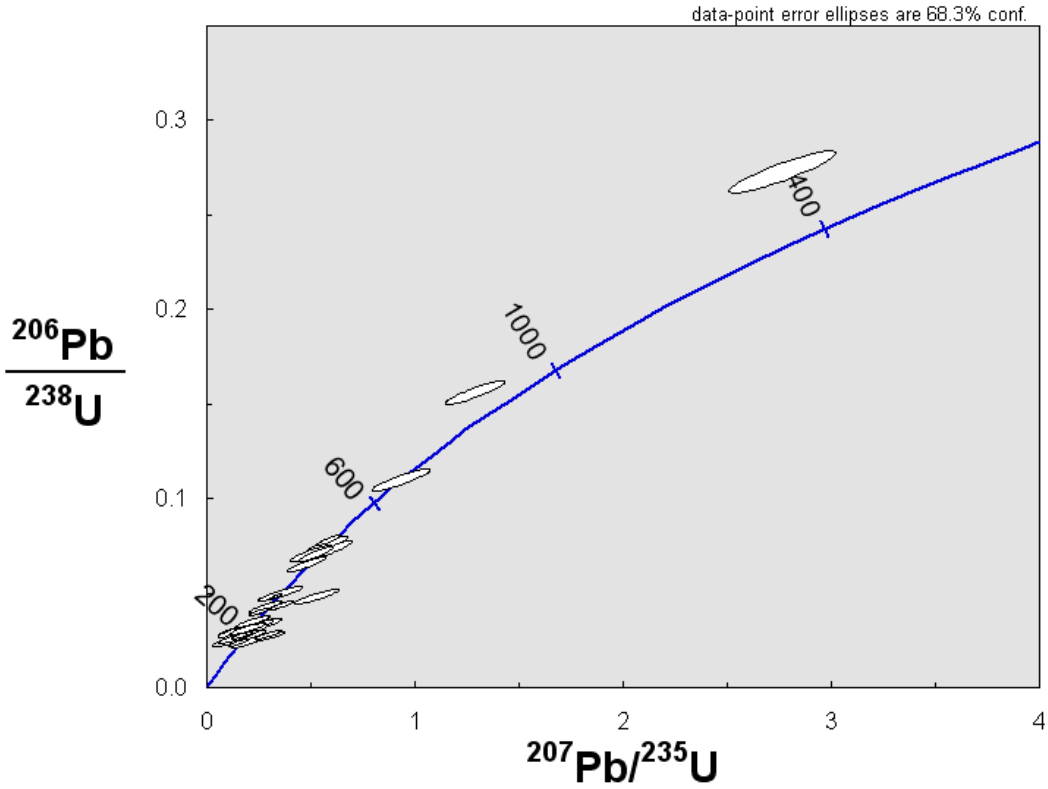

Figure. 5.4 U-Pb concordia plot of single zircon analysis from sample 8 (Mckee Formation), showing the residual twenty seven concordant/near-concordant crystals (1σ error ellipses) used in further age interpretation.

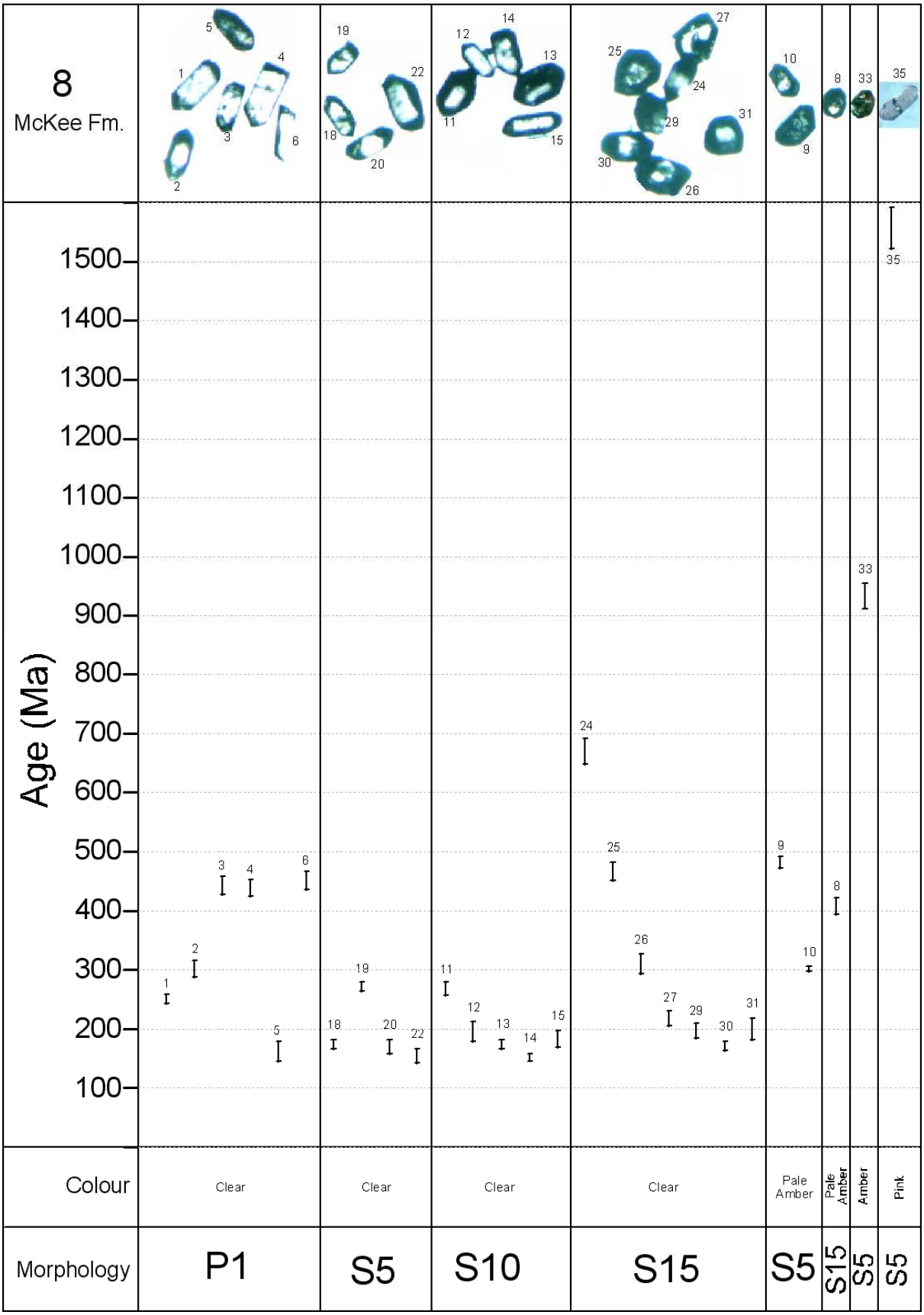

Figure. 5.5 $^{206}Pb/^{238}$ age distribution for sample 8 (McKee Formation), with zircon morphology and colour outlined. Visual representation of zircon morphology (for Pupin (1980) morphologies see Appendix V) and colour subdivisions given.

Sample 12 (Turi Formation)

Eighteen zircon grains were analysed for this sample with 14 having concordant/near-concordant ages. Figure 5.6 shows individual crystal error ellipses with 1σ uncertainty. Most crystals appear to be concordant with only two near-concordant crystals. There does not appear to be significant clustering of ages, with a fairly even spread between 100 – 350 Ma. Figure 5.7 shows the individual $^{206}Pb/^{238}U$ ages plotted with respect to crystal morphology and colour. $^{206}Pb/^{238}U$ ages range from 102 – 572 Ma, with 86% falling below 300 Ma and 71% below 210 Ma. Only two Pupin (1980) morphologies were identified (P1 and S5) and only clear crystals were found in the sample. There does not appear to be any relationship between morphology and age (Fig. 5.7).

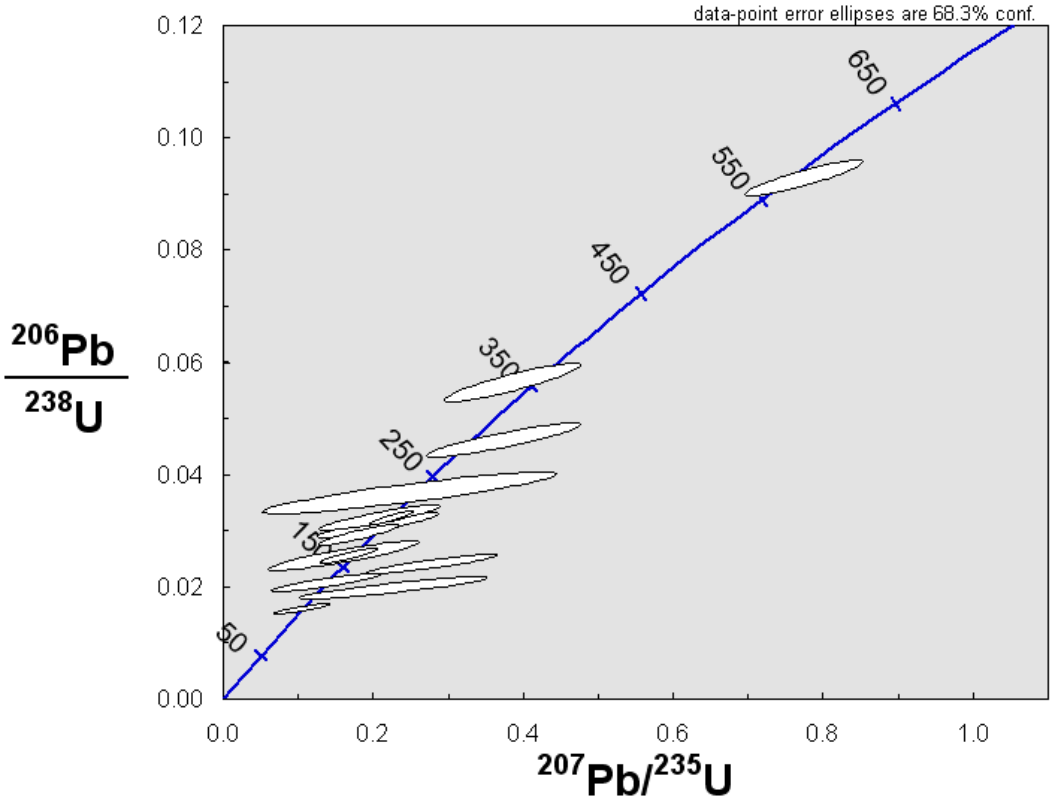

Figure. 5.6 U-Pb concordia plot of single zircon analysis from sample 12 (Turi Formation), showing the residual fourteen concordant/near-concordant crystals (1σ error ellipses) used in further age interpretation.

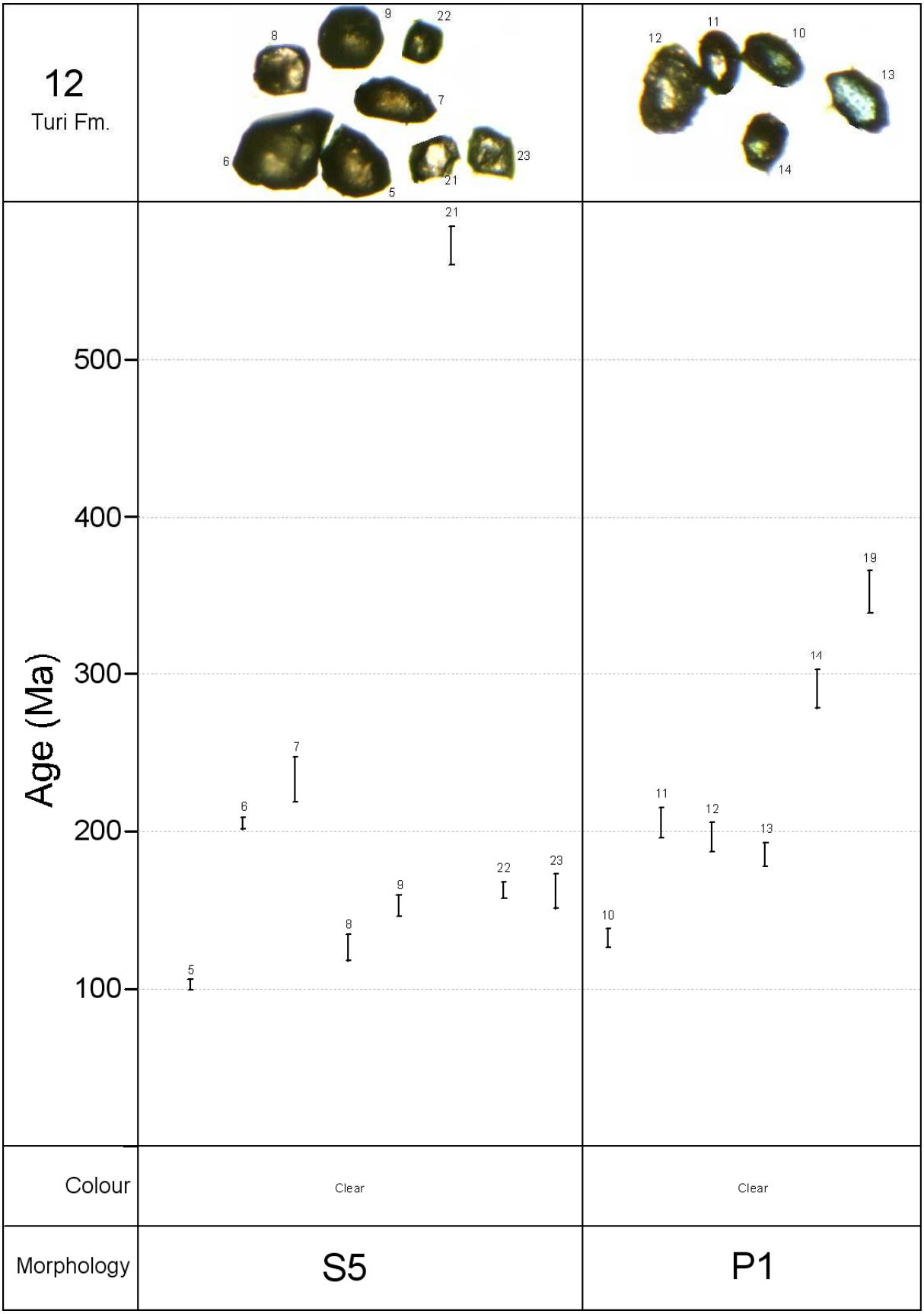

Figure. 5.7 $^{206}Pb/^{238}$ age distribution for sample 12 (Turi Formation), with zircon morphology and colour outlined. Visual representation of zircon morphology (for Pupin (1980) morphologies see Appendix V) and colour subdivisions given.

Sample 15 (Otaihanga Outlier)

Twenty six zircon grains were analysed in this sample, with all being concordant/near-concordant ages. Figure 5.8 is a concordia plot showing individual crystal error ellipses with 1σ uncertainty. Most crystals appear to be concordant with the exception of one near-concordant determination at around 500 Ma. Although there is a fairly large age range in the data there is an obvious cluster of ages between 200 – 300 Ma. Figure 5.9 shows individual $^{206}Pb/^{238}U$ ages plotted against crystal morphology and colour. $^{206}Pb/^{238}U$ ages range from 212.9 to 1103.4 Ma with 73% of ages occurring between 210 and 290 Ma. Pupin (1980) morphologies identified include P2, S10 and S15 subtypes. However, there was no apparent relationship between grain morphology and age. Analysed crystals were dominantly clear, however 10 crystals had pale amber and amber colours observed under reflected light. The two oldest $^{206}Pb/^{238}U$ ages included one pale amber and one amber crystal, and the other eight coloured crystals possessed similar ages to those that were clear (Fig. 5.9).

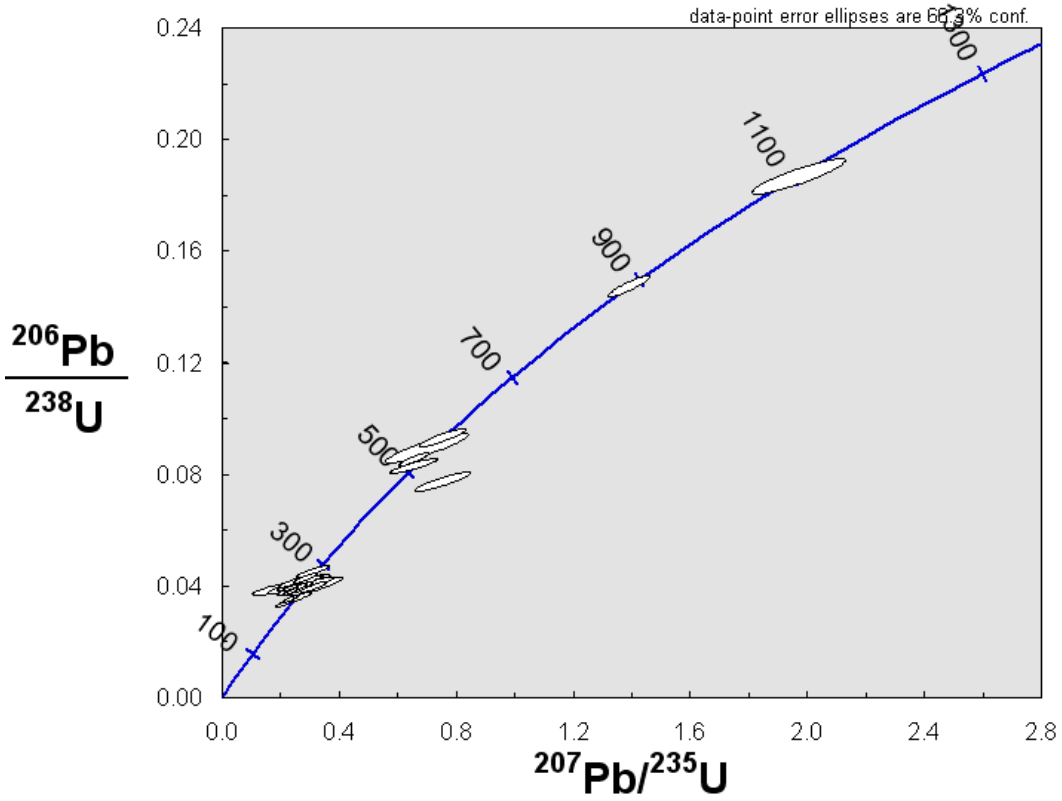

Figure. 5.8 U-Pb concordia plot of single zircon analysis from sample 15 (Otaihanga Outlier), showing the twenty six concordant /near-concordant crystals (1σ error ellipses) used in further age interpretation.

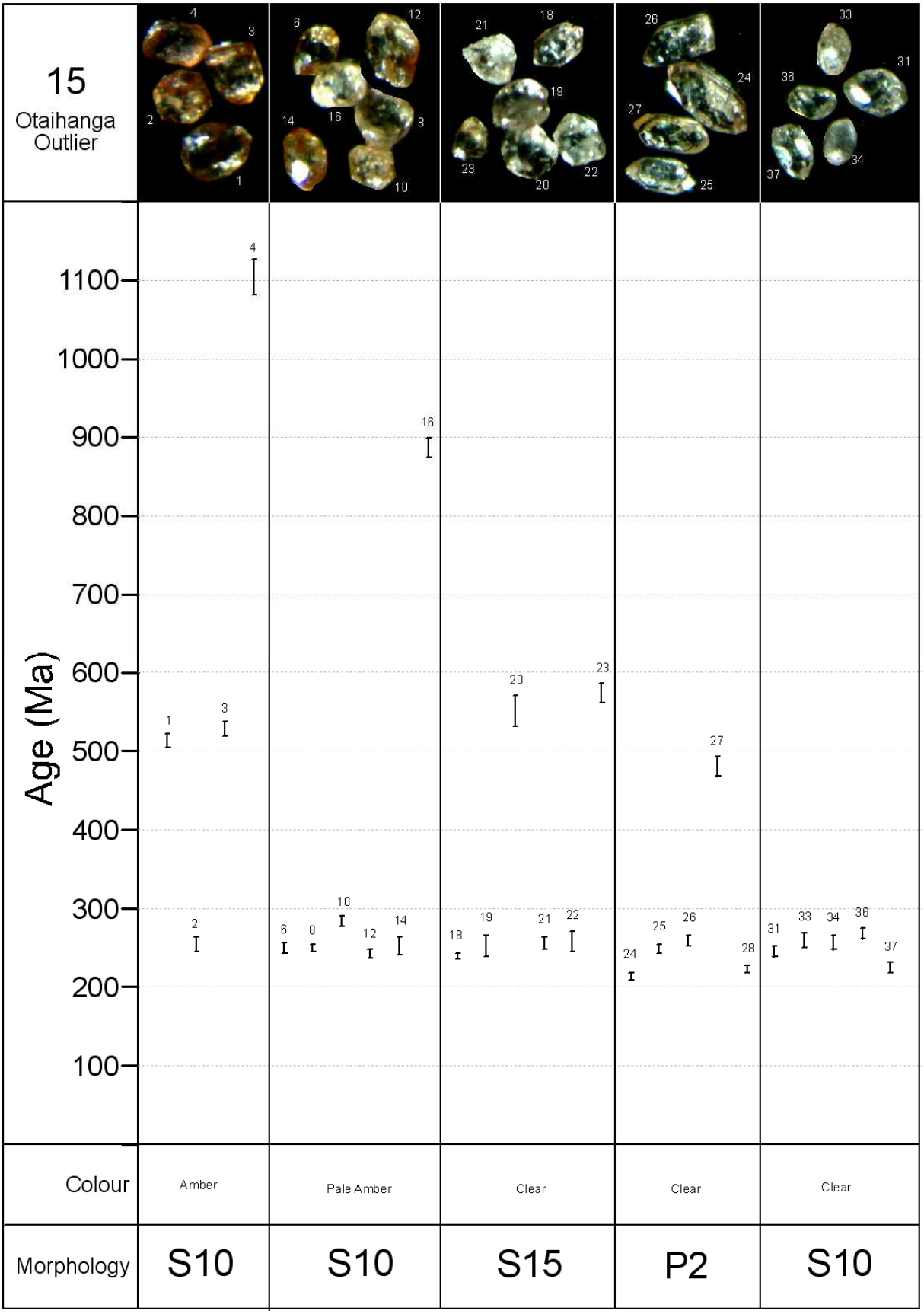

Figure. 5.9 $^{206}Pb/^{238}$ age distribution for sample 15 (Otaihanga Outlier), with zircon morphology and colour outlined. Visual representation of zircon morphology (for Pupin (1980) morphologies see Appendix V) and colour subdivisions given.

Sample 10 (Matapo Sandstone)

Thirty two zircon grains were analysed in this sample with 29 concordant/near-concordant ages. Figure 5.10 is a concordia plot showing individual crystal error ellipses with 1σ uncertainty. Most crystals appear to be concordant with an even spread of ages between 150 – 350 Ma. Figure 5.11 shows individual $^{206}Pb/^{238}U$ ages plotted against crystal morphology and colour. $^{206}Pb/^{238}U$ ages range from 115.5 to 396.8 Ma with 76% of ages falling below 300 Ma and 41% below 200. Unlike other samples where relatively young (<200 Ma) clusters are present, there appears to be much more spread of ages through to 350 Ma within this population. Pupin (1980) morphologies identified include P1, P2, S5 and S15 subtypes. However, there was no apparent relationships between morphology and age. Only clear crystals were identified and analysed in this sample (Fig. 5.11).

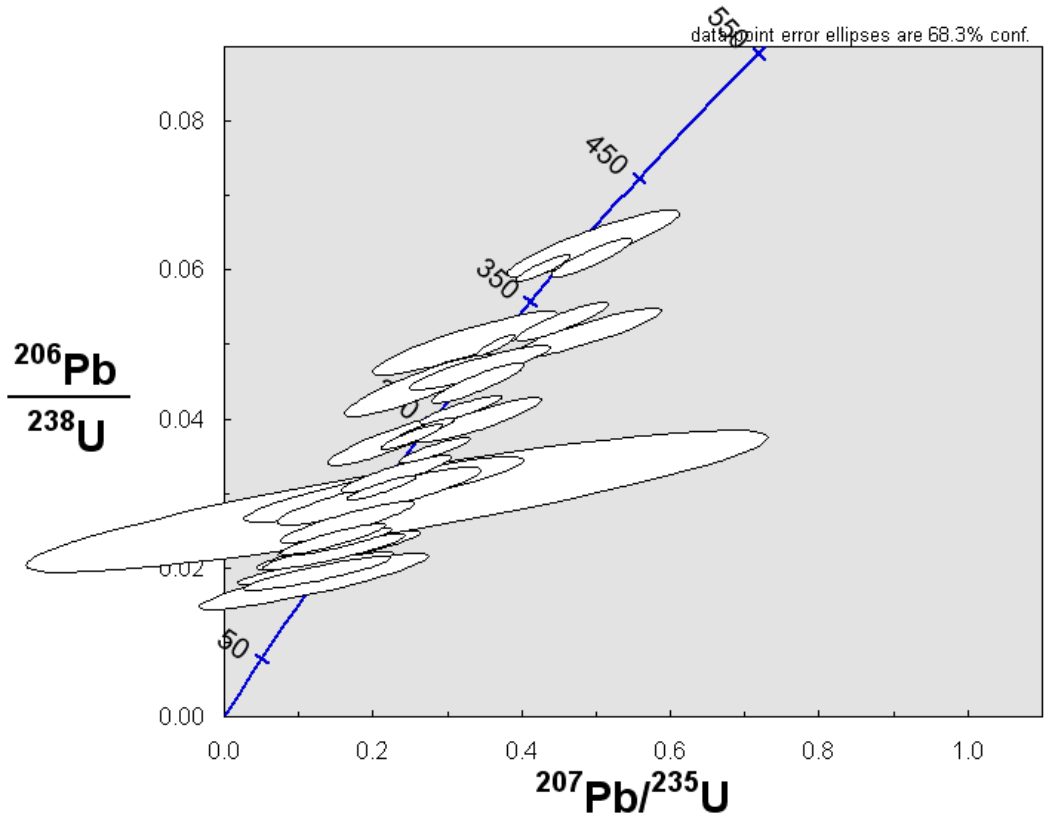

Figure. 5.10 U-Pb concordia plot of single zircon analysis from sample 10 (Matapo Sandstone), showing the residual twenty nine concordant/near-concordant crystals (1σ error ellipses) used in further age interpretation. Note the very large error ellipse, reflecting high $^{207}U/^{235}U$ error.

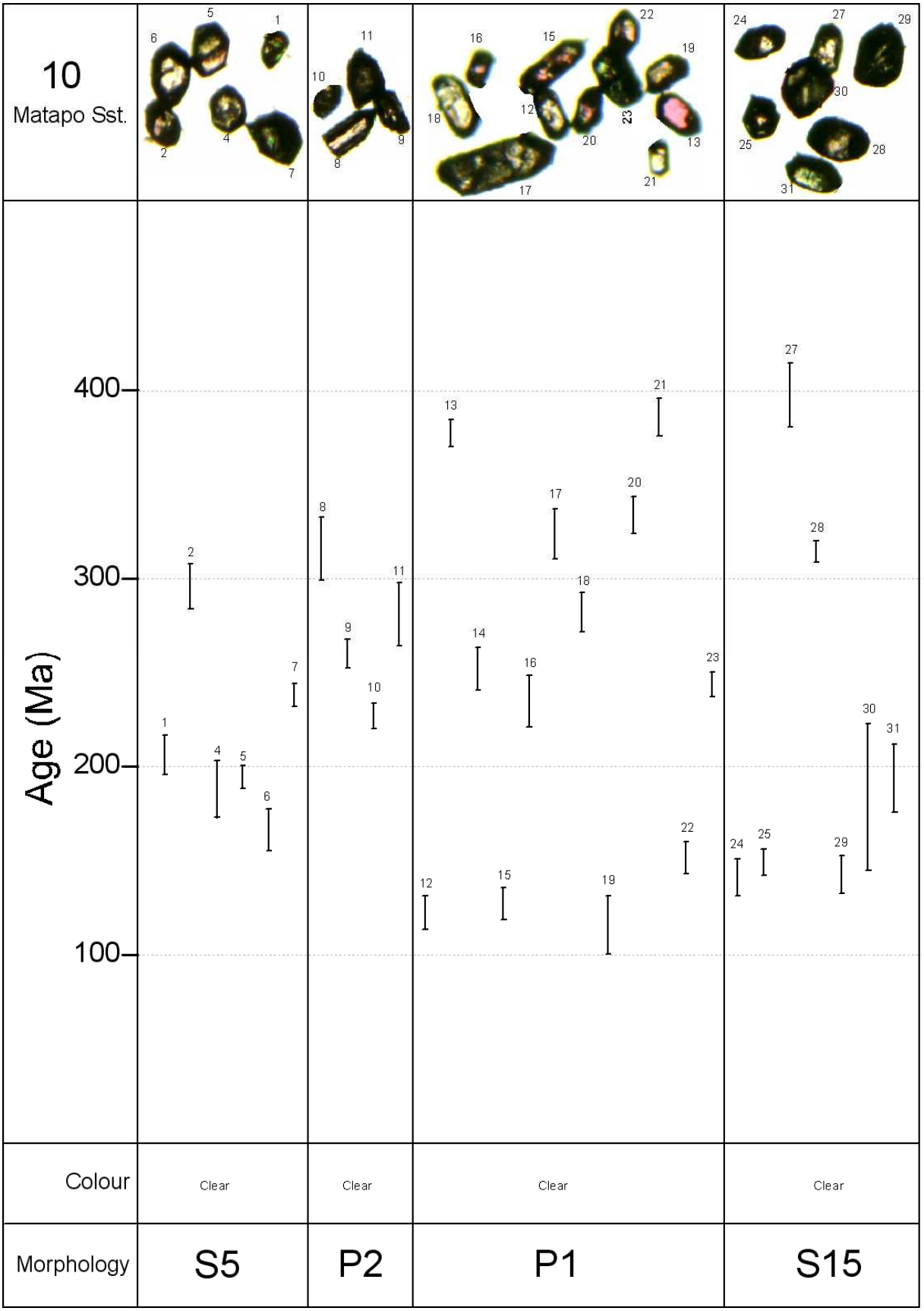

Figure. 5.11 $^{206}Pb/^{238}$ age distribution for sample 10 (Matapo Sandstone), with zircon morphology and colour outlined. Visual representation of zircon morphology (for Pupin (1980) morphologies see Appendix V) and colour subdivisions given.

Sample 7 (Taumarunui quartz sandstone)

Thirty three zircon grains were analysed in this sample with 31 concordant/near-concordant ages. Figure 5.12 is a concordia plot showing individual crystal error ellipses with 1σ uncertainty. Most crystals appear to be concordant with several near-concordant older (>500 Ma) and younger (<300 Ma) ages. There appears to be a dominant cluster between 150 – 400 Ma. Figure 5.13 shows individual $^{206}Pb/^{238}U$ ages plotted against crystal morphology and colour. $^{206}Pb/^{238}U$ ages range from 145.9 to 859.8 Ma with 81% appearing below 300 Ma and 45% below 200 Ma. Pupin (1980) morphologies identified include P1, P2, P3, S3, S4 and S8 subtypes. However, there was no apparent relationship between morphology and age. Only clear crystals were found and analysed in this sample (Fig. 5.13).

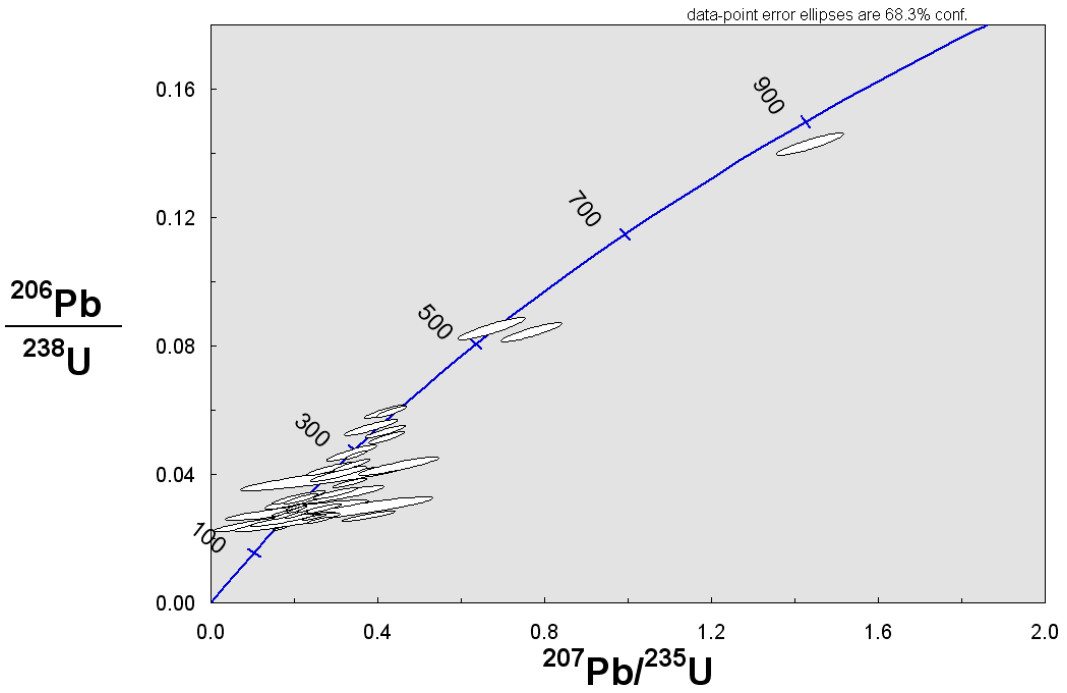

Figure. 5.12 U-Pb concordia plot of single zircon analysis from sample 7 (Taumarunui quartz sandstone), showing the residual thirty one concordant/near-concordant crystals (1σ error ellipses) used in further age interpretation.

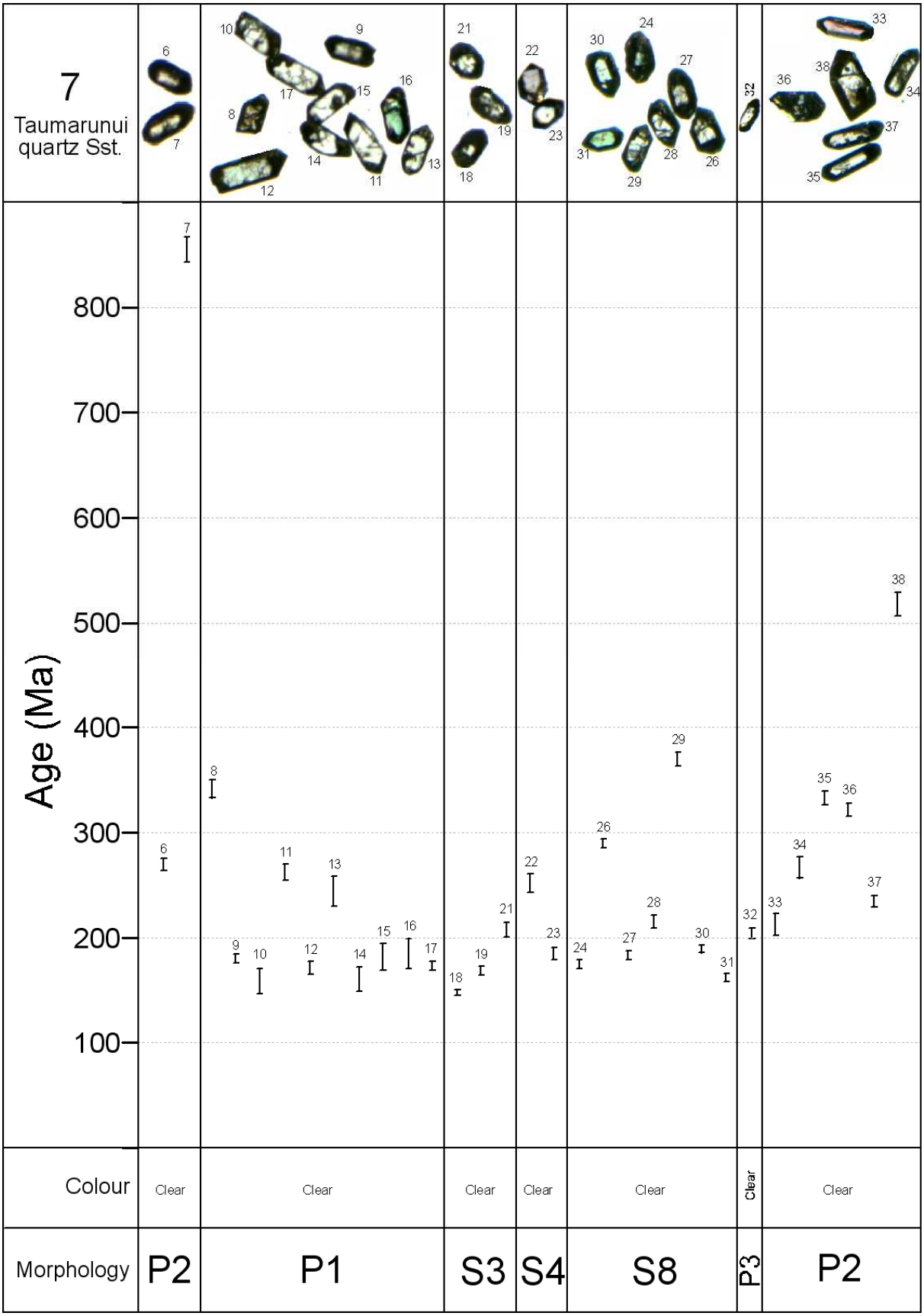

Figure. 5.13 $^{206}Pb/^{238}$ age distribution for sample 7 (Taumarunui quartz sandstone), with zircon morphology and colour outlined. Visual representation of zircon morphology (for Pupin (1980) morphologies see Appendix V) and colour subdivisions given.

Sample 1 (Ahirau Sandstone)

Twenty five zircon grains were analysed for this sample, with all being concordant/near-concordant ages. Figure 5.14 is a concordia plot showing individual crystal error ellipses with 1σ uncertainty. Compared with other samples most of the error ellipses for this sample appear much smaller, due to smaller error associated with $^{207}Pb/^{235}U$ measurements. Most crystal ages appear to be concordant and many of the smaller ellipses appear to be near-concordant. There appears to be an even spread of ages between 100 and 300 Ma. Figure 5.15 shows individual $^{206}Pb/^{238}U$ ages plotted against crystal morphology and colour. $^{206}Pb/^{238}U$ ages range from 104.7 to 433.4 Ma with 88% of ages falling below 280 Ma and 52% below 200 Ma. Unlike other samples where there is a cluster of ages <200 Ma this sample shows a spread of ages through to 300 Ma. Pupin (1980) morphologies identified include P1, S5, S10 and S15 subtypes. However, there are no apparent relationships between morphology and age. Only clear crystals were found and analysed in this sample (Fig. 5.15).

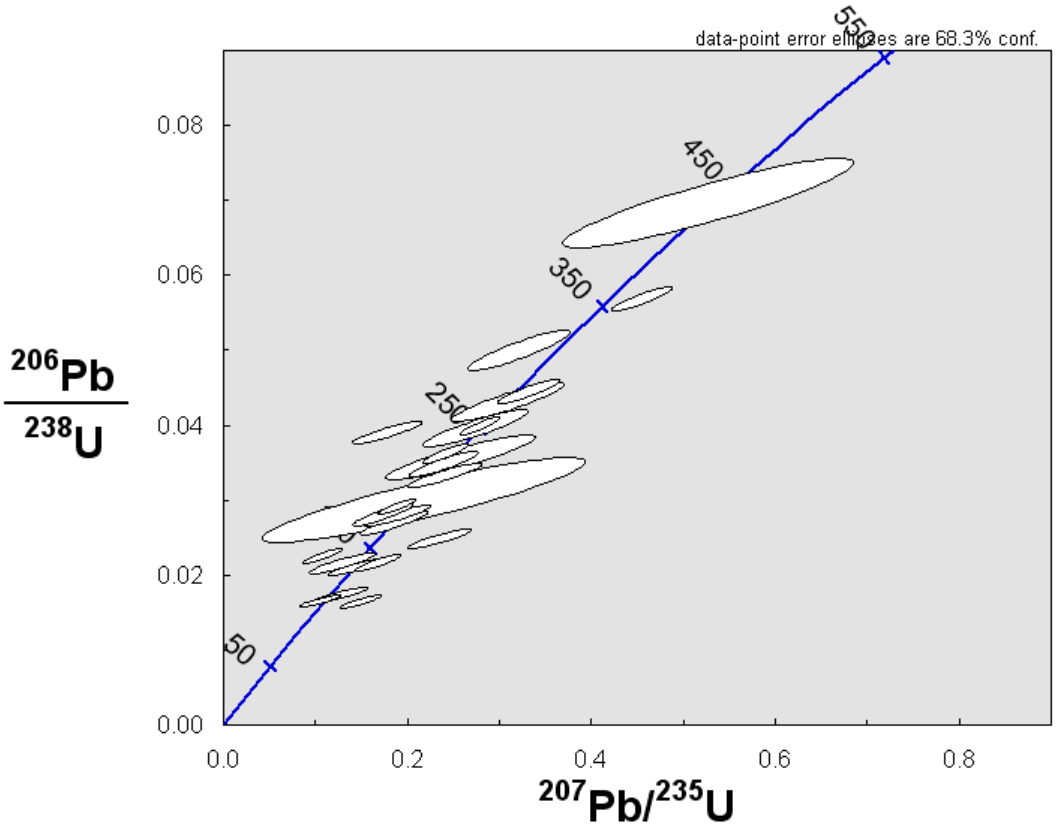

Figure. 5.14 U-Pb concordia plot of single zircon analysis from sample 1 (Ahirau Sandstone), showing the twenty five concordant/near-concordant crystals (1σ error ellipses) used in further age interpretation.

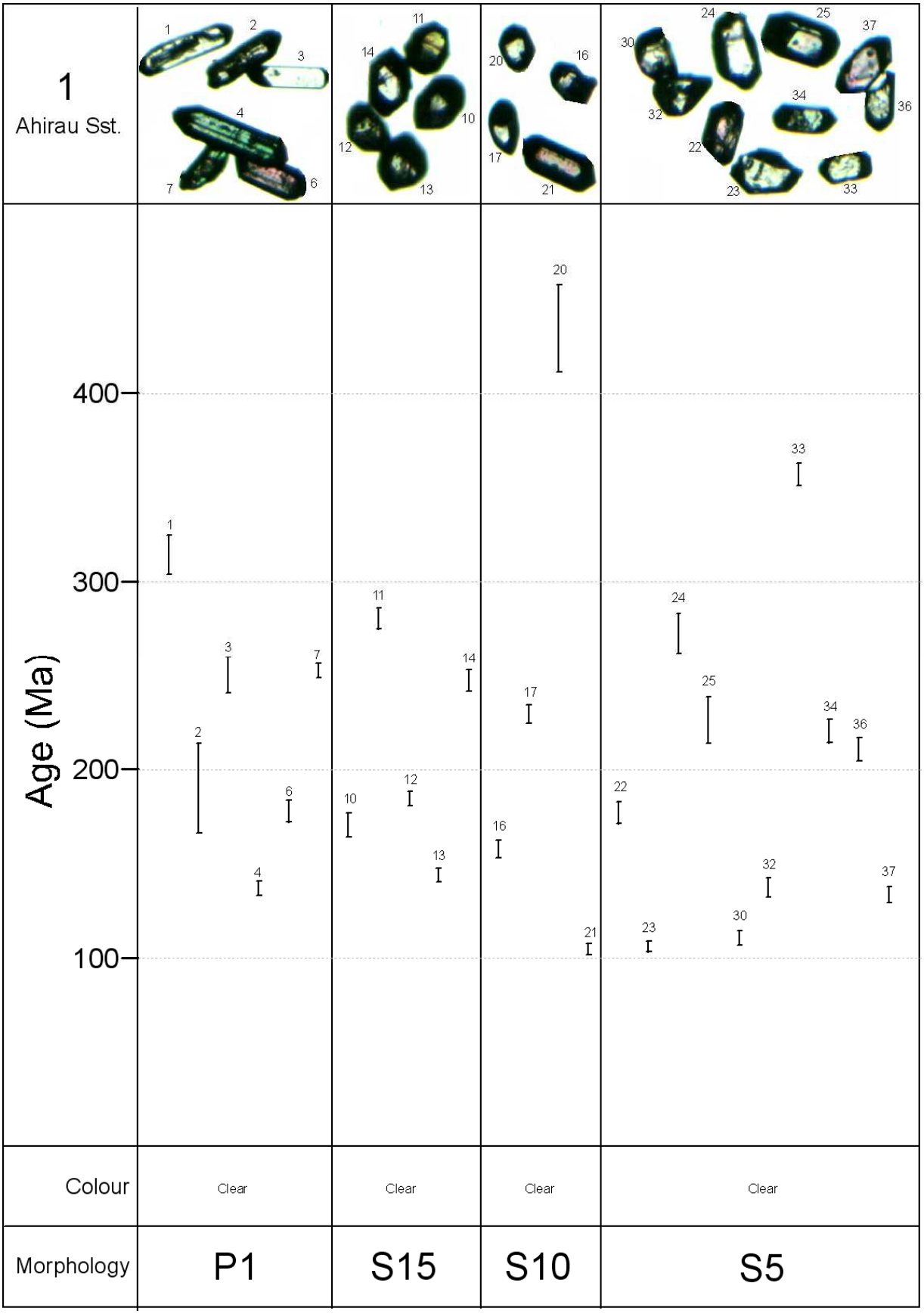

Figure. 5.15 $^{206}Pb/^{238}$ age distribution for sample 1 (Ahirau Sandstone), with zircon morphology and colour outlined. Visual representation of zircon morphology (for Pupin (1980) morphologies see Appendix V) and colour subdivisions given.

Sample 2 (Ahirau Sandstone)

Twenty eight single zircon grains were analysed in this sample, with 27 showing concordant/near-concordant ages. Figure 5.16 is a concordia plot showing individual crystal error ellipses with 1σ uncertainty. All crystals appear to be concordant with a cluster of ages around 150 Ma. Figure 5.17 shows individual $^{206}Pb/^{238}U$ ages plotted against crystal morphology and colour. $^{206}Pb/^{238}U$ ages range from 132.8 to 1066.9 Ma with 74% of ages falling below 300 Ma and 56% below 200 Ma. Pupin (1980) morphologies identified include P1, S5, S9 and S10 subtypes. However, there are no apparent relationships between morphology and age. Only clear crystals were found and analysed for this sample (Fig. 5.17).

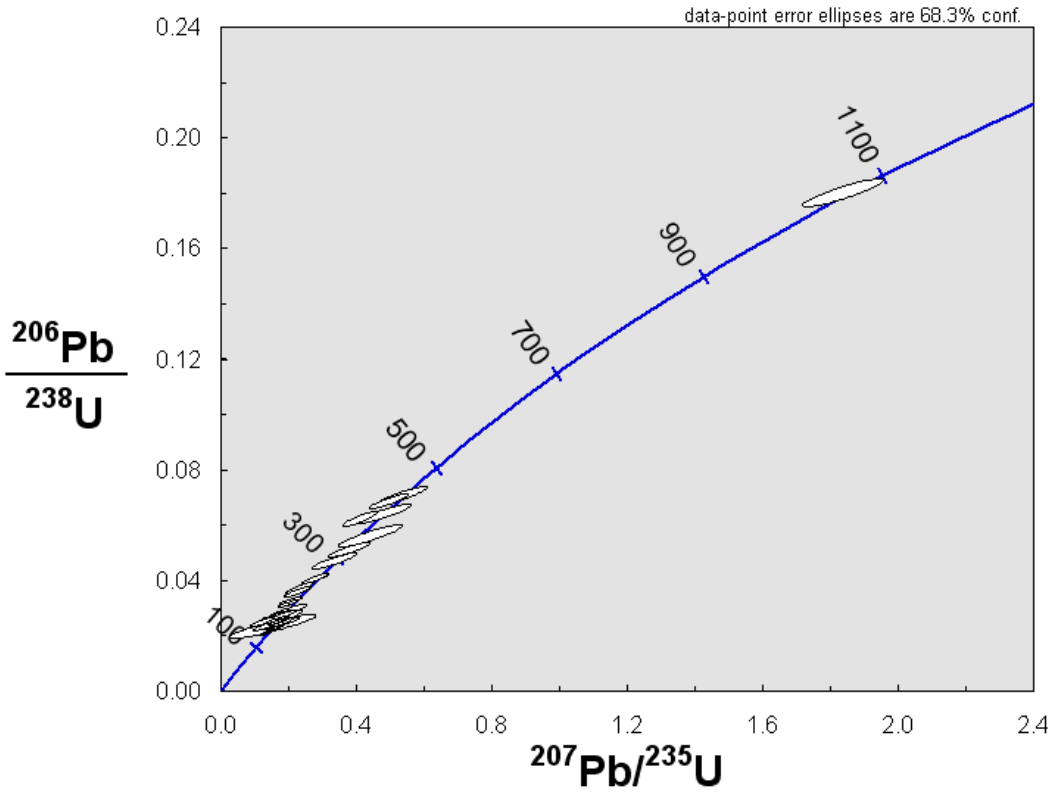

Figure. 5.16 U-Pb concordia plot of single zircon analysis from sample 2 (Ahirau Sandstone), showing the residual twenty seven concordant/near-concordant crystals (1σ error ellipses) used in further age interpretation.

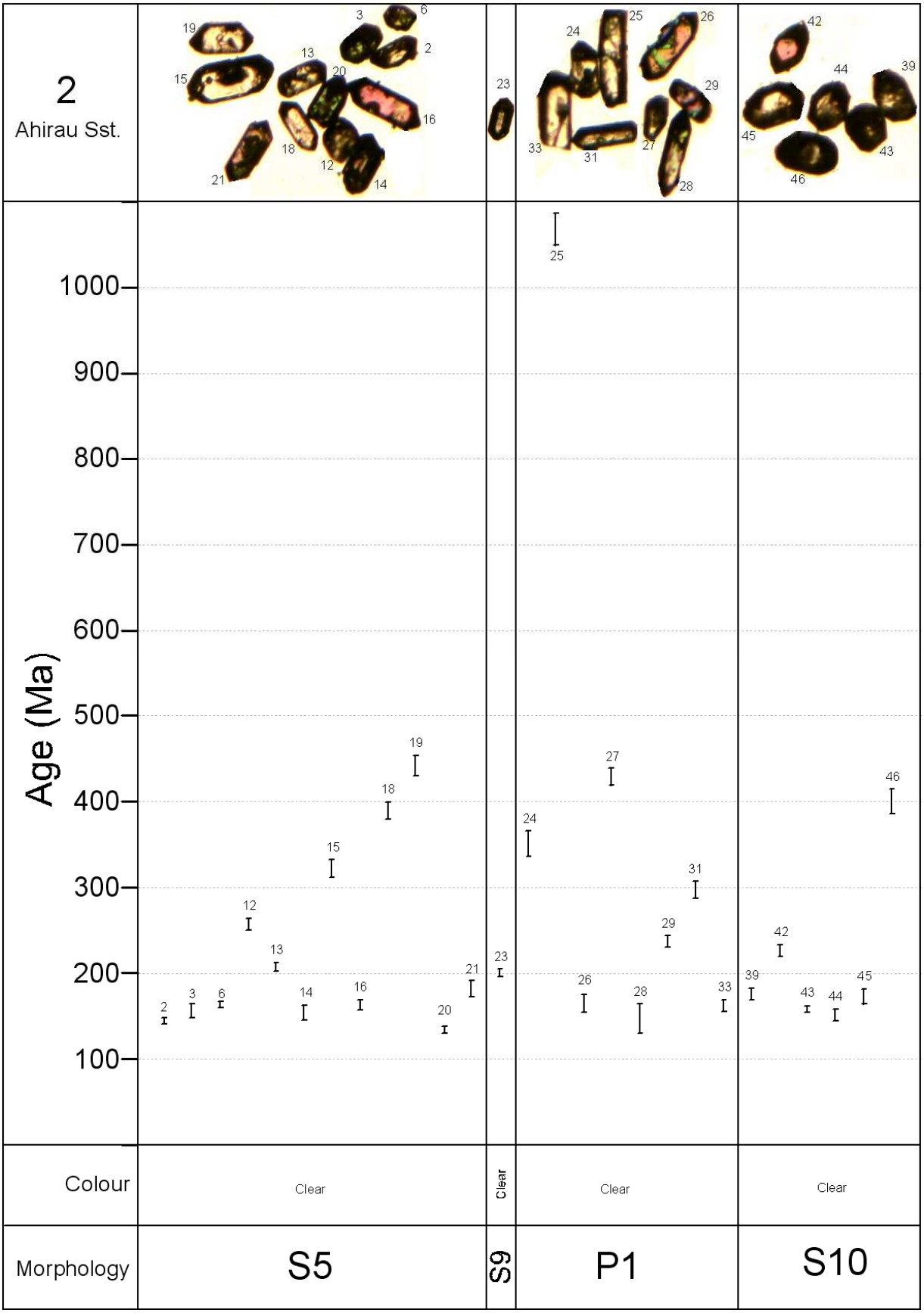

Figure. 5.17 $^{206}Pb/^{238}$ age distribution for sample 2 (Ahirau Sandstone), with zircon morphology and colour outlined. Visual representation of zircon morphology (for Pupin (1980) morphologies see Appendix V) and colour subdivisions given.

Sample 3 (Ahirau Sandstone)

Thirty one single zircon grains were analysed in this sample, with 27 showing concordant/near-concordant ages. Figure 5.18 is a concordia plot showing individual crystal error ellipses with 1σ uncertainty. Many crystals appear near-concordant or discordant for this sample but have been kept on plots with a suspicion that the $^{207}Pb/^{235}U$ measurements may be causing the apparent discordance. A dominant cluster of ages is present between 200 – 250 Ma. Figure 5.19 shows individual $^{206}Pb/^{238}U$ ages plotted against crystal morphology and colour. $^{206}Pb/^{238}U$ ages range from 120.5 to 373.5 Ma with 81% of ages falling below 300 Ma and 52% between 190 – 250 Ma. Pupin (1980) morphologies identified include P1, P2, S5, S10 and S15 subtypes. However, there is no apparent relationship between morphology and age. Only clear crystals were found and analysed for this sample (Fig. 5.19).

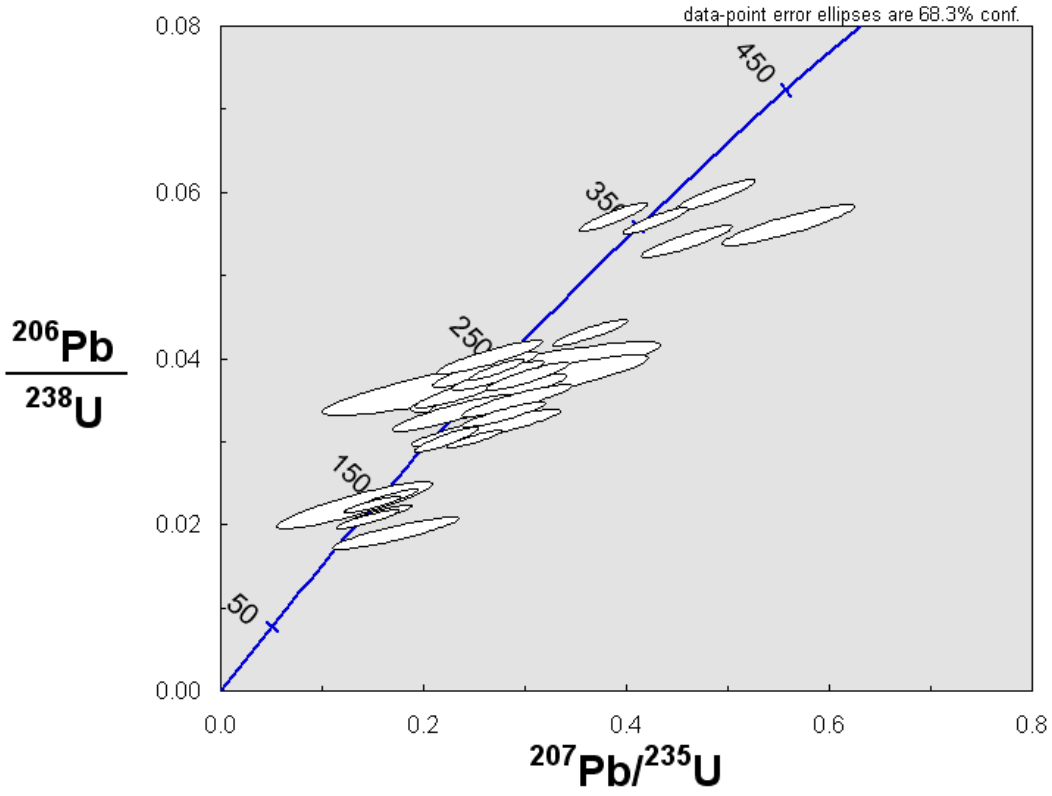

Figure. 5.18 U-Pb concordia plot of single zircon analysis from sample 3 (Ahirau Sandstone), showing the residual twenty seven concordant/near-concordant crystals (1σ error ellipses) used in further age interpretation.

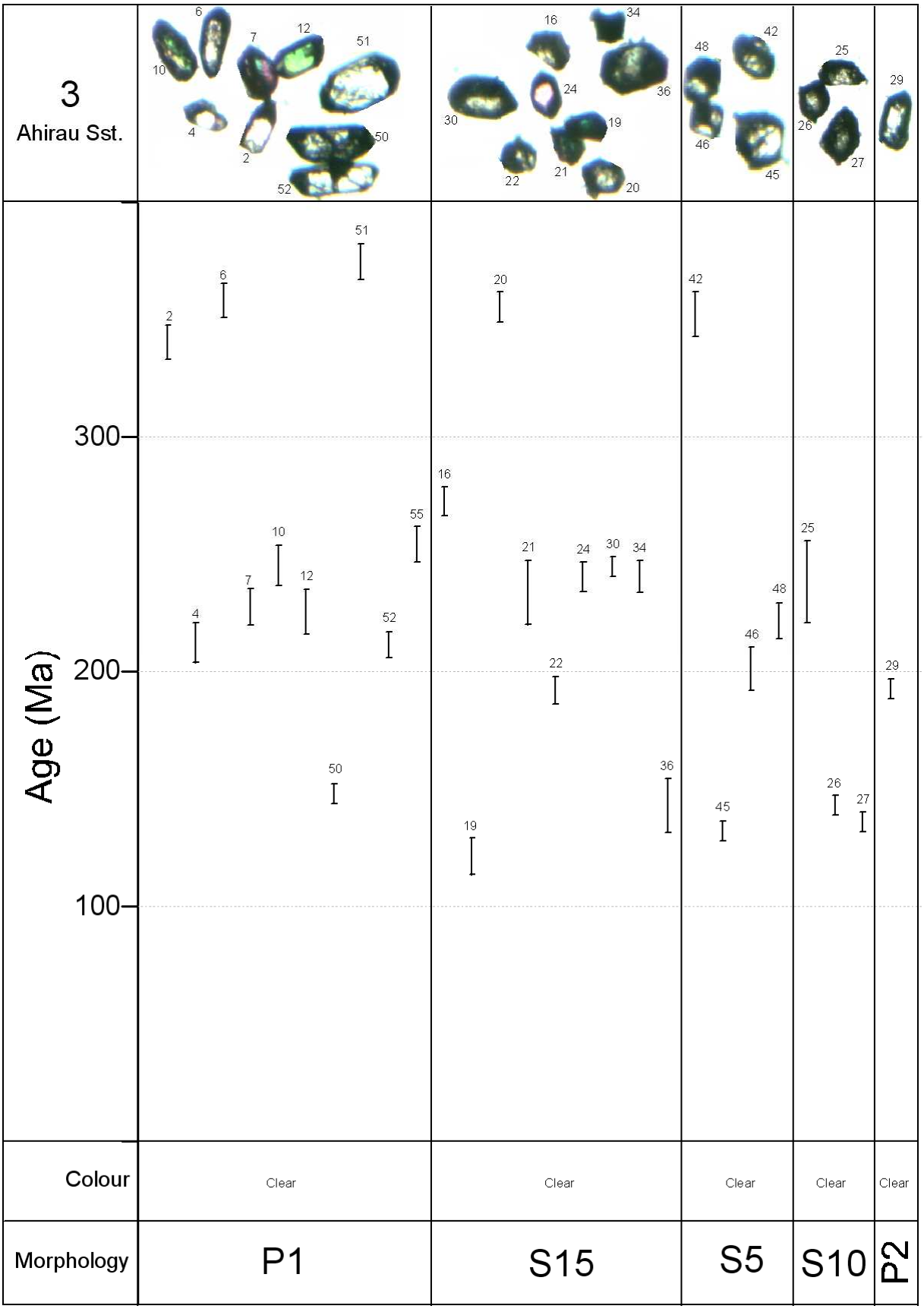

Figure. 5.19 $^{206}Pb/^{238}$ age distribution for sample 3 (Ahirau Sandstone), with zircon morphology and colour outlined. Visual representation of zircon morphology (for Pupin (1980) morphologies see Appendix V) and colour subdivisions given.

Sample 9 (Tariki Sandstone)

Thirty zircon grains were analysed in this sample with a resulting 27 concordant/near-concordant ages used in interpretation. Figure 5.20 is a concordia plot showing individual crystal error ellipses with 1σ uncertainty. Compared with other samples, there appears to be a lot more error associated with $^{207}Pb/^{235}U$ measurements, which is shown by ellipse elongation in the left/right direction. This was possibly due to high ^{207}Pb background levels in the sample chamber that were present on this day of probing. There does however appear to be a dominant cluster between 100 and 150 Ma. Figure 5.21 shows individual $^{206}Pb/^{238}U$ ages plotted against crystal morphology and colour. $^{206}Pb/^{238}U$ ages range from 112.2 to 377.6 Ma with 89% of ages falling below 300 Ma and 59% below 150 Ma. Pupin (1980) morphologies identified include P1, P2, L5, S5 and S15. However, there are no apparent relationships between morphology and age. All crystals found and analysed in this sample were clear (Fig. 5.21).

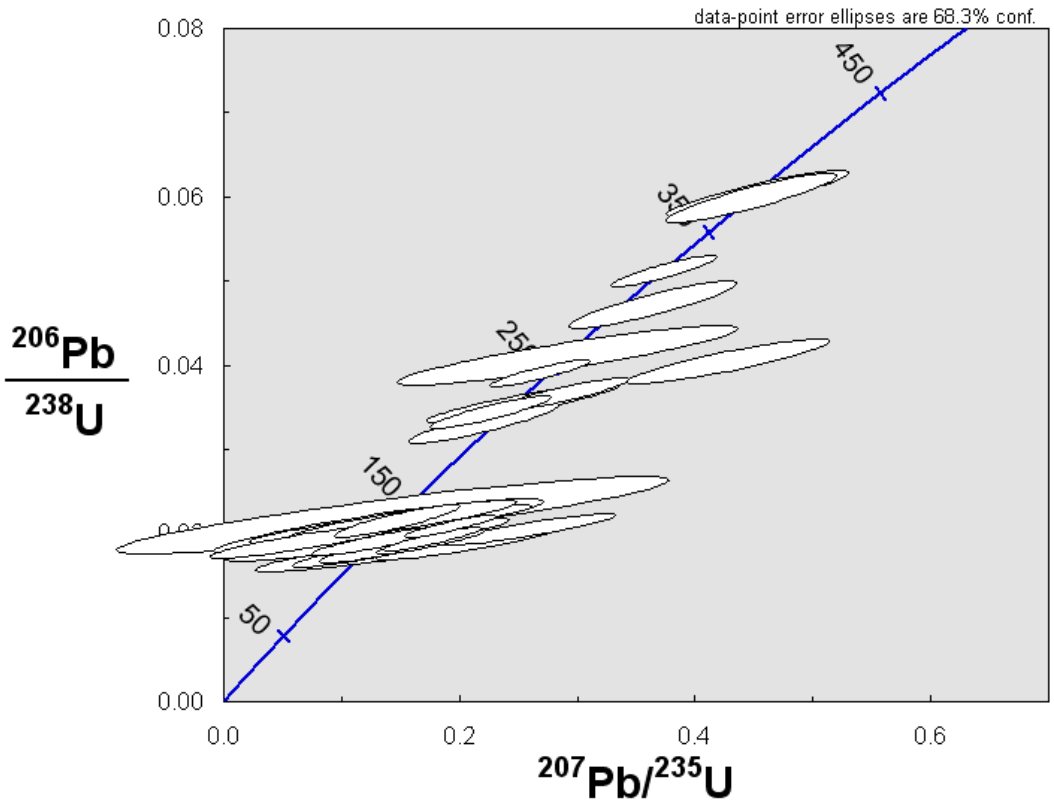

Figure. 5.20 U-Pb concordia plot of single zircon analysis from sample 9 (Tariki Sandstone), showing the residual twenty seven concordant/near-concordant crystals (1σ error ellipses) used in further age interpretation.

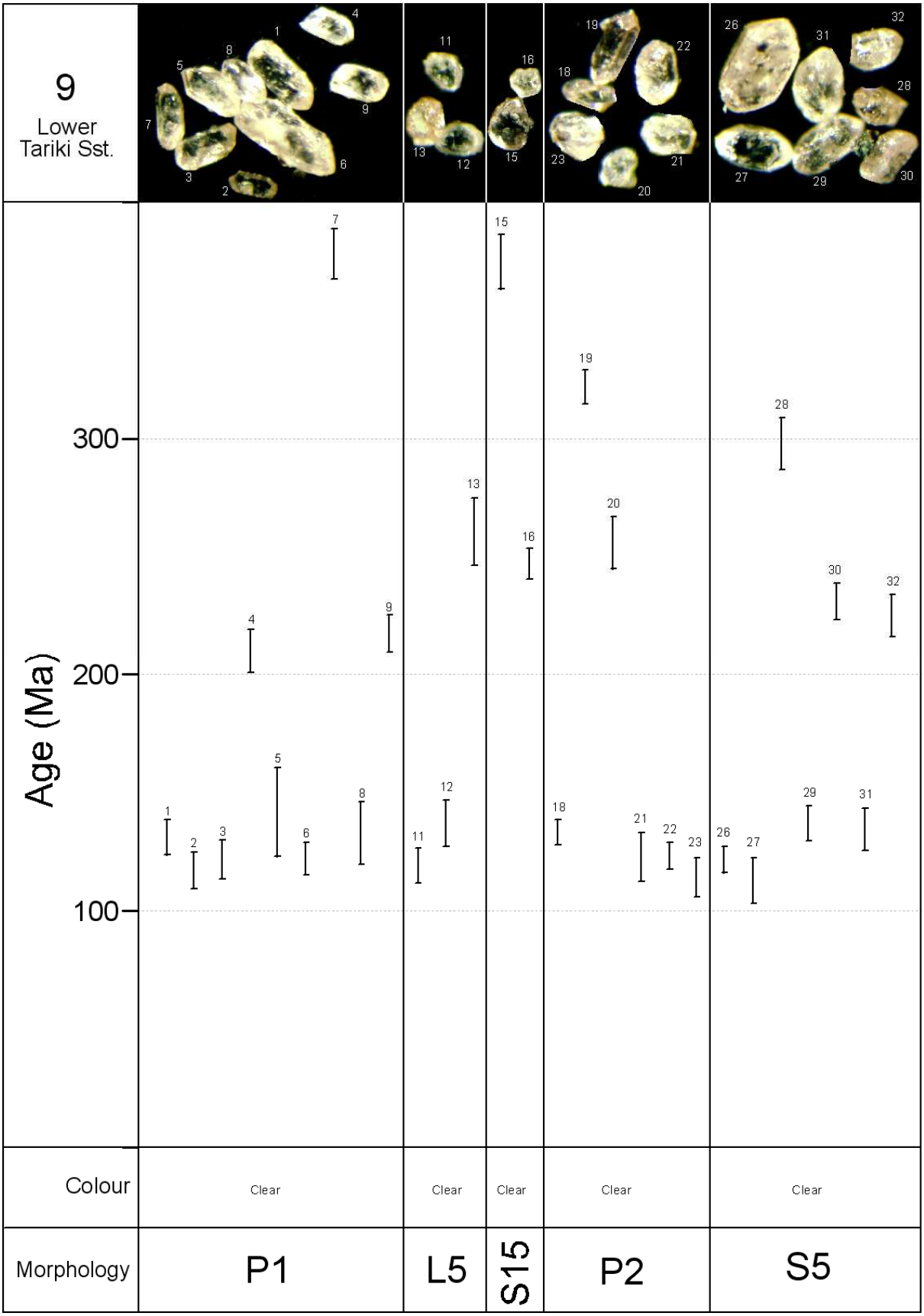

Figure. 5.21 $^{206}Pb/^{238}$ age distribution for sample 9 (Tariki Sandstone), with zircon morphology and colour outlined. Visual representation of zircon morphology (for Pupin (1980) morphologies see Appendix V) and colour subdivisions given.

Sample 13 (Tariki Sandstone)

Thirty one zircon grains were analysed in this sample with a resulting 29 concordant/near-concordant ages. Figure 5.22 is a concordia plot showing individual crystal error ellipses with 1σ uncertainty. Most crystals are concordant with a clusters around 125, 250 and 350 Ma. Figure 5.23 shows individual $^{206}Pb/^{238}U$ ages plotted against crystal morphology and colour. $^{206}Pb/^{238}U$ ages range from 110 to 363.9 Ma with 66% of ages falling below 200 Ma and 52% below 150 Ma. Pupin (1980) morphologies identified include P1, P2, S5 and S20 subtypes. However, there was no apparent relationships between morphology and age. All crystals found and analysed in this sample were clear (Fig. 5.23).

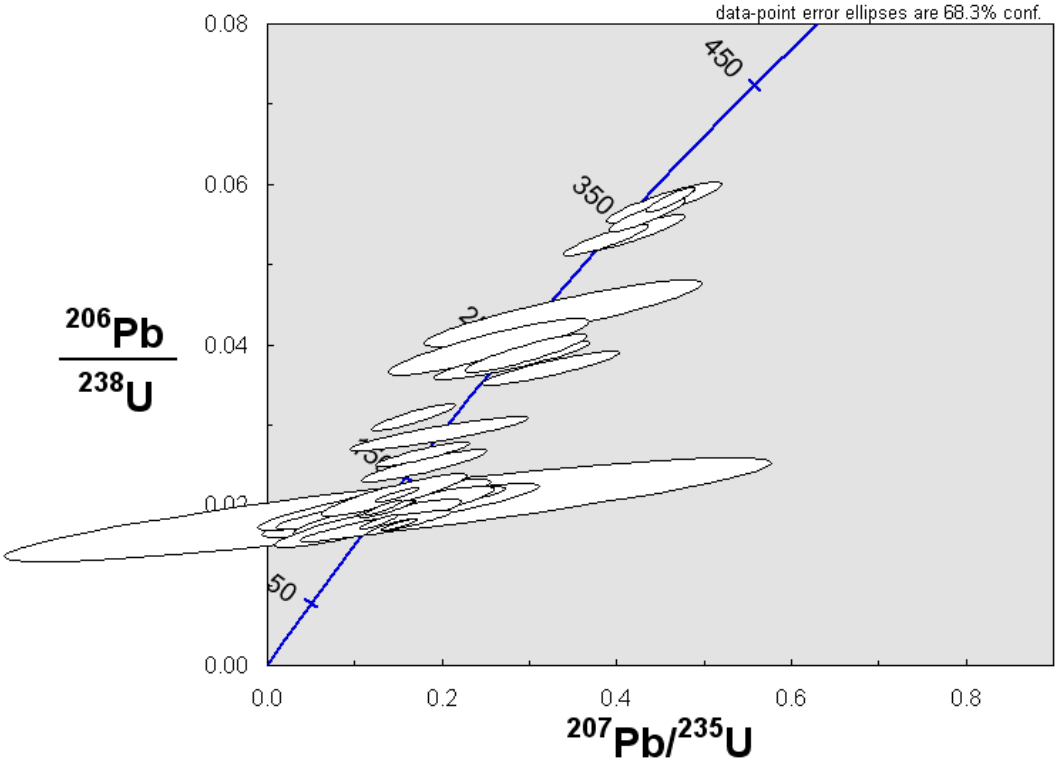

Figure. 5.22 U-Pb concordia plot of single zircon analysis from sample 13 (Tariki Sandstone), showing the residual twenty nine concordant/near-concordant crystals (1σ error ellipses) used in further age interpretation.

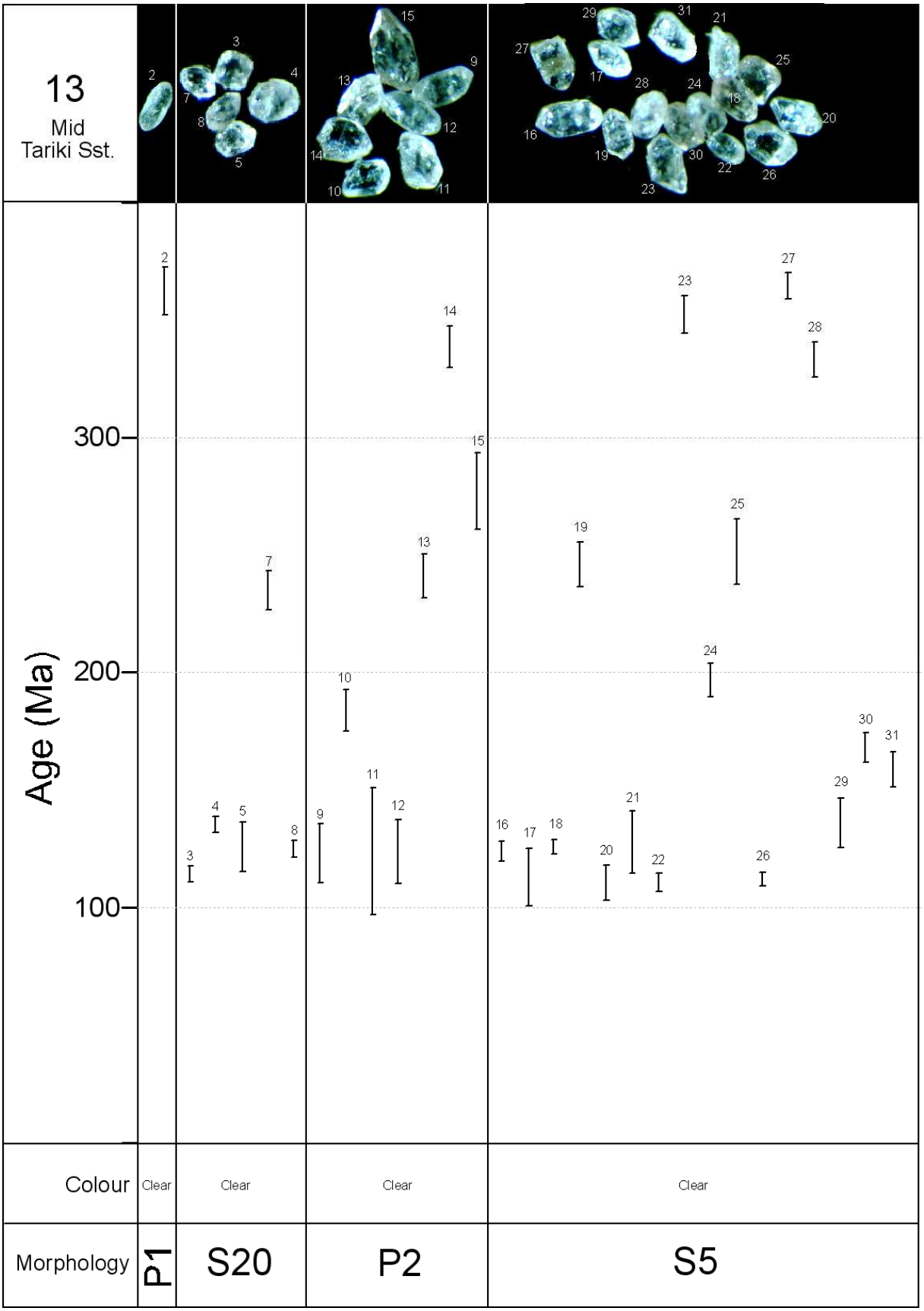

Figure. 5.23 $^{206}Pb/^{238}$ age distribution for sample 13 (Tariki Sandstone), with zircon morphology and colour outlined. Visual representation of zircon morphology (for Pupin (1980) morphologies see Appendix V) and colour subdivisions given.

Sample 14 (Tariki Sandstone)

Twenty nine single zircon grains were analysed in this sample with 23 concordant/near-concordant ages. Figure 5.24 is a concordia plot showing individual crystal error ellipses with 1σ uncertainty. There appears to be several near-concordant ellipses and compared with other samples there is more error associated with the $^{207}Pb/^{235}U$ measurements, which is shown by more ellipse elongation in the left/right direction. This was possibly due to high ^{207}Pb background levels in the sample chamber on this day of probing. Figure 5.25 shows individual $^{206}Pb/^{238}U$ ages plotted against crystal morphology and colour. $^{206}Pb/^{238}U$ ages range from 114.7 to 374.6 Ma with 70% of ages falling below 250 Ma and 39% below 150 Ma. Pupin (1980) morphologies identified include P1, P2, S5, S10, S15 and S20 subtypes. Analysed crystals were dominantly clear, however there were two pink crystals identified in the sample. There does not appear to be any relationships between morphology and age or crystal discolouration and age (Fig. 5.25).

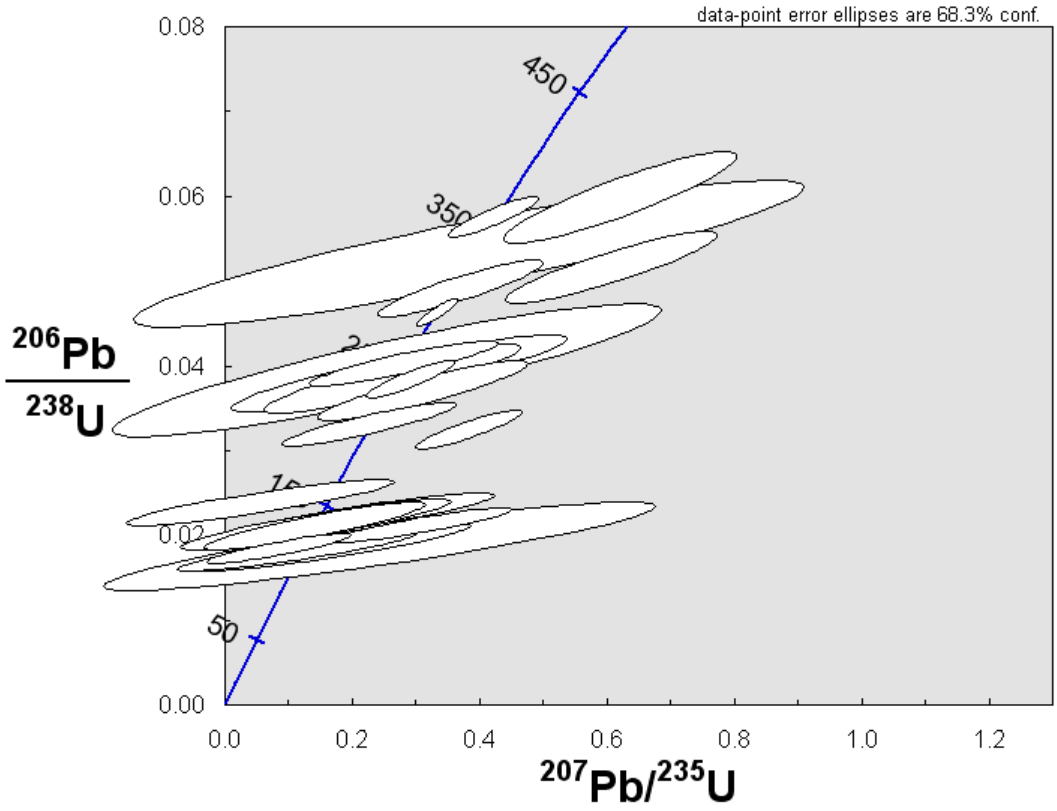

Figure. 5.24 U-Pb concordia plot of single zircon analysis from sample 14 (Tariki Sandstone), showing the residual twenty three concordant/near-concordant crystals (1σ error ellipses) used in further age interpretation.

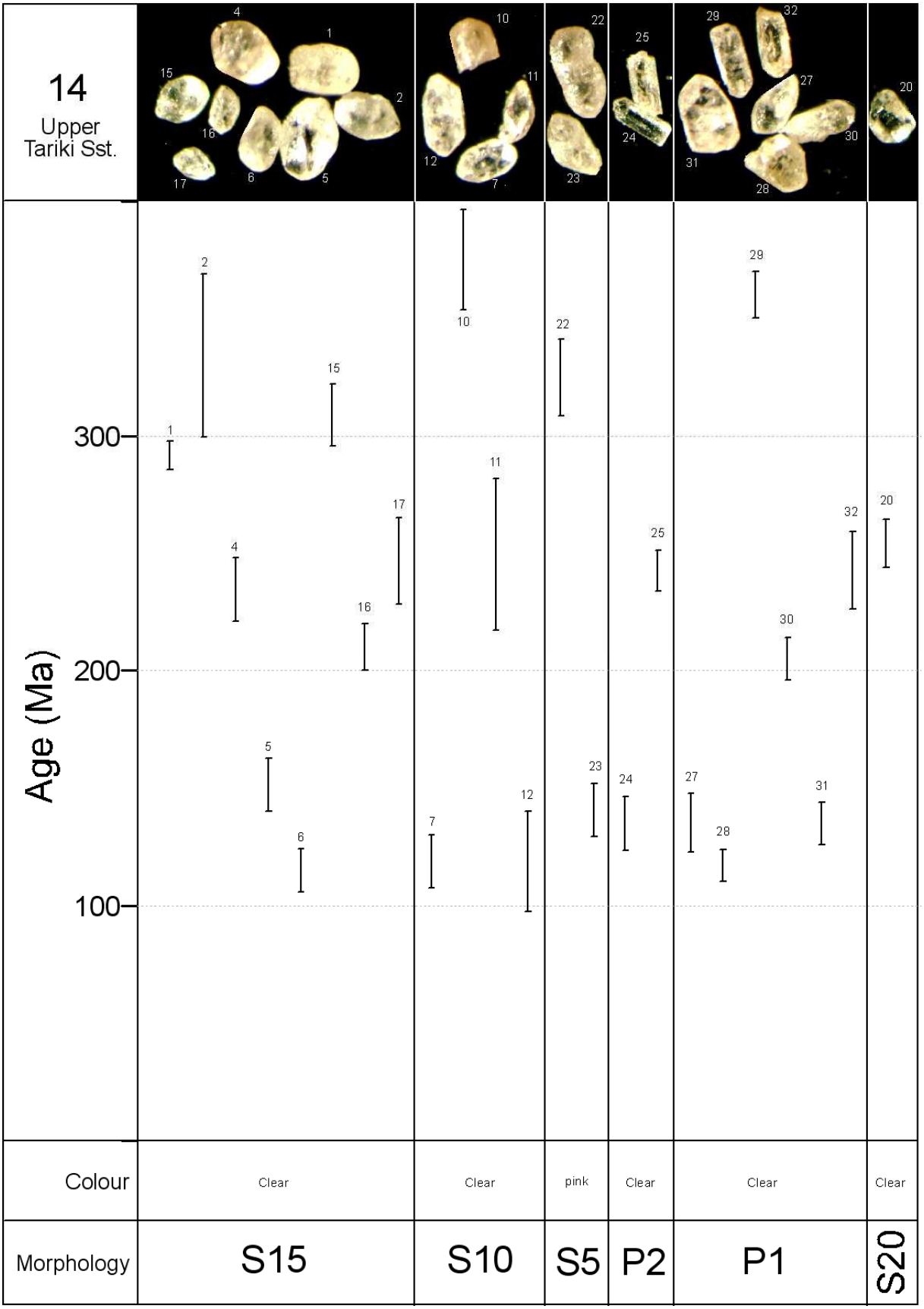

Figure. 5.25 $^{206}Pb/^{238}$ age distribution for sample 14 (Tariki Sandstone), with zircon morphology and colour outlined. Visual representation of zircon morphology (for Pupin (1980) morphologies see Appendix V) and colour subdivisions given.

Sample 5 (Hauturu Sandstone)

Thirty three zircon grains were analysed in this sample, with a resulting 32 concordant/near-concordant ages. Figure 5.26 is a concordia plot showing individual crystal error ellipses with 1σ uncertainty. Most crystals appear to be concordant with a dominant cluster of ages between 100 – 150 Ma. Figure 5.27 shows individual $^{206}Pb/^{238}U$ ages plotted against crystal morphology and colour. $^{206}Pb/^{238}U$ ages range from 100.6 to 605.2 Ma with 81% of ages falling below 200 Ma and 68% below 150 Ma. Pupin (1980) morphologies identified include P1, P2, S10 and S15 subtypes. However, there are no apparent relationships between morphology and age. Only clear crystals were found and analysed in this sample (Fig.5.27).

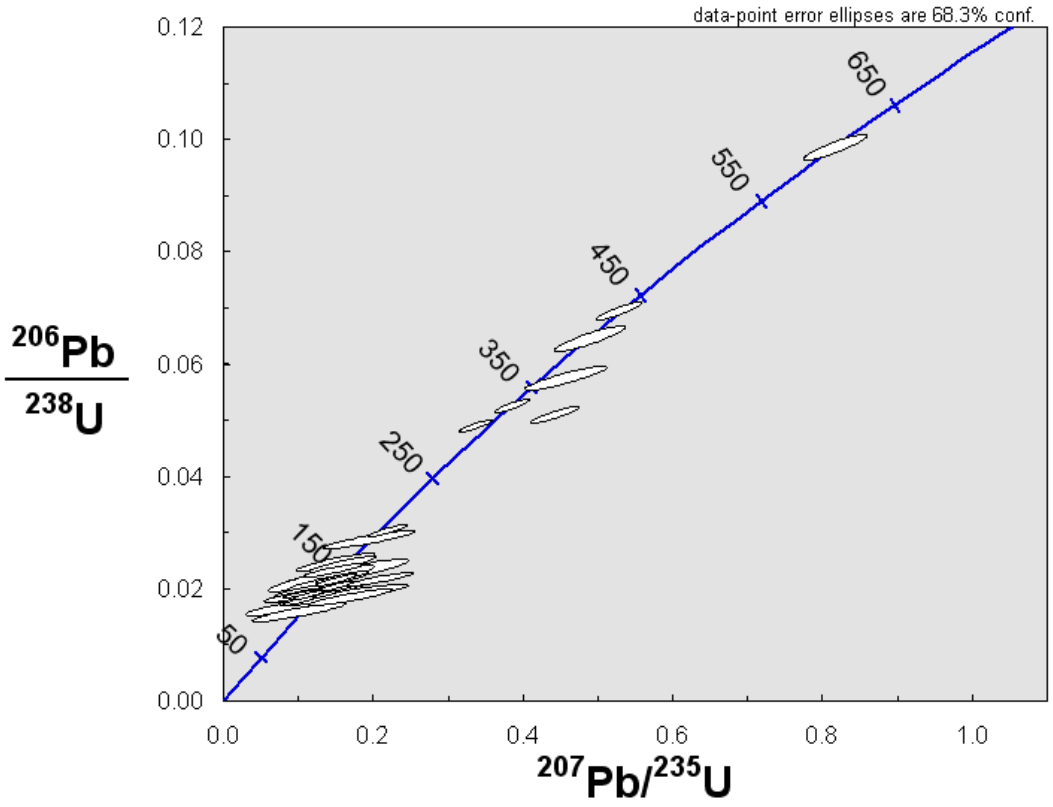

Figure. 5.26 U-Pb concordia plot of single zircon analysis from sample 5 (Hauturu Sandstone), showing the residual thirty one concordant/near-concordant crystals (1σ error ellipses) used in further age interpretation.

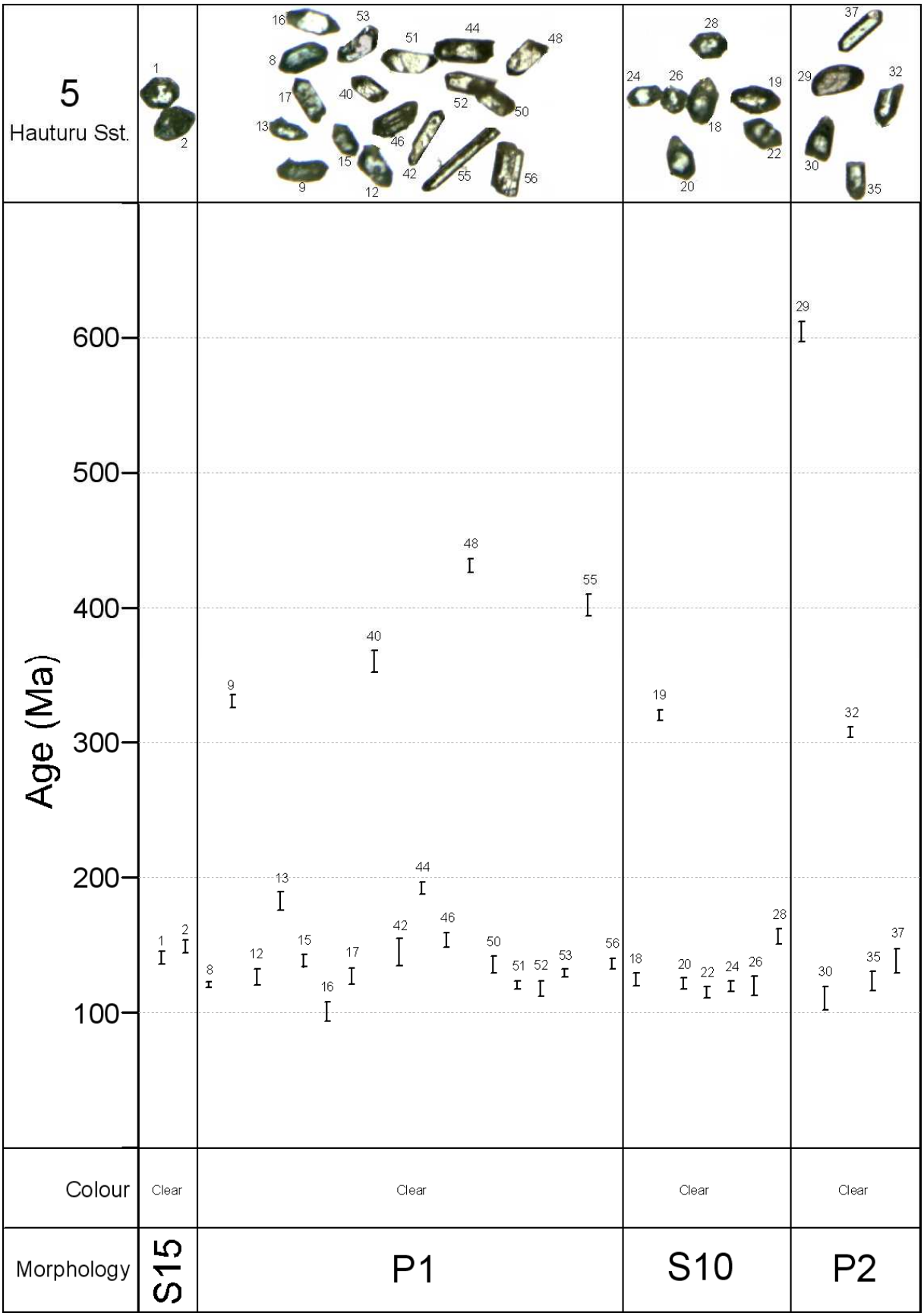

Figure. 5.27 $^{206}Pb/^{238}$ age distribution for sample 5 (Hauturu Sandstone), with zircon morphology and colour outlined. Visual representation of zircon morphology (for Pupin (1980) morphologies see Appendix V) and colour subdivisions given.

Sample 6 (Hauturu Sandstone)

Eighteen zircon grains were analysed in this sample, with a resulting 17 concordant/near-concordant ages used in interpretation. Figure 5.28 is a concordia plot showing individual crystal error ellipses with 1σ uncertainty. Most crystals are concordant for this sample and there is no dominant cluster of ages, but rather a spread of ages between 150 – 350 Ma. Figure 5.29 shows individual $^{206}Pb/^{238}U$ ages plotted against crystal morphology and colour. $^{206}Pb/^{238}U$ ages range from 110 to 361.3 Ma with 41% of ages falling between 300 – 365 Ma and 53% below 200 Ma. Pupin (1980) morphologies identified include P1, P2, S5 and S15 subtypes. However, there are no apparent relationships between morphology and age. Only clear crystals were found and analysed in this sample (Fig. 5.29).

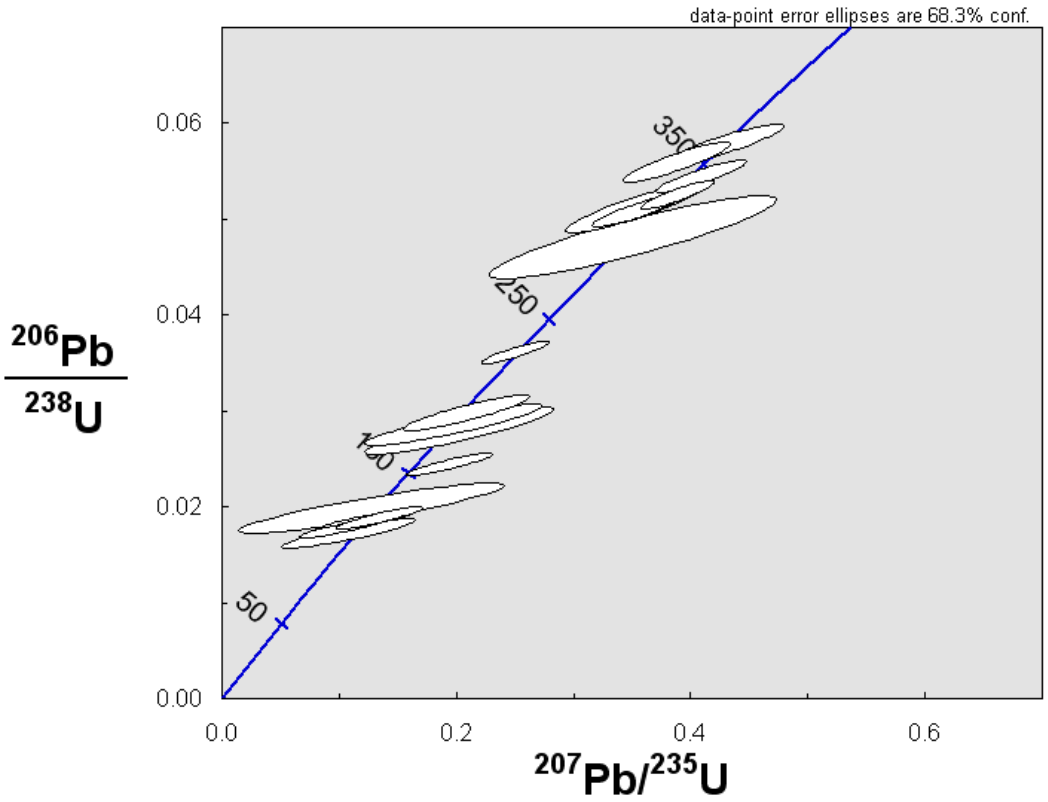

Figure. 5.28 U-Pb concordia plot of single zircon analysis from sample 6 (Hauturu Sandstone), showing the residual seventeen concordant/near-concordant crystals (1σ error ellipses) used in further age interpretation.

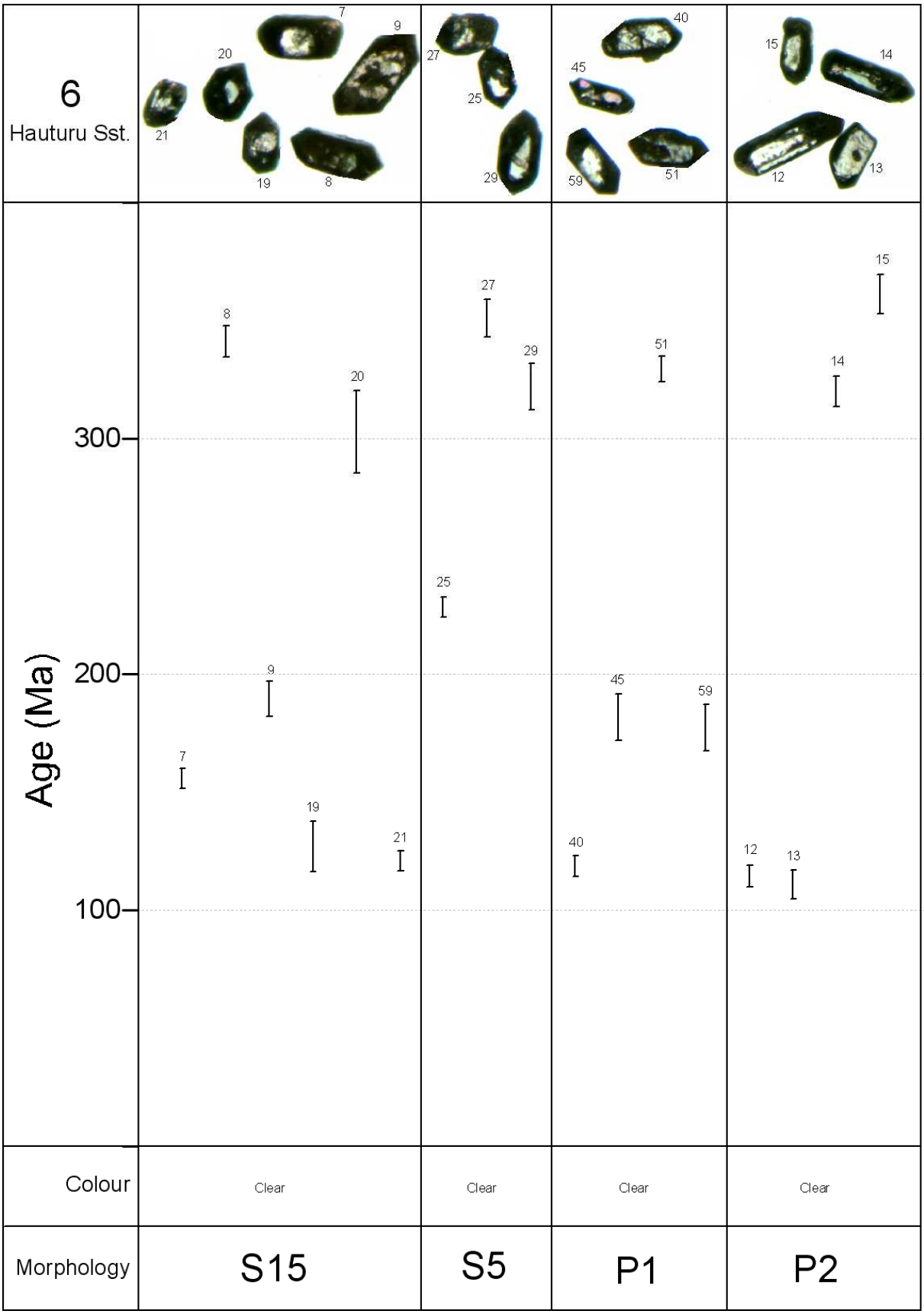

Figure. 5.29 $^{206}Pb/^{238}$ age distribution for sample 6 (Hauturu Sandstone), with zircon morphology and colour outlined. Visual representation of zircon morphology (for Pupin (1980) morphologies see Appendix V) and colour subdivisions given.

5.3.3 Probability distribution plots

This following section discusses $^{206}Pb/^{238}U$ age probability density plots prepared as simple histogram and probability density functions using Isoplot 3.00 software for each of the 13 sample populations analysed. These plots allow dominant age peaks and age distributions to be identified for U-Pb age interpretation. A full set of $^{207}Pb/^{235}U$ and $^{206}Pb/^{238}U$ GLITTER software isotope ratios and age estimate data are provided in Appendix VII.

Sample 8 (McKee Formation)

Zircon $^{206}Pb/^{238}U$ age data from sample 8 (McKee Formation) show a very dominant age peak at 169 Ma (Middle Jurassic), with significant minor peaks for the intervals 270 – 302 Ma (Middle Permian to Late Carboniferous) and 444 – 476 Ma (Late Ordovician to Early Ordovician), and the remainder having scattered Neoproterozoic and Mesoproterozoic ages (Fig. 5.30).

Sample 12 (Turi Formation)

Figure 5.31 illustrates that the majority of ages lie in the range 100 – 200 Ma. Significant peaks occur at 103 Ma (late – Early Cretaceous), 131 Ma (Early Cretaceous), 161 (Middle Jurassic) and within the interval 189 – 204 Ma (Early Jurassic to Middle Triassic) for sample 12 (Turi Formation). The remaining peaks have Permian, Carboniferous and Neoproterozoic ages.

Sample 15 (Otaihanga Outlier)

Zircon $^{206}Pb/^{238}U$ age data for sample 15 (Otaihanga Outlier) show a very dominant age peak at 249 Ma (Early Triassic), with a significant minor peak at 220 Ma (Late Triassic), and the remainder scattered Ordovician to Neoproterozoic and Mesoproterozoic ages (Fig. 5.32).

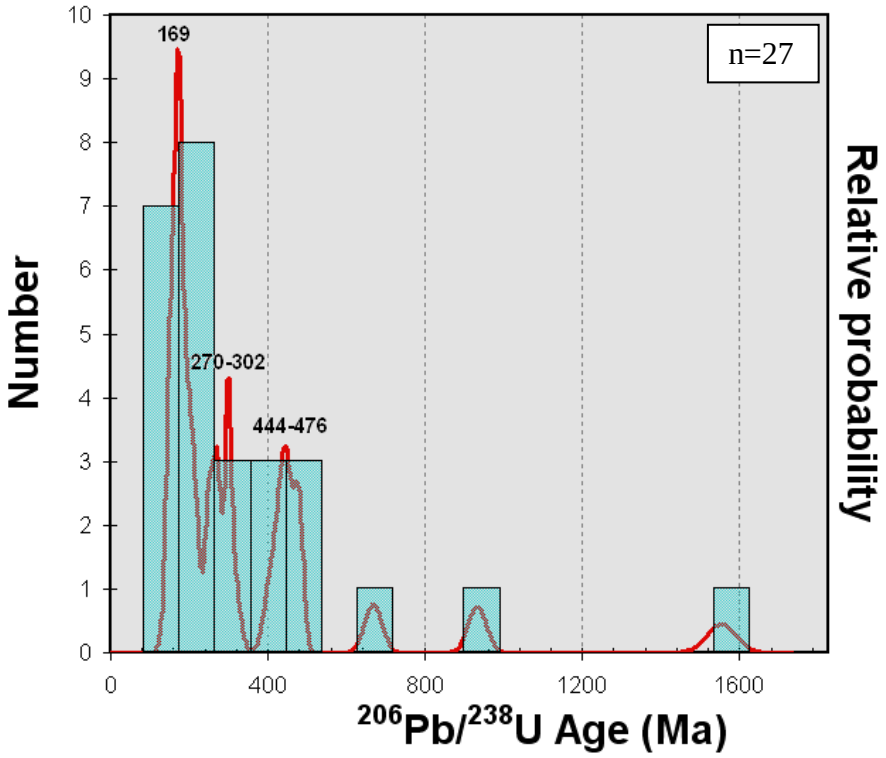

Figure. 5.30 $^{206}Pb/^{238}U$ age probability distribution function for sample 8 (McKee Formation), with number of crystals per age range (bin) represented as a simple histogram. Note dominant peak at 169 Ma.

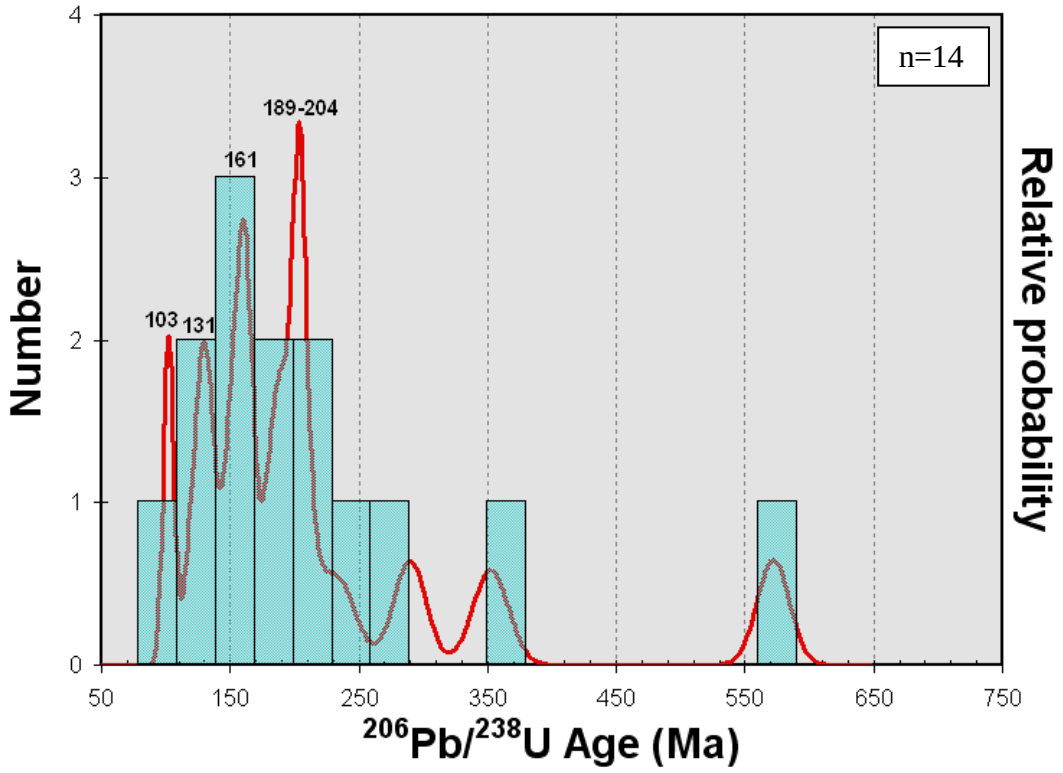

Figure. 5.31 $^{206}Pb/^{238}U$ age probability distribution function for sample 12 (Turi Formation), with number of crystals per age range (bin) represented as a simple histogram. Note significant peaks at 103 Ma, 131 Ma, 161 Ma and between 189 – 204 Ma.

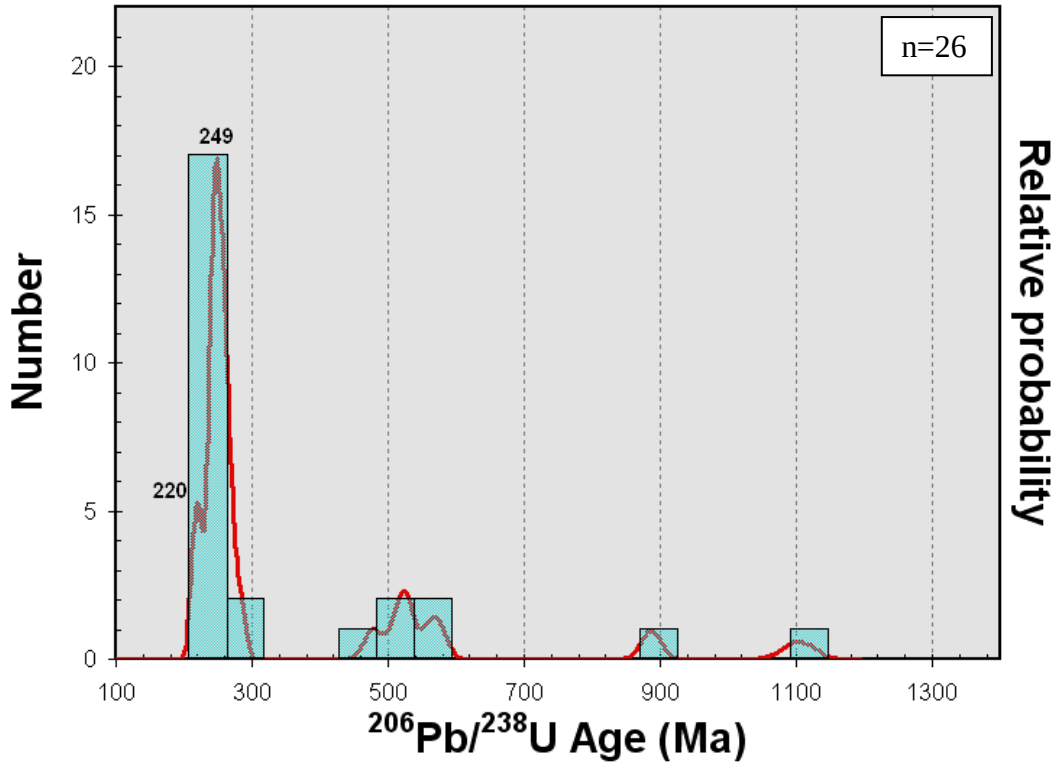

Figure. 5.32 $^{206}Pb/^{238}U$ age probability distribution function for sample 15 (Otaihanga Outlier), with number of crystals per age range (bin) represented as a simple histogram. Note the very dominant peak at 249 Ma.

Sample 10 (Matapo Sandstone)

Zircon $^{206}Pb/^{238}U$ age data for sample 10 (Matapo Sandstone) show no dominant peak, but rather a cluster of peaks with Early Cretaceous to Late Devonian ages (Fig. 5.33). The more significant peaks occur at 131 Ma (Early Cretaceous), 149 Ma (Late Jurassic), 196 Ma (Early Jurassic), 241 Ma (Middle Triassic) and 315 Ma (Late Carboniferous). The remainder and less significant peaks have Early Permian and Late Devonian ages.

Sample 7 (Taumarunui quartz sandstone)

Zircon $^{206}Pb/^{238}U$ age data for sample 7 (Taumarunui quartz sandstone) show a dominant age peak at 173 – 185 Ma (Middle to Early Jurassic) with significant minor peaks at 147 Ma (Late Jurassic), 208 Ma (Late Triassic) and 265 Ma (Middle Permian) (Fig. 5.34). The remaining ages are Late Triassic to Early Permian, Early Carboniferous to Late Permian, Early Cambrian and Neoproterozoic.

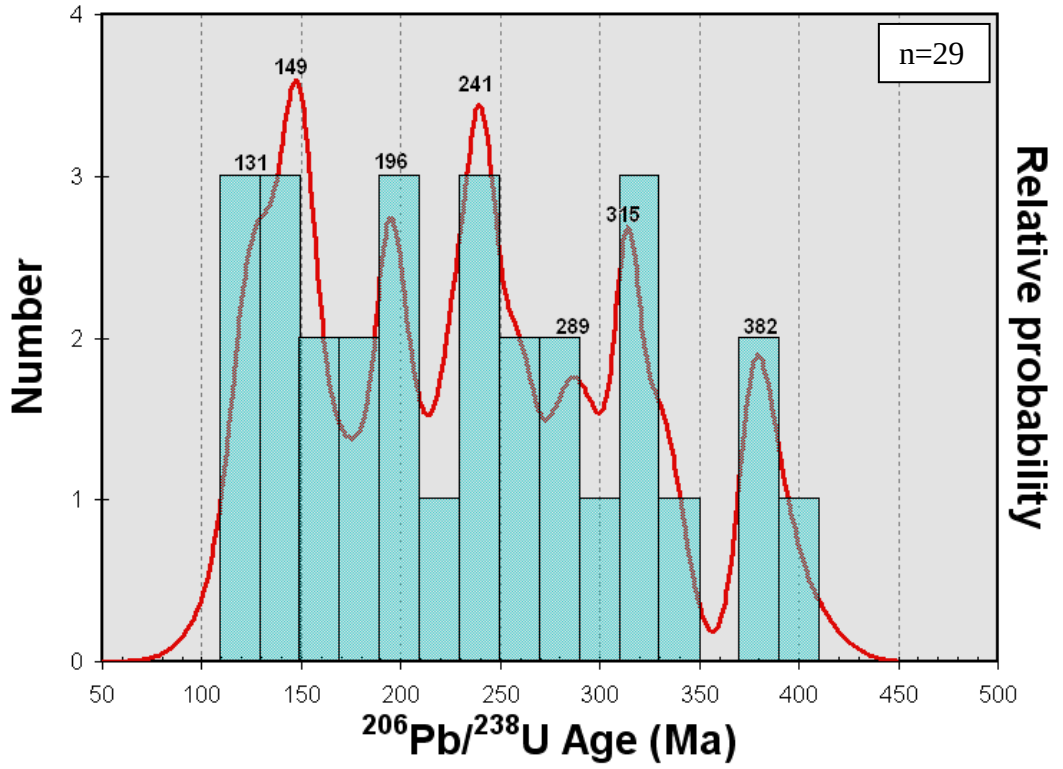

Figure. 5.33 $^{206}Pb/^{238}U$ age probability distribution function for sample 10 (Matapo Sandstone), with number of crystals per age range (bin) represented as a simple histogram. Note distribution of significant peaks from 131 to 382 Ma.

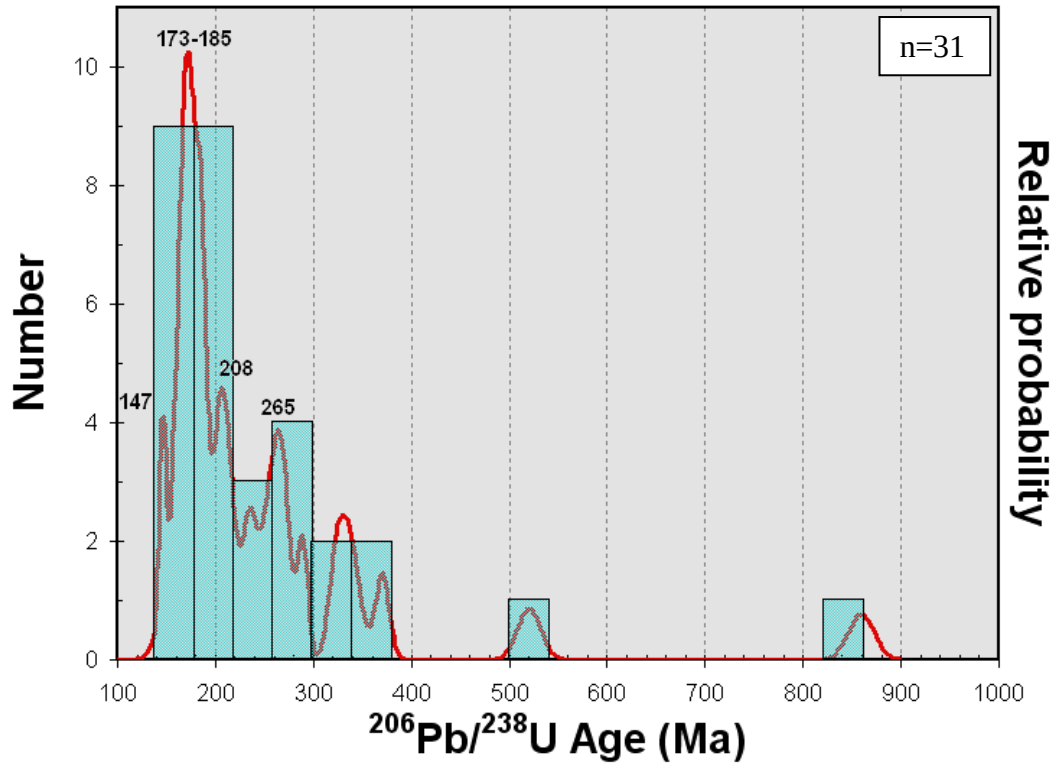

Figure. 5.34 $^{206}Pb/^{238}U$ age probability distribution function for sample 7 (Taumarunui quartz sandstone), with number of crystals per age range (bin) represented as a simple histogram. Note distribution of dominant peak occurring between 173 – 185 Ma.

Sample 1 (Ahirau Sandstone)

Zircon $^{206}Pb/^{238}U$ age data for sample 1 (Ahirau Sandstone) show dominant age peaks at 106 Ma (Early Cretaceous) and 136 Ma (Early Cretaceous), with significant minor peaks at 181 Ma (Early Jurassic) and 250 Ma (Early Triassic), and the remainder have scattered Middle Jurassic, Late Triassic to Early Permian, Carboniferous and Silurian ages (Fig. 5.35).

Sample 2 (Ahirau Sandstone)

Zircon $^{206}Pb/^{238}U$ age data for sample 2 (Ahirau Sandstone) show a very dominant age peak at 159 Ma (Middle Jurassic), with less significant peaks of Late to Early Triassic, Carboniferous, Middle Devonian to Middle Silurian and Mesoproterozoic ages (Fig. 5.36).

Sample 3 (Ahirau Sandstone)

Zircon $^{206}Pb/^{238}U$ age data from sample 3 (Ahirau Sandstone) show no dominant peaks, and rather a cluster of peaks with Early Cretaceous to Carboniferous ages. The more significant of these peaks occur between 136 – 143 Ma (Early Cretaceous), at 193 Ma (Early Jurassic), 218 Ma (Late Triassic), 242 Ma (Middle Triassic) and 356 (Early Carboniferous) (Fig. 5.37).

Aggregated Ahirau Sandstone (samples 1,2 and 3)

Aggregated Ahirau Sandstone $^{206}Pb/^{238}U$ zircon age data for samples 1, 2 and 3 show dominant age peaks at 141 – 159 Ma (Early Cretaceous – Late Jurassic) and 229 – 243 Ma (Late - Early Triassic) with less significant peaks at 105 Ma (Early Cretaceous) and 356 Ma (Carboniferous) (Fig. 5.38).

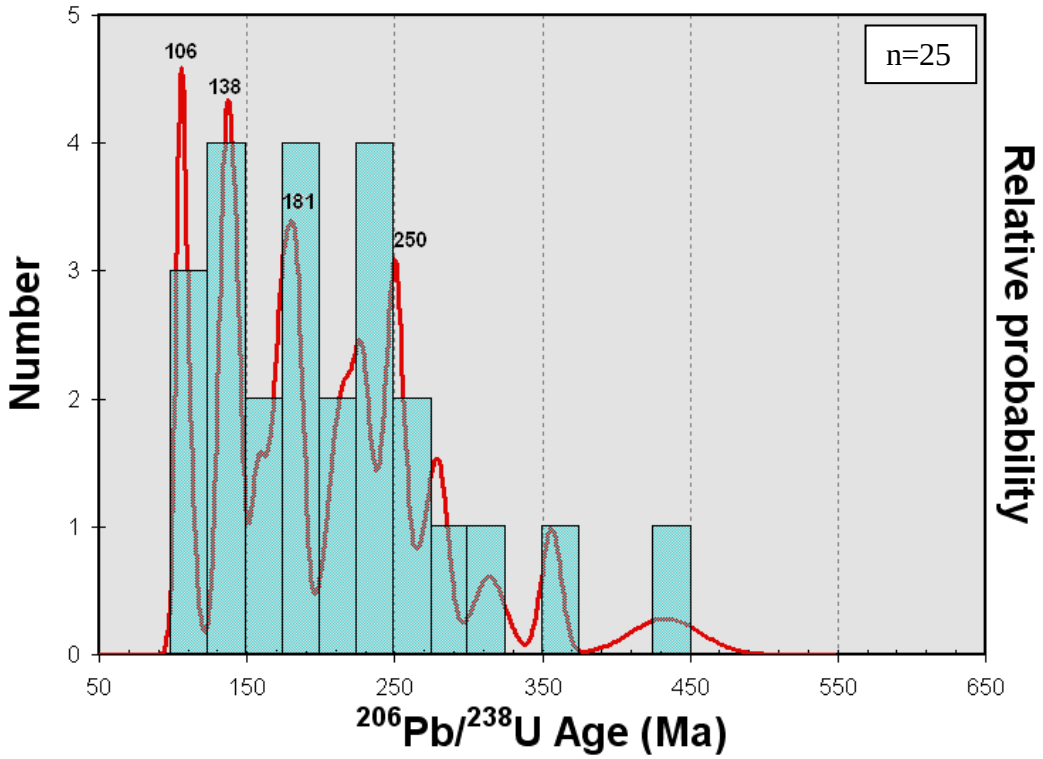

Figure. 5.35 $^{206}Pb/^{238}U$ age probability distribution function for sample 1 (Ahirau Sandstone), with number of crystals per age range (bin) represented as a simple histogram. Note range of significant peaks, occurring at 106 Ma, 138 Ma, 181 Ma and 250 Ma.

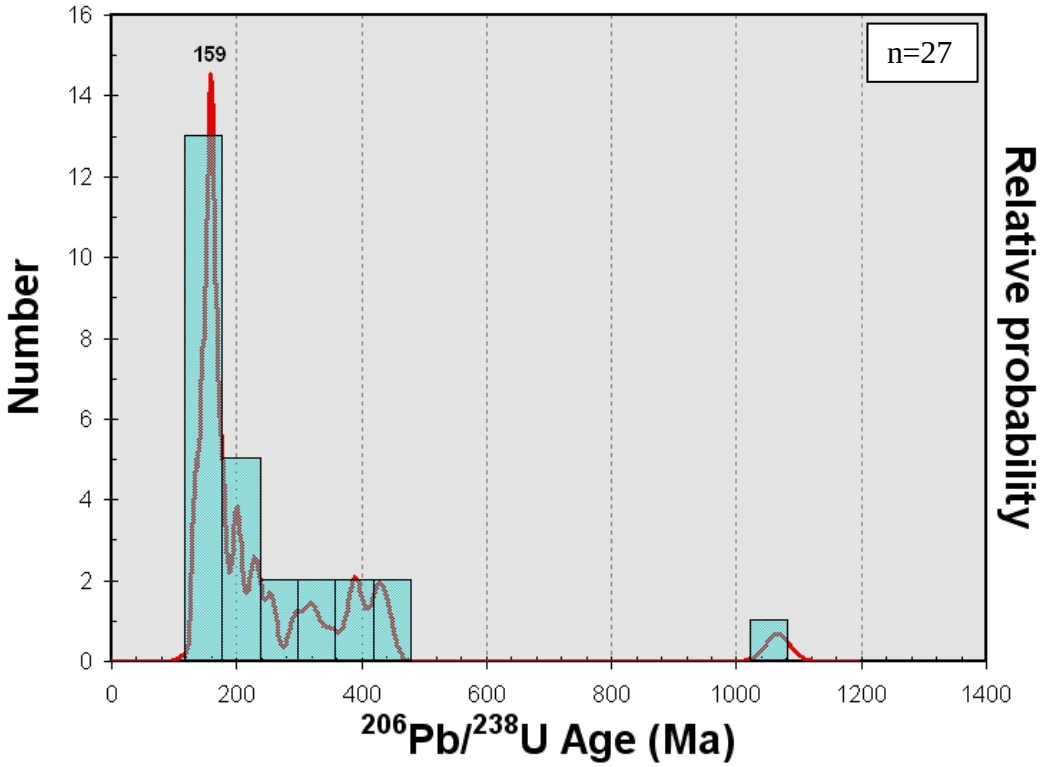

Figure. 5.36 $^{206}Pb/^{238}U$ age probability distribution function for sample 2 (Ahirau Sandstone), with number of crystals per age range (bin) represented as a simple histogram. Note very dominant peak at 159 Ma.

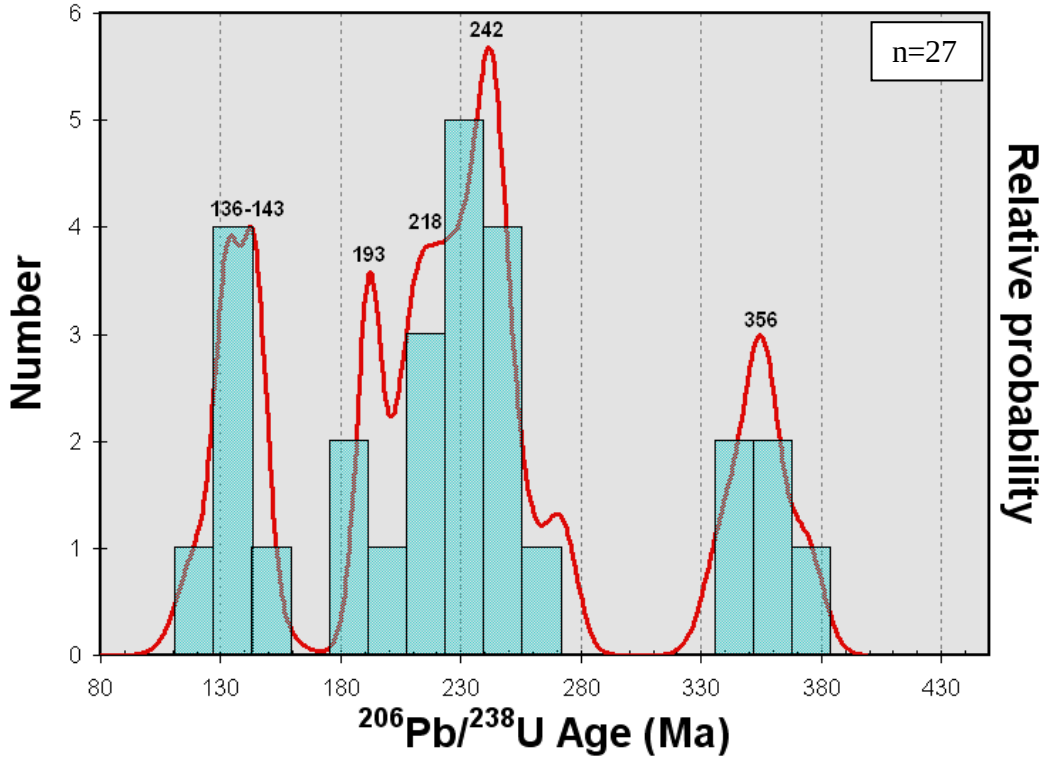

Figure. 5.37 $^{206}Pb/^{238}U$ age probability distribution function for sample 3 (Ahirau Sandstone), with number of crystals per age range (bin) represented as a simple histogram. Note age range of significant peaks, occurring between 136 – 143 Ma, at 193 Ma, 218 Ma, 242 Ma and 356 Ma.

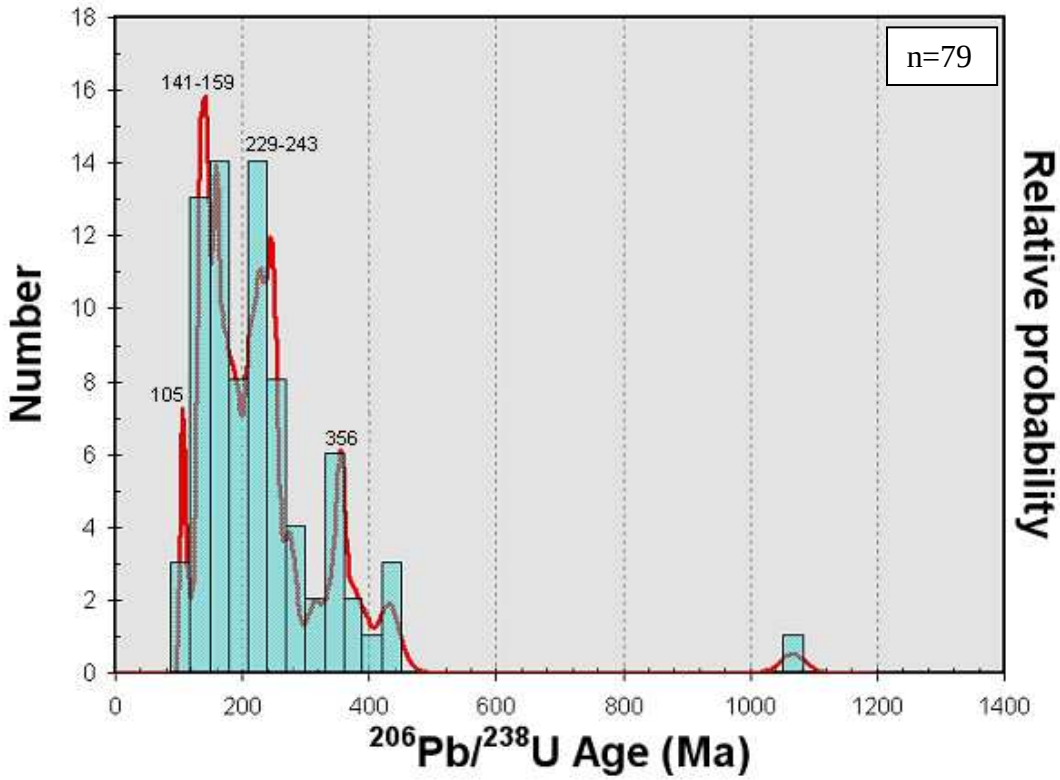

Figure. 5.38 $^{206}Pb/^{238}U$ age probability distribution function for aggregated Ahirau Sandstone samples, with number of crystals per age range (bin) represented as a simple histogram. Note age range of dominant peaks, occurring between 141 – 159 Ma and 243 - 229.

Sample 9 (Tariki Sandstone)

Zircon $^{206}Pb/^{238}U$ age data for sample 9 (Tariki Sandstone) show a dominant age peak at 123 Ma (Early Cretaceous), and the remaining ages are scattered Late Triassic to mid-Carboniferous and Middle Devonian ages (Fig. 5.39).

Sample 13 (Tariki Sandstone)

Zircon $^{206}Pb/^{238}U$ age data from sample 13 (Tariki Sandstone) show a dominant age peak at 112 – 124 Ma (Early Cretaceous), and the remaining ages are Middle to Early Jurassic, Middle Jurassic and Early Carboniferous to late Devonian ages (Fig. 5.40).

Sample 14 (Tariki Sandstone)

Zircon $^{206}Pb/^{238}U$ age data for sample 14 (Tariki Sandstone) show a dominant age peak at 124 – 136 Ma (Early Cretaceous), with significant minor peaks at 221 Ma (Early Triassic), 246 Ma (Early Triassic) and 293 Ma (Early Permian), and the remainder have scattered Carboniferous ages (Fig. 5.41).

Aggregated Tariki Sandstone (samples 9, 13 and 14)

Aggregated Tariki Sandstone $^{206}Pb/^{238}U$ zircon age data for samples 9, 13 and 14 show a very dominant age peak within the interval 116 – 124 Ma (Early Cretaceous) (Fig. 5.42). Significant minor peaks occur between 202 and 365 Ma (Late Devonian – Late Triassic).

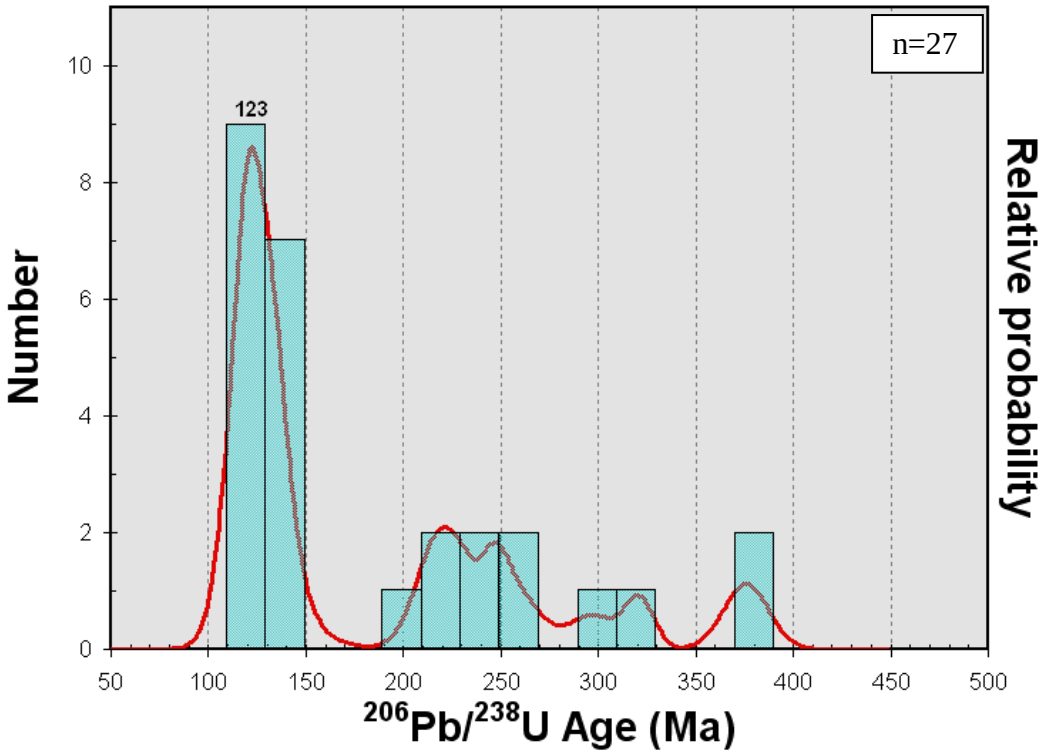

Figure. 5.39 $^{206}Pb/^{238}U$ age probability distribution function for sample 9 (Tariki Sandstone), with number of crystals per age range (bin) represented as a simple histogram. Note dominant peak at 123 Ma.

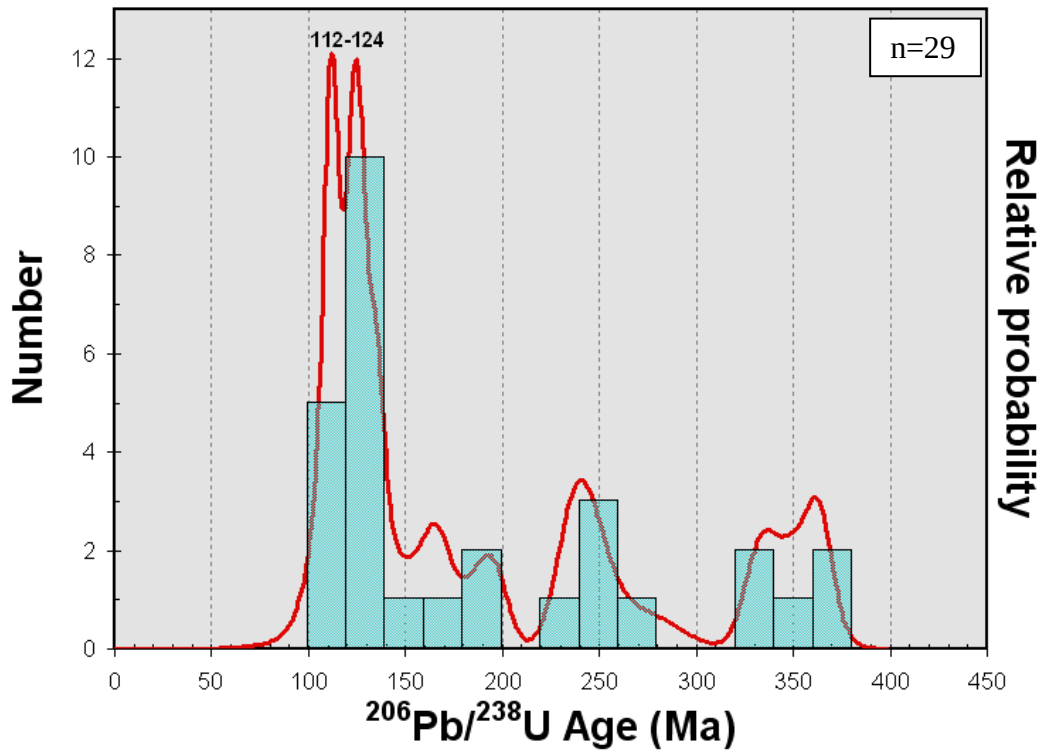

Figure. 5.40 $^{206}Pb/^{238}U$ age probability distribution function for sample 13 (Tariki Sandstone), with number of crystals per age range (bin) represented as a simple histogram. Note dominant peaks between 112 – 124 Ma.

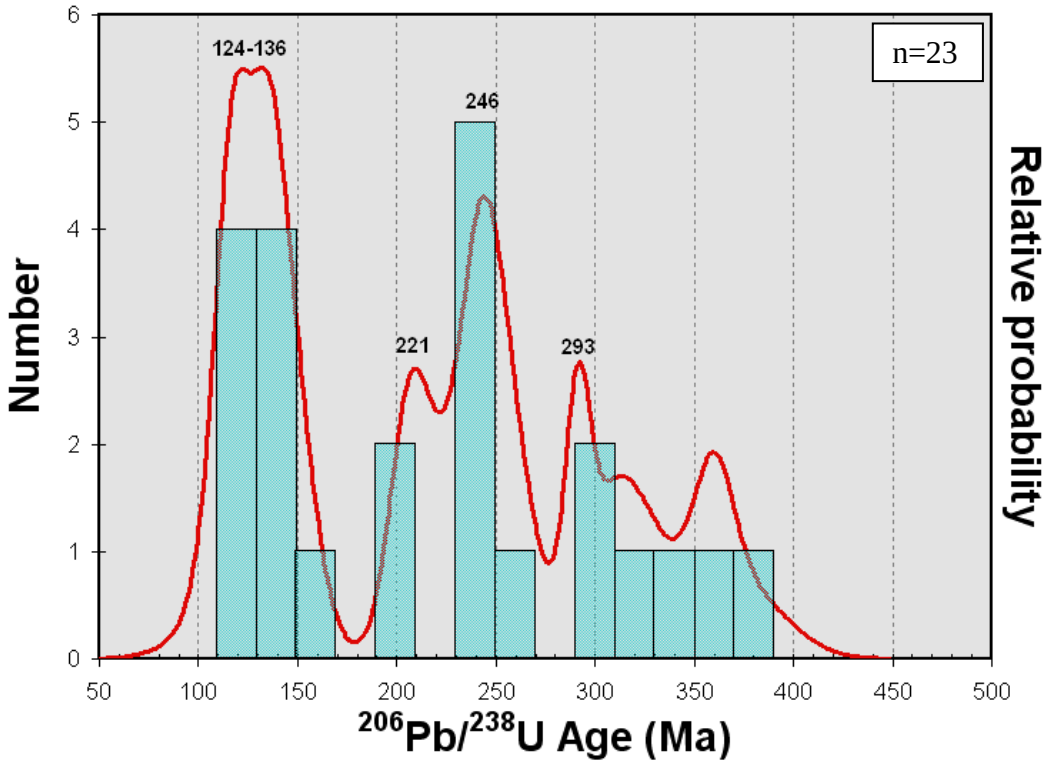

Figure. 5.41 $^{206}Pb/^{238}U$ age probability distribution function for sample 14 (Tariki Sandstone), with number of crystals per age range (bin) represented as a simple histogram. Note dominant peak between 124 – 136 Ma, and large age range of significant minor peaks.

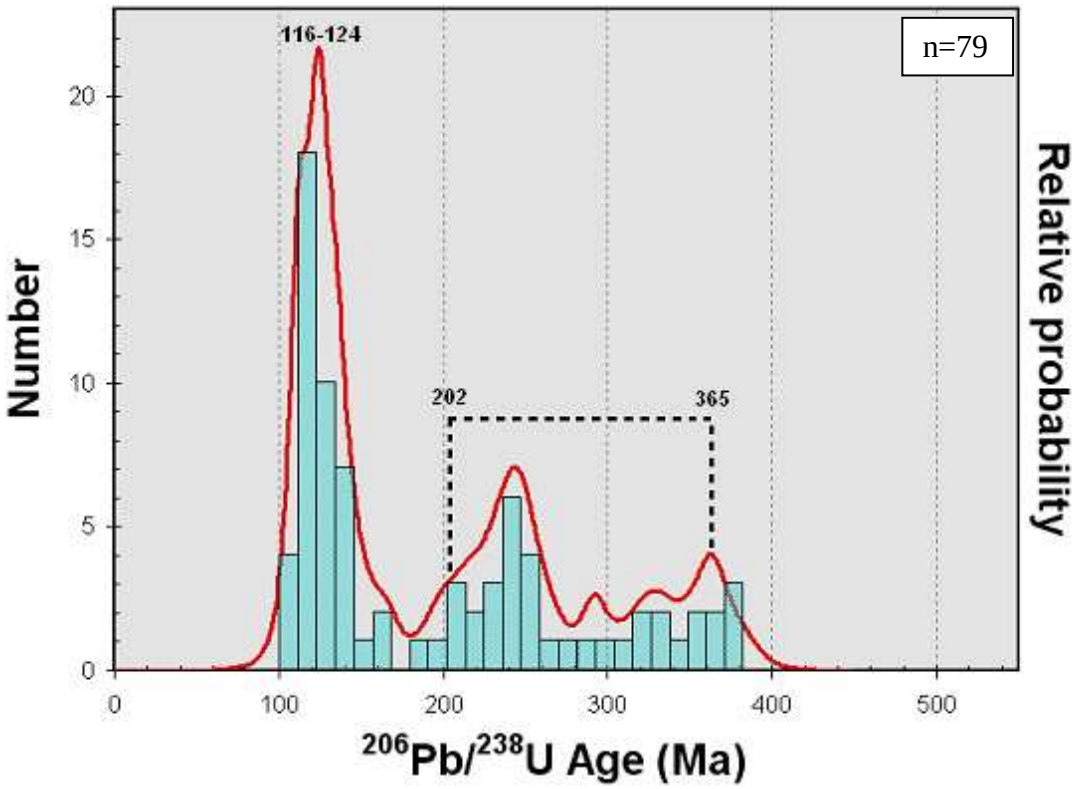

Figure. 5.42 $^{206}Pb/^{238}U$ age probability distribution function for aggregated Tariki Sandstone samples, with number of crystals per age range (bin) represented as a simple histogram. Note dominant age peak, occurring between 116 – 124 Ma.

Sample 5 (Hauturu Sandstone)

Zircon $^{206}Pb/^{238}U$ age data for sample 5 (Hauturu Sandstone) show a very dominant age peak at 120 Ma (Early Cretaceous) and a significant minor peak at 135 Ma (Early Cretaceous), with less significant peaks showing Late and Early Jurassic, Carboniferous to Silurian and Neoproterozoic ages (Fig. 5.43).

Sample 6 (Hauturu Sandstone)

Zircon $^{206}Pb/^{238}U$ age data for sample 6 (Hauturu Sandstone) show a dominant age peak at 117 Ma (Early Cretaceous) and a significant minor peak at 328 – 345 Ma (Carboniferous) (Fig. 5.44). The remaining ages show minor peaks of Late and Early Jurassic and Late Triassic ages.

Aggregated Hauturu Sandstone (samples 5 and 6)

Complied Hauturu Sandstone zircon $^{206}Pb/^{238}U$ age data for samples 5 and 6 show a dominant age peak at 121 Ma (Early Cretaceous) with less significant peaks at 136 (Early Cretaceous), 154 (Late Jurassic) and 328 Ma (Carboniferous) (Fig. 5.45).

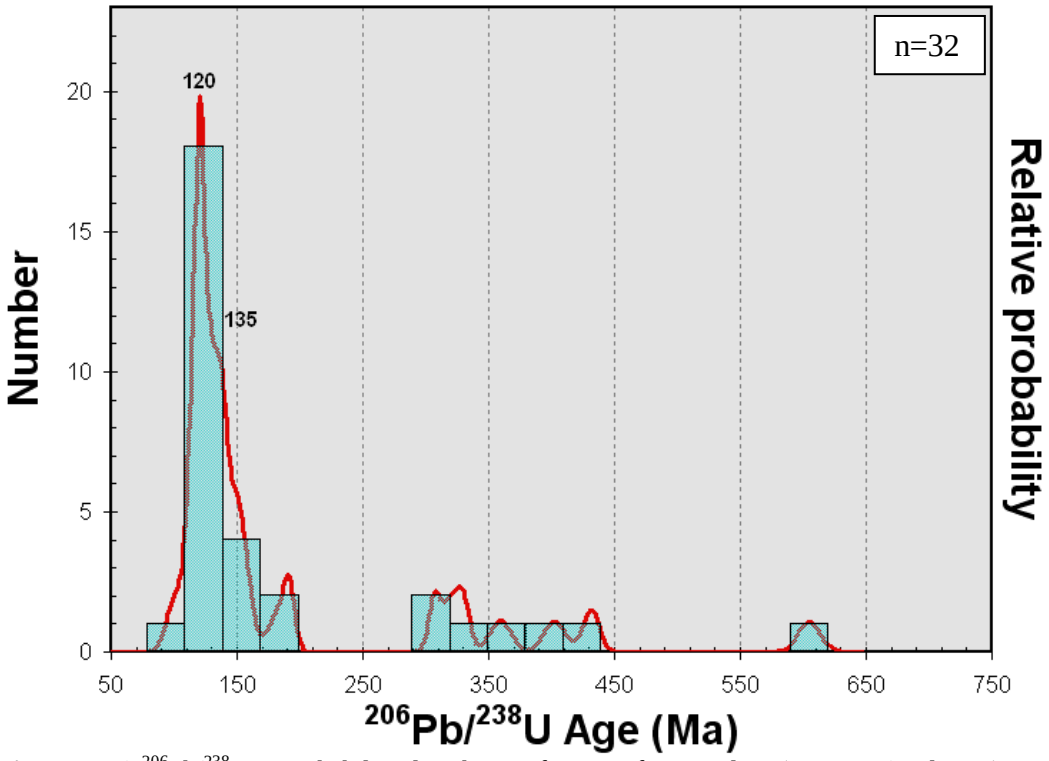

Figure. 5.43 $^{206}Pb/^{238}$ age probability distribution function for sample 5 (Hauturu Sandstone), with number of crystals per age range (bin) represented as a simple histogram. Note very dominant peak at 120 Ma.

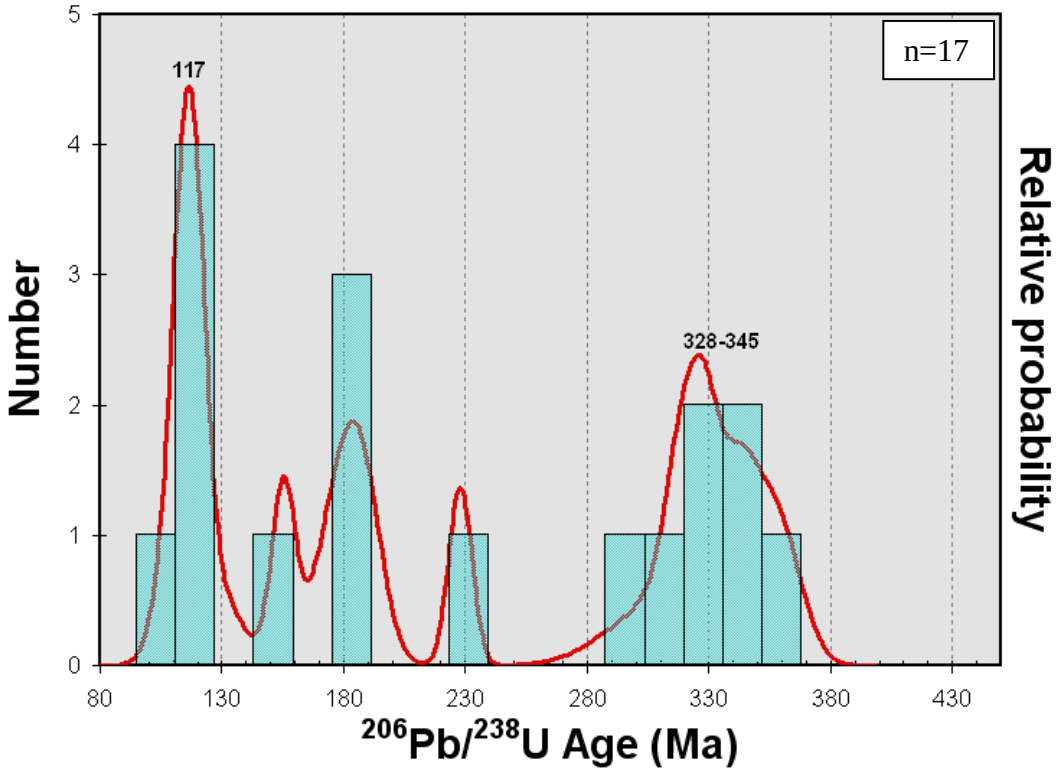

Figure. 5.44 $^{206}Pb/^{238}U$ age probability distribution function for sample 6 (Hauturu Sandstone), with number of crystals per age range (bin) represented as a simple histogram. Note very dominant peak at 117 Ma.

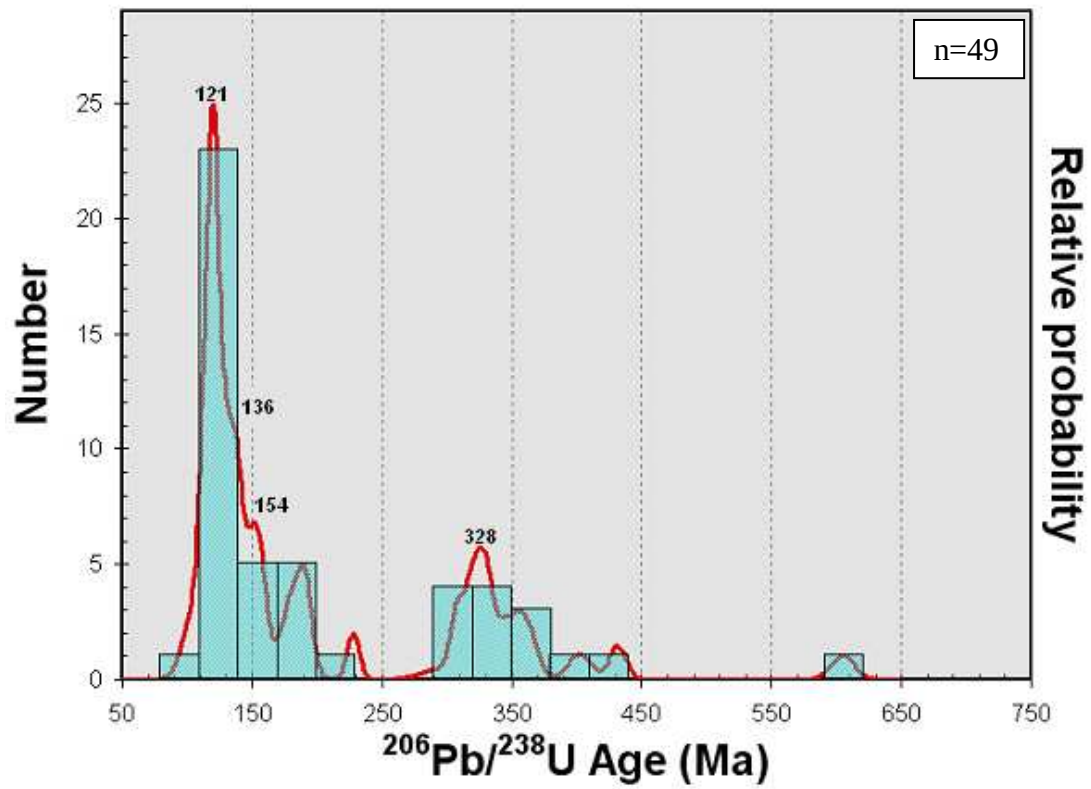

Figure. 5.45 $^{206}Pb/^{238}U$ age probability distribution function for aggregated Hauturu Sandstone samples, with number of crystals per age range (bin) represented as a simple histogram. Note very dominant age peak at 121 Ma.

5.4 INTERPRETATION OF SEDIMENT PROVENANCES

If the U-Pb age or age distributions of potential source rocks supplying sediments to a sedimentary basin are known, U-Pb dating of detrital zircon within basin sediments may be used to constrain the provenance of those sediments (Campbell et al. 2005). In some cases there may be a direct correlation between U-Pb ages in the source areas versus the sediments. However, the situation may be more problematic due to a range of factors including the recycling of zircon from pre-existing sediments as well as multiple first cycle sources such as plutons. Campbell et al. (2005) describe first-cycle zircons as those that crystallised during the orogenic event that created the topography from which the zircons were exhumed in the most recent cycle of erosion and sedimentation. Multi-cycle zircons are those that are derived from pre-existing sedimentary rocks. The U-Pb dating technique applied in this study does not directly give an indication of whether or not crystals are first cycle, or have been derived from an igneous source. Provenance interpretation can also become quite ambiguous if populations show mixed zircon age patterns such as bimodal/multimodal peaks on age probability distribution plots (Campbell et al. 2005).

Age patterns expressed in age probability distribution plots (as included in Section 5.3.3) can be used to constrain provenance if the U-Pb ages of zircons within potential source terranes are known (Campbell et al. 2005). Many workers have contributed to determination of the U-Pb ages of zircons within New Zealand basement terranes. These data have been compiled by Mortimer (2004) for Cretaceous to Devonian terranes of volcanic, sedimentary and plutonic heritage, some of which exhibit metamorphic overprinting. For the 13 sample populations analysed in this thesis, grains with ages less than about 200 Ma have possibly been derived from igneous plutonic sources, grains greater than 500 Ma probably have more complex histories as multi-cycle zircons.

5.5 CONCLUSIONS

As zircon is a common accessory mineral in most rock types, U-Pb dating is a widely applied technique to determine constraints on formation ages. With technology developments over the last decade U-Pb geochronology via laser ablation ICP-MS has proved to be a reasonably precise and valuable tool. This

chapter has outlined data quality issues encountered while performing laser ablation ICP-MS dating on zircon populations from 13 Late Eocene – Oligocene sedimentary rocks from Taranaki Basin and North Island equivalents, including the Te Kuiti Group exposed onshore in central-western North Island. By plotting concordia diagrams for the data derived for each of the samples, the degree of concordance, or otherwise, of the grains can be determined as an important means of control on the quality of the data. The geological interpretation of the U-Pb data is best made by plotting the $^{206}Pb/^{238}U$ age data on probability distribution plots. This gives a spectra of the detrital ages for each sample and hence the dominant ages.

CHAPTER 6

PROVENANCE AND PALEOGEOGRAPHY

6.1 INTRODUCTION

This chapter summarises the U-Pb zircon ages for New Zealand terranes/sub-terranes (Fig. 6.1) and discusses their general petrography. The provenance of Late Eocene – Oligocene sedimentary units investigated in this study are subsequently interpreted using petrographic and U-Pb geochronology data developed in the preceding chapters. The chapter concludes by discussing the paleogeographic evolution of eastern Taranaki Basin margin for five intervals through the Late Eocene to earliest Miocene.

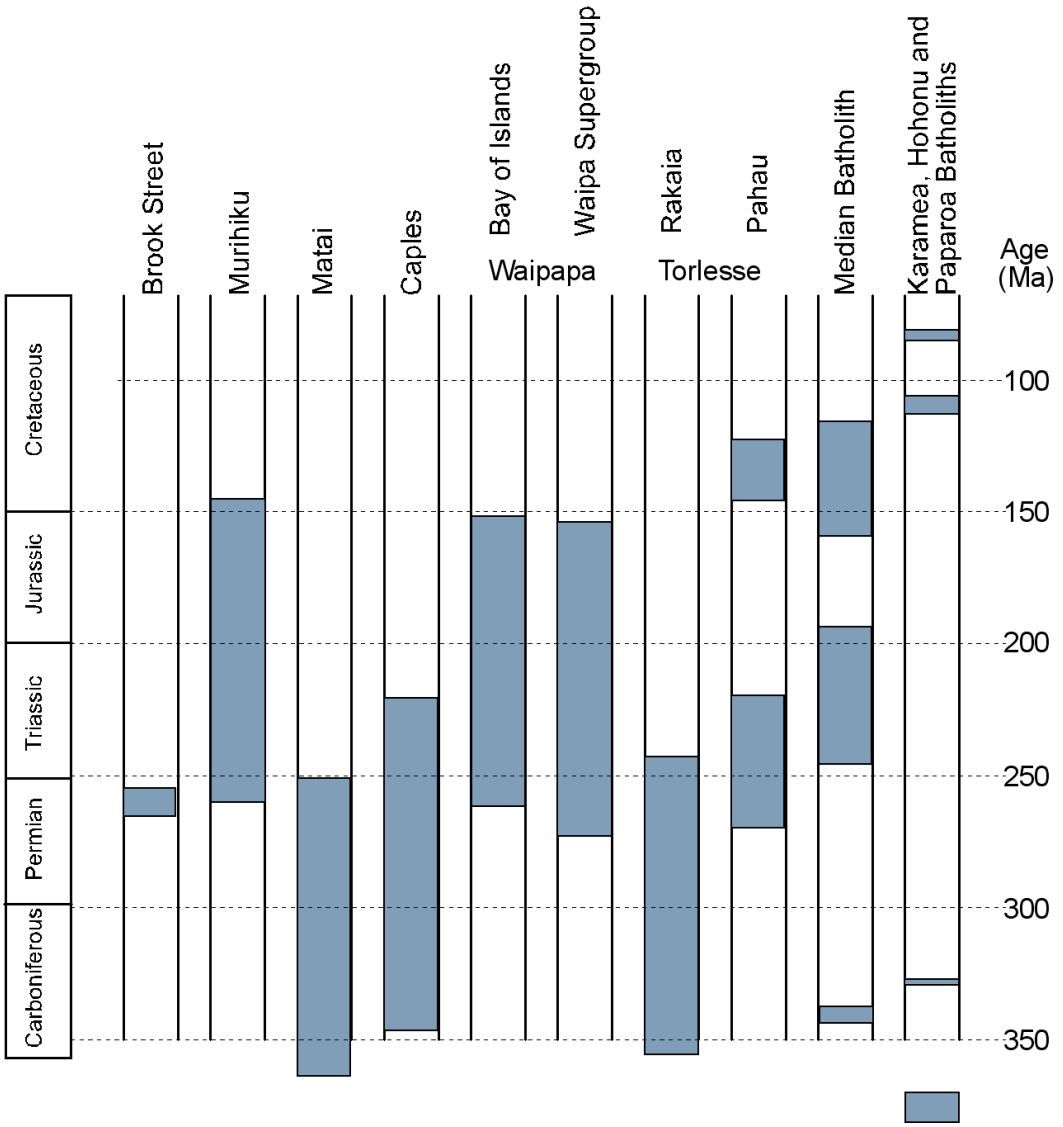

Figure 6.1. The dominant U-Pb zircon age ranges for New Zealand basement. Adapted from Kimbrough et al. 1994; Muir et al. 1996; Waight et al. 1997; Cawood et al. 1999; Adams et al. 2002; Wandres et al. 2004a; Wandres et al. 2004b; Adams et al. 2007.

6.2 U-Pb ZIRCON AGE AND LITHOLOGY OF BASEMENT TERRANES

Brook Street Terrane

The Brook Street Terrane is a primitive intraoceanic island arc assemblage dominated by basaltic volcanics, basaltic to andesitic breccias, volcaniclastics and associated sediments including limestone (Landis et al. 1999; Mortimer 2004; Spandler et al. 2005). The Brook Street Terrane is situated west of the Murihiku Terrane in the Nelson area and in the subsurface to the north (Taranaki Basin) and south of the Southland Syncline (Murihiku Terrane) in eastern Southland (Fig. 2.8). In Adams et al. (2007) U-Pb zircon ages have been derived for the Brook Street Terrane in the Nelson area. Most U-Pb zircon ages range from middle to Late Permian (265 –256 Ma), coinciding with the stratigraphic age of the Brook Street Terrane. A minor peak of significantly older (>300 Ma) ages are possibly derived from inherited grains.

Murihiku Terrane

The Murihiku Terrane is an andesitic volcaniclastic sandstone succession dominated by volcanic rock fragments and feldspar with much less abundant detrital quartz (see Section 4.5) (Briggs et al. 2004). The Murihiku Terrane occurs in outcrop along the western margin of the North Island from Awakino to Port Waikato, and in Southland (Fig. 2.8). The terrane is inferred to occur in the subsurface south of Awakino and to the north of Port Waikato. In Adams et al. (2007) U-Pb zircon ages have been derived for the Murihiku Terrane in the North Island (Waikato Region) and South Island (Southland/Otago) areas. Most U-Pb zircon ages range from latest Devonian to Late Jurassic (361 – 141 Ma). The U-Pb zircon ages are within the stratigraphic age of the terrane, which varies between ~260 and 145 Ma (Late Permian – latest Jurassic) (Adams et al. 2007). The youngest U-Pb zircon ages constrain the youngest age of magmatism in the source region of the Murihiku Terrane, whereas the oldest zircons are possibly inherited or recycled.

Maitai Terrane

The Maitai Terrane consists of an Early Permian ophiolite belt (Dun Mountain Belt) overlain by Permian – Triassic volcaniclastic siltstone and sandstone (Matai Group) (Adams et al. 2002). The Matai Terrane is situated east of the Murihiku Terrane between Nelson and Auckland, and north of the Murihiku Terrane in the Southland area (Fig. 2.8). In Adams et al. (2002; 2007) U-Pb zircon ages have been derived for the Maitai Terrane in the Southland and Nelson areas. Most U-Pb zircon ages range from Late Devonian to Late Permian (364 – 251 Ma), with a less significant older peak at >400 Ma). The younger group of ages are mainly in the range 270 – 251 Ma and help constrain the youngest age of magmatism in the source region (Adams et al. 2002). The old zircon grains are possibly inherited (recycled) from other terranes.

Caples Terrane

Caples Terrane is a weakly metamorphosed sequence of volcaniclastic (mostly andesitic) greywacke and argillite with rare lavas, chert and limestone (Roser et al. 1993; Mortimer 2004, after MacKinnon 1983). The Caples Terrane is situated in east Nelson and in northern Southland and west Otago (Fig. 2.8). U-Pb zircon ages for the Caples Terrane in west Otago, and Nelson range from 347 to 221 Ma (Carboniferous – Late Triassic) with the dominant age peaks at 260 and 221 Ma (Late Permian – Late Triassic). The youngest ages (~221 Ma) correspond to the depositional age of the Caples Terrane, which is 230 – 220 Ma (Adams et al. 2007).

Waipapa Terrane – Hunua - Bay of Islands Terrane

The Hunua - Bay of Islands Terrane (Bay of Islands Terrane) consists of basalt, chert and limestone associations with mudstone and quartz rich sandstone (Mortimer 2004, after, Black 1994) and crop out along the east coast of Auckland and Northland, including the Bay of Islands (Fig. 2.8). In Adams et al. (2007) U-Pb zircon ages have been derived from the Bay of Islands Terrane in the North Auckland and Northland regions with two distinct age groups recognised, the first between 158 and 152 Ma (mid – Late Jurassic) and the second between 262 and

207 Ma (Middle Permian – Late Triassic). Both age groups correspond with the approximate depositional age of the Bay of Islands Terrane (Adams et al. 2007).

Waipapa Terrane – Waipa Supergroup

The Waipa Supergroup of Kear and Mortimer (2003) is a Median Batholith-derived (granite dominated) volcaniclastic blanket of Late Jurassic to Early Cretaceous age (Mortimer 2004). The Waipa Supergroup is located along much of the east coast of the North Island including Bay of Plenty and eastern Waikato areas (Fig. 2.8). In Adams et al. (2007) and Cawood et al. (1999) U-Pb zircon ages have been obtained for the Waipa Supergroup from the Waikato and eastern Bay of Plenty regions yielding mostly Early Permian to Late Jurassic (274 – 154 Ma) U-Pb ages, the youngest of which corresponds to the depositional age of the Waipa Supergroup, which is 160 to 133 Ma (Adams et al. 2007).

Torlesse Terrane – (Rakaia Sub-terrane)

The Rakaia Sub-terrane (terrane) is mostly a turbiditic sequence of quartzofeldspathic sandstone and mudstone of Permian to Late Triassic age (Mortimer 2004). The Rakaia terrane occurs in central North Island, east Nelson and over much of central South Island (Fig. 2.8). In Wandres et al. (2004b), U-Pb zircon ages for the Rakaia terrane have been derived from igneous clasts (both volcanic and plutonic) obtained from terrane in South Island. The igneous clasts produced U-Pb peaks at 292 to 243 Ma (Early Permian – Middle Triassic), 325 to 356 Ma (Carboniferous) and 497 and 517 Ma (Cambrian) (Wandres et al. 2004b). Ages have also been determined for two Rakaia sandstone samples, being mostly of Carboniferous – Triassic (349 – 237 Ma) age, with grains as old as 1,500 Ma (Mesoproterozoic). The youngest ages determined were ~ 238 Ma (Middle Triassic) reflecting the age of plutons contributing erosion products to the terrane (Wandres et al. 2004b).

Torlesse Terrane – (Pahau Sub-terrane)

The Pahau Sub-terrane (terrane) has an inferred recycled Rakaia terrane and Median Batholith provenance, with mostly quartzose sandstone and mudstone

sequences with rare limestone and chert. Pahau terrane occurs in central North Island and in northeastern South Island (Kaikoura area) (Fig. 2.8). In Wandres et al. (2004a) U-Pb zircon ages for the Pahau terrane have been derived from igneous clasts (both volcanic and plutonic) from conglomerate and from sandstone conglomerate clasts. The igneous clasts have Middle Permian to Late Triassic and Late Jurassic to Early Cretaceous ages, ranging between 270 to 220 Ma and 147 to 123 Ma (Wandres et al. 2004a; Adams et al. 2007*)*. Age determinations for the sandstone matrix are mainly of Early Cretaceous age (140 – 120 Ma), with the youngest being 111.7 Ma.

The Pahau Sub-terrane was probably derived from granitiods of the Median Tectonic Zone (Darren Suite and Electric Granite) and the older parts of the Rakaia terrane (Wandres et al. 2004a). A Pahau terrane provenance is not likely for the Late Eocene – Oligocene sediments in Taranaki Basin as this terrane was possibly not exhumed during this period, being buried beneath the bathyal Paleogene succession in Marlborough and eastern North Island.

Median Batholith Terrane

The Median Batholith is a composite batholith comprising dozens of small (1-10 km size) gabbroic to granitic batholiths (see Section 2.4) (Mortimer 2004) situated in the offshore western North Island, northwest Nelson and Southland/Fiordland areas (Fig. 2.8). In Scott and Palin (2008), intrusives from the Darran/Median Suite have yielded Middle Jurassic to Early Cretaceous ages (160.6 - 127.9 Ma). Zircons from the younger Separation Point Suite have yielded Early Cretaceous U-Pb zircon ages (123.5 - 116.3 Ma). In Kimbrough et al. (1994) most plutonic units from the Median Batholith have Middle Jurassic to Early Cretaceous U-Pb zircon ages. However, plutons of the Median Batholith Suite with older Early Triassic to Early Jurassic (247 – 195 Ma) and Carboniferous (343 and 337 Ma) U-Pb zircon ages have also been identified (Kimbrough et al. 1994).

Karamea, Hohonu and Paparoa Batholiths

The Karamea, Hohonu and Paparoa Batholiths are granite-dominated (Mortimer 2004) and are situated in northwestern South Island (Fig. 2.8) for which U-Pb

zircon ages have been derived (Muir et al. 1996). U-Pb zircon ages yielded from the Karamea Batholith are of Late Devonian age, ranging between 380.4 to 370.7 Ma. Zircon ages from the Paparoa Batholith are younger and of Carboniferous age (328.6 – 327.3 Ma) (Muir et al. 1996). The Hohonu Batholith has mostly Early Cretaceous ages (113.5 to 108.7 Ma) with peaks at 381.2 Ma (Late Devonian) and 81.7 Ma (Late Cretaceous) (Waight et al. 1997).

6.3 PROVENANCE OF LATE EOCENE-OLIGOCENE UNITS

In the following section the possible source rocks of the Late Eocene – Oligocene Taranaki Basin and Te Kuiti units are inferred from comparison of the U-Pb age characteristics of samples (Section 5.3.3) with the U-Pb ages of zircons from New Zealand terranes (Section 6.2). Potential basement sources are then supported or discounted based on the comparison of the petrographic characteristics of samples and basement.

6.3.1 McKee Formation

The youngest and dominant U-Pb zircon age peak of 169 Ma (Fig. 5.30) is consistent with the dominant U-Pb zircon peak ages of the Murihiku Terrane and Waipapa Terrane (Bay of Islands Terrane and Waipa Supergroup). A quartz content of ~34% (Section 4.4.3) is much higher than Murihiku Terrane rocks, discounting them as the primary source rocks for the McKee Formation. The Waipapa Terrane has a similar quartz content to the McKee Formation. The abundance (~45%) of very fine-grained sedimentary rock fragments in McKee Formation samples (Section 4.4.3) also supports a possible Waipapa Terrane provenance.

6.3.2 Turi Formation

On Fig. 5.31 for the Turi Formation four major age peaks occur at 103, 131, 161 and 189 – 204 Ma. The youngest age (103 Ma) does not fall within the dominant U-Pb zircon age range of any New Zealand terranes (Fig. 6.1), however, Torlesse sediments in the Wellington and Bay of Plenty areas have yielded U-Pb zircon ages of 106±5 Ma and 100±2 Ma respectively (Cawood et al. 1999; Pickard et al.

2000) that are likely sourced from granites of the Median Tectonic zone. The 131 Ma age peak on Fig. 5.31 is consistent with the U-Pb zircon age of the Darran/Median Suite of the Median Batholith. The 161 Ma peak on Figure 5.31 is consistent with the U-Pb zircon age range of the Murihiku and Waipapa terranes. The main peak on Figure 5.31 (189 – 204 Ma) is consistent with the main U-Pb zircon age peak for the Brook Street Terrane, Murihiku Terrane and Waipapa Terrane. The abundance of fine-grained sedimentary rock fragments (52%) and quartz grains (30%) in Turi Formation (Section 4.4.3) discounts the Murihiku and Brook Street terranes and supports a dominant Waipapa Terrane provenance similar to that for McKee Formation, with an additional Median Tectonic Zone and Darran/Median Suite source accounting for younger age peaks of 103 and 131 Ma, respectively.

6.3.3 Otaihanga Outlier

The U-Pb zircon age probability distribution peak of 249 Ma (Fig. 5.32) is consistent with the dominant U-Pb zircon ages of the Murihiku Terrane, Caples Terrane, Waipapa Terrane and the Rakaia terrane. Although no petrographic data were obtained for this unit in this study the Otaihanga Outlier has been described as a quartzose sandstone by King and Thrasher (1996), discounting quartz poor terranes (Murihiku Terrane) as dominant source rocks. A dominant Waipapa Terrane, Caples Terrane and/or Rakaia terrane provenance are the most likely sources of the Otaihanga Outlier.

6.3.4 Matapo Sandstone

The Matapo Sandstone has seven significant age peaks (Fig. 5.33) between 382 and 131 Ma, the younger of which are possibly more diagnostic of particular source rocks. The 131 Ma peak is consistent with the main U-Pb zircon ages for the Darran/Median Suite of the Median Batholith. The 149 Ma peak (Fig. 5.33) is consistent with ages for the Murihiku Terrane as well as the Darran/Median Suite. The 196 Ma peak (Fig. 5.33) is consistent with the main U-Pb zircon ages for the Murihiku Terrane, Waipapa Terrane (Bay of Islands Terrane and Waipa Supergroup) and Median Batholith. The older age peaks on Fig. 5.33 (382 Ma, 315 Ma, 289 Ma and 241 Ma) are consistent with a wide range of New Zealand

terranes (including Brook Street Terrane, Murihiku Terrane, Matai Terrane, Caples Terrane, Waipapa Terrane, Torlesse Terrane and the Median Batholith). Matapo Sandstone has abundant fine-grained sedimentary rock fragments and relatively minor quartz (in the sample examined) suggesting the Waipapa and/or Caples Terrane as a principal source rocks. However the occurrence of the younger (149 and 131 Ma) zircons suggest a Median Batholith source contributed to Matapo Sandstone as well. The oldest peak ages (382 Ma; Fig. 5.33) are consistent with U-Pb zircon ages from the Karamea Batholith.

6.3.5 Taumarunui quartz sandstone

The main U-Pb zircon age peak between 185 and 173 Ma (Fig. 5.34) for the Taumarunui quartz sandstone is consistent with the main U-Pb zircon ages for the Murihiku Terrane and Waipapa Terrane (Bay of Islands Terrane and Waipa Supergroup). The youngest age peak (147 Ma) is consistent with the youngest parts of the Murihiku Terrane and the Darran/Median Suite of the Median Batholith. The high quartz component (57%) of the Taumarunui quartz sandstone (Section 4.4.3) discounts the quartz poor Murihiku Terranes as dominant source rocks, leaving the Waipapa Terrane and Median Batholith as the main provenance. The abundance of fine-grained sedimentary rock fragments (22%) in the quartz sandstone may also point to the Waipapa Terrane as the chief provenance.

6.3.6 Ahirau Sandstone Member

U-Pb zircon ages for aggregated Ahirau Sandstone samples have Carboniferous to Early Cretaceous ages (356 – 105 Ma) (Fig. 5.38). The youngest age peak of 105 Ma (sample 1) is consistent with ages yielded from Torlesse sediments (i.e. 106 Ma, Pickard et al. 2000), which were likely derived from Median Batholith plutons. The age peaks of 159 and 141 Ma (Late Jurassic - Early Cretaceous) (Fig. 5.35) are consistent with the main U-Pb ages of the Darran/Median Suite of the Median Batholith. The significant Middle Triassic to Late Triassic age peaks (243 – 229 Ma) observed (Fig. 5.38) are consistent with the U-Pb zircon ages of many New Zealand terranes, including Murihiku Terrane, Caples Terrane, Waipapa Terrane and the Median Batholith. These Late Triassic to Early Jurassic ages are

likely derived from a mixture of Waipapa, Caples and Murihiku Terranes. Dominant derivation from the Median Batholith (i.e. the Darran/Median Suite), the Waipapa Terrane and/or Caples Terrane and the Murihiku Terrane is supported by the abundant quartz component (~55 %) and sedimentary rock fragment component (~18%), large orthoclase feldspar grains, minor volcanic rock fragments and the very abundant amphibole components (Section 4.4.3). The oldest significant minor ages of Fig. 5.38 are possibly derived from the Rakaia terrane.

6.3.7 Tariki Sandstone Member

Aggregated U-Pb ages for several Tariki Sandstone samples identify an Early Cretaceous (124 – 116 Ma) peak (Fig. 5.42), which is the same as the U-Pb zircon age range of the Separation Point Suite of the Median Batholith. The high quartz component (~51 %), trace granitic rock fragments, epidote and sphene content (Section 4.3.3) of the sandstone supports a main Separation Point Suite (granitic) provenance. The abundant sedimentary rock fragment component (21%), trace amounts of orthoclase feldspar (4%) and volcanic rock fragments (4%) observed in Tariki Sandstone samples (Section 4.4.3) however suggests an additional sedimentary basement source (e.g. Waipapa Terrane), and possibly to a lesser extent a volcaniclastic sedimentary source (e.g. Murihiku Terrane). The older peaks that occur between 365 and 202 Ma (Late Permian – Late Triassic) (Fig. 5.42) support Waipapa, Caples and Murihiku Terranes provenance. A dominant Separation Point Suite source is therefore inferred for Tariki Sandstone, with additional Waipapa Terrane and minor Murihiku Terrane, Caples Terrane and/or Rakaia terrane provenance.

6.3.8 Hauturu Sandstone Member

The dominant Early Cretaceous U-Pb zircon age peak of 121 Ma (Fig. 5.45) yielded for 2 aggregated Hauturu Sandstone samples is very similar to that of the Tariki Sandstone Member, consistent with a main Separation Point Suite provenance. This is supported by the abundant quartz component (65 %) and trace occurrence of epidote observed in samples (Section 4.3.3). A significant minor U-Pb zircon age peak of 136 Ma (Fig. 5.45) suggests an additional Darran/Median

Suite source. Additional significant minor age peaks of 189 and 154 Ma (Fig. 5.45) correspond with the dominant U-Pb zircon age ranges of the Waipapa and Murihiku Terranes. The minor Carboniferous (~328) peak (Fig. 5.45) corresponds to the zircon ages for the Matai Terrane, Caples Terrane and Rakaia terrane of the Torlesse Supergroup. The abundant sedimentary rock fragments (10 %) (Section 4.4.3) in Tariki Sandstone discounts the Murihiku and Matai Terranes supporting an additional sedimentary basement source, most likely being the Waipapa and/or Caples Terrane and Rakaia terrane.

6.4 PALEOGEOGRAPHIC INTERPRETATIONS

The paleogeography of the eastern margin, Taranaki Basin, is discussed in this section for five key intervals during accumulation of the Late Eocene to earliest Miocene succession. Paleogeographic interpretations are based on the integration of lithostratigraphy, biostratigraphy, U-Pb geochronology, petrography and interpreted paleo-depositional environments as developed in the preceding chapter. Three new paleogeography maps are presented for the Runangan (Late Eocene), Lower Whaingaroan (Early Oligocene) and Upper Whaingaroan (Early mid-Oligocene), displaying interpreted paleobathymetry, depositional extent and potential provenance with associated sediment migration pathways. New paleogeography maps are presented for the Taranaki Basin area, drawn with reference to a 30 Ma (Oligocene) distribution of New Zealand basement terranes (Furlong and Kamp *in press)* (Fig. 6.2). Paleogeography maps of the Waikato Region from Tripathi (2009) are integrated with the new Taranaki Basin maps.

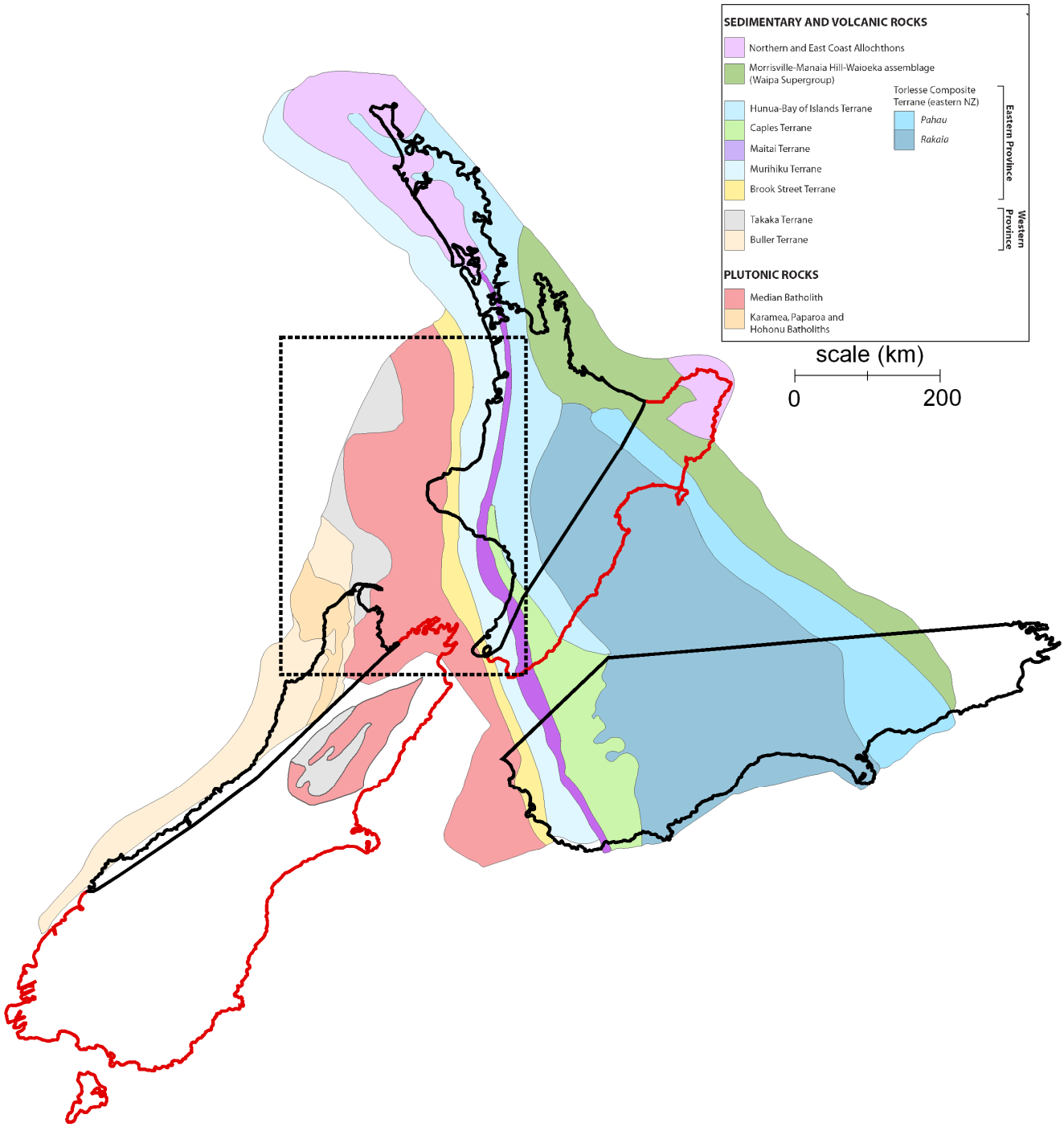

Figure 6.2. An Early Oligocene (~30 Ma) interpretation of the distribution of New Zealand Terrane. Black outline represents the inferred location of the New Zealand continent, and the red outline represent the modern day New Zealand Outline. The dashed box represents the mapped area of Figures 6.3 - 6.6. From Furlong and Kamp *in press.*

6.4.1 Runangan (Late Eocene)

A new Runangan (Late Eocene) paleogeography map for the Taranaki Basin area is presented in Fig. 6.3. Because of post Oligocene shortening across the Taranaki Fault Zone, the late Eocene and Oligocene location of this fault has been shifted ~10 km to the east, accommodating a wider shelf adjacent to Taranaki Fault than previously illustrated (i.e. King & Thrasher 1996). Regional subsidence and southward directed onlap resulted in expansion of the Eocene marine embayment in southern Taranaki Basin to the southeast, forming a northwest facing and deepening marine embayment bounded by land to the south and east (King & Thrasher 1996). In the Wanganui Basin area, Late Miocene inversion has stripped away much of the pre-Miocene sedimentary record (Vonk & Kamp 2008), making it difficult to interpret the pre-Miocene paleogeography. King and Thrasher (1996) report that during the Late Eocene the northwest Nelson area was possibly still emergent with a deeply weathered land barrier separating the west coast of the South Island from the Eocene embayment in southern Taranaki Basin. Late Eocene coal measures followed by shallow marine strata were subsequently deposited in estuarine environments in fault controlled grabens in southern Taranaki Basin (i.e. Takaka, Aorere and Surville Sub-basins) (King & Thrasher 1996). This marginal marine/estuarine/fluvial environment was likely present over a large area in southern Taranaki Basin with a fluvial system passing eastward through the area of the Otaihanga Outlier. A dominant Waipapa Terrane provenance is inferred for the McKee and Turi Formations, with an additional Median Batholith source. With reference to the Oligocene (~30 Ma) location of these identified source rocks (Fig. 6.3), it is likely these sediments were derived from a landmass that existed to the east and southeast of the Wellington area, with subsequent migration of sediments northward to Taranaki Basin. McKee Formation sediments were subsequently deposited in marginal marine/coastal areas and Turi Formation sediments were deposited in inner shelf environments. Fine to coarse grained deep marine sandstone of the Tangaroa Formation were deposited on a northwest-facing slope. The dominant Waipapa Terrane and/or Rakaia Sub-terrane provenance inferred for the Otaihanga Outlier also supports derivation from an eastern landmass. Farrelly (1988) reported a granitic provenance for Tangaroa Formation sediments. It is likely these sediments have a similar McKee/Turi Formation provenance, with dominant derivation from the

Waipapa Terrane with additional Median Batholith (granitic) input. In the Waikato region the Waikato Coal measures were deposited on basement in wide valleys with southward onlap (Edbrooke et al. 1994).

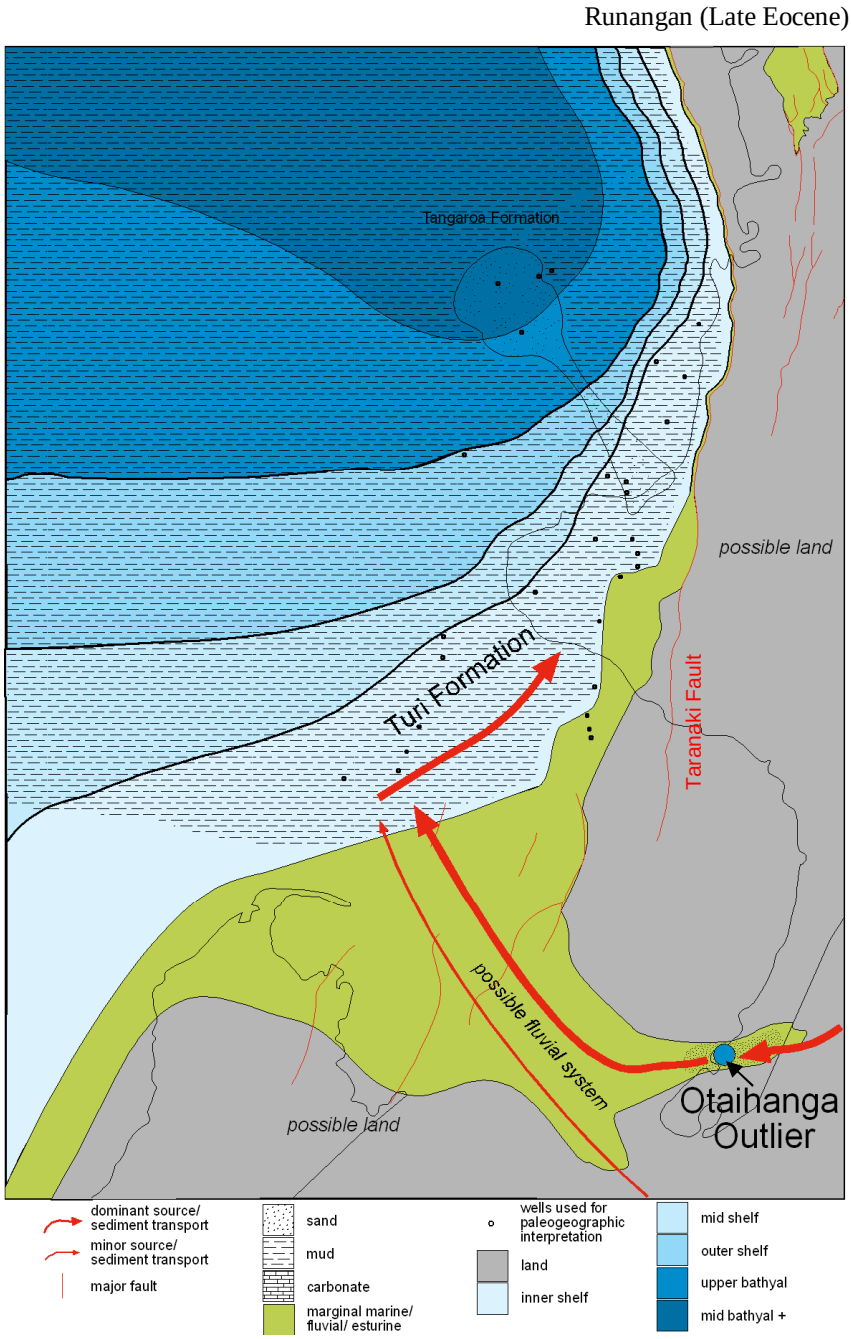

Figure 6.3. A new Runangan (Late Eocene) paleogeographic interpretation for the Taranaki Basin area illustrating the Turi Formation and Otaihanga Outlier depositional setting, a northwest facing marine embayment paleogeographic setting. Adapted from King and Thrasher 1996; Tripathi 2009.

6.4.2 Lower Whaingaroan (Early Oligocene)

A new Lower Whaingaroan (Early Oligocene) paleogeographic map for the Taranaki Basin area is presented in Fig. 6.4. As for the Runangan paleogeographic map, the location of the Taranaki Fault has been shifted ~10 km to the east. Because deposition of the condensed Matapo Sandstone Member was associated with ongoing subsidence and basin deepening, there was expansion of the Eocene marine embayment beyond that during the Runangan, possibly extending further to the southeast then previously understood. This is supported by the presence of a possibly Lower Whaingaroan correlative of the Matapo Sandstone Member outcropping in the Otaihanga area (see Section 2.6.3). A dominant Waipapa/Caples provenance with additional sediment derived from the Median Batholith is inferred for the Matapo Sandstone suggesting derivation from a land area to the east and southeast of Wellington. The sediment dispersal pathway was to the north and onto the contemporary Taranaki Basin shelf. The Taumarunui quartz sandstone possibly had a similar provenance, with sediment transport along a shoreline into a coastal environment in the Taumarunui area. Marine conditions became established across most of the Waikato region with deposition of the Glen Massey Formation, including the Ahirau Sandstone Member at inner to mid shelf depths. The provenance of Ahirau Sandstone included a significant input from Murihiku basement, but the age of the zircon grains and the quartz content of the sandstone suggests a source including the Median Batholith. A southern tidal seaway possibly connected the Waikato with Taranaki, allowing sediment to migrate along a shoreline from Taranaki Basin through into the Te Kuiti Group depocentre where it mixed with sediment eroded off the Herangi High.

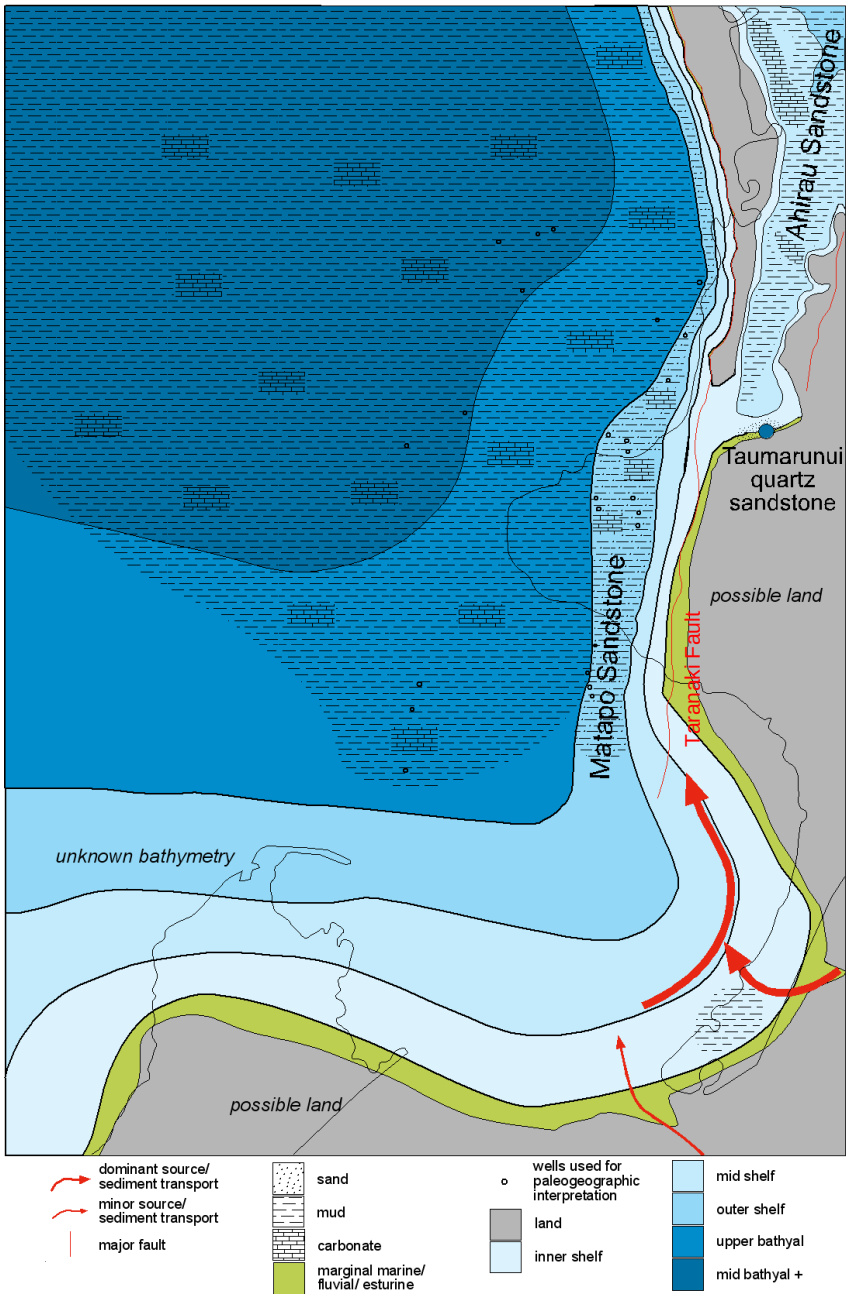

Figure 6.4. A new Lower Whaingaroan (Early Oligocene) paleogeographic interpretation for the Taranaki Basin area illustrating the Matapo Sandstone, Taumarunui quartz sandstone and Ahirau Sandstone depositional setting and the expansion of the northwest facing Eocene marine embayment. Adapted from Tripathi (2009).

6.4.3 Upper Whaingaroan (mid-Oligocene)

A new Upper Whaingaroan (mid-Oligocene) paleogeographic map for the Taranaki Basin area is presented in Figure 6.5. In contrast to the Lower Whaingaroan map, the Taranaki Fault is placed at its modern day location as reversal and shortening across the Taranaki Fault zone had begun by this time. During the Upper Whaingaroan Taranaki Basin subsided resulting in upper to middle bathyal depths in the foredeep trough adjacent to Taranaki Fault. A Separation Point Suite (Median Batholith) provenance is inferred for both the Tariki Sandstone and Hauturu Sandstone implying sediment transport from the south. Figure 6.2 indicates that during the Oligocene (~30 Ma), part of the Median Batholith was situated to the south and southeast of the Wellington area, and this was probably the part of the batholith that sourced the Tariki and Hauturu sediments. Much of this part of the batholith has been distended, deformed and eroded through subsequent plate boundary displacements as the Alpine Fault subsequently formed through this region. The significance of sourcing the sediments from this part of the batholith is that it places the source on the eastern side of Taranaki Basin during the Upper Whaingaroan. Sediments likely migrated northward along a north–south trending shoreline attached to the Patea-Tongaporutu High. The Tariki sediments may have moved along a shoreline on the western side of the high, while the Hauturu sediments migrated along a shoreline along the eastern side of the high. The Tariki sediments were possibly captured by channels across a narrow shelf, and fed downslope to accumulate in the foredeep trough at upper to mid bathyal depths. Episodic uplift of the Taranaki Fault may have helped trigger the turbidity current and sandy debris flows that comprise the Tariki Sandstone. Hauturu Sandstone sediments were re-worked across the inner shelf by littoral drift and deposited as shoreface deposits in the Te Kuiti Group depocentre to the east of the Herangi High (Tripathi & Kamp 2008). The Tariki Sandstone is localised to the Taranaki Peninsula area adjacent to Taranaki Fault, with deposits intersected from McKee-1 in the north to Rimu-B1 in the south (southern Taranaki Peninsula) (Higgs et al. 2004). Elsewhere in Taranaki Basin Otaraoa Formation accumulation occurred at upper to mid bathyal depths.

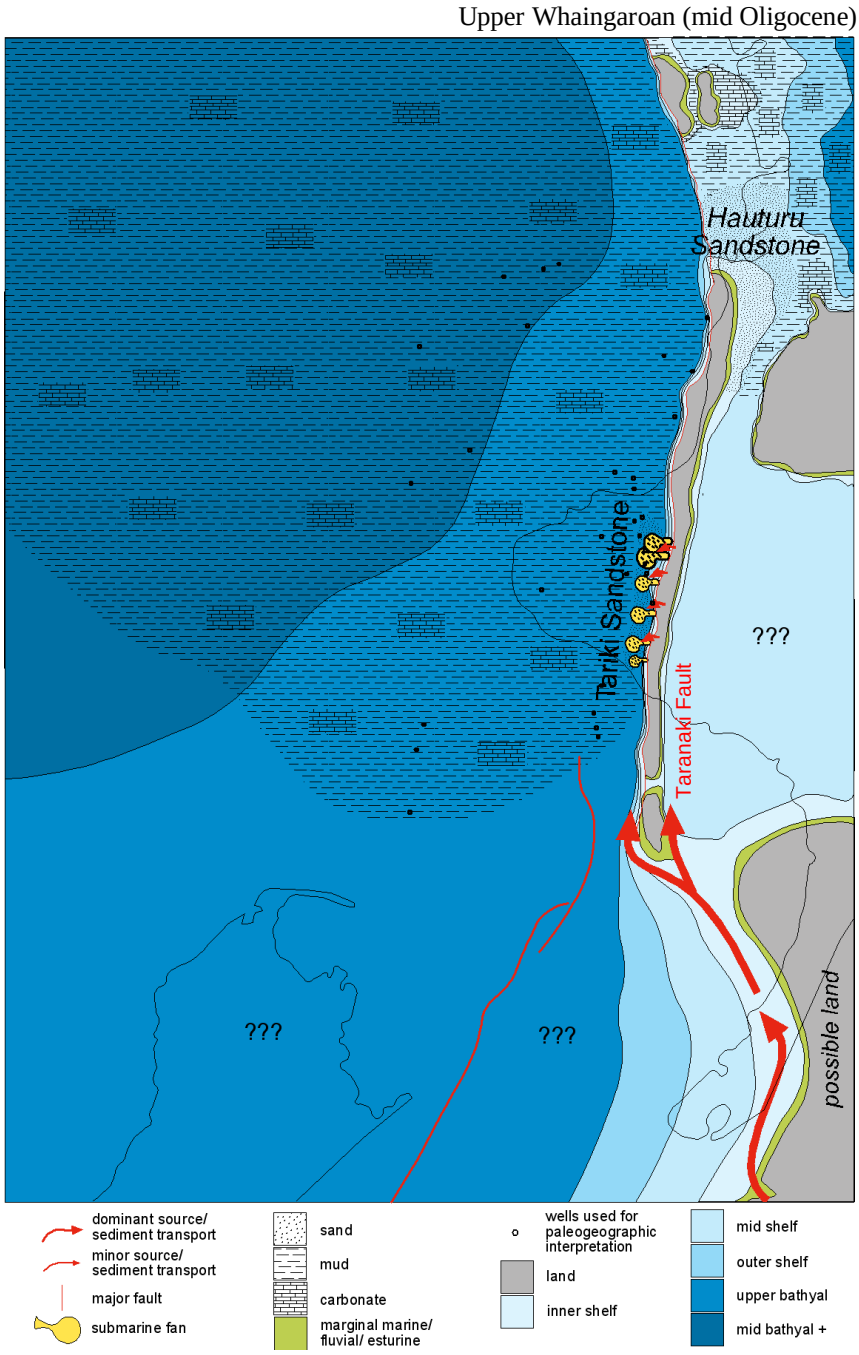

Figure 6.5. A new Upper Whaingaroan (Early - mid Oligocene) paleogeographic interpretation for the Taranaki Basin area illustrating the Tariki Sandstone/Hauturu Sandstone foredeep trough paleogeographic setting of the Taranaki Basin area. Adapted from King and Thrasher 1996; Tripathi 2009.

6.4.4 Lower Waitakian (Late Oligocene)

By the Lower Waitakian carbonate sediment influx into eastern Taranaki Basin had become very significant. An Early Miocene paleogeographic map from King and Thrasher (1996) (Fig. 6.6) illustrates this latest Oligocene – earliest Miocene paleogeographic setting, with the presence of a very narrow shelf along the eastern margin of the basin and bathyal water depths over much of Taranaki Basin. A carbonate factory located along the inner shelf around a rocky shoreline atop the Patea-Tongaporutu Herangi High sourced the carbonate sediment shed into Taranaki Basin to accumulate as the Tikorangi Formation (Hood et al. 2003). For much of the Oligocene a pelagic carbonate facies (Tikorangi basinal facies) accumulated in distal (western) parts of the basin. A Tikorangi Formation correlative, the Otorohanga Limestone, accumulated at shelf depths in the Waikato Region to the east of the Herangi High, and the Takaka Limestone accumulated at mid-shelf water depths in the northwest Nelson area (Hayward et al. 1984).

6.4.5 Upper Waitakian (Early Miocene)

During the Upper Waitakian a terrigenous source delivering muddy sediment to Taranaki Basin was re-established. This expressed itself in the calcareous mudstone of the Taimana Formation. A narrow shelf still existed west of the Patea-Tongaporutu Herangi High where shelf carbonate sediment was still being supplied to the slope to the west, a similar paleogeographic setting to that illustrated in Fig. 6.6. More extensive shelf carbonate was still accumulating as Otorohanga Limestone to the east of Herangi High. The increase in terrigenous mud supply to the basin reflects the developing plate boundary zone through New Zealand and associated tectonic movements. In the Waikato Region, basal Waitemata Group and Mahoenui Group sediments were deposited following inversion, uplift and erosion of parts of the Te Kuiti Group during the latest Waitakian. By the Altonian (Early Miocene) high rates of terrigenous sediment was being supplied to the basin, resulting in cessation of accumulation of the Ngatoro Group and the change to accumulation of the Wai-iti Group.

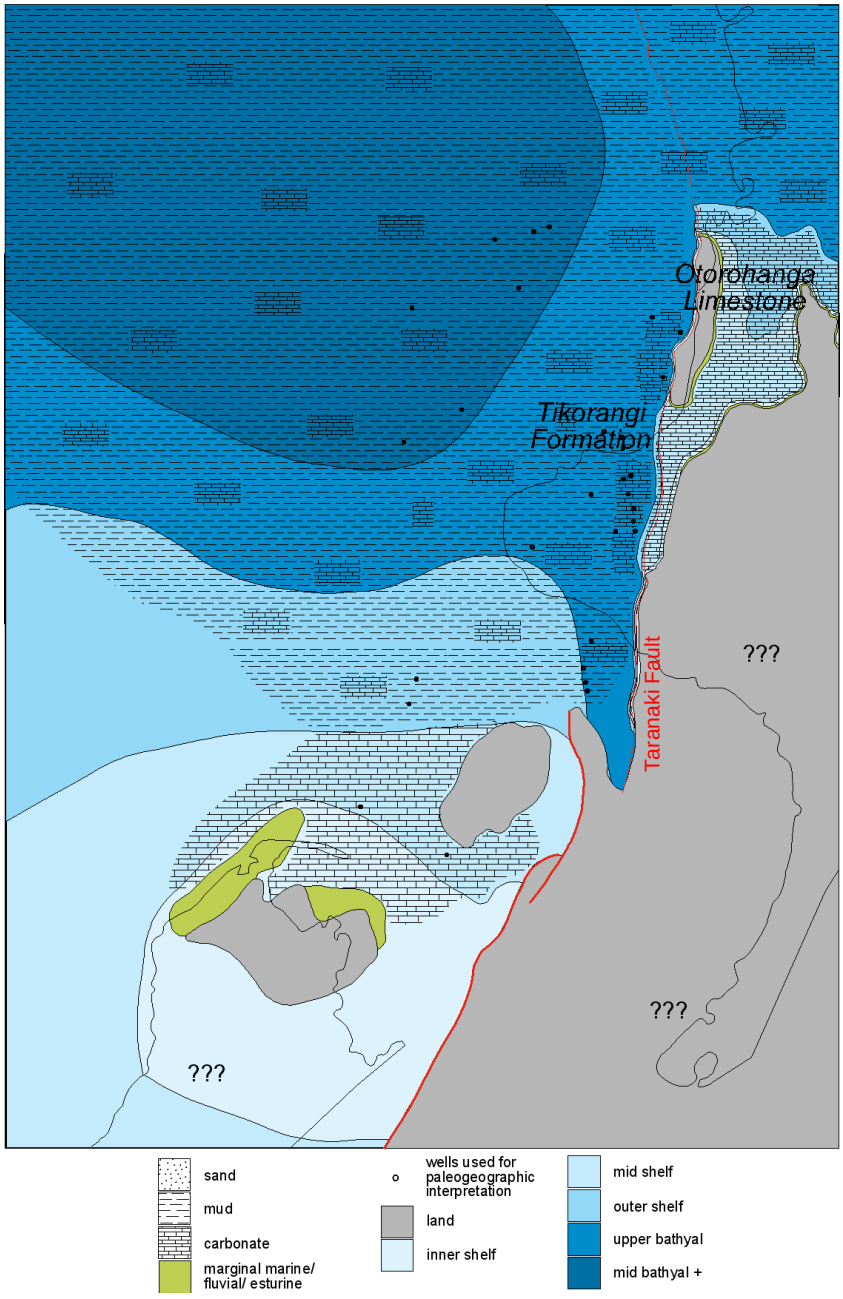

Figure 6.6. A Waitakian (Early Miocene) paleogeographic interpretation for the Taranaki Basin area illustrating the depositional setting of the Tikorangi Formation. From King and Thrasher 1996; Tripathi 2009.

6.5 EVALUATION OF TARANAKI FAULT DISPLACEMENT MODELS

Evidence of the timing of the start of shortening across the Taranaki Fault Zone may be evident stratigraphically within Taranaki Basin. If shortening across this fault started during the Middle Eocene (e.g. Stagpoole & Nicol 2008) then one might expect to see a middle-Late Eocene stratigraphic signal of this, particularly along the eastern margin of the basin. Although the Late Eocene Tangaroa Sandstone fan may have a tectonic origin, Early Oligocene sediments in the basin have condensed character which is not really consistent with reverse fault movement and the uplift and erosion that might be associated with it. Moreover, King & Thrasher (1996) have suggested that there may have been normal fault movement associated with the development of sub-basins in southern Taranaki during the Late Eocene and Early Oligocene. This "passive margin" sedimentation phase continued until the end of the Lower Whaingaroan as reflected in the condensed nature of the calcareous and glauconitic Matapo Sandstone Member. Although the Matapo Sandstone and Tariki Sandstone are separated by only a few metres stratigraphically, during the Upper Whaingaroan the sea floor to the eastern part of the basin lay at upper to mid bathyal depths and a foredeep had developed along the eastern margin within which the Tariki Sandstone accumulated.

The northward transport of shoreline sediments to supply the Tariki Sandstone fan and the shoreline deposits of the Hauturu Sandstone is a reflection of the development of Taranaki Fault as a reverse fault during the upper Whaingaroan. The displacement on Taranaki Fault uplifted basement on the hanging wall. Without this structural high (Patea-Tongaporutu-Herangi High) shoreline sediments sourced from the south would not have been able to migrate northward and be emplaced from the east into the foredeep, or to migrate into the Waikato region. An Upper Whaingaroan age for the start of reverse movement on Taranaki Fault is more likely than a Middle Eocene age taking into account the character of the Late Eocene and Oligocene sediments in Taranaki Basin and in the Te Kuiti Group.

6.6 CONCLUSIONS

Based upon sediment petrography and detrital U-Pb zircon ages, new information about Taranaki Basin sediment provenance and paleogeography has been established. For most sedimentary units analysed (i.e. McKee Formation, Turi Formation, Otaihanga Outlier, Matapo Sandstone and the Taumarunui quartz sandstone) the Waipapa Terrane has been identified as a likely significant basement source rock, with additional input from other New Zealand terranes, particularly the Median Batholith, Rakaia terrane, Caples Terrane and Murihiku Terrane. Separation Point Suite is evidently an important source for Tariki Sandstone and Hauturu Sandstone sediments. The Median Batholith and Waipapa Terrane contributed components to the Ahirau Sandstone together with Murihiku Terrane.

With reference to the ~30 Ma New Zealand Terrane reconstruction of Furlong and Kamp (*in press)* it is apparent that the sediments analysed in this study may have been largely derived from the parts of the New Zealand basement terranes that lay to the southeast of the southern part of Taranaki Basin, rather than having been derived from due south of the basin, being the Northwest Nelson area. In the southeastern area numerous Late Paleozoic and Mesozoic basement terranes were juxtaposed and the Median Batholith lay on the south side, contiguous with the parts to the northwest, now cropping out west of Nelson in the Golden Bay area. Three new paleogeography maps have been presented for key intervals in the basin's development. These maps illustrate the significant paleoenvironmental and paleogeographic changes that occurred between accumulation of the Matapo Sandstone and the Tariki Sandstone. There was probably an extensive northwest facing marine embayment in the Lower Whaingaroan, which was truncated in the east by reversement on the Taranaki Fault, uplift of basement immediately east of it as hanging wall, and subsidence immediately to the west forming a foredeep trough.

CHAPTER 7
SUMMARY AND CONCLUSIONS

7.1 GEOLOGICAL SETTING AND BASIN EVOLUTION

Taranaki Basin is located along the western margin of North Island, New Zealand, in a back-arc position behind the Taupo Volcanic Zone (TVZ) and Hikurangi Margin subduction zone. Structurally, the basin is subdivided into two broad zones, the Western Stable Platform (WSP), a relatively featureless section of seafloor encompassing the western region of the basin, and the Eastern Mobile Belt (EMB), a structurally complex eastern region of the basin. The north-south striking Taranaki Fault, which moved mainly during the Late Oligocene and Miocene is identified as one of the major structural features of the basin, on which basement was thrust westwards into the basin. The basin has evolved since the mid-Cretaceous break-up of New Zealand from eastern Gondwanaland. Of particular interest in this study is the culmination of the Paleocene to Early Oligocene passive margin phase and the development of shortening across the eastern margin, associated with development of the Australian-Pacific plate boundary through New Zealand during the mid-Oligocene to Early Miocene. This change in basin style and the associated changes in paleogeography are reflected in the subsurface Late Eocene – Oligocene sedimentary succession of the basin, particularly the eastern margin.

7.2 STRATIGRAPHY

Taranaki Basin has a Cretaceous-Cenozoic sedimentary fill that is mainly in the subsurface. The Late Eocene – Oligocene succession is dominated by calcareous rocks of the Ngatoro Group, which are of Oligocene to earliest Miocene in age. Underlying the Ngatoro Group are the terrestrial/intercalated marginal marine and shallow marine (inner shelf) strata of the Kapuni and Moa Groups. Overlying is the Wai-iti Group, dominantly a terrigenous succession making up most of the thickness of the Miocene succession in Taranaki Basin. Well cuttings from the McKee Formation, Turi Formation, Matapo Sandstone Member, Otaraoa Formation, Tariki Sandstone Member and Taimana Formation have been obtained

in this study for the purpose of wireline log calibration, to investigate the sedimentary petrography and to undertake U-Pb dating of zircon grains. Onshore North Island correlative units have also been sampled, including Te Kuiti Group sandstone units (Ahirau Sandstone and Hauturu Sandstone), a quartz sandstone from the Taumarunui area (Taumarunui quartz sandstone), and a quartzose sandstone from the Otaihanga area (Otaihanga Outlier), all obtained for sedimentary petrography and U-Pb dating to help constrain interpretations of Late Eocene – Oligocene paleogeography.

7.3 WIRELINE MOTIFS

A comprehensive assessment of Late Eocene – Oligocene subsurface stratigraphy using geophysical well logs has been undertaken. A suite of distinctive wireline motifs were defined for Late Eocene – Oligocene units using the geometric appearance of major log types. The relatively homogenous mud-dominated Turi Formation interval was subdivided into three wireline motifs. The Tu1 motif represents background Turi Formation with relatively smooth and 'featureless' appearance of major log types. The Tu2 motif indicates a sandy facies and Tu3 represents a large semi-caved and/or washed out interbedded zone. The thin (~5 m) and condensed Matapo Sandstone Member was subdivided into two wireline motifs. Motif Ma1, the dominant Matapo wireline motif identified, indicates an upward fining in lithology or upward decreasing carbonate content. Motif Ma2 that normally occurs in association with, and below Ma1, commonly displays a medium to high value GR log suggesting a finer grained facies then Ma2. The calcareous mud-dominated Otaraoa Formation was subdivided into three wireline motifs, of which Ot1 represents most of the Otaraoa Formation, characterised by a relatively smooth and stable, medium to high value, relatively cylindrical-shaped GR log. Motif Ot2 represents sections that display a medium to low value GR log with log character suggesting carbonate-dominated zones. Similarly motif Ot3, characterised by a medium to low value GR log and tightly serrated SP log, suggests an interbedded and carbonate-dominated zone. The Tariki Sandstone Member was subdivided into three wireline motifs. Motif Ta1 is characterised by a relatively smooth to serrated, blocky and cylindrical GR log, reflecting amalgamated sandstone packages. Motif Ta2, characterised by a relatively smooth

and featureless, medium to high value GR log suggests a relatively homogenous and fine-grained succession. Ta3 is a log character suggesting an interbedded succession. The very highly calcareous Tikorangi formation was subdivided into three wireline motifs. Motif Tk1 is characterised by a very smooth, featureless and stable, cylindrical-shaped, low value GR log, indicative of very high carbonate content. Motif Tk2 is a log character indicative of an interbedded succession with a very high carbonate content. Tk3 is similar to Tk2 but coarser grained. The fairly homogenous, highly calcareous mud dominated interval of Taimana Formation was subdivided into two wireline motifs. Motif Tm1 is indicative of a fairly homogenous lithology with some interbedding apparent. Tm2 displays a very serrated, variably low to high value GR log indicative of mudstone intercalated with sandstone.

7.4 BIOSTRATIGRAPHY AND DEPOSITIONAL ENVIRONMENTS

Turi Formation generally has a Bortonian (Middle Eocene) to Upper Whaingaroan (Late Oligocene) age and was deposited in an inner shelf (0 – 30 m water depth) depositional environment under neritic water mass conditions. The Turi Formation reflects marine inundation of the basin, and overlies sandy coastal plain/marginal marine facies of the Mangahewa and McKee Formations. The Matapo Sandstone in the Taranaki Peninsula area has a Runangan (Late Eocene) to Lower Whaingaroan (Early Oligocene) age and was deposited in outer shelf to upper bathyal water depths (100 – 400 m). Matapo Sandstone deposition reflects a decrease in terrigenous sediment input to the shelf indicated by its stratigraphic condensation and abundant glauconite content. The Otaraoa Formation has an Upper Whaingaroan (Middle Oligocene) to mid Waitakian (earliest Miocene) age and was deposited in an upper to mid-bathyal depositional environment, around 400 – 600 m of water depth. Deposition of the Otaraoa Formation occurred in response to the development of a foredeep along the eastern margin of central parts of Taranaki Basin. The Tariki Sandstone is observed to have a strictly Upper Whaingaroan (Middle Oligocene) age and was deposited in upper bathyal water depths. Tariki Sandstone is restricted to the Taranaki Peninsula area, representing turbidite deposits that accumulated in a north-south trending foredeep along the eastern margin of the basin. The Tikorangi Formation in the Taranaki Peninsula

area has a Waitakian (latest Oligocene – earliest Miocene) age and represents redeposited carbonate that accumulated on a moderate westward dipping continental slope at outer shelf and upper bathyal water depths. The Taimana Formation has an upper Waitakian (earliest Miocene) to Otaian (Early Miocene) age and was deposited at bathyal water depths (200 – 1000 m). The Taimana Formation reflects the start of terrigenous input to the basin that persisted during the Neogene and reflects the development of the plate boundary through New Zealand.

7.5 MODAL PETROGRAPHY

The modal composition of Late Eocene – Oligocene sediments has been determined as a preliminary assessment of sediment provenance. Modal composition data of the light mineral fraction for Late Eocene – Oligocene Taranaki Basin and onshore North Island units plotted on QFL plots reveal three distinct groupings of samples. The Matapo Sandstone Member plots by itself, near the lithics pole, dominated by fine-grained sedimentary rock fragments (80%) with a minor quartz component (5%), indicative of a fine-grained sedimentary, quartz poor provenance. The McKee Formation and Turi Formation plot closely, nearest to the lithics pole. McKee and Turi sediments are dominated by fine-grained sedimentary rock fragments (45% and 52%) and angular quartz grains (34% and 30%). A significant sedimentary rock provenance is likely for McKee and Turi Formation, possibly a greywacke source. Most other samples cluster near the quartz pole, including those from the Taumarunui quartz sandstone, Ahirau Sandstone, Tariki Sandstone and Hauturu Sandstone. The dominant quartz (56%) and sedimentary rock fragments (22%) of the Taumarunui quartz sandstone suggest a fine-grained, quartz rich sedimentary provenance. The dominant quartz (~55%), sedimentary rock fragment (~18%) and very abundant heavy mineral amphibole component observed in Ahirau Sandstone samples suggests more than one source area, possibly a dominant Murihiku Terrane contribution, but it also includes sediment derived from a granitic source area. Tariki Sandstone samples have major quartz (~51%), plagioclase feldspar (~21%) and sedimentary rock fragment (~21%) components, suggesting a fine-grained sedimentary provenance, possibly a greywacke source and an additional granitic source. The primary quartz

(~65%) component observed in Hauturu Sandstone samples is consistent with derivation from a quartz rich basement such as a granitoid belt or quartz rich sedimentary basement. An increasing quartz content with decreasing age relationship is apparent between samples, suggesting an increase in the importance of a granitic provenance for the Late Eocene – Oligocene Taranaki Basin sediments over time.

7.6 U-Pb GEOCHRONOLOGY

U-Pb geochronology has been adopted as a tool to assess the provenance of Late Eocene – Oligocene sediments. The U-Pb ages of more than 350 detrital zircon grains were determined in this study from 13 Late Eocene – Oligocene aged samples, using a U-Pb zircon LA-ICP-MS dating technique. Results were plotted on concordia plots allowing discordant ages to be removed and concordant/near concordant ages to be used in further interpretations. $^{206}Pb/^{238}U$ ages yielded from samples ranged from the Mesoproterozoic to Early Cretaceous. $^{206}Pb/^{238}U$ ages prepared as probability density plots revealed the dominant age peaks and age distributions of samples. The dominant age peak of the McKee Formation was 169 Ma. The Turi Formation had multiple significant peaks that occurred between 204 and 103 Ma. Similarly, Matapo Sandstone had a cluster of age peaks from Late Devonian Early Cretaceous. The Otaihanga Outlier had a dominant age peak of 249 Ma, and the Taumarunui quartz sandstone had age peaks between 185 and 173 Ma. The Ahirau Sandstone has multiple peaks between 356 and 105 Ma. The Tariki Sandstone has a dominant 124 – 116 Ma age peak and the Hauturu Sandstone has a dominant 121 Ma age peak.

7.7 PROVENANCE

The provenance of Late Eocene – Oligocene units was interpreted by integrating $^{206}Pb/^{238}U$ zircon age data with modal petrography data and comparisons to New Zealand basement. The McKee Formation has a possible Waipapa Terrane provenance. The Turi Formation also has an inferred Waipapa Terrane provenance similar to that for McKee Formation, with an additional Median Tectonic Zone and Darran/Median Suite source. Although no petrographic data were obtained for the Otaihanga Outlier, a Waipapa Terrane/Caples Terrane

and/or Rakaia Sub-terrane provenance are the most likely sources. The Waipapa and/or Caples Terrane is the likely principal source rocks for the Matapo Sandstone with an additional source from the Darran/Median Suite of the Median Batholith and possibly a minor source from the Karamea Batholith. For the Taumarunui quartz sandstone, a dominant Waipapa Terrane and Median Batholith provenance is likely. Dominant derivation from the Median Batholith (i.e. the Darran/Median Suite), the Waipapa Terrane and/or Caples Terrane and the Murihiku Terrane is inferred for the Ahirau Sandstone. The Tariki Sandstone has dominant Separation Point Suite (Median Batholith) provenance with minor derivation from the Waipapa, Caples and Murihiku Terranes and similarly, Hauturu Sandstone has a main Separation Point Suite provenance with an additional Darran/Median Suite, Waipapa and/or Caples Terrane and Rakaia terrane source.

7.8 PALEOGEOGRAPHY

A reassessment of the paleogeographic evolution of eastern Taranaki Basin margin at key intervals through the Late Eocene – Oligocene has been undertaken. Paleogeography discussions and interpretations are based on integration of data as developed in the preceding chapters of this thesis. Derivation of sediments from a landmass that existed to the east and southeast of the Wellington area has been inferred for the Late Eocene – Oligocene, with subsequent migration of sediments northward to Taranaki Basin and to the Waikato Region. Three new paleogeography maps are presented for the Runangan (Late Eocene), Lower Whaingaroan (Early Oligocene) and Upper Whaingaroan (Early-Middle Oligocene). In the Runangan, a northwest facing and deepening marine embayment bounded by land to the south and east existed in southern Taranaki Basin. A marginal marine/estuarine/fluvial environment was present over this area, with a fluvial system likely passing eastward through the area of the Otaihanga Outlier. Sediments of the McKee and Turi Formations derived from the southeast migrated northward accumulating in Taranaki Basin. By the Lower Whaingaroan, the Eocene marine embayment had expanded, possibly extending farther to the southeast then previously understood, inundating the area of the Otaihanga Outlier. A southern tidal seaway possibly connected the Waikato with

Taranaki Basin. Sediments migrating northward to Taranaki Basin were deposited at outer shelf depths as Matapo Sandstone and along a shoreline from Taranaki Basin to the Te Kuiti Group depocentre, accumulating in a coastal environment in the Taumarunui area (i.e. Taumarunui quartz sandstone deposition) and at inner to mid shelf depths in the Waikato region (i.e. Ahirau Sandstone deposition). During the Upper Whaingaroan most of Taranaki Basin had subsided to upper to middle bathyal depths and a foredeep trough had formed adjacent to Taranaki Fault. Sediment transport from the south, derived from the Separation Point Suite (Median Batholith), likely migrated northward along a north-south trending shoreline attached to the Patea-Tongaporutu High. The Tariki sediments may have moved along a shoreline on the western side of the high with subsequent deposition in the Taranaki Peninsula area, while the Hauturu sediments migrated along a shoreline along the eastern side of the high depositing in the Te Kuiti Group depocentre. By the Lower Waitakian, carbonate sediment influx into eastern Taranaki Basin had become very significant and sourced from an inner shelf around a rocky shoreline atop the Patea-Tongaporutu-Herangi High to the west, accumulating as Tikorangi Formation on a west-dipping slope. During the Upper Waitakian a terrigenous source delivering muddy sediment to Taranaki Basin was re-established, however carbonate sediment was still being supplied to the slope (to the west) expressed as the calcareous mudstone of the Taimana Formation.

7.9 TARANAKI FAULT DISPLACEMENT

The hypothesis that the lower and upper parts of the Ngatoro Group have different stratigraphic and sedimentologic characteristics, reflecting accumulation in different tectonic settings has been tested by reviewing the stratigraphic and sedimentologic signals evident within the Late Eocene – Oligocene sedimentary succession in Taranaki Basin, along with new paleogeographic data determined in this study. The condensed nature of the calcareous and glauconitic Matapo Sandstone (Lower Whaingaroan) is not really consistent with reverse movement on the Taranaki Fault and the uplift and erosion that might be associated with it, suggesting deposition during a passive margin phase. Although the Matapo Sandstone and Tariki Sandstone (Upper Whaingaroan) are separated by only a

few metres stratigraphically, Tariki Sandstone and Hauturu Sandstone (age correlatives) deposition is a reflection of the development of Taranaki Fault as a reverse fault during the Upper Whaingaroan. Without this structural high (Patea-Tongaporutu-Herangi High) associated with shortening and displacement on Taranaki Fault, shoreline sediments sourced from the south would not have been able to migrate northward and be emplaced from the east into the foredeep, or to migrate into the Waikato region. An Upper Whaingaroan age for the start of reverse movement on Taranaki Fault is most likely taking into account the character of the Late Eocene – Oligocene sediments in Taranaki Basin and in the Te Kuiti Group.

REFERENCES

Adams EA, Palmer J, Patchett J; Petroleum Corporation of NZ Exploration Ltd 1980. Toko-1 Well Completion Report. PPL 38034. Ministry of Economic Development New Zealand Unpublished Petroleum Report PR761.

Adams CJ, Campbell HJ, Griffin WL 2007. Provenance comparisons of Permian to Jurassic tectonostratigraphic terranes in New Zealand: perspectives from detrital zircon age patterns. Geological Magazine 144: 701-729.

Adams CJ, Barley ME, Maas R, Doyle MG 2002. Provenance of Permian-Triassic volcaniclastic sedimentary terranes in New Zealand: evidence from their radiogenic isotope characteristics and detrital mineral age patterns. New Zealand Journal of Geology and Geophysics 45: 221-242.

Asquith GB 1982. Basic well log analysis for geologists. American Association of Petroleum Geologists, Methods in Exploration Series. 216 p.

Black LP, Kamo SL, Allen CM, Davis DW, Aleinikoff JN, Valley JW, Mundil R, Campbell IH, Korsch RJ, Williams IS, Foudoulis C 2004. Improved $^{206}Pb/^{238}U$ microprobe geochronology by the monitoring of a trace-element-related matrix effect; SHRIMP, ID-TIMS, ELA-ICP-MS and oxygen isotope documentation for a series of zircon standards. Chemical Geology 205: 115-140.

Briggs RM, Middleton MP, Nelson CS 2004. Provenance history of a Late Triassic-Jurassic Gondwana margin forearc basin, Murihiku Terrane, North Island, New Zealand: petrographic and geochemical constraints. New Zealand Journal of Geology and Geophysics 47: 589-602.

Campbell IH, Reiners PW, Allen CM, Nicolescu S, Upadhyay R 2005. He-Pd double dating of detrital zircons from the Ganges and Indus Rivers: implication for quantifying sediment recycling and provenance studies. Earth and Planetary Science Letters 237 n.3-4: 402-432.

Cant DJ 1992. Subsurface facies analysis. In: Walker RG, James NP eds. Facies Models: response to sea level change. Geological Association of Canada: Pp. 297-310.

Carozzi AV 1993. Sedimentary Petrography. PTR Prentice Hall, Englewood Cliffs, New Jersey. 263 p.

Carter M; Petroleum Corporation of NZ Exploration Ltd 1983. Kaimiro-1 Well Completion Report. Ministry of Economic Development New Zealand Unpublished Petroleum Report PR936.

Carter M, Rainey S; Petroleum Corporation of NZ Exploration Ltd 1988. Totara-1 Well Completion Report. PPL 38034. Ministry of Economic Development New Zealand Unpublished Petroleum Report PR1348.

Carter M, Kelly C, Lammerink W; Petroleum Corporation of NZ Exploration Ltd 1987a. Ahuroa-1, Ahuroa-1A Well Completion Report. PPL 38034. Ministry of Economic Development New Zealand Unpublished Petroleum Report PR1260.

Carter M, Kelly C, Lammerink W, Longson C; Petroleum Corporation of NZ Exploration Ltd 1987b. Tariki-1, Tariki-1A Well Completion Report. PPL 38034. Ministry of Economic Development New Zealand Unpublished Petroleum Report PR1248.

Cartwright SJ 2003. Cenozoic geological evolution of the central-eastern King Country Basin, North Island. MSc Thesis, University of Waikato, Hamilton, New Zealand.

Catanzaro EJ 1968. The interpretation of zircon ages. In: Hamilton EI, Farquhar RM eds. Radiometric dating for geologists. Interscience Publishers. Pp. 225-258.

Cawood PA, Nemchin AA, Leverenz A, Saeed A, Ballance PF 1999. U/Pb dating of detrital zircons: implications for the provenance record of Gondwana margin terranes. Geological Society of America Bulletin 111: 1107-1119.

Crown Minerals. Taranaki Basin. http://www.crownminerals.govt.nz/cms/petroleum/petroleum-basins/taranaki-basin. (2007).

de Bock JF, Palmer JF, Lock RG 1990. Tariki Sandstone Early Oligocene hydrocarbon reservoir, eastern Taranaki, New Zealand. In: 1989 Petroleum Conference Proceedings 214-224. Ministry of Commerce, Wellington.

de Bock JF, True T, Lammerink W, Kelly C, McDowell P; Petroleum Corporation of NZ Exploration Ltd 1985. Awakino-1 Well Completion Report. PPL 38094. Ministry of Economic Development New Zealand Unpublished Petroleum Report PR1140.

Dickin AP 2005. Radiogenic Isotope Geology. Cambridge University Press. Pp. 101-114

Dickinson WR, Suczek CA 1979. Plate tectonics and sandstone compositions. American Association of Petroleum Geologists Bulletin 63: 2164-2183.

Dickinson WR, Beard LS, Brackenridge GR, Erjavec JL, Ferguson RC, Inman KF, Knepp RA, Lindenberg FA, Ryberg PT 1983. Provenance of North American Phanerozoic sandstones in relation to tectonic setting. Geological Society of America Bulletin 94: 222-235.

Doveton JH 1994. Geologic log interpretation. Society of Economic Paleontologists and Mineralogists Short Course No. 29. Tulsa, USA. 169 p.

Edbrooke SW, Sykes R, Pocknall DT 1994. Geology of the Waikato Coal Measures, Waikato Coal Region, New Zealand. Institute of Geological and Nuclear Sciences Monograph 6. Institute of Geological and Nuclear Sciences, Lower Hutt, New Zealand.

Farrelly JJ; AMOCO New Zealand Oil Company 1988. Te Kumi-1 Geological Well Report. Ministry of Economic Development New Zealand Unpublished Petroleum Report PR1386.

Furlong KP, Kamp PJJ 2009. The lithospheric geodynamics of plate boundary transpression in New Zealand: initiating and emplacing subduction along the Hikorangi Margin, and the tectonic evolution of the Alpine Fault System. Tectonophysics, In Review.

Garver JI, Kamp PJJ 2002. Integration of zircon colour and zircon fission track zonation patterns in orogenic belts: application of the Southern Alps, New Zealand. Tectonophysics 349 n.1-4: 203-219

Gordon T, Boothby P, Roth S; ARCO Petroleum NZ Inc. 1993. Waihi-1, Waihi-1A Well Completion Report. PPL 38453. Ministry of Economic Development New Zealand Unpublished Petroleum Report PR1862.

Hansen RJ, Kamp PJJ 2006. An integrated biostratigraphy and seismic stratigraphy for the late Neogene continental margin succession in northern Taranaki Basin, New Zealand. New Zealand Journal of Geology and Geophysics 49: 39-56.

Hayward BW, Midenhall DC, Beu AG; NZ Geological Survey 1984. Biostratigraphy of Surville-1 offshore well Tasman Bay. PPL 38125. Ministry of Economic Development New Zealand Unpublished Petroleum Report PR1058.

Hayward BW, Grenfell HR, Reid CM, Hayward KA 1999. Recent New Zealand shallow-water benthic foraminifera: taxonomy, ecological distribution, biogeography, and use in paleoenvironmental assessment. Institute of Geological and Nuclear Sciences Monograph 21. 258 p. Institute of Geological and Nuclear Sciences, Lower Hutt, New Zealand.

Higgs KE, King PR, Browne GH, Morgans HEG 2004. Oligocene submarine fan systems in Taranaki: a proven reservoir and an outcrop comparison. 2004 New Zealand Petroleum Conference Proceedings.

Hood SD, Nelson CS, Kamp PJJ 2003. Lithostratigraphy and depositional episodes of the Oligocene carbonate-rich Tikorangi Formation, Taranaki Basin, New Zealand. New Zealand Journal of Geology and Geophysics 46: 363-386.

Jackson SE, Pearson NJ, Griffin WL, Belousova EA 2004. The application of laser ablation-inductively coupled plasma-mass spectrometry to in situ U-Pb zircon geochronology. Chemical Geology 211: 47-69.

Kamp PJJ 1986. The mid-Cenozoic Challenger Rift System of western New Zealand and its implication for the age of alpine fault inception. Geological Society of America Bulletin 97: 255-281.

Kear D, Schofield JC 1959. Te Kuiti Group. New Zealand Journal of Geology and Geophysics 2: 685-717.

Kear D, Mortimer N 2003. Waipa Supergroup, New Zealand: a proposal. Journal of the Royal Society of New Zealand 33 n.1: 149-1633.

Keary P, Brooks M 1991. An introduction to geophysical exploration. Blackwell Scientific Publications, Oxford. 254 p.

Kimbrough DL, Tullock AJ, Coombs DS, Landis CA, Johnston MR, Mattinson JM 1994. Uranium-lead ages from the Median Tectonic Zone, New Zealand. New Zealand Journal of Geology and Geophysics 37: 393-419

King PR 2000. Tectonic reconstructions of New Zealand: 40 Ma to the present. New Zealand Journal of Geology and Geophysics 43: 611-638.

King PR, Thrasher GP 1996. Cretaceous-Cenozoic geology and petroleum systems of the Taranaki Basin, New Zealand. Institute of Geological and Nuclear Sciences, Monograph 13. 243 p. 6 enclosures. Institute of Geological and Nuclear Sciences Ltd, Lower Hutt, New Zealand.

Košler J, Fonneland H, Sylvester P, Tubrett M, Pedersen R 2002. U-Pb dating of detrital zircons for sediment provenance studies – a comparison of laser ablation ICP-MS and SIMS techniques. Chemical Geology 182: 605-618.

Landis CA, Campbell HJ, Aslund T, Cawood PA, Douglas A 1999. Permian-Jurassic strata at Productus Creek Southland, New Zealand: implications for terrane dynamics of the eastern Gondwanaland margin. New Zealand Journal of Geology and Geophysics 42: 255-278.

Lock R; Petroleum Corporation of NZ Exploration Ltd 1983. Stratford-1 Well Completion Report. PPL 38034. Ministry of Economic Development New Zealand Unpublished Petroleum Report PR968.

Marsaglia KM, Ingersoll RV 1992. Compositional trends in arc-related, deep-marine sand and sandstones: a reassessment of magmatic-arc provenance. Geological Society of America Bulletin 104: 1637-1649.

McRae SC 1972. Glauconite. Earth-Science Reviews 8: 397-440

Morgans HE 2008. Pers comm. Micropaleontologist, Institute of Geological and Nuclear Sciences Ltd. Lower Hutt, New Zealand.

Mortimer N 2004. New Zealand's Geological Foundations. Gondwana Research 7 n.1: 261-272

Mortimer N, Smith Lyttle B 2001. New Zealand's geological foundations. Institute of Geological and Nuclear Sciences. Dunedin, New Zealand.

Muir RJ, Ireland TR, Weaver SD, Bradshaw JD 1994. Ion microprobe U-Pb zircon geochronology of granitic magmatism in the Western Province of the

South Island, New Zealand. Chemical Geology (Isotope Geoscience Section) 113: 171-189.

Muir RJ, Ireland TR, Weaver SD, Bradshaw JD 1996. Ion microprobe dating of Paleozoic Granitoids: Devonian magmatism in New Zealand and correlations with Australia and Antarctica. Chemical Geology (Isotope Geoscience Section) 127: 191-210.

Murray D; Fletcher Challenge Energy Taranaki 2000. Pohokura-1 Well Completion Report. Ministry of Economic Development New Zealand Unpublished Petroleum Report PR2491.

Murray D; Fletcher Challenge Energy Taranaki 2001. Pohokura South-1 Well Completion Report. PPL38705. Ministry of Economic Development New Zealand Unpublished Petroleum Report PR2588.

Palmer JA 1985. Pre-Miocene lithostratigraphy of Taranaki Basin, New Zealand. New Zealand Journal of Geology and Geophysics 28: 197-21.

Pickard AL, Adams CJ, Barley ME 2000. Australian provenances for Upper Permian to Cretaceous rocks forming accretionary complexes on the New Zealand sector of the Gondwanaland margin. Australian Journal of Earth Sciences 47: 987-1007.

Pupin JP 1980. Zircon and Granite petrology. Contributions to Mineralogy and Petrology 73: 207-220.

Rider MH 1986. The geological interpretation of well logs. Blackie and Sons Ltd, Glasgow. 168 p.

Roser BP, Mortimer N, Turnbull IN, Landis CA 1993. Geology and geochemistry of the Caples terrane, Otago, New Zealand: compositional variations near a Permo-Triassic arc margin. In: Ballance PF ed. South Pacific sedimentary basins, sedimentary basins of the world, 2. Elsevier, Amsterdam. Pp. 3-19.

SBPT; Shell BP and Todd Oil Services Ltd 1975. Well resume Turi-1. Ministry of Economic Development New Zealand Unpublished Petroleum Report PR659.

Scott JM, Palin JM 2008. LA-ICP-MS U-Pb zircon ages from Mesozoic plutonic rocks in eastern Fiordland, New Zealand. New Zealand Journal of Geology and Geophysics 51: 105-113.

Sheriff RE 1989. Geophysical Methods. Prentice Hall, New Jersey. 605 p.

Smale D 1992. Provenance of sediments in the Taranaki Basin: an assessment from heavy minerals. 1991 New Zealand Oil Exploration Conference Proceedings: 245-254.

Smale D 1996. Petrographic summaries of Taranaki petroleum reports. Institute of Geological and Nuclear Sciences report 96/1. Lower Hutt, New Zealand.

Smale D, Morton AC 1987. Heavy mineral suites of core samples from the McKee Formation (Eocene-lower Oligocene), Taranaki: implications for provenance and diagenesis. New Zealand Journal of Geology and Geophysics 30: 299-306.

Spandler C, Worden K, Arculus R, Eggins S 2005. Igneous rocks of the Brook Street Terrane, New Zealand: implications for Permian tectonics of eastern Gondwana and magma genesis in modern intra-oceanic volcanic arcs. New Zealand Journal of Geology and Geophysics 48: 167-183.

Stagpoole V, Nicol A 2008. Regional structure and kinematic history of a large subduction back thrust: Taranaki Fault, New Zealand. Journal of Geophysical Research 113: 1-19.

STOS; Shell BP Todd Oil Services Ltd 1988. Well resume Mokau-1. PPL38098. Ministry of Economic Development New Zealand Unpublished Petroleum Report PR1396.

Thrasher GP 1990. Tectonics of the Taranaki Rift. 1989 New Zealand Oil Exploration Conference Proceedings.

Tripathi A 2009. Basin analysis of the Late Eocene – Oligocene Te Kuiti Group, western North Island, New Zealand. Unpublished PhD thesis, University of Waikato, Hamilton, New Zealand.

Tripathi A, Kamp PJJ 2008. Timing of initiation of reverse displacement on the Taranaki Fault, northern Taranaki Basin: constraints from the on land record. 2008 New Zealand Petroleum Conference Proceedings.

Turnbull IM 1979. Stratigraphy and sedimentology of the Caples terrane of the Thomson Mountains, northern Southland, New Zealand. New Zealand Journal of Geology and Geophysics 22: 555-574.

Vermeesch P 2004. How many grains are needed for a provenance study? Earth and Planetary Science Letters 224: 441-451.

Vonk A, Kamp PJJ 2008. The Late Miocene Southern and Central Taranaki Inversion Phase (SCTIP) and related sequence stratigraphy and paleogeography. 2008 New Zealand Petroleum Conference Proceedings, Auckland, NZ Ministry of Economic Development.

Waight TE, Weaver SD, Ireland TR, Maas R, Muir RJ, Shelley D 1997. Field characteristics, petrography, and geochronology of the Hohonu Batholith and the adjacent Granite Hill Complex, North Westland, New Zealand. New Zealand Journal of Geology and Geophysics 40: 1-17.

Wandres AM, Bradshaw JD, Weaver S, Maas R, Ireland T, Eby N 2004a. Provenance analysis using conglomerate class lithologies: a case study from the Pahau terrane of New Zealand. Sedimentary Geology 167: 57-89.

Wandres AM, Bradshaw JD, Weaver S, Maas R, Ireland T, Eby N 2004b. Provenance of the sedimentary Rakaia sub-terrane, Torlesse terrane, South Island, New Zealand: the use of igneous class compositions to define the source. Sedimentary Geology 168: 193-226.

Webster M, Rainey S; Petroleum Corporation of NZ Exploration Ltd 1987. Te Kiri-1 Well Completion Report. PPL 38034. Ministry of Economic Development New Zealand Unpublished Petroleum Report PR1249.

White PJ, Waterhouse BC 1993. Lithostratigraphy of the Te Kuiti Group: a revision. New Zealand Journal of Geology and Geophysics 36: 255-266.

Young J, Carter M; Petrocorp Exploration Ltd 1989. Waihapa-5 Well Completion Report. PML 38140. Ministry of Economic Development New Zealand Unpublished Petroleum Report PR1851.

APPENDIX I

SAMPLE INFORMATION

I.1 – Subsurface sample numbers (well cutting samples) and types of analysis.

Well	Formation/member	Depth (m)	Carbonate content/grain size sample No.	Petrography sample No.	U-Pb geochronology sample No.	UOW number	Coments
Ahuroa-1	Matapo Sandstone	3210-3213	-	-	-	-	Sample returned to MED
		3213-3216	2	-	-	-	Remainder of sample returned to MED
		3216-3219	-	-	-	-	Sample returned to MED
Ahuroa-1	Matapo Sandstone	3222-3225	3	-	-	-	Remainder of sample returned to MED
		3228-3231	-	-	-	-	Sample returned to MED
Awakino-1	Taimana Formation	1878-1881	-	-	-	-	Sample returned to MED
		1881-1884	4	-	-	-	Remainder of sample returned to MED
		1884-1887	-	-	-	-	Sample returned to MED
		1887-1890	-	-	-	-	Sample returned to MED
Kaimiro-1	Taimana Formation	2998-3001	-	-	-	-	Sample returned to MED
		3001-3004	-	-	-	-	Sample returned to MED
		3004-3007	5	-	-	-	Remainder of sample returned to MED
		3007-3010	-	-	-	-	Sample returned to MED
Kaimrio-1	Taimana Formation	3139-3142	-	-	-	-	Sample returned to MED
		3142-3145	-	-	-	-	Sample returned to MED
		3145-3148	6	-	-	-	Remainder of sample returned to MED
		3148-3151	-	-	-	-	Sample returned to MED
Kaimiro-1	McKee Formation	3739-3742	-	-	-	-	-
		3742-3745	-	-	-	-	-
		3745-3748	-	-	-	-	-
		3748-3751	-	-	-	-	-
		3751-3754	-	-	-	-	-
		3754-3757	-	-	-	-	-
		3757-3760	-	-	-	-	Sample retained and returned to MED
		3760-3763	-	-	-	-	-
		3763-3766	-	-	-	-	-
		3766-3769	-	8	8	20090400	Aggregated depths 3739-3769 (excluding 3757-3760 m)
Mokau-1	Otaraoa Formation	2700-2710	8	-	-	-	Remainder of sample returned to MED
Mokau-1	Otaraoa Formation	2740-2750	7	-	-	-	Remainder of sample returned to MED
Ngatoro-1	Matapo Sandstone	3550-3553	-	-	-	-	-
		3553-3556	-	-	-	-	-
		3556-3559	-	-	-	-	-
		3559-3562	-	-	-	-	-
		3562-3565	-	-	-	-	-
		3565-3568	-	-	-	-	-
		3568-3571	-	-	-	-	-
		3571-3574	-	-	-	-	-
		3574-3577	-	-	-	-	-
		3577-3580	-	-	-	-	Sample retained and returned to MED
		3580-3583	-	-	-	-	-
		3583-3586	-	-	-	-	-
		3586-3589	-	-	-	-	-
		3589-3592	-	-	-	-	-
		3592-3595	-	-	-	-	-
		3595-3598	-	-	-	-	-
		3598-3601	-	10	10	20090401	Aggregated depths 3550-3601 (excluding 3577-3580 m)
Pohokura-1	Turi Formation	3305	-	-	-	-	Sample returned to MED
		3312	10	-	-	-	Remainder of sample returned to MED
Pohokura-1	Turi Formation	3384	-	-	-	-	Sample returned to MED
		3390	11	-	-	-	Remainder of sample returned to MED
Pohokura-1	Turi Formation	3423-3426	-	-	-	-	-
		3426-3429	-	-	-	-	-
		3429-3432	-	-	-	-	-
		3432-3435	-	-	-	-	-
		3435-3438	-	-	-	-	-
		3438-3441	-	-	-	-	-
		3441-3444	-	-	-	-	-
		3444-3447	-	-	-	-	-
		3447-3450	-	-	-	-	Sample retained and returned to MED
		3450-3453	-	-	-	-	-
		3453-3456	-	-	-	-	-
		3456-3459	-	-	-	-	-
		3459-3462	-	-	-	-	-
		3462-3465	-	-	-	-	-
		3465-3468	-	-	-	-	-
		3468-3471	-	12	12	20090402	Aggregated depths 3423-3471 (excluding 3447-3450 m)

Subsurface sample numbers continued.

Tariki-1	Otaraoa Formation	2340-2343	-	-	-		Sample returned to MED
		2343-2346	-	-	-		Sample returned to MED
		2346-2349	13	-	-		Remainder of sample returned to MED
Tariki-1	Otaraoa Formation	2580-2583	-	-	-		Sample returned to MED
		2583-2586	14	-	-		Remainder of sample returned to MED
		2586-2589	-	-	-		Sample returned to MED
Tariki-1	Tariki Sandstone	2808-2811	-	-	-	-	-
		2811-2814	-	-	-	-	-
		2814-2817	-	-	-	-	-
		2817-2820	-	-	-	-	-
		2820-2823	-	-	-	-	-
		2820-2823	-	-	-	-	-
		2823-2826	-	-	-	-	-
		2826-2829	-	-	-	-	-
		2829-2832	-	-	-	-	-
		2832-2835	-	-	-	-	Sample retained and returned to MED
		2835-2838	-	-	-	-	-
		2838-2841	-	-	-	-	-
		2841-2844	-	-	-	-	-
		2844-2847	-	-	-	-	-
		2847-2850	-	-	-	-	-
		2850-2853	-	-	-	-	-
		2853-2856	-	-	-	-	-
		2856-2859	-	-	14	20090403	Aggregated depths 2808-2859 (excluding 2832-2835 m)
Tariki-1	Tariki Sandstone	2868-2871	-	-	-	-	-
		2871-2874	-	-	-	-	-
		2877-2880	-	-	-	-	-
		2883-2886	-	-	-	-	-
		2886-2889	-	-	-	-	-
		2889-2892	-	-	-	-	-
		2892-2895	-	-	-	-	-
		2895-2898	-	-	-	-	Sample retained and returned to MED
		2898-2901	-	-	-	-	-
		2901-2904	-	-	-	-	-
		2904-2907	-	-	-	-	-
		2907-2910	-	-	-	-	-
		2910-2913	-	-	-	-	-
		2913-2916	-	-	-	-	-
		2916-2919	-	-	-	-	-
		2919-2922	-	13	13	20090404	Aggregated depths 2868-2922 (excluding 2895-2898 m)
Tariki-1	Tariki Sandstone	2940-2941	-	-	-	-	-
		2941-2942	-	-	-	-	-
		2942-2943	-	-	-	-	-
		2943-2944	-	-	-	-	-
		2944-2945	-	-	-	-	-
		2945-2946	-	-	-	-	-
		2946-2947	-	-	-	-	-
		2947-2948.5	-	-	-	-	-
		2948.5-2952	-	-	-	-	-
		2952-2955	-	-	-	-	-
		2955-2958	-	-	-	-	-
		2958-2961	-	-	-	-	-
		2961-2964	-	-	-	-	Sample retained and returned to MED
		2964-2967	-	-	-	-	-
		2967-2970	-	-	-	-	-
		2970-2973	-	-	-	-	-
		2973-2976	-	-	-	-	-
		2976-2979	-	-	-	-	-
		2979-2982	-	-	-	-	-
		2982-2985	-	-	-	-	-
		2985-2988	-	-	-	-	-
		2988-2991	-	9	9	20090405	Aggregated depths 2940-2991 (excluding 2961-2964 m)
Tariki-1	Matapo Sandstone	3021-3024	-	-	-		Sample returned to MED
		3024-3027	18	-	-		Remainder of sample returned to MED
		3027-3030	-	-	-		Sample returned to MED
Toetoe-1	Otaraoa Intra	2109-2112	-	-	-		Sample returned to MED
		2112-2115	-	-	-		Sample returned to MED
		2115-2118	19	-	-		Remainder of sample returned to MED
		2119-2121	-	-	-		Sample returned to MED
Toetoe-1	Otaraoa Intra	2091-2094	-	-	-		Sample returned to MED
		2094-2097	20	-	-		Remainder of sample returned to MED
		2097-2100	-	-	-		Sample returned to MED
Toko-1	Taimana Formation	2860-2863	-	-	-		Sample returned to MED
		2863-2866	21	-	-		Remainder of sample returned to MED
		2866-2869	-	-	-		Sample returned to MED
Toko-1	Taimana Formation	2911-2914	-	-	-		Sample returned to MED
		2914-2917	22	-	-		Remainder of sample returned to MED
		2917-2920	-	-	-		Sample returned to MED

Well location map.

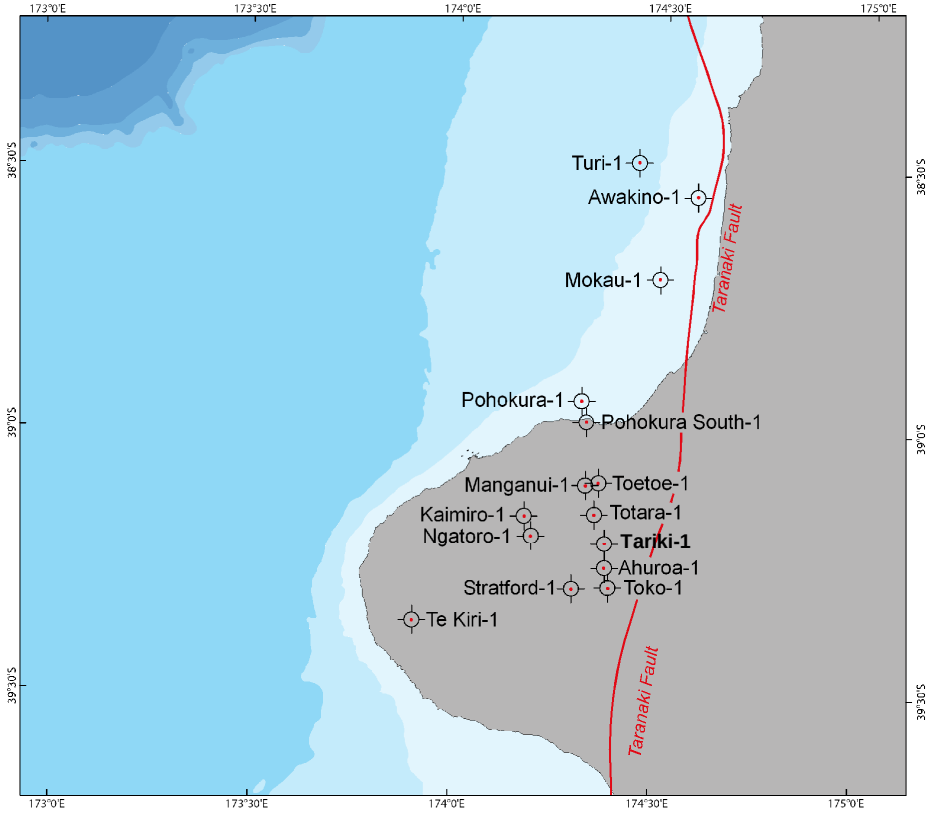

I.2 – Onshore samples

Onshore sample summary, with sampled well, formation/member and sample purpose.

Sample area	Formation/ member	Sample purpose
Port Waikato	Glen Massey Formation (Ahirau Sandstone Member)	Petrography and U-Pb geochronology
Aotea Harbour	Glen Massey Formation (Ahirau Sandstone Member)	Petrography and U-Pb geochronology
Awamarino	Glen Massey Formation (Ahirau Sandstone Member)	Petrography and U-Pb geochronology
Hautapu Hill	Aotea Formation (Hauturu Sandstone Member)	Petrography and U-Pb geochronology
Kihi Road	Aotea Formation (Hauturu Sandstone Member)	Petrography and U-Pb geochronology
Taumarunui	Taumarunui quartz sandstone	Petrography and U-Pb geochronology
Otaihanga	Otaihanga Outlier	Petrography and U-Pb geochronology

Sample 1 – Ahirau Sandstone

Location: Sunset Farm, Waikaretu, Port Waikato

Grid reference: longitude – 2664798, latitude – 6417568

Sample description: Light blue-grey to brownish-grey, well cemented sandstone.

Note: Sampled as part of Tripathi's (2008) thesis (samples: WO33-016, 015, 018, 019).

Sample 2 – Ahirau Sandstone

Location: Orotangi Cliffs, Okapu Station, Aotea Harbour

Grid reference: longitude – 2673640, latitude – 6353050

Sample description: Light blue-grey to brownish-grey, well cemented sandstone.

Note: Sampled as part of Tripathi's (2008) thesis (samples: WO33-318, 319, 320, 321).

Sample 3 – Ahirau Sandstone

Location: Kairimu Road, South of Awamarino

Grid reference: longitude – 2668370, latitude – 6320399

Sample description: Light blue-grey to brownish-grey, well cemented sandstone.

Note: Sampled as part of Tripathi's (2008) thesis (samples: WO33-461, 461).

Sample 4 – Hauturu Sandstone

Location: Hautapu Hill, south of Hauturu

Grid reference: longitude – 2678955, latitude – 6342499

Sample description: Light blue-grey to brownish-grey, well cemented sandstone.

Note: Sampled as part of Tripathi's (2008) thesis (samples: WO33-342, 343, 344, 345, 346).

Sample 5 – Hauturu Sandstone

Location: 2 km east of Hauturu, south of Kihi Road

Grid reference: longitude – 2681500, latitude – 6342500

Sample description: Light blue-grey to brownish-grey, well cemented sandstone.

Note: Sampled as part of Tripathi's (2008) thesis (samples: WO33-358, 359, 363).

Sample 7 – Taumarunui quartz sandstone

Location: Oruaiwi, Taumarunui

Grid reference: easting – 2722240, northing – 3262868

Sample description: Medium to coarse grained, quartz rich sandstone.

Note: Sampled as part of Cartwright's (2003) thesis.

Sample 15 – Otaihanga Outlier

Location: Otaihanga

Grid reference: unknown

Sample description: Quartz rich sandstone.

Note: Sample of zircons only, provided by Professor Peter Kamp (sample: 9801-63).

Onshore North Island sample location map.

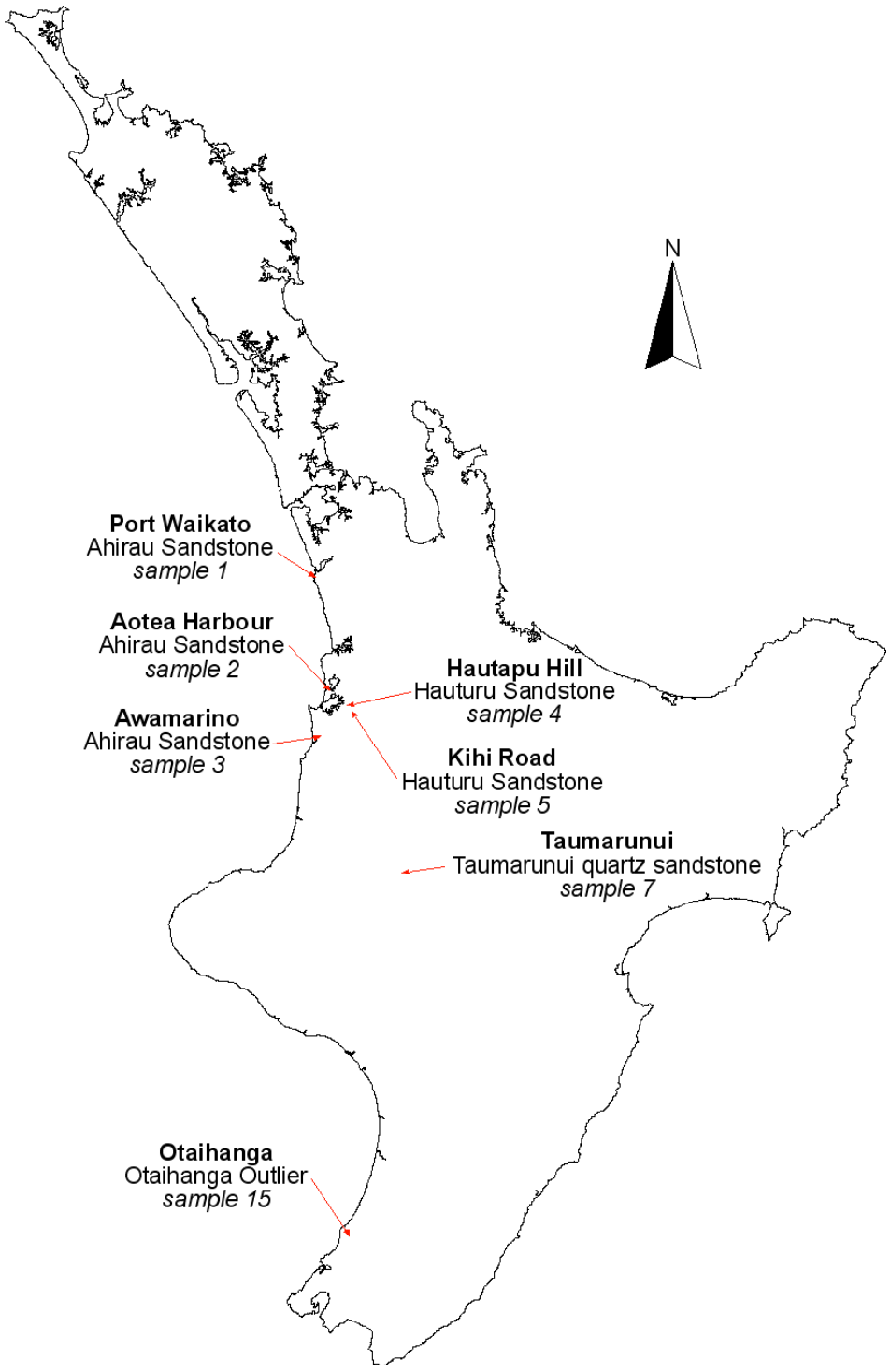

APPENDIX II

WIRELINE MOTIFS IN SELECTED WELLS

II.1 – Wireline motif subdivisions in selected wells

The following figures present the wireline motifs that have been identified through the Late Eocene – Oligocene succession for the 15 selected wells in this study. Figures are adapted from well cards supplied by the Institute of Geological and Nuclear Sciences Limited.

Ahuroa-1

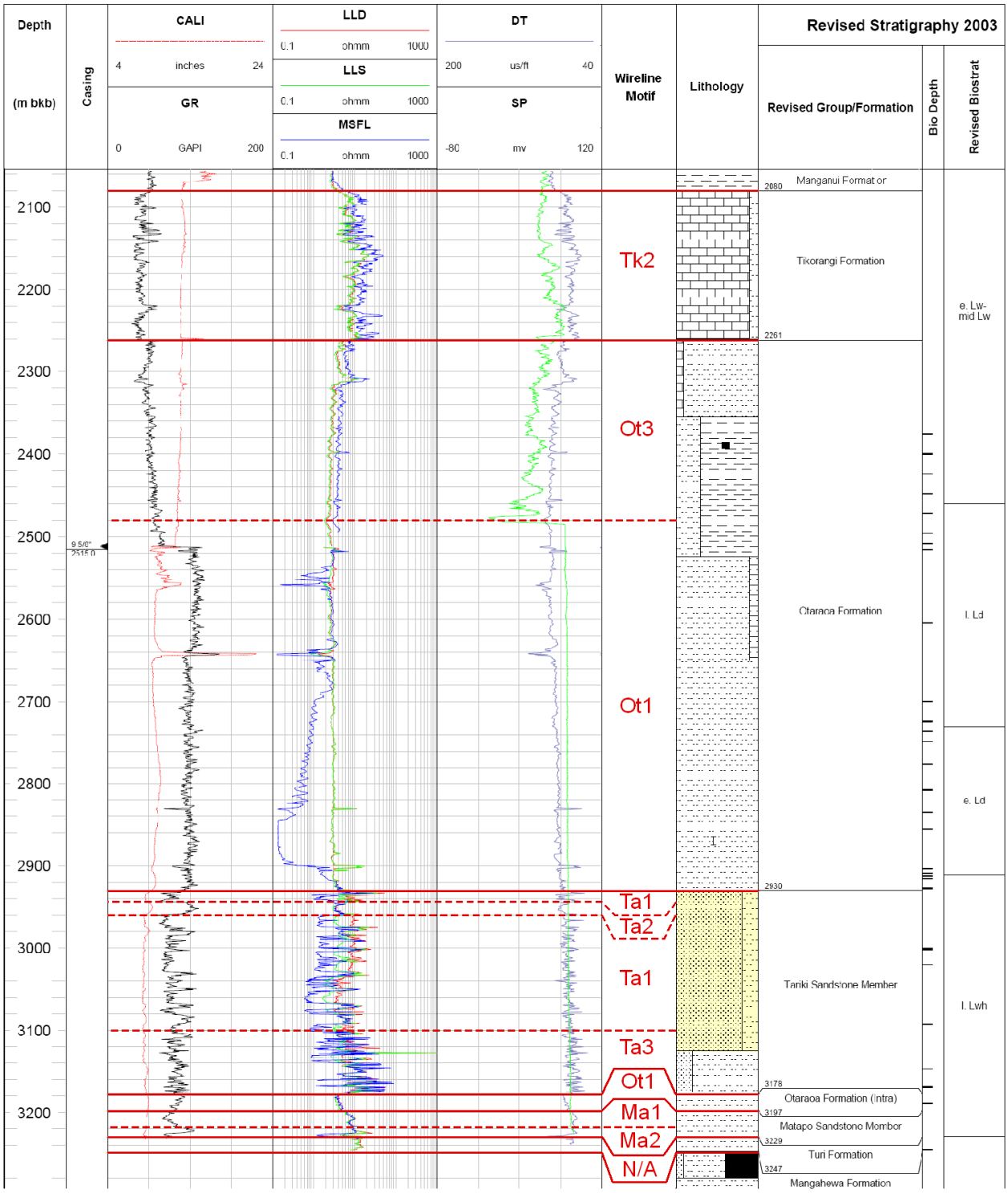

Tk1: 2080 m – 2261 m
Ot3: 2261 m – 2480 m
Ot1: 2480 m – 2930 m
Ta1: 2930 m – 2944 m
Ta2: 2944 m – 2960 m
Ta1: 2960 m – 3100 m
Ta3: 3100 m – 3178 m
Ot1: 3178 m – 3197 m
Ma1: 3197 m – 3211 m
Ma2 3211 m – 3229 m

Awakino-1

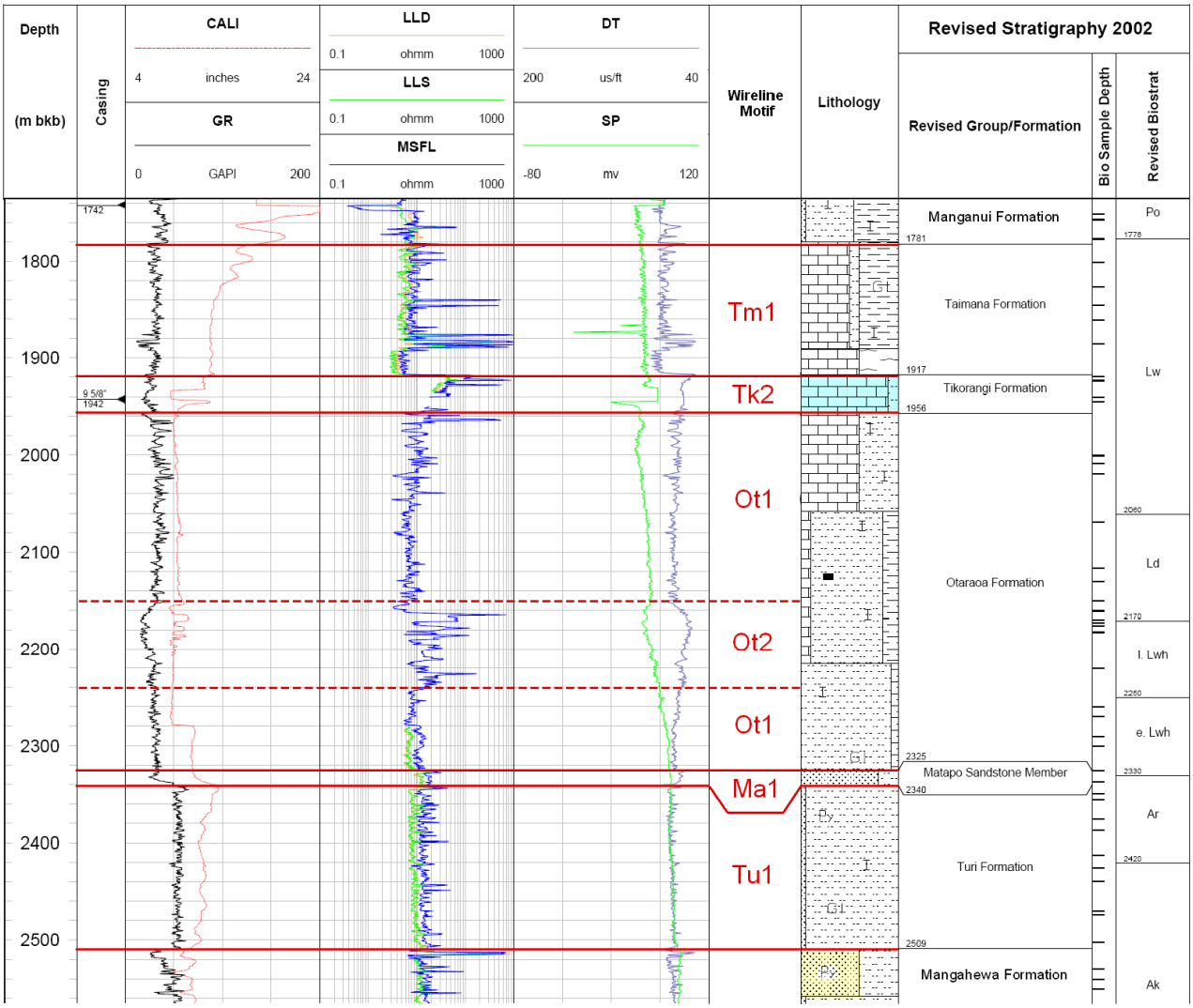

Tm1: 1781 m – 1917 m
Tk2: 1917 m – 1956 m
Ot1: 1956 m – 2150 m
Ot2: 2150 m – 2240 m
Ot3: 2240 m – 2325 m
Ma1: 2325 m – 2340 m
Tu1: 2340 m – 2509 m

Kaimiro-1

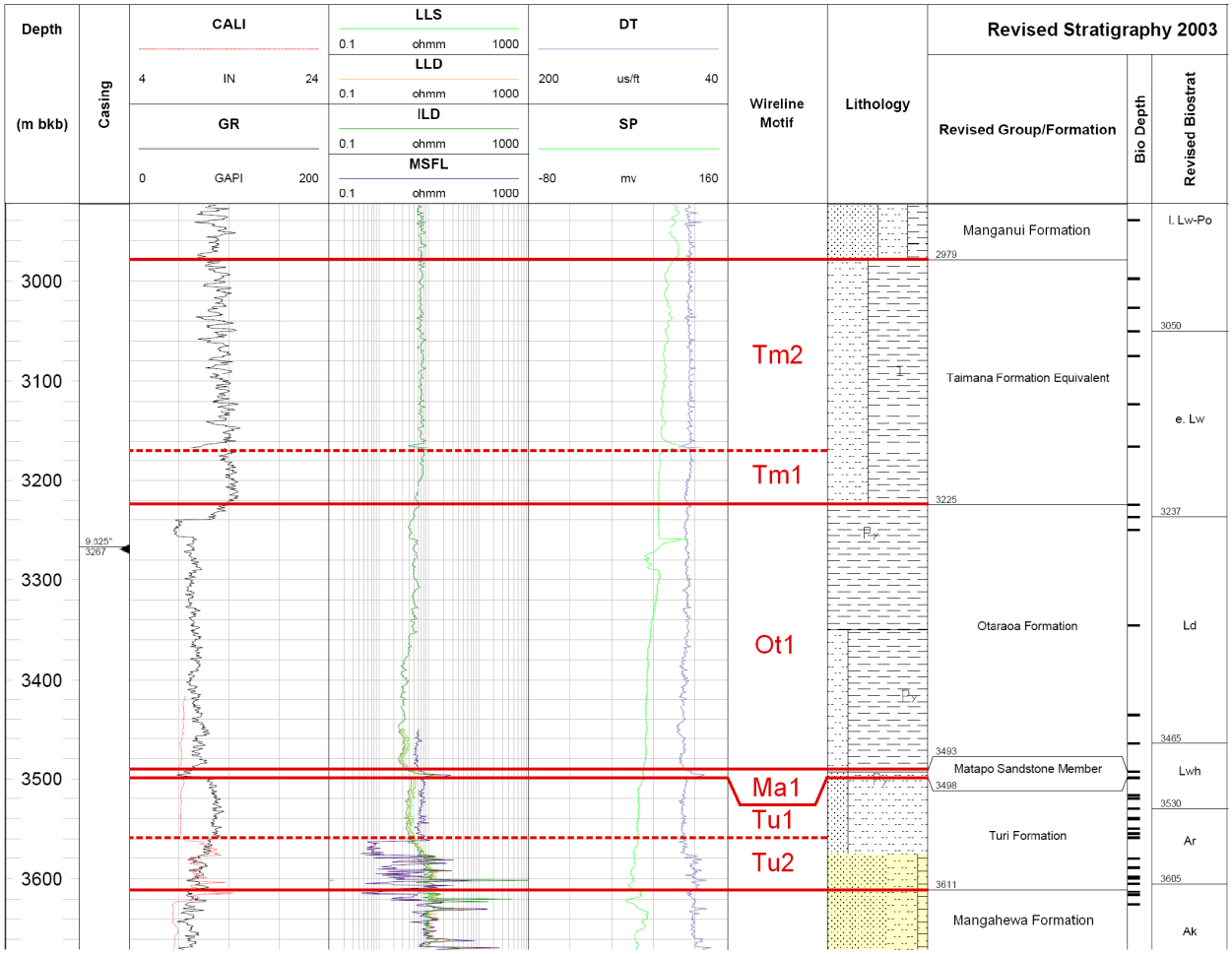

Tm2: 2979 m – 3170 m
Tm1: 3170 m – 3225 m
Ot1: 3225 m – 3493 m
Ma1: 3493 m – 3498 m
Tu1: 3498 m – 3558 m
Tu2: 3558 m – 3611 m

Manganui-1

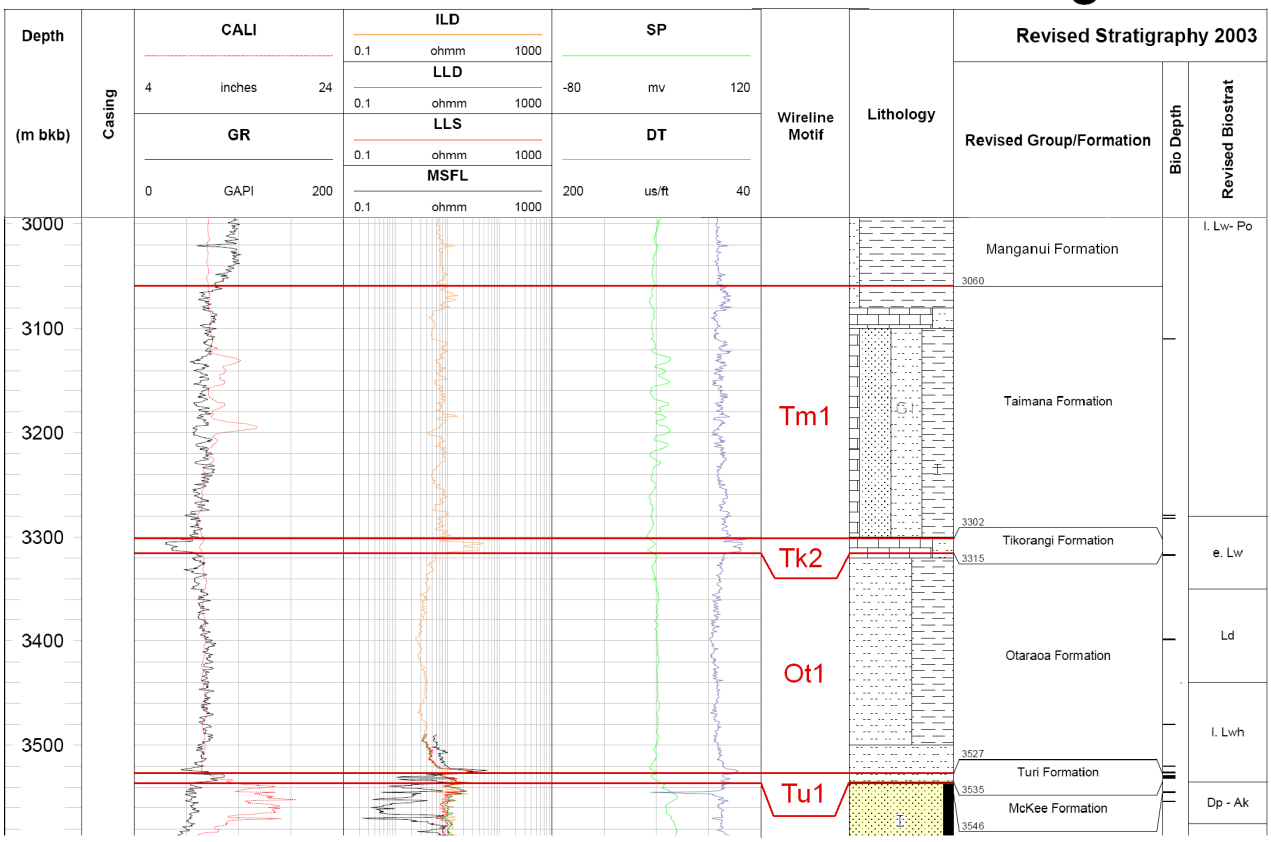

Tm1: 3060 m – 3302 m
Tk2: 3302 m – 3315 m
Ot1: 3315 m – 3527 m
Tu1: 3527 m – 3535 m

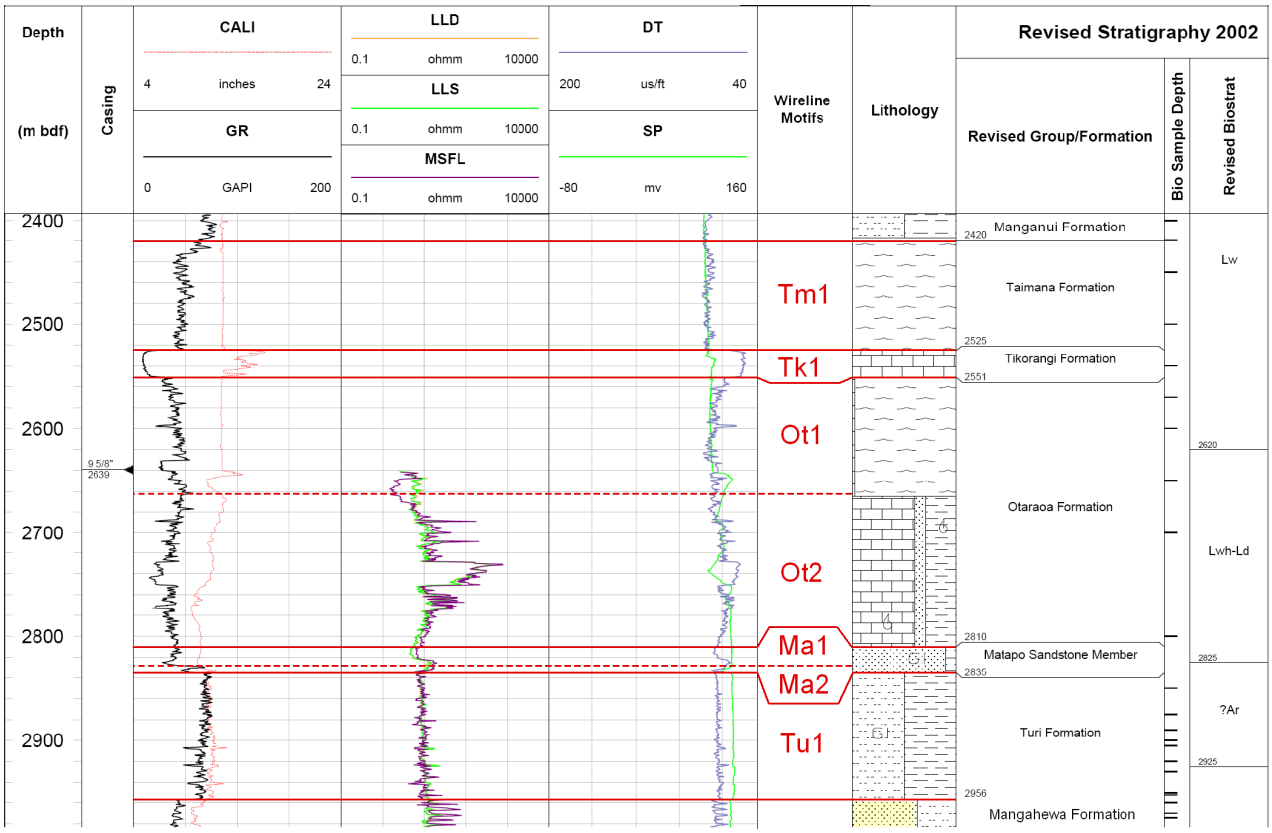

Tm1: 2420 m – 2525 m
Tk2: 2525 m – 2551 m
Ot1: 2551 m – 2600 m
Ot2: 2600 m – 2810 m
Ma1: 2810 m – 2828 m
Ma2: 2828 m – 2836 m
Tu1: 2836 m – 2956 m

Ngatoro-1

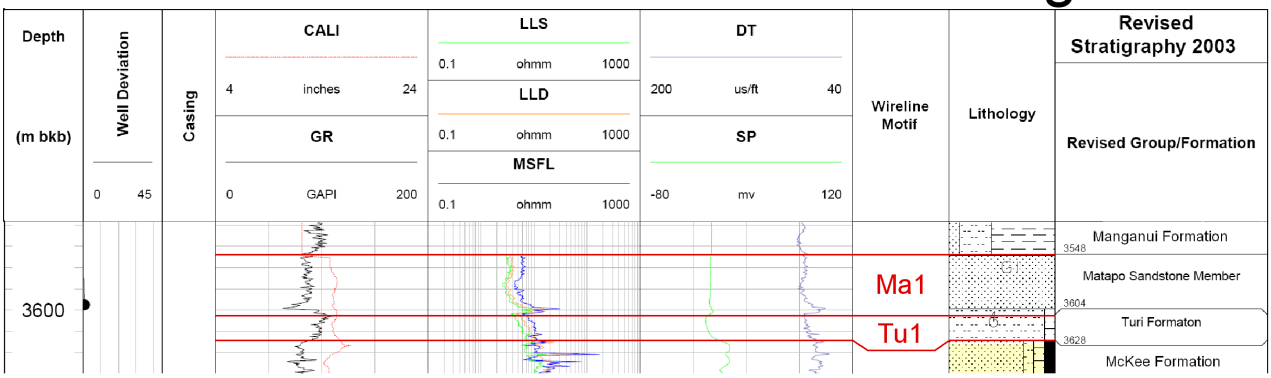

Ma1: 3548 m – 3604 m
Tu1: 3604 m – 3628 m

Pohokura-1

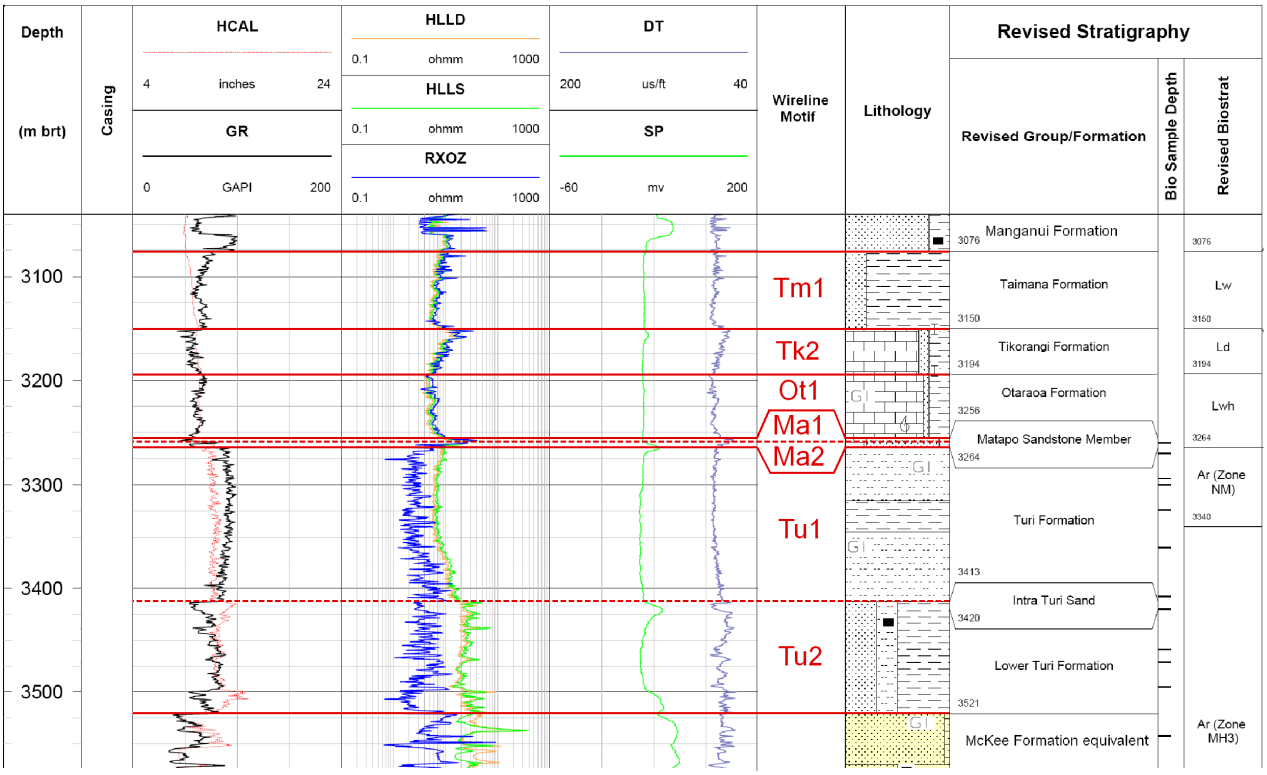

Tm1: 3076 m – 3150 m
Tk2: 3150 m – 3194 m
Ot1: 3194 m – 3256 m
Ma1: 3256 m – 3261 m
Ma2: 3261 m – 3264 m
Tu1: 3264 m – 3413 m
Tu2: 3413 m – 3521 m

Pohokura South-1

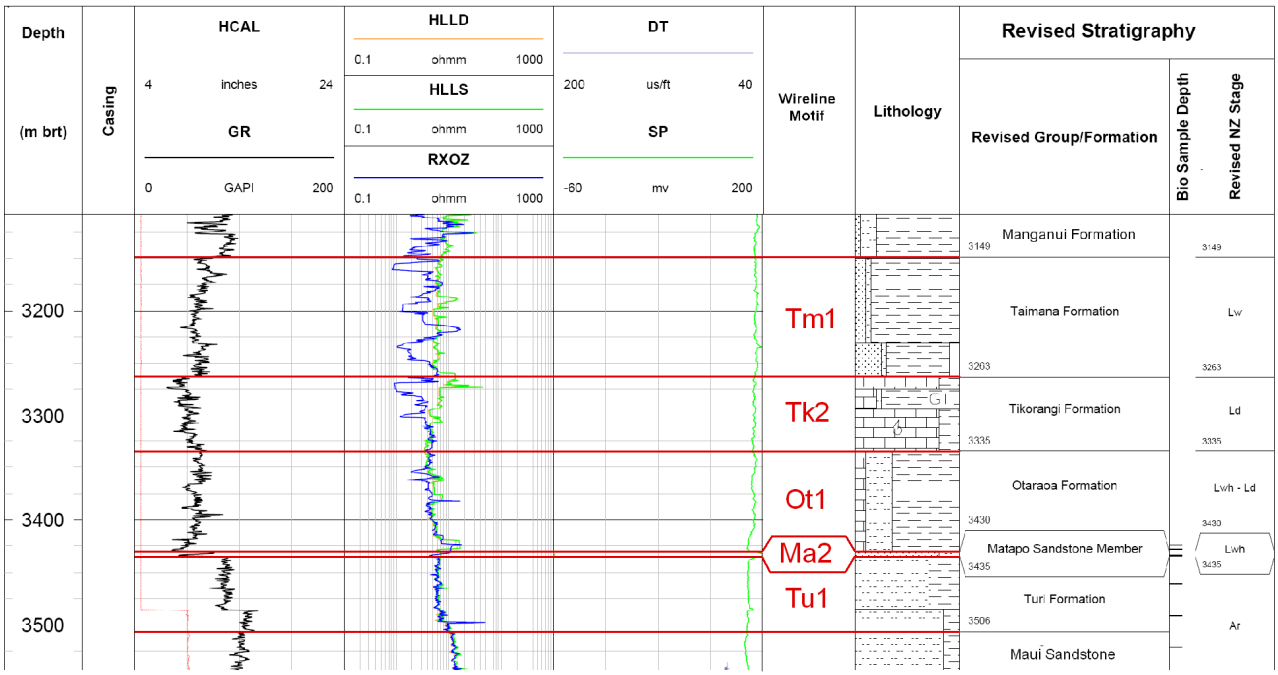

Tm1: 3149 m – 3263 m
Tk2: 3263 m – 3335 m
Ot1: 3335 m – 3430 m
Ma2: 3430 m –3435 m
Tu1: 3435 m – 3506 m

Stratford-1

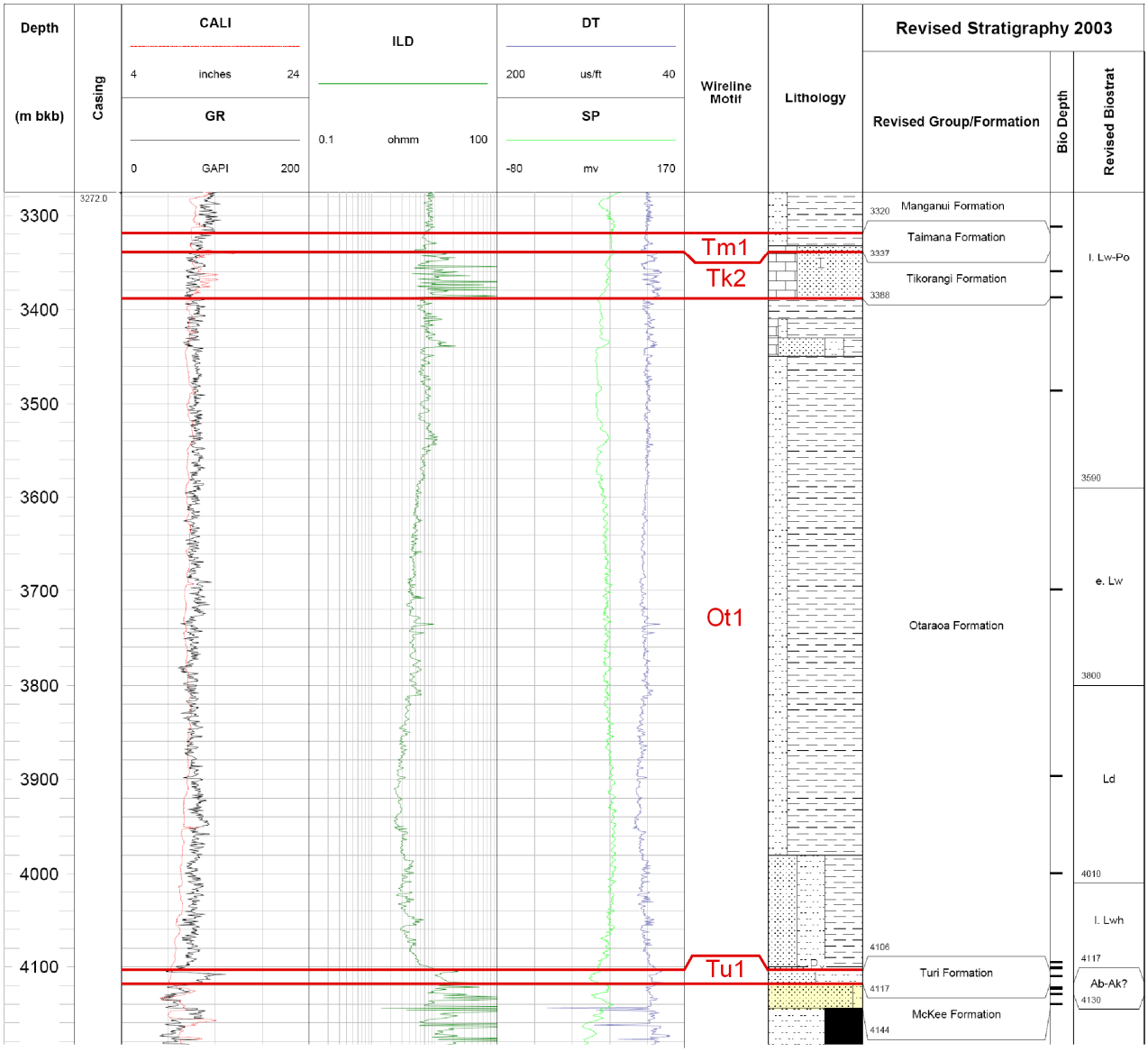

Tm1: 3320 m – 3337 m
Tk2: 3337 m – 3388 m
Ot1: 3388 m – 4106 m
Tu1: 4106 m – 4117 m

Tariki-1

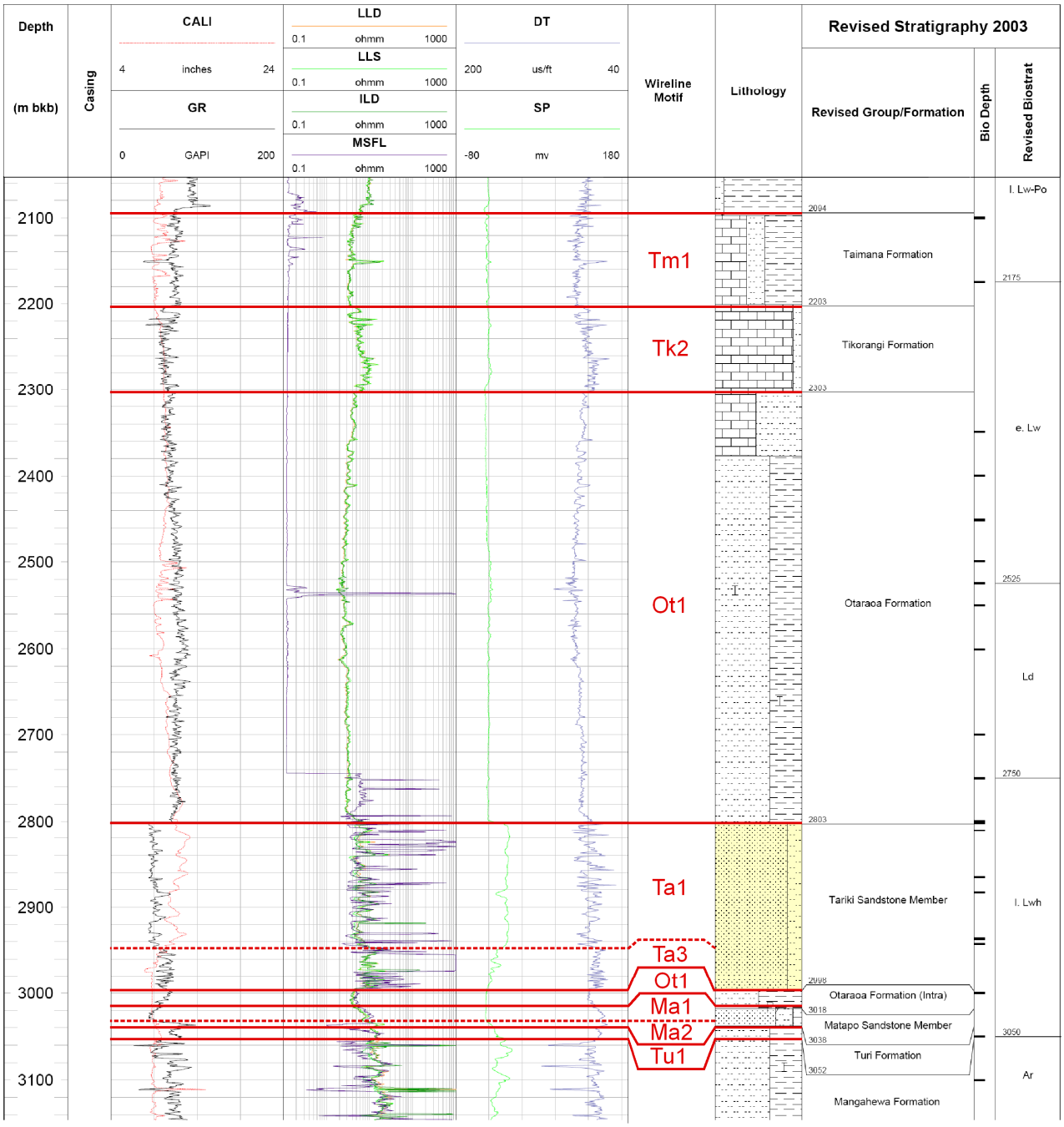

Tm1: 2094 m – 2203 m
Tk2: 2203 m – 3303 m
Ot1: 3303 m – 2803 m
Ta1: 2803 m – 2949 m
Ta3: 2949 m – 2998 m
Ot1: 2998 m – 3018 m
Ma1: 3018 m – 3033 m
Ma2: 3033 m – 3038 m
Tu1: 3038 m – 3052 m

Te Kiri-1

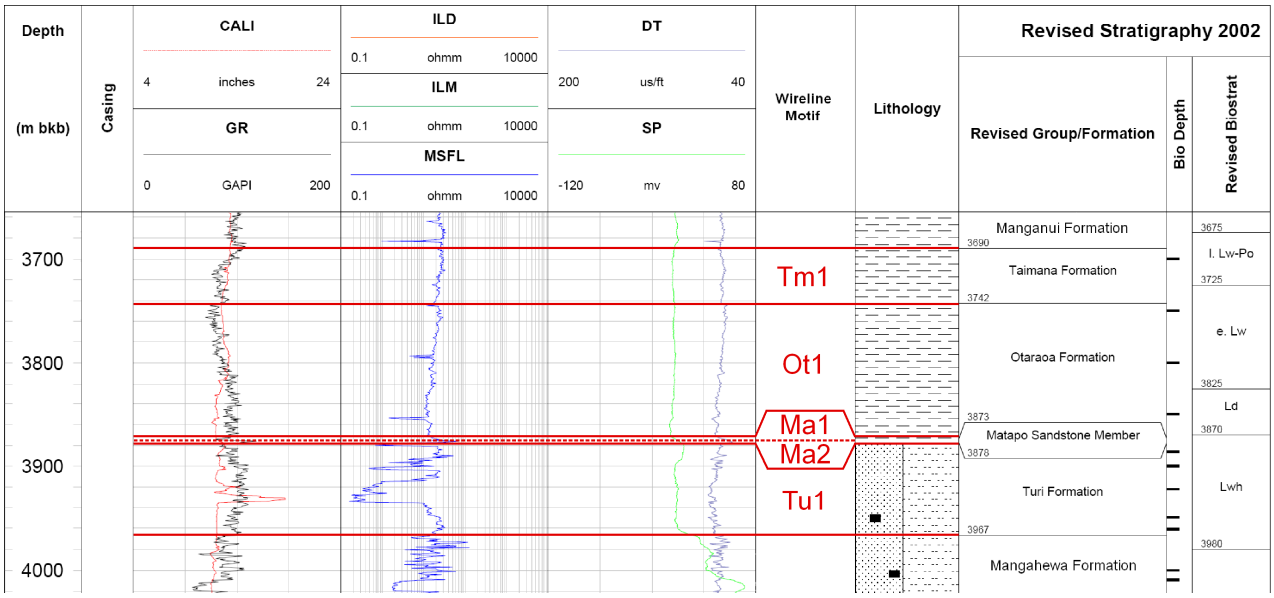

Tm1: 3690 m – 3742 m
Ot1: 2742 m – 2873 m
Ma1: 2873 m – 2876 m
Ma2: 2876 m – 2878 m
Tu1: 2878 m –2967 m

Toetoe-1

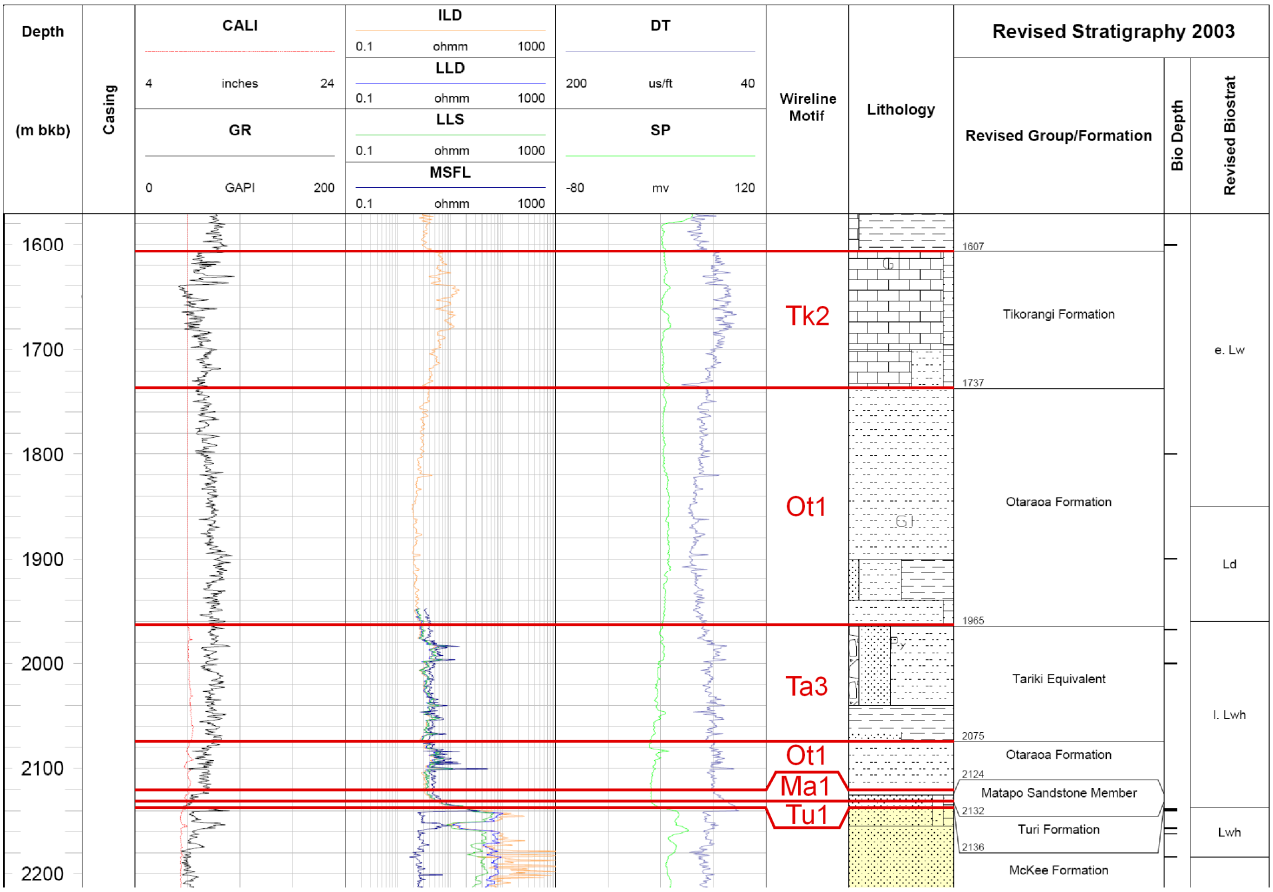

Tk2: 1607 m – 1737 m
Ot1: 1737 m – 1965 m
Ta3: 1965 m – 2075 m
Ot3: 2075 m – 2124 m
Ma1: 2124 m – 2132 m
Tu1: 2132 m – 2136 m

Toko-1

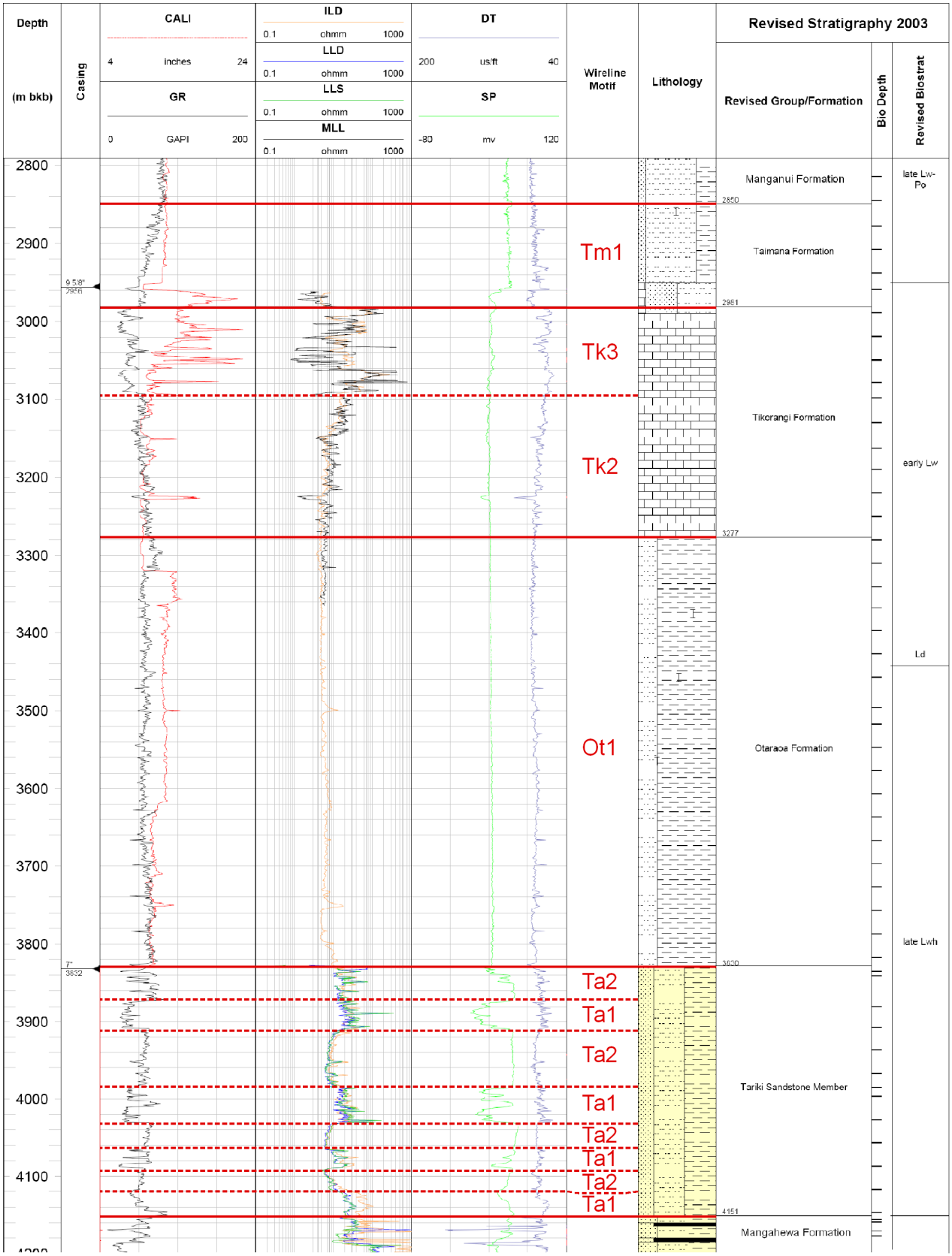

Tm1: 2850 m – 2981 m
Tk3: 2981 m – 3100 m
Tk2: 3100 m – 3277 m
Ot1: 3277 m – 3830 m
Ta2: 3830 m – 3870 m
Ta1: 3870 m – 3912 m
Ta2: 3912 m – 3982 m
Ta1: 3982 m – 4033 m
Ta2: 4033 m – 4062 m
Ta1: 4062 m – 4094 m
Ta2: 4094 m – 4110 m
Ta1: 4110 m – 4151 m

Totara-1

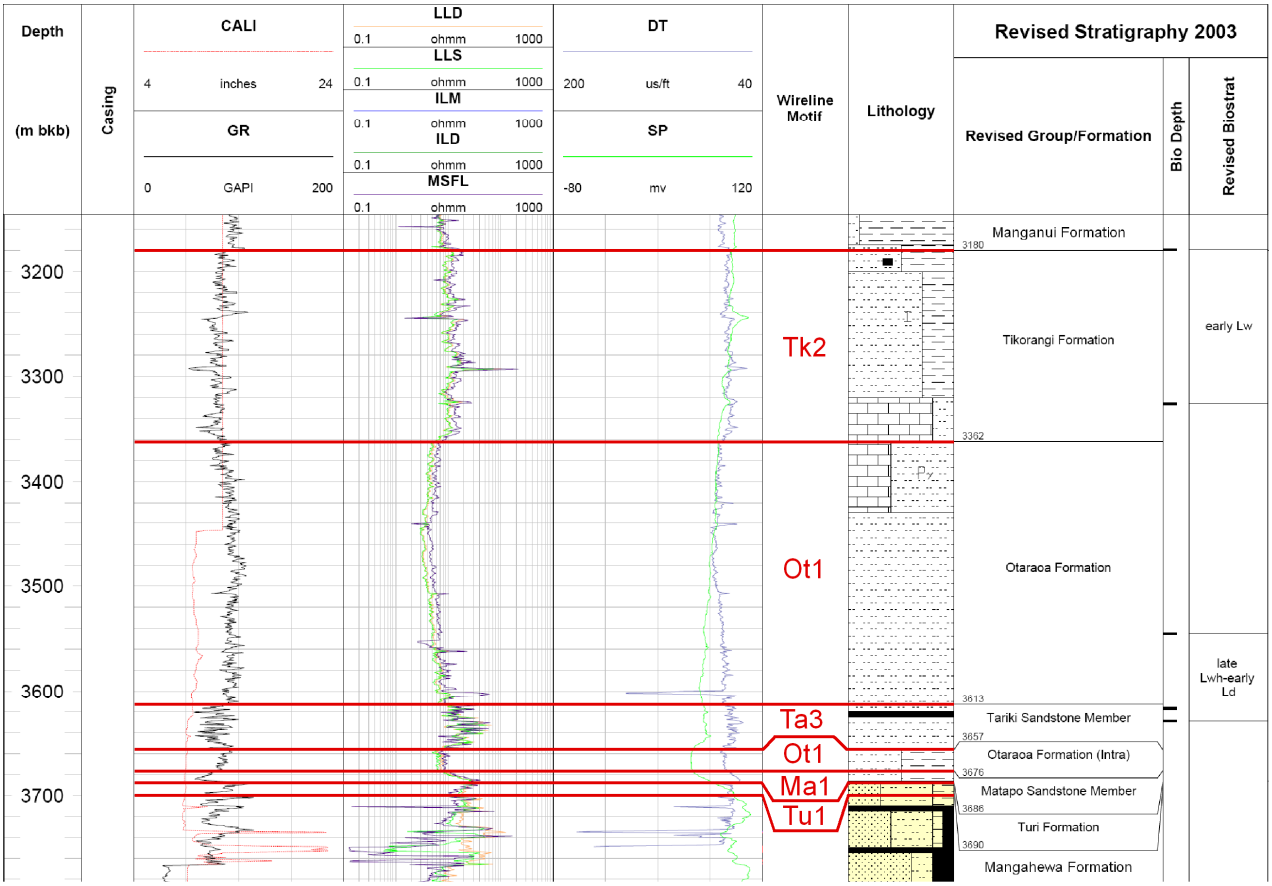

Tk2: 3180 m – 3362 m
Ot1: 3362 m – 3613 m
Ta3: 3613 m – 3657 m
Ot1: 3657 m – 3676 m
Ma1: 3676 m – 3686 m
Tu1: 3686 m – 3690 m

Turi-1

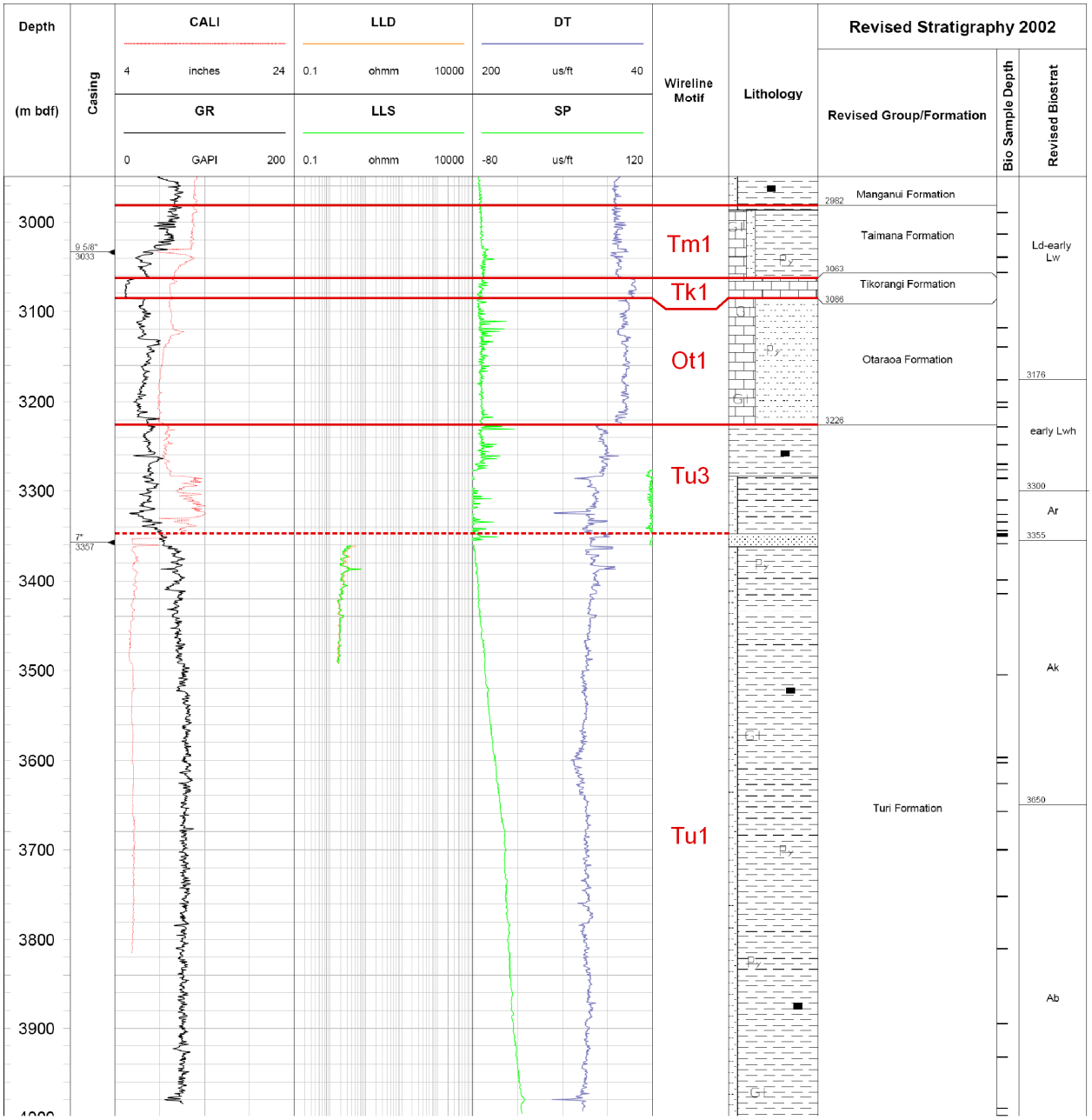

Tm1: 2982 m – 3063 m
Tk1: 3063 m – 3086 m
Ot1: 3086 m – 3226 m
Tu3: 3220 m – 3347 m
Tu1: 3347 m +

APPENDIX III

CARBONATE CONTENT AND GRAIN SIZE

III.1 – Samples for carbonate digestion and grain size determination

Carbonate digestion and grain size sample numbers with associated sampled well, formation/member and depth.

Well	Formation/Member	Depth (m)	Carbonate digestion/ grain size sample number
Kaimiro-1	Taimana Formation	3145 - 3148	**6**
Kaimiro-1	Taimana Formation	3004 - 3007	**5**
Toko-1	Taimana Formation	2914 - 2917	**22**
Toko-1	Taimana Formation	2863 - 2866	**21**
Awakino-1	Taimana Formation	1881 - 1884	**4**
Mokau-1	Otaraoa Formation	2740 - 2750	**7**
Mokau-1	Otaraoa Formation	2700 - 2710	**8**
Tariki-1	Otaraoa Formation	2583 - 2586	**14**
Tariki-1	Otaraoa Formation	2346 - 2349	**13**
Toetoe-1	Otaraoa Formation (*intra* Member)	2115 - 2118	**19**
Toetoe-1	Otaraoa Formation (*intra* Member)	2094 - 2097	**20**
Ahuroa-1	Otaraoa Formation (Matapo Sandstone Member)	3222 - 3225	**3**
Ahuroa-1	Otaraoa Formation (Matapo Sandstone Member)	3213 - 3216	**2**
Tariki-1	Otaraoa Formation (Matapo Sandstone Member)	3024 - 3027	**18**
Pohokura-1	Turi Formation	3390	**11**
Pohokura-1	Turi Formation	3312	**10**

III.2 – Carbonate content

Carbonate digestion raw data. Note that the sample number refers to carbonate digestion/grain size sample numbers referred to above.

Sample No.	Sample (g)	Filter Paper (g)	Filter Paper + Residue (g)	Residue (g)	CO_3 (g)	$\%CO_3$		% Error
2	4.95	1.82	3.94	2.12	2.83	**57.2**	±	*0.126 %*
3	5.04	1.82	4.94	3.12	1.92	**38.1**	±	*0.176 %*
4	4.94	1.82	3.79	1.97	2.97	**60.1**	±	*0.121 %*
5	5.35	1.82	6.54	4.72	0.63	**11.8**	±	*0.495 %*
6	5.17	1.82	6.55	4.73	0.44	**8.5**	±	*0.701 %*
7	5.89	1.82	4.12	2.3	3.59	**61.0**	±	*0.101 %*
8	4.65	1.82	3.71	1.89	2.76	**59.4**	±	*0.130 %*
10	5.04	1.12	5.63	4.51	0.53	**10.5**	±	*0.586 %*
11	4.51	1.82	5.92	4.1	0.41	**9.1**	±	*0.754 %*
13	4.85	1.82	4.55	2.73	2.12	**43.7**	±	*0.162 %*
14	5.23	1.82	5.64	3.82	1.41	**27.0**	±	*0.232 %*
18	5.18	1.82	3.79	1.97	3.21	**62.0**	±	*0.113 %*
19	5.32	1.82	4.45	2.63	2.69	**50.6**	±	*0.130 %*
20	5.24	1.12	4.05	2.93	2.31	**44.1**	±	*0.149 %*
21	5.15	1.12	5.5	4.38	0.77	**15.0**	±	*0.409 %*
22	5.1	1.82	6.07	4.25	0.85	**16.7**	±	*0.373 %*

III.3 – Grain size

The following figures illustrate the grain size characteristic data for analysed samples. Data have been obtained from a Malvern-Mastersizer S instrument. Note that the sample number refers to carbonate digestion/ grain size sample numbers referred to above.

MALVERN INSTRUMENTS

MASTERSIZER 2000

Result Analysis Report

Sample Name: 2	**SOP Name:** Marine Sediment	**Measured:** Thursday, 14 August 2008 1:37:28 p.m.	
Sample Source & type:	**Measured by:** bsh3	**Analysed:** Thursday, 14 August 2008 1:37:29 p.m.	
Sample bulk lot ref:	**Result Source:** Measurement		
Particle Name: Marine Sediment	**Accessory Name:** None	**Analysis model:** General purpose	**Sensitivity:** Enhanced
Particle RI: 1.500	**Absorption:** 0	**Size range:** 0.020 to 2000.000 um	**Obscuration:** 18.08 %
Dispersant Name: Water	**Dispersant RI:** 1.330	**Weighted Residual:** 0.626 %	**Result Emulation:** Off
Concentration: 0.0211 %Vol	**Span :** 3.053	**Uniformity:** 1.07	**Result units:** Volume
Specific Surface Area: 0.629 m^2/g	**Surface Weighted Mean D[3,2]:** 9.546 um	**Vol. Weighted Mean D[4,3]:** 24.154 um	

d(0.1): 3.981 um **d(0.5):** 15.325 um **d(0.9):** 50.766 um

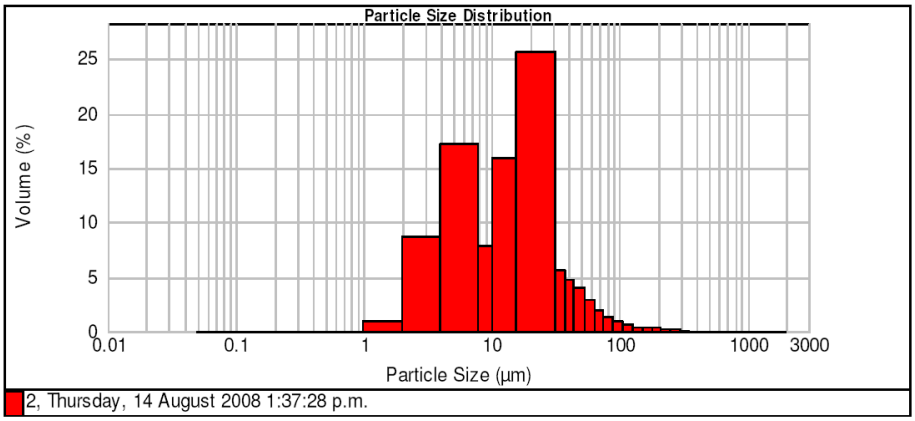

Size (µm)	Vol Under %	Size (µm)	Vol Under %	Size (µm)	Vol Under %	Size (µm)	Vol Under %	Size (µm)	Vol Under %	Size (µm)	Vol Under %
0.050	0.00	0.980	0.00	31.000	76.38	88.000	96.92	250.000	99.74	710.000	100.00
0.060	0.00	2.000	0.93	37.000	82.03	105.000	97.79	300.000	99.94	840.000	100.00
0.120	0.00	3.900	9.60	44.000	86.77	125.000	98.36	350.000	100.00	1000.000	100.00
0.240	0.00	7.800	26.83	53.000	90.85	149.000	98.78	420.000	100.00	2000.000	100.00
0.490	0.00	10.000	34.72	63.000	93.68	177.000	99.14	500.000	100.00		
0.700	0.00	15.600	50.67	74.000	95.56	210.000	99.46	590.000	100.00		

Operator notes:

Malvern Instruments Ltd.
Malvern, UK

Mastersizer 2000 Ver. 5.22
Serial Number : MAL102144

File name: Brad
Record Number: 2

MALVERN INSTRUMENTS

MASTERSIZER 2000

Result Analysis Report

Sample Name: 3	**SOP Name:** Marine Sediment	**Measured:** Thursday, 14 August 2008 1:49:52 p.m.	
Sample Source & type:	**Measured by:** bsh3	**Analysed:** Thursday, 14 August 2008 1:49:53 p.m.	
Sample bulk lot ref:	**Result Source:** Measurement		
Particle Name: Marine Sediment	**Accessory Name:** None	**Analysis model:** General purpose	**Sensitivity:** Enhanced
Particle RI: 1.500	**Absorption:** 0	**Size range:** 0.020 to 2000.000 um	**Obscuration:** 16.88 %
Dispersant Name: Water	**Dispersant RI:** 1.330	**Weighted Residual:** 0.387 %	**Result Emulation:** Off
Concentration: 0.0238 %Vol	**Span :** 3.429	**Uniformity:** 2.25	**Result units:** Volume
Specific Surface Area: 0.518 m^2/g	**Surface Weighted Mean D[3,2]:** 11.591 um	**Vol. Weighted Mean D[4,3]:** 58.895 um	

d(0.1): 4.512 um **d(0.5):** 21.581 um **d(0.9):** 78.518 um

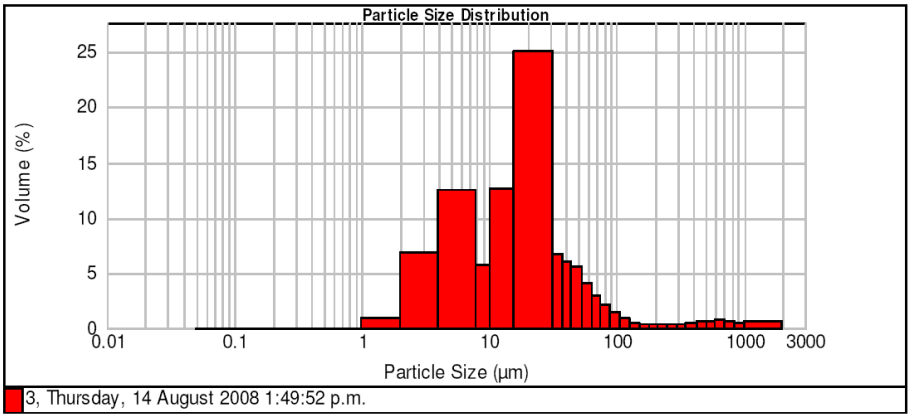

Size (µm)	Vol Under %	Size (µm)	Vol Under %	Size (µm)	Vol Under %	Size (µm)	Vol Under %	Size (µm)	Vol Under %	Size (µm)	Vol Under %
0.050	0.00	0.980	0.00	31.000	63.87	88.000	91.34	250.000	95.07	710.000	98.23
0.060	0.00	2.000	0.93	37.000	70.52	105.000	92.77	300.000	95.43	840.000	98.85
0.120	0.00	3.900	7.77	44.000	76.53	125.000	93.61	350.000	95.80	1000.000	99.39
0.240	0.00	7.800	20.28	53.000	82.10	149.000	94.12	420.000	96.31	2000.000	100.00
0.490	0.00	10.000	26.05	63.000	86.24	177.000	94.47	500.000	96.88		
0.700	0.00	15.600	38.71	74.000	89.15	210.000	94.76	590.000	97.50		

Operator notes:

MALVERN INSTRUMENTS

MASTERSIZER 2000

Result Analysis Report

Sample Name: 4	**SOP Name:** Marine Sediment	**Measured:** Thursday, 14 August 2008 3:01:07 p.m.	
Sample Source & type:	**Measured by:** bsh3	**Analysed:** Thursday, 14 August 2008 3:01:08 p.m.	
Sample bulk lot ref:	**Result Source:** Measurement		

Particle Name: Marine Sediment	**Accessory Name:** None	**Analysis model:** General purpose	**Sensitivity:** Enhanced
Particle RI: 1.500	**Absorption:** 0	**Size range:** 0.020 to 2000.000 um	**Obscuration:** 14.06 %
Dispersant Name: Water	**Dispersant RI:** 1.330	**Weighted Residual:** 0.520 %	**Result Emulation:** Off

Concentration: 0.0163 %Vol	**Span :** 6.464	**Uniformity:** 3.07	**Result units:** Volume
Specific Surface Area: 8.21 m²/g	**Surface Weighted Mean D[3,2]:** 0.731 um	**Vol. Weighted Mean D[4,3]:** 42.261 um	

d(0.1): 0.192 um **d(0.5):** 12.477 um **d(0.9):** 80.844 um

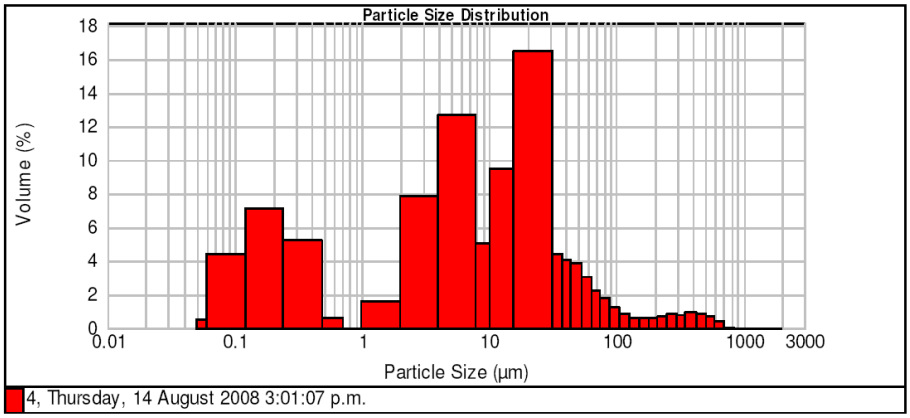

Size (µm)	Vol Under %	Size (µm)	Vol Under %	Size (µm)	Vol Under %	Size (µm)	Vol Under %	Size (µm)	Vol Under %	Size (µm)	Vol Under %
0.050	0.31	0.980	18.13	31.000	71.40	88.000	90.79	250.000	95.37	710.000	99.93
0.060	0.76	2.000	19.75	37.000	75.80	105.000	92.03	300.000	96.22	840.000	100.00
0.120	5.20	3.900	27.62	44.000	79.88	125.000	92.87	350.000	97.01	1000.000	100.00
0.240	12.29	7.800	40.33	53.000	83.78	149.000	93.50	420.000	97.97	2000.000	100.00
0.490	17.50	10.000	45.37	63.000	86.80	177.000	94.06	500.000	98.83		
0.700	18.13	15.600	54.86	74.000	89.02	210.000	94.66	590.000	99.50		

Operator notes:

Malvern Instruments Ltd.
Malvern, UK

Mastersizer 2000 Ver. 5.22
Serial Number : MAL102144

File name: Brad
Record Number: 8

MASTERSIZER 2000

Result Analysis Report

Sample Name: 5	**SOP Name:** Marine Sediment	**Measured:** Thursday, 14 August 2008 4:30:39 p.m.	
Sample Source & type:	**Measured by:** bsh3	**Analysed:** Thursday, 14 August 2008 4:30:40 p.m.	
Sample bulk lot ref:	**Result Source:** Measurement		
Particle Name: Marine Sediment	**Accessory Name:** None	**Analysis model:** General purpose	**Sensitivity:** Enhanced
Particle RI: 1.500	**Absorption:** 0	**Size range:** 0.020 to 2000.000 um	**Obscuration:** 17.23 %
Dispersant Name: Water	**Dispersant RI:** 1.330	**Weighted Residual:** 0.368 %	**Result Emulation:** Off
Concentration: 0.0204 %Vol	**Span :** 18.621	**Uniformity:** 5.79	**Result units:** Volume
Specific Surface Area: 7.91 m^2/g	**Surface Weighted Mean D[3,2]:** 0.759 um	**Vol. Weighted Mean D[4,3]:** 91.238 um	

d(0.1): 0.204 um **d(0.5):** 15.014 um **d(0.9):** 279.775 um

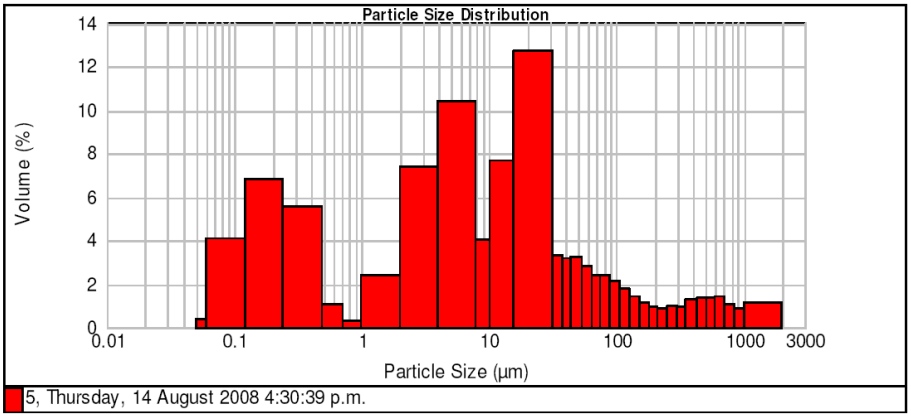

Size (µm)	Vol Under %	Size (µm)	Vol Under %	Size (µm)	Vol Under %	Size (µm)	Vol Under %	Size (µm)	Vol Under %	Size (µm)	Vol Under %
0.050	0.28	0.980	18.64	31.000	63.48	88.000	80.95	250.000	89.40	710.000	96.87
0.060	0.70	2.000	21.06	37.000	66.79	105.000	83.08	300.000	90.39	840.000	97.99
0.120	4.82	3.900	28.49	44.000	69.97	125.000	84.86	350.000	91.35	1000.000	98.87
0.240	11.67	7.800	38.92	53.000	73.24	149.000	86.34	420.000	92.65	2000.000	100.00
0.490	17.24	10.000	42.98	63.000	76.09	177.000	87.51	500.000	94.04		
0.700	18.33	15.600	50.69	74.000	78.55	210.000	88.49	590.000	95.41		

Operator notes:

Malvern Instruments Ltd.
Malvern, UK

Mastersizer 2000 Ver. 5.22
Serial Number : MAL102144

File name: Brad
Record Number: 15

MASTERSIZER 2000

Result Analysis Report

Sample Name: 6	**SOP Name:** Marine Sediment	**Measured:** Thursday, 14 August 2008 4:17:52 p.m.	
Sample Source & type:	**Measured by:** bsh3	**Analysed:** Thursday, 14 August 2008 4:17:53 p.m.	
Sample bulk lot ref:	**Result Source:** Measurement		
Particle Name: Marine Sediment	**Accessory Name:** None	**Analysis model:** General purpose	**Sensitivity:** Enhanced
Particle RI: 1.500	**Absorption:** 0	**Size range:** 0.020 to 2000.000 um	**Obscuration:** 15.27 %
Dispersant Name: Water	**Dispersant RI:** 1.330	**Weighted Residual:** 0.444 %	**Result Emulation:** Off
Concentration: 0.0146 %Vol	**Span :** 7.084	**Uniformity:** 2.99	**Result units:** Volume
Specific Surface Area: 8.64 m^2/g	**Surface Weighted Mean D[3,2]:** 0.695 um	**Vol. Weighted Mean D[4,3]:** 31.307 um	

d(0.1): 0.190 um **d(0.5):** 9.499 um **d(0.9):** 67.483 um

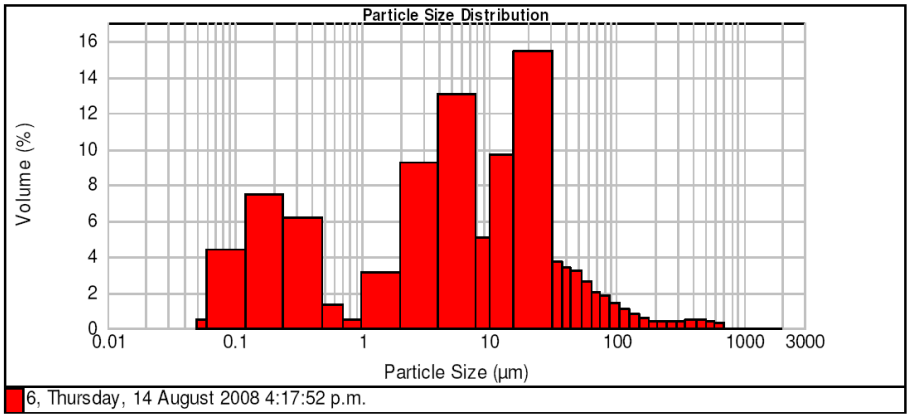

Size (µm)	Vol Under %	Size (µm)	Vol Under %	Size (µm)	Vol Under %	Size (µm)	Vol Under %	Size (µm)	Vol Under %	Size (µm)	Vol Under %
0.050	0.30	0.980	20.54	31.000	76.17	88.000	92.92	250.000	97.58	710.000	100.00
0.060	0.75	2.000	23.68	37.000	79.89	105.000	94.36	300.000	97.97	840.000	100.00
0.120	5.16	3.900	32.93	44.000	83.26	125.000	95.44	350.000	98.34	1000.000	100.00
0.240	12.58	7.800	45.98	53.000	86.50	149.000	96.24	420.000	98.84	2000.000	100.00
0.490	18.76	10.000	51.07	63.000	89.09	177.000	96.80	500.000	99.34		
0.700	20.07	15.600	60.70	74.000	91.12	210.000	97.22	590.000	99.74		

Operator notes:

Malvern Instruments Ltd.
Malvern, UK

Mastersizer 2000 Ver. 5.22
Serial Number : MAL102144

File name: Brad
Record Number: 14

MASTERSIZER 2000

Result Analysis Report

Sample Name: 7	**SOP Name:** Marine Sediment	**Measured:** Thursday, 14 August 2008 3:40:10 p.m.	
Sample Source & type:	**Measured by:** bsh3	**Analysed:** Thursday, 14 August 2008 3:40:11 p.m.	
Sample bulk lot ref:	**Result Source:** Measurement		
Particle Name: Marine Sediment	**Accessory Name:** None	**Analysis model:** General purpose	**Sensitivity:** Enhanced
Particle RI: 1.500	**Absorption:** 0	**Size range:** 0.020 to 2000.000 um	**Obscuration:** 16.35 %
Dispersant Name: Water	**Dispersant RI:** 1.330	**Weighted Residual:** 0.531 %	**Result Emulation:** Off
Concentration: 0.0154 %Vol	**Span :** 4.108	**Uniformity:** 1.42	**Result units:** Volume
Specific Surface Area: 9.69 m²/g	**Surface Weighted Mean D[3,2]:** 0.619 um	**Vol. Weighted Mean D[4,3]:** 12.887 um	

d(0.1): 0.161 um **d(0.5):** 7.293 um **d(0.9):** 30.121 um

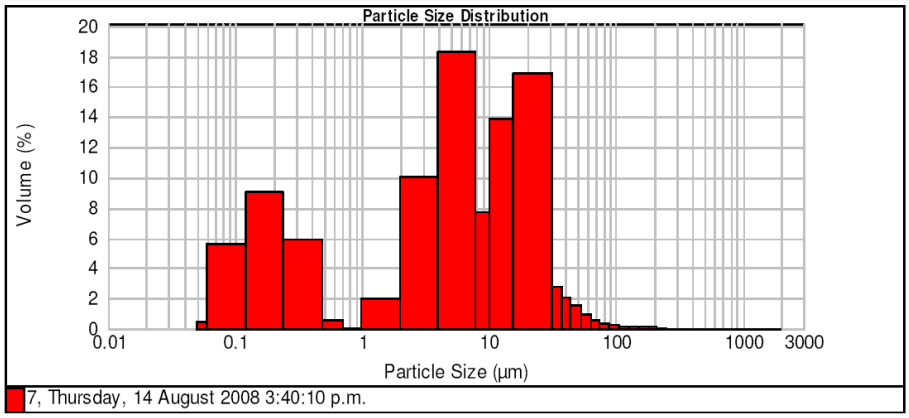

Size (µm)	Vol Under %	Size (µm)	Vol Under %	Size (µm)	Vol Under %	Size (µm)	Vol Under %	Size (µm)	Vol Under %	Size (µm)	Vol Under %
0.050	0.16	0.980	21.68	31.000	90.52	88.000	98.94	250.000	100.00	710.000	100.00
0.060	0.66	2.000	23.62	37.000	93.32	105.000	99.19	300.000	100.00	840.000	100.00
0.120	6.21	3.900	33.69	44.000	95.40	125.000	99.38	350.000	100.00	1000.000	100.00
0.240	15.22	7.800	52.03	53.000	97.00	149.000	99.56	420.000	100.00	2000.000	100.00
0.490	21.08	10.000	59.76	63.000	97.98	177.000	99.74	500.000	100.00		
0.700	21.67	15.600	73.66	74.000	98.56	210.000	99.90	590.000	100.00		

Operator notes:

Malvern Instruments Ltd.
Malvern, UK

Mastersizer 2000 Ver. 5.22
Serial Number : MAL102144

File name: Brad
Record Number: 11

MASTERSIZER 2000

Result Analysis Report

Sample Name: 8	**SOP Name:** Marine Sediment	**Measured:** Thursday, 14 August 2008 2:13:57 p.m.	
Sample Source & type:	**Measured by:** bsh3	**Analysed:** Thursday, 14 August 2008 2:13:58 p.m.	
Sample bulk lot ref:	**Result Source:** Measurement		
Particle Name: Marine Sediment	**Accessory Name:** None	**Analysis model:** General purpose	**Sensitivity:** Enhanced
Particle RI: 1.500	**Absorption:** 0	**Size range:** 0.020 to 2000.000 um	**Obscuration:** 17.64 %
Dispersant Name: Water	**Dispersant RI:** 1.330	**Weighted Residual:** 0.550 %	**Result Emulation:** Off
Concentration: 0.0196 %Vol	**Span :** 4.422	**Uniformity:** 1.53	**Result units:** Volume
Specific Surface Area: 8.68 m^2/g	**Surface Weighted Mean D[3,2]:** 0.691 um	**Vol. Weighted Mean D[4,3]:** 16.907 um	

d(0.1): 0.164 um **d(0.5):** 9.031 um **d(0.9):** 40.102 um

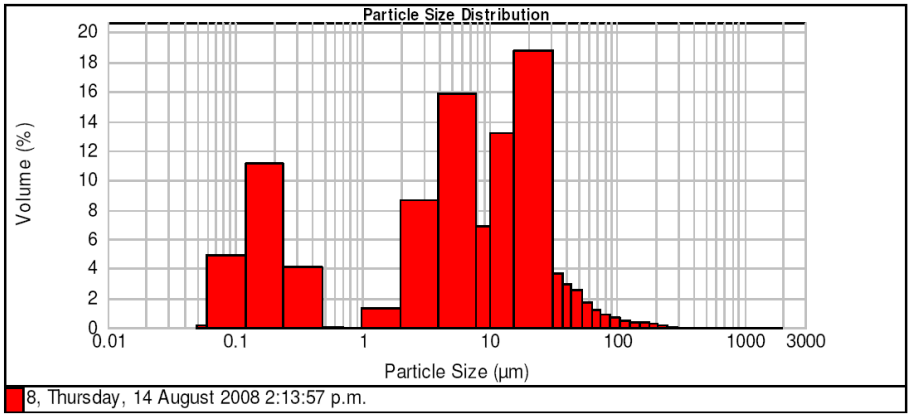

Size (µm)	Vol Under %	Size (µm)	Vol Under %	Size (µm)	Vol Under %	Size (µm)	Vol Under %	Size (µm)	Vol Under %	Size (µm)	Vol Under %
0.050	0.00	0.980	20.27	31.000	84.83	88.000	97.75	250.000	99.95	710.000	100.00
0.060	0.11	2.000	21.56	37.000	88.53	105.000	98.39	300.000	100.00	840.000	100.00
0.120	4.97	3.900	30.17	44.000	91.52	125.000	98.86	350.000	100.00	1000.000	100.00
0.240	16.11	7.800	46.00	53.000	94.01	149.000	99.25	420.000	100.00	2000.000	100.00
0.490	20.23	10.000	52.88	63.000	95.72	177.000	99.56	500.000	100.00		
0.700	20.27	15.600	66.05	74.000	96.87	210.000	99.80	590.000	100.00		

Operator notes:

Malvern Instruments Ltd.
Malvern, UK

Mastersizer 2000 Ver. 5.22
Serial Number : MAL102144

File name: Brad
Record Number: 5

MASTERSIZER 2000

Result Analysis Report

Sample Name: 10	**SOP Name:** Marine Sediment	**Measured:** Thursday, 14 August 2008 3:26:19 p.m.	
Sample Source & type:	**Measured by:** bsh3	**Analysed:** Thursday, 14 August 2008 3:26:20 p.m.	
Sample bulk lot ref:	**Result Source:** Measurement		
Particle Name: Marine Sediment	**Accessory Name:** None	**Analysis model:** General purpose	**Sensitivity:** Enhanced
Particle RI: 1.500	**Absorption:** 0	**Size range:** 0.020 to 2000.000 um	**Obscuration:** 19.31 %
Dispersant Name: Water	**Dispersant RI:** 1.330	**Weighted Residual:** 0.506 %	**Result Emulation:** Off
Concentration: 0.0320 %Vol	**Span :** 37.869	**Uniformity:** 8.77	**Result units:** Volume
Specific Surface Area: 0.445 m^2/g	**Surface Weighted Mean D[3,2]:** 13.479 um	**Vol. Weighted Mean D[4,3]:** 247.449 um	

d(0.1): 4.928 um **d(0.5):** 26.828 um **d(0.9):** 1020.883 um

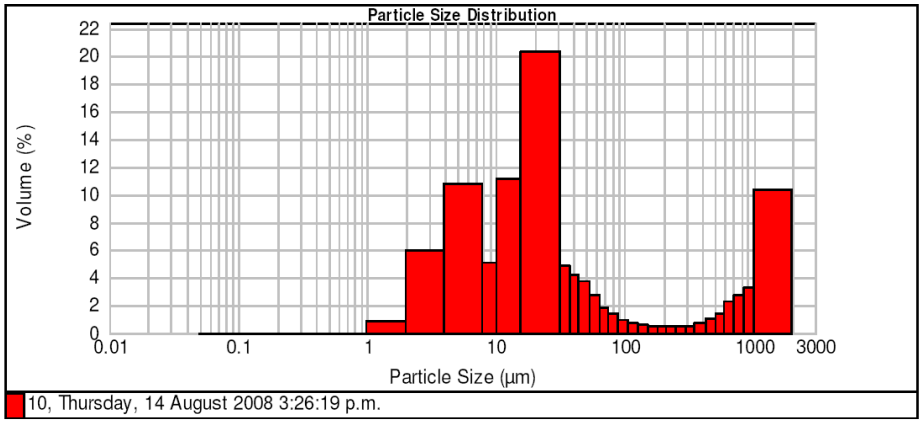

Size (µm)	Vol Under %	Size (µm)	Vol Under %	Size (µm)	Vol Under %	Size (µm)	Vol Under %	Size (µm)	Vol Under %	Size (µm)	Vol Under %
0.050	0.00	0.980	0.00	31.000	54.27	88.000	73.19	250.000	76.96	710.000	83.57
0.060	0.00	2.000	0.88	37.000	59.16	105.000	74.18	300.000	77.51	840.000	86.28
0.120	0.00	3.900	6.84	44.000	63.40	125.000	74.88	350.000	78.02	1000.000	89.59
0.240	0.00	7.800	17.67	53.000	67.17	149.000	75.45	420.000	78.79	2000.000	100.00
0.490	0.00	10.000	22.78	63.000	69.88	177.000	75.96	500.000	79.84		
0.700	0.00	15.600	33.90	74.000	71.76	210.000	76.46	590.000	81.29		

Operator notes:

Malvern Instruments Ltd.
Malvern, UK

Mastersizer 2000 Ver. 5.22
Serial Number : MAL102144

File name: Brad
Record Number: 10

MASTERSIZER 2000

Result Analysis Report

Sample Name: 11	**SOP Name:** Marine Sediment	**Measured:** Thursday, 14 August 2008 3:52:32 p.m.	
Sample Source & type:	**Measured by:** bsh3	**Analysed:** Thursday, 14 August 2008 3:52:33 p.m.	
Sample bulk lot ref:	**Result Source:** Measurement		
Particle Name: Marine Sediment	**Accessory Name:** None	**Analysis model:** General purpose	**Sensitivity:** Enhanced
Particle RI: 1.500	**Absorption:** 0	**Size range:** 0.020 to 2000.000 um	**Obscuration:** 18.50 %
Dispersant Name: Water	**Dispersant RI:** 1.330	**Weighted Residual:** 0.435 %	**Result Emulation:** Off
Concentration: 0.0227 %Vol	**Span :** 3.965	**Uniformity:** 1.42	**Result units:** Volume
Specific Surface Area: 7.88 m^2/g	**Surface Weighted Mean D[3,2]:** 0.761 um	**Vol. Weighted Mean D[4,3]:** 24.067 um	

d(0.1): 0.201 um **d(0.5):** 13.796 um **d(0.9):** 54.902 um

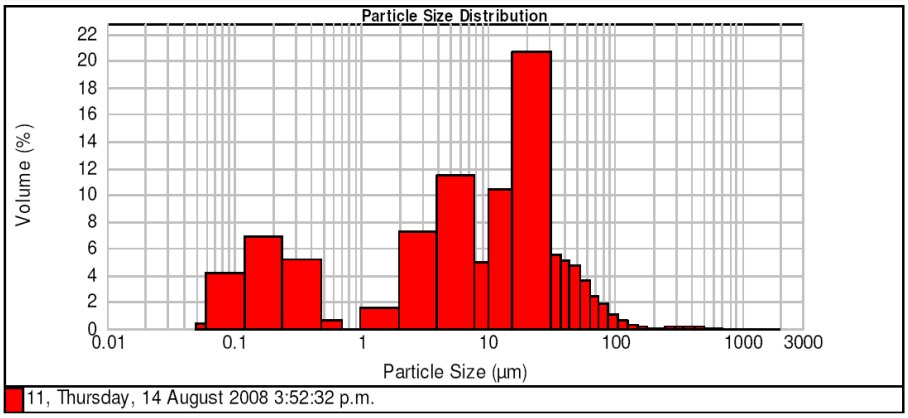

Size (µm)	Vol Under %	Size (µm)	Vol Under %	Size (µm)	Vol Under %	Size (µm)	Vol Under %	Size (µm)	Vol Under %	Size (µm)	Vol Under %
0.050	0.29	0.980	17.62	31.000	73.81	88.000	97.06	250.000	99.34	710.000	100.00
0.060	0.72	2.000	19.15	37.000	79.39	105.000	98.18	300.000	99.47	840.000	100.00
0.120	4.92	3.900	26.37	44.000	84.46	125.000	98.77	350.000	99.60	1000.000	100.00
0.240	11.79	7.800	37.79	53.000	89.21	149.000	99.04	420.000	99.76	2000.000	100.00
0.490	16.98	10.000	42.70	63.000	92.75	177.000	99.16	500.000	99.90		
0.700	17.62	15.600	53.13	74.000	95.22	210.000	99.25	590.000	100.00		

Operator notes:

Malvern Instruments Ltd.
Malvern, UK

Mastersizer 2000 Ver. 5.22
Serial Number : MAL102144

File name: Brad
Record Number: 12

MALVERN INSTRUMENTS

MASTERSIZER 2000

Result Analysis Report

Sample Name: 13	**SOP Name:** Marine Sediment	**Measured:** Thursday, 14 August 2008 4:04:41 p.m.	
Sample Source & type:	**Measured by:** bsh3	**Analysed:** Thursday, 14 August 2008 4:04:42 p.m.	
Sample bulk lot ref:	**Result Source:** Measurement		
Particle Name: Marine Sediment	**Accessory Name:** None	**Analysis model:** General purpose	**Sensitivity:** Enhanced
Particle RI: 1.500	**Absorption:** 0	**Size range:** 0.020 to 2000.000 um	**Obscuration:** 21.95 %
Dispersant Name: Water	**Dispersant RI:** 1.330	**Weighted Residual:** 0.377 %	**Result Emulation:** Off
Concentration: 0.0286 %Vol	**Span :** 4.692	**Uniformity:** 1.8	**Result units:** Volume
Specific Surface Area: 8.55 m^2/g	**Surface Weighted Mean D[3,2]:** 0.702 um	**Vol. Weighted Mean D[4,3]:** 25.176 um	

d(0.1): 0.168 um **d(0.5):** 11.926 um **d(0.9):** 56.118 um

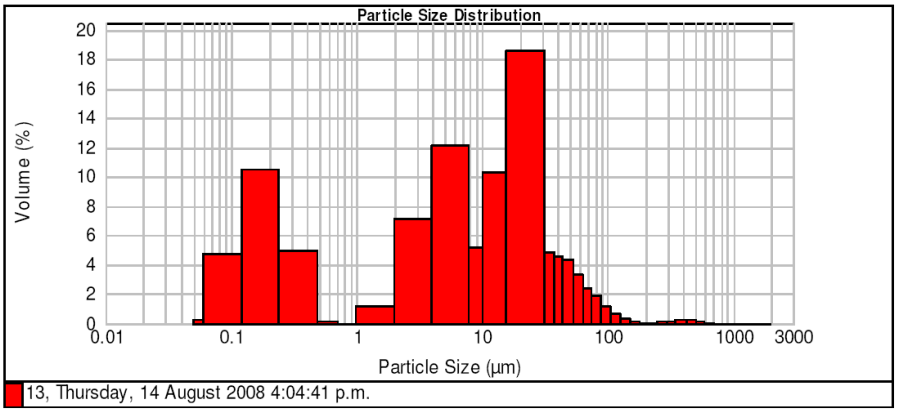

Size (µm)	Vol Under %	Size (µm)	Vol Under %	Size (µm)	Vol Under %	Size (µm)	Vol Under %	Size (µm)	Vol Under %	Size (µm)	Vol Under %
0.050	0.00	0.980	20.45	31.000	75.05	88.000	96.42	250.000	98.89	710.000	100.00
0.060	0.21	2.000	21.66	37.000	79.96	105.000	97.61	300.000	99.05	840.000	100.00
0.120	4.95	3.900	28.75	44.000	84.50	125.000	98.27	350.000	99.24	1000.000	100.00
0.240	15.41	7.800	40.90	53.000	88.82	149.000	98.58	420.000	99.49	2000.000	100.00
0.490	20.34	10.000	46.08	63.000	92.15	177.000	98.71	500.000	99.72		
0.700	20.45	15.600	56.42	74.000	94.56	210.000	98.79	590.000	99.90		

Operator notes:

Malvern Instruments Ltd.
Malvern, UK

Mastersizer 2000 Ver. 5.22
Serial Number : MAL102144

File name: Brad
Record Number: 13

MASTERSIZER 2000

Result Analysis Report

Sample Name: 14	**SOP Name:** Marine Sediment	**Measured:** Thursday, 14 August 2008 3:13:41 p.m.	
Sample Source & type:	**Measured by:** bsh3	**Analysed:** Thursday, 14 August 2008 3:13:42 p.m.	
Sample bulk lot ref:	**Result Source:** Measurement		
Particle Name: Marine Sediment	**Accessory Name:** None	**Analysis model:** General purpose	**Sensitivity:** Enhanced
Particle RI: 1.500	**Absorption:** 0	**Size range:** 0.020 to 2000.000 um	**Obscuration:** 22.78 %
Dispersant Name: Water	**Dispersant RI:** 1.330	**Weighted Residual:** 0.351 %	**Result Emulation:** Off
Concentration: 0.0363 %Vol	**Span :** 26.059	**Uniformity:** 6.7	**Result units:** Volume
Specific Surface Area: 8.84 m^2/g	**Surface Weighted Mean D[3,2]:** 0.679 um	**Vol. Weighted Mean D[4,3]:** 125.898 um	

d(0.1): 0.165 um **d(0.5):** 18.059 um **d(0.9):** 470.779 um

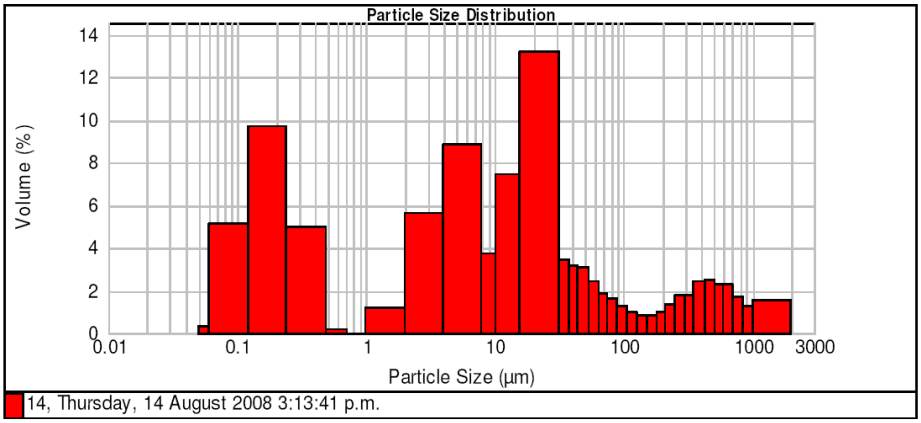

Size (µm)	Vol Under %	Size (µm)	Vol Under %	Size (µm)	Vol Under %	Size (µm)	Vol Under %	Size (µm)	Vol Under %	Size (µm)	Vol Under %
0.050	0.12	0.980	20.43	31.000	60.55	88.000	76.10	250.000	82.37	710.000	95.47
0.060	0.44	2.000	21.66	37.000	63.97	105.000	77.36	300.000	84.14	840.000	97.15
0.120	5.55	3.900	27.31	44.000	67.14	125.000	78.33	350.000	85.94	1000.000	98.42
0.240	15.29	7.800	36.15	53.000	70.20	149.000	79.18	420.000	88.38	2000.000	100.00
0.490	20.24	10.000	39.86	63.000	72.63	177.000	80.04	500.000	90.86		
0.700	20.43	15.600	47.32	74.000	74.50	210.000	81.06	590.000	93.17		

Operator notes:

Malvern Instruments Ltd.
Malvern, UK

Mastersizer 2000 Ver. 5.22
Serial Number : MAL102144

File name: Brad
Record Number: 9

MALVERN INSTRUMENTS

MASTERSIZER 2000

Result Analysis Report

Sample Name: 18	**SOP Name:** Marine Sediment	**Measured:** Thursday, 14 August 2008 1:24:34 p.m.	
Sample Source & type:	**Measured by:** bsh3	**Analysed:** Thursday, 14 August 2008 1:24:35 p.m.	
Sample bulk lot ref:	**Result Source:** Measurement		

Particle Name: Marine Sediment	**Accessory Name:** None	**Analysis model:** General purpose	**Sensitivity:** Enhanced
Particle RI: 1.500	**Absorption:** 0	**Size range:** 0.020 to 2000.000 um	**Obscuration:** 15.93 %
Dispersant Name: Water	**Dispersant RI:** 1.330	**Weighted Residual:** 1.451 %	**Result Emulation:** Off

Concentration: 0.0157 %Vol	**Span :** 2.893	**Uniformity:** 0.917	**Result units:** Volume
Specific Surface Area: 0.729 m²/g	**Surface Weighted Mean D[3,2]:** 8.230 um	**Vol. Weighted Mean D[4,3]:** 17.833 um	

d(0.1): 3.586 um **d(0.5):** 12.318 um **d(0.9):** 39.220 um

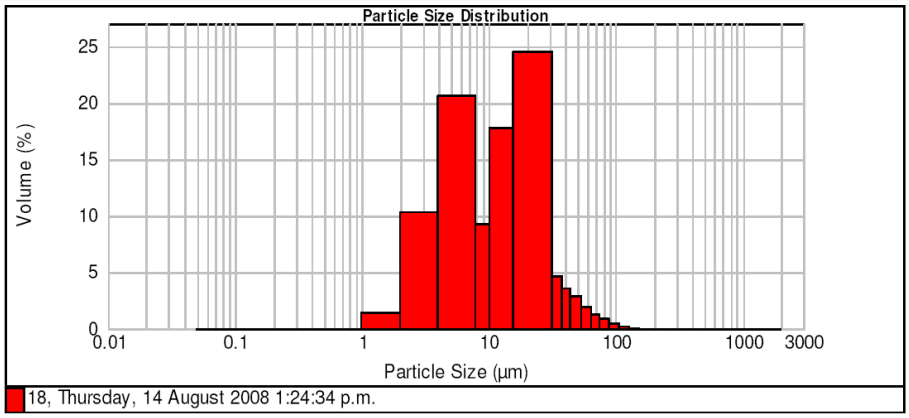

Size (µm)	Vol Under %	Size (µm)	Vol Under %	Size (µm)	Vol Under %	Size (µm)	Vol Under %	Size (µm)	Vol Under %	Size (µm)	Vol Under %
0.050	0.00	0.980	0.00	31.000	84.10	88.000	99.24	250.000	100.00	710.000	100.00
0.060	0.00	2.000	1.48	37.000	88.69	105.000	99.77	300.000	100.00	840.000	100.00
0.120	0.00	3.900	11.85	44.000	92.29	125.000	99.97	350.000	100.00	1000.000	100.00
0.240	0.00	7.800	32.44	53.000	95.21	149.000	100.00	420.000	100.00	2000.000	100.00
0.490	0.00	10.000	41.73	63.000	97.14	177.000	100.00	500.000	100.00		
0.700	0.00	15.600	59.55	74.000	98.37	210.000	100.00	590.000	100.00		

Operator notes:

Malvern Instruments Ltd.
Malvern, UK

Mastersizer 2000 Ver. 5.22
Serial Number : MAL102144

File name: Brad
Record Number: 1

MASTERSIZER 2000

Result Analysis Report

Sample Name: 19	**SOP Name:** Marine Sediment	**Measured:** Thursday, 14 August 2008 4:42:43 p.m.	
Sample Source & type:	**Measured by:** bsh3	**Analysed:** Thursday, 14 August 2008 4:42:44 p.m.	
Sample bulk lot ref:	**Result Source:** Measurement		
Particle Name: Marine Sediment	**Accessory Name:** None	**Analysis model:** General purpose	**Sensitivity:** Enhanced
Particle RI: 1.500	**Absorption:** 0	**Size range:** 0.020 to 2000.000 um	**Obscuration:** 18.63 %
Dispersant Name: Water	**Dispersant RI:** 1.330	**Weighted Residual:** 0.443 %	**Result Emulation:** Off
Concentration: 0.0199 %Vol	**Span :** 2.980	**Uniformity:** 1.01	**Result units:** Volume
Specific Surface Area: 0.685 m^2/g	**Surface Weighted Mean D[3,2]:** 8.763 um	**Vol. Weighted Mean D[4,3]:** 20.743 um	

d(0.1): 3.722 um **d(0.5):** 13.591 um **d(0.9):** 44.220 um

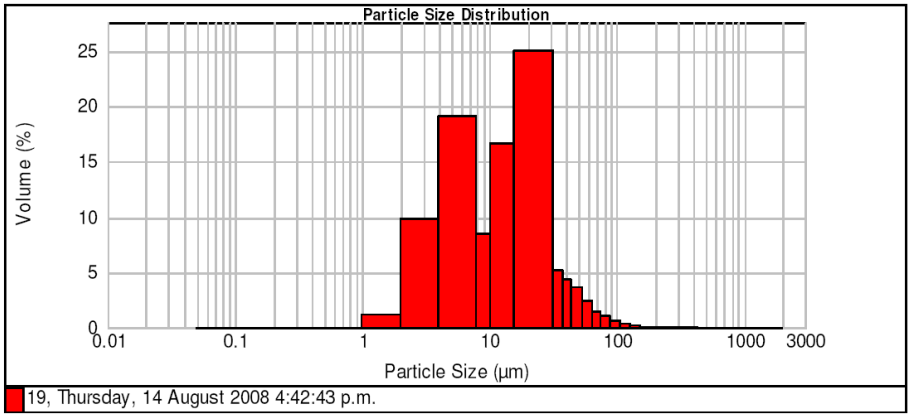

Size (µm)	Vol Under %	Size (µm)	Vol Under %	Size (µm)	Vol Under %	Size (µm)	Vol Under %	Size (µm)	Vol Under %	Size (µm)	Vol Under %
0.050	0.00	0.980	0.00	31.000	80.36	88.000	98.42	250.000	99.77	710.000	100.00
0.060	0.00	2.000	1.15	37.000	85.60	105.000	98.99	300.000	99.88	840.000	100.00
0.120	0.00	3.900	11.00	44.000	89.89	125.000	99.28	350.000	99.97	1000.000	100.00
0.240	0.00	7.800	30.17	53.000	93.48	149.000	99.44	420.000	100.00	2000.000	100.00
0.490	0.00	10.000	38.67	63.000	95.89	177.000	99.56	500.000	100.00		
0.700	0.00	15.600	55.27	74.000	97.40	210.000	99.67	590.000	100.00		

Operator notes:

Malvern Instruments Ltd.
Malvern, UK

Mastersizer 2000 Ver. 5.22
Serial Number : MAL102144

File name: Brad
Record Number: 16

MASTERSIZER 2000

Result Analysis Report

Sample Name: 20	**SOP Name:** Marine Sediment	**Measured:** Thursday, 14 August 2008 2:02:06 p.m.	
Sample Source & type:	**Measured by:** bsh3	**Analysed:** Thursday, 14 August 2008 2:02:07 p.m.	
Sample bulk lot ref:	**Result Source:** Measurement		
Particle Name: Marine Sediment	**Accessory Name:** None	**Analysis model:** General purpose	**Sensitivity:** Enhanced
Particle RI: 1.500	**Absorption:** 0	**Size range:** 0.020 to 2000.000 um	**Obscuration:** 16.88 %
Dispersant Name: Water	**Dispersant RI:** 1.330	**Weighted Residual:** 0.651 %	**Result Emulation:** Off
Concentration: 0.0193 %Vol	**Span :** 4.378	**Uniformity:** 1.68	**Result units:** Volume
Specific Surface Area: 0.624 m^2/g	**Surface Weighted Mean D[3,2]:** 9.613 um	**Vol. Weighted Mean D[4,3]:** 37.141 um	

d(0.1): 3.738 um **d(0.5):** 17.340 um **d(0.9):** 79.653 um

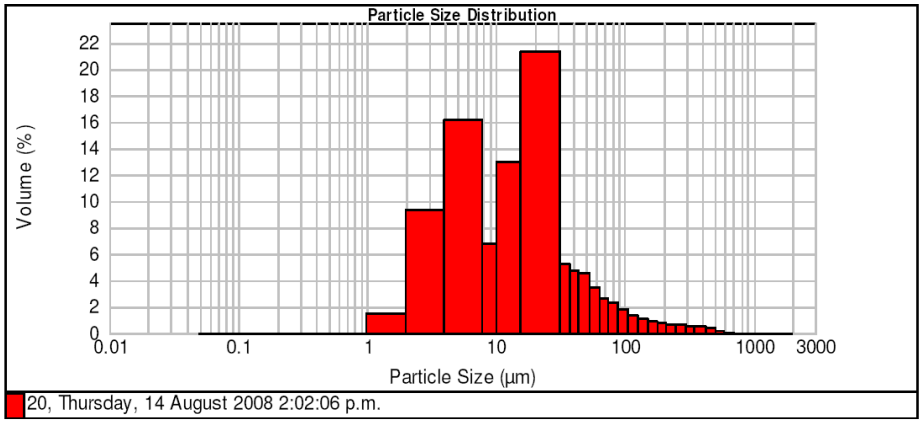

Size (µm)	Vol Under %	Size (µm)	Vol Under %	Size (µm)	Vol Under %	Size (µm)	Vol Under %	Size (µm)	Vol Under %	Size (µm)	Vol Under %
0.050	0.00	0.980	0.00	31.000	68.19	88.000	91.26	250.000	97.75	710.000	100.00
0.060	0.00	2.000	1.47	37.000	73.45	105.000	93.08	300.000	98.39	840.000	100.00
0.120	0.00	3.900	10.82	44.000	78.21	125.000	94.45	350.000	98.90	1000.000	100.00
0.240	0.00	7.800	27.03	53.000	82.71	149.000	95.52	420.000	99.43	2000.000	100.00
0.490	0.00	10.000	33.78	63.000	86.25	177.000	96.38	500.000	99.83		
0.700	0.00	15.600	46.76	74.000	88.95	210.000	97.09	590.000	99.99		

Operator notes:

Malvern Instruments Ltd.
Malvern, UK

Mastersizer 2000 Ver. 5.22
Serial Number : MAL102144

File name: Brad
Record Number: 4

MALVERN INSTRUMENTS

MASTERSIZER 2000

Result Analysis Report

Sample Name: 21	**SOP Name:** Marine Sediment	**Measured:** Thursday, 14 August 2008 2:28:43 p.m.	
Sample Source & type:	**Measured by:** bsh3	**Analysed:** Thursday, 14 August 2008 2:28:44 p.m.	
Sample bulk lot ref:	**Result Source:** Measurement		

Particle Name: Marine Sediment	**Accessory Name:** None	**Analysis model:** General purpose	**Sensitivity:** Enhanced
Particle RI: 1.500	**Absorption:** 0	**Size range:** 0.020 to 2000.000 um	**Obscuration:** 22.05 %
Dispersant Name: Water	**Dispersant RI:** 1.330	**Weighted Residual:** 0.569 %	**Result Emulation:** Off

Concentration: 0.0217 %Vol	**Span :** 8.845	**Uniformity:** 5.77	**Result units:** Volume
Specific Surface Area: 11.8 m^2/g	**Surface Weighted Mean D[3,2]:** 0.510 um	**Vol. Weighted Mean D[4,3]:** 40.497 um	

d(0.1): 0.145 um **d(0.5):** 6.703 um **d(0.9):** 59.427 um

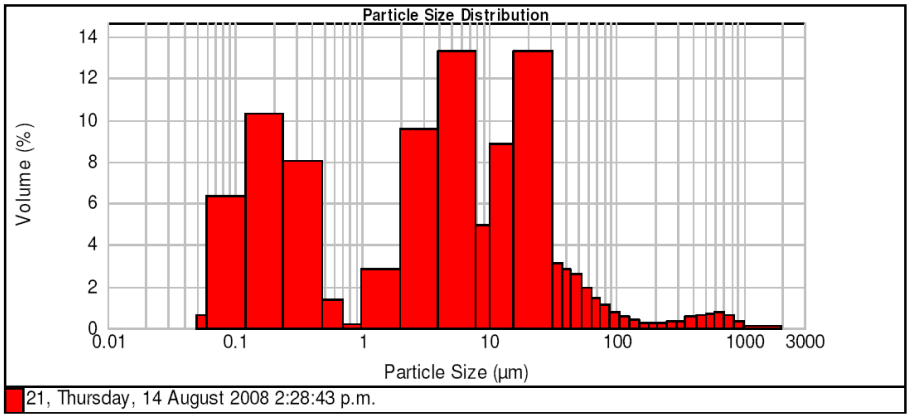

Size (µm)	Vol Under %	Size (µm)	Vol Under %	Size (µm)	Vol Under %	Size (µm)	Vol Under %	Size (µm)	Vol Under %	Size (µm)	Vol Under %
0.050	0.43	0.980	27.31	31.000	80.13	88.000	93.12	250.000	95.57	710.000	98.94
0.060	1.08	2.000	30.16	37.000	83.27	105.000	93.90	300.000	95.89	840.000	99.53
0.120	7.39	3.900	39.70	44.000	86.07	125.000	94.42	350.000	96.24	1000.000	99.90
0.240	17.70	7.800	53.00	53.000	88.66	149.000	94.79	420.000	96.79	2000.000	100.00
0.490	25.73	10.000	57.95	63.000	90.61	177.000	95.07	500.000	97.44		
0.700	27.11	15.600	66.79	74.000	92.01	210.000	95.32	590.000	98.15		

Operator notes:

Malvern Instruments Ltd.
Malvern, UK

Mastersizer 2000 Ver. 5.22
Serial Number : MAL102144

File name: Brad
Record Number: 6

MALVERN INSTRUMENTS

MASTERSIZER 2000

Result Analysis Report

Sample Name: 22	**SOP Name:** Marine Sediment	**Measured:** Thursday, 14 August 2008 2:49:11 p.m.	
Sample Source & type:	**Measured by:** bsh3	**Analysed:** Thursday, 14 August 2008 2:49:12 p.m.	
Sample bulk lot ref:	**Result Source:** Measurement		
Particle Name: Marine Sediment	**Accessory Name:** None	**Analysis model:** General purpose	**Sensitivity:** Enhanced
Particle RI: 1.500	**Absorption:** 0	**Size range:** 0.020 to 2000.000 um	**Obscuration:** 22.22 %
Dispersant Name: Water	**Dispersant RI:** 1.330	**Weighted Residual:** 0.655 %	**Result Emulation:** Off
Concentration: 0.0231 %Vol	**Span :** 6.932	**Uniformity:** 2.79	**Result units:** Volume
Specific Surface Area: 11.2 m²/g	**Surface Weighted Mean D[3,2]:** 0.536 um	**Vol. Weighted Mean D[4,3]:** 21.739 um	

d(0.1): 0.147 um **d(0.5):** 7.065 um **d(0.9):** 49.120 um

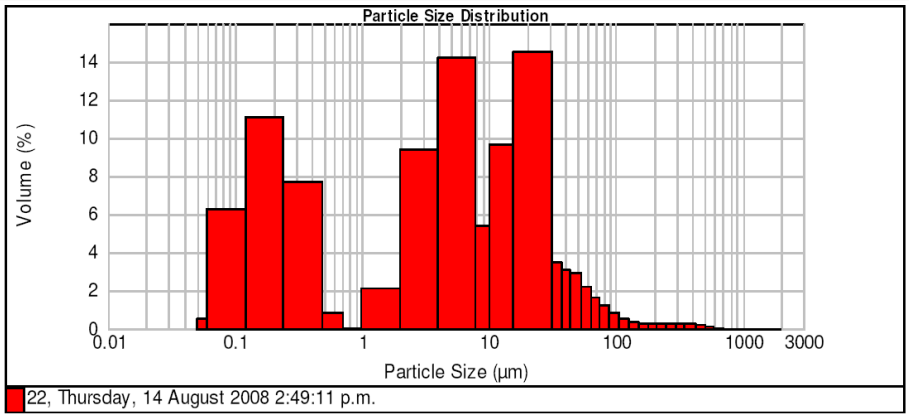

Size (µm)	Vol Under %	Size (µm)	Vol Under %	Size (µm)	Vol Under %	Size (µm)	Vol Under %	Size (µm)	Vol Under %	Size (µm)	Vol Under %
0.050	0.16	0.980	26.49	31.000	81.65	88.000	96.18	250.000	98.73	710.000	100.00
0.060	0.70	2.000	28.62	37.000	85.11	105.000	97.04	300.000	99.03	840.000	100.00
0.120	6.99	3.900	37.96	44.000	88.22	125.000	97.58	350.000	99.29	1000.000	100.00
0.240	18.01	7.800	52.13	53.000	91.13	149.000	97.94	420.000	99.57	2000.000	100.00
0.490	25.68	10.000	57.52	63.000	93.33	177.000	98.21	500.000	99.79		
0.700	26.48	15.600	67.14	74.000	94.93	210.000	98.46	590.000	99.93		

Operator notes:

Malvern Instruments Ltd.
Malvern, UK

Mastersizer 2000 Ver. 5.22
Serial Number : MAL102144

File name: Brad
Record Number: 7

APPENDIX IV
PETROGRAPHY

IV.1 – Petrography samples

Subsurface and onshore samples analysed petrographically with associated petrography sample numbers.

Sample location	Formation/Member	Depth (m)	Sample number
Port Waikato	Glen Massey Formation (Ahirau Sandstone Member)	~	**1**
Aotea Harbour	Glen Massey Formation (Ahirau Sandstone Member)	~	**2**
Hautapu Hill	Aotea Formation (Hauturu Sandstone Member)	~	**4**
Kihi Road	Aotea Formation (Hauturu Sandstone Member)	~	**5**
Taumarunui	Taumarunui quartz sandstone	~	**7**
Kaimiro-1	McKee Formation	3784 - 3740	**8**
Tariki-1	Otaraoa Formation (Tariki Sandstone Member)	2940 - 2990	**9**
Ngatoro-1	Otaraoa Formation (Matapo Sandstone Member)	3550 - 3600	**10**
Pohokura-1	Turi Formation	3420 - 3470	**12**
Tariki-1	Otaraoa Formation (Tariki Sandstone Member)	2870 - 2920	**13**

IV.2 – Light mineral fraction

Table summarising light mineral fraction composition data obtained by point counting. Values expressed as percentage of total.

Sample No.	Quartz	Plagioclase	Orthoclase	Sed. Rock	Volc. Rock	Sphene	Epidote	Glauconite	Opaque	Microcline	Other
1	61.5	4.9	5.7	17.4	3.4	0.4	0.0	3.0	1.1	0.0	2.6
2	47.6	8.1	2.9	19.0	5.5	0.0	0.7	8.1	2.6	0.0	5.5
4	67.4	13.0	5.7	11.9	1.0	0.0	0.0	1.0	0.0	0.0	0.0
5	63.3	14.5	5.5	7.8	2.3	0.0	0.0	4.3	0.8	0.4	1.2
7	56.3	12.7	3.0	21.7	6.0	0.0	0.0	0.0	0.3	0.0	0.0
8	34.3	9.3	0.7	45.3	6.7	0.0	0.0	0.0	2.0	0.3	1.3
9	49.7	15.7	5.0	24.3	4.0	0.0	0.0	0.3	0.7	0.0	0.3
10	5.0	3.0	1.7	80.0	9.0	0.0	0.0	0.3	0.3	0.0	0.7
12	30.0	10.0	4.0	52.0	4.0	0.0	0.0	0.0	0.0	0.0	2.0
13	50.7	26.7	2.7	16.7	3.0	0.0	0.0	0.0	0.3	0.0	0.0

IV.3 – Heavy magnetic mineral fraction

Table summarising heavy magnetic mineral fraction composition data obtained by point counting. Values expressed as percentages of total. Note samples 8 and 10 do not have data expressed as percentages. Descriptions of these two samples are given below.

Sample No.	Opaque	Limonite	Glauconite	Sed. Rock	Volc. Rock	Amphibole	Sphene	Other
1	77.0	8.0	3.7	1.0	1.3	0.7	1.0	7.4
2	63.0	2.0	9.3	0.0	0.3	23.7	0.3	1.3
4	47.3	8.0	32.0	1.7	0.0	3.3	0.0	7.6
5	47.0	5.0	33.3	2.3	0.3	3.0	0.0	9.0
7	17.7	67.5	0.0	1.8	0.4	0.7	0.0	11.8
8	~	~	~	~	~	~	~	~
9	6.7	8.0	3.3	28.7	14.7	0.0	0.7	28.0
10	~	~	~	~	~	~	~	~
12	8.7	21.3	2.0	16.3	13.0	0.0	0.0	39.3
13	13.0	16.7	4.3	15.0	2.7	0.0	0.7	24.4

Sample number 8 is mostly composed of indistinguishable volcanic and sedimentary rock fragments with some glauconite and plagioclase feldspar.

Sample number 10 is mostly composed of sedimentary rock fragments with some glauconite, opaque minerals and limonite.

IV.4 – QFL (quartz, feldspar, lithics) data

Table summarising quartz feldspar and lithics percentages determined for the light mineral fraction of samples.

Sample No.	Feldspar	Quartz	Lithics
1	11.4	66.3	22.4
2	13.2	57.3	29.5
4	18.8	68.1	13.1
5	21.7	67.5	10.8
7	15.7	56.5	27.8
8	10.7	35.5	53.8
9	20.9	50.3	28.7
10	4.7	5.1	90.2
12	14.0	30.0	56.0
13	29.4	50.8	19.7

APPENDIX V

LA-ICP-MS AND MORPHOLOGIES

V.1 – LA-ICP-MS specifications

The following summarises LA-ICP-MS operating conditions and data acquisition parameters.

ICP-MS

Model		Elan 6100 DRCII ICP-MS (Perkin Elmer Sciex)
Gas Flows		
	Plasma (Ar)	15 L/min
	Auxillary (Ar)	1.2 L/min
	Carrier (He)	1.0 L/min
	Nebuliser	0.63 L/min
Sheild torch		Used for most analyses
Vacuum pressure		1×10^{-5} Torr
Software		Elan 3.3

LA

Model	New Wave UP-213 Deep Nd YAG - Tempest 20 Hz
Wavelength	5th Harmonic @ 213 nm
Repitition rate	10 Hz
Pre-ablation laser warm-up	Laser Fired Continously
Pulse duration (FWHM)	<4 ns (stablilty 3%)
Beam - expander setting	0
Focussing objective	5X, f.l. = 40 mm
Degree of defocusing	Not known
Spot size	30-60 nm
Incident pulse energy	ca. > 1 mJ per pulse
Energy density on sample	ca. > 3 mJ
Software	New Wave Research (Merchantek) Laser Ablation System 1.8.13.1

Data Acqusition Parameters

Data Acqusition Protocol	Time resolved anyalses
Scanning mode	Peak hopping, 1 point per peak
Detector mode	Pulse counting, dead time correction applied
Isotopes determined	^{206}Pb, ^{207}Pb, ^{208}Pb, ^{232}Th, ^{238}U, ^{29}Si, ^{87}Sr, ^{89}Y, ^{91}Zr, ^{177}Hf
Dwell time per isotope	15, 30, 10, 10, 15, 5, 5, 5, 5, 5 ms respectively
Quadrapole settling time	ca. 2 ms
Time/scan	ca. 89 ms
Data acqusition (s)	180 s (60 s gas blank, up to 120 s ablation)
Software	GLITTER (Version 4.4.1). Gemoc Laser ICP-MS Total Trace Element Reduction

Samples & Standards

Mounts	25 mm diameter polished grain mounts
Standard:	and standard mounts
	Gem Zircon "GJ-1", 609 Ma.
	NIST 610 - Doped Glass standard
	Gem Zircon "Temora 2", 416 Ma

V.2 – Zircon morphologies

The following figure illustrates the zircon morphology classification used in this study, that proposed by Pupin (1980). Different morphologies reflect a difference in the arrangement of crystal faces.

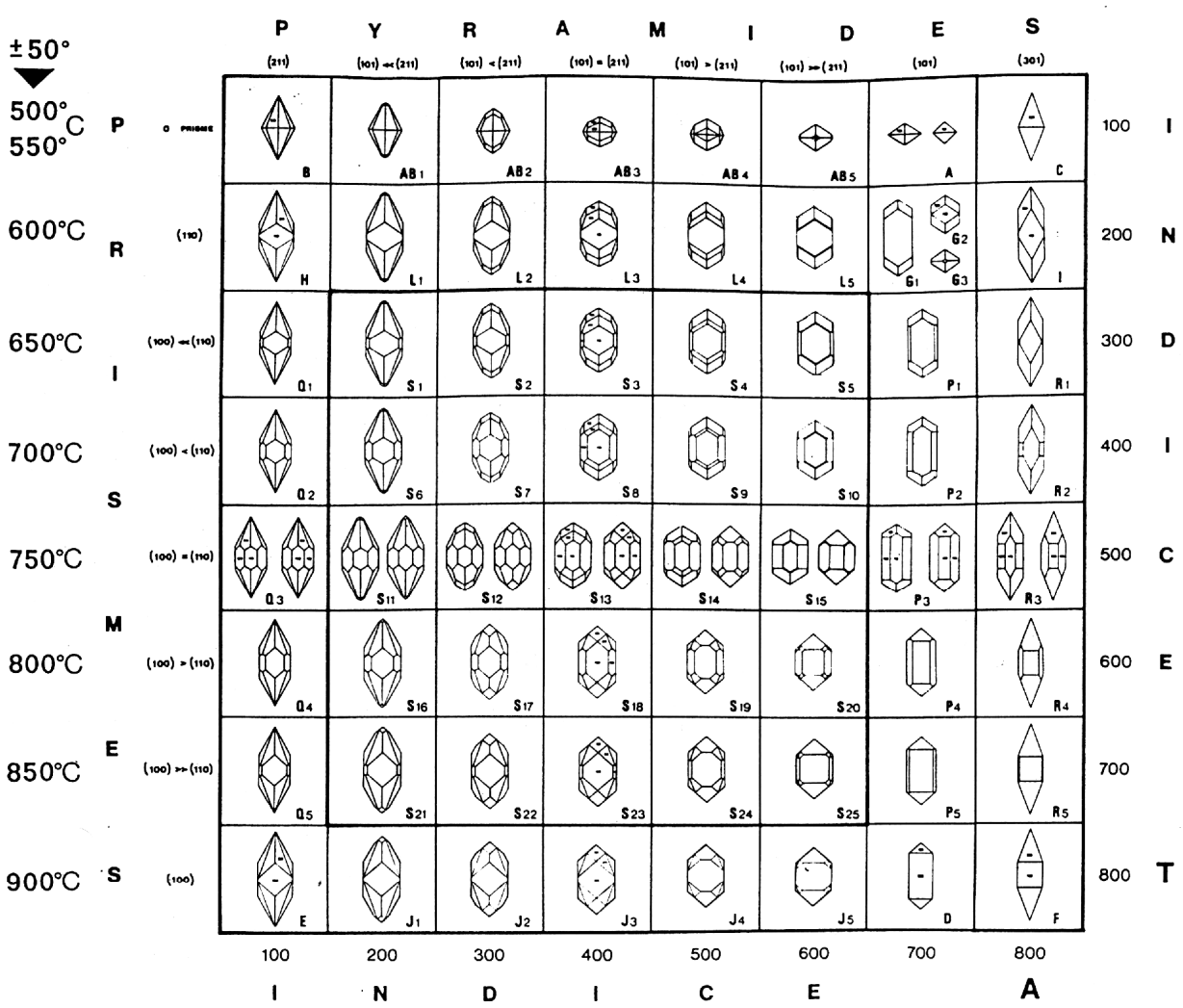

Fig. 1. Main types and subtypes of the typologic classification and corresponding geothermometric scale. The approximative temperature scale proposed (Pupin and Turco 1972c) was calibrated from the confrontation of the typology zircon data with the temperatures normally accepted in literature for crystallization of pluto-volcanic rocks and minerals. In this work, we have particularly considered: The limit of stability of the minerals (i.e., the muscovite in granitic and metamorphic rocks); – the geothermometric data obtained with other methods (i.e., on pyroxenes from charnockitic and volcanic rocks; on vitreous inclusions); – the temperature ranges for gneiss anatexy; – the temperature ranges for the beginning and the end of the magmatic crystallization in granites, diorites, gabbros and effusive equivalents; – the temperatures of formation of minerals with which zircon synerystallized (i.e., fluorite, late-magmatic

APPENDIX VI

SIGNAL SELECTION

VI.1 – Signal selection images

The following images display signal selections for individual crystal analysis exported from GLITTER software.

Example ^{206}Pb signal.

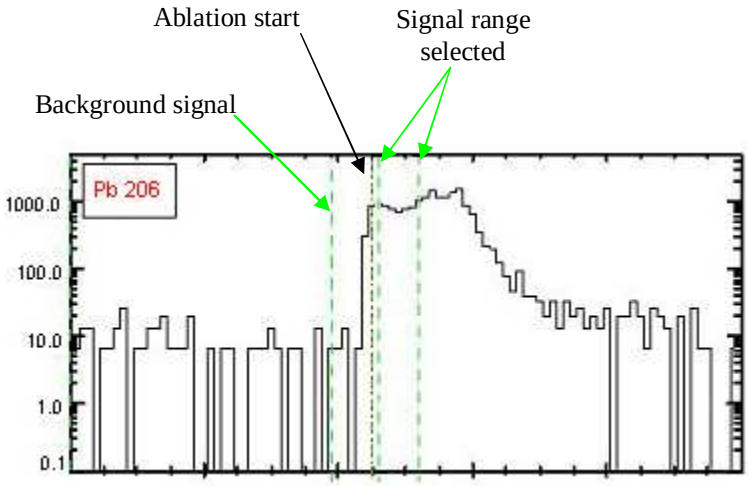

8 – McKee Formation

1.

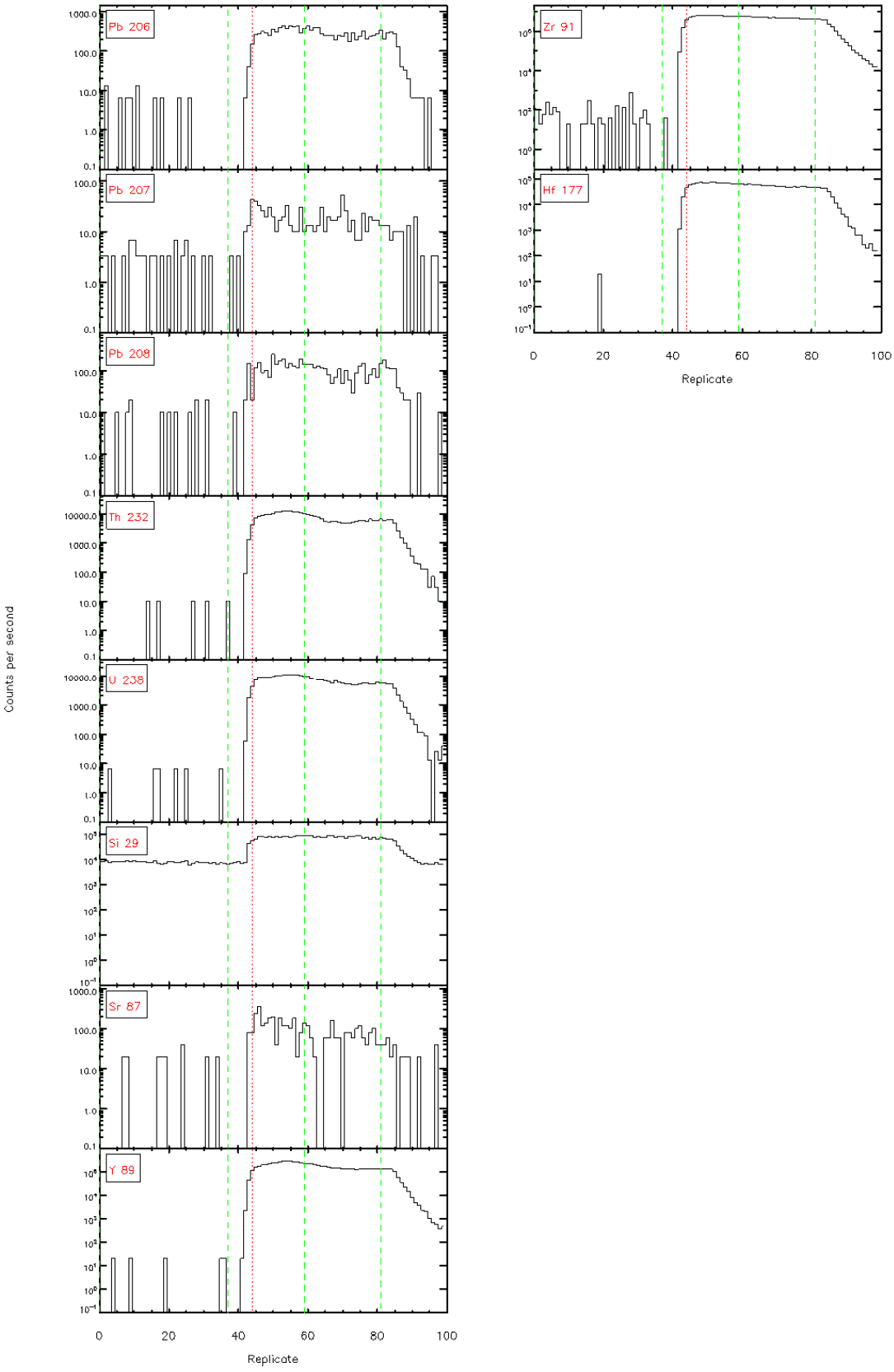

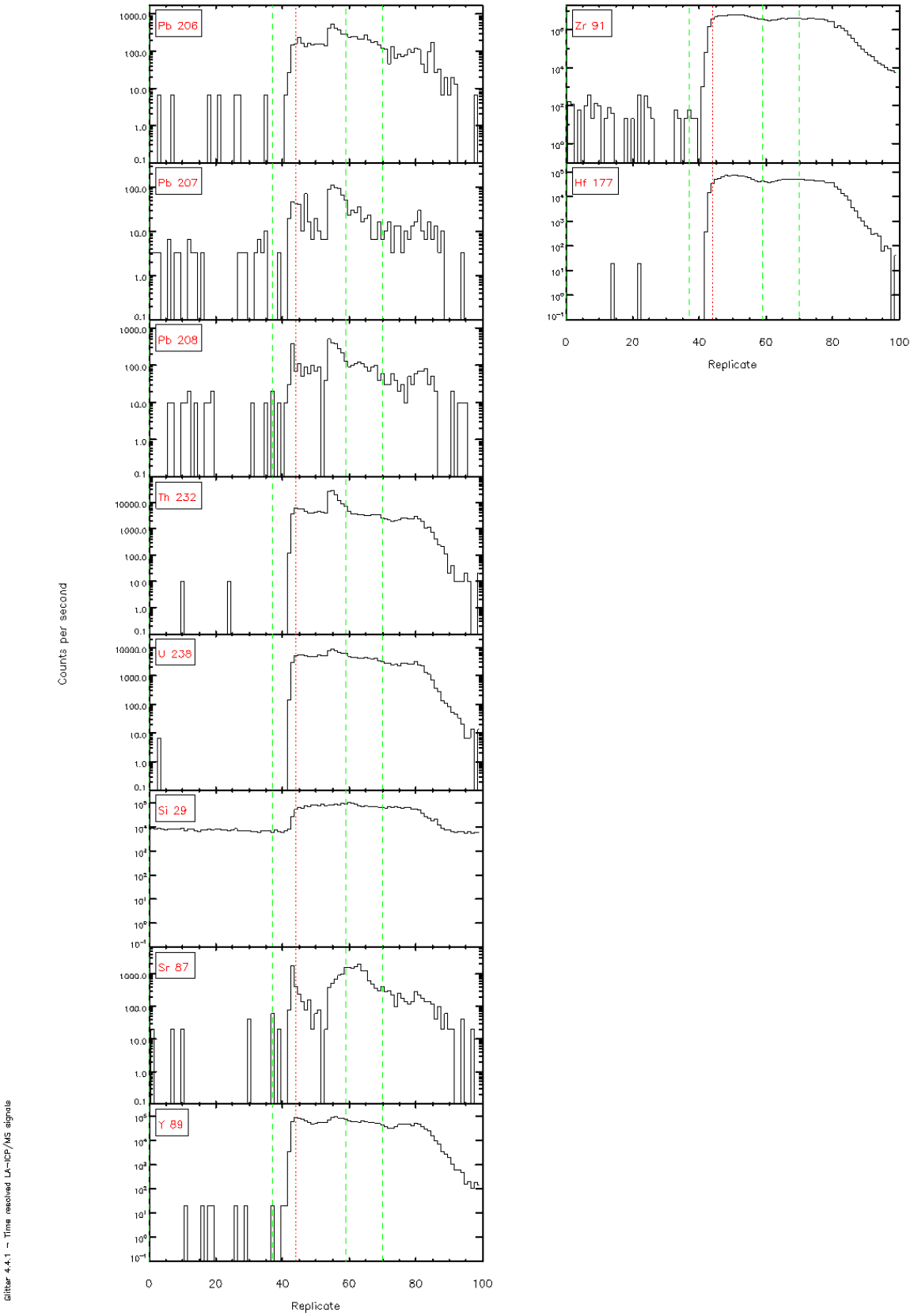
Pb 206
Pb 207
Pb 208
Th 232
U 238
Si 29
Sr 87
Y 89
Zr 91
Hf 177
Counts per second
Replicate
Glitter 4.4.1 – Time resolved LA-ICP/MS signals

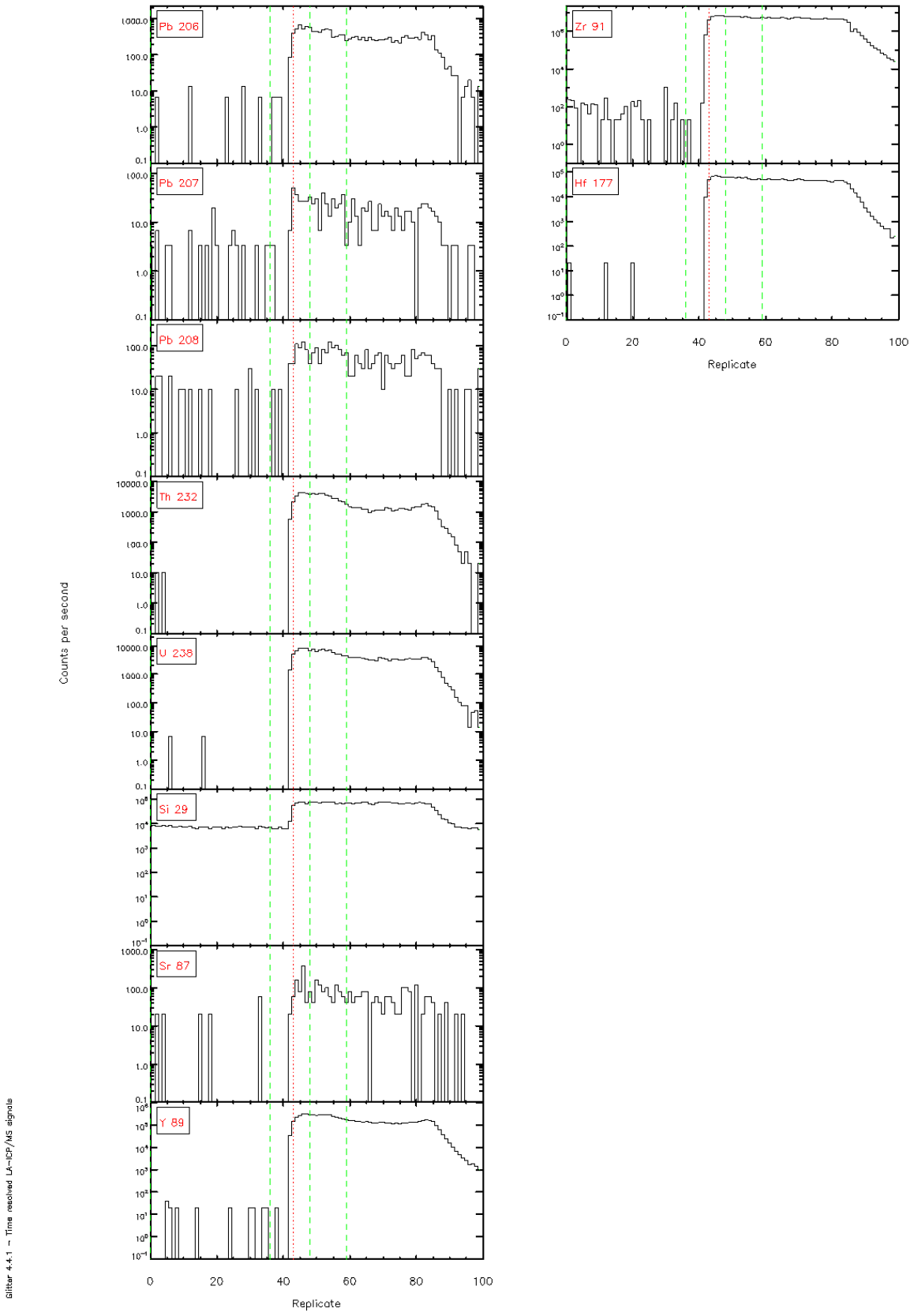
Pb 206
Pb 207
Pb 208
Th 232
U 238
Si 29
Sr 87
Y 89
Zr 91
Hf 177
Counts per second
Replicate
Glitter 4.4.1 – Time resolved LA-ICP/MS signals

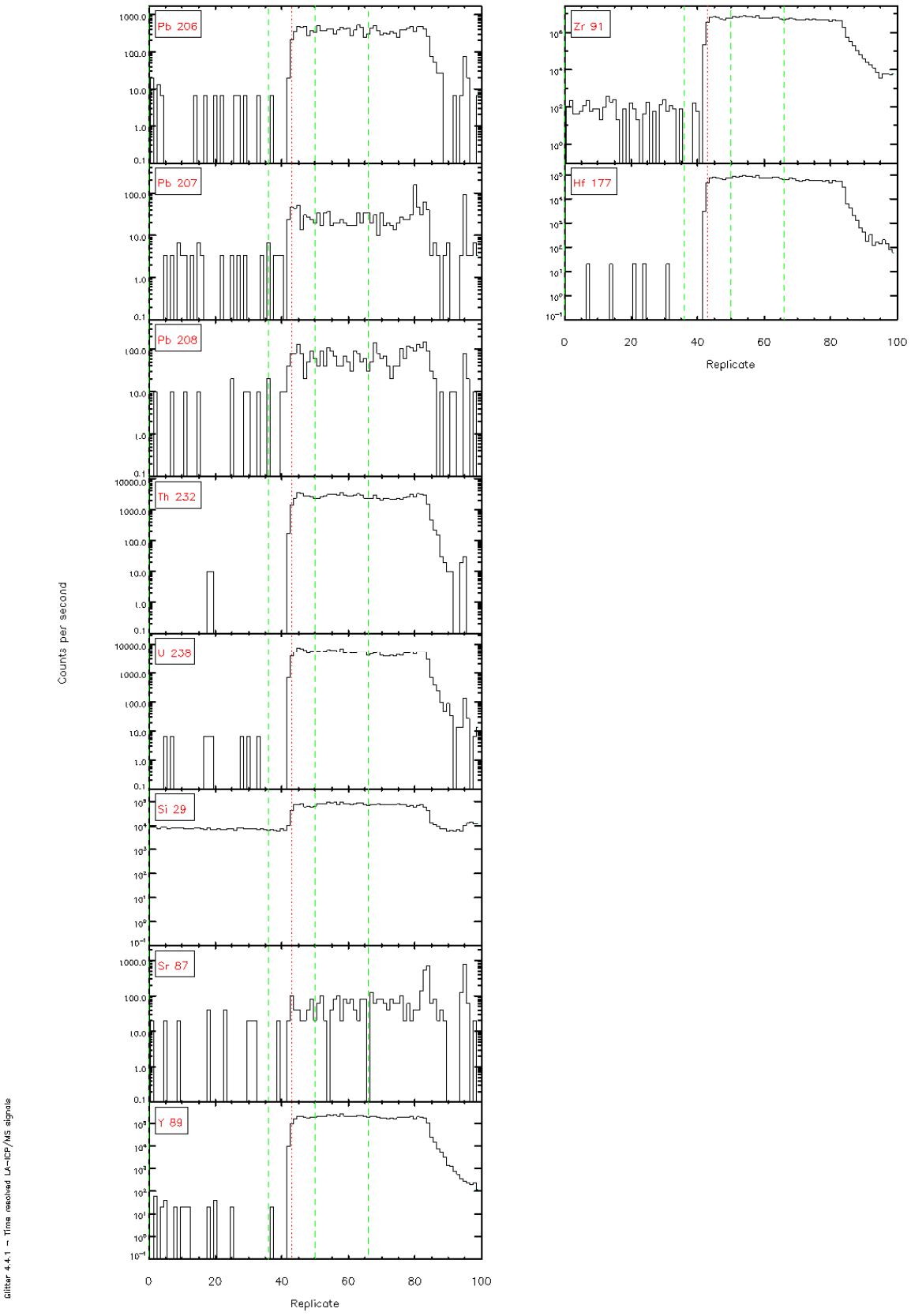
Pb 206
Pb 207
Pb 208
Th 232
U 238
Si 29
Sr 87
Y 89
Zr 91
Hf 177
Counts per second
Replicate
Glitter 4.4.1 – Time resolved LA-ICP/MS signals

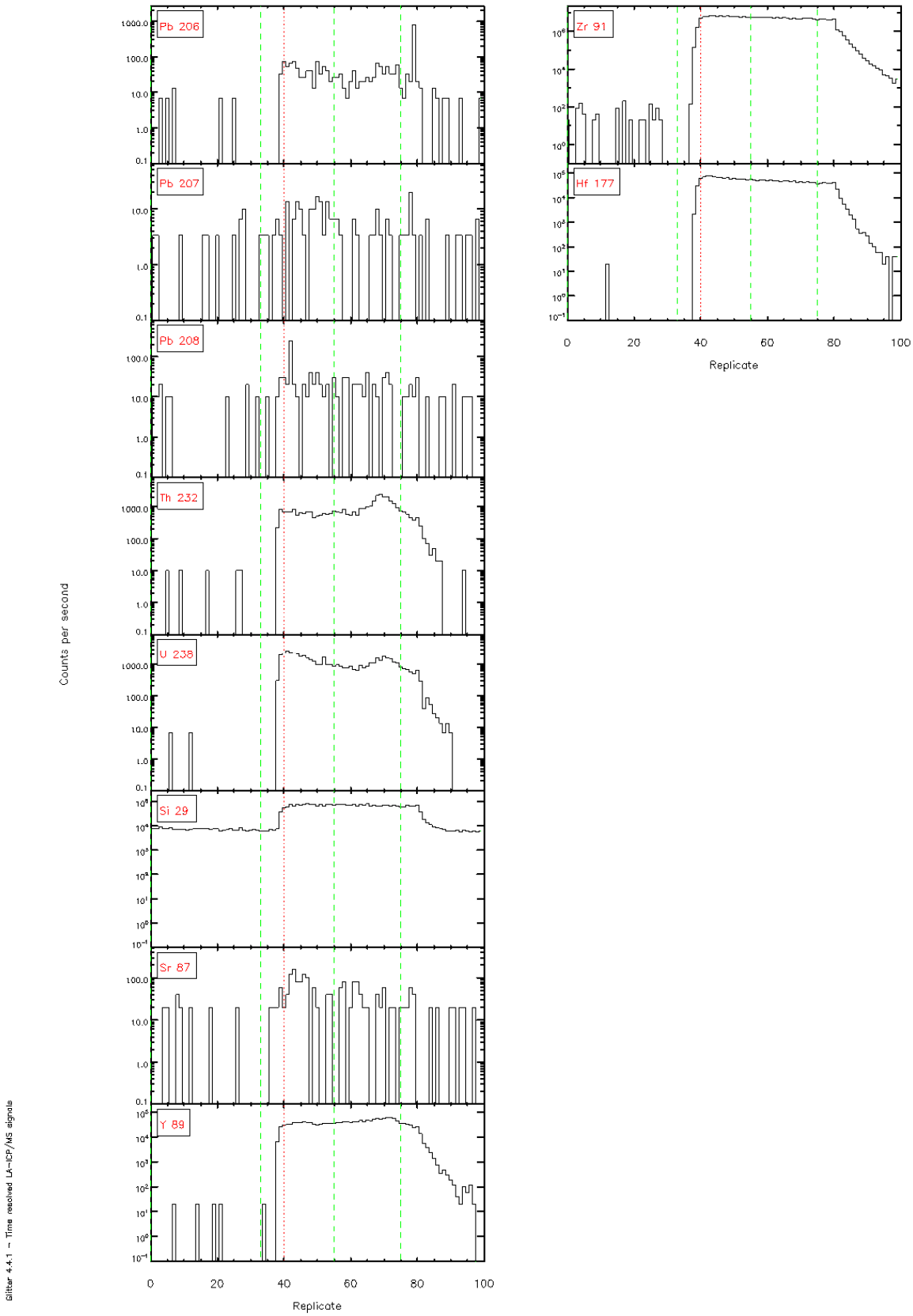
Pb 206
Pb 207
Pb 208
Th 232
U 238
Si 29
Sr 87
Y 89
Zr 91
Hf 177
Counts per second
Replicate
Glitter 4.4.1 – Time resolved LA-ICP/MS signals

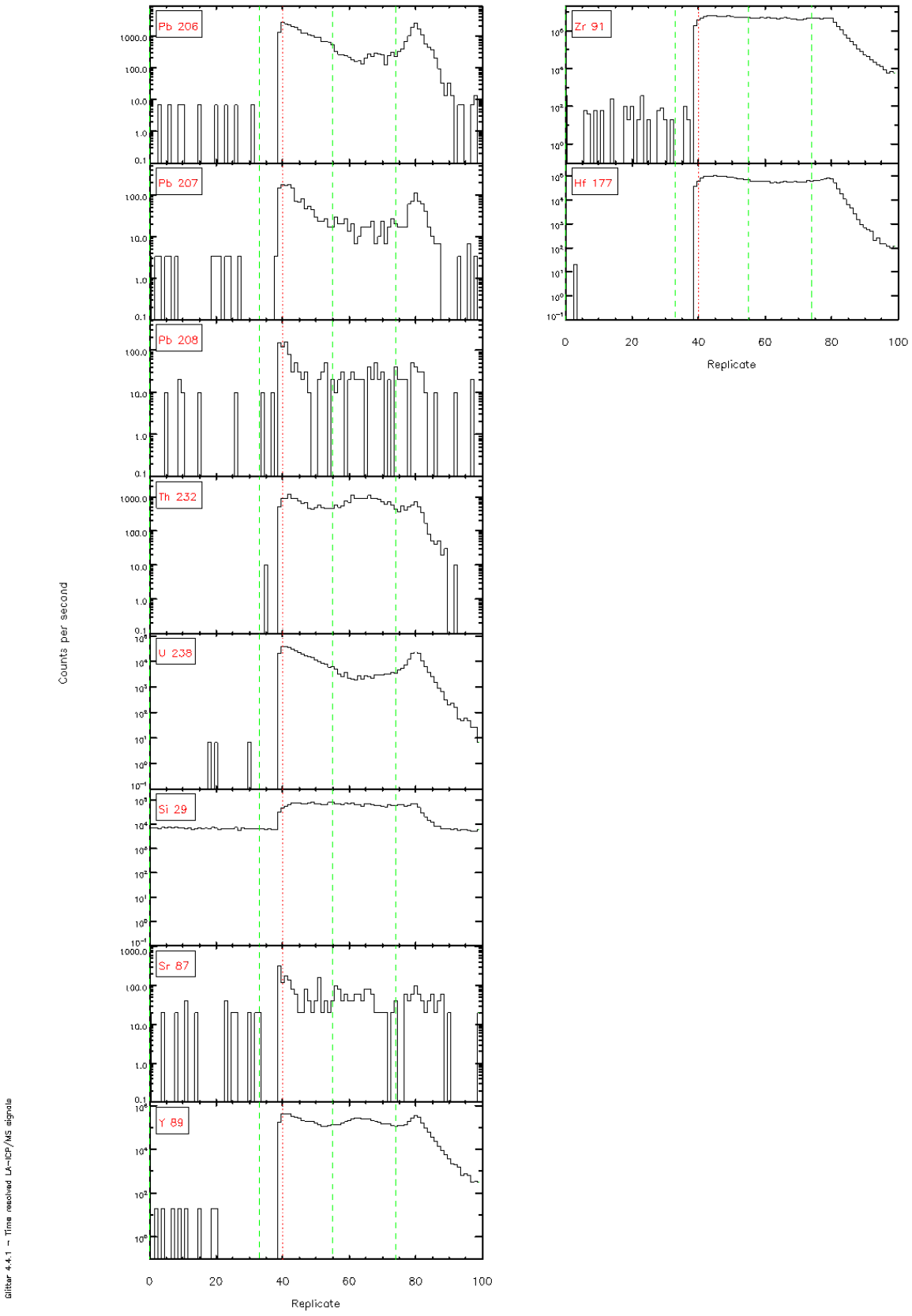
Pb 206
Pb 207
Pb 208
Th 232
U 238
Si 29
Sr 87
Y 89
Zr 91
Hf 177
Counts per second
Replicate
Glitter 4.4.1 – Time resolved LA-ICP/MS signals

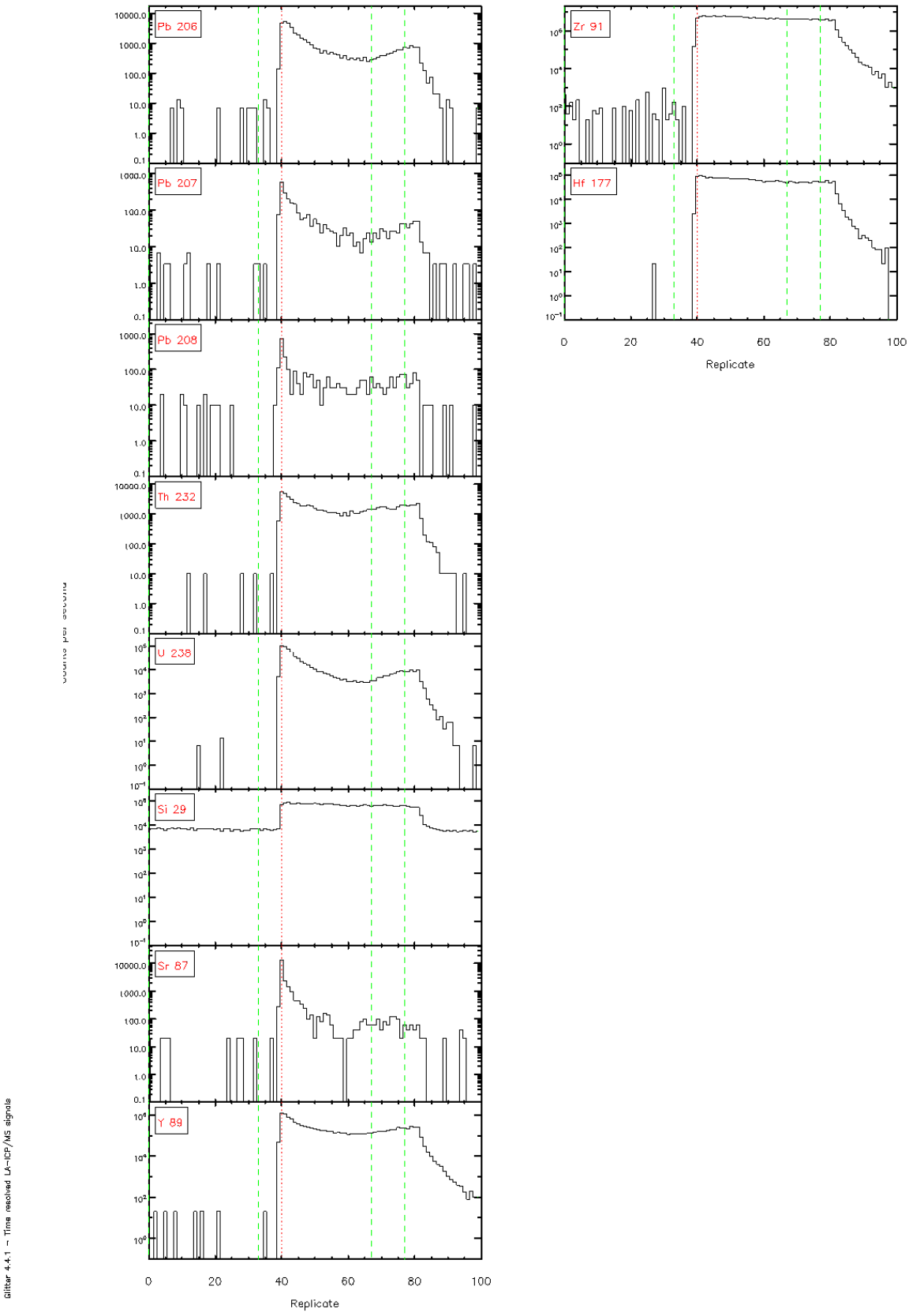
Pb 206
Pb 207
Pb 208
Th 232
U 238
Si 29
Sr 87
Y 89
Zr 91
Hf 177
Replicate
Glitter 4.4.1 – Time resolved LA-ICP/MS signals

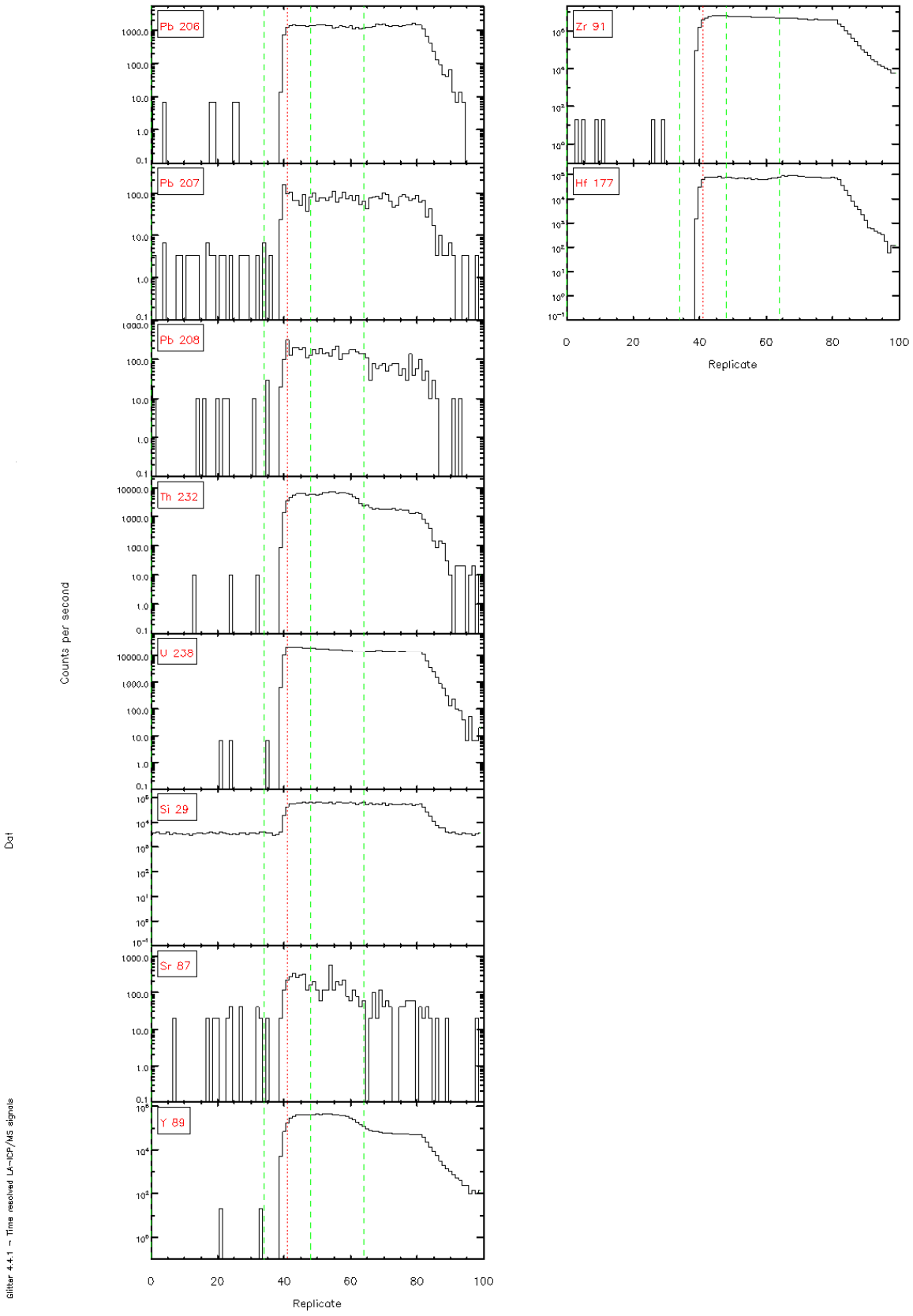
Pb 206
Pb 207
Pb 208
Th 232
U 238
Si 29
Sr 87
Y 89
Zr 91
Hf 177
Counts per second
Replicate
Glitter 4.4.1 – Time resolved LA-ICP/MS signals
Dat

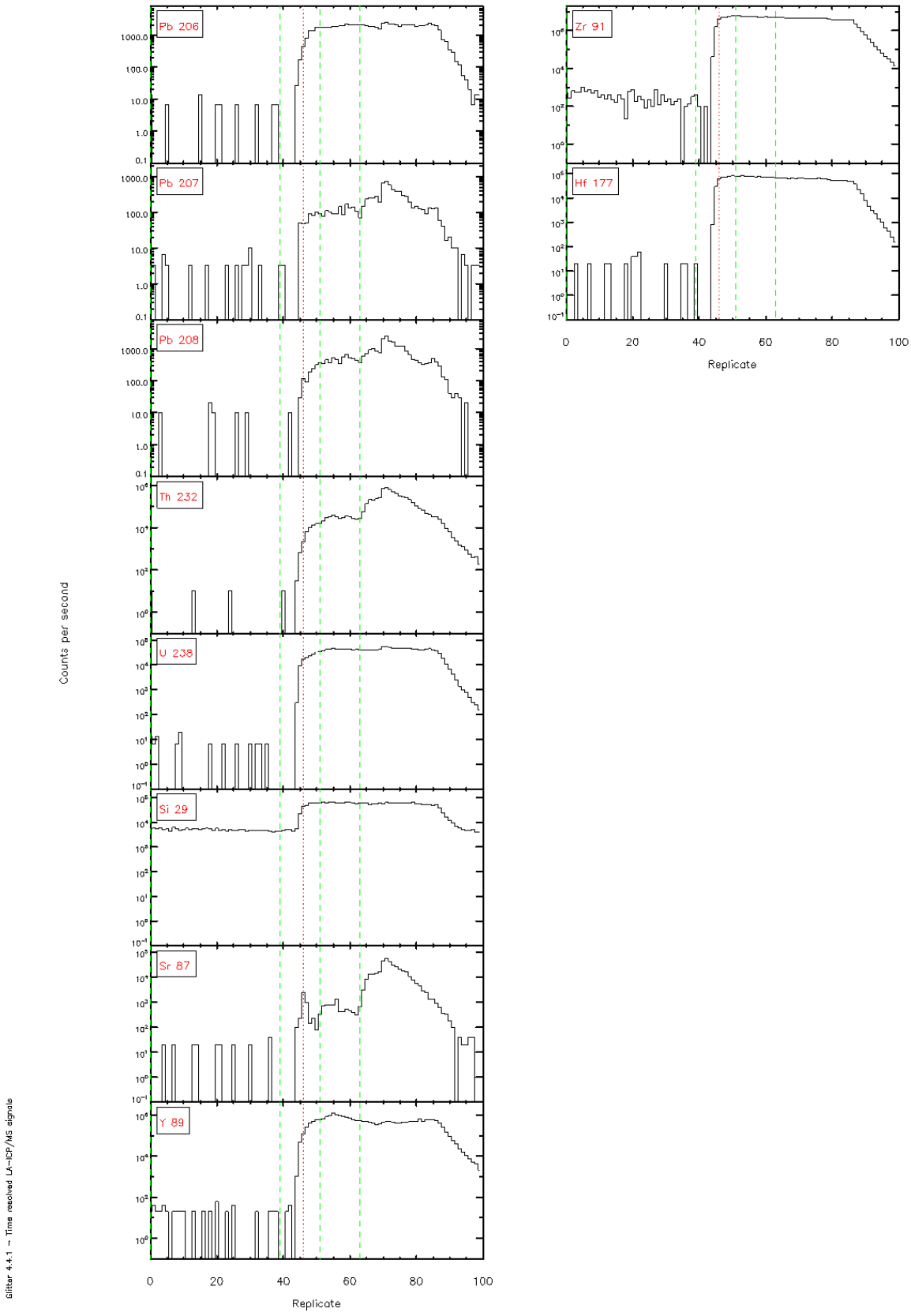
Pb 206
Pb 207
Pb 208
Th 232
U 238
Si 29
Sr 87
Y 89
Zr 91
Hf 177
Counts per second
Replicate
Replicate
Glitter 4.4.1 – Time resolved LA-ICP/MS signals

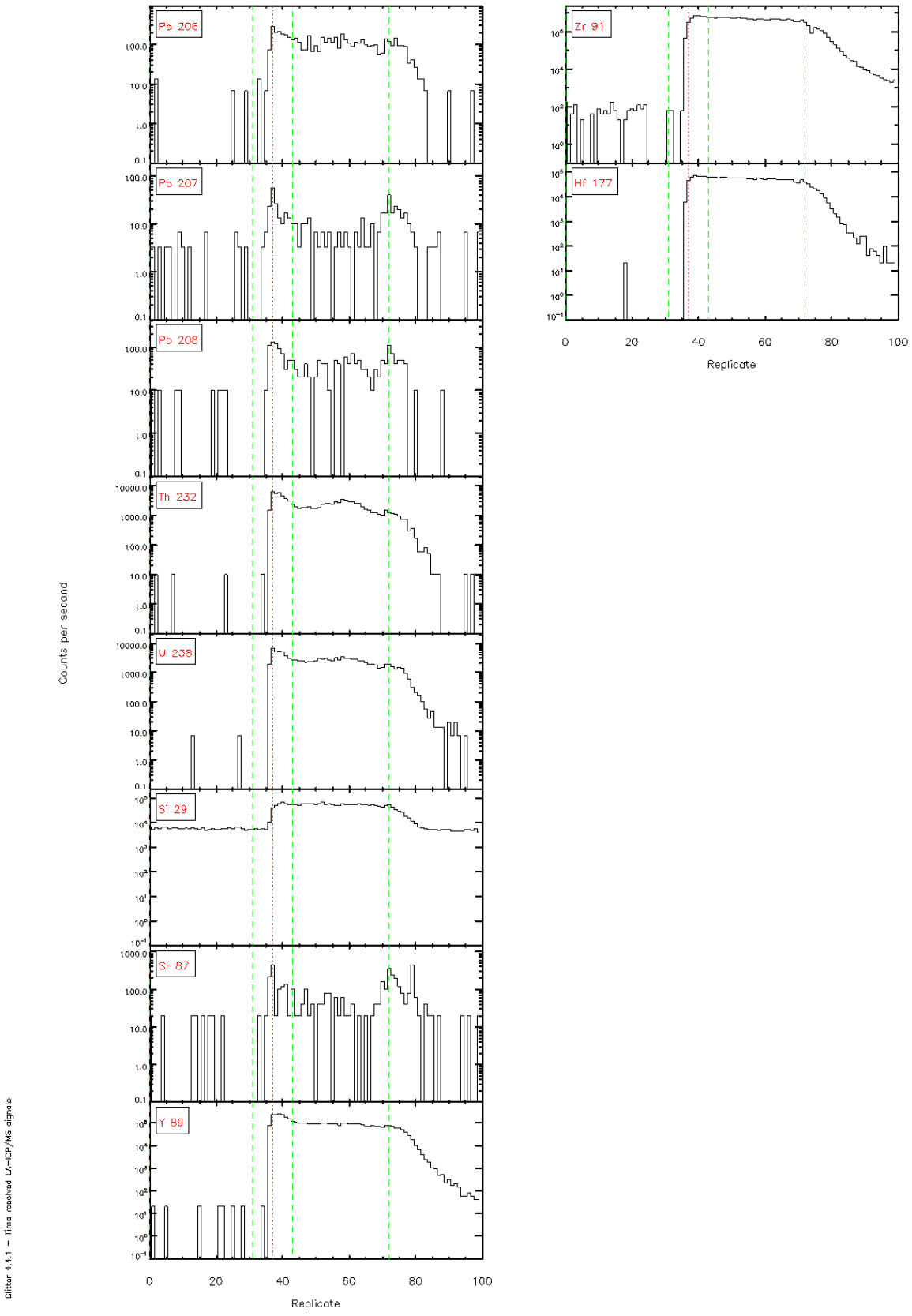
Pb 206
Pb 207
Pb 208
Th 232
U 238
Si 29
Sr 87
Y 89
Zr 91
Hf 177
Counts per second
Replicate
Glitter 4.4.1 – Time resolved LA-ICP/MS signals

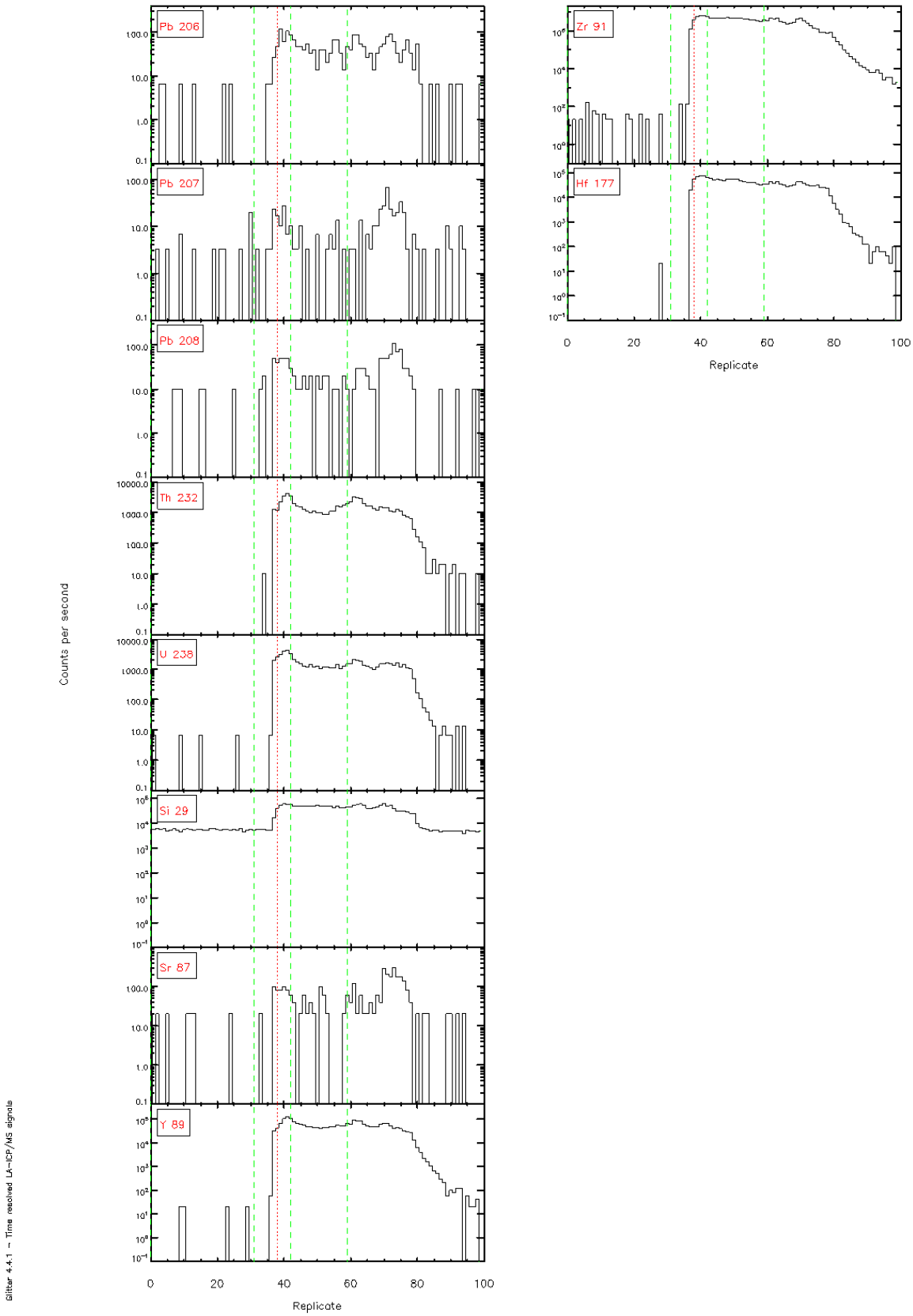
Pb 206
Pb 207
Pb 208
Th 232
U 238
Si 29
Sr 87
Y 89
Zr 91
Hf 177
Counts per second
Replicate
Glitter 4.4.1 – Time resolved LA-ICP/MS signals

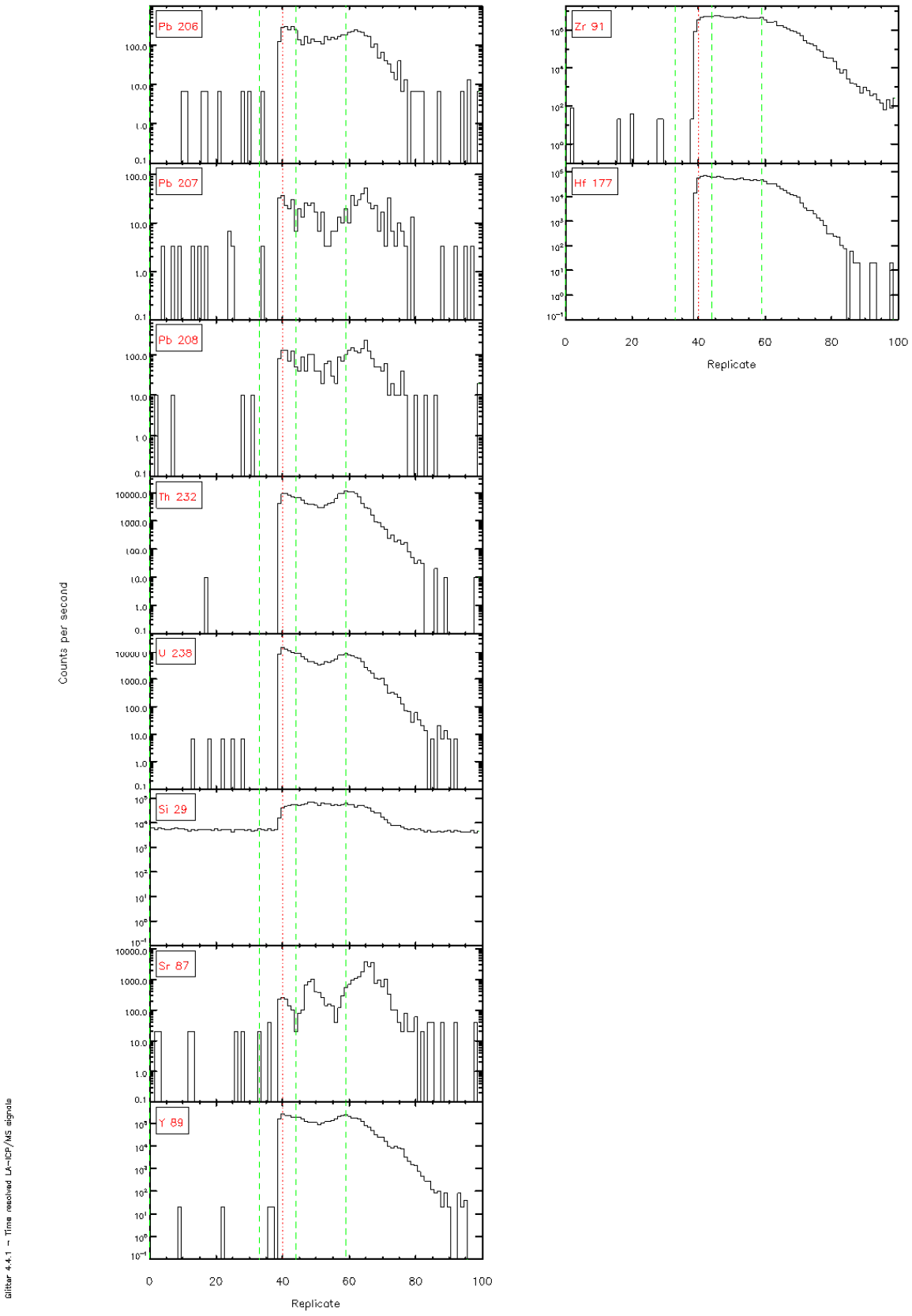
Pb 206
Pb 207
Pb 208
Th 232
U 238
Si 29
Sr 87
Y 89
Zr 91
Hf 177
Counts per second
Replicate
Glitter 4.4.1 – Time resolved LA-ICP/MS signals

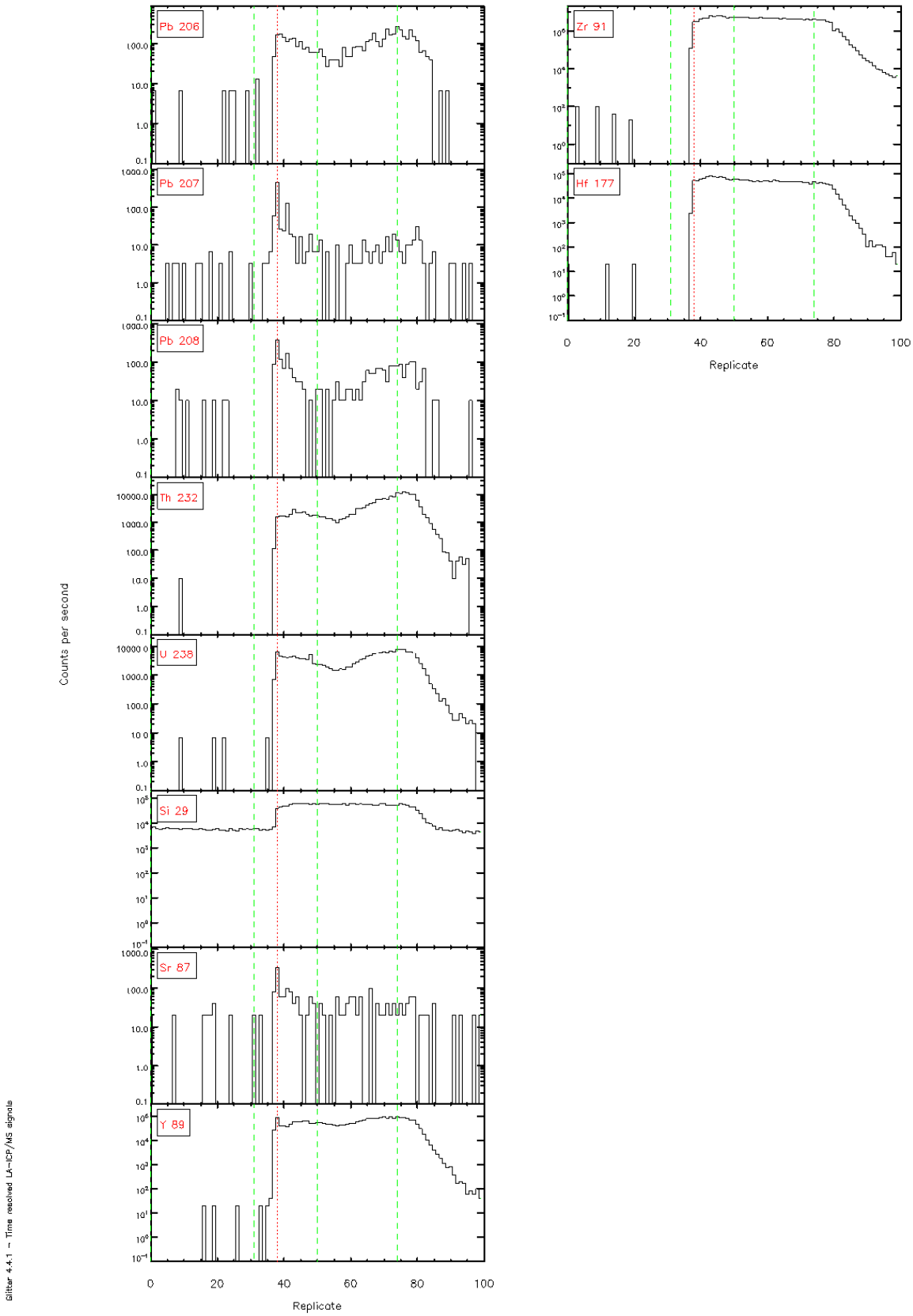
Pb 206
Pb 207
Pb 208
Th 232
U 238
Si 29
Sr 87
Y 89
Zr 91
Hf 177
Counts per second
Replicate
Replicate
Glitter 4.4.1 – Time resolved LA-ICP/MS signals

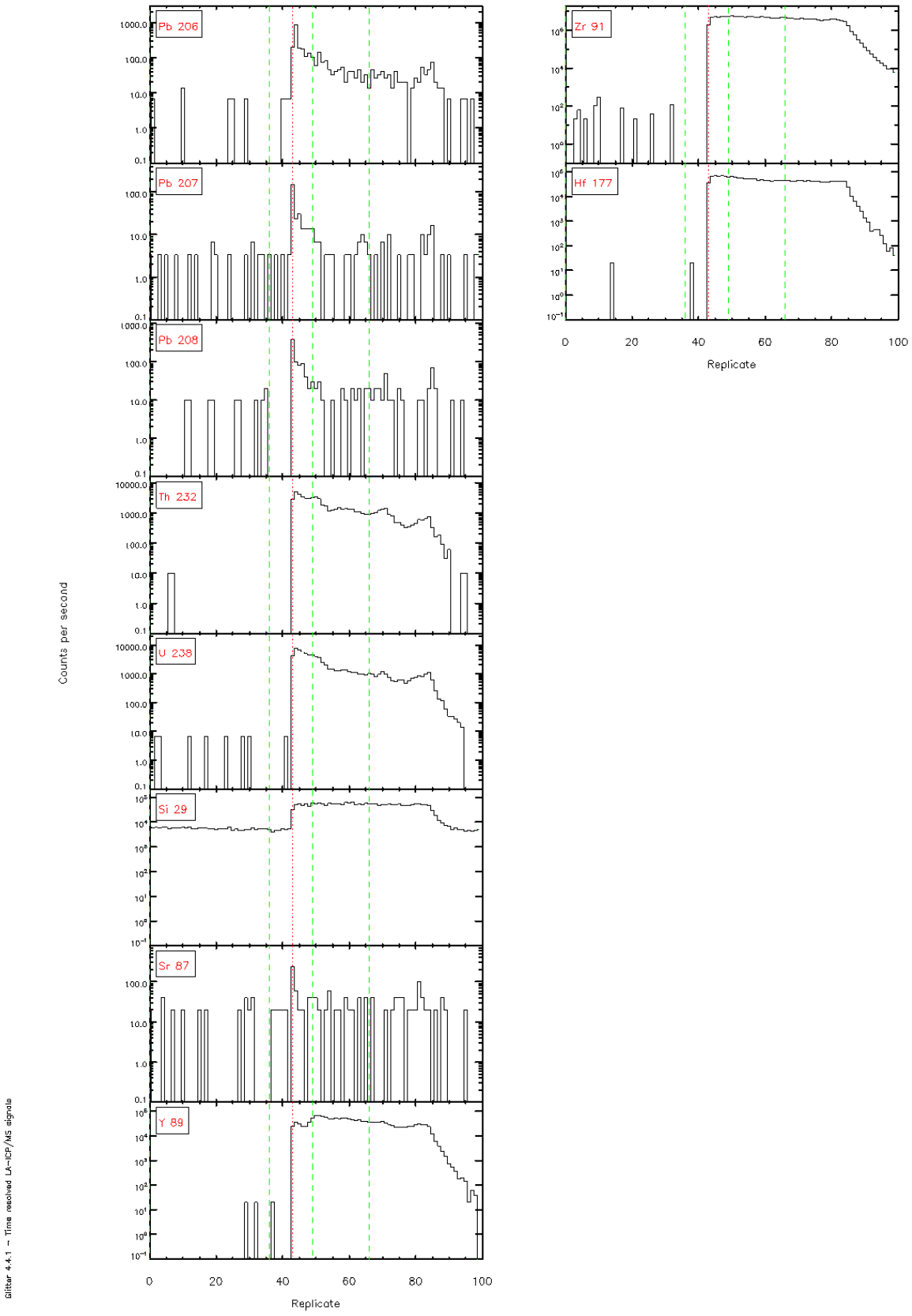
Pb 206
Pb 207
Pb 208
Th 232
U 238
Si 29
Sr 87
Y 89
Zr 91
Hf 177
Counts per second
Replicate
Glitter 4.4.1 – Time resolved LA-ICP/MS signals

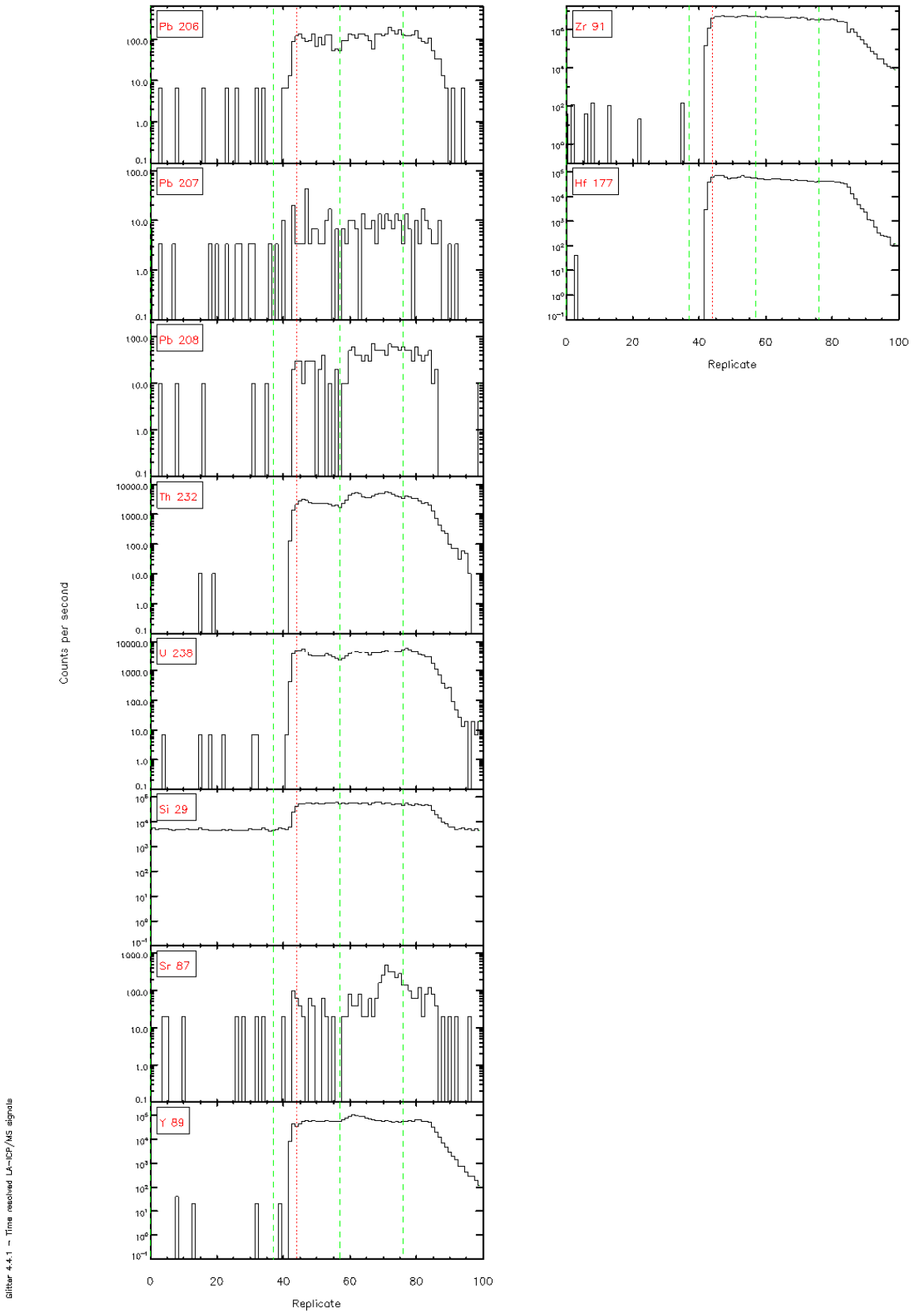
Pb 206
Pb 207
Pb 208
Th 232
U 238
Si 29
Sr 87
Y 89
Zr 91
Hf 177
Counts per second
Replicate
Glitter 4.4.1 – Time resolved LA-ICP/MS signals

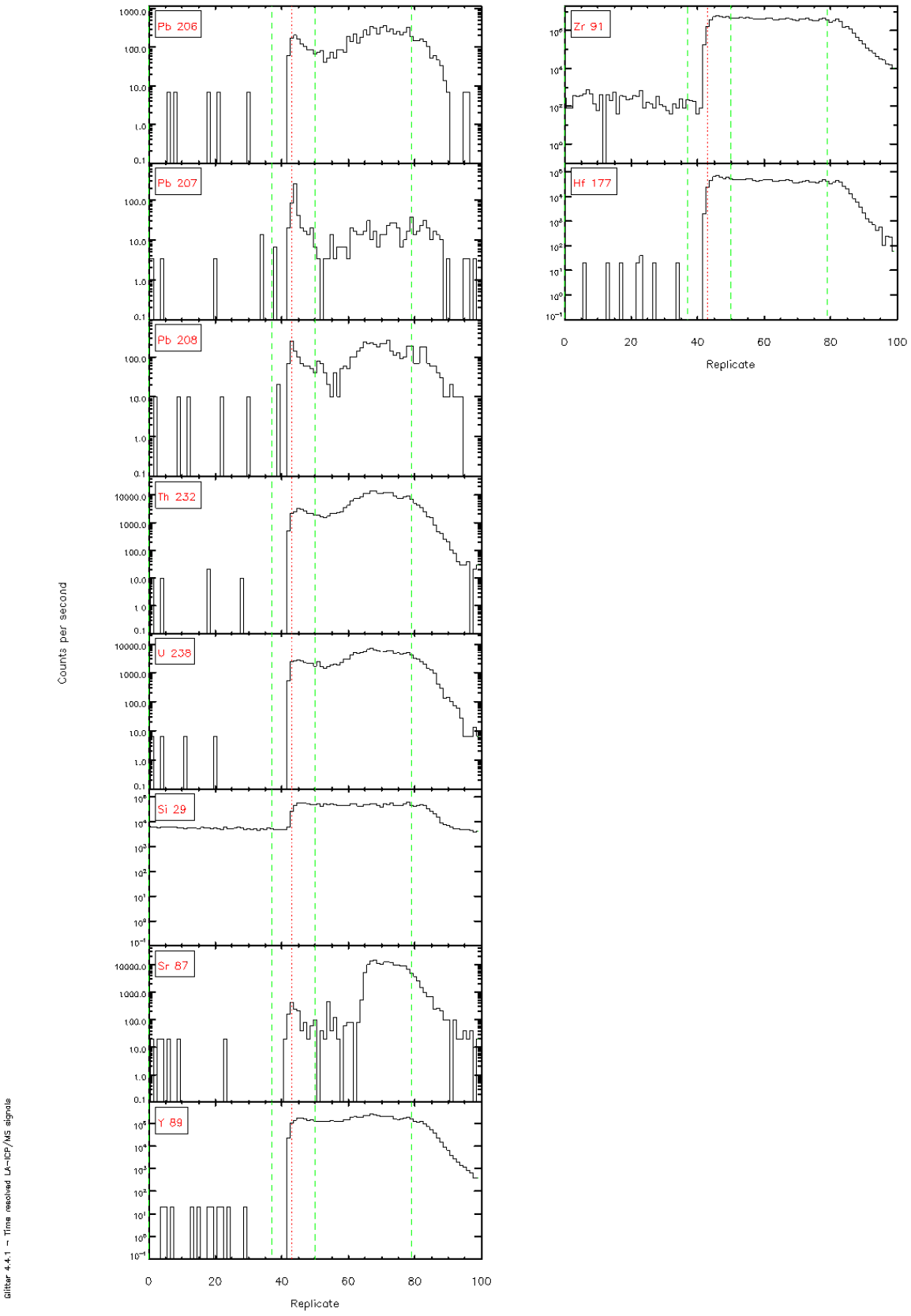
Pb 206
Pb 207
Pb 208
Th 232
U 238
Si 29
Sr 87
Y 89
Zr 91
Hf 177
Counts per second
Replicate
Glitter 4.4.1 – Time resolved LA-ICP/MS signals

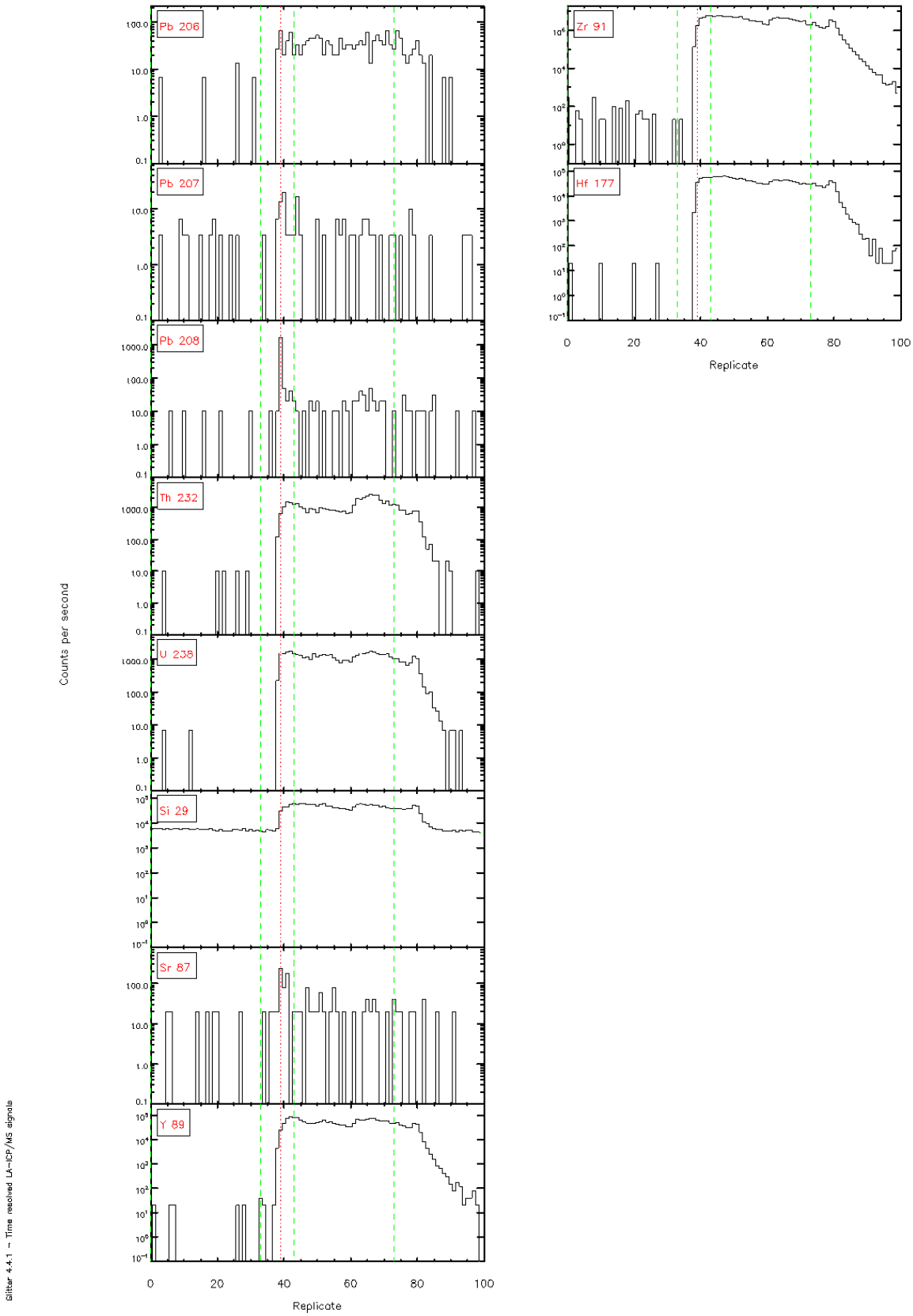
Pb 206
Pb 207
Pb 208
Th 232
U 238
Si 29
Sr 87
Y 89
Zr 91
Hf 177
Counts per second
Replicate
Glitter 4.4.1 – Time resolved LA-ICP/MS signals

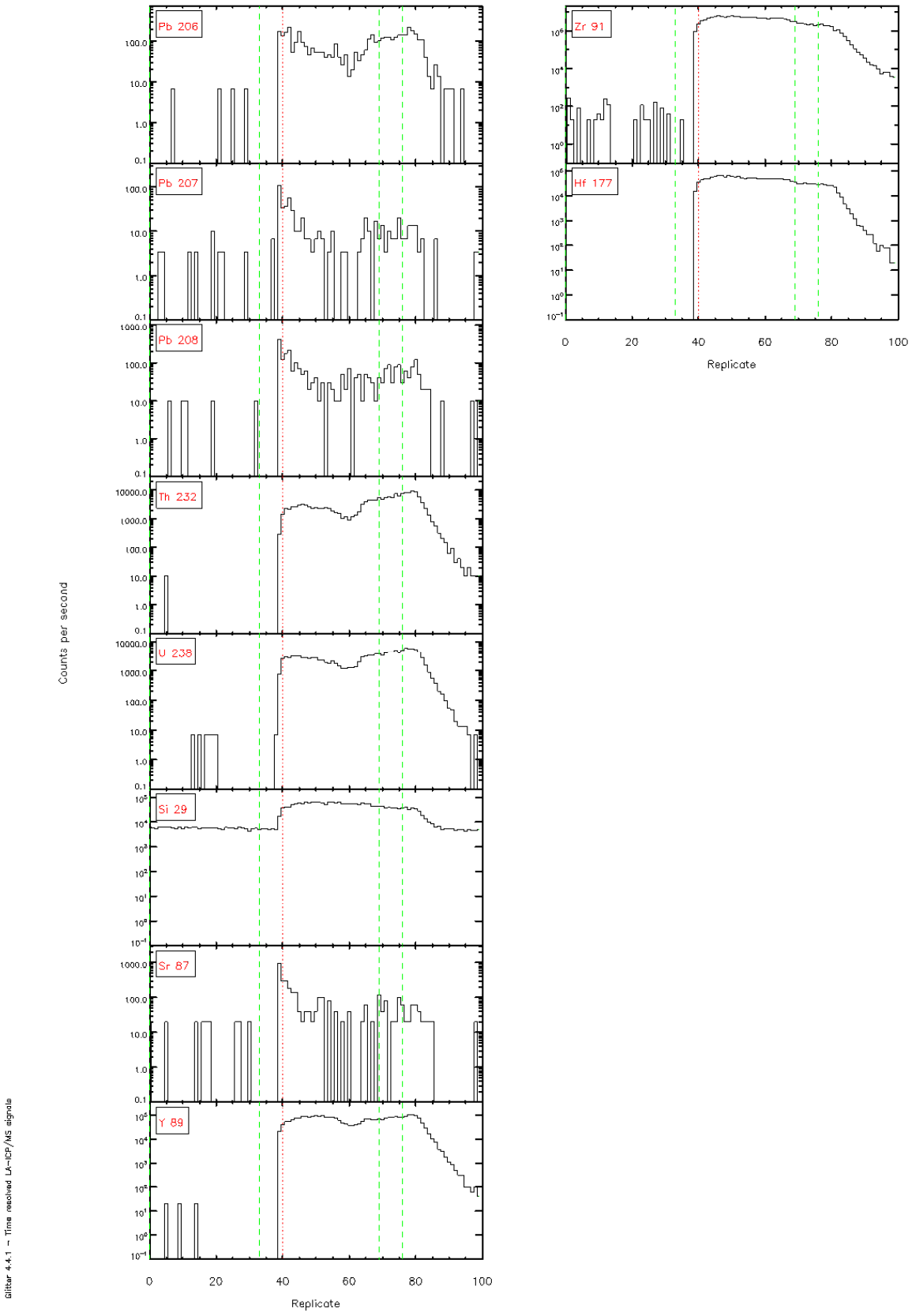
Pb 206
Pb 207
Pb 208
Th 232
U 238
Si 29
Sr 87
Y 89
Zr 91
Hf 177
Counts per second
Replicate
Glitter 4.4.1 – Time resolved LA-ICP/MS signals

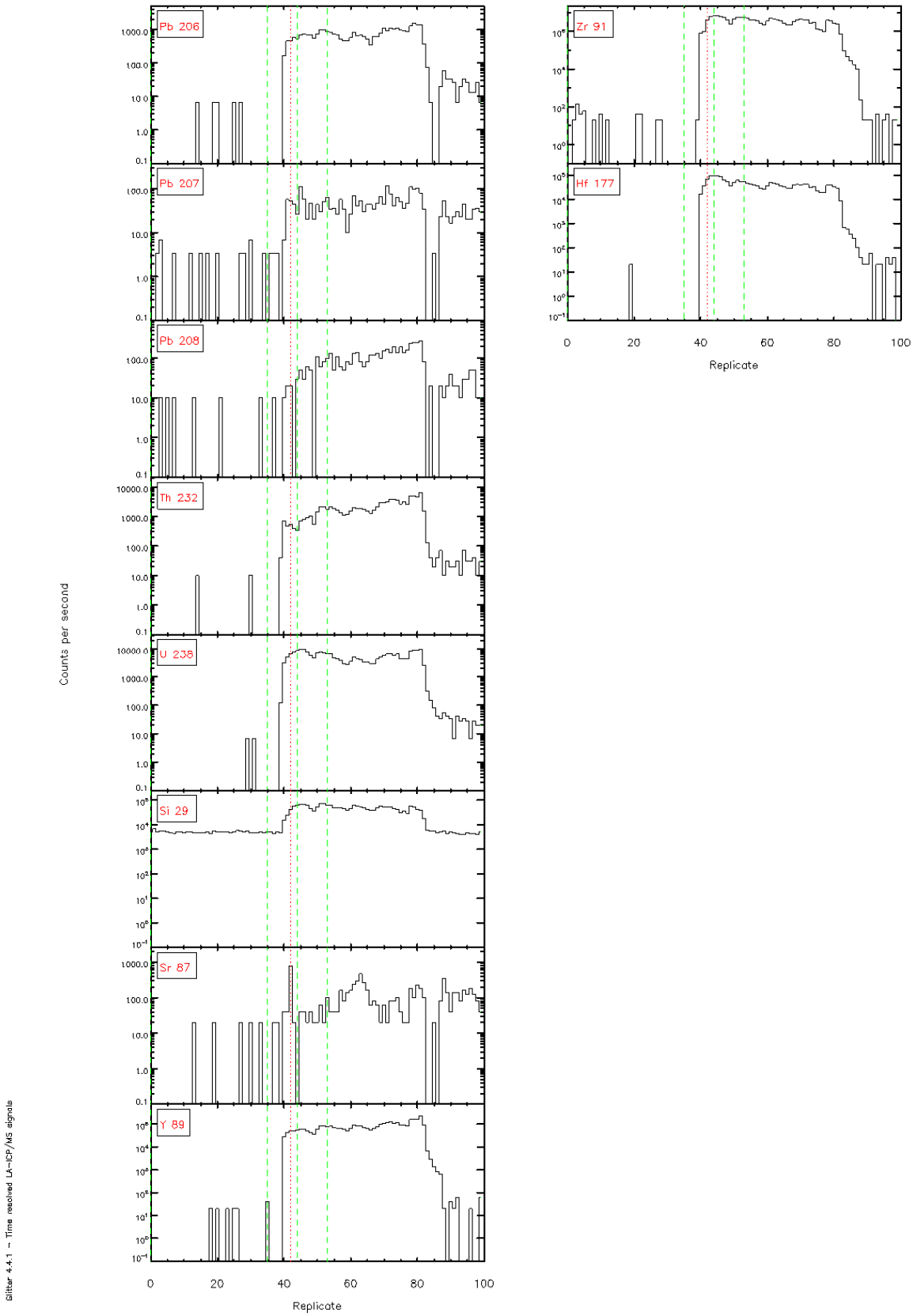
Pb 206
Pb 207
Pb 208
Th 232
U 238
Si 29
Sr 87
Y 89
Zr 91
Hf 177
Counts per second
Replicate
Glitter 4.4.1 – Time resolved LA-ICP/MS signals

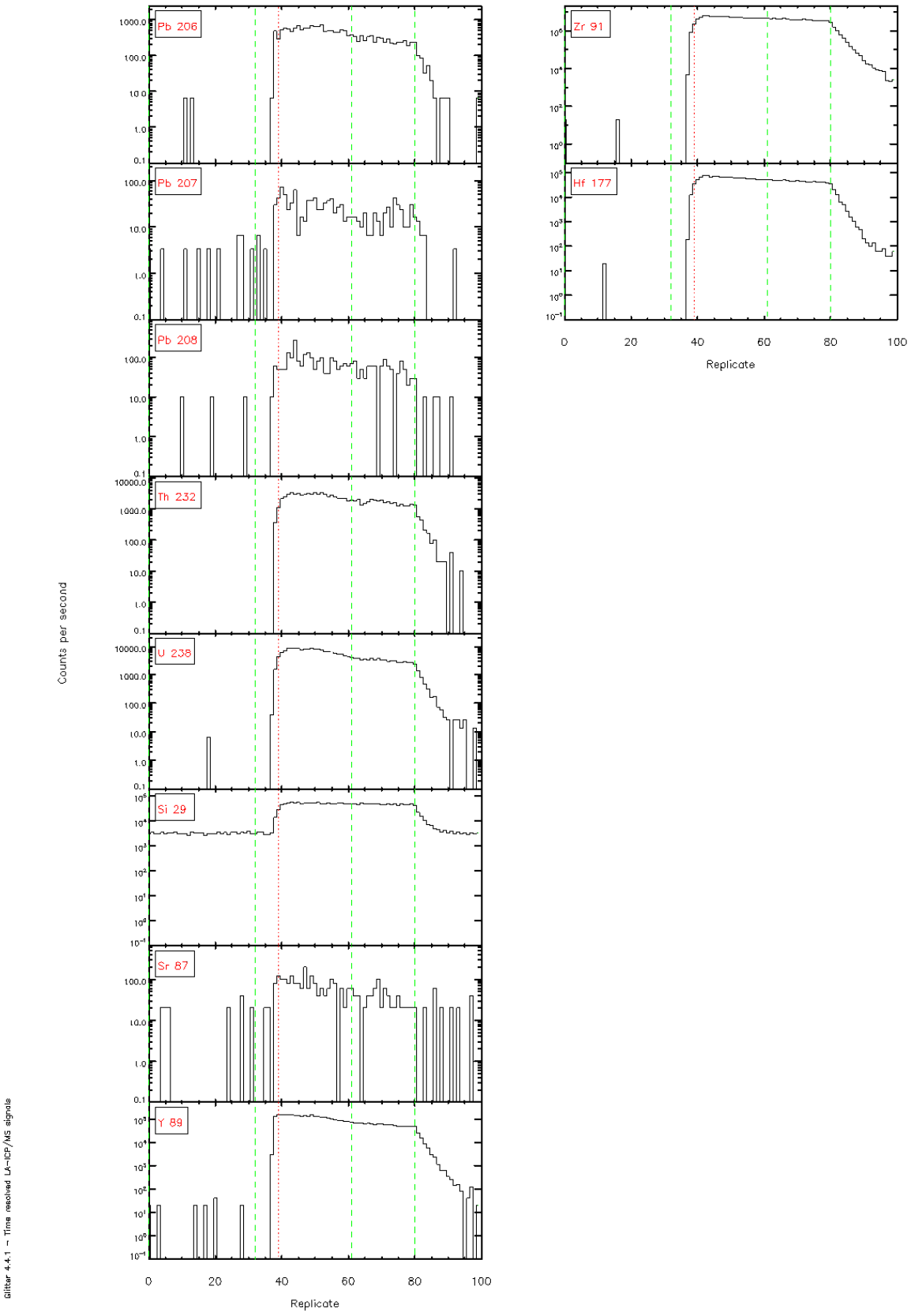
Pb 206
Pb 207
Pb 208
Th 232
U 238
Si 29
Sr 87
Y 89
Zr 91
Hf 177
Counts per second
Replicate
Glitter 4.4.1 – Time resolved LA-ICP/MS signals

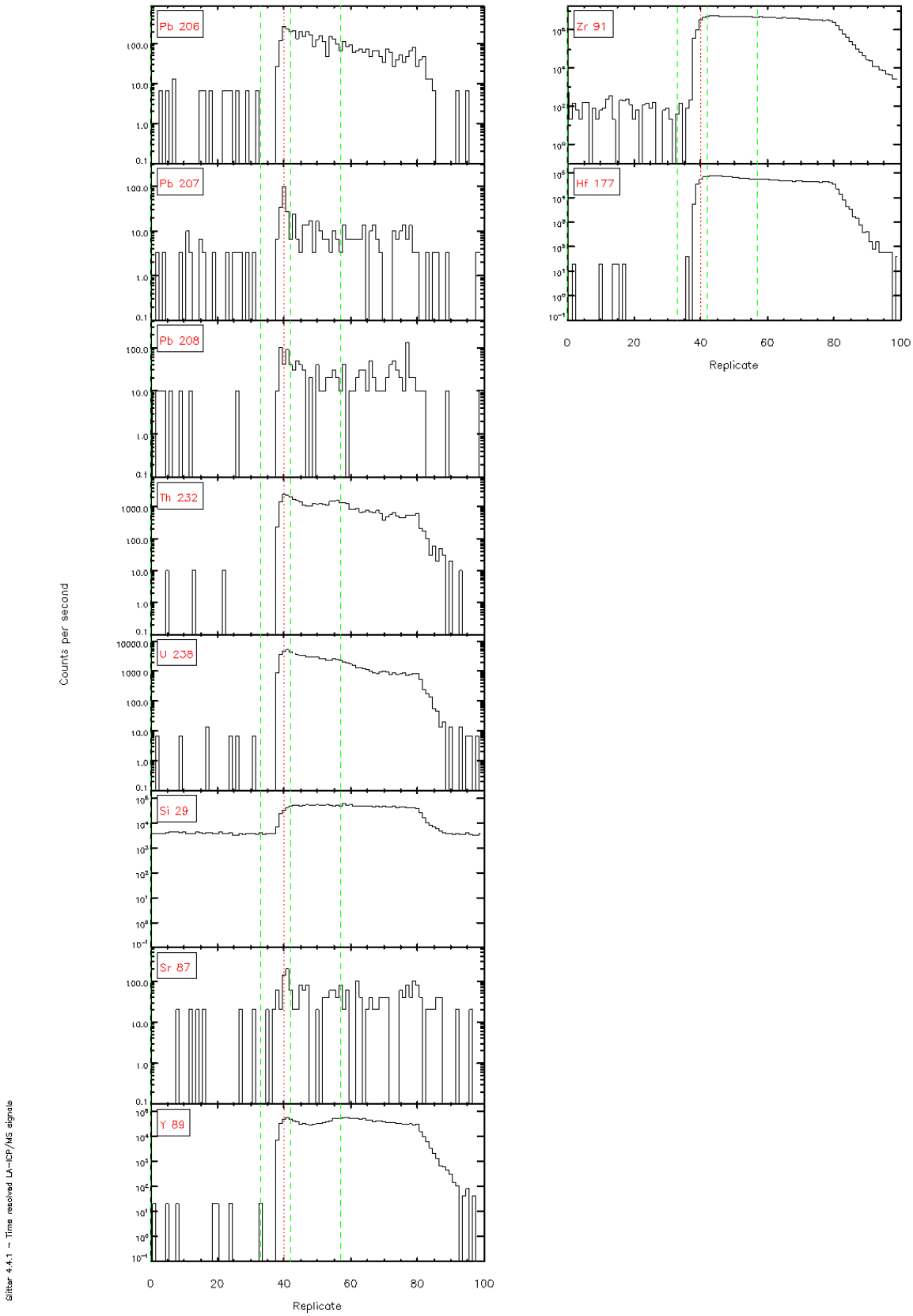
Pb 206
Pb 207
Pb 208
Th 232
U 238
Si 29
Sr 87
Y 89
Zr 91
Hf 177
Counts per second
Replicate
Glitter 4.4.1 – Time resolved LA-ICP/MS signals

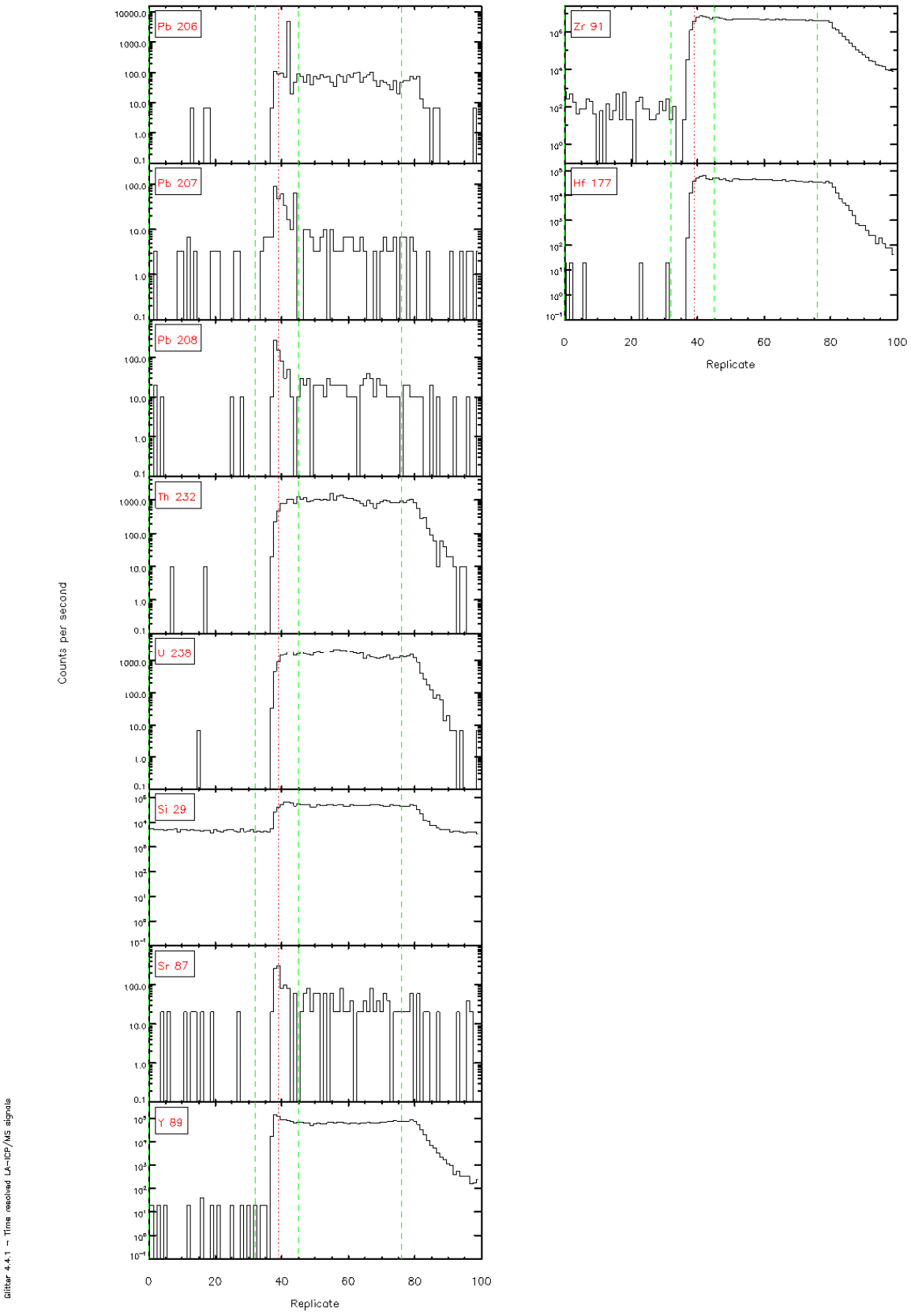
Pb 206
Pb 207
Pb 208
Th 232
U 238
Si 29
Sr 87
Y 89
Zr 91
Hf 177
Counts per second
Replicate
Glitter 4.4.1 – Time resolved LA-ICP/MS signals

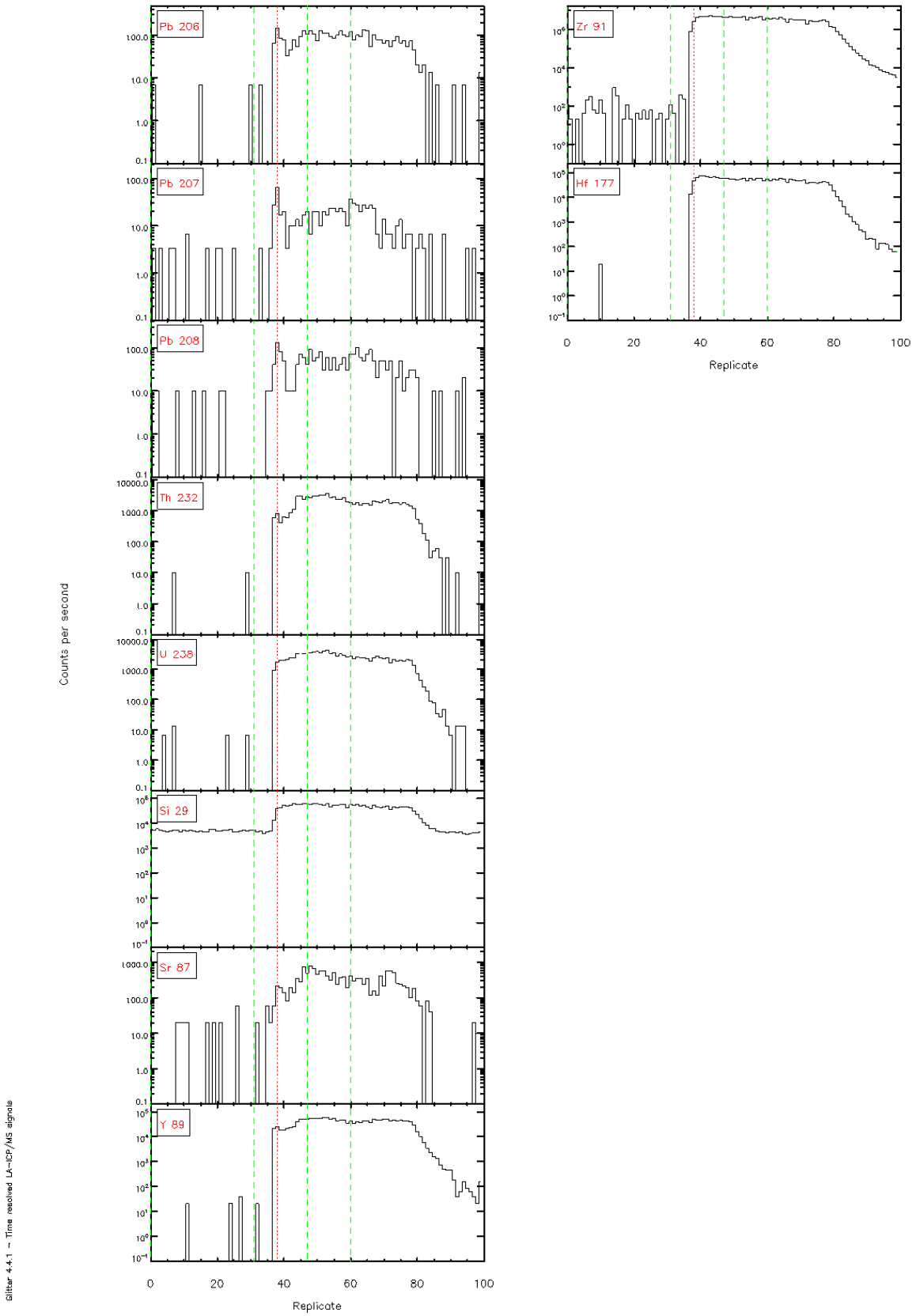
Pb 206
Pb 207
Pb 208
Th 232
U 238
Si 29
Sr 87
Y 89
Zr 91
Hf 177
Counts per second
Replicate
Glitter 4.4.1 – Time resolved LA-ICP/MS signals

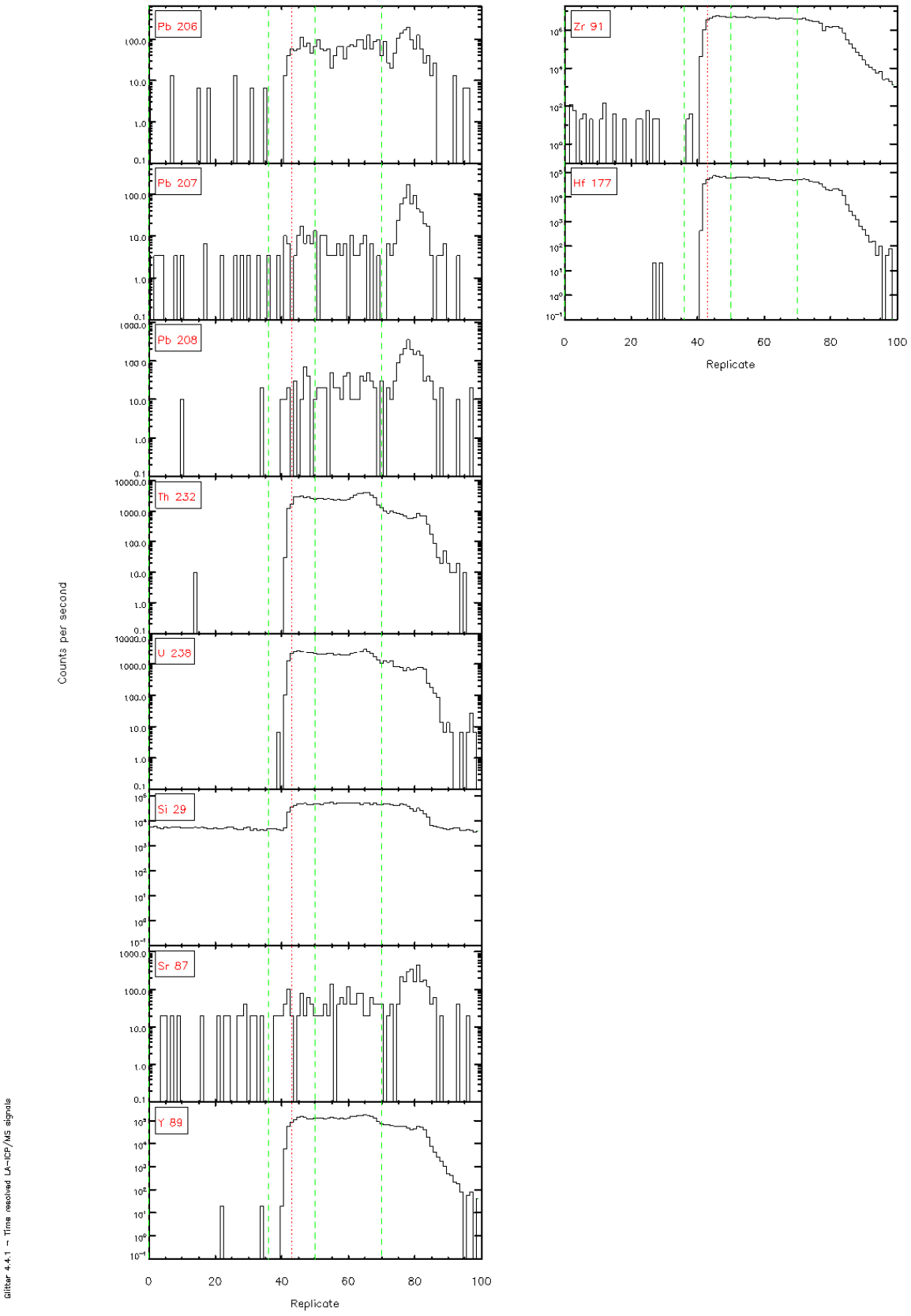
Pb 206
Pb 207
Pb 208
Th 232
U 238
Si 29
Sr 87
Y 89
Zr 91
Hf 177
Counts per second
Replicate
Glitter 4.4.1 – Time resolved LA-ICP/MS signals

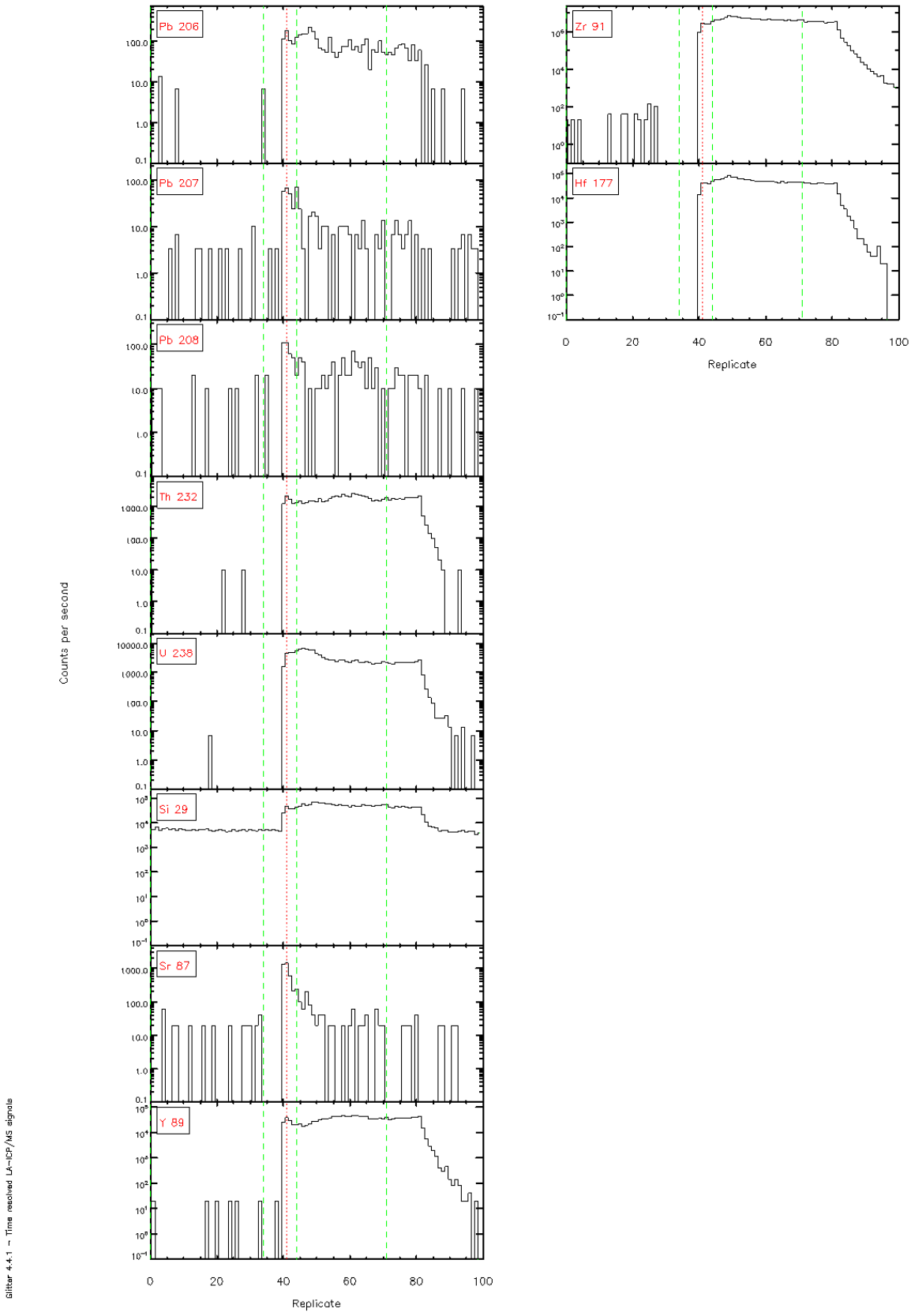
Pb 206
Pb 207
Pb 208
Th 232
U 238
Si 29
Sr 87
Y 89
Zr 91
Hf 177
Counts per second
Replicate
Glitter 4.4.1 – Time resolved LA-ICP/MS signals

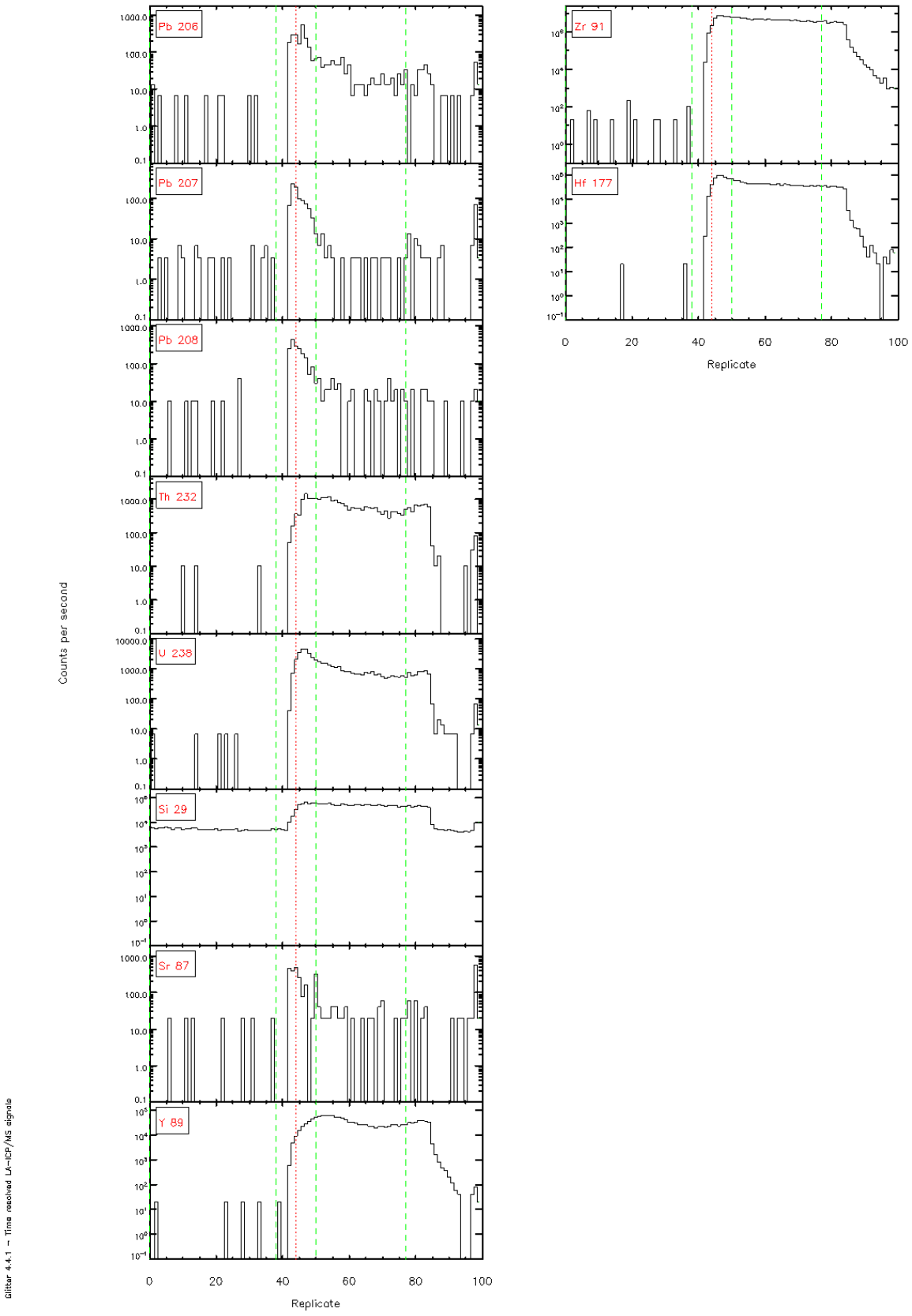
Pb 206
Pb 207
Pb 208
Th 232
U 238
Si 29
Sr 87
Y 89
Zr 91
Hf 177
Counts per second
Replicate
Glitter 4.4.1 – Time resolved LA-ICP/MS signals

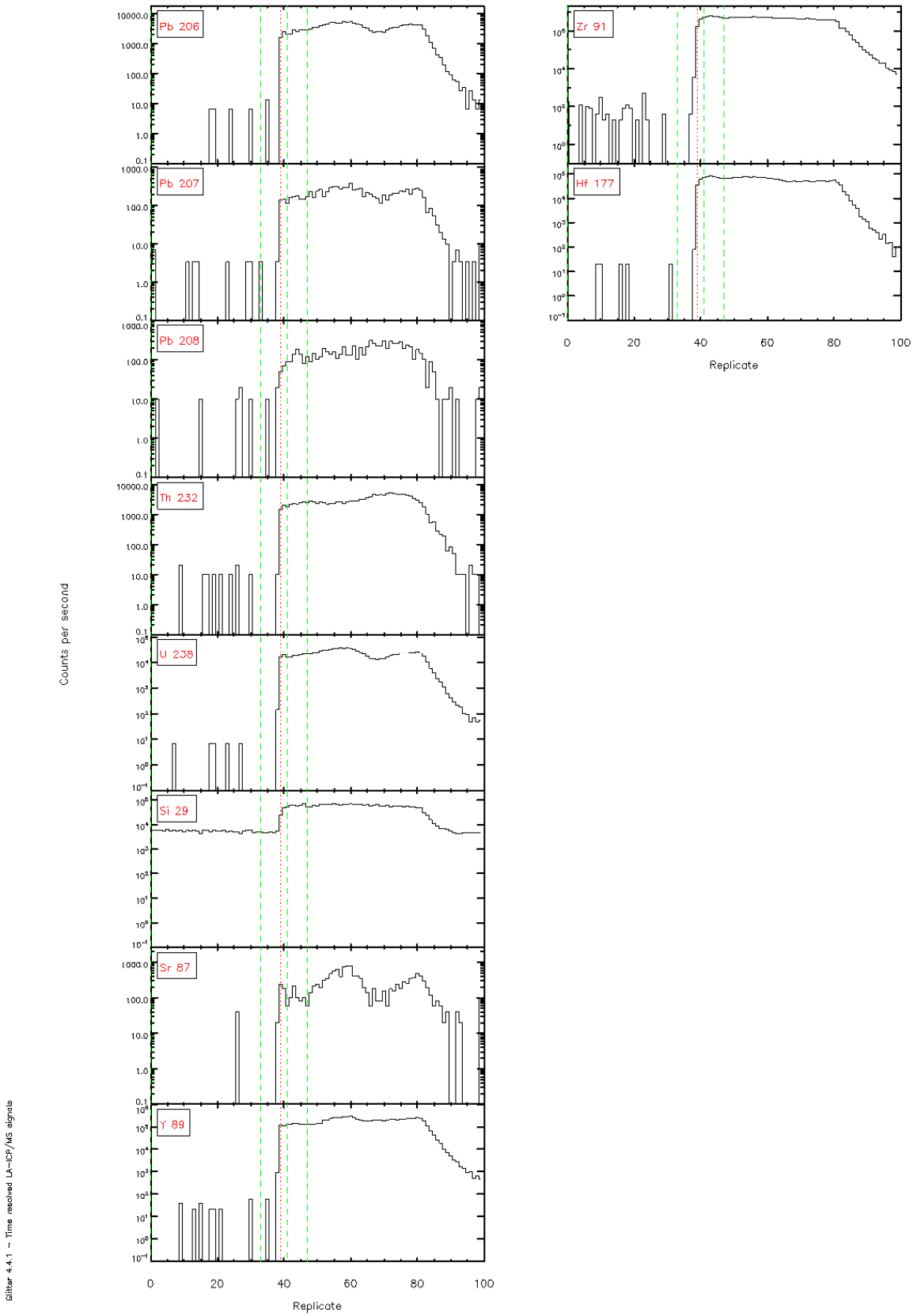
Pb 206
Pb 207
Pb 208
Th 232
U 238
Si 29
Sr 87
Y 89
Zr 91
Hf 177
Counts per second
Replicate
Replicate
Glitter 4.4.1 – Time resolved LA-ICP/MS signals

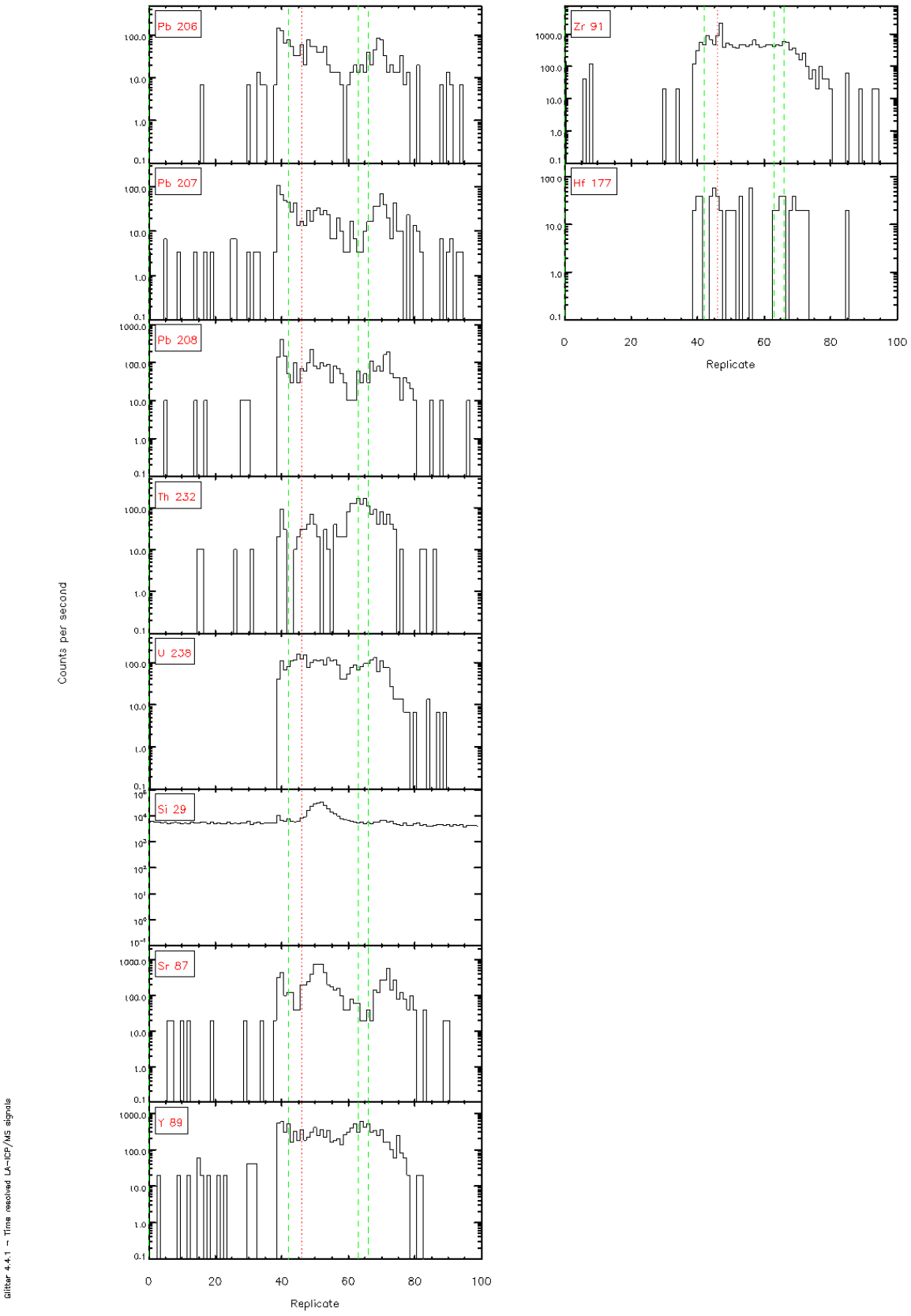
Pb 206
Pb 207
Pb 208
Th 232
U 238
Si 29
Sr 87
Y 89
Zr 91
Hf 177
Counts per second
Replicate
Glitter 4.4.1 – Time resolved LA-ICP/MS signals

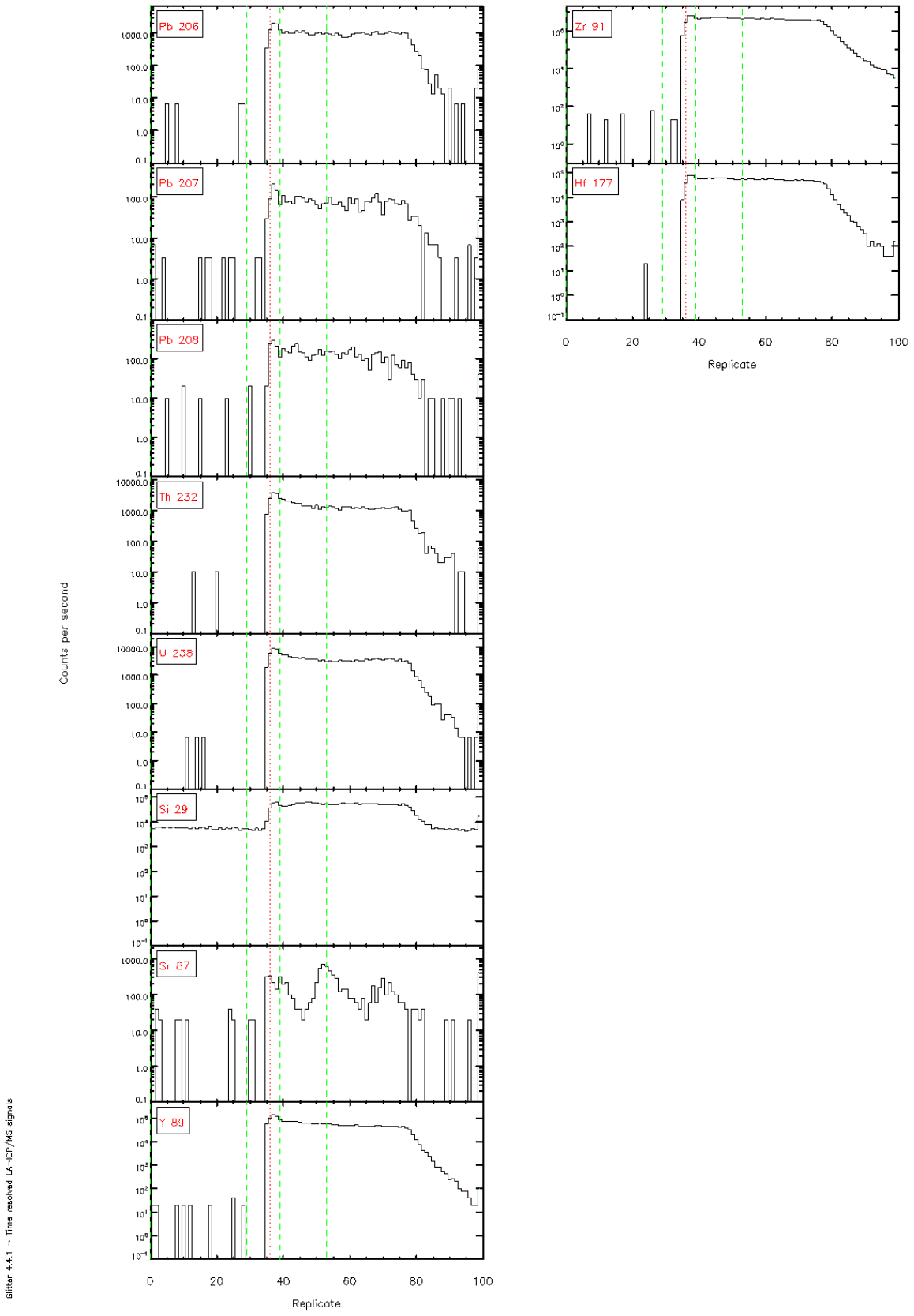
Pb 206
Pb 207
Pb 208
Th 232
U 238
Si 29
Sr 87
Y 89
Zr 91
Hf 177
Counts per second
Replicate
Replicate
Glitter 4.4.1 – Time resolved LA-ICP/MS signals

12 – Turi Formation

1.

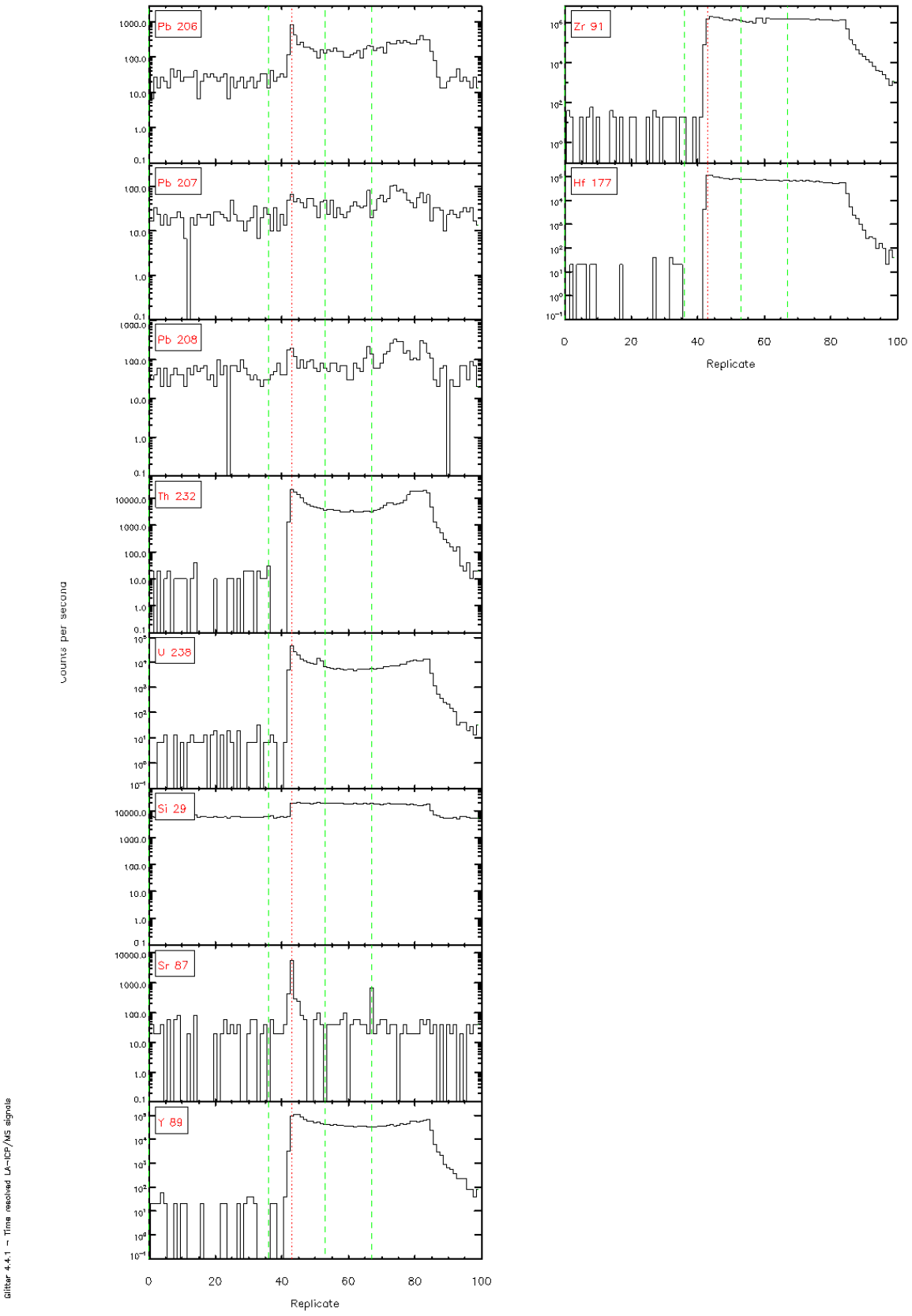

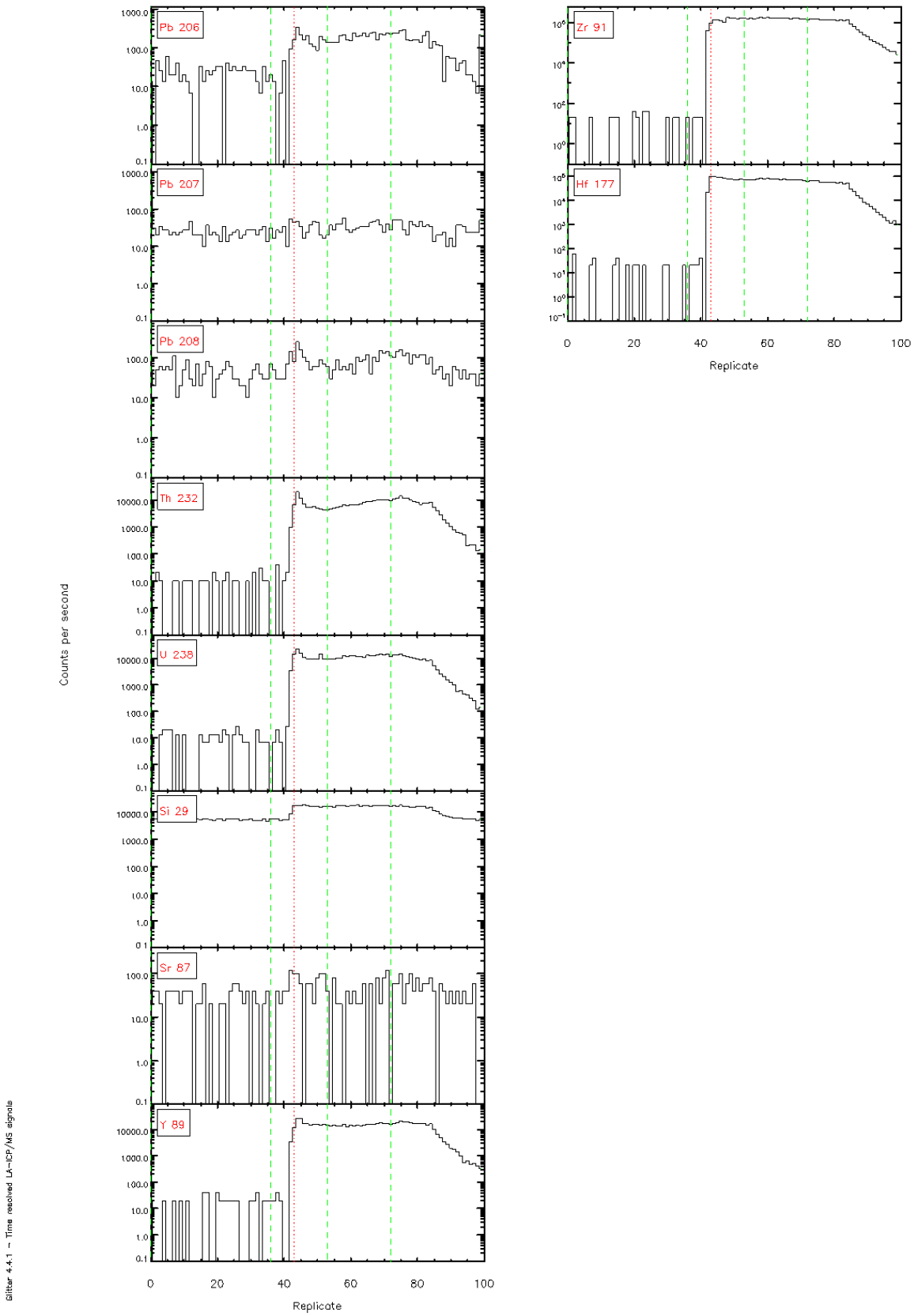
Pb 206
Pb 207
Pb 208
Th 232
U 238
Si 29
Sr 87
Y 89
Zr 91
Hf 177
Counts per second
Replicate
Glitter 4.4.1 – Time resolved LA-ICP/MS signals

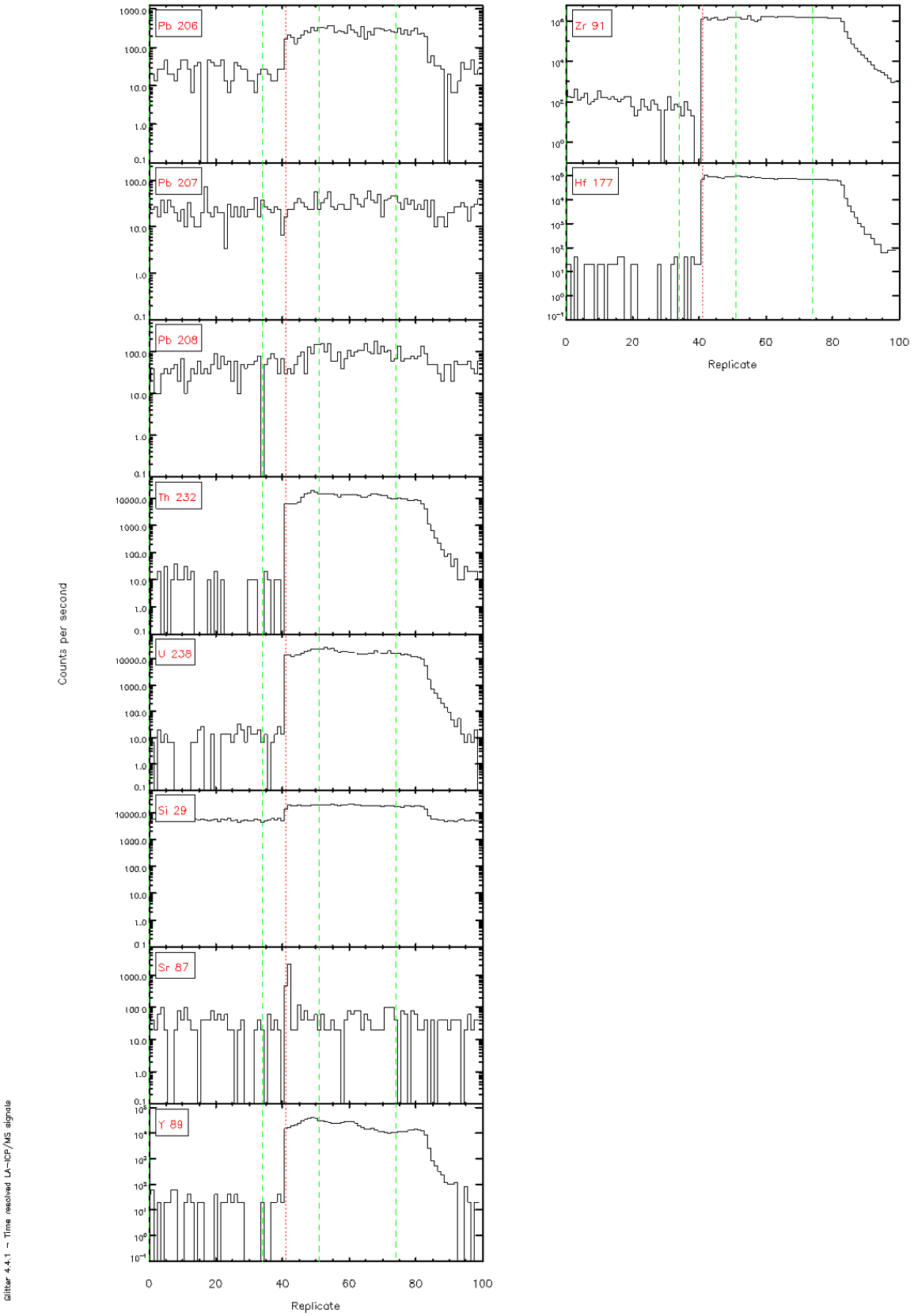
Pb 206
Pb 207
Pb 208
Th 232
U 238
Si 29
Sr 87
Y 89
Zr 91
Hf 177
Counts per second
Replicate
Glitter 4.4.1 – Time resolved LA-ICP/MS signals

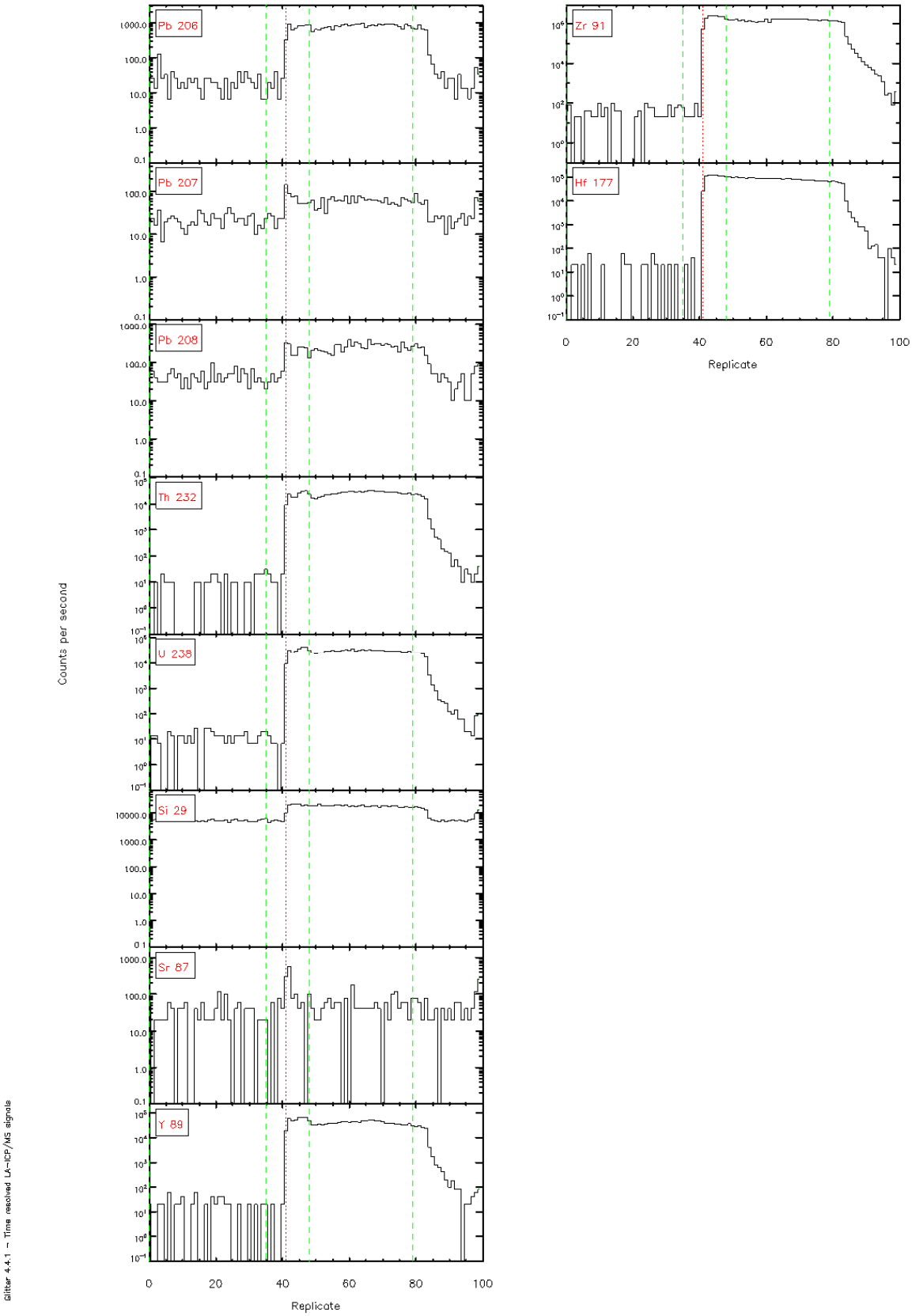
Pb 206
Pb 207
Pb 208
Th 232
U 238
Si 29
Sr 87
Y 89
Zr 91
Hf 177
Counts per second
Replicate
Glitter 4.4.1 – Time resolved LA-ICP/MS signals

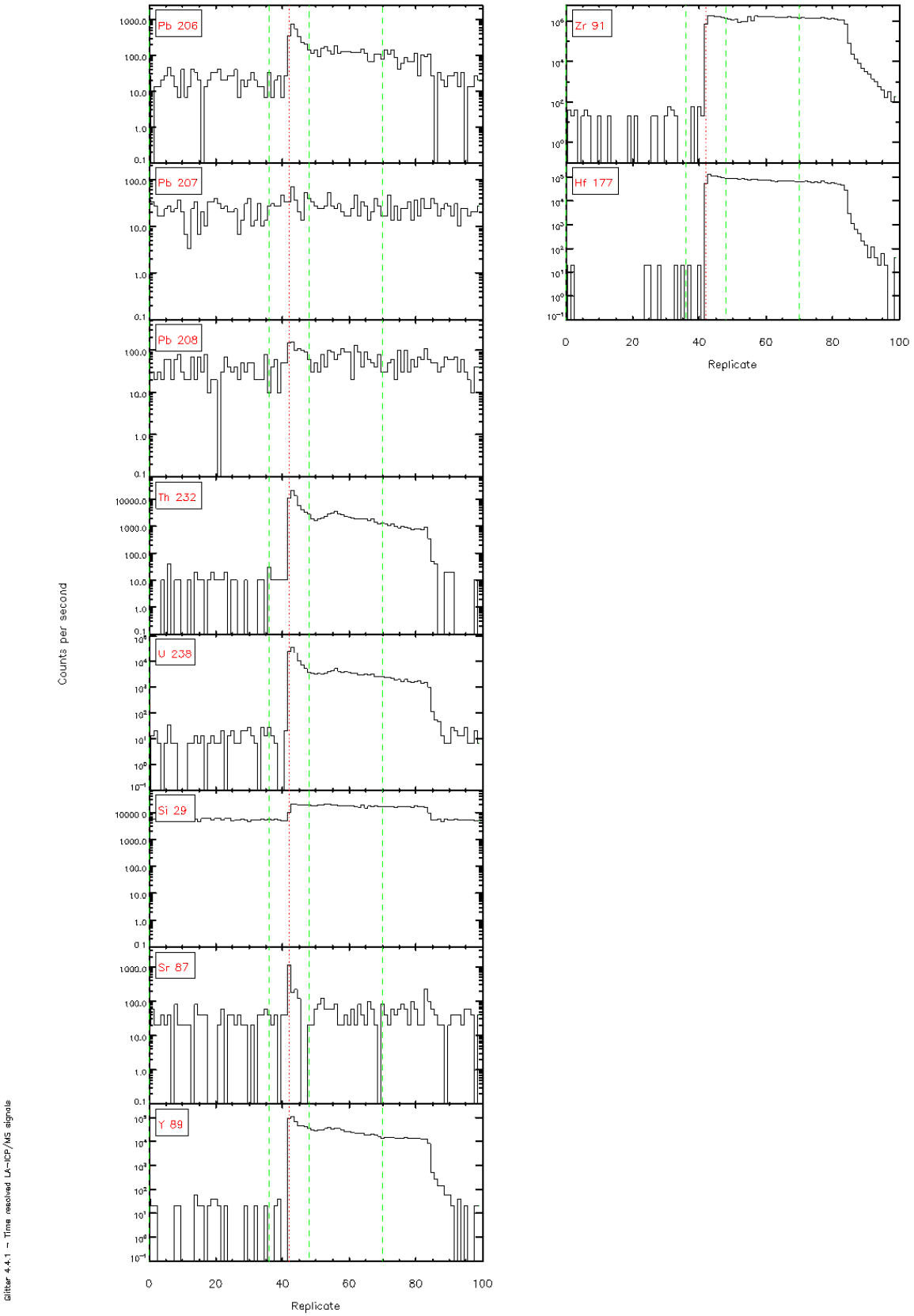
Pb 206
Pb 207
Pb 208
Th 232
U 238
Si 29
Sr 87
Y 89
Zr 91
Hf 177
Counts per second
Replicate
Glitter 4.4.1 – Time resolved LA-ICP/MS signals

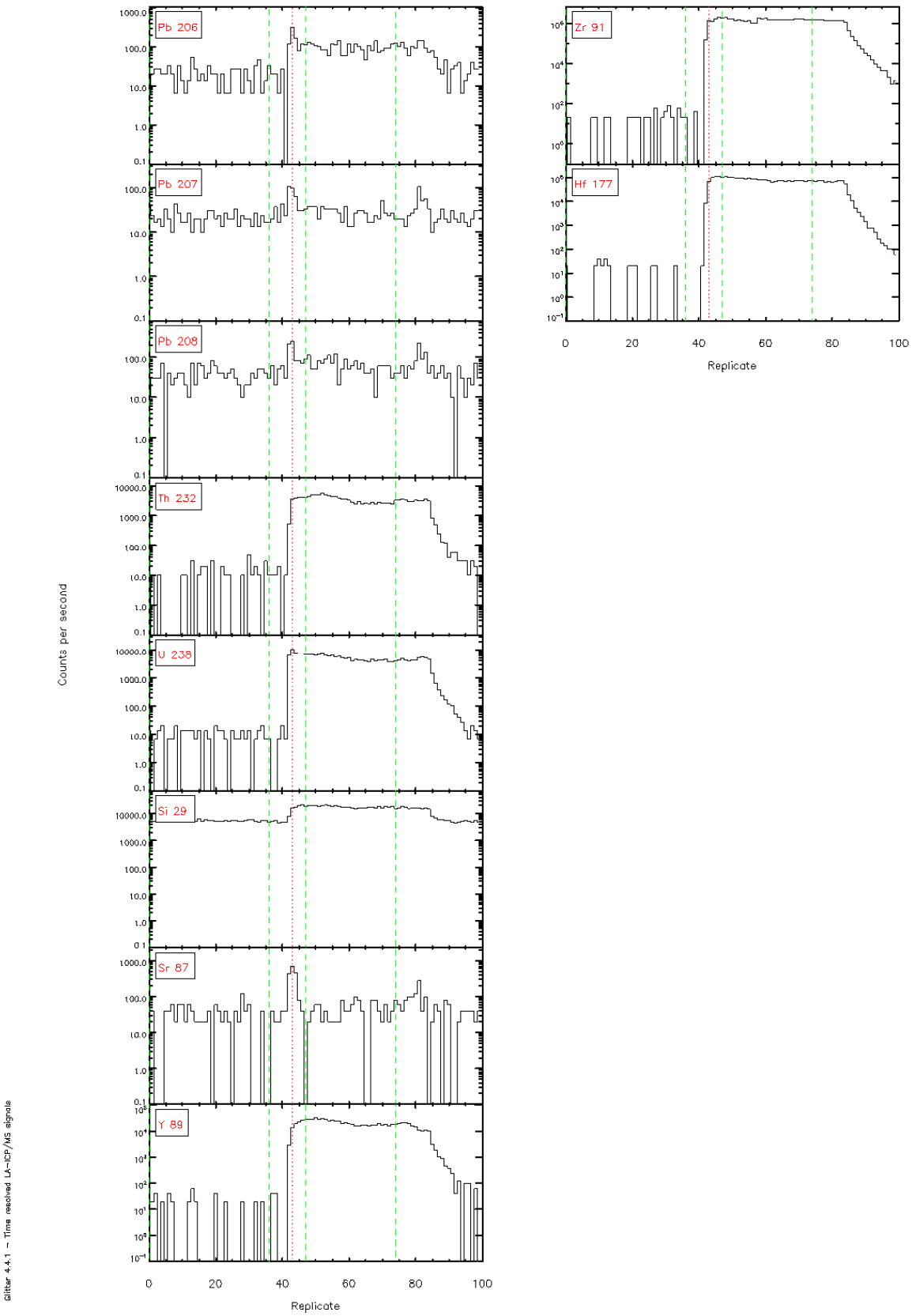
Pb 206
Pb 207
Pb 208
Th 232
U 238
Si 29
Sr 87
Y 89
Zr 91
Hf 177
Counts per second
Replicate
Glitter 4.4.1 – Time resolved LA-ICP/MS signals

9.

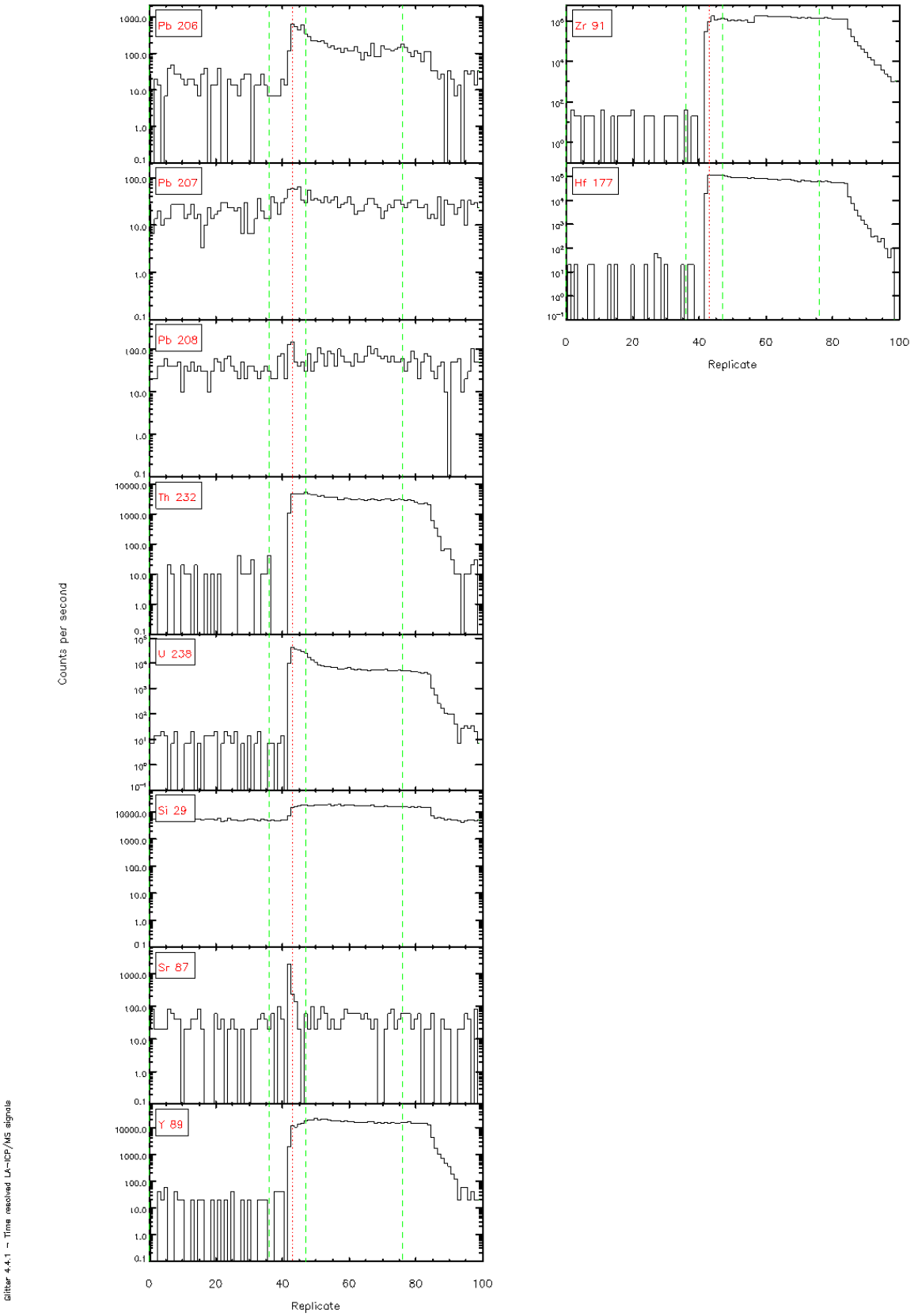
Pb 206
Pb 207
Pb 208
Th 232
U 238
Si 29
Sr 87
Y 89
Zr 91
Hf 177
Counts per second
Replicate
Glitter 4.4.1 – Time resolved LA-ICP/MS signals

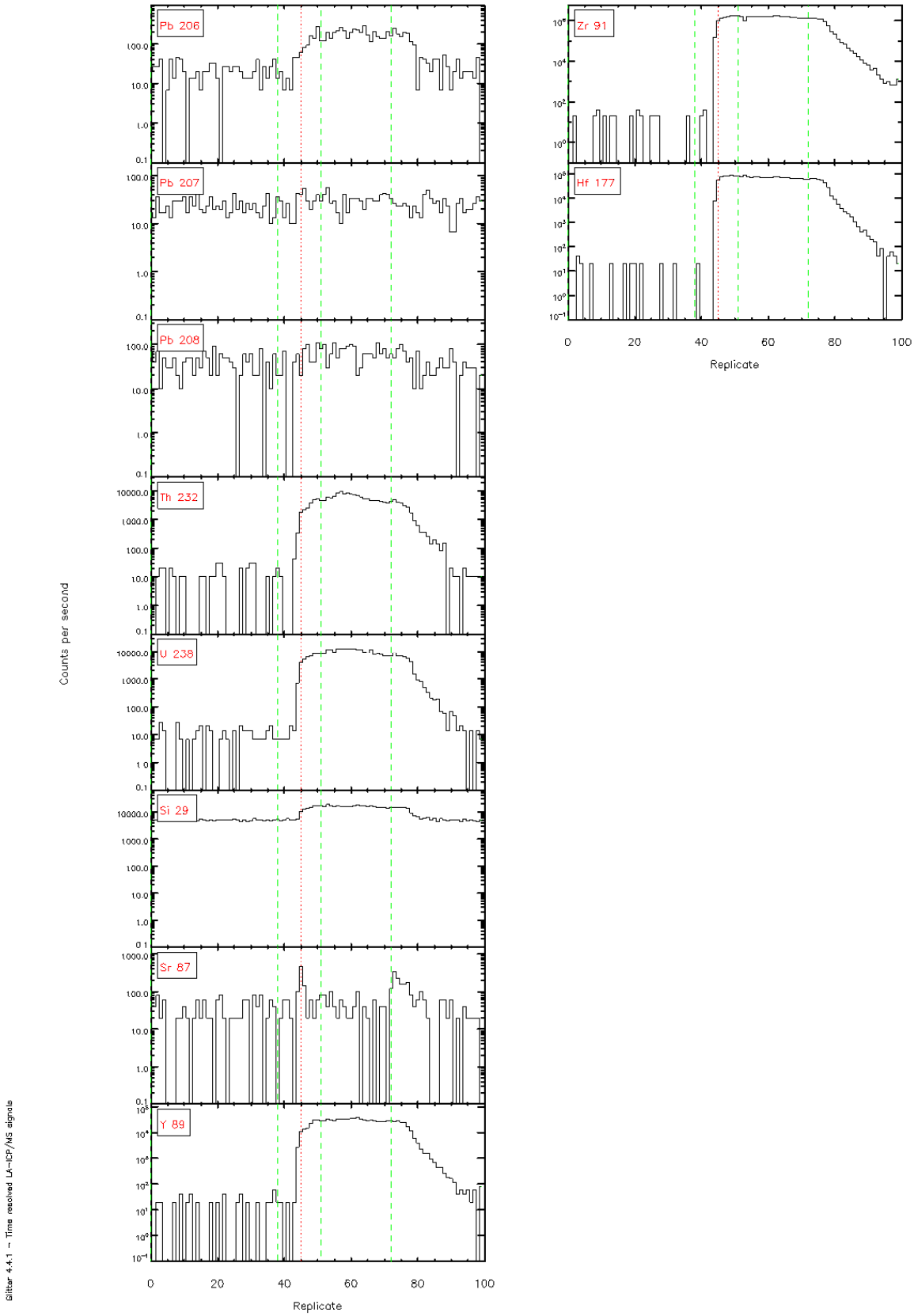
Pb 206
Pb 207
Pb 208
Th 232
U 238
Si 29
Sr 87
Y 89
Zr 91
Hf 177
Counts per second
Replicate
Glitter 4.4.1 – Time resolved LA-ICP/MS signals

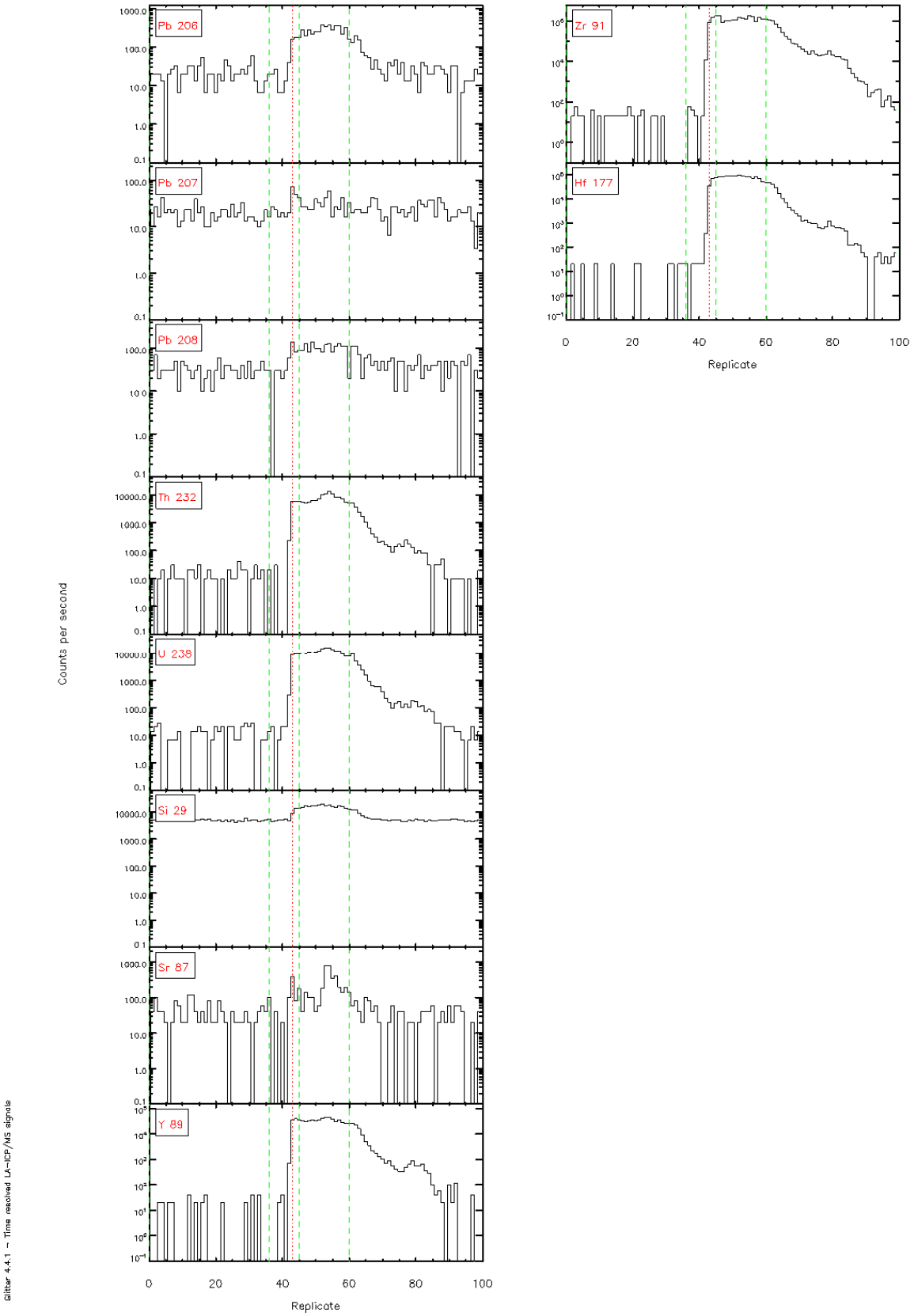
Pb 206
Pb 207
Pb 208
Th 232
U 238
Si 29
Sr 87
Y 89
Zr 91
Hf 177
Counts per second
Replicate
Glitter 4.4.1 – Time resolved LA-ICP/MS signals

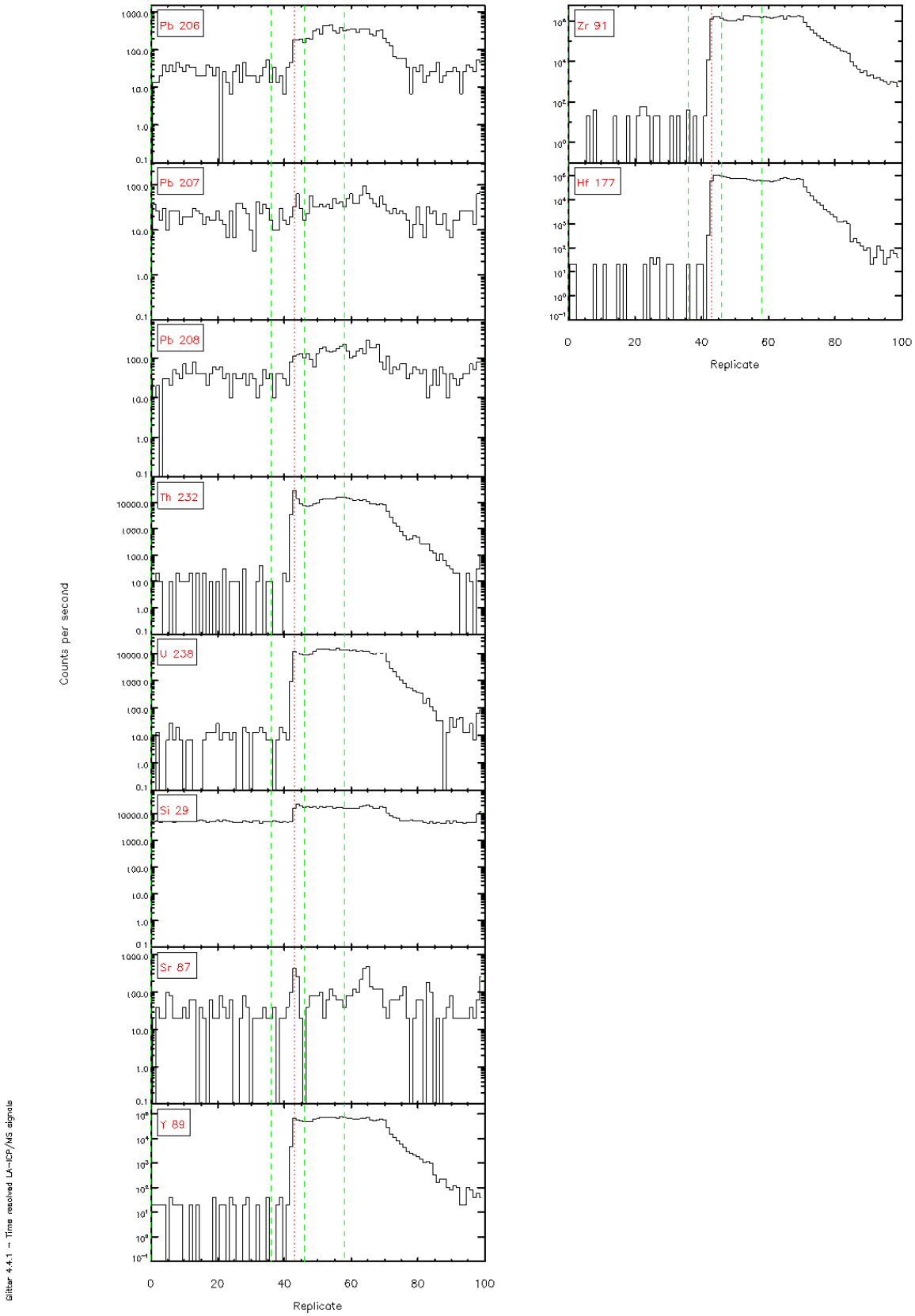
Pb 206
Pb 207
Pb 208
Th 232
U 238
Si 29
Sr 87
Y 89
Zr 91
Hf 177
Counts per second
Replicate
Glitter 4.4.1 – Time resolved LA-ICP/MS signals

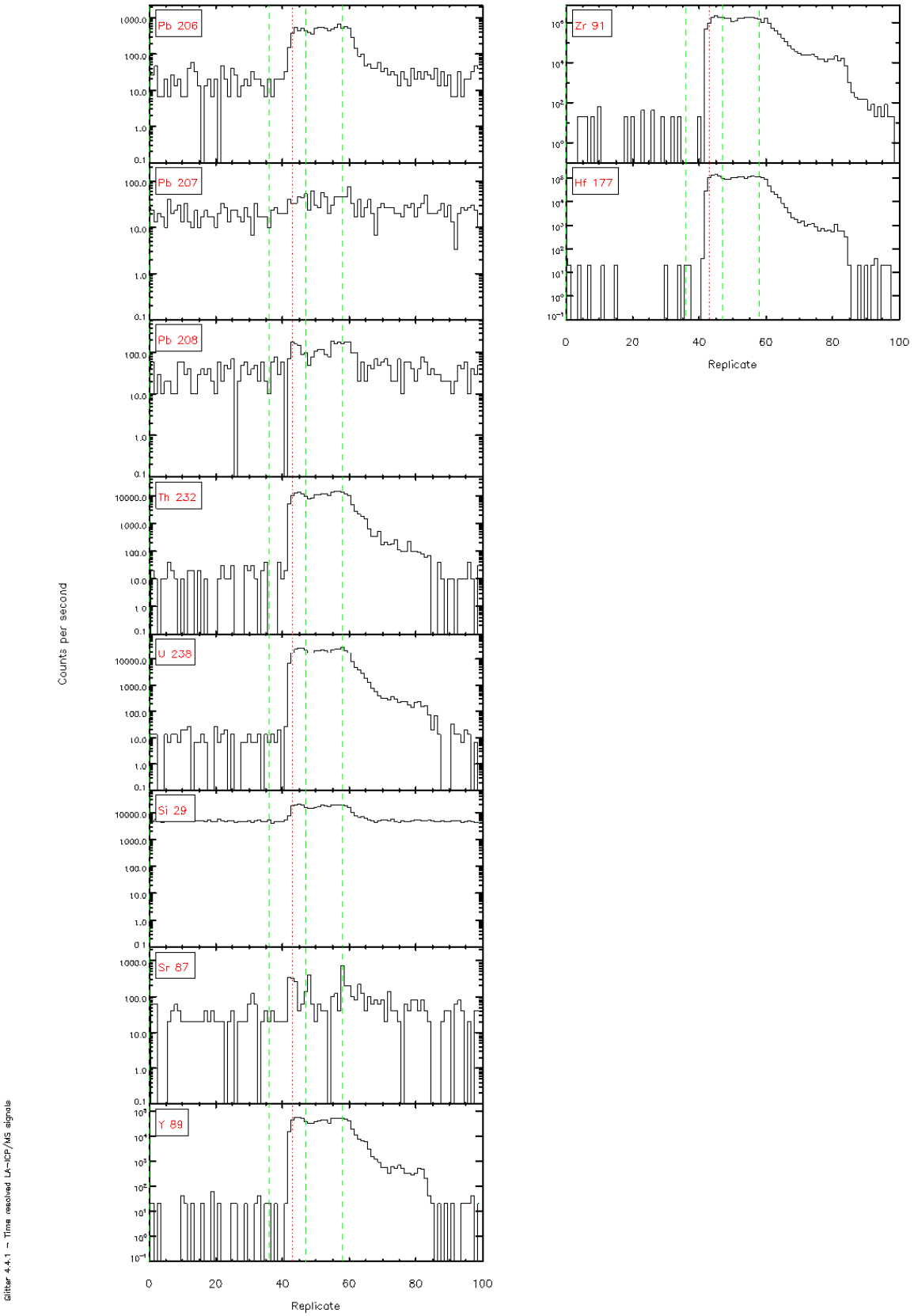
Pb 206
Pb 207
Pb 208
Th 232
U 238
Si 29
Sr 87
Y 89
Zr 91
Hf 177
Counts per second
Replicate
Glitter 4.4.1 – Time resolved LA-ICP/MS signals

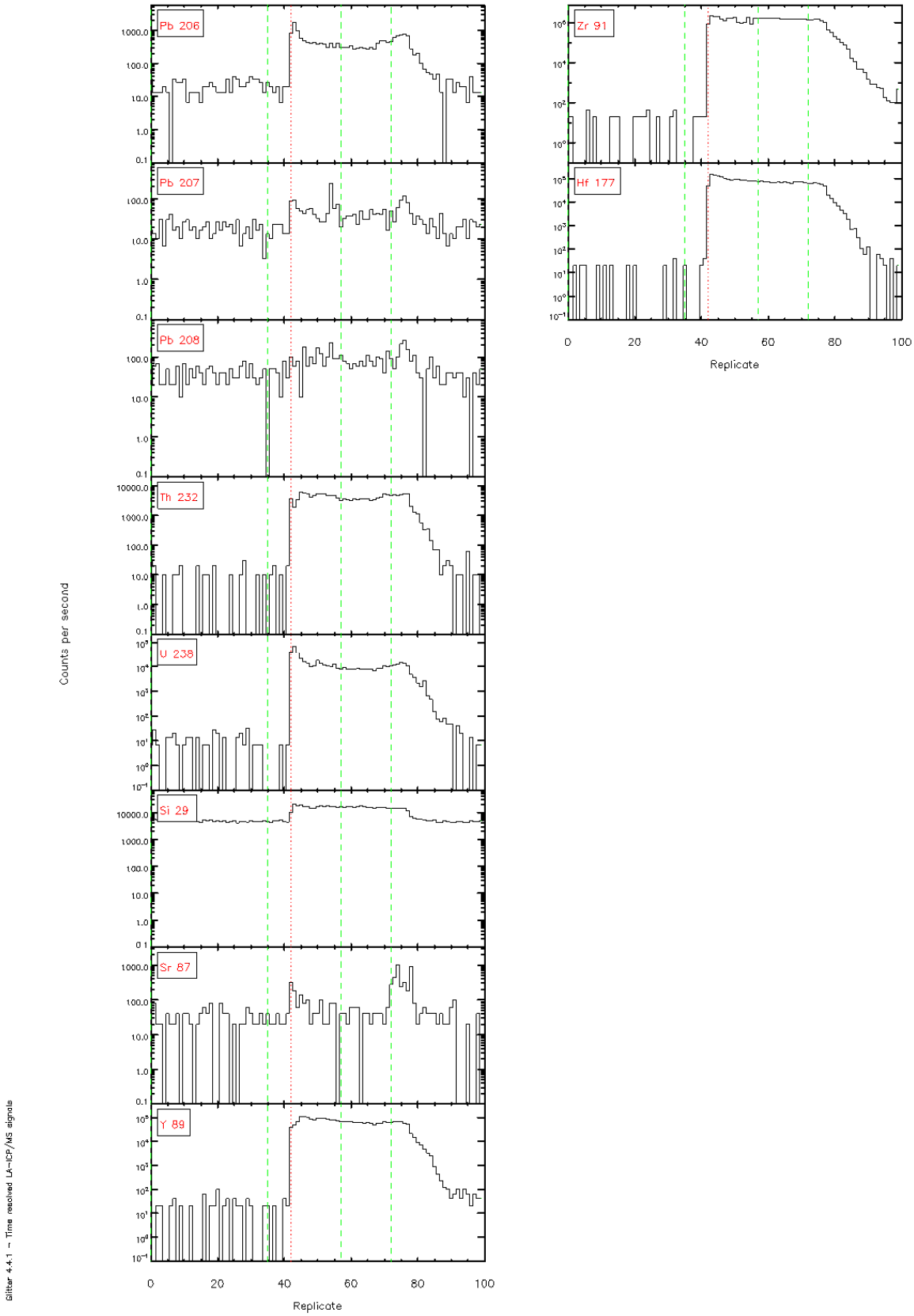
Pb 206
Pb 207
Pb 208
Th 232
U 238
Si 29
Sr 87
Y 89
Zr 91
Hf 177
Counts per second
Replicate
Glitter 4.4.1 – Time resolved LA-ICP/MS signals

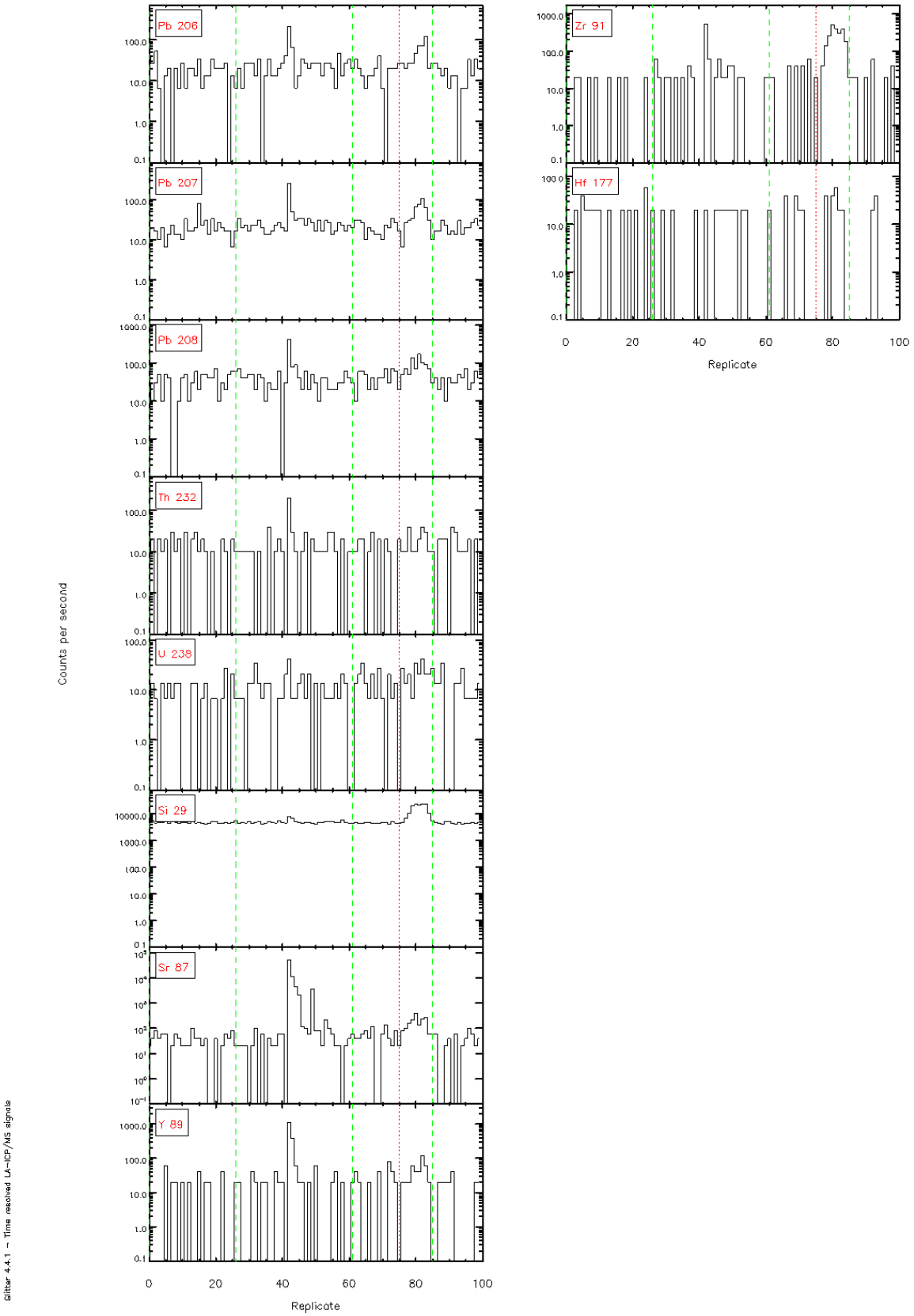
Pb 206
Pb 207
Pb 208
Th 232
U 238
Si 29
Sr 87
Y 89
Zr 91
Hf 177
Counts per second
Replicate
Glitter 4.4.1 – Time resolved LA-ICP/MS signals

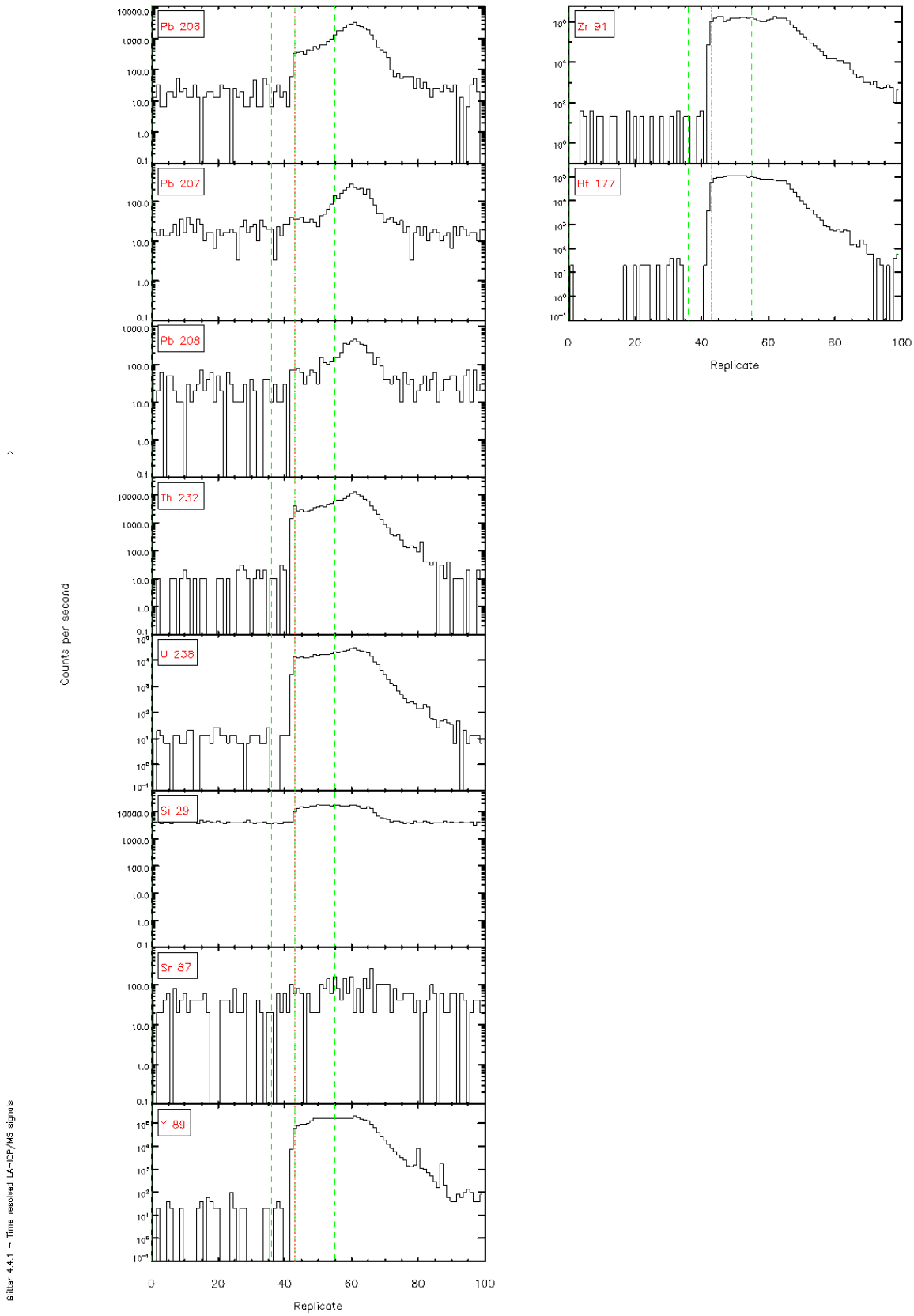
Pb 206
Pb 207
Pb 208
Th 232
U 238
Si 29
Sr 87
Y 89
Zr 91
Hf 177
Counts per second
Replicate
Glitter 4.4.1 - Time resolved LA-ICP/MS signals

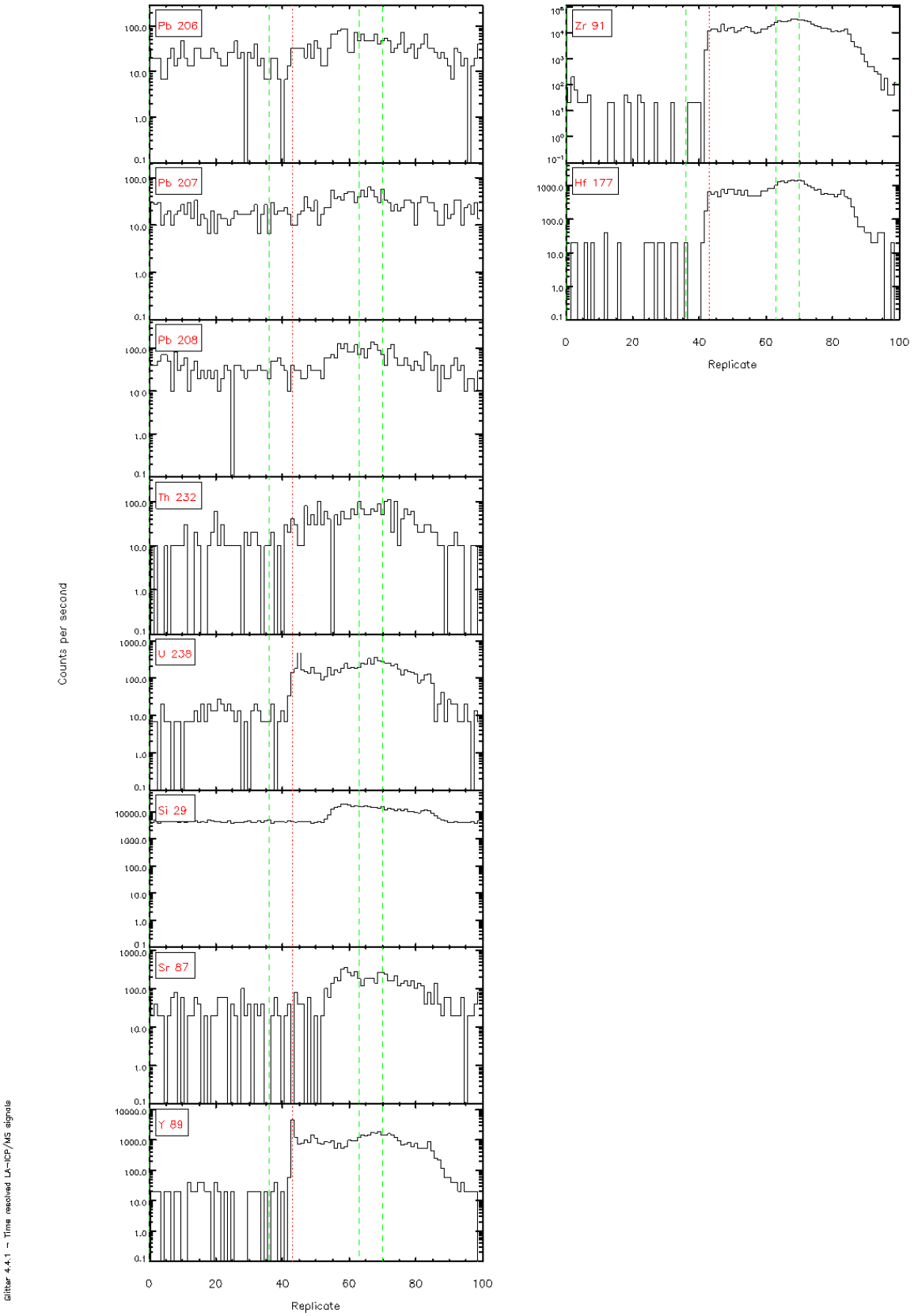
Pb 206
Pb 207
Pb 208
Th 232
U 238
Si 29
Sr 87
Y 89
Zr 91
Hf 177
Counts per second
Replicate
Glitter 4.4.1 – Time resolved LA-ICP/MS signals

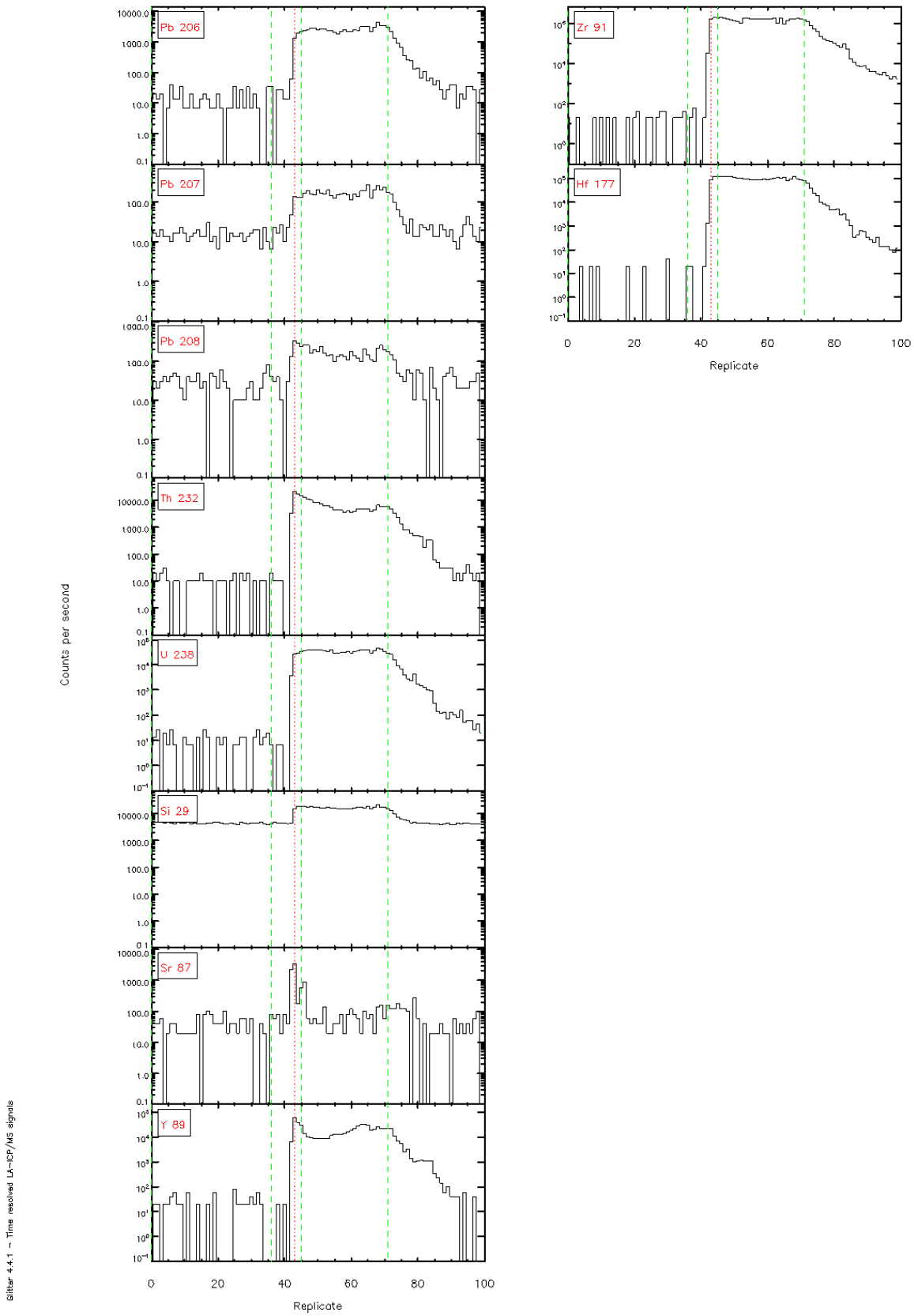
Pb 206
Pb 207
Pb 208
Th 232
U 238
Si 29
Sr 87
Y 89
Zr 91
Hf 177
Counts per second
Replicate
Glitter 4.4.1 – Time resolved LA-ICP/MS signals

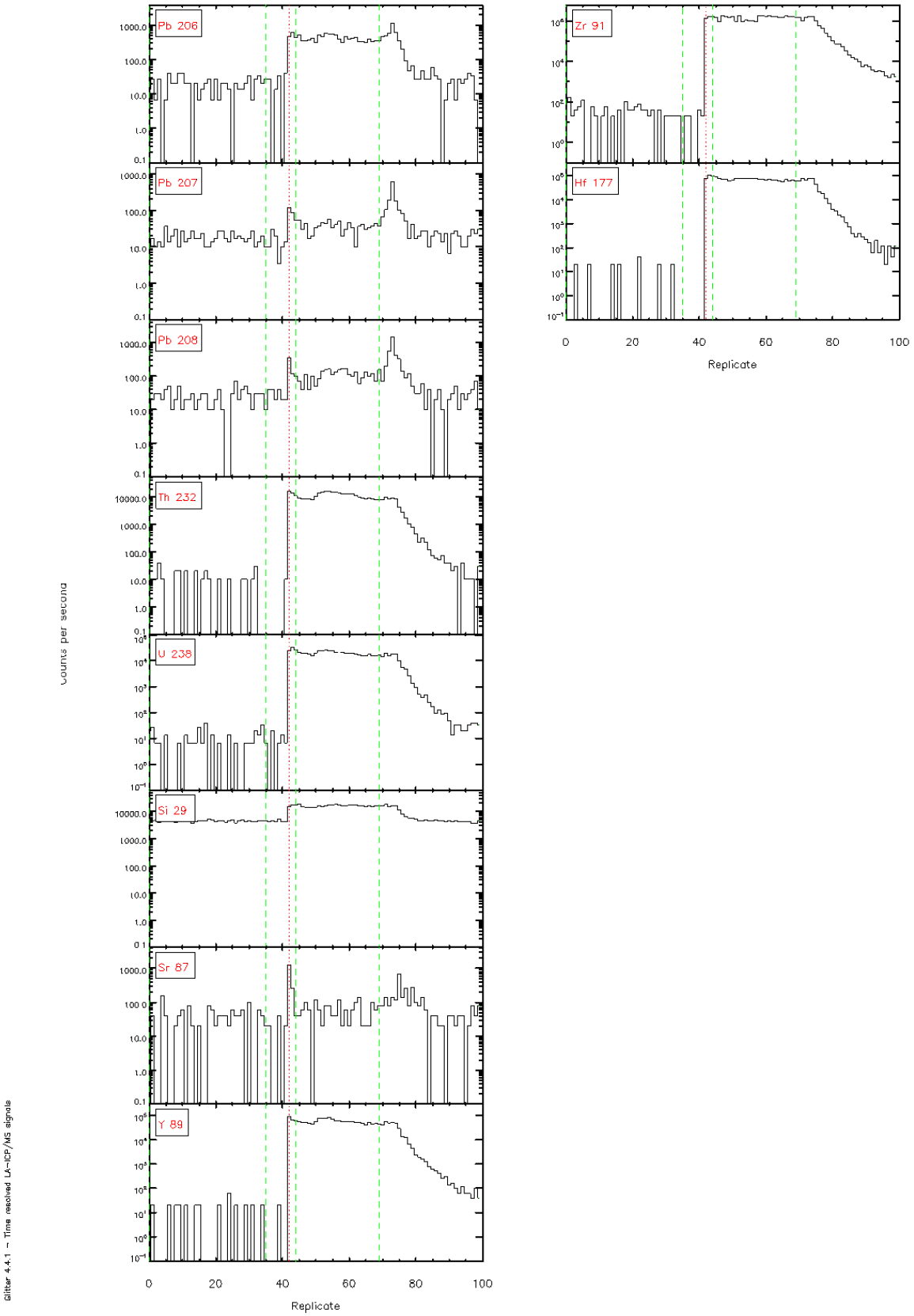
Pb 206
Pb 207
Pb 208
Th 232
U 238
Si 29
Sr 87
Y 89
Zr 91
Hf 177
Counts per second
Replicate
Glitter 4.4.1 – Time resolved LA-ICP/MS signals

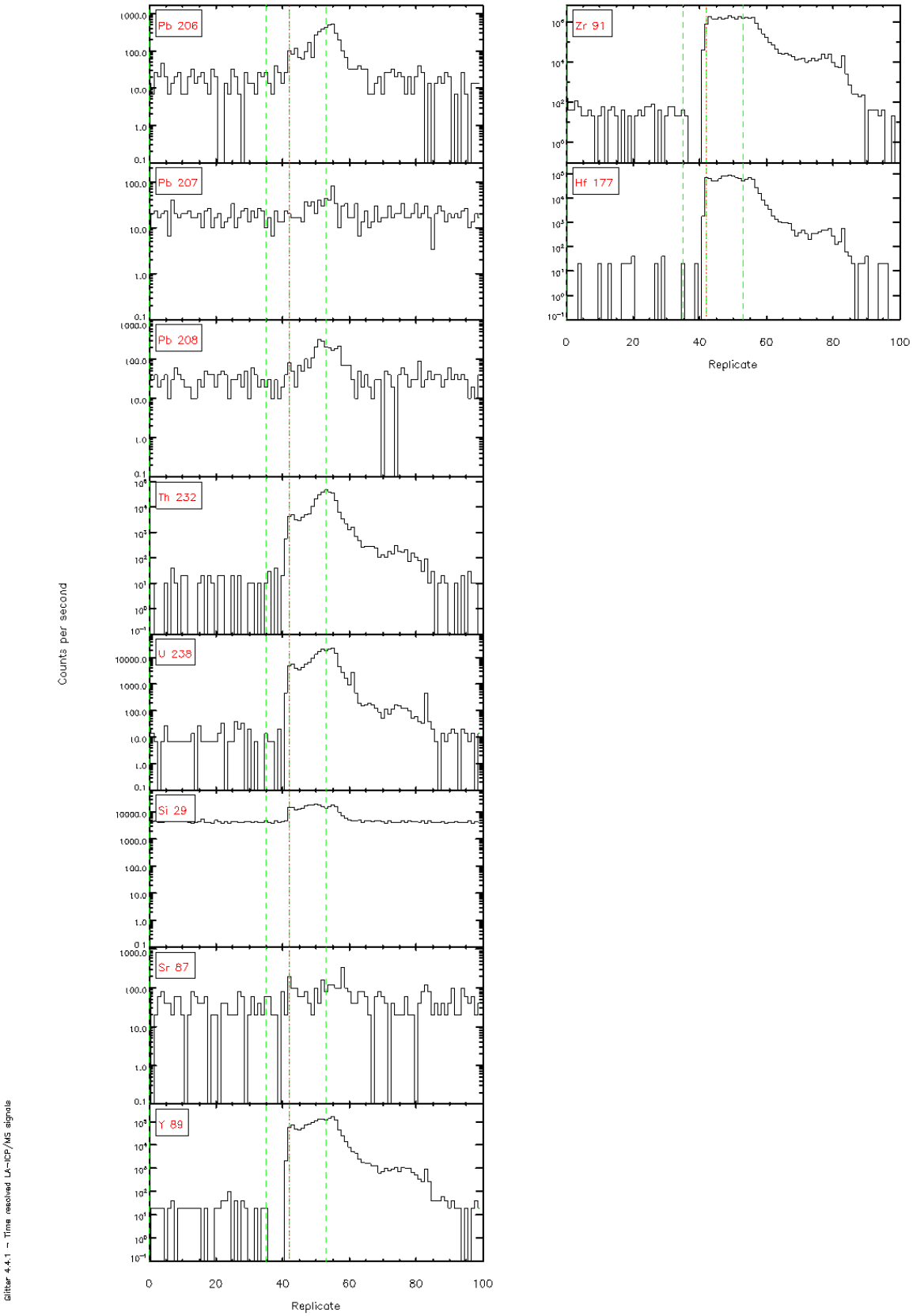
Pb 206
Pb 207
Pb 208
Th 232
U 238
Si 29
Sr 87
Y 89
Zr 91
Hf 177
Counts per second
Replicate
Glitter 4.4.1 – Time resolved LA-ICP/MS signals

15 – Otaihanga Outlier

1.

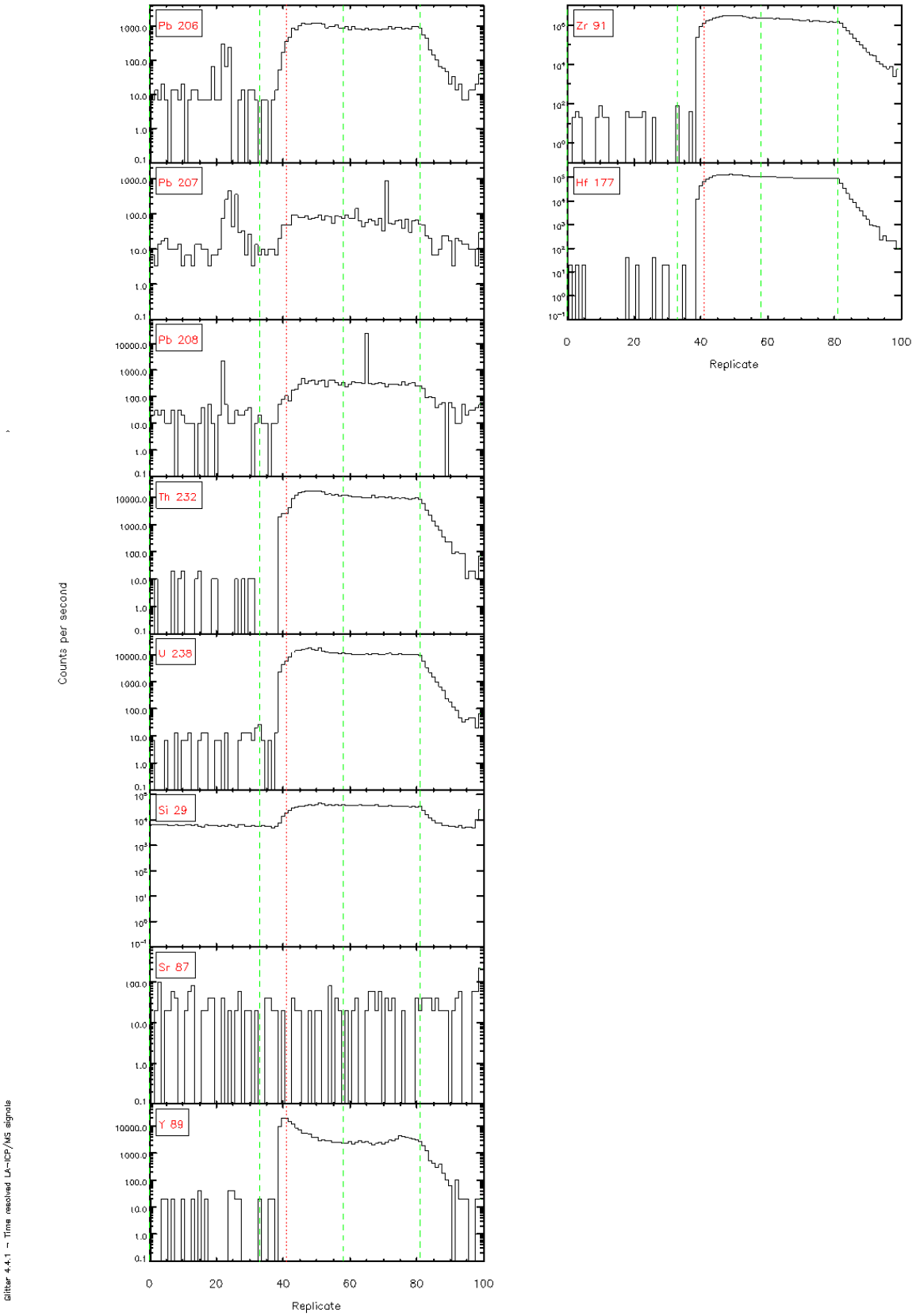

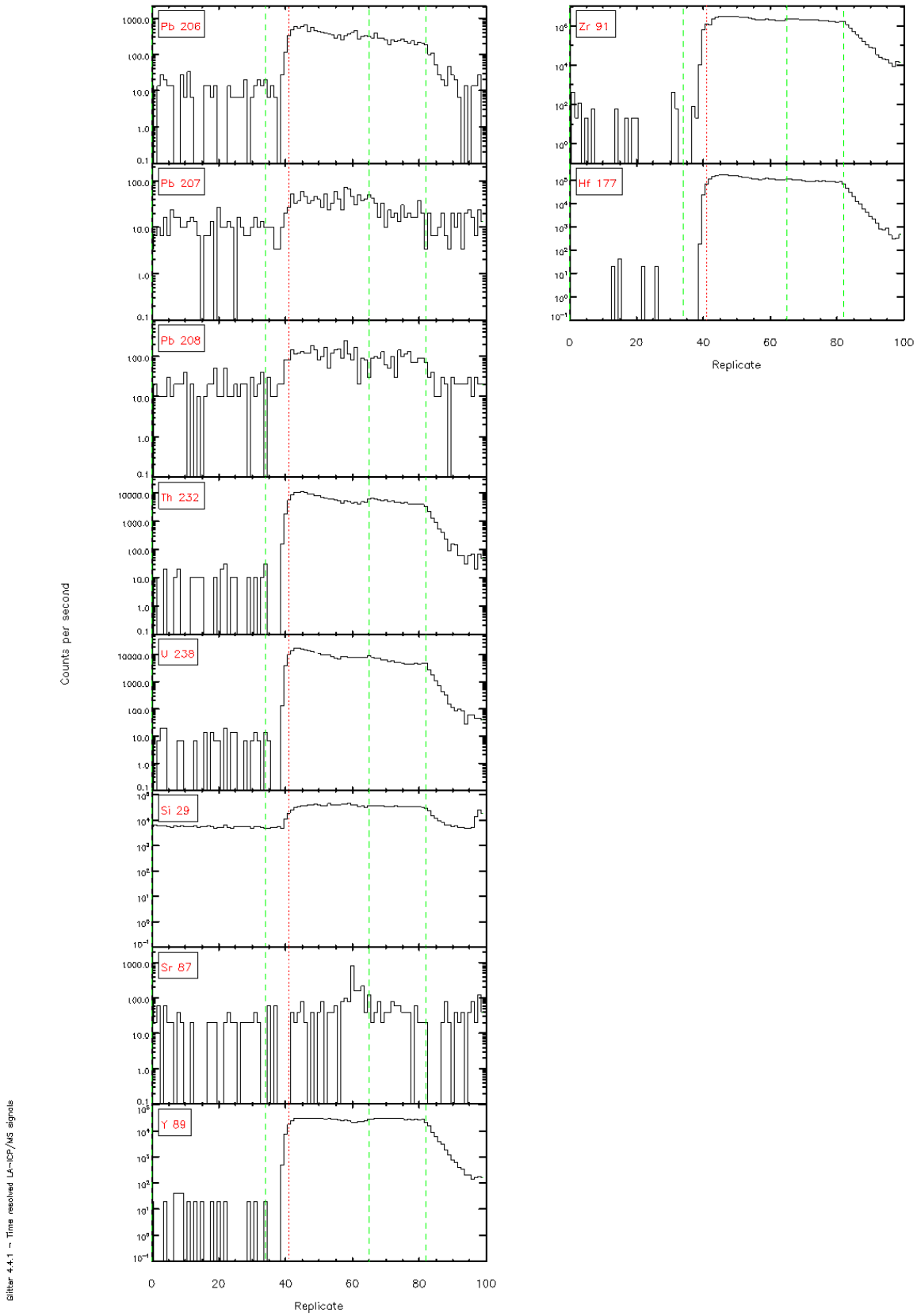
Pb 206
Pb 207
Pb 208
Th 232
U 238
Si 29
Sr 87
Y 89
Zr 91
Hf 177
Counts per second
Replicate
Glitter 4.4.1 - Time resolved LA-ICP/MS signals

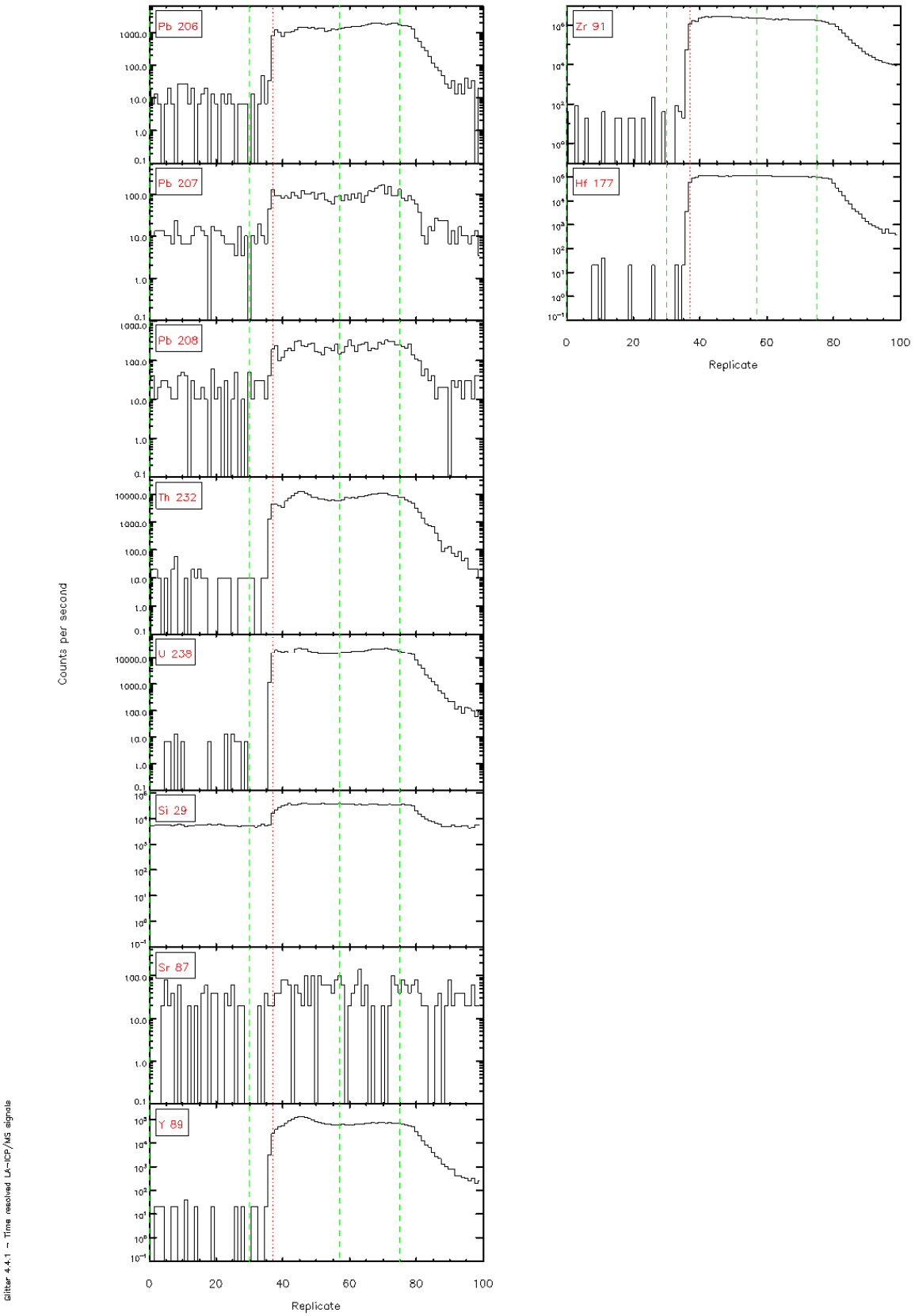
Pb 206
Pb 207
Pb 208
Th 232
U 238
Si 29
Sr 87
Y 89
Zr 91
Hf 177
Counts per second
Replicate
Glitter 4.4.1 – Time resolved LA-ICP/MS signals

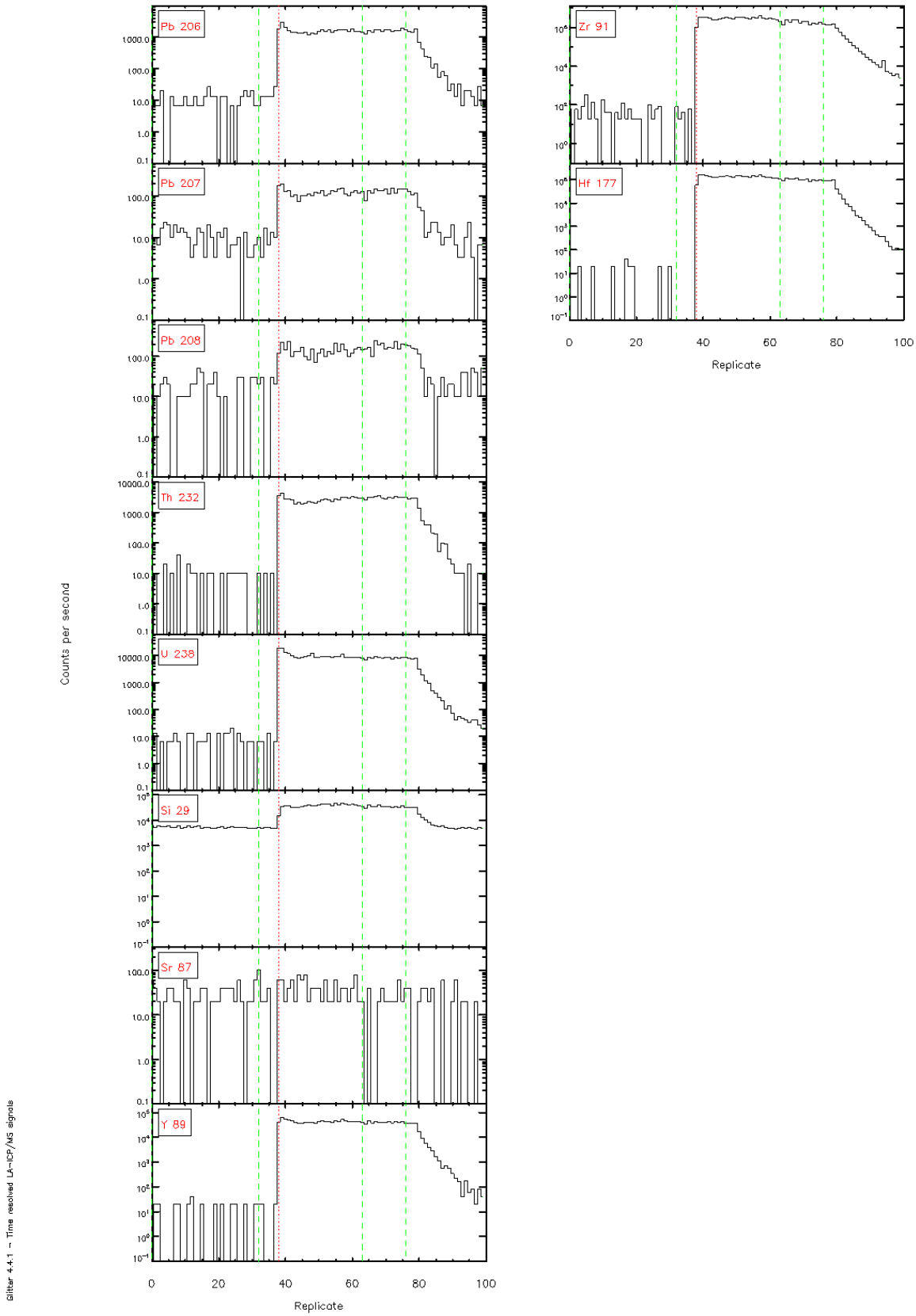
Pb 206
Pb 207
Pb 208
Th 232
U 238
Si 29
Sr 87
Y 89
Zr 91
Hf 177
Counts per second
Replicate
Glitter 4.4.1 - Time resolved LA-ICP/MS signals

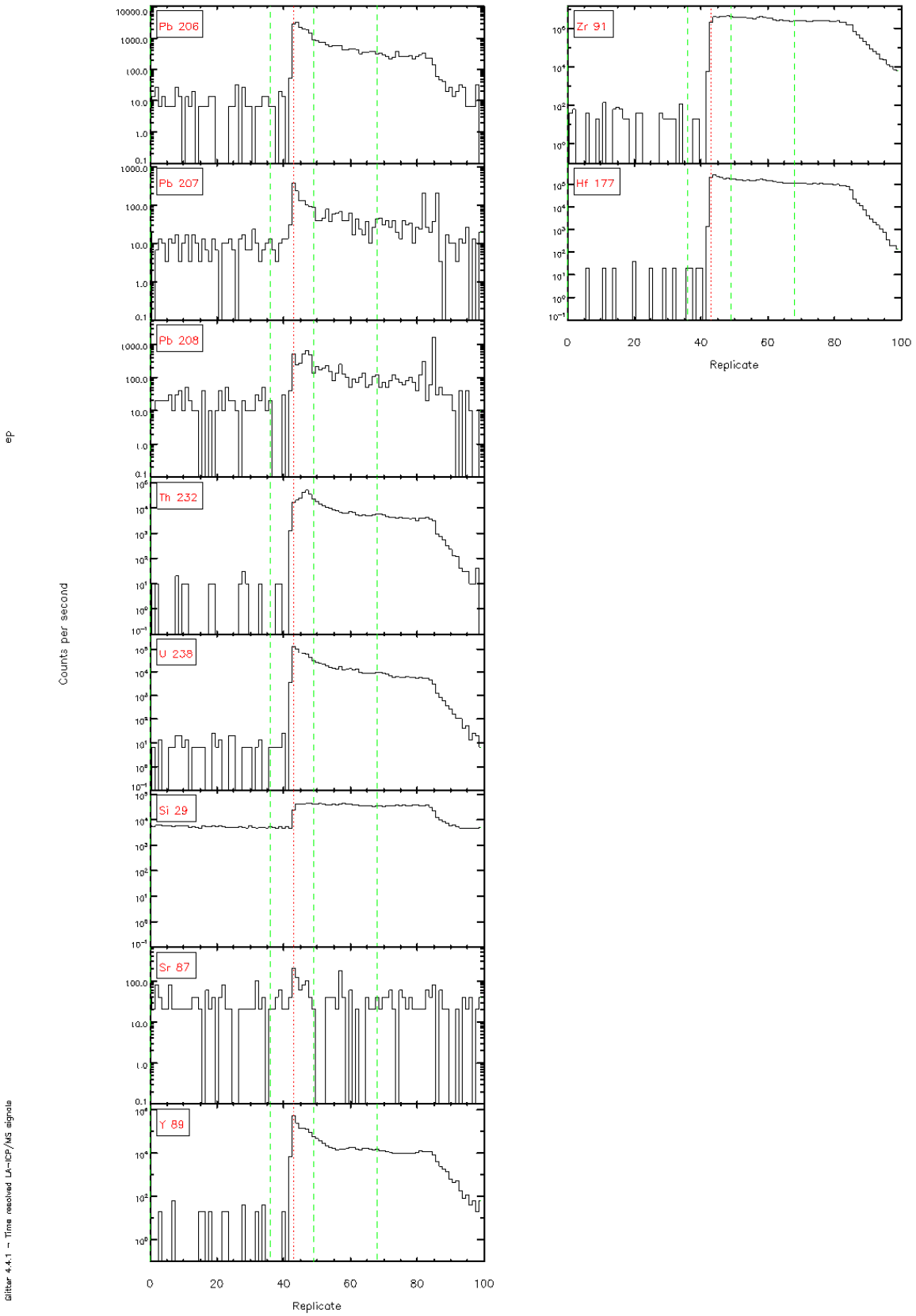
Pb 206
Pb 207
Pb 208
Th 232
U 238
Si 29
Sr 87
Y 89
Zr 91
Hf 177
Counts per second
Replicate
0
20
40
60
80
100
ep
Glitter 4.4.1 - Time resolved LA-ICP/MS signals

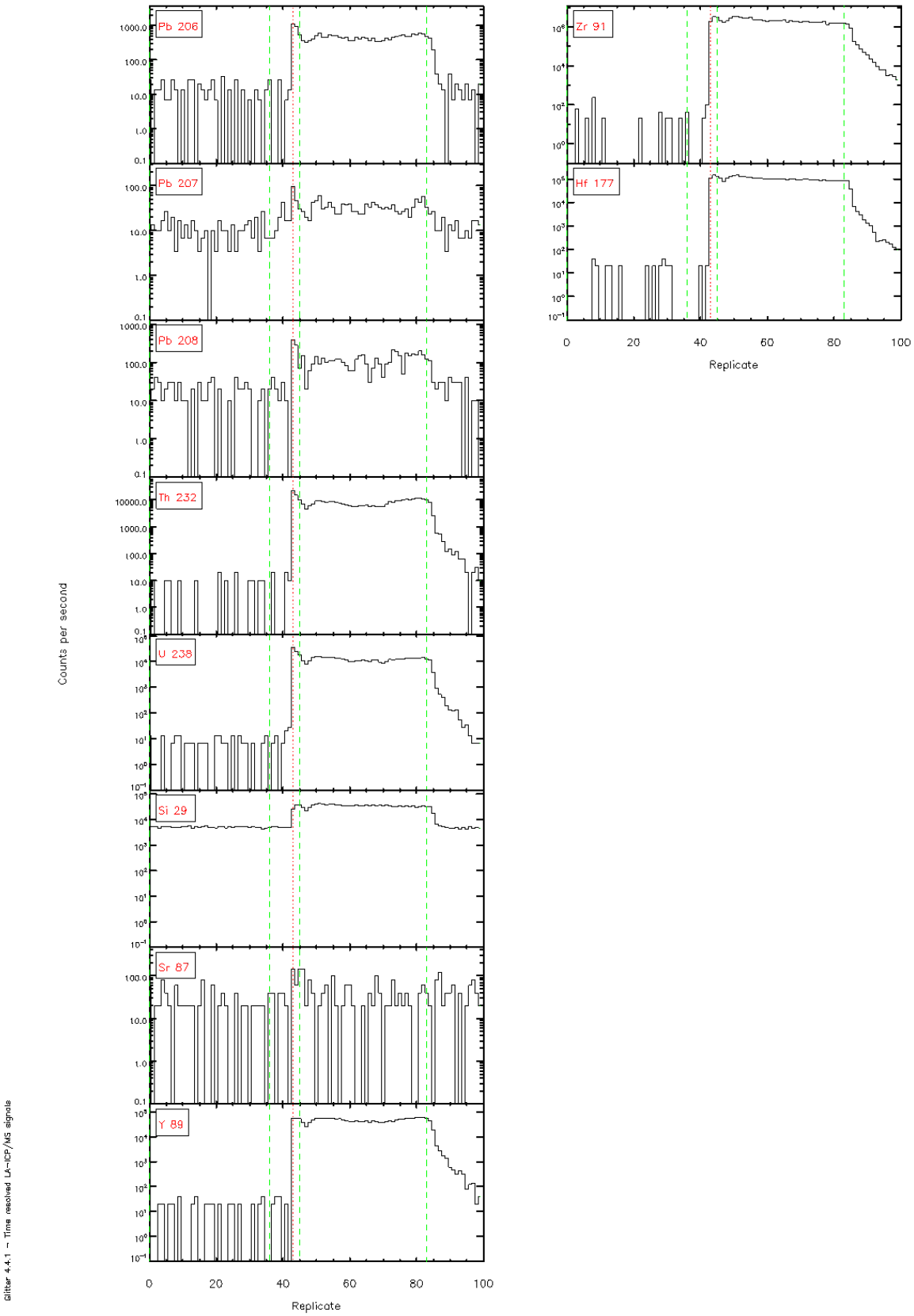
Pb 206
Pb 207
Pb 208
Th 232
U 238
Si 29
Sr 87
Y 89
Zr 91
Hf 177
Counts per second
Replicate
Glitter 4.4.1 - Time resolved LA-ICP/MS signals

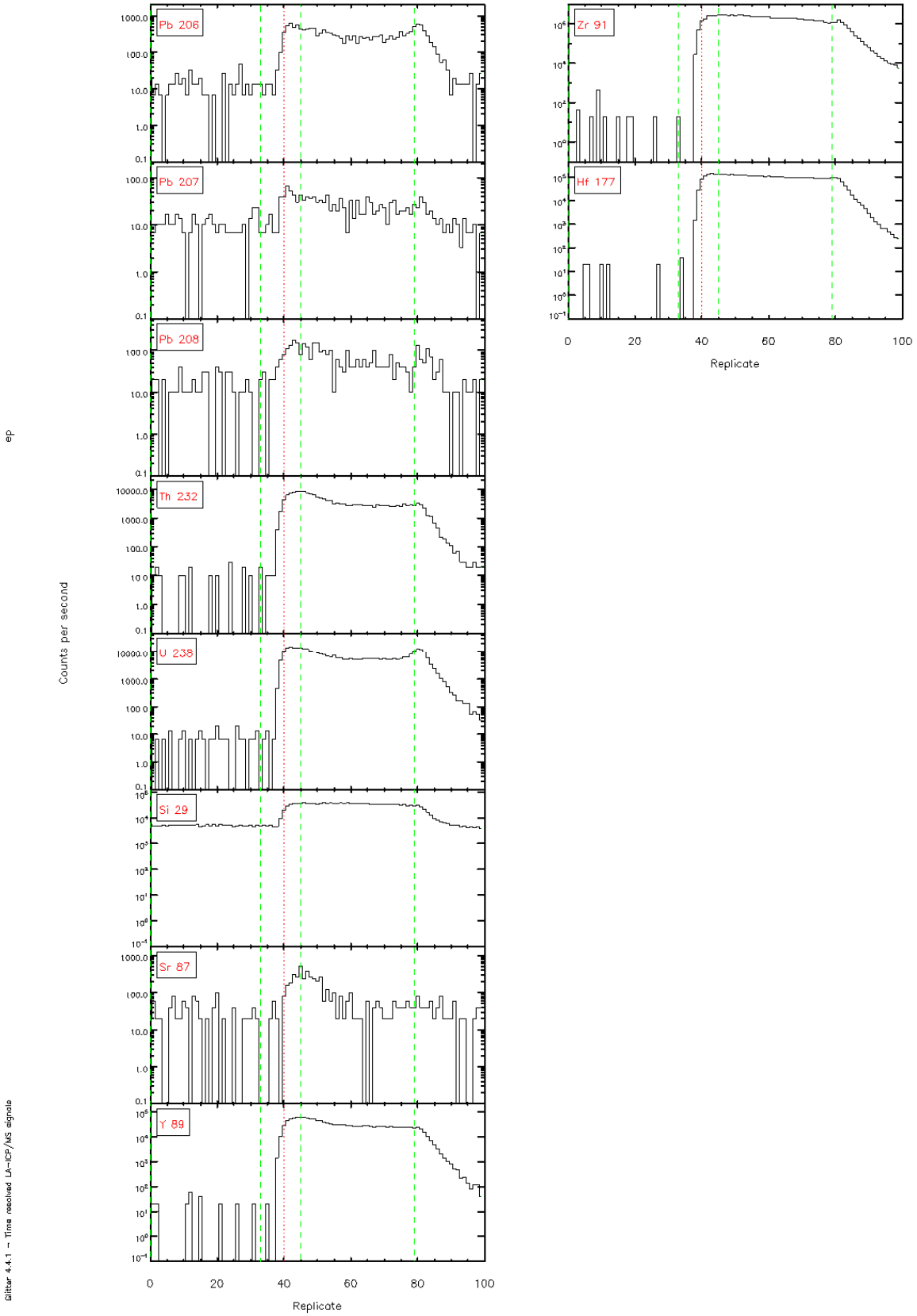
Pb 206
Pb 207
Pb 208
Th 232
U 238
Si 29
Sr 87
Y 89
Zr 91
Hf 177
Counts per second
Replicate
Glitter 4.4.1 - Time resolved LA-ICP/MS signals

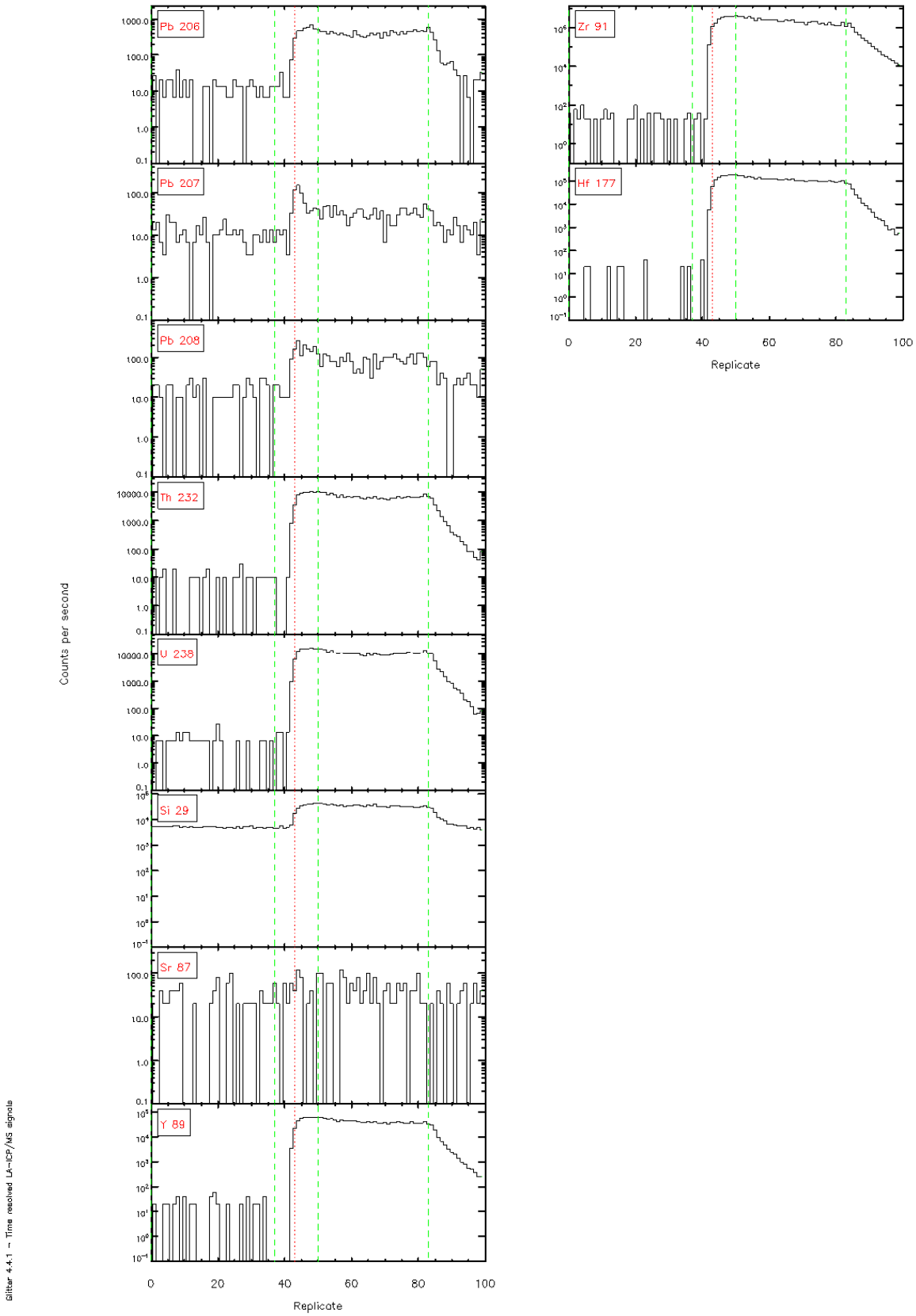
Pb 206
Pb 207
Pb 208
Th 232
U 238
Si 29
Sr 87
Y 89
Zr 91
Hf 177
Counts per second
Replicate
Glitter 4.4.1 - Time resolved LA-ICP/MS signals

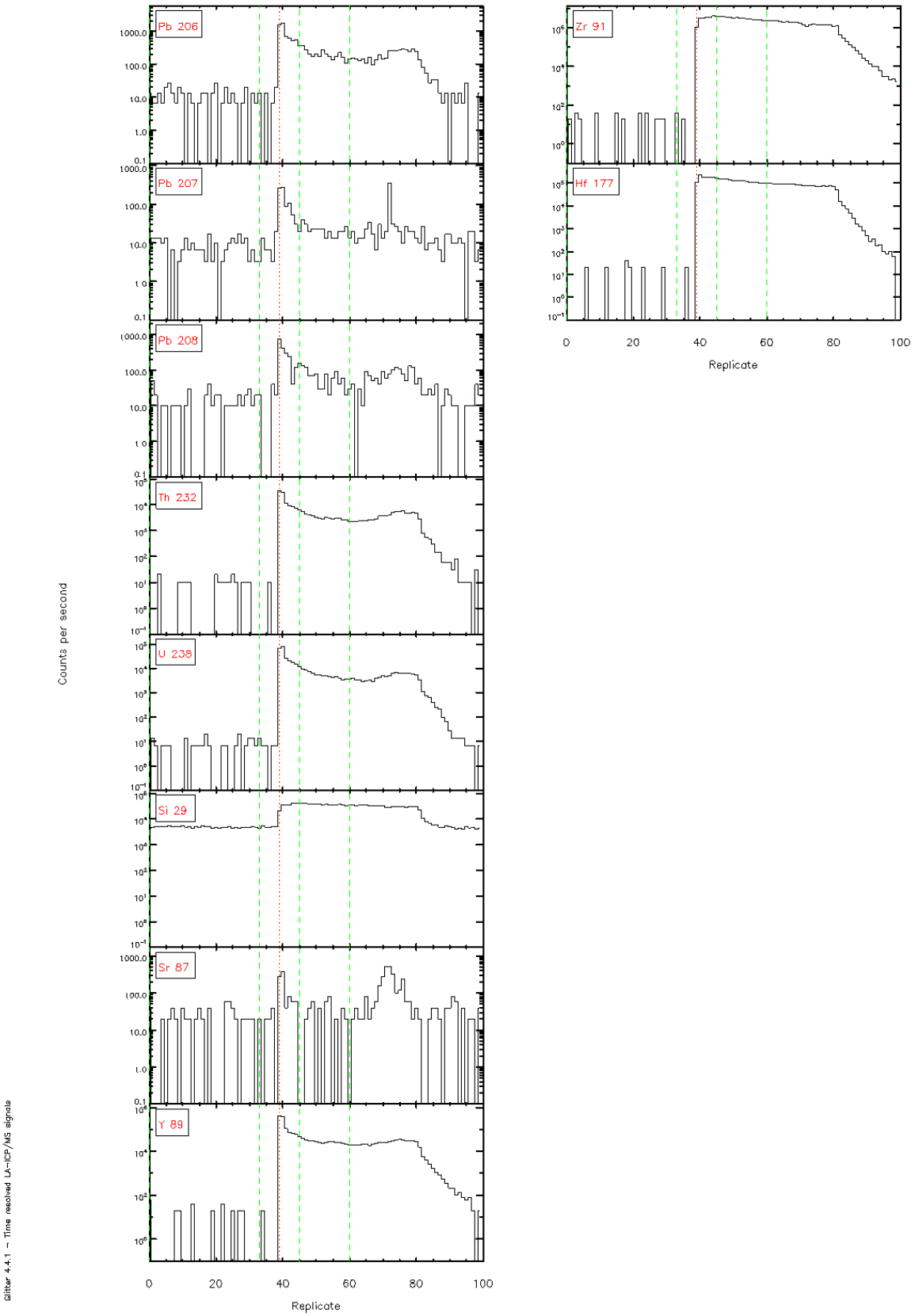
Pb 206
Pb 207
Pb 208
Th 232
U 238
Si 29
Sr 87
Y 89
Zr 91
Hf 177
Counts per second
Replicate
Glitter 4.4.1 - Time resolved LA-ICP/MS signals

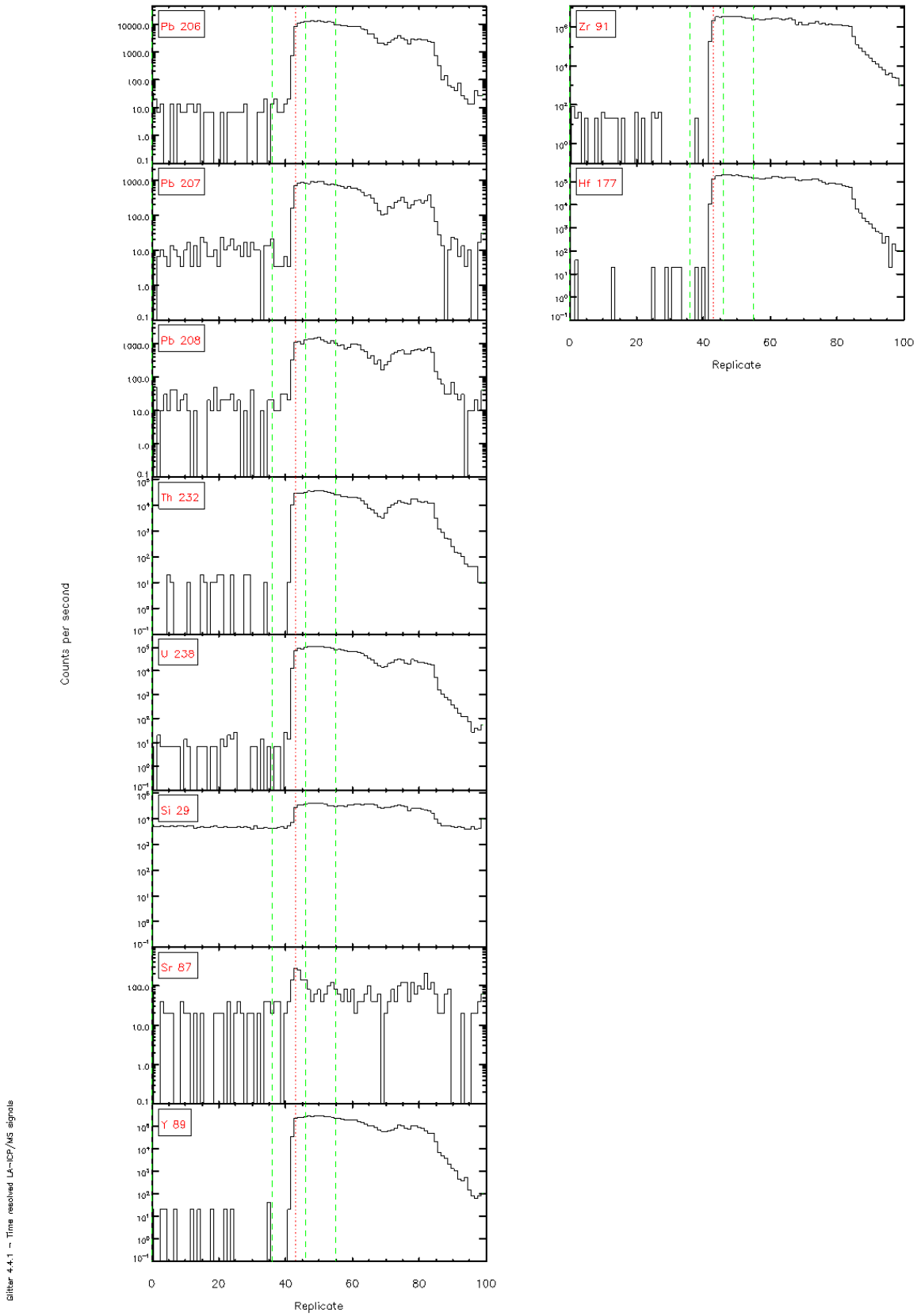
Pb 206
Pb 207
Pb 208
Th 232
U 238
Si 29
Sr 87
Y 89
Zr 91
Hf 177
Counts per second
Replicate
Glitter 4.4.1 - Time resolved LA-ICP/MS signals

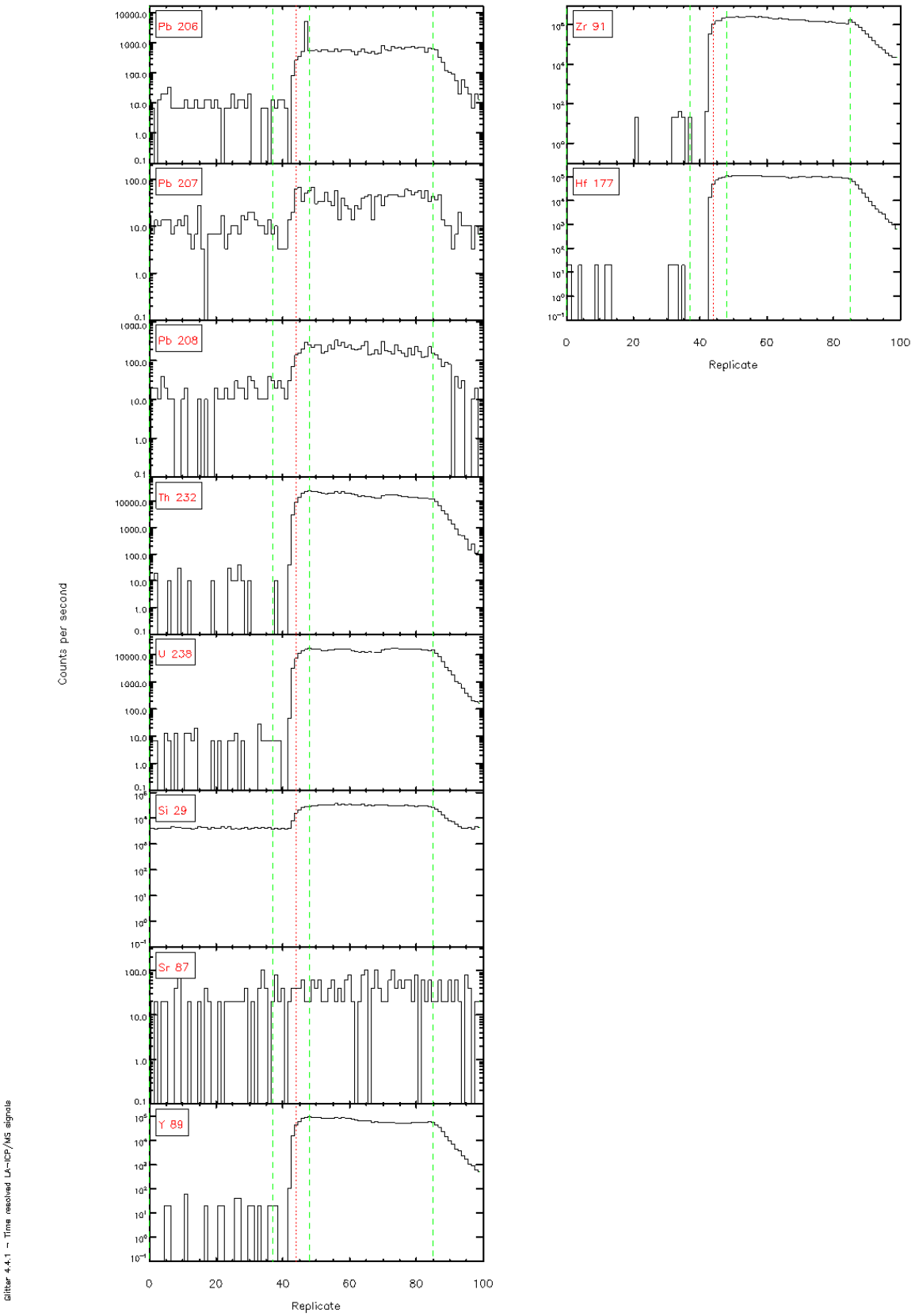
Pb 206
Pb 207
Pb 208
Th 232
U 238
Si 29
Sr 87
Y 89
Zr 91
Hf 177
Counts per second
Replicate
Glitter 4.4.1 - Time resolved LA-ICP/MS signals

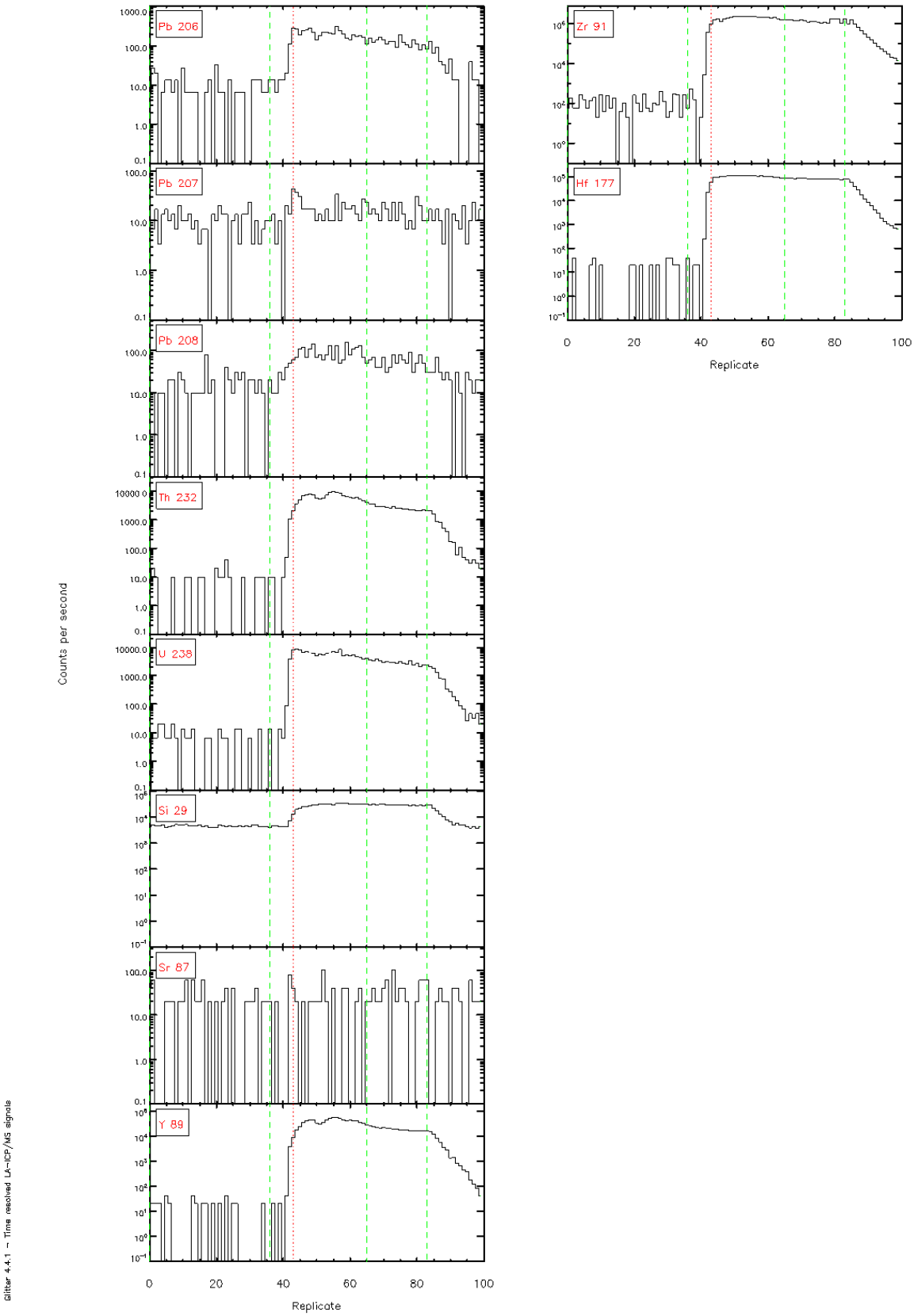
Pb 206
Pb 207
Pb 208
Th 232
U 238
Si 29
Sr 87
Y 89
Zr 91
Hf 177
Counts per second
Replicate
Glitter 4.4.1 - Time resolved LA-ICP/MS signals

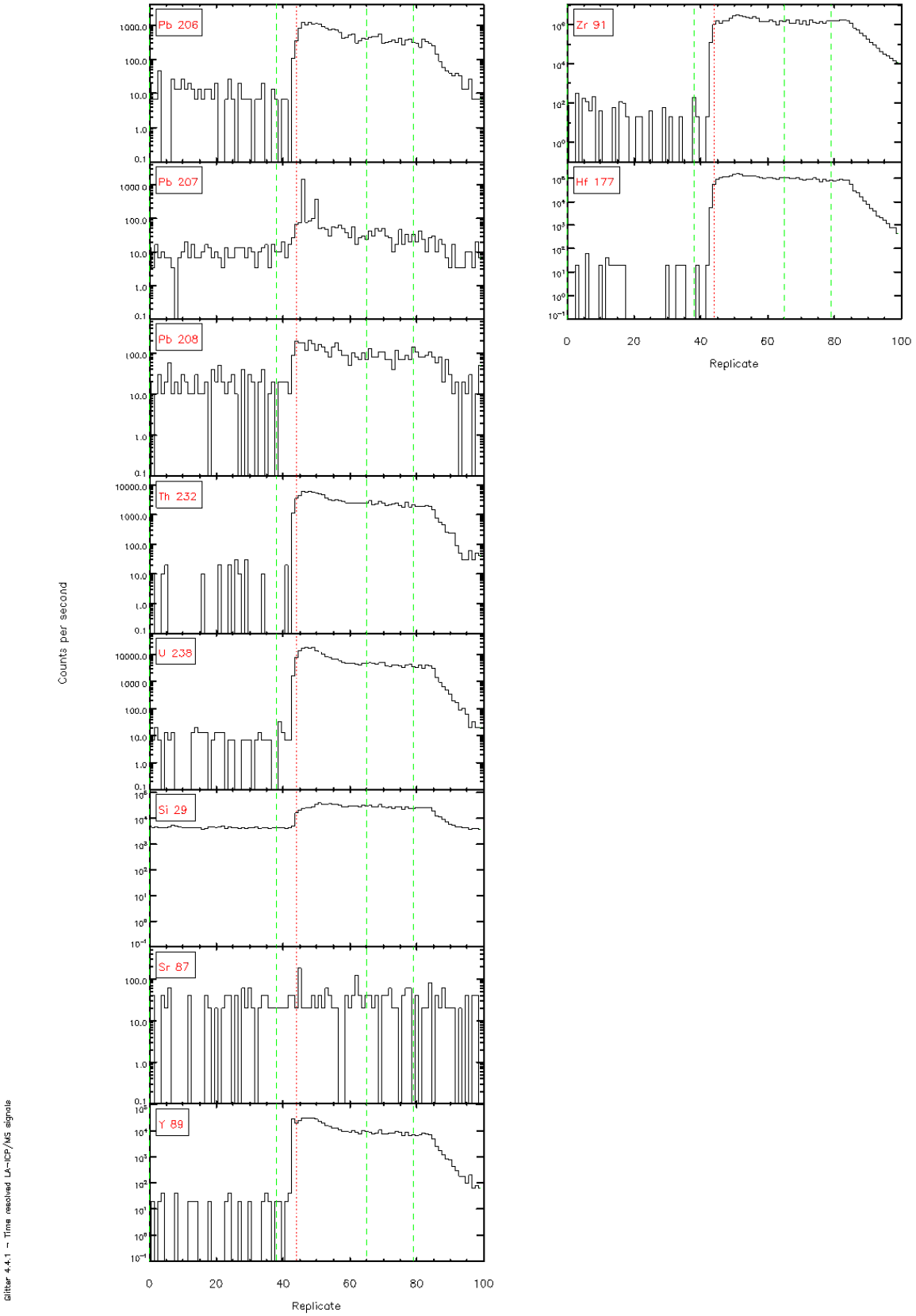
Pb 206
Pb 207
Pb 208
Th 232
U 238
Si 29
Sr 87
Y 89
Zr 91
Hf 177
Counts per second
Replicate
Glitter 4.4.1 - Time resolved LA-ICP/MS signals

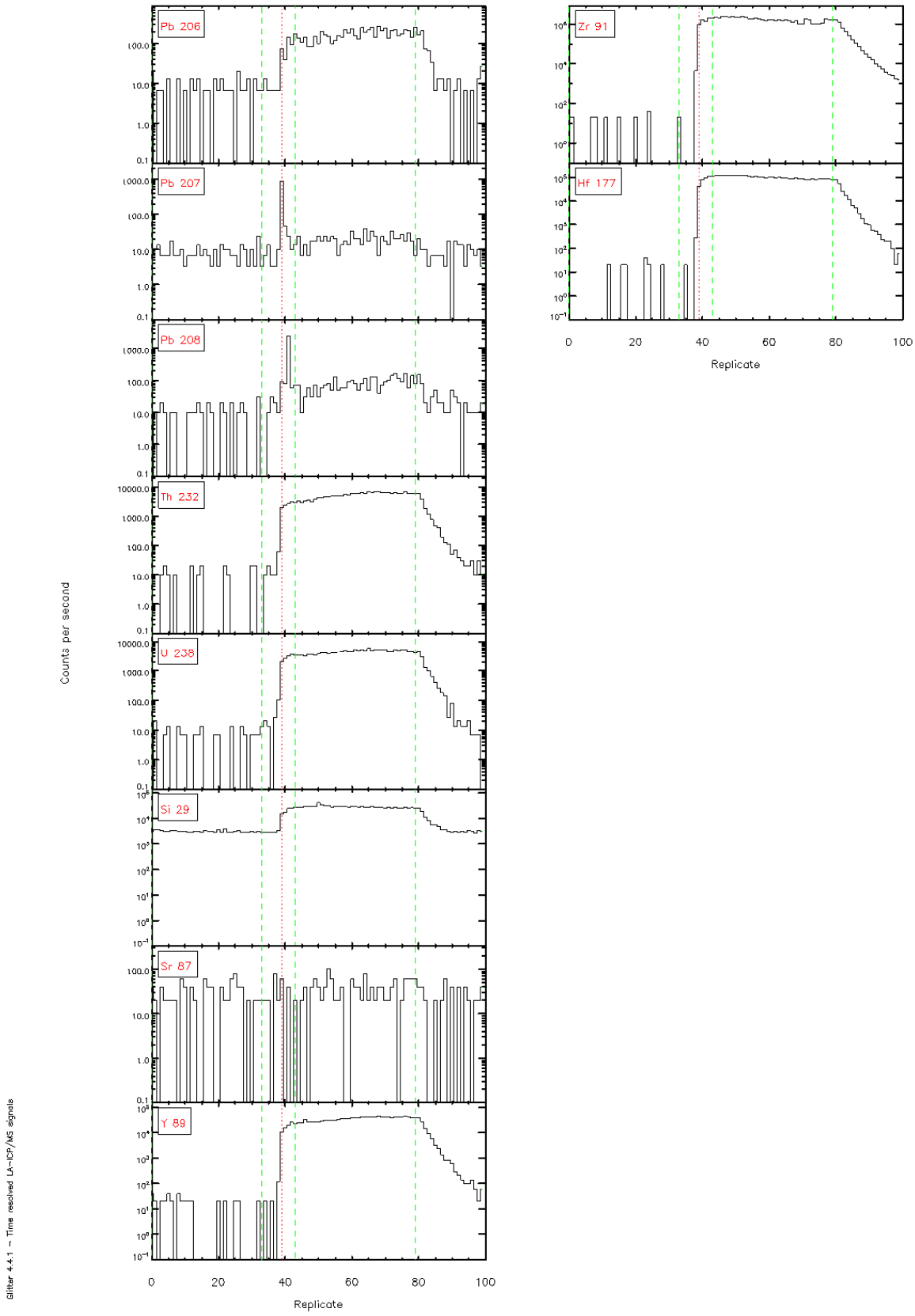
Pb 206
Pb 207
Pb 208
Th 232
U 238
Si 29
Sr 87
Y 89
Zr 91
Hf 177
Counts per second
Replicate
Glitter 4.4.1 - Time resolved LA-ICP/MS signals

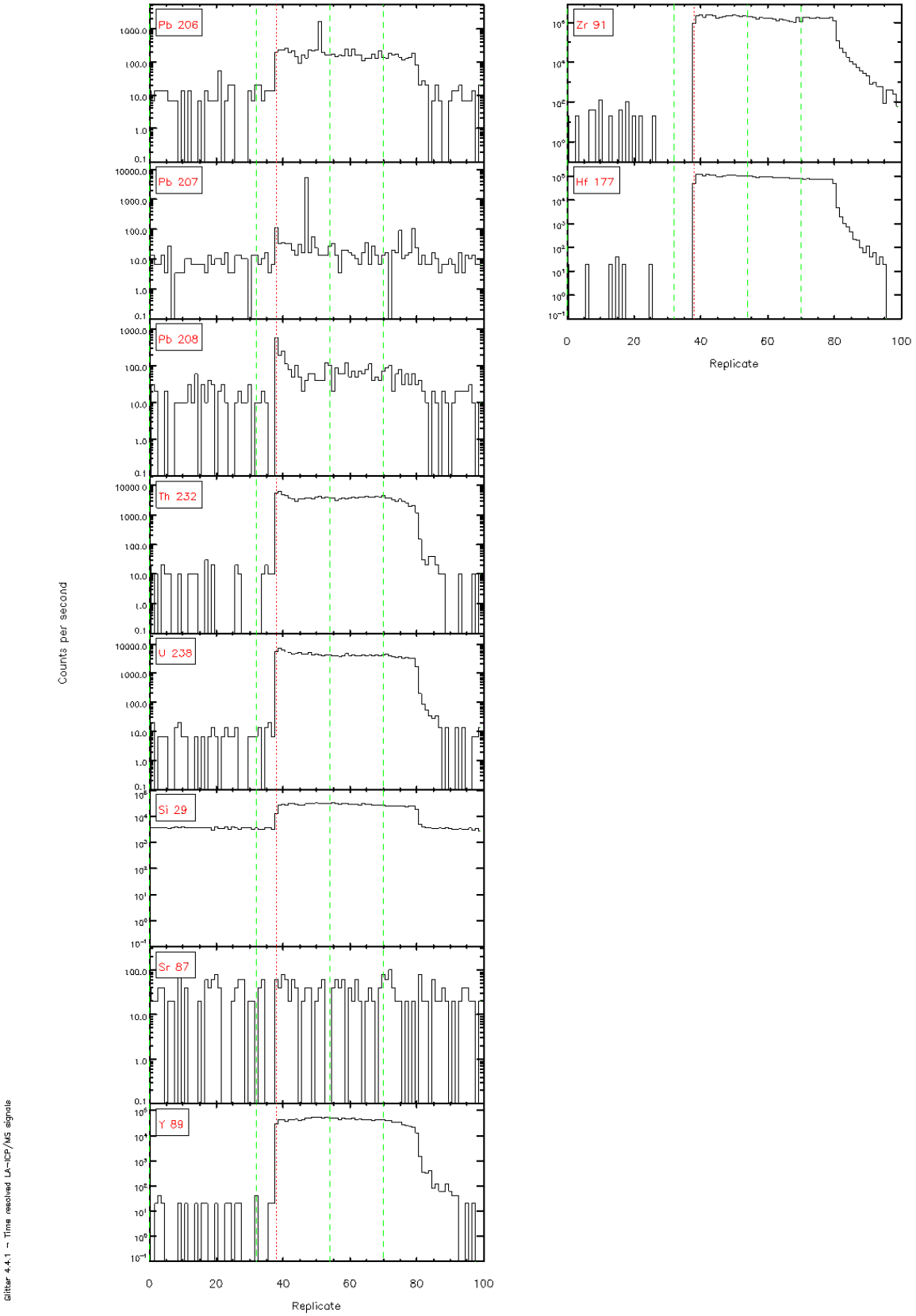
Pb 206
Pb 207
Pb 208
Th 232
U 238
Si 29
Sr 87
Y 89
Zr 91
Hf 177
Counts per second
Replicate
Glitter 4.4.1 - Time resolved LA-ICP/MS signals

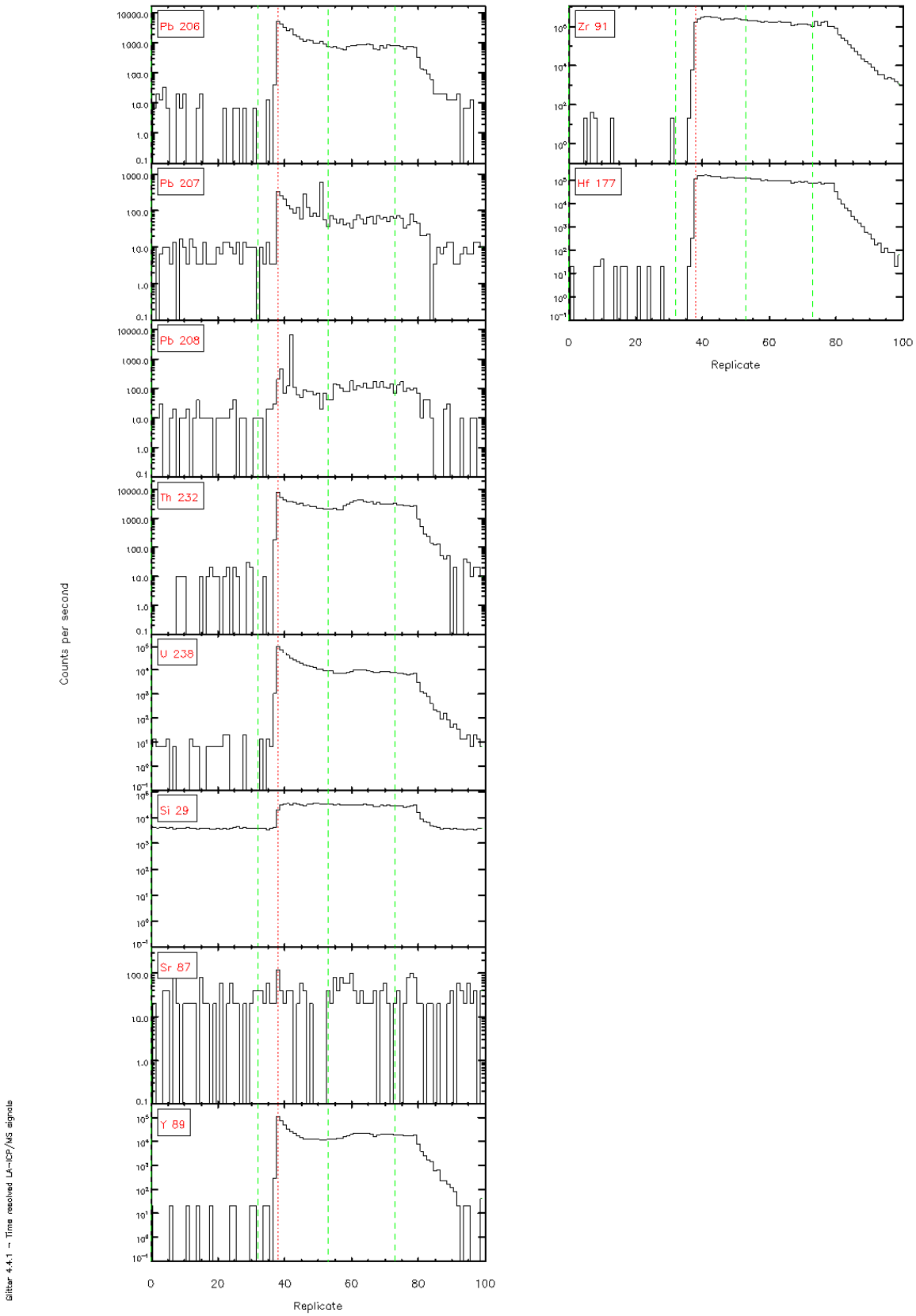
Pb 206
Pb 207
Pb 208
Th 232
U 238
Si 29
Sr 87
Y 89
Zr 91
Hf 177
Counts per second
Replicate
Glitter 4.4.1 – Time resolved LA-ICP/MS signals

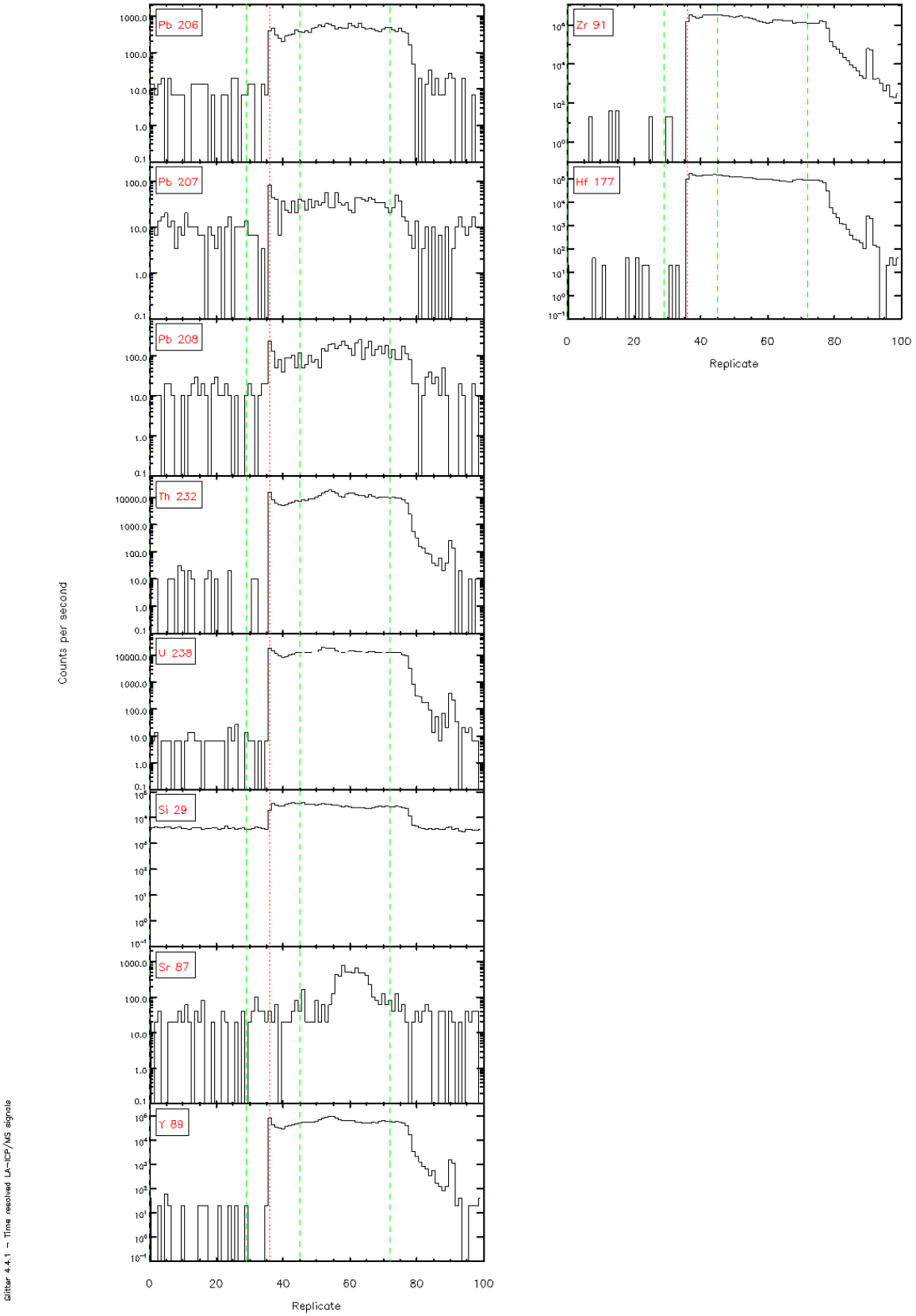
Pb 206
Pb 207
Pb 208
Th 232
U 238
Si 29
Sr 87
Y 89
Zr 91
Hf 177
Counts per second
Replicate
Glitter 4.4.1 – Time resolved LA-ICP/MS signals

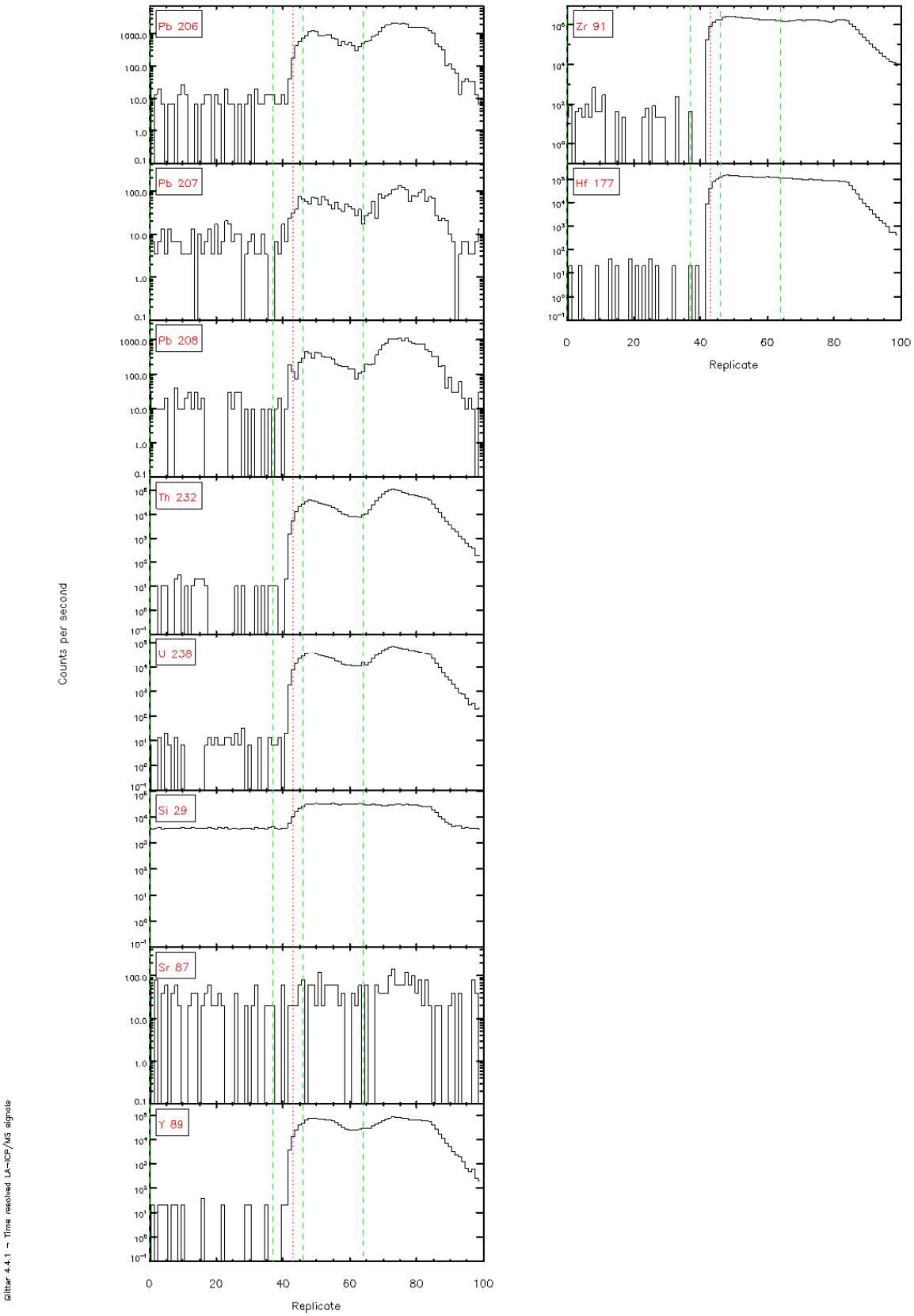
Pb 206
Pb 207
Pb 208
Th 232
U 238
Si 29
Sr 87
Y 89
Zr 91
Hf 177
Counts per second
Replicate
Glitter 4.4.1 - Time resolved LA-ICP/MS signals

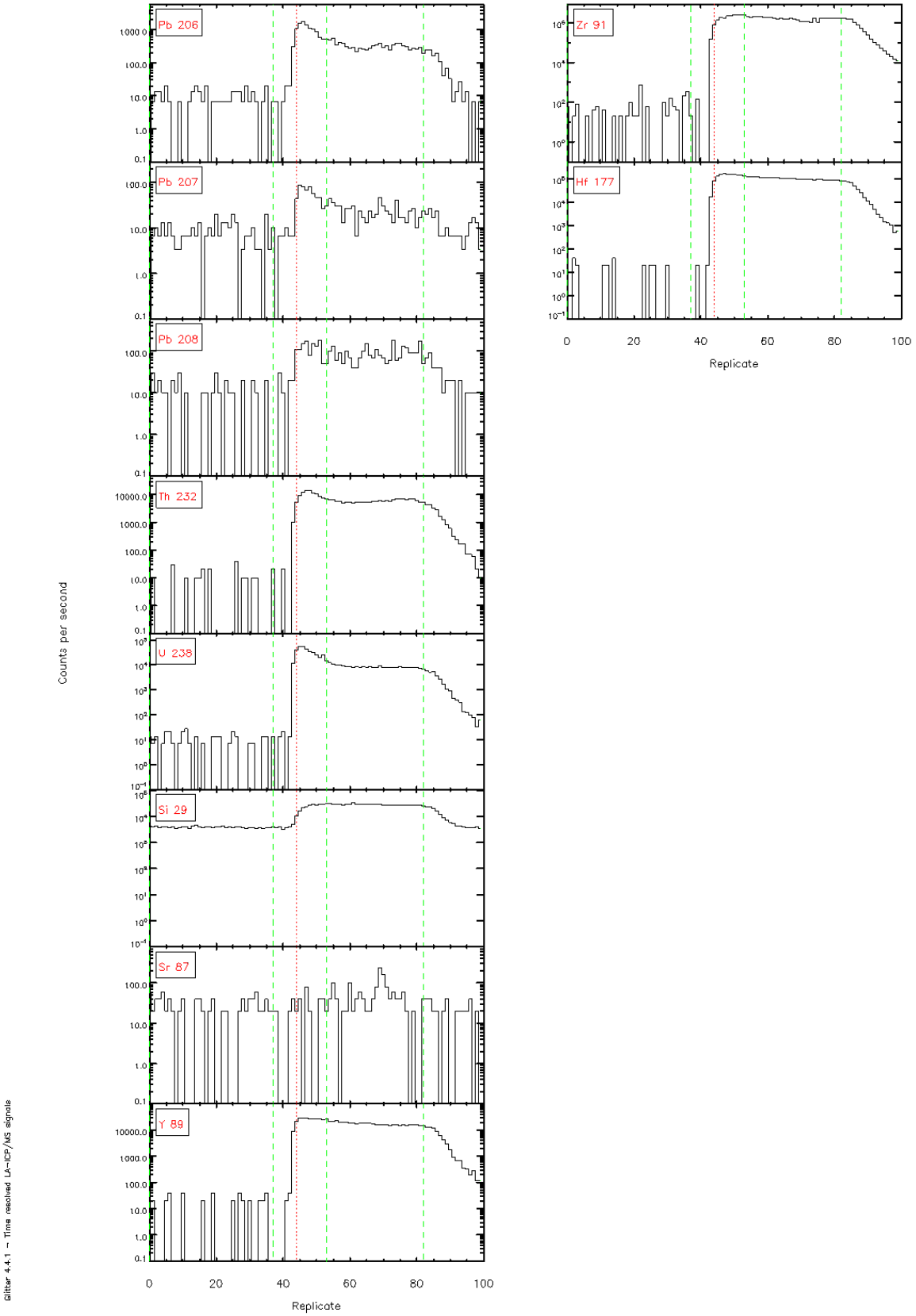
Pb 206
Pb 207
Pb 208
Th 232
U 238
Si 29
Sr 87
Y 89
Zr 91
Hf 177
Counts per second
Replicate
Glitter 4.4.1 - Time resolved LA-ICP/MS signals

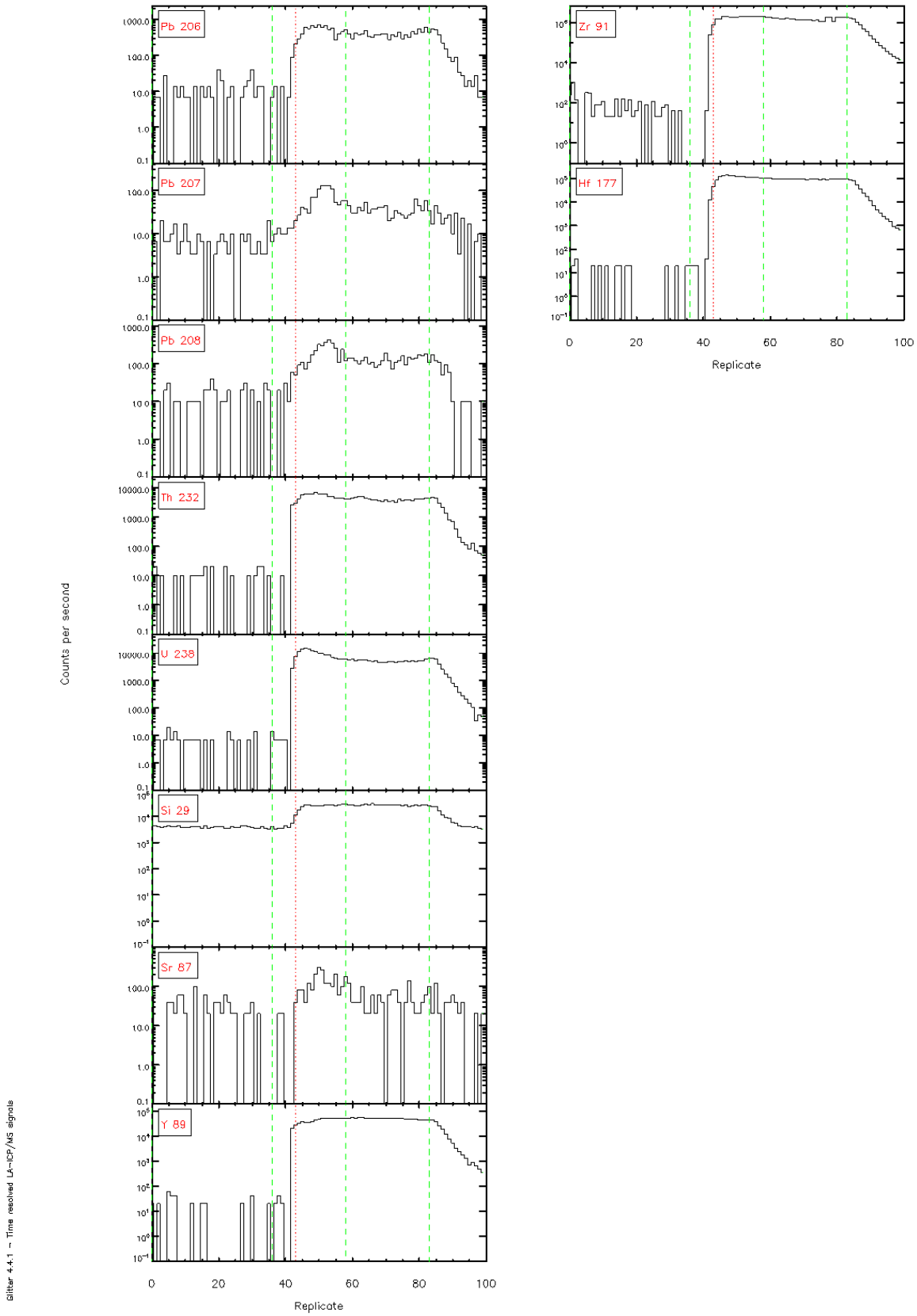
Pb 206
Pb 207
Pb 208
Th 232
U 238
Si 29
Sr 87
Y 89
Zr 91
Hf 177
Counts per second
Replicate
Glitter 4.4.1 - Time resolved LA-ICP/MS signals

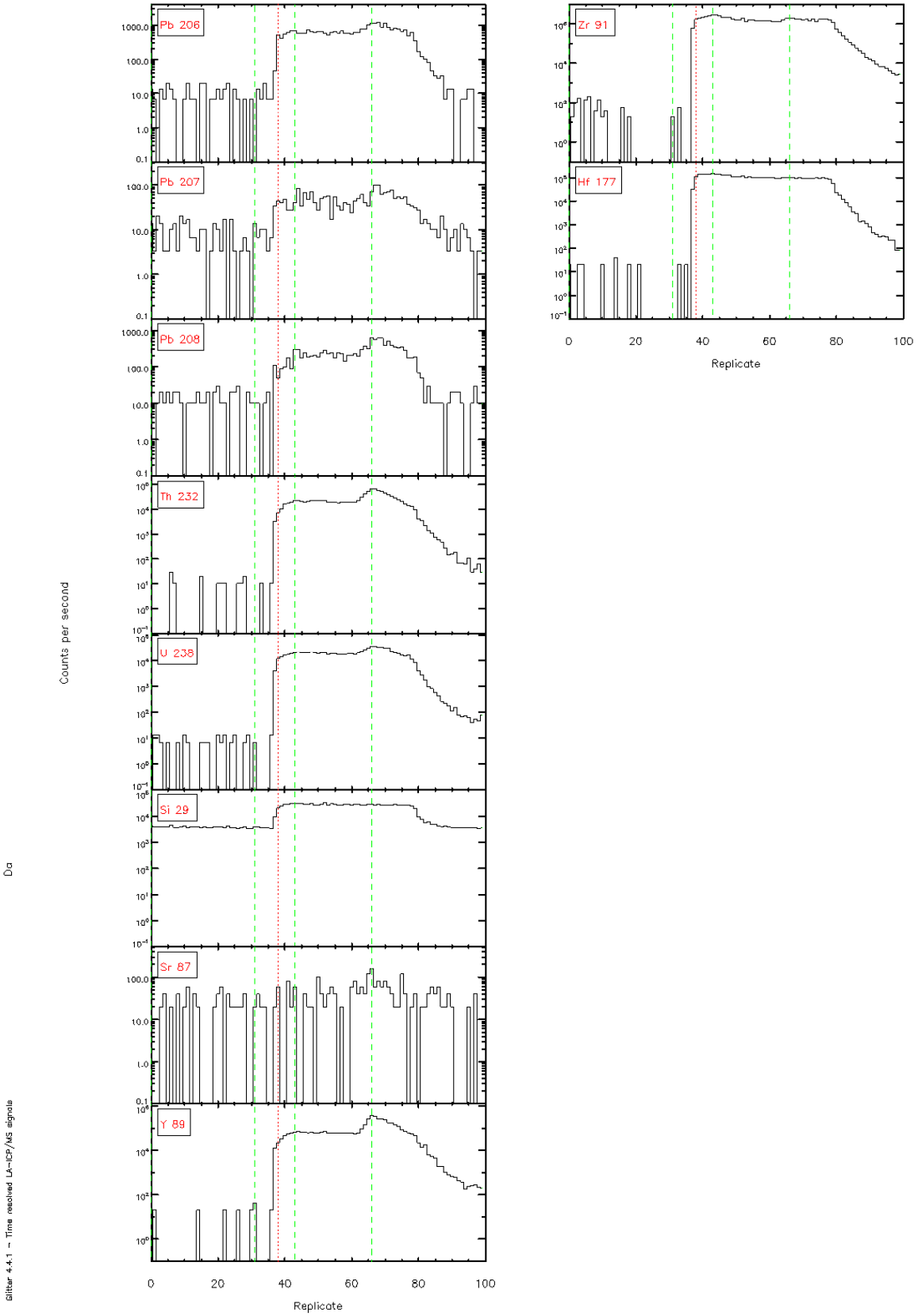
Pb 206
Pb 207
Pb 208
Th 232
U 238
Si 29
Sr 87
Y 89
Zr 91
Hf 177
Counts per second
Replicate
0
20
40
60
80
100
Da
Glitter 4.4.1 - Time resolved LA-ICP/MS signals

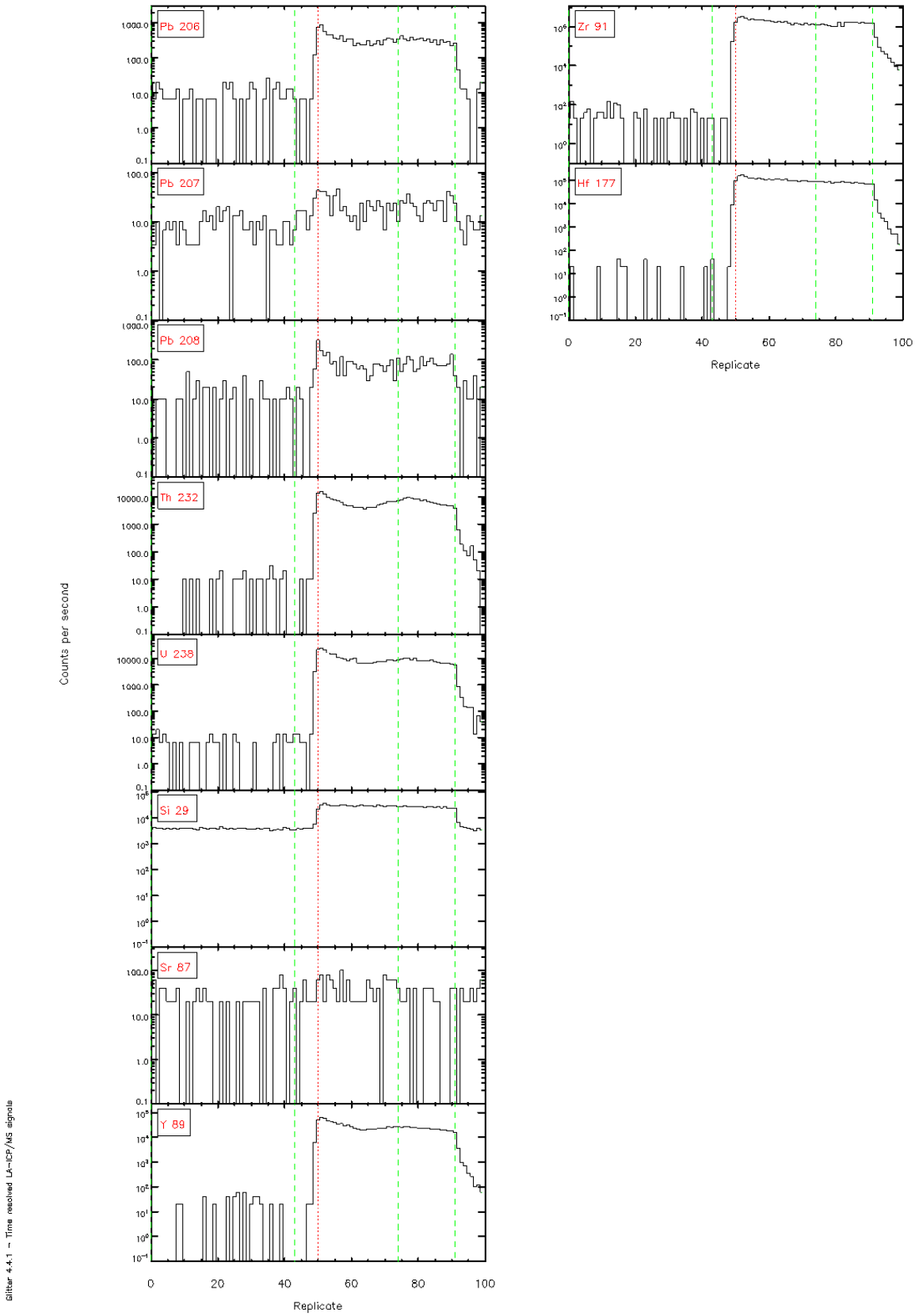
Pb 206
Pb 207
Pb 208
Th 232
U 238
Si 29
Sr 87
Y 89
Zr 91
Hf 177
Counts per second
Replicate
Glitter 4.4.1 - Time resolved LA-ICP/MS signals

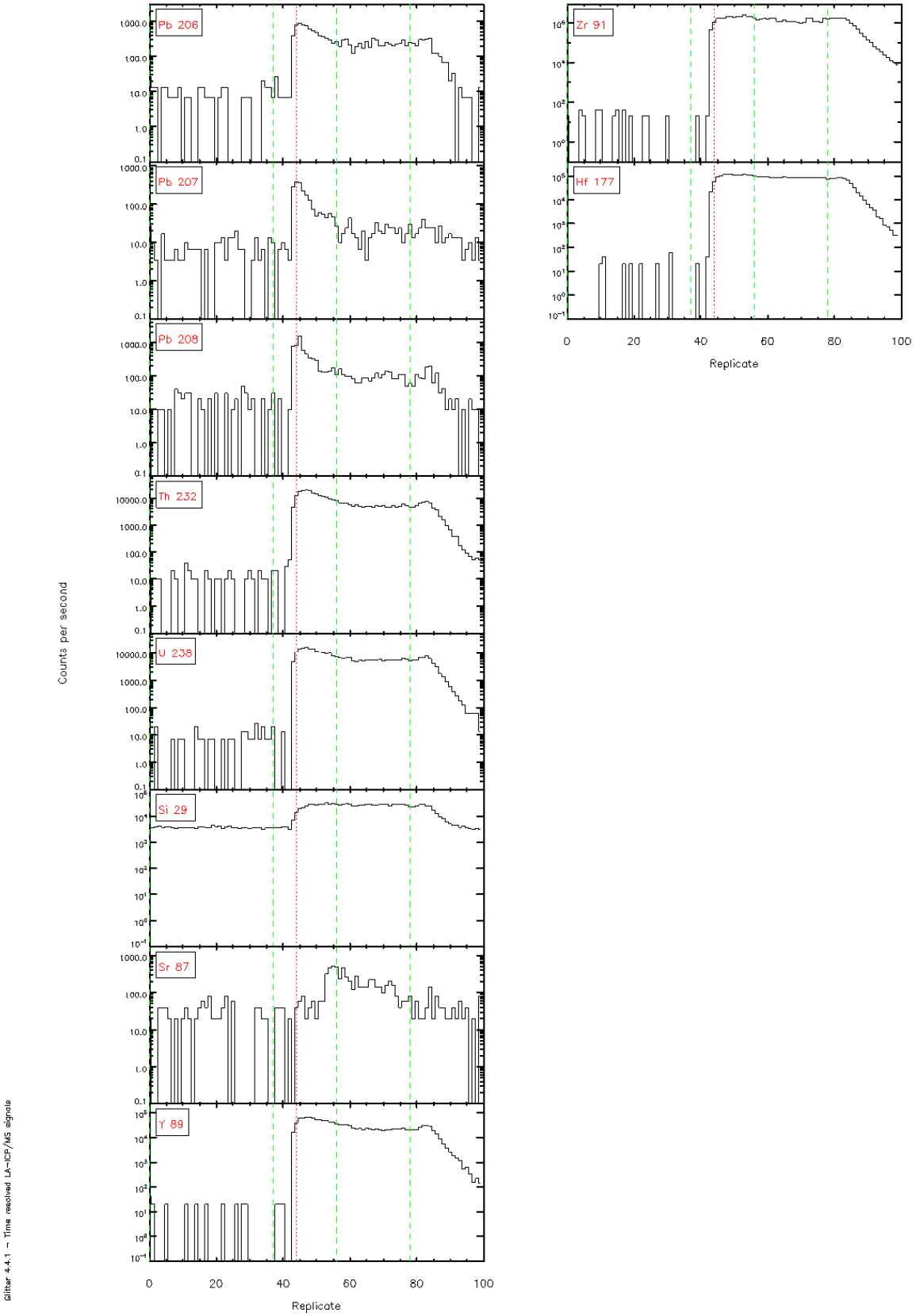
Pb 206
Pb 207
Pb 208
Th 232
U 238
Si 29
Sr 87
Y 89
Zr 91
Hf 177
Counts per second
Replicate
Glitter 4.4.1 - Time resolved LA-ICP/MS signals

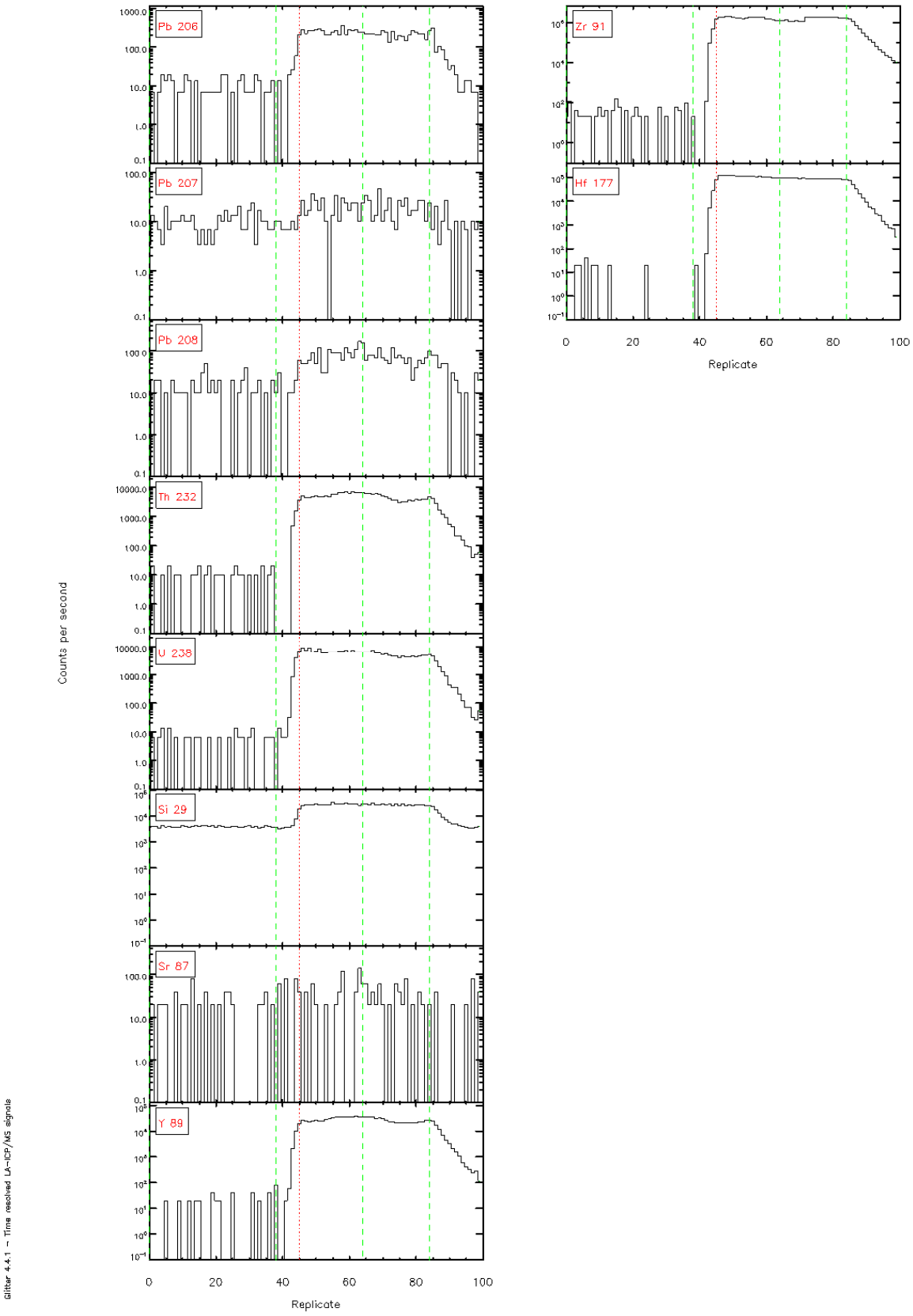
Pb 206
Pb 207
Pb 208
Th 232
U 238
Si 29
Sr 87
Y 89
Zr 91
Hf 177
Counts per second
Replicate
Glitter 4.4.1 - Time resolved LA-ICP/MS signals

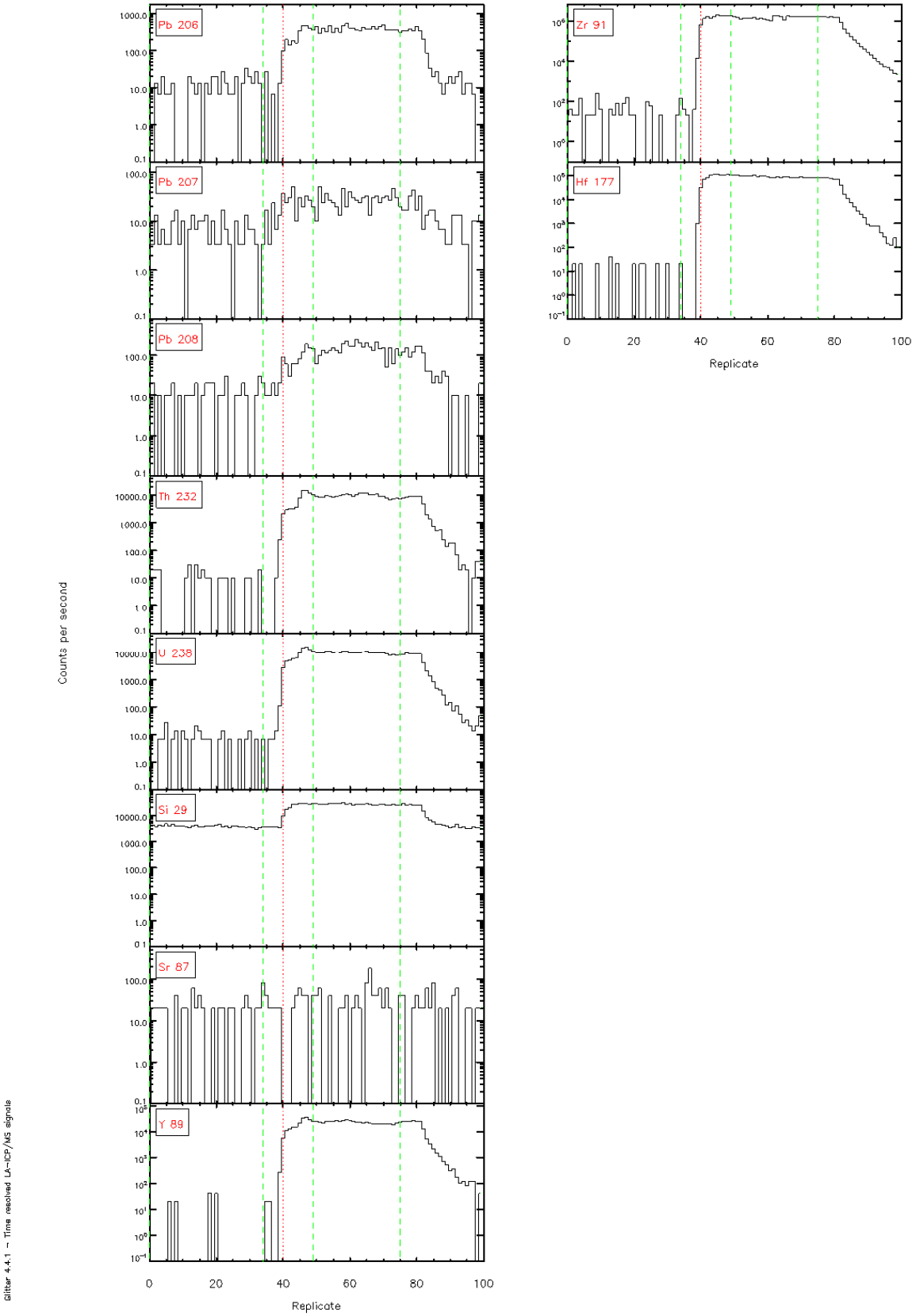
Pb 206
Pb 207
Pb 208
Th 232
U 238
Si 29
Sr 87
Y 89
Zr 91
Hf 177
Counts per second
Replicate
Glitter 4.4.1 – Time resolved LA-ICP/MS signals

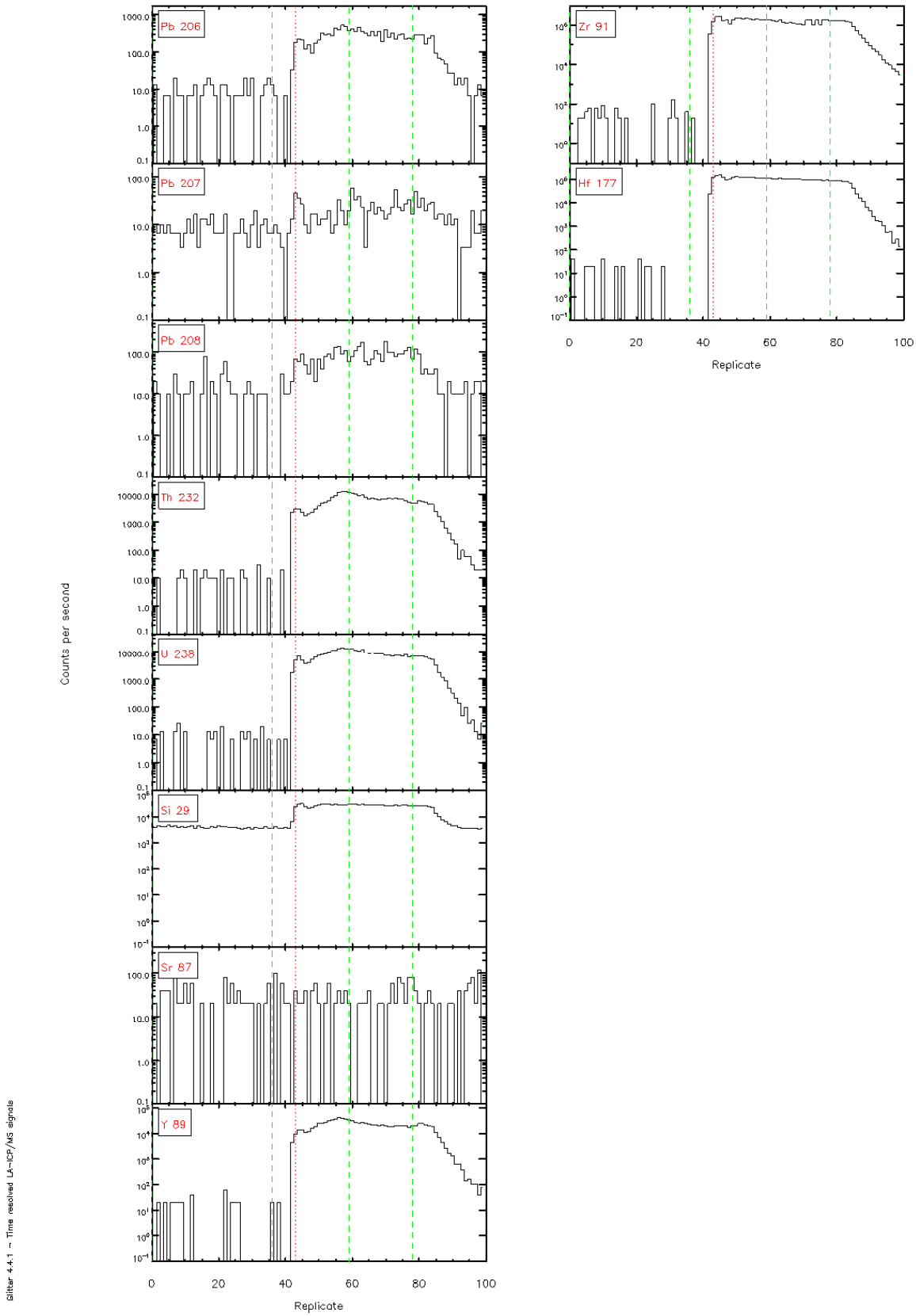
Pb 206
Pb 207
Pb 208
Th 232
U 238
Si 29
Sr 87
Y 89
Zr 91
Hf 177
Counts per second
Replicate
Glitter 4.4.1 - Time resolved LA-ICP/MS signals

10 – Matapo Sandstone

1.

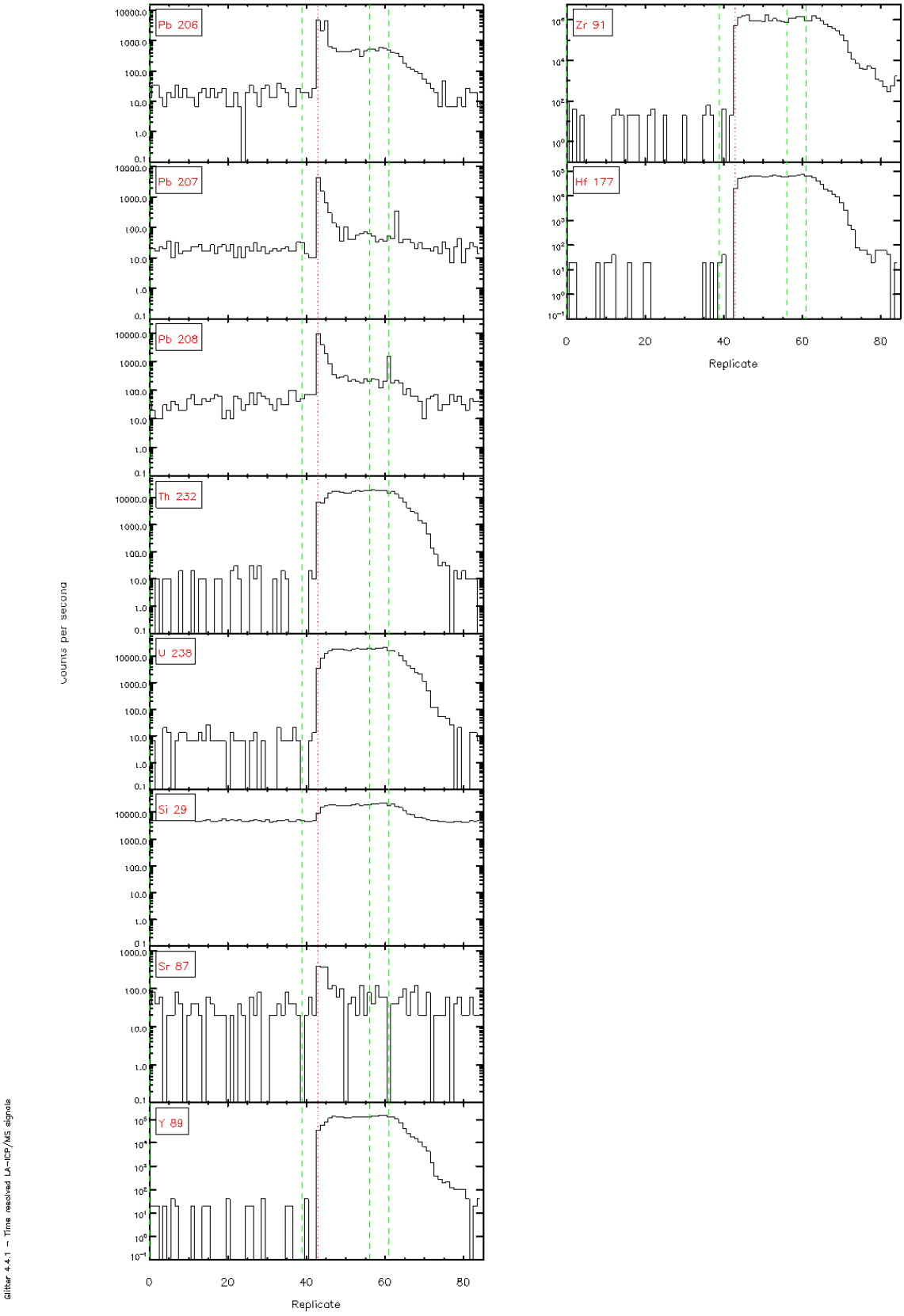

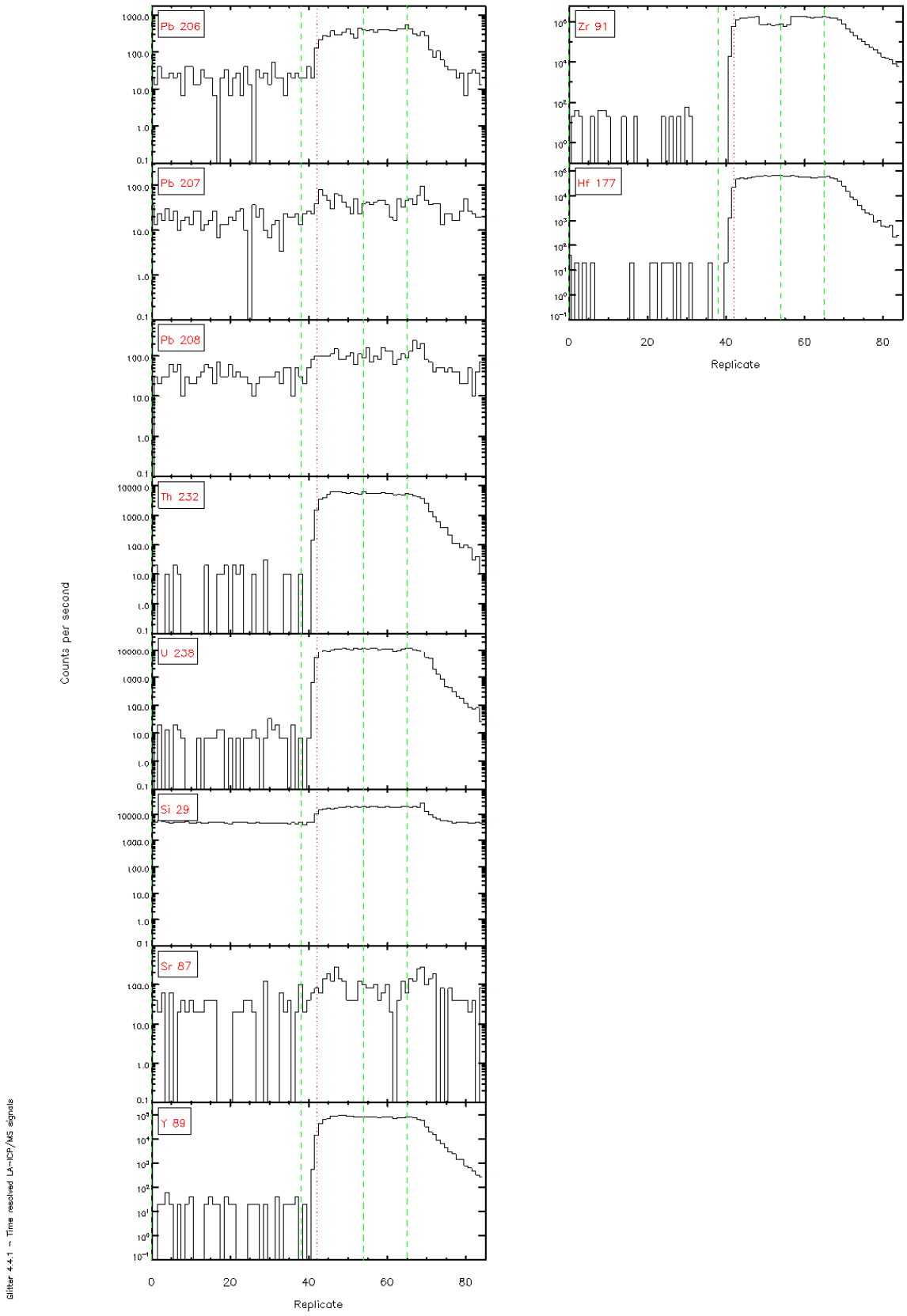
Pb 206
Pb 207
Pb 208
Th 232
U 238
Si 29
Sr 87
Y 89
Zr 91
Hf 177
Counts per second
Replicate
Glitter 4.4.1 - Time resolved LA-ICP/MS signals

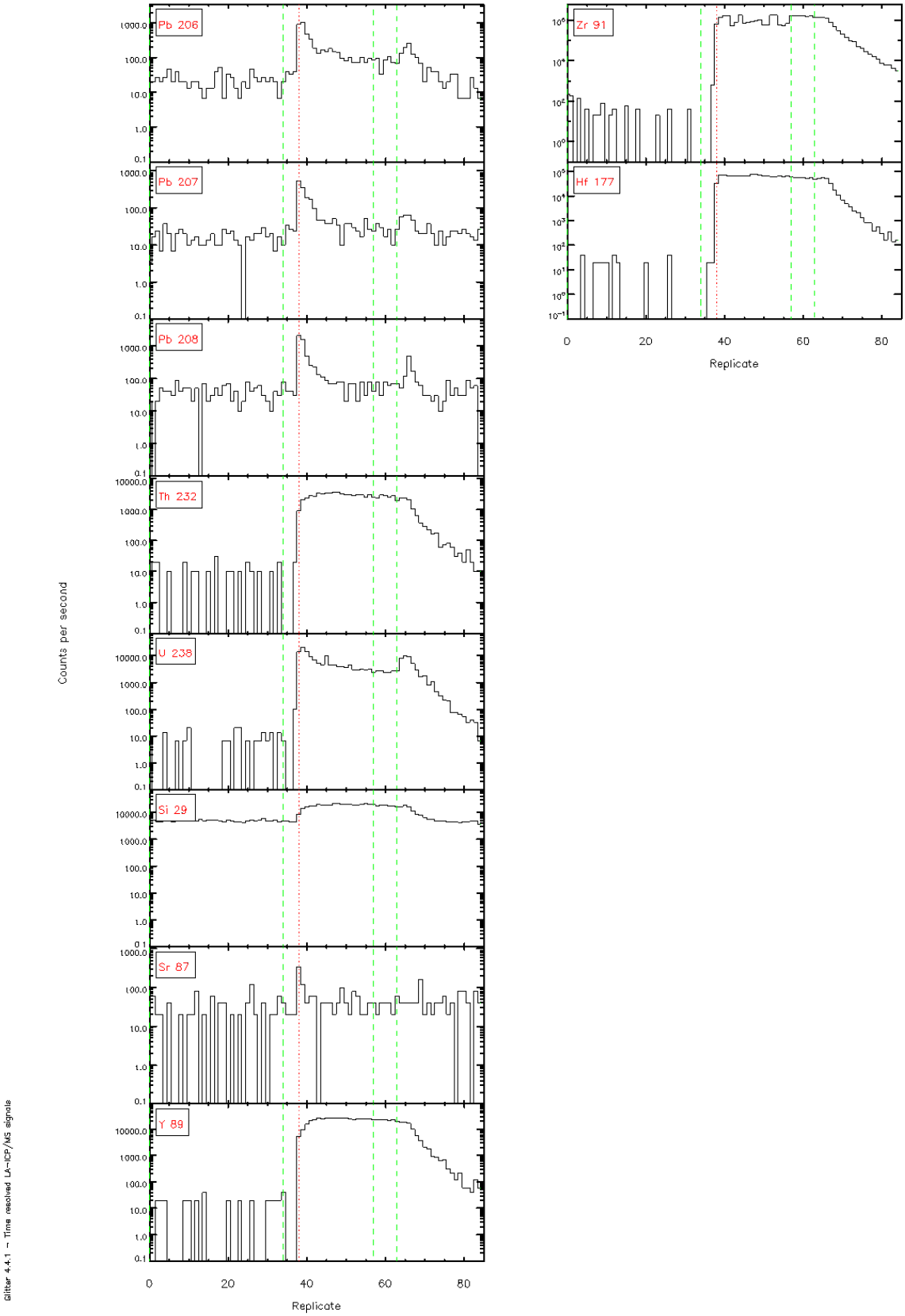
Pb 206
Pb 207
Pb 208
Th 232
U 238
Si 29
Sr 87
Y 89
Zr 91
Hf 177
Counts per second
Replicate
0
20
40
60
80
Glitter 4.4.1 - Time resolved LA-ICP/MS signals

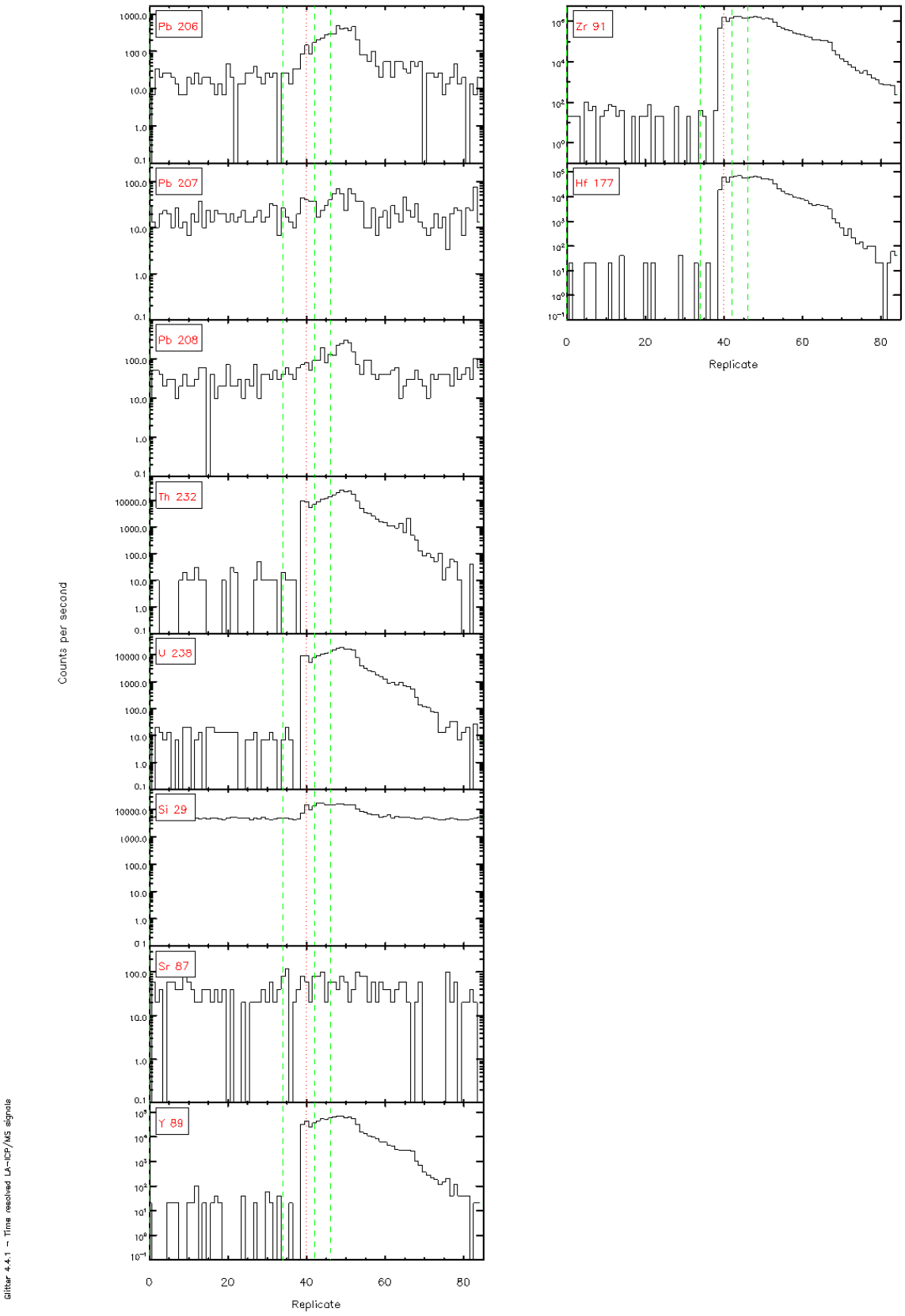
Pb 206
Pb 207
Pb 208
Th 232
U 238
Si 29
Sr 87
Y 89
Zr 91
Hf 177
Counts per second
Replicate
Glitter 4.4.1 - Time resolved LA-ICP/MS signals

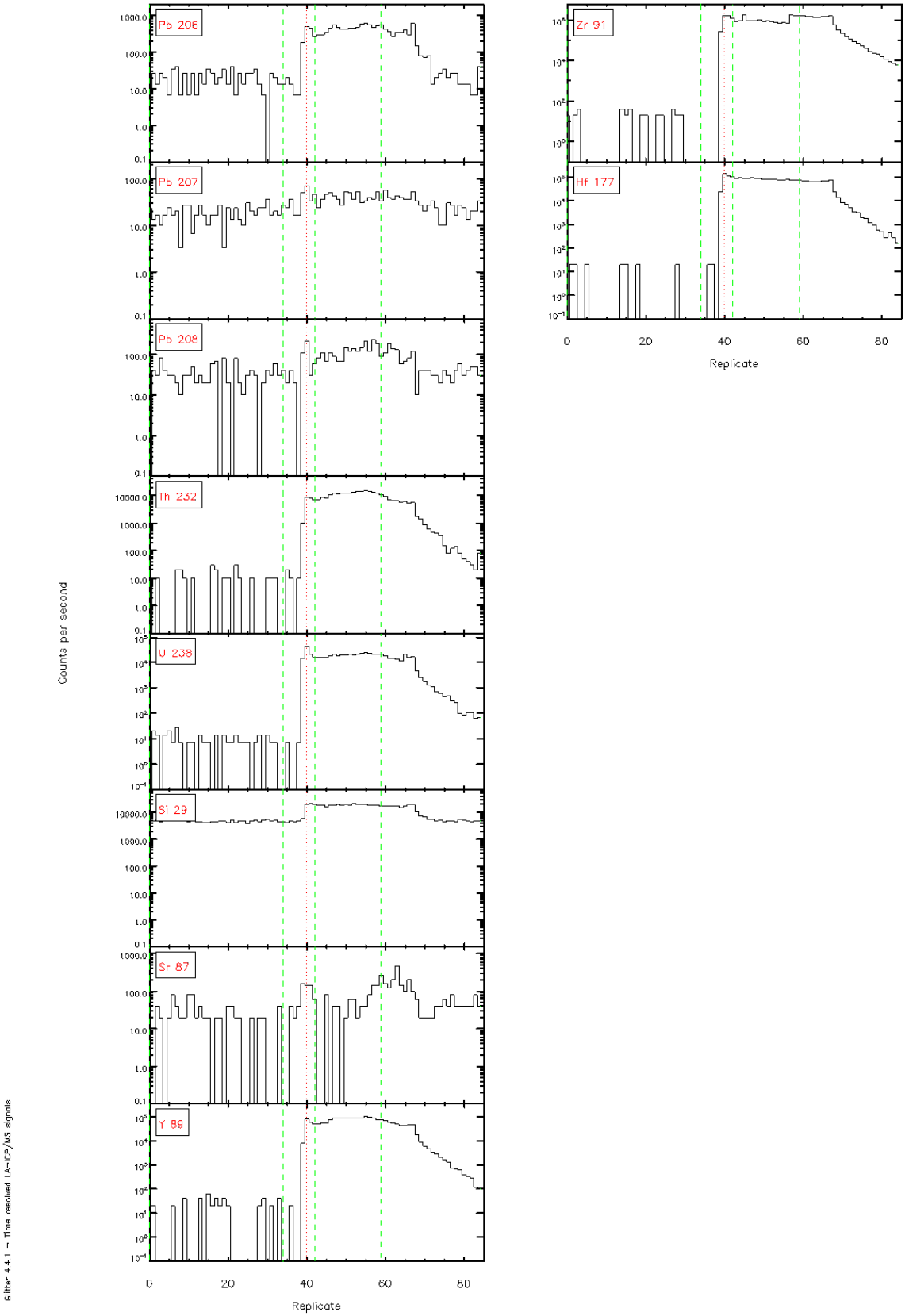
Pb 206
Pb 207
Pb 208
Th 232
U 238
Si 29
Sr 87
Y 89
Zr 91
Hf 177
Counts per second
Replicate
Glitter 4.4.1 – Time resolved LA-ICP/MS signals

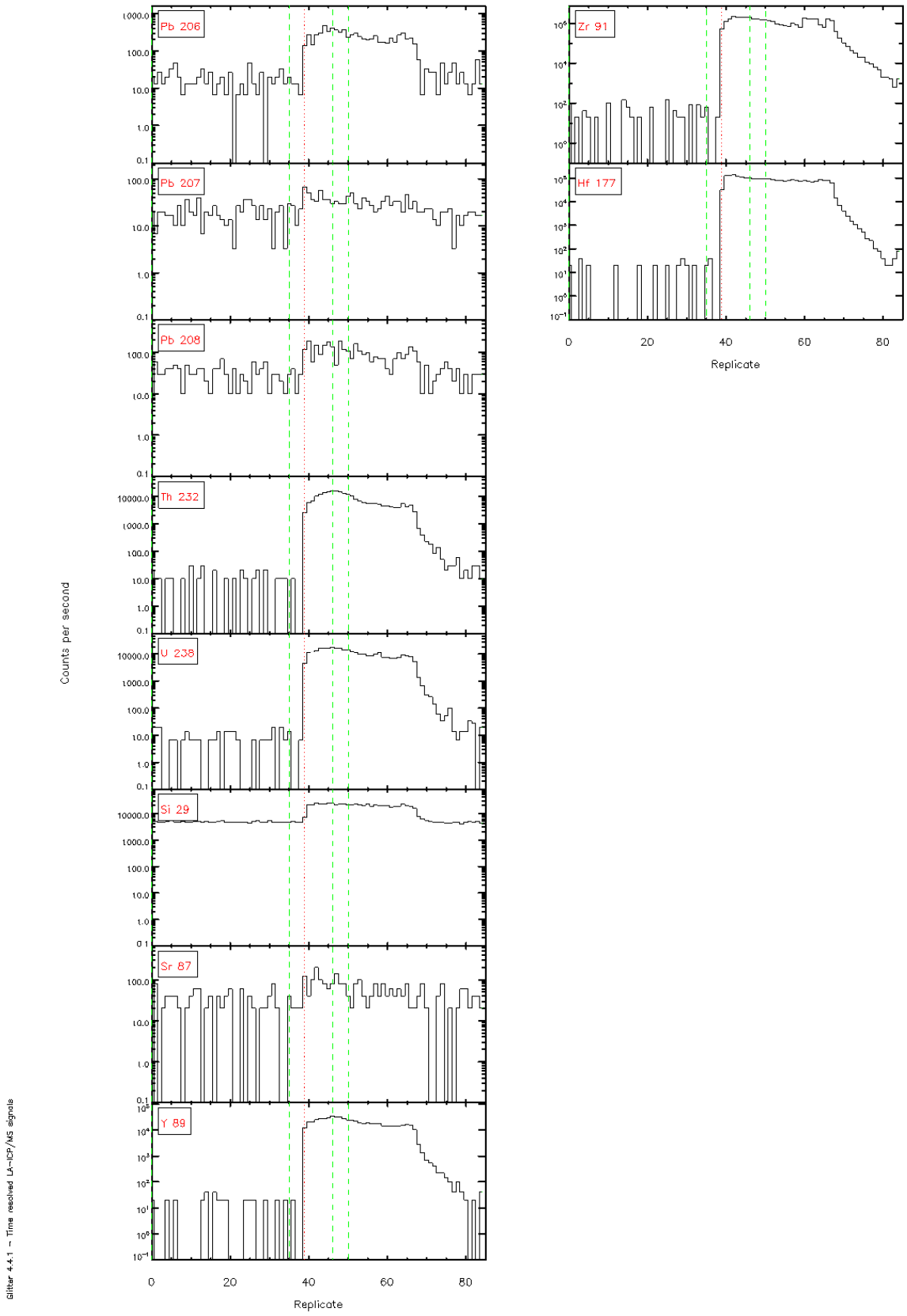
Pb 206
Pb 207
Pb 208
Th 232
U 238
Si 29
Sr 87
Y 89
Zr 91
Hf 177
Counts per second
Replicate
Glitter 4.4.1 - Time resolved LA-ICP/MS signals

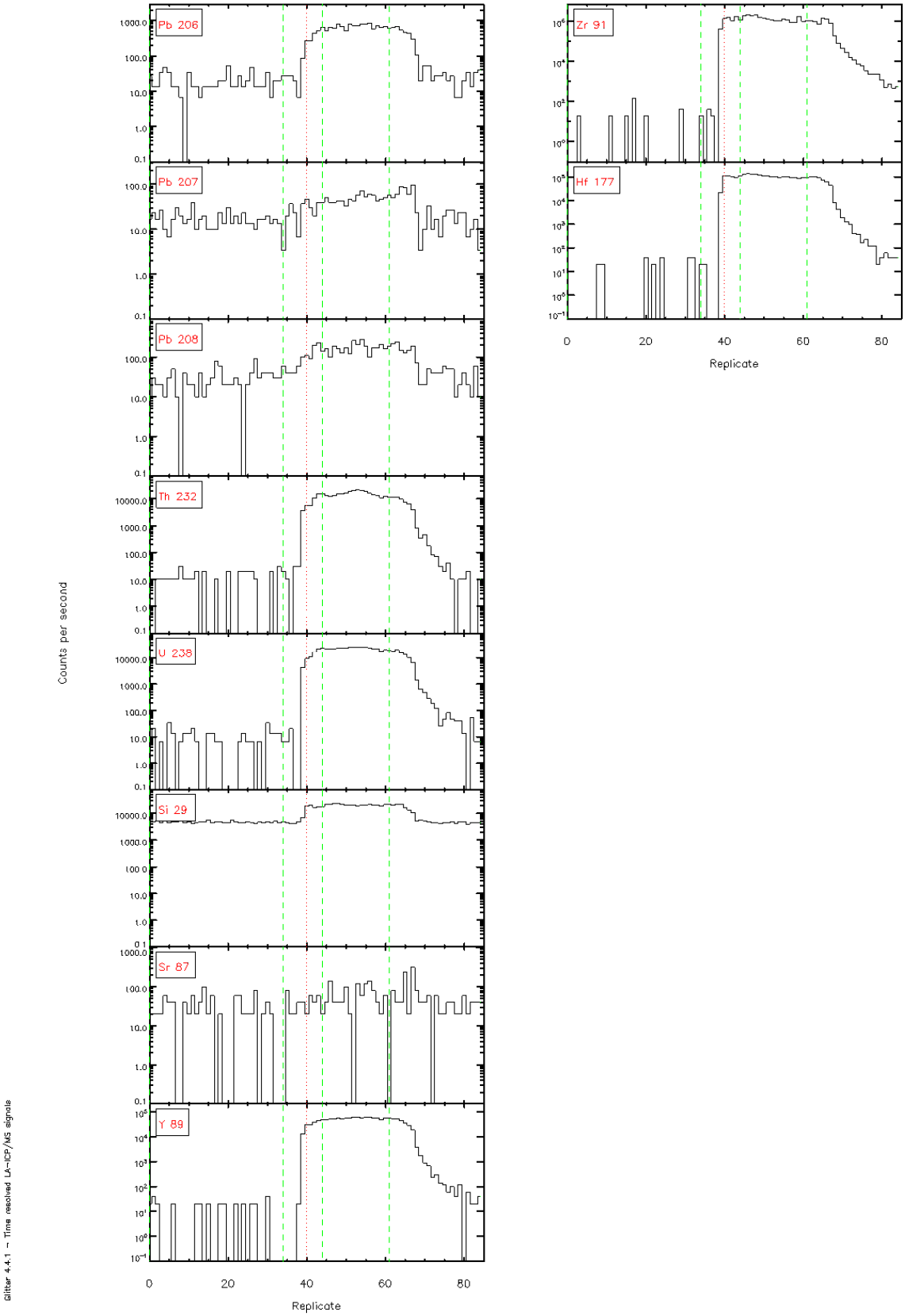
Pb 206
Pb 207
Pb 208
Th 232
U 238
Si 29
Sr 87
Y 89
Zr 91
Hf 177
Counts per second
Replicate
Glitter 4.4.1 - Time resolved LA-ICP/MS signals

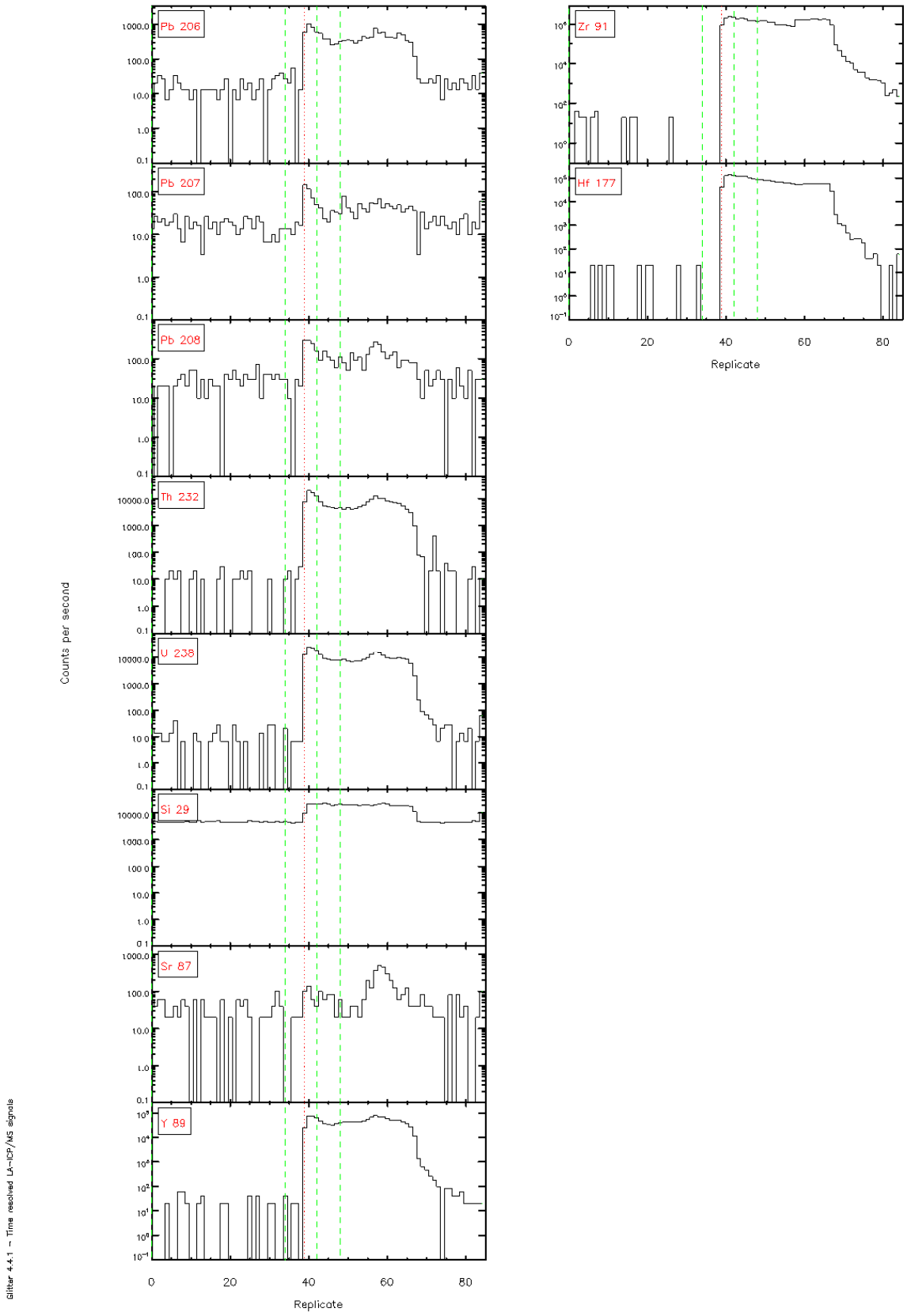
Pb 206
Pb 207
Pb 208
Th 232
U 238
Si 29
Sr 87
Y 89
Zr 91
Hf 177
Counts per second
Replicate
Glitter 4.4.1 - Time resolved LA-ICP/MS signals

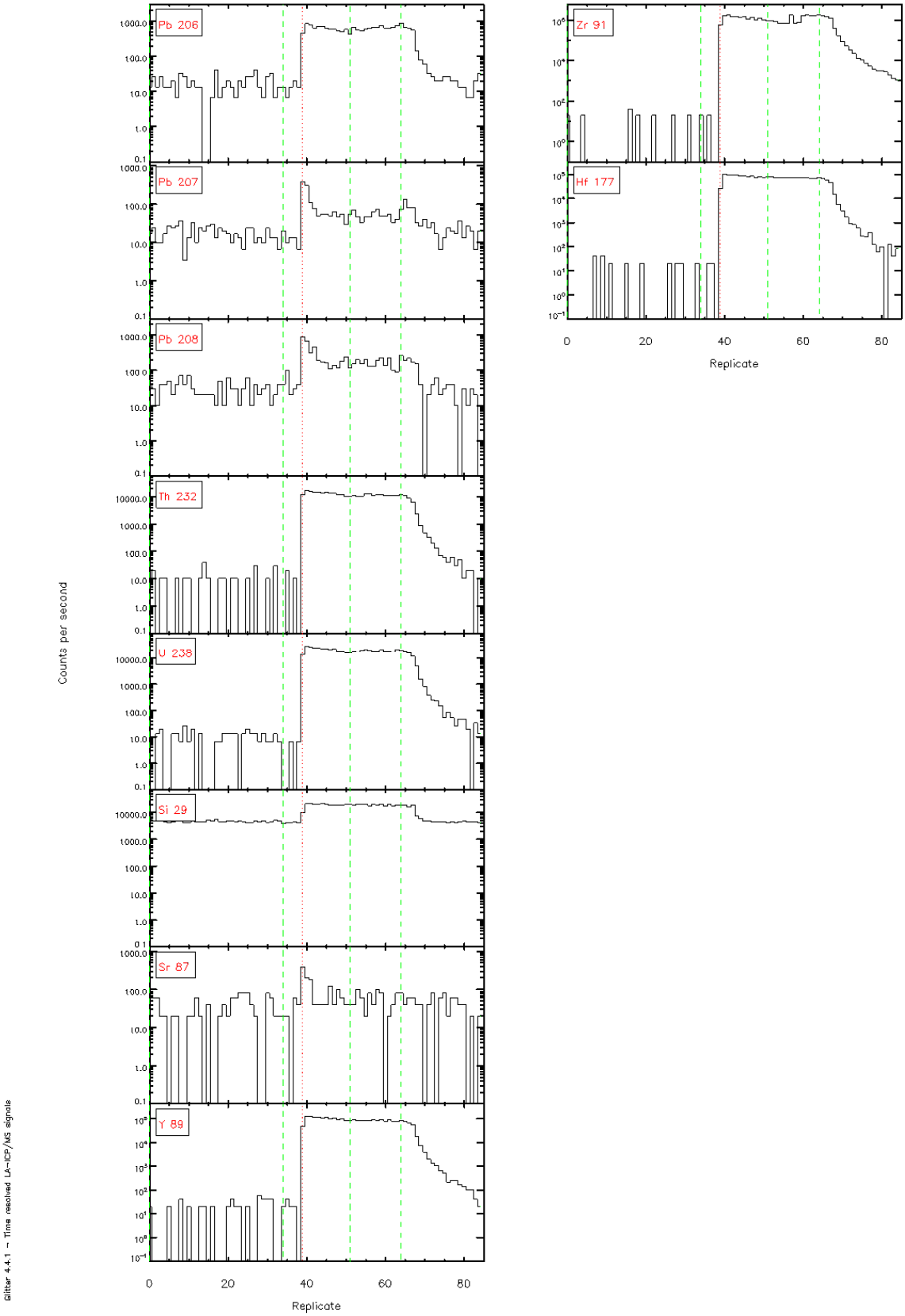
Pb 206
Pb 207
Pb 208
Th 232
U 238
Si 29
Sr 87
Y 89
Zr 91
Hf 177
Counts per second
Replicate
Glitter 4.4.1 - Time resolved LA-ICP/MS signals

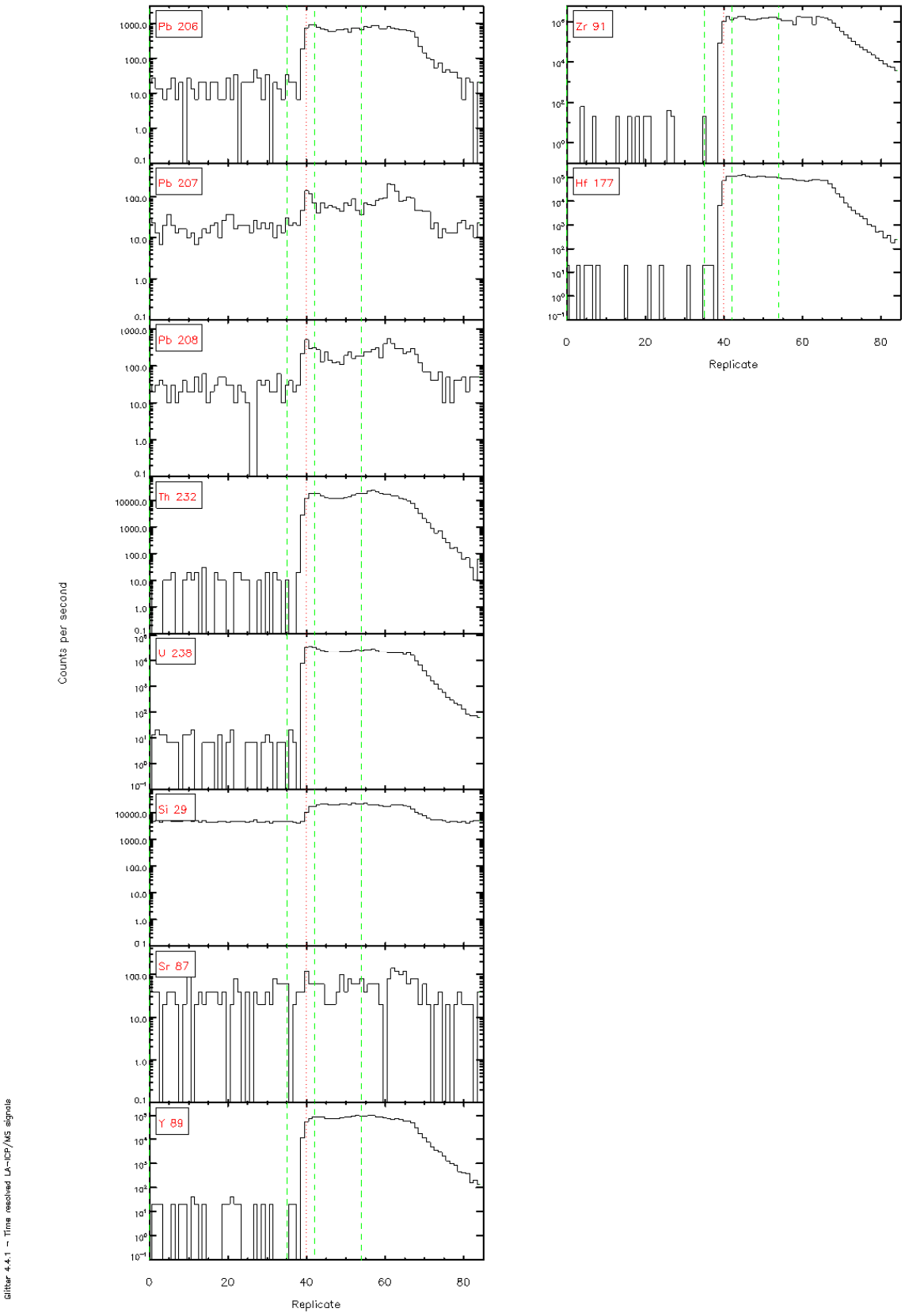
Pb 206
Pb 207
Pb 208
Th 232
U 238
Si 29
Sr 87
Y 89
Zr 91
Hf 177
Counts per second
Replicate
Glitter 4.4.1 - Time resolved LA-ICP/MS signals

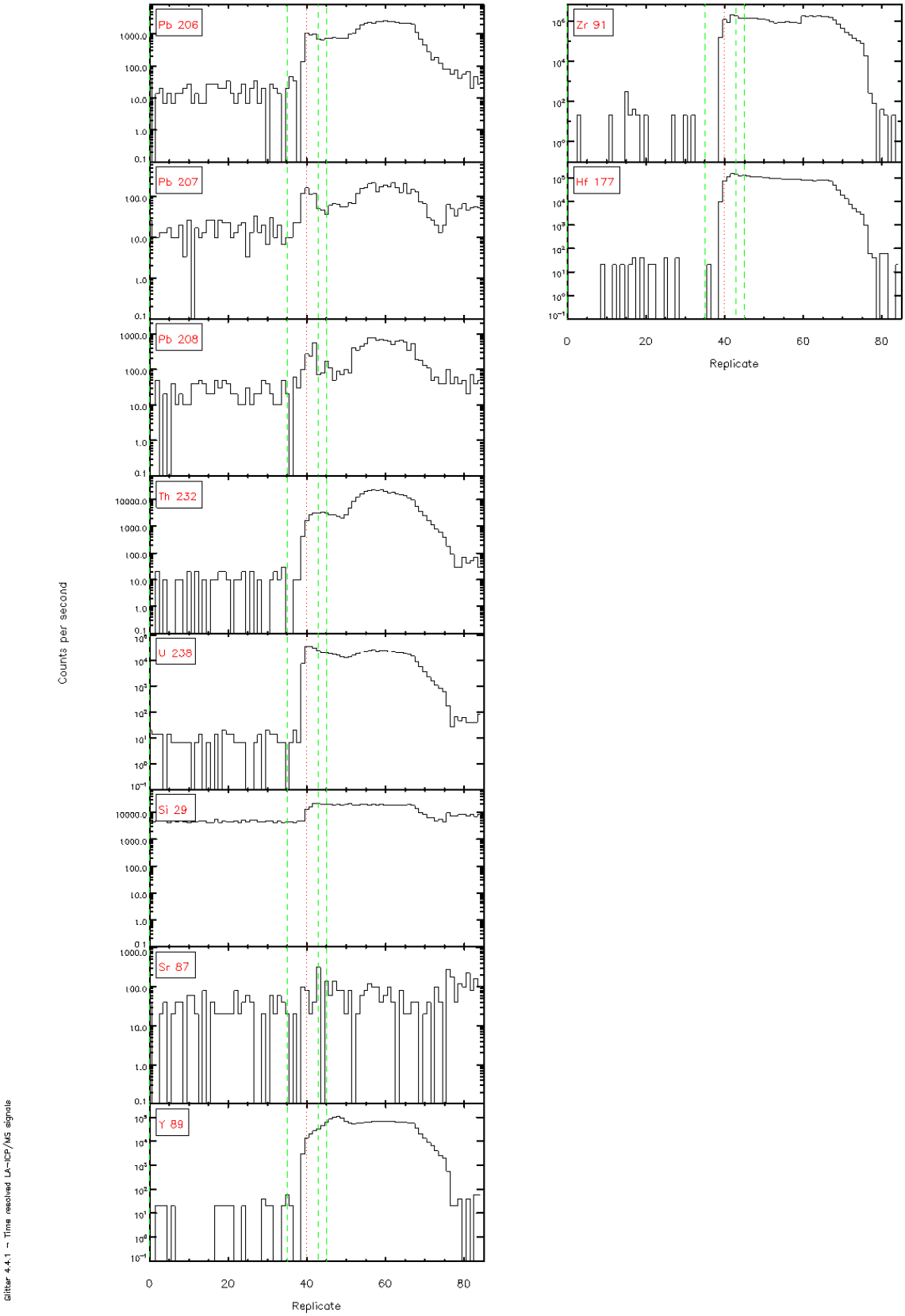
Pb 206
Pb 207
Pb 208
Th 232
U 238
Si 29
Sr 87
Y 89
Zr 91
Hf 177
Counts per second
Replicate
Glitter 4.4.1 - Time resolved LA-ICP/MS signals

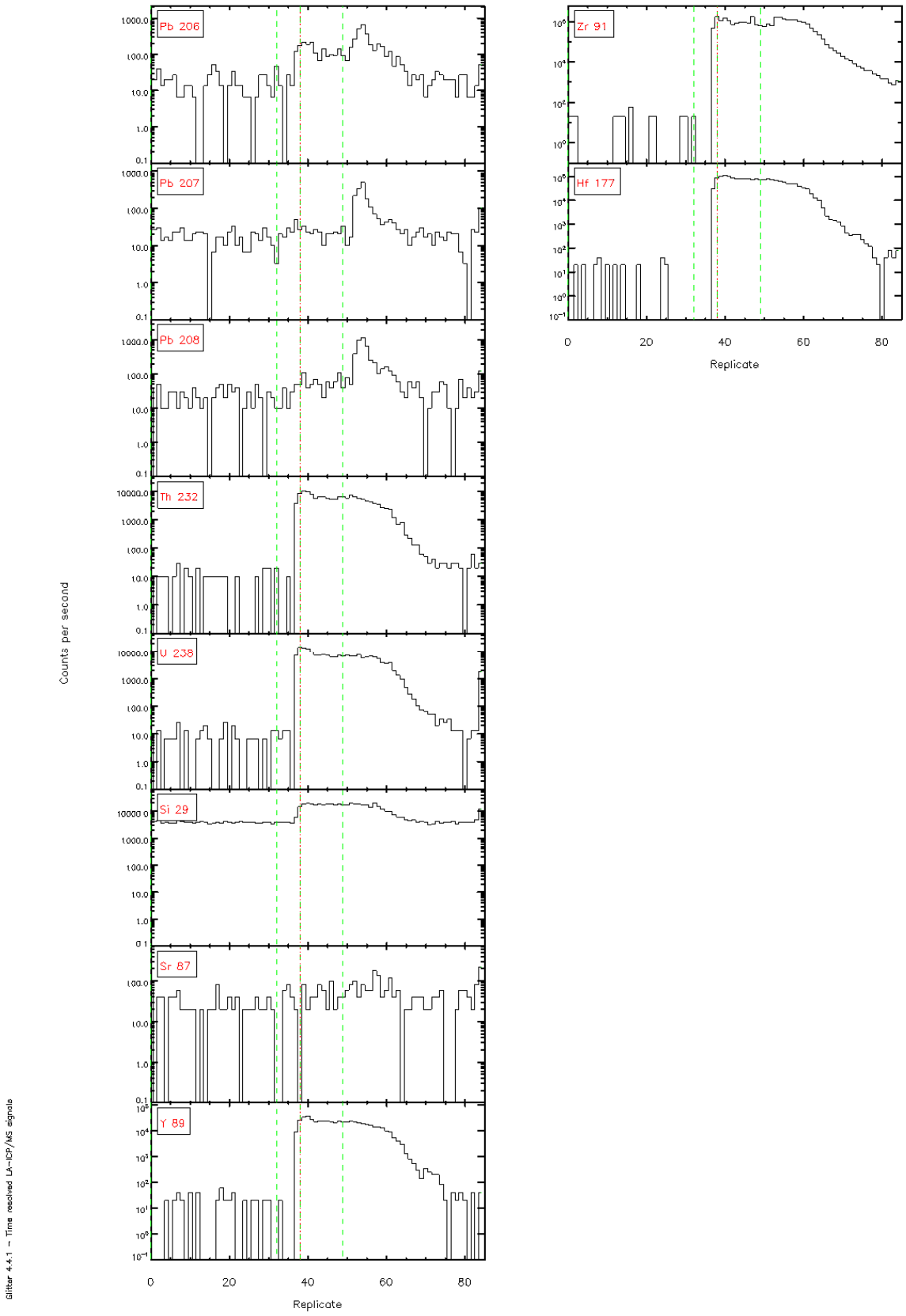
Pb 206
Pb 207
Pb 208
Th 232
U 238
Si 29
Sr 87
Y 89
Zr 91
Hf 177
Counts per second
Replicate
Glitter 4.4.1 - Time resolved LA-ICP/MS signals

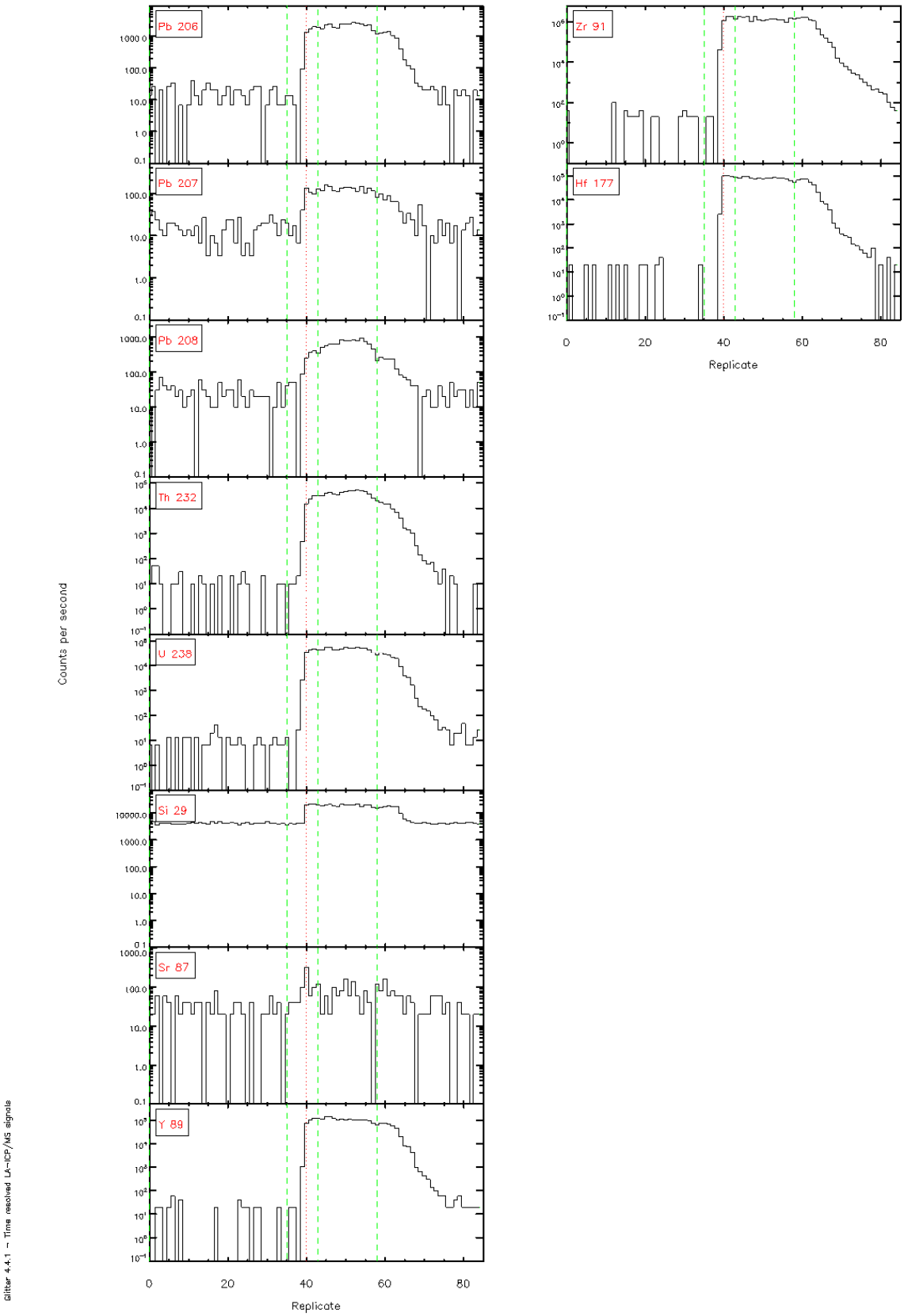
Pb 206
Pb 207
Pb 208
Th 232
U 238
Si 29
Sr 87
Y 89
Zr 91
Hf 177
Counts per second
Replicate
Glitter 4.4.1 - Time resolved LA-ICP/MS signals

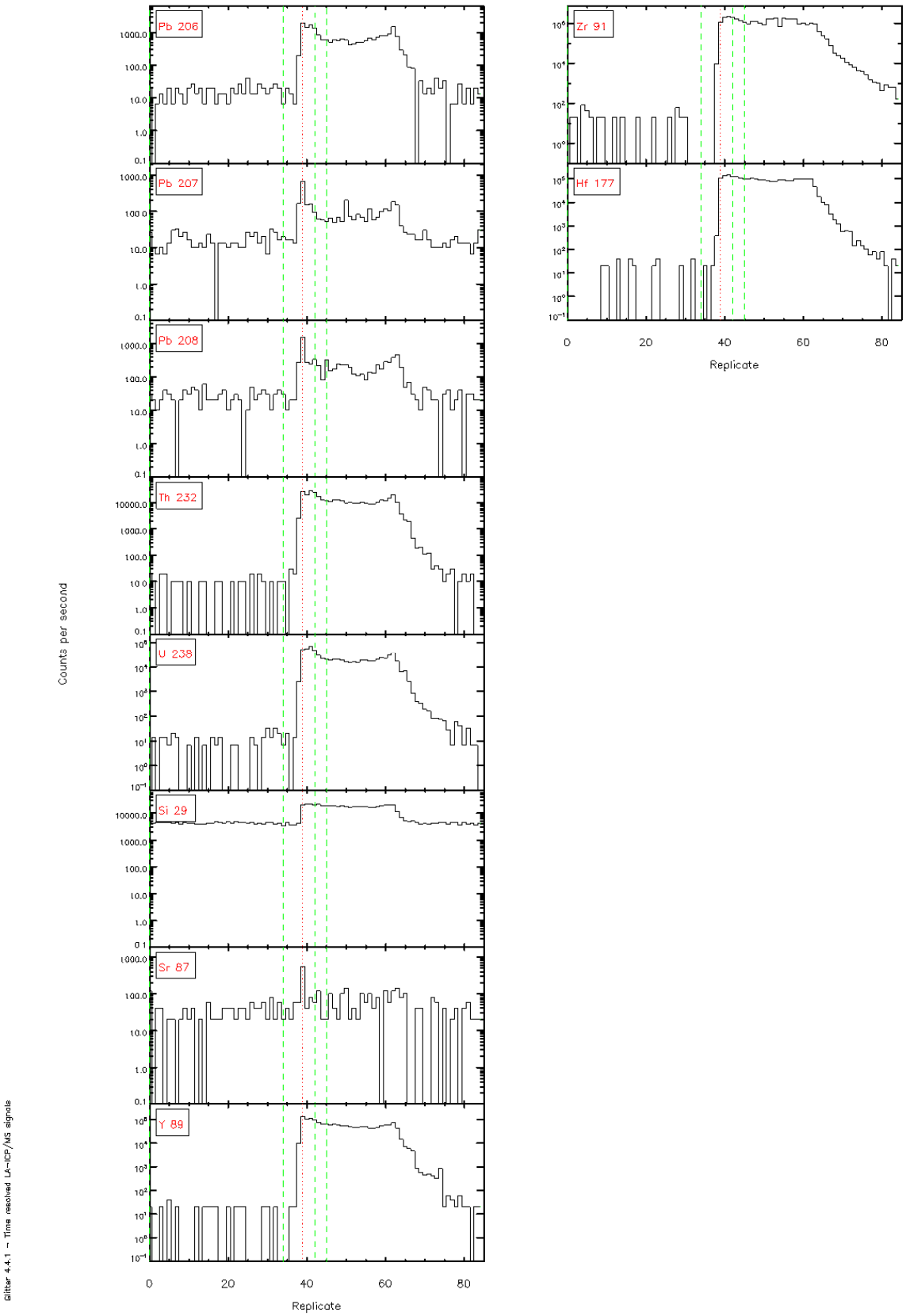
Pb 206
Pb 207
Pb 208
Th 232
U 238
Si 29
Sr 87
Y 89
Zr 91
Hf 177
Counts per second
Replicate
Glitter 4.4.1 - Time resolved LA-ICP/MS signals

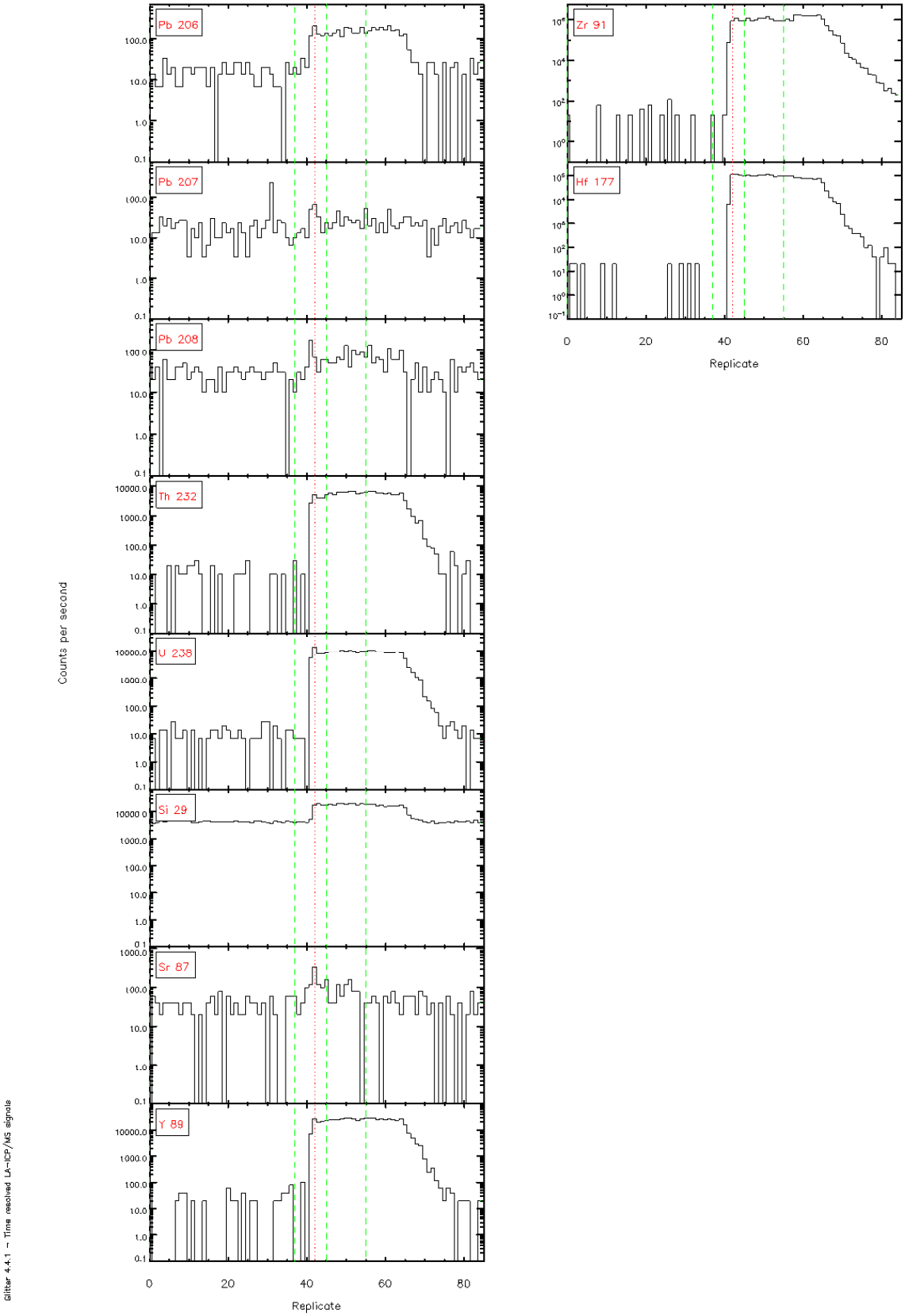
Pb 206
Pb 207
Pb 208
Th 232
U 238
Si 29
Sr 87
Y 89
Zr 91
Hf 177
Counts per second
Replicate
Glitter 4.4.1 - Time resolved LA-ICP/MS signals

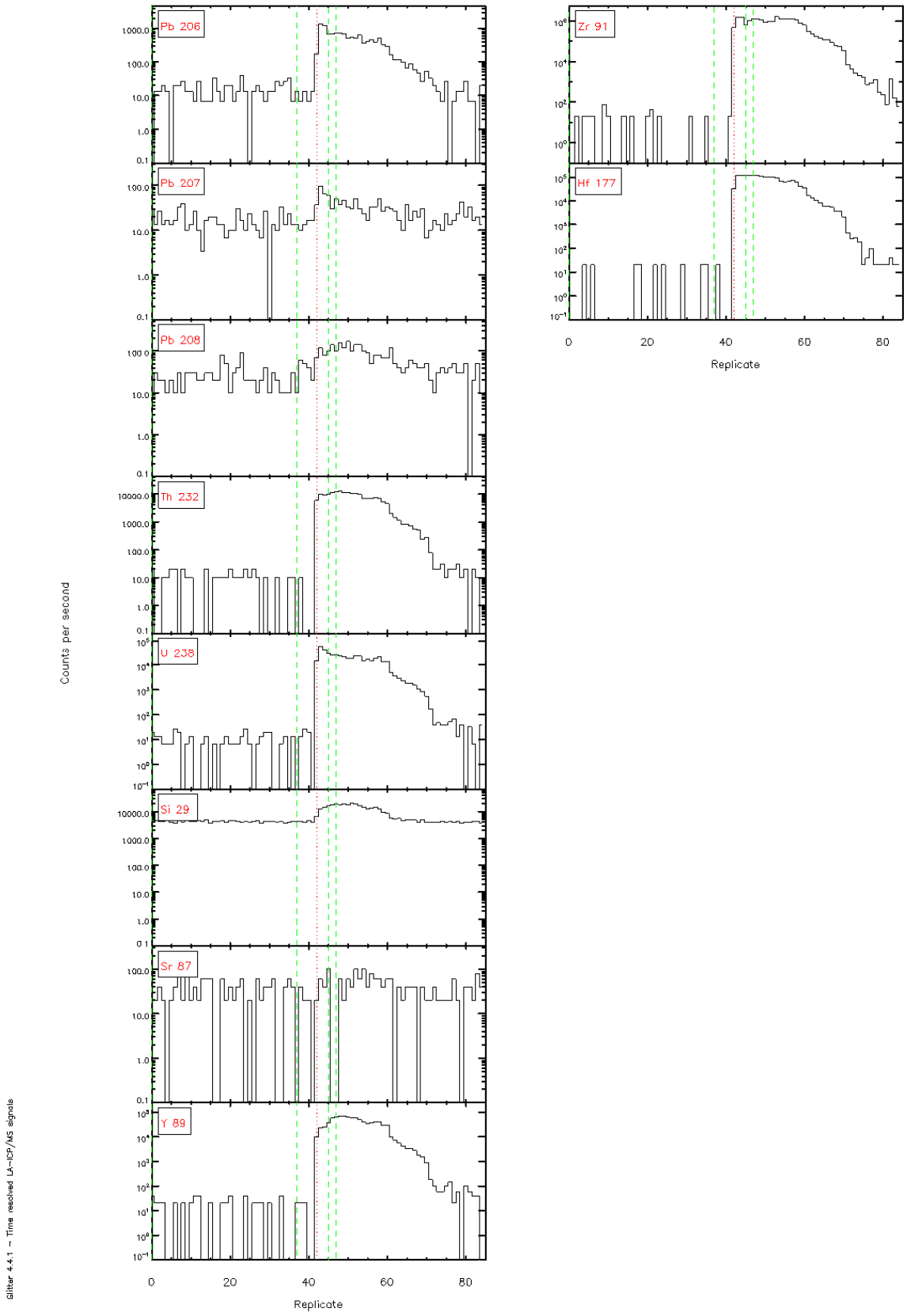
Pb 206
Pb 207
Pb 208
Th 232
U 238
Si 29
Sr 87
Y 89
Zr 91
Hf 177
Counts per second
Replicate
Glitter 4.4.1 - Time resolved LA-ICP/MS signals

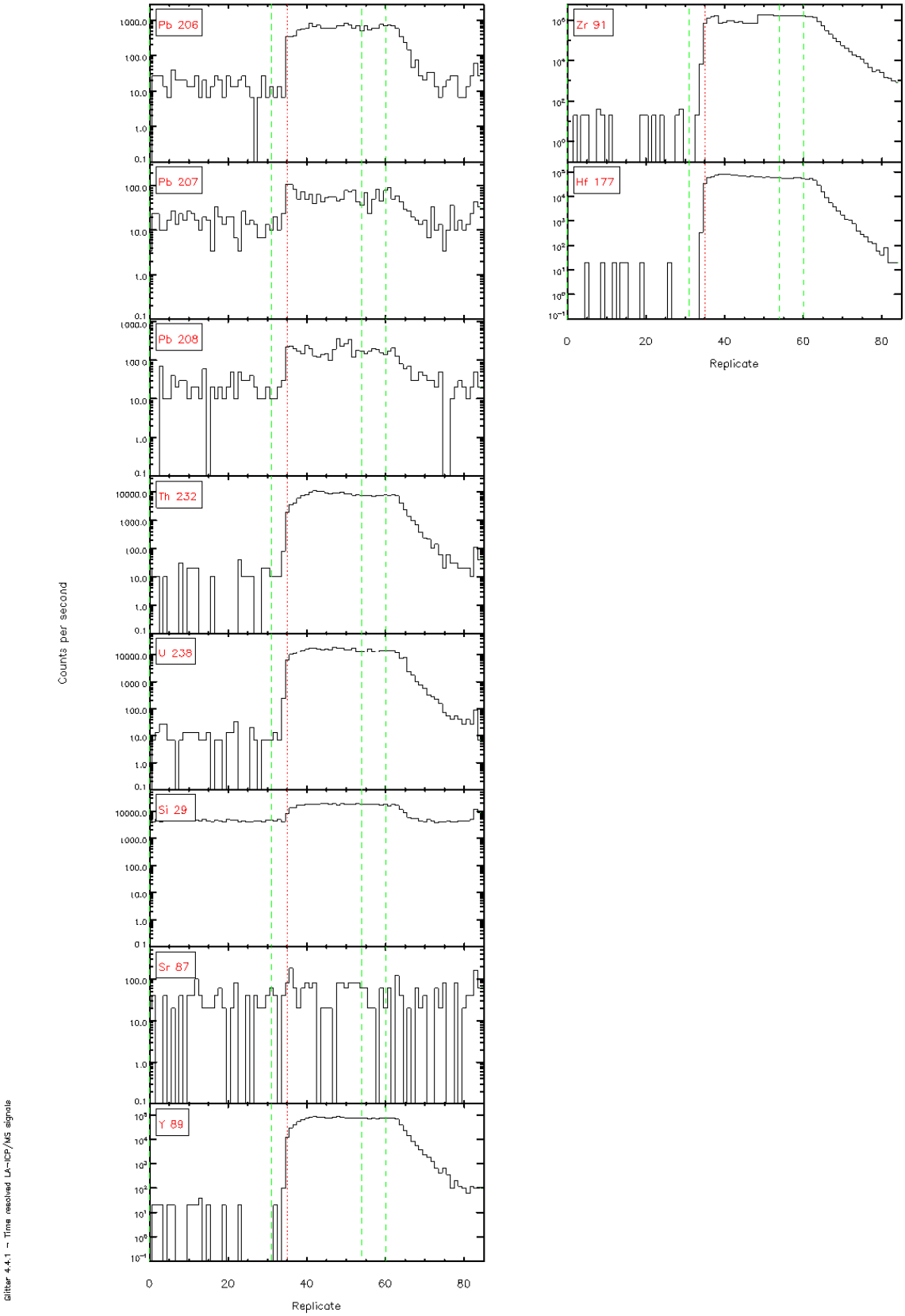
Pb 206
Pb 207
Pb 208
Th 232
U 238
Si 29
Sr 87
Y 89
Zr 91
Hf 177
Counts per second
Replicate
Glitter 4.4.1 – Time resolved LA-ICP/MS signals

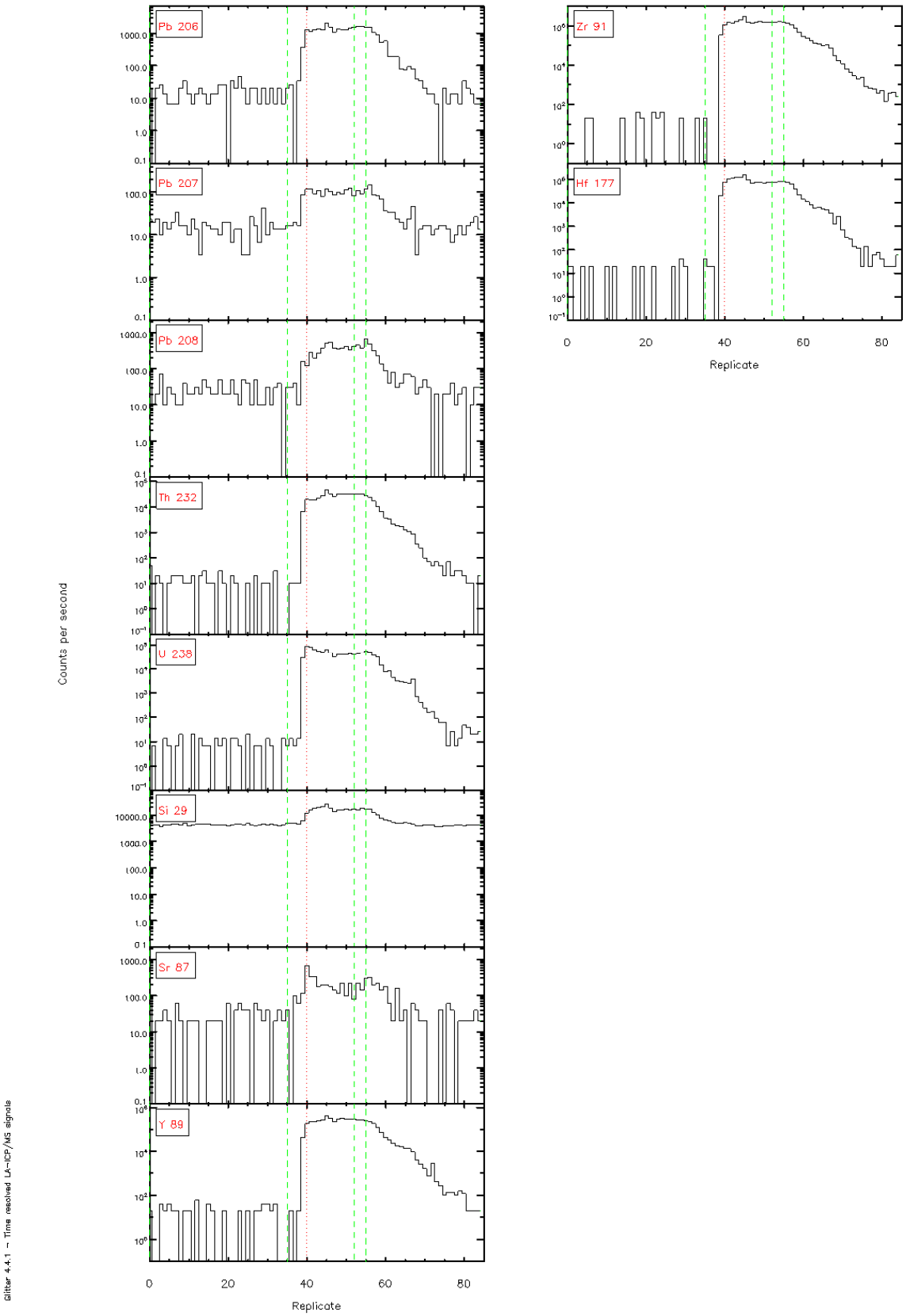
Pb 206
Pb 207
Pb 208
Th 232
U 238
Si 29
Sr 87
Y 89
Zr 91
Hf 177
Counts per second
Replicate
Glitter 4.4.1 - Time resolved LA-ICP/MS signals

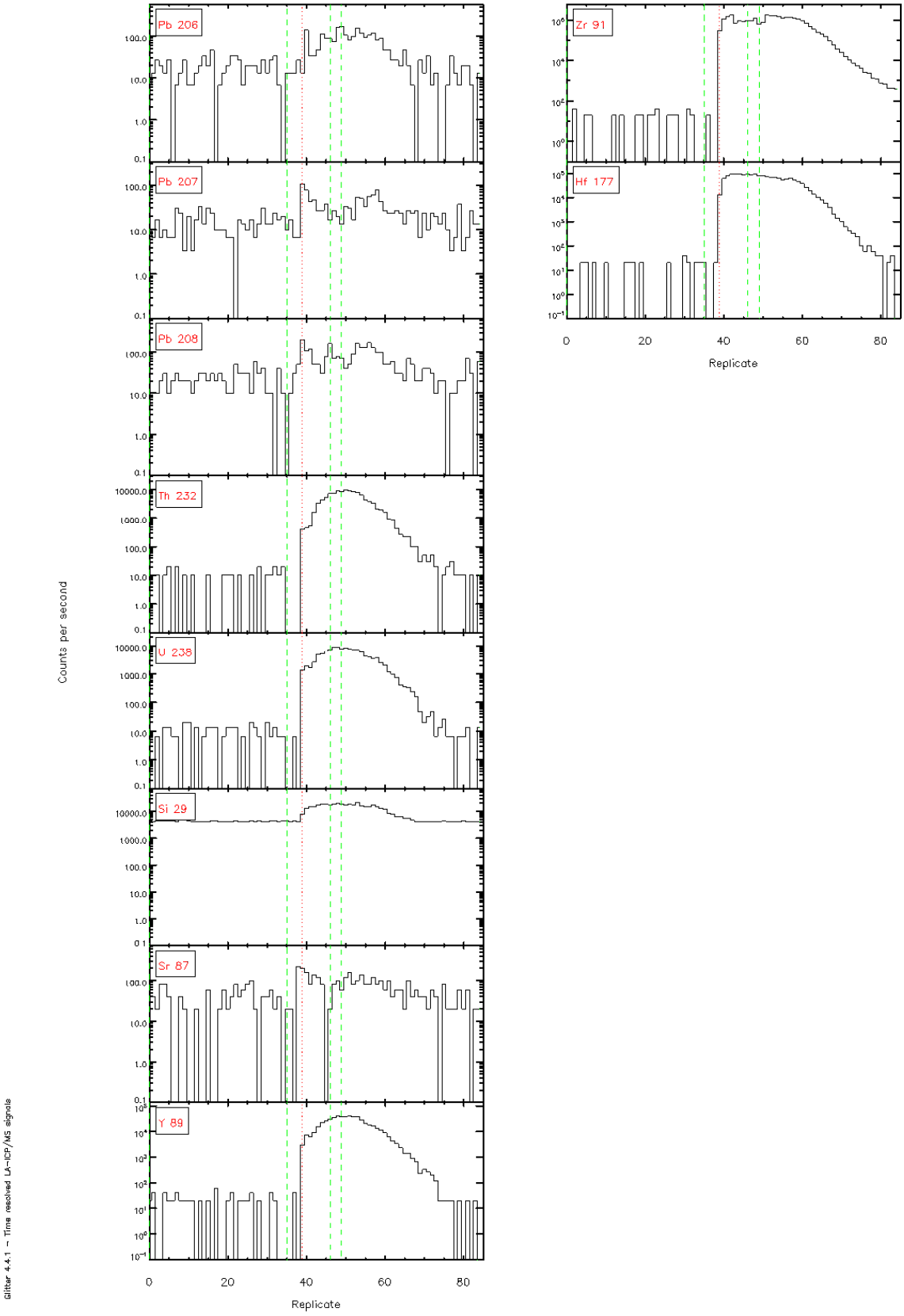
Pb 206
Pb 207
Pb 208
Th 232
U 238
Si 29
Sr 87
Y 89
Zr 91
Hf 177
Counts per second
Replicate
Glitter 4.4.1 - Time resolved LA-ICP/MS signals

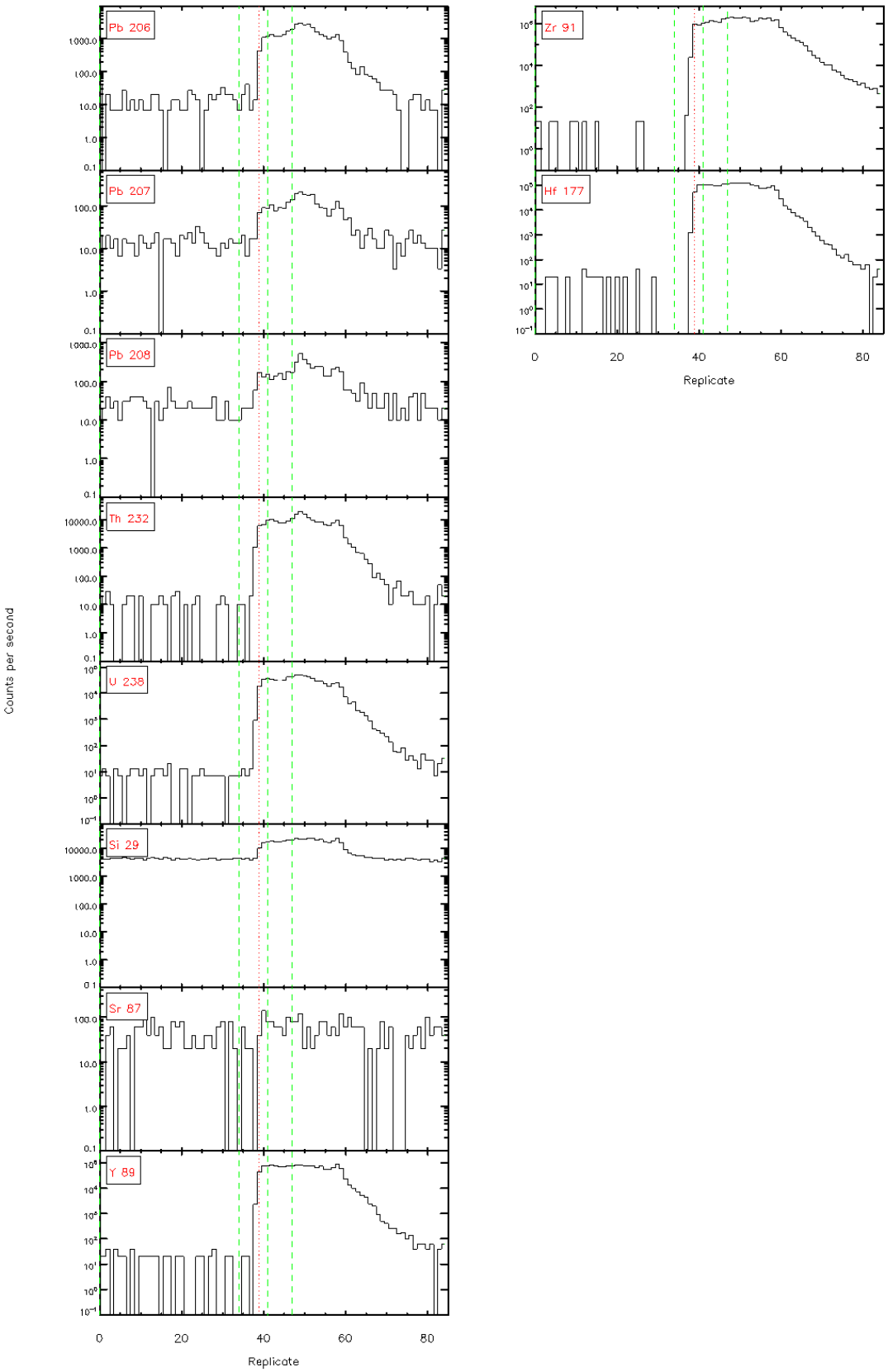
Pb 206
Pb 207
Pb 208
Th 232
U 238
Si 29
Sr 87
Y 89
Zr 91
Hf 177
Counts per second
Replicate
Glitter 4.4.1 - Time resolved LA-ICP/MS signals

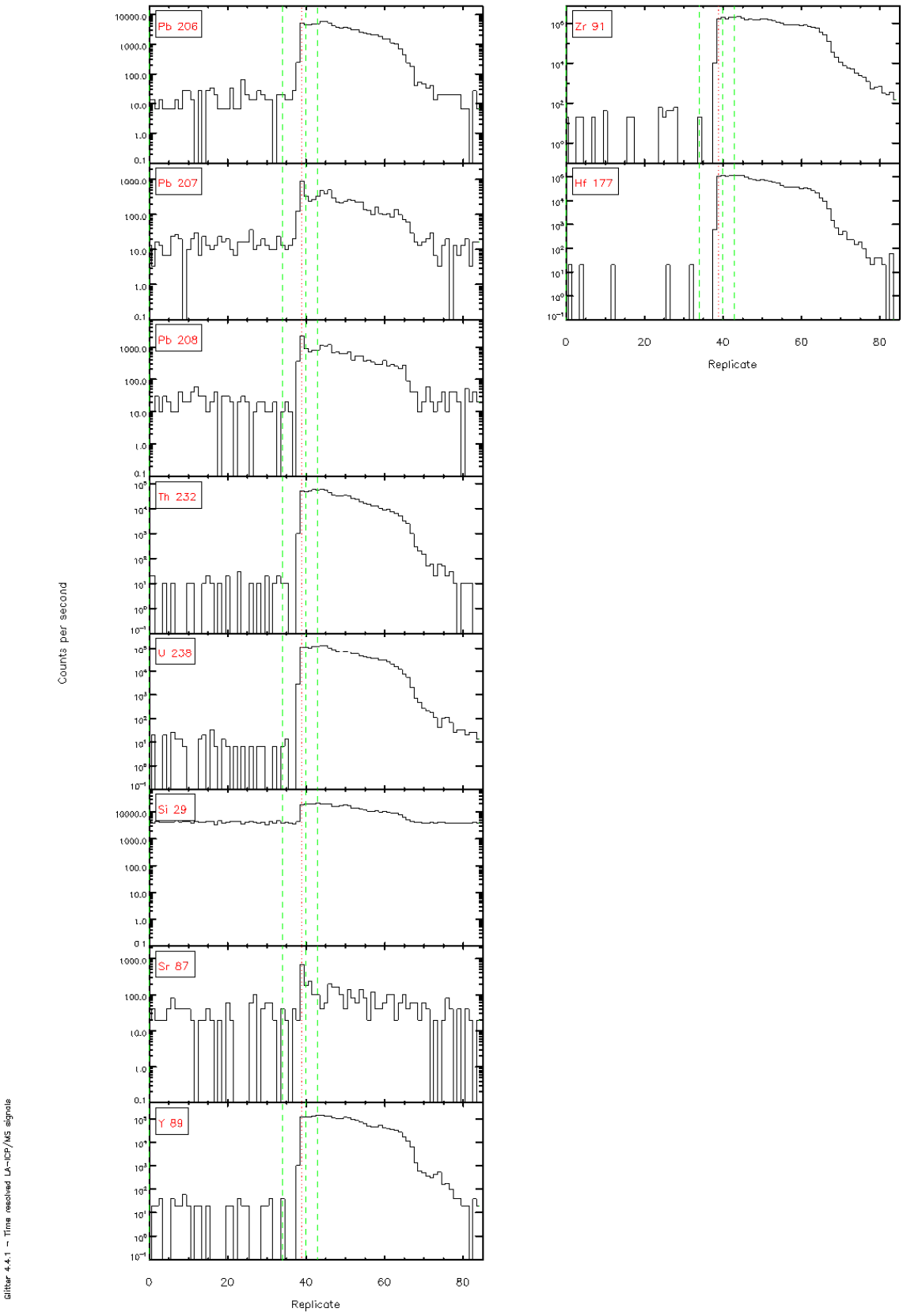
Pb 206
Pb 207
Pb 208
Th 232
U 238
Si 29
Sr 87
Y 89
Zr 91
Hf 177
Counts per second
Replicate
Glitter 4.4.1 - Time resolved LA-ICP/MS signals

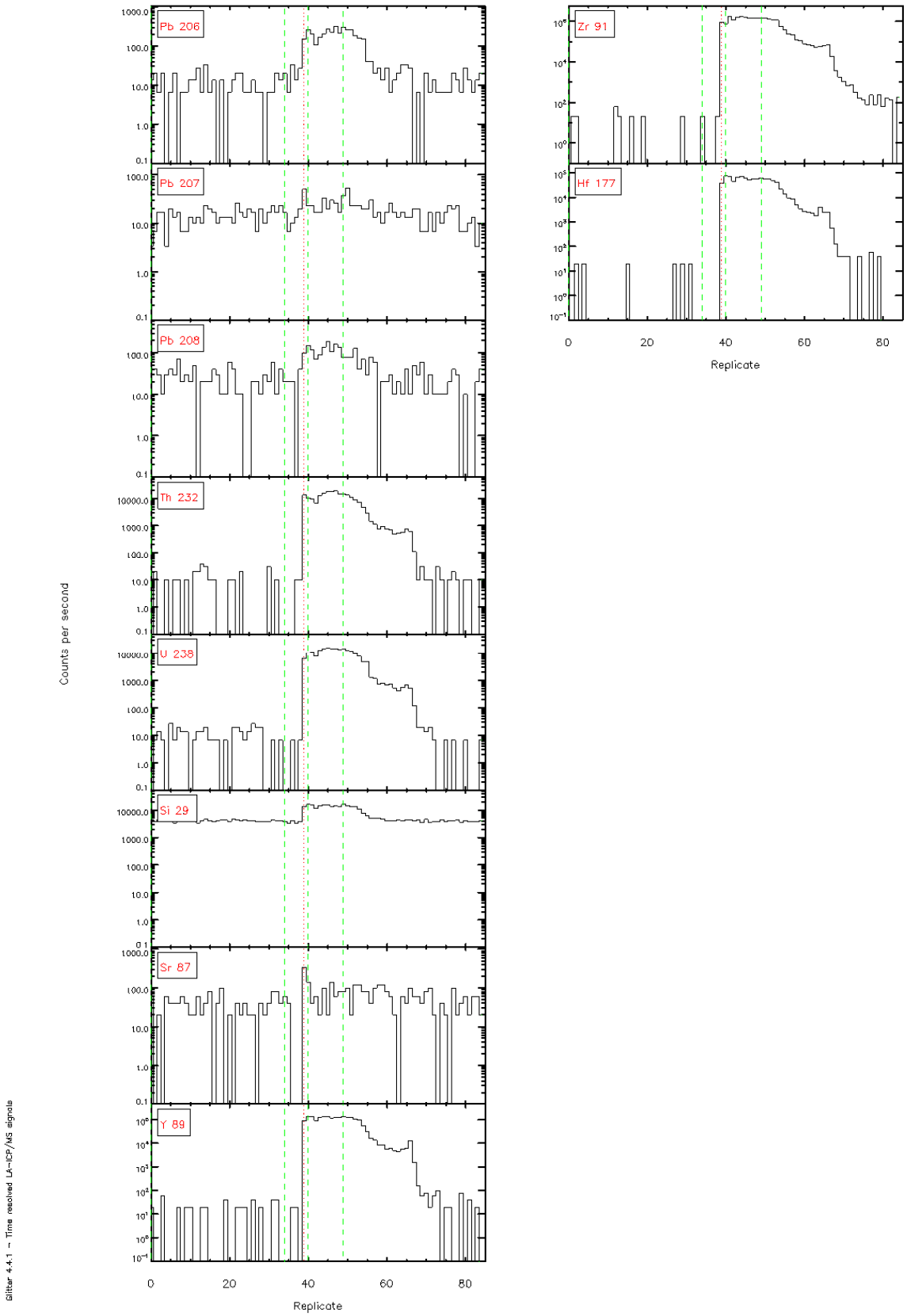
Pb 206
Pb 207
Pb 208
Th 232
U 238
Si 29
Sr 87
Y 89
Zr 91
Hf 177
Counts per second
Replicate
Glitter 4.4.1 - Time resolved LA-ICP/MS signals

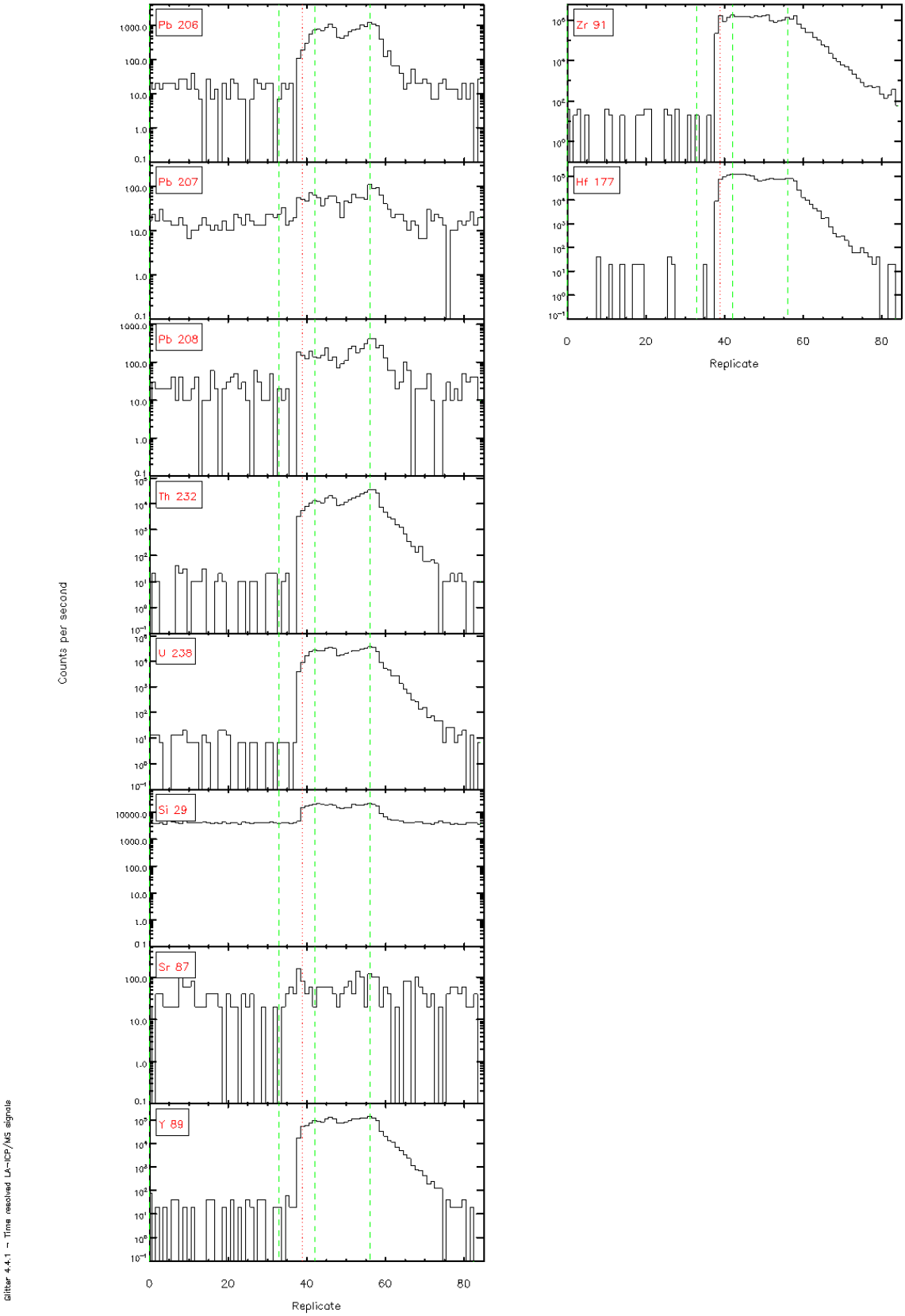
Pb 206
Pb 207
Pb 208
Th 232
U 238
Si 29
Sr 87
Y 89
Zr 91
Hf 177
Counts per second
Replicate
Glitter 4.4.1 - Time resolved LA-ICP/MS signals

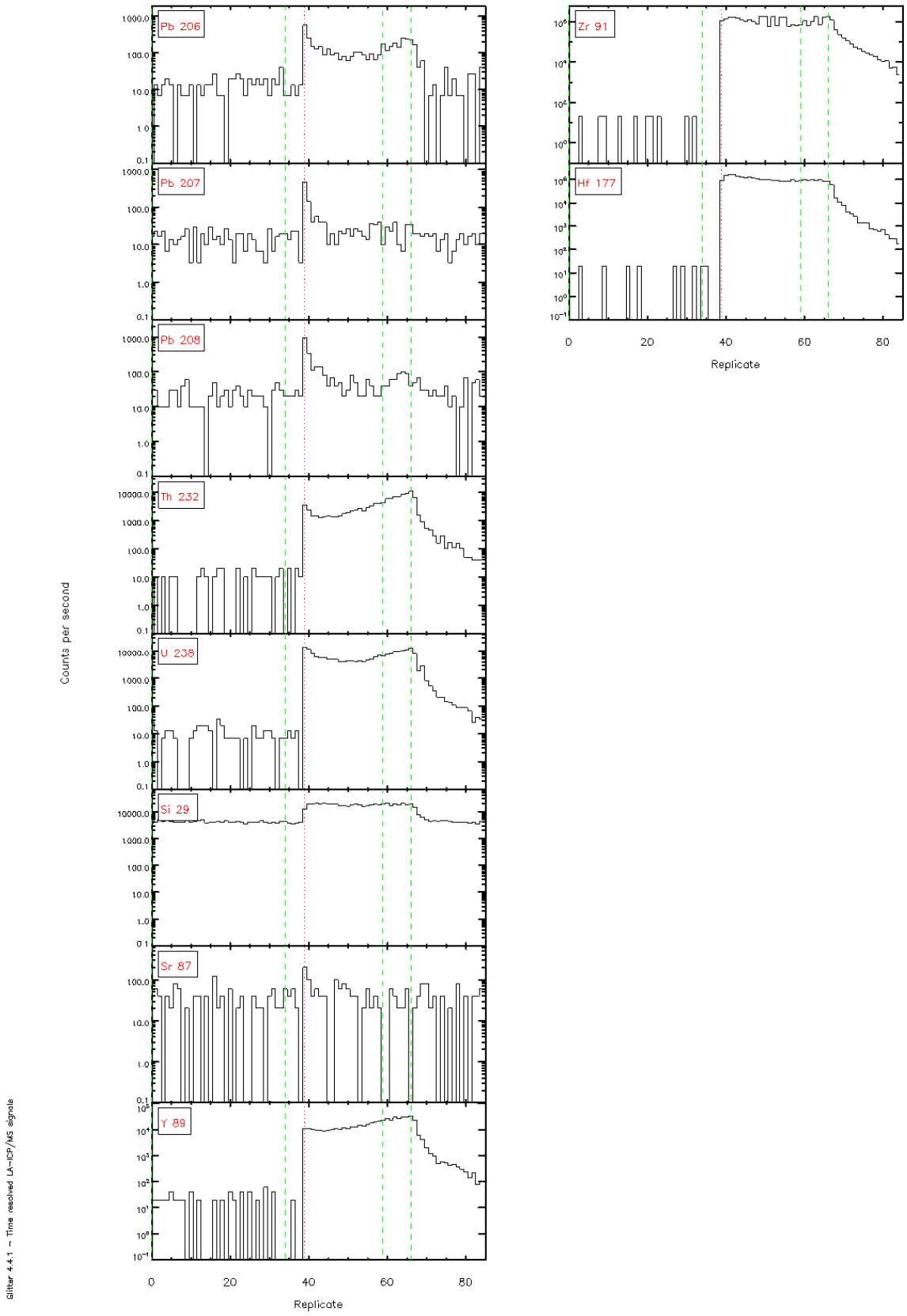
Pb 206
Pb 207
Pb 208
Th 232
U 238
Si 29
Sr 87
Y 89
Zr 91
Hf 177
Counts per second
Replicate
Glitter 4.4.1 - Time resolved LA-ICP/MS signals

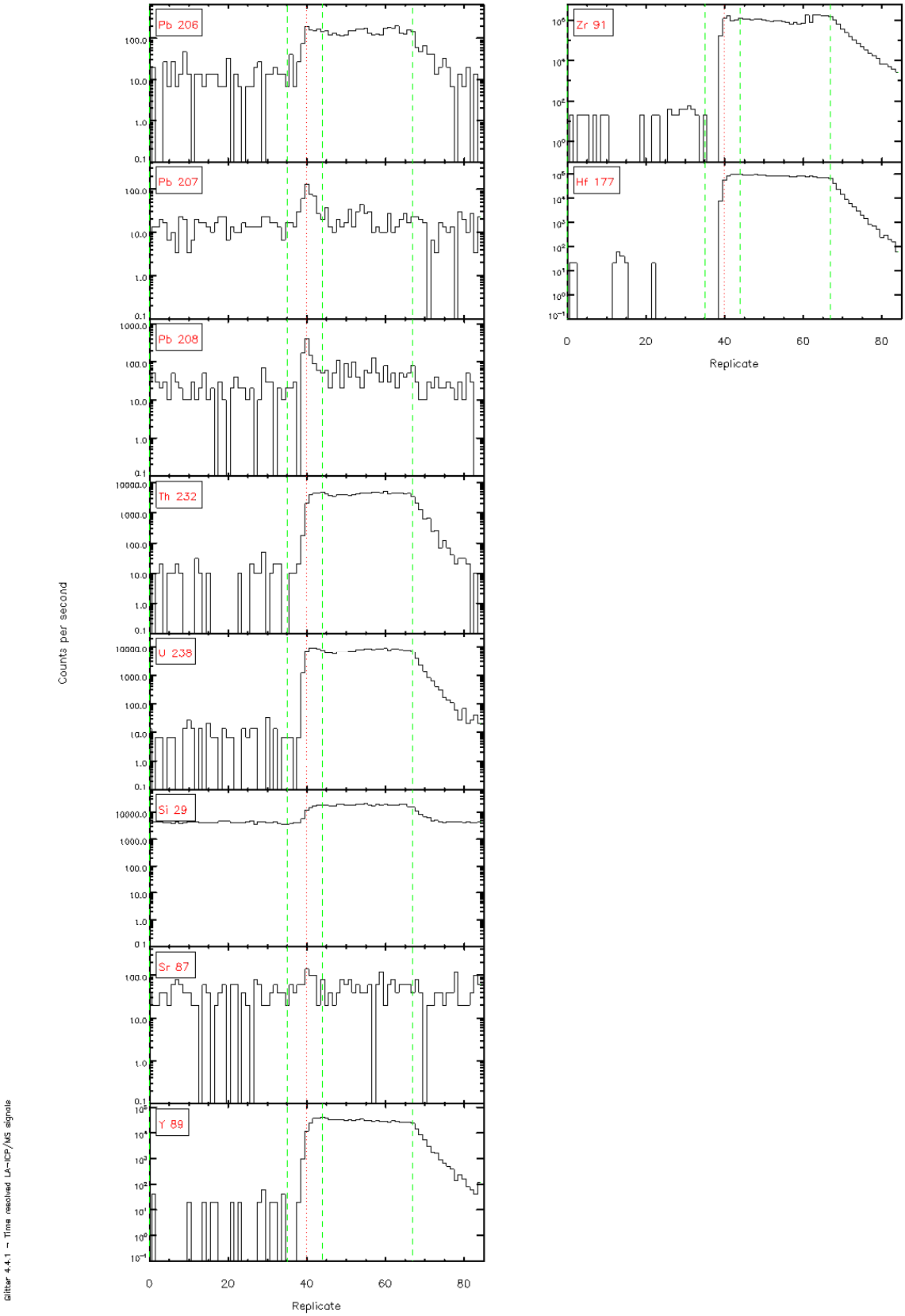
Pb 206
Pb 207
Pb 208
Th 232
U 238
Si 29
Sr 87
Y 89
Zr 91
Hf 177
Counts per second
Replicate
Glitter 4.4.1 - Time resolved LA-ICP/MS signals

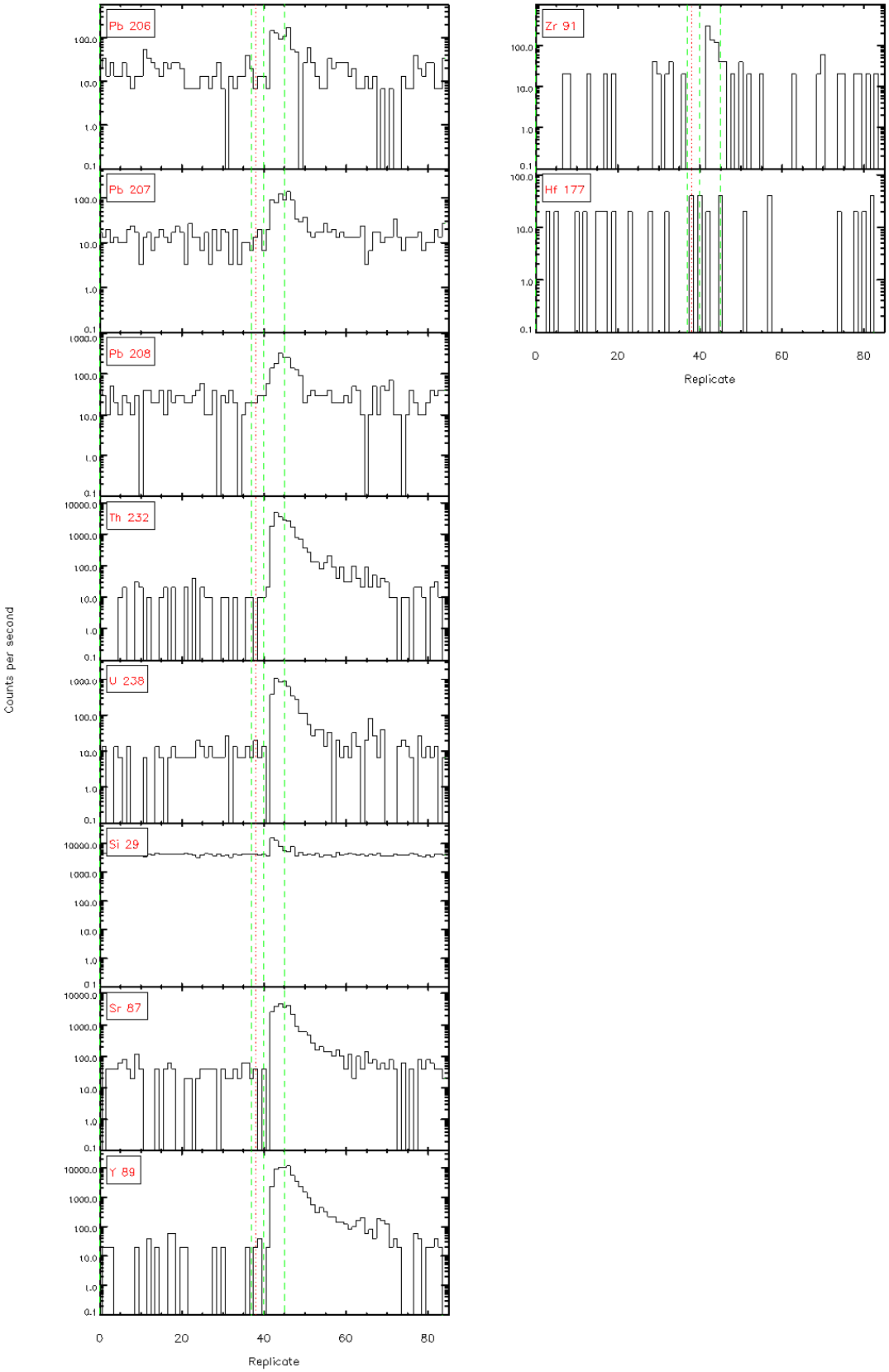
Pb 206
Pb 207
Pb 208
Th 232
U 238
Si 29
Sr 87
Y 89
Zr 91
Hf 177
Counts per second
Replicate
Glitter 4.4.1 - Time resolved LA-ICP/MS signals

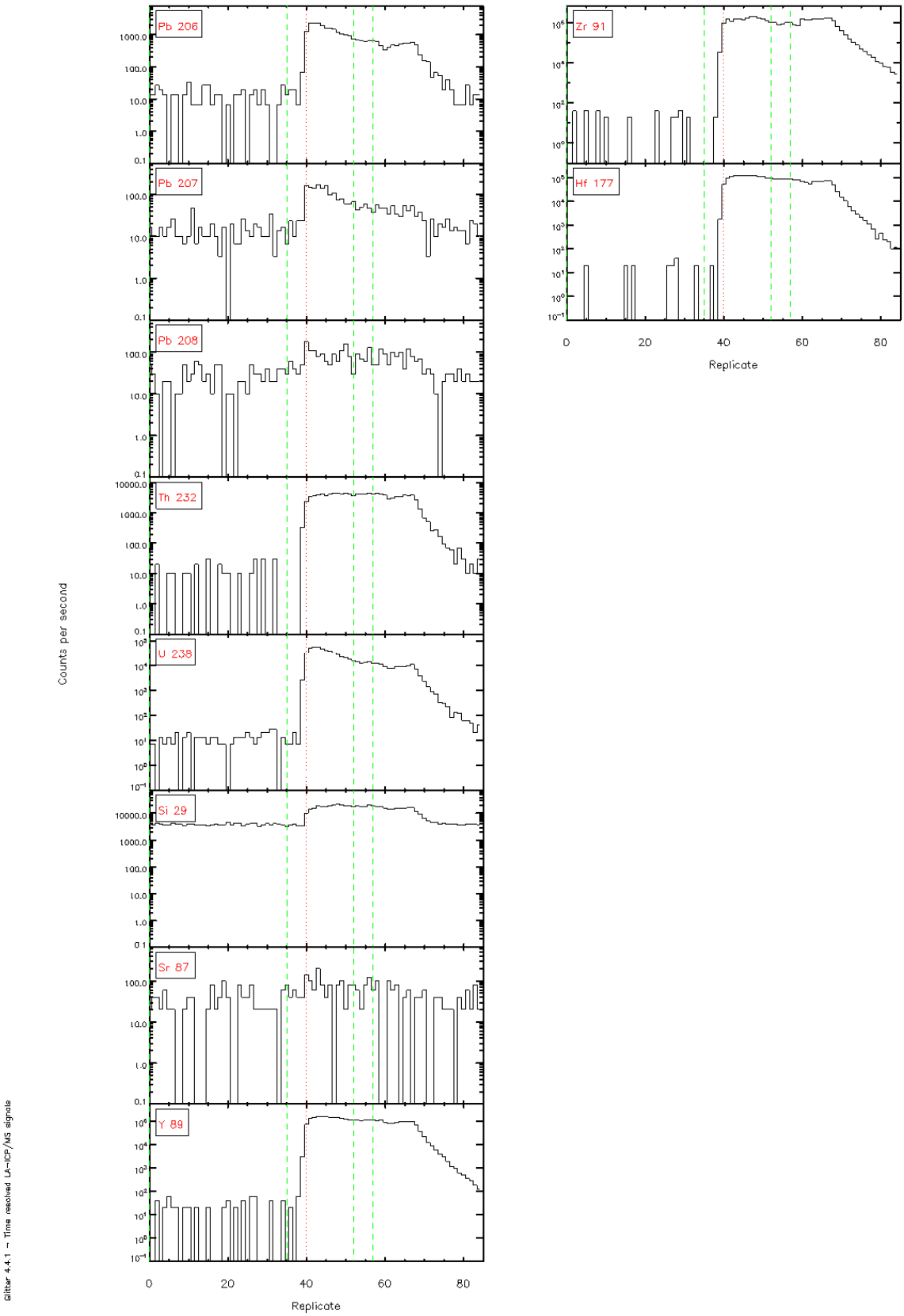
Pb 206
Pb 207
Pb 208
Th 232
U 238
Si 29
Sr 87
Y 89
Zr 91
Hf 177
Counts per second
Replicate
Glitter 4.4.1 - Time resolved LA-ICP/MS signals

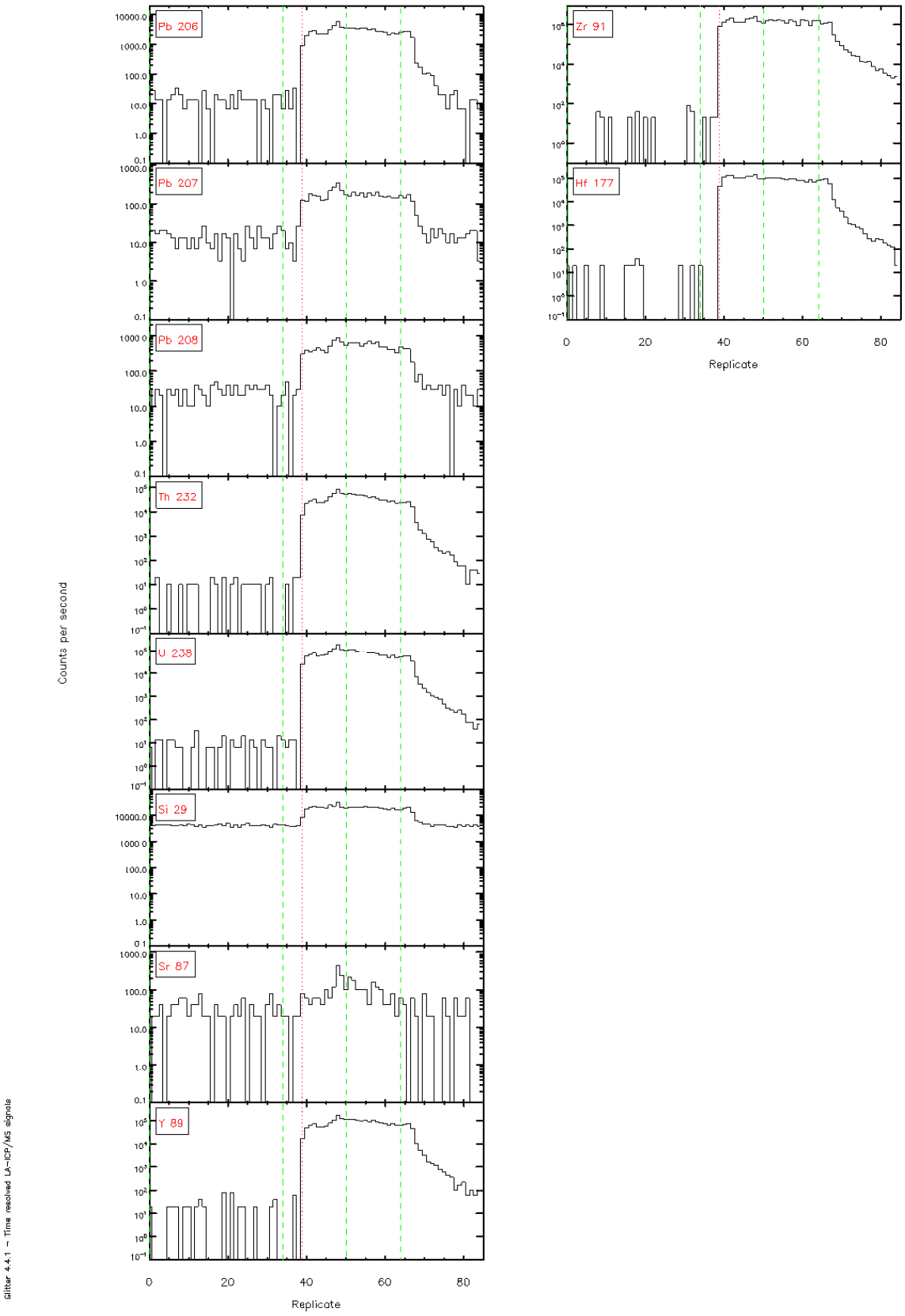
Pb 206
Pb 207
Pb 208
Th 232
U 238
Si 29
Sr 87
Y 89
Zr 91
Hf 177
Counts per second
Replicate
Glitter 4.4.1 - Time resolved LA-ICP/MS signals

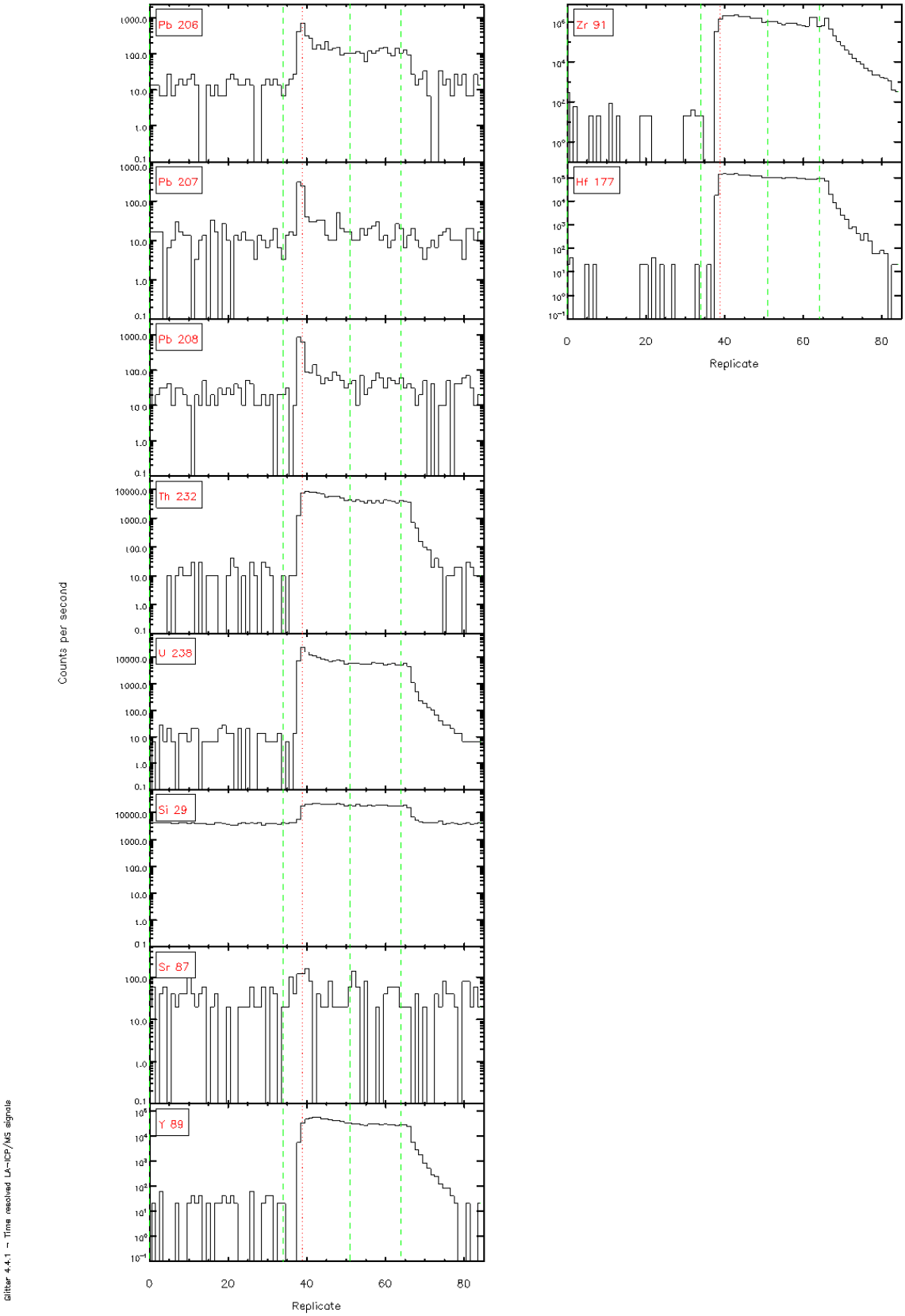
Pb 206
Pb 207
Pb 208
Th 232
U 238
Si 29
Sr 87
Y 89
Zr 91
Hf 177
Counts per second
Replicate
Glitter 4.4.1 - Time resolved LA-ICP/MS signals

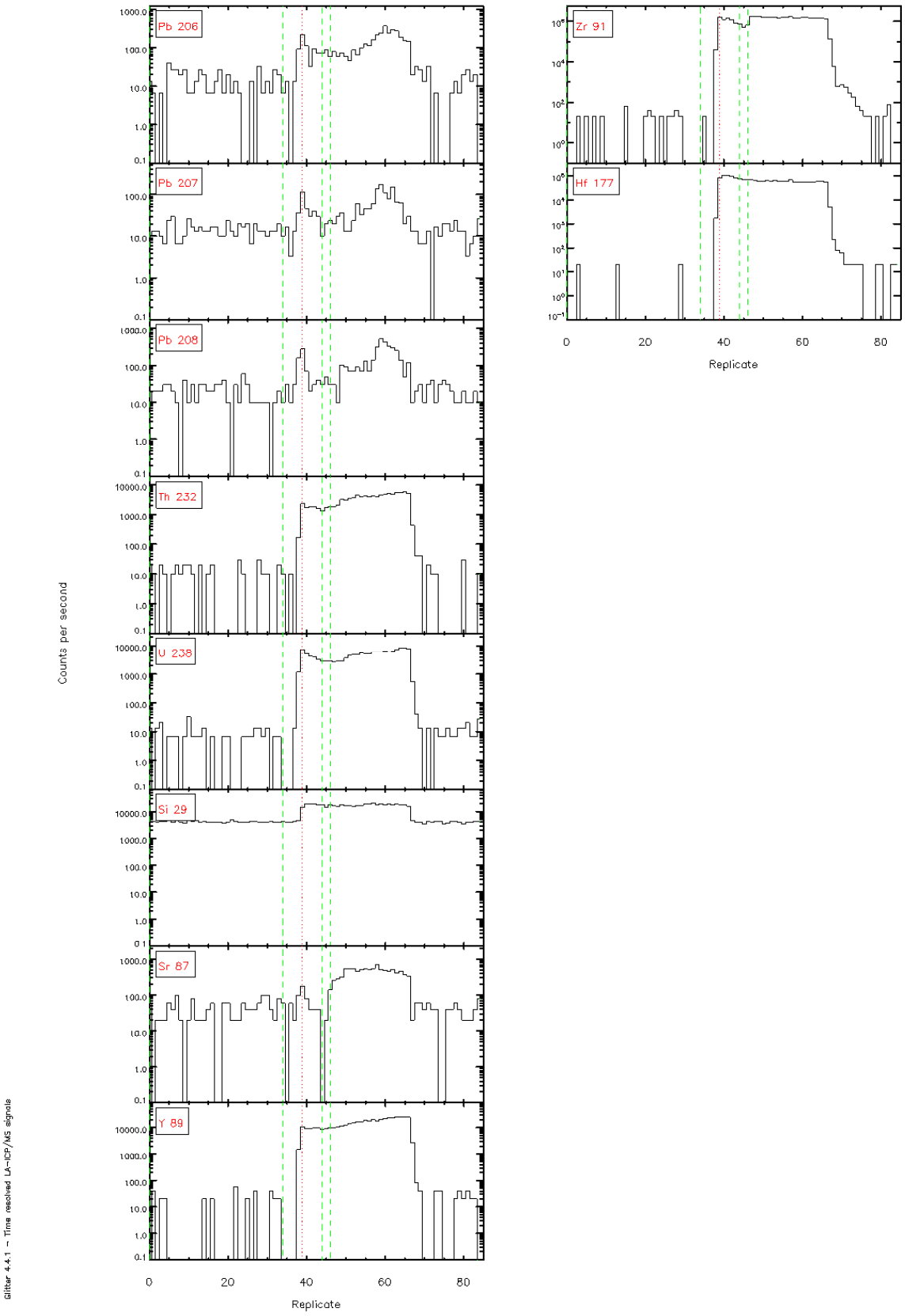
Pb 206
Pb 207
Pb 208
Th 232
U 238
Si 29
Sr 87
Y 89
Zr 91
Hf 177
Counts per second
Replicate
Glitter 4.4.1 - Time resolved LA-ICP/MS signals

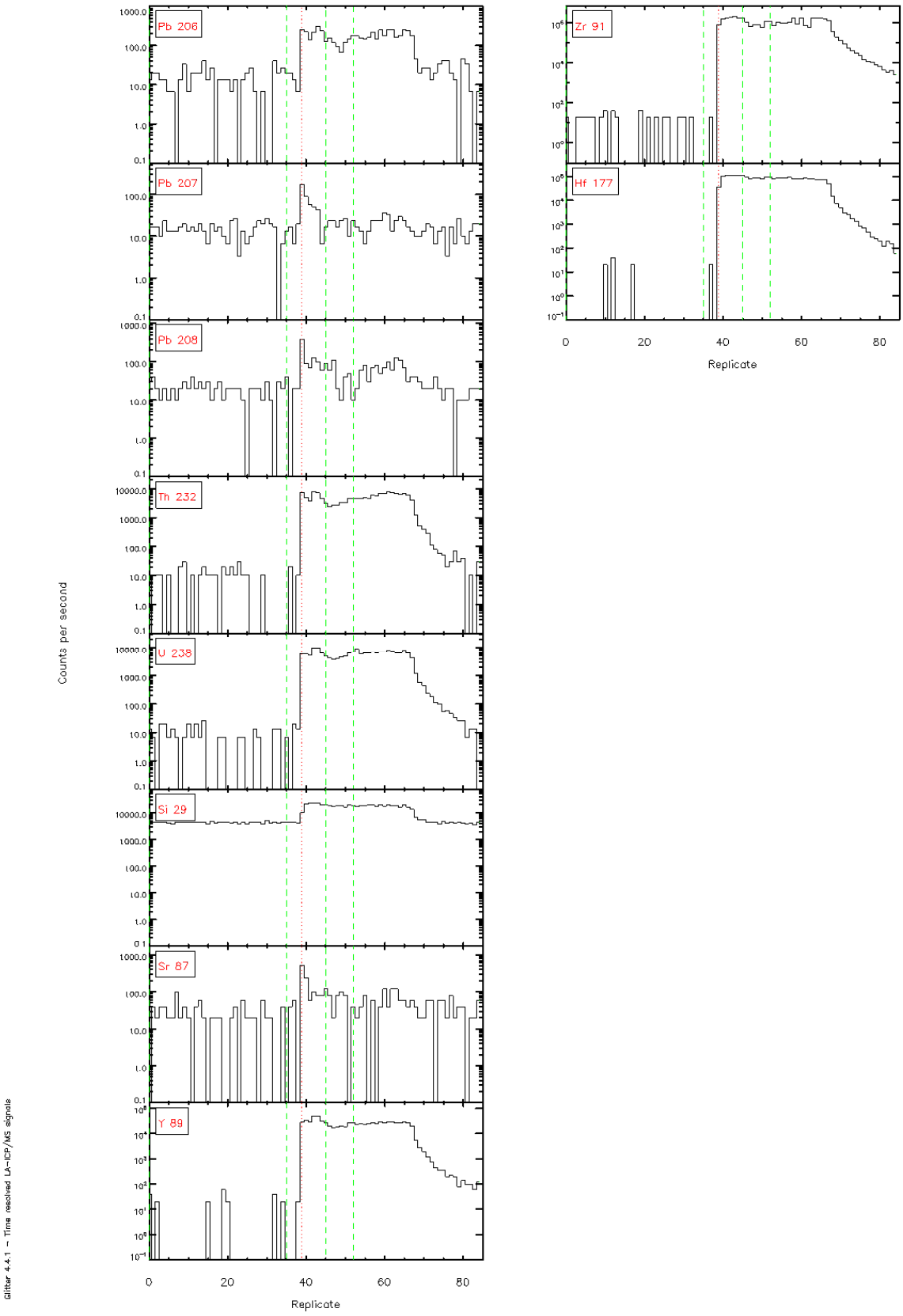
Pb 206
Pb 207
Pb 208
Th 232
U 238
Si 29
Sr 87
Y 89
Zr 91
Hf 177
Counts per second
Replicate
Glitter 4.4.1 – Time resolved LA-ICP/MS signals

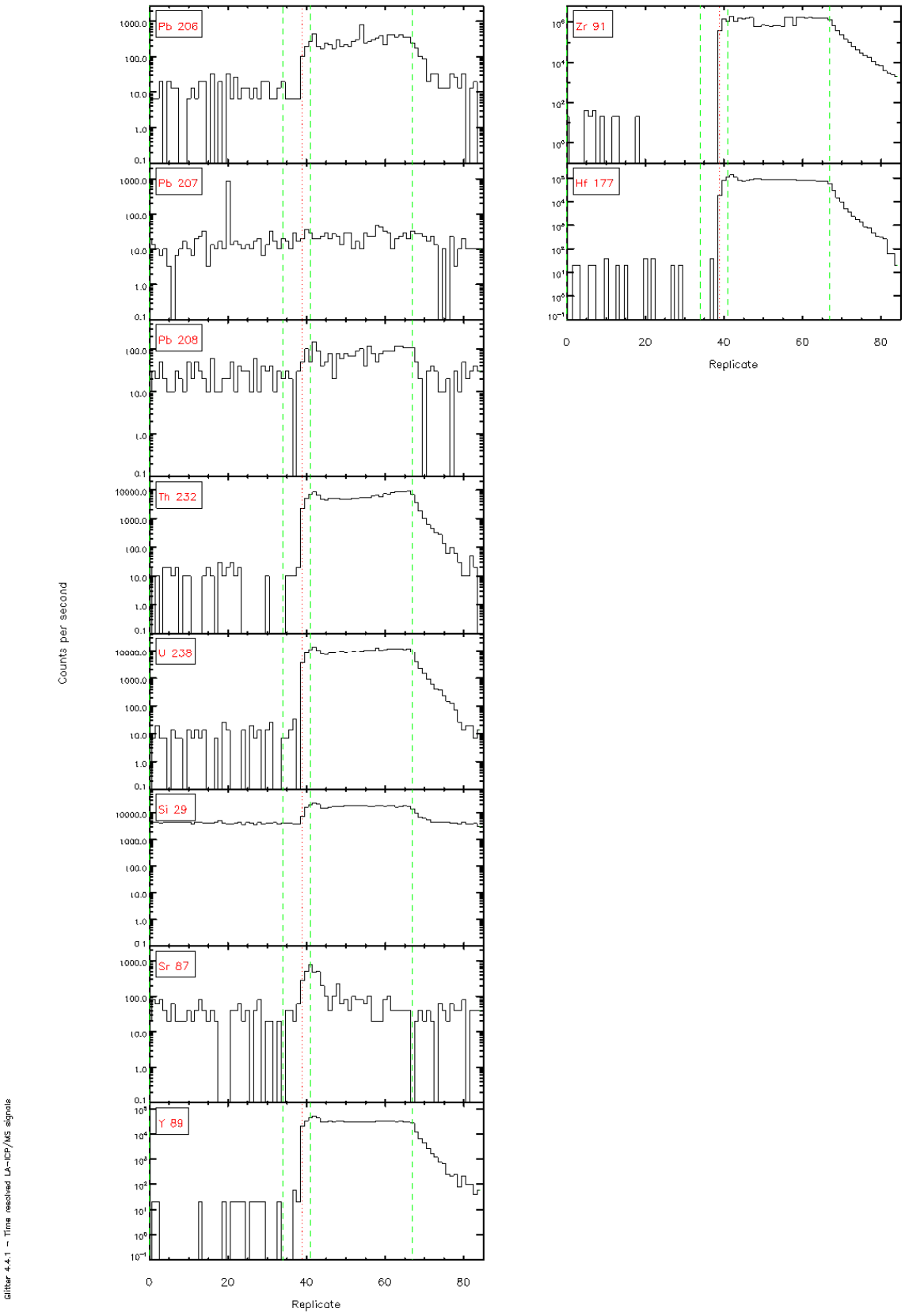
Pb 206
Pb 207
Pb 208
Th 232
U 238
Si 29
Sr 87
Y 89
Zr 91
Hf 177
Counts per second
Replicate
Glitter 4.4.1 - Time resolved LA-ICP/MS signals

7 – Taumarunui quartz sandstone

6.

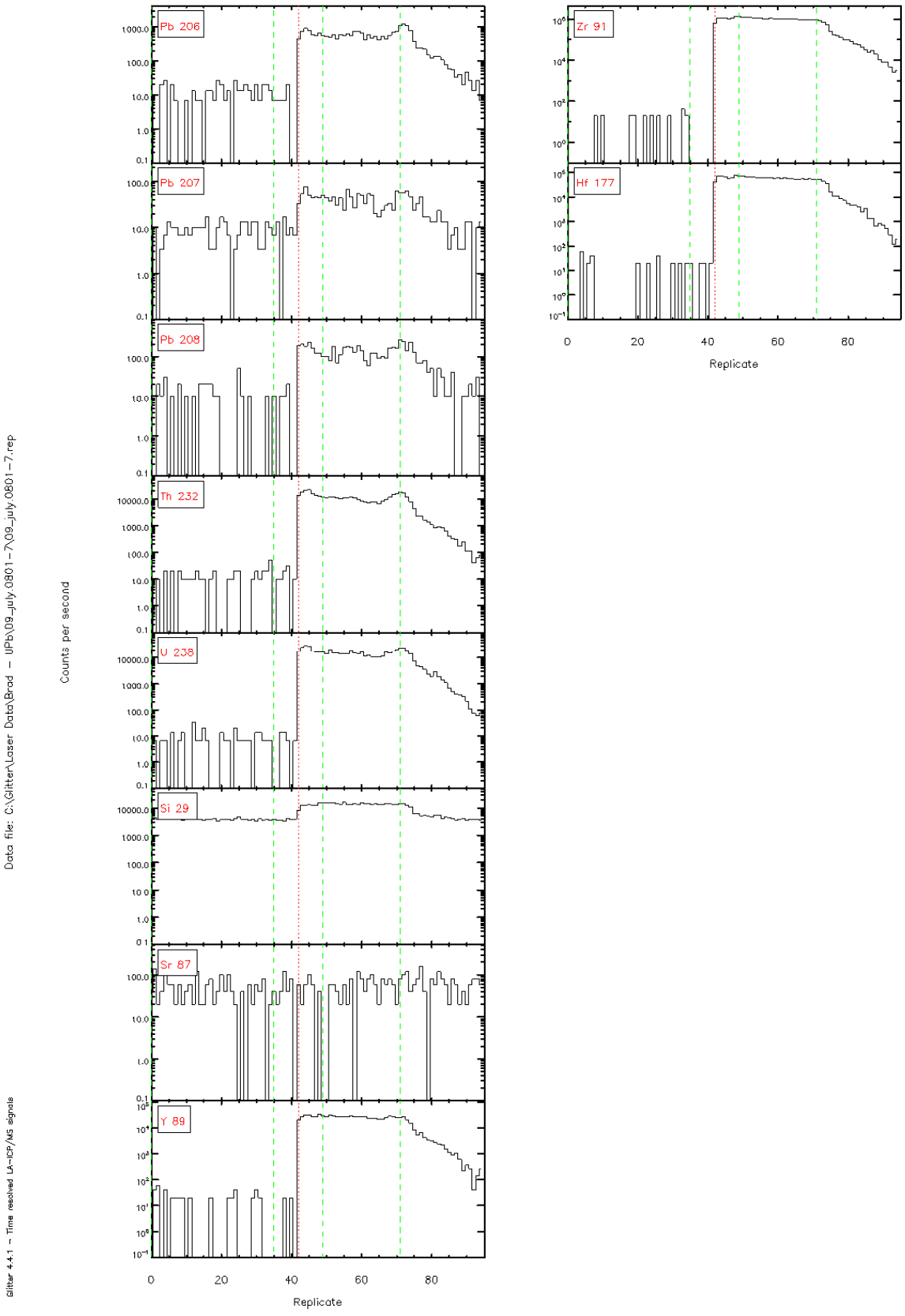

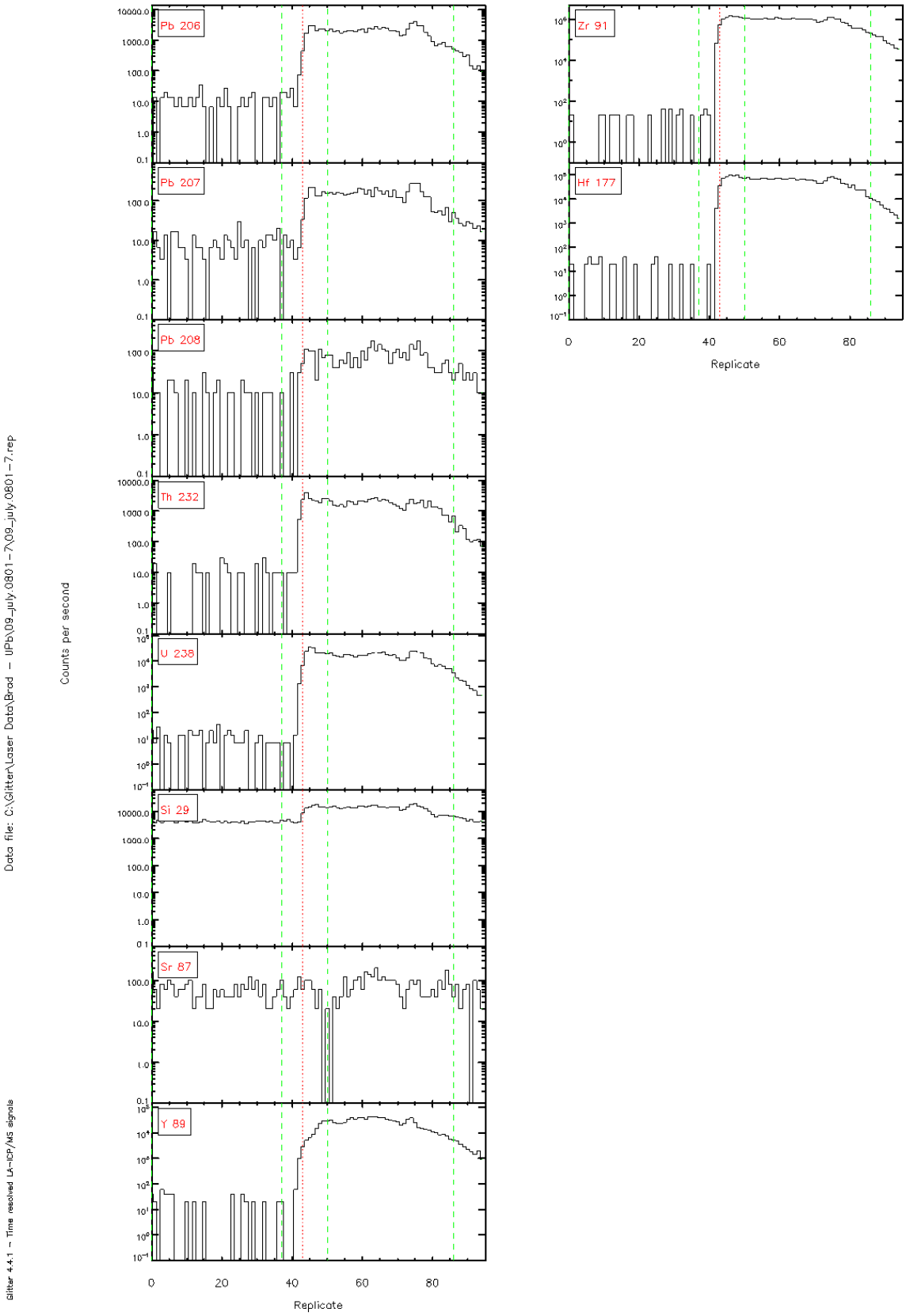
Pb 206
Pb 207
Pb 208
Th 232
U 238
Si 29
Sr 87
Y 89
Zr 91
Hf 177
Counts per second
Replicate
Data file: C:\Glitter\Laser Data\Brad - UPb\09_july.0801-7\09_july.0801-7.rep
Glitter 4.4.1 - Time resolved LA-ICP/MS signals

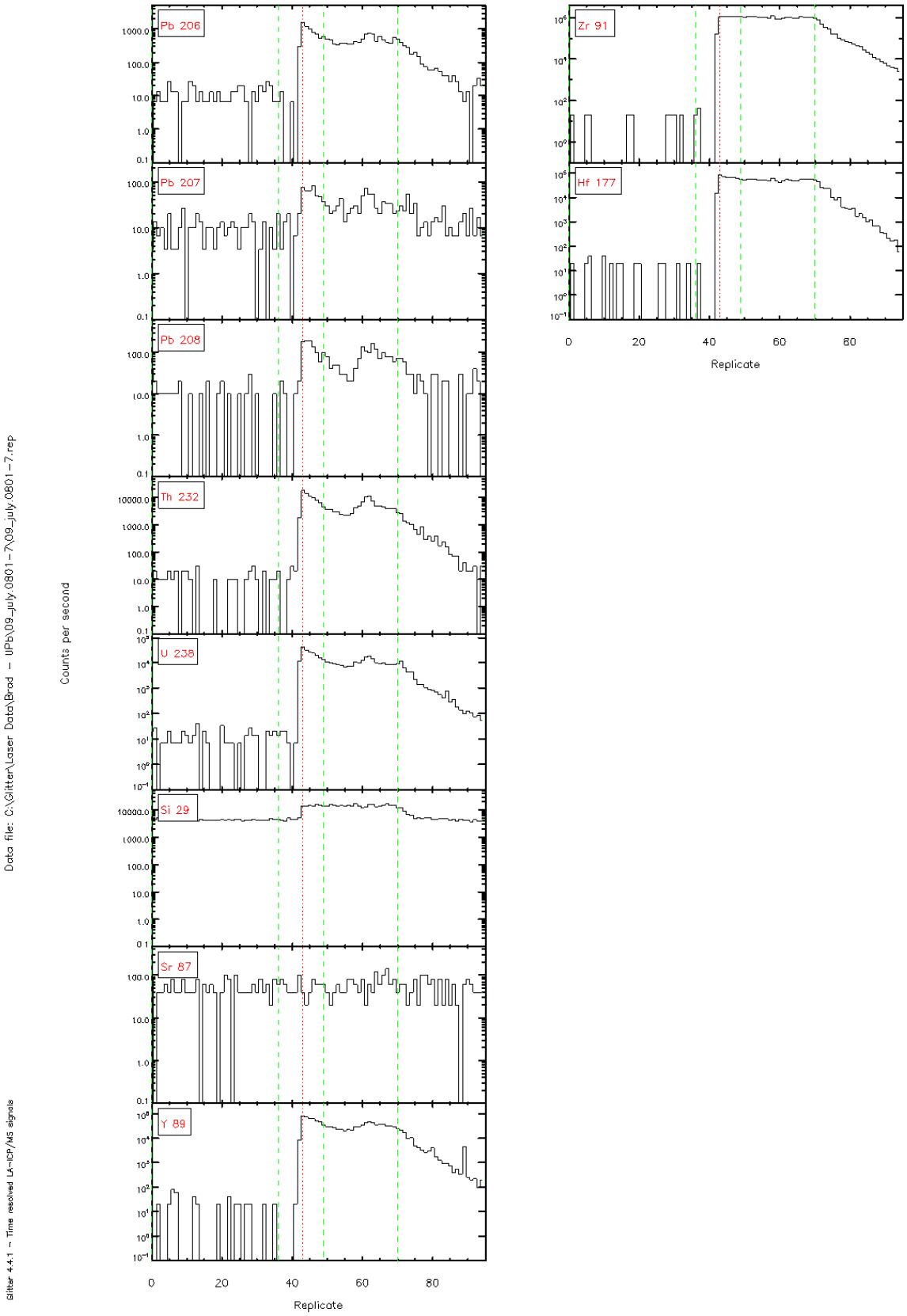
Pb 206
Pb 207
Pb 208
Th 232
U 238
Si 29
Sr 87
Y 89
Zr 91
Hf 177
Counts per second
Replicate
Data file: C:\Glitter\Laser Data\Brad - UPb\09_july.0801-7\09_july.0801-7.rep
Glitter 4.4.1 - Time resolved LA-ICP/MS signals

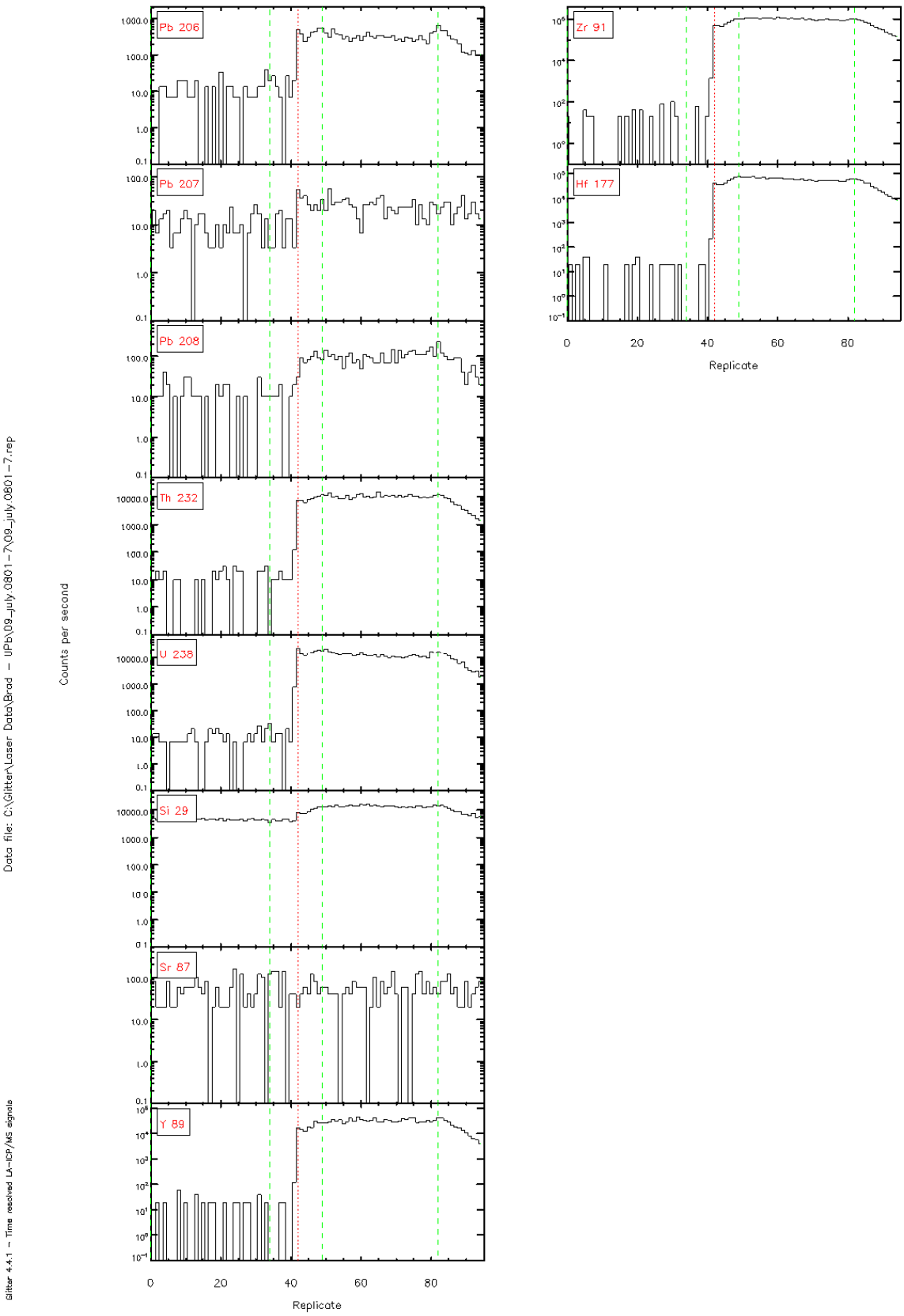
Pb 206
Pb 207
Pb 208
Th 232
U 238
Si 29
Sr 87
Y 89
Zr 91
Hf 177
Counts per second
Replicate
Data file: C:\Glitter\Laser Data\Brad - UPb\09_july.0801-7\09_july.0801-7.rep
Glitter 4.4.1 - Time resolved LA-ICP/MS signals

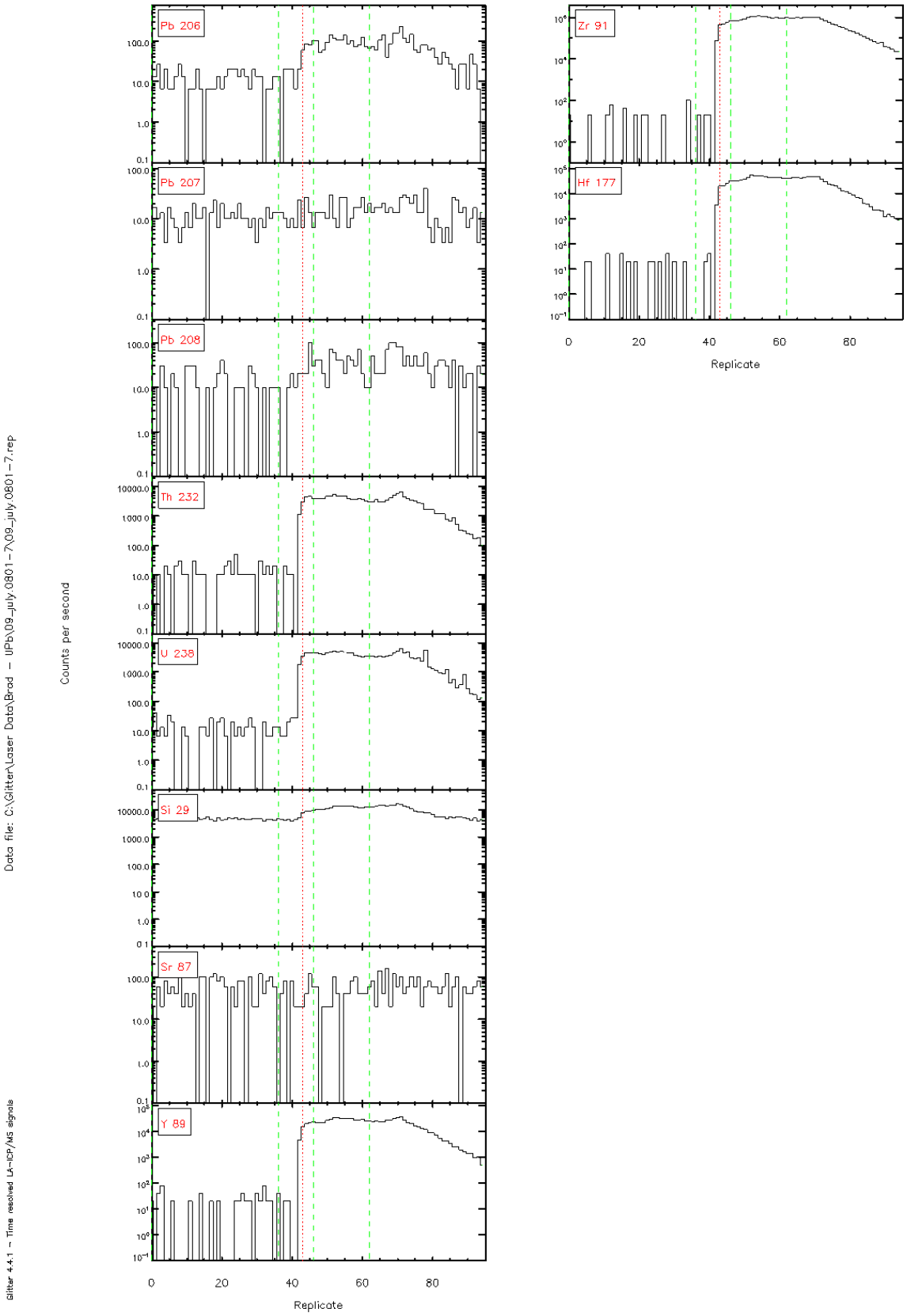
Pb 206
Pb 207
Pb 208
Th 232
U 238
Si 29
Sr 87
Y 89
Zr 91
Hf 177
Counts per second
Replicate
Data file: C:\Glitter\Laser Data\Brad - UPb\09_july.0801-7\09_july.0801-7.rep
Glitter 4.4.1 - Time resolved LA-ICP/MS signals

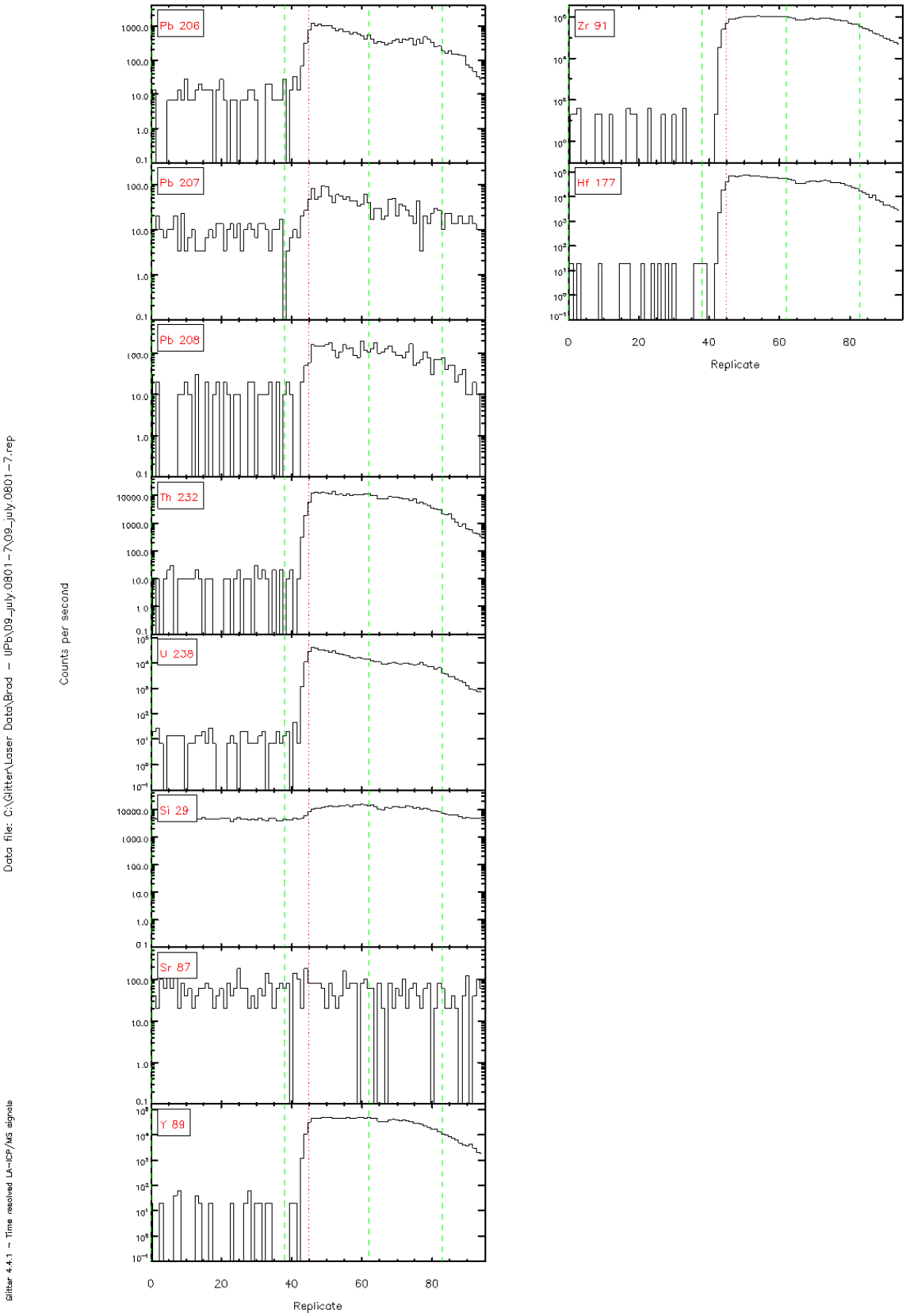
Pb 206
Pb 207
Pb 208
Th 232
U 238
Si 29
Sr 87
Y 89
Zr 91
Hf 177
Counts per second
Replicate
Data file: C:\Glitter\Laser Data\Brad - UPb\09_july.0801-7\09_july.0801-7.rep
Glitter 4.4.1 - Time resolved LA-ICP/MS signals

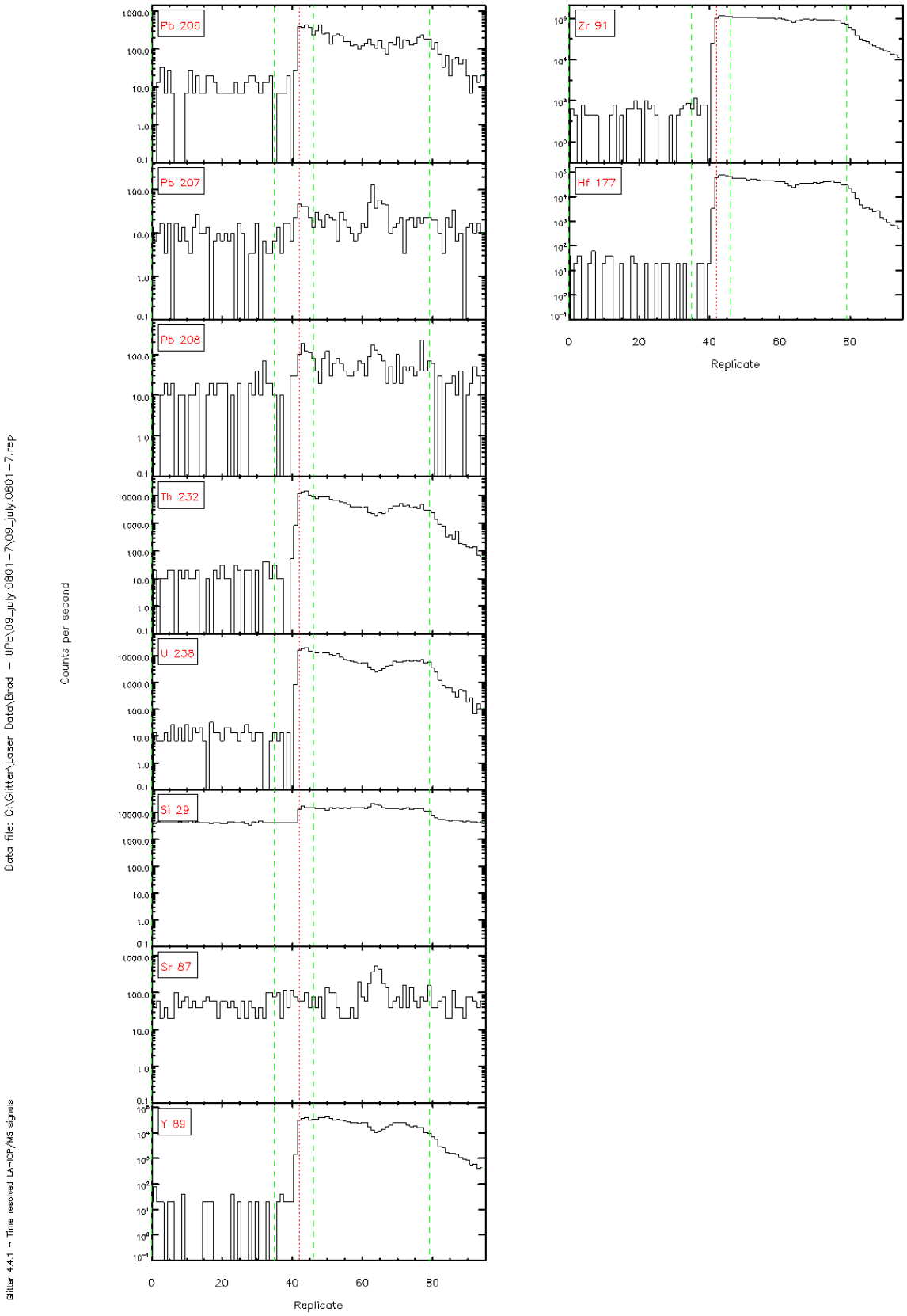
Pb 206
Pb 207
Pb 208
Th 232
U 238
Si 29
Sr 87
Y 89
Zr 91
Hf 177
Counts per second
Replicate
Data file: C:\Glitter\Laser Data\Brad - UPb\09_july.0801-7\09_july.0801-7.rep
Glitter 4.4.1 - Time resolved LA-ICP/MS signals

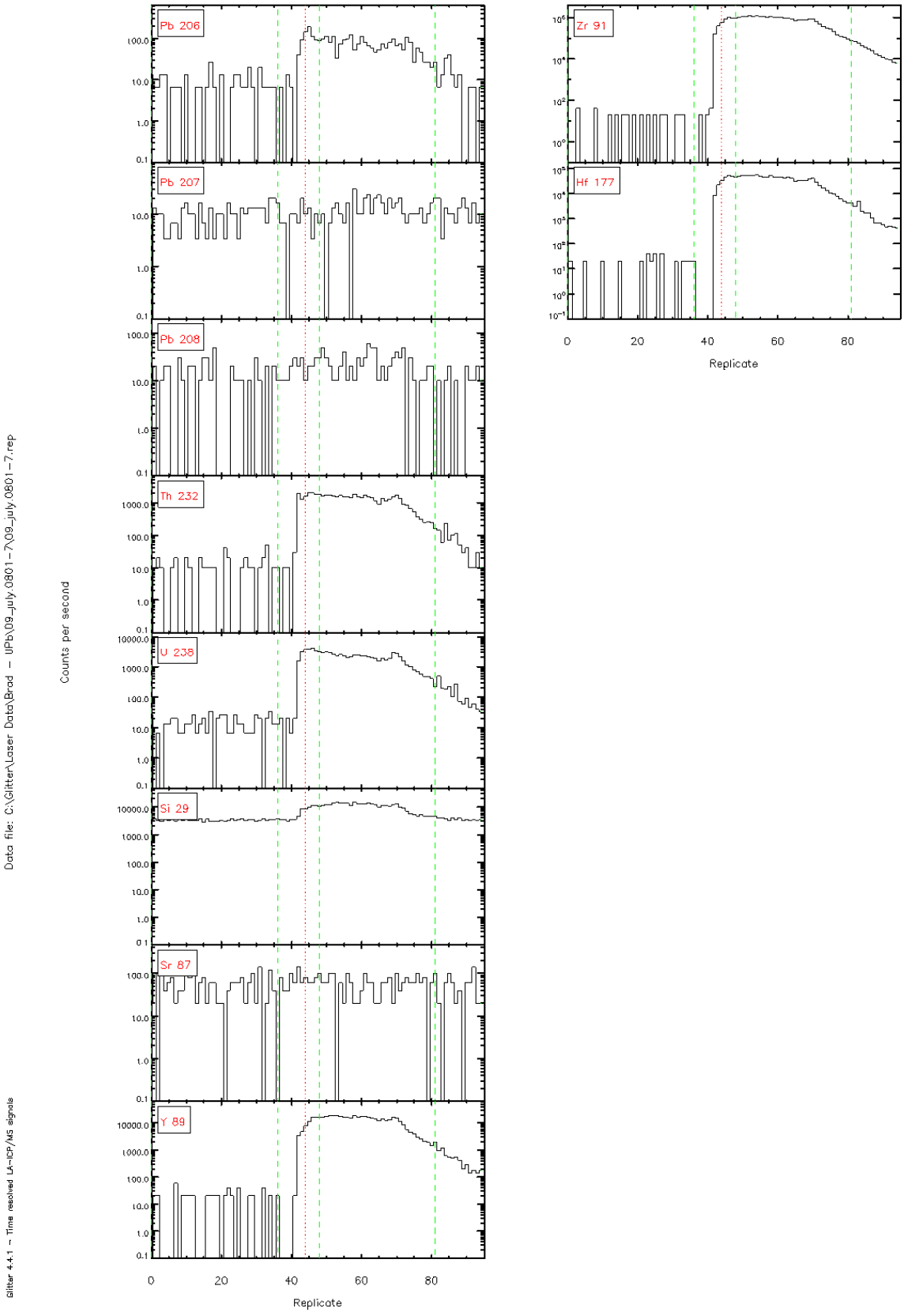
Pb 206
Pb 207
Pb 208
Th 232
U 238
Si 29
Sr 87
Y 89
Zr 91
Hf 177
Counts per second
Replicate
Data file: C:\Glitter\Laser Data\Brad - UPb\09_july.0801-7\09_july.0801-7.rep
Glitter 4.4.1 - Time resolved LA-ICP/MS signals

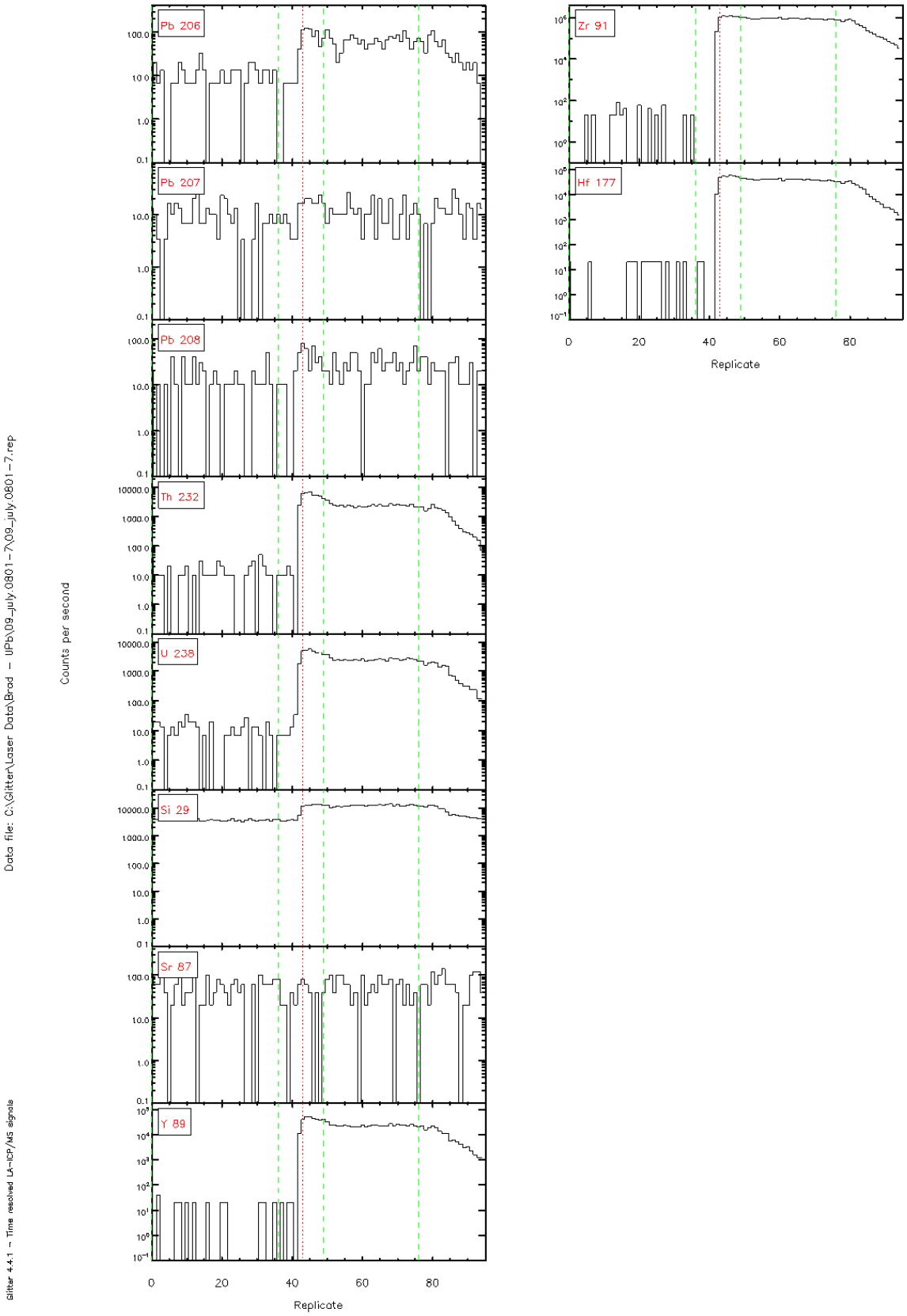
Pb 206
Pb 207
Pb 208
Th 232
U 238
Si 29
Sr 87
Y 89
Zr 91
Hf 177
Counts per second
Replicate
Data file: C:\Glitter\Laser Data\Brad - UPb\09_july.0801-7\09_july.0801-7.rep
Glitter 4.4.1 - Time resolved LA-ICP/MS signals

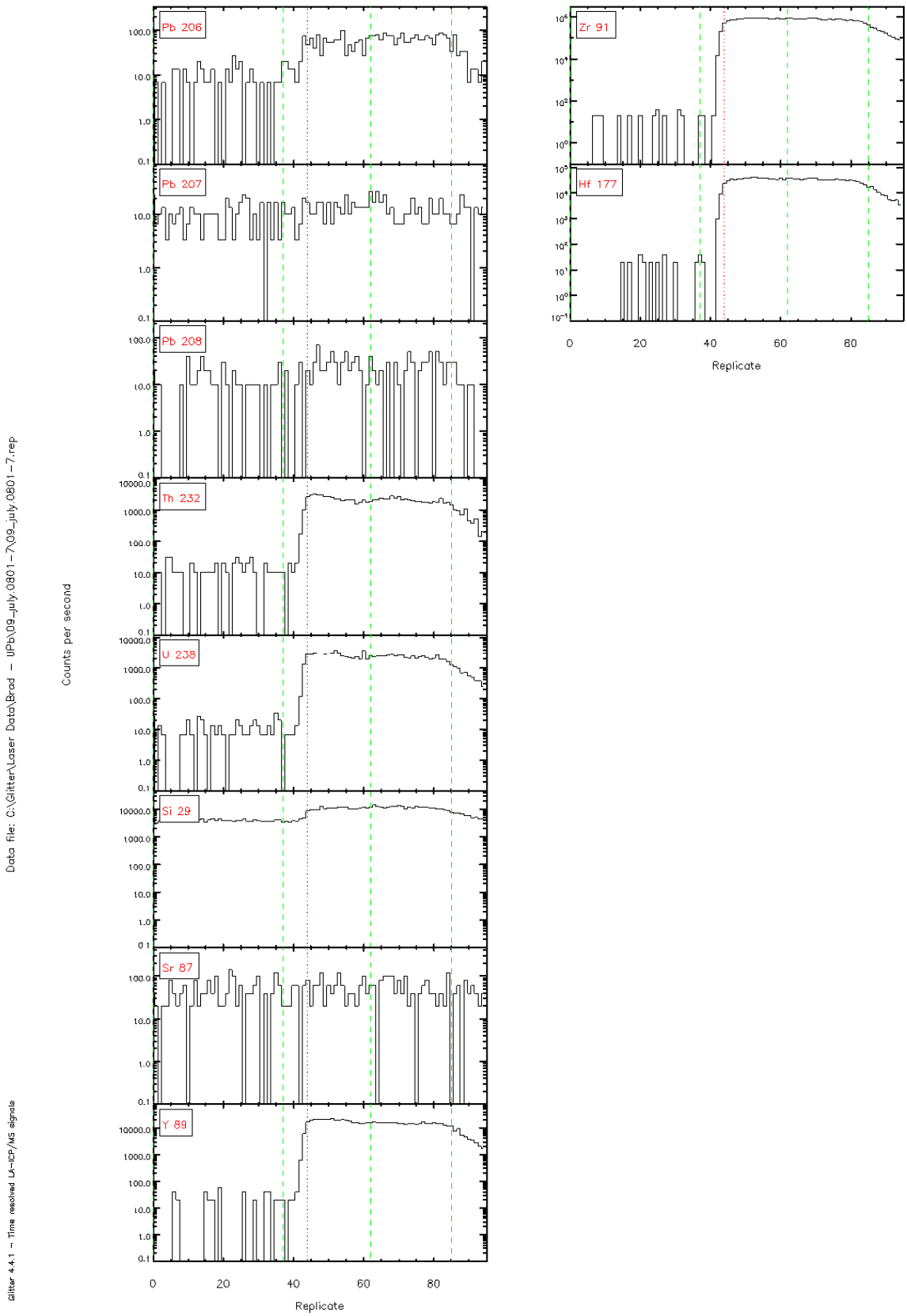
Pb 206
Pb 207
Pb 208
Th 232
U 238
Si 29
Sr 87
Y 89
Zr 91
Hf 177
Counts per second
Replicate
Data file: C:\Glitter\Laser Data\Brad - UPb\09_july.0801-7\09_july.0801-7.rep
Glitter 4.4.1 - Time resolved LA-ICP/MS signals

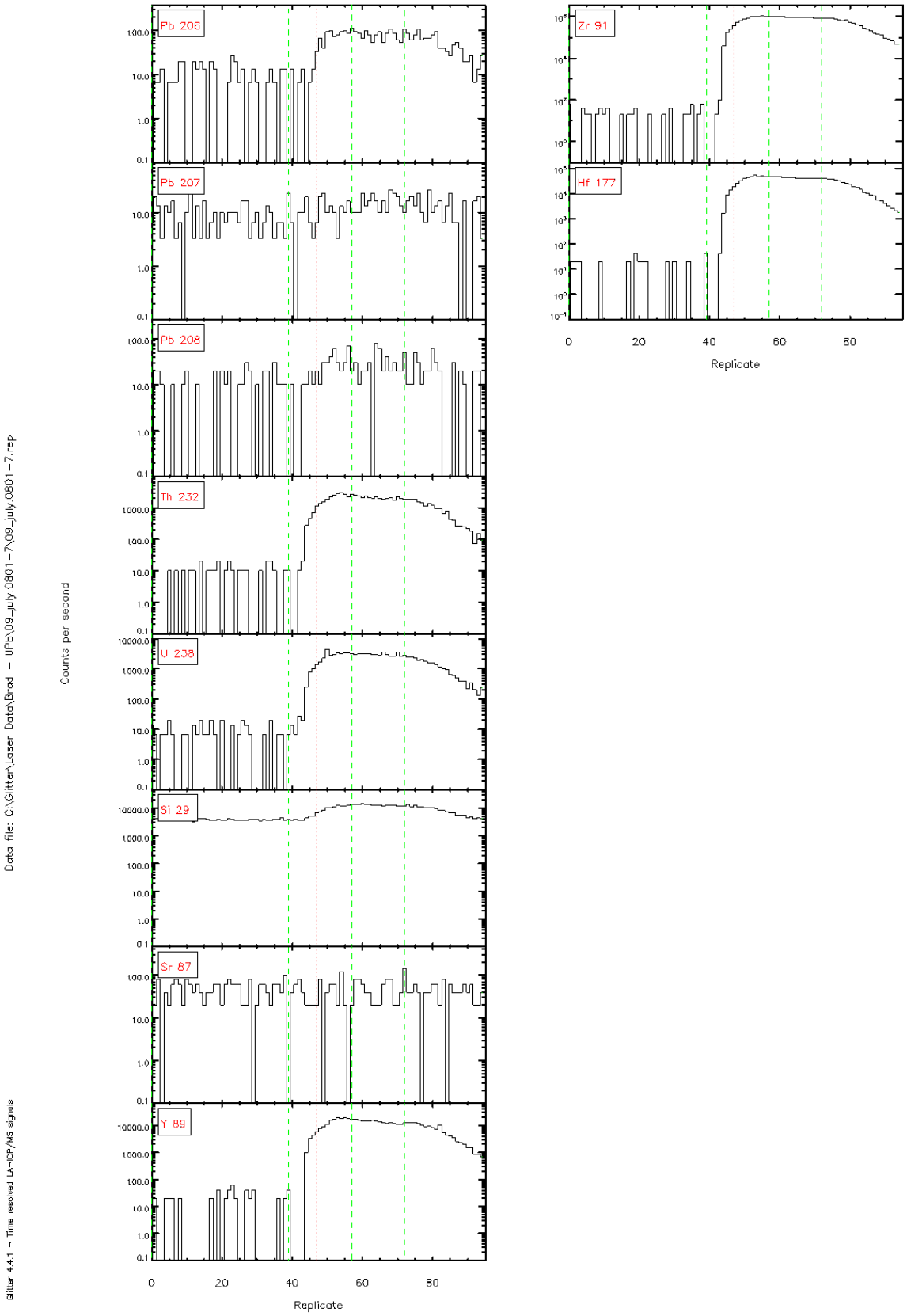
Pb 206
Pb 207
Pb 208
Th 232
U 238
Si 29
Sr 87
Y 89
Zr 91
Hf 177
Counts per second
Replicate
Data file: C:\Glitter\Laser Data\Brad - UPb\09_july.0801-7\09_july.0801-7.rep
Glitter 4.4.1 - Time resolved LA-ICP/MS signals

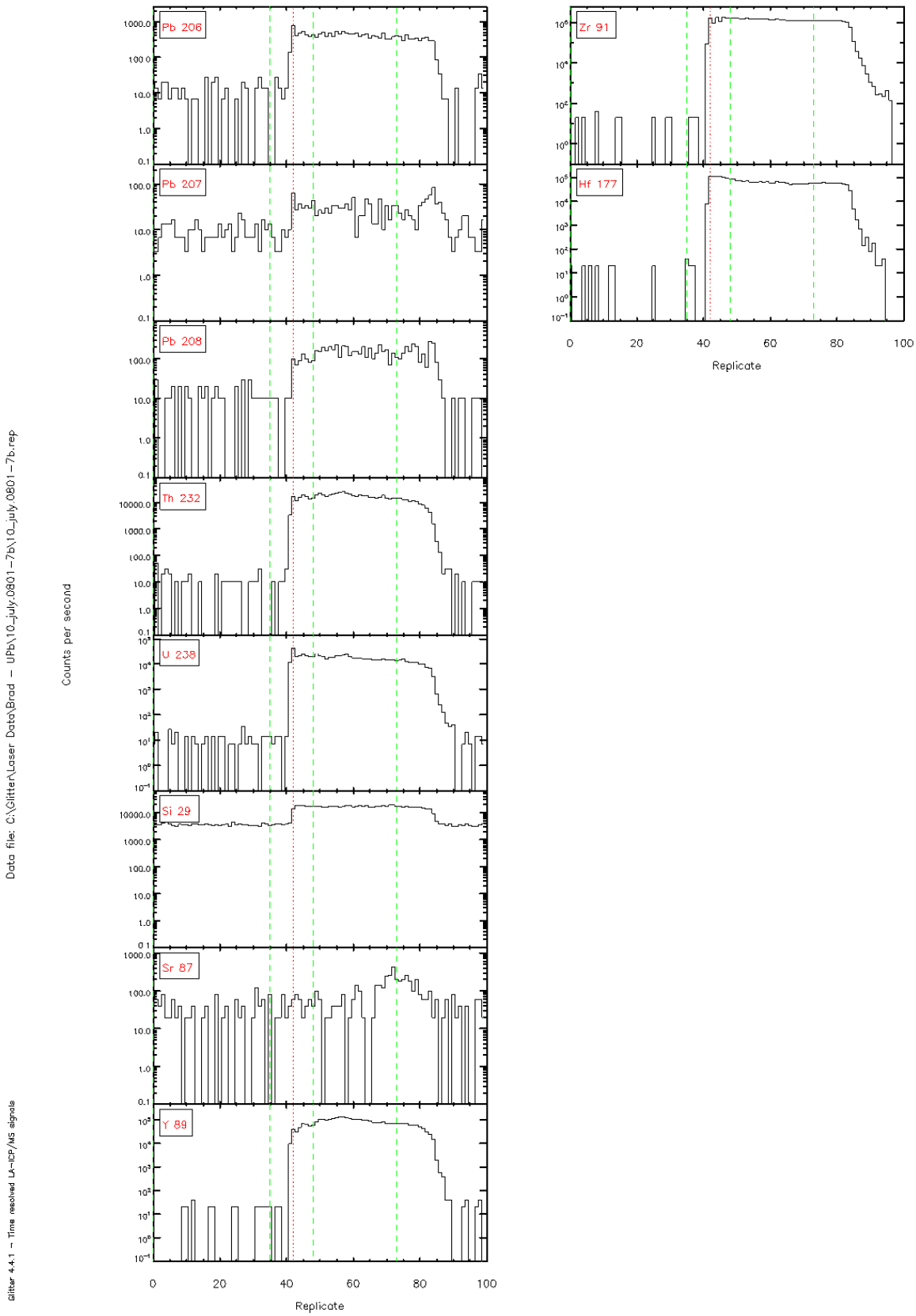
Pb 206
Pb 207
Pb 208
Th 232
U 238
Si 29
Sr 87
Y 89
Zr 91
Hf 177
Counts per second
Replicate
Data file: C:\Glitter\Laser Data\Brad – UPb\10_july.0801–7b\10_july.0801–7b.rep
Glitter 4.4.1 – Time resolved LA-ICP/MS signals

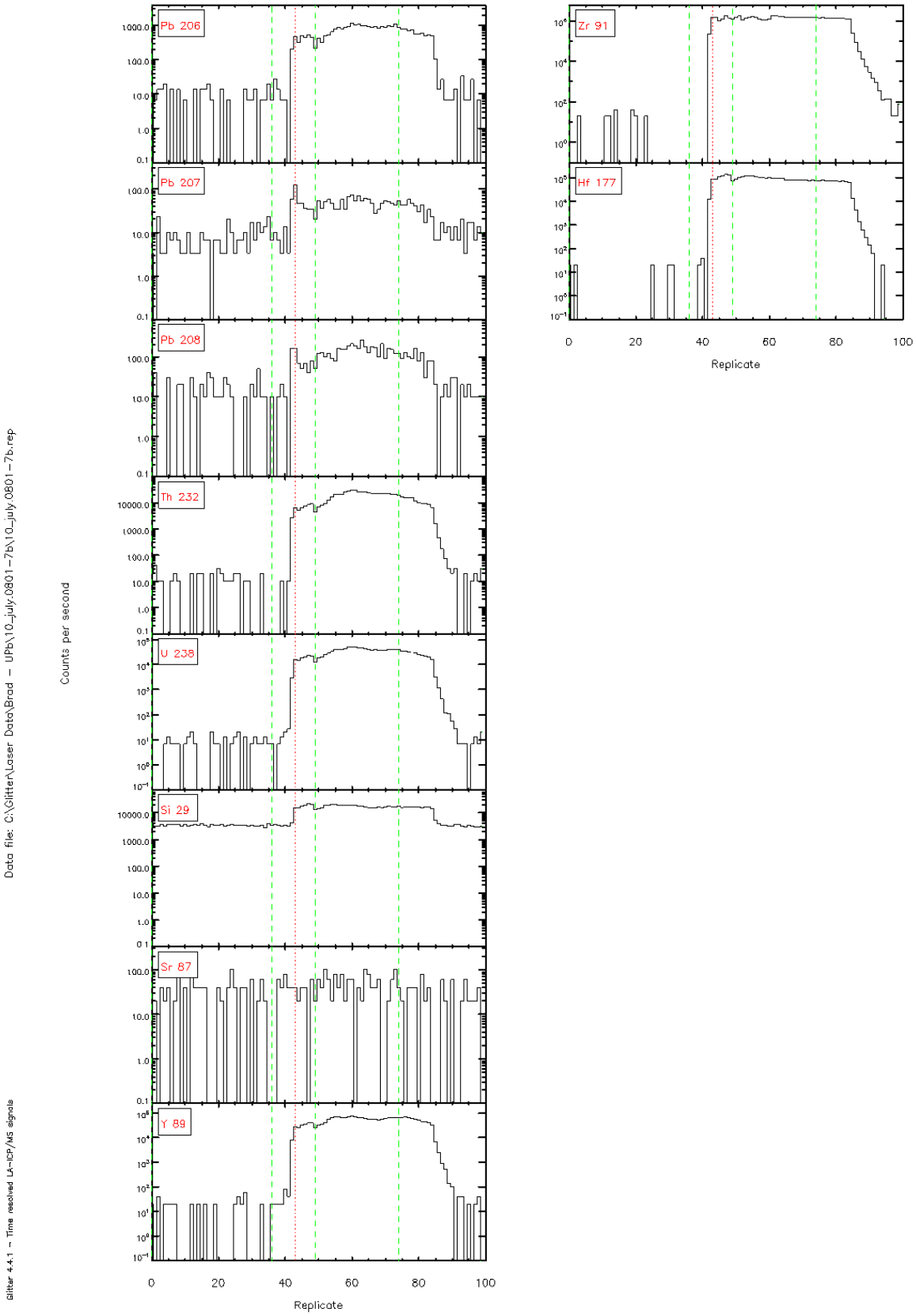
Pb 206
Pb 207
Pb 208
Th 232
U 238
Si 29
Sr 87
Y 89
Zr 91
Hf 177
Counts per second
Replicate
Data file: C:\Glitter\Laser Data\Brad - UPb\10_july.0801-7b\10_july.0801-7b.rep
Glitter 4.4.1 - Time resolved LA-ICP/MS signals

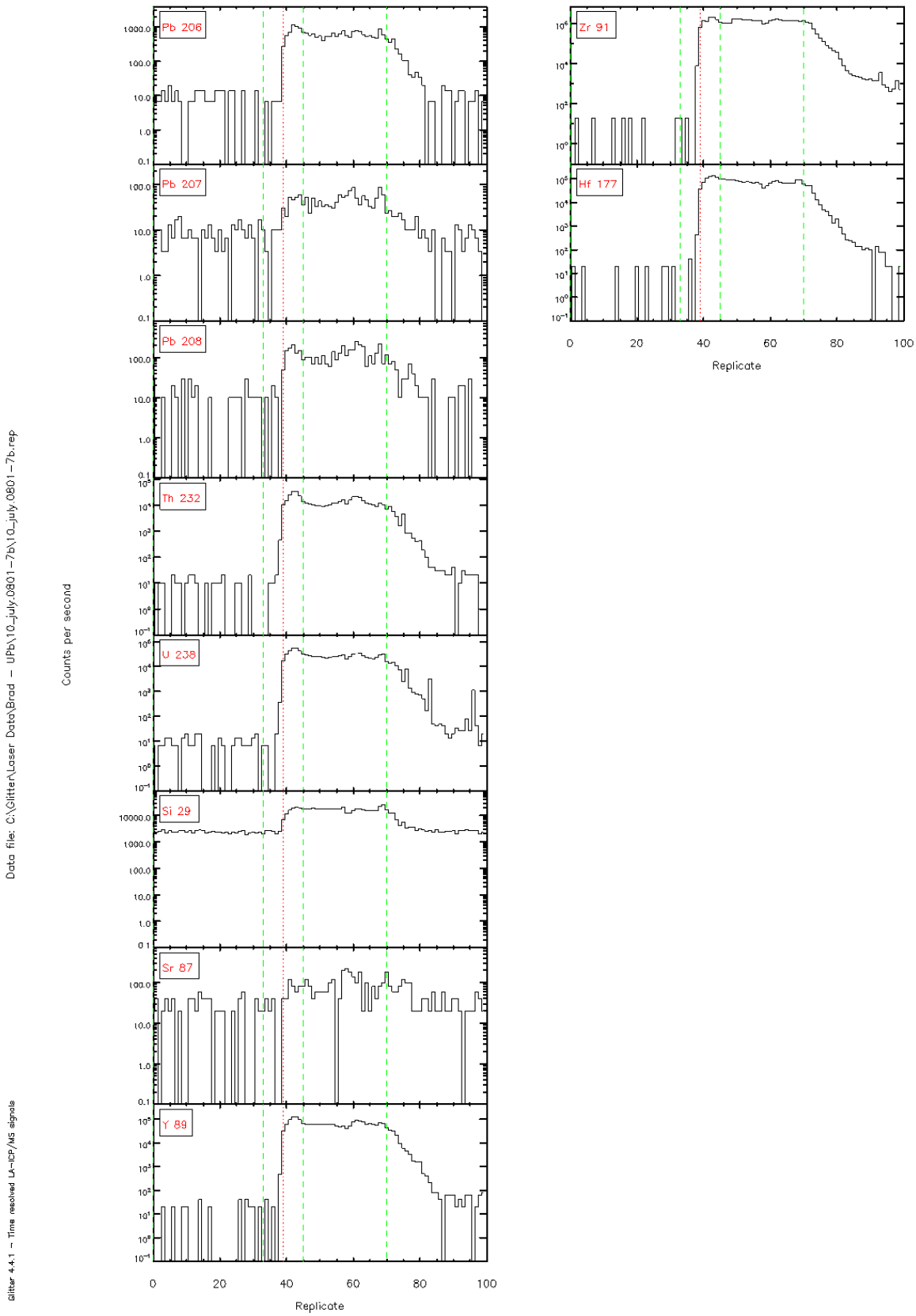
Pb 206
Pb 207
Pb 208
Th 232
U 238
Si 29
Sr 87
Y 89
Zr 91
Hf 177
Counts per second
Replicate
Data file: C:\Glitter\Laser Data\Brad – UPb\10_july.0801–7b\10_july.0801–7b.rep
Glitter 4.4.1 – Time resolved LA-ICP/MS signals

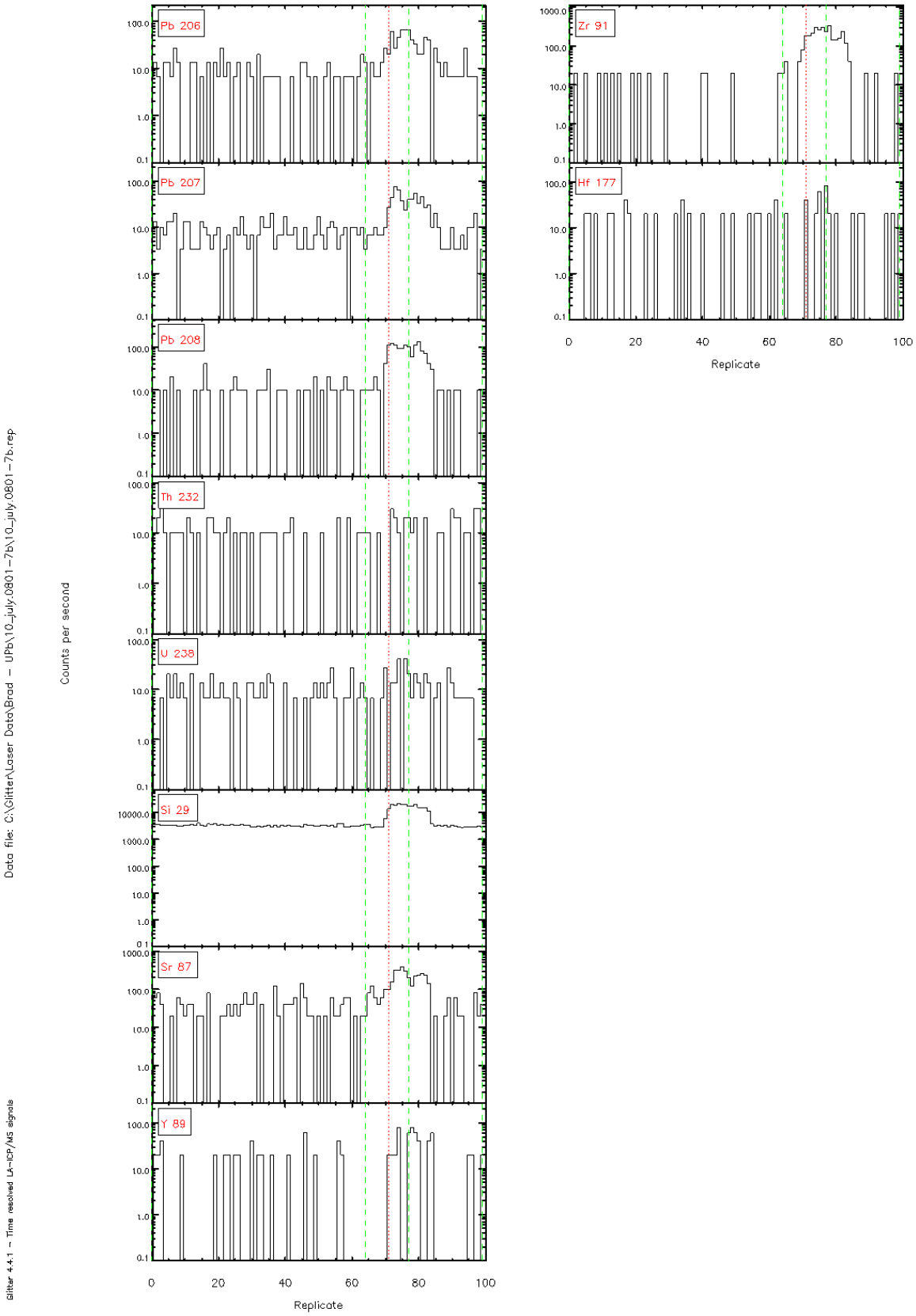
Pb 206
Pb 207
Pb 208
Th 232
U 238
Si 29
Sr 87
Y 89
Zr 91
Hf 177
Counts per second
Replicate
Data file: C:\Glitter\Laser Data\Brad - UPb\10_july.0801-7b\10_july.0801-7b.rep
Glitter 4.4.1 - Time resolved LA-ICP-MS signals

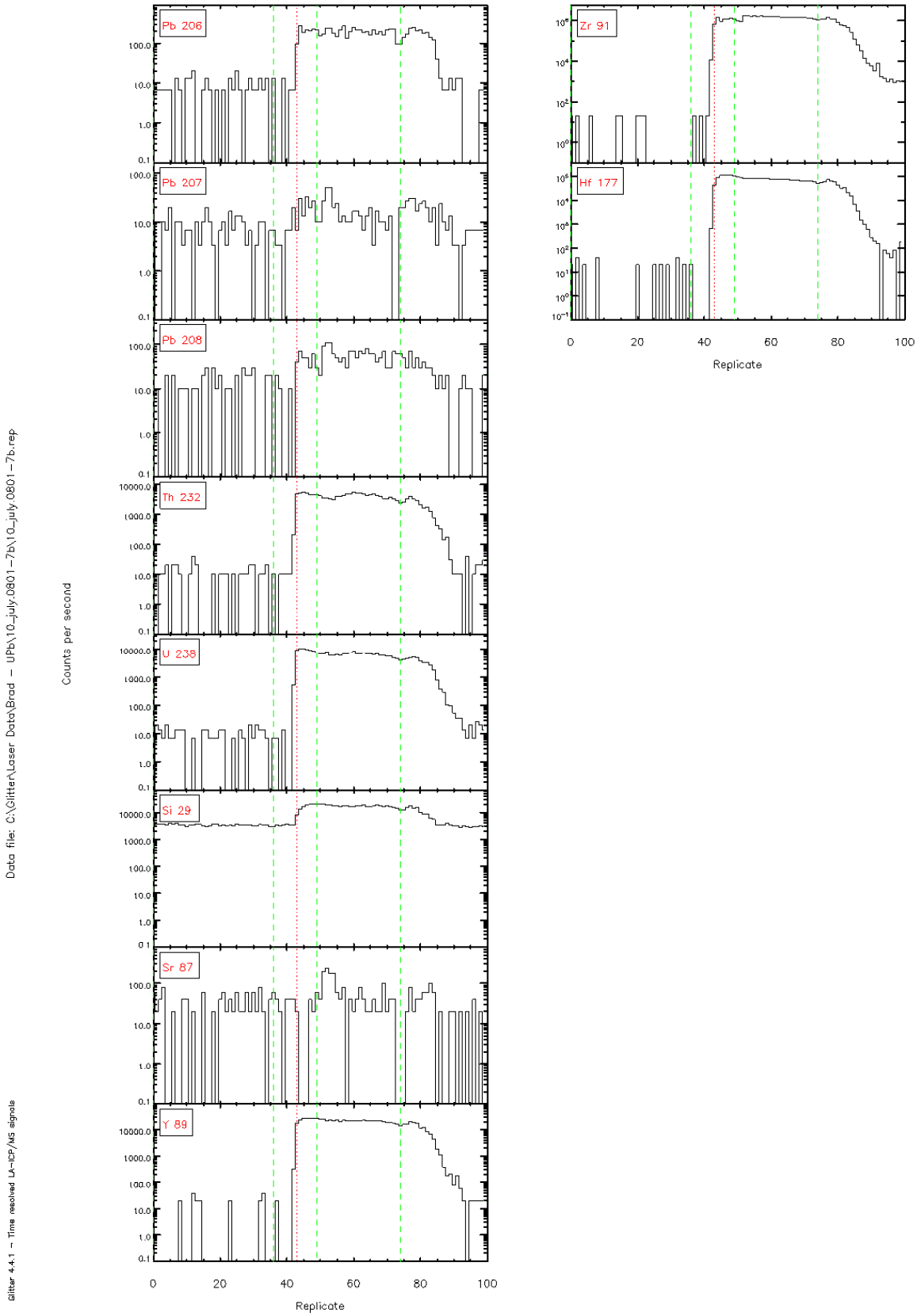
Pb 206
Pb 207
Pb 208
Th 232
U 238
Si 29
Sr 87
Y 89
Zr 91
Hf 177
Counts per second
Replicate
0
20
40
60
80
100
Data file: C:\Glitter\Laser Data\Brad – UPb\10_july.0801–7b\10_july.0801–7b.rep
Glitter 4.4.1 – Time resolved LA-ICP/MS signals

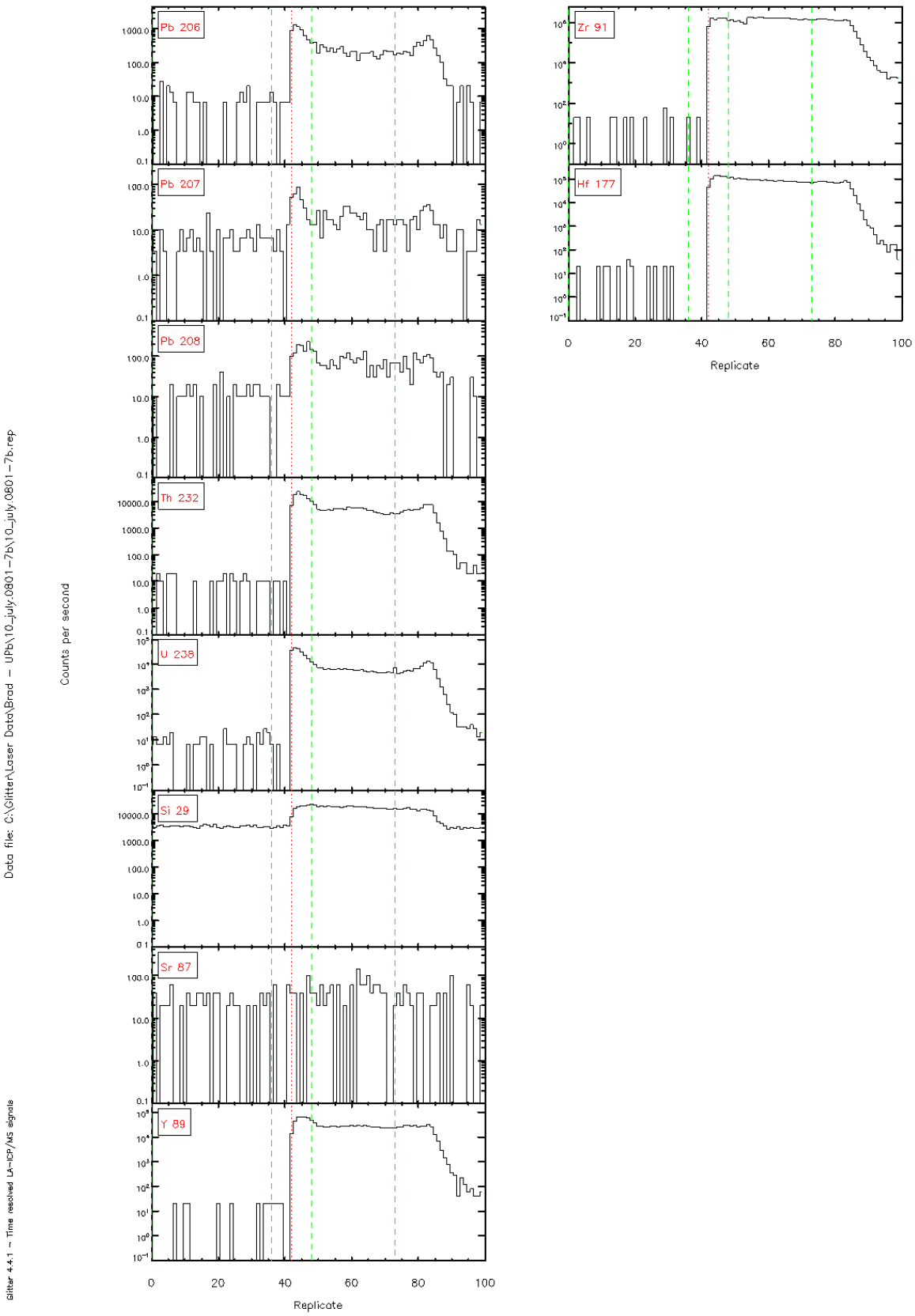
Pb 206
Pb 207
Pb 208
Th 232
U 238
Si 29
Sr 87
Y 89
Zr 91
Hf 177
Counts per second
Replicate
Data file: C:\Glitter\Laser Data\Brad - UPb\10_july.0801-7b\10_july.0801-7b.rep
Glitter 4.4.1 - Time resolved LA-ICP-MS signals

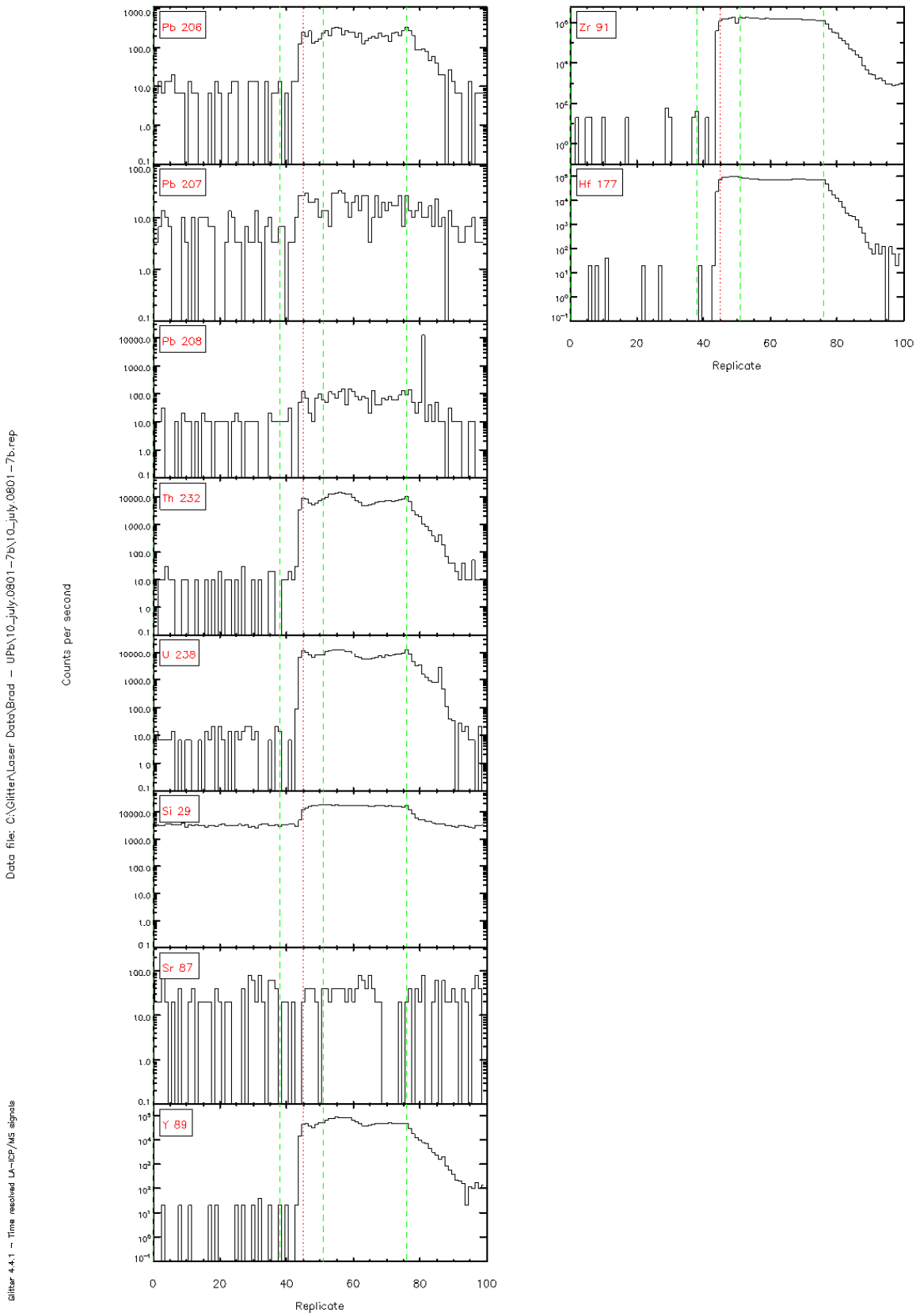
Pb 206
Pb 207
Pb 208
Th 232
U 238
Si 29
Sr 87
Y 89
Zr 91
Hf 177
Counts per second
Replicate
Data file: C:\Glitter\Laser Data\Brad – UPb\10_july.0801–7b\10_july.0801–7b.rep
Glitter 4.4.1 – Time resolved LA-ICP/MS signals

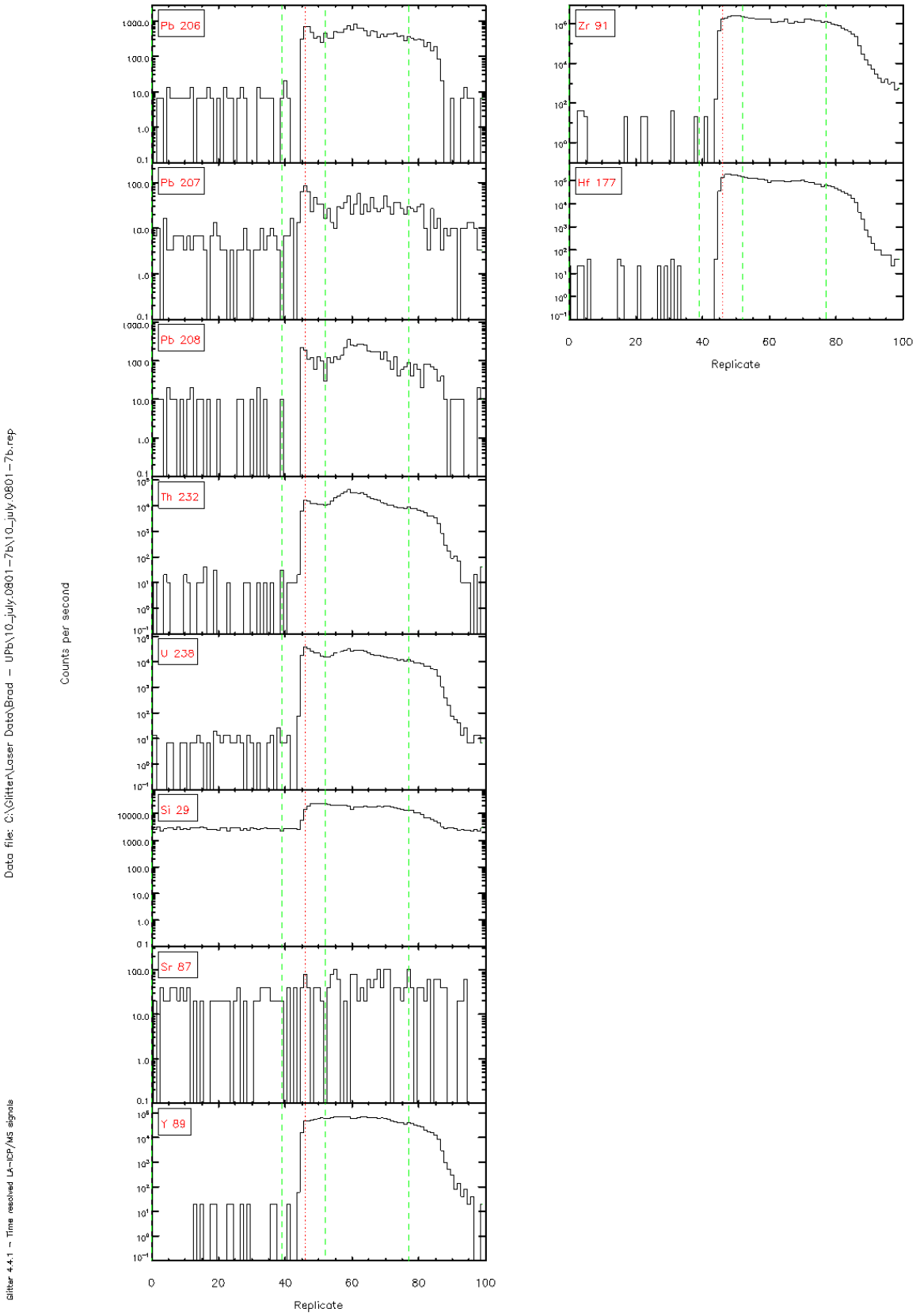
Pb 206
Pb 207
Pb 208
Th 232
U 238
Si 29
Sr 87
Y 89
Zr 91
Hf 177
Counts per second
Replicate
Data file: C:\Glitter\Laser Data\Brad - UPb\10_july.0801-7b\10_july.0801-7b.rep
Glitter 4.4.1 - Time resolved LA-ICP/MS signals

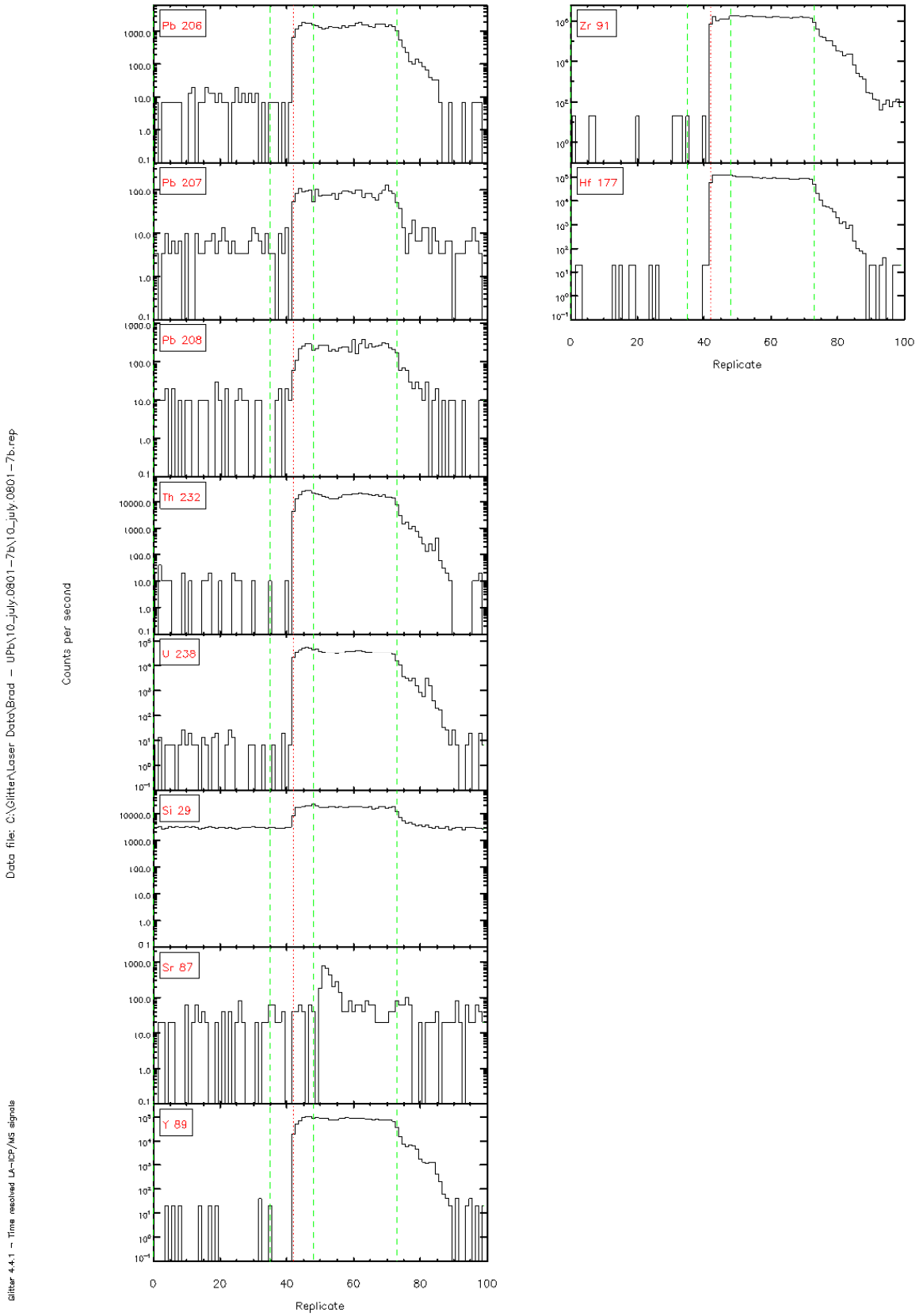
Pb 206
Pb 207
Pb 208
Th 232
U 238
Si 29
Sr 87
Y 89
Zr 91
Hf 177
Counts per second
Replicate
Data file: C:\Glitter\Laser Data\Brad – UPb\10_july.0801–7b\10_july.0801–7b.rep
Glitter 4.4.1 – Time resolved LA-ICP/MS signals

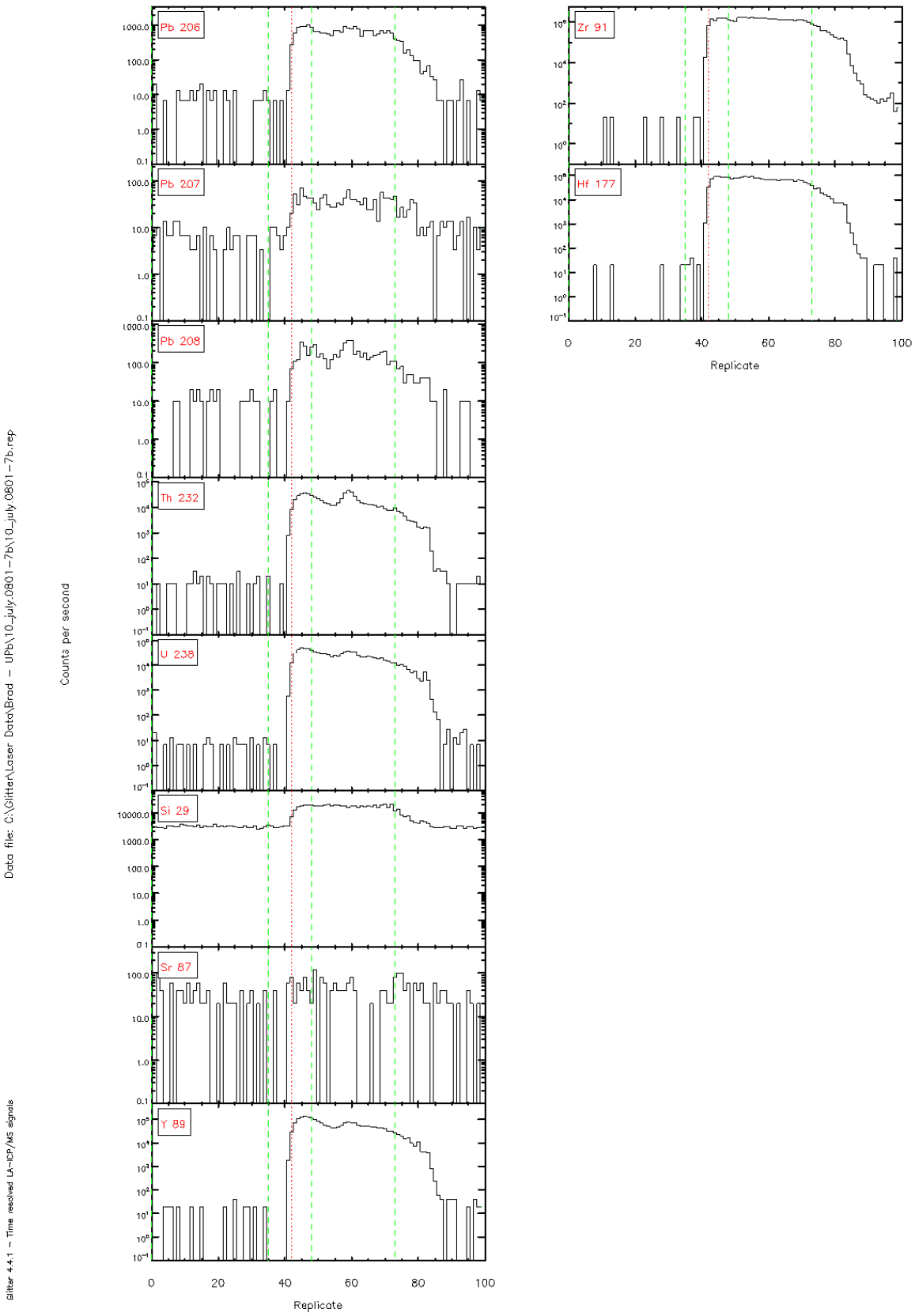
Pb 206
Pb 207
Pb 208
Th 232
U 238
Si 29
Sr 87
Y 89
Zr 91
Hf 177
Counts per second
Replicate
Data file: C:\Glitter\Laser Data\Brad - UPb\10_july.0801-7b\10_july.0801-7b.rep
Glitter 4.4.1 - Time resolved LA-ICP/MS signals

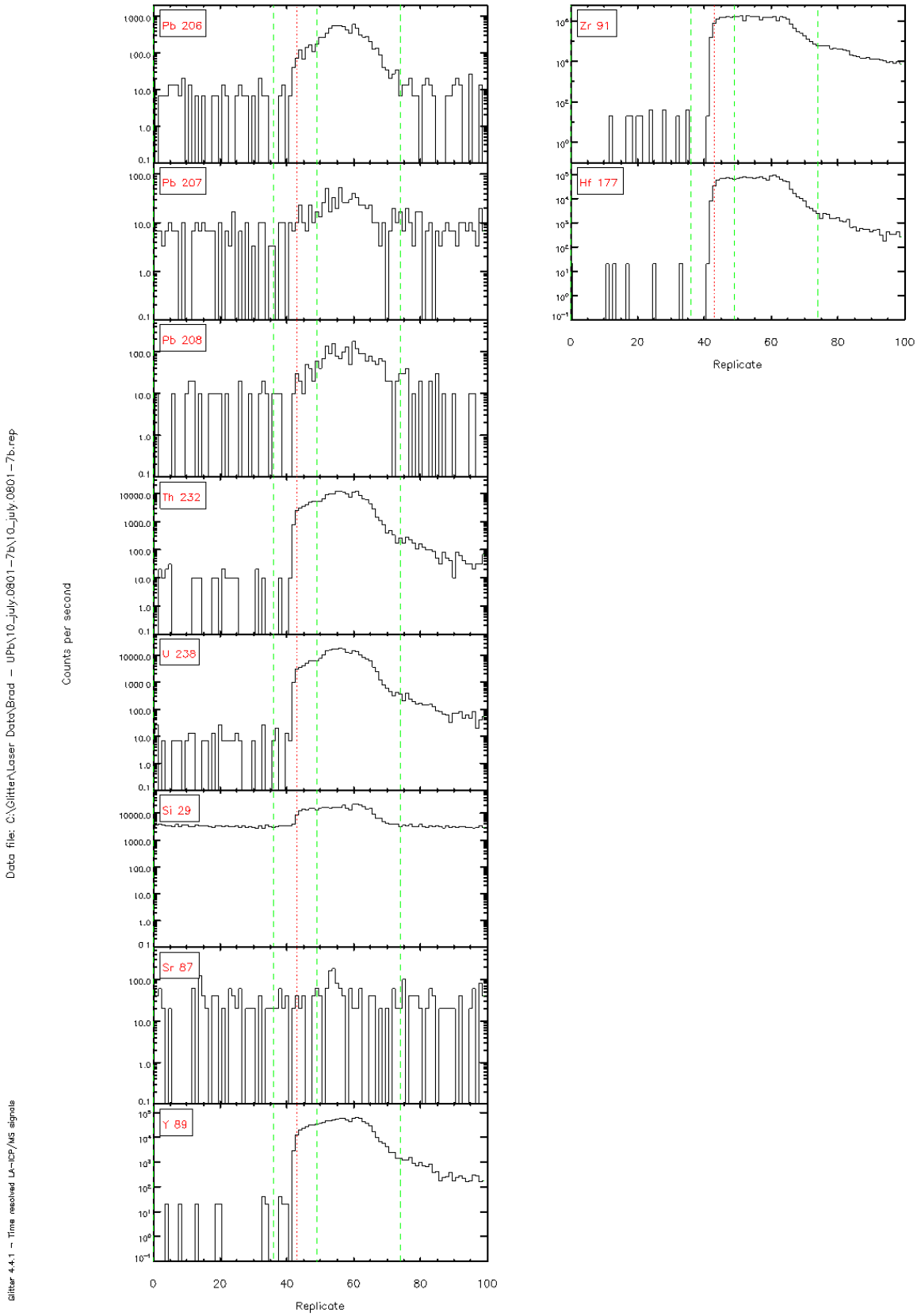
Pb 206
Pb 207
Pb 208
Th 232
U 238
Si 29
Sr 87
Y 89
Zr 91
Hf 177
Counts per second
Replicate
Data file: C:\Glitter\Laser Data\Brad – UPb\10_july.0801–7b\10_july.0801–7b.rep
Glitter 4.4.1 – Time resolved LA-ICP/MS signals

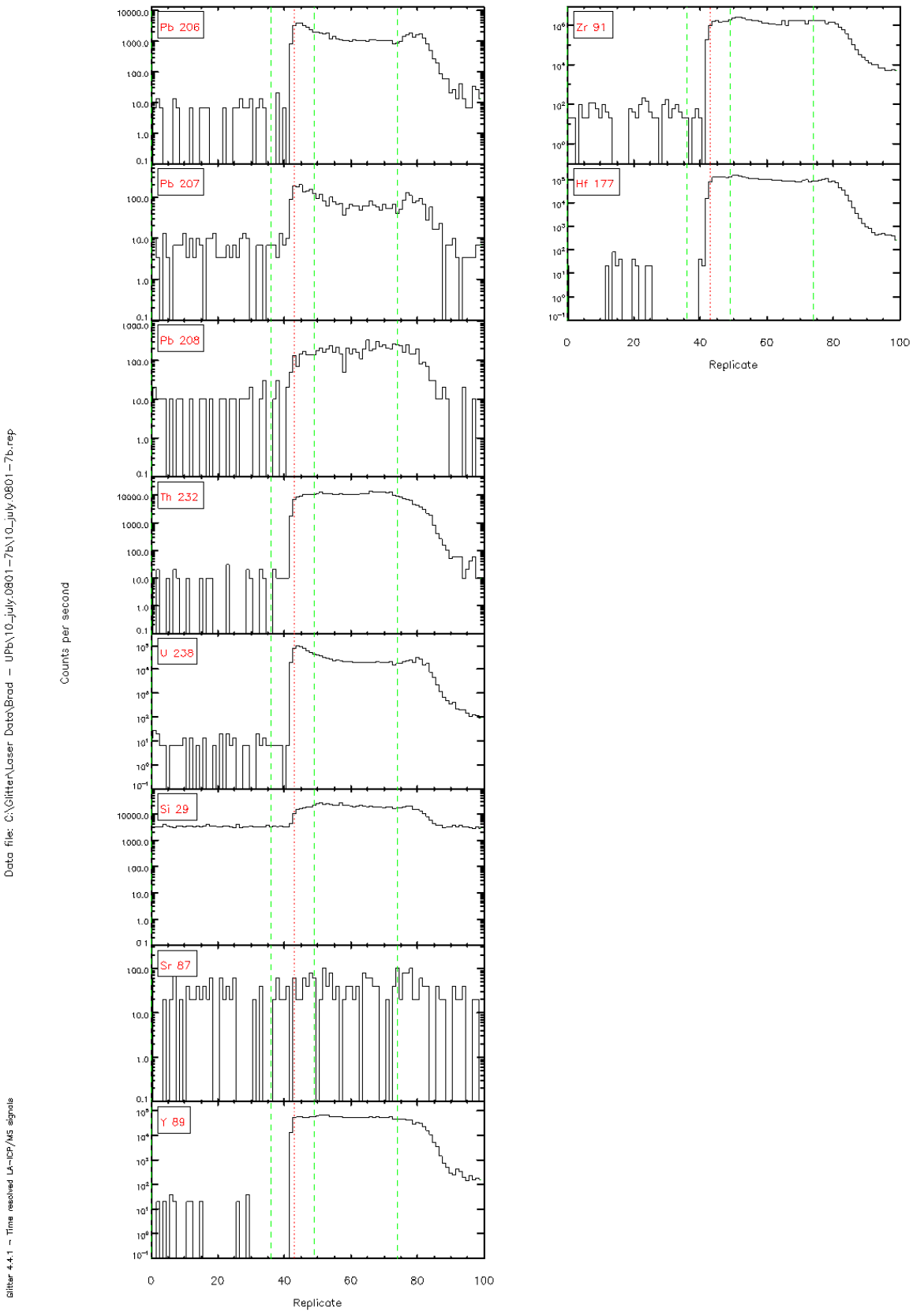
Pb 206
Pb 207
Pb 208
Th 232
U 238
Si 29
Sr 87
Y 89
Zr 91
Hf 177
Counts per second
Replicate
Data file: C:\Glitter\Laser Data\Brad - UPb\10_july.0801-7b\10_july.0801-7b.rep
Glitter 4.4.1 - Time resolved LA-ICP/MS signals

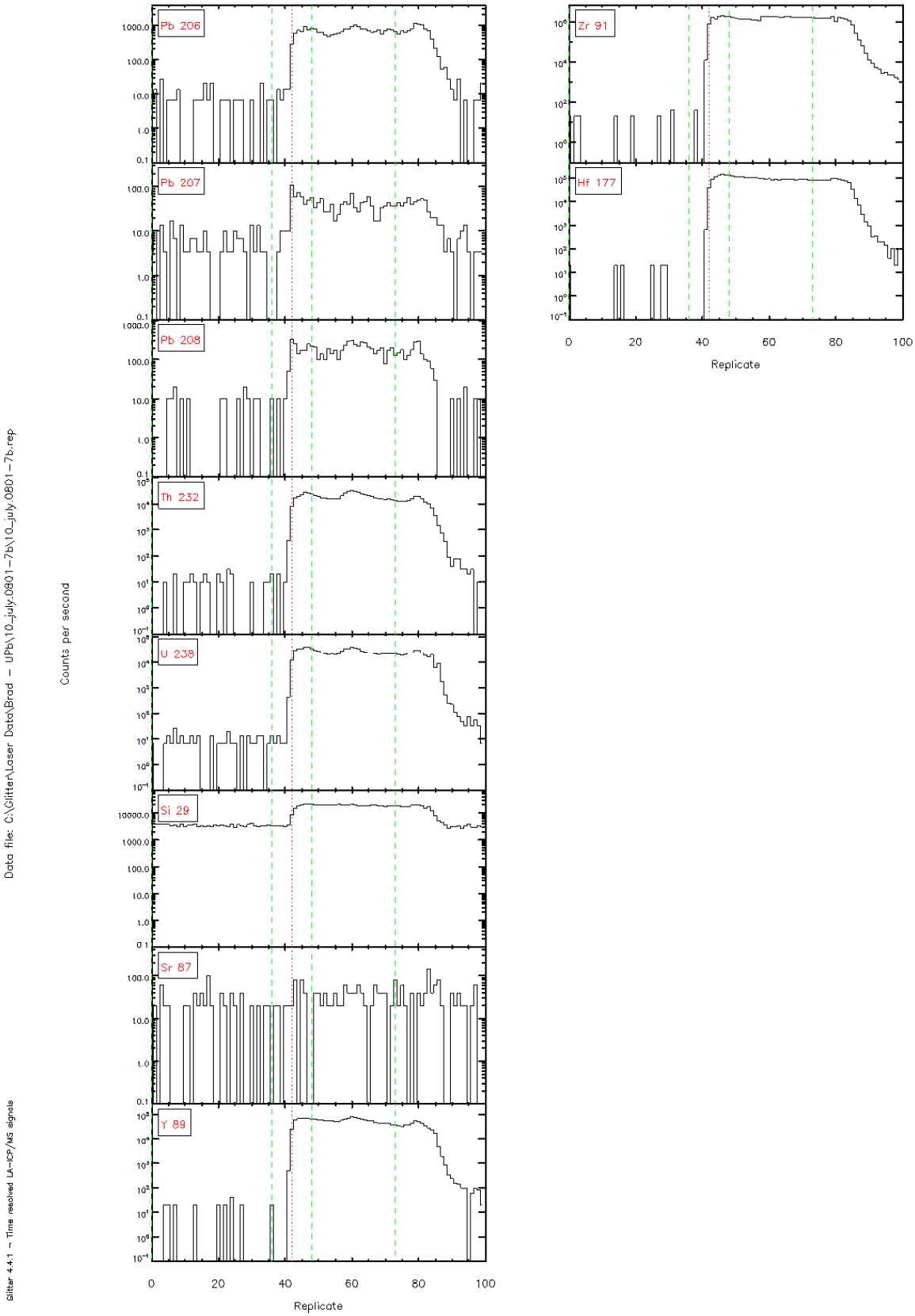
Pb 206
Pb 207
Pb 208
Th 232
U 238
Si 29
Sr 87
Y 89
Zr 91
Hf 177
Counts per second
Replicate
Data file: C:\Glitter\Laser Data\Brad – UPb\10_july.0801–7b\10_july.0801–7b.rep
Glitter 4.4.1 – Time resolved LA-ICP/MS signals

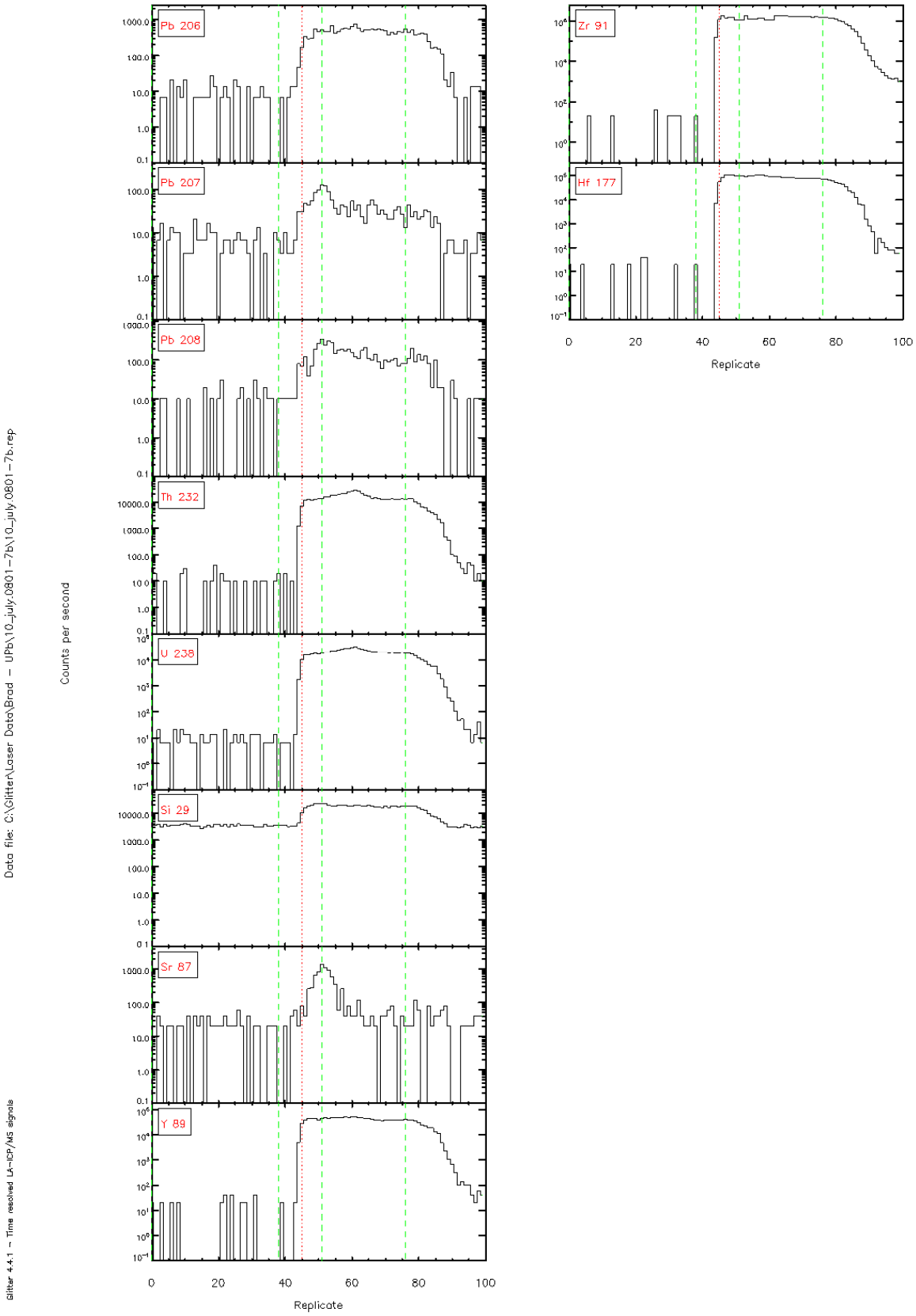
Pb 206
Pb 207
Pb 208
Th 232
U 238
Si 29
Sr 87
Y 89
Zr 91
Hf 177
Counts per second
Replicate
Data file: C:\Glitter\Laser Data\Brad - UPb\10_july.0801-7b\10_july.0801-7b.rep
Glitter 4.4.1 - Time resolved LA-ICP/MS signals

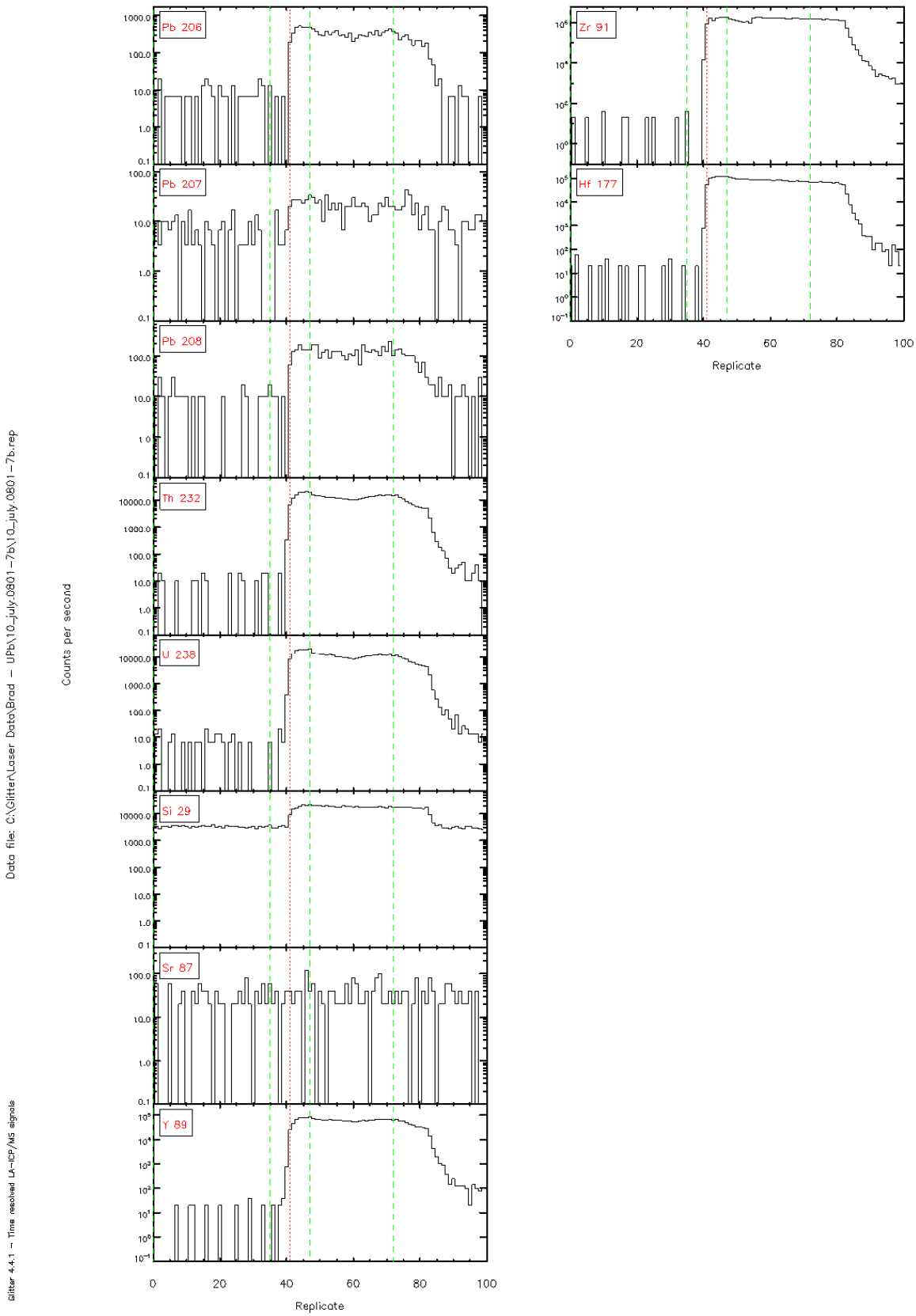
Pb 206
Pb 207
Pb 208
Th 232
U 238
Si 29
Sr 87
Y 89
Zr 91
Hf 177
Counts per second
Replicate
Data file: C:\Glitter\Laser Data\Brad – UPb\10_july.0801–7b\10_july.0801–7b.rep
Glitter 4.4.1 – Time resolved LA-ICP/MS signals

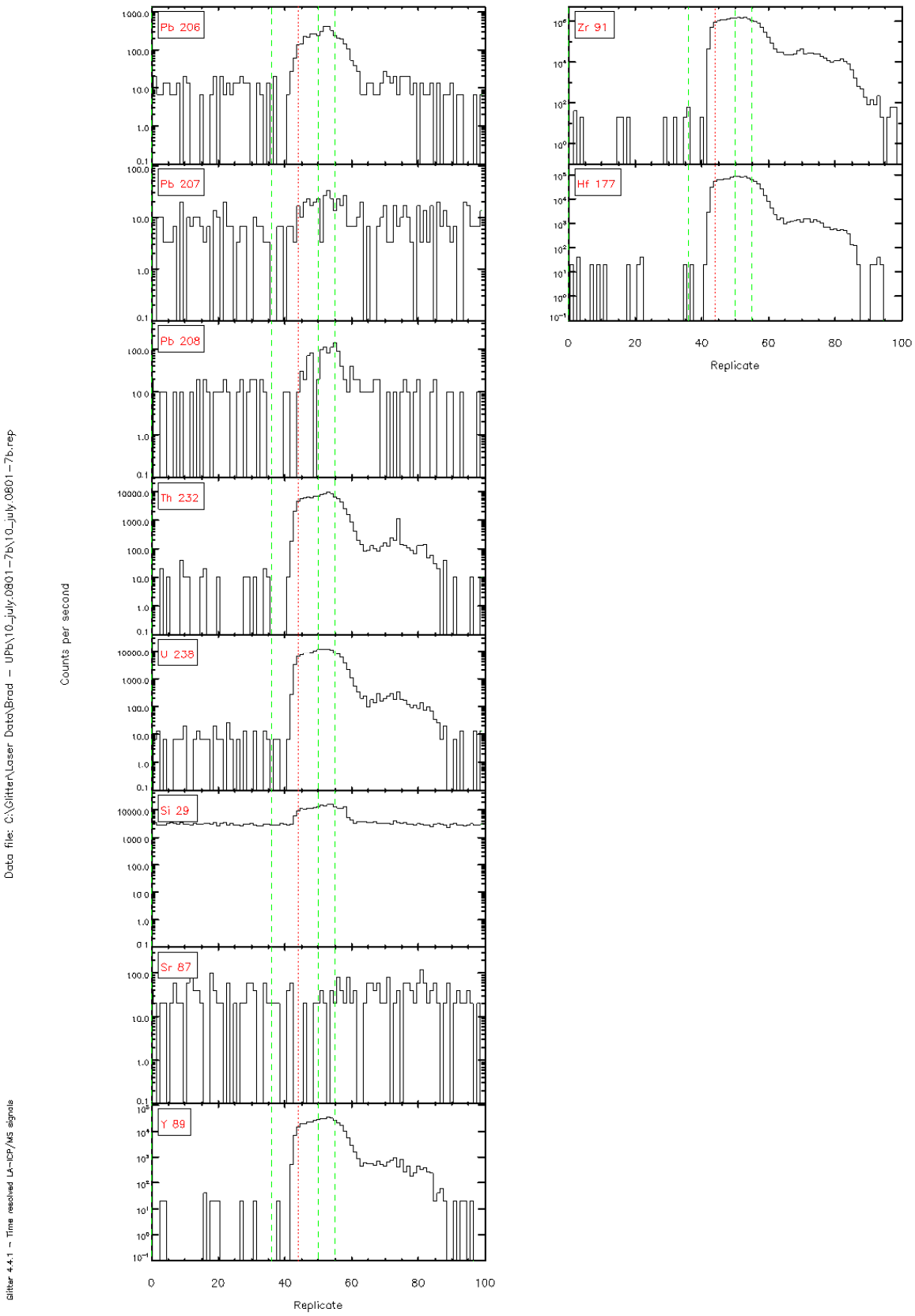
Pb 206
Pb 207
Pb 208
Th 232
U 238
Si 29
Sr 87
Y 89
Zr 91
Hf 177
Counts per second
Replicate
Data file: C:\Glitter\Laser Data\Brad - UPb\10_july.0801-7b\10_july.0801-7b.rep
Glitter 4.4.1 - Time resolved LA-ICP-MS signals

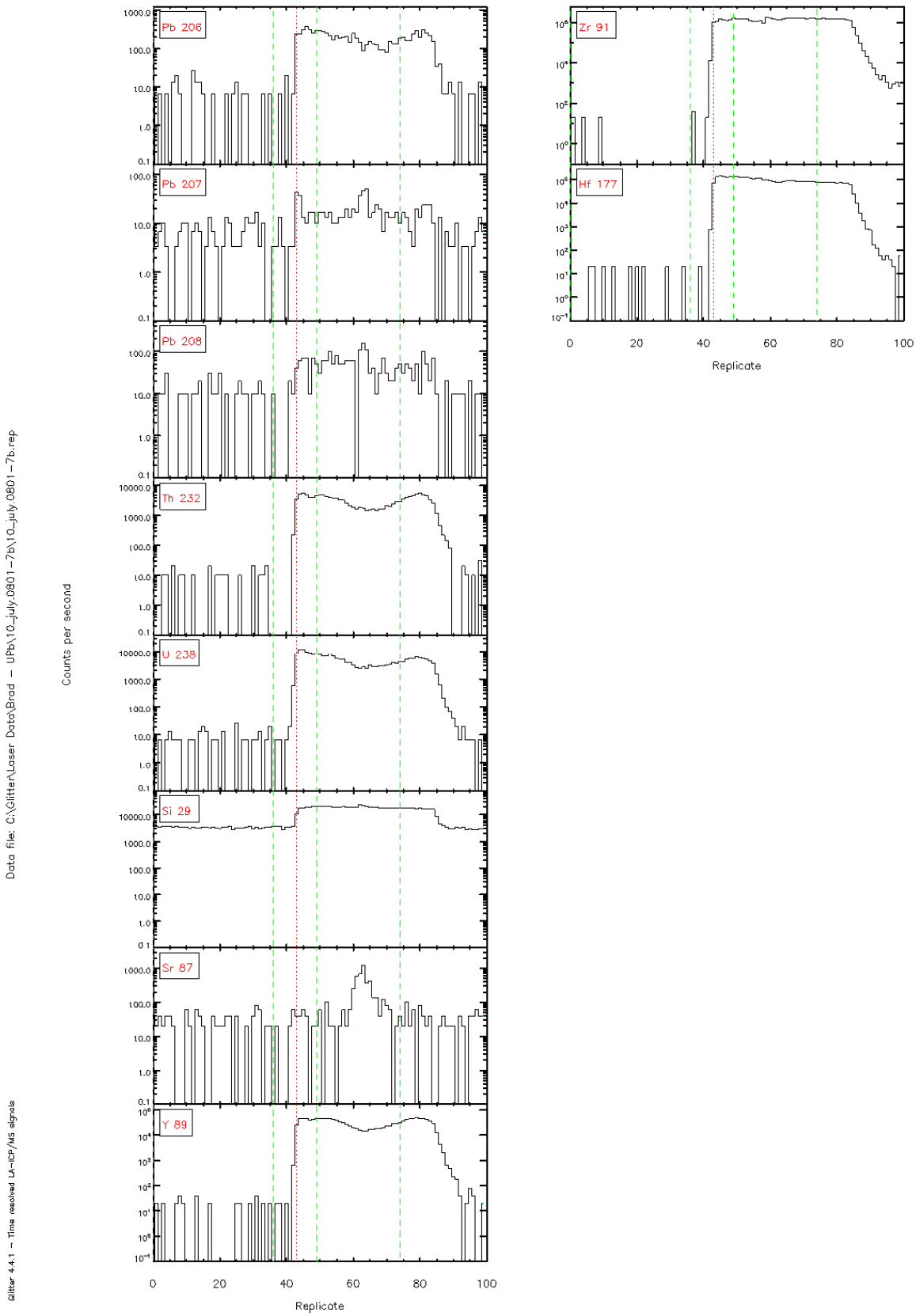
Pb 206
Pb 207
Pb 208
Th 232
U 238
Si 29
Sr 87
Y 89
Zr 91
Hf 177
Counts per second
Replicate
Data file: C:\Glitter\Laser Data\Brad – UPb\10_july.0801–7b\10_july.0801–7b.rep
Glitter 4.4.1 – Time resolved LA-ICP/MS signals

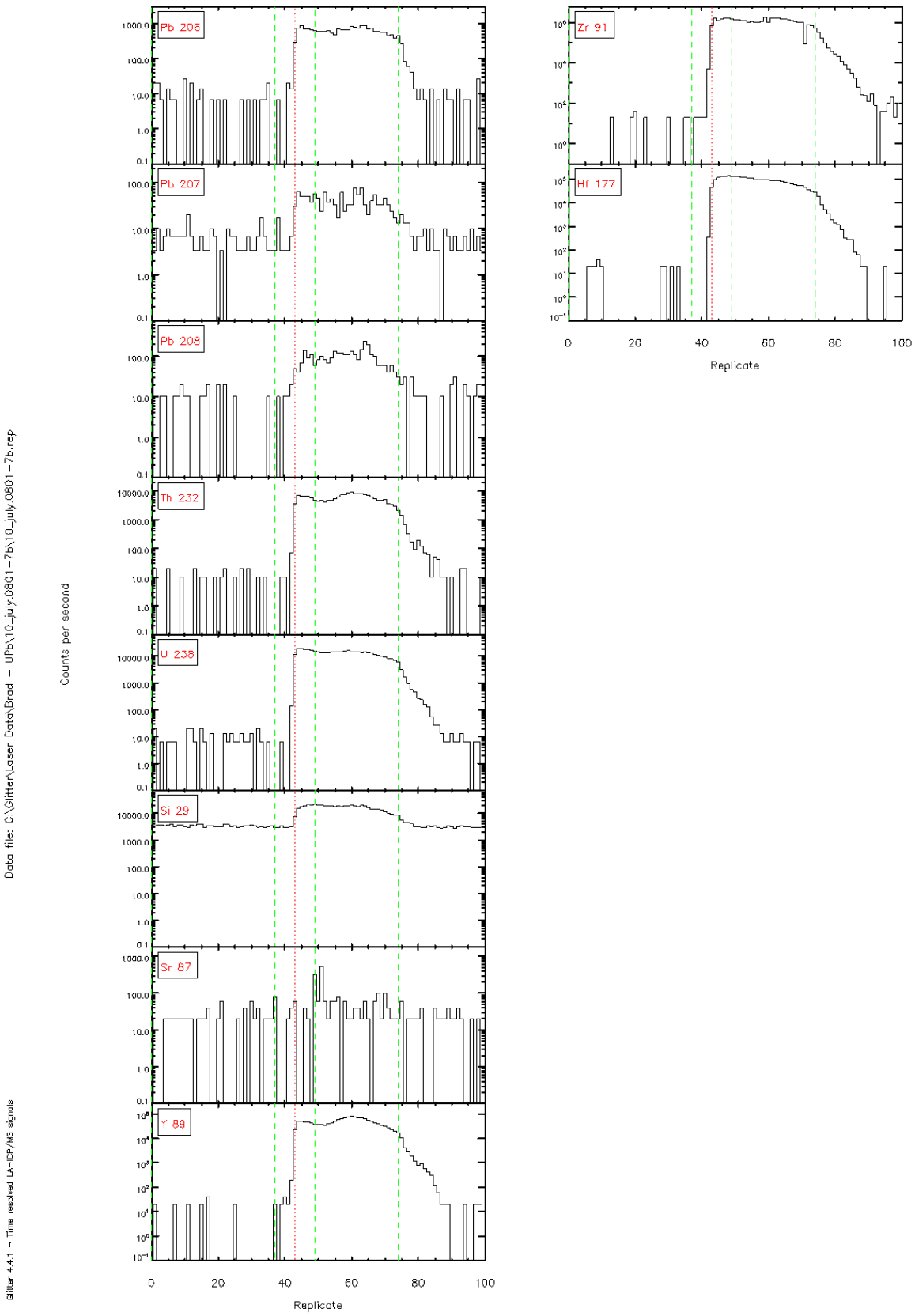
Pb 206
Pb 207
Pb 208
Th 232
U 238
Si 29
Sr 87
Y 89
Zr 91
Hf 177
Counts per second
Replicate
Data file: C:\Glitter\Laser Data\Brad - UPb\10_july.0801-7b\10_july.0801-7b.rep
Glitter 4.4.1 - Time resolved LA-ICP-MS signals

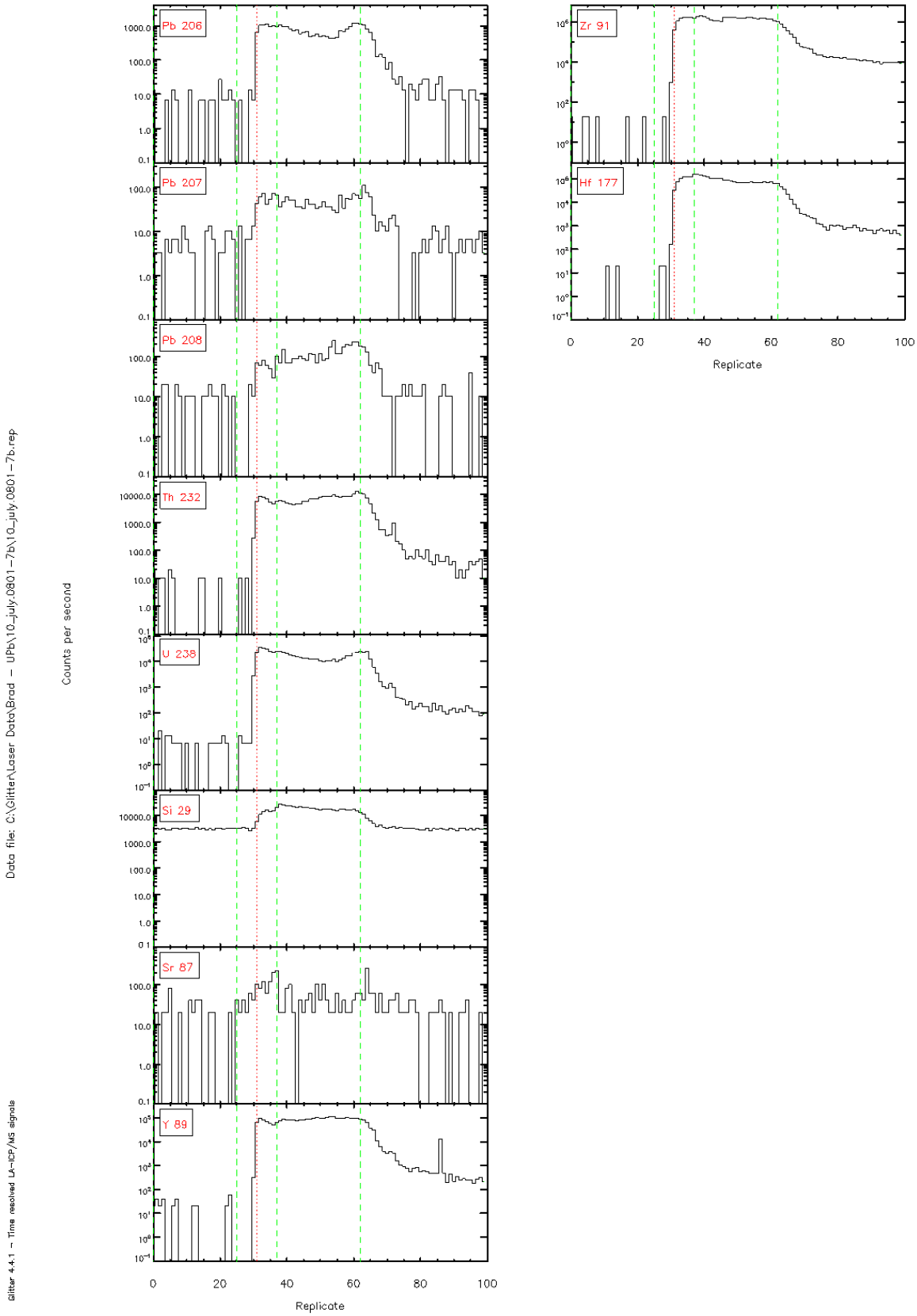
Pb 206
Pb 207
Pb 208
Th 232
U 238
Si 29
Sr 87
Y 89
Zr 91
Hf 177
Counts per second
Replicate
Data file: C:\Glitter\Laser Data\Brad – UPb\10_july.0801–7b\10_july.0801–7b.rep
Glitter 4.4.1 – Time resolved LA-ICP/MS signals

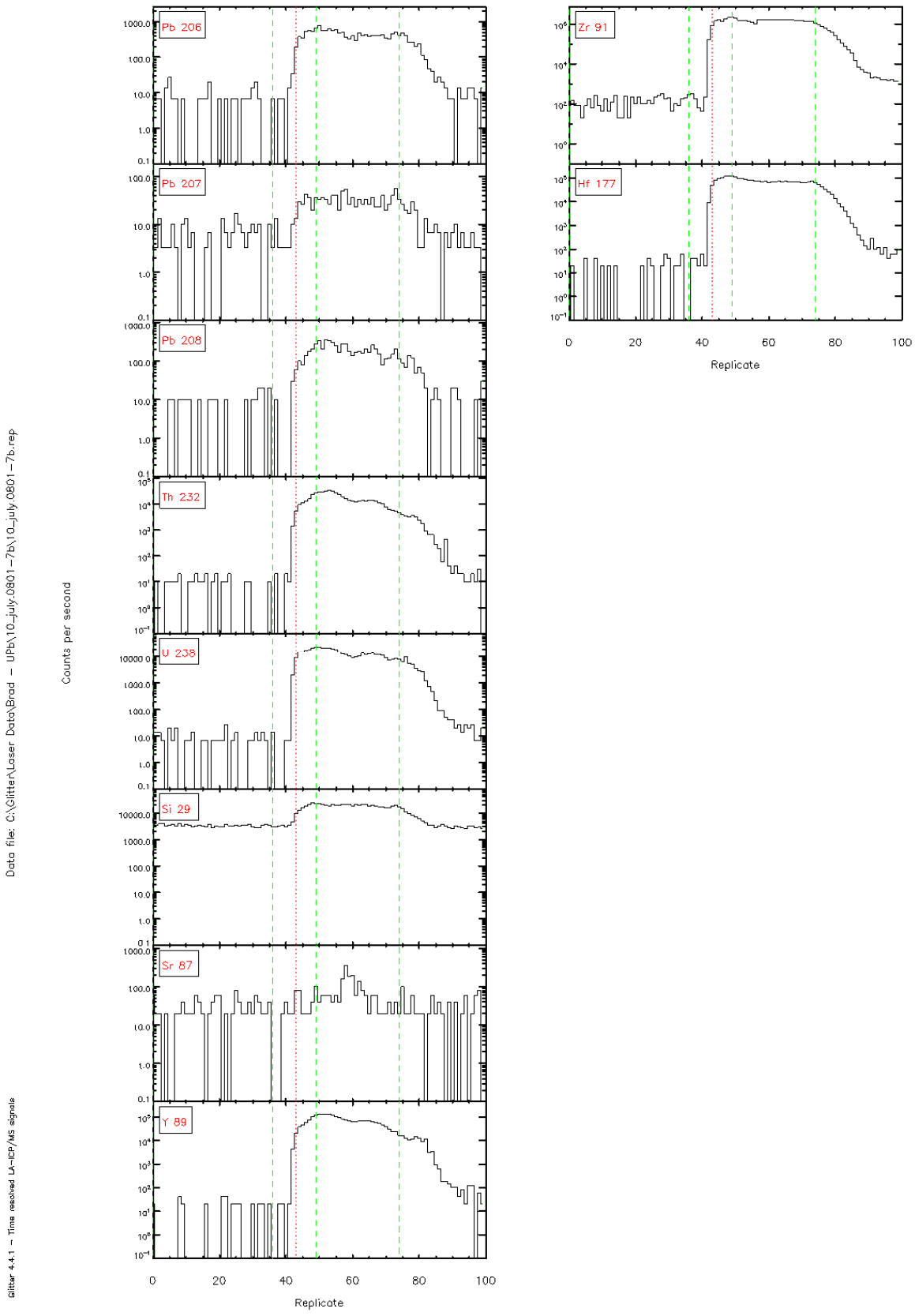
Pb 206
Pb 207
Pb 208
Th 232
U 238
Si 29
Sr 87
Y 89
Zr 91
Hf 177
Counts per second
Replicate
Data file: C:\Glitter\Laser Data\Brad – UPb\10_july.0801-7b\10_july.0801-7b.rep
Glitter 4.4.1 – Time resolved LA-ICP/MS signals

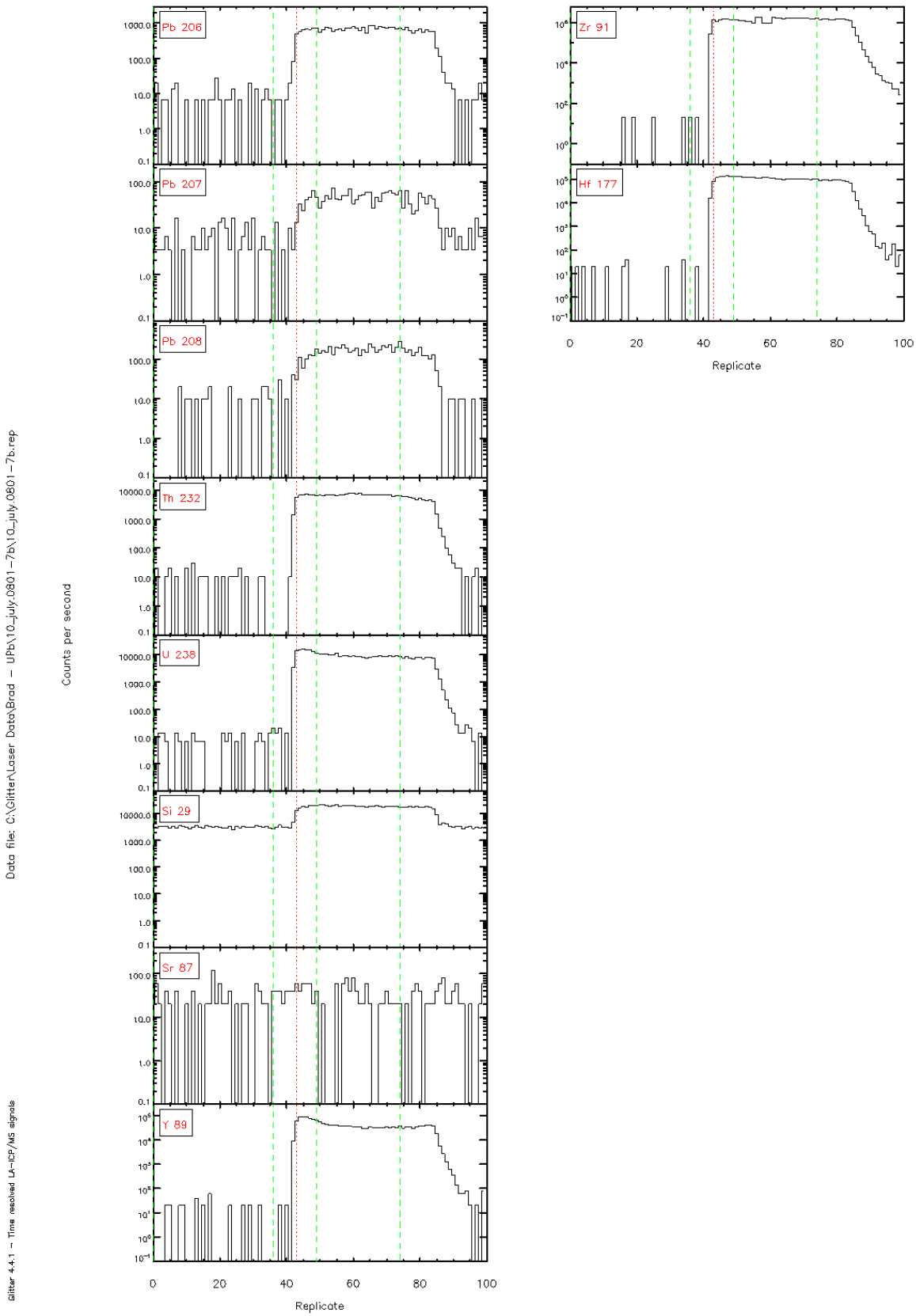
Pb 206
Pb 207
Pb 208
Th 232
U 238
Si 29
Sr 87
Y 89
Zr 91
Hf 177
Counts per second
Replicate
Data file: C:\Glitter\Laser Data\Brad – UPb\10_july.0801–7b\10_july.0801–7b.rep
Glitter 4.4.1 – Time resolved LA-ICP/MS signals

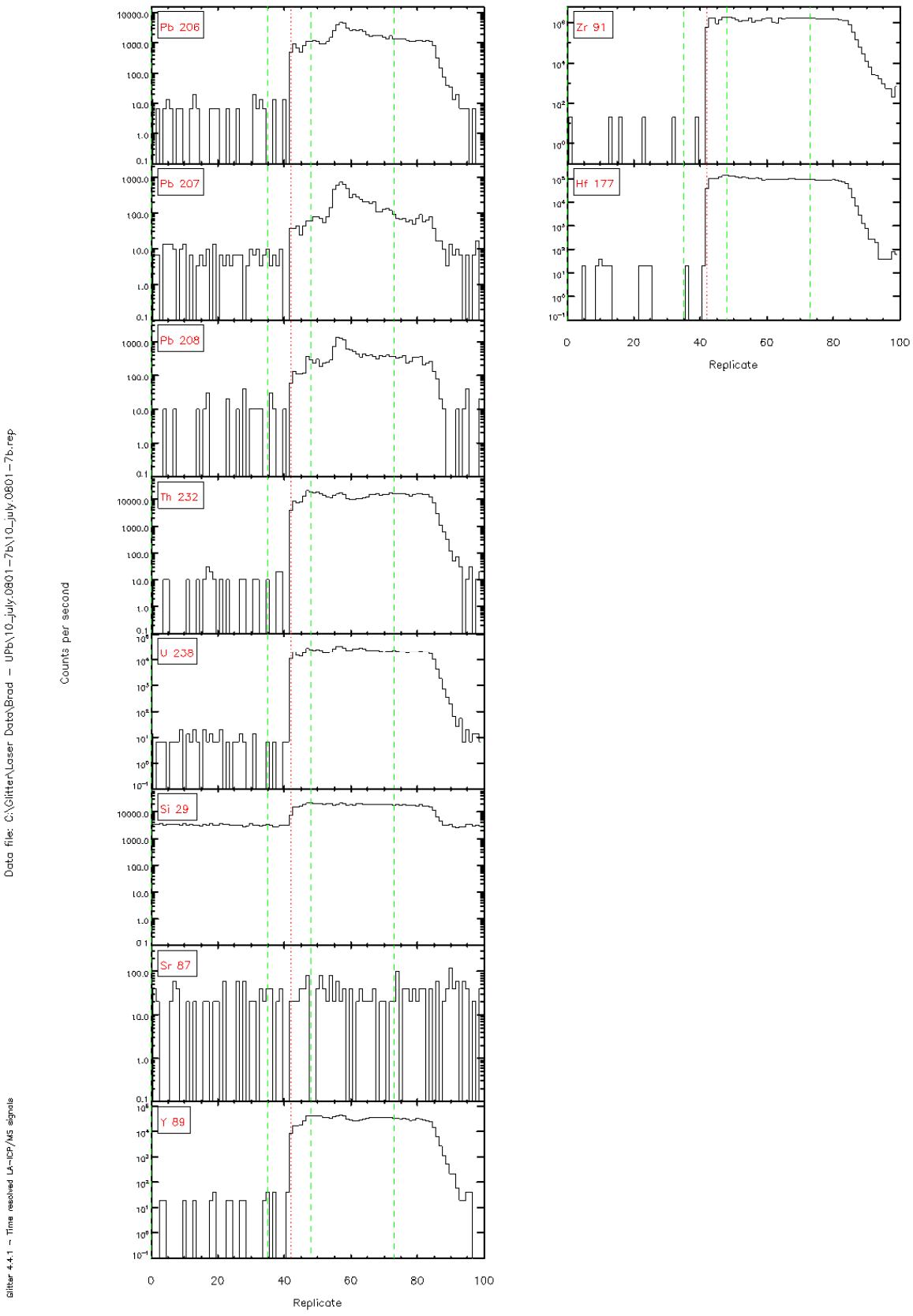
Pb 206
Pb 207
Pb 208
Th 232
U 238
Si 29
Sr 87
Y 89
Zr 91
Hf 177
Counts per second
Replicate
Data file: C:\Glitter\Laser Data\Brad – UPb\10_july.0801–7b\10_july.0801–7b.rep
Glitter 4.4.1 – Time resolved LA–ICP/MS signals

1 – Ahirau Sandstone

1.

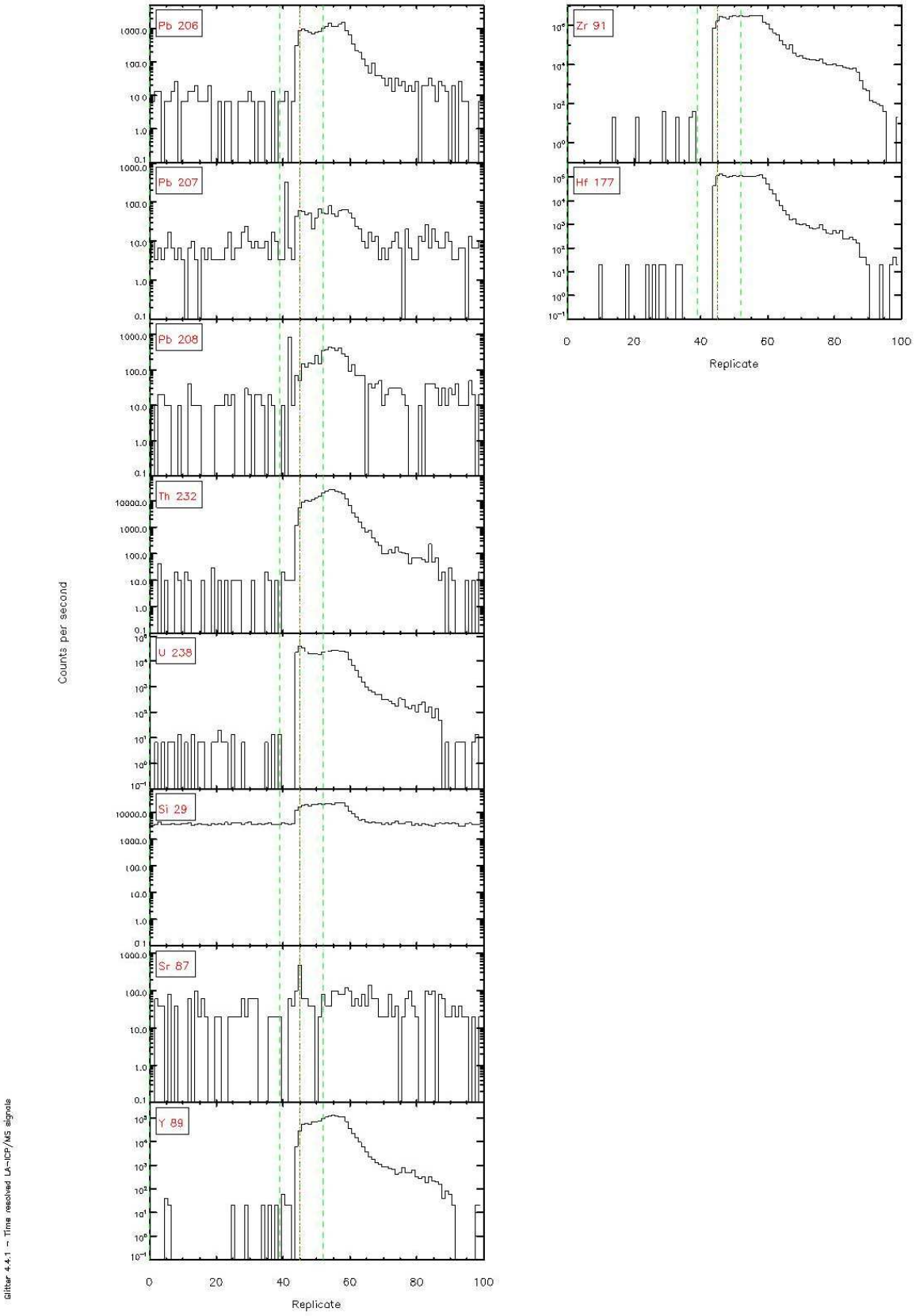

2.

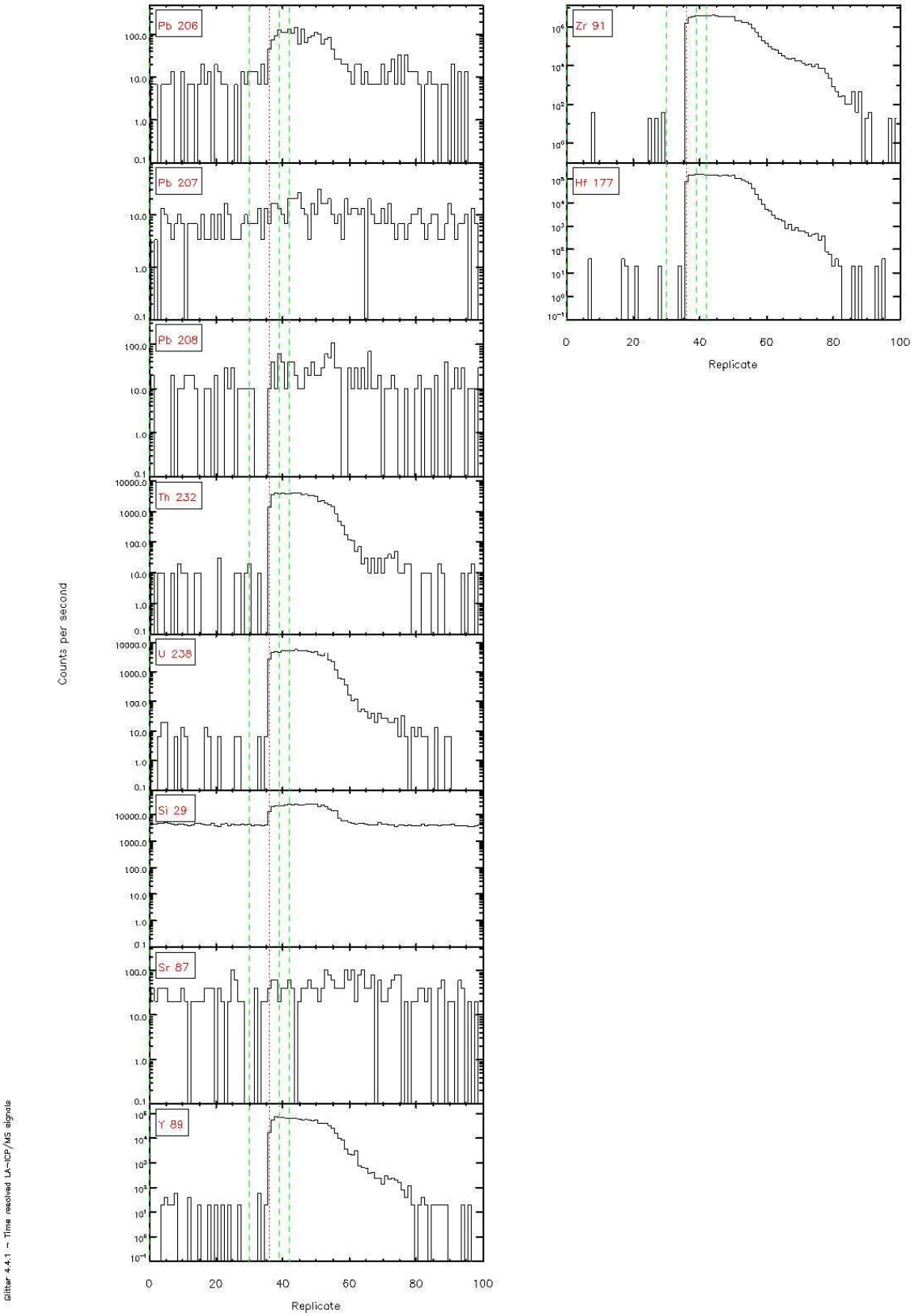
Pb 206
Pb 207
Pb 208
Th 232
U 238
Si 29
Sr 87
Y 89
Zr 91
Hf 177
Counts per second
Replicate
Glitter 4.4.1 – Time resolved LA-ICP/MS signals

3.

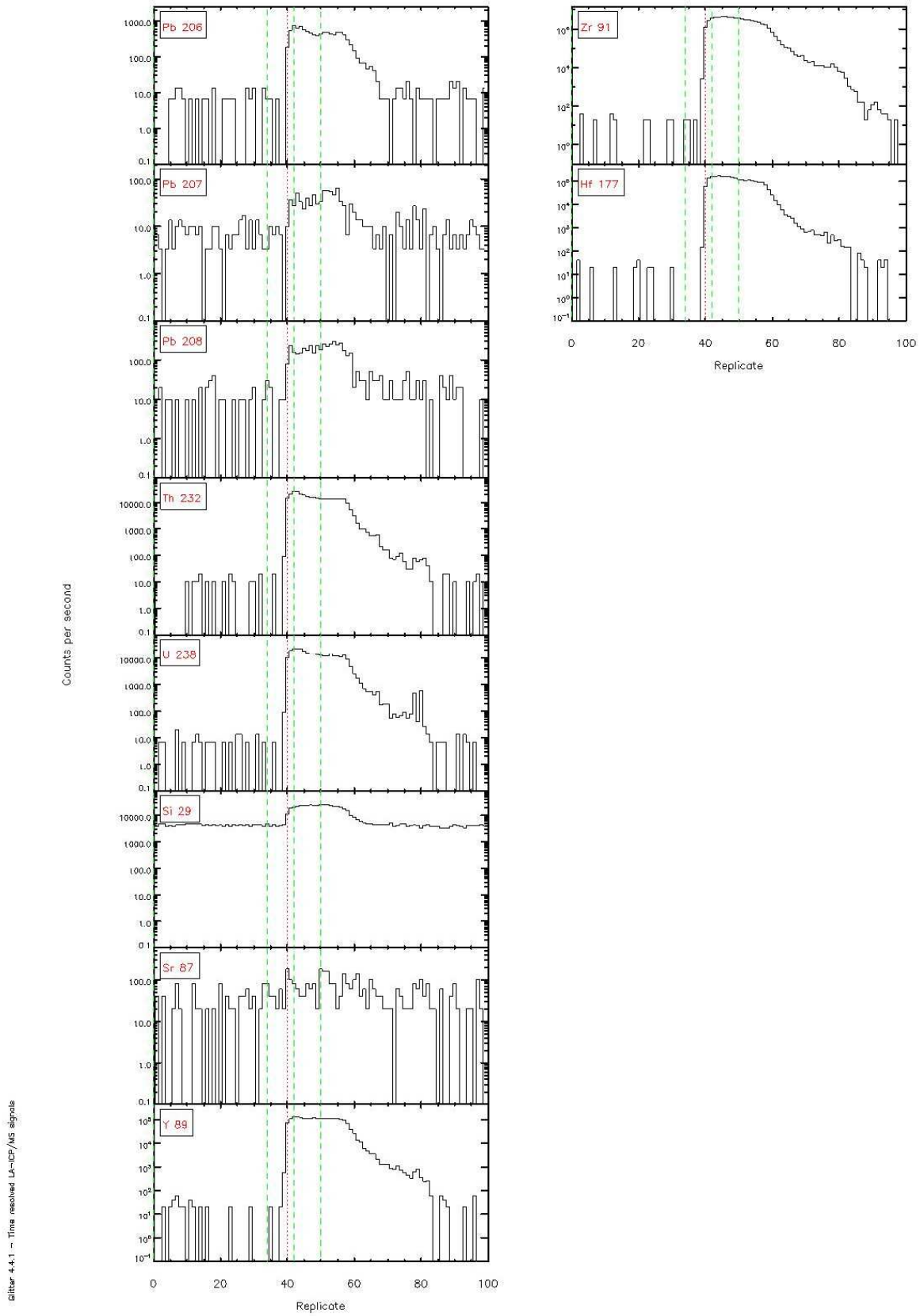
Pb 206
Pb 207
Pb 208
Th 232
U 238
Si 29
Sr 87
Y 89
Zr 91
Hf 177
Counts per second
Replicate
Glitter 4.4.1 - Time resolved LA-ICP/MS signals

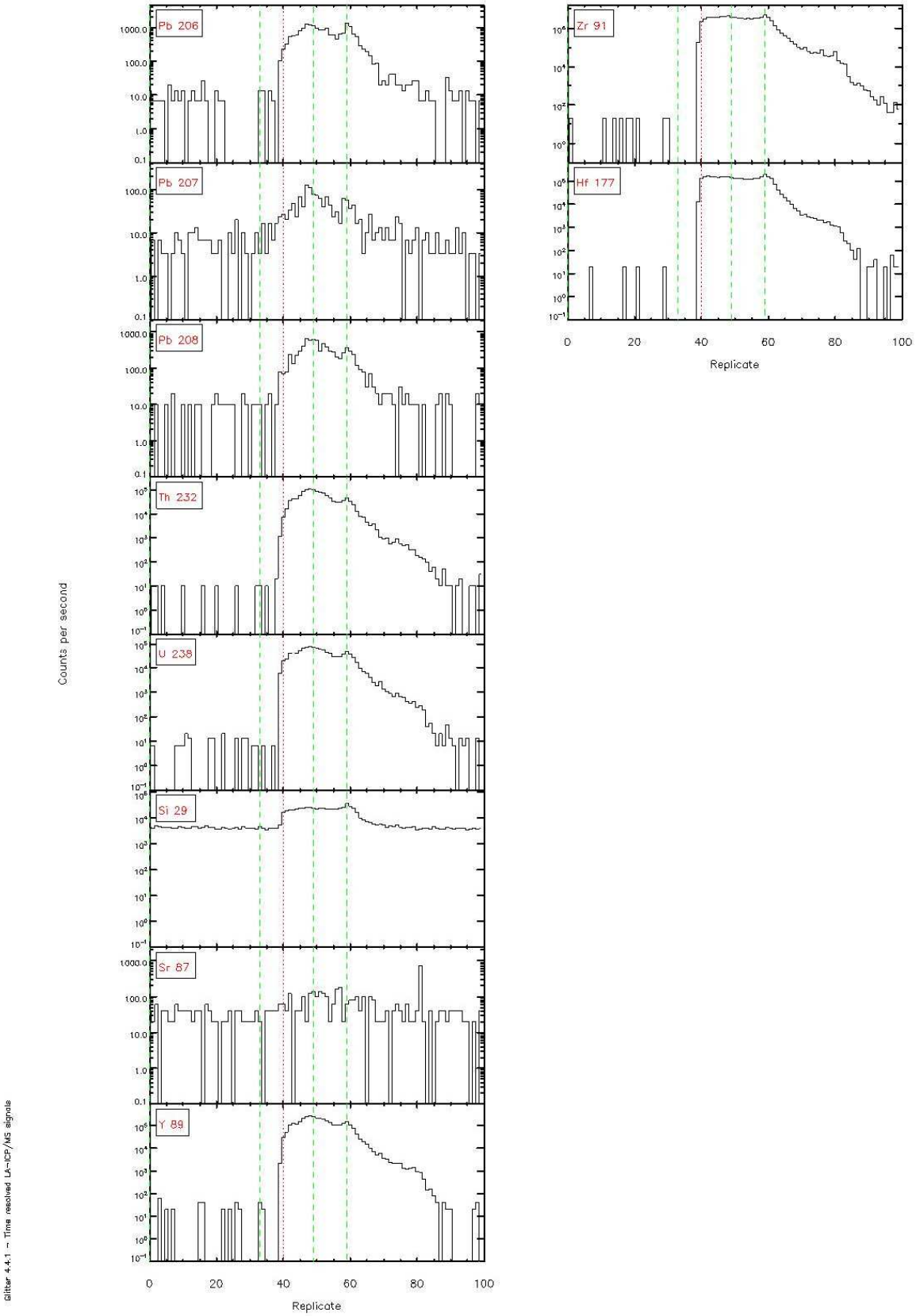
Pb 206
Pb 207
Pb 208
Th 232
U 238
Si 29
Sr 87
Y 89
Zr 91
Hf 177
Counts per second
Replicate
Glitter 4.4.1 – Time resolved LA-ICP/MS signals

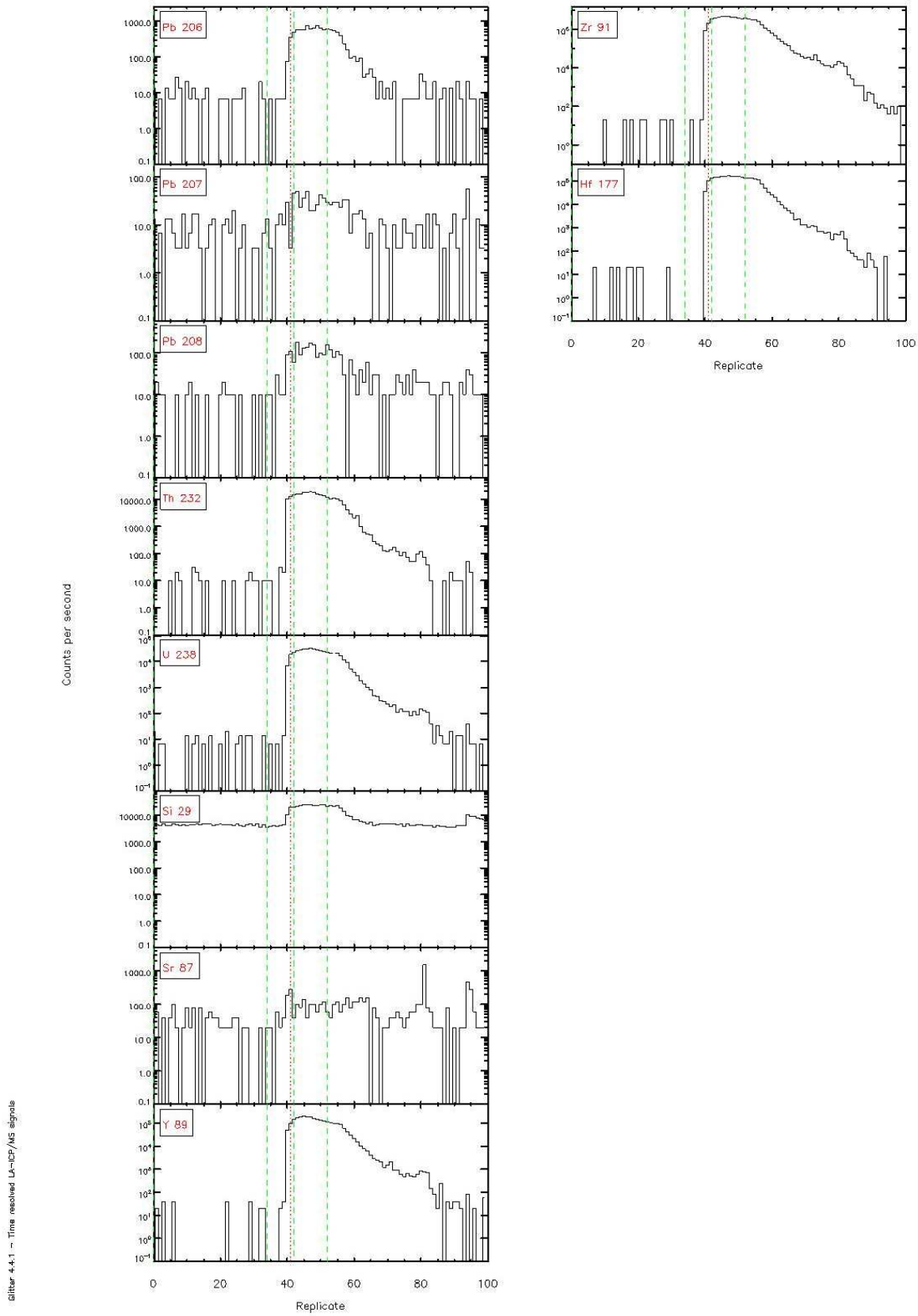
Pb 206
Pb 207
Pb 208
Th 232
U 238
Si 29
Sr 87
Y 89
Zr 91
Hf 177
Counts per second
Replicate
Glitter 4.4.1 - Time resolved LA-ICP/MS signals

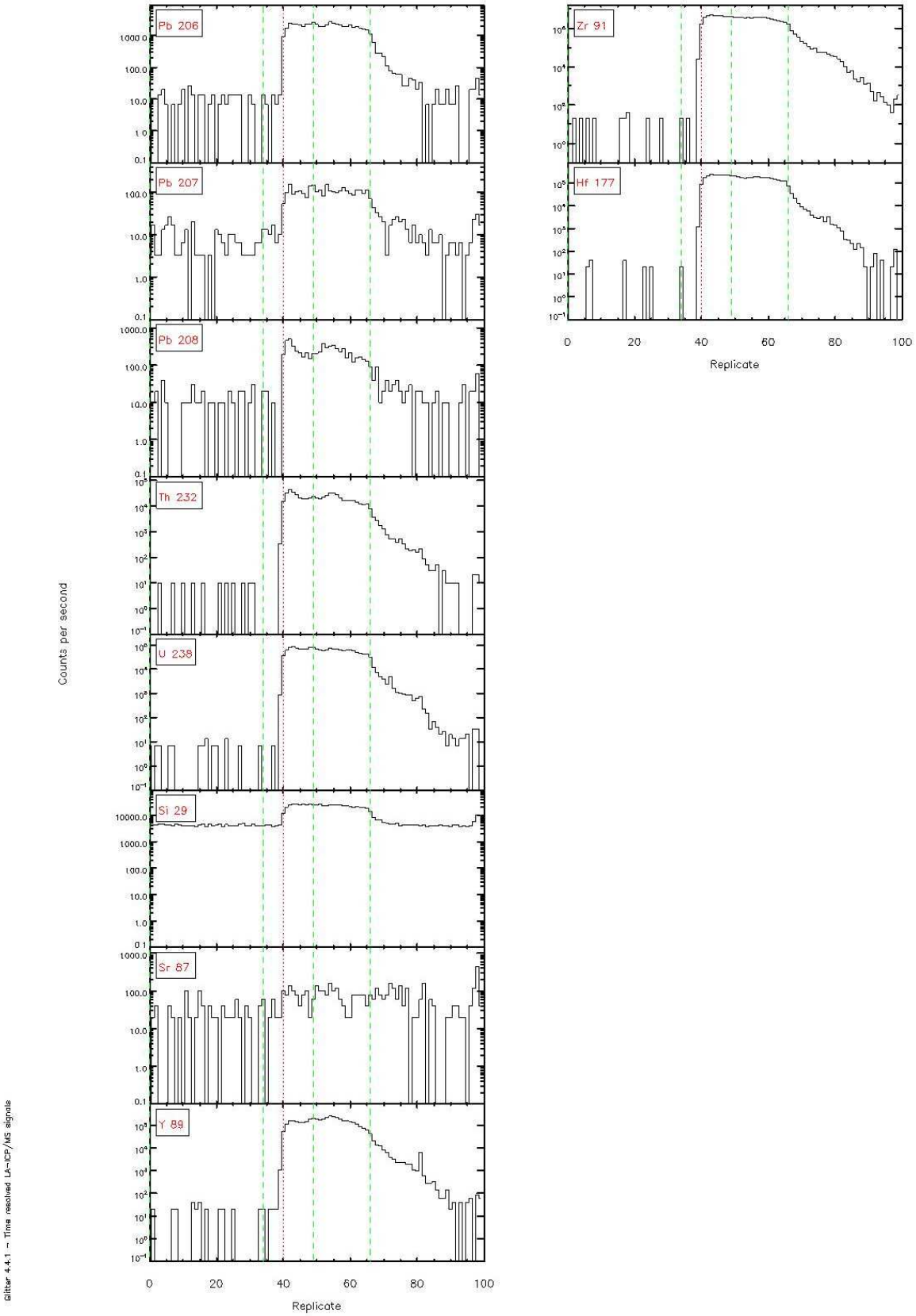
Pb 206
Pb 207
Pb 208
Th 232
U 238
Si 29
Sr 87
Y 89
Zr 91
Hf 177
Counts per second
Replicate
Glitter 4.4.1 – Time resolved LA-ICP/MS signals

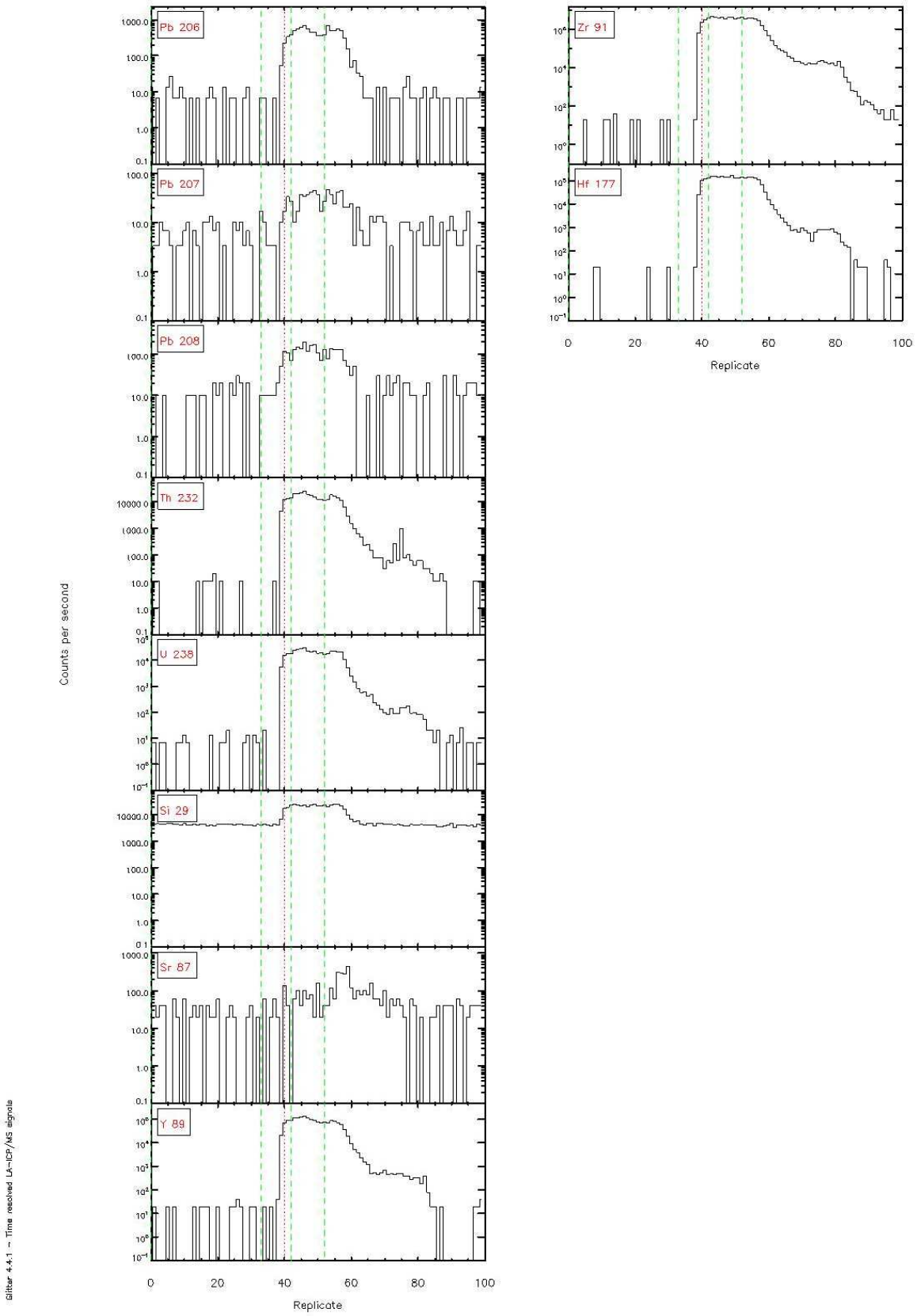
Pb 206
Pb 207
Pb 208
Th 232
U 238
Si 29
Sr 87
Y 89
Zr 91
Hf 177
Counts per second
Replicate
Glitter 4.4.1 – Time resolved LA-ICP/MS signals

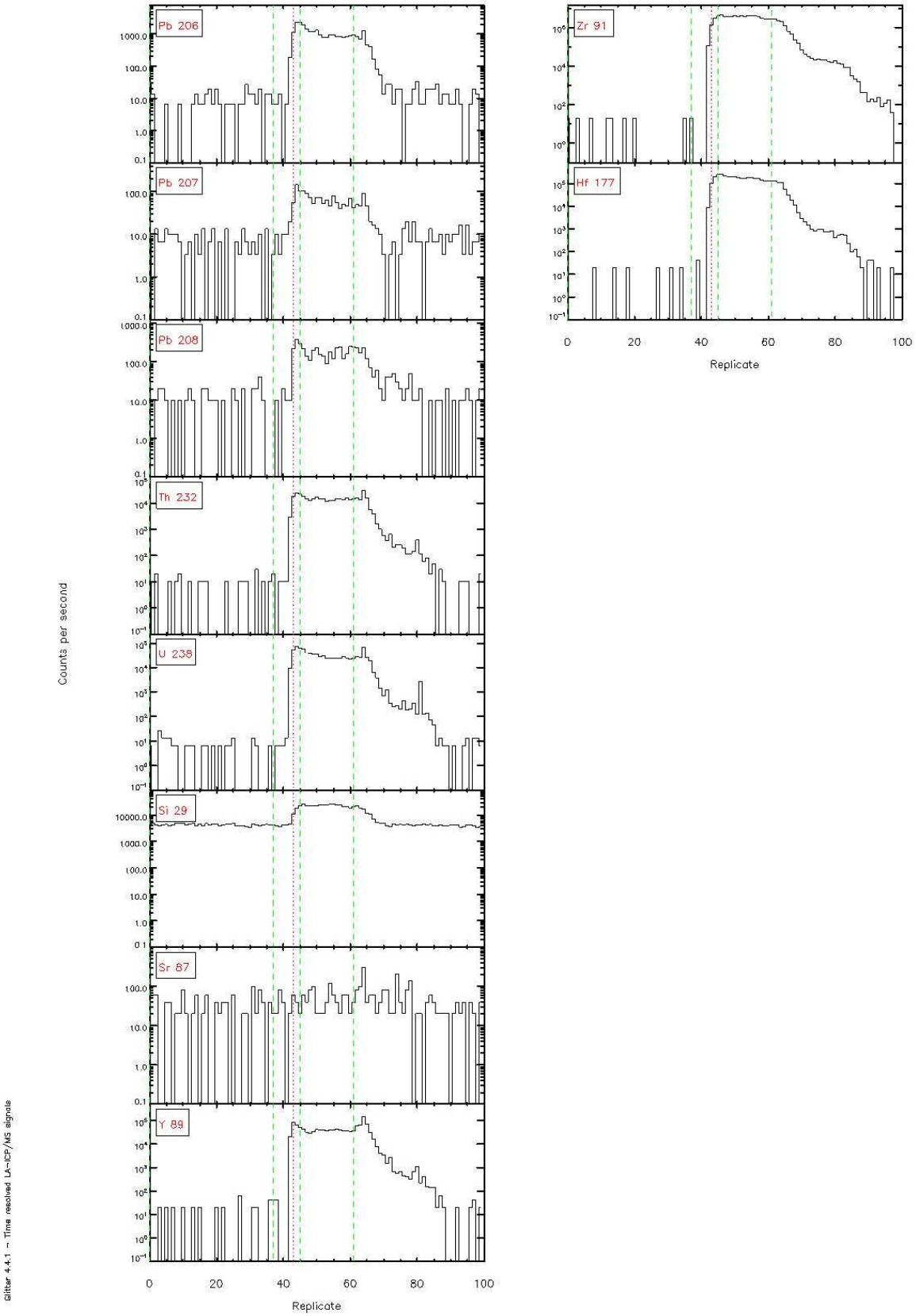
Pb 206
Pb 207
Pb 208
Th 232
U 238
Si 29
Sr 87
Y 89
Zr 91
Hf 177
Counts per second
Replicate
Glitter 4.4.1 - Time resolved LA-ICP/MS signals

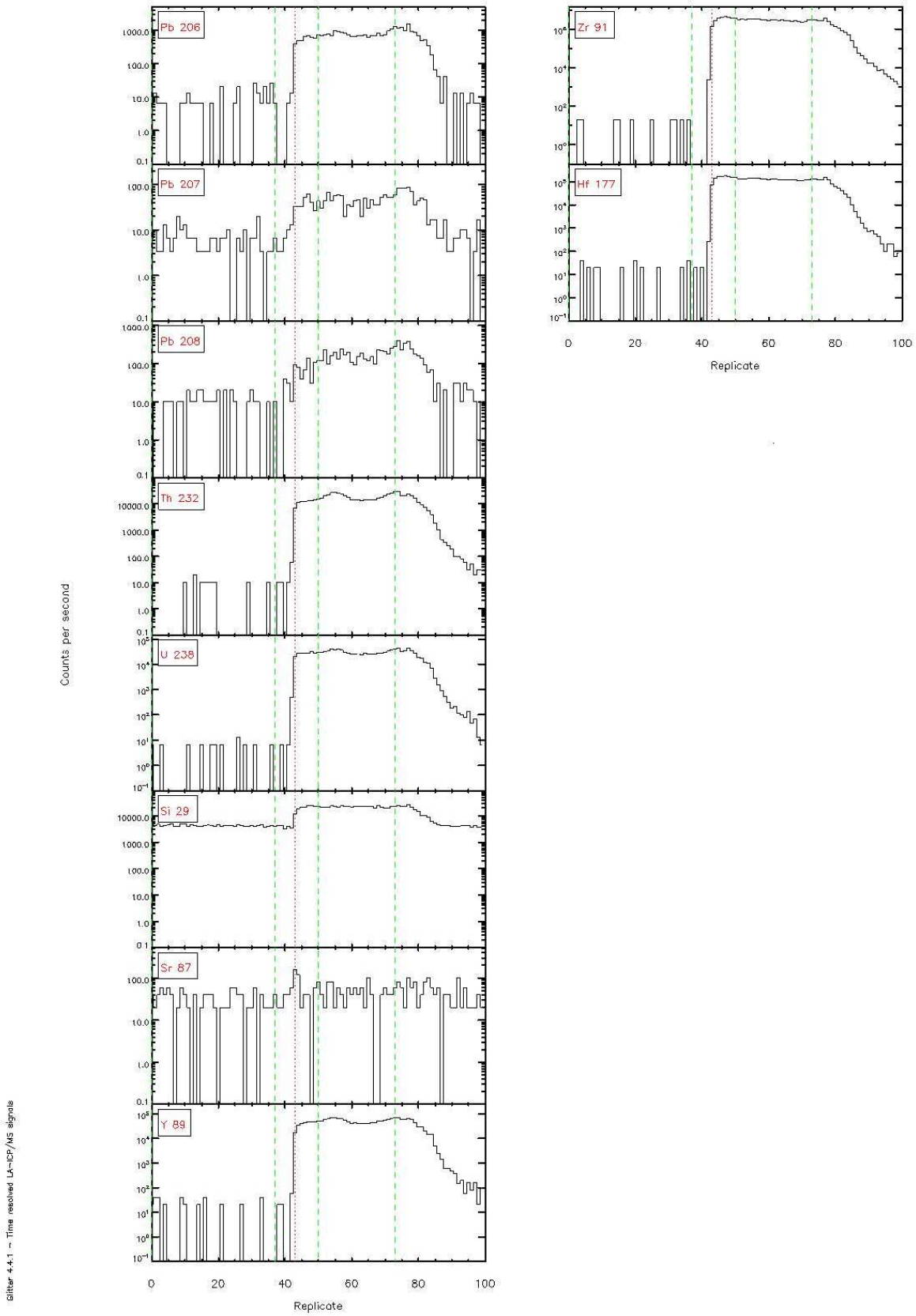
Pb 206
Pb 207
Pb 208
Th 232
U 238
Si 29
Sr 87
Y 89
Zr 91
Hf 177
Counts per second
Replicate
Glitter 4.4.1 – Time resolved LA-ICP/MS signals

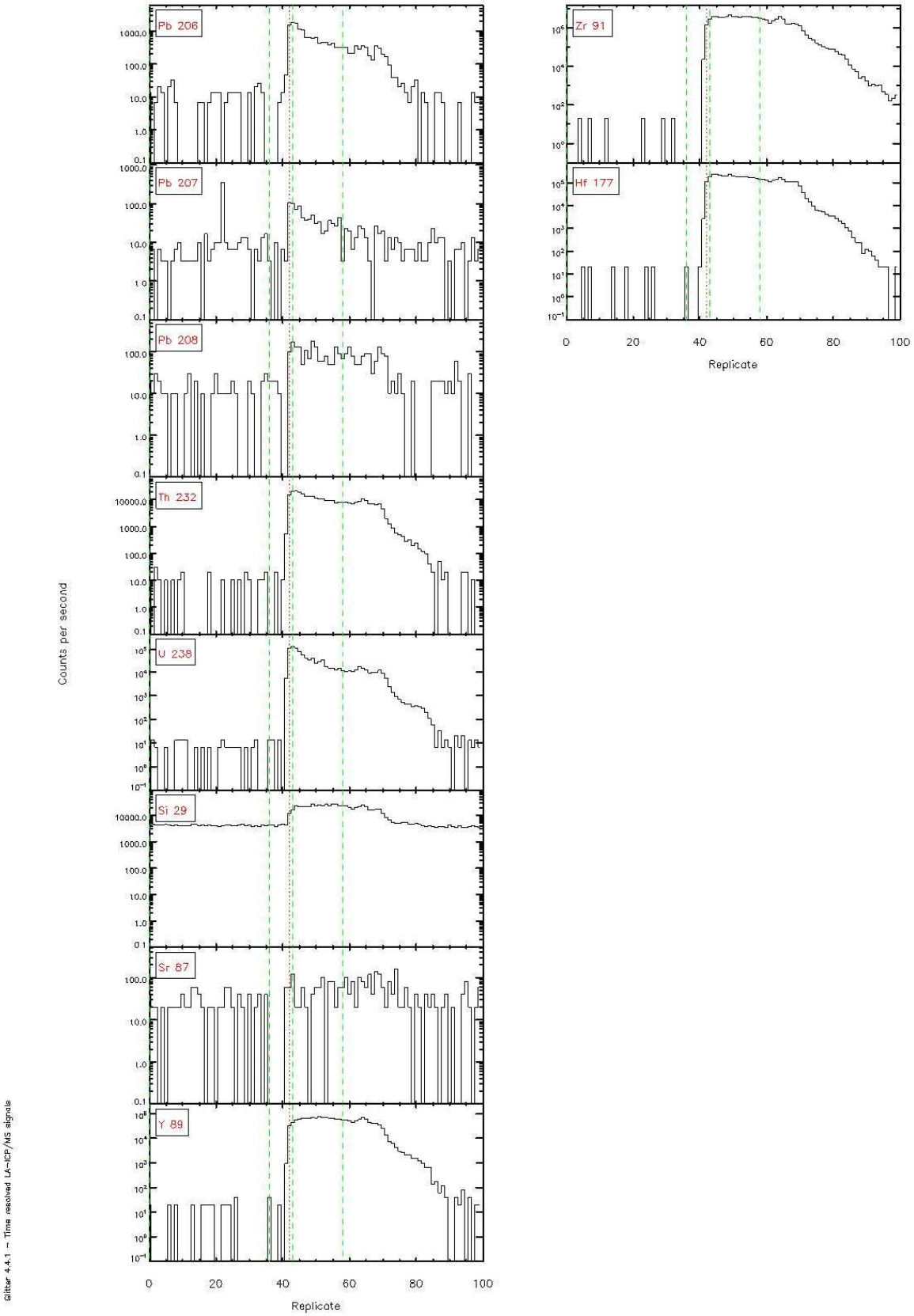
Pb 206
Pb 207
Pb 208
Th 232
U 238
Si 29
Sr 87
Y 89
Zr 91
Hf 177
Counts per second
Replicate
Glitter 4.4.1 – Time resolved LA-ICP/MS signals

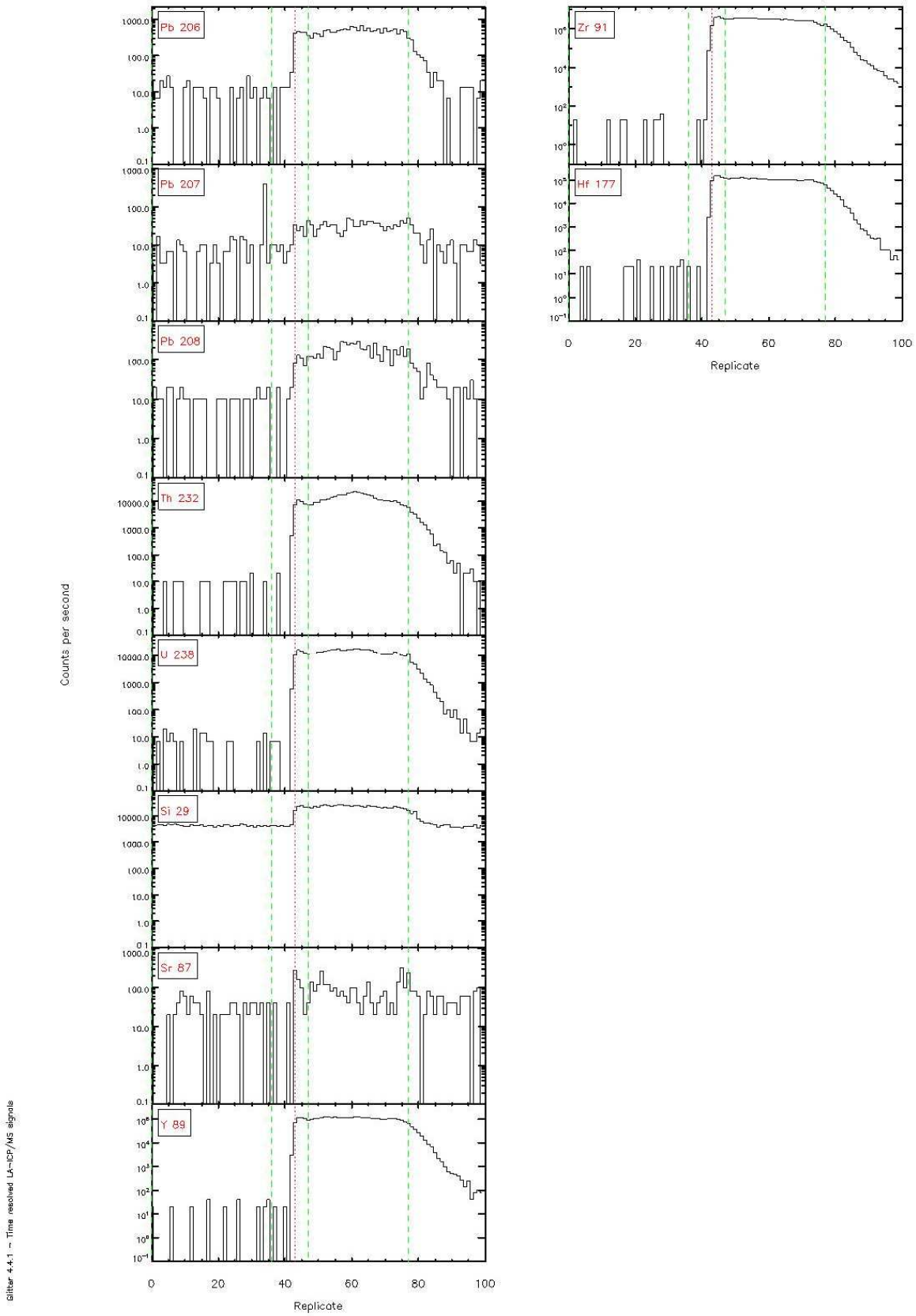
Pb 206
Pb 207
Pb 208
Th 232
U 238
Si 29
Sr 87
Y 89
Zr 91
Hf 177
Counts per second
Replicate
Glitter 4.4.1 – Time resolved LA-ICP/MS signals

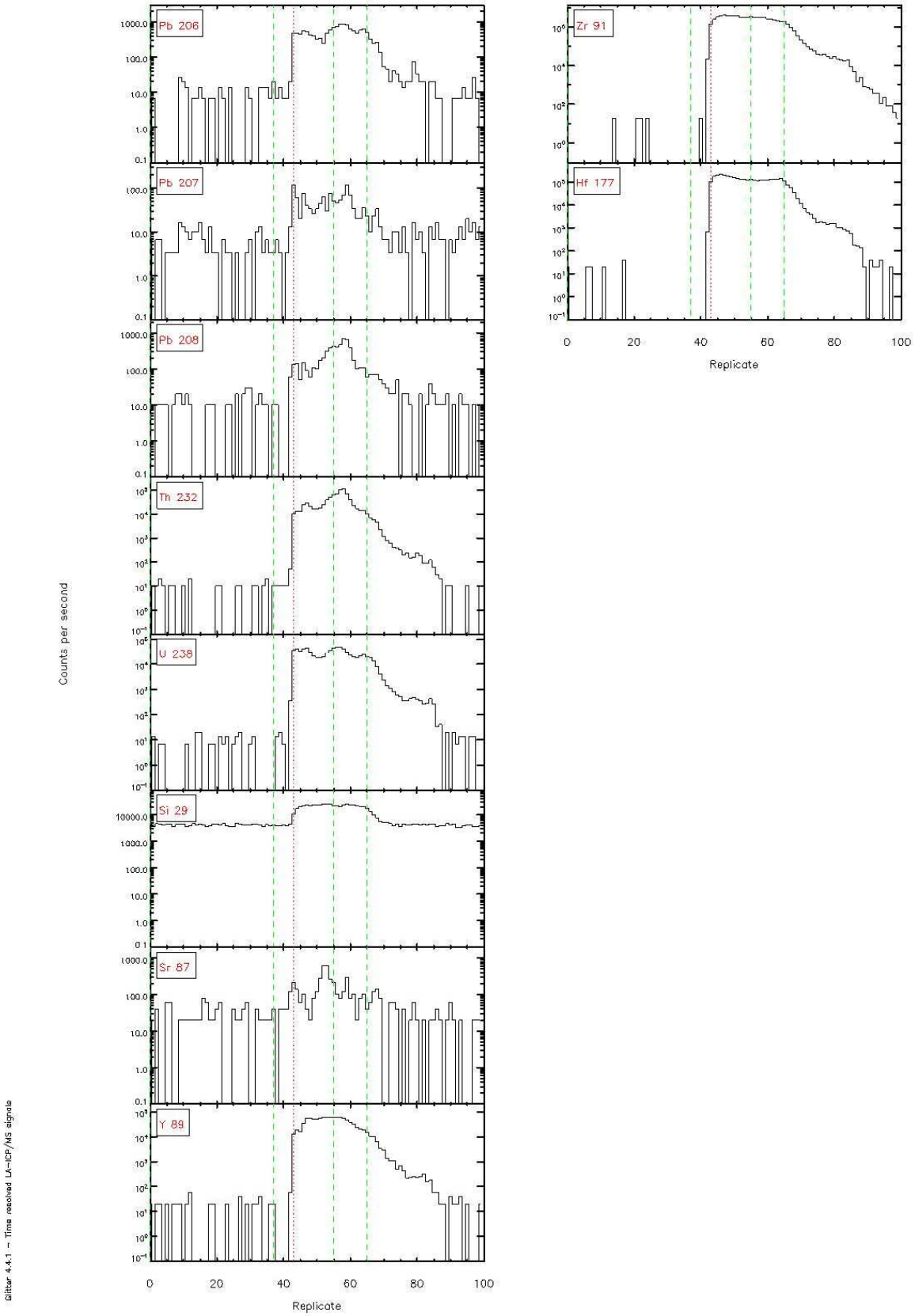
Pb 206
Pb 207
Pb 208
Th 232
U 238
Si 29
Sr 87
Y 89
Zr 91
Hf 177
Counts per second
Replicate
Glitter 4.4.1 – Time resolved LA-ICP/MS signals

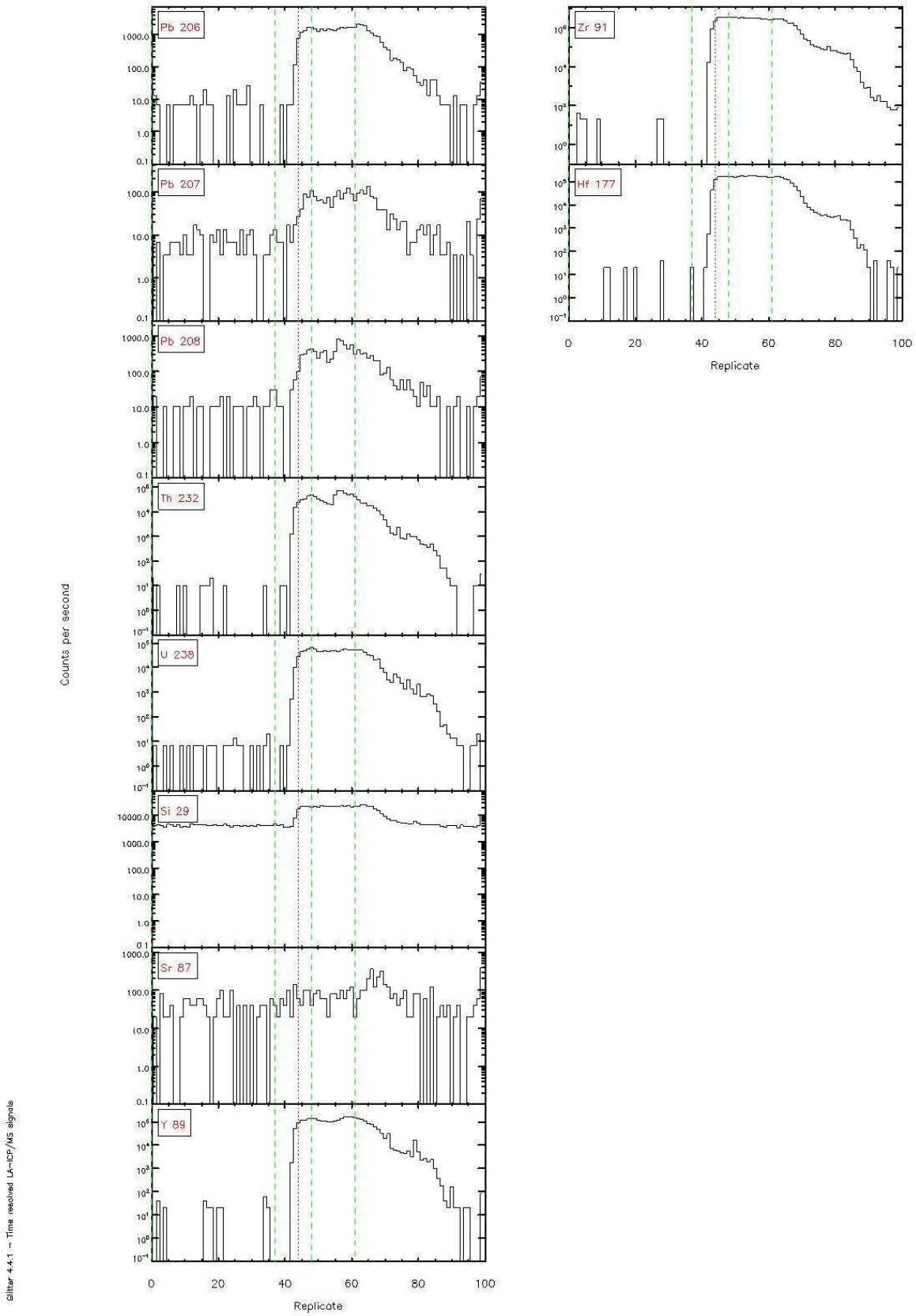
Pb 206
Pb 207
Pb 208
Th 232
U 238
Si 29
Sr 87
Y 89
Zr 91
Hf 177
Counts per second
Replicate
Glitter 4.4.1 – Time resolved LA-ICP/MS signals

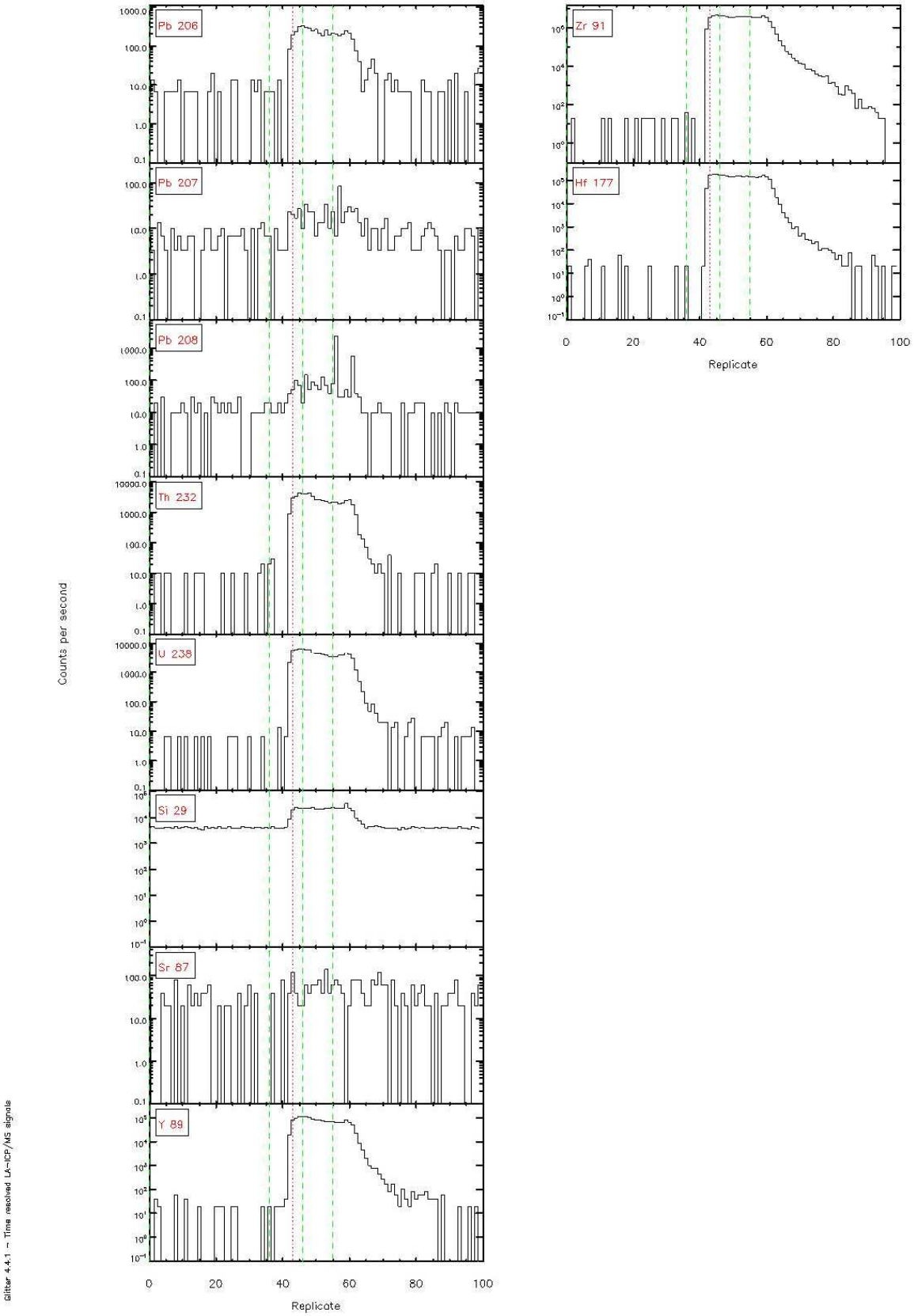
Pb 206
Pb 207
Pb 208
Th 232
U 238
Si 29
Sr 87
Y 89
Zr 91
Hf 177
Counts per second
Replicate
Glitter 4.4.1 – Time resolved LA-ICP/MS signals

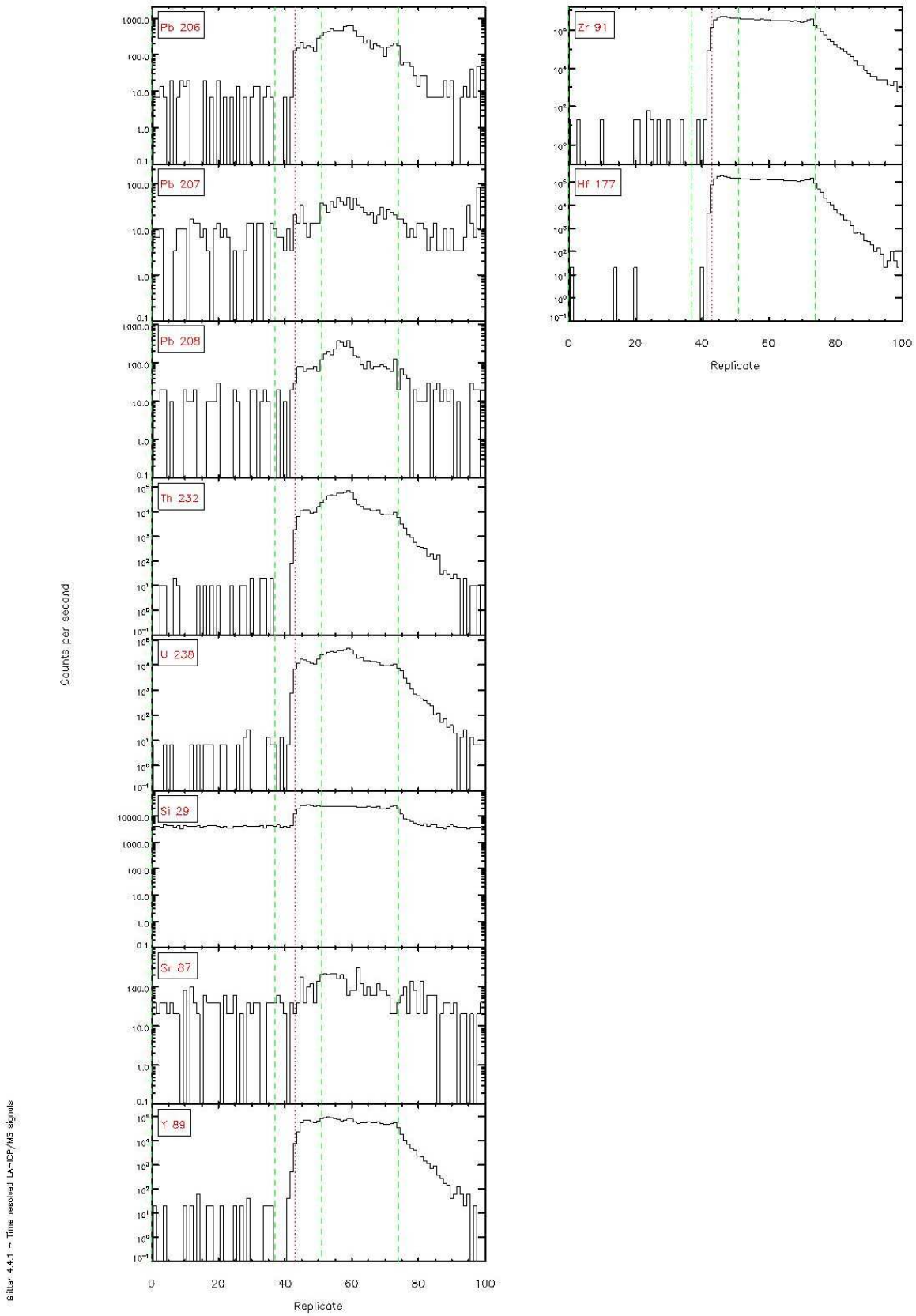
Pb 206
Pb 207
Pb 208
Th 232
U 238
Si 29
Sr 87
Y 89
Zr 91
Hf 177
Counts per second
Replicate
Glitter 4.4.1 – Time resolved LA-ICP/MS signals

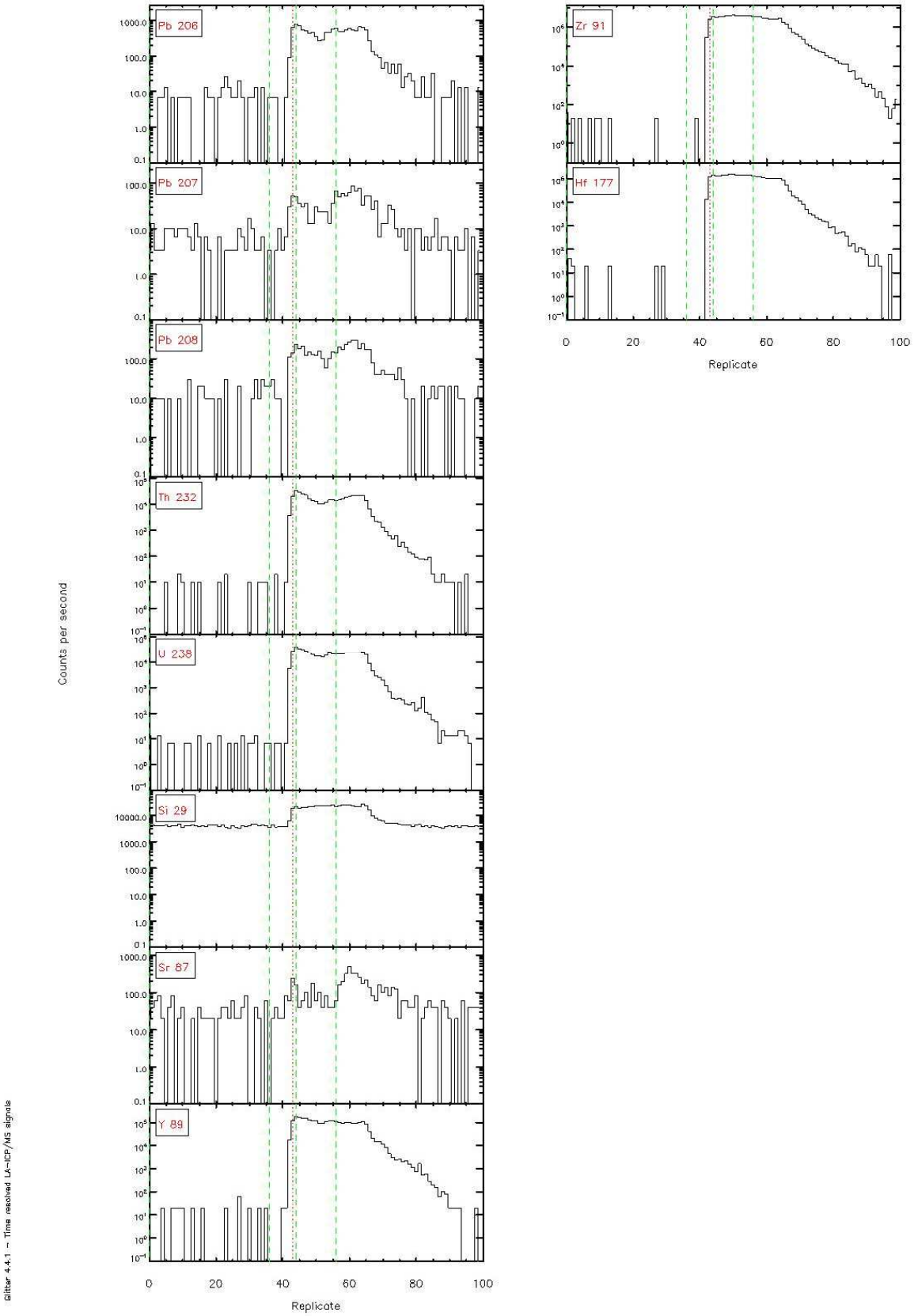
Pb 206
Pb 207
Pb 208
Th 232
U 238
Si 29
Sr 87
Y 89
Zr 91
Hf 177
Counts per second
Replicate
Glitter 4.4.1 – Time resolved LA-ICP/MS signals

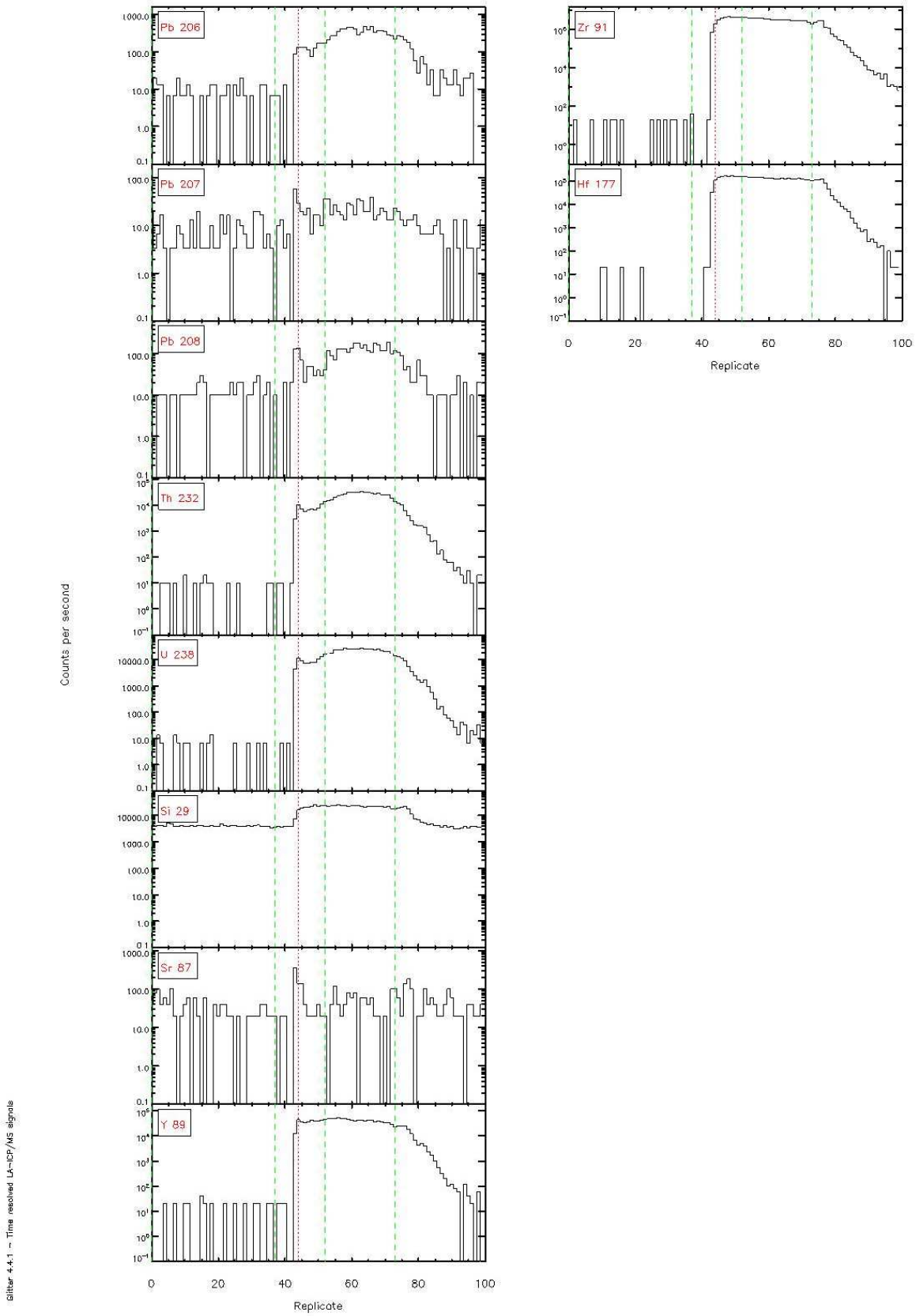
Pb 206
Pb 207
Pb 208
Th 232
U 238
Si 29
Sr 87
Y 89
Zr 91
Hf 177
Counts per second
Replicate
Glitter 4.4.1 – Time resolved LA-ICP/MS signals

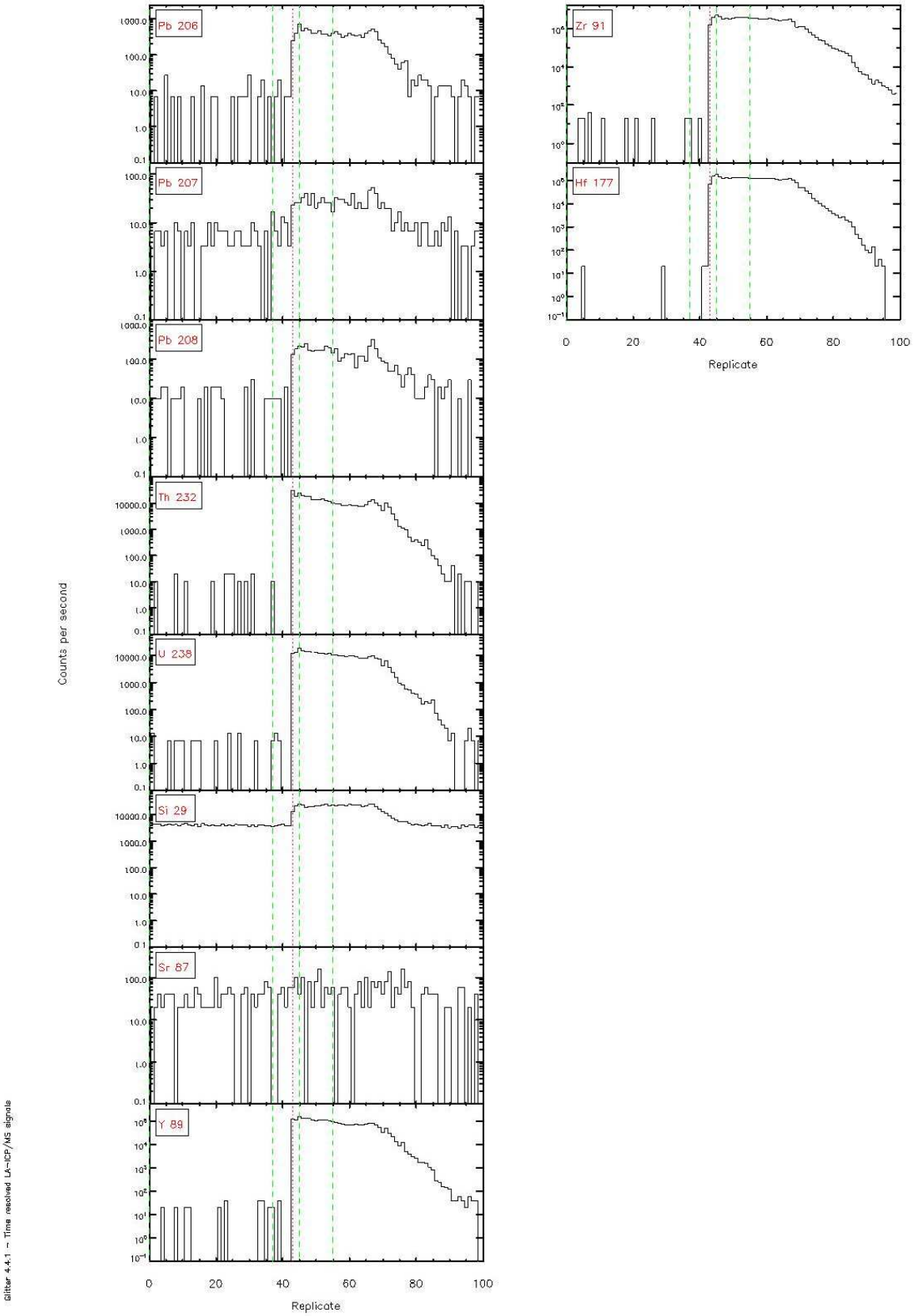
Pb 206
Pb 207
Pb 208
Th 232
U 238
Si 29
Sr 87
Y 89
Zr 91
Hf 177
Counts per second
Replicate
Glitter 4.4.1 – Time resolved LA-ICP/MS signals

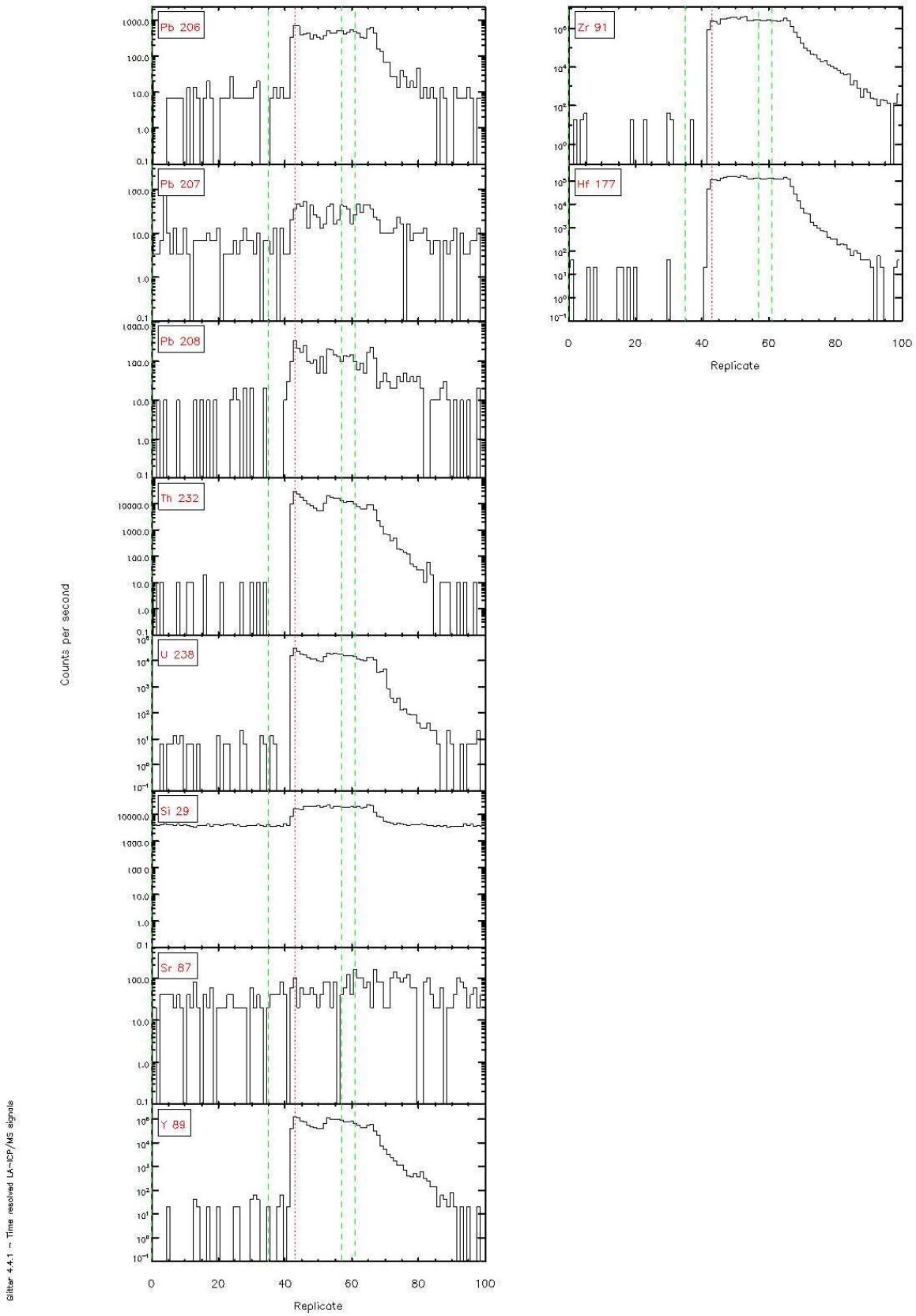
Pb 206
Pb 207
Pb 208
Th 232
U 238
Si 29
Sr 87
Y 89
Zr 91
Hf 177
Counts per second
Replicate
Glitter 4.4.1 – Time resolved LA-ICP/MS signals

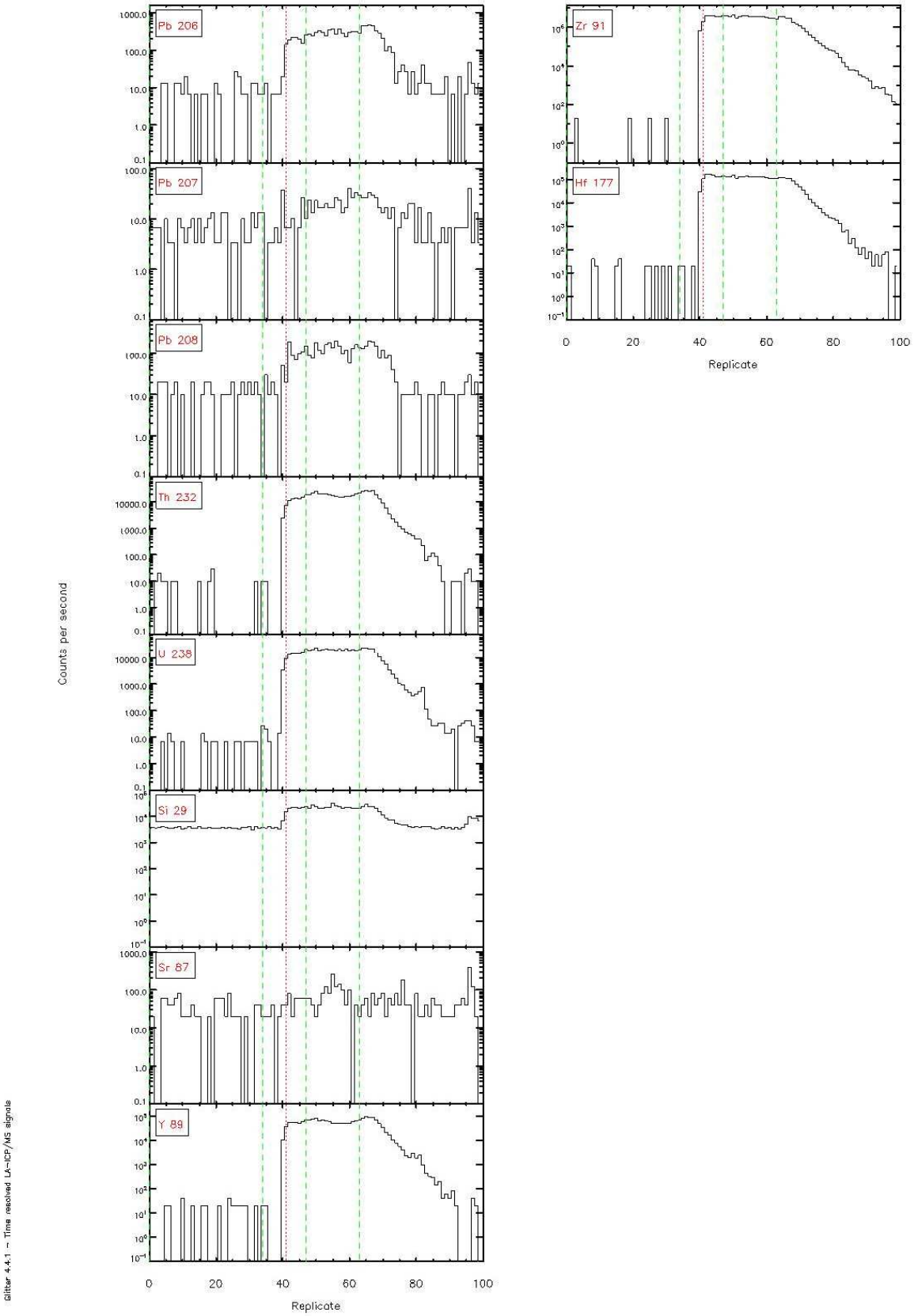
Pb 206
Pb 207
Pb 208
Th 232
U 238
Si 29
Sr 87
Y 89
Zr 91
Hf 177
Counts per second
Replicate
Glitter 4.4.1 – Time resolved LA-ICP/MS signals

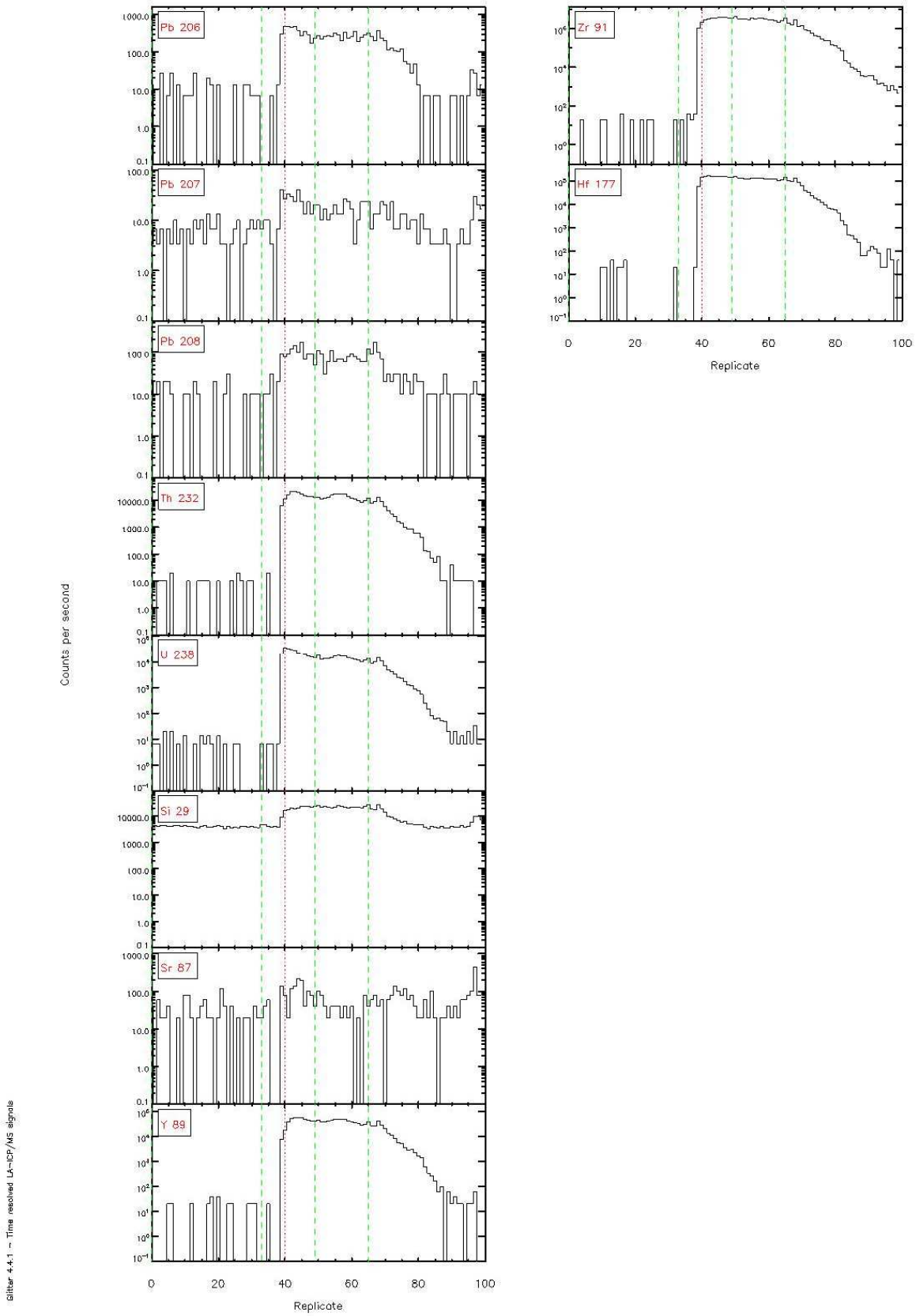
Pb 206
Pb 207
Pb 208
Th 232
U 238
Si 29
Sr 87
Y 89
Zr 91
Hf 177
Counts per second
Replicate
Glitter 4.4.1 – Time resolved LA-ICP/MS signals

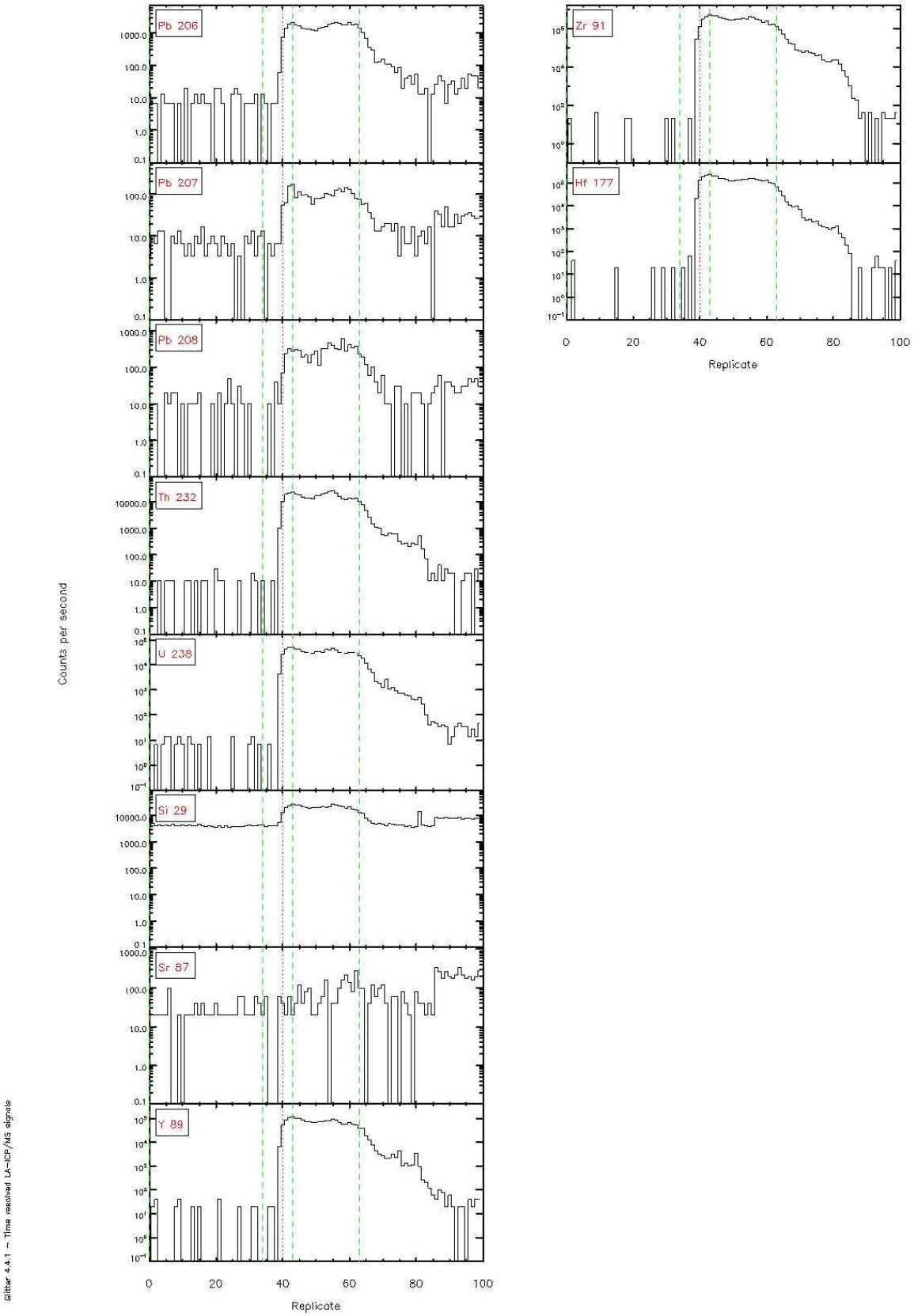
Pb 206
Pb 207
Pb 208
Th 232
U 238
Si 29
Sr 87
Y 89
Zr 91
Hf 177
Counts per second
Replicate
Glitter 4.4.1 – Time resolved LA-ICP/MS signals

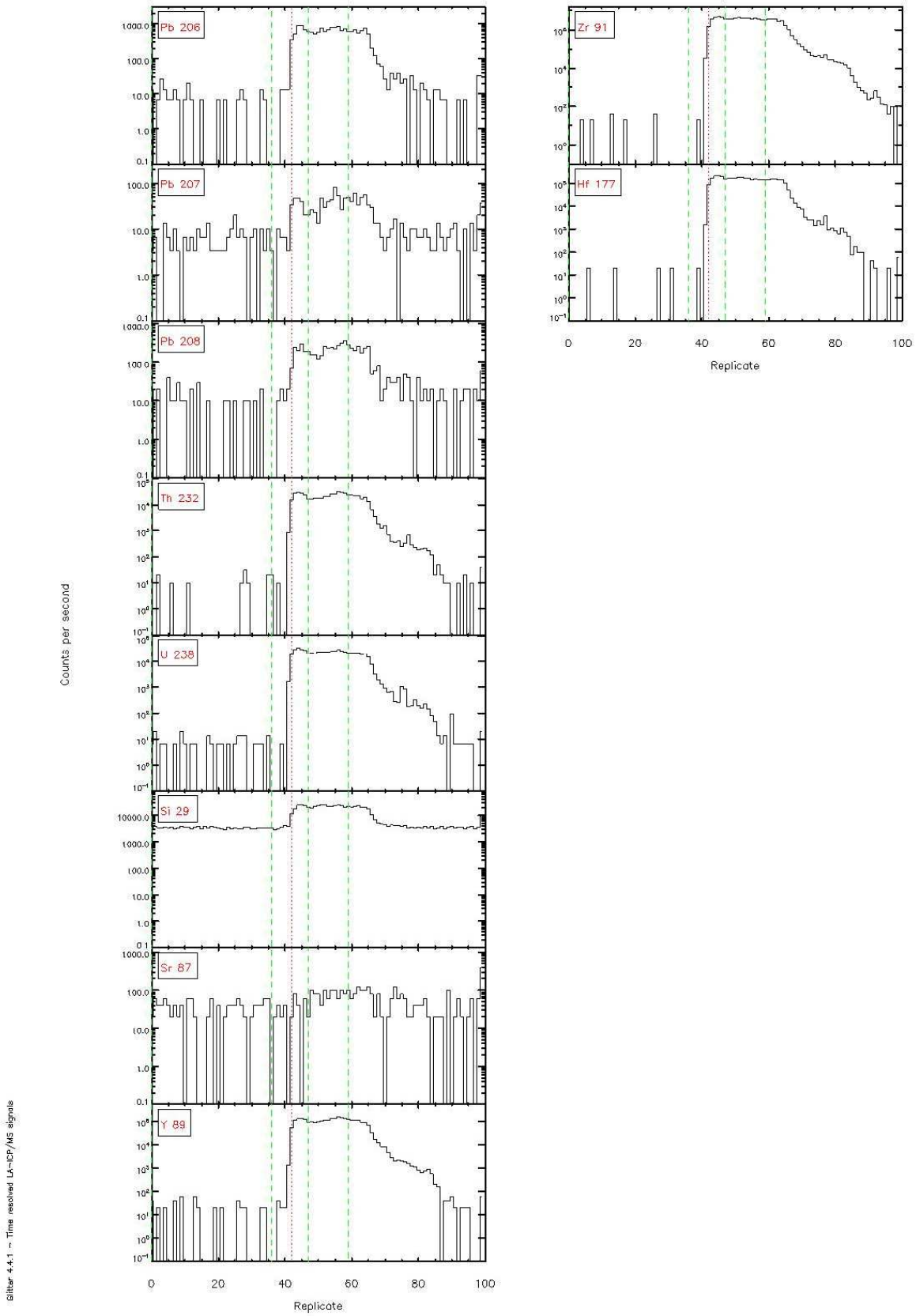
Pb 206
Pb 207
Pb 208
Th 232
U 238
Si 29
Sr 87
Y 89
Zr 91
Hf 177
Counts per second
Replicate
Glitter 4.4.1 – Time resolved LA-ICP/MS signals

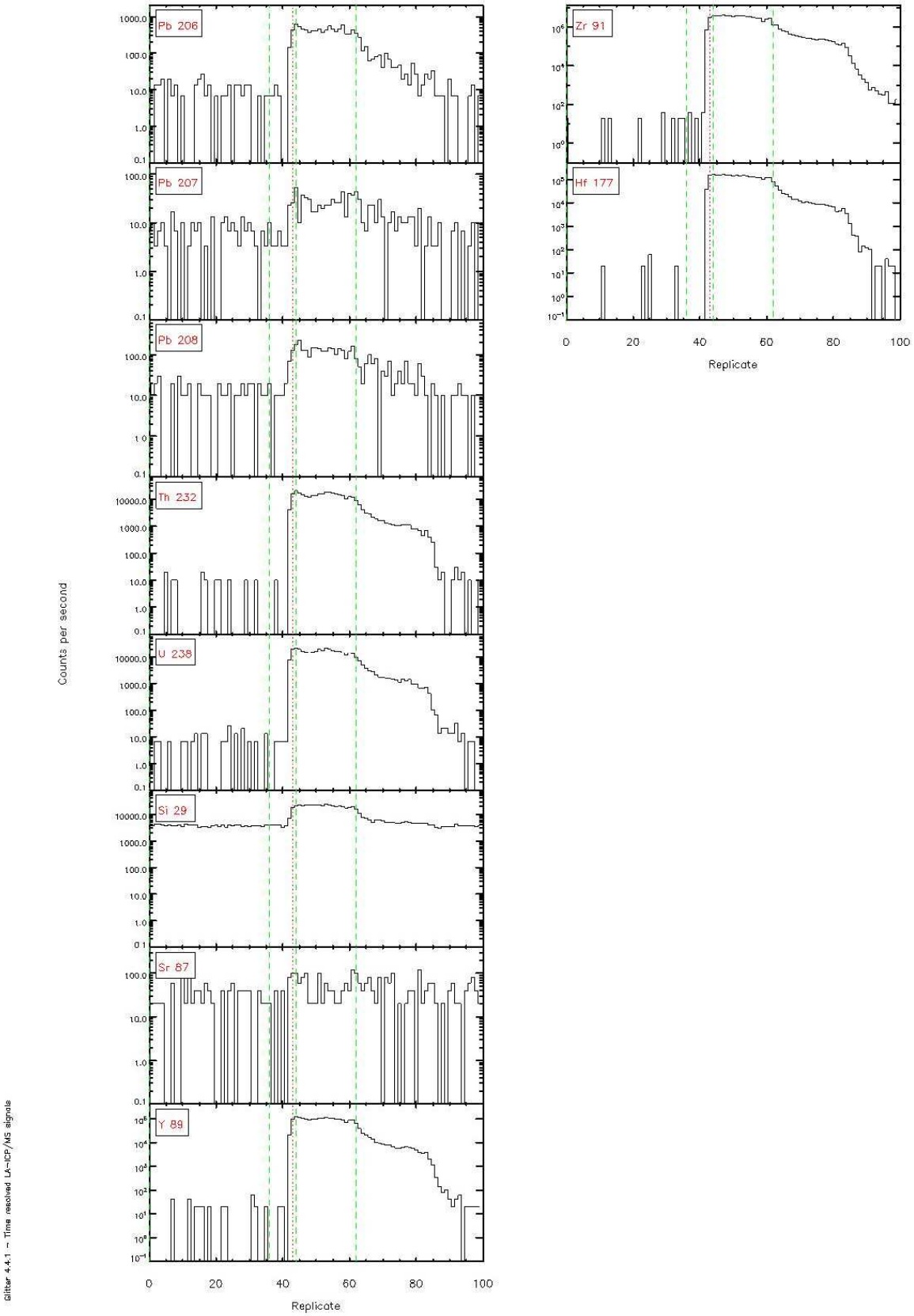
Pb 206
Pb 207
Pb 208
Th 232
U 238
Si 29
Sr 87
Y 89
Zr 91
Hf 177
Counts per second
Replicate
Glitter 4.4.1 – Time resolved LA-ICP/MS signals

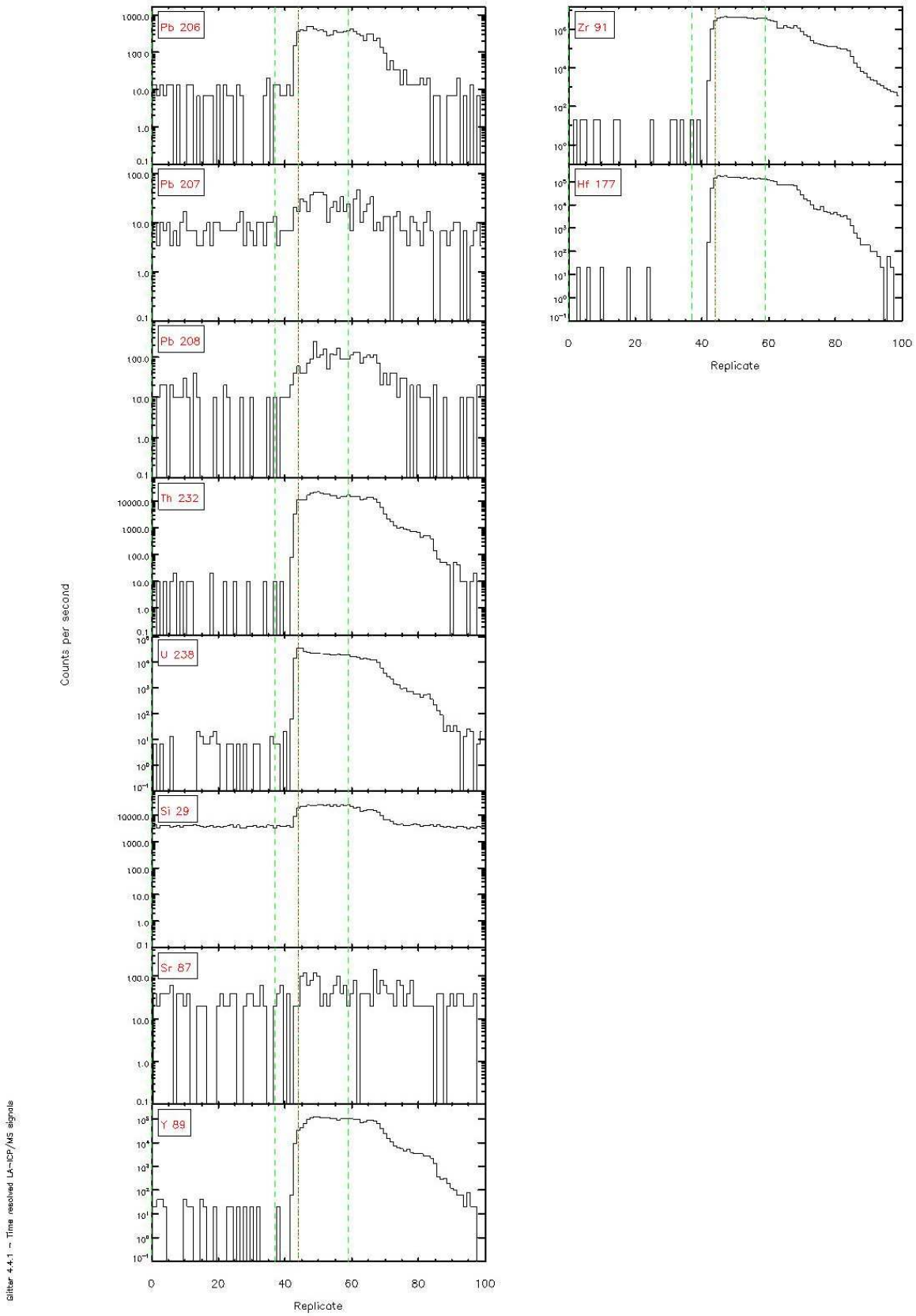
Pb 206
Pb 207
Pb 208
Th 232
U 238
Si 29
Sr 87
Y 89
Zr 91
Hf 177
Counts per second
Replicate
Glitter 4.4.1 – Time resolved LA-ICP/MS signals

2 – Ahirau Sandstone

1.

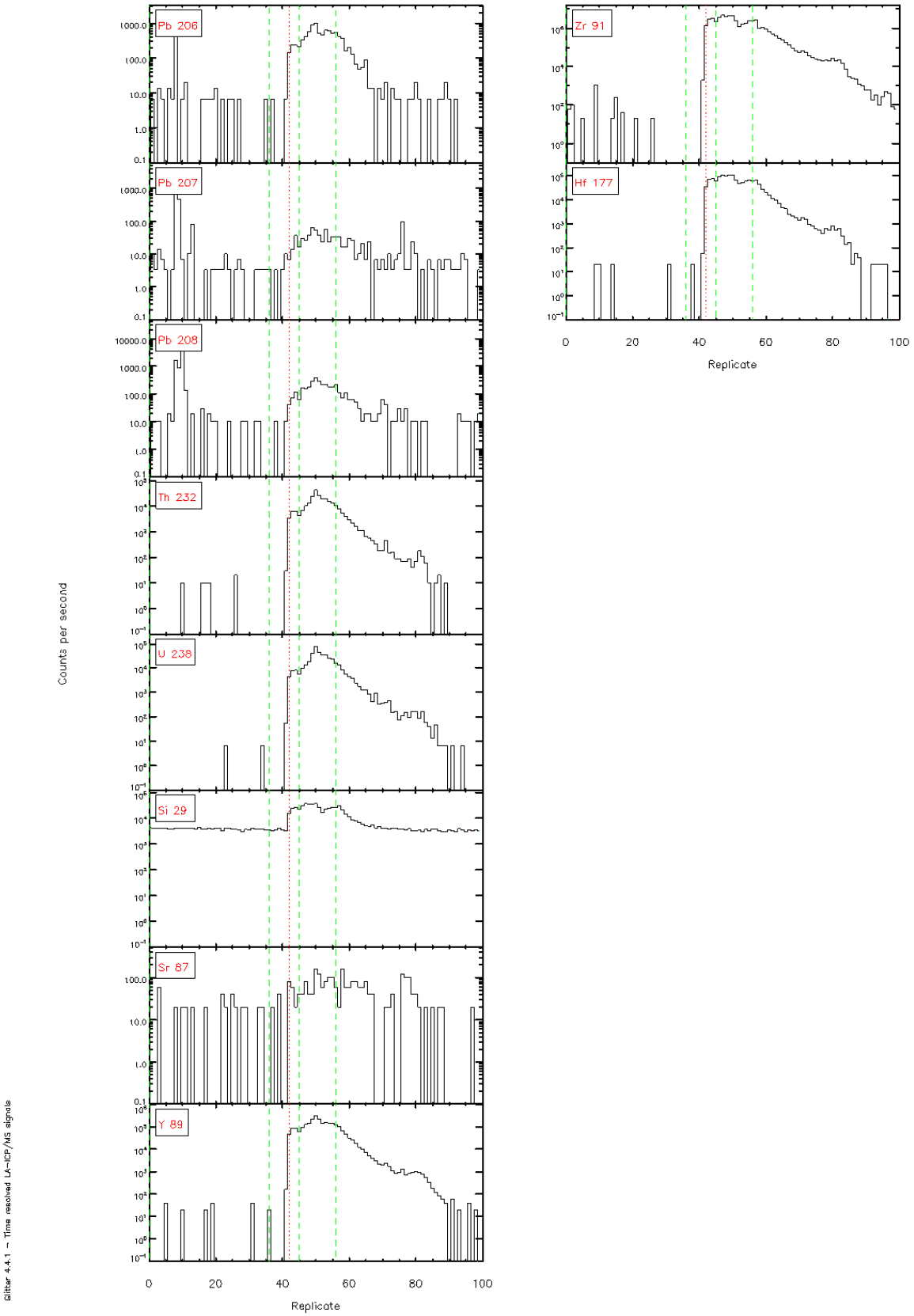

2.

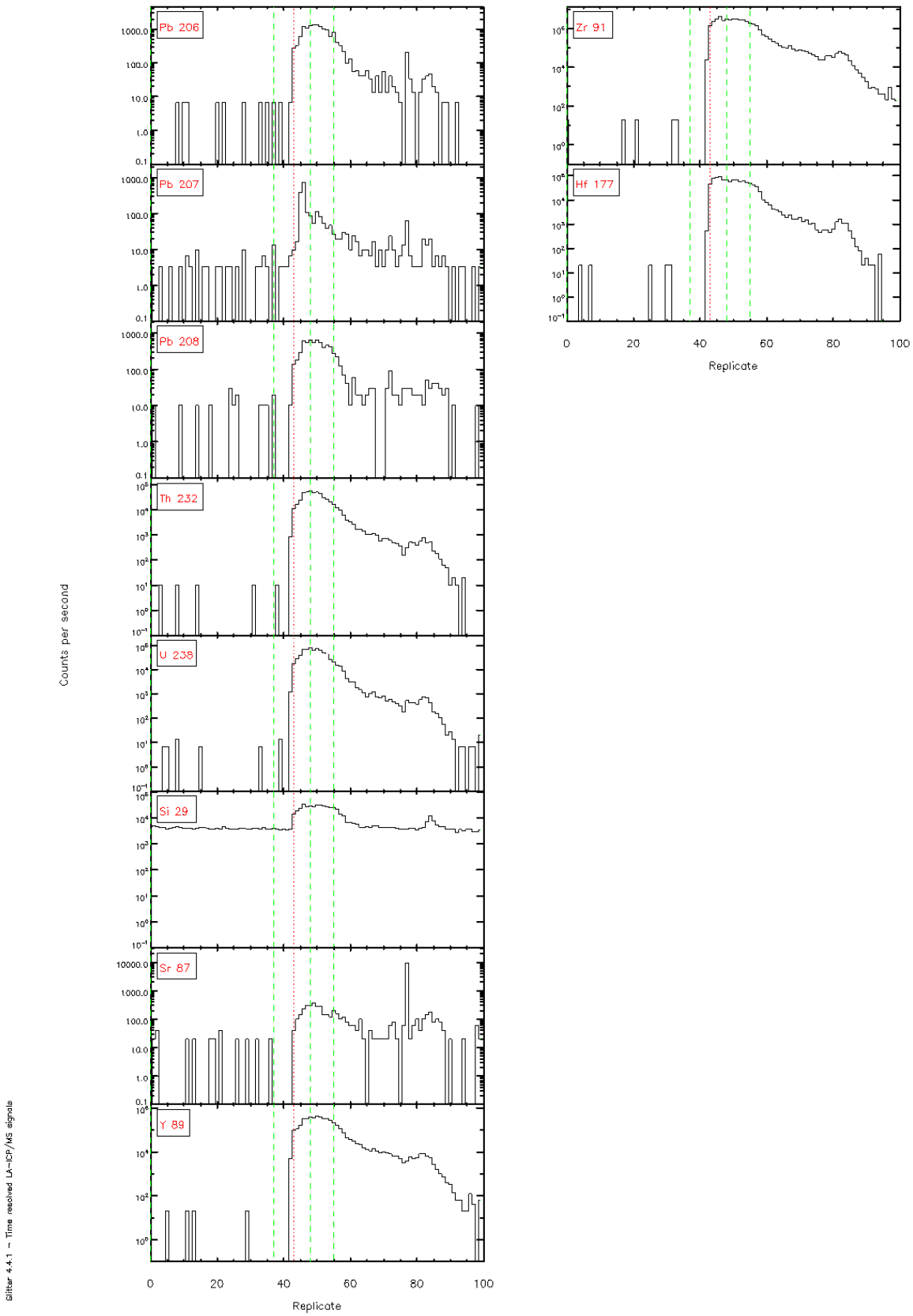
Pb 206
Pb 207
Pb 208
Th 232
U 238
Si 29
Sr 87
Y 89
Zr 91
Hf 177
Counts per second
Replicate
Glitter 4.4.1 - Time resolved LA-ICP/MS signals

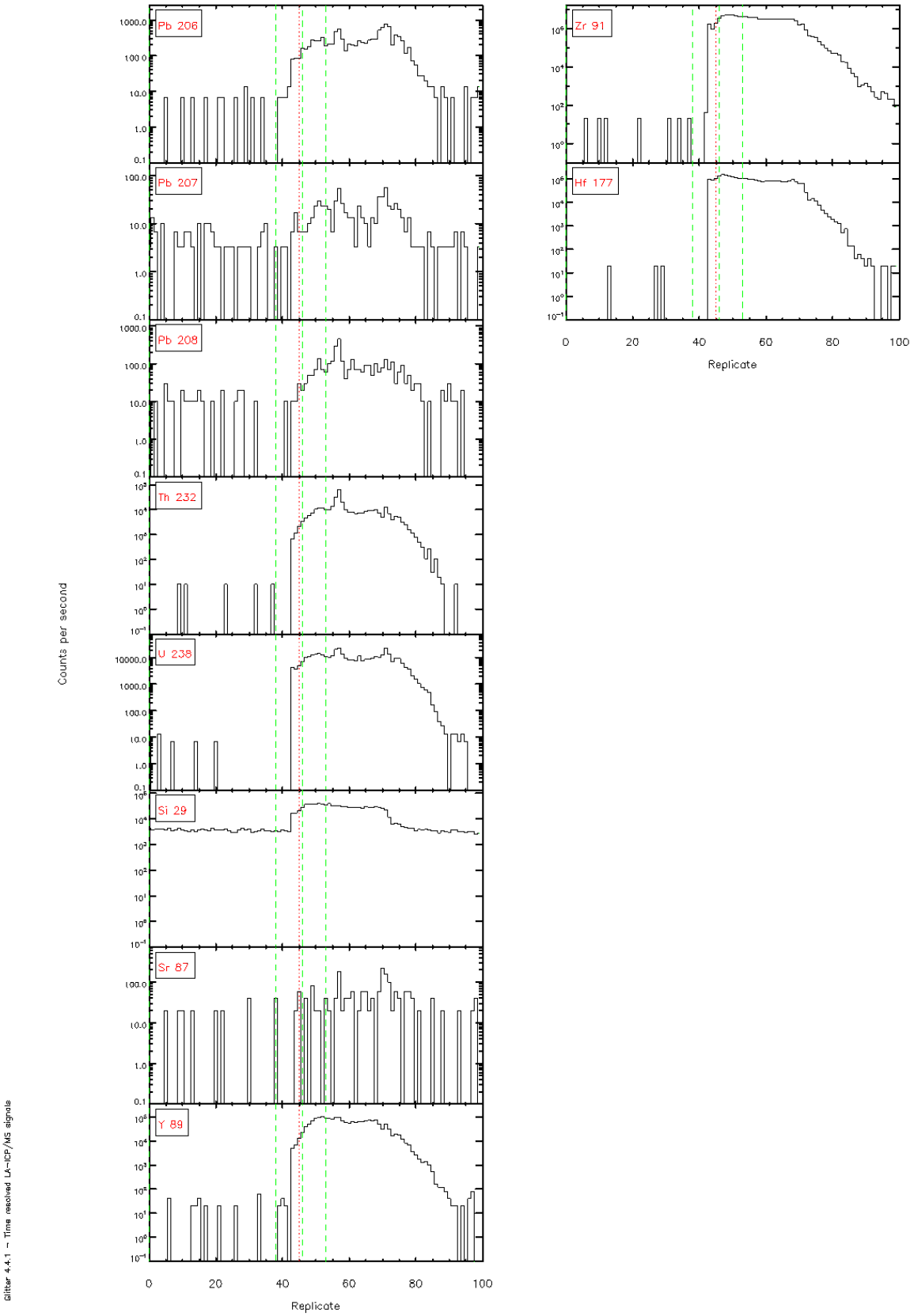
Pb 206
Pb 207
Pb 208
Th 232
U 238
Si 29
Sr 87
Y 89
Zr 91
Hf 177
Counts per second
Replicate
Glitter 4.4.1 – Time resolved LA-ICP/MS signals

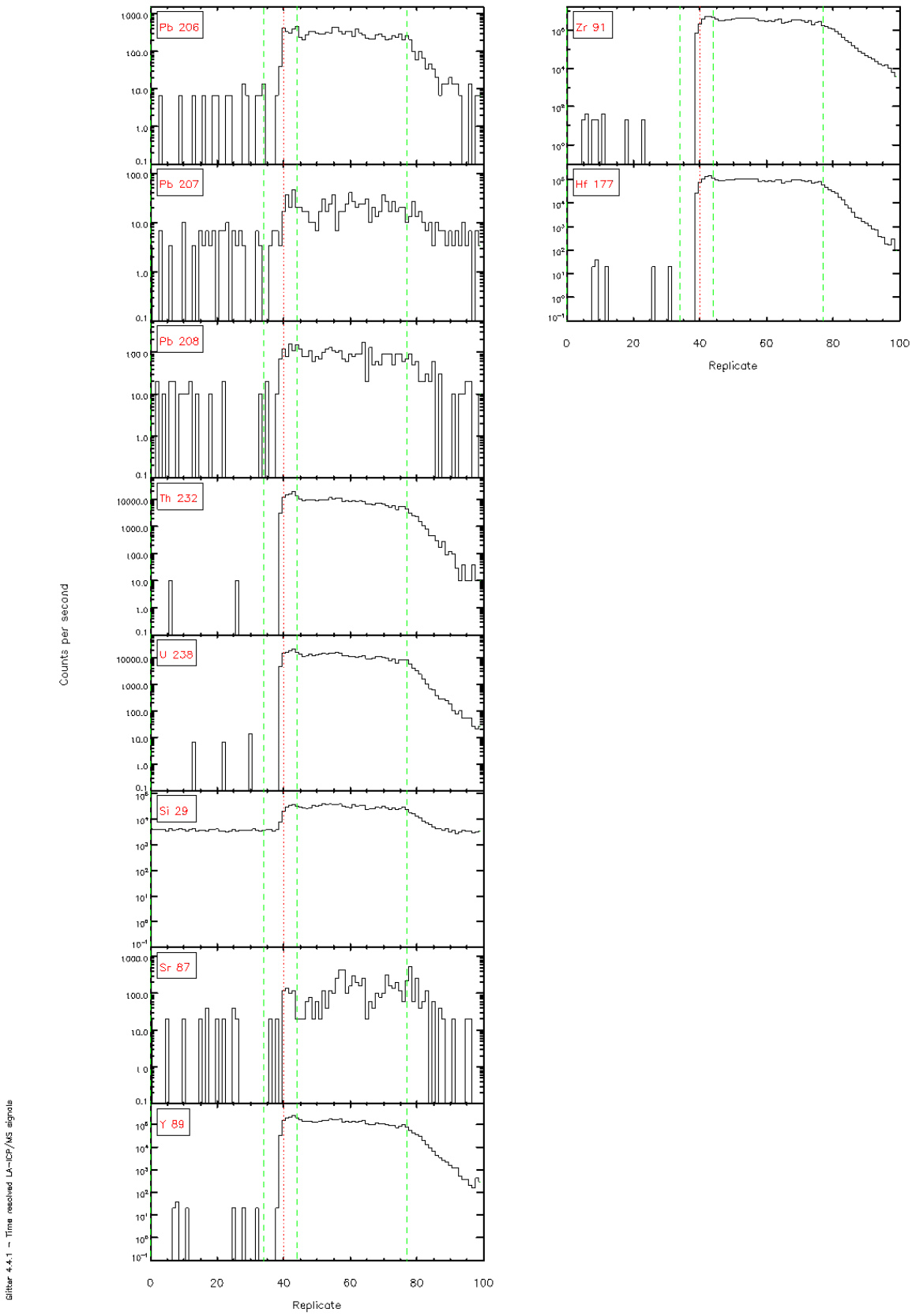
Pb 206
Pb 207
Pb 208
Th 232
U 238
Si 29
Sr 87
Y 89
Zr 91
Hf 177
Counts per second
Replicate
Glitter 4.4.1 - Time resolved LA-ICP/MS signals

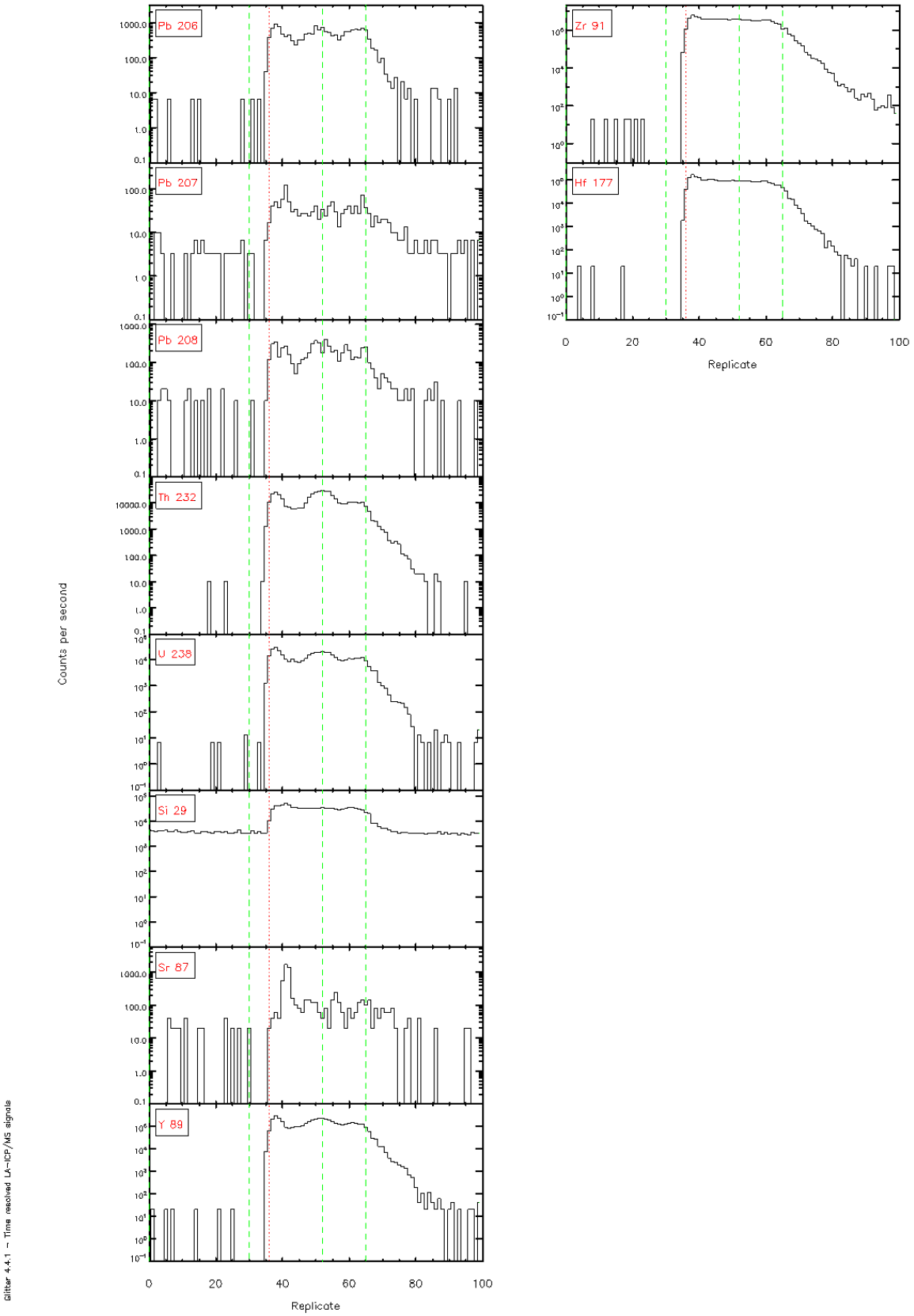
Pb 206
Pb 207
Pb 208
Th 232
U 238
Si 29
Sr 87
Y 89
Zr 91
Hf 177
Counts per second
Replicate
Glitter 4.4.1 – Time resolved LA-ICP/MS signals

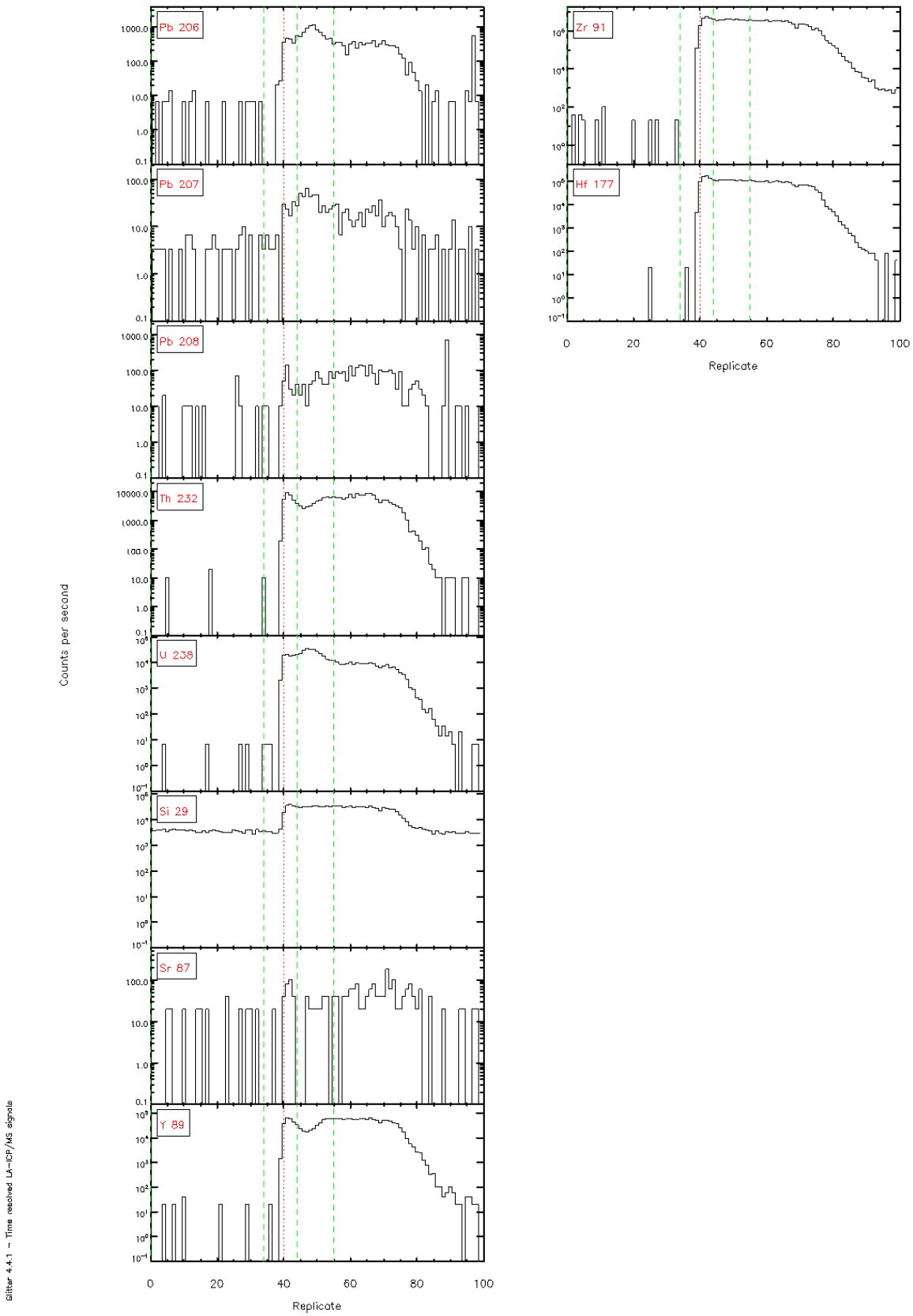
Pb 206
Pb 207
Pb 208
Th 232
U 238
Si 29
Sr 87
Y 89
Zr 91
Hf 177
Counts per second
Replicate
Glitter 4.4.1 - Time resolved LA-ICP/MS signals

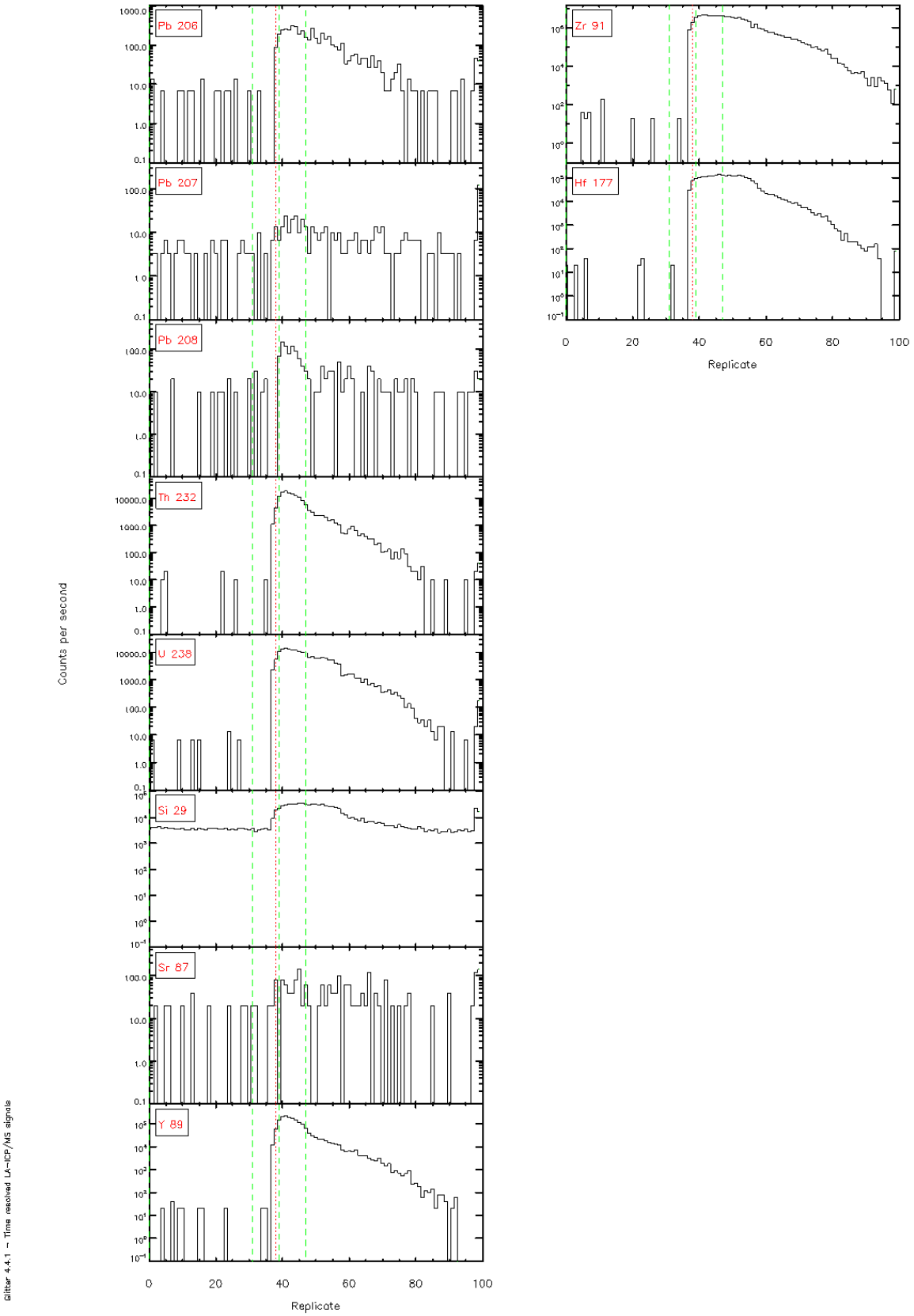
Pb 206
Pb 207
Pb 208
Th 232
U 238
Si 29
Sr 87
Y 89
Zr 91
Hf 177
Counts per second
Replicate
Glitter 4.4.1 – Time resolved LA-ICP/MS signals

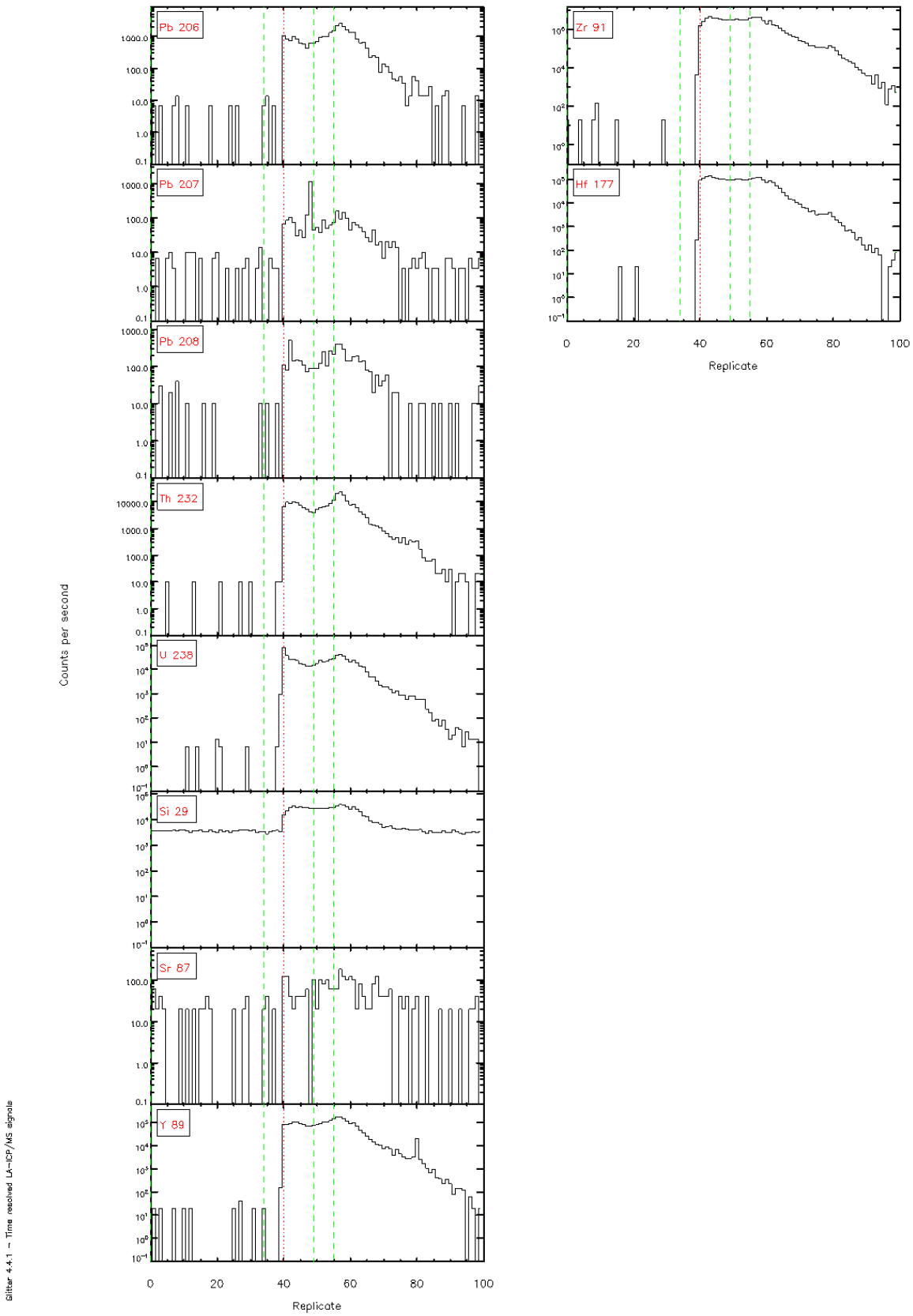
Pb 206
Pb 207
Pb 208
Th 232
U 238
Si 29
Sr 87
Y 89
Zr 91
Hf 177
Counts per second
Replicate
Glitter 4.4.1 - Time resolved LA-ICP/MS signals

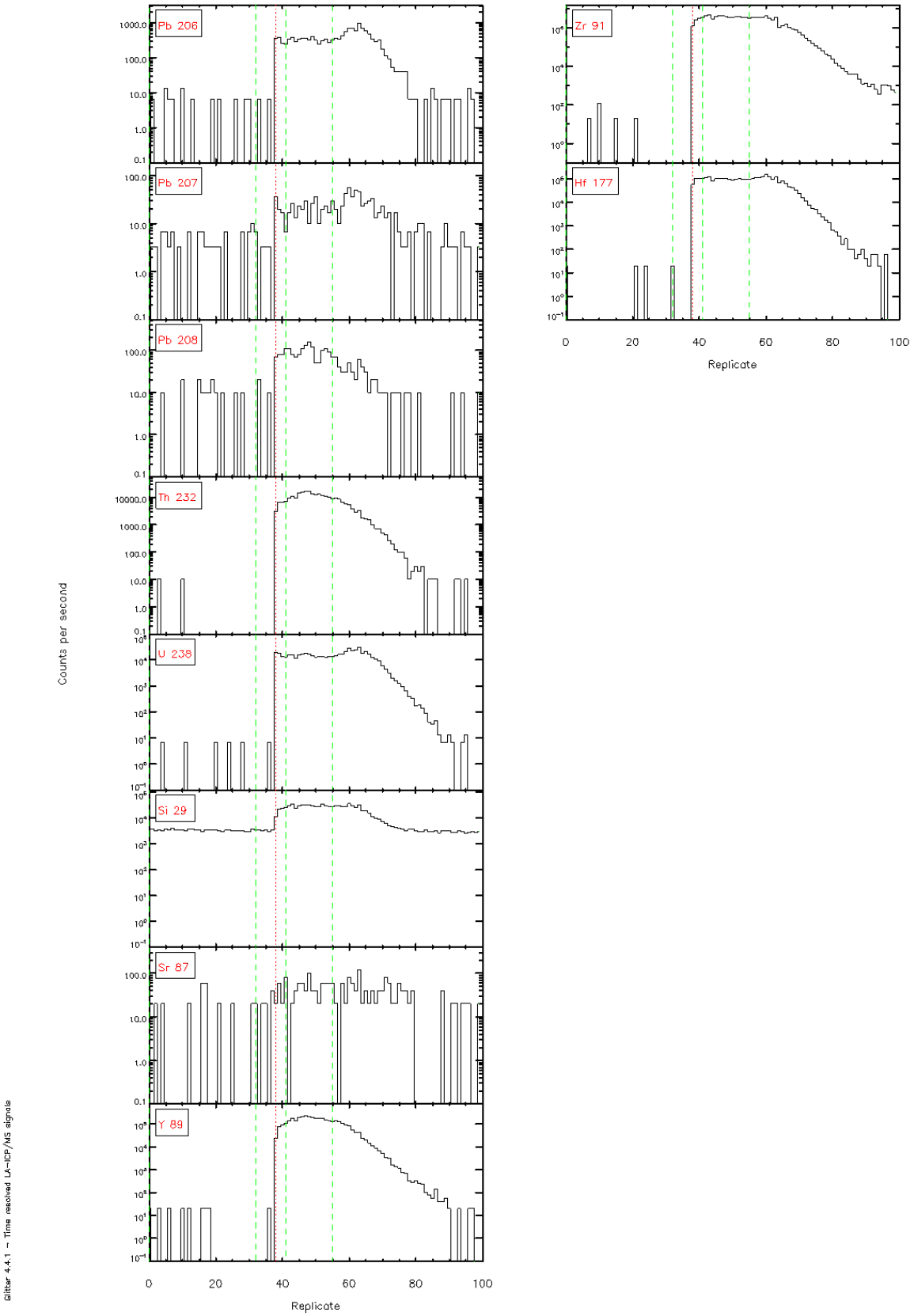
Pb 206
Pb 207
Pb 208
Th 232
U 238
Si 29
Sr 87
Y 89
Zr 91
Hf 177
Counts per second
Replicate
Glitter 4.4.1 – Time resolved LA-ICP/MS signals

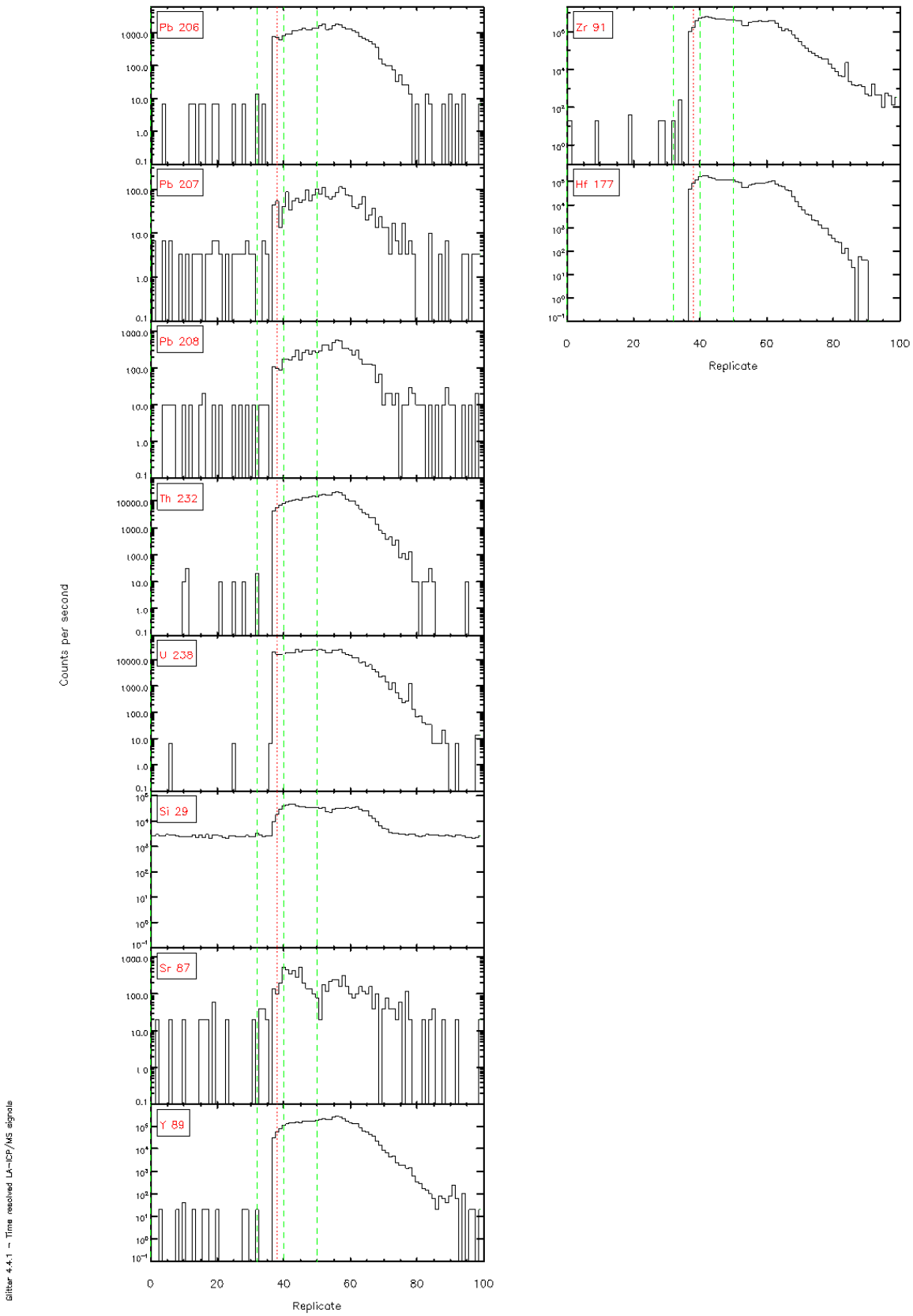
Pb 206
Pb 207
Pb 208
Th 232
U 238
Si 29
Sr 87
Y 89
Zr 91
Hf 177
Counts per second
Replicate
Glitter 4.4.1 - Time resolved LA-ICP/MS signals

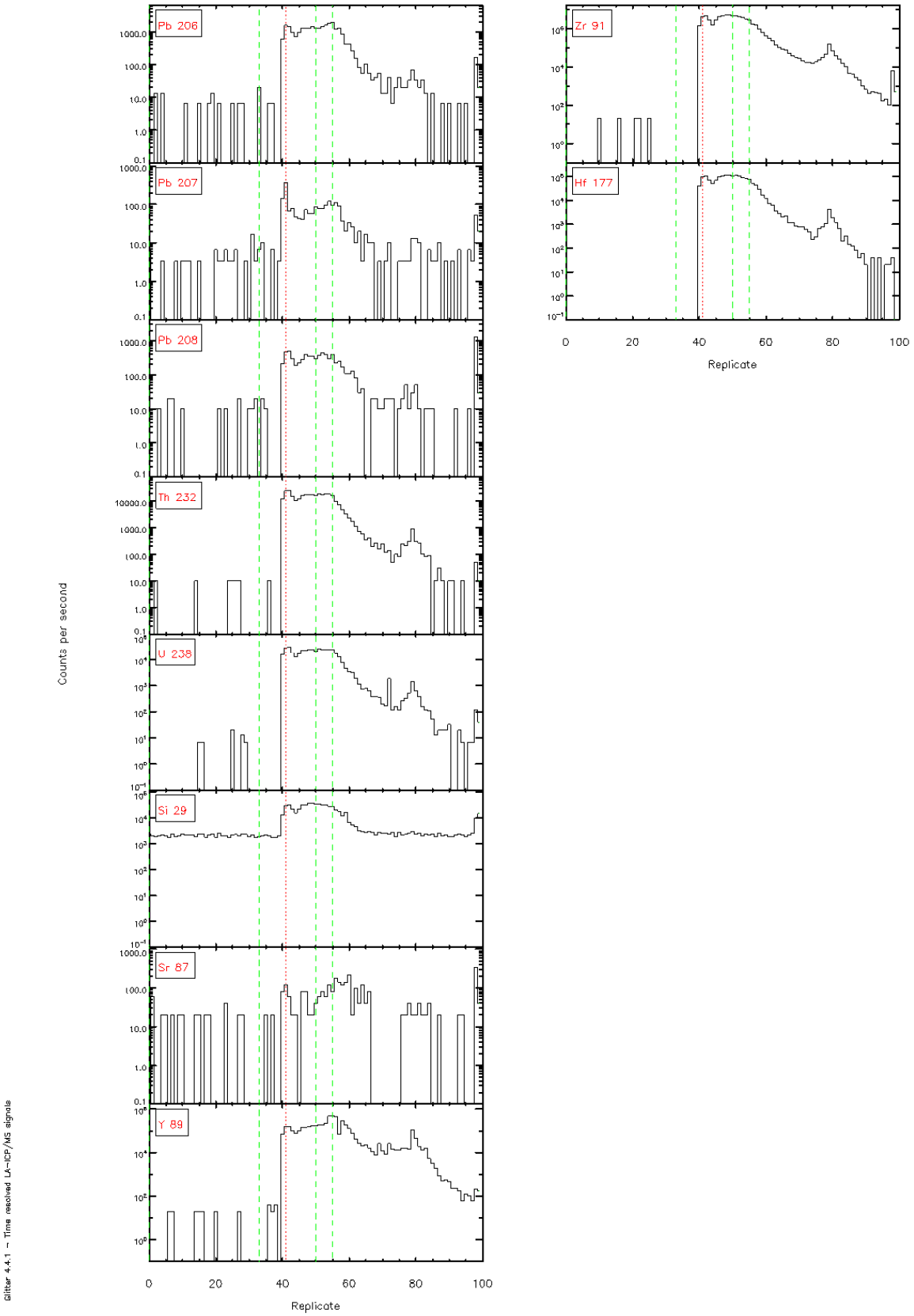
Pb 206
Pb 207
Pb 208
Th 232
U 238
Si 29
Sr 87
Y 89
Zr 91
Hf 177
Counts per second
Replicate
Glitter 4.4.1 – Time resolved LA-ICP/MS signals

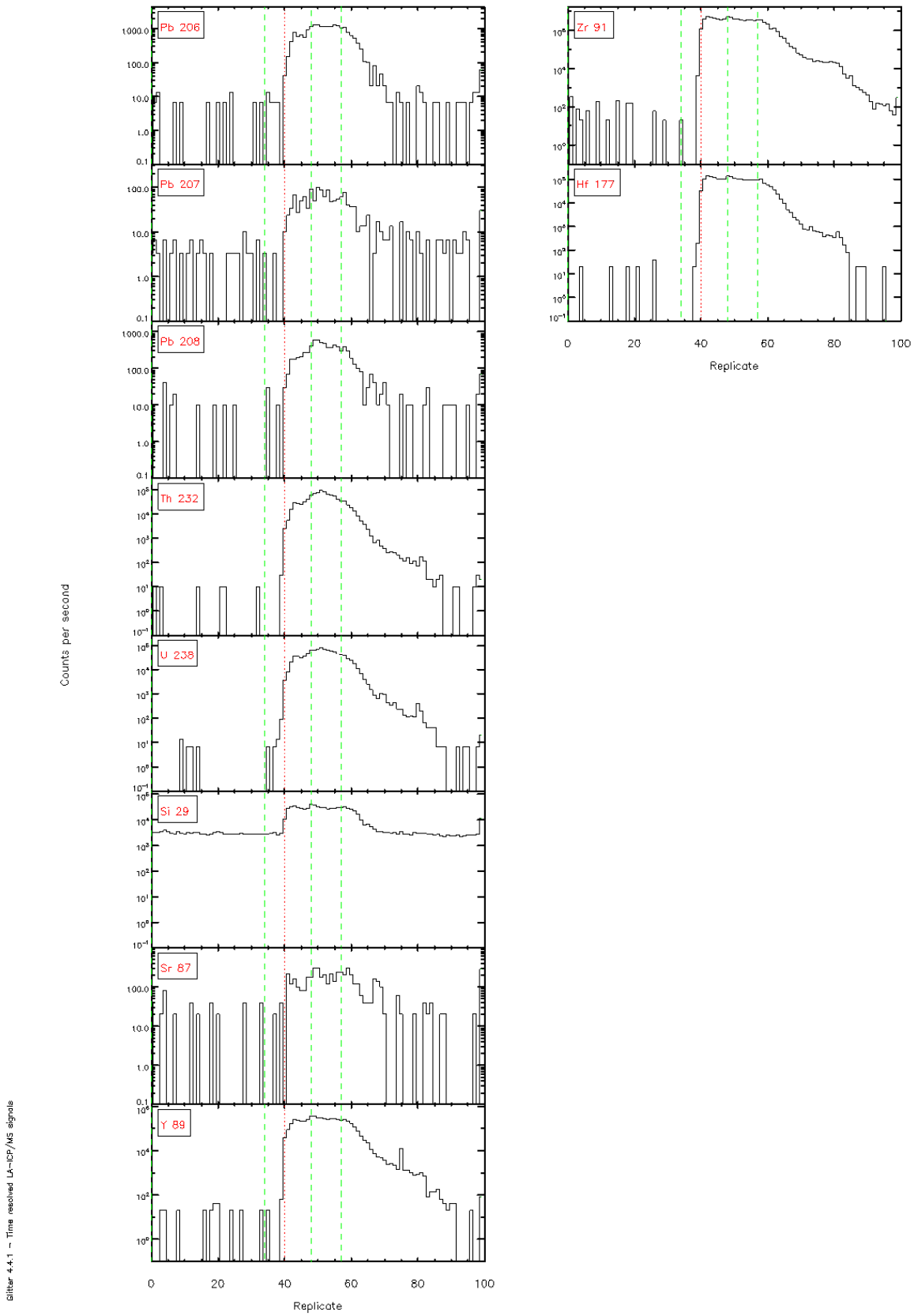
Pb 206
Pb 207
Pb 208
Th 232
U 238
Si 29
Sr 87
Y 89
Zr 91
Hf 177
Counts per second
Replicate
Replicate
Glitter 4.4.1 - Time resolved LA-ICP/MS signals

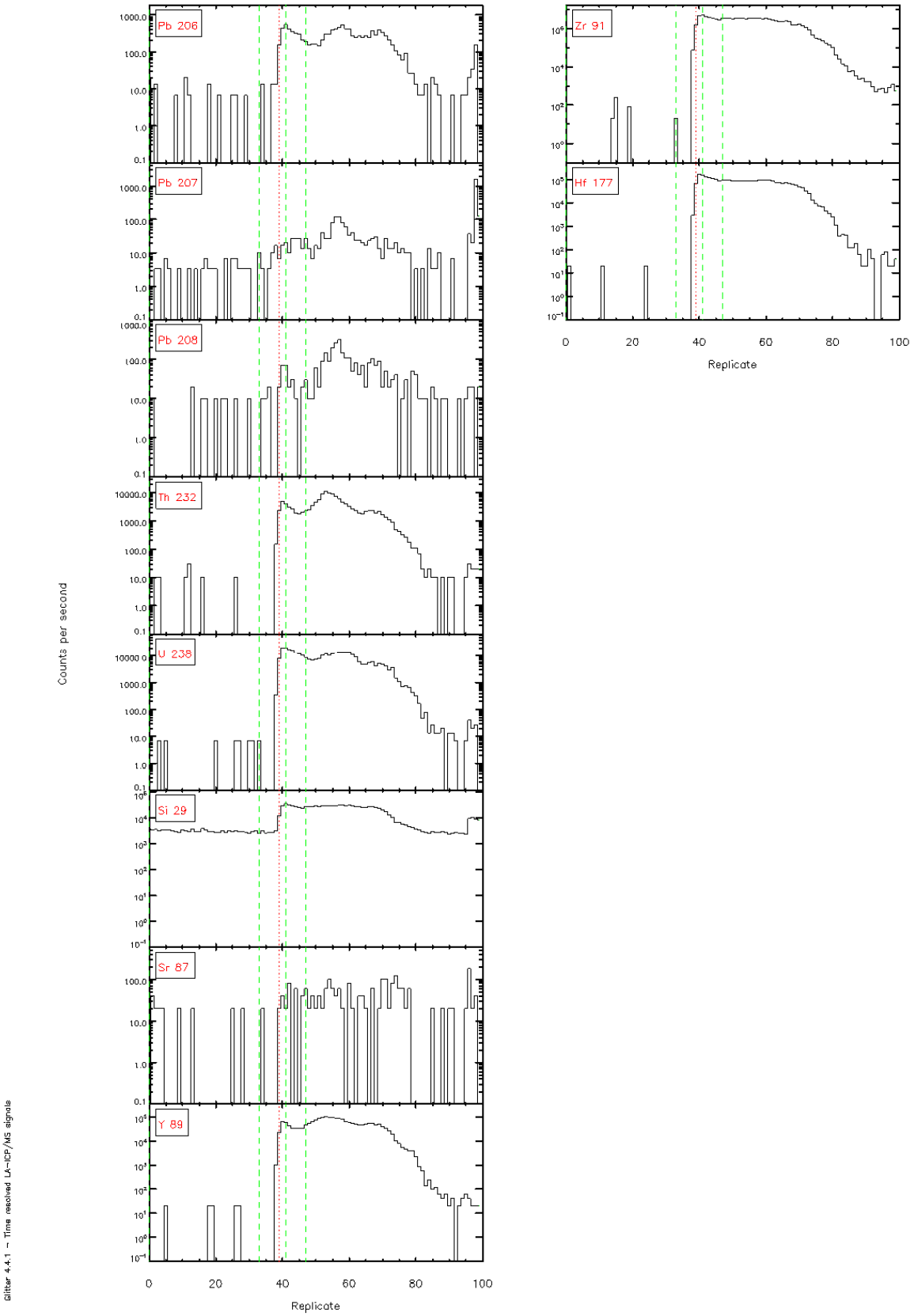
Pb 206
Pb 207
Pb 208
Th 232
U 238
Si 29
Sr 87
Y 89
Zr 91
Hf 177
Counts per second
Replicate
Glitter 4.4.1 – Time resolved LA-ICP/MS signals

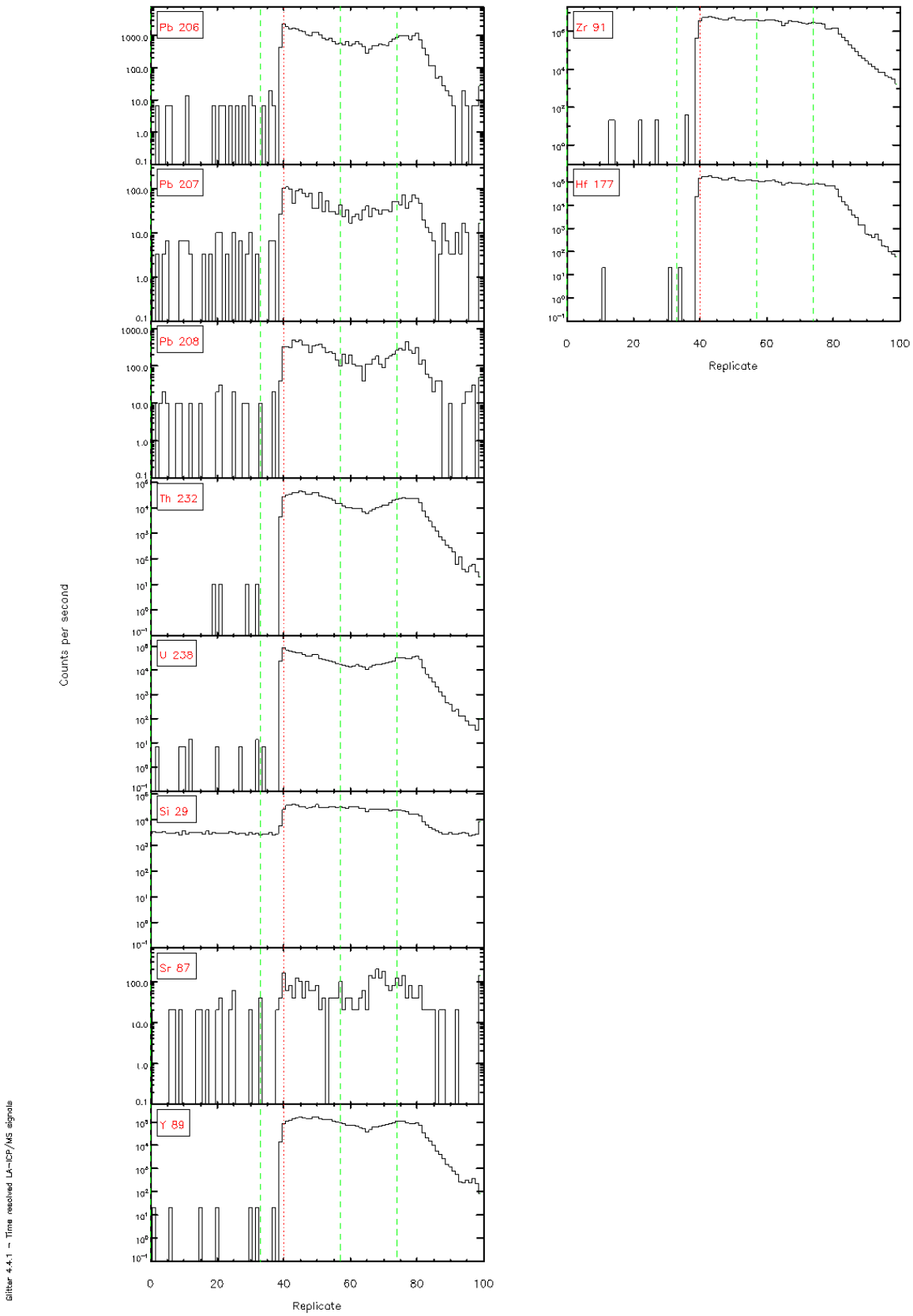
Pb 206
Pb 207
Pb 208
Th 232
U 238
Si 29
Sr 87
Y 89
Zr 91
Hf 177
Counts per second
Replicate
Glitter 4.4.1 - Time resolved LA-ICP/MS signals

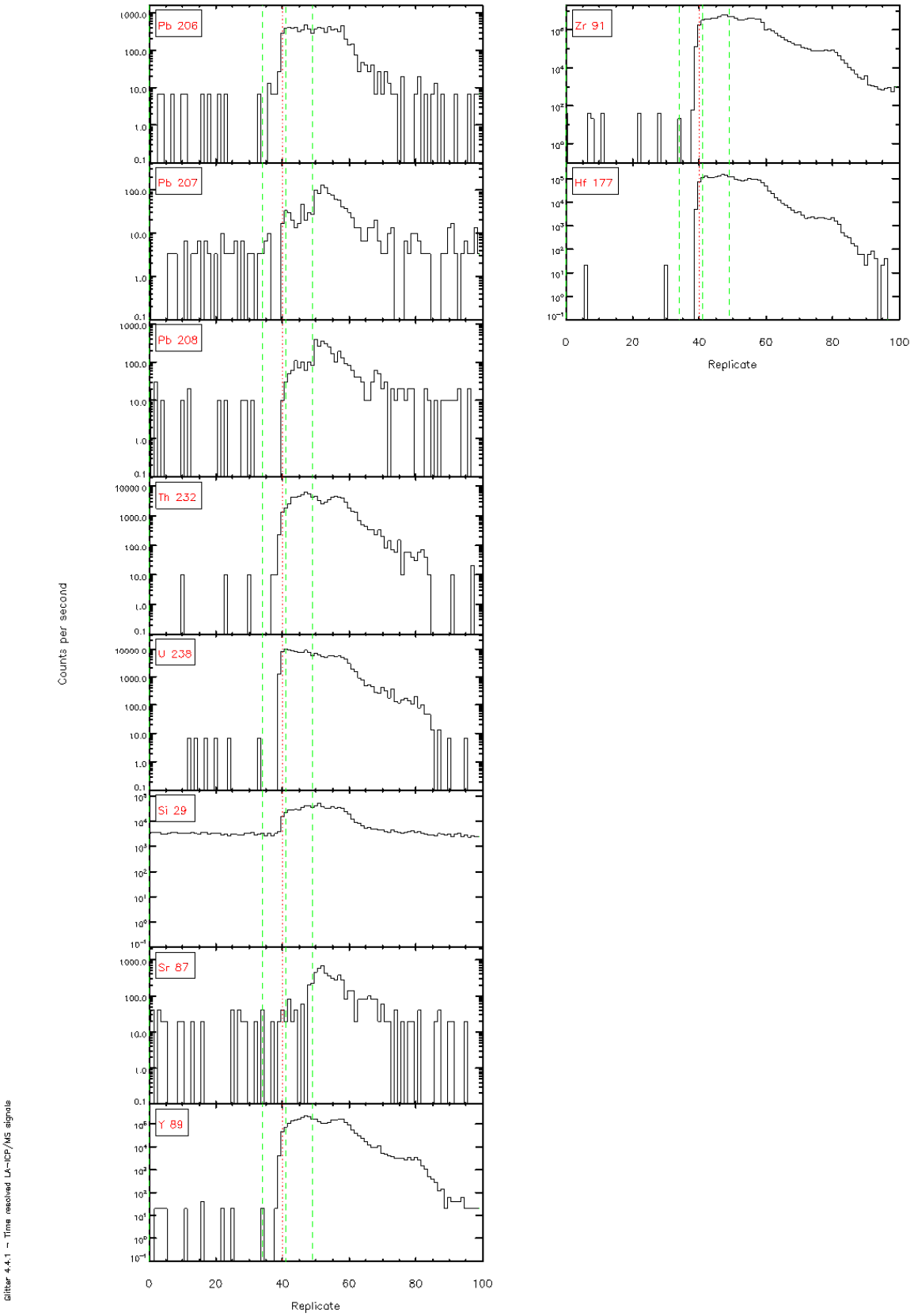
Pb 206
Pb 207
Pb 208
Th 232
U 238
Si 29
Sr 87
Y 89
Zr 91
Hf 177
Counts per second
Replicate
Glitter 4.4.1 – Time resolved LA-ICP/MS signals

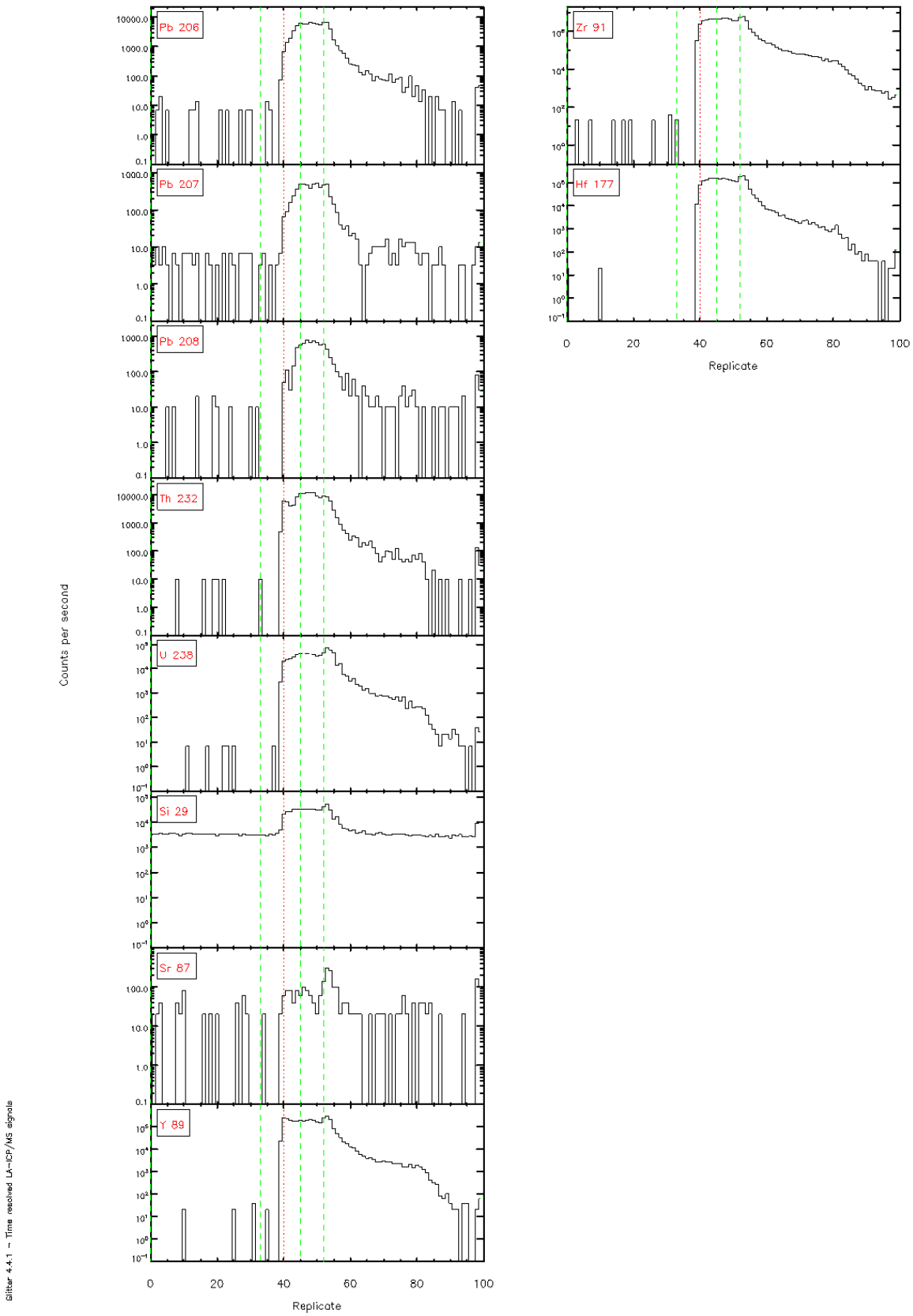
Pb 206
Pb 207
Pb 208
Th 232
U 238
Si 29
Sr 87
Y 89
Zr 91
Hf 177
Counts per second
Replicate
Glitter 4.4.1 - Time resolved LA-ICP/MS signals

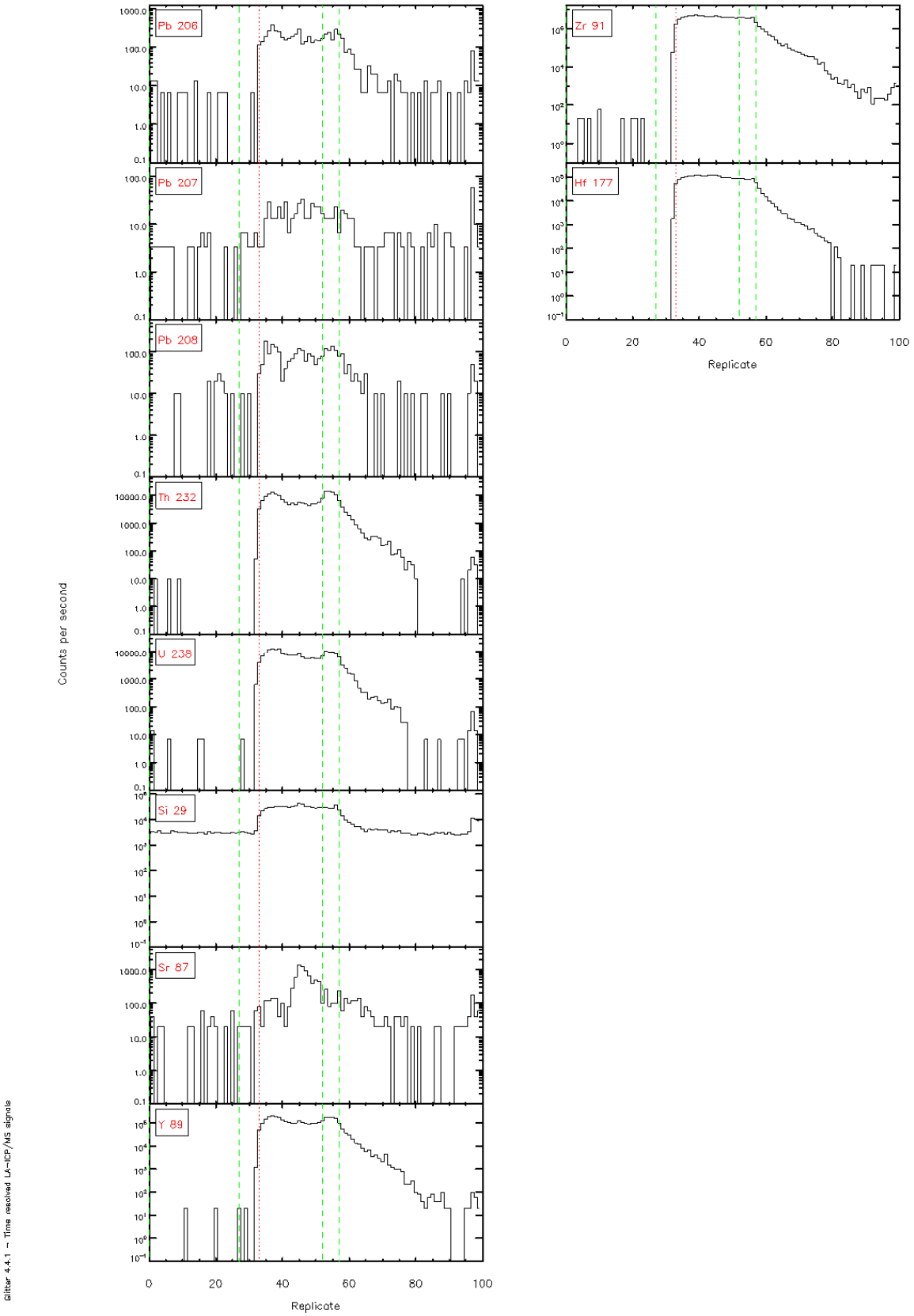
Pb 206
Pb 207
Pb 208
Th 232
U 238
Si 29
Sr 87
Y 89
Zr 91
Hf 177
Counts per second
Replicate
Glitter 4.4.1 – Time resolved LA-ICP/MS signals

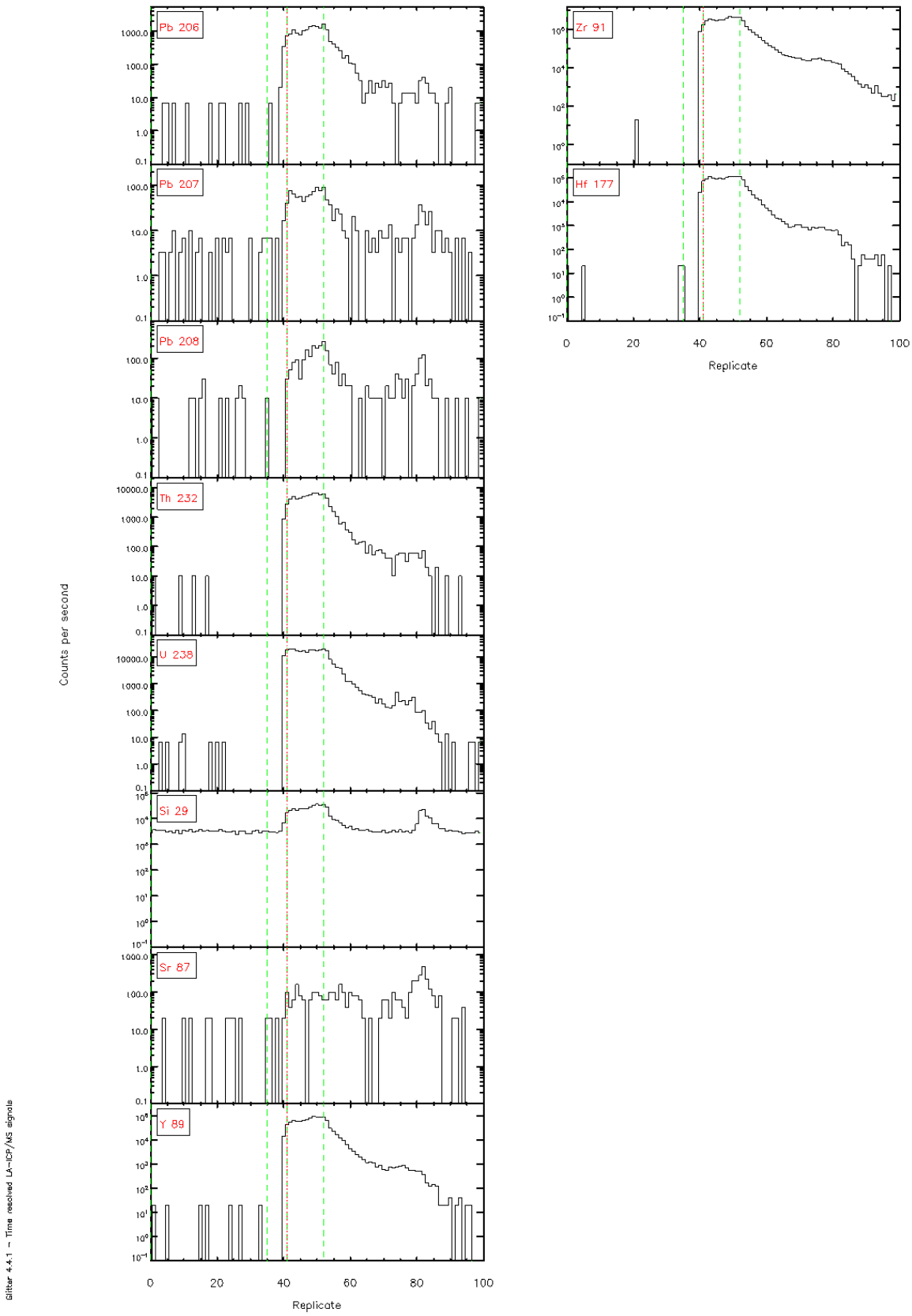
Pb 206
Pb 207
Pb 208
Th 232
U 238
Si 29
Sr 87
Y 89
Zr 91
Hf 177
Counts per second
Replicate
Glitter 4.4.1 - Time resolved LA-ICP/MS signals

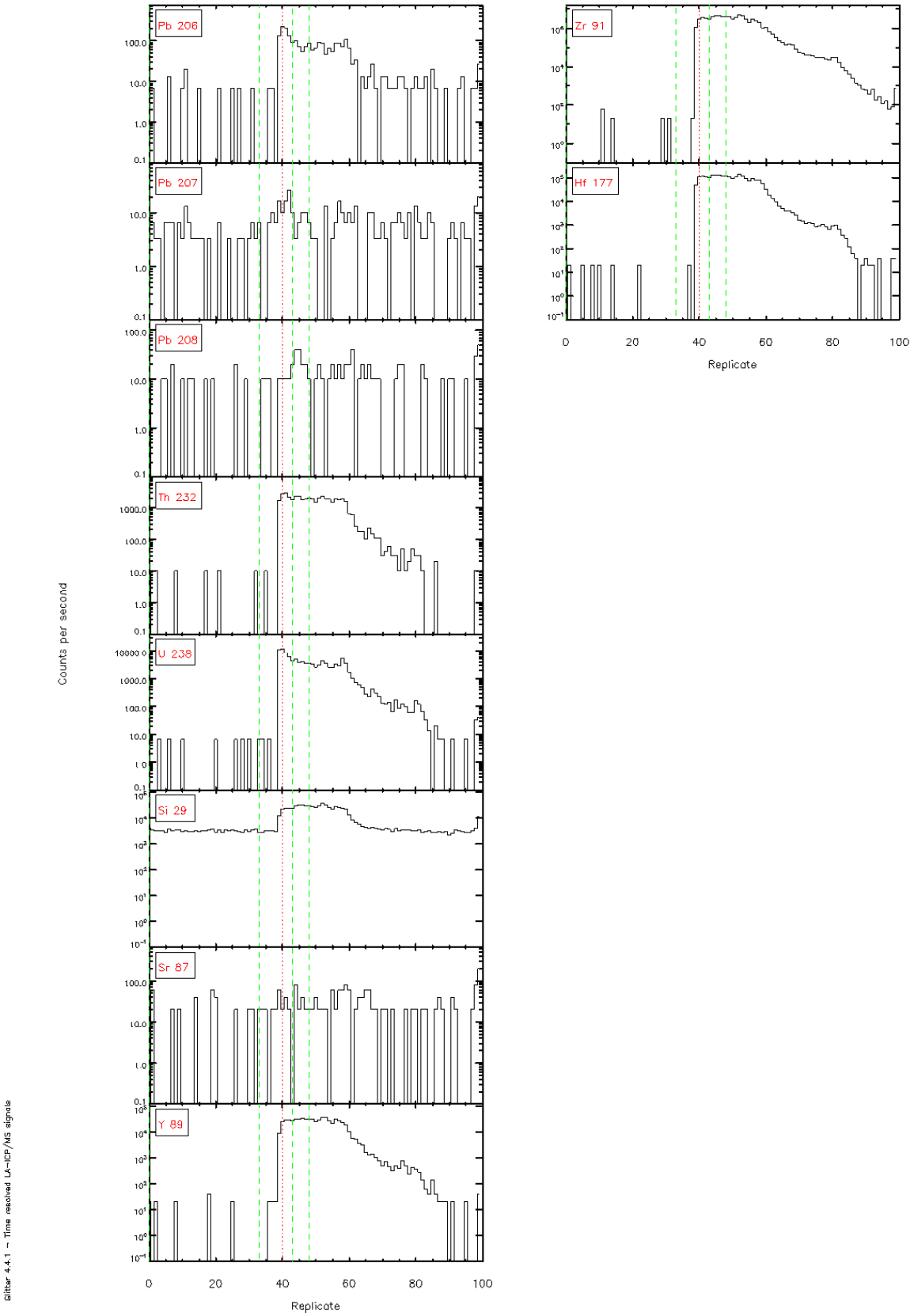
Pb 206
Pb 207
Pb 208
Th 232
U 238
Si 29
Sr 87
Y 89
Zr 91
Hf 177
Counts per second
Replicate
Glitter 4.4.1 – Time resolved LA-ICP/MS signals

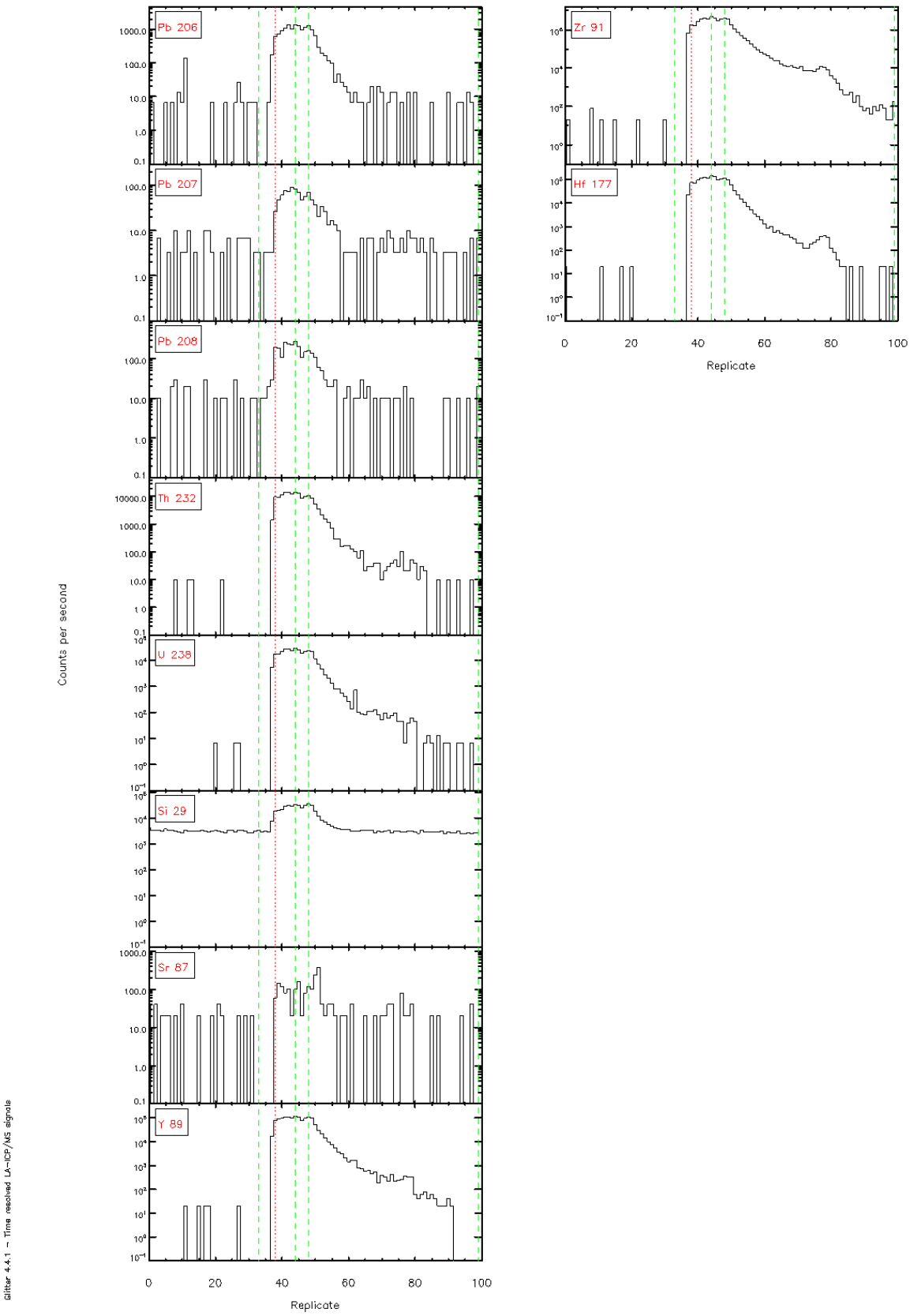
Pb 206
Pb 207
Pb 208
Th 232
U 238
Si 29
Sr 87
Y 89
Zr 91
Hf 177
Counts per second
Replicate
Glitter 4.4.1 - Time resolved LA-ICP/MS signals

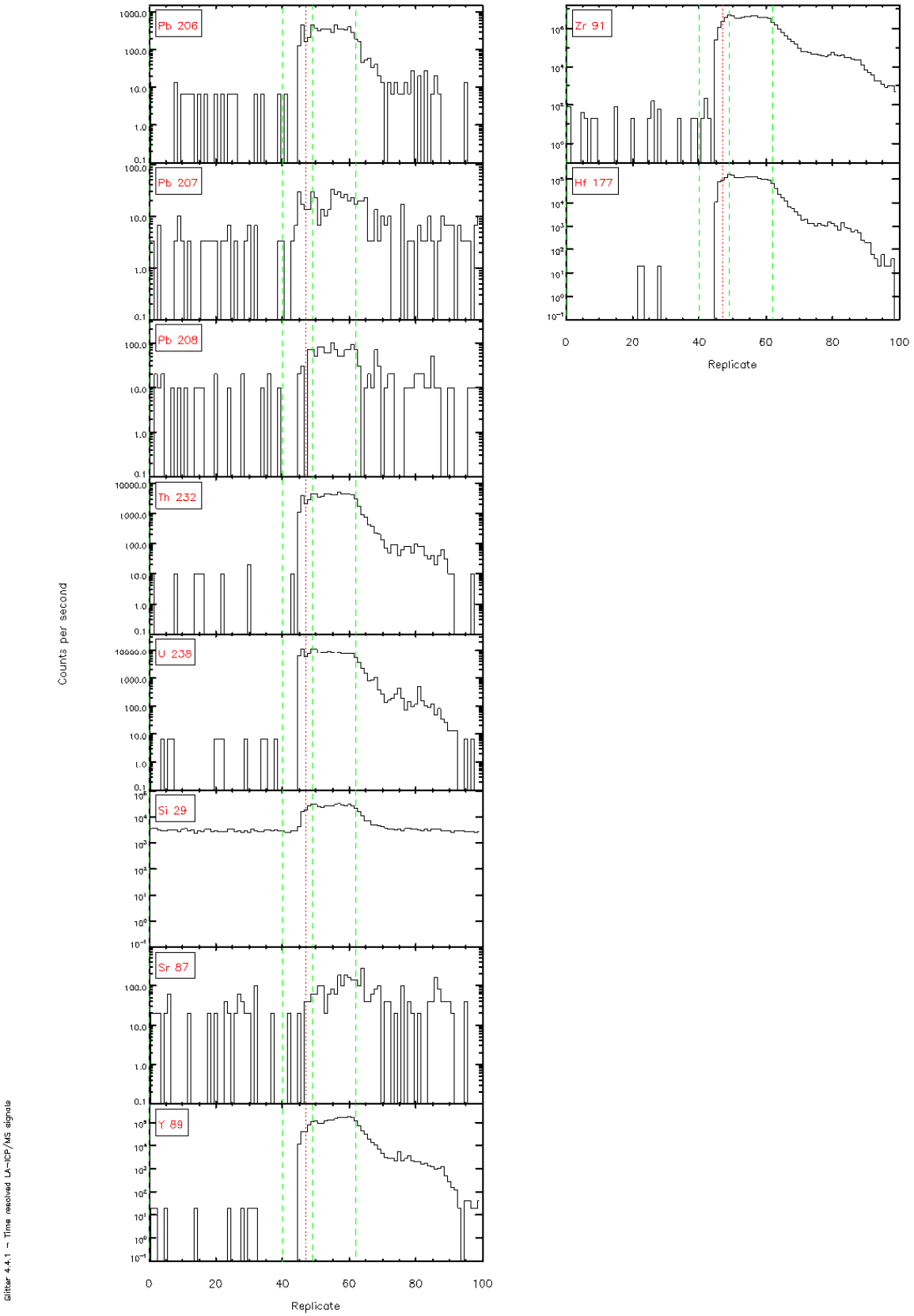
Pb 206
Pb 207
Pb 208
Th 232
U 238
Si 29
Sr 87
Y 89
Zr 91
Hf 177
Counts per second
Replicate
Glitter 4.4.1 – Time resolved LA-ICP/MS signals

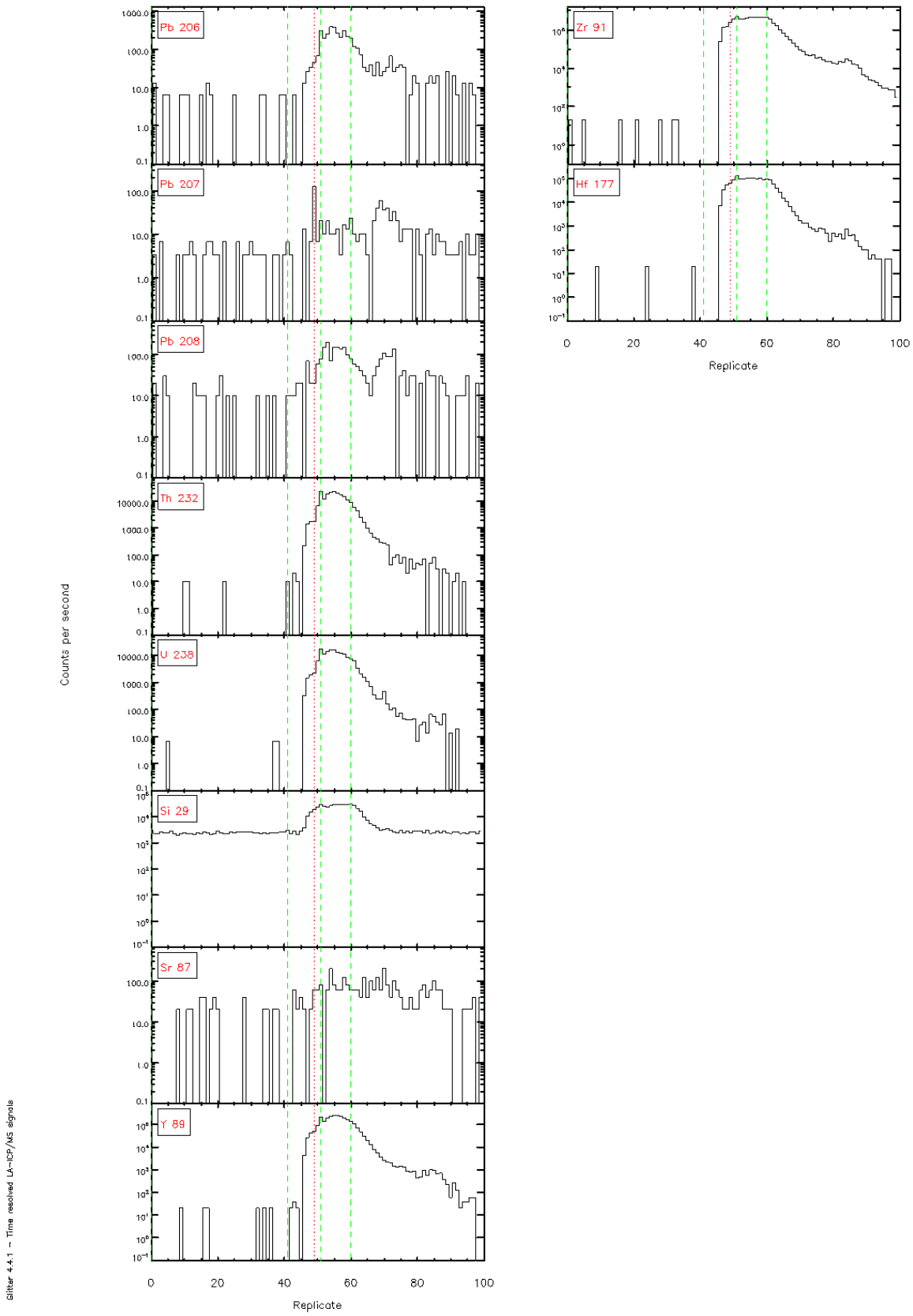
Pb 206
Pb 207
Pb 208
Th 232
U 238
Si 29
Sr 87
Y 89
Zr 91
Hf 177
Counts per second
Replicate
Glitter 4.4.1 - Time resolved LA-ICP/MS signals

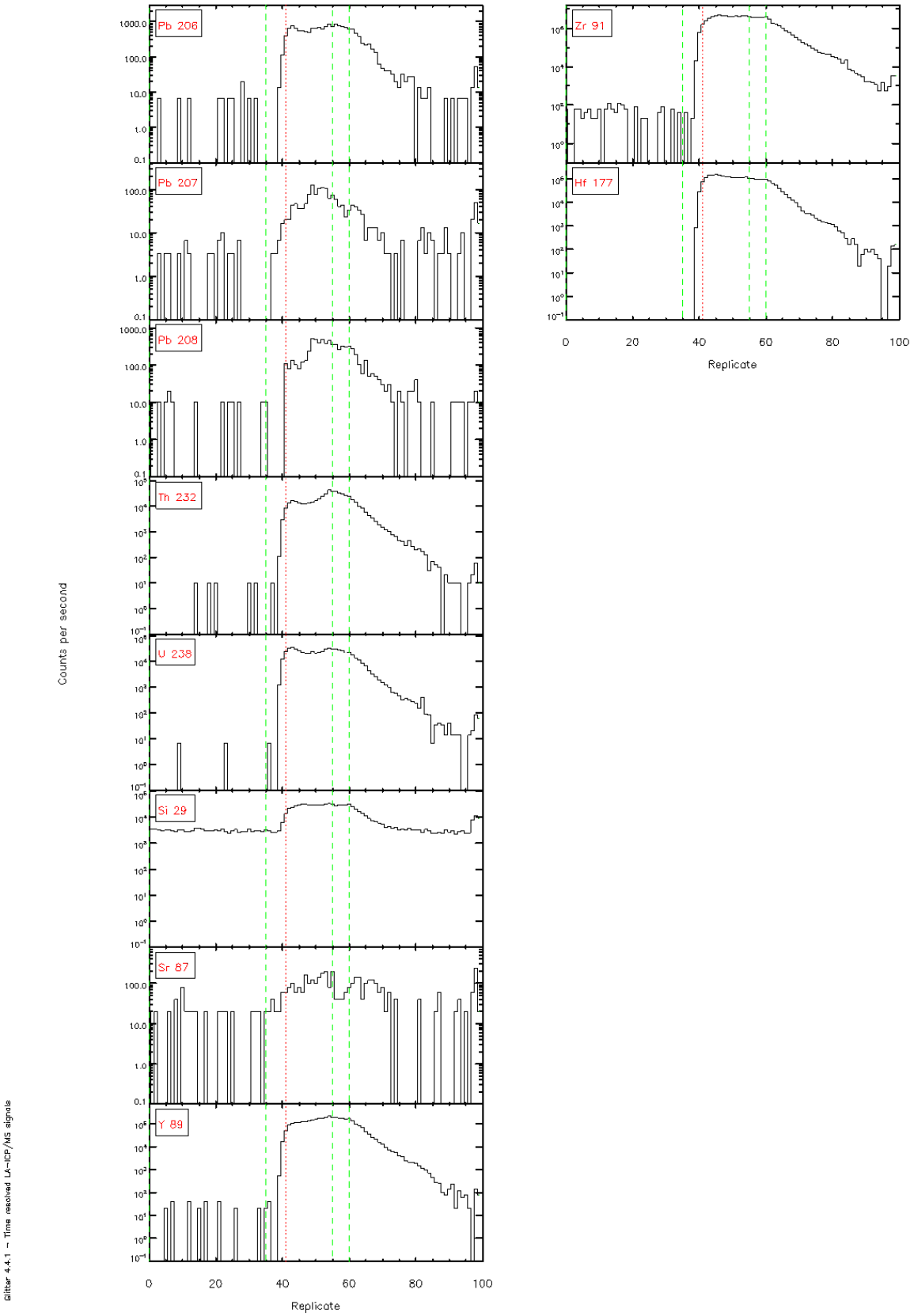
Pb 206
Pb 207
Pb 208
Th 232
U 238
Si 29
Sr 87
Y 89
Zr 91
Hf 177
Counts per second
Replicate
Glitter 4.4.1 – Time resolved LA-ICP/MS signals

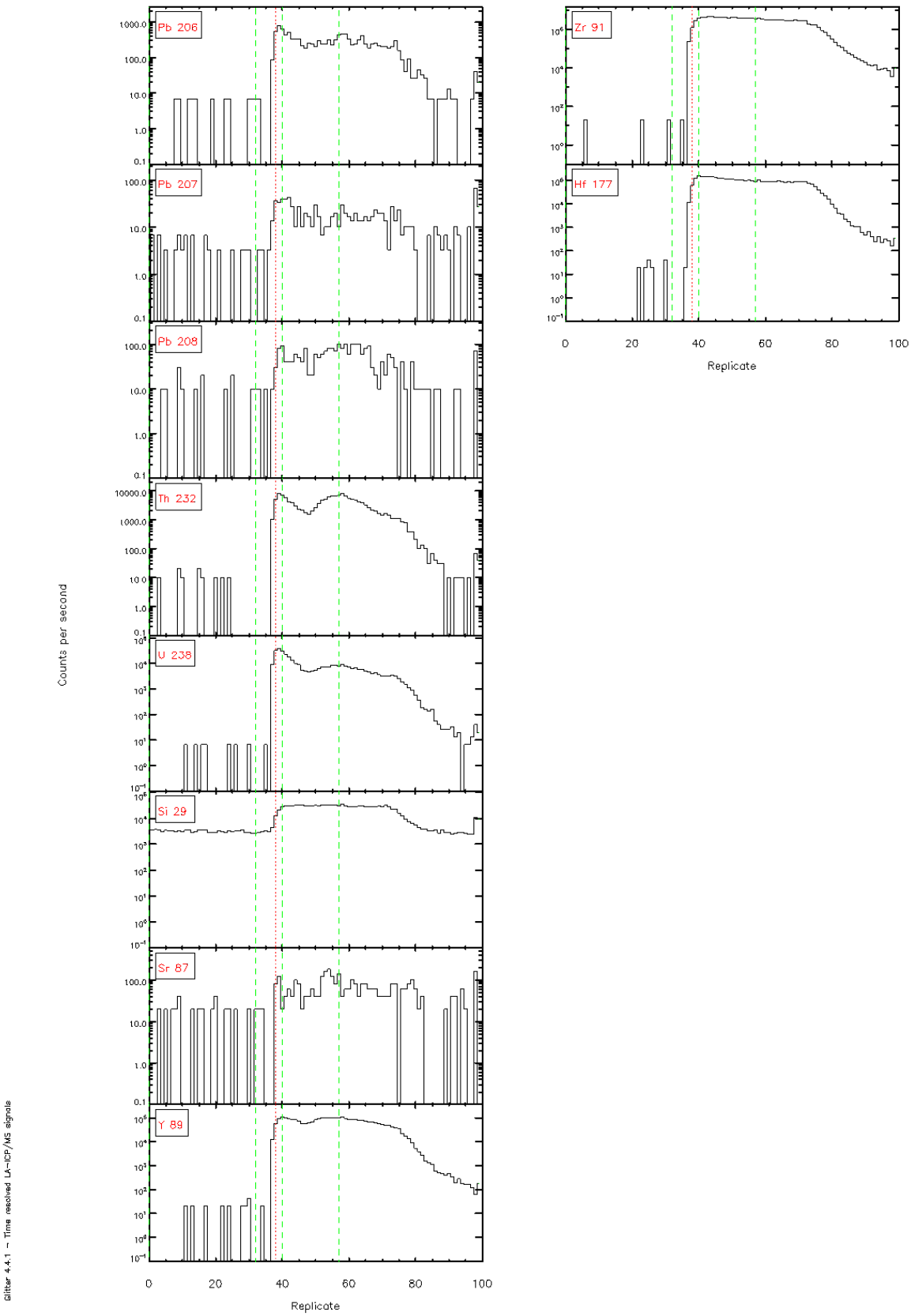
Pb 206
Pb 207
Pb 208
Th 232
U 238
Si 29
Sr 87
Y 89
Zr 91
Hf 177
Counts per second
Replicate
Glitter 4.4.1 - Time resolved LA-ICP/MS signals

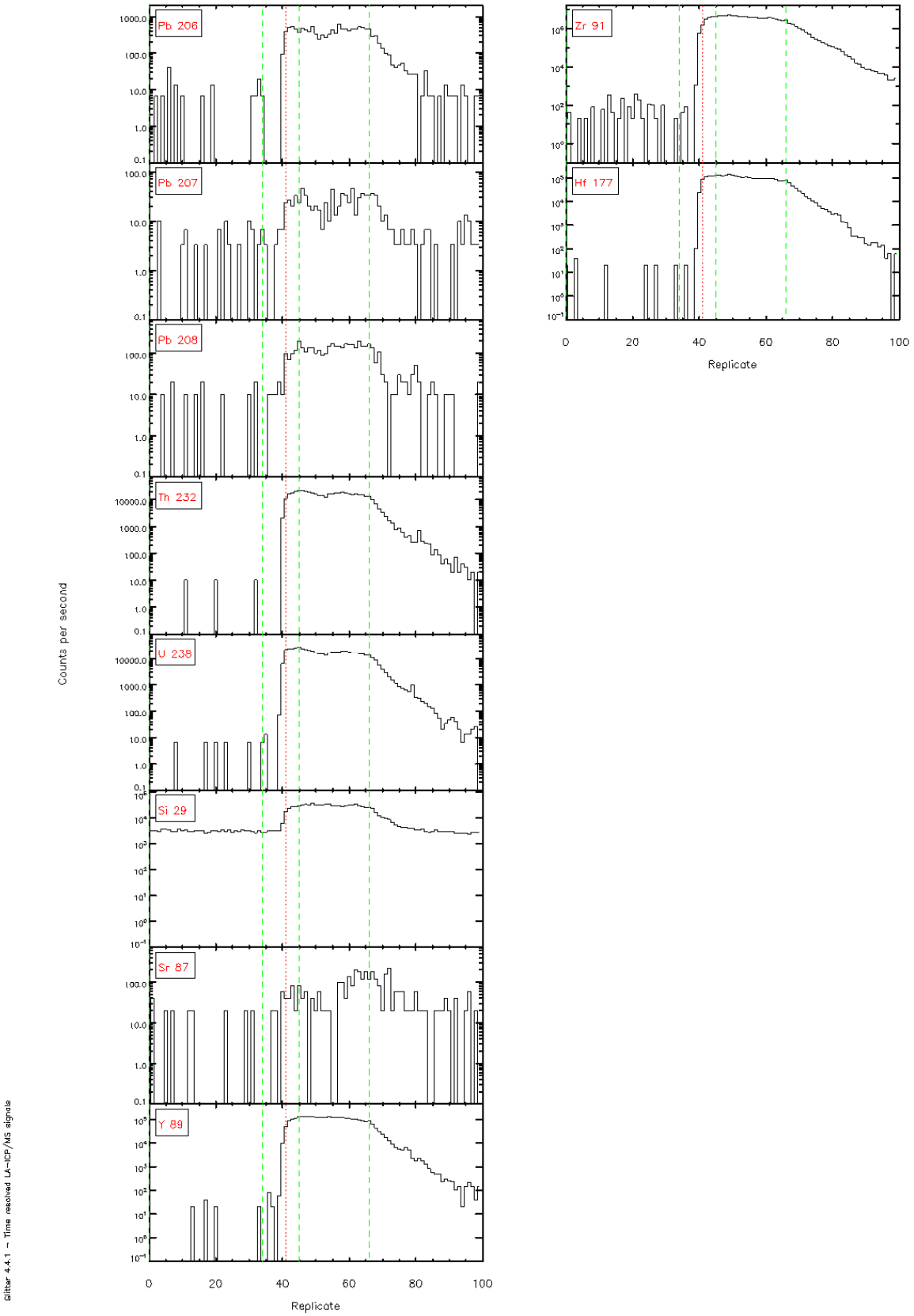
Pb 206
Pb 207
Pb 208
Th 232
U 238
Si 29
Sr 87
Y 89
Zr 91
Hf 177
Counts per second
Replicate
Glitter 4.4.1 – Time resolved LA-ICP/MS signals

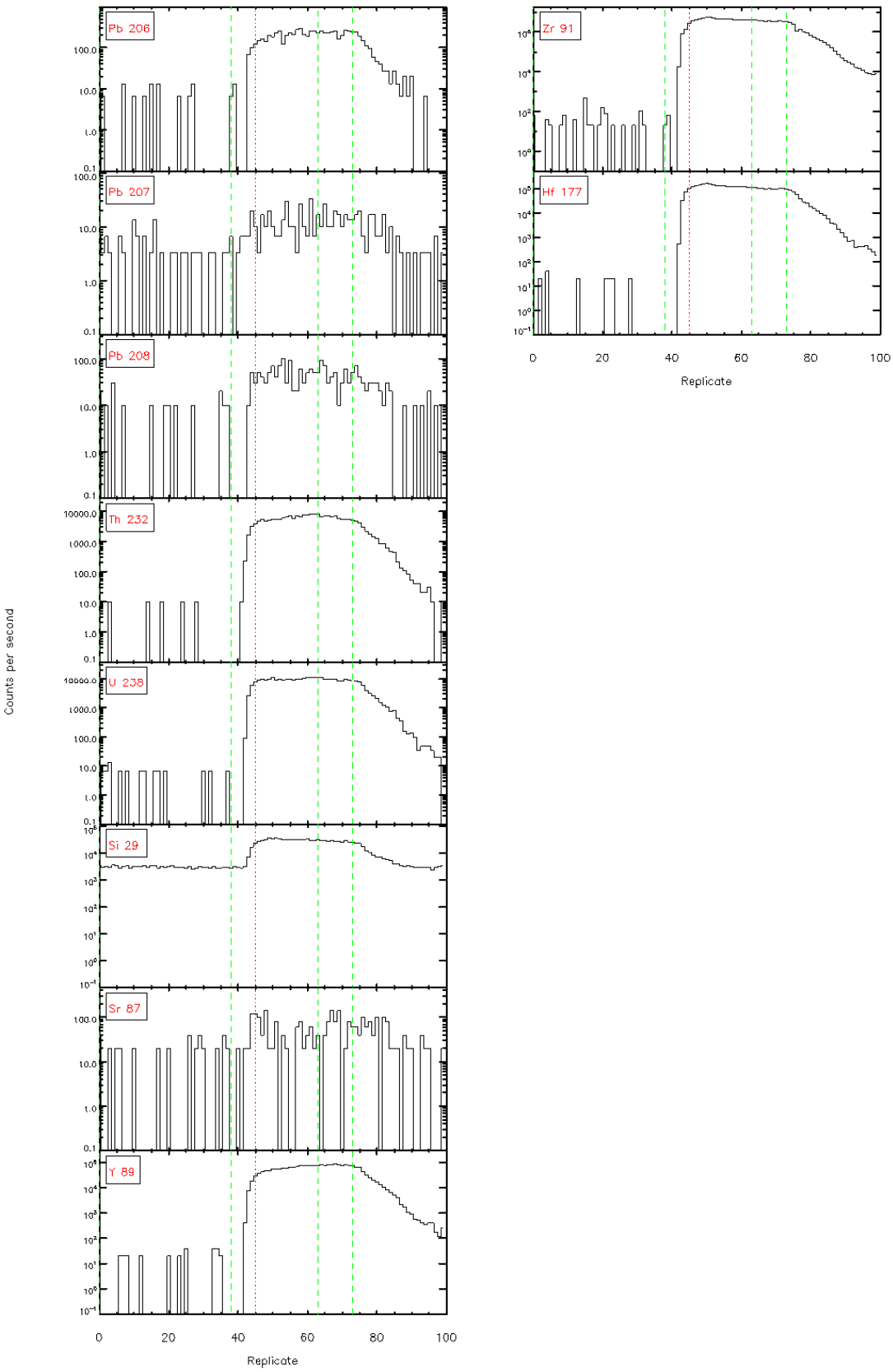
Pb 206
Pb 207
Pb 208
Th 232
U 238
Si 29
Sr 87
Y 89
Zr 91
Hf 177
Counts per second
Replicate
Glitter 4.4.1 - Time resolved LA-ICP/MS signals

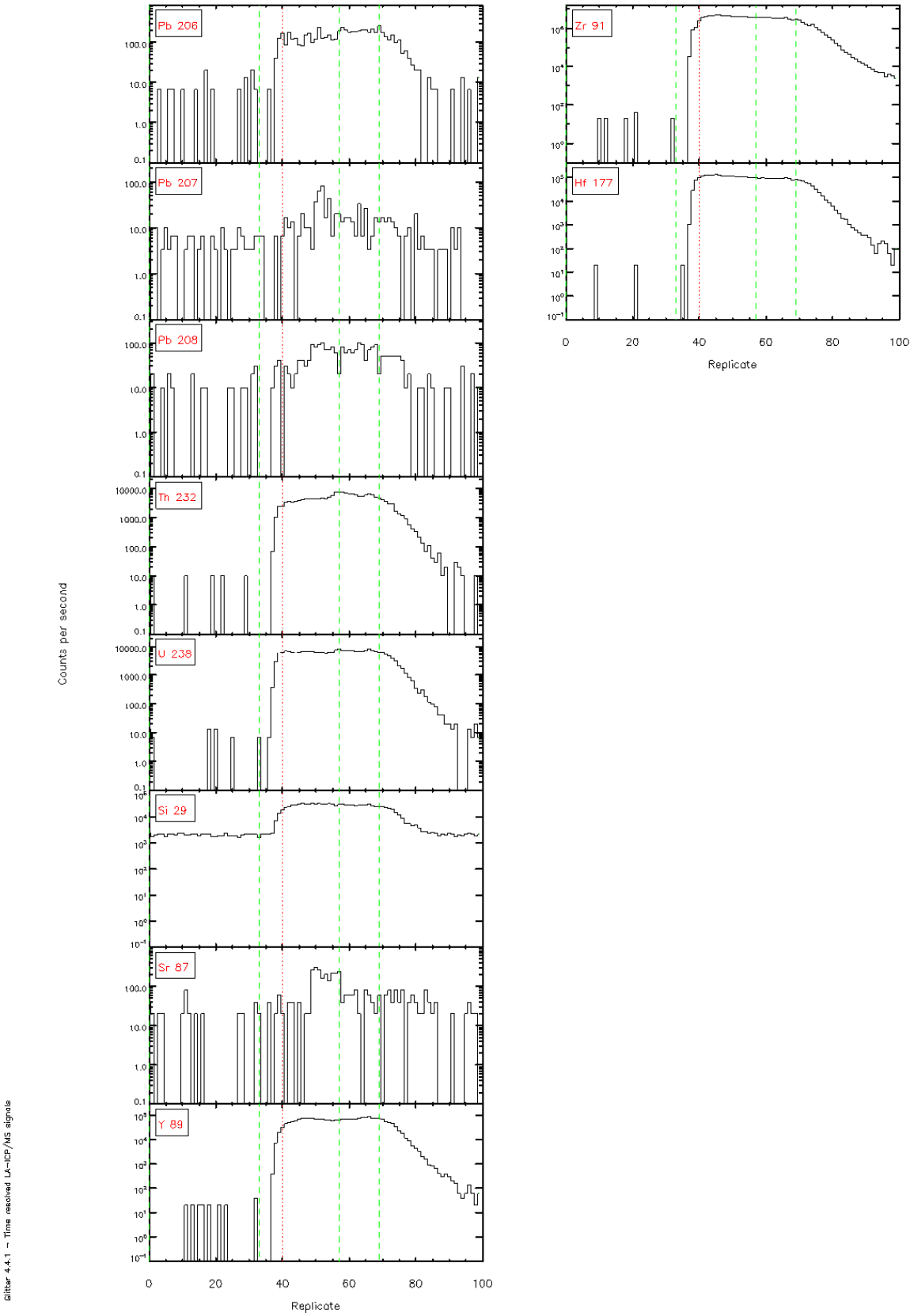
Pb 206
Pb 207
Pb 208
Th 232
U 238
Si 29
Sr 87
Y 89
Zr 91
Hf 177
Counts per second
Replicate
Glitter 4.4.1 – Time resolved LA-ICP/MS signals

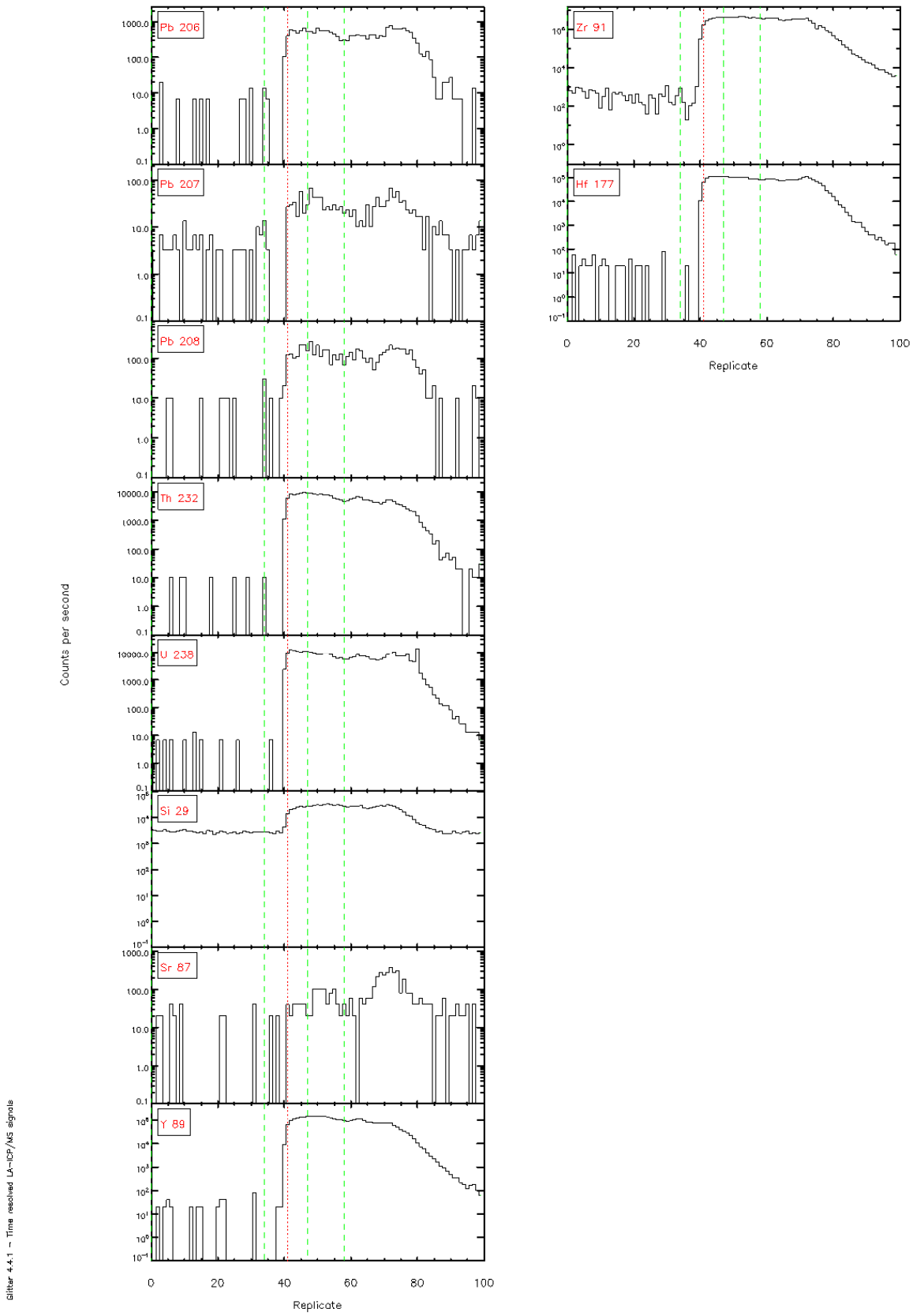
Pb 206
Pb 207
Pb 208
Th 232
U 238
Si 29
Sr 87
Y 89
Zr 91
Hf 177
Counts per second
Replicate
Replicate
Glitter 4.4.1 - Time resolved LA-ICP/MS signals

3 – Ahirau Sandstone

2.

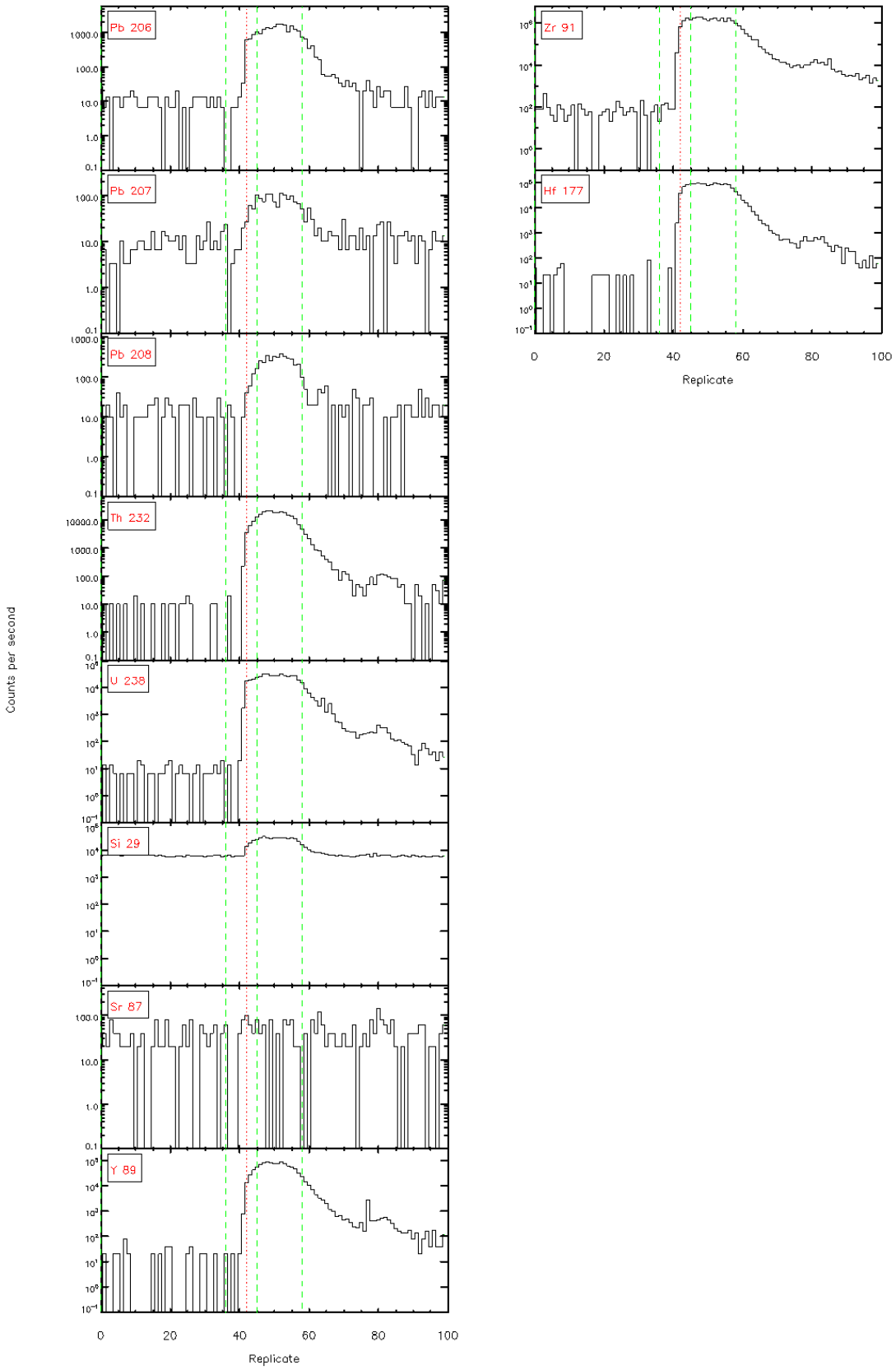

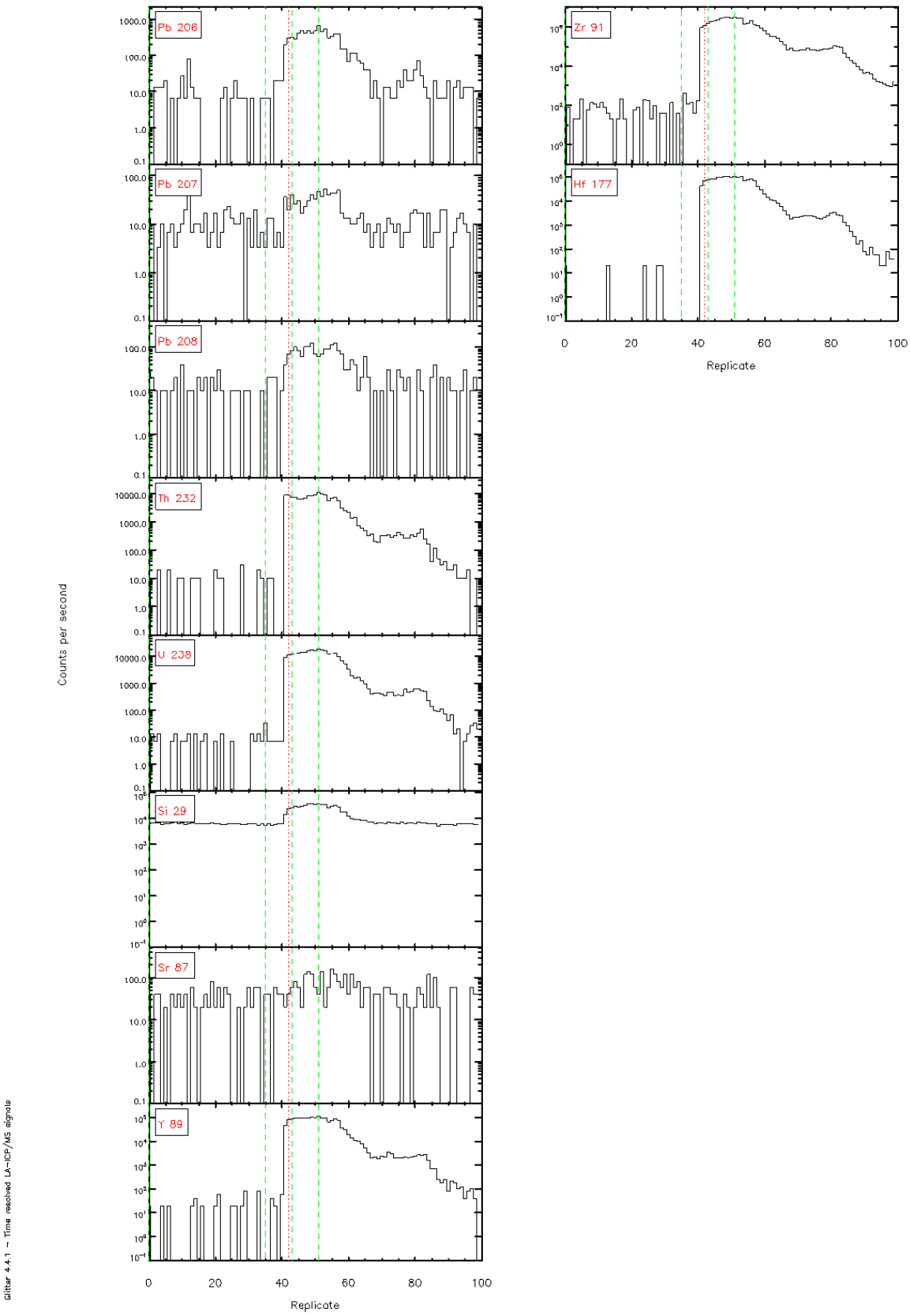
Pb 206
Pb 207
Pb 208
Th 232
U 238
Si 29
Sr 87
Y 89
Zr 91
Hf 177
Counts per second
Replicate
Glitter 4.4.1 - Time resolved LA-ICP/MS signals

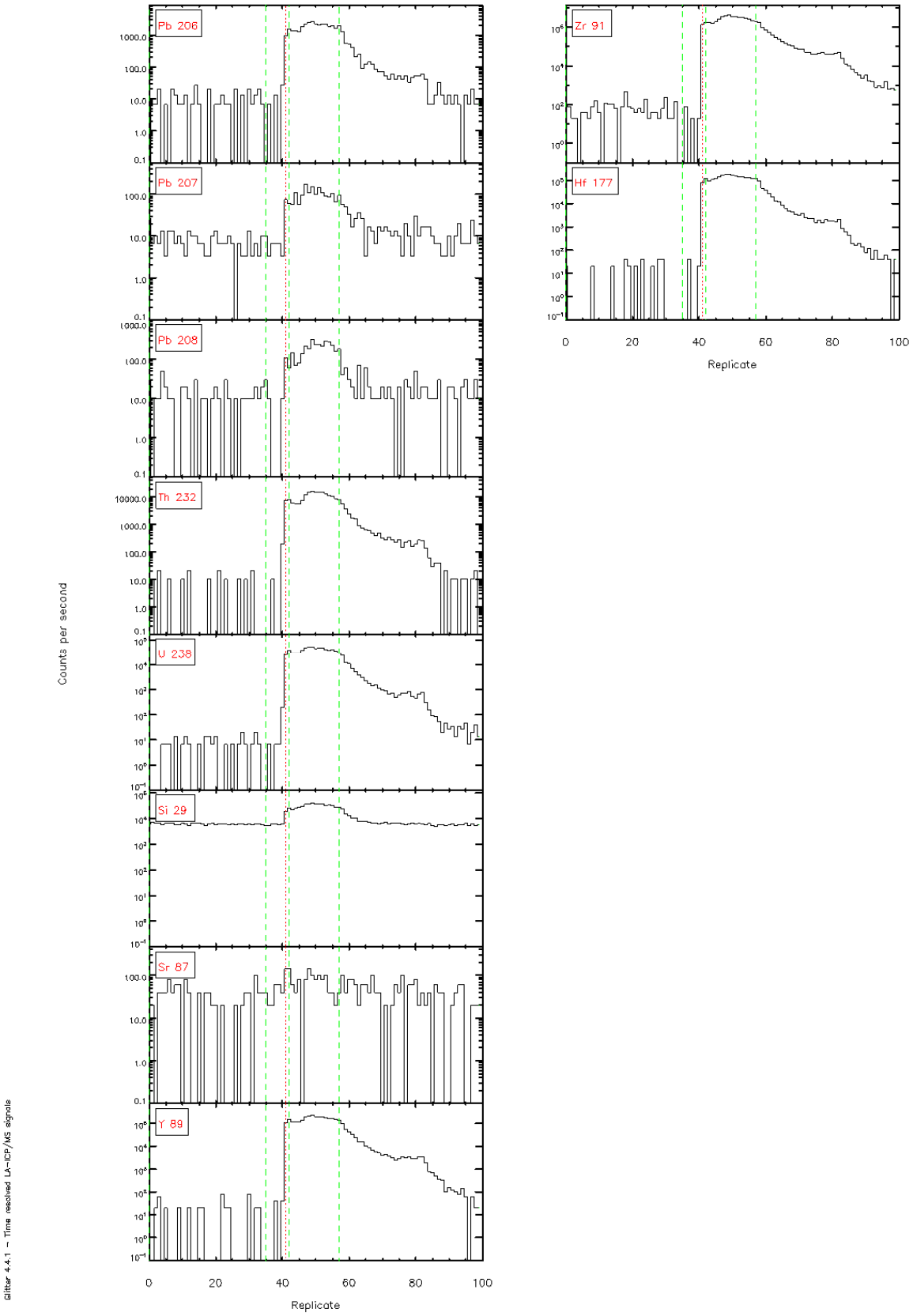
Pb 206
Pb 207
Pb 208
Th 232
U 238
Si 29
Sr 87
Y 89
Zr 91
Hf 177
Counts per second
Replicate
Glitter 4.4.1 – Time resolved LA-ICP/MS signals

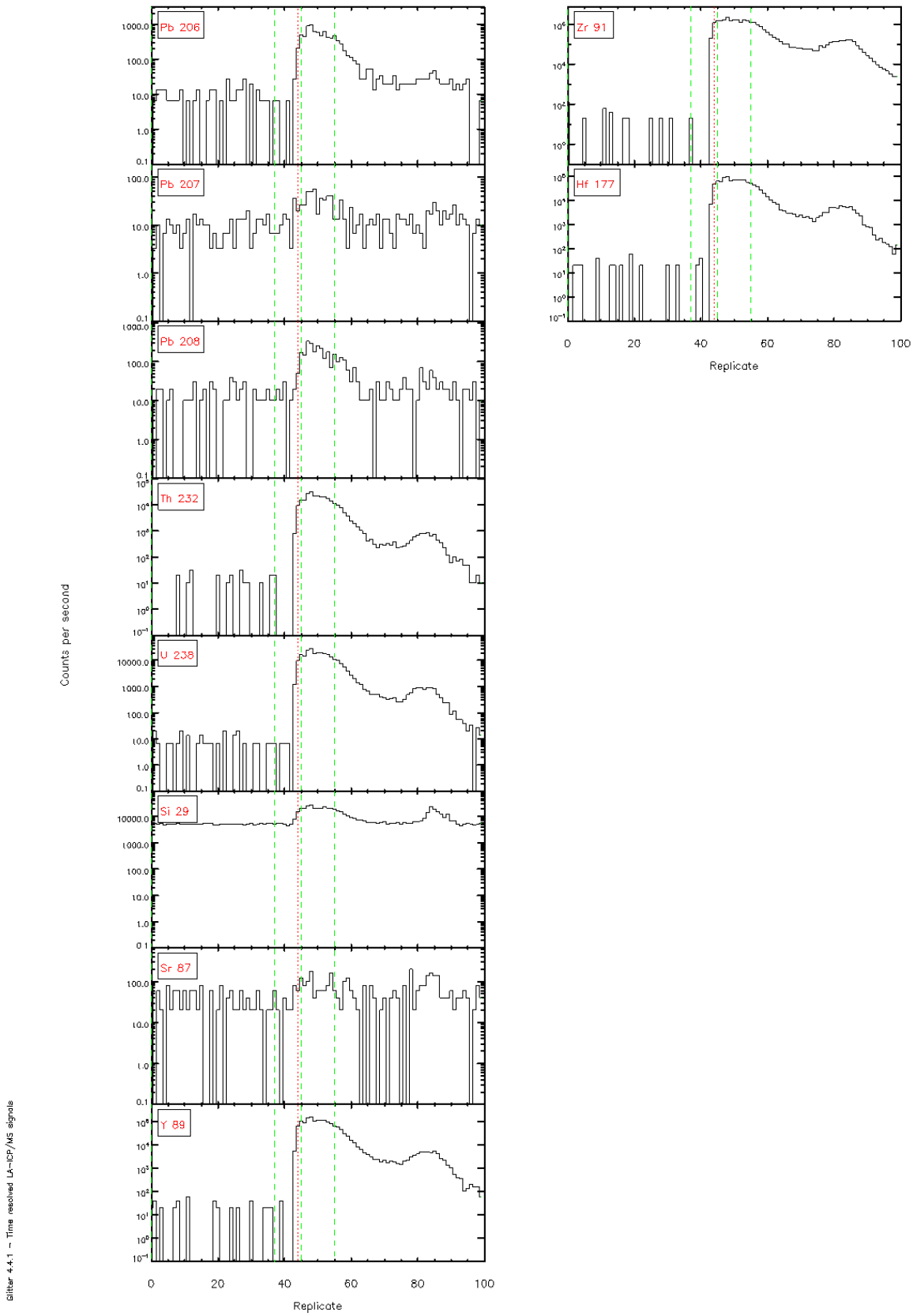
Pb 206
Pb 207
Pb 208
Th 232
U 238
Si 29
Sr 87
Y 89
Zr 91
Hf 177
Counts per second
Replicate
Glitter 4.4.1 - Time resolved LA-ICP/MS signals

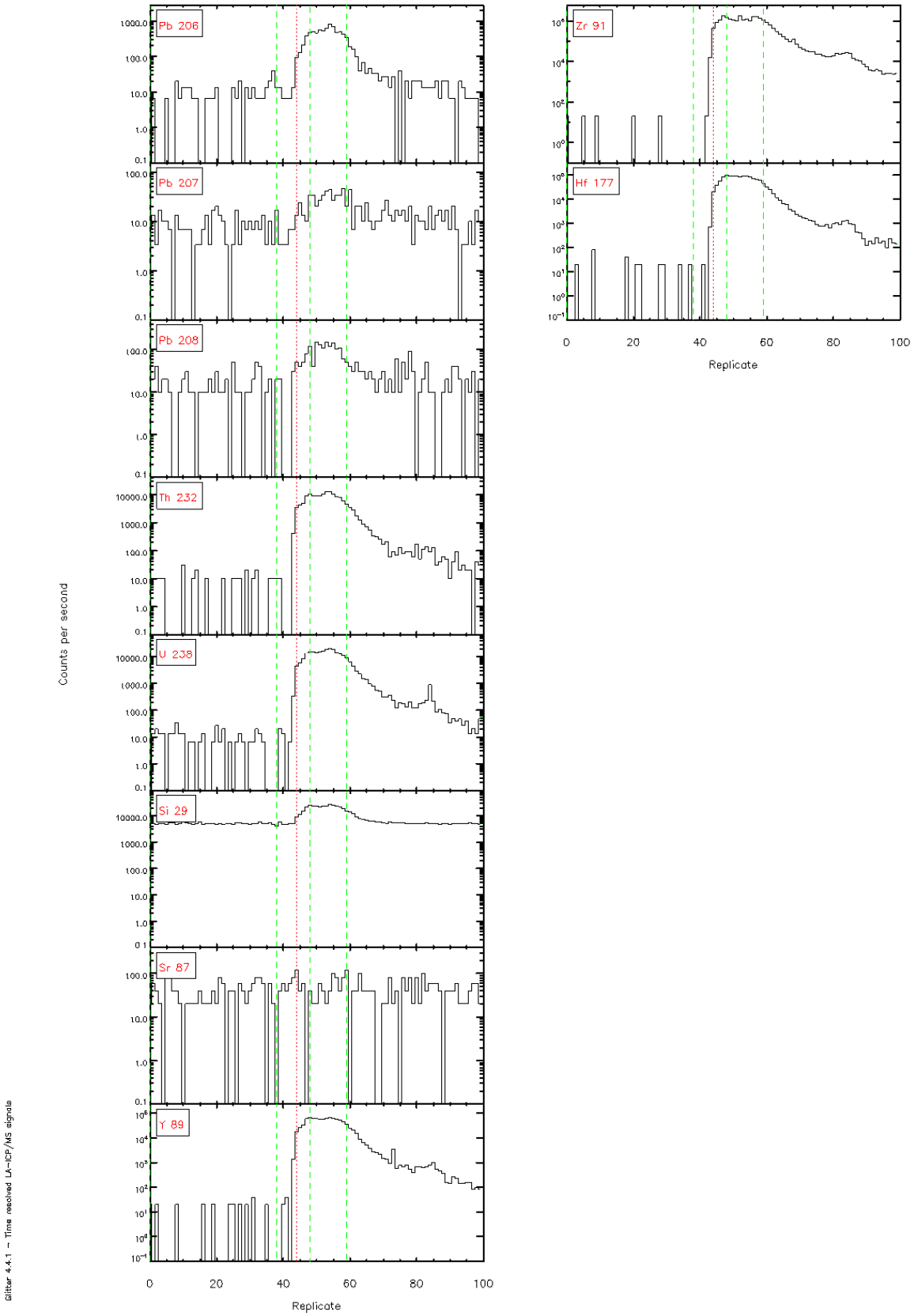
Pb 206
Pb 207
Pb 208
Th 232
U 238
Si 29
Sr 87
Y 89
Zr 91
Hf 177
Counts per second
Replicate
Glitter 4.4.1 - Time resolved LA-ICP/MS signals

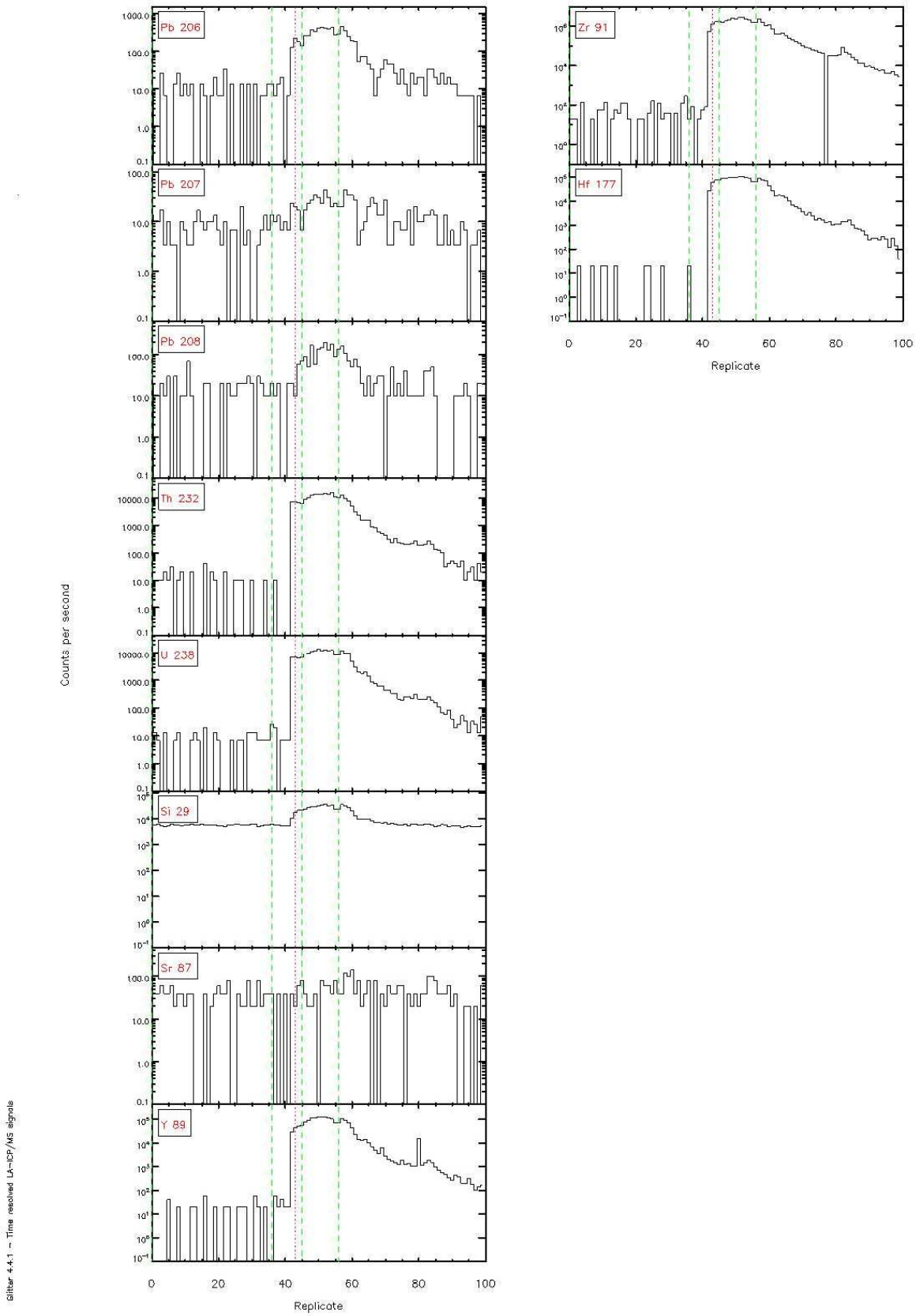
Pb 206
Pb 207
Pb 208
Th 232
U 238
Si 29
Sr 87
Y 89
Zr 91
Hf 177
Counts per second
Replicate
Glitter 4.4.1 – Time resolved LA-ICP/MS signals

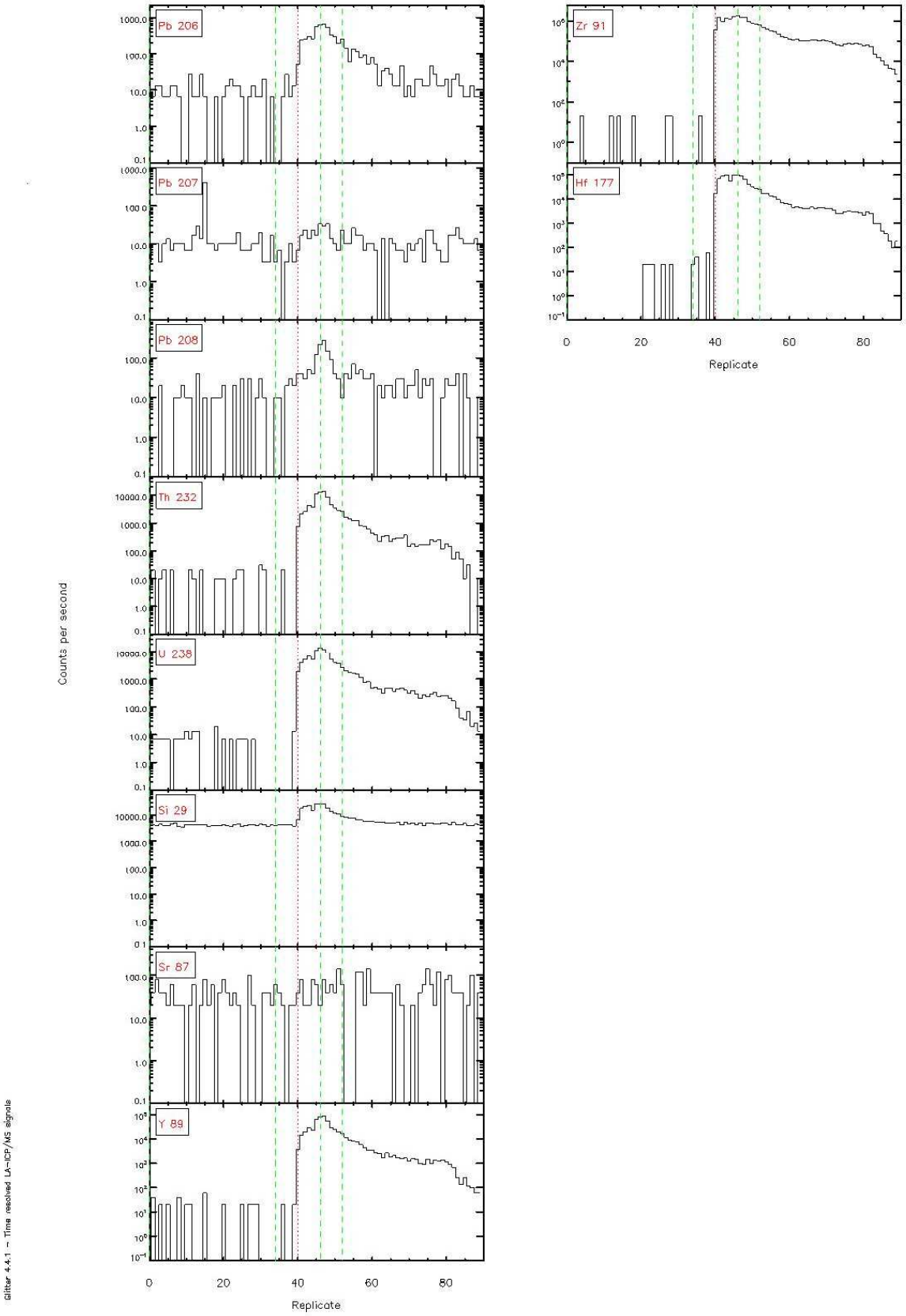
Pb 206
Pb 207
Pb 208
Th 232
U 238
Si 29
Sr 87
Y 89
Zr 91
Hf 177
Counts per second
Replicate
Glitter 4.4.1 – Time resolved LA-ICP/MS signals

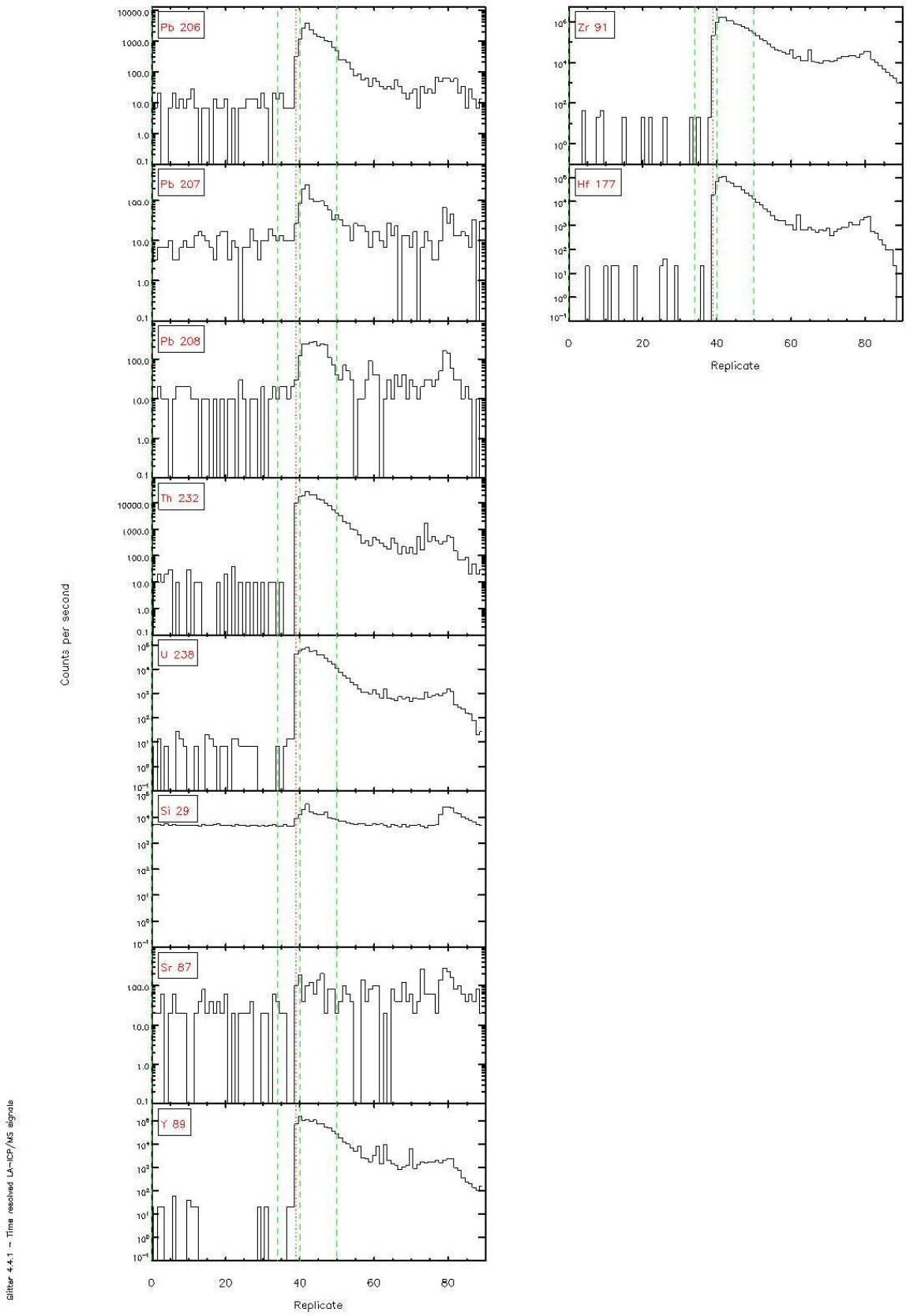
Pb 206
Pb 207
Pb 208
Th 232
U 238
Si 29
Sr 87
Y 89
Zr 91
Hf 177
Counts per second
Replicate
Glitter 4.4.1 – Time resolved LA-ICP/MS signals

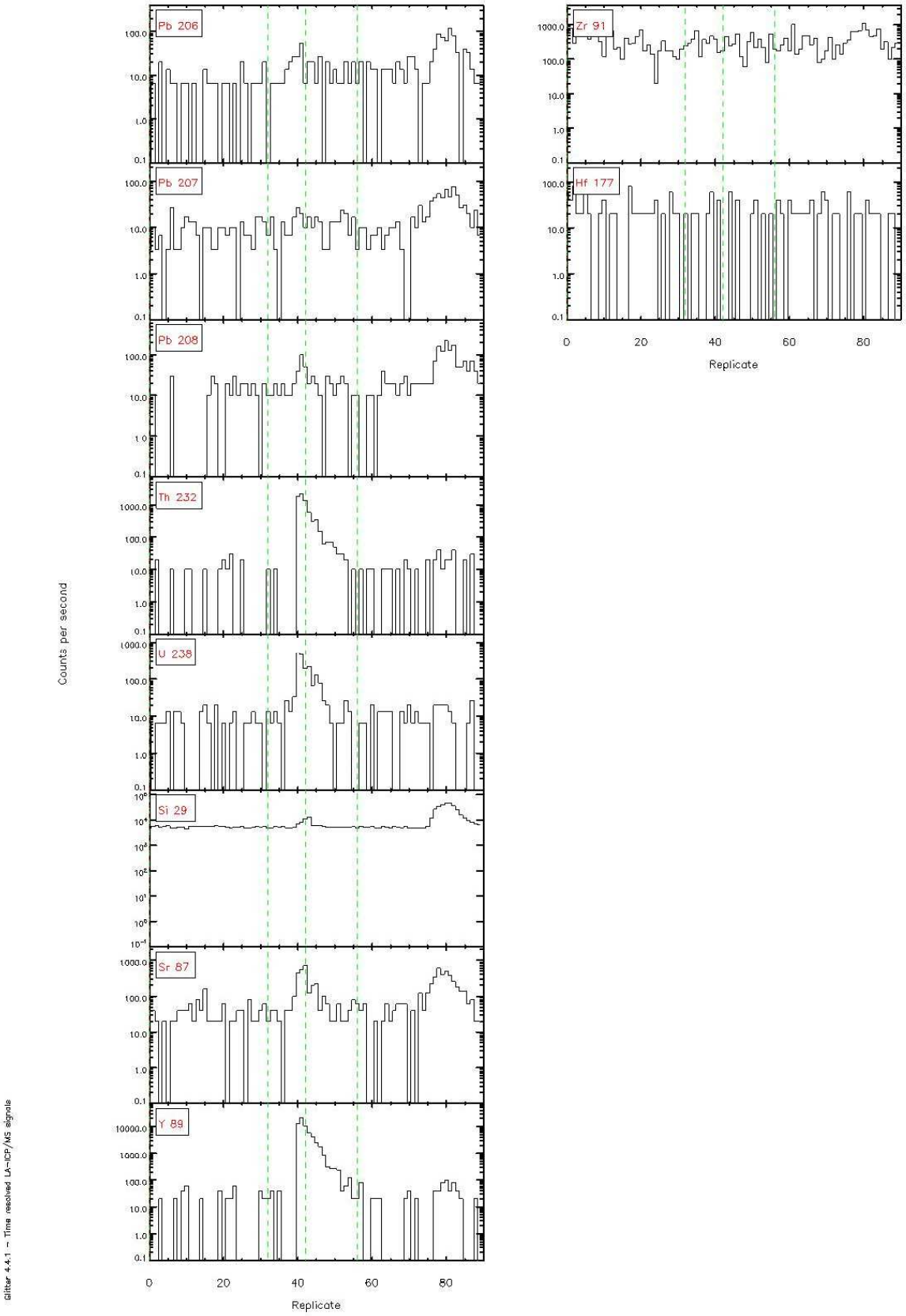
Pb 206
Pb 207
Pb 208
Th 232
U 238
Si 29
Sr 87
Y 89
Zr 91
Hf 177
Counts per second
Replicate
Glitter 4.4.1 - Time resolved LA-ICP/MS signals

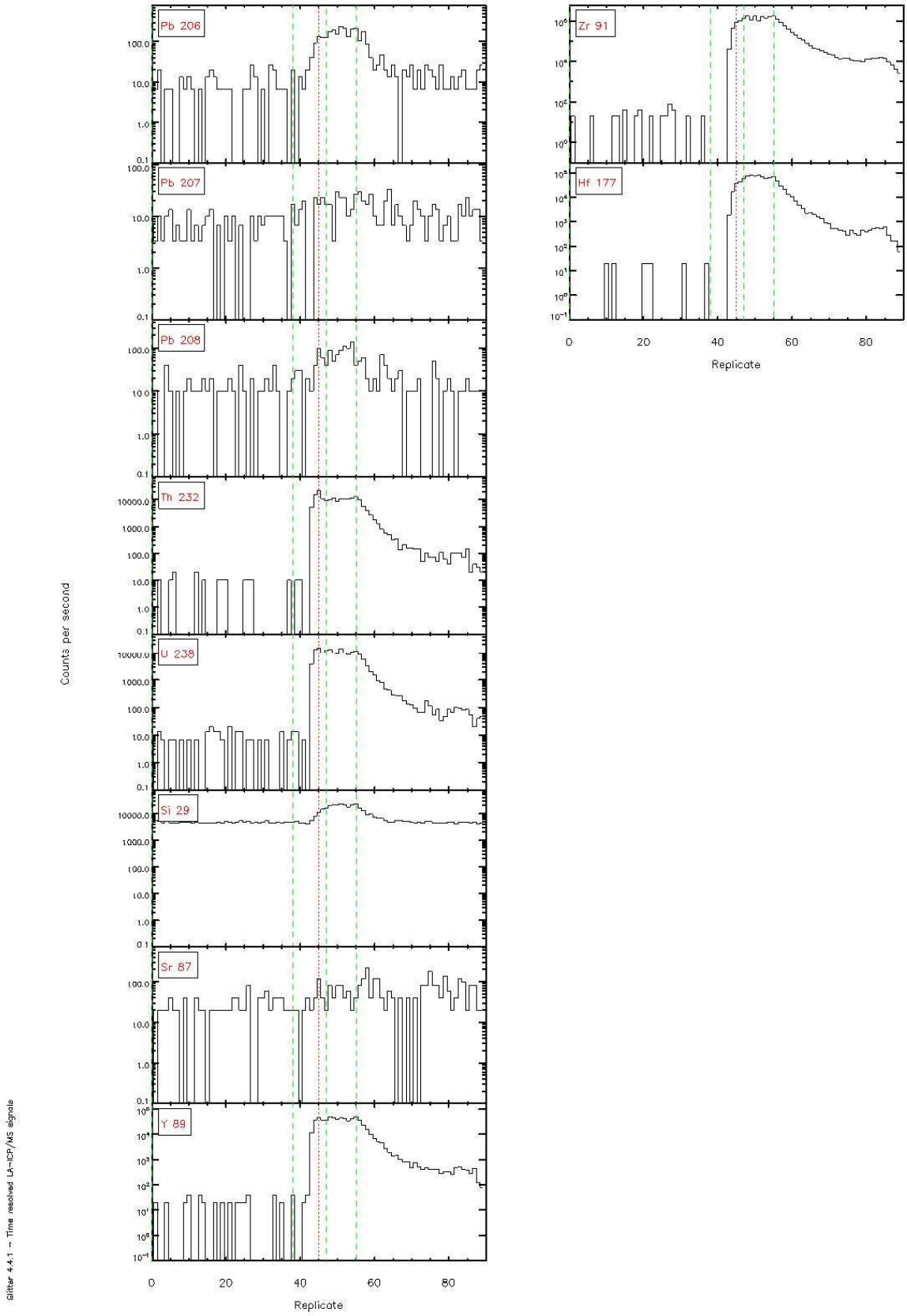
Pb 206
Pb 207
Pb 208
Th 232
U 238
Si 29
Sr 87
Y 89
Zr 91
Hf 177
Counts per second
Replicate
Glitter 4.4.1 – Time resolved LA-ICP/MS signals

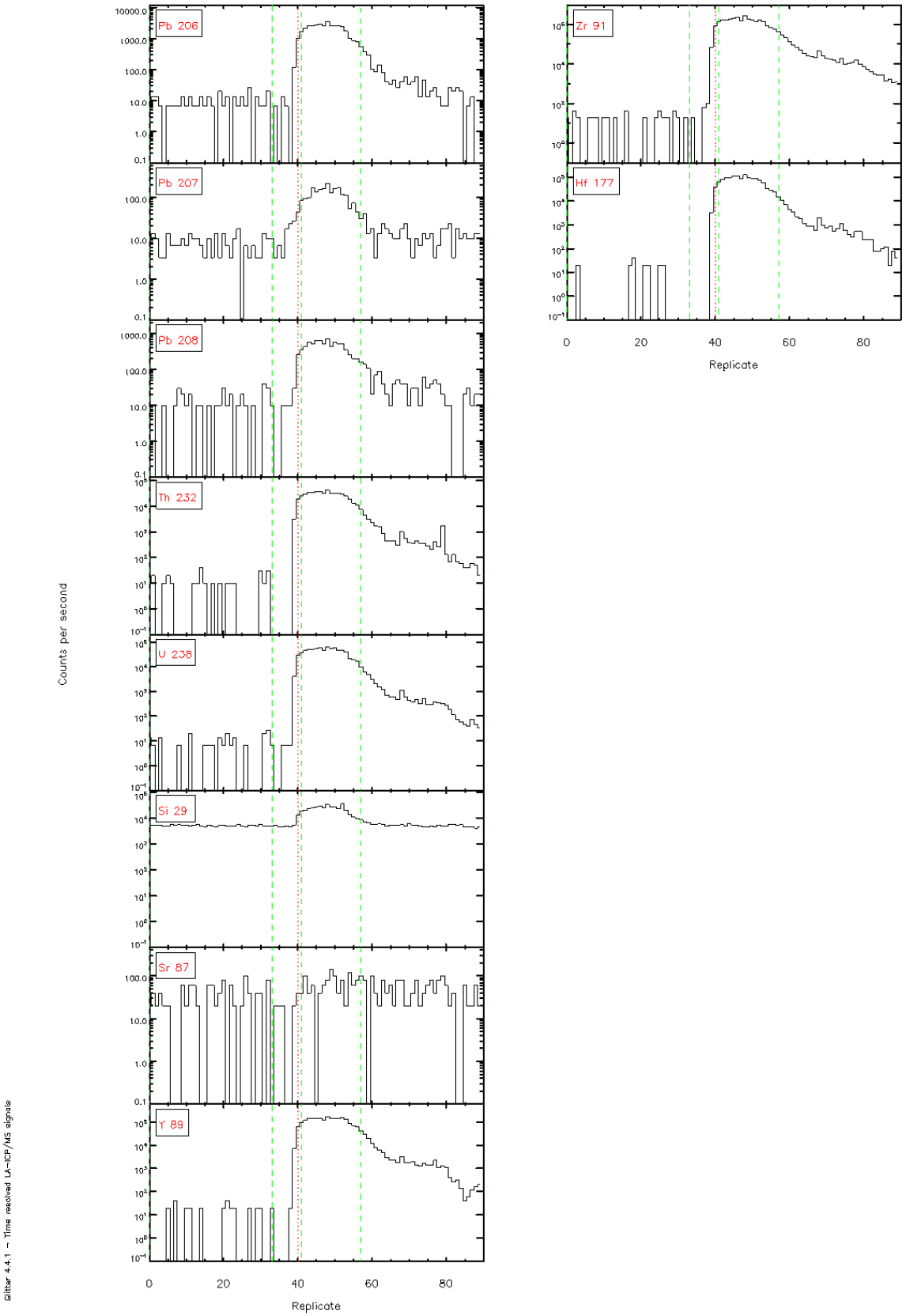
Pb 206
Pb 207
Pb 208
Th 232
U 238
Si 29
Sr 87
Y 89
Zr 91
Hf 177
Counts per second
Replicate
Glitter 4.4.1 - Time resolved LA-ICP/MS signals

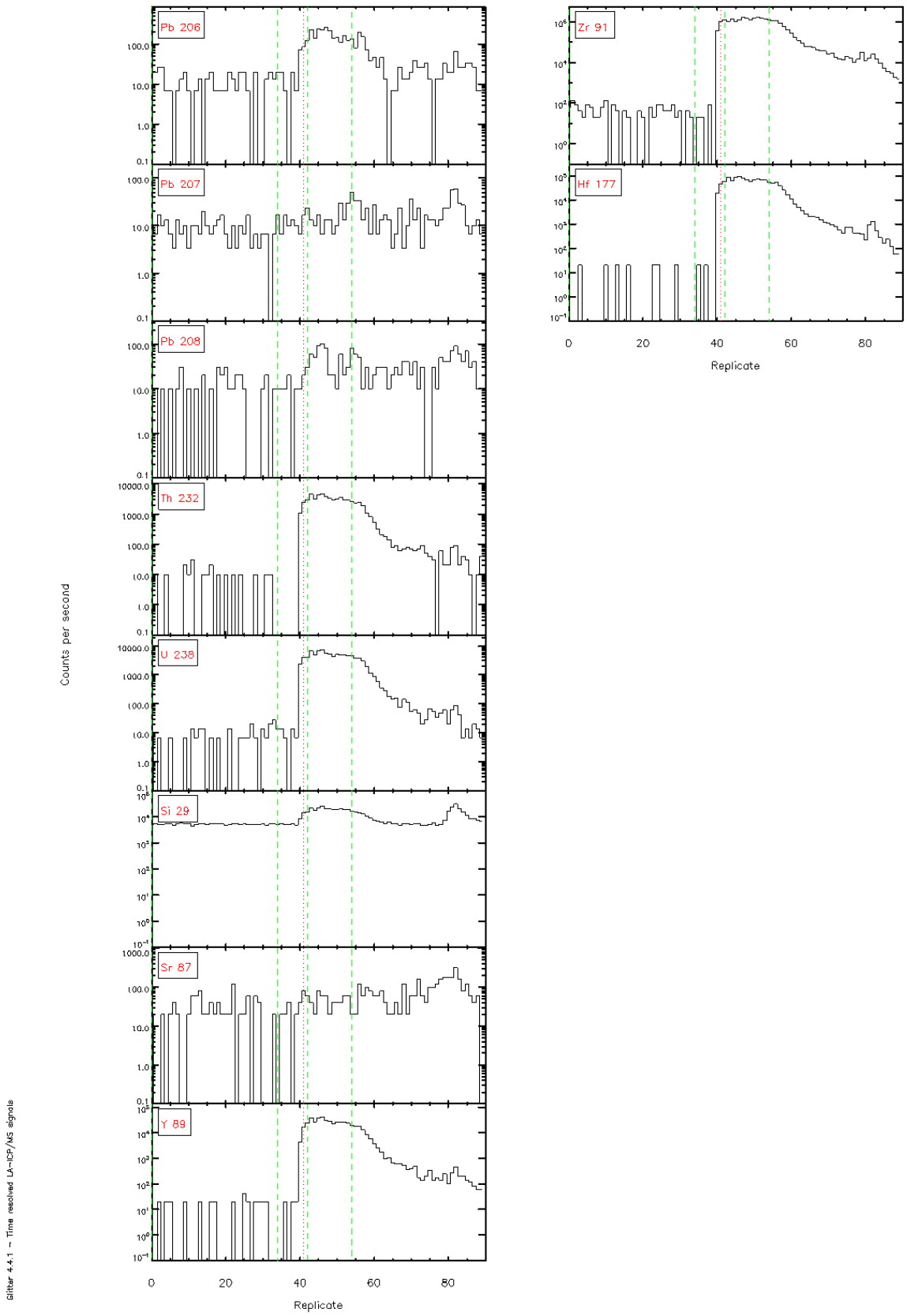
Pb 206
Pb 207
Pb 208
Th 232
U 238
Si 29
Sr 87
Y 89
Zr 91
Hf 177
Counts per second
Replicate
Glitter 4.4.1 – Time resolved LA-ICP/MS signals

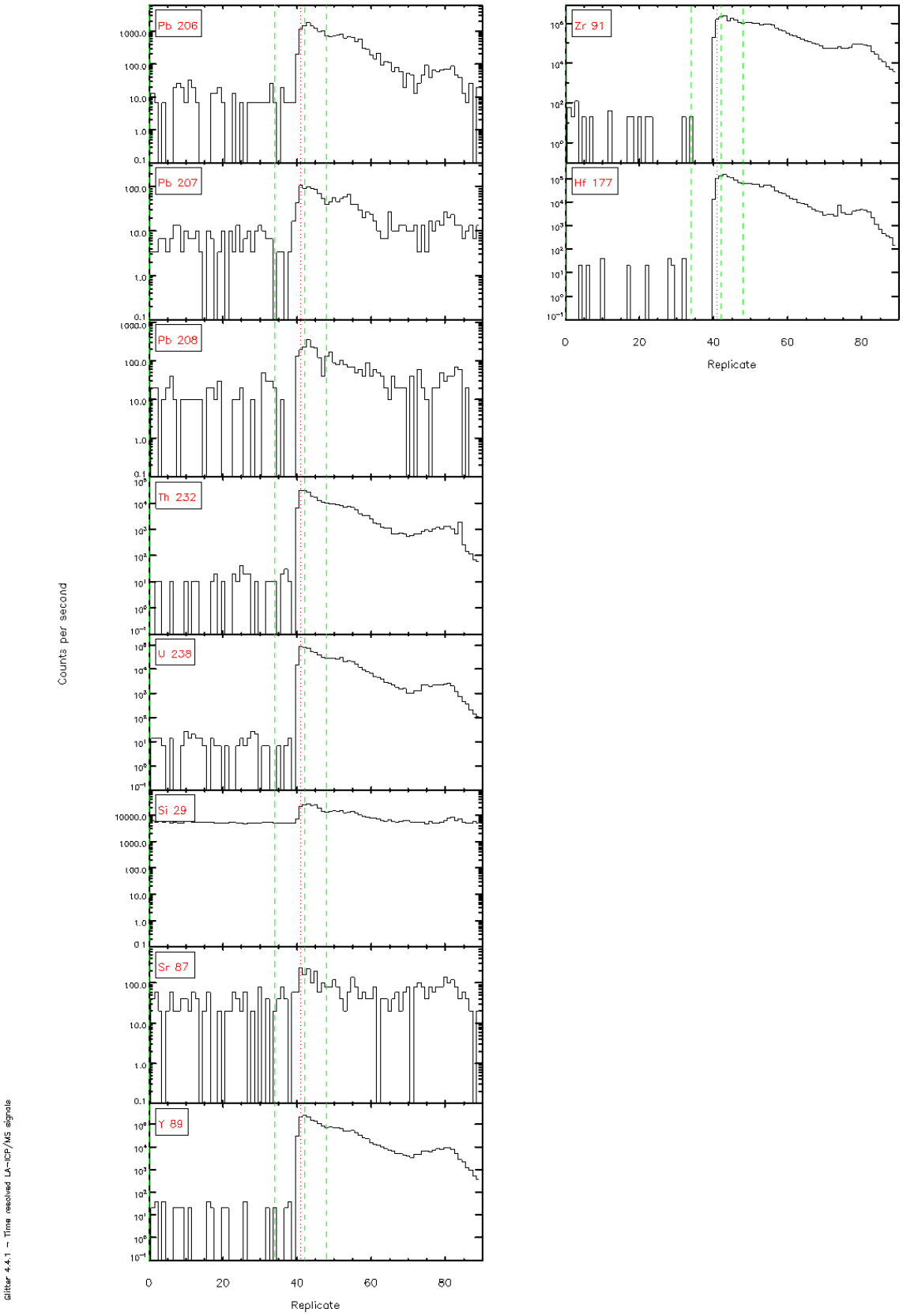
Pb 206
Pb 207
Pb 208
Th 232
U 238
Si 29
Sr 87
Y 89
Zr 91
Hf 177
Counts per second
Replicate
Glitter 4.4.1 – Time resolved LA-ICP/MS signals

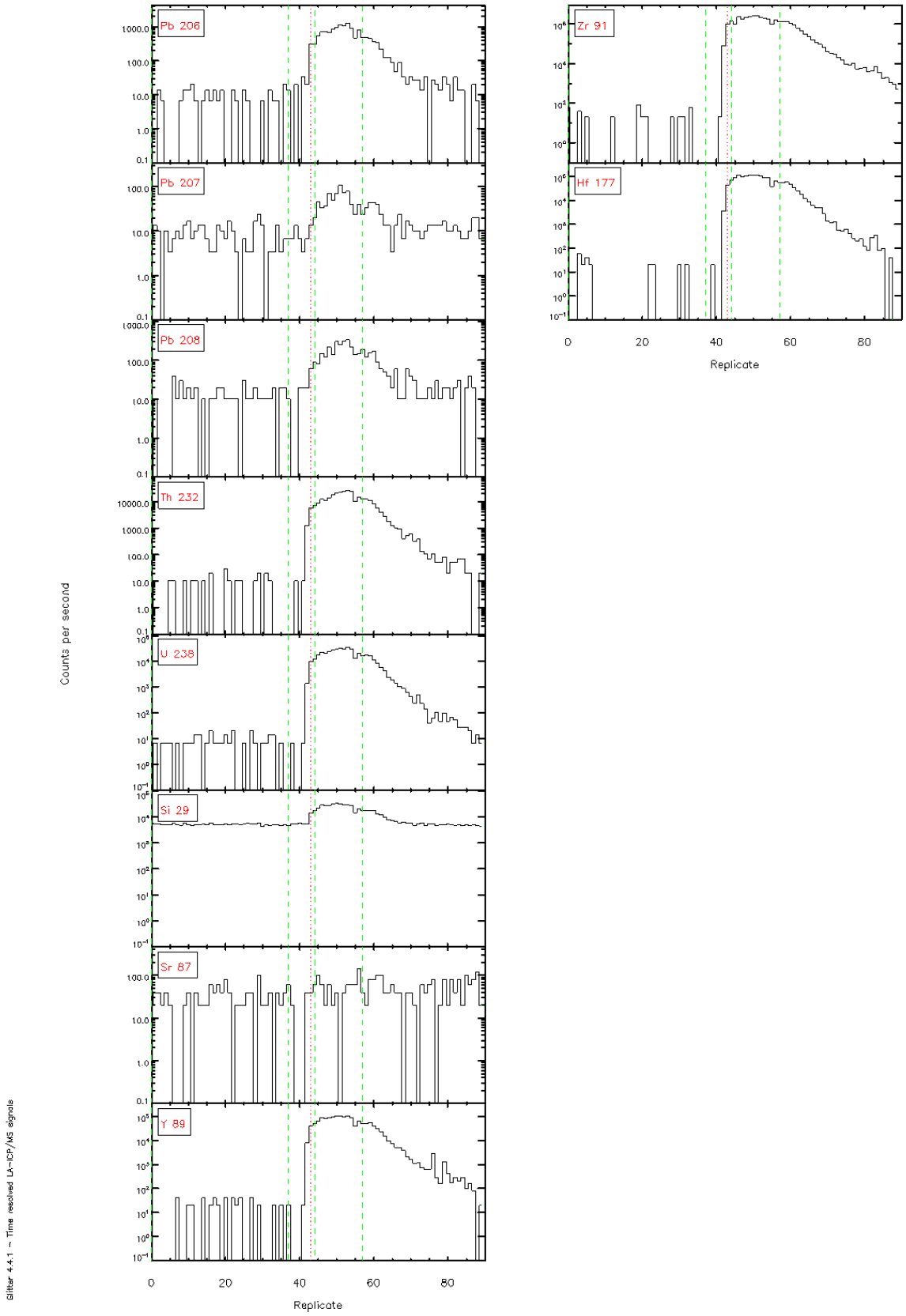
Pb 206
Pb 207
Pb 208
Th 232
U 238
Si 29
Sr 87
Y 89
Zr 91
Hf 177
Counts per second
Replicate
Glitter 4.4.1 - Time resolved LA-ICP/MS signals

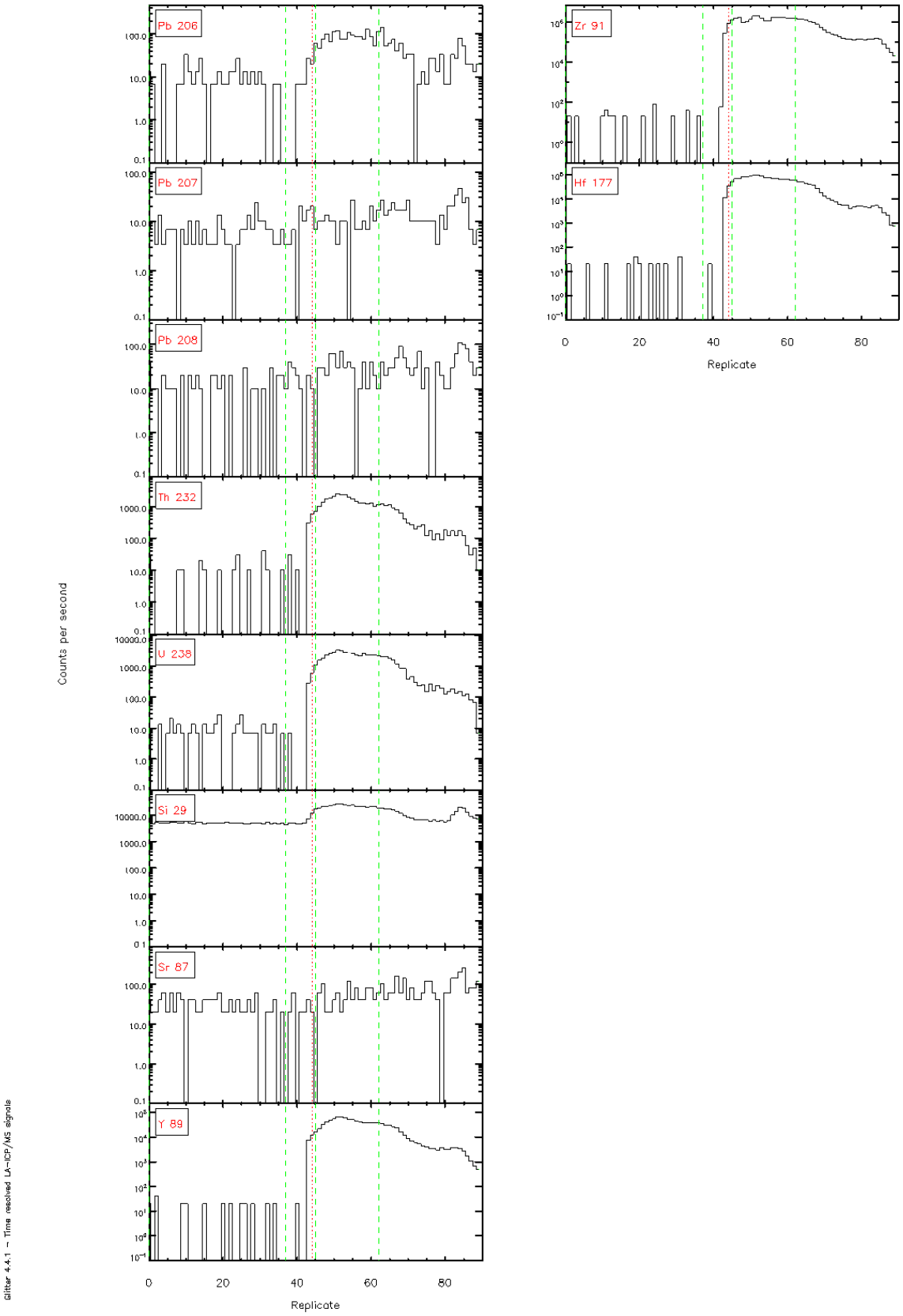
Pb 206
Pb 207
Pb 208
Th 232
U 238
Si 29
Sr 87
Y 89
Zr 91
Hf 177
Counts per second
Replicate
Glitter 4.4.1 – Time resolved LA-ICP/MS signals

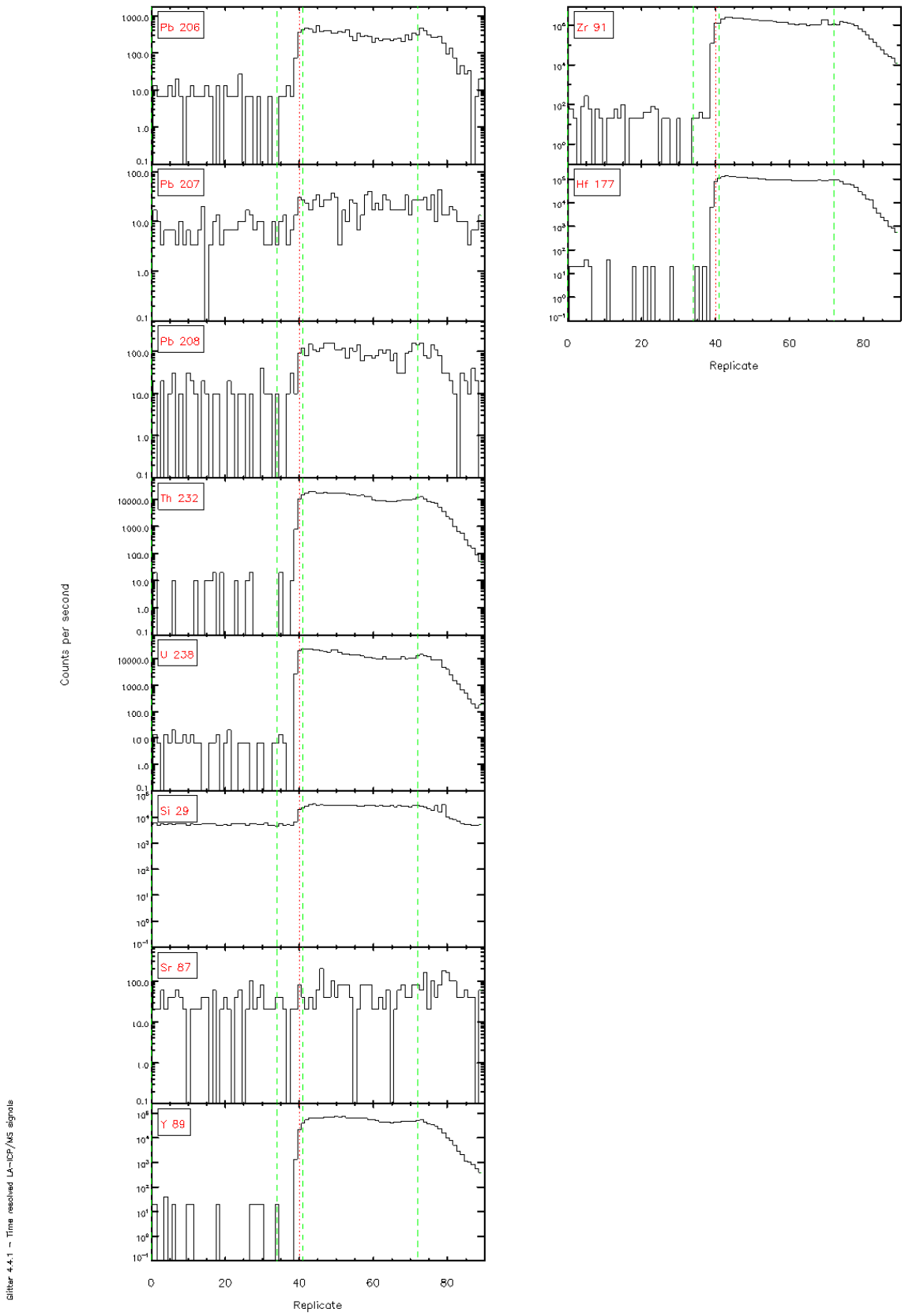
Pb 206
Pb 207
Pb 208
Th 232
U 238
Si 29
Sr 87
Y 89
Zr 91
Hf 177
Counts per second
Replicate
Glitter 4.4.1 - Time resolved LA-ICP/MS signals

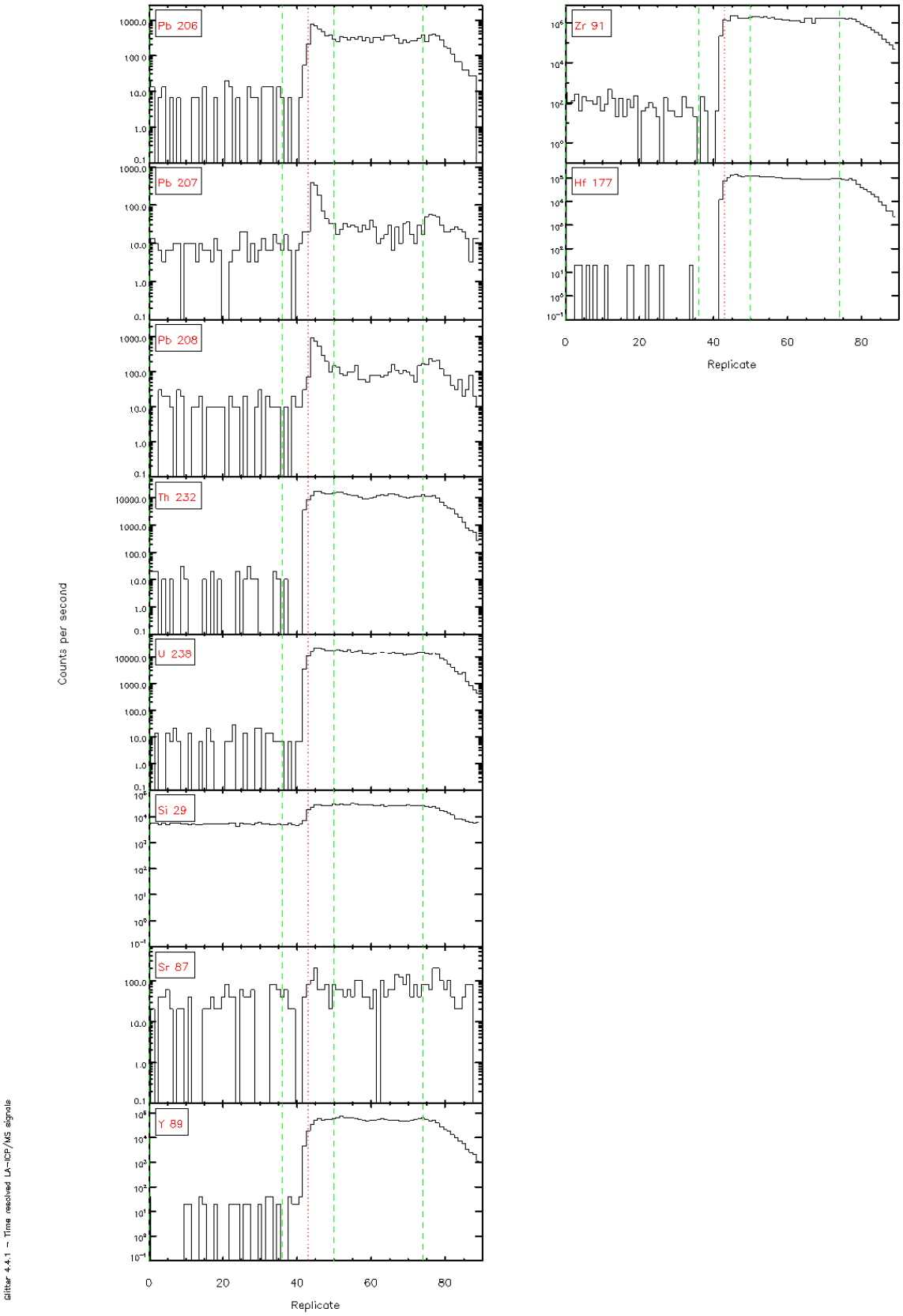
Pb 206
Pb 207
Pb 208
Th 232
U 238
Si 29
Sr 87
Y 89
Zr 91
Hf 177
Counts per second
Replicate
Glitter 4.4.1 – Time resolved LA-ICP/MS signals

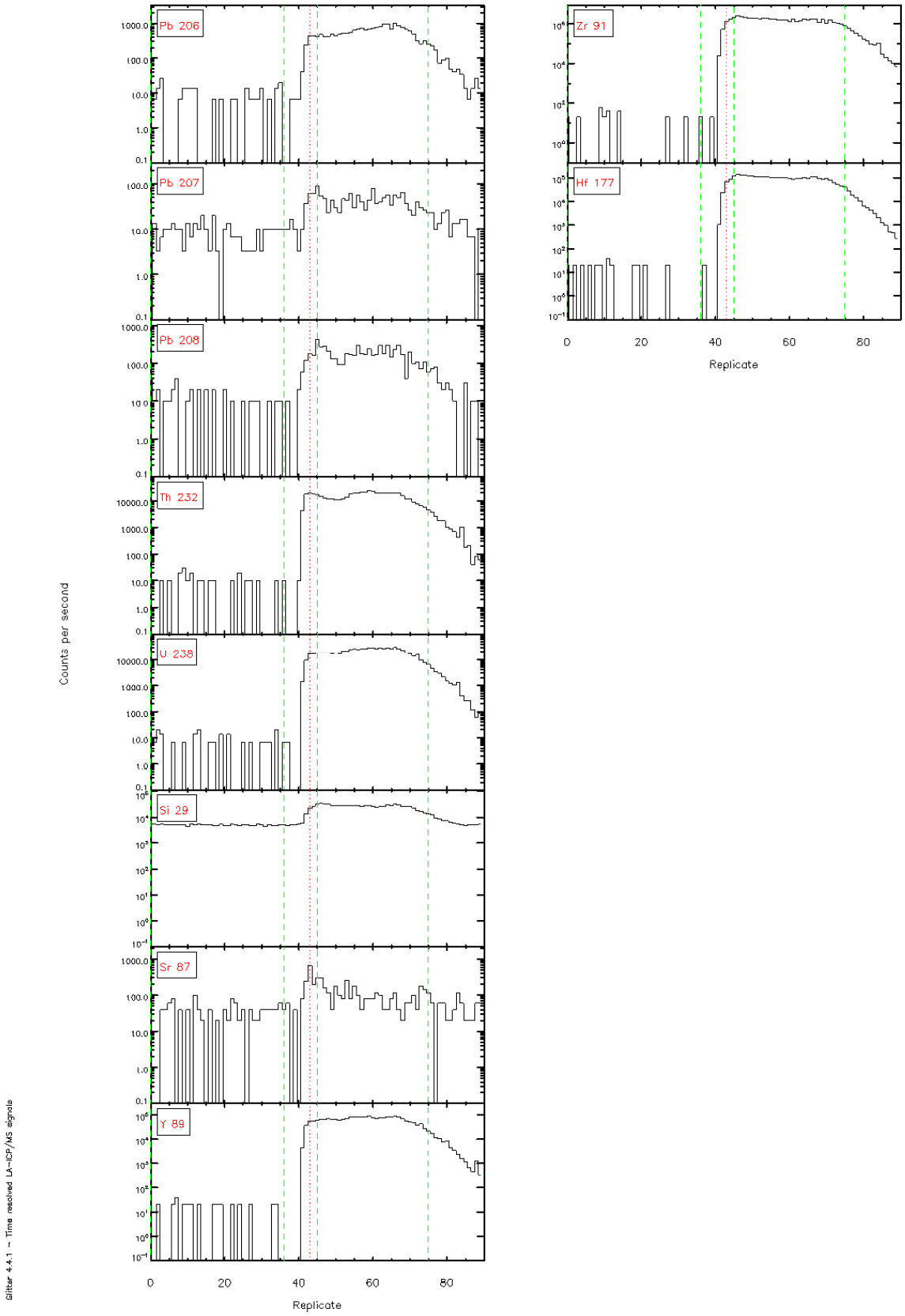
Pb 206
Pb 207
Pb 208
Th 232
U 238
Si 29
Sr 87
Y 89
Zr 91
Hf 177
Counts per second
Replicate
Glitter 4.4.1 - Time resolved LA-ICP/MS signals

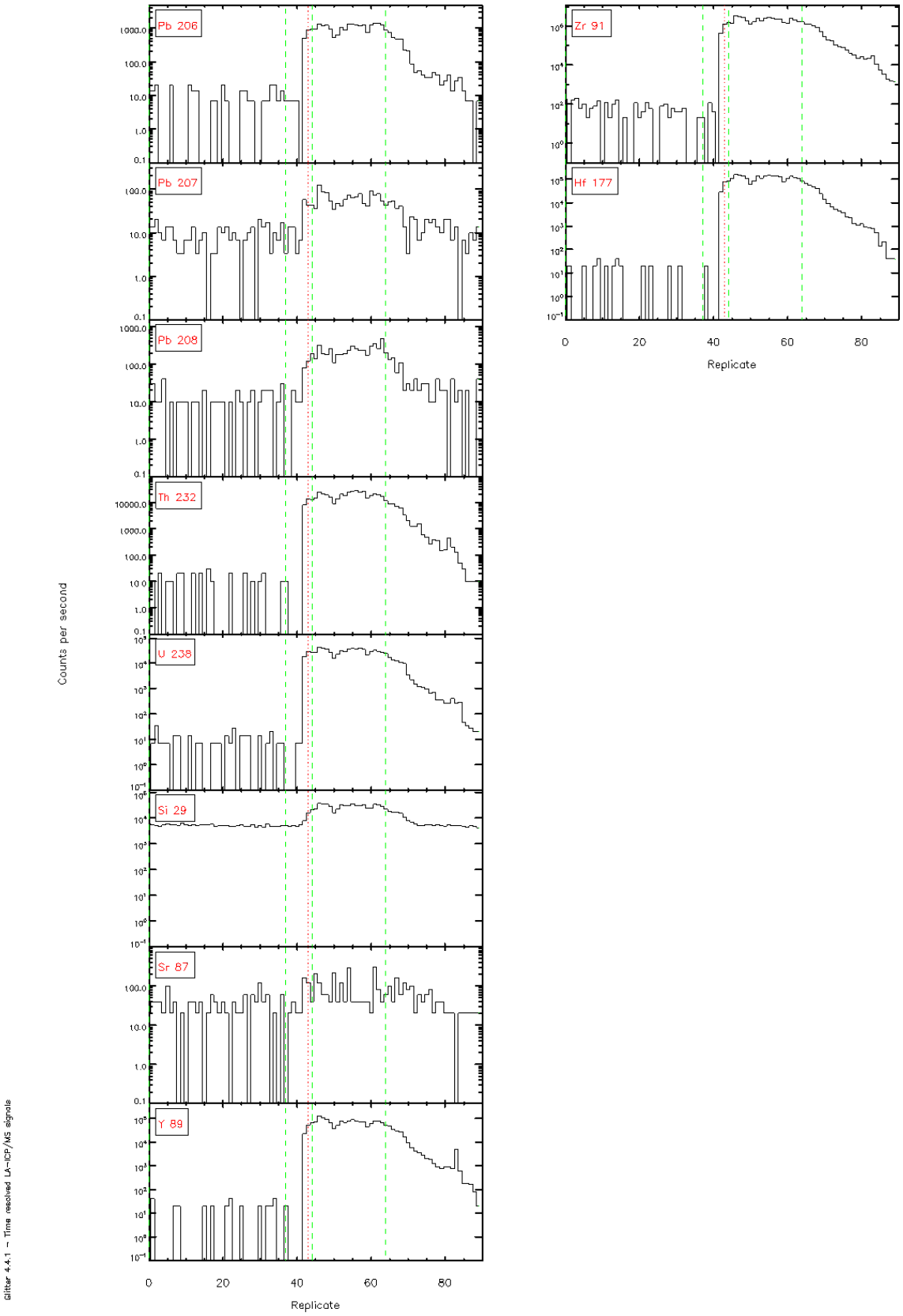
Pb 206
Pb 207
Pb 208
Th 232
U 238
Si 29
Sr 87
Y 89
Zr 91
Hf 177
Counts per second
Replicate
Glitter 4.4.1 – Time resolved LA-ICP/MS signals

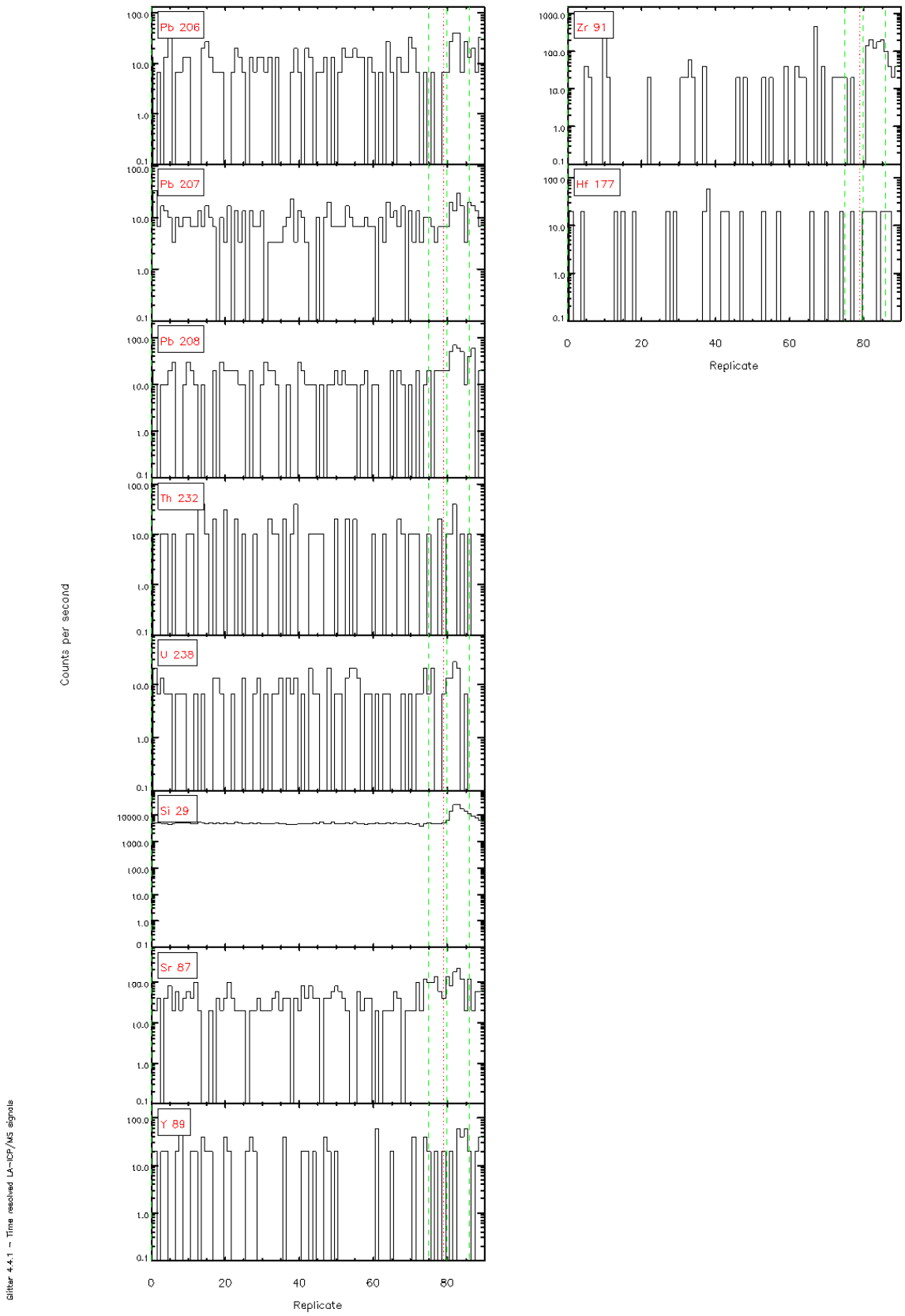
Pb 206
Pb 207
Pb 208
Th 232
U 238
Si 29
Sr 87
Y 89
Zr 91
Hf 177
Counts per second
Replicate
Glitter 4.4.1 – Time resolved LA-ICP/MS signals

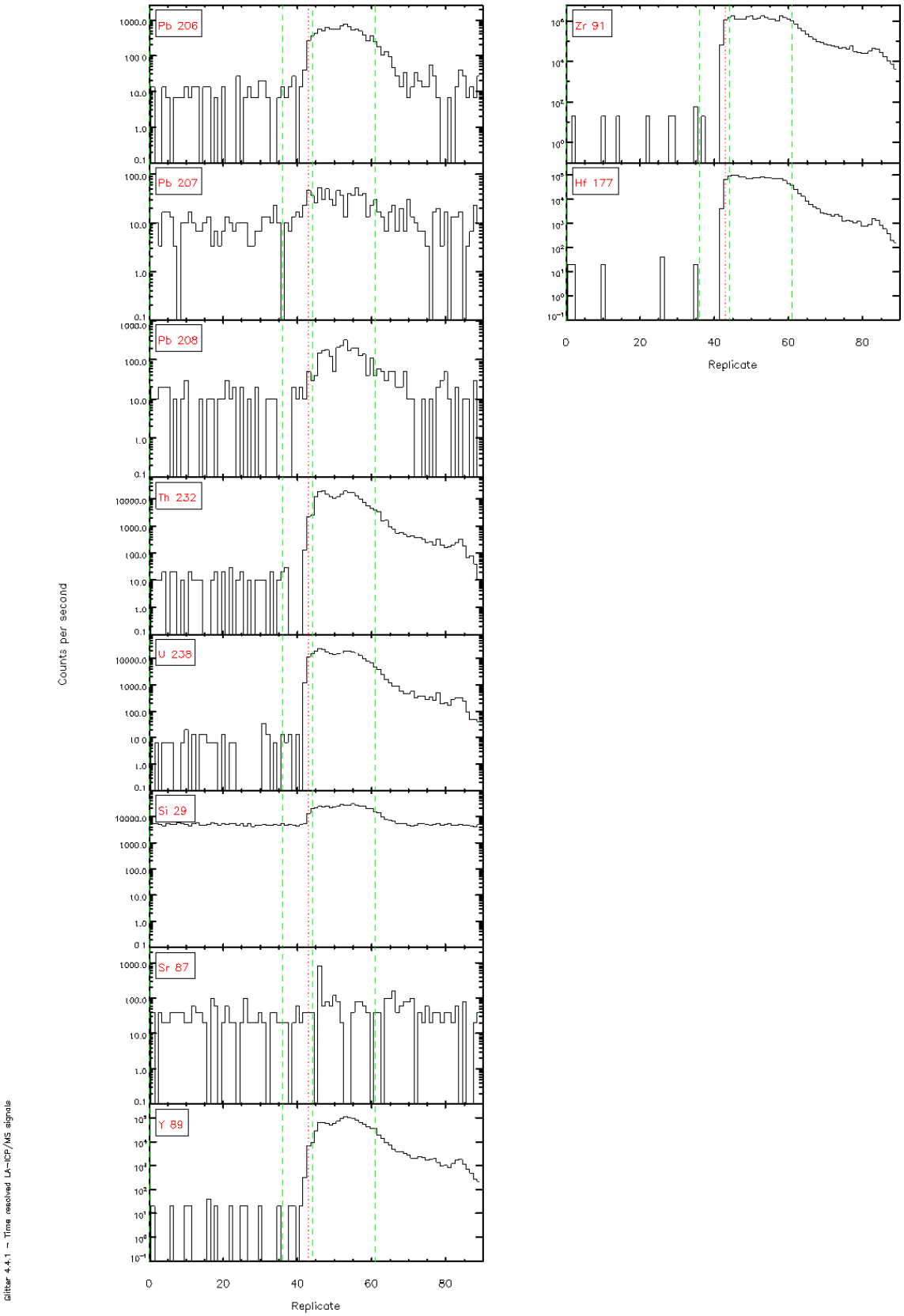
Pb 206
Pb 207
Pb 208
Th 232
U 238
Si 29
Sr 87
Y 89
Zr 91
Hf 177
Counts per second
Replicate
Glitter 4.4.1 - Time resolved LA-ICP/MS signals

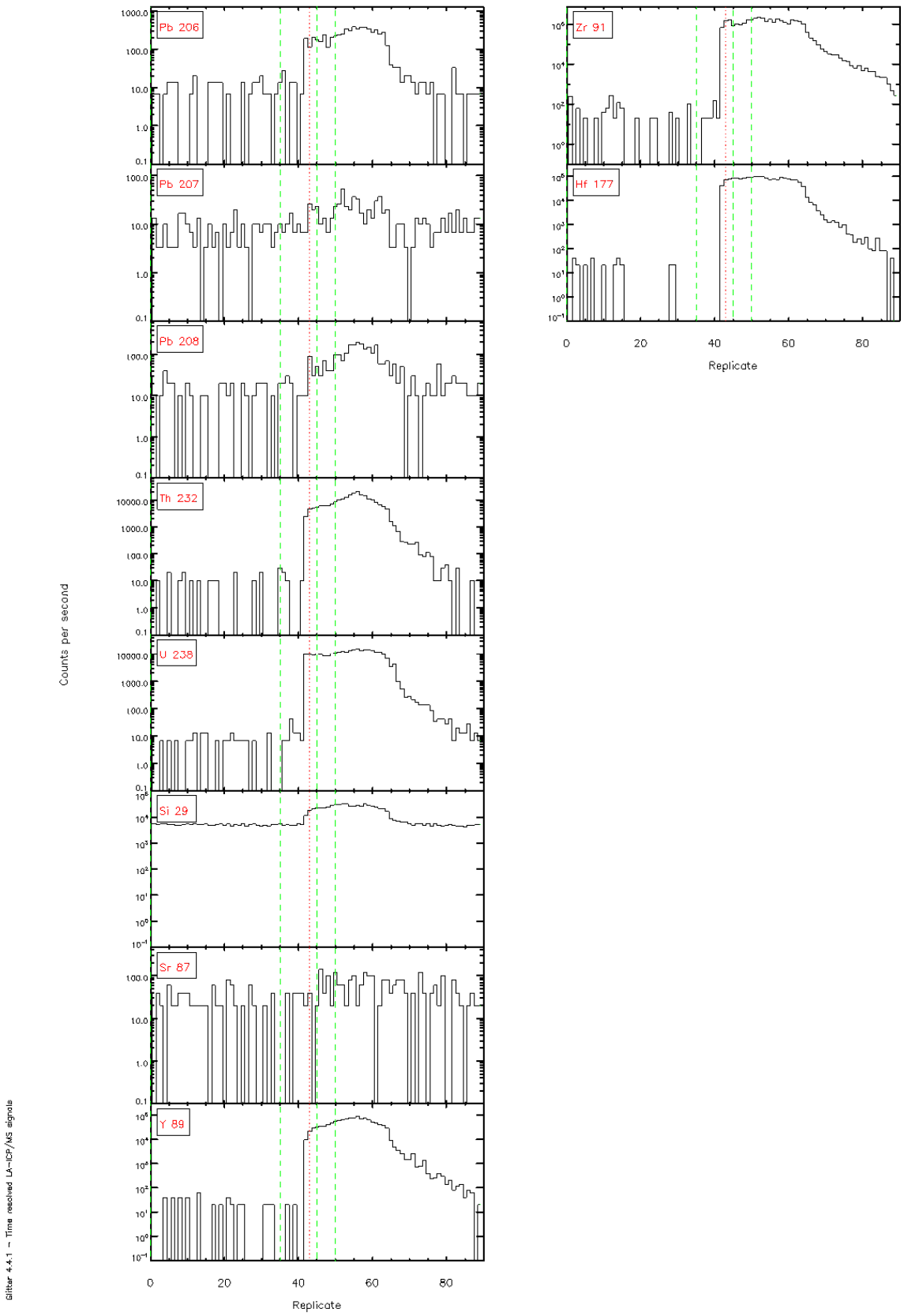
Pb 206
Pb 207
Pb 208
Th 232
U 238
Si 29
Sr 87
Y 89
Zr 91
Hf 177
Counts per second
Replicate
Glitter 4.4.1 - Time resolved LA-ICP/MS signals

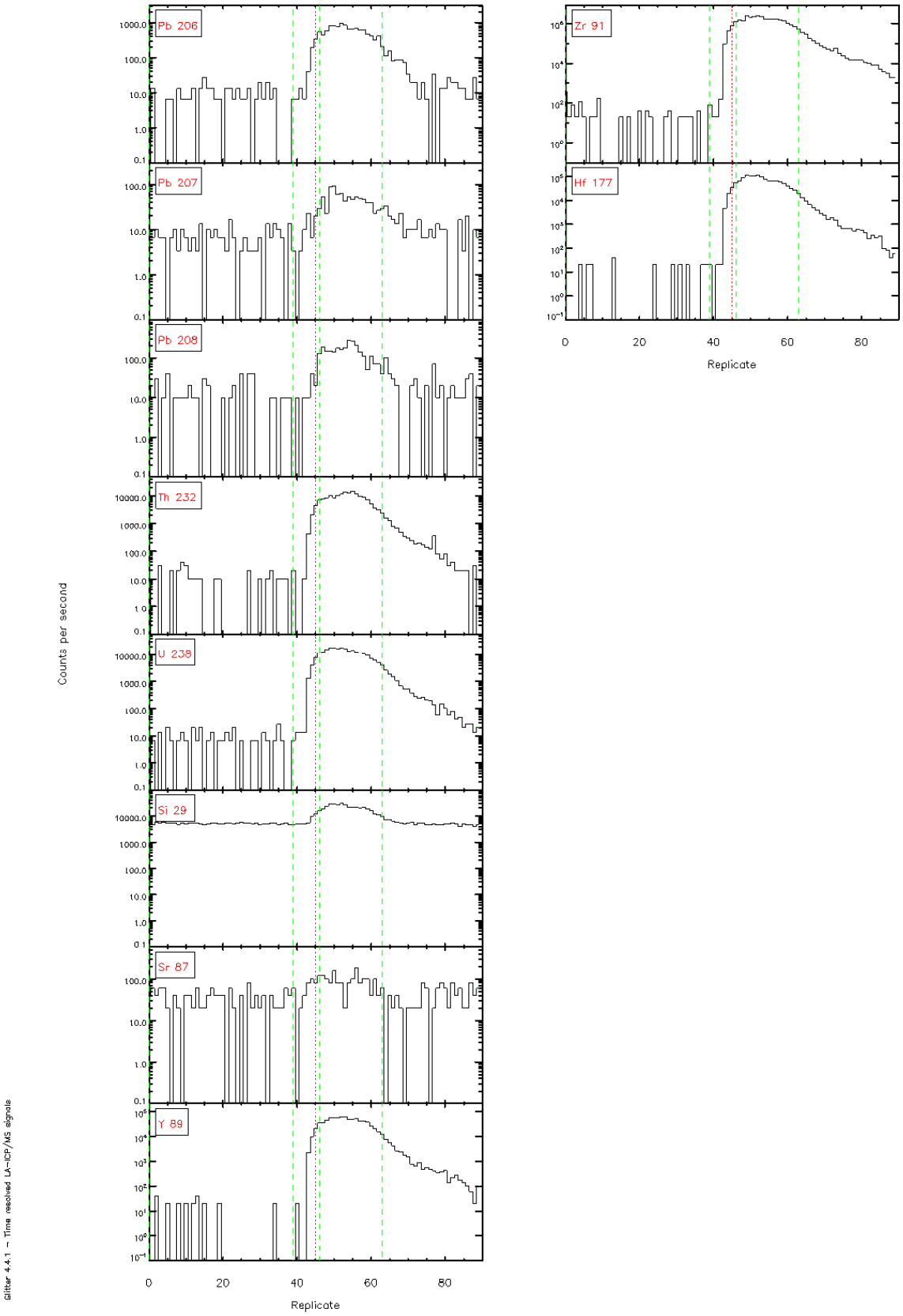
Pb 206
Pb 207
Pb 208
Th 232
U 238
Si 29
Sr 87
Y 89
Zr 91
Hf 177
Counts per second
Replicate
Glitter 4.4.1 – Time resolved LA-ICP/MS signals

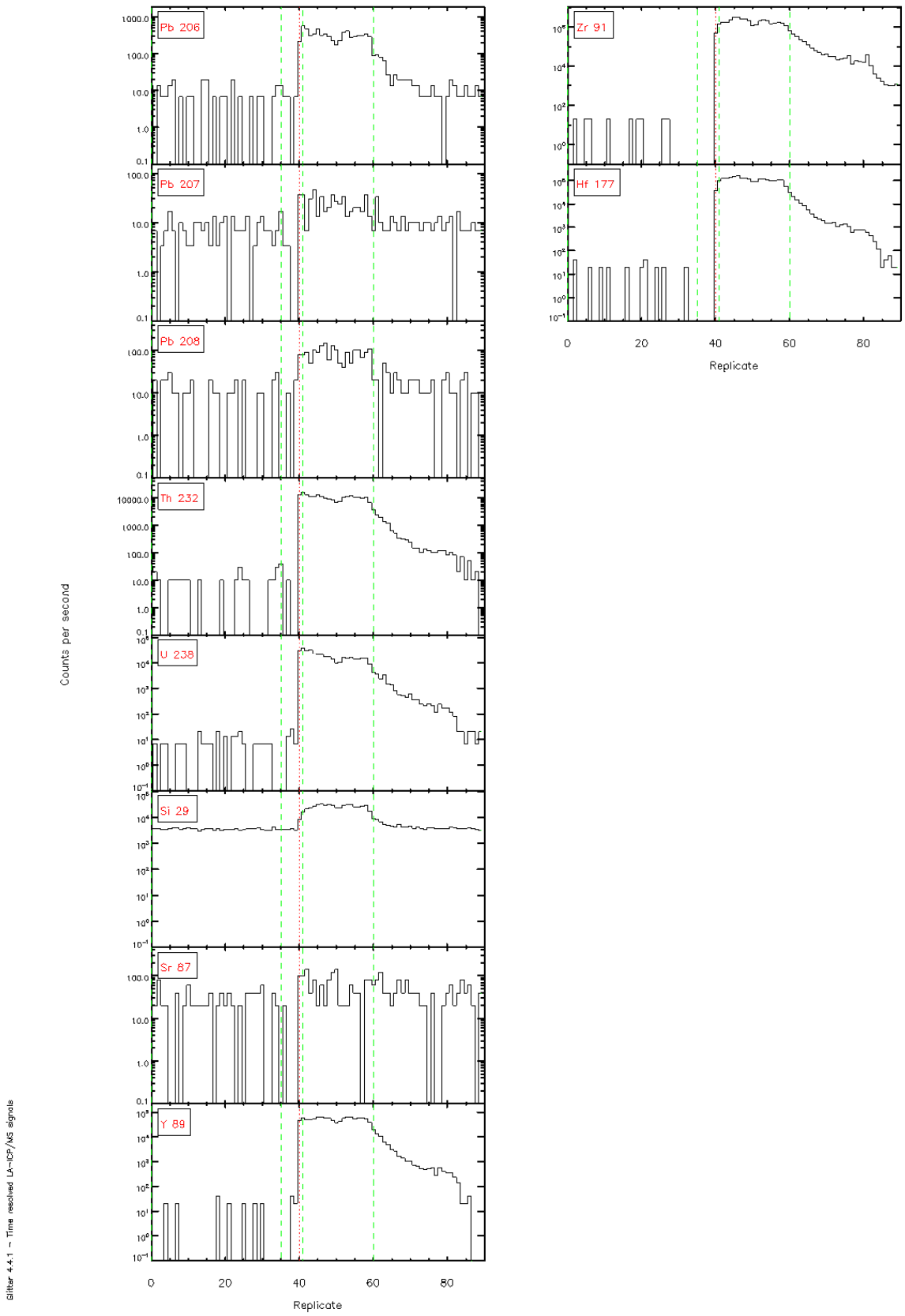
Pb 206
Pb 207
Pb 208
Th 232
U 238
Si 29
Sr 87
Y 89
Zr 91
Hf 177
Counts per second
Replicate
Glitter 4.4.1 - Time resolved LA-ICP/MS signals

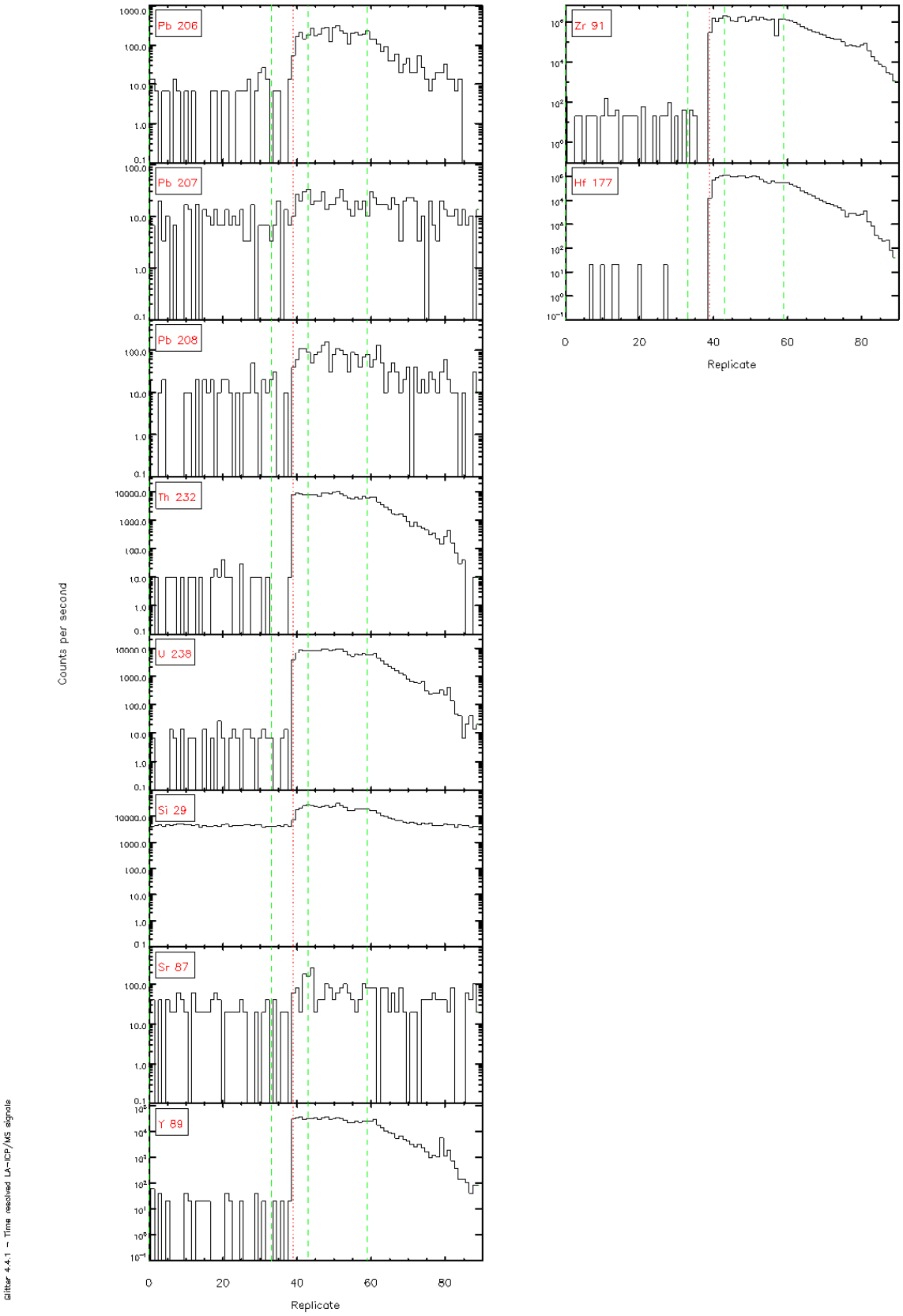
Pb 206
Pb 207
Pb 208
Th 232
U 238
Si 29
Sr 87
Y 89
Zr 91
Hf 177
Counts per second
Replicate
Glitter 4.4.1 - Time resolved LA-ICP/MS signals

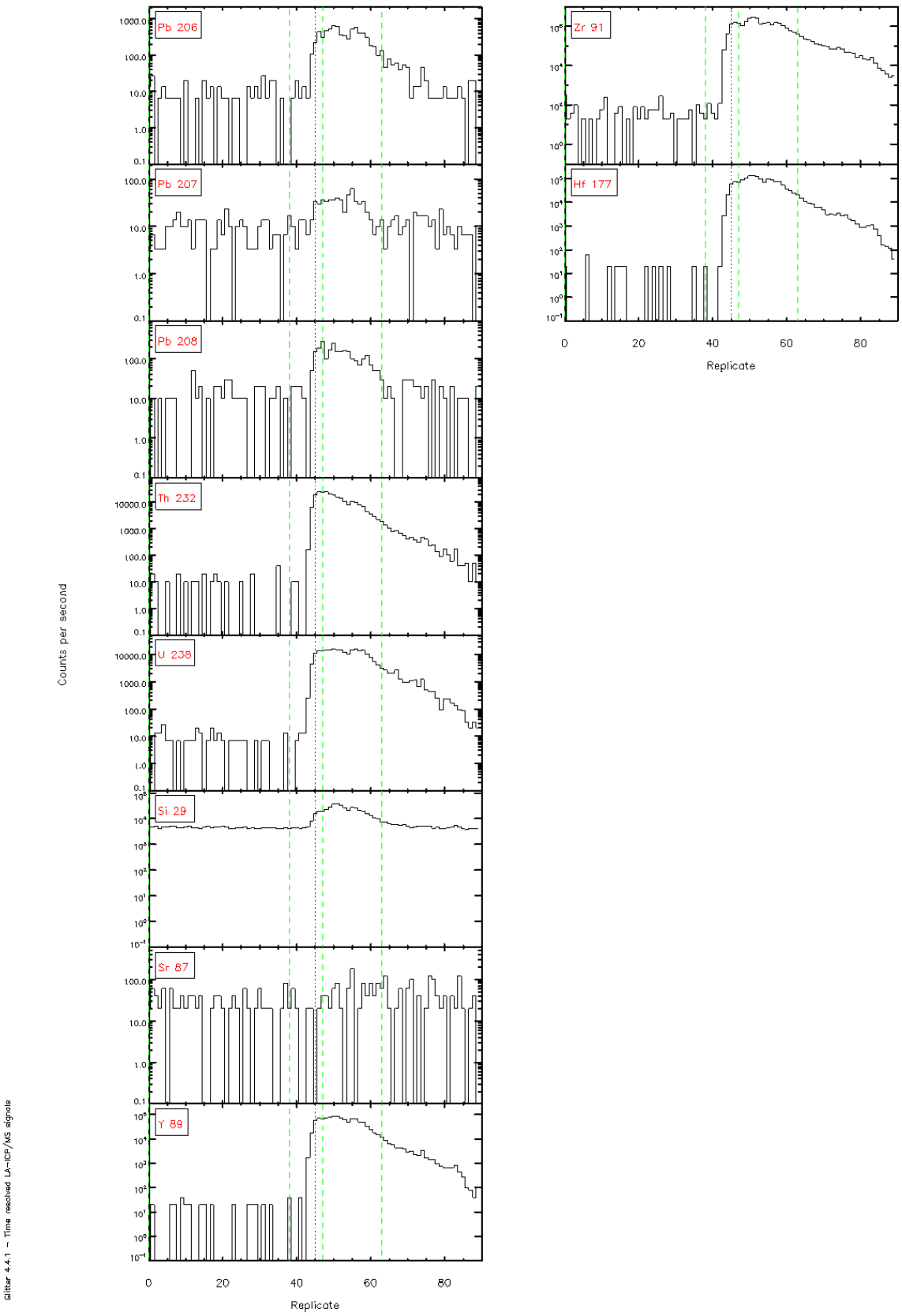
Pb 206
Pb 207
Pb 208
Th 232
U 238
Si 29
Sr 87
Y 89
Zr 91
Hf 177
Counts per second
Replicate
Glitter 4.4.1 - Time resolved LA-ICP/MS signals

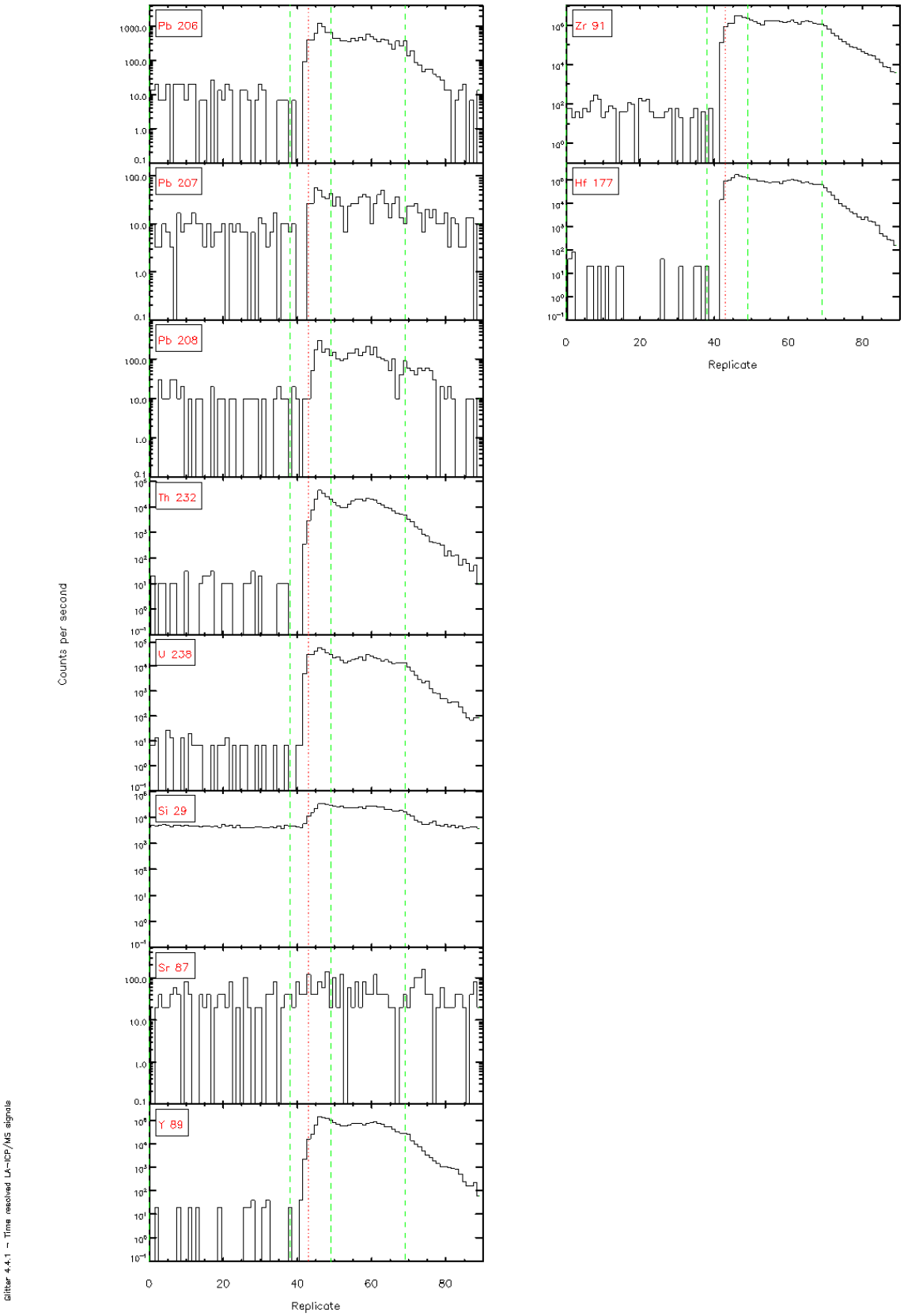
Pb 206
Pb 207
Pb 208
Th 232
U 238
Si 29
Sr 87
Y 89
Zr 91
Hf 177
Counts per second
Replicate
Glitter 4.4.1 – Time resolved LA-ICP/MS signals

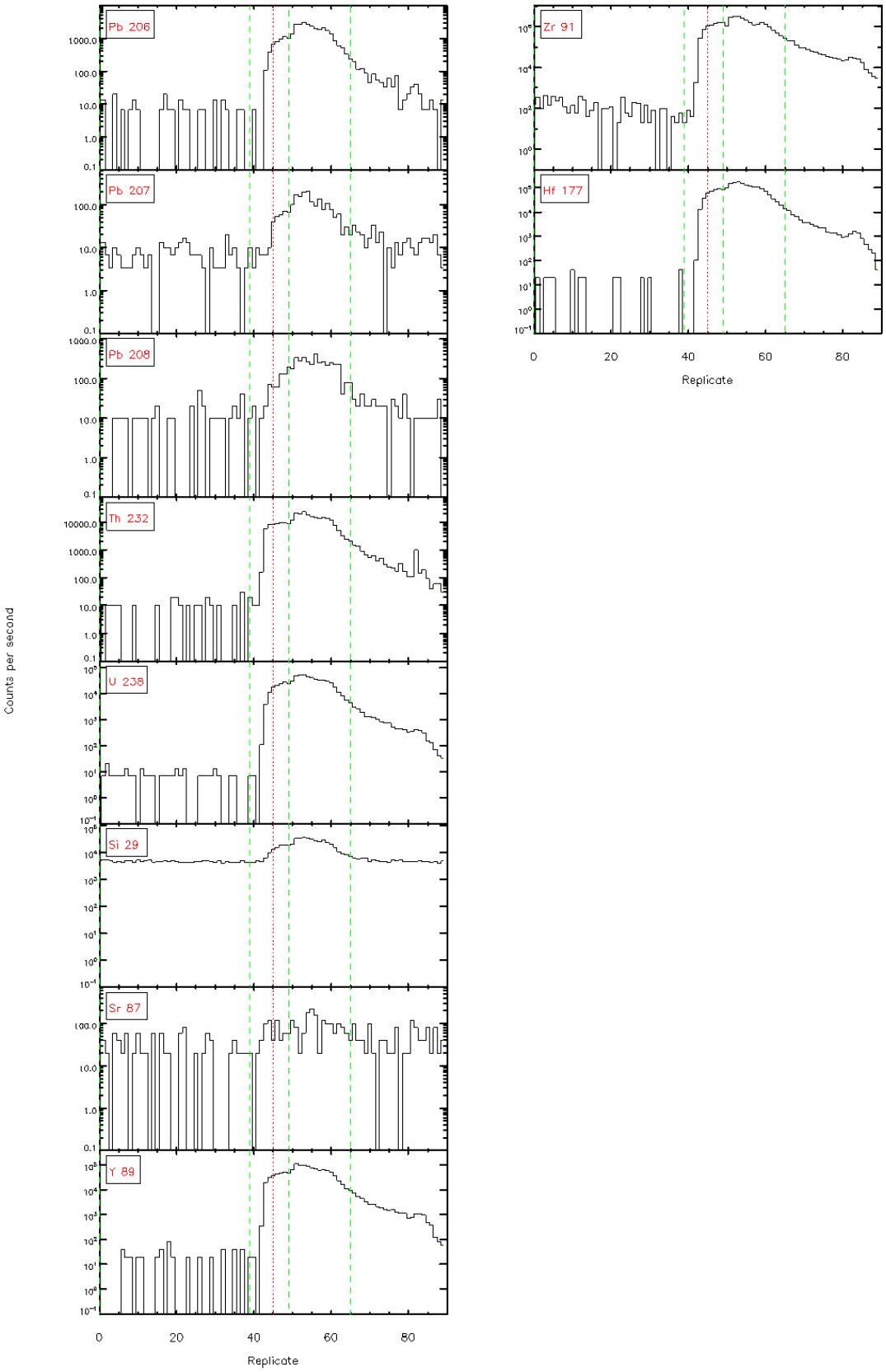
Pb 206
Pb 207
Pb 208
Th 232
U 238
Si 29
Sr 87
Y 89
Zr 91
Hf 177
Counts per second
Replicate
Glitter 4.4.1 - Time resolved LA-ICP/MS signals

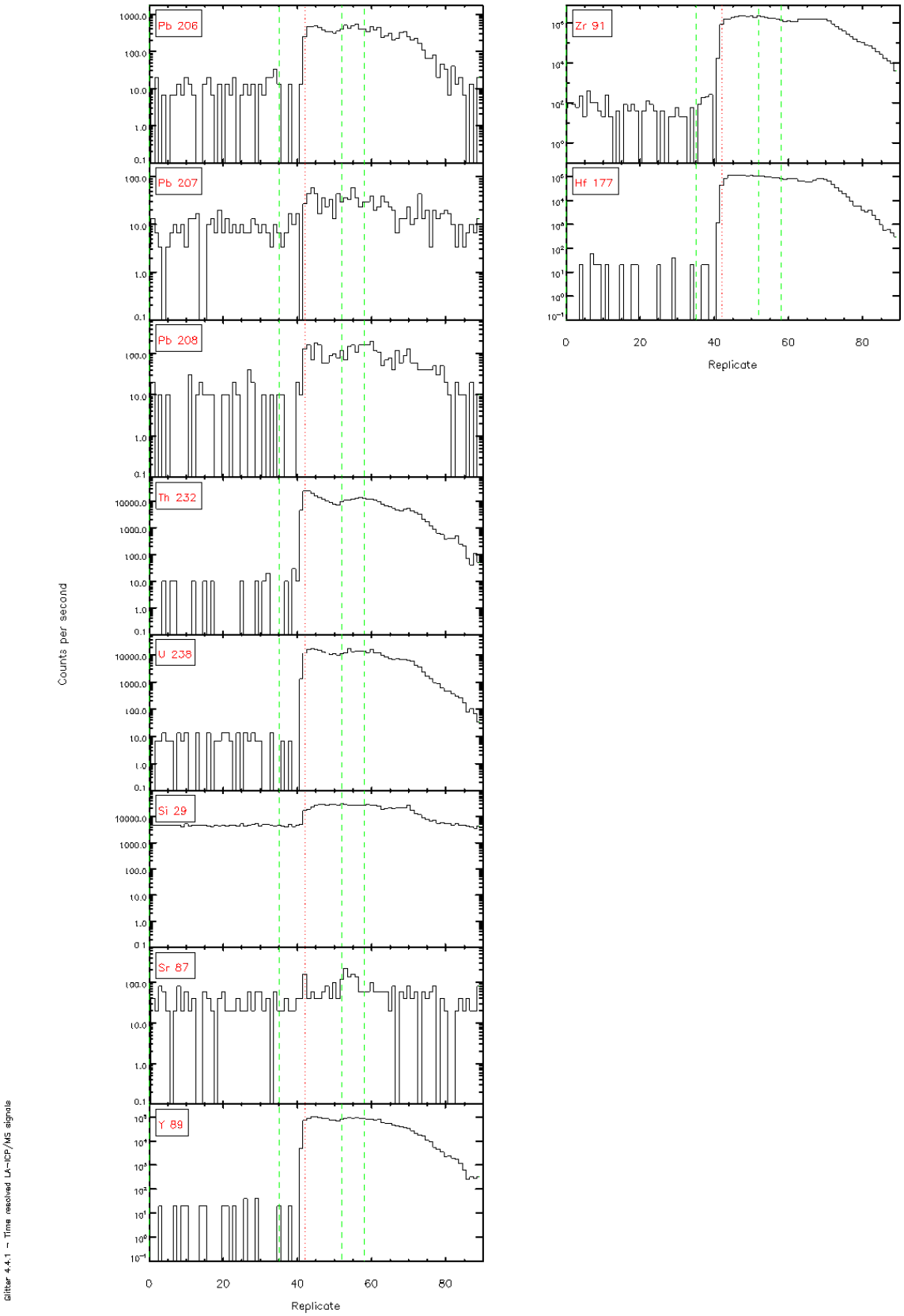
Pb 206
Pb 207
Pb 208
Th 232
U 238
Si 29
Sr 87
Y 89
Zr 91
Hf 177
Counts per second
Replicate
Glitter 4.4.1 – Time resolved LA-ICP/MS signals

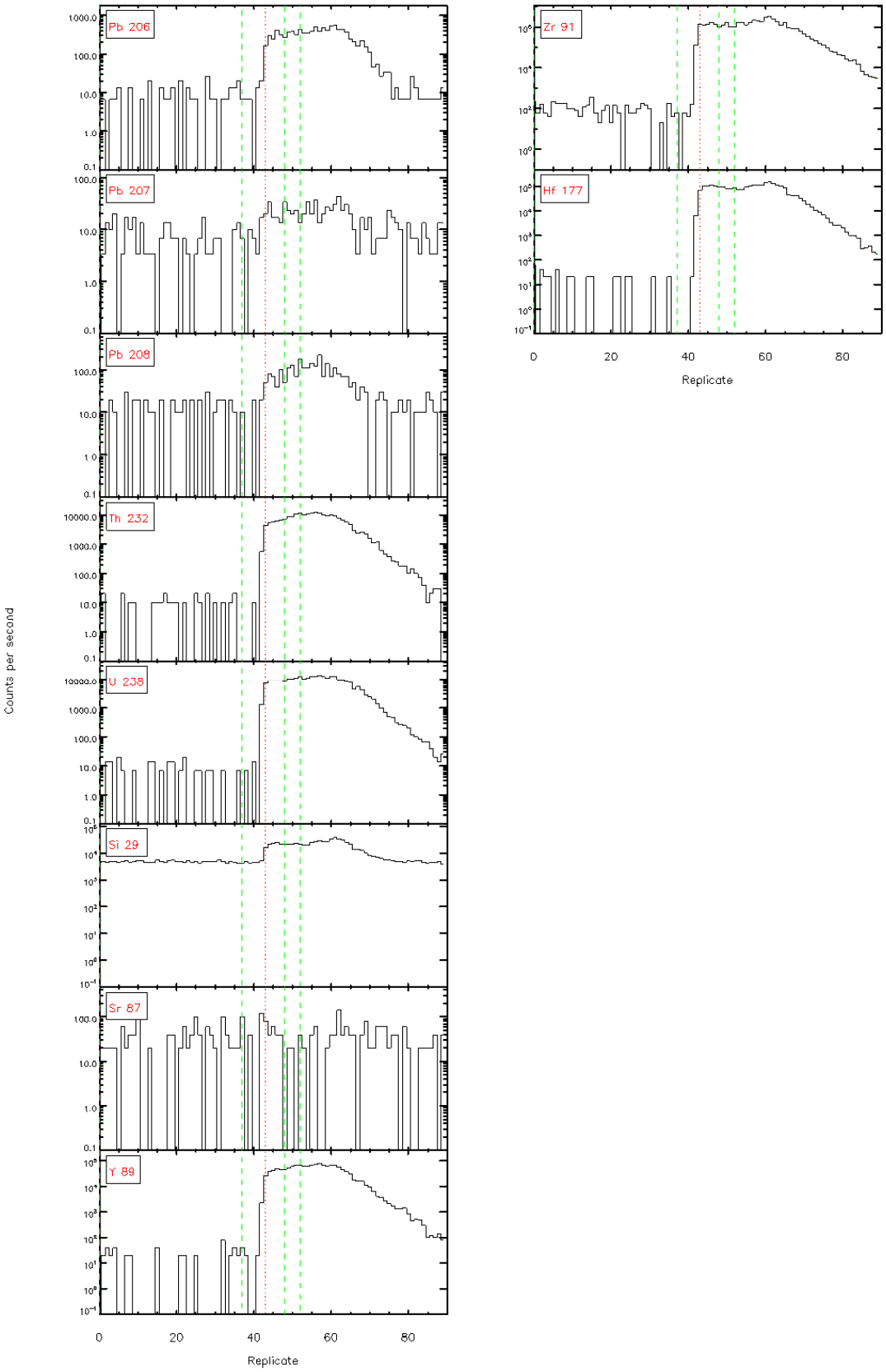
Pb 206
Pb 207
Pb 208
Th 232
U 238
Si 29
Sr 87
Y 89
Zr 91
Hf 177
Counts per second
Replicate
Glitter 4.4.1 - Time resolved LA-ICP/MS signals

9 – Tariki Sandstone

1.

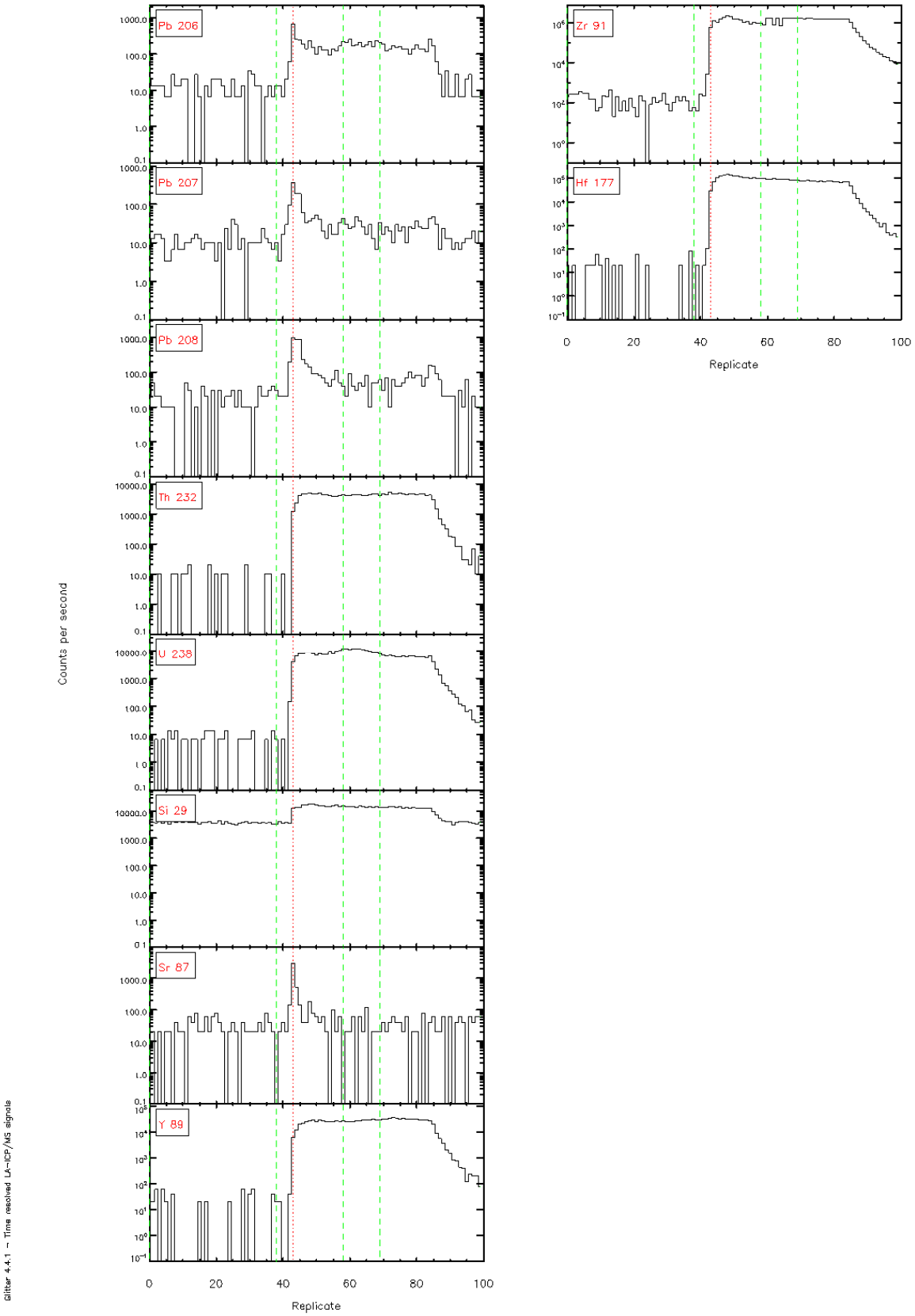

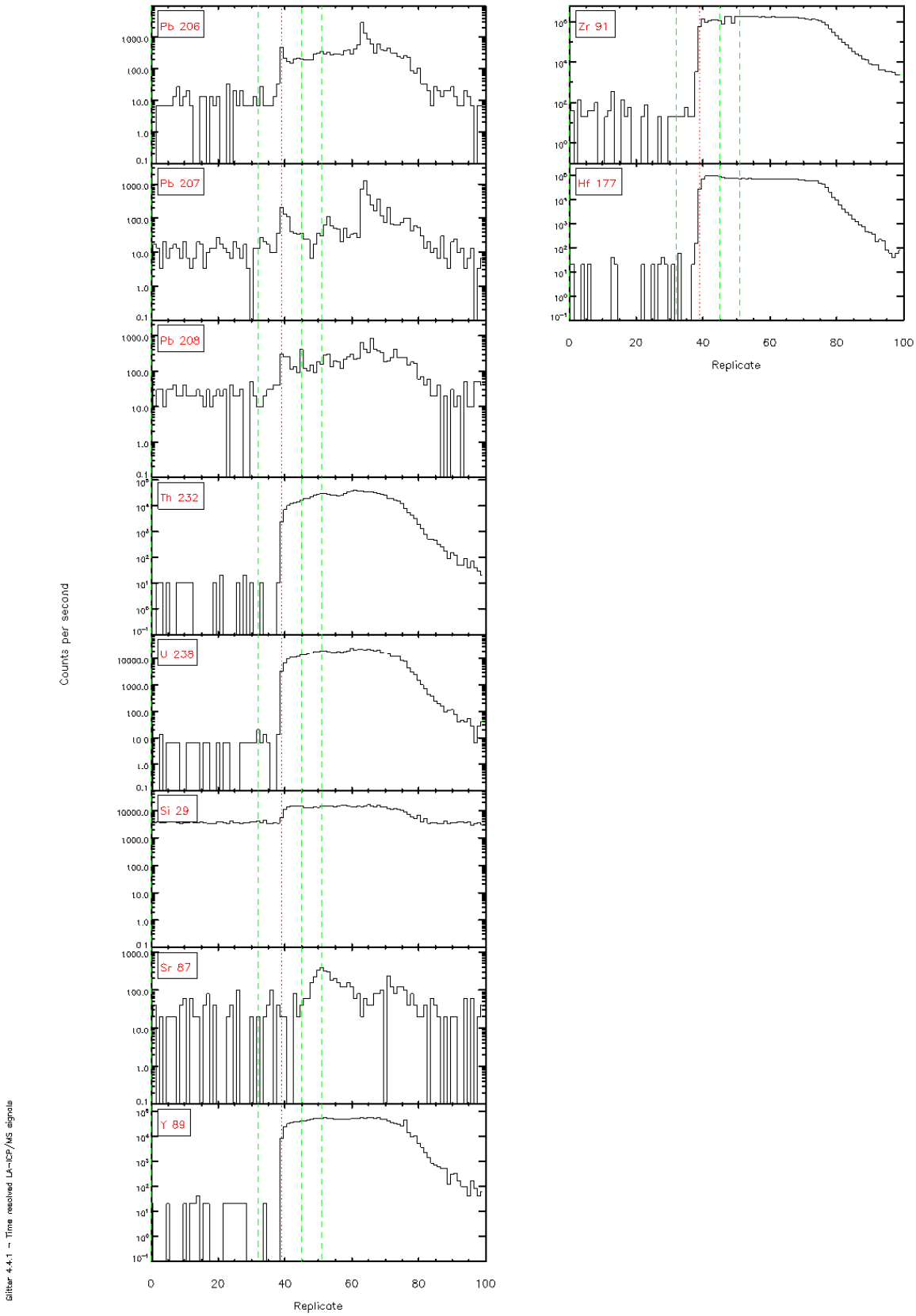
Pb 206
Pb 207
Pb 208
Th 232
U 238
Si 29
Sr 87
Y 89
Zr 91
Hf 177
Counts per second
Replicate
Glitter 4.4.1 – Time resolved LA-ICP/MS signals

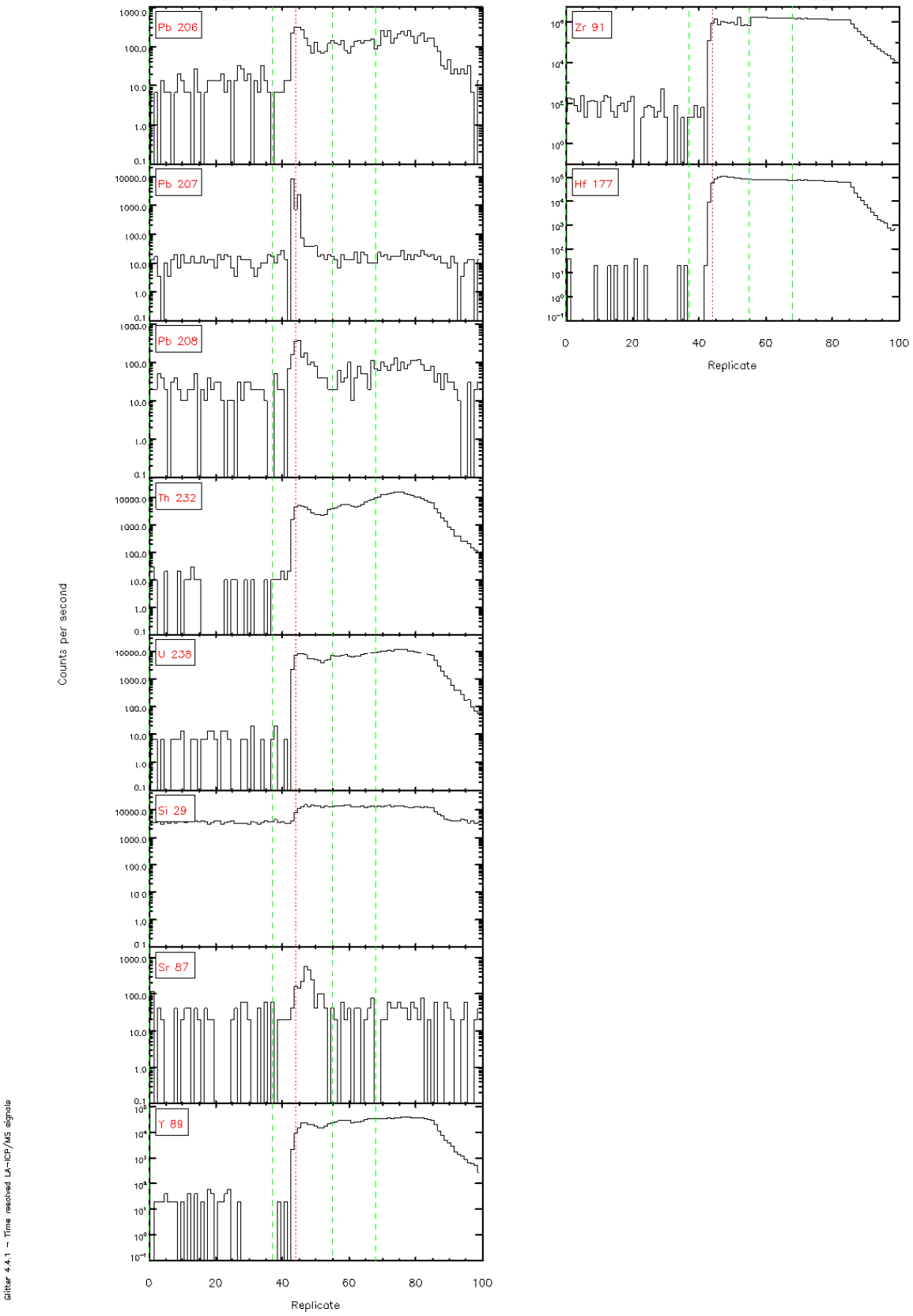
Pb 206
Pb 207
Pb 208
Th 232
U 238
Si 29
Sr 87
Y 89
Zr 91
Hf 177
Counts per second
Replicate
Glitter 4.4.1 - Time resolved LA-ICP/MS signals

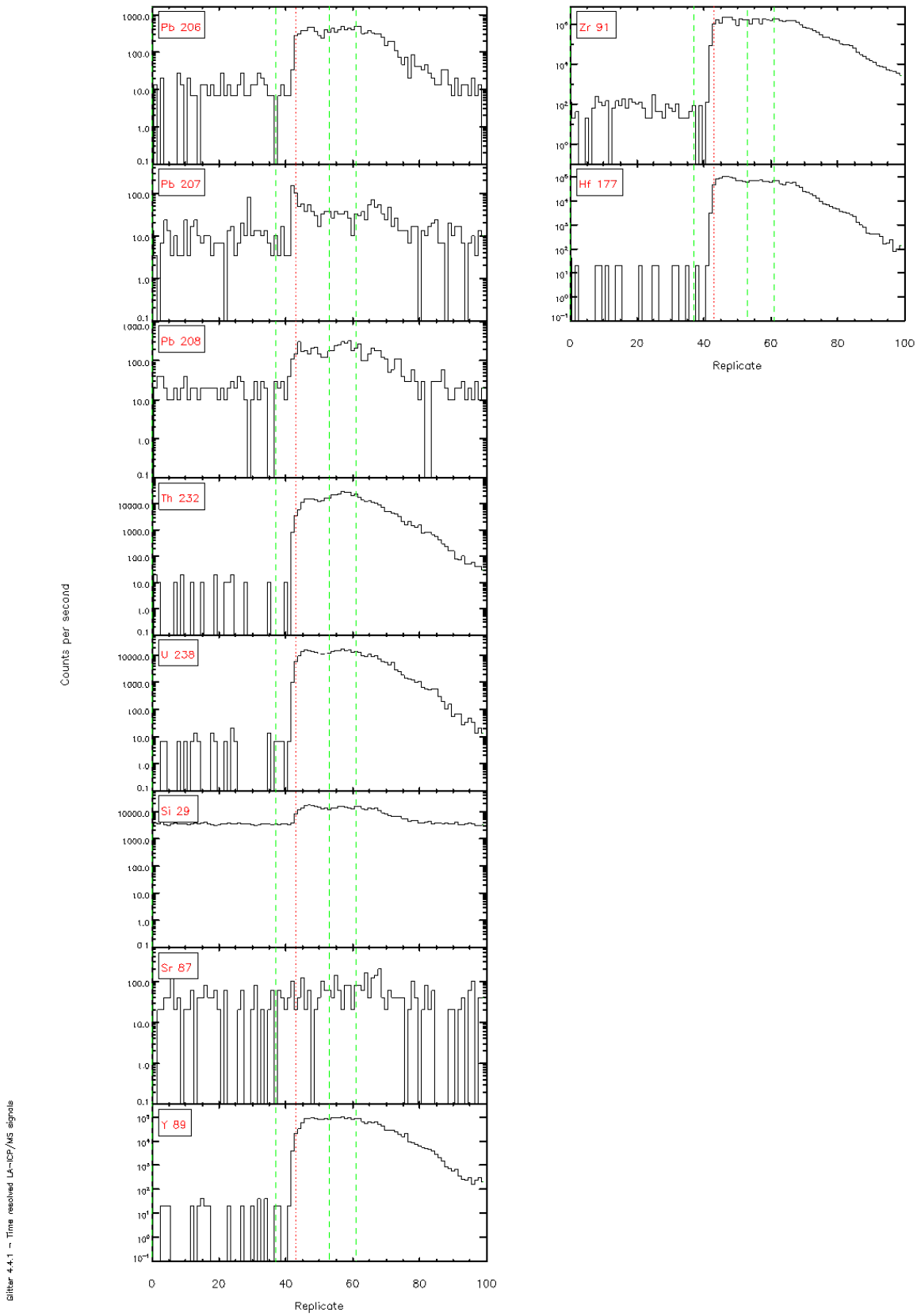
Pb 206
Pb 207
Pb 208
Th 232
U 238
Si 29
Sr 87
Y 89
Zr 91
Hf 177
Counts per second
Replicate
Glitter 4.4.1 - Time resolved LA-ICP/MS signals

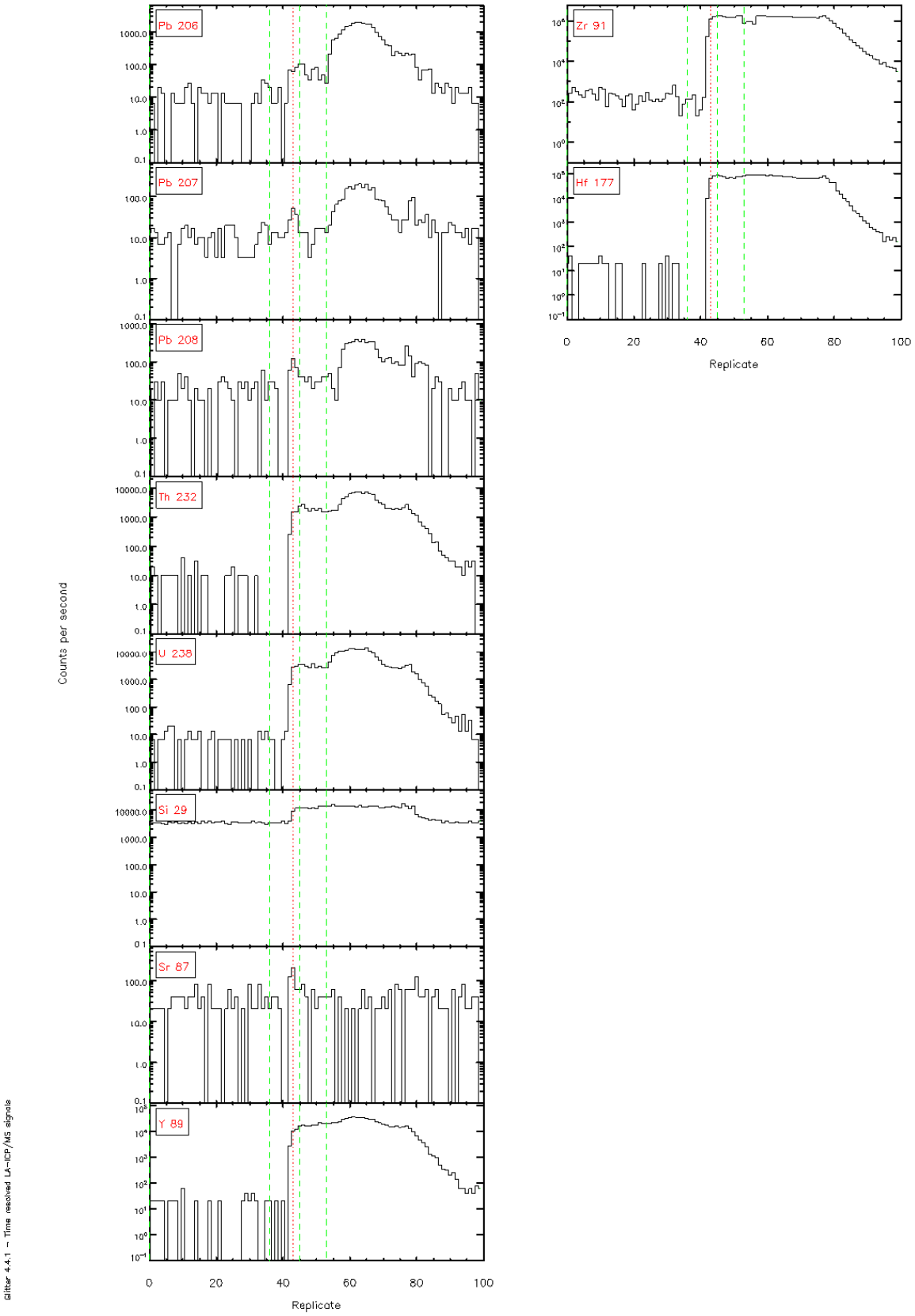
Pb 206
Pb 207
Pb 208
Th 232
U 238
Si 29
Sr 87
Y 89
Zr 91
Hf 177
Counts per second
Replicate
Glitter 4.4.1 - Time resolved LA-ICP/MS signals

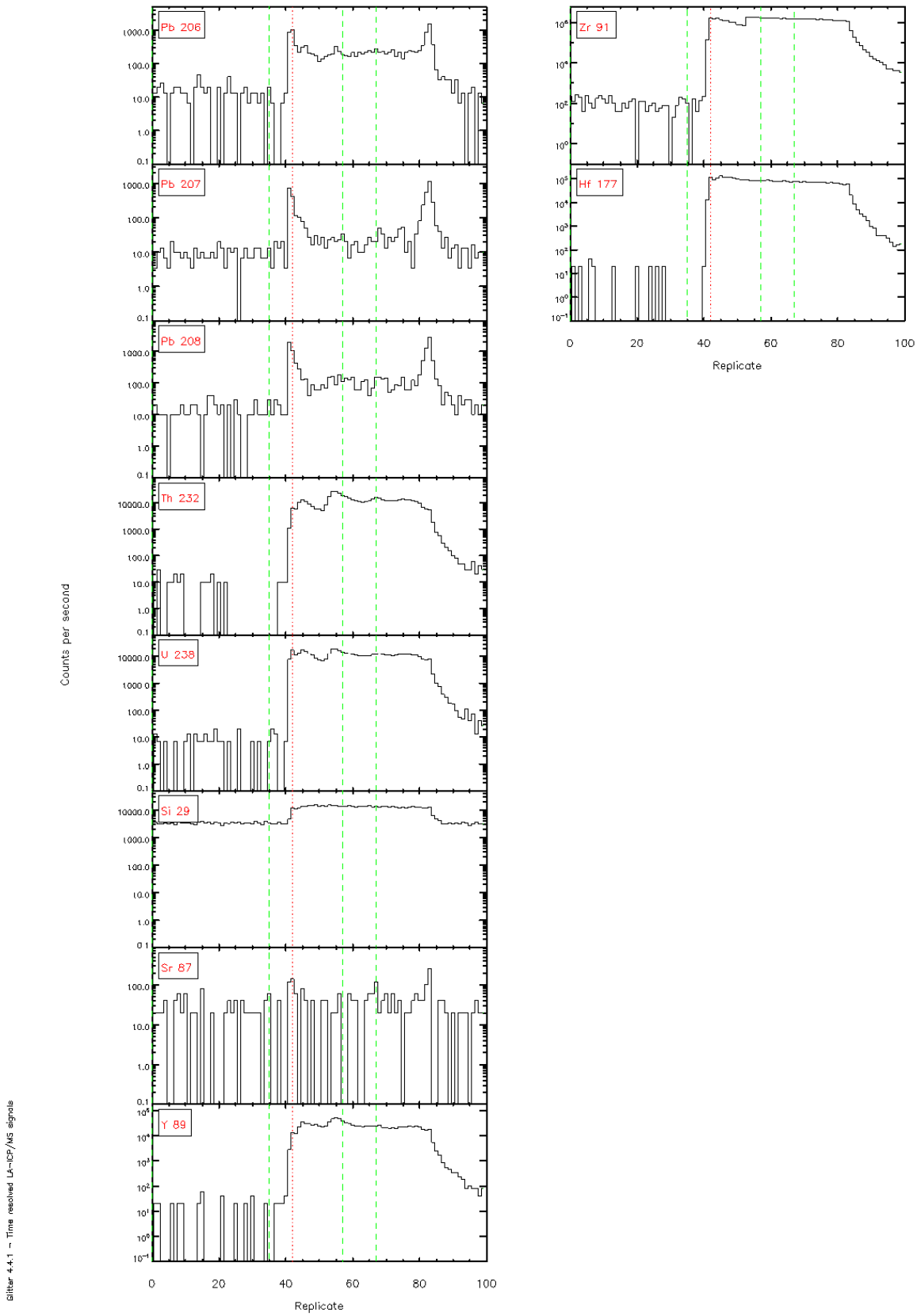
Pb 206
Pb 207
Pb 208
Th 232
U 238
Si 29
Sr 87
Y 89
Zr 91
Hf 177
Counts per second
Replicate
Glitter 4.4.1 - Time resolved LA-ICP/MS signals

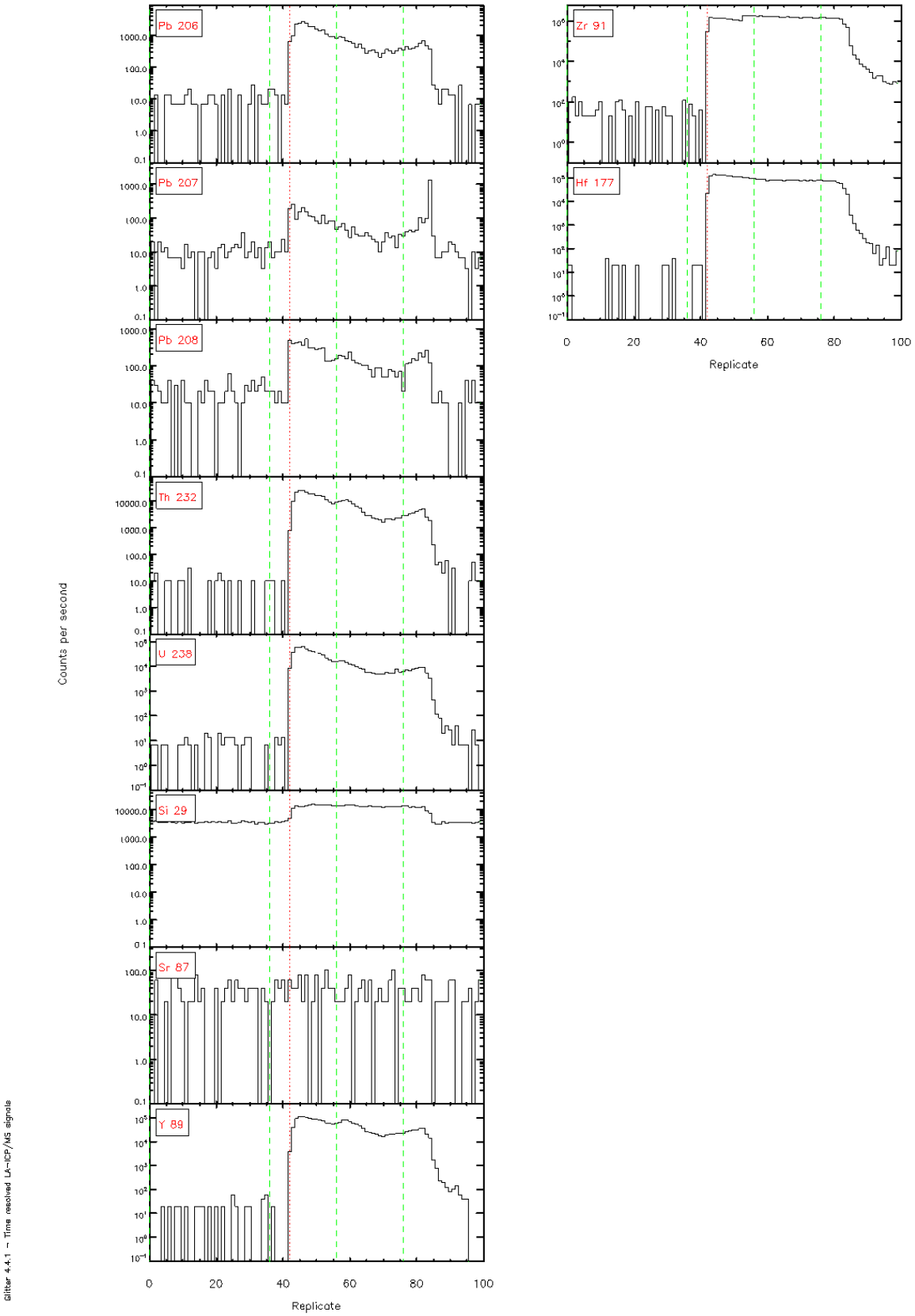
Pb 206
Pb 207
Pb 208
Th 232
U 238
Si 29
Sr 87
Y 89
Zr 91
Hf 177
Counts per second
Replicate
Glitter 4.4.1 - Time resolved LA-ICP/MS signals

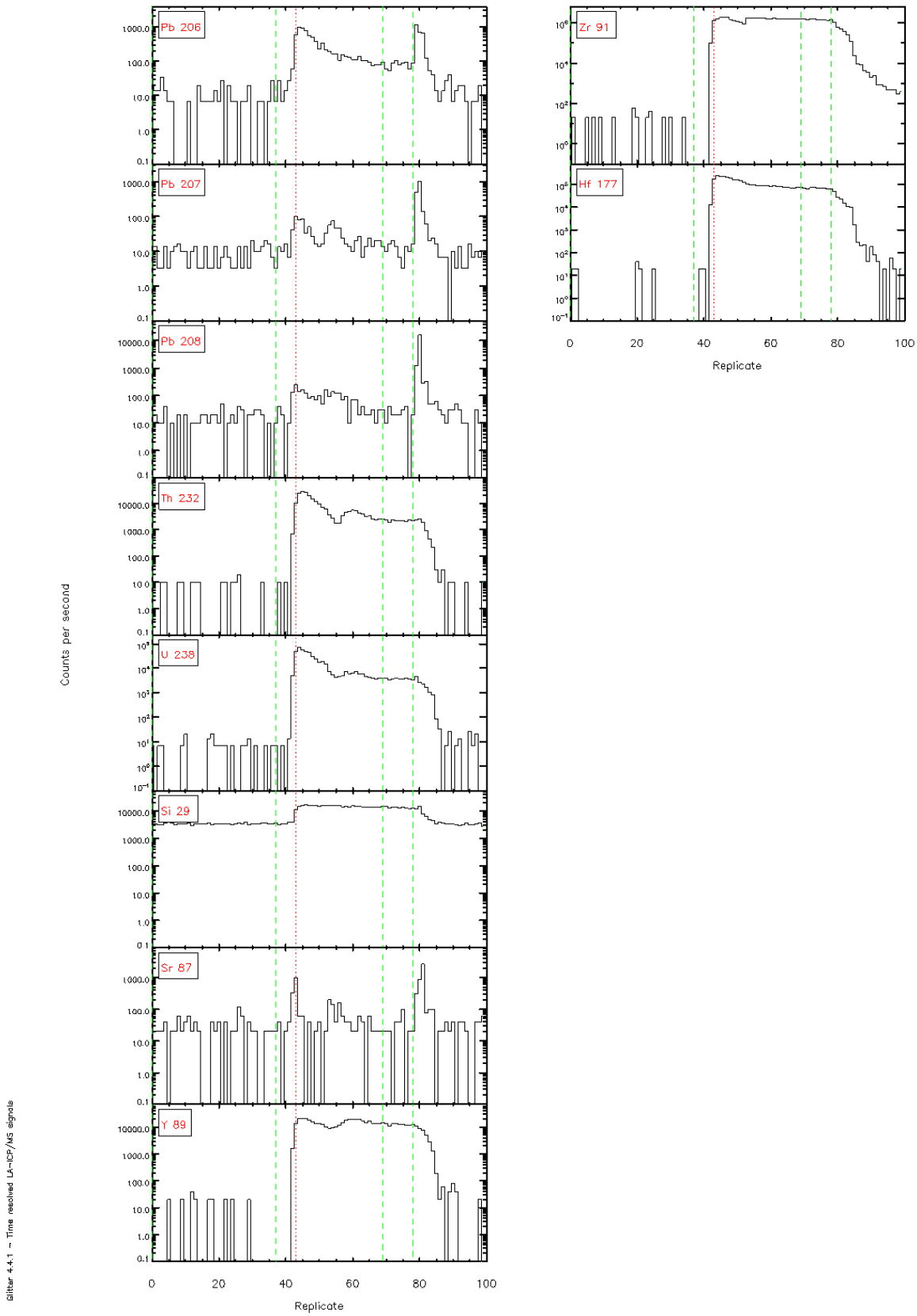
Pb 206
Pb 207
Pb 208
Th 232
U 238
Si 29
Sr 87
Y 89
Zr 91
Hf 177
Counts per second
Replicate
Glitter 4.4.1 - Time resolved LA-ICP/MS signals

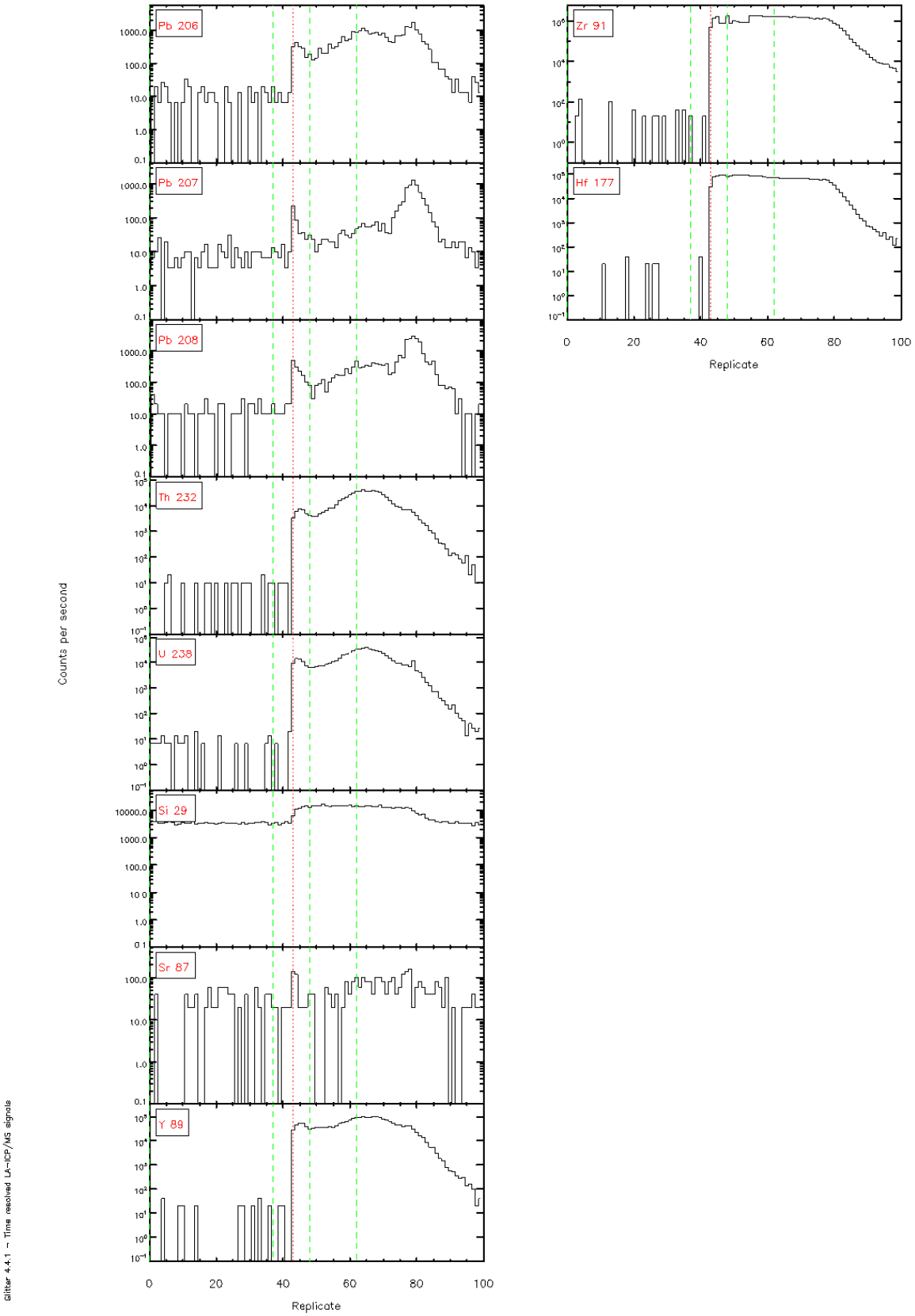
Pb 206
Pb 207
Pb 208
Th 232
U 238
Si 29
Sr 87
Y 89
Zr 91
Hf 177
Counts per second
Replicate
Glitter 4.4.1 - Time resolved LA-ICP/MS signals

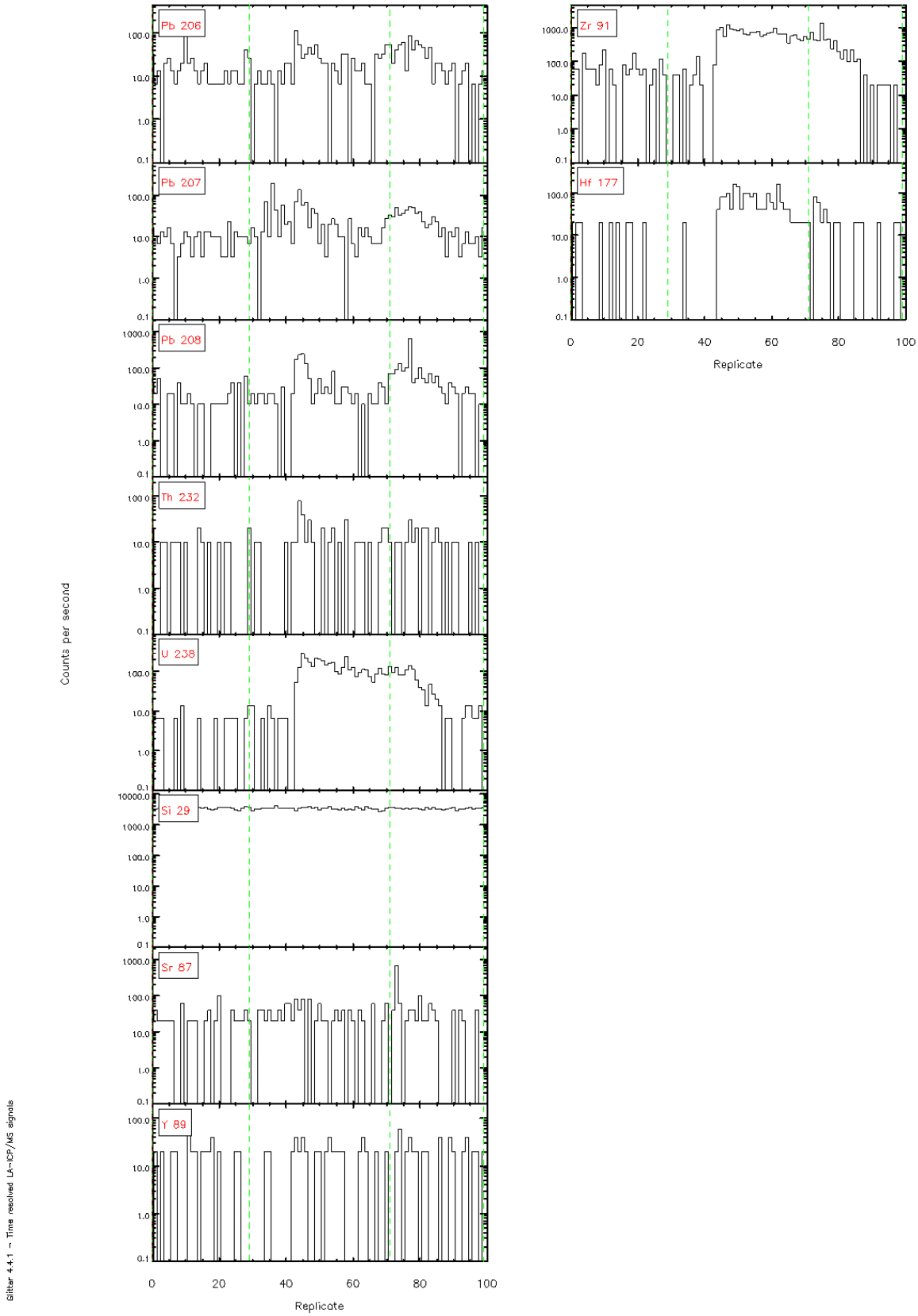
Pb 206
Pb 207
Pb 208
Th 232
U 238
Si 29
Sr 87
Y 89
Zr 91
Hf 177
Counts per second
Replicate
Glitter 4.4.1 – Time resolved LA-ICP/MS signals

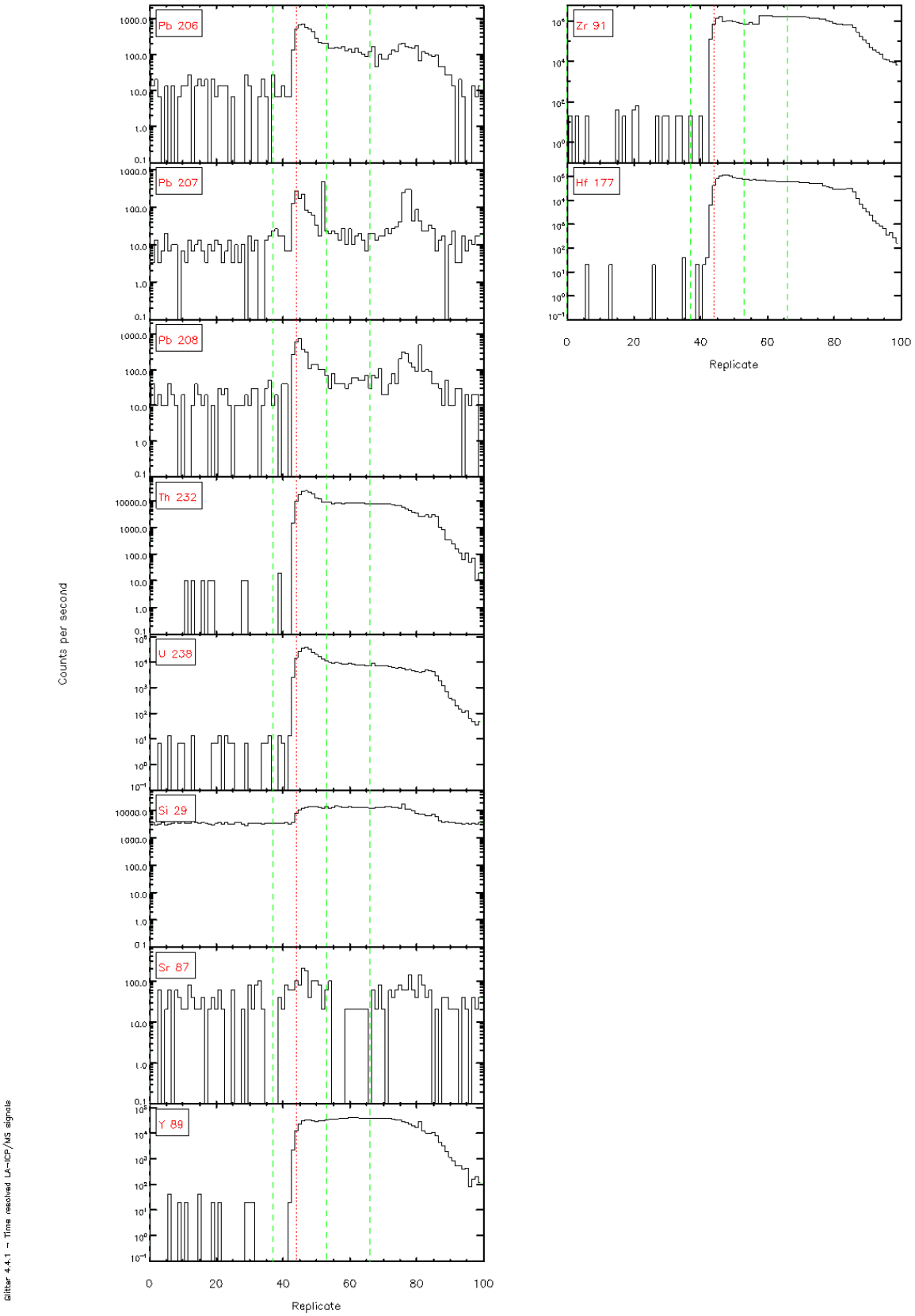
Pb 206
Pb 207
Pb 208
Th 232
U 238
Si 29
Sr 87
Y 89
Zr 91
Hf 177
Counts per second
Replicate
Glitter 4.4.1 - Time resolved LA-ICP/MS signals

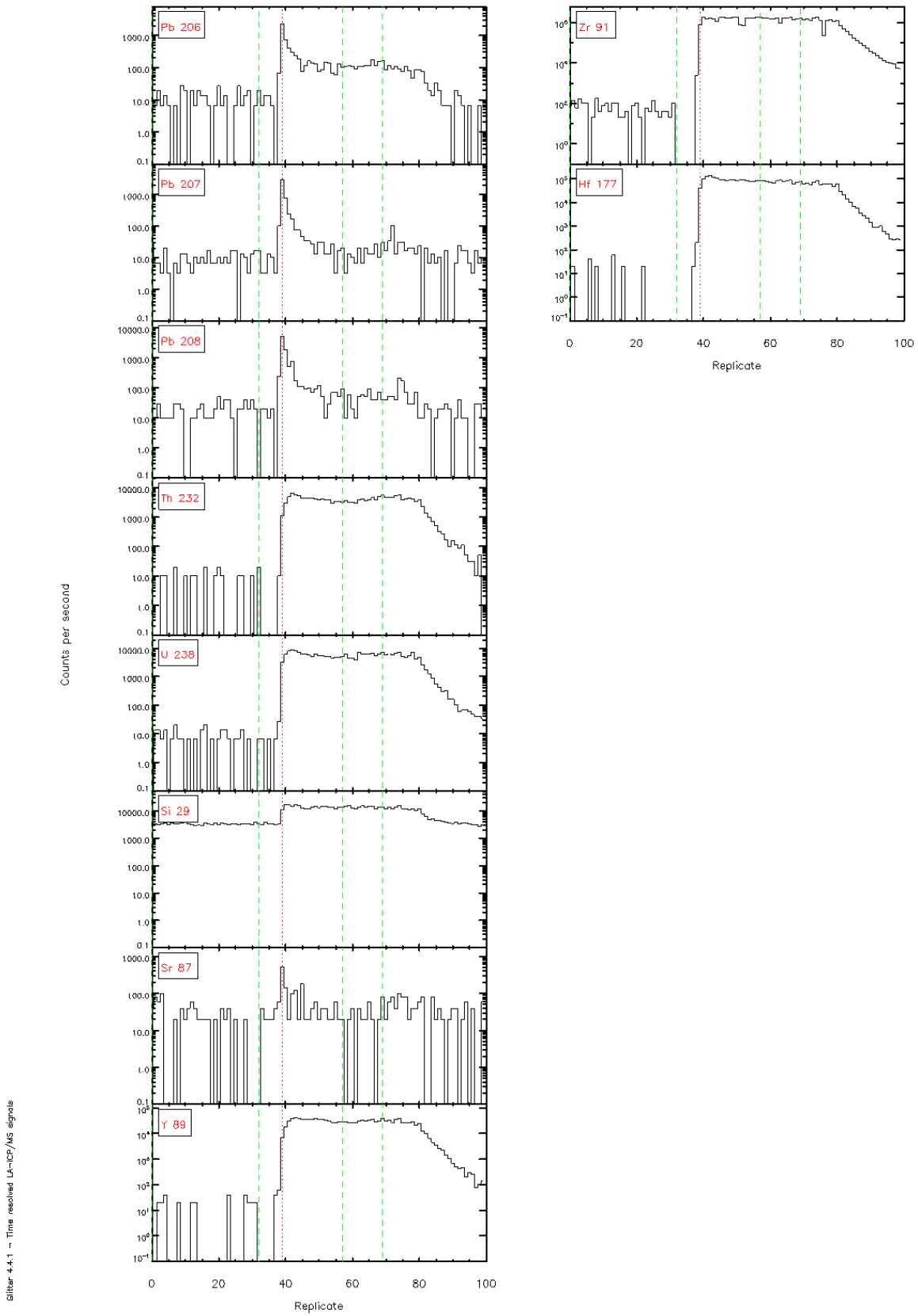
Pb 206
Pb 207
Pb 208
Th 232
U 238
Si 29
Sr 87
Y 89
Zr 91
Hf 177
Counts per second
Replicate
Glitter 4.4.1 - Time resolved LA-ICP/MS signals

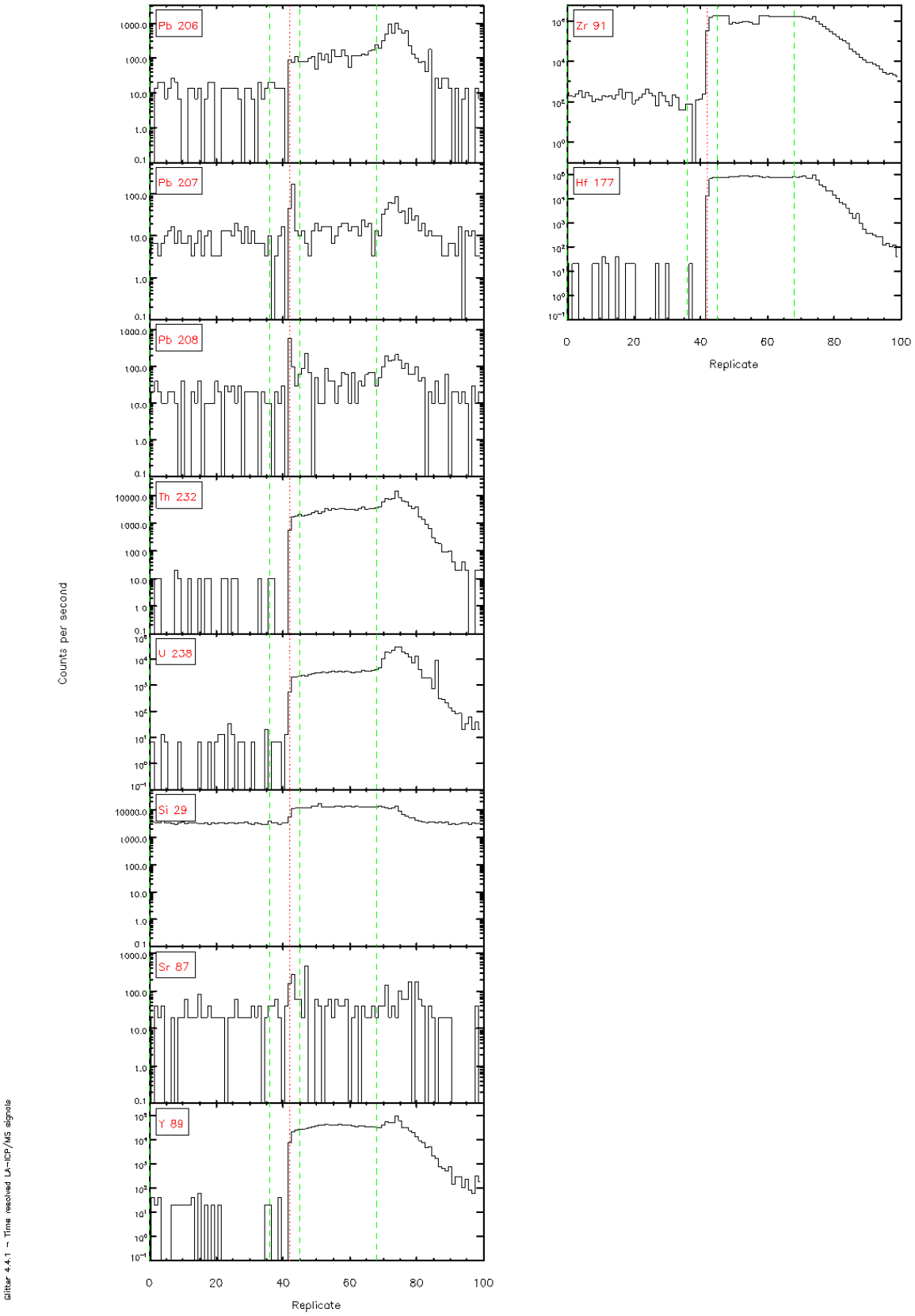
Pb 206
Pb 207
Pb 208
Th 232
U 238
Si 29
Sr 87
Y 89
Zr 91
Hf 177
Counts per second
Replicate
Glitter 4.4.1 - Time resolved LA-ICP/MS signals

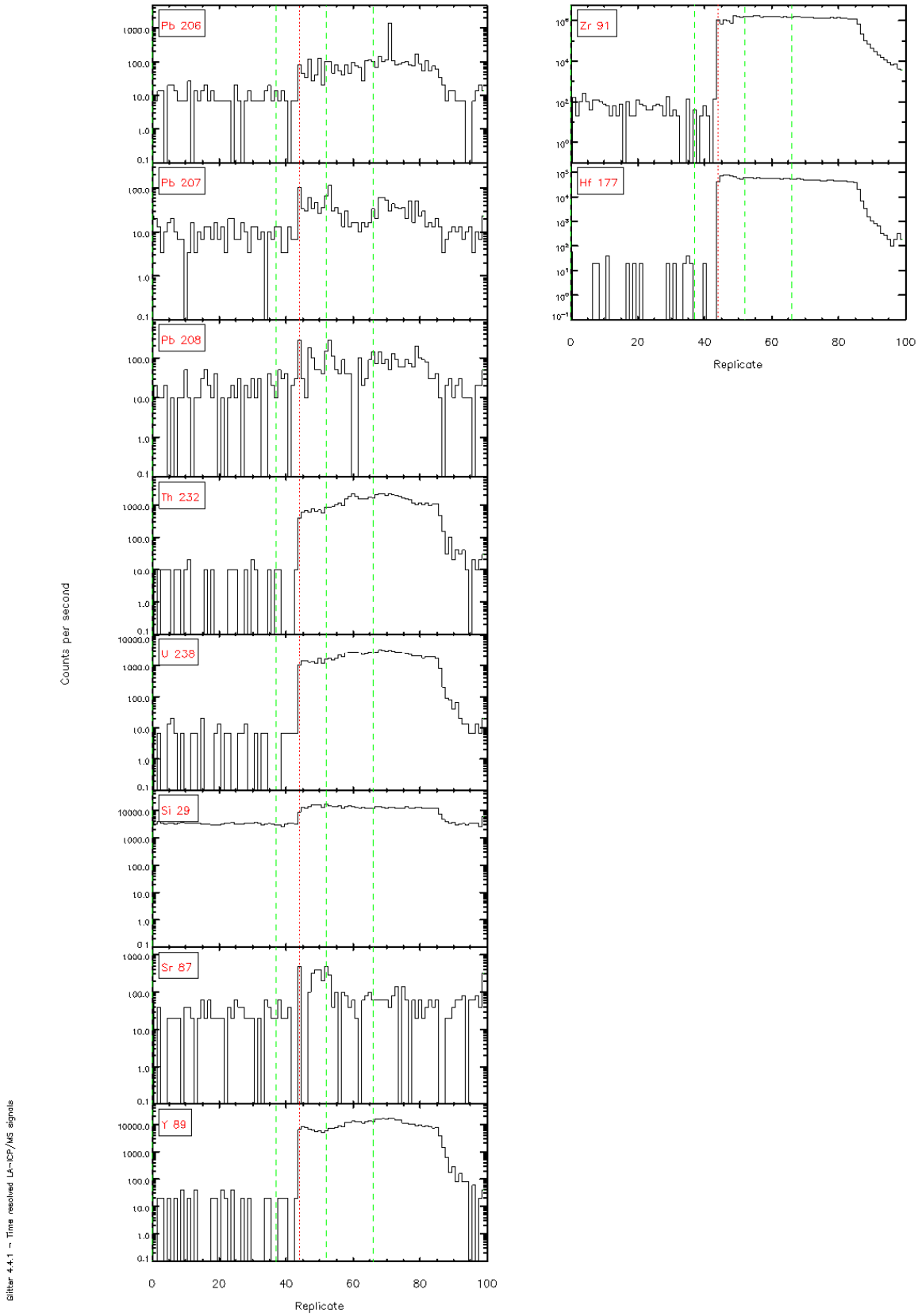
Pb 206
Pb 207
Pb 208
Th 232
U 238
Si 29
Sr 87
Y 89
Zr 91
Hf 177
Counts per second
Replicate
Glitter 4.4.1 - Time resolved LA-ICP/MS signals

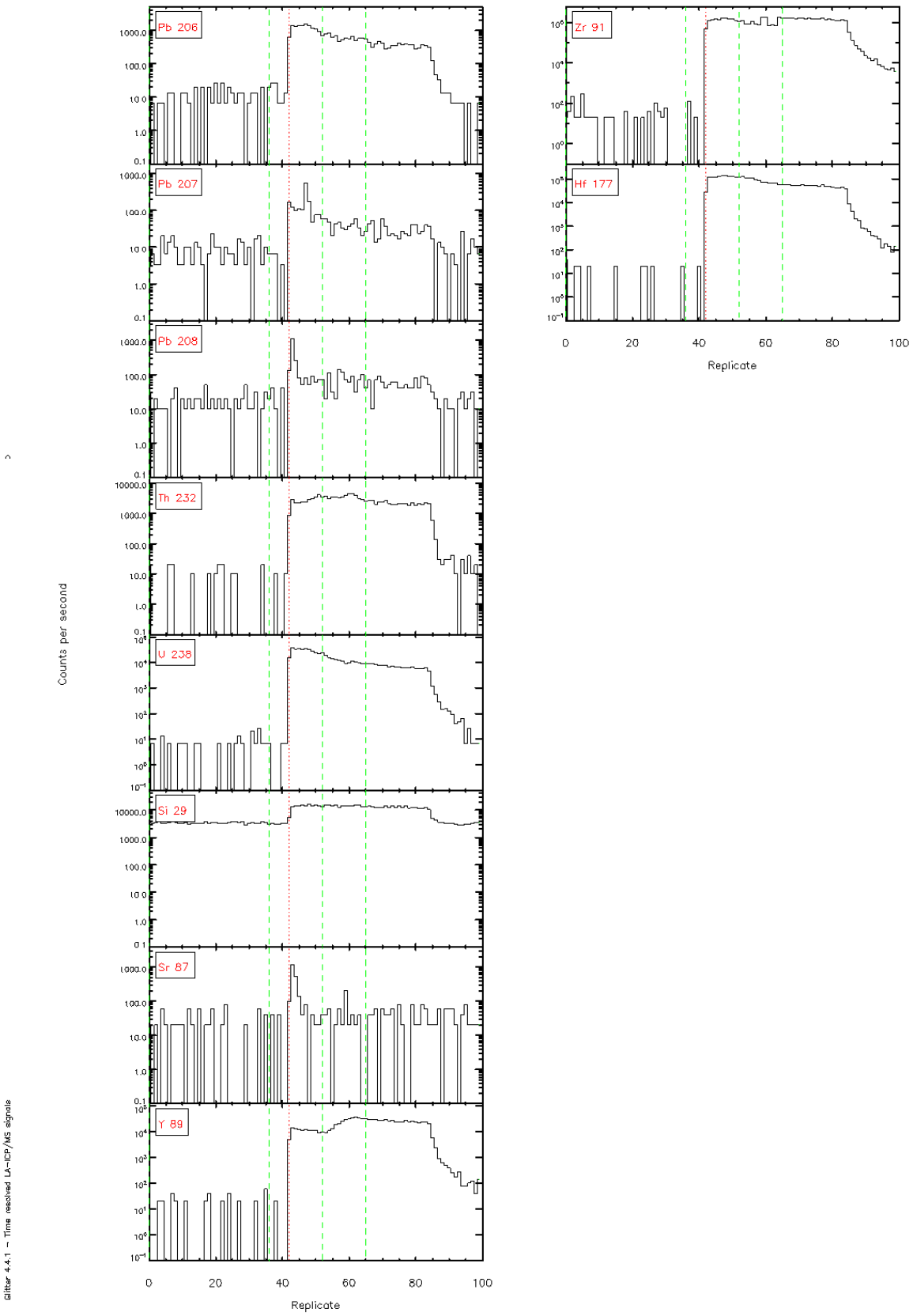
Pb 206
Pb 207
Pb 208
Th 232
U 238
Si 29
Sr 87
Y 89
Zr 91
Hf 177
Counts per second
Replicate
Glitter 4.4.1 - Time resolved LA-ICP/MS signals

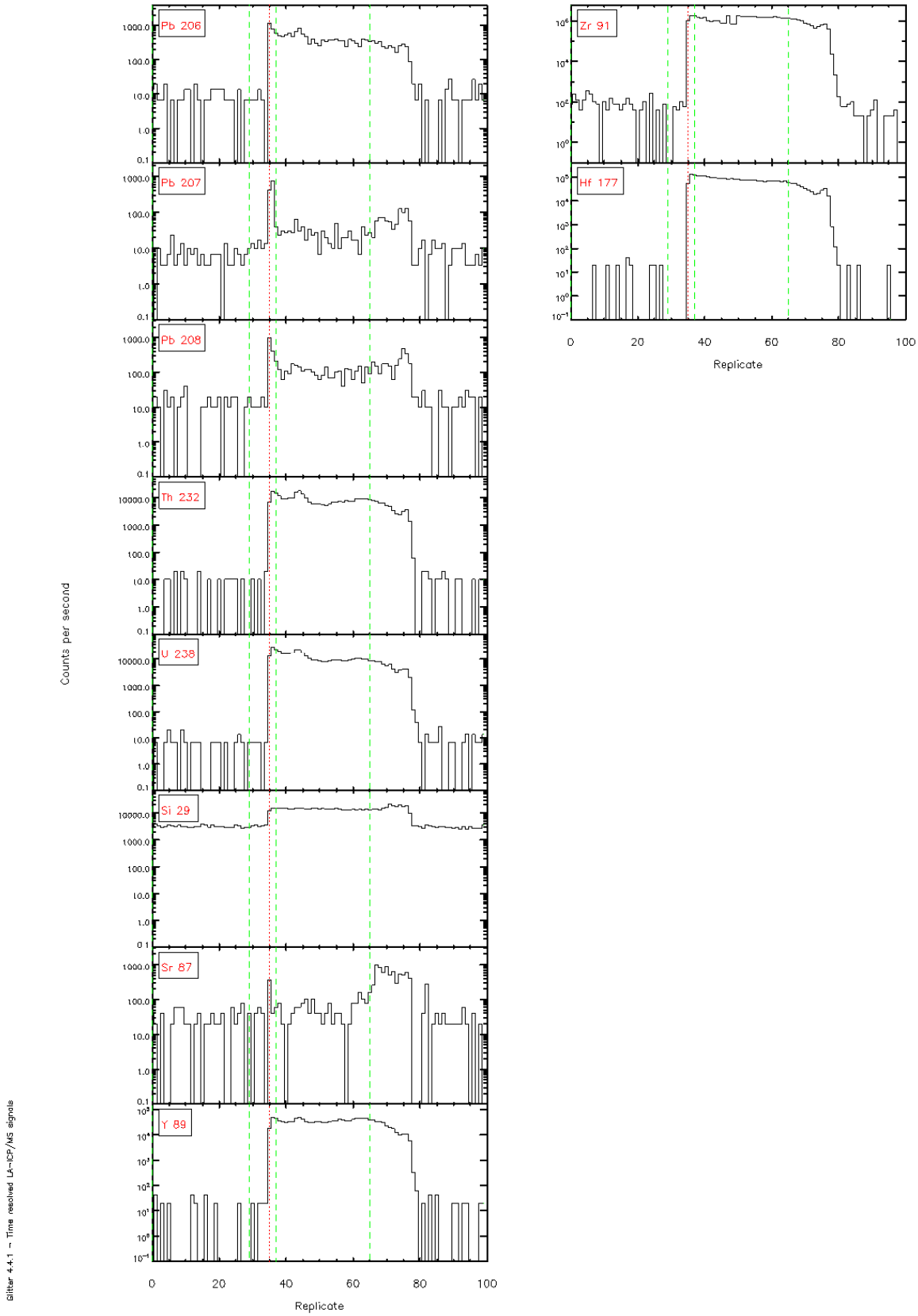
Pb 206
Pb 207
Pb 208
Th 232
U 238
Si 29
Sr 87
Y 89
Zr 91
Hf 177
Counts per second
Replicate
Glitter 4.4.1 - Time resolved LA-ICP/MS signals

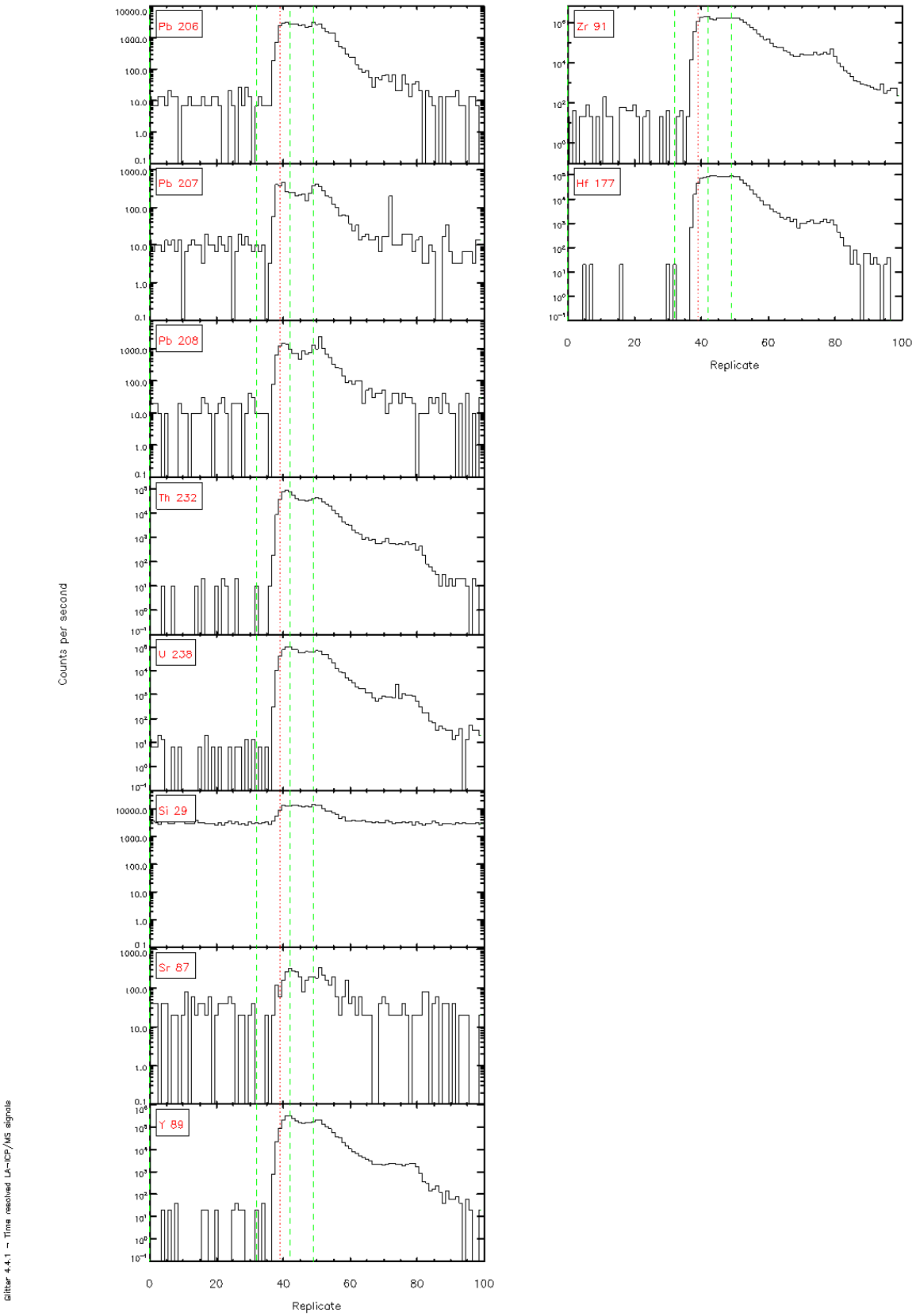
Pb 206
Pb 207
Pb 208
Th 232
U 238
Si 29
Sr 87
Y 89
Zr 91
Hf 177
Counts per second
Replicate
Glitter 4.4.1 – Time resolved LA-ICP/MS signals

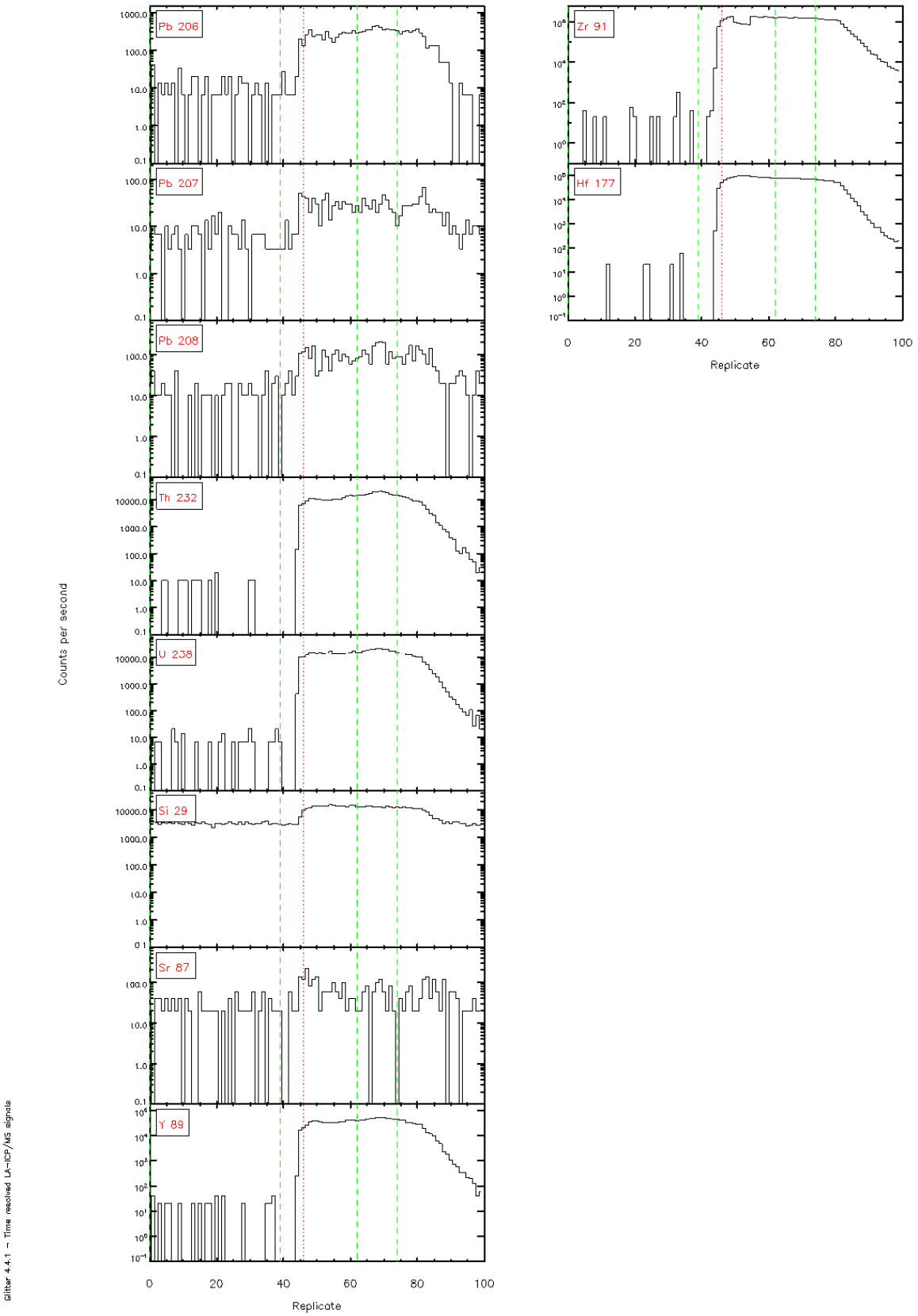
Pb 206
Pb 207
Pb 208
Th 232
U 238
Si 29
Sr 87
Y 89
Zr 91
Hf 177
Counts per second
Replicate
Glitter 4.4.1 – Time resolved LA-ICP/MS signals

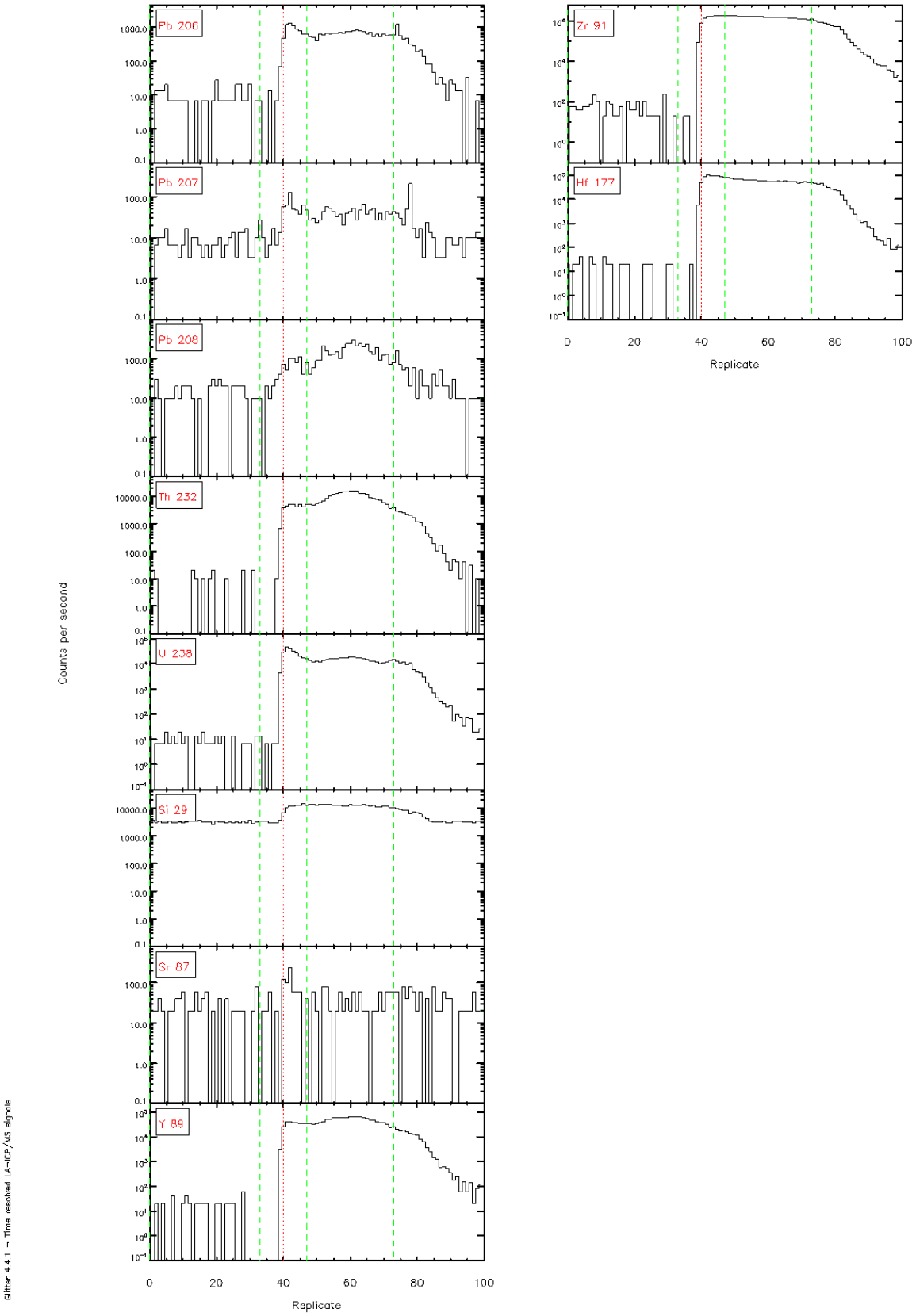
Pb 206
Pb 207
Pb 208
Th 232
U 238
Si 29
Sr 87
Y 89
Zr 91
Hf 177
Counts per second
Replicate
Glitter 4.4.1 - Time resolved LA-ICP/MS signals

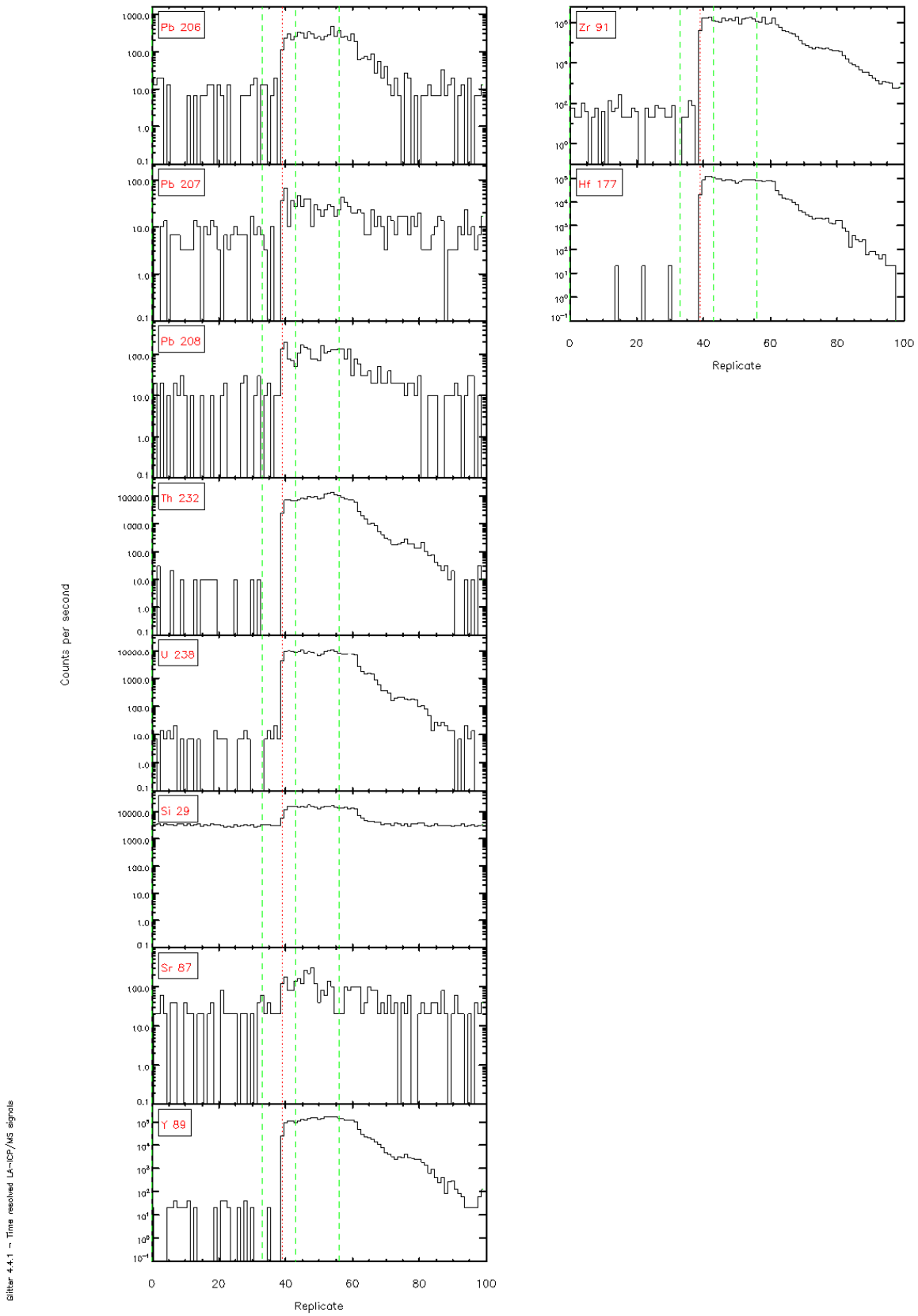
Pb 206
Pb 207
Pb 208
Th 232
U 238
Si 29
Sr 87
Y 89
Zr 91
Hf 177
Counts per second
Replicate
Glitter 4.4.1 - Time resolved LA-ICP/MS signals

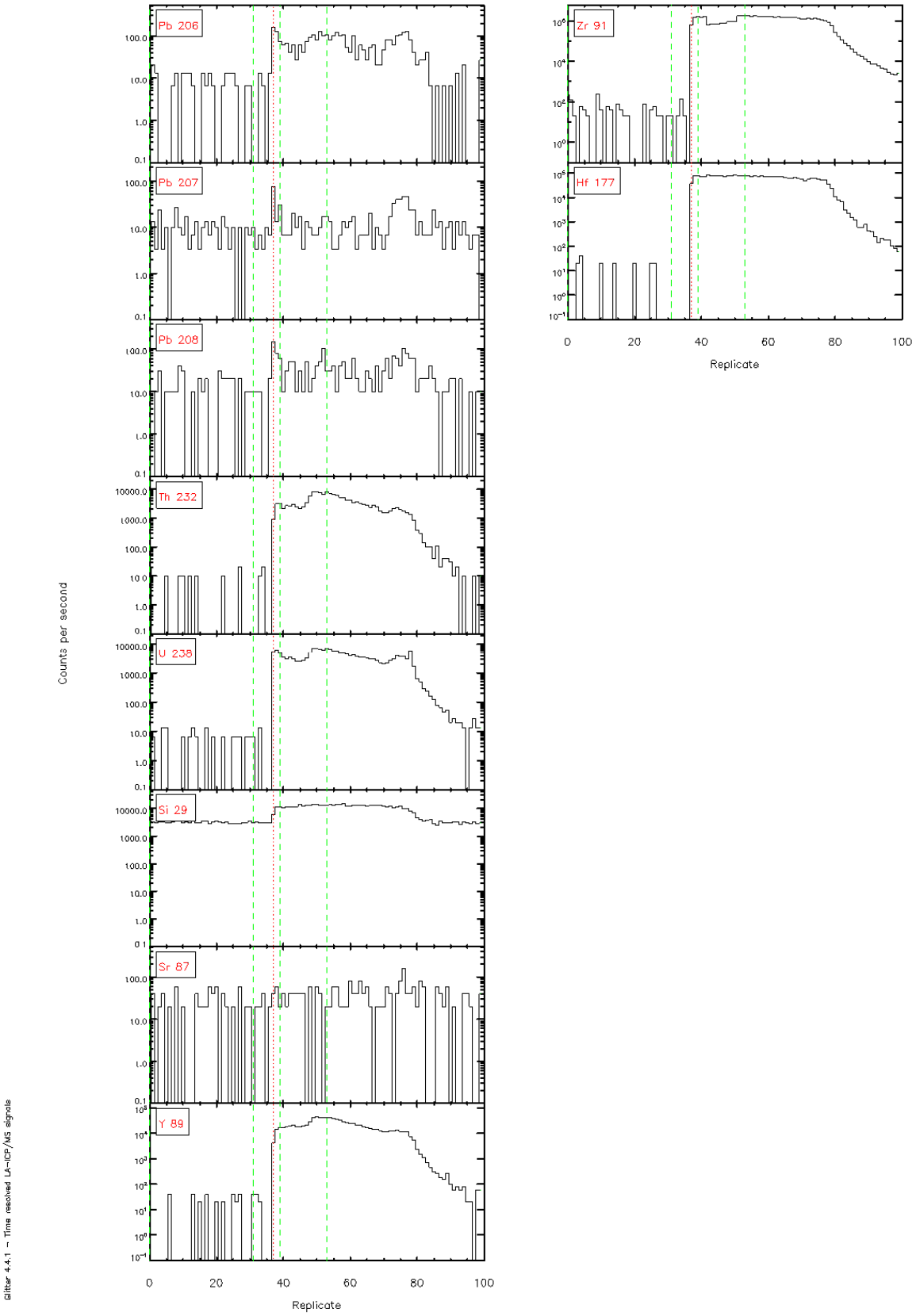
Pb 206
Pb 207
Pb 208
Th 232
U 238
Si 29
Sr 87
Y 89
Zr 91
Hf 177
Counts per second
Replicate
Glitter 4.4.1 - Time resolved LA-ICP/MS signals

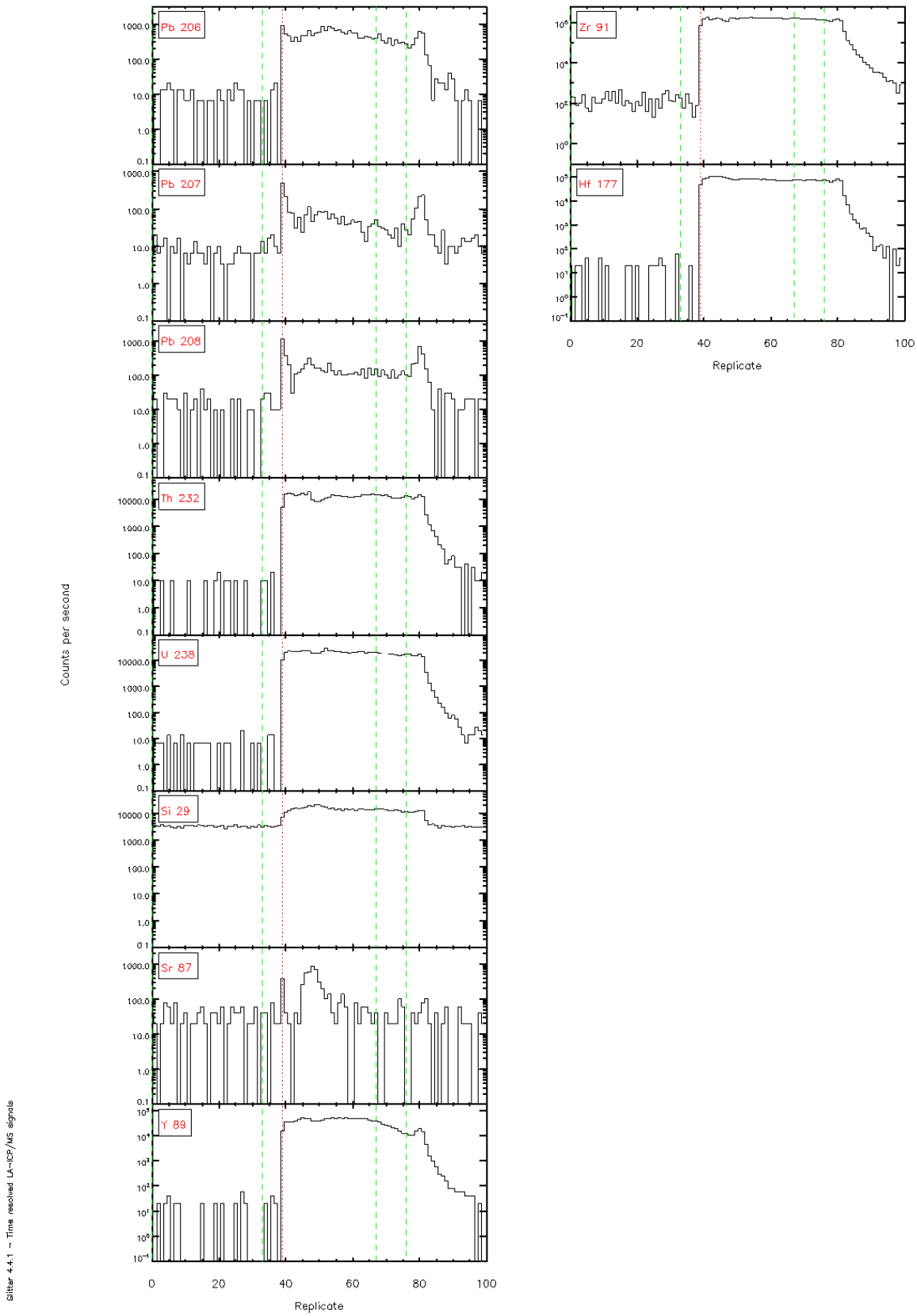
Pb 206
Pb 207
Pb 208
Th 232
U 238
Si 29
Sr 87
Y 89
Zr 91
Hf 177
Counts per second
Replicate
Glitter 4.4.1 - Time resolved LA-ICP/MS signals

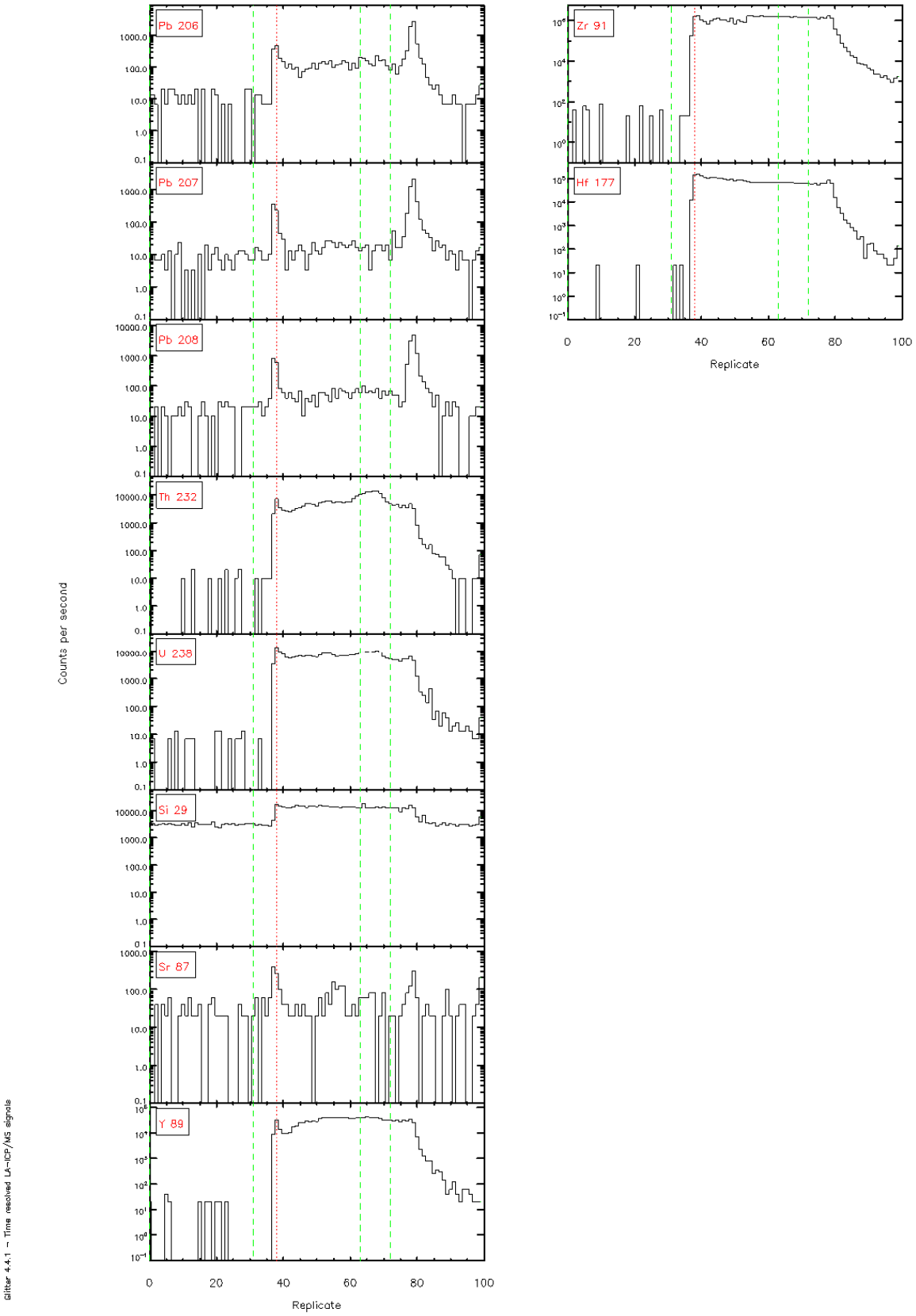
Pb 206
Pb 207
Pb 208
Th 232
U 238
Si 29
Sr 87
Y 89
Zr 91
Hf 177
Counts per second
Replicate
Glitter 4.4.1 - Time resolved LA-ICP/MS signals

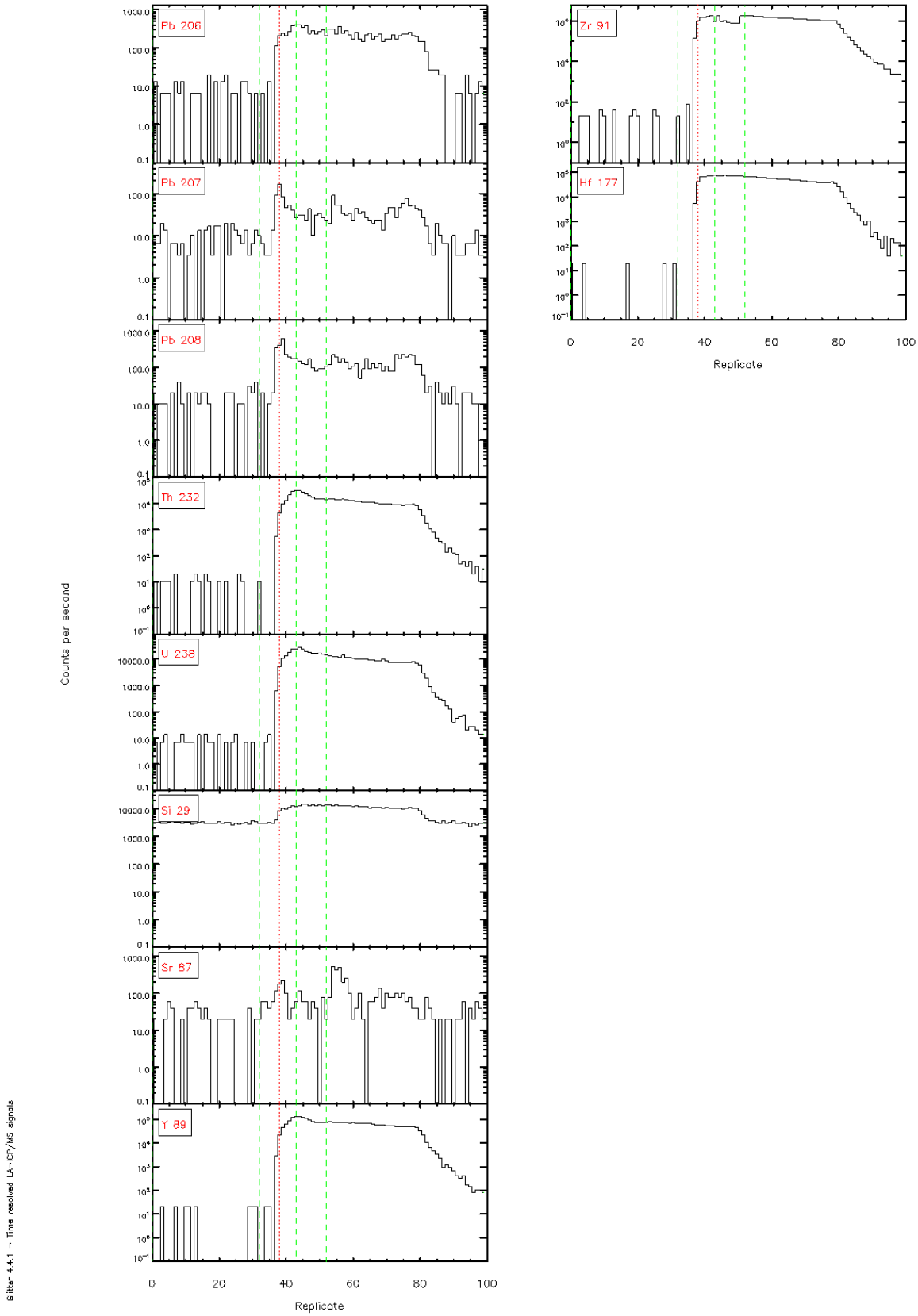
Pb 206
Pb 207
Pb 208
Th 232
U 238
Si 29
Sr 87
Y 89
Zr 91
Hf 177
Counts per second
Replicate
Glitter 4.4.1 - Time resolved LA-ICP/MS signals

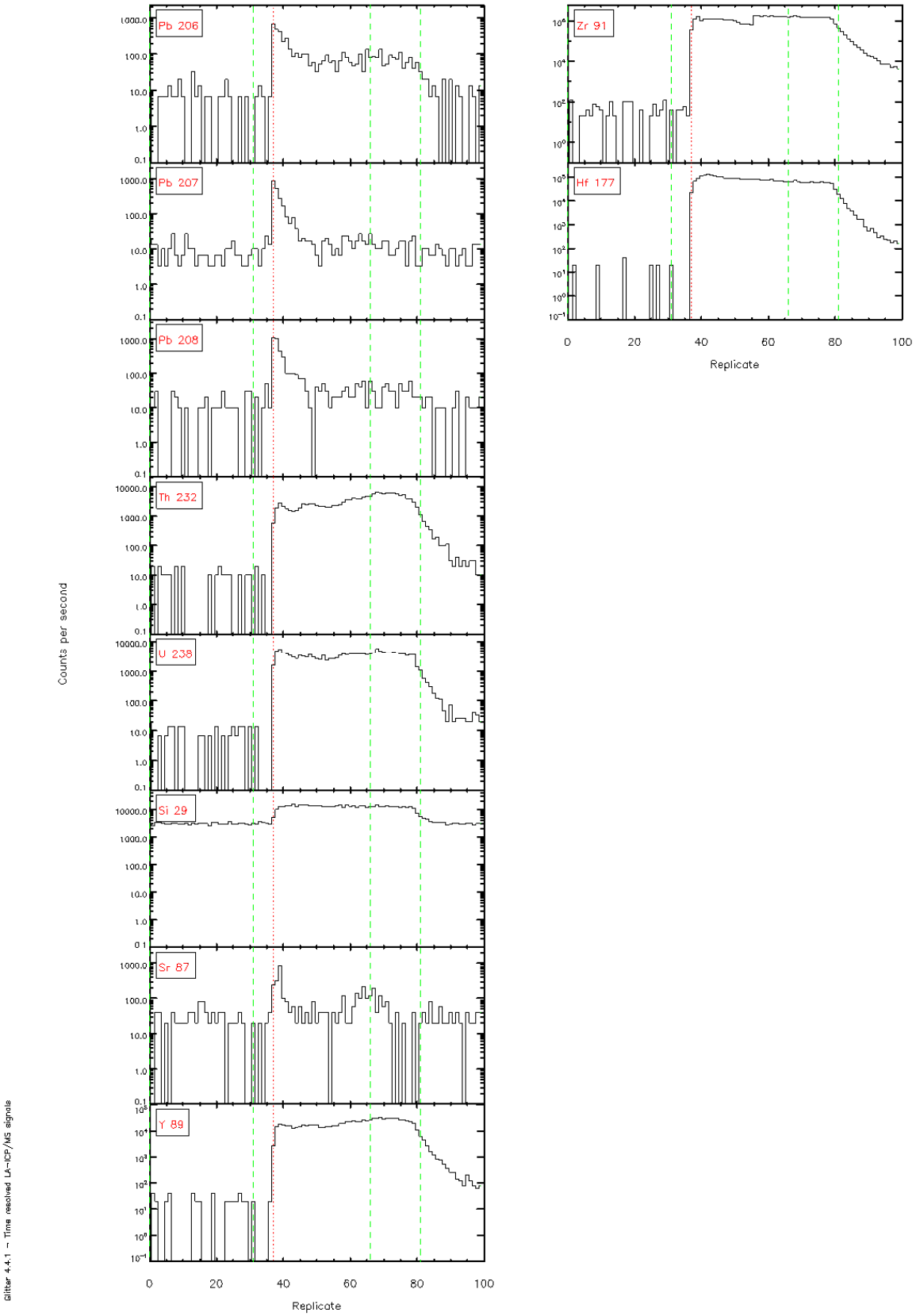
Pb 206
Pb 207
Pb 208
Th 232
U 238
Si 29
Sr 87
Y 89
Zr 91
Hf 177
Counts per second
Replicate
Glitter 4.4.1 - Time resolved LA-ICP/MS signals

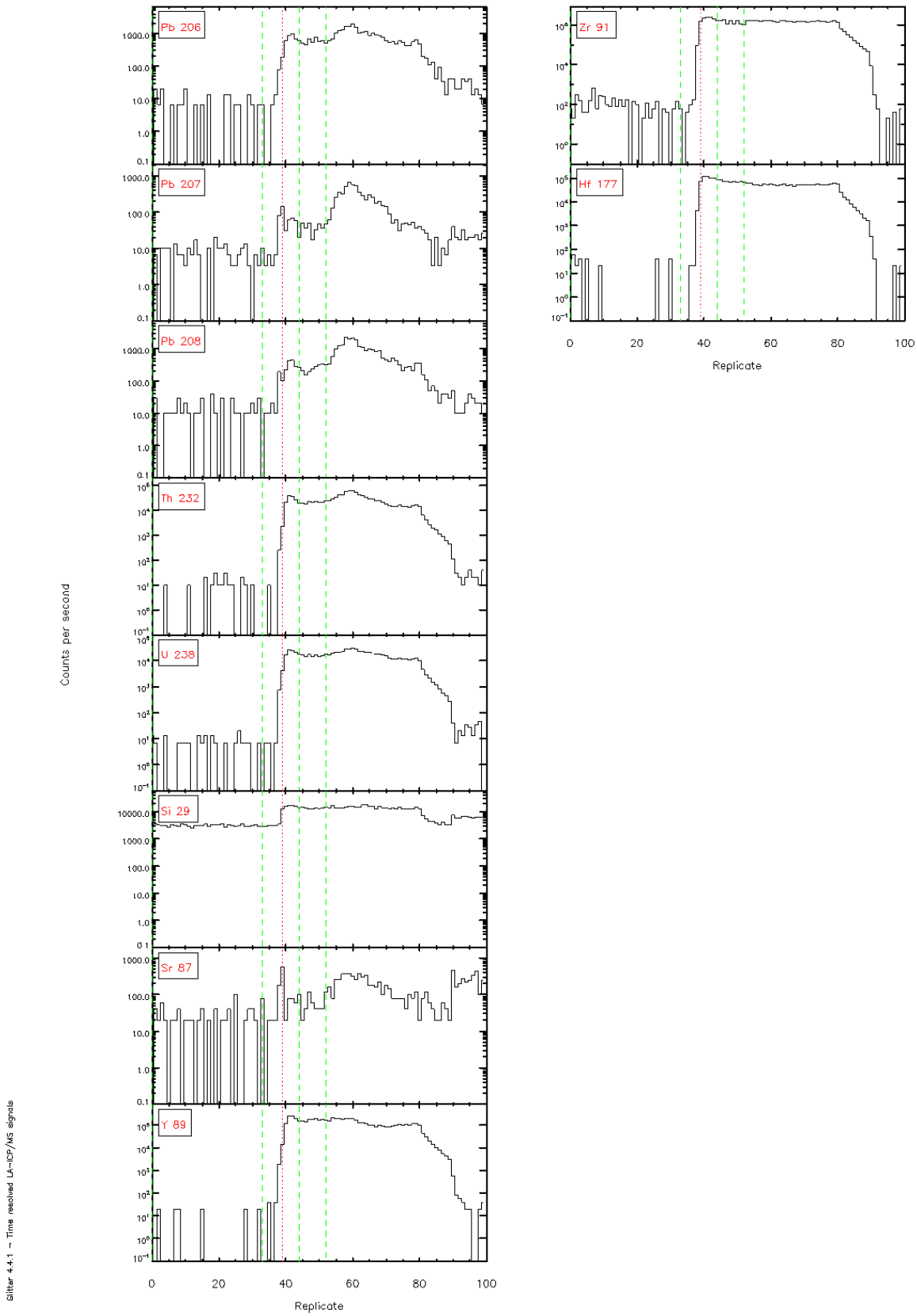
Pb 206
Pb 207
Pb 208
Th 232
U 238
Si 29
Sr 87
Y 89
Zr 91
Hf 177
Counts per second
Replicate
Glitter 4.4.1 - Time resolved LA-ICP/MS signals

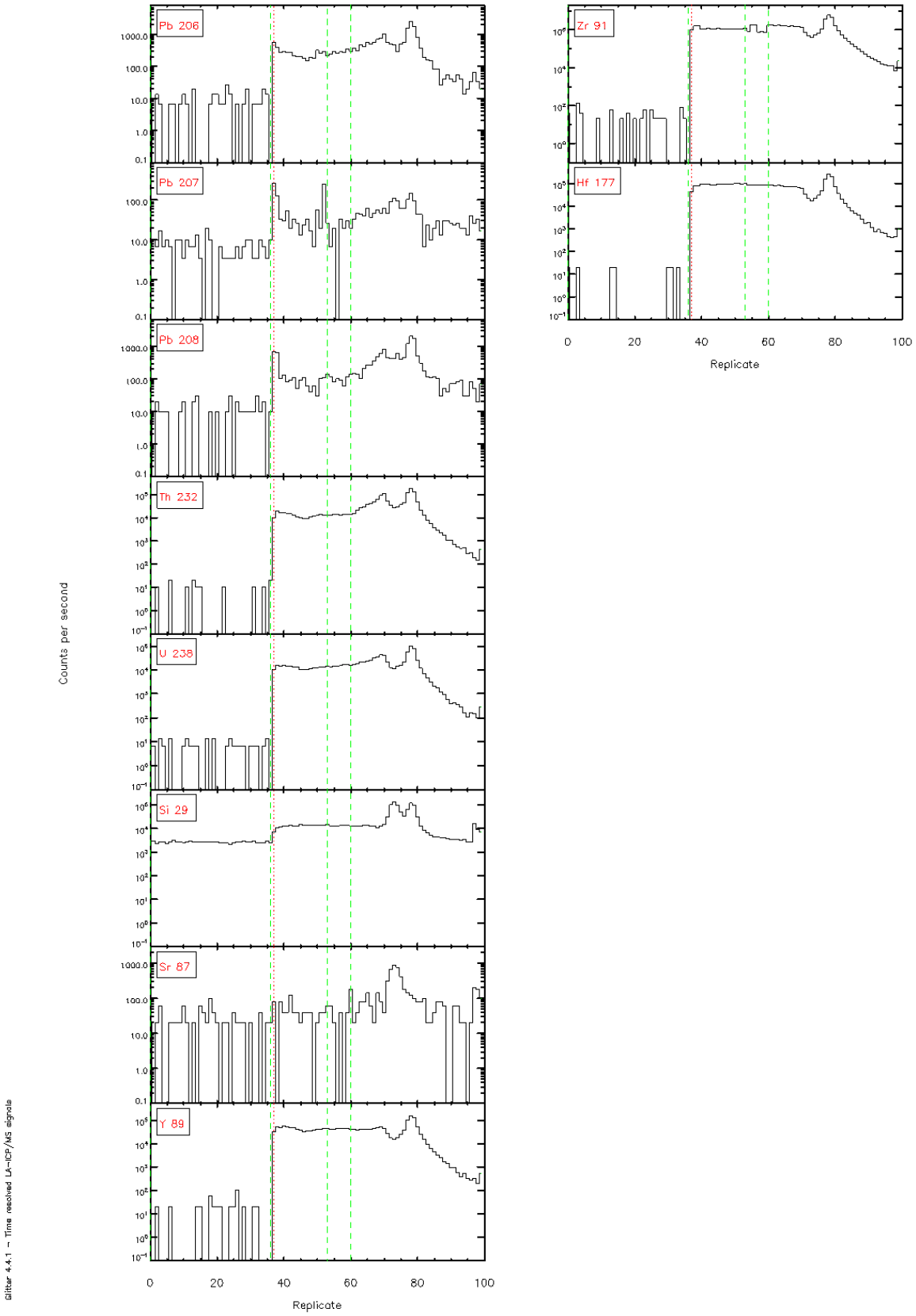
Pb 206
Pb 207
Pb 208
Th 232
U 238
Si 29
Sr 87
Y 89
Zr 91
Hf 177
Counts per second
Replicate
Glitter 4.4.1 - Time resolved LA-ICP/MS signals

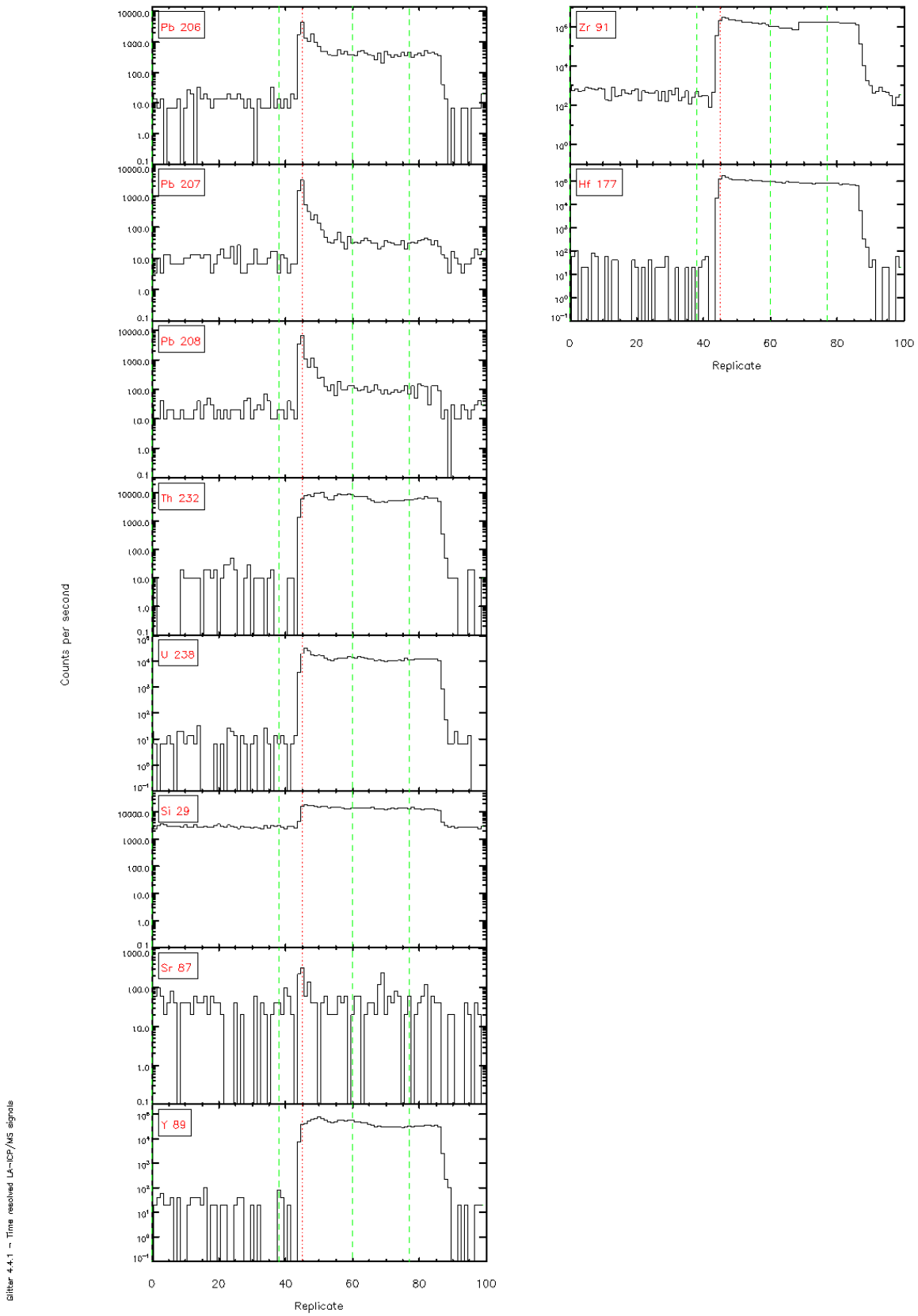
Pb 206
Pb 207
Pb 208
Th 232
U 238
Si 29
Sr 87
Y 89
Zr 91
Hf 177
Counts per second
Replicate
Glitter 4.4.1 - Time resolved LA-ICP/MS signals

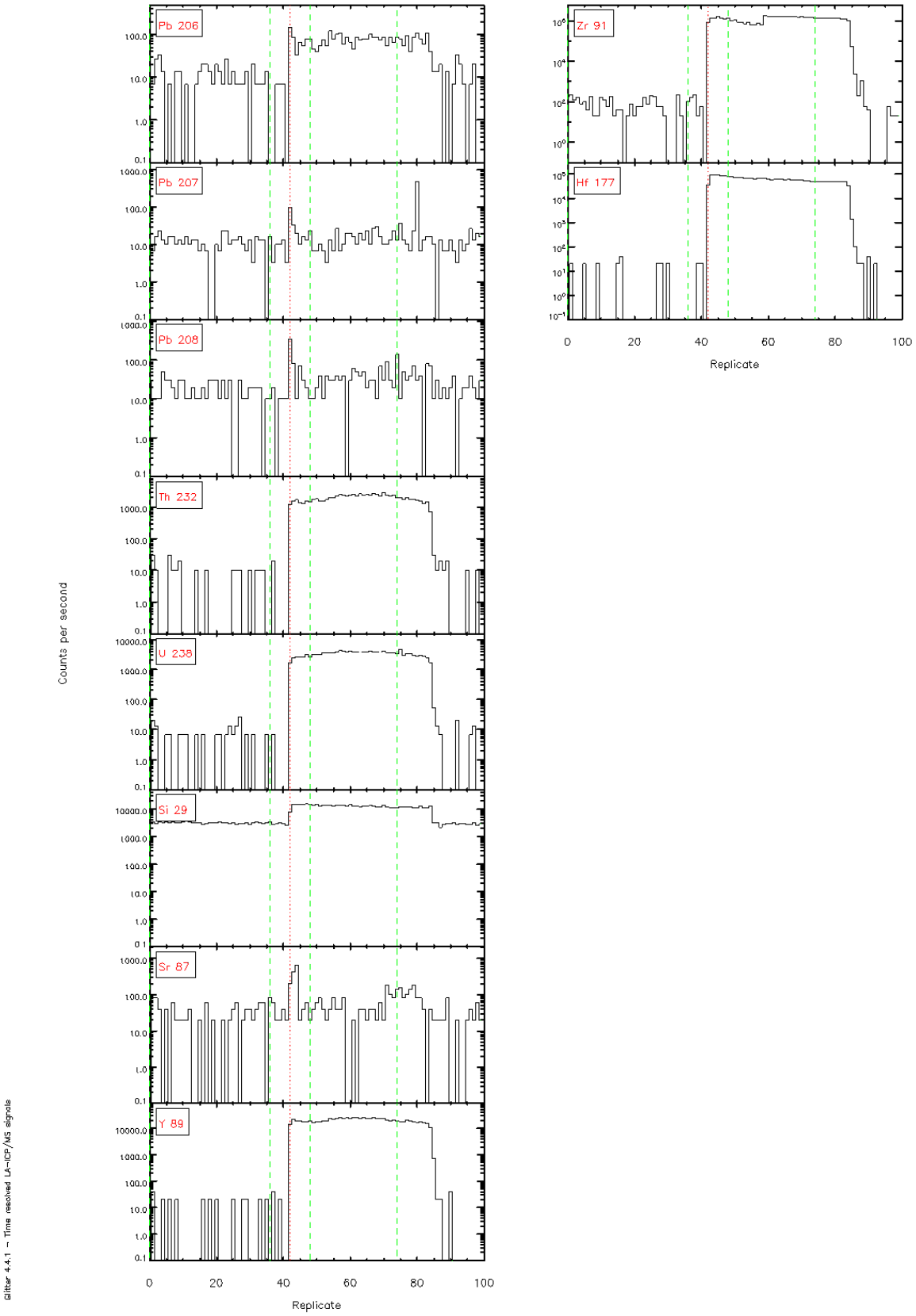
Pb 206
Pb 207
Pb 208
Th 232
U 238
Si 29
Sr 87
Y 89
Zr 91
Hf 177
Counts per second
Replicate
Glitter 4.4.1 - Time resolved LA-ICP/MS signals

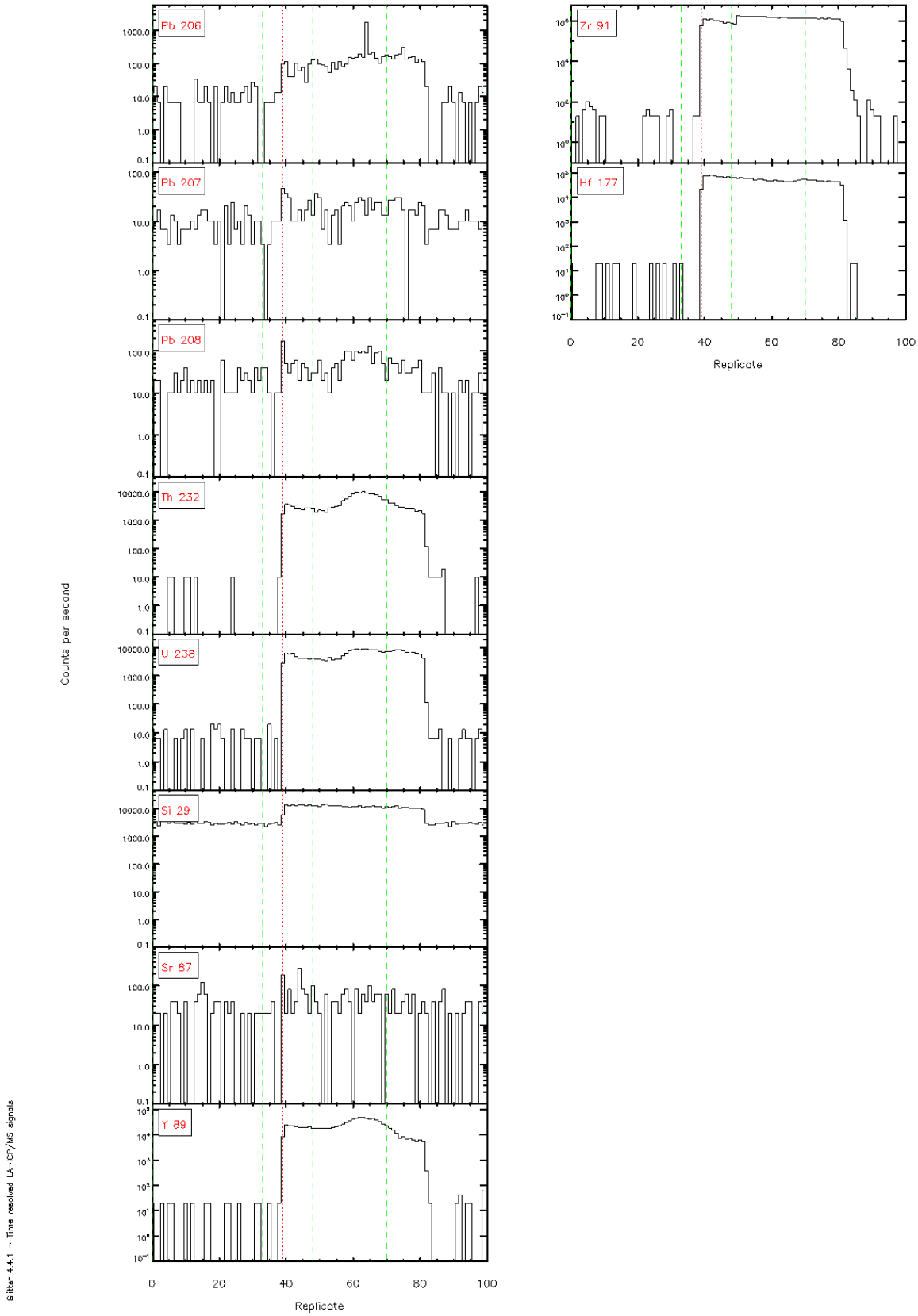
Pb 206
Pb 207
Pb 208
Th 232
U 238
Si 29
Sr 87
Y 89
Zr 91
Hf 177
Counts per second
Replicate
Glitter 4.4.1 - Time resolved LA-ICP/MS signals

13 – Tariki Sandstone

1.

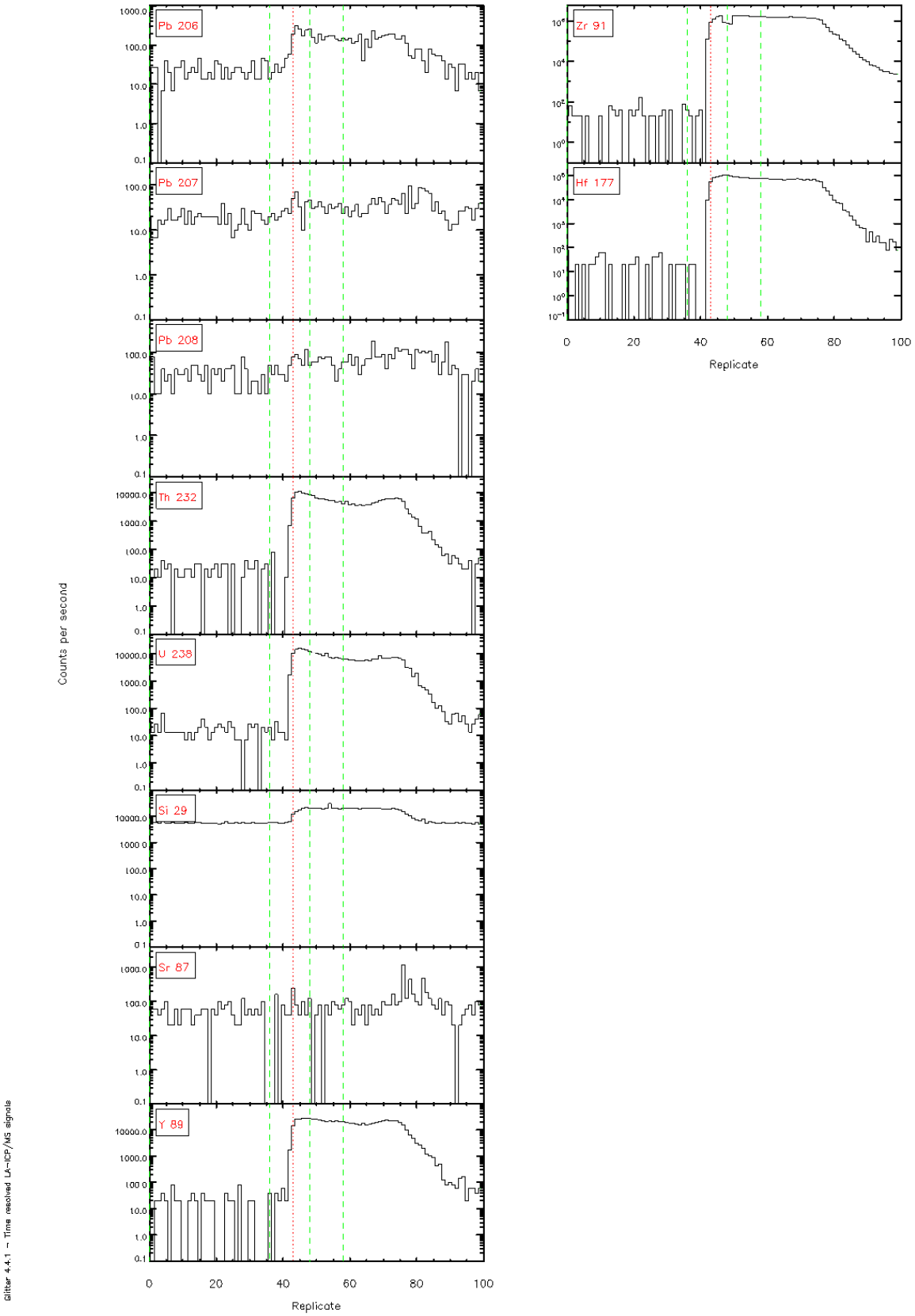

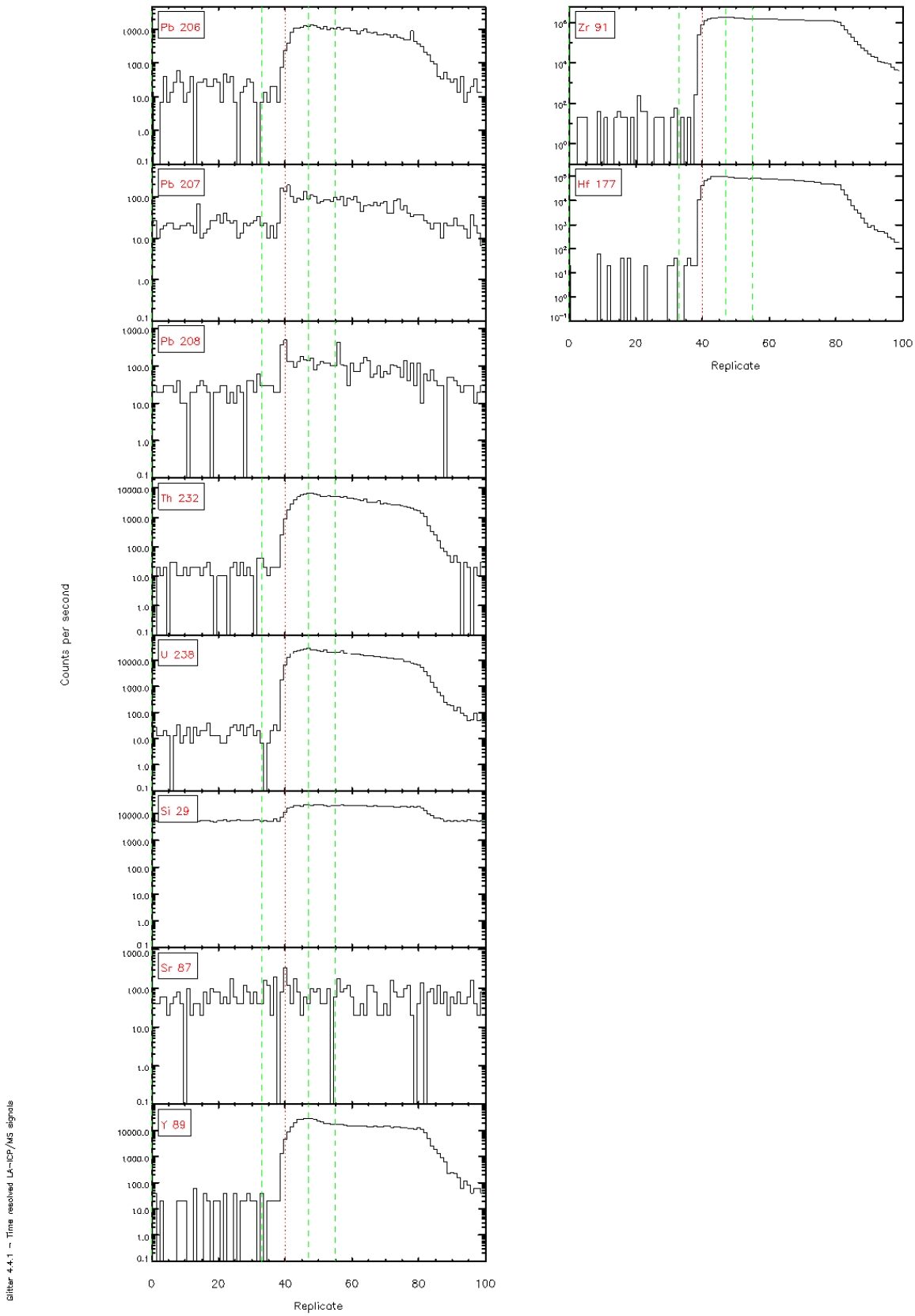
Pb 206
Pb 207
Pb 208
Th 232
U 238
Si 29
Sr 87
Y 89
Zr 91
Hf 177
Counts per second
Replicate
Glitter 4.4.1 ~ Time resolved LA-ICP/MS signals

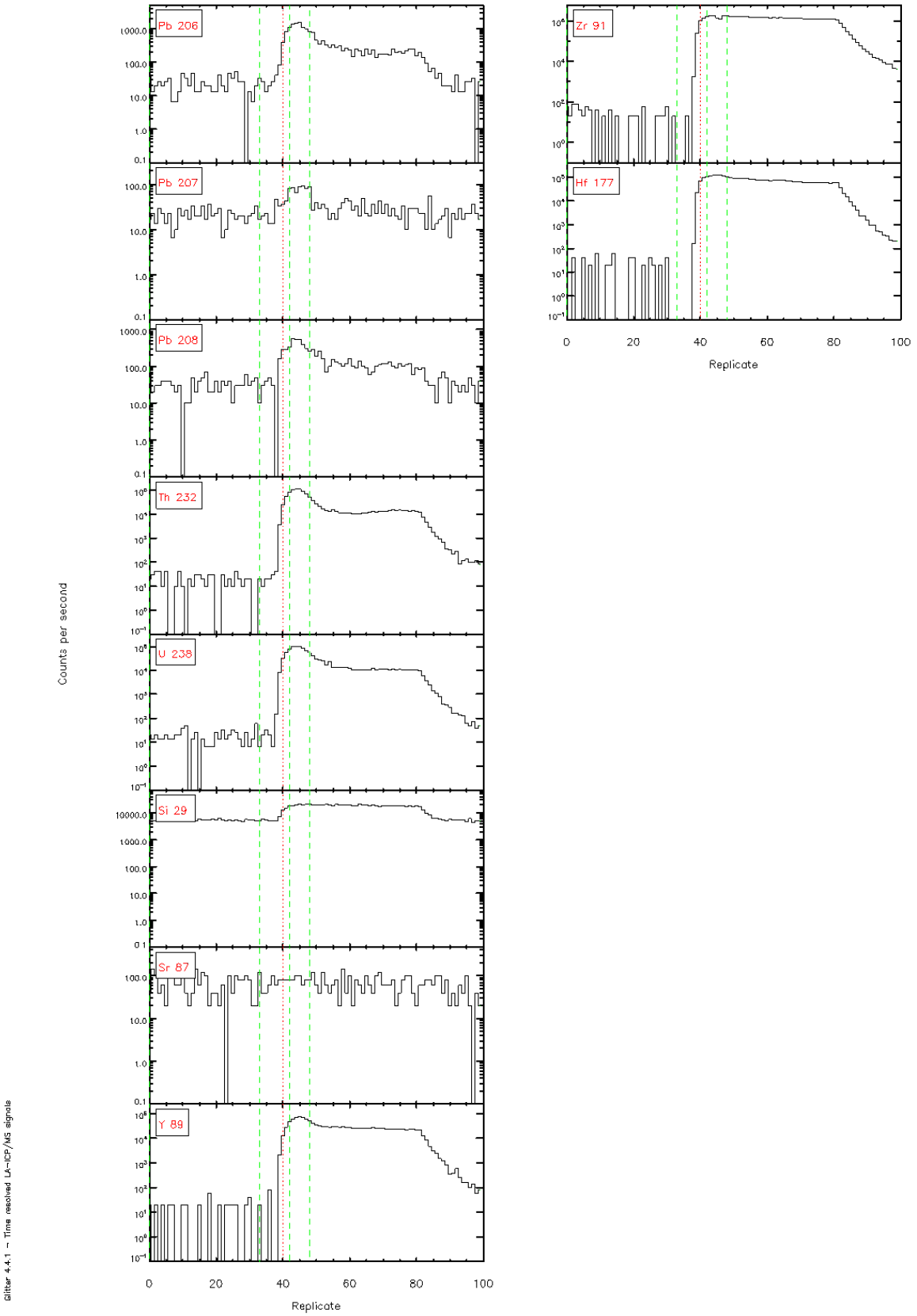
Pb 206
Pb 207
Pb 208
Th 232
U 238
Si 29
Sr 87
Y 89
Zr 91
Hf 177
Counts per second
Replicate
Glitter 4.4.1 - Time resolved LA-ICP/MS signals

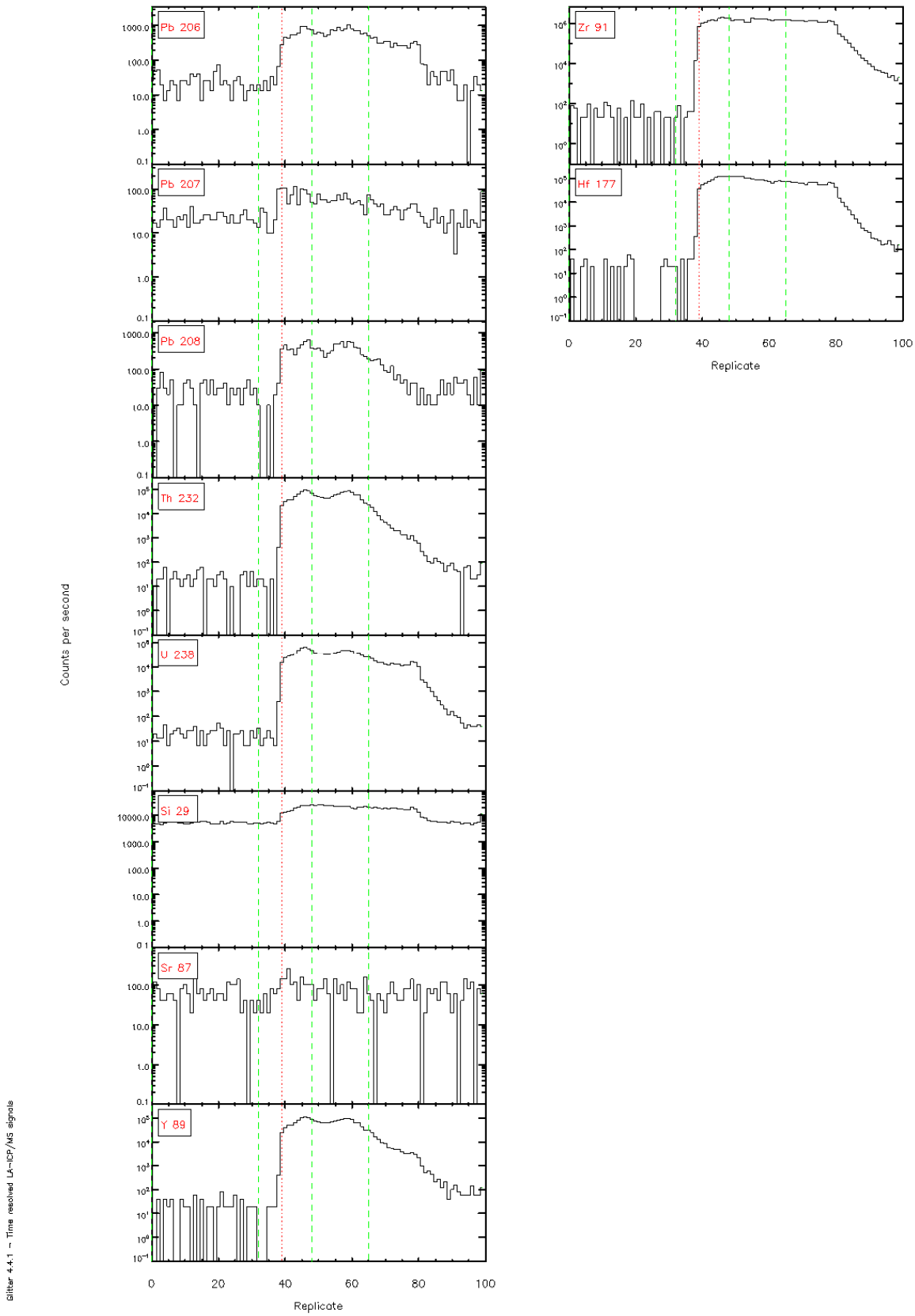
Pb 206
Pb 207
Pb 208
Th 232
U 238
Si 29
Sr 87
Y 89
Zr 91
Hf 177
Counts per second
Replicate
Glitter 4.4.1 - Time resolved LA-ICP/MS signals

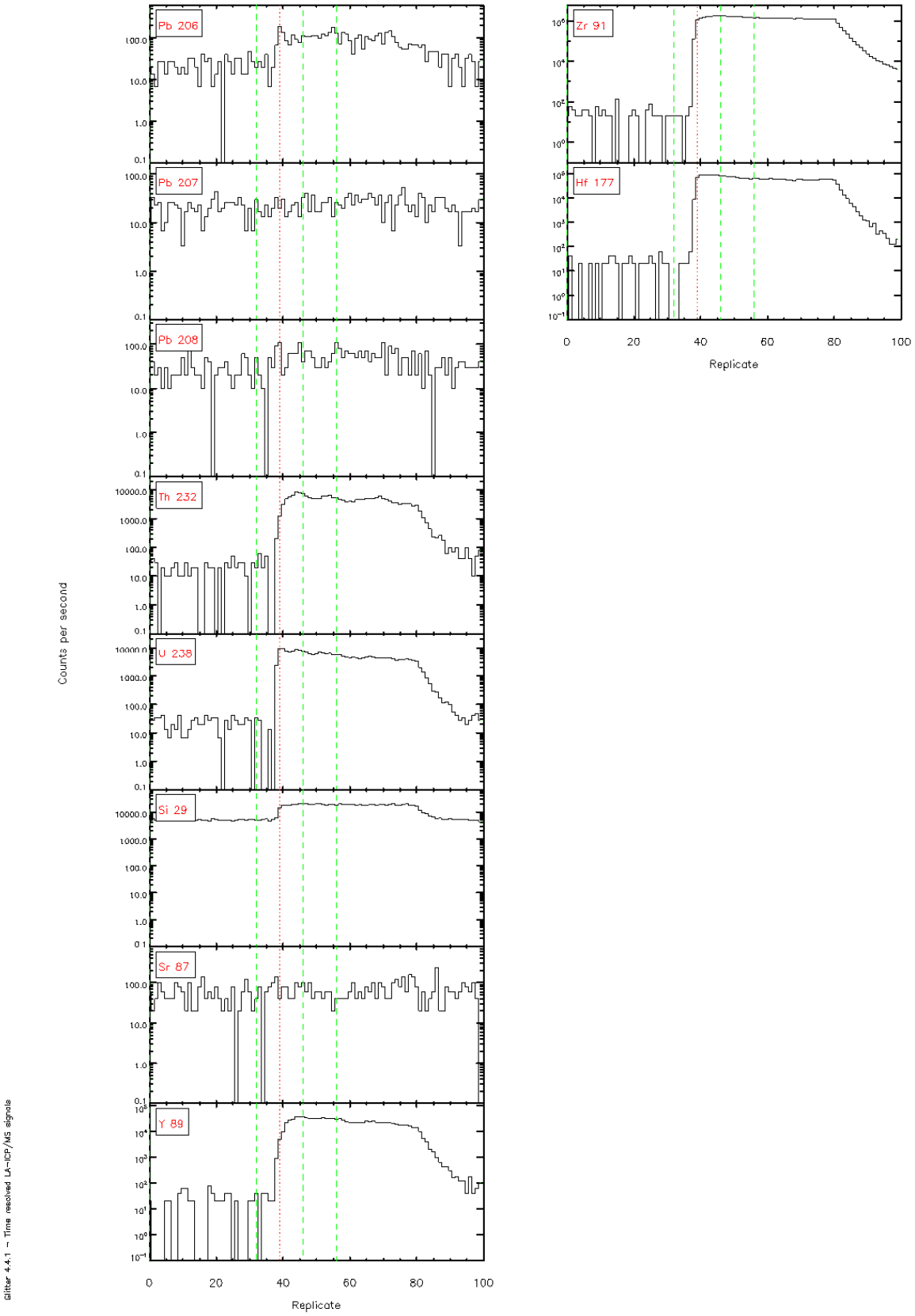
Pb 206
Pb 207
Pb 208
Th 232
U 238
Si 29
Sr 87
Y 89
Zr 91
Hf 177
Counts per second
Replicate
Glitter 4.4.1 - Time resolved LA-ICP/MS signals

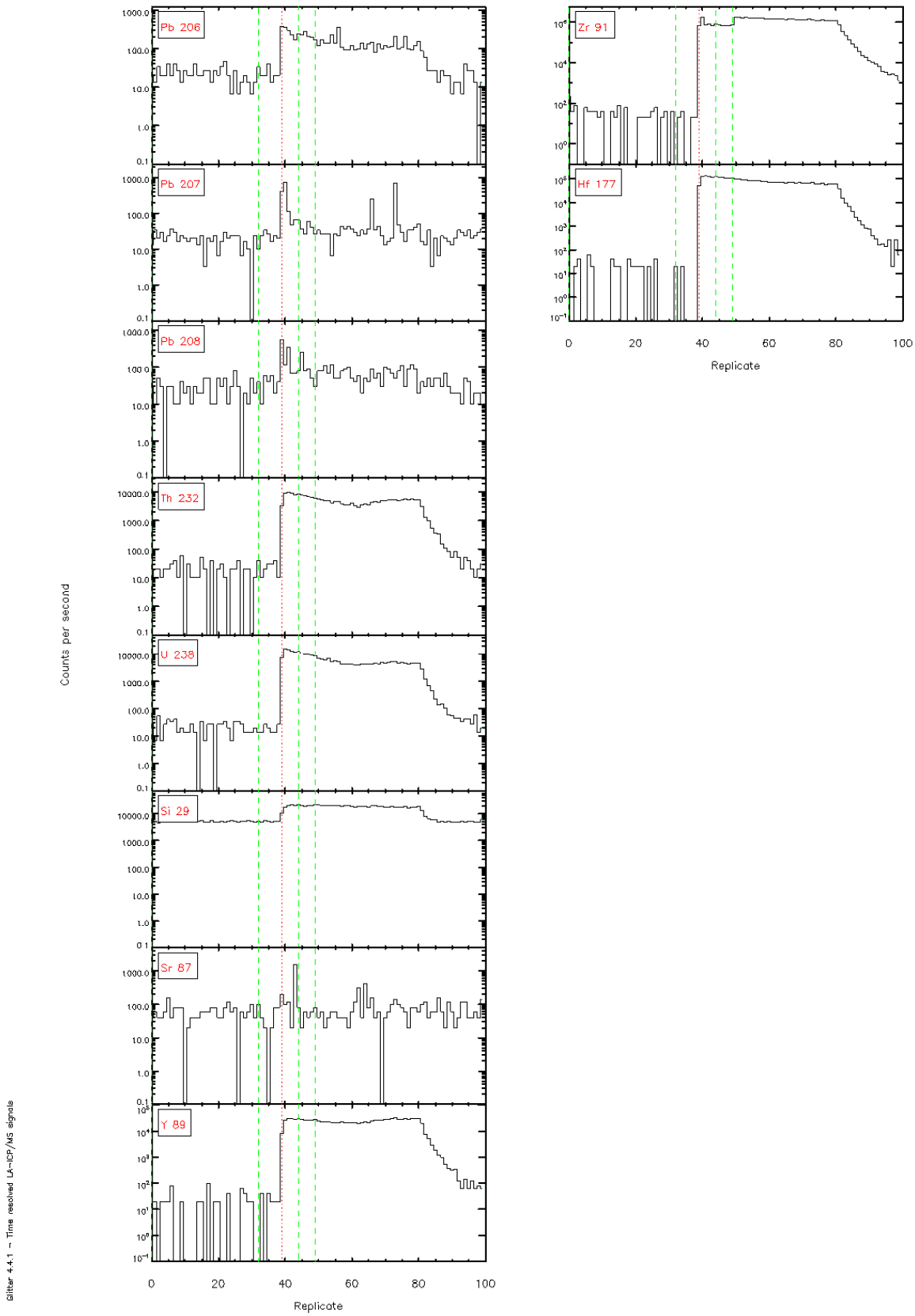
Pb 206
Pb 207
Pb 208
Th 232
U 238
Si 29
Sr 87
Y 89
Zr 91
Hf 177
Counts per second
Replicate
Glitter 4.4.1 - Time resolved LA-ICP/MS signals

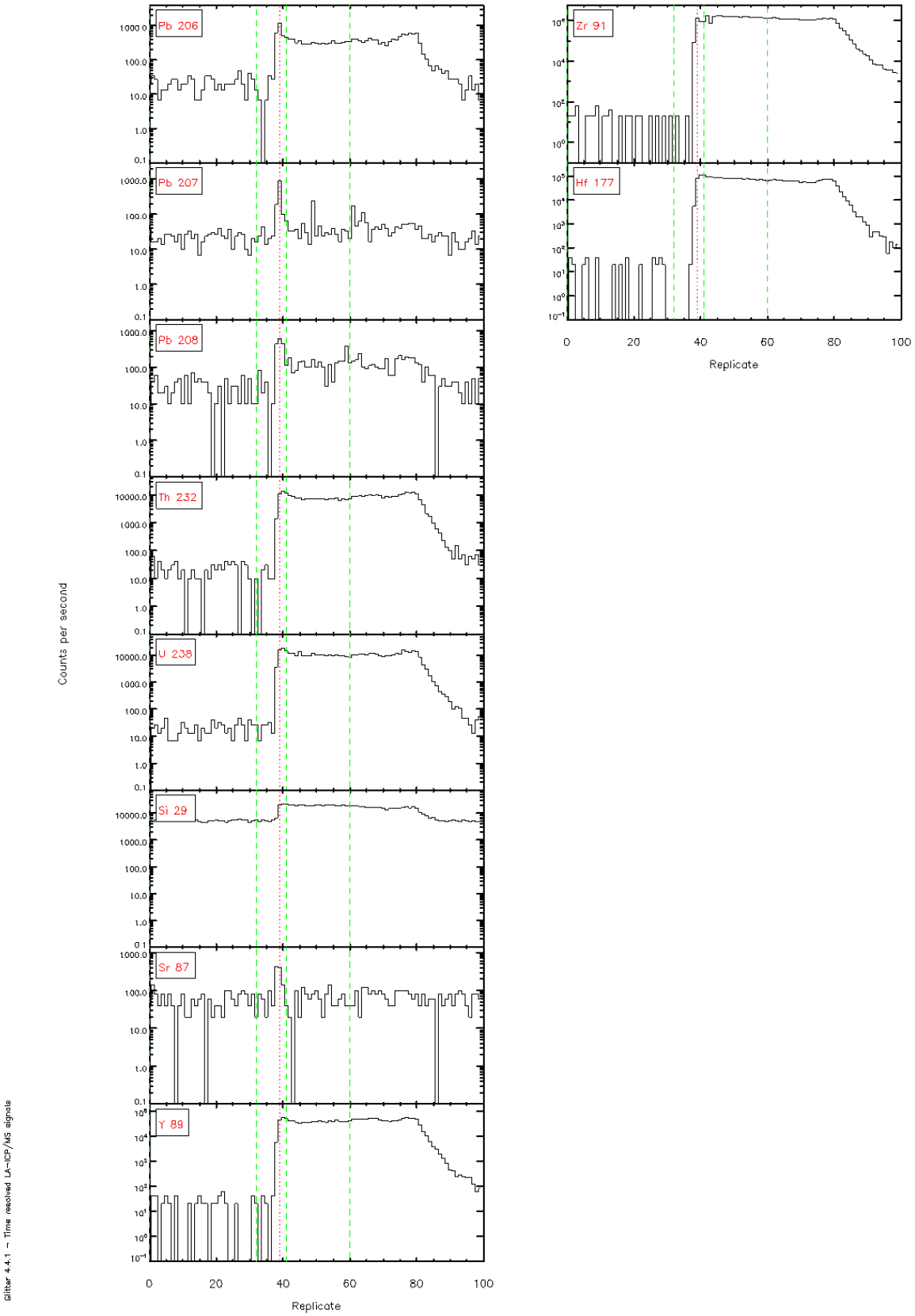
Pb 206
Pb 207
Pb 208
Th 232
U 238
Si 29
Sr 87
Y 89
Zr 91
Hf 177
Counts per second
Replicate
Glitter 4.4.1 - Time resolved LA-ICP/MS signals

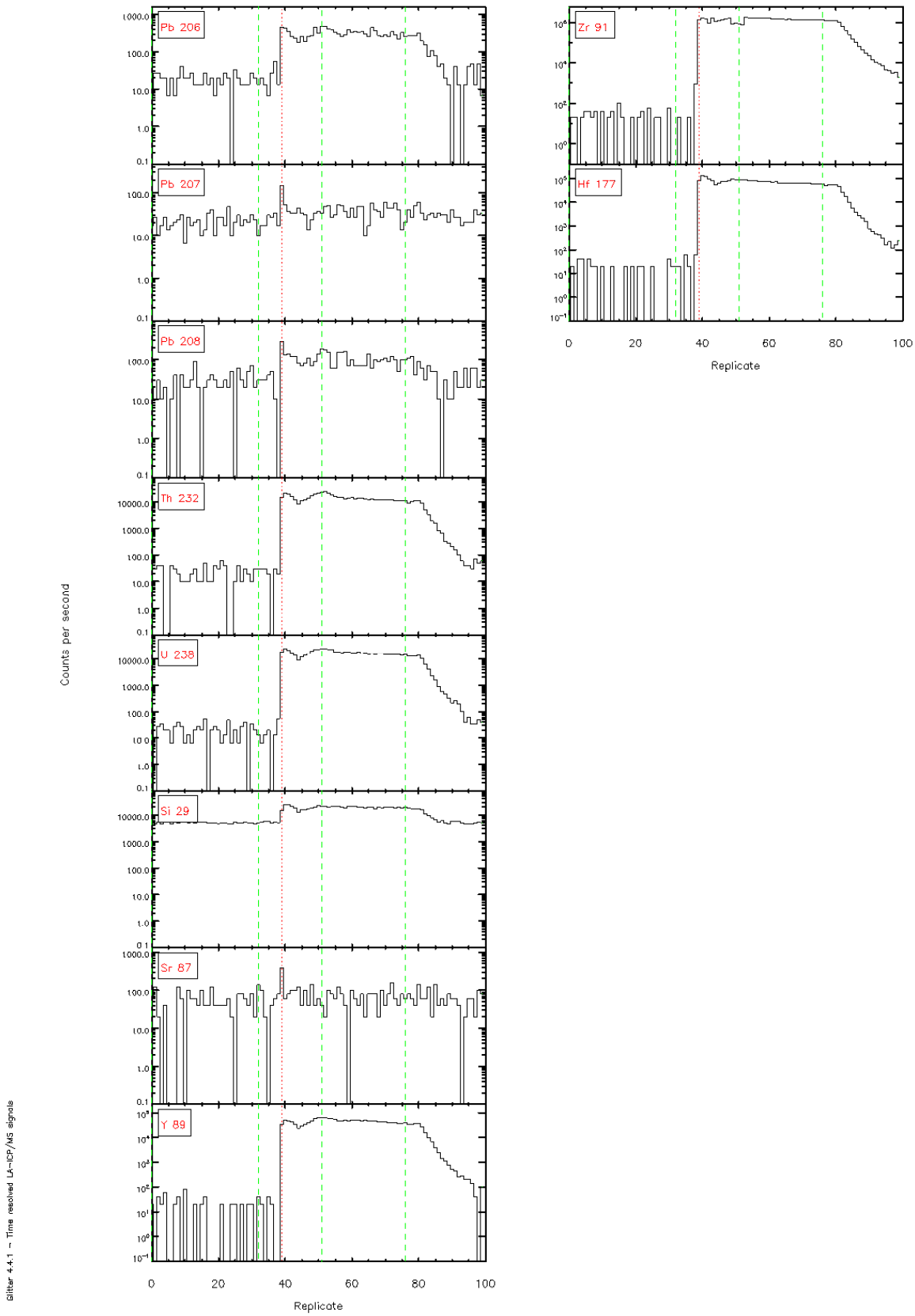
Pb 206
Pb 207
Pb 208
Th 232
U 238
Si 29
Sr 87
Y 89
Zr 91
Hf 177
Counts per second
Replicate
Glitter 4.4.1 - Time resolved LA-ICP/MS signals

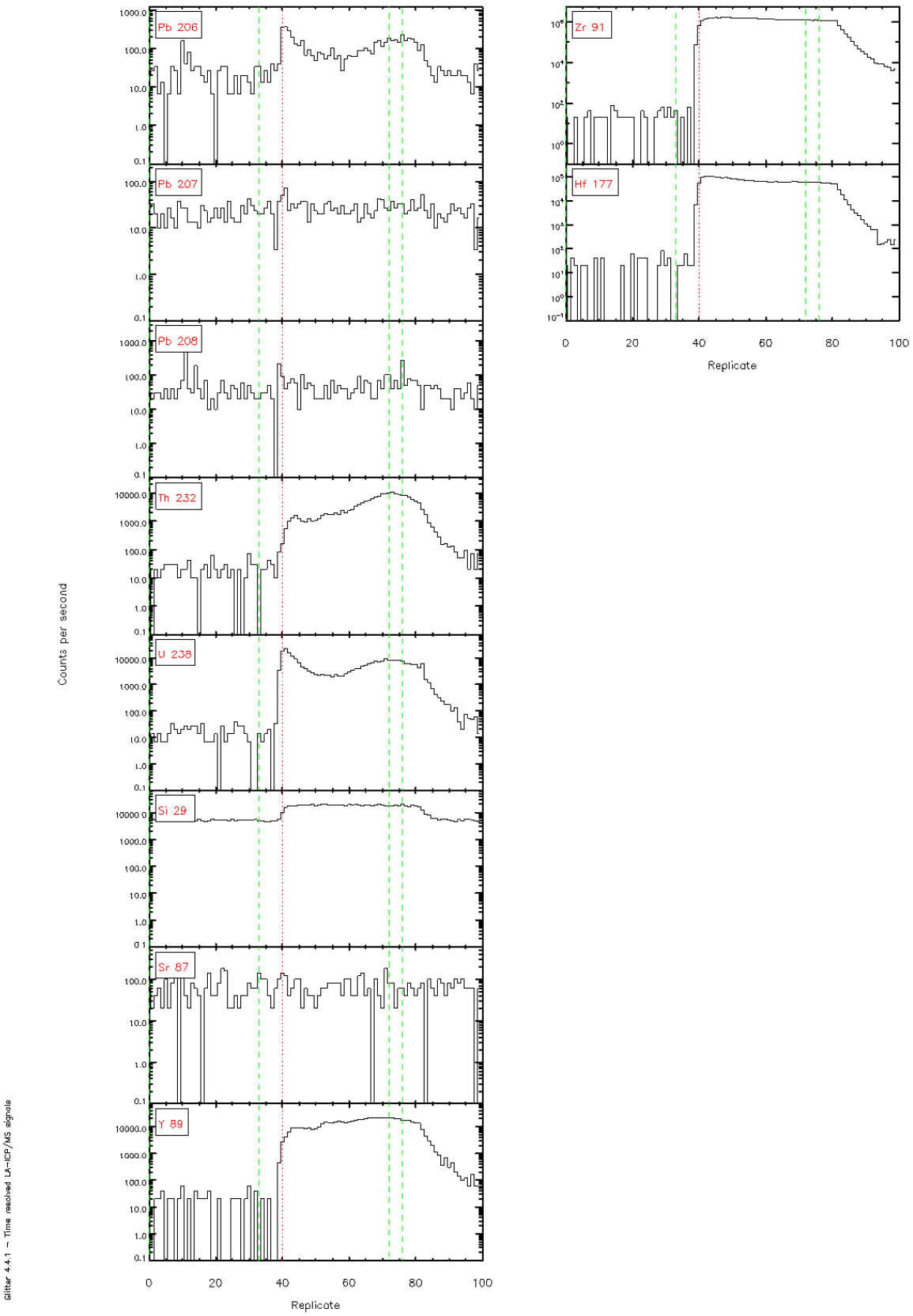
Pb 206
Pb 207
Pb 208
Th 232
U 238
Si 29
Sr 87
Y 89
Zr 91
Hf 177
Counts per second
Replicate
Glitter 4.4.1 - Time resolved LA-ICP/MS signals

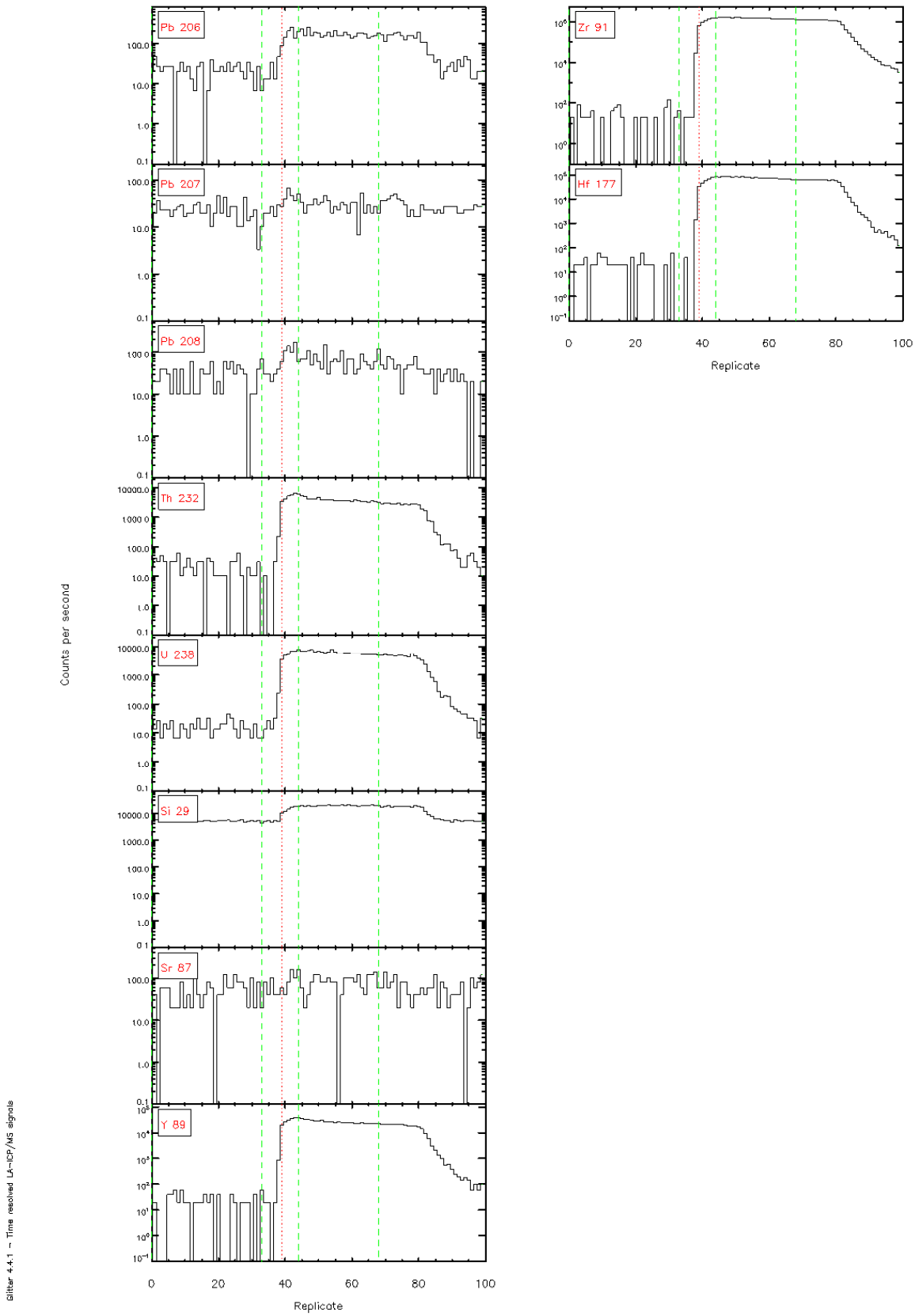
Pb 206
Pb 207
Pb 208
Th 232
U 238
Si 29
Sr 87
Y 89
Zr 91
Hf 177
Counts per second
Replicate
Glitter 4.4.1 ~ Time resolved LA-ICP/MS signals

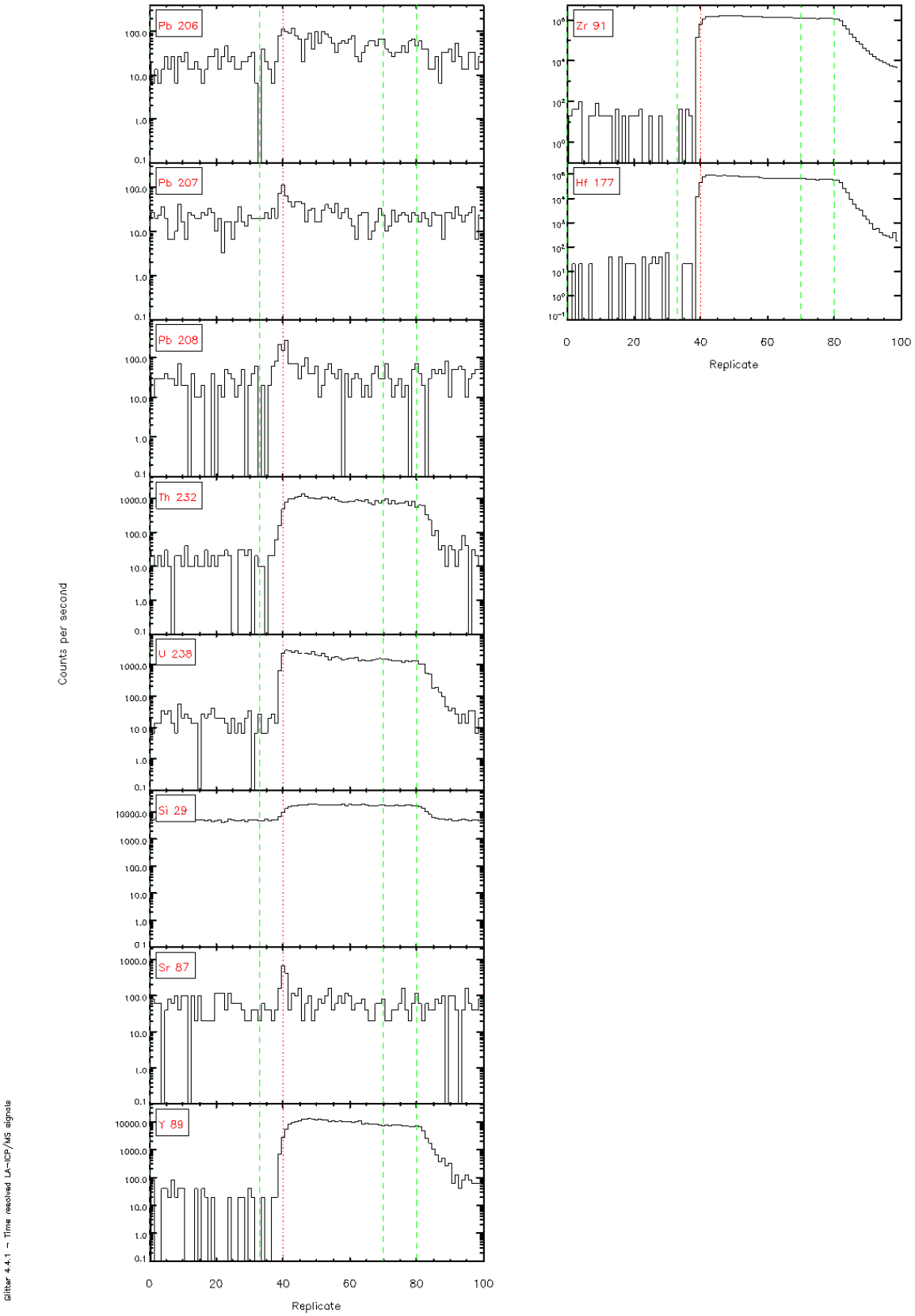
Pb 206
Pb 207
Pb 208
Th 232
U 238
Si 29
Sr 87
Y 89
Zr 91
Hf 177
Counts per second
Replicate
Glitter 4.4.1 - Time resolved LA-ICP/MS signals

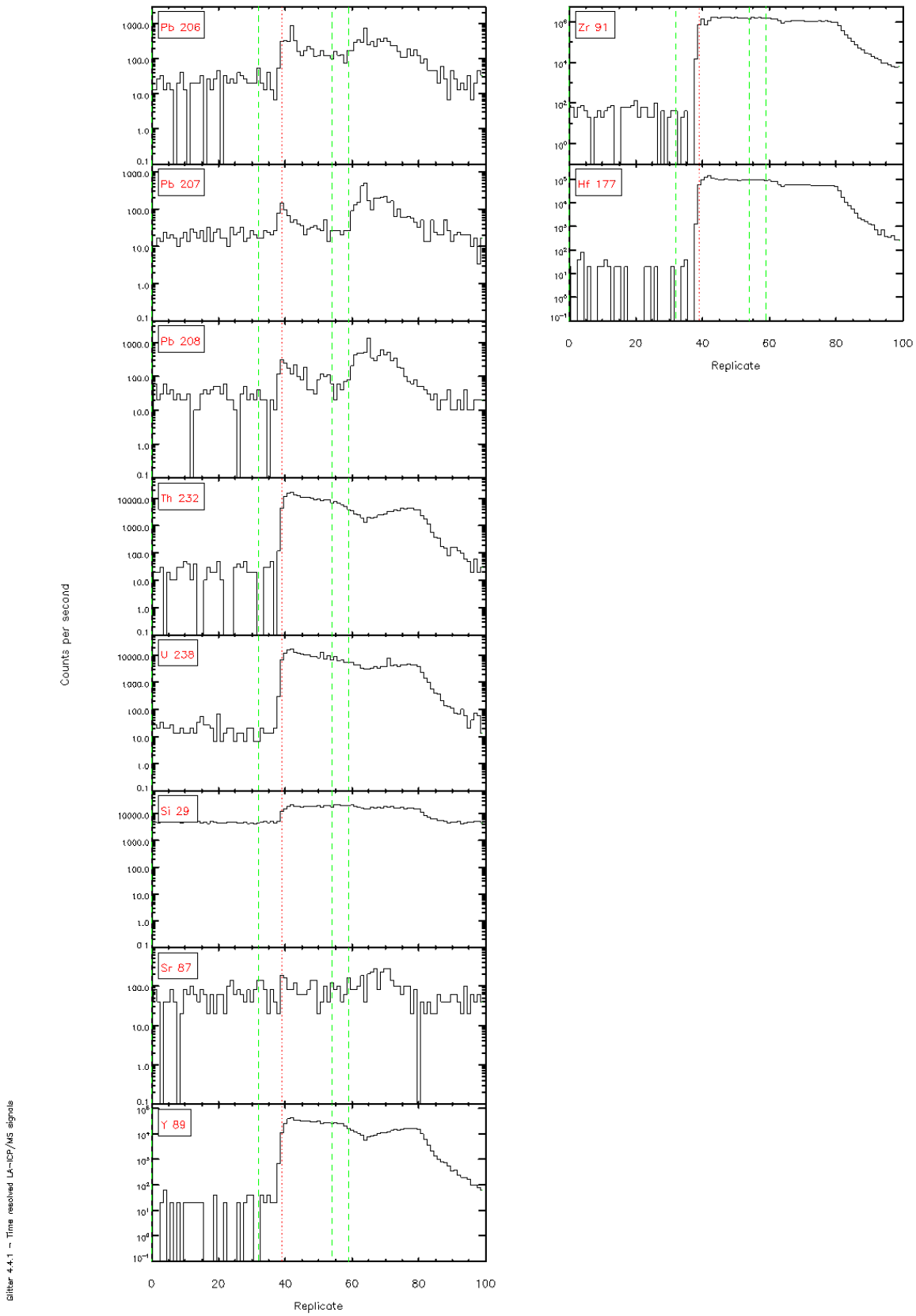
Pb 206
Pb 207
Pb 208
Th 232
U 238
Si 29
Sr 87
Y 89
Zr 91
Hf 177
Counts per second
Replicate
Glitter 4.4.1 - Time resolved LA-ICP/MS signals

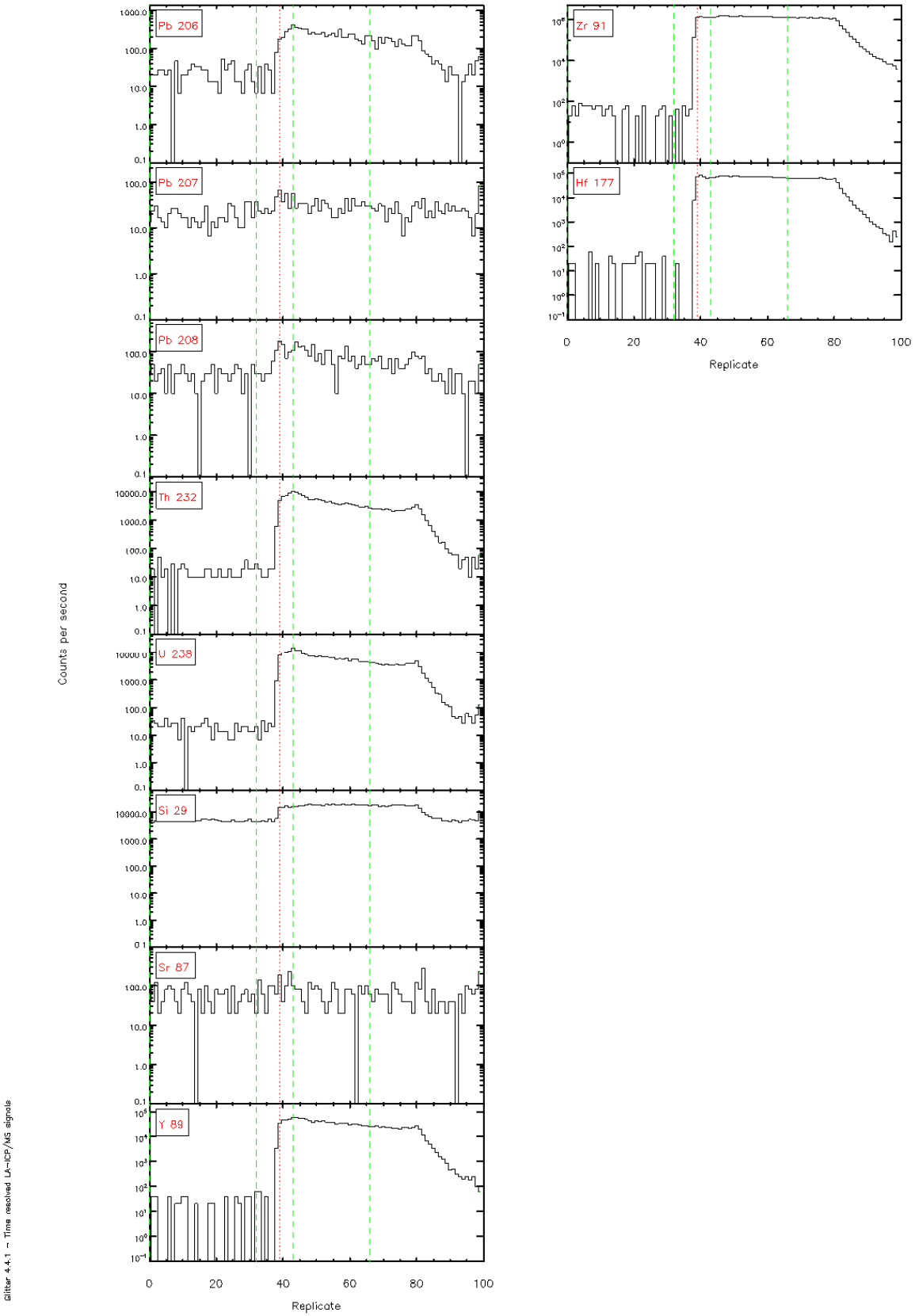
Pb 206
Pb 207
Pb 208
Th 232
U 238
Si 29
Sr 87
Y 89
Zr 91
Hf 177
Counts per second
Replicate
Glitter 4.4.1 - Time resolved LA-ICP/MS signals

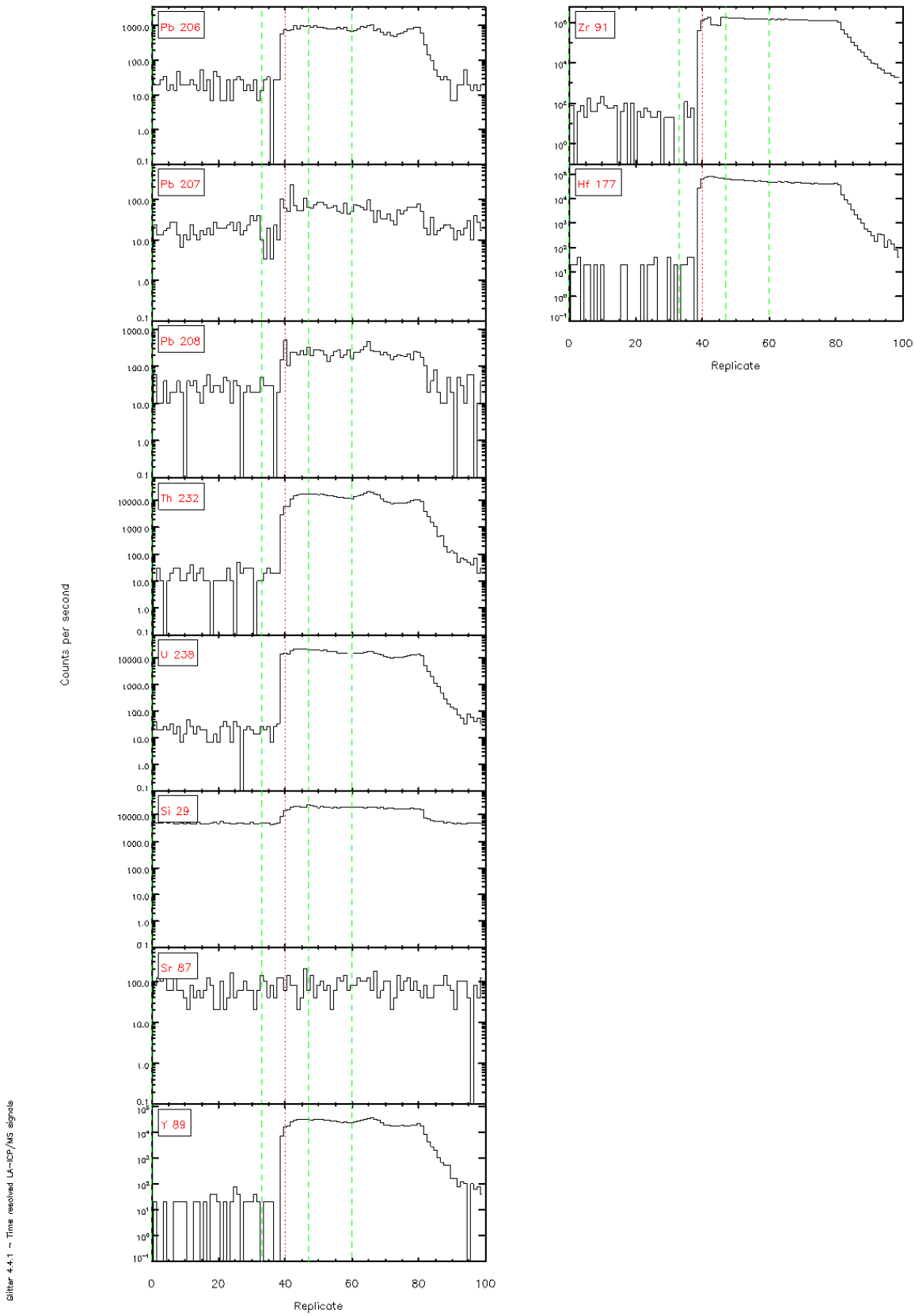
Pb 206
Pb 207
Pb 208
Th 232
U 238
Si 29
Sr 87
Y 89
Zr 91
Hf 177
Counts per second
Replicate
Glitter 4.4.1 - Time resolved LA-ICP/MS signals

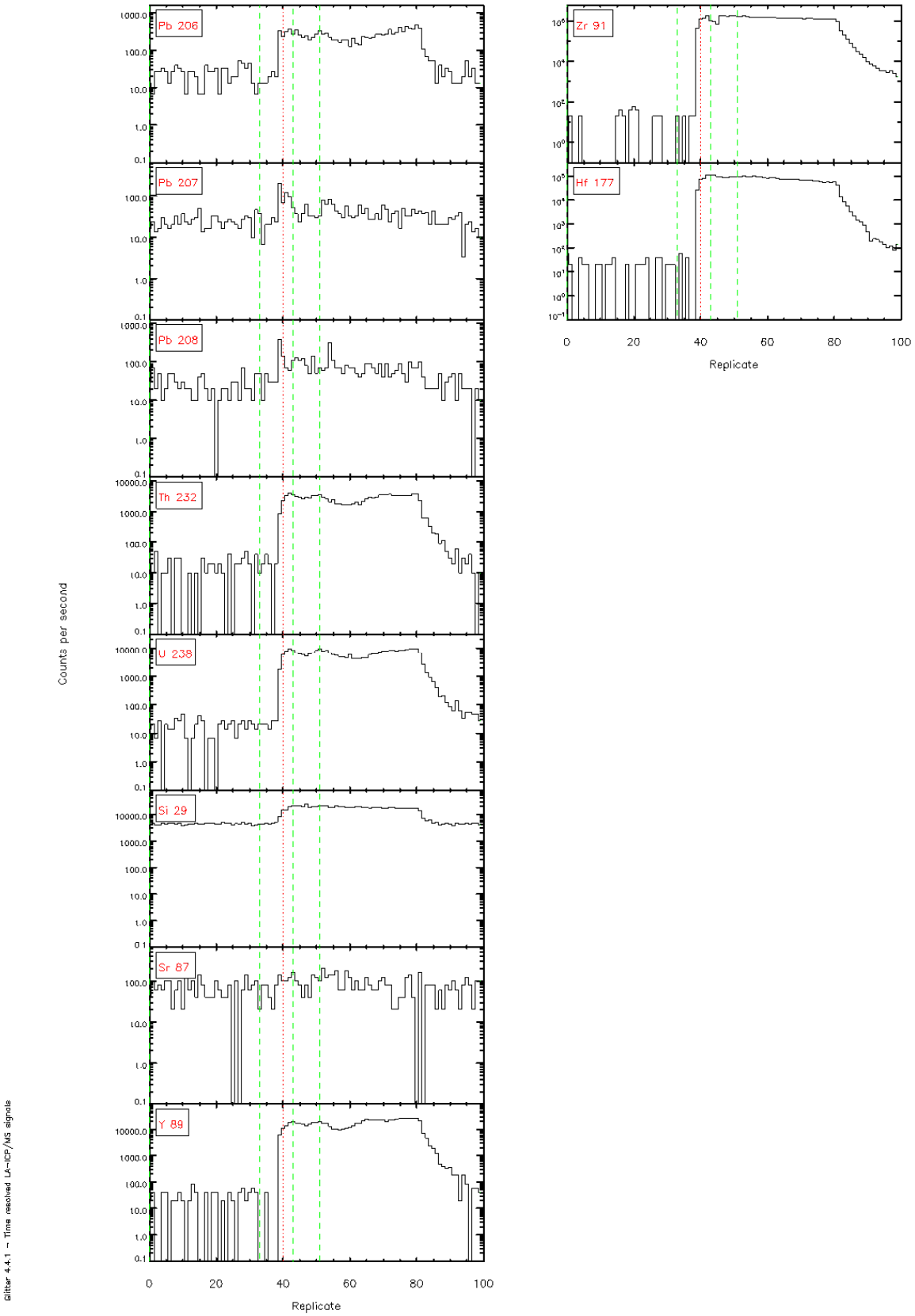
Pb 206
Pb 207
Pb 208
Th 232
U 238
Si 29
Sr 87
Y 89
Zr 91
Hf 177
Counts per second
Replicate
Glitter 4.4.1 - Time resolved LA-ICP/MS signals

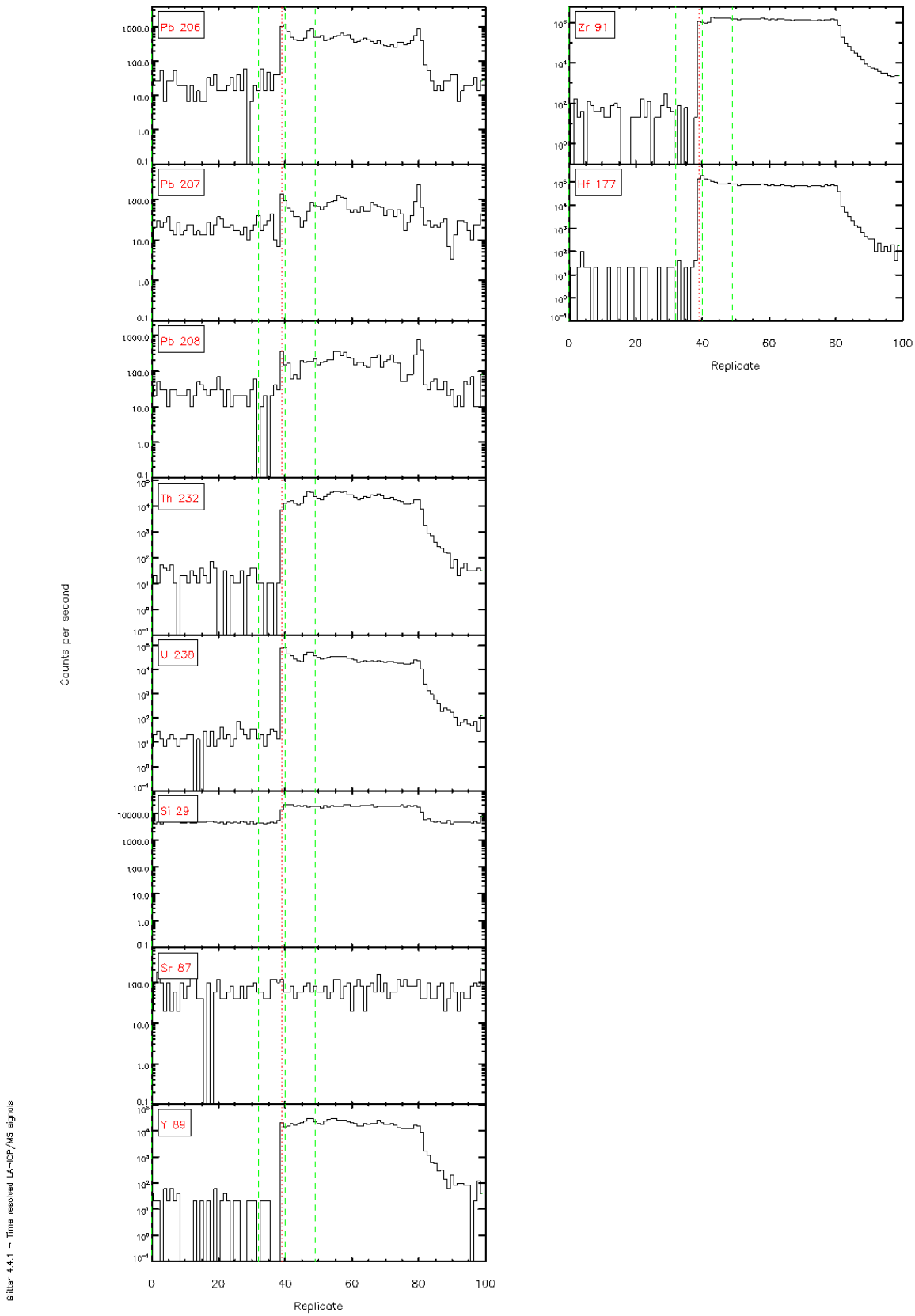
Pb 206
Pb 207
Pb 208
Th 232
U 238
Si 29
Sr 87
Y 89
Zr 91
Hf 177
Counts per second
Replicate
Glitter 4.4.1 ~ Time resolved LA-ICP/MS signals

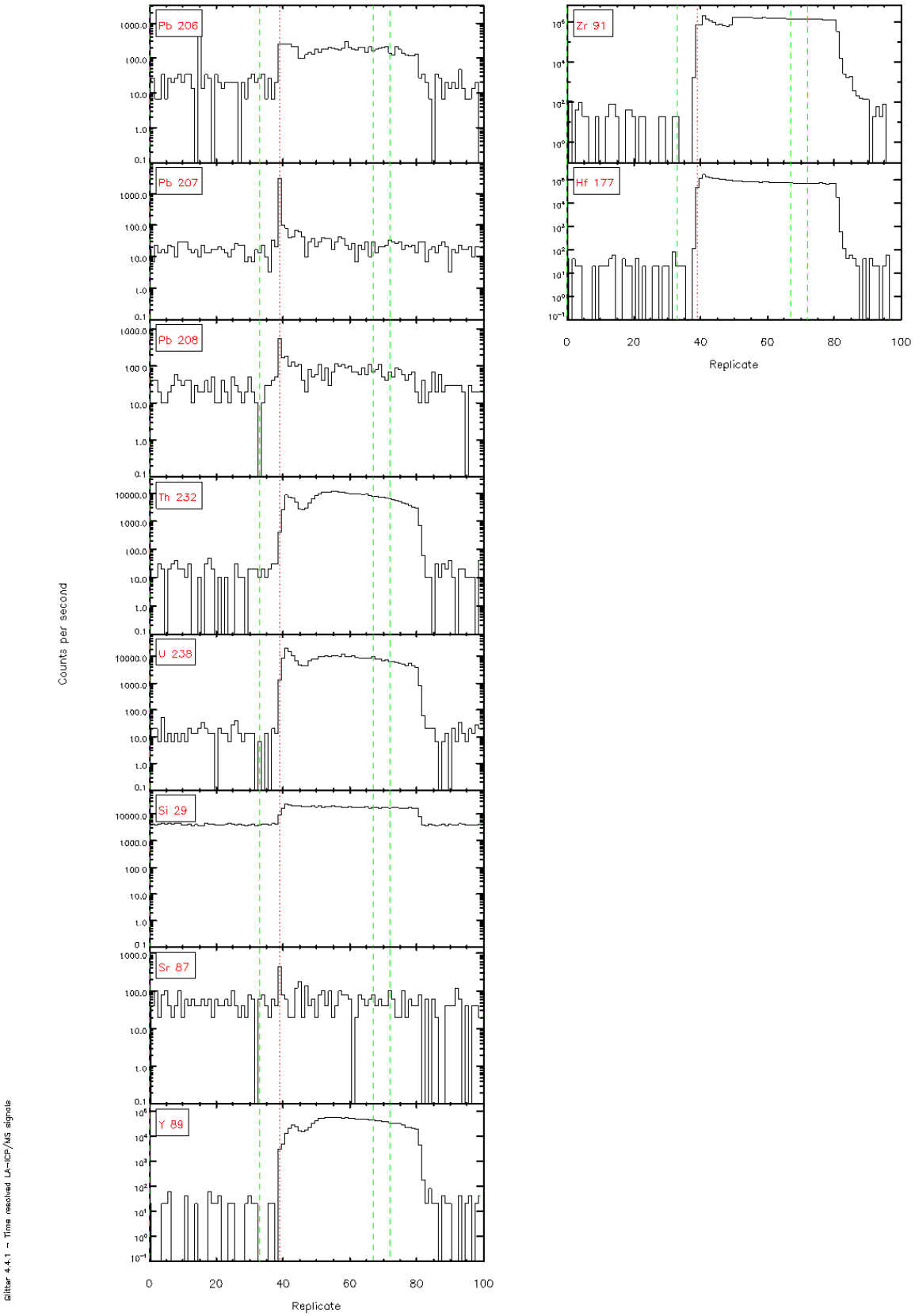
Pb 206
Pb 207
Pb 208
Th 232
U 238
Si 29
Sr 87
Y 89
Zr 91
Hf 177
Counts per second
Replicate
Glitter 4.4.1 - Time resolved LA-ICP/MS signals

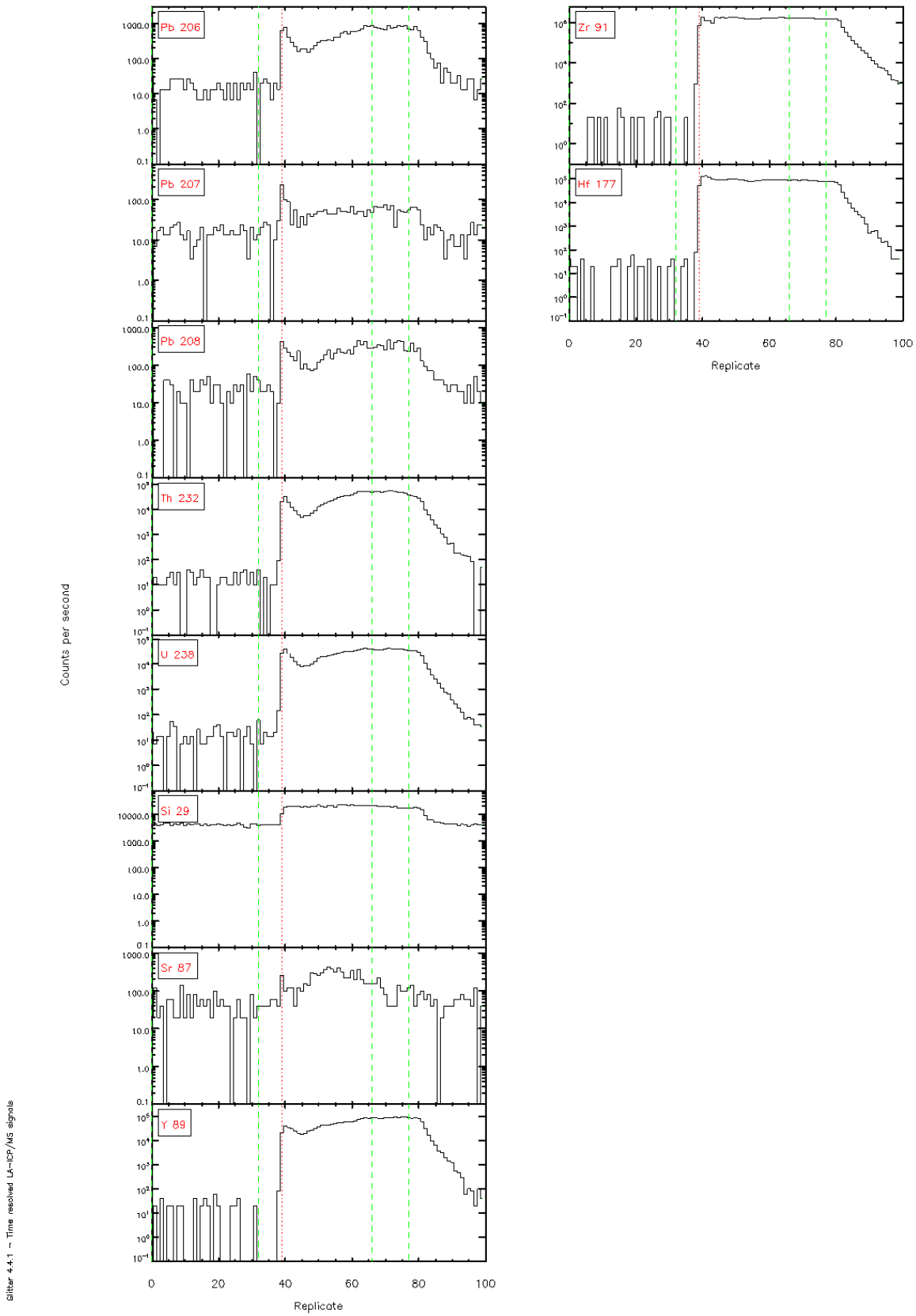
Pb 206
Pb 207
Pb 208
Th 232
U 238
Si 29
Sr 87
Y 89
Zr 91
Hf 177
Counts per second
Replicate
Glitter 4.4.1 - Time resolved LA-ICP/MS signals

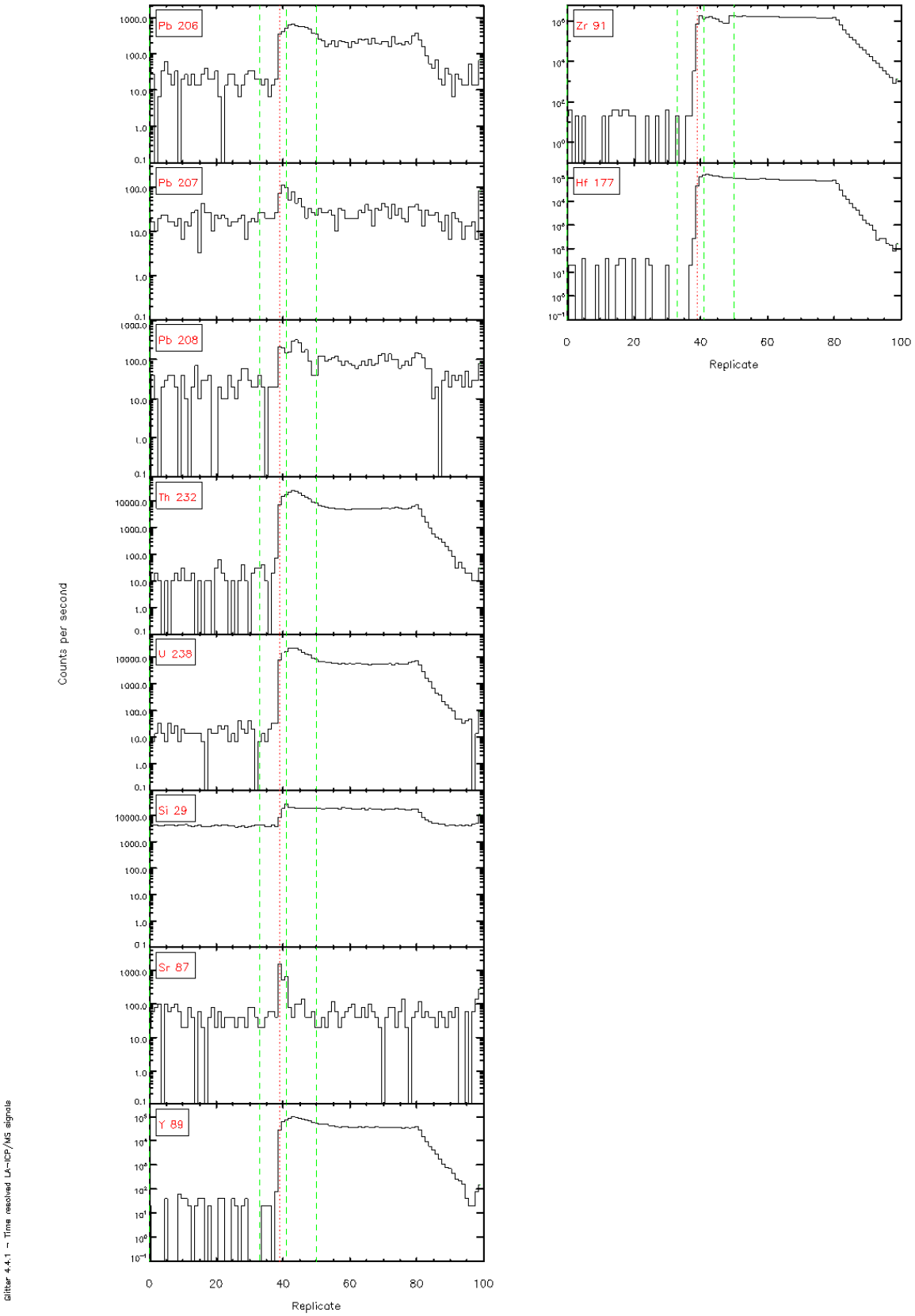
Pb 206
Pb 207
Pb 208
Th 232
U 238
Si 29
Sr 87
Y 89
Zr 91
Hf 177
Counts per second
Replicate
Glitter 4.4.1 - Time resolved LA-ICP/MS signals

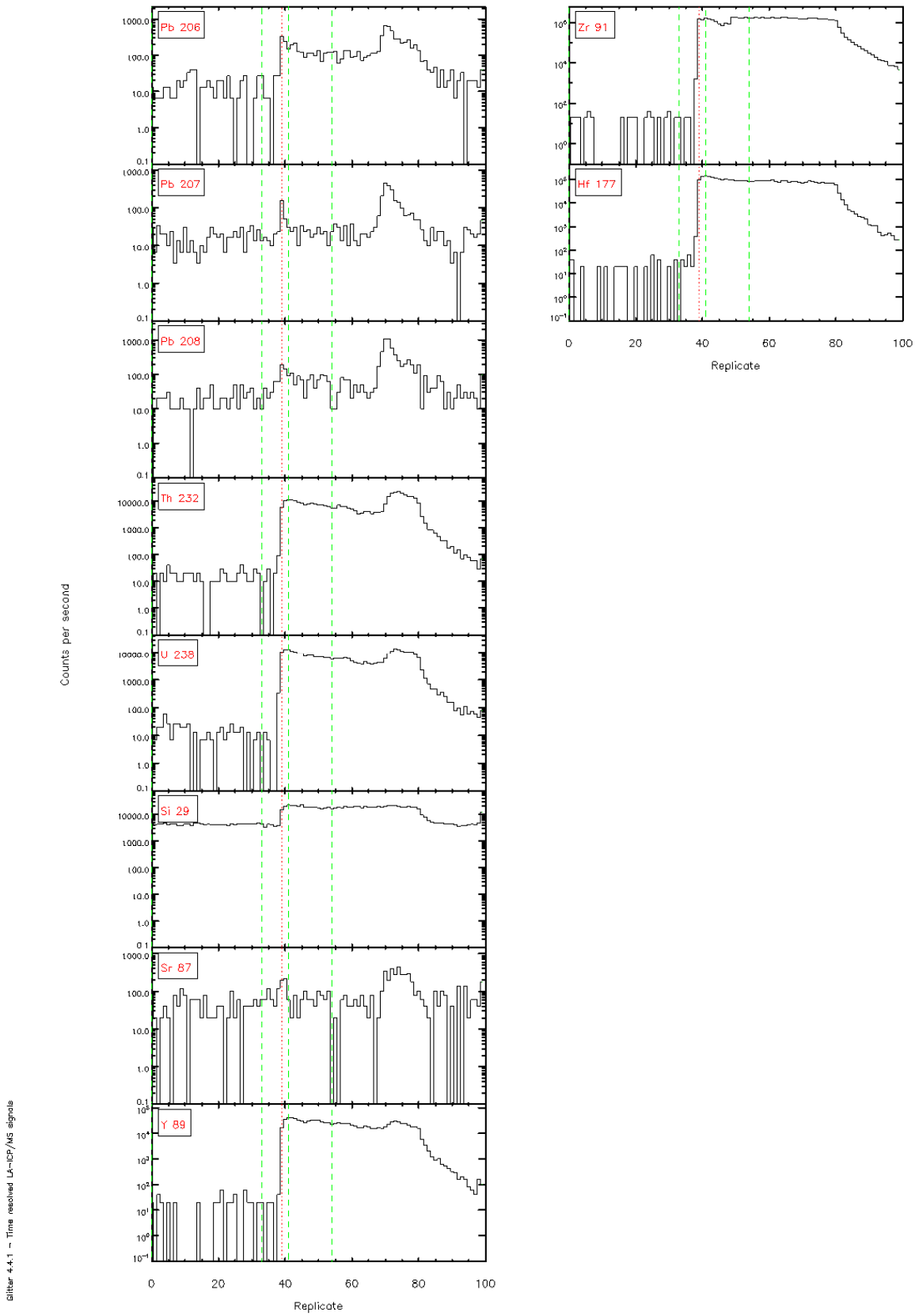
Pb 206
Pb 207
Pb 208
Th 232
U 238
Si 29
Sr 87
Y 89
Zr 91
Hf 177
Counts per second
Replicate
Glitter 4.4.1 ~ Time resolved LA-ICP/MS signals

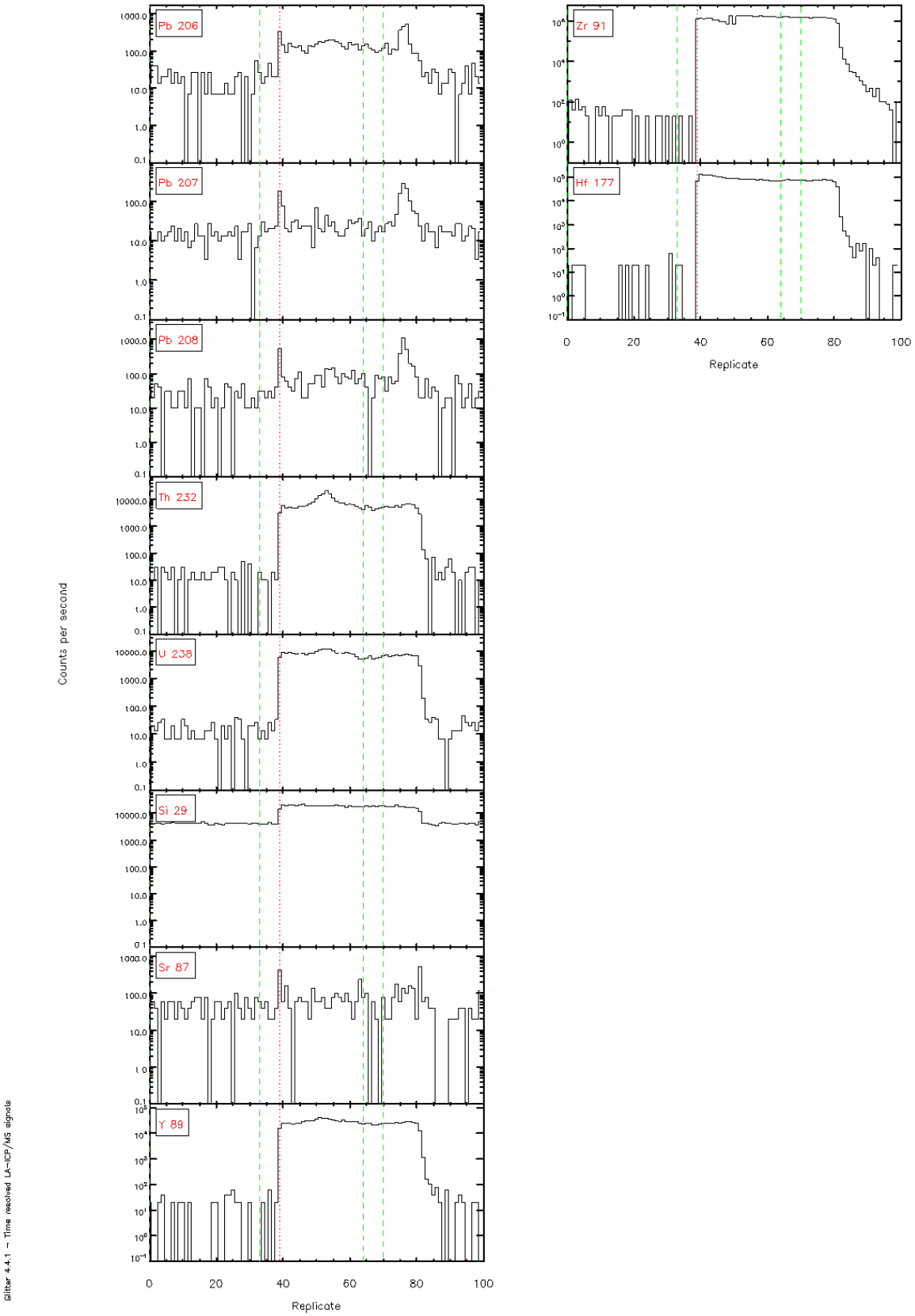
Pb 206
Pb 207
Pb 208
Th 232
U 238
Si 29
Sr 87
Y 89
Zr 91
Hf 177
Counts per second
Replicate
Glitter 4.4.1 - Time resolved LA-ICP/MS signals

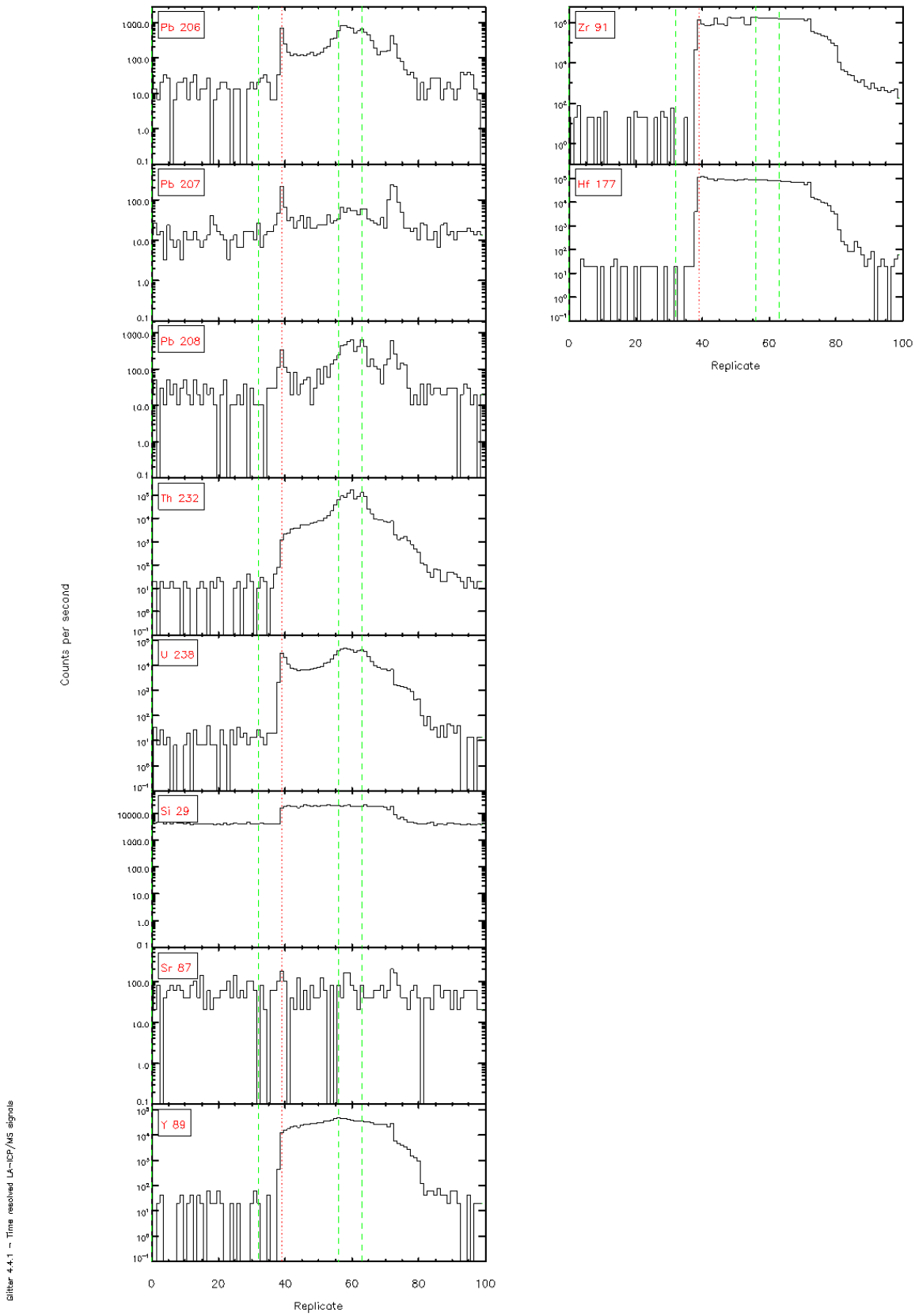
Pb 206
Pb 207
Pb 208
Th 232
U 238
Si 29
Sr 87
Y 89
Zr 91
Hf 177
Counts per second
Replicate
Glitter 4.4.1 ~ Time resolved LA-ICP/MS signals

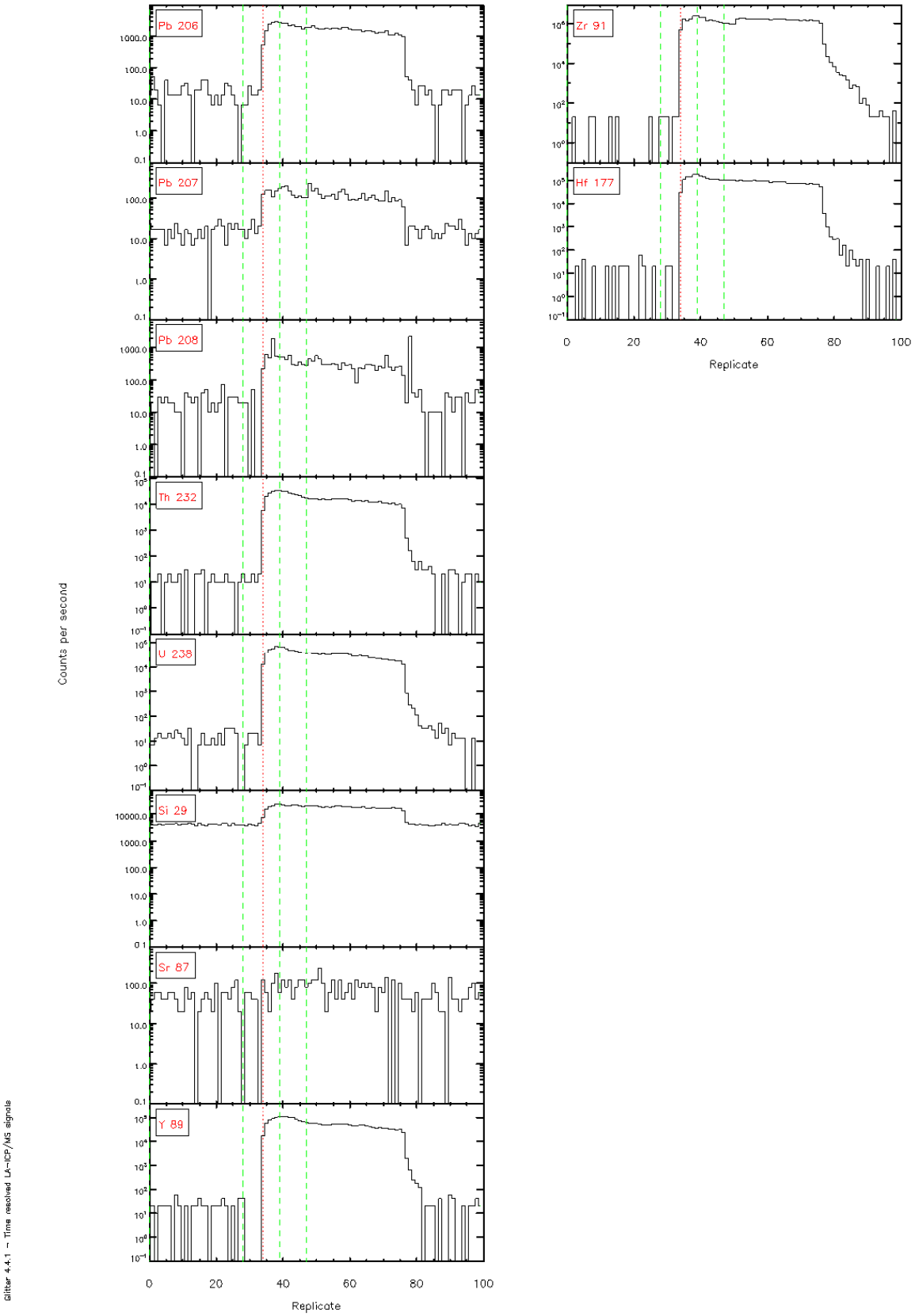
Pb 206
Pb 207
Pb 208
Th 232
U 238
Si 29
Sr 87
Y 89
Zr 91
Hf 177
Counts per second
Replicate
Glitter 4.4.1 - Time resolved LA-ICP/MS signals

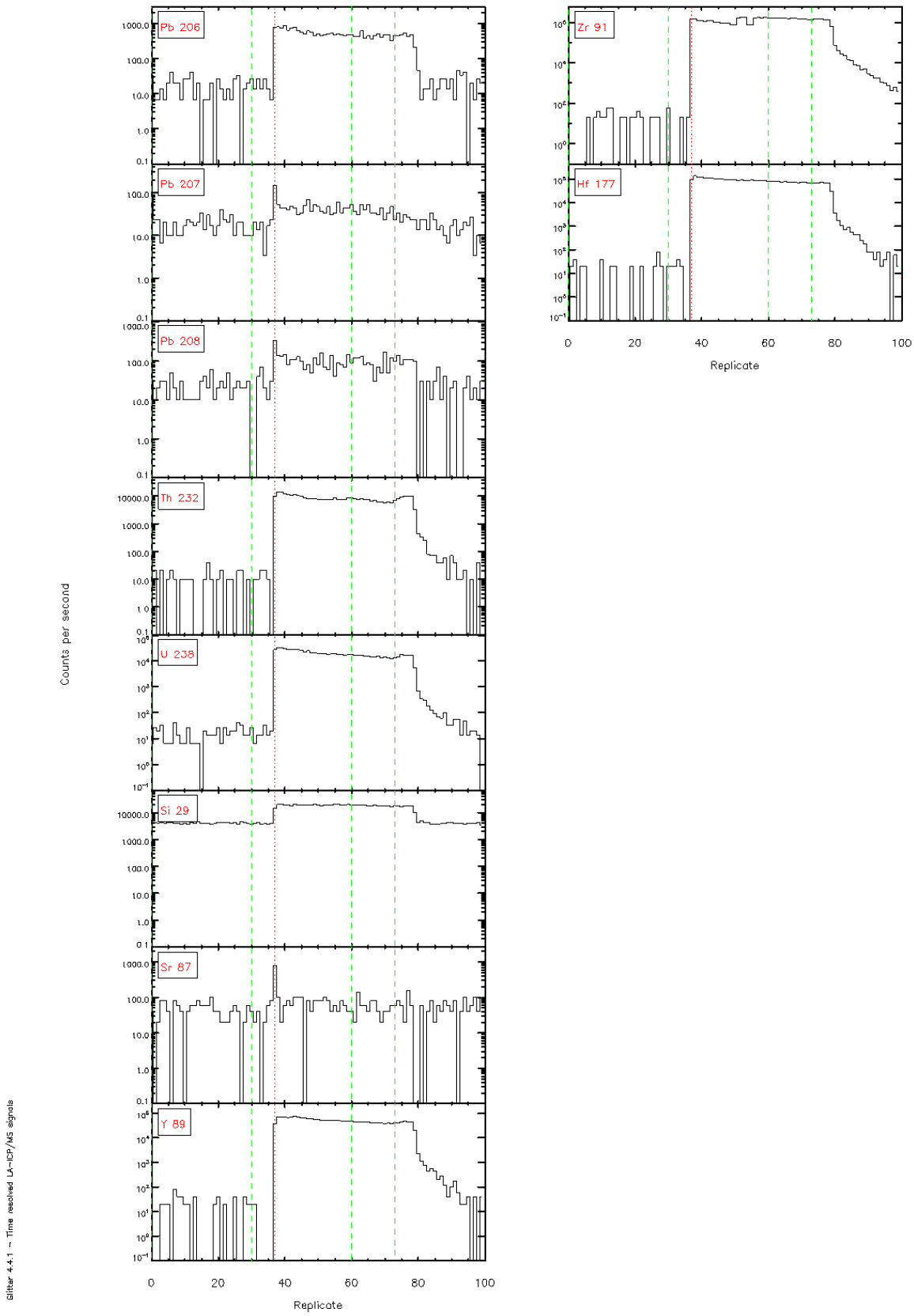
Pb 206
Pb 207
Pb 208
Th 232
U 238
Si 29
Sr 87
Y 89
Zr 91
Hf 177
Counts per second
Replicate
Glitter 4.4.1 - Time resolved LA-ICP/MS signals

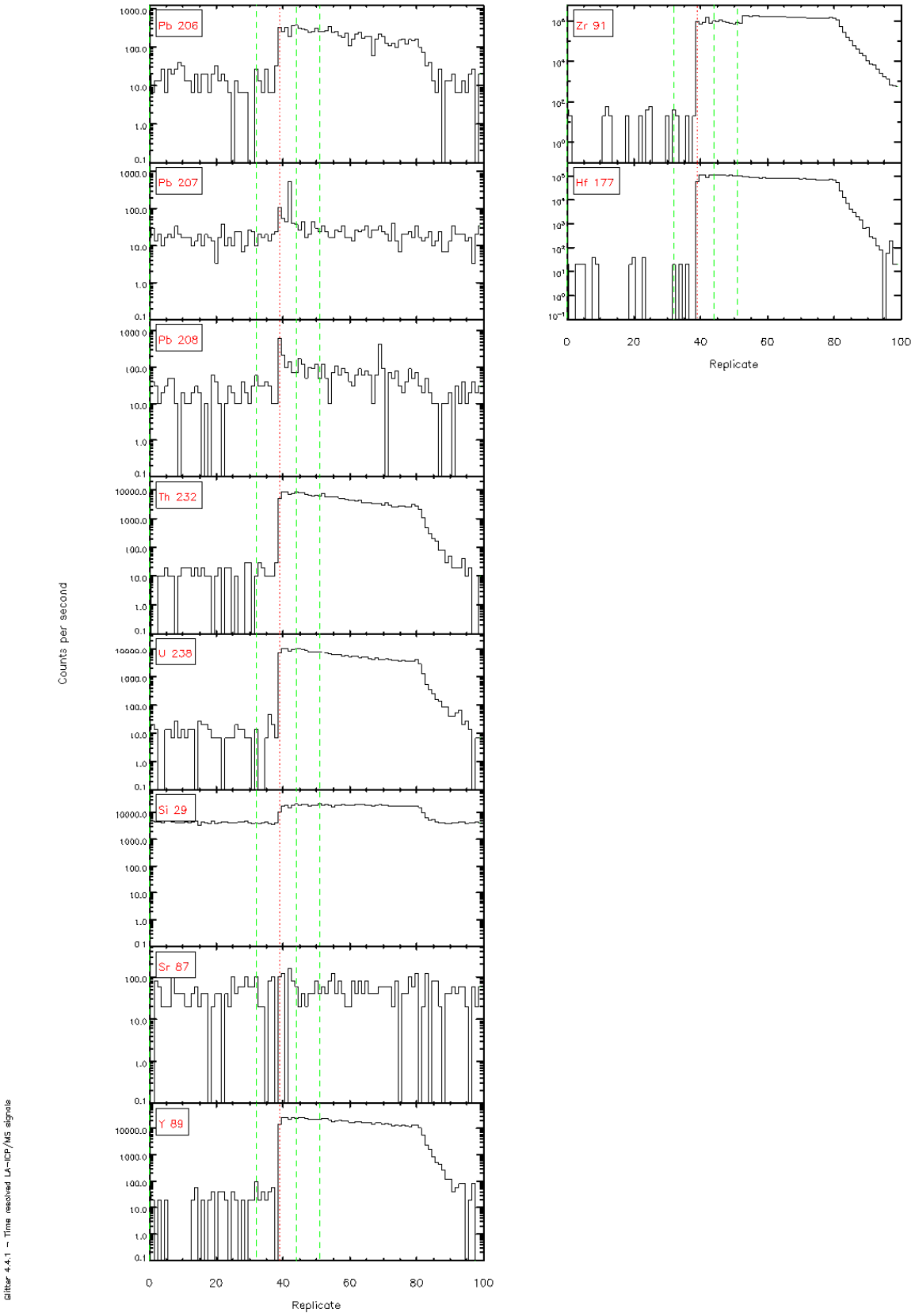
Pb 206
Pb 207
Pb 208
Th 232
U 238
Si 29
Sr 87
Y 89
Zr 91
Hf 177
Counts per second
Replicate
Glitter 4.4.1 - Time resolved LA-ICP/MS signals

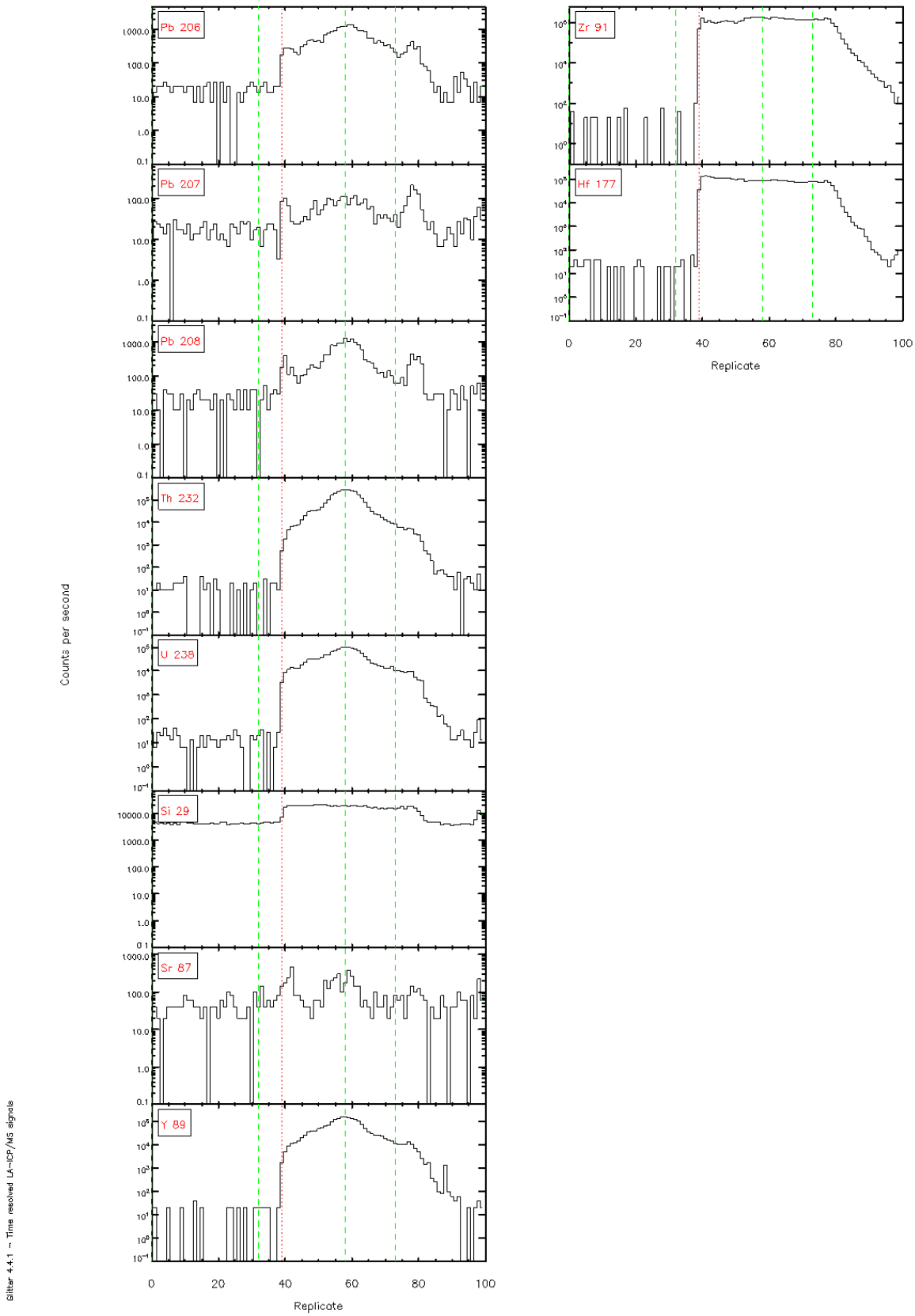
Pb 206
Pb 207
Pb 208
Th 232
U 238
Si 29
Sr 87
Y 89
Zr 91
Hf 177
Counts per second
Replicate
Glitter 4.4.1 - Time resolved LA-ICP/MS signals

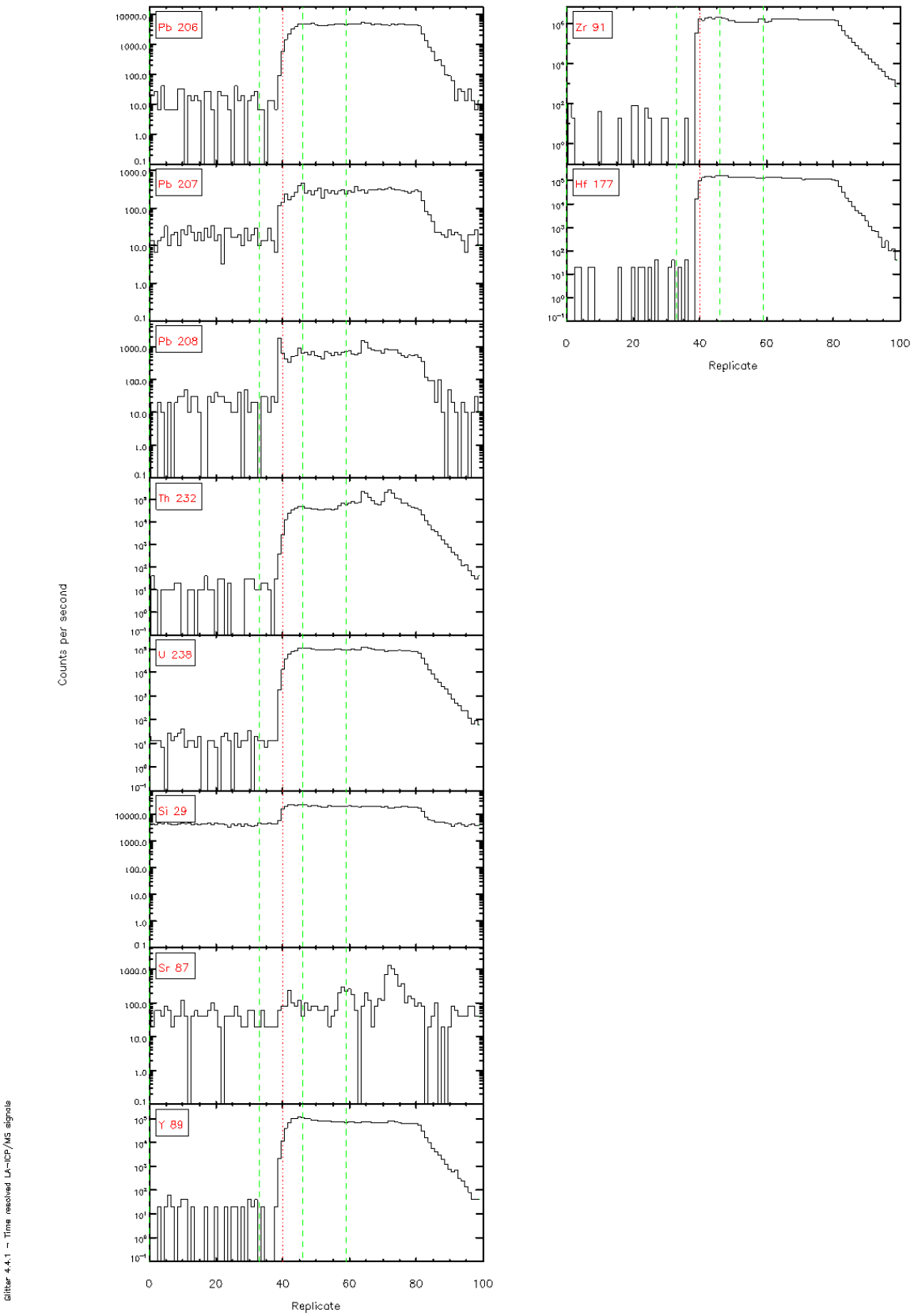
Pb 206
Pb 207
Pb 208
Th 232
U 238
Si 29
Sr 87
Y 89
Zr 91
Hf 177
Counts per second
Replicate
Glitter 4.4.1 - Time resolved LA-ICP/MS signals

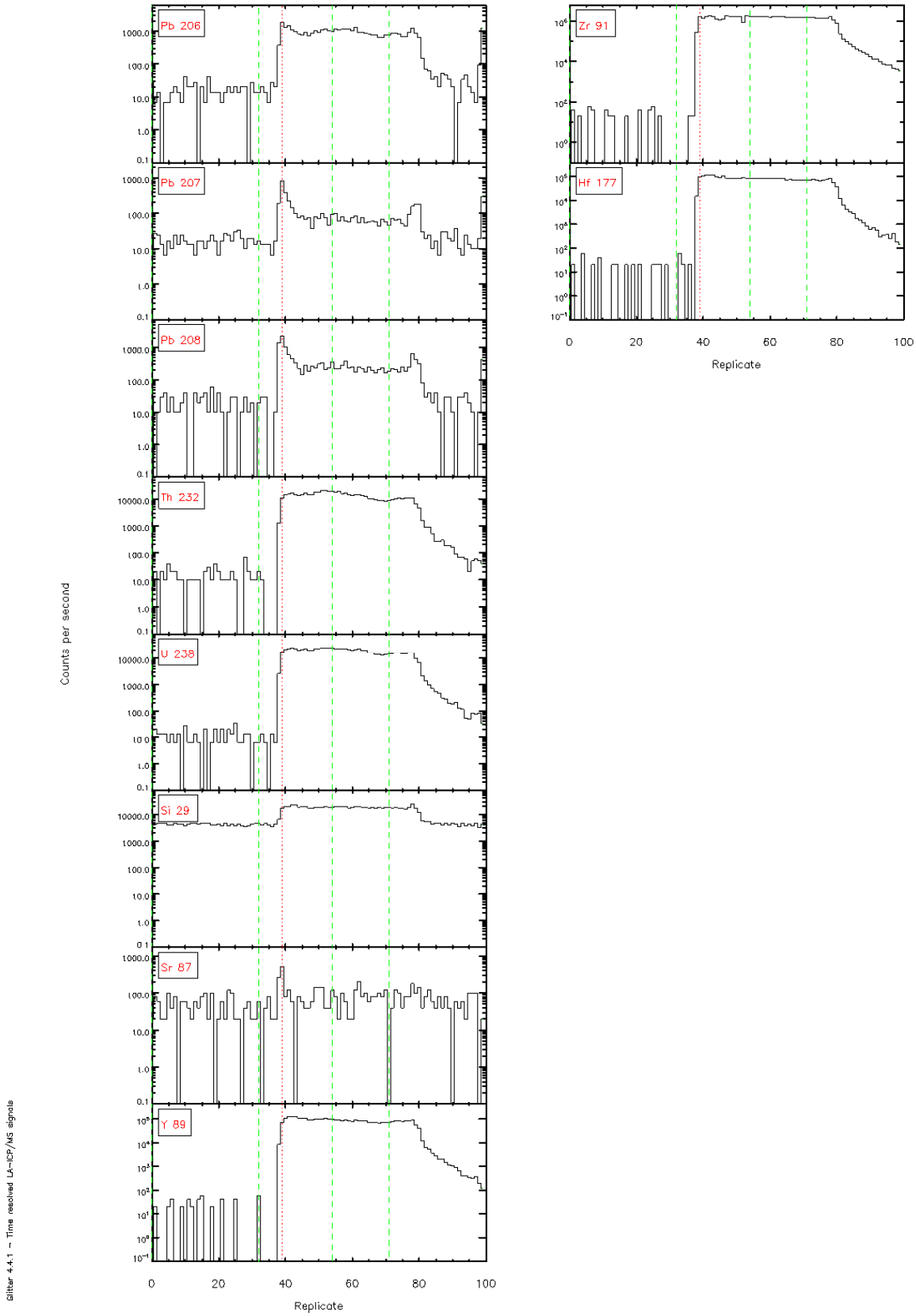
Pb 206
Pb 207
Pb 208
Th 232
U 238
Si 29
Sr 87
Y 89
Zr 91
Hf 177
Counts per second
Replicate
Glitter 4.4.1 - Time resolved LA-ICP/MS signals

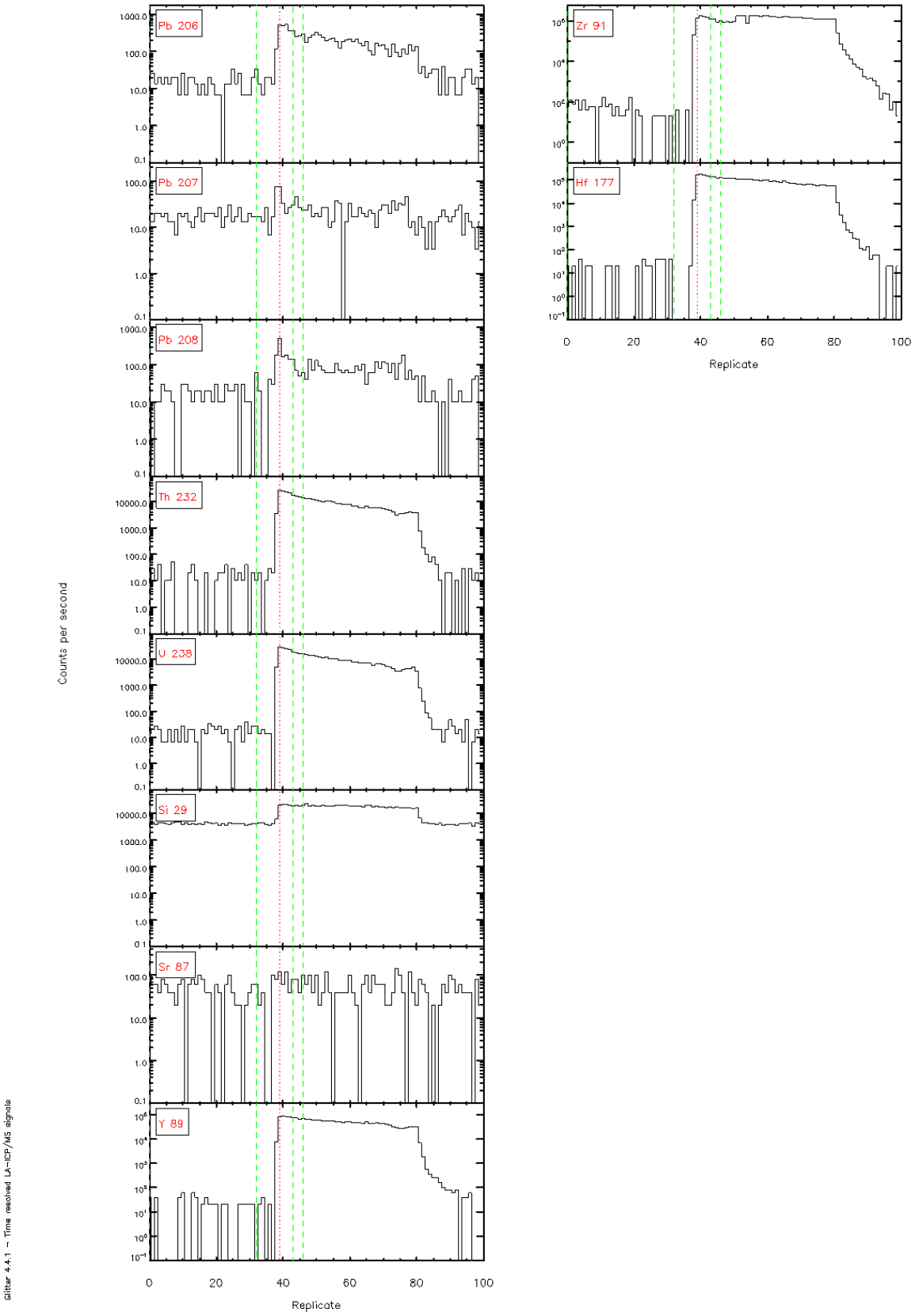
Pb 206
Pb 207
Pb 208
Th 232
U 238
Si 29
Sr 87
Y 89
Zr 91
Hf 177
Counts per second
Replicate
Glitter 4.4.1 - Time resolved LA-ICP/MS signals

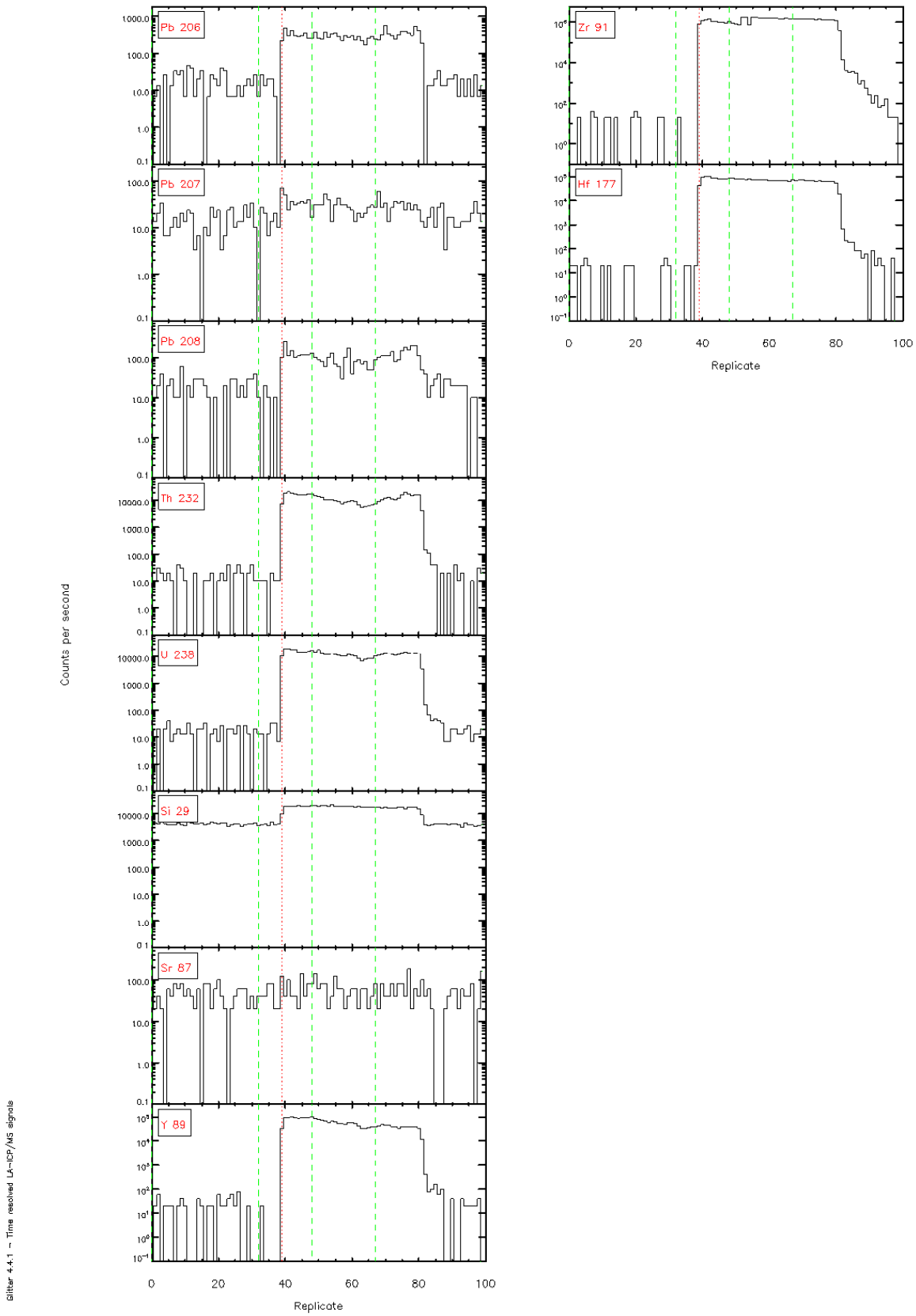
Pb 206
Pb 207
Pb 208
Th 232
U 238
Si 29
Sr 87
Y 89
Zr 91
Hf 177
Counts per second
Replicate
Glitter 4.4.1 - Time resolved LA-ICP/MS signals

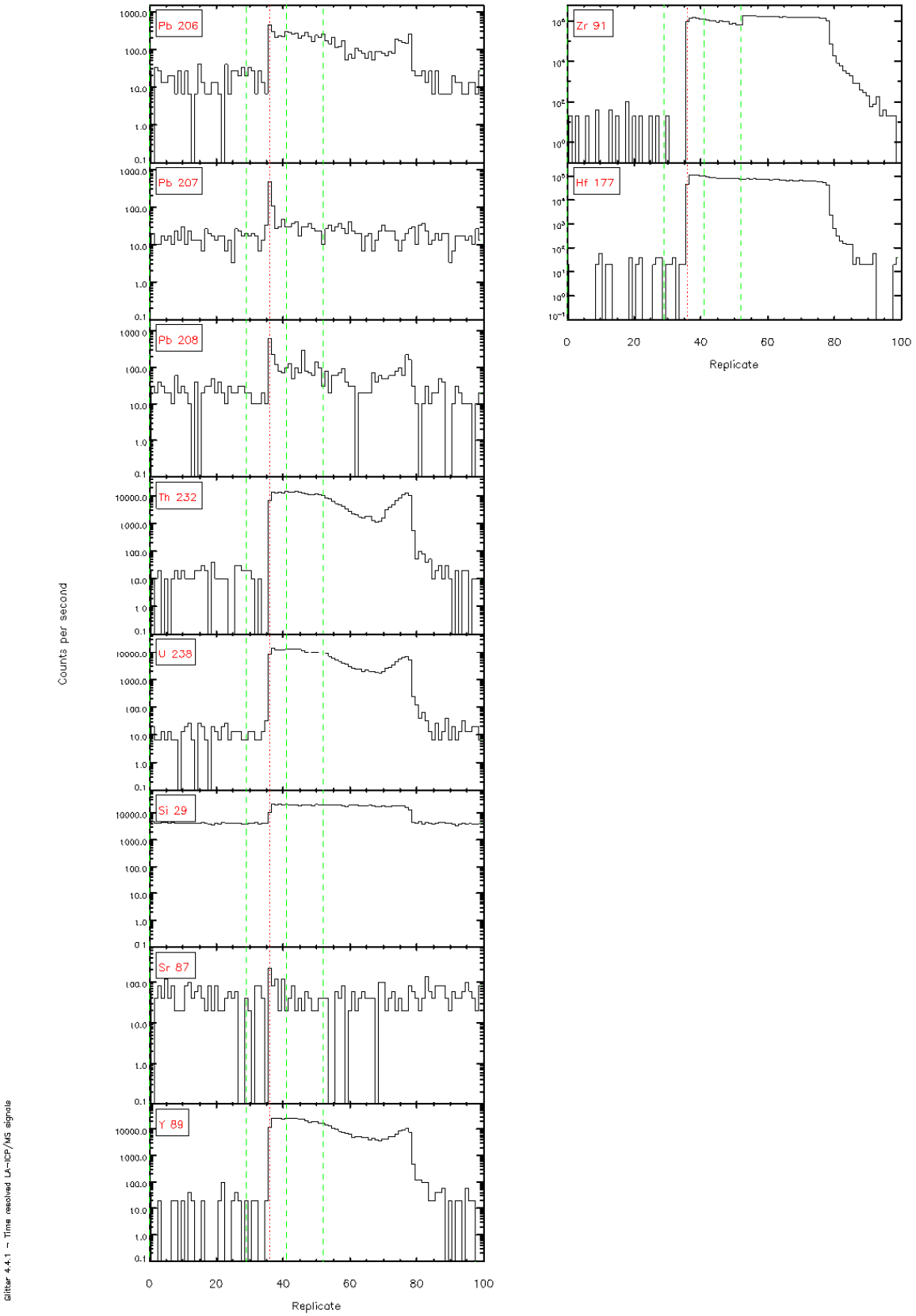
Pb 206
Pb 207
Pb 208
Th 232
U 238
Si 29
Sr 87
Y 89
Zr 91
Hf 177
Counts per second
Replicate
Glitter 4.4.1 - Time resolved LA-ICP/MS signals

14 – Tariki Sandstone

1.

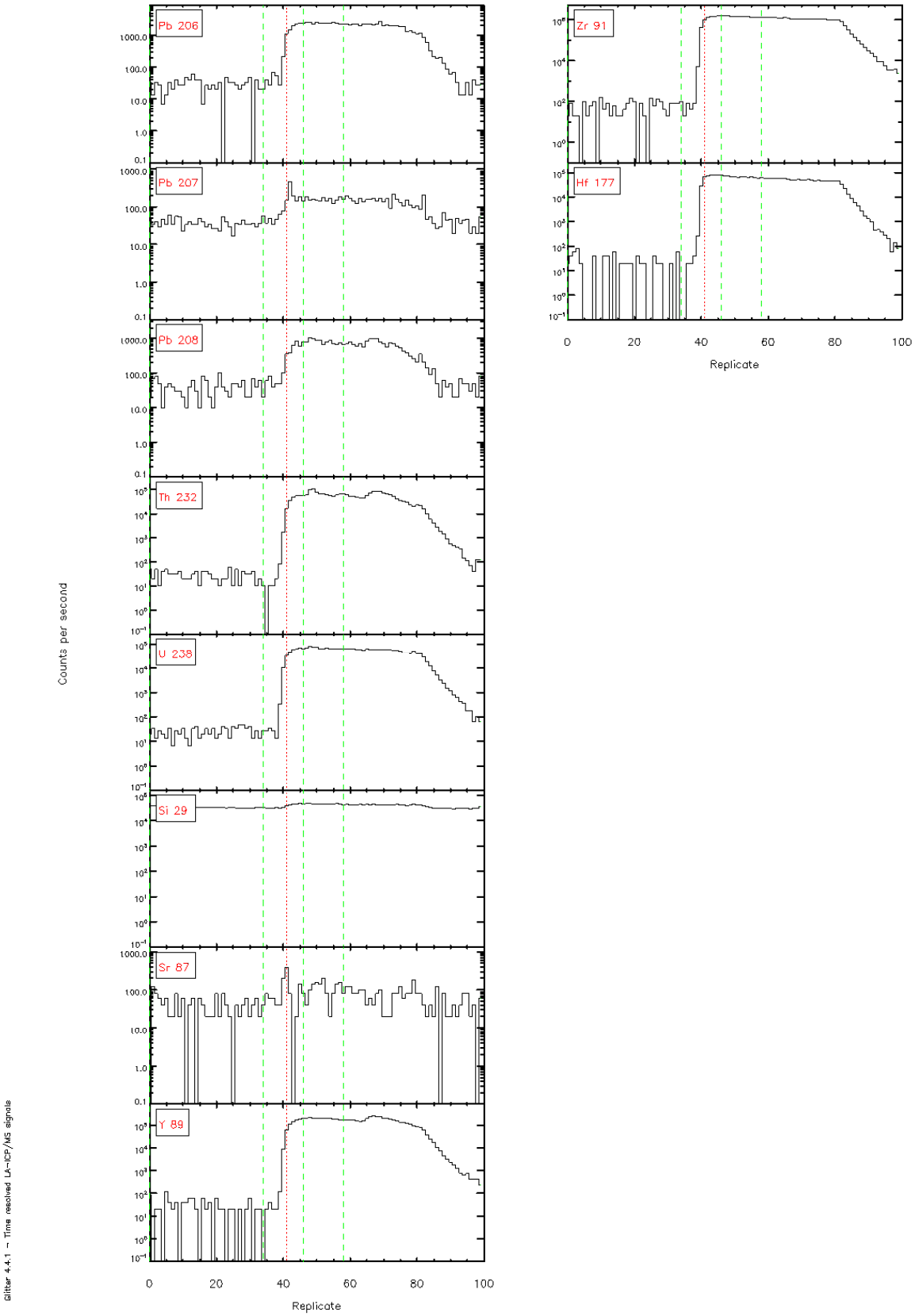

2.

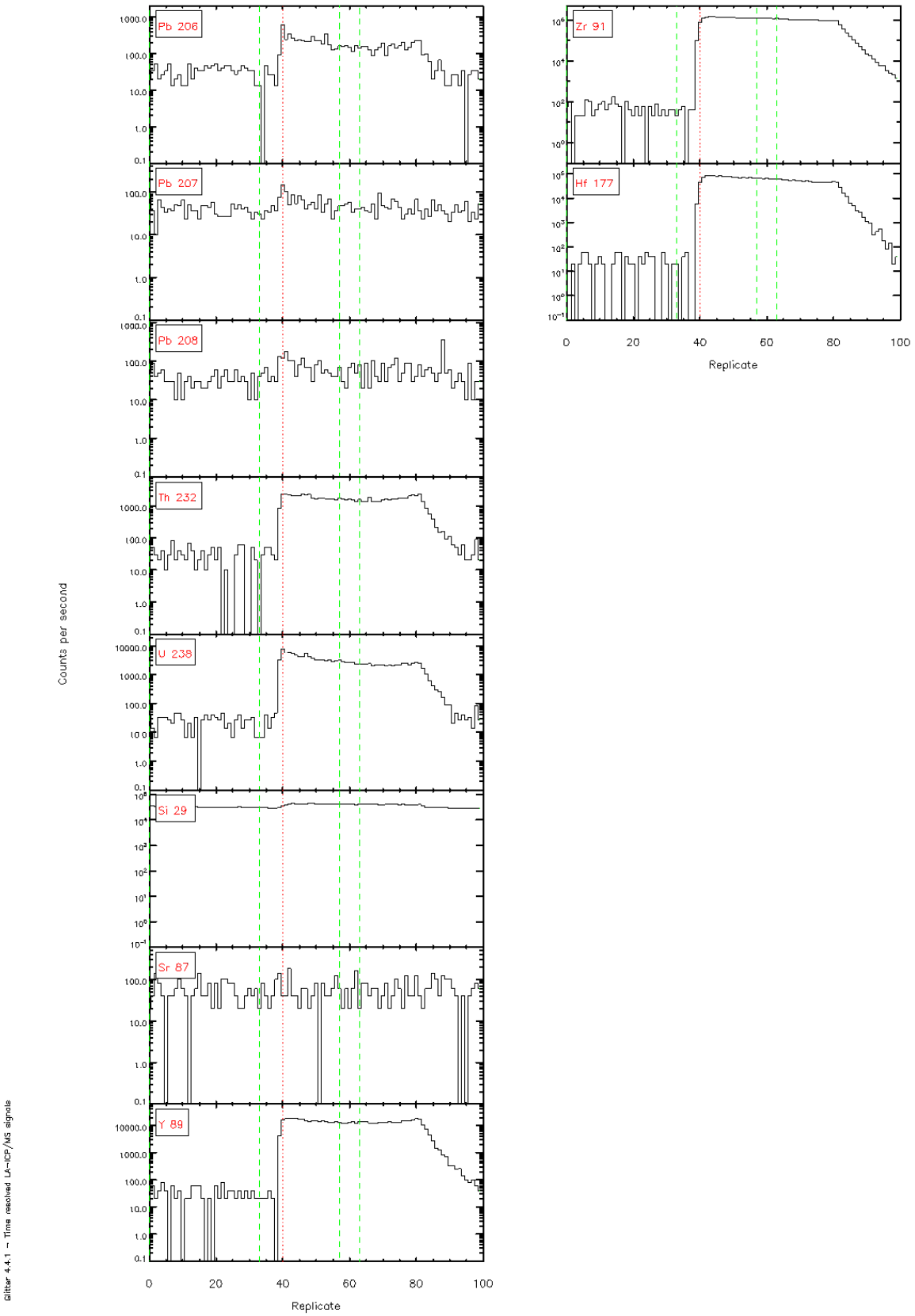
Pb 206
Pb 207
Pb 208
Th 232
U 238
Si 29
Sr 87
Y 89
Zr 91
Hf 177
Counts per second
Replicate
Glitter 4.4.1 - Time resolved LA-ICP/MS signals

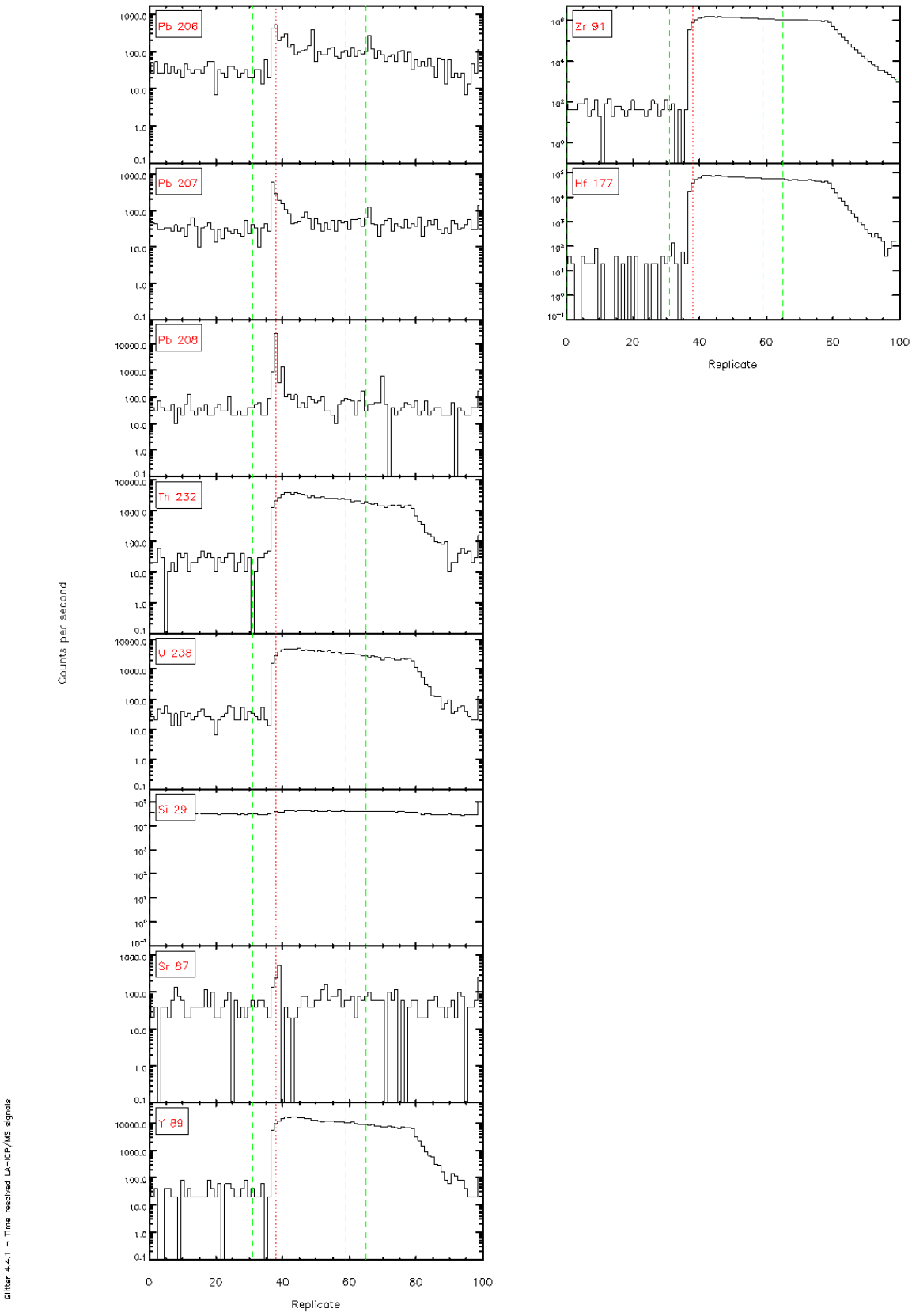
Pb 206
Pb 207
Pb 208
Th 232
U 238
Si 29
Sr 87
Y 89
Zr 91
Hf 177
Counts per second
Replicate
Glitter 4.4.1 - Time resolved LA-ICP/MS signals

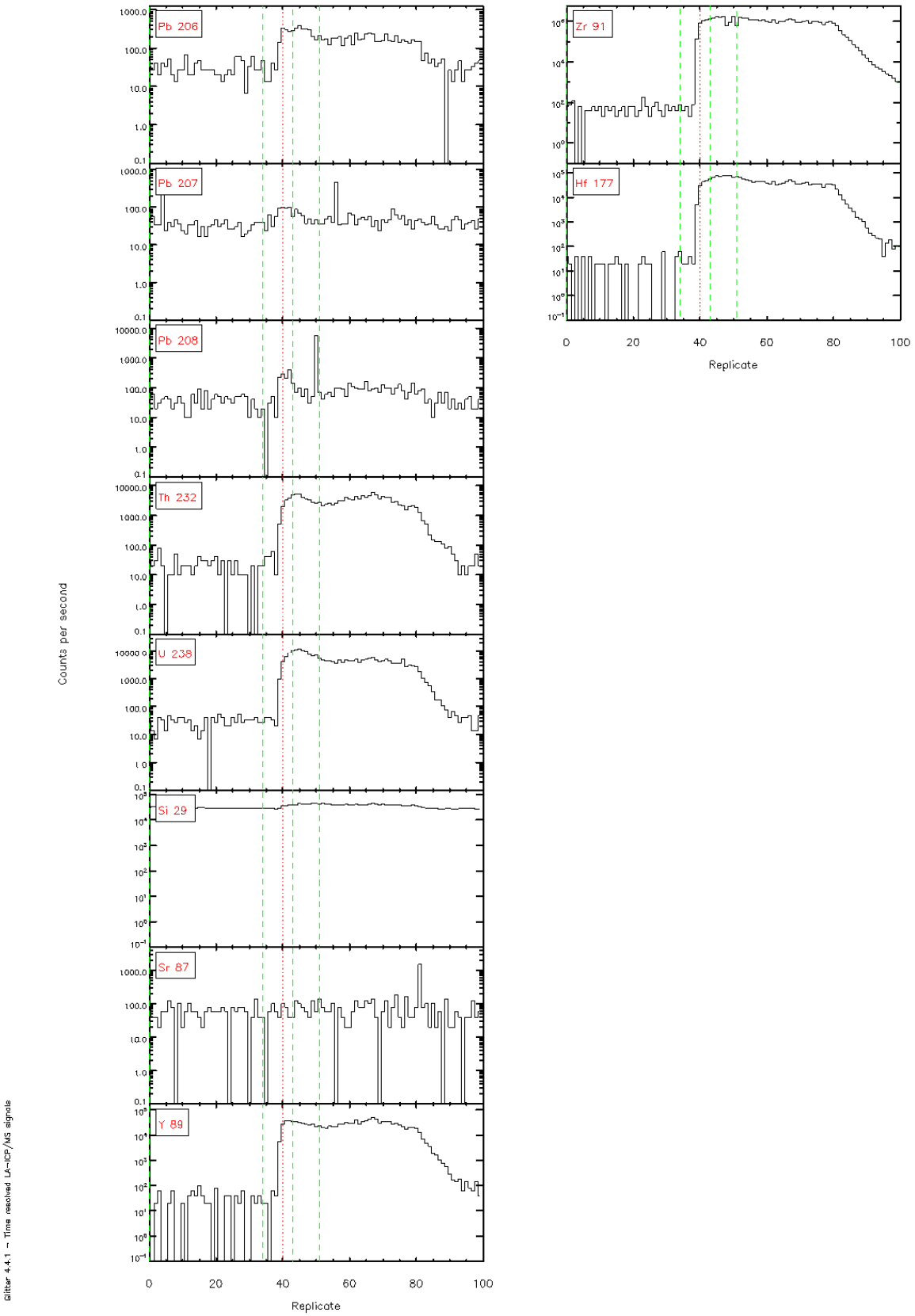
Pb 206
Pb 207
Pb 208
Th 232
U 238
Si 29
Sr 87
Y 89
Zr 91
Hf 177
Counts per second
Replicate
Glitter 4.4.1 - Time resolved LA-ICP/MS signals

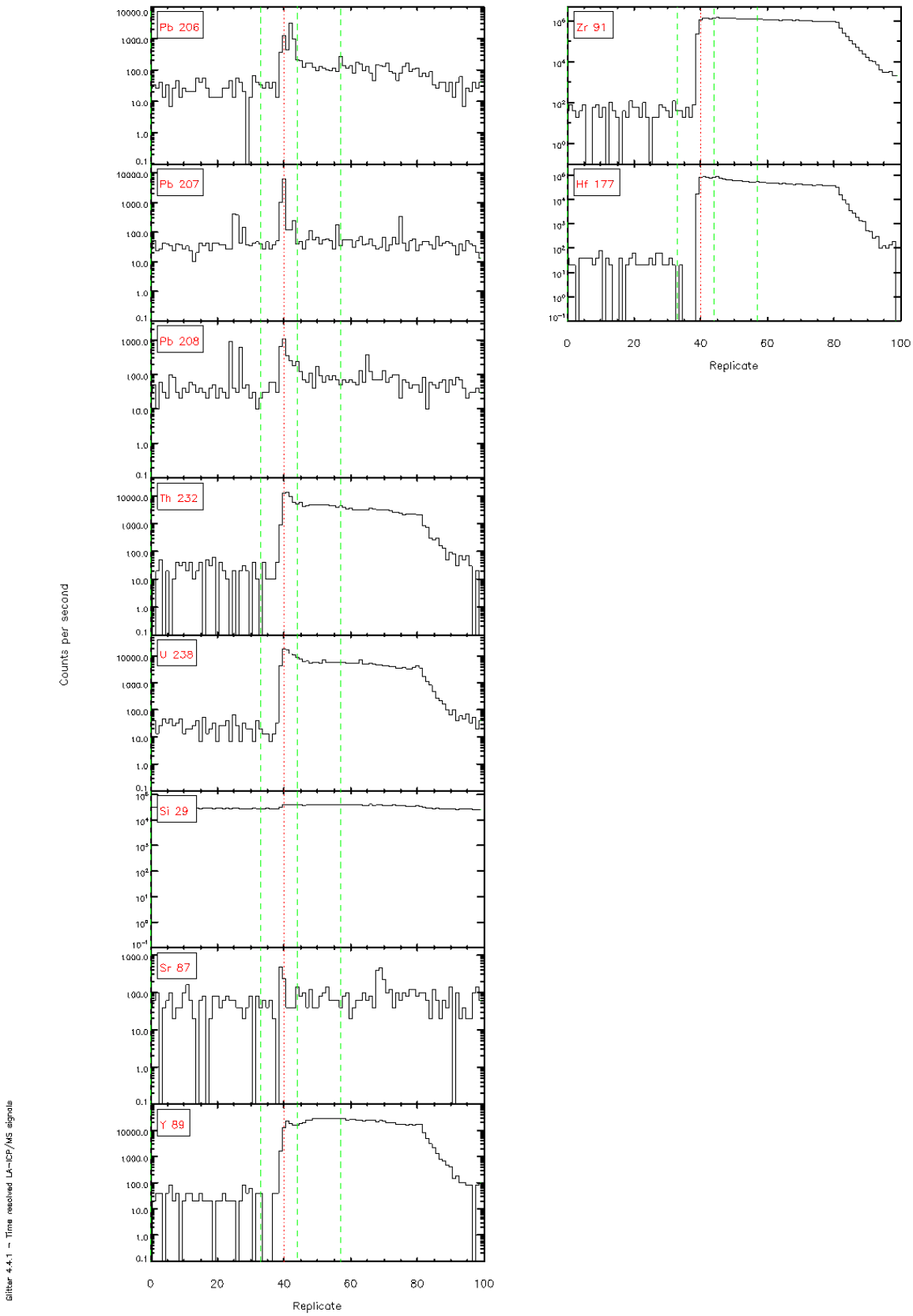
Pb 206
Pb 207
Pb 208
Th 232
U 238
Si 29
Sr 87
Y 89
Zr 91
Hf 177
Counts per second
Replicate
Glitter 4.4.1 – Time resolved LA-ICP/MS signals

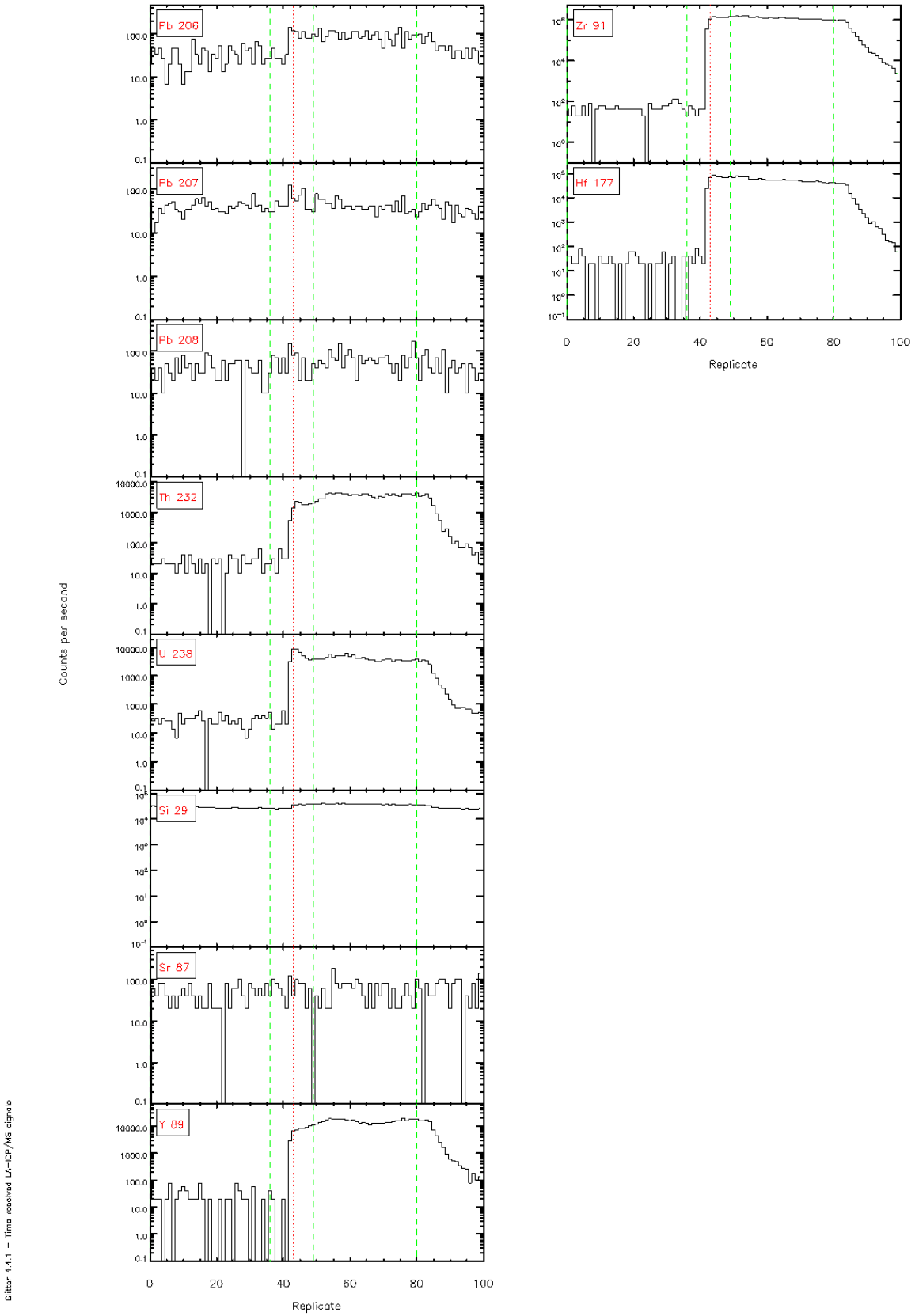
Pb 206
Pb 207
Pb 208
Th 232
U 238
Si 29
Sr 87
Y 89
Zr 91
Hf 177
Counts per second
Replicate
Glitter 4.4.1 – Time resolved LA-ICP/MS signals

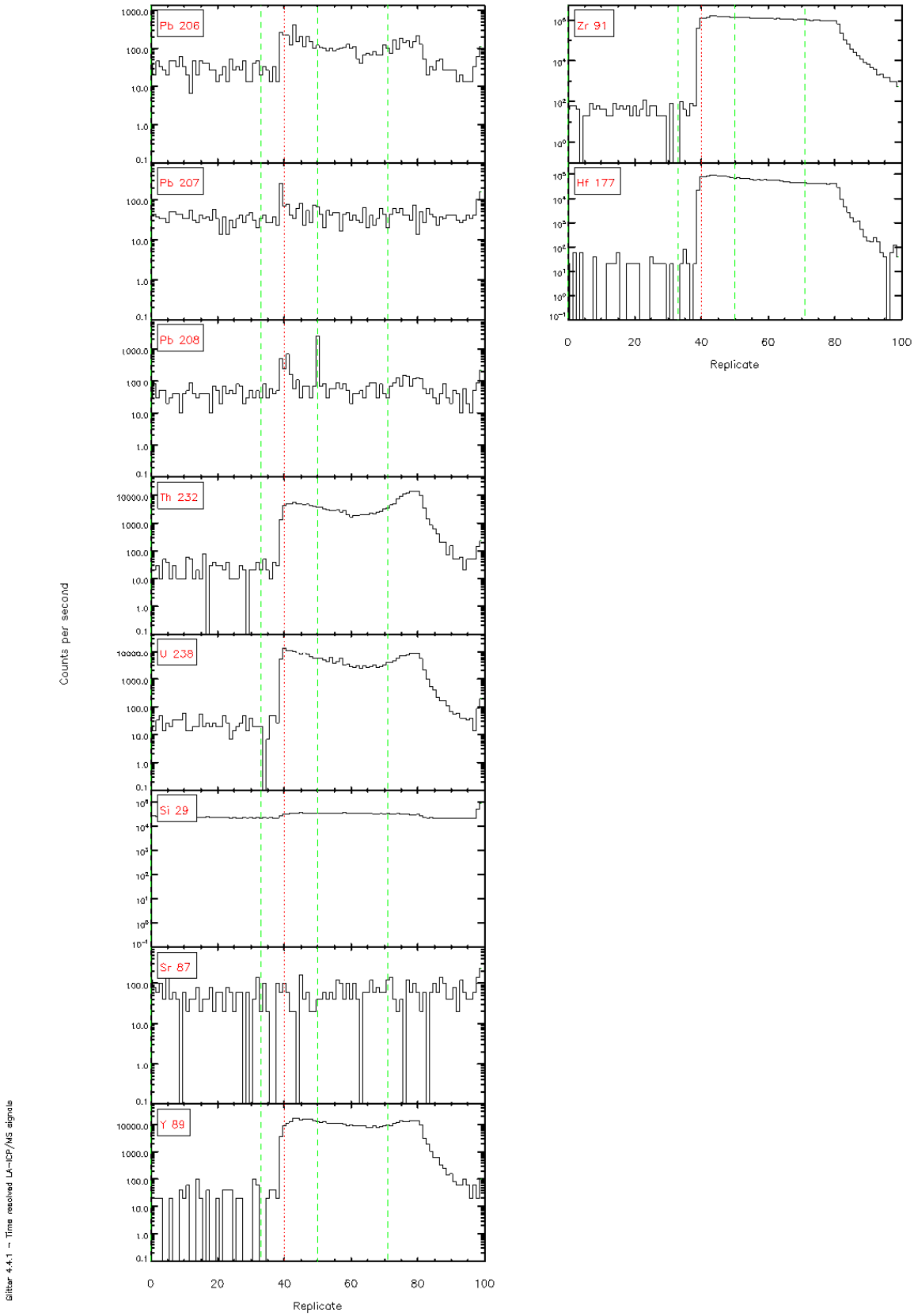
Pb 206
Pb 207
Pb 208
Th 232
U 238
Si 29
Sr 87
Y 89
Zr 91
Hf 177
Counts per second
Replicate
Glitter 4.4.1 – Time resolved LA-ICP/MS signals

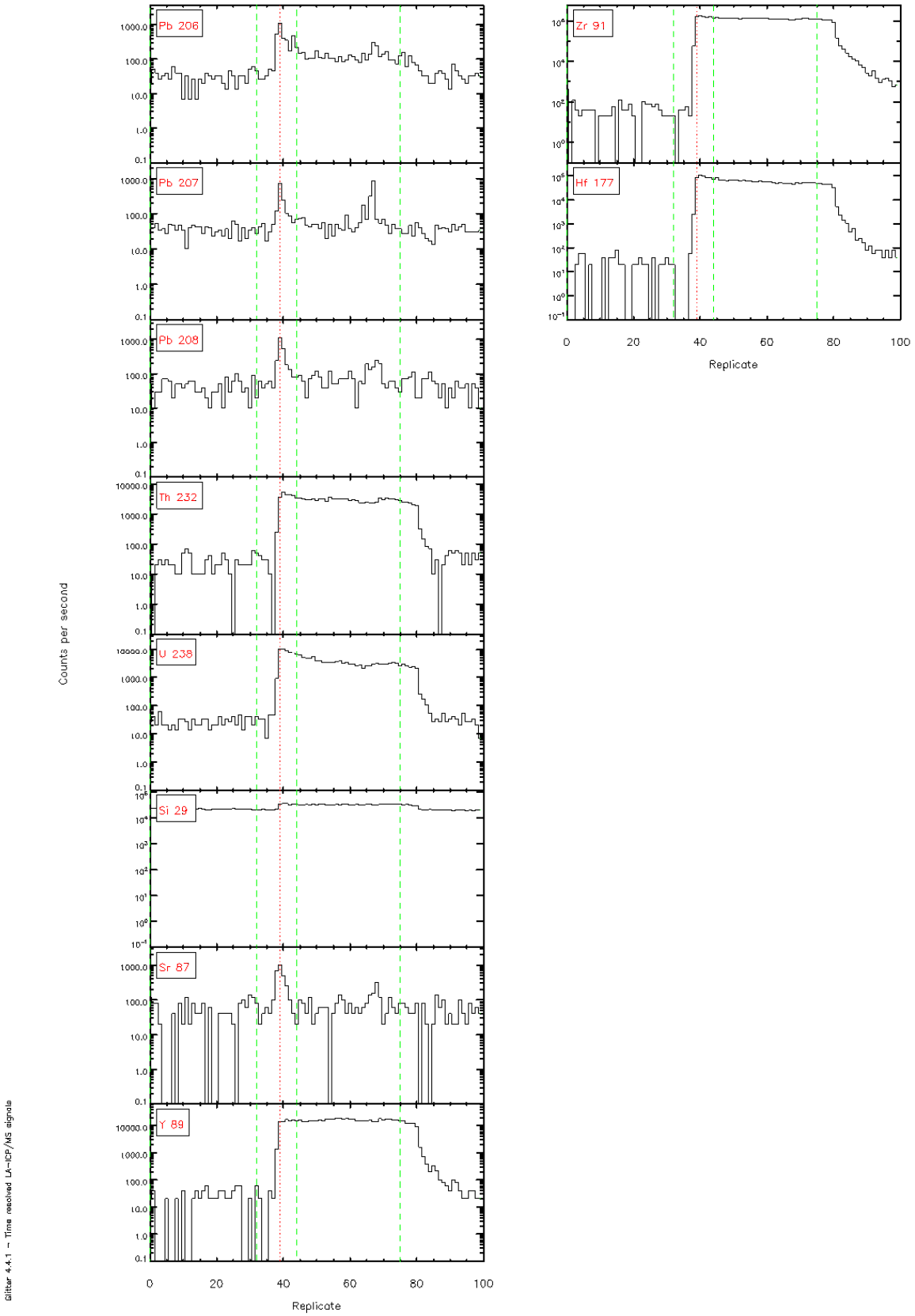
Pb 206
Pb 207
Pb 208
Th 232
U 238
Si 29
Sr 87
Y 89
Zr 91
Hf 177
Counts per second
Replicate
Glitter 4.4.1 – Time resolved LA-ICP/MS signals

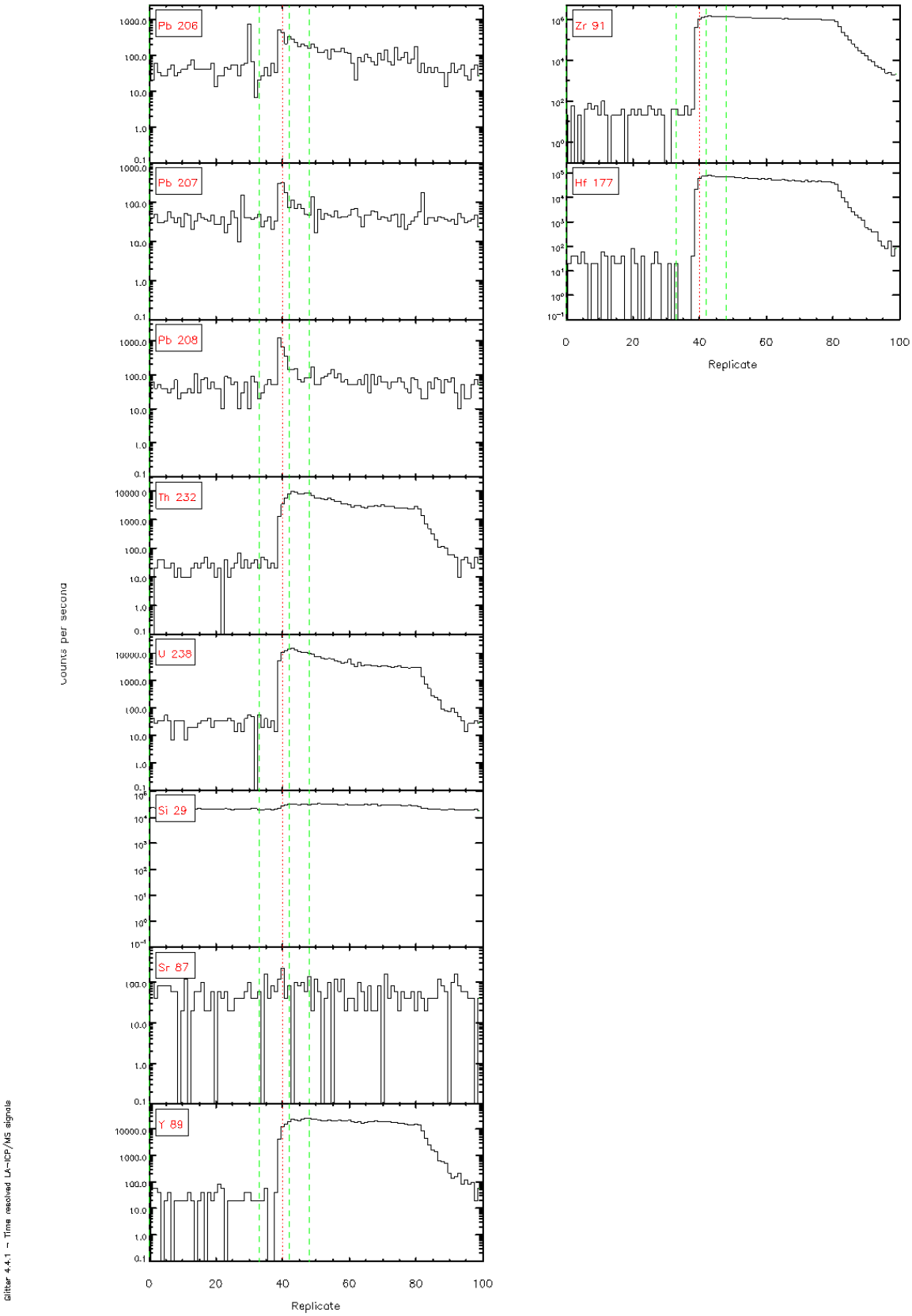
Pb 206
Pb 207
Pb 208
Th 232
U 238
Si 29
Sr 87
Y 89
Zr 91
Hf 177
Counts per second
Replicate
Glitter 4.4.1 – Time resolved LA-ICP/MS signals

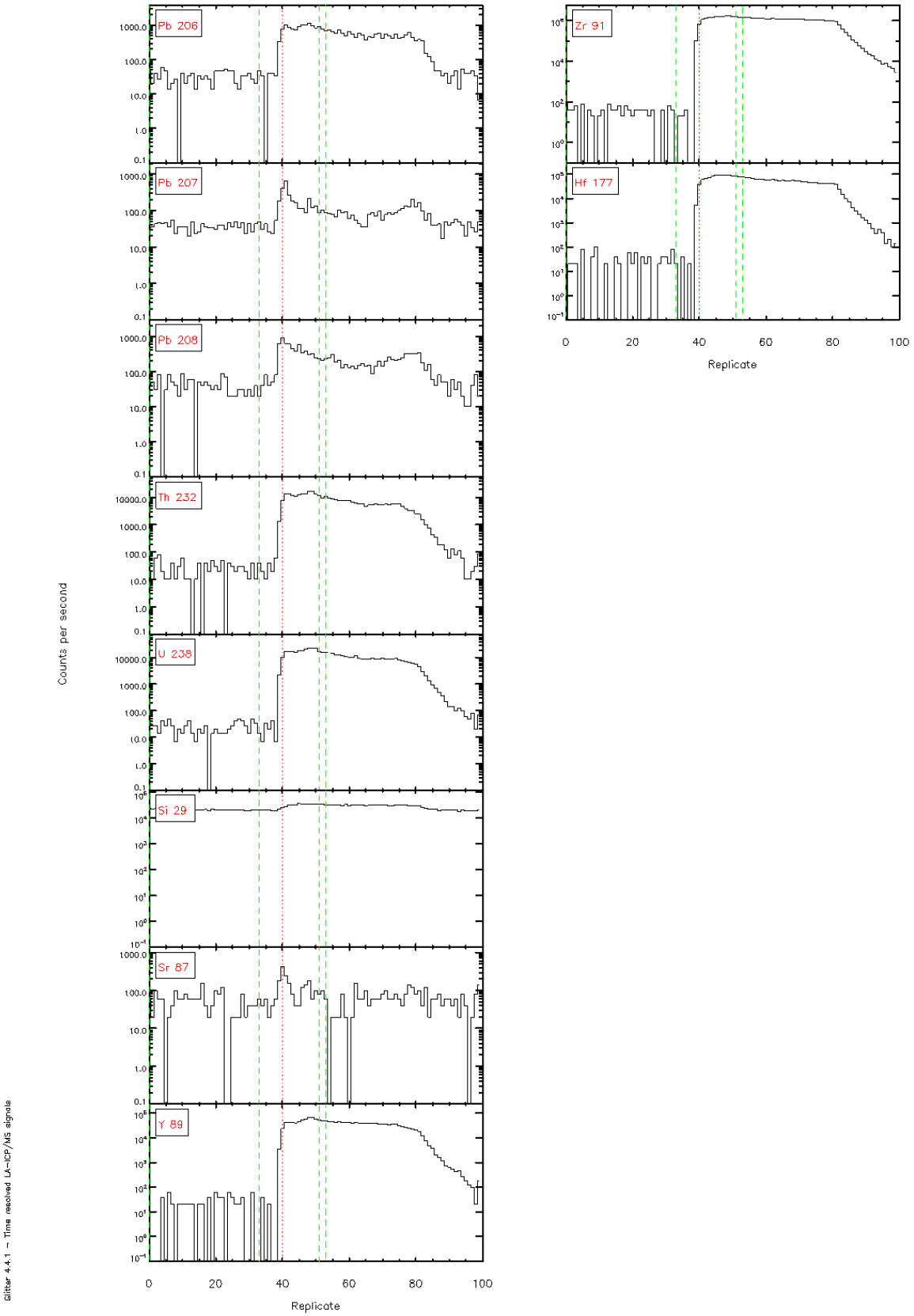
Pb 206
Pb 207
Pb 208
Th 232
U 238
Si 29
Sr 87
Y 89
Zr 91
Hf 177
Counts per second
Replicate
Glitter 4.4.1 – Time resolved LA-ICP/MS signals

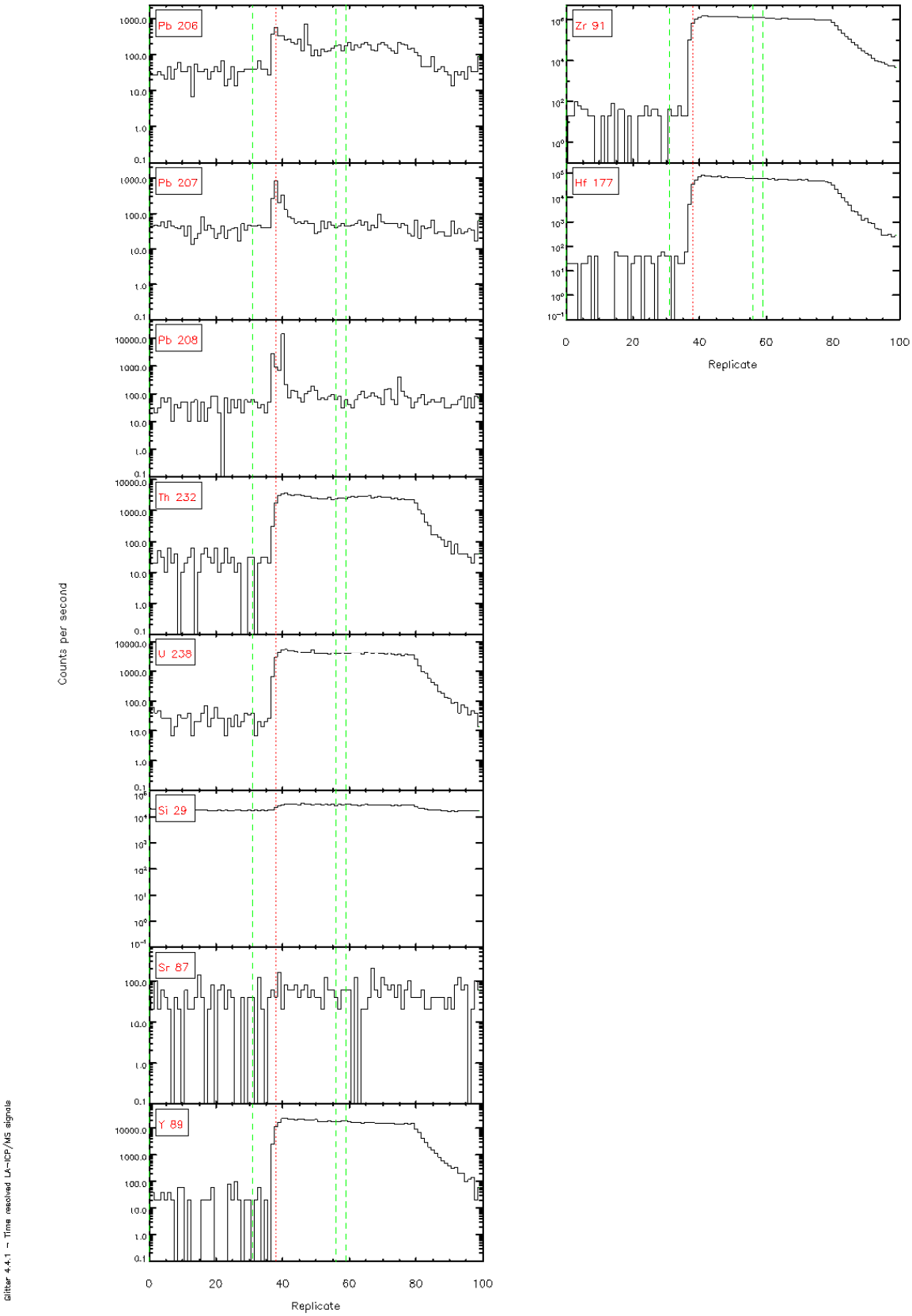
Pb 206
Pb 207
Pb 208
Th 232
U 238
Si 29
Sr 87
Y 89
Zr 91
Hf 177
Counts per second
Replicate
Glitter 4.4.1 – Time resolved LA-ICP/MS signals

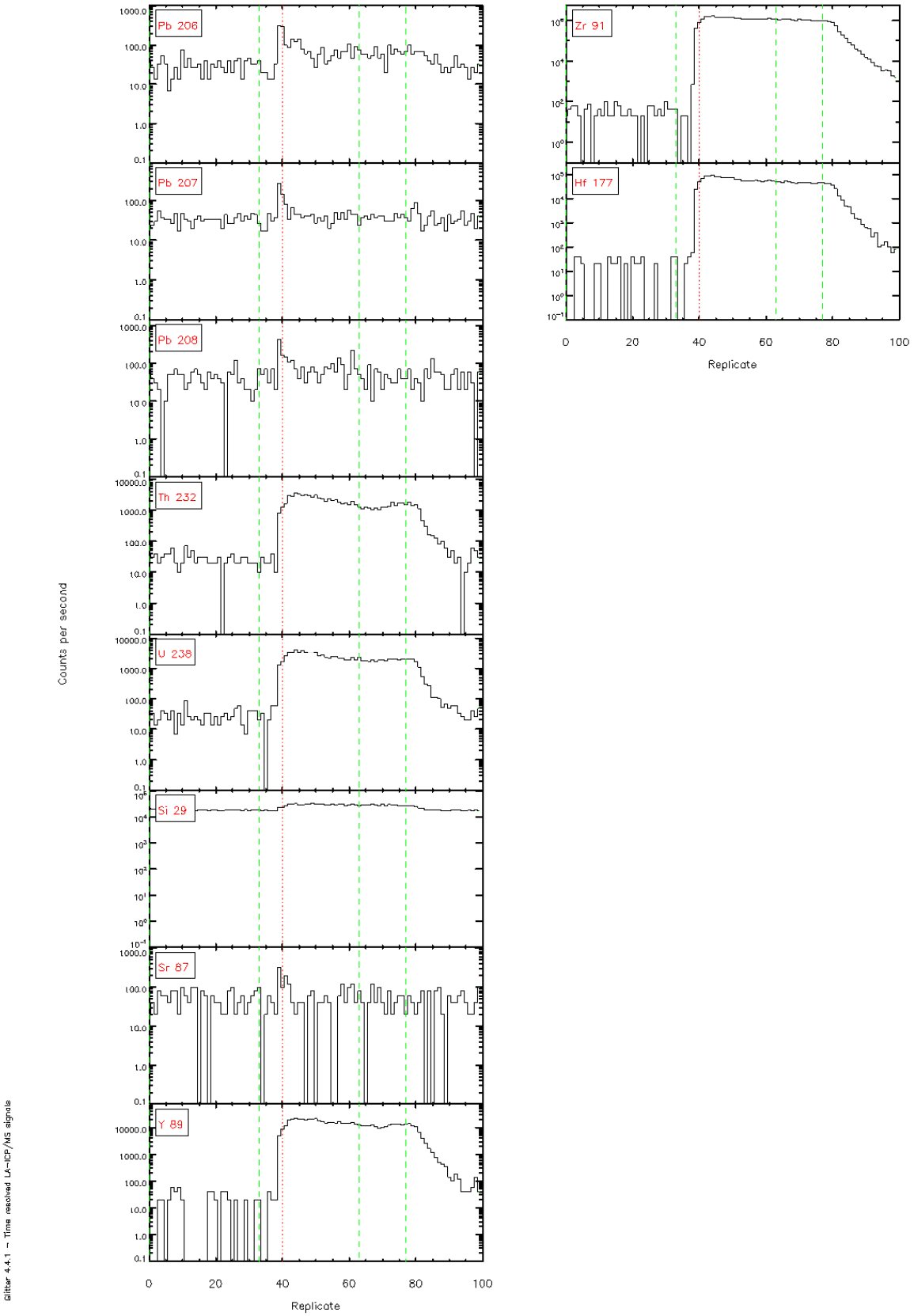
Pb 206
Pb 207
Pb 208
Th 232
U 238
Si 29
Sr 87
Y 89
Zr 91
Hf 177
Counts per second
Replicate
Glitter 4.4.1 – Time resolved LA-ICP/MS signals

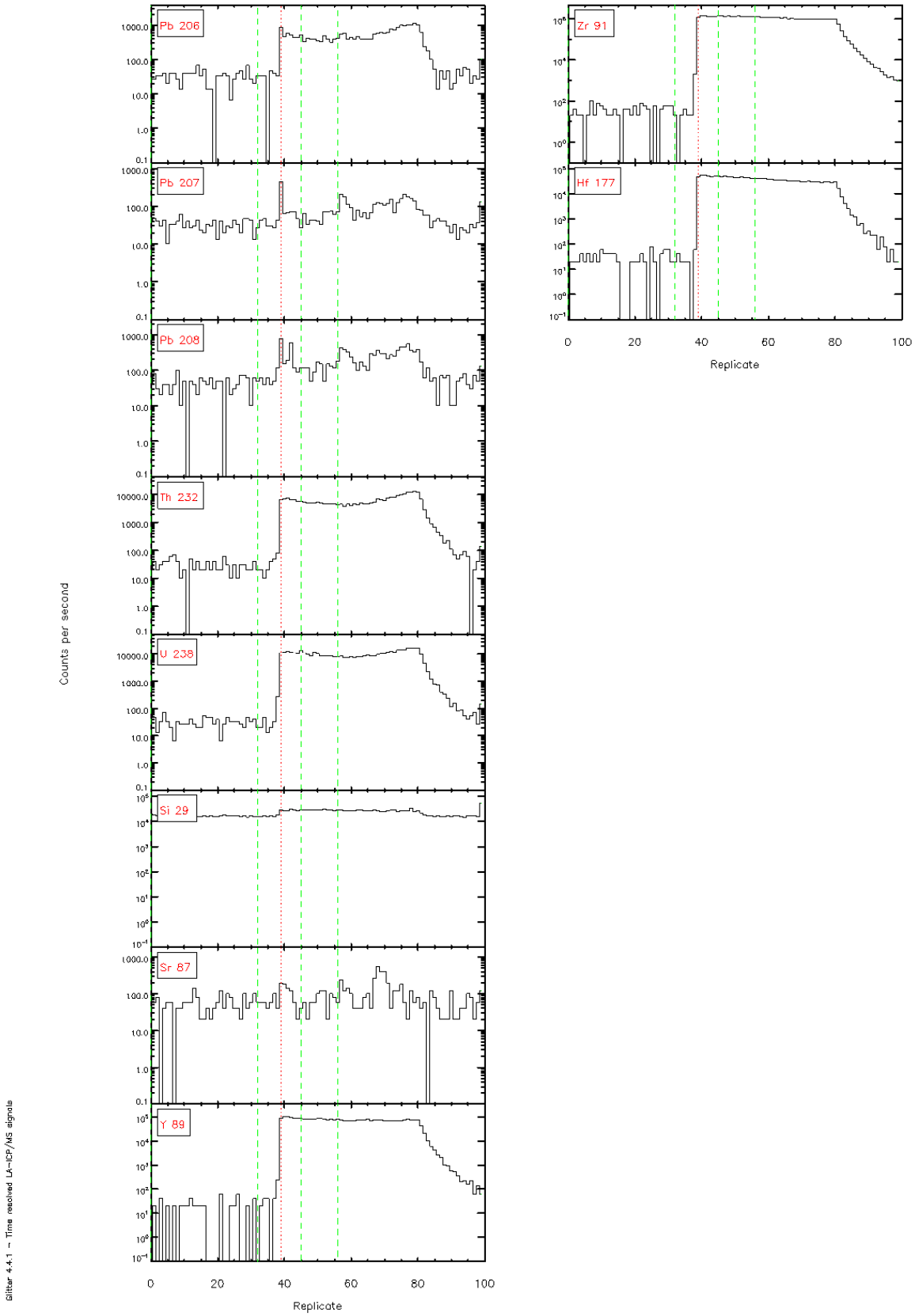
Pb 206
Pb 207
Pb 208
Th 232
U 238
Si 29
Sr 87
Y 89
Zr 91
Hf 177
Counts per second
Replicate
Glitter 4.4.1 – Time resolved LA-ICP/MS signals

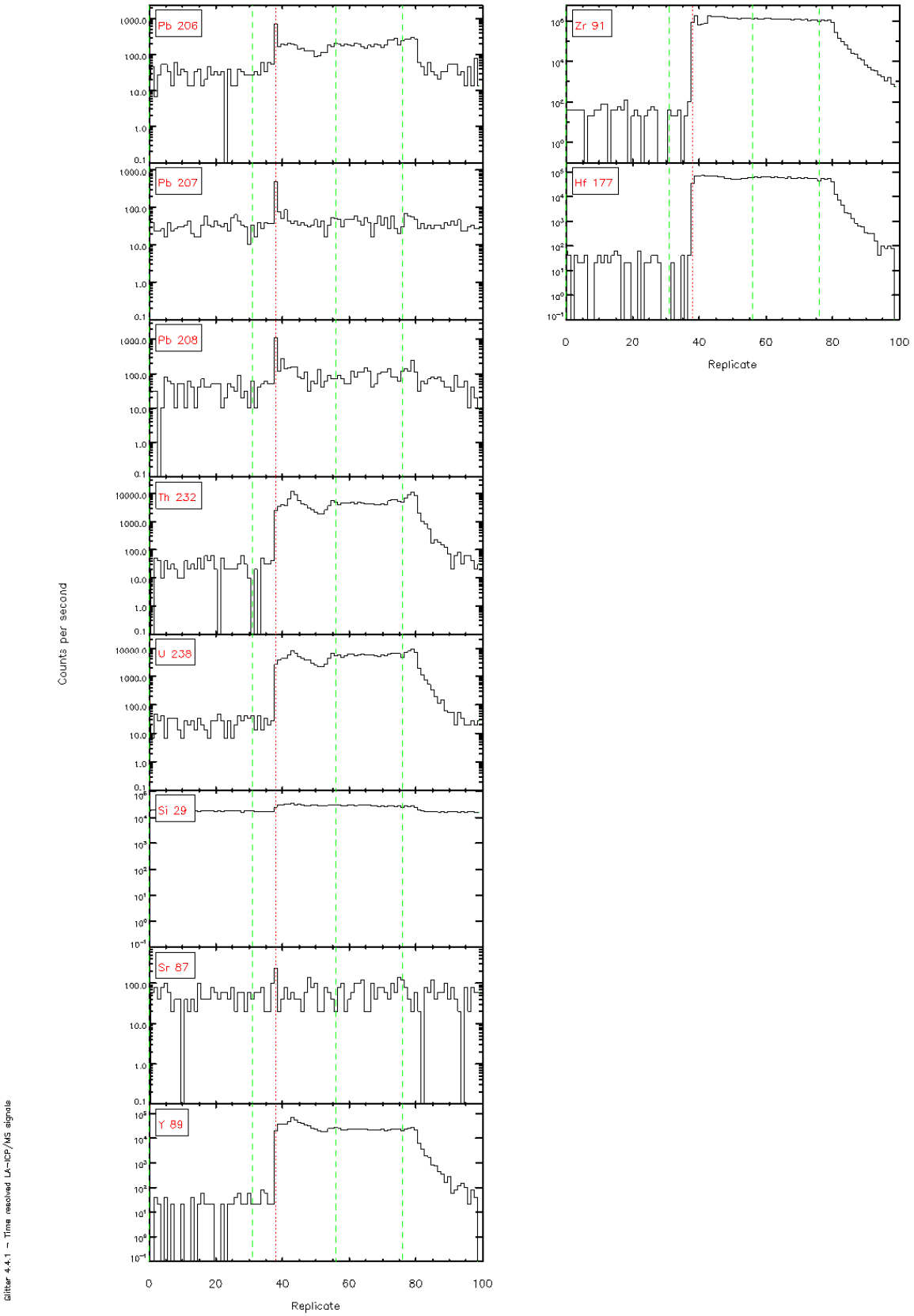
Pb 206
Pb 207
Pb 208
Th 232
U 238
Si 29
Sr 87
Y 89
Zr 91
Hf 177
Counts per second
Replicate
Glitter 4.4.1 – Time resolved LA-ICP/MS signals

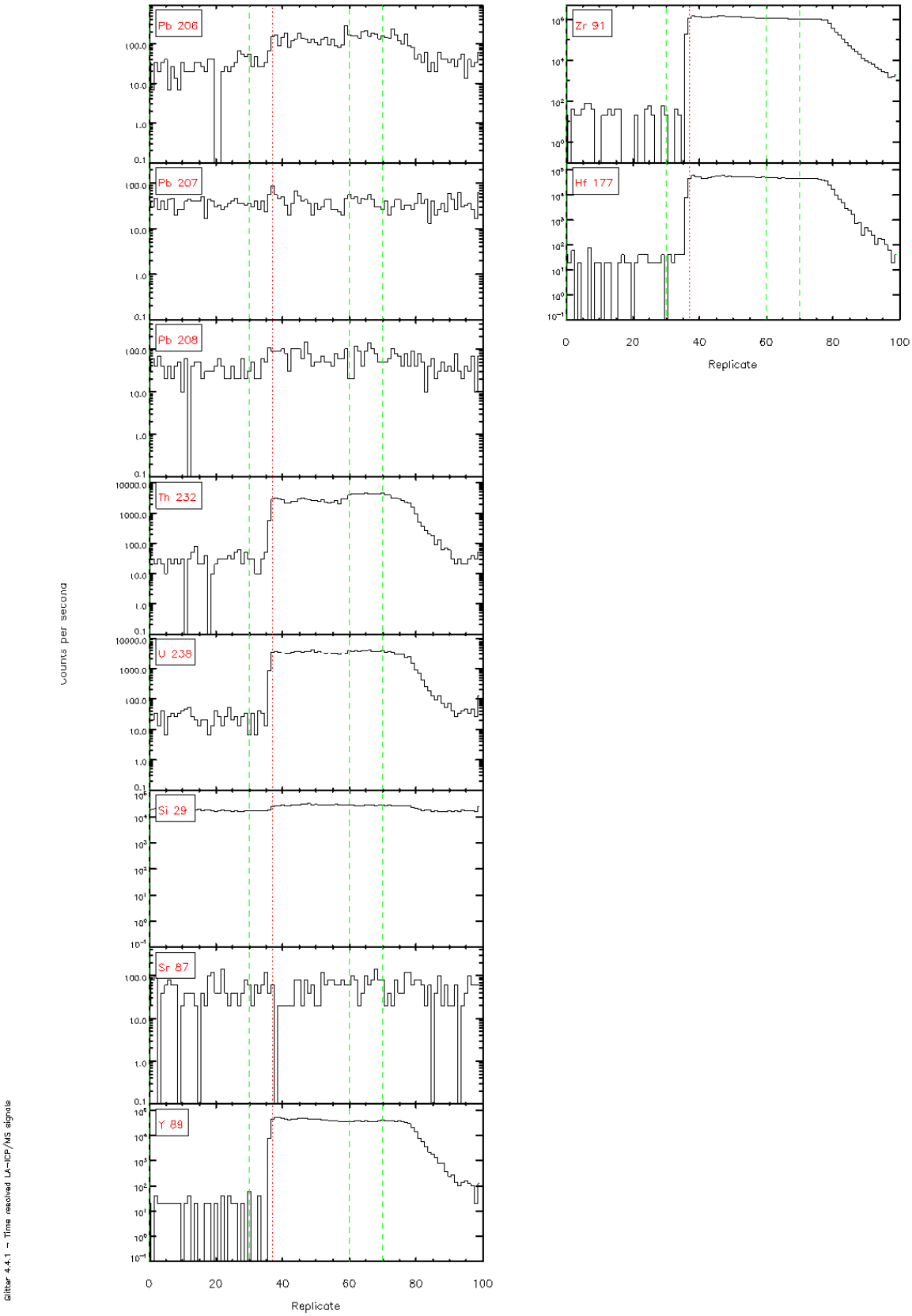
Pb 206
Pb 207
Pb 208
Th 232
U 238
Si 29
Sr 87
Y 89
Zr 91
Hf 177
Counts per second
Replicate
Glitter 4.4.1 – Time resolved LA-ICP/MS signals

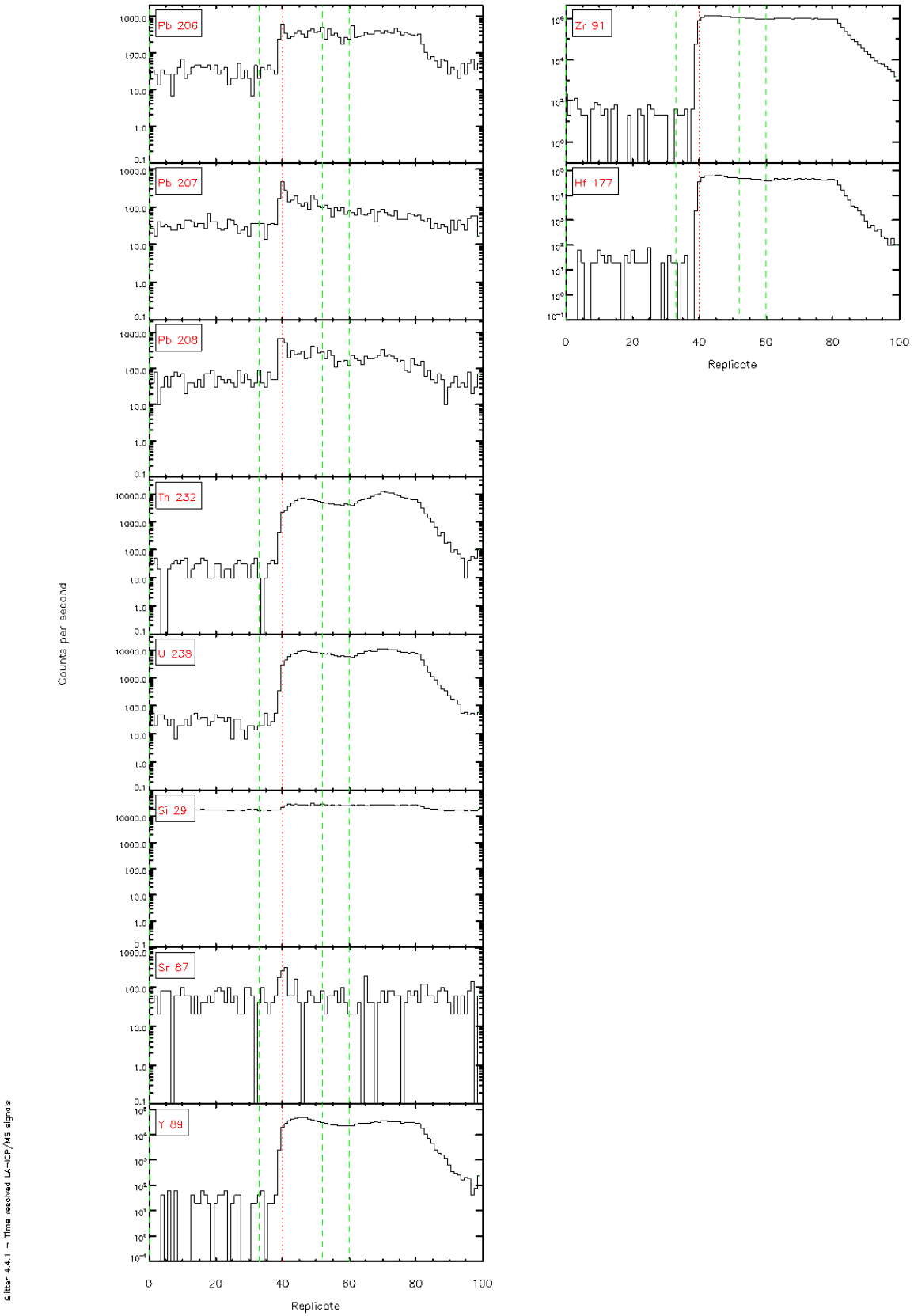
Pb 206
Pb 207
Pb 208
Th 232
U 238
Si 29
Sr 87
Y 89
Zr 91
Hf 177
Counts per second
Replicate
Glitter 4.4.1 – Time resolved LA-ICP/MS signals

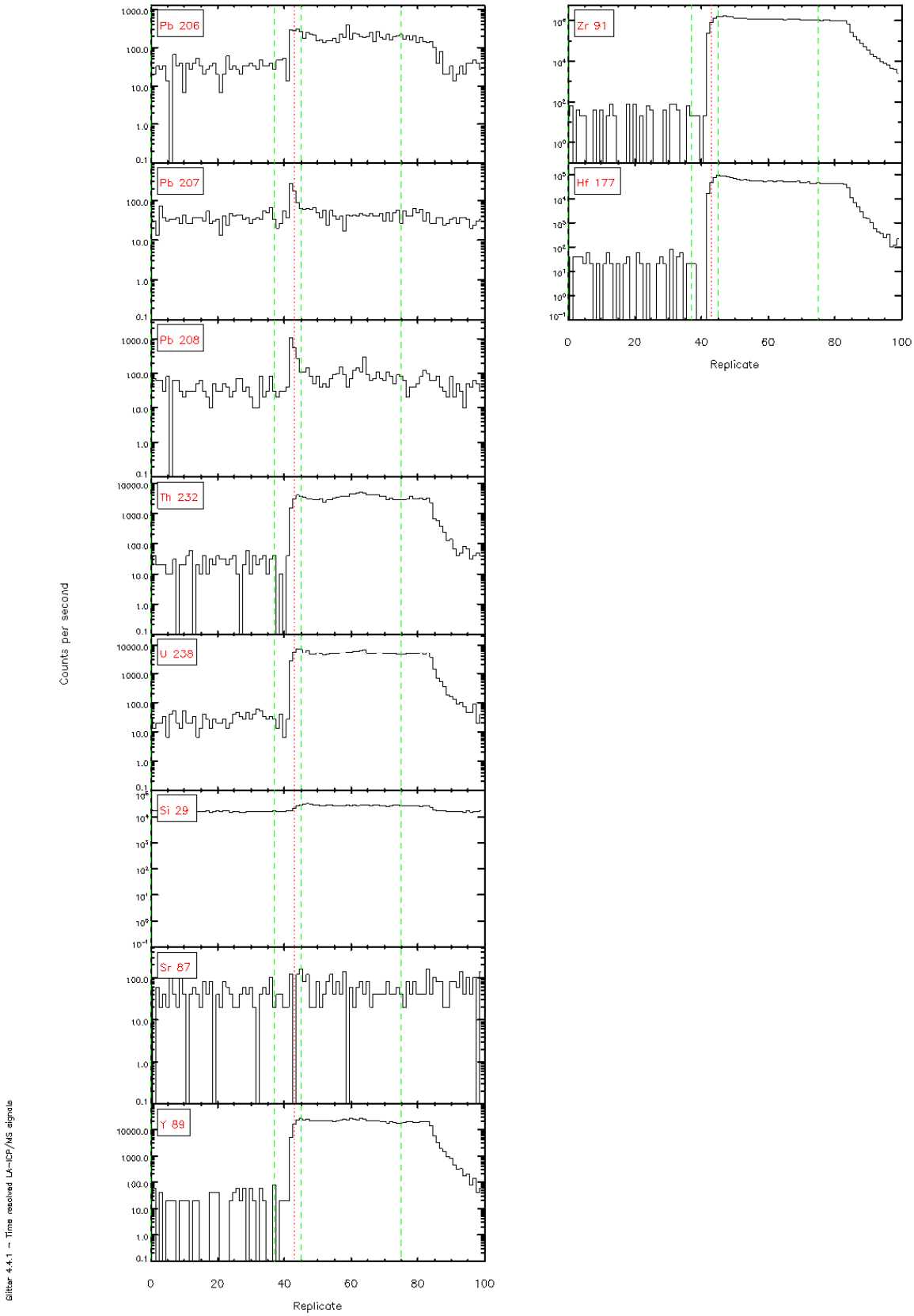
Pb 206
Pb 207
Pb 208
Th 232
U 238
Si 29
Sr 87
Y 89
Zr 91
Hf 177
Counts per second
Replicate
Glitter 4.4.1 – Time resolved LA-ICP/MS signals

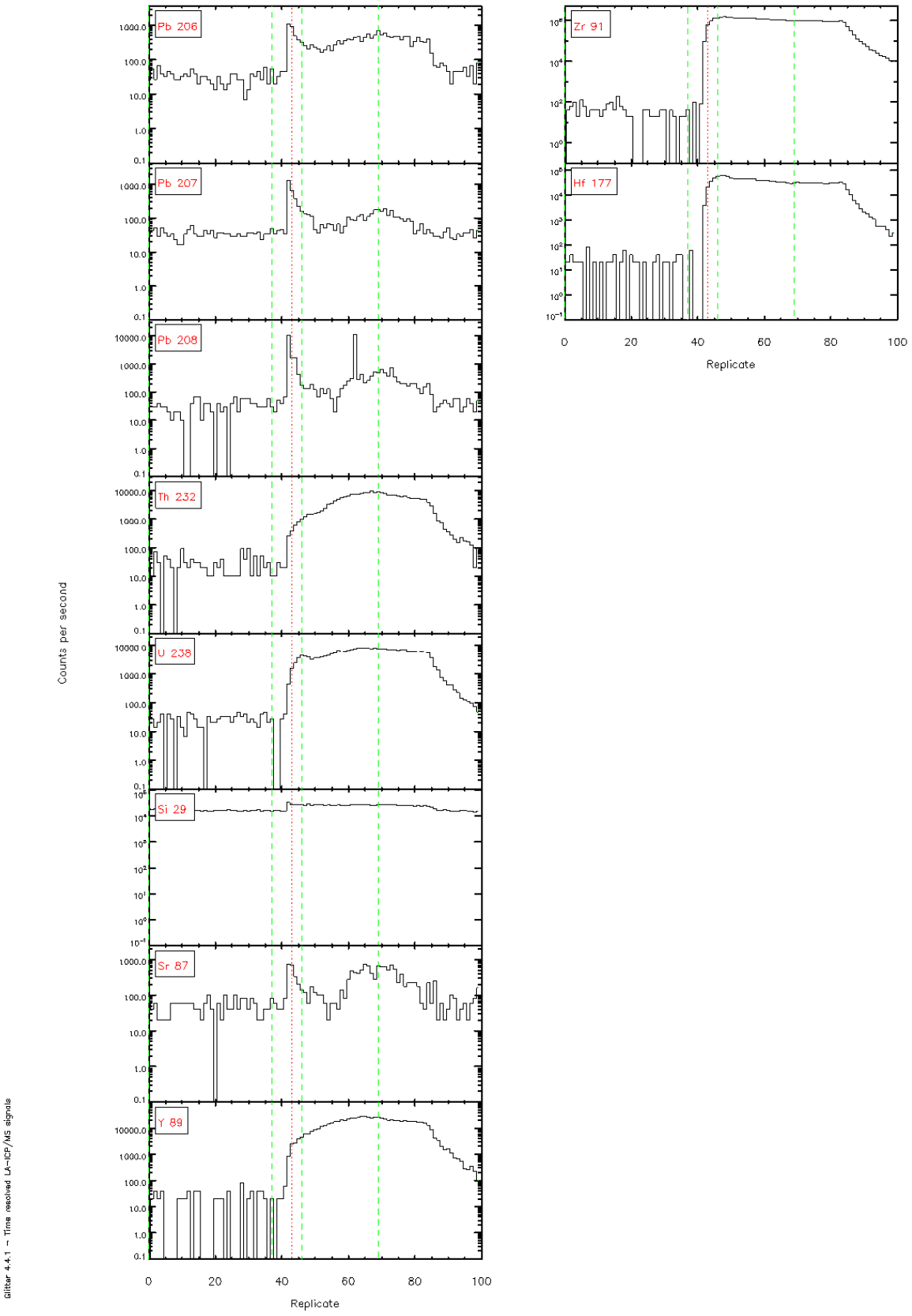
Pb 206
Pb 207
Pb 208
Th 232
U 238
Si 29
Sr 87
Y 89
Zr 91
Hf 177
Counts per second
Replicate
Glitter 4.4.1 – Time resolved LA-ICP/MS signals

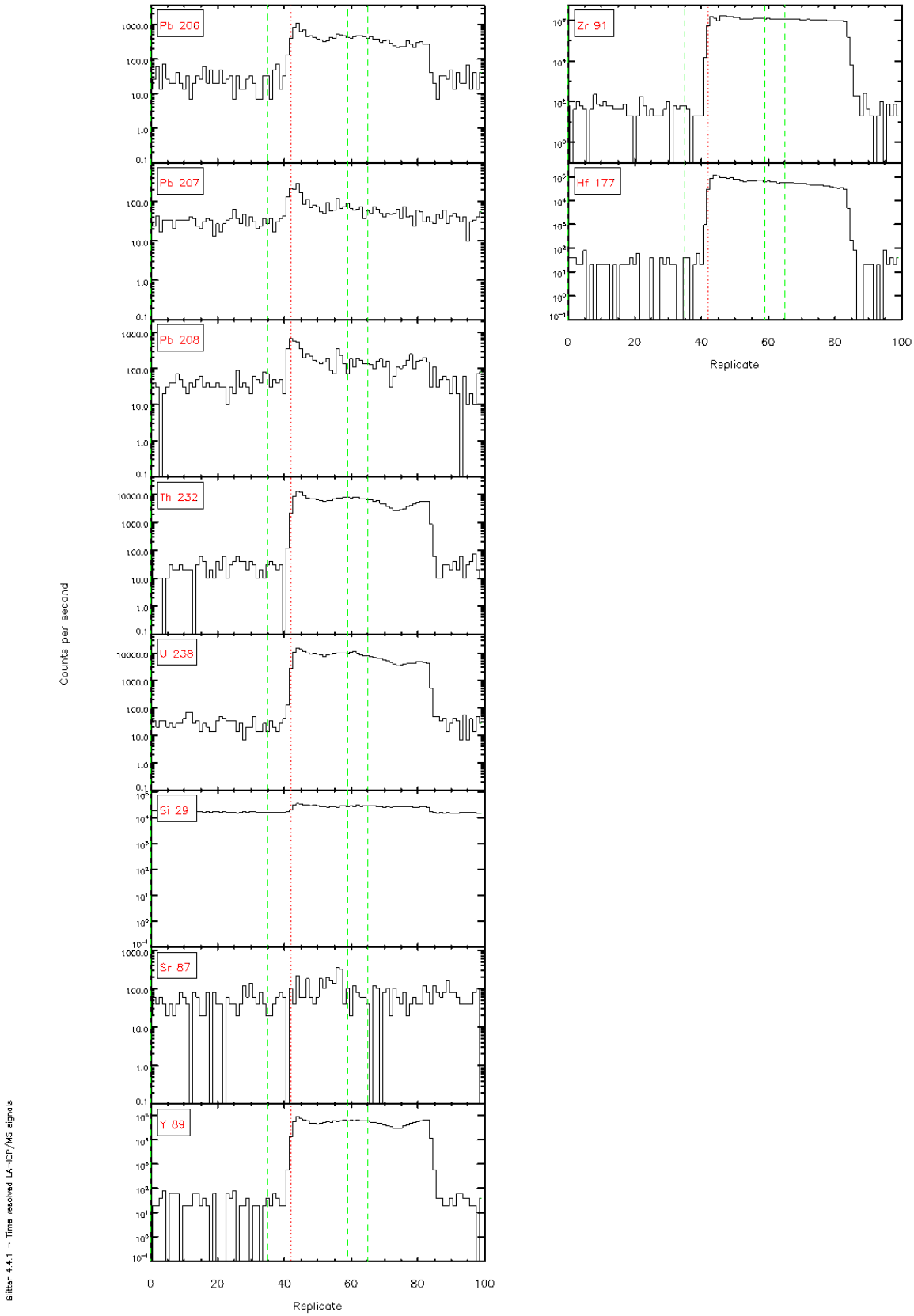
Pb 206
Pb 207
Pb 208
Th 232
U 238
Si 29
Sr 87
Y 89
Zr 91
Hf 177
Counts per second
Replicate
Glitter 4.4.1 – Time resolved LA-ICP/MS signals

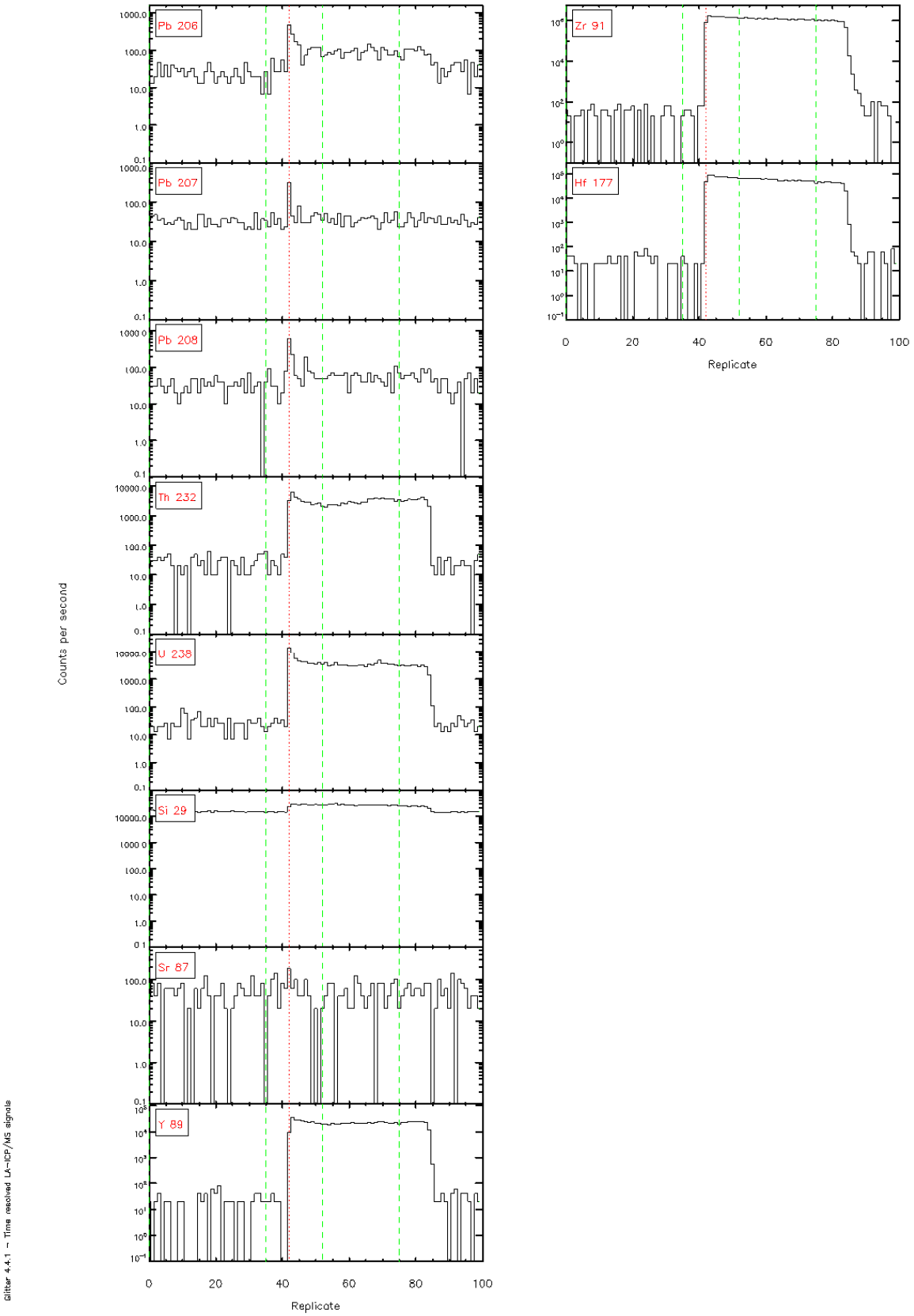
Pb 206
Pb 207
Pb 208
Th 232
U 238
Si 29
Sr 87
Y 89
Zr 91
Hf 177
Counts per second
Replicate
Glitter 4.4.1 – Time resolved LA-ICP/MS signals

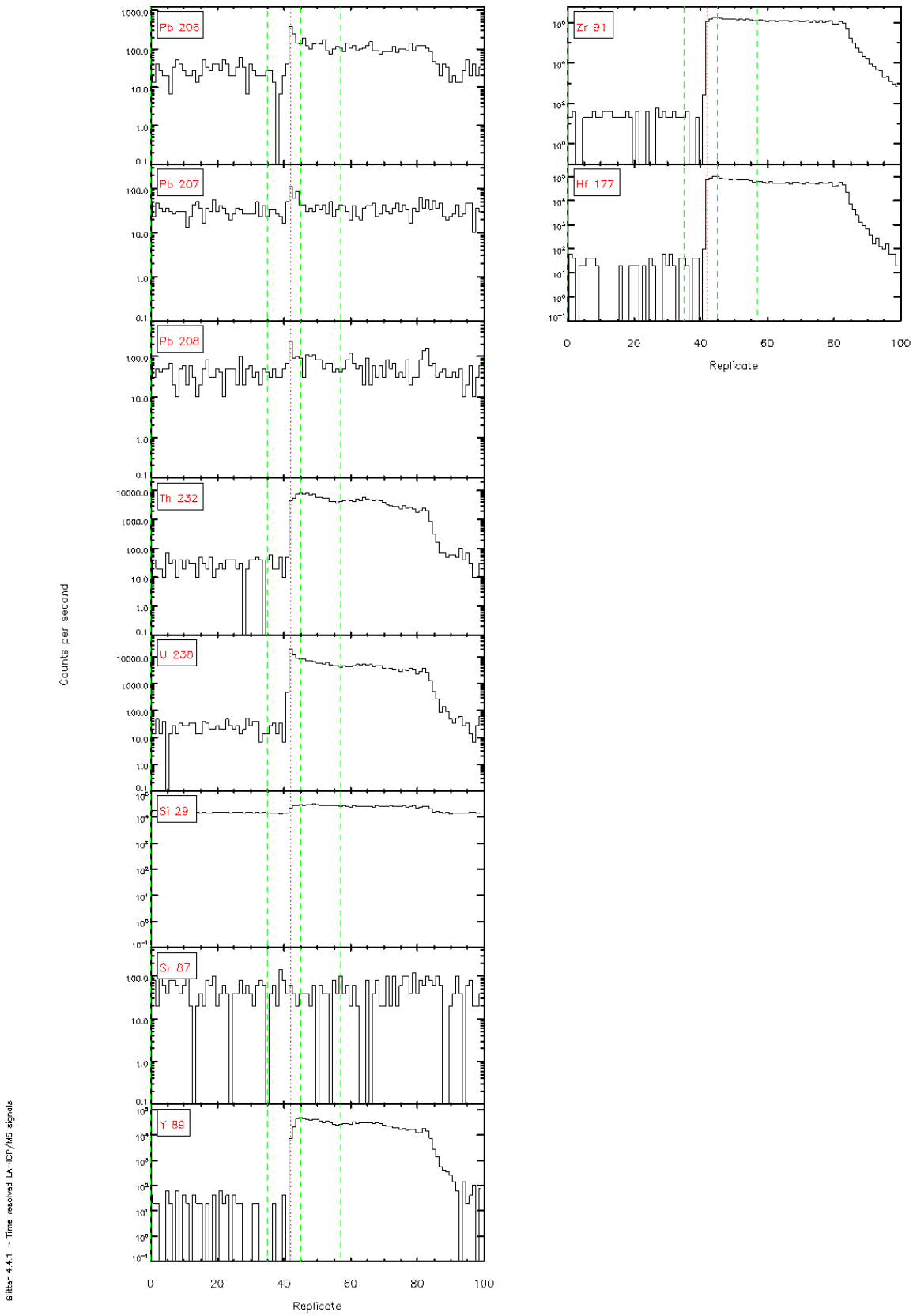
Pb 206
Pb 207
Pb 208
Th 232
U 238
Si 29
Sr 87
Y 89
Zr 91
Hf 177
Counts per second
Replicate
Glitter 4.4.1 – Time resolved LA-ICP/MS signals

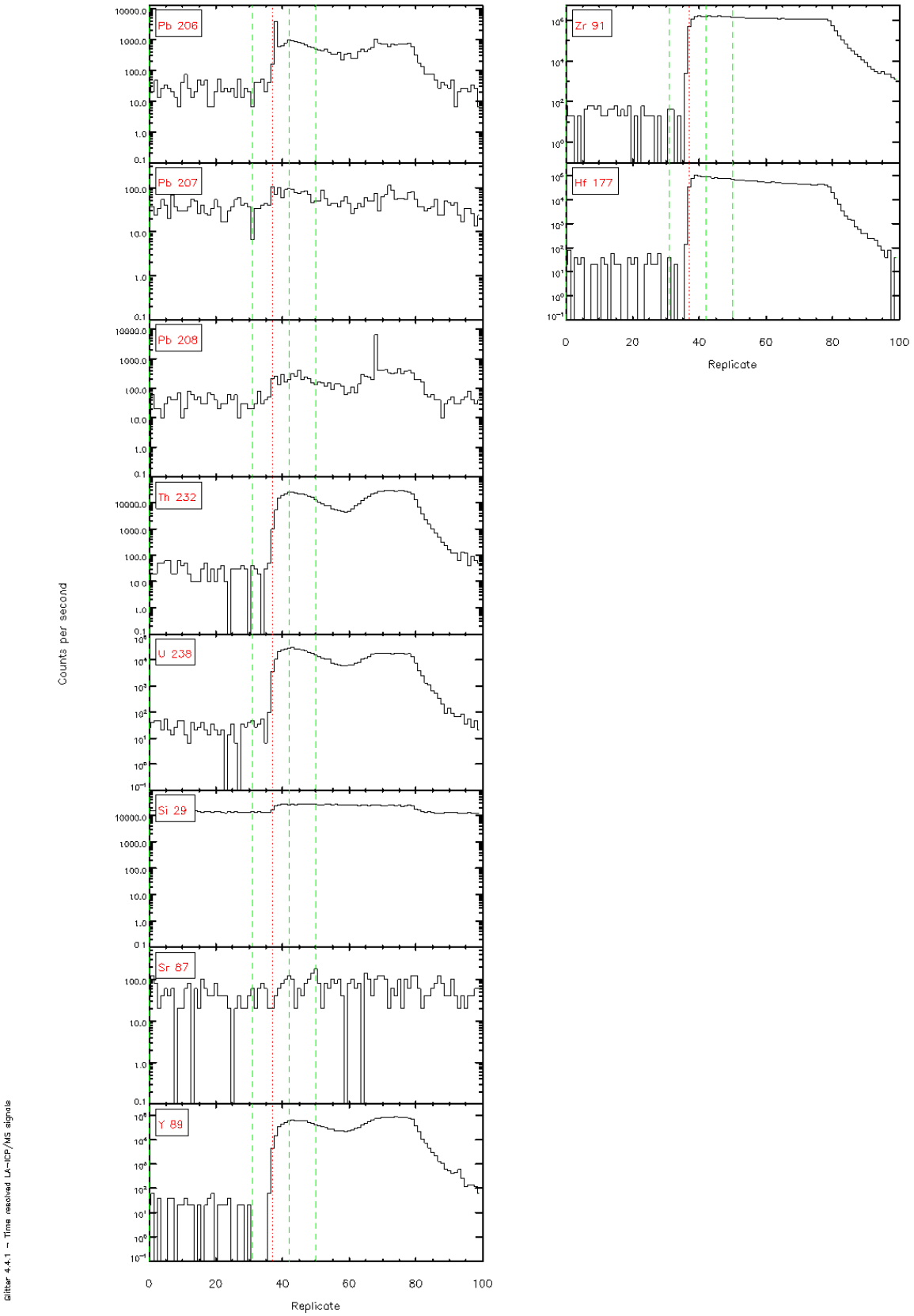
Pb 206
Pb 207
Pb 208
Th 232
U 238
Si 29
Sr 87
Y 89
Zr 91
Hf 177
Counts per second
Replicate
Glitter 4.4.1 – Time resolved LA-ICP/MS signals

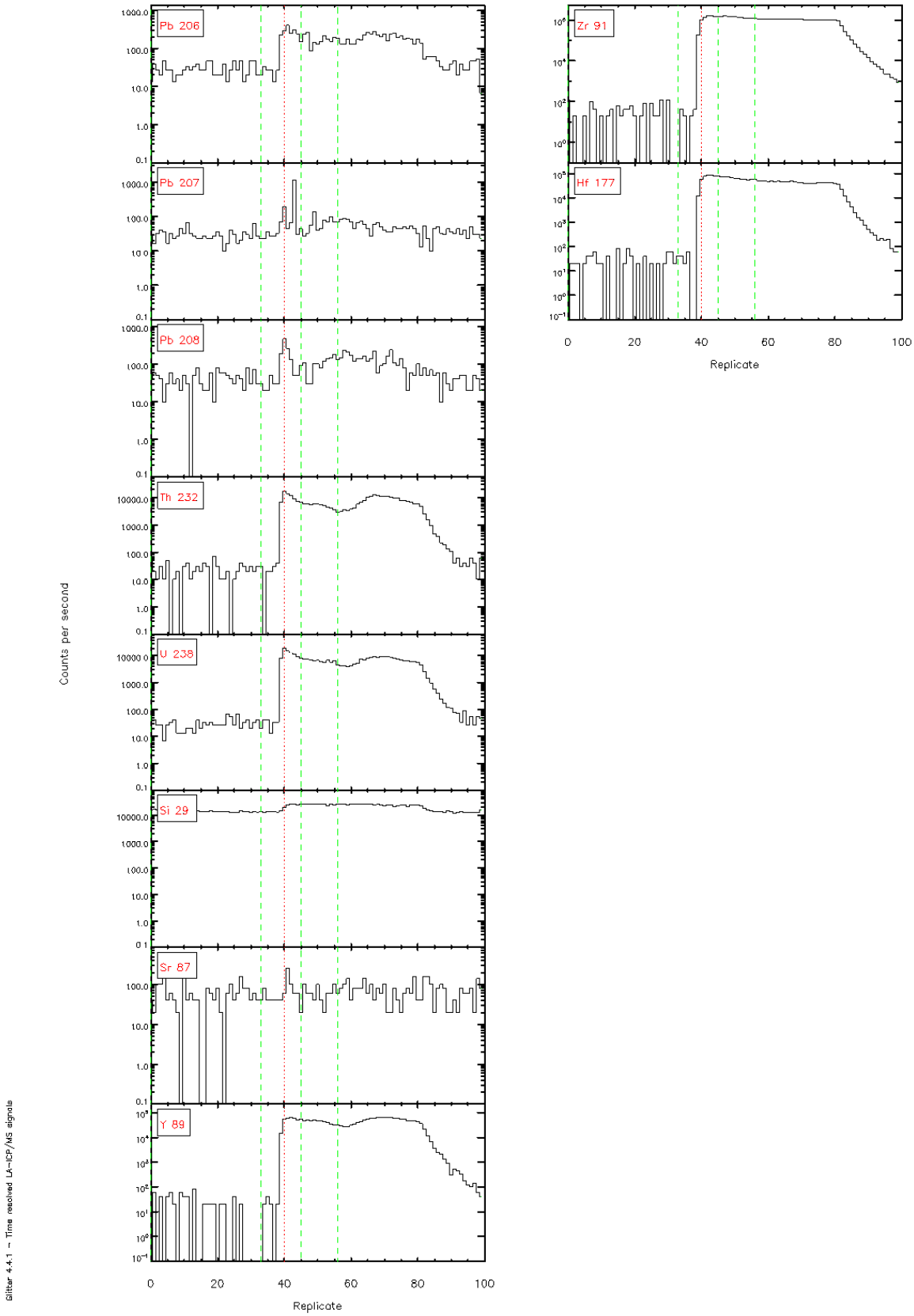
Pb 206
Pb 207
Pb 208
Th 232
U 238
Si 29
Sr 87
Y 89
Zr 91
Hf 177
Counts per second
Replicate
Glitter 4.4.1 – Time resolved LA-ICP/MS signals

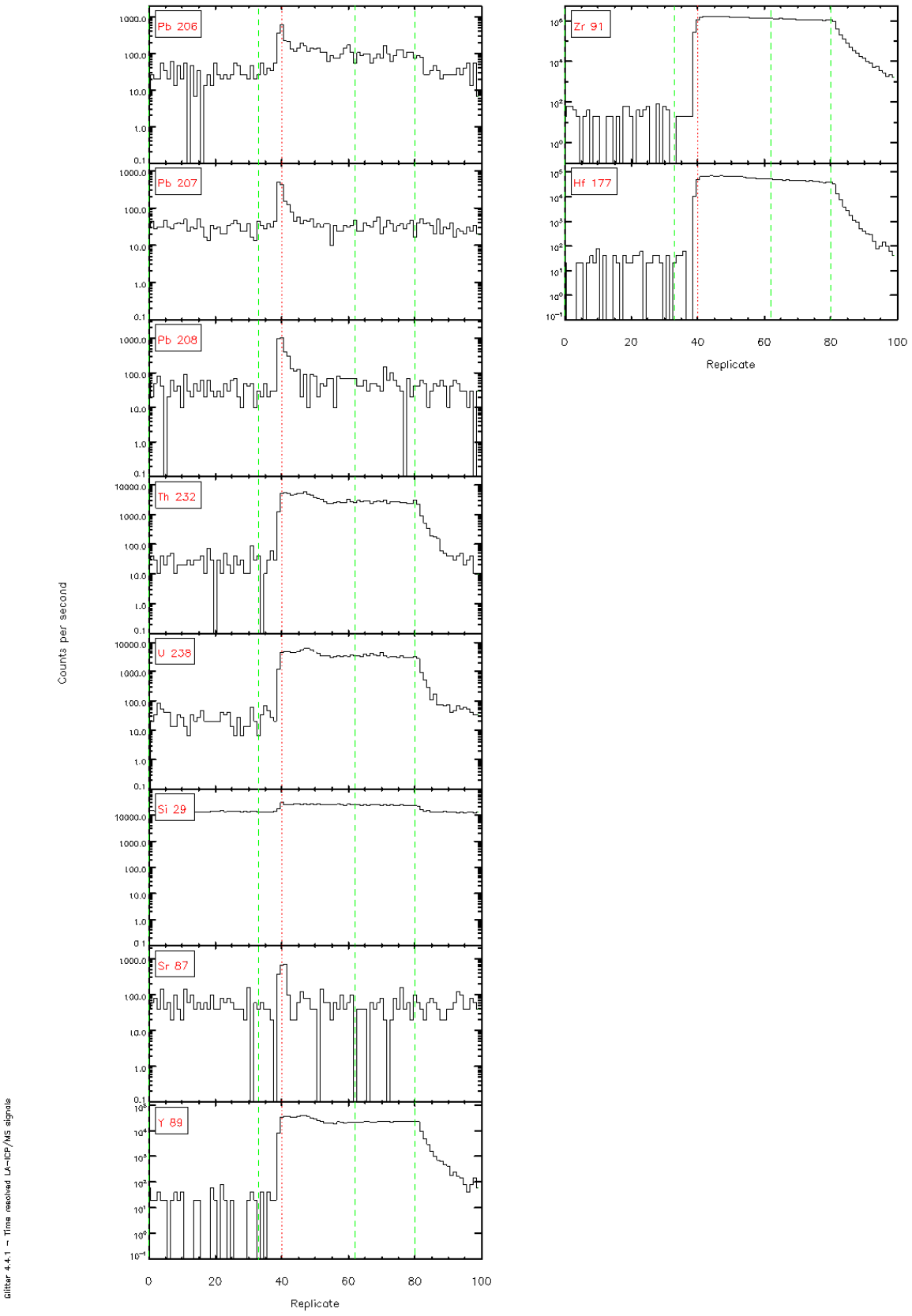
Pb 206
Pb 207
Pb 208
Th 232
U 238
Si 29
Sr 87
Y 89
Zr 91
Hf 177
Counts per second
Replicate
Glitter 4.4.1 – Time resolved LA-ICP/MS signals

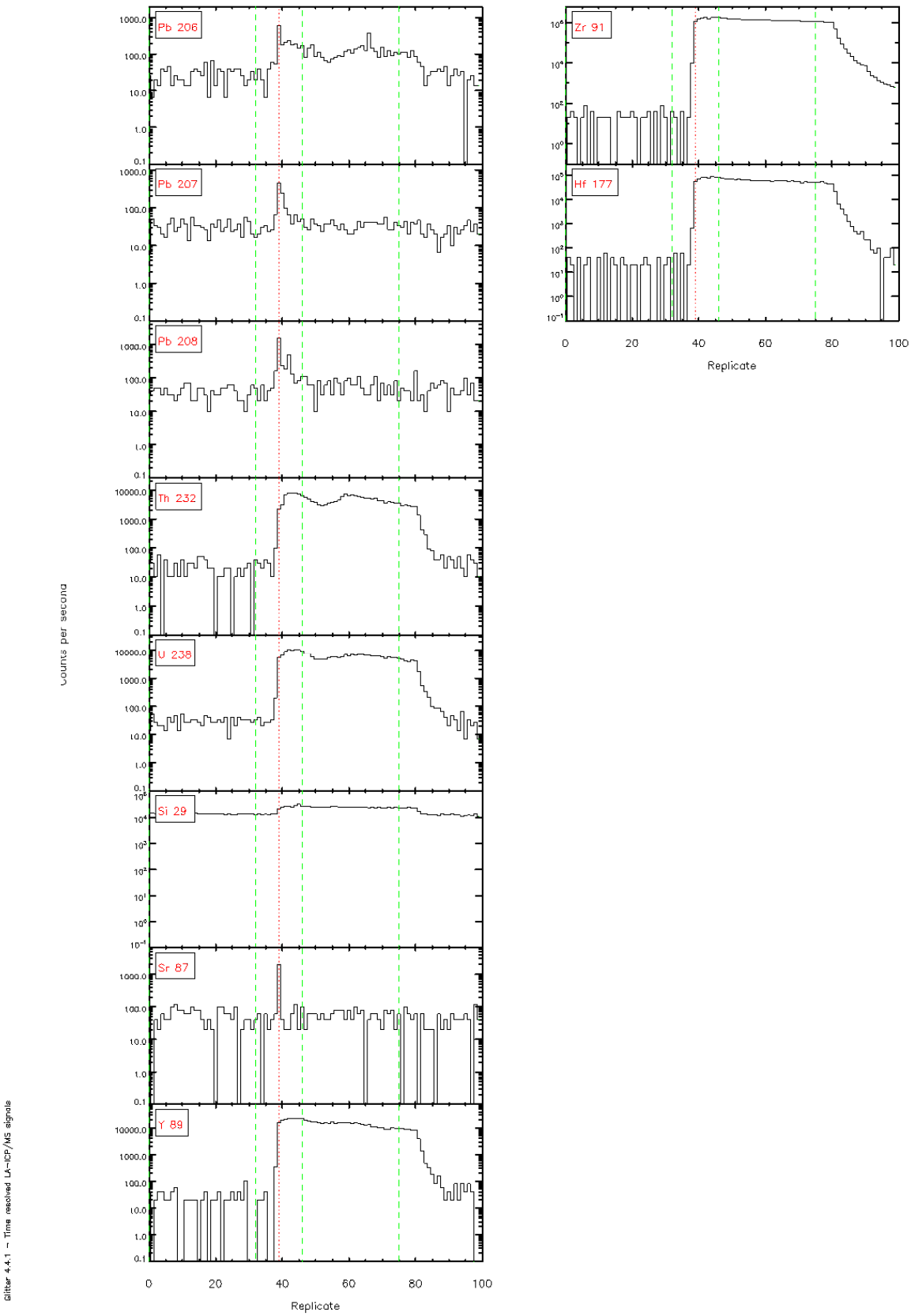
Pb 206
Pb 207
Pb 208
Th 232
U 238
Si 29
Sr 87
Y 89
Zr 91
Hf 177
Counts per second
Replicate
Glitter 4.4.1 – Time resolved LA-ICP/MS signals

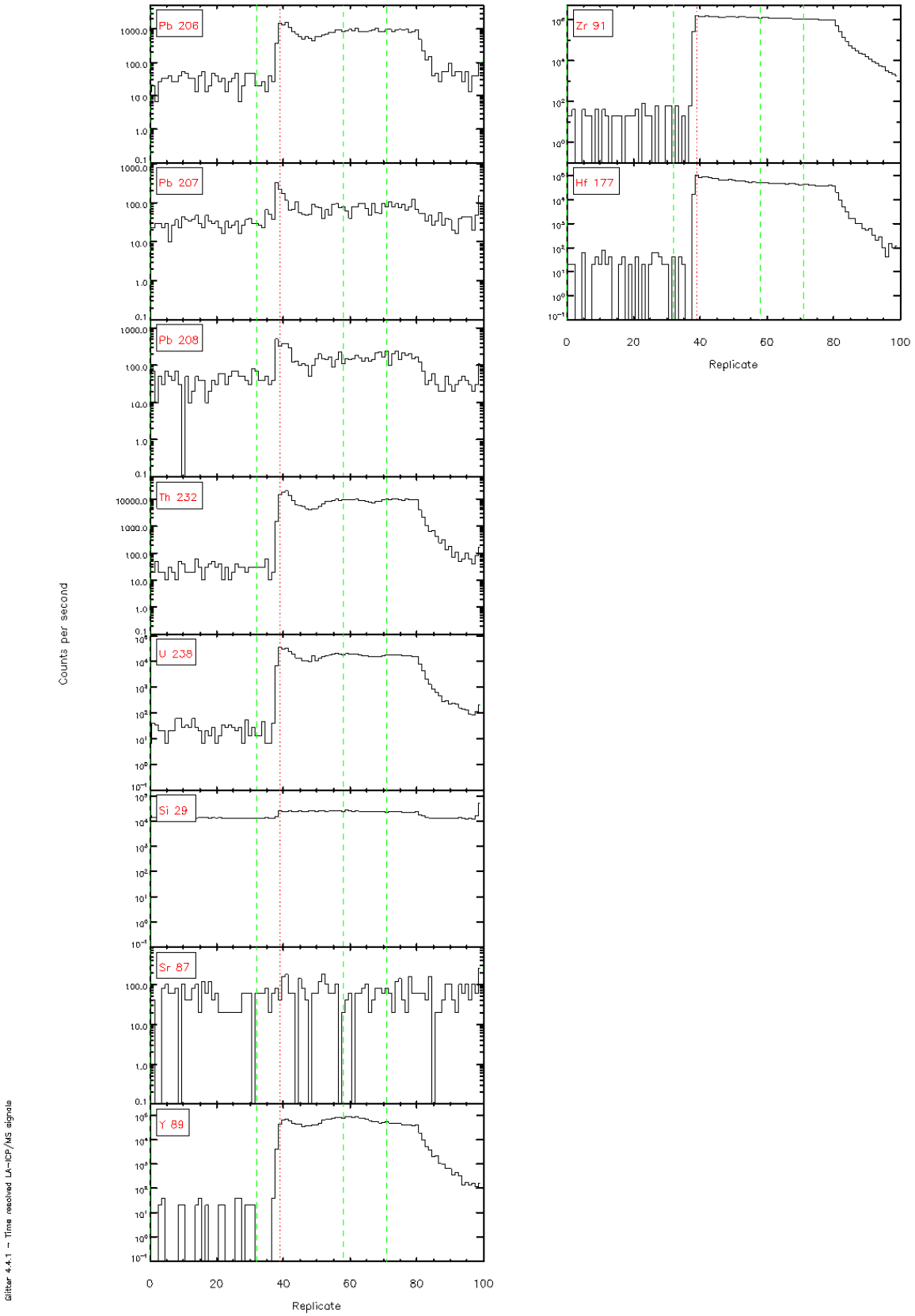
Pb 206
Pb 207
Pb 208
Th 232
U 238
Si 29
Sr 87
Y 89
Zr 91
Hf 177
Counts per second
Replicate
Glitter 4.4.1 – Time resolved LA-ICP/MS signals

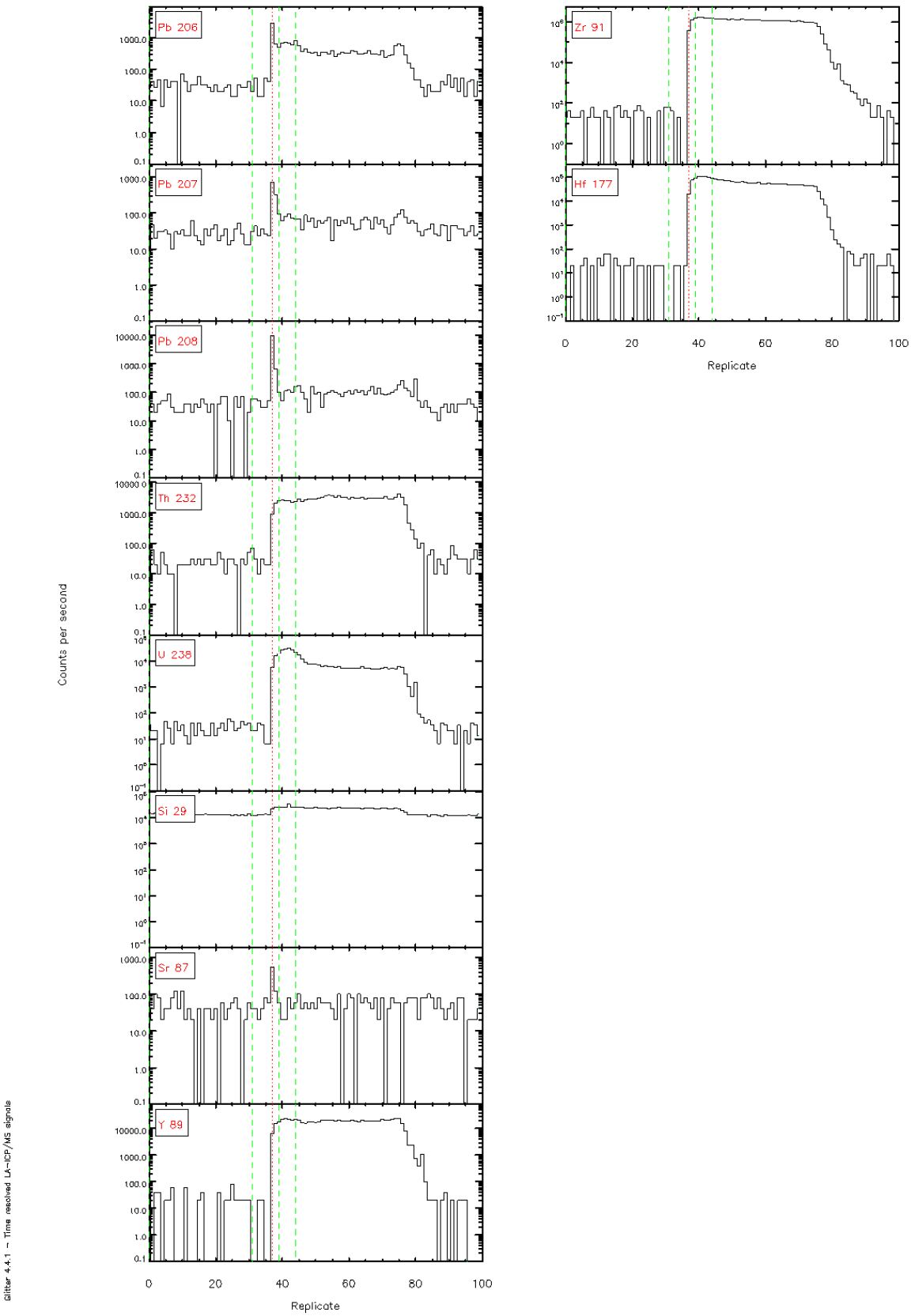
Pb 206
Pb 207
Pb 208
Th 232
U 238
Si 29
Sr 87
Y 89
Zr 91
Hf 177
Counts per second
Replicate
Glitter 4.4.1 – Time resolved LA-ICP/MS signals

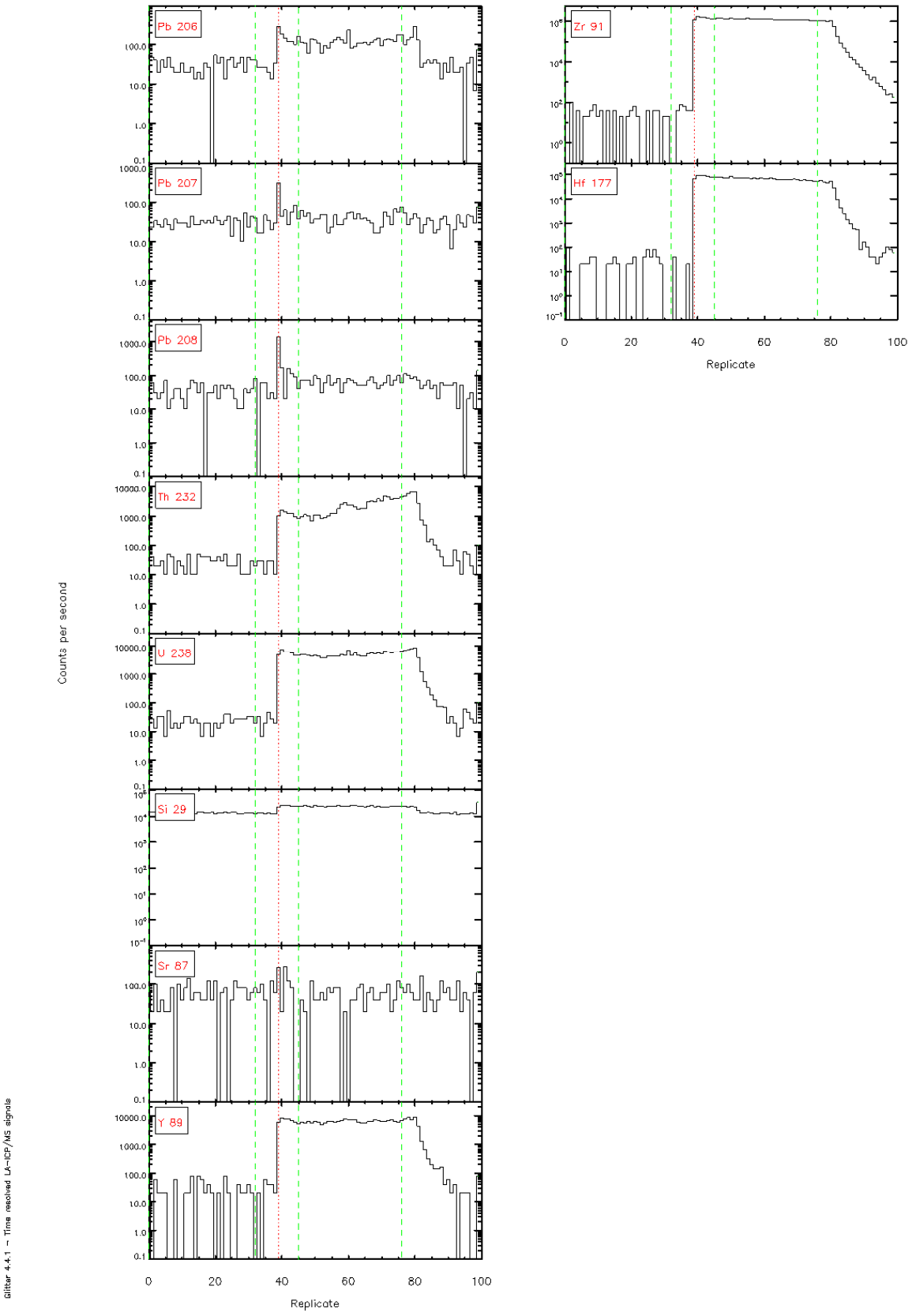
Pb 206
Pb 207
Pb 208
Th 232
U 238
Si 29
Sr 87
Y 89
Zr 91
Hf 177
Counts per second
Replicate
Glitter 4.4.1 – Time resolved LA-ICP/MS signals

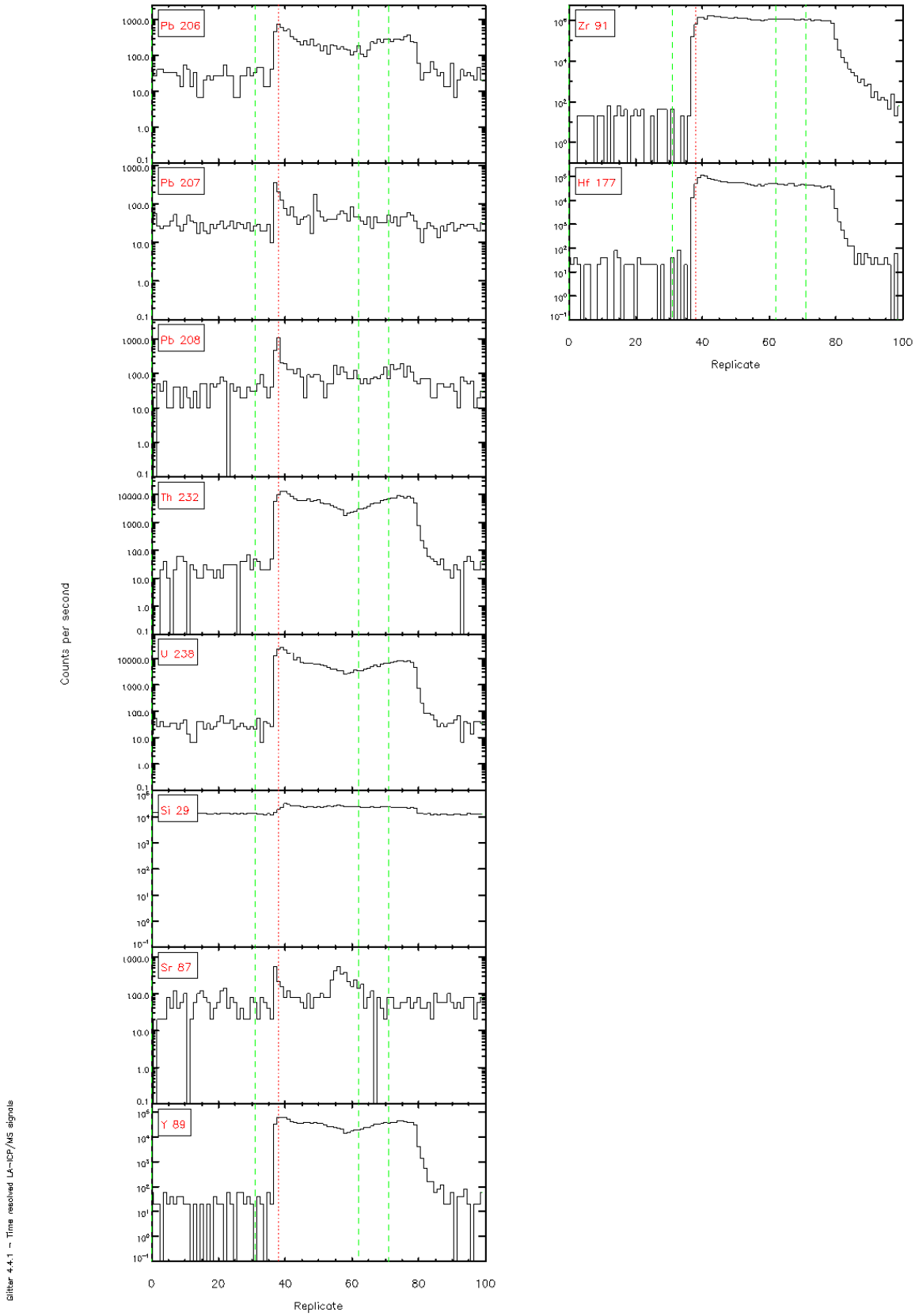
Pb 206
Pb 207
Pb 208
Th 232
U 238
Si 29
Sr 87
Y 89
Zr 91
Hf 177
Counts per second
Replicate
Glitter 4.4.1 – Time resolved LA-ICP/MS signals

5 – Hauturu Sandstone

1.

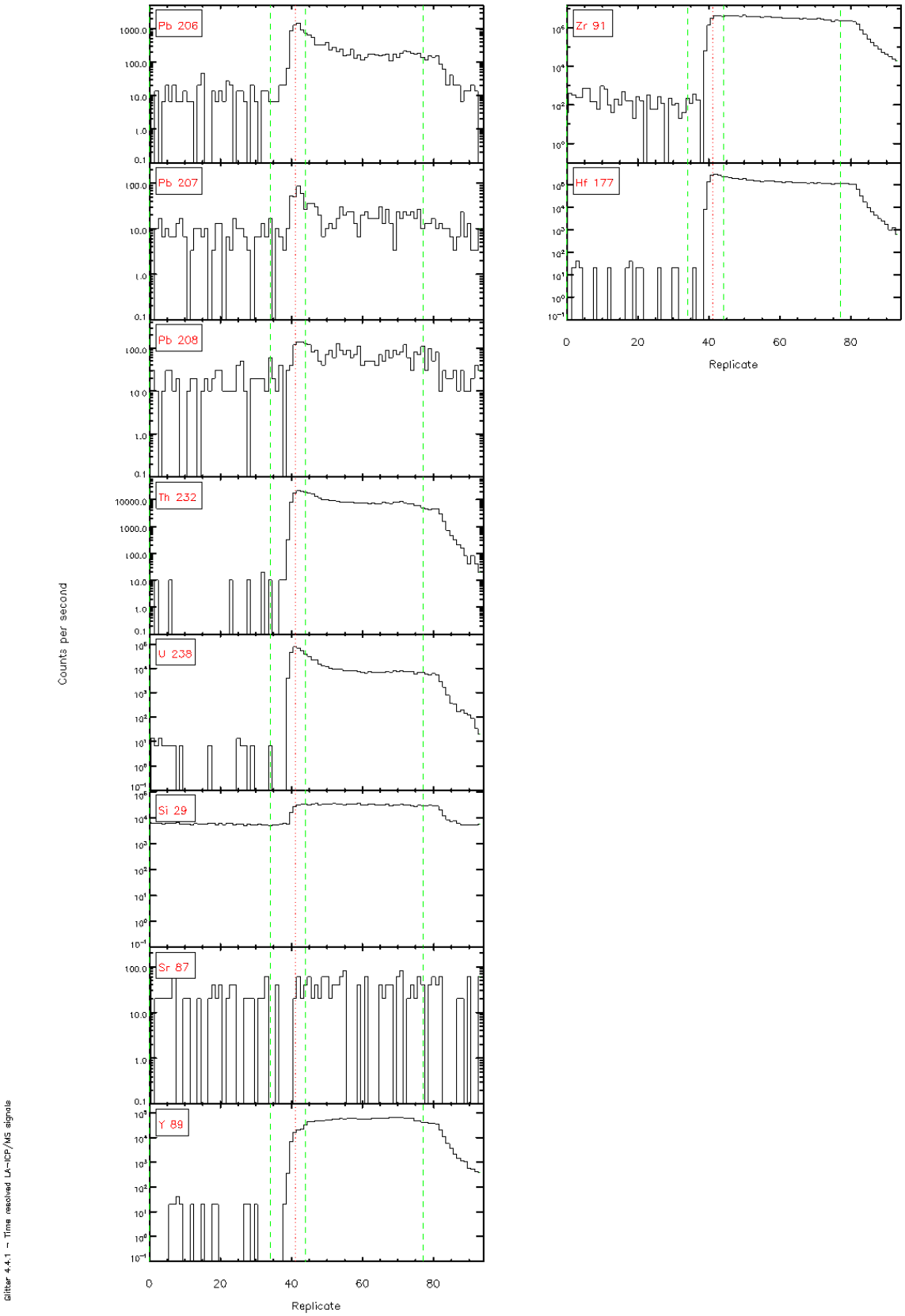

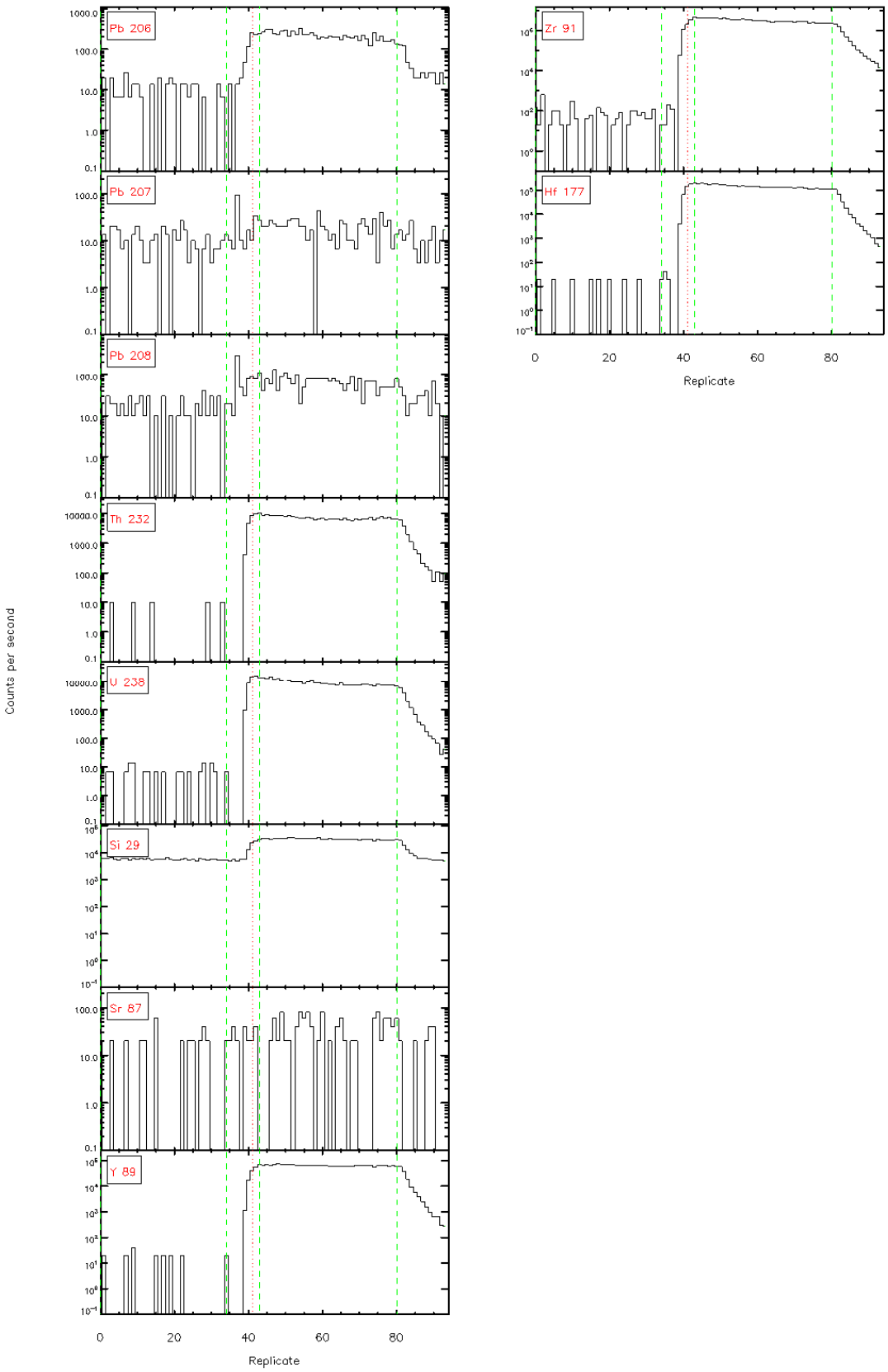
Pb 206
Pb 207
Pb 208
Th 232
U 238
Si 29
Sr 87
Y 89
Zr 91
Hf 177
Counts per second
Replicate
Glitter 4.4.1 - Time resolved LA-ICP/MS signals

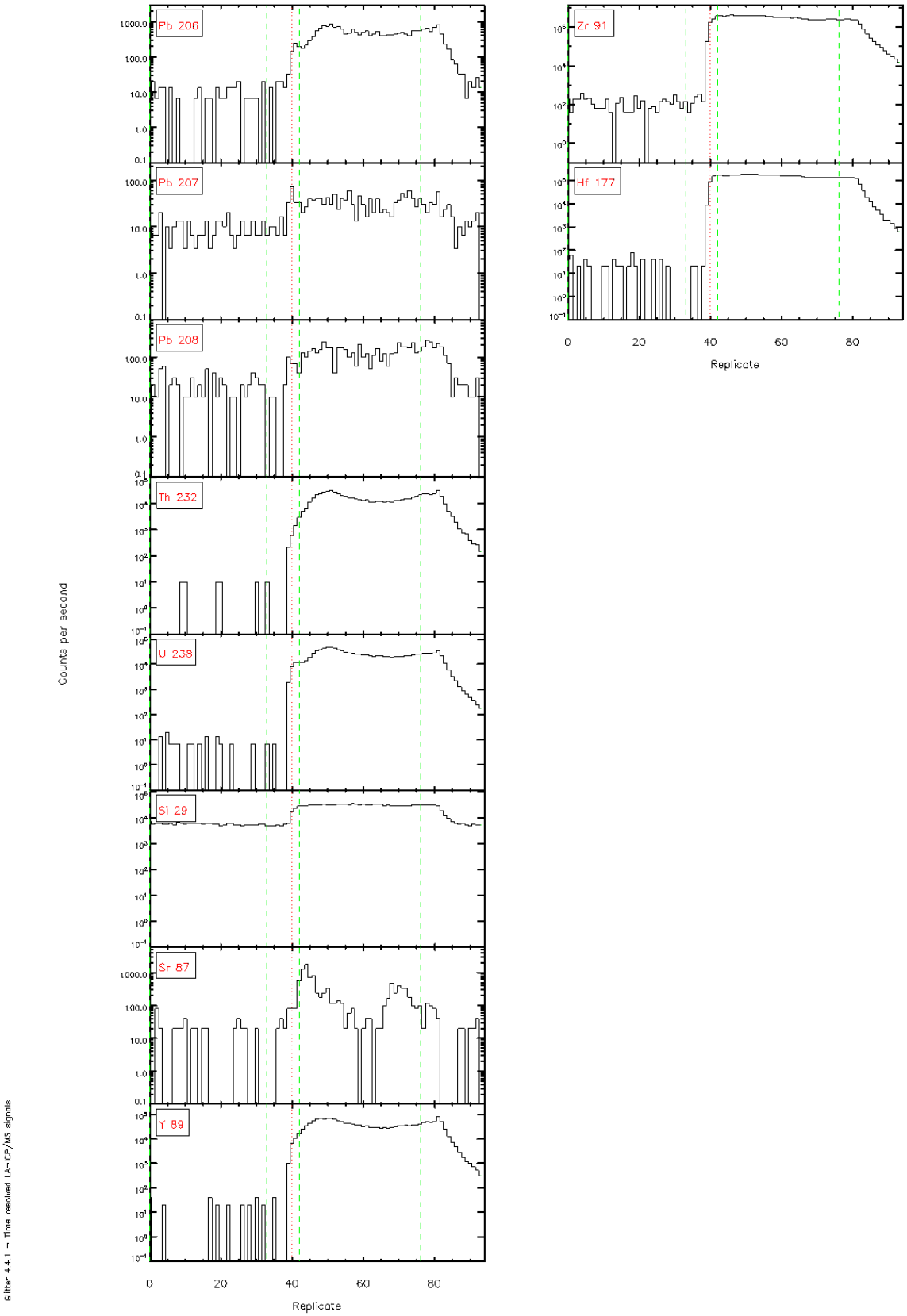
Pb 206
Pb 207
Pb 208
Th 232
U 238
Si 29
Sr 87
Y 89
Zr 91
Hf 177
Counts per second
Replicate
Glitter 4.4.1 - Time resolved LA-ICP/MS signals

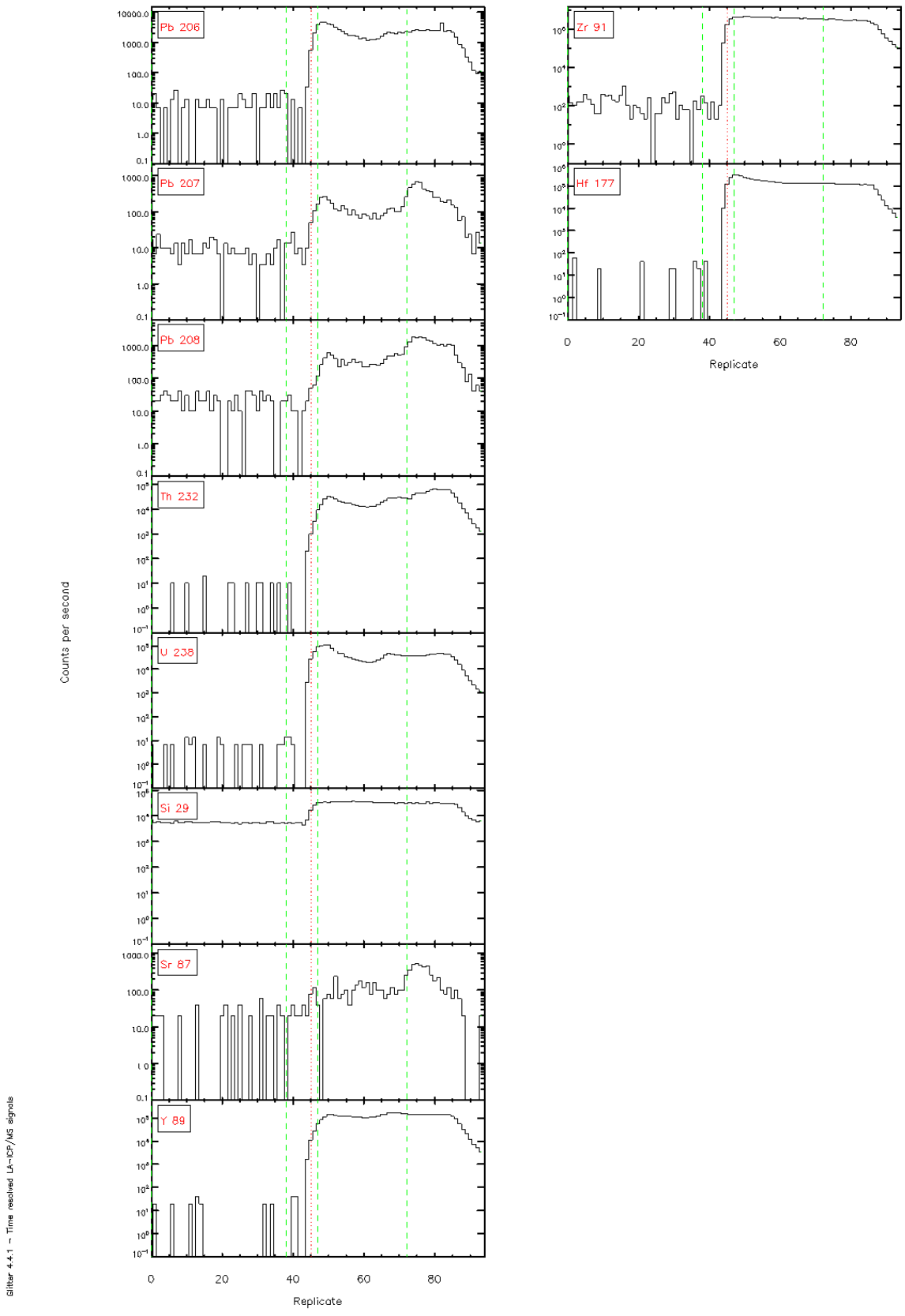
Pb 206
Pb 207
Pb 208
Th 232
U 238
Si 29
Sr 87
Y 89
Zr 91
Hf 177
Counts per second
Replicate
Glitter 4.4.1 – Time resolved LA-ICP/MS signals

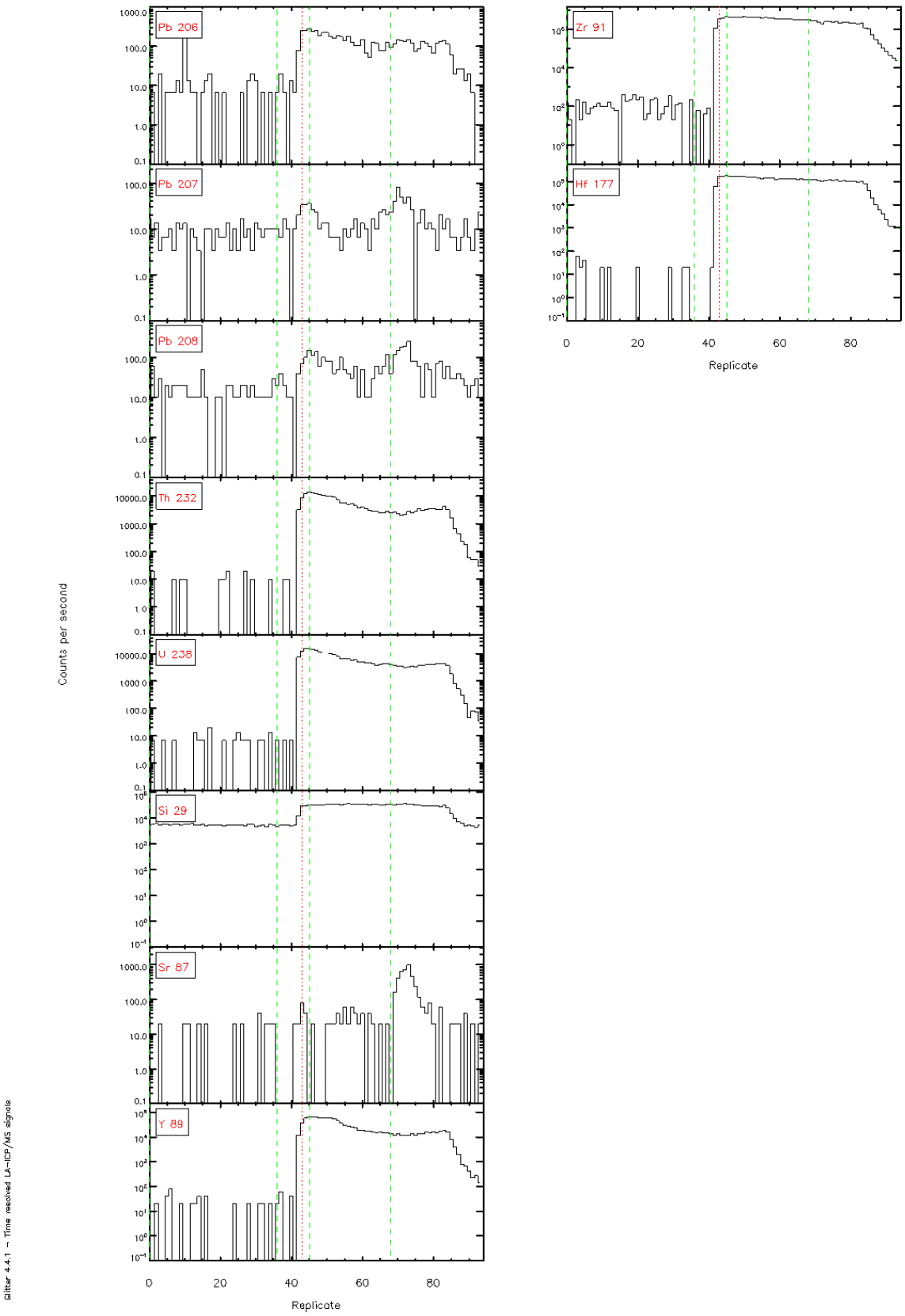
Pb 206
Pb 207
Pb 208
Th 232
U 238
Si 29
Sr 87
Y 89
Zr 91
Hf 177
Counts per second
Replicate
Glitter 4.4.1 - Time resolved LA-ICP/MS signals

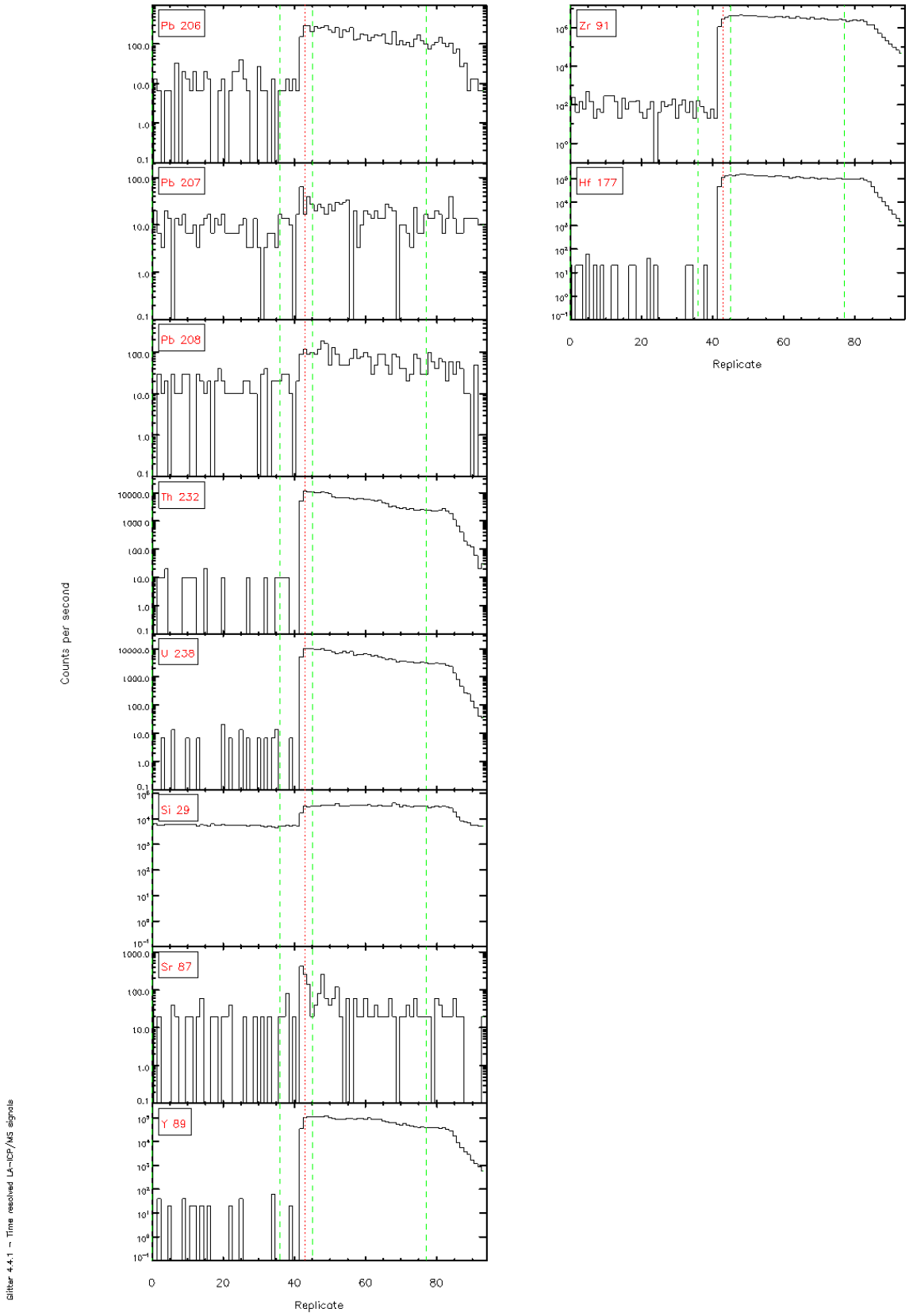
Pb 206
Pb 207
Pb 208
Th 232
U 238
Si 29
Sr 87
Y 89
Zr 91
Hf 177
Counts per second
Replicate
Glitter 4.4.1 - Time resolved LA-ICP/MS signals

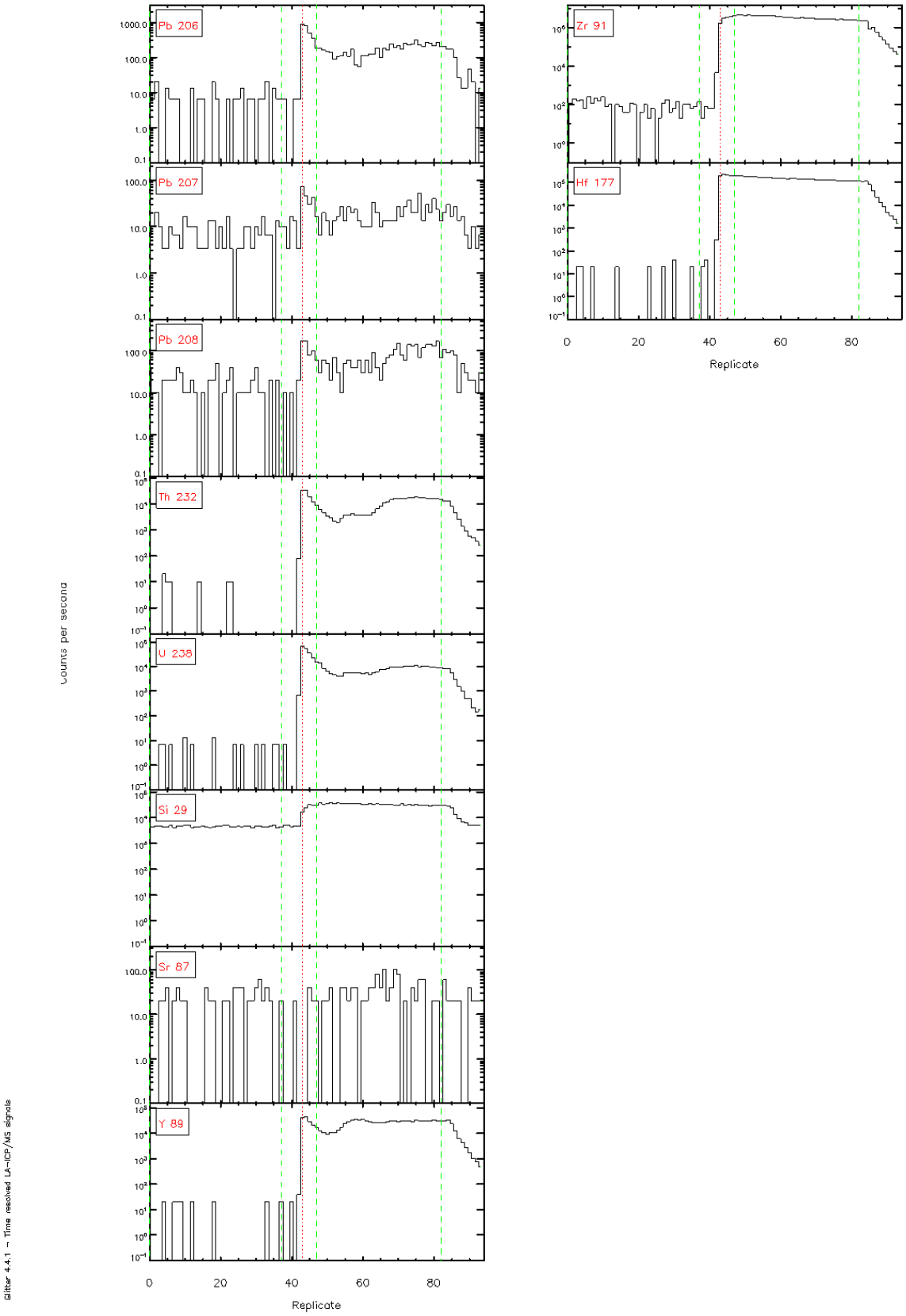
Pb 206
Pb 207
Pb 208
Th 232
U 238
Si 29
Sr 87
Y 89
Zr 91
Hf 177
Counts per second
Replicate
Glitter 4.4.1 - Time resolved LA-ICP/MS signals

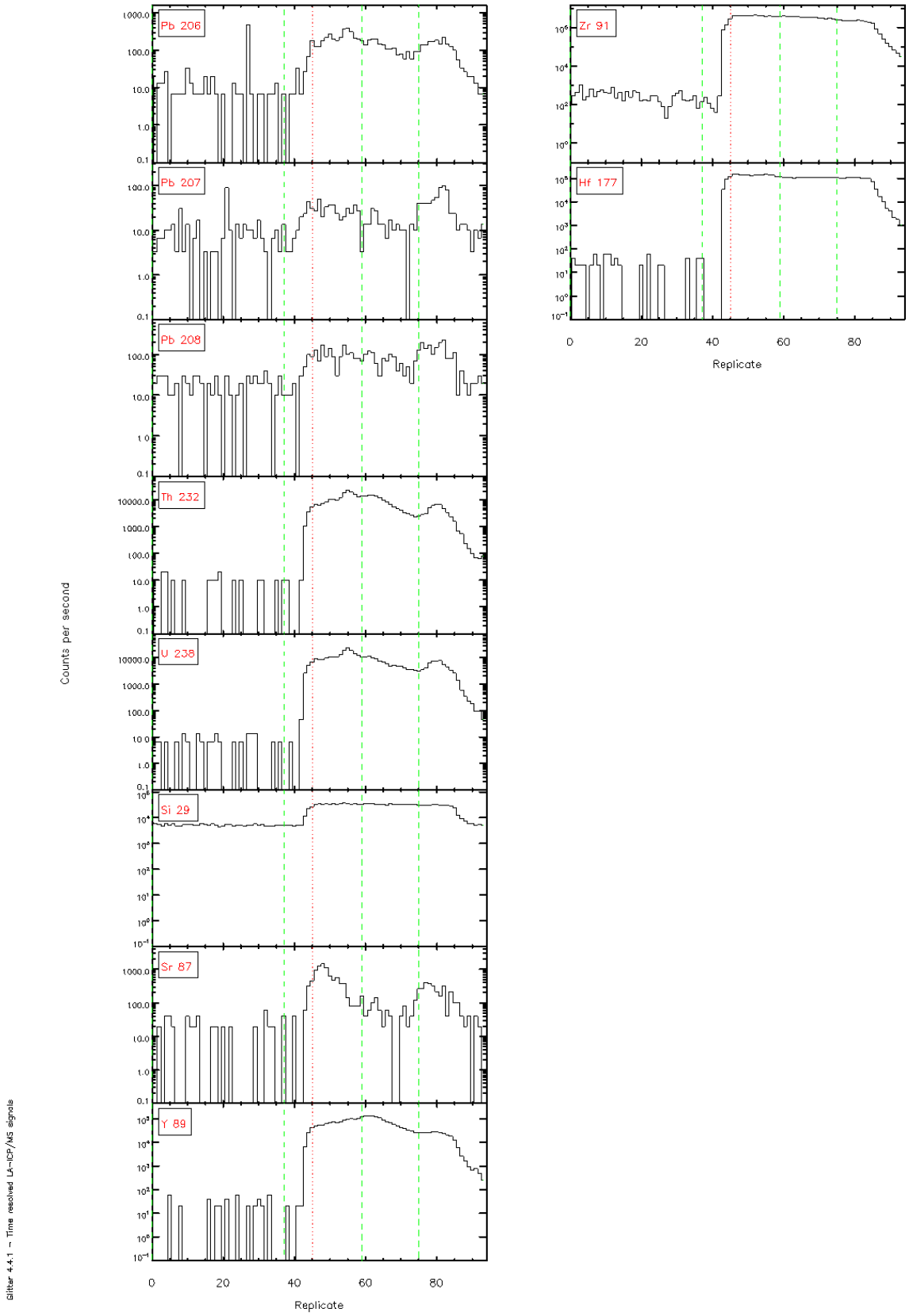
Pb 206
Pb 207
Pb 208
Th 232
U 238
Si 29
Sr 87
Y 89
Zr 91
Hf 177
Counts per second
Replicate
Glitter 4.4.1 - Time resolved LA-ICP/MS signals

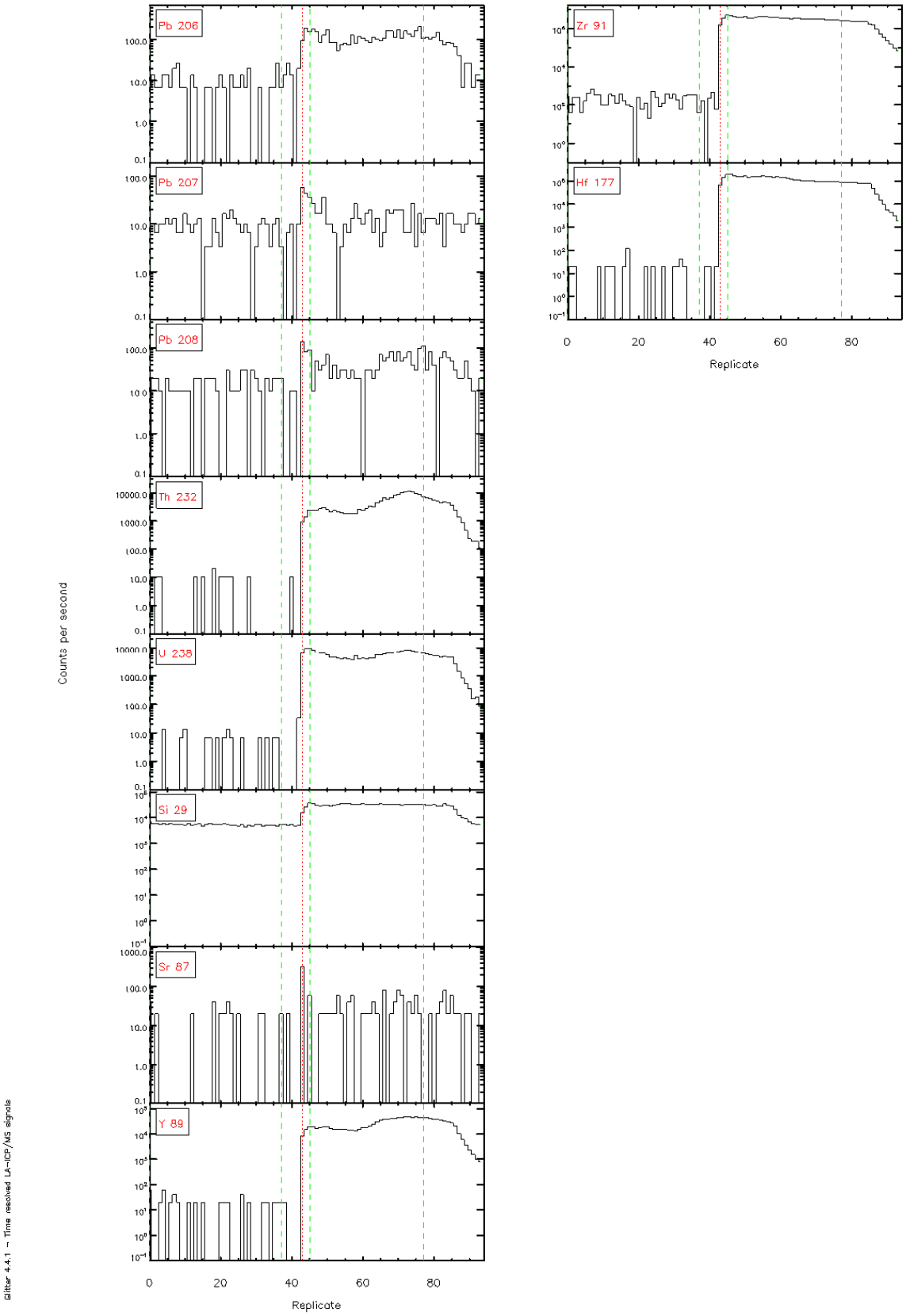
Pb 206
Pb 207
Pb 208
Th 232
U 238
Si 29
Sr 87
Y 89
Zr 91
Hf 177
Counts per second
Replicate
Glitter 4.4.1 - Time resolved LA-ICP/MS signals

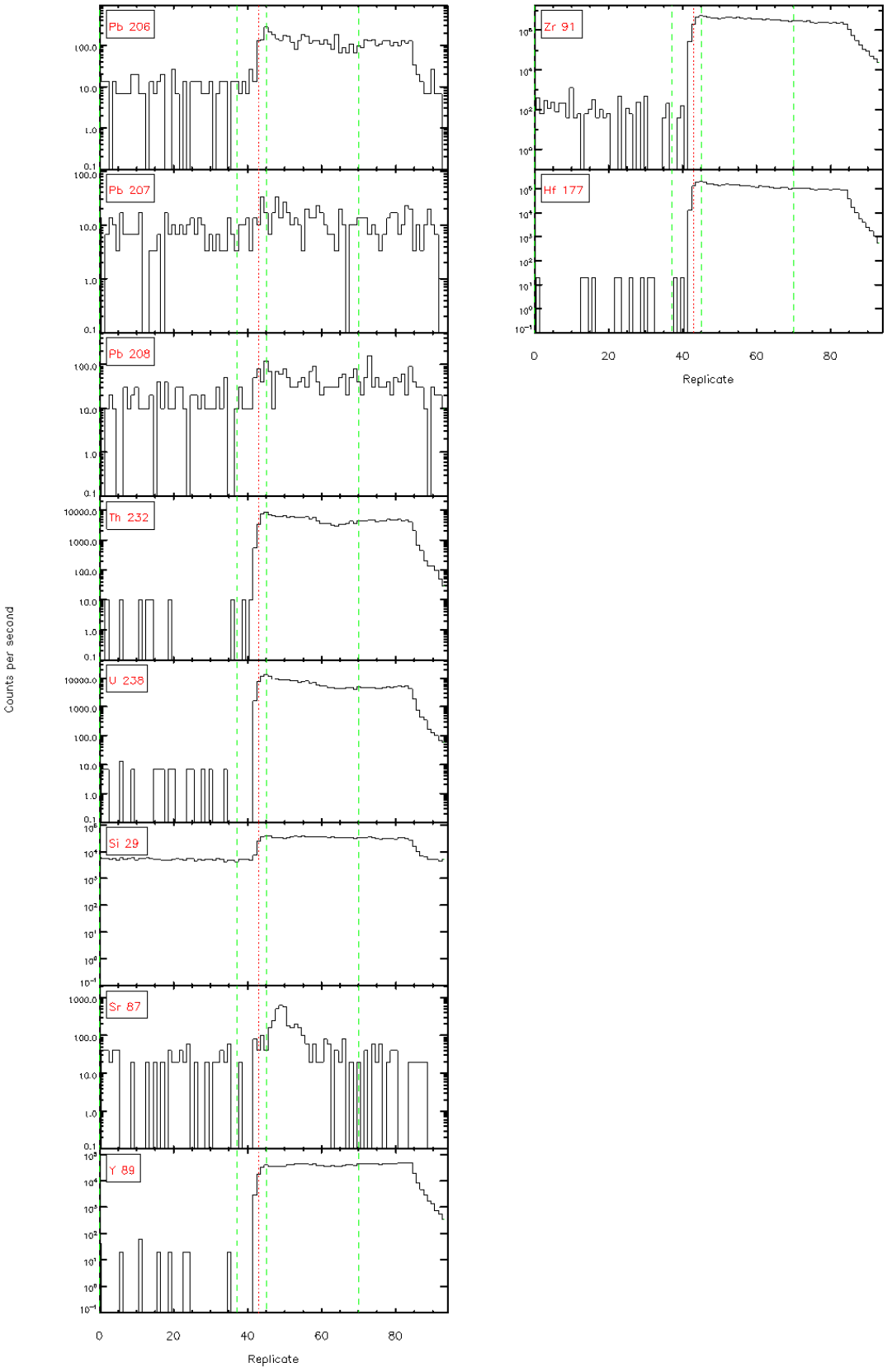
Pb 206
Pb 207
Pb 208
Th 232
U 238
Si 29
Sr 87
Y 89
Zr 91
Hf 177
Counts per second
Replicate
Glitter 4.4.1 - Time resolved LA-ICP/MS signals

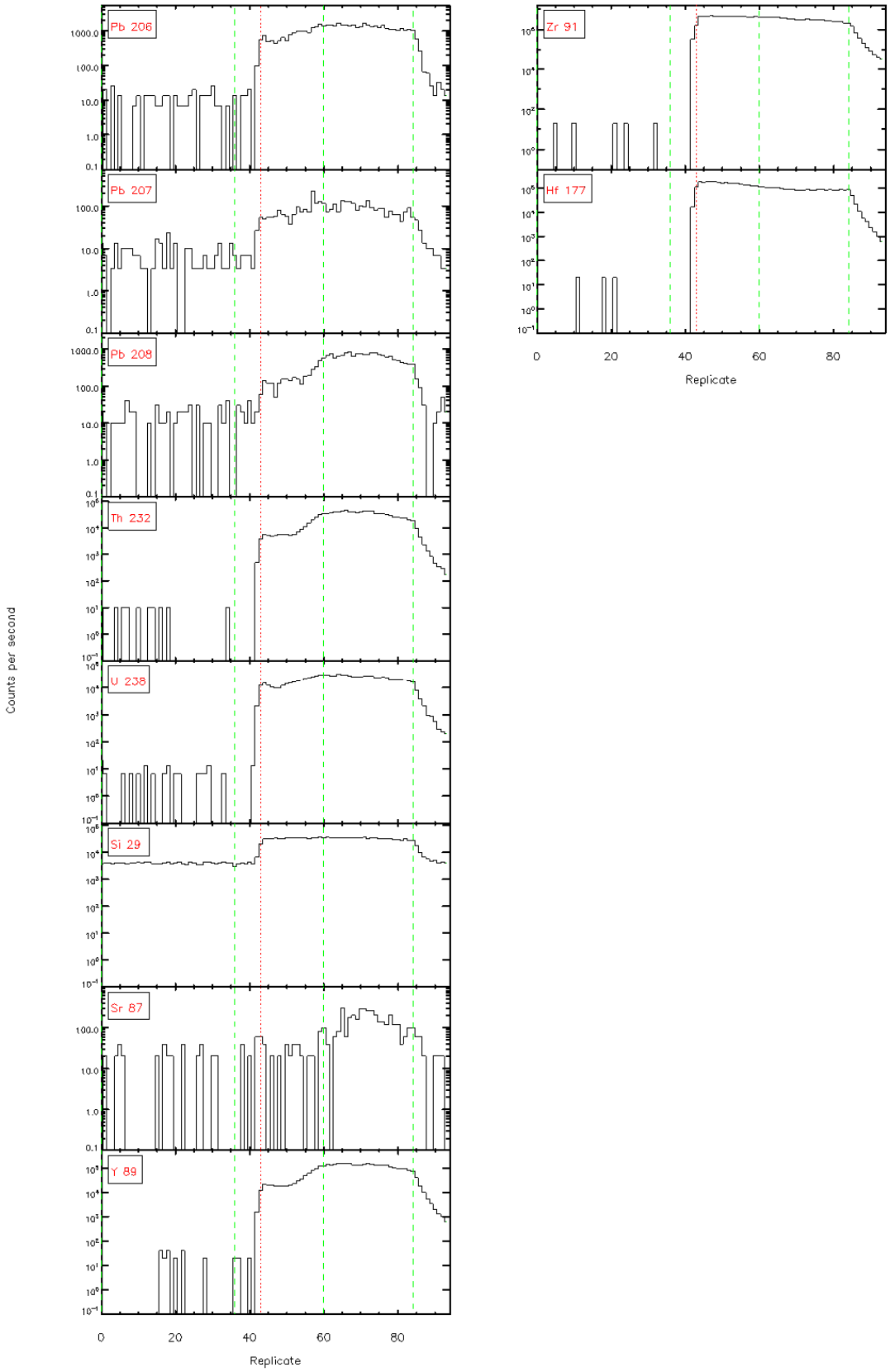
Pb 206
Pb 207
Pb 208
Th 232
U 238
Si 29
Sr 87
Y 89
Zr 91
Hf 177
Counts per second
Replicate
Glitter 4.4.1 - Time resolved LA-ICP/MS signals

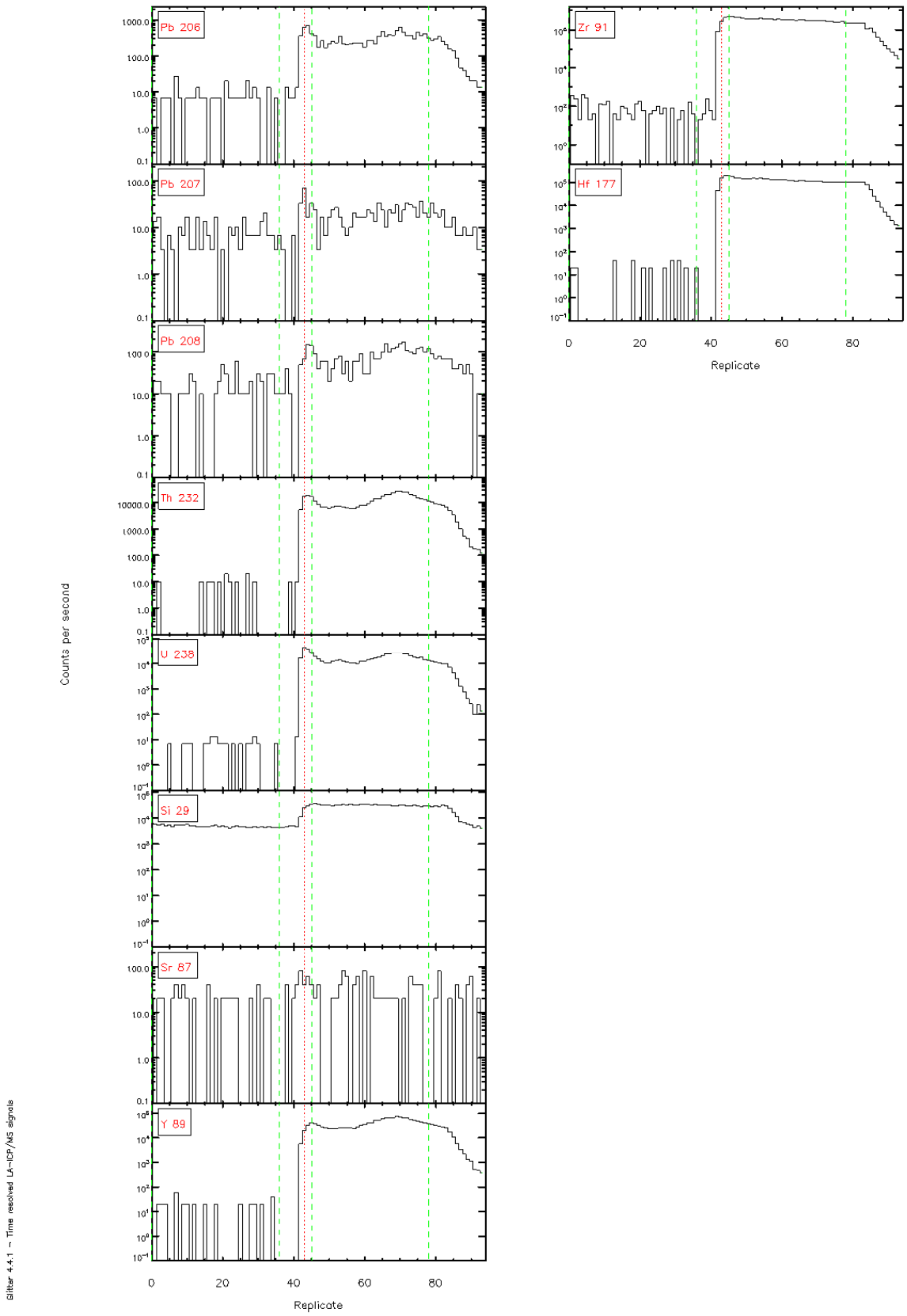
Pb 206
Pb 207
Pb 208
Th 232
U 238
Si 29
Sr 87
Y 89
Zr 91
Hf 177
Counts per second
Replicate
Glitter 4.4.1 - Time resolved LA-ICP/MS signals

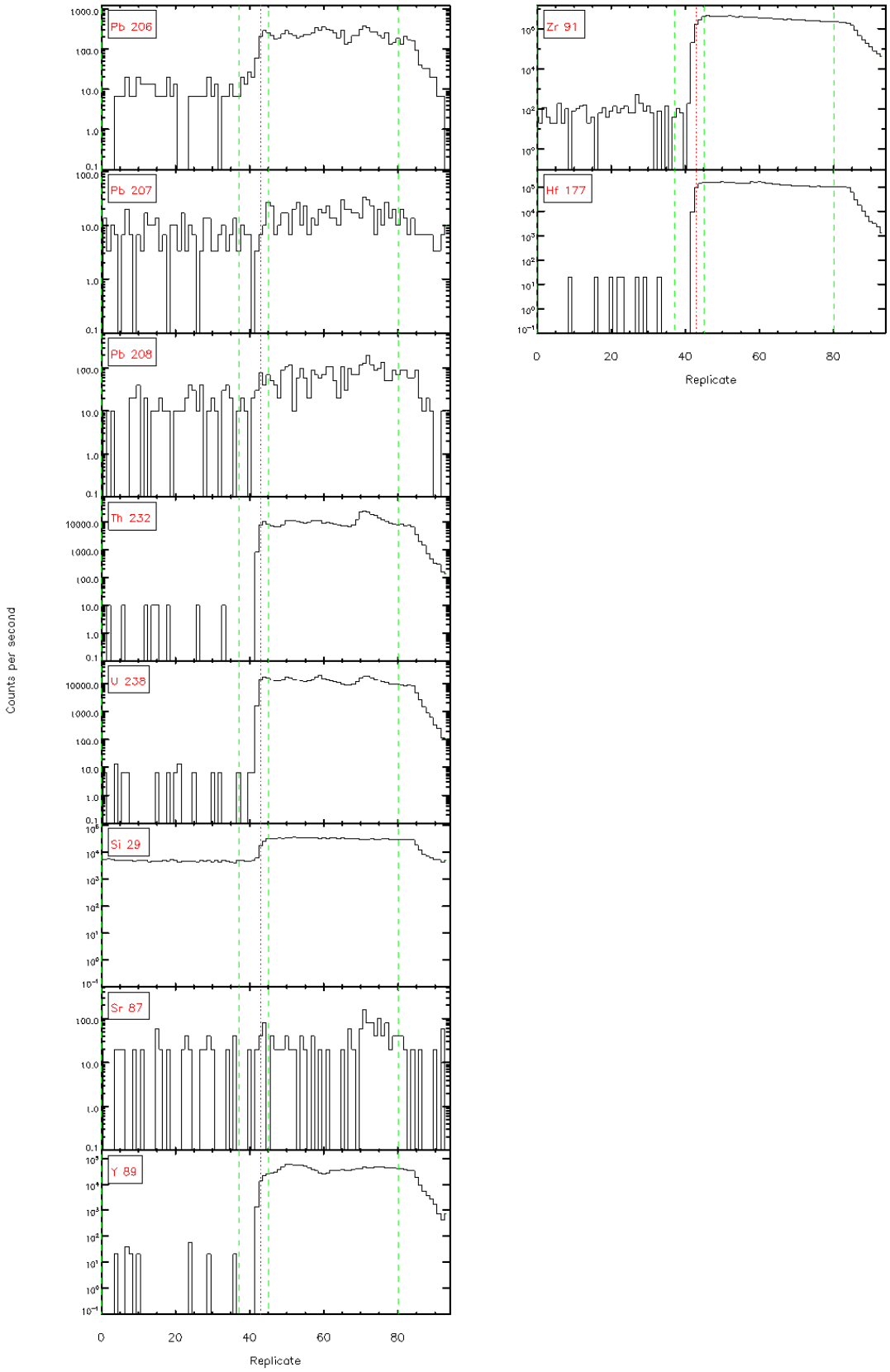
Pb 206
Pb 207
Pb 208
Th 232
U 238
Si 29
Sr 87
Y 89
Zr 91
Hf 177
Counts per second
Replicate
Glitter 4.4.1 - Time resolved LA-ICP/MS signals

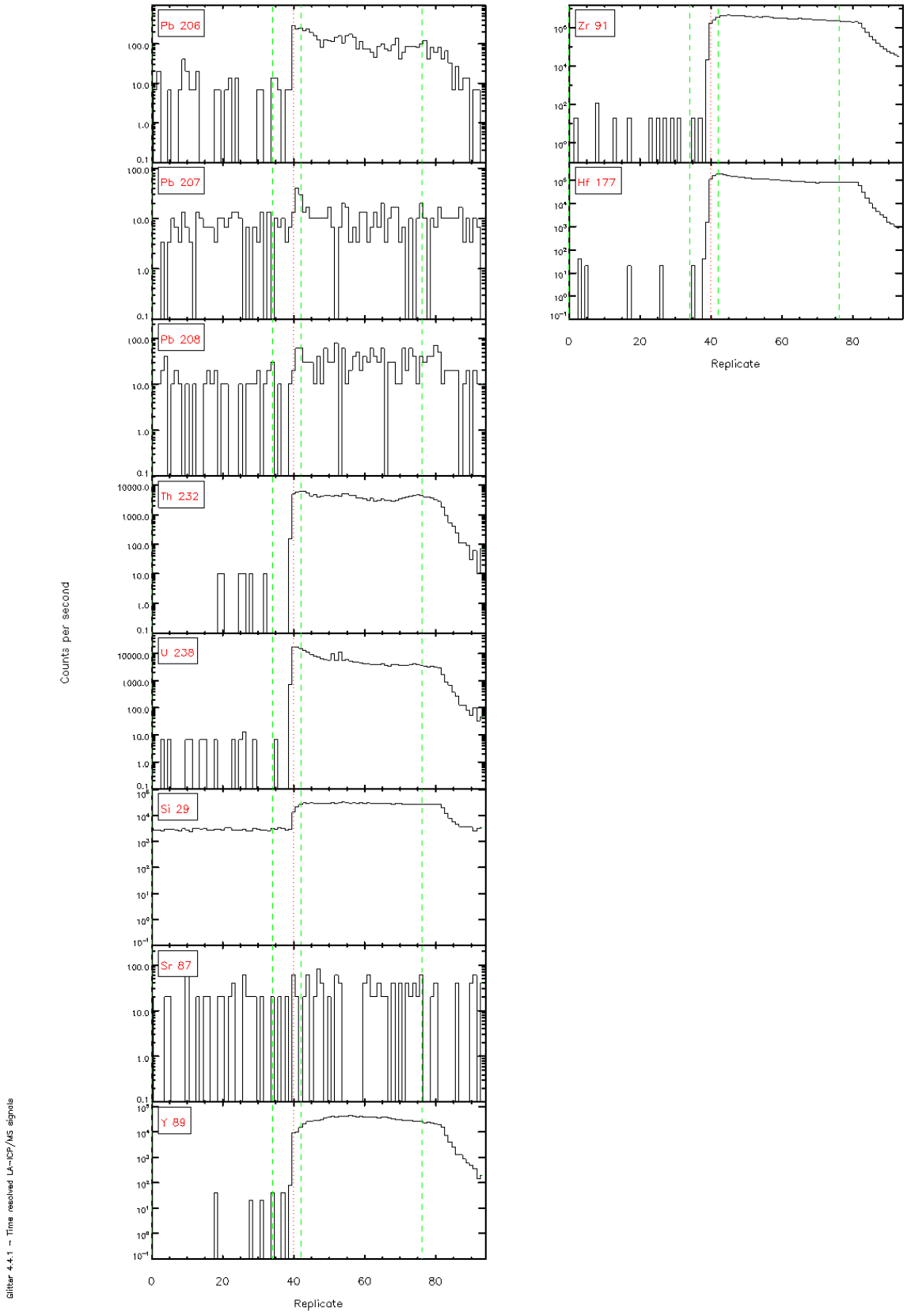
Pb 206
Pb 207
Pb 208
Th 232
U 238
Si 29
Sr 87
Y 89
Zr 91
Hf 177
Counts per second
Replicate
Glitter 4.4.1 - Time resolved LA-ICP/MS signals

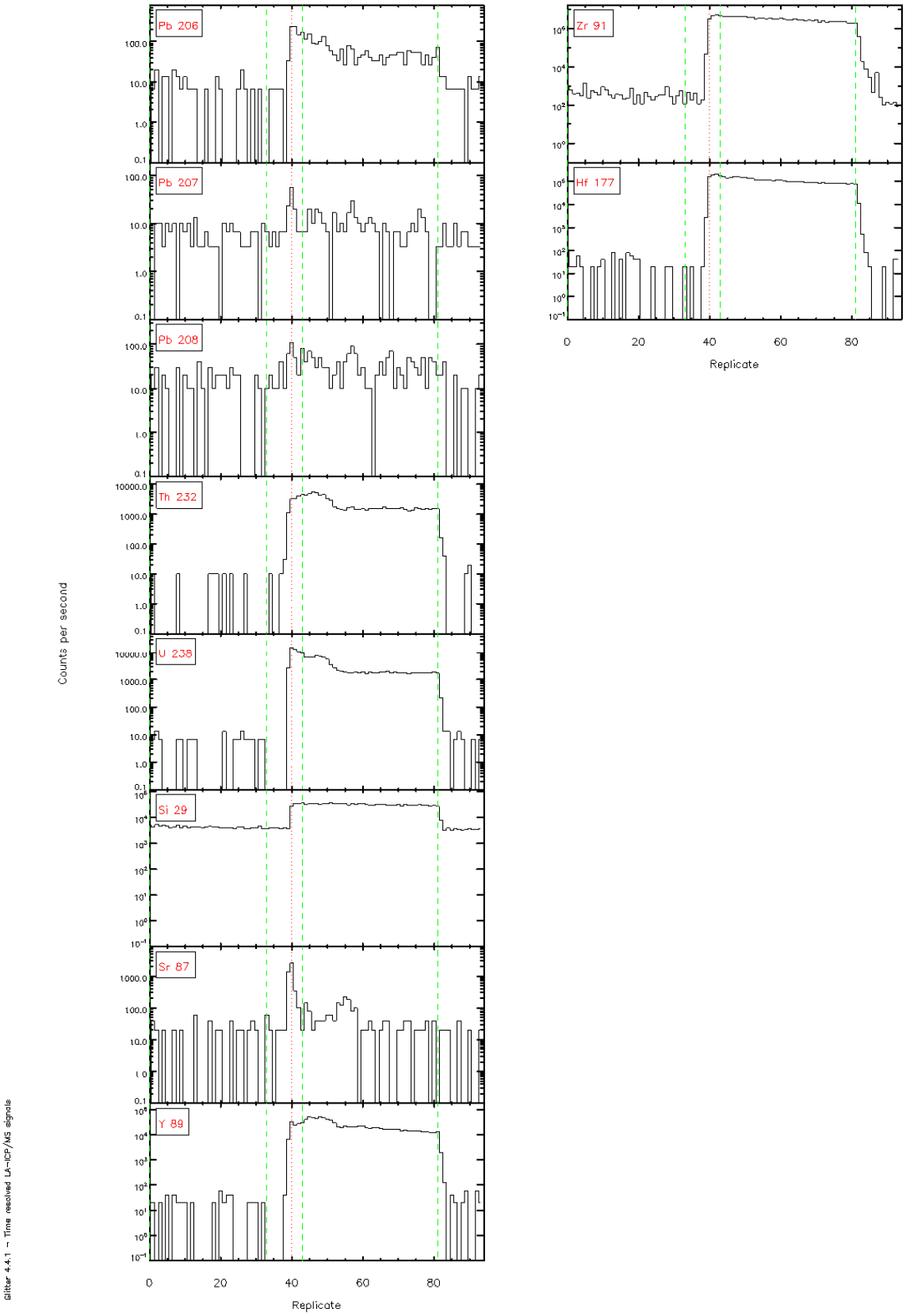
Pb 206
Pb 207
Pb 208
Th 232
U 238
Si 29
Sr 87
Y 89
Zr 91
Hf 177
Counts per second
Replicate
Glitter 4.4.1 - Time resolved LA-ICP/MS signals

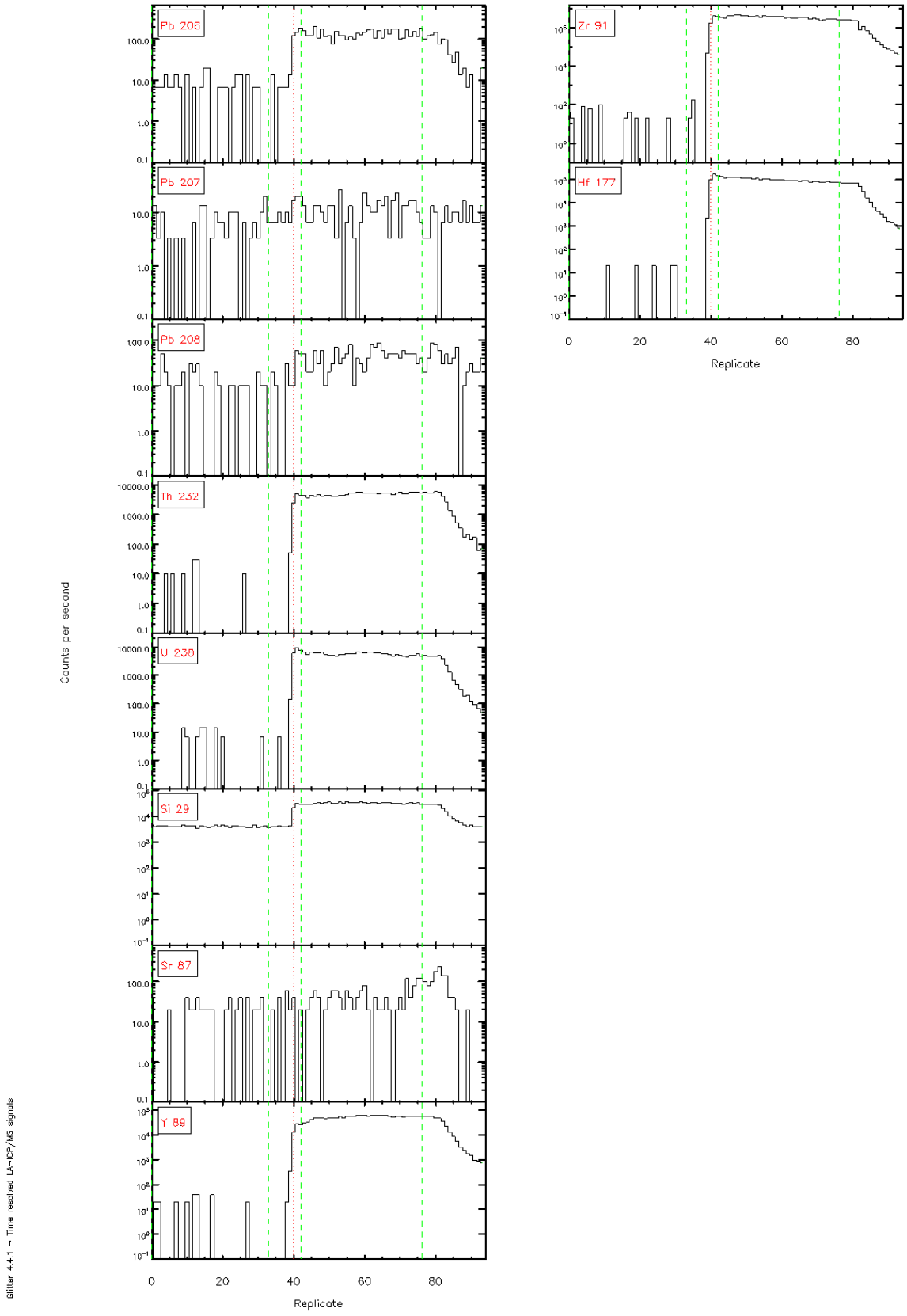
Pb 206
Pb 207
Pb 208
Th 232
U 238
Si 29
Sr 87
Y 89
Zr 91
Hf 177
Counts per second
Replicate
Glitter 4.4.1 - Time resolved LA-ICP/MS signals

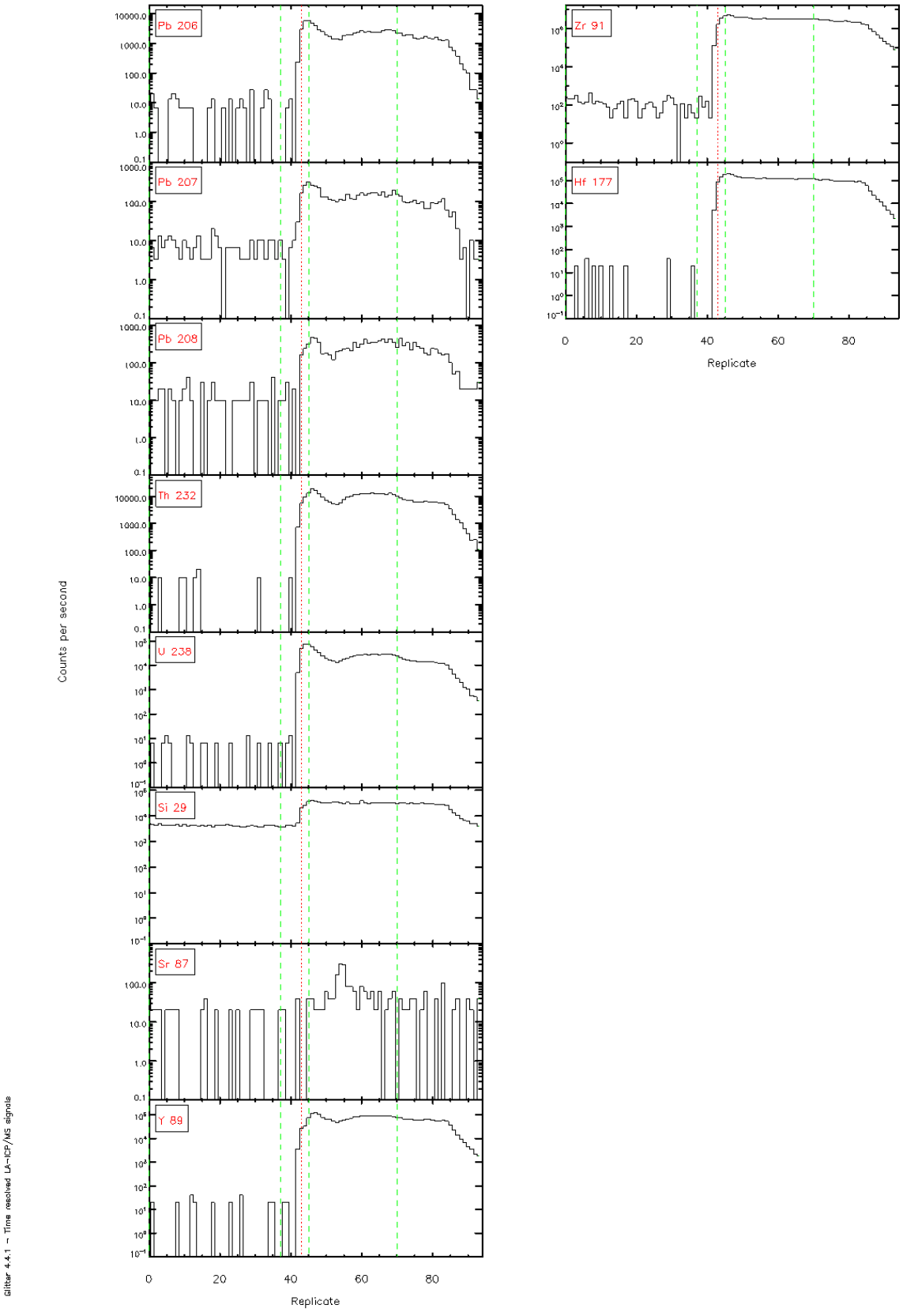
Pb 206
Pb 207
Pb 208
Th 232
U 238
Si 29
Sr 87
Y 89
Zr 91
Hf 177
Counts per second
Replicate
Glitter 4.4.1 - Time resolved LA-ICP/MS signals

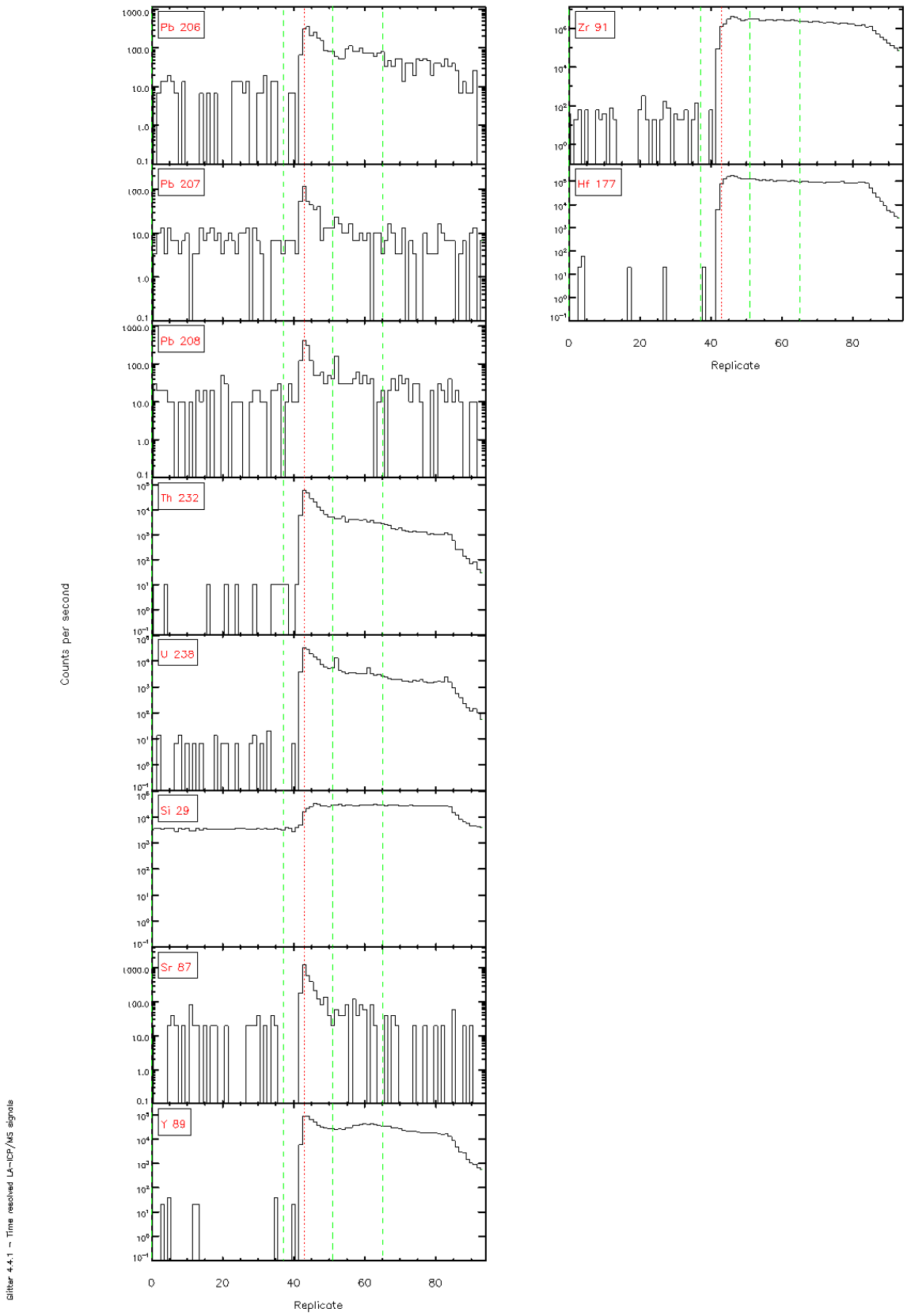
Pb 206
Pb 207
Pb 208
Th 232
U 238
Si 29
Sr 87
Y 89
Zr 91
Hf 177
Counts per second
Replicate
Glitter 4.4.1 - Time resolved LA-ICP/MS signals

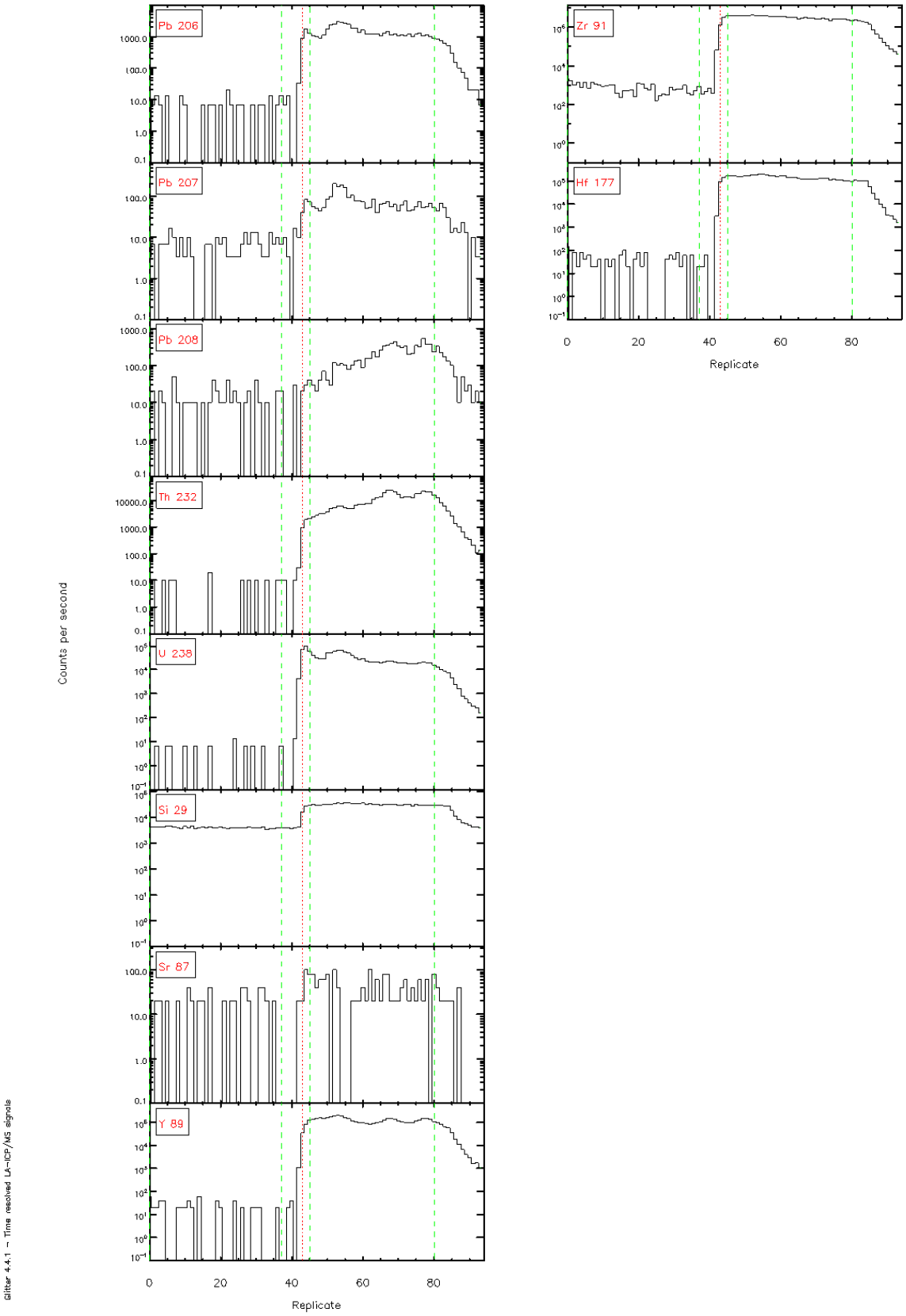
Pb 206
Pb 207
Pb 208
Th 232
U 238
Si 29
Sr 87
Y 89
Zr 91
Hf 177
Counts per second
Replicate
Glitter 4.4.1 - Time resolved LA-ICP/MS signals

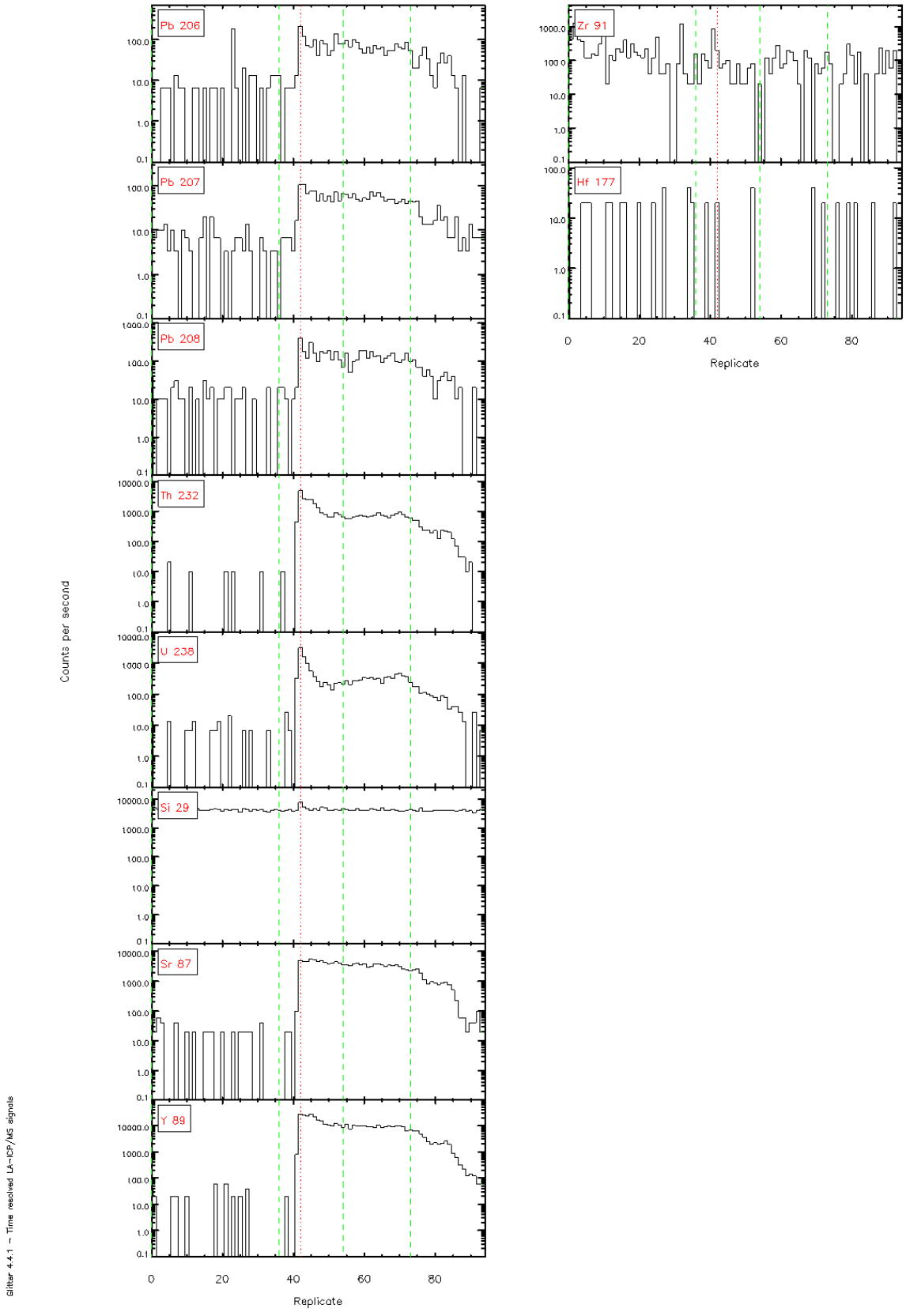
Pb 206
Pb 207
Pb 208
Th 232
U 238
Si 29
Sr 87
Y 89
Zr 91
Hf 177
Counts per second
Replicate
Glitter 4.4.1 - Time resolved LA-ICP/MS signals

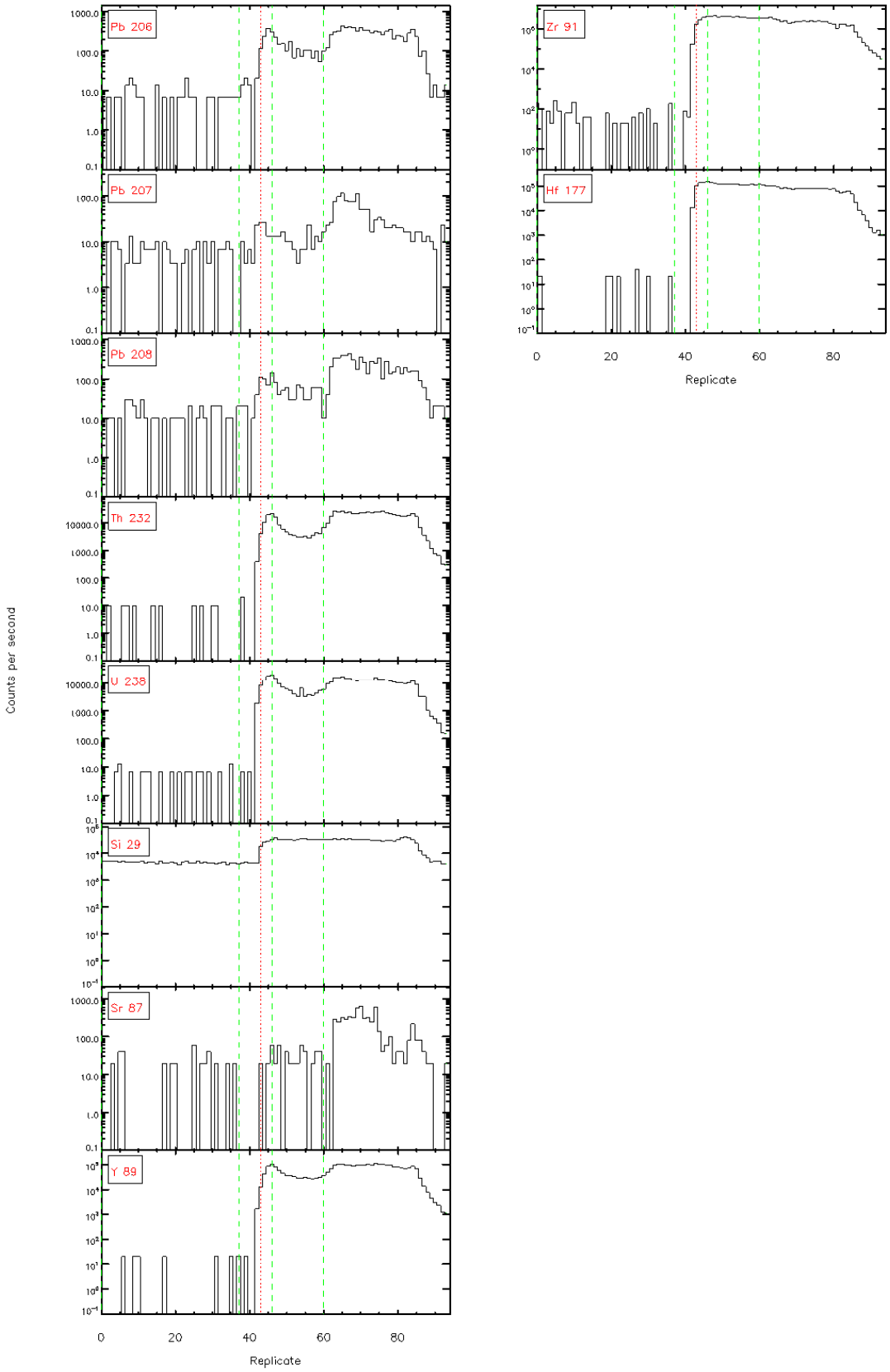
Pb 206
Pb 207
Pb 208
Th 232
U 238
Si 29
Sr 87
Y 89
Zr 91
Hf 177
Counts per second
Replicate
Glitter 4.4.1 - Time resolved LA-ICP/MS signals

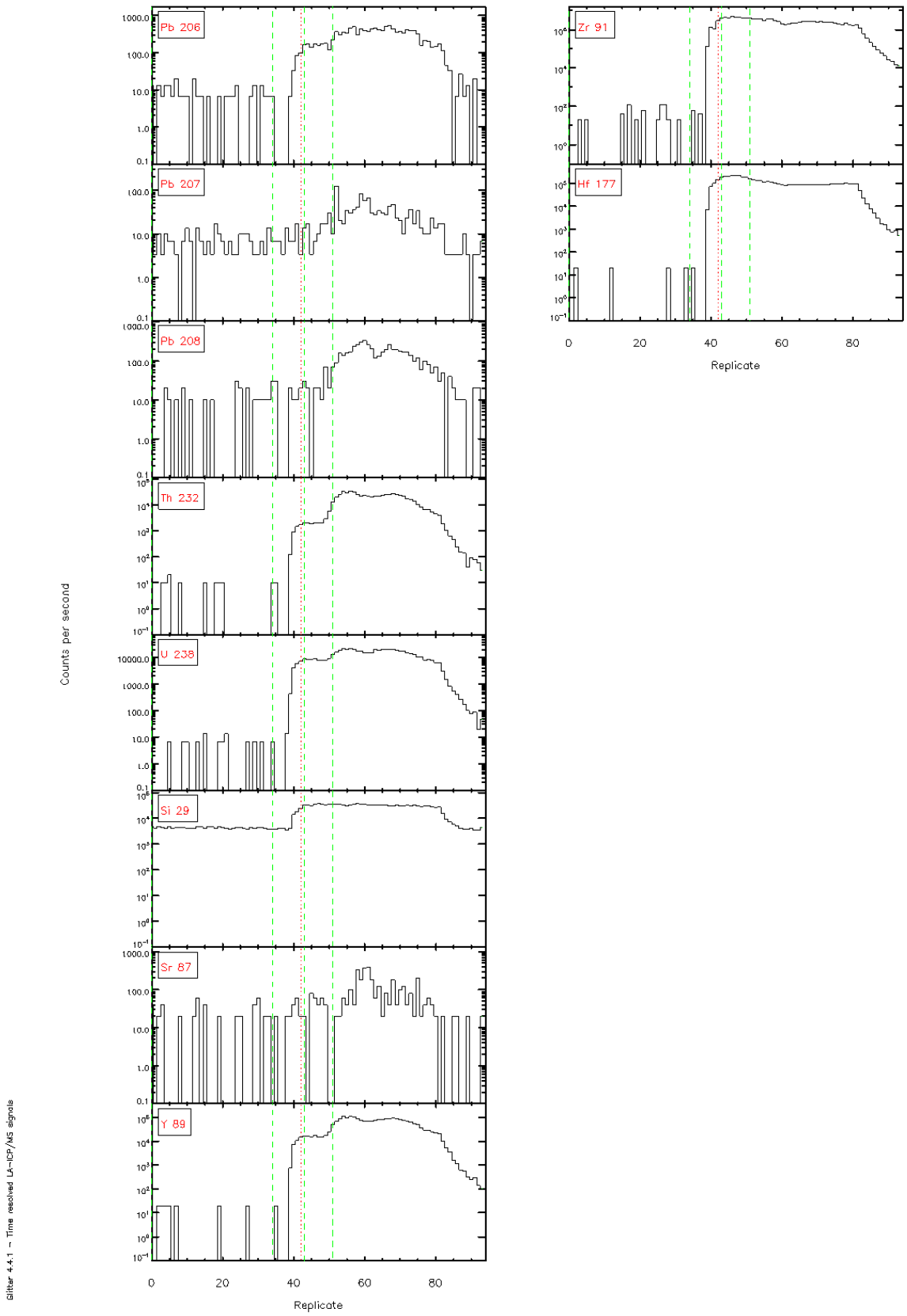
Pb 206
Pb 207
Pb 208
Th 232
U 238
Si 29
Sr 87
Y 89
Zr 91
Hf 177
Counts per second
Replicate
Glitter 4.4.1 - Time resolved LA-ICP/MS signals

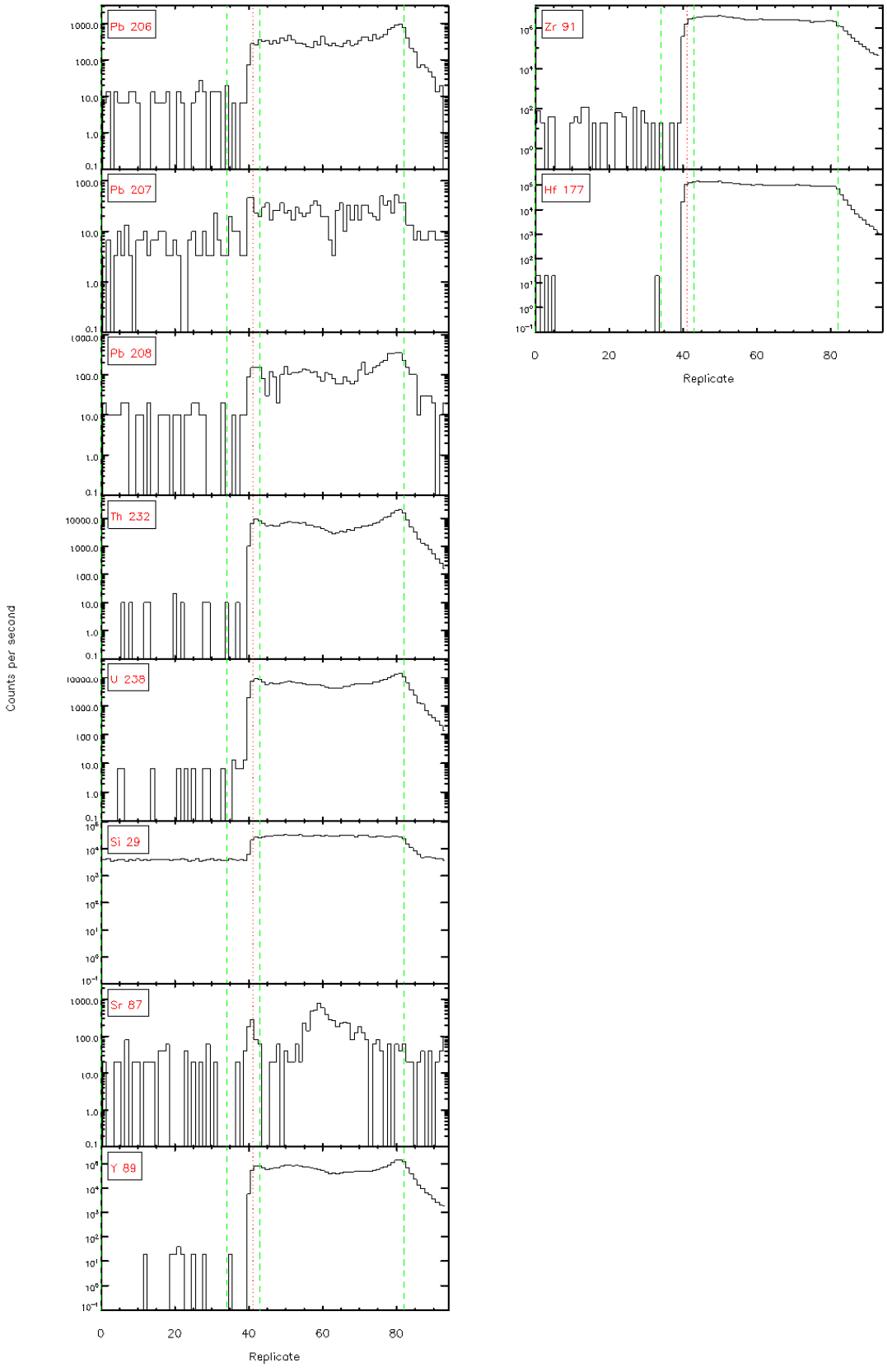
Pb 206
Pb 207
Pb 208
Th 232
U 238
Si 29
Sr 87
Y 89
Zr 91
Hf 177
Counts per second
Replicate
Glitter 4.4.1 - Time resolved LA-ICP/MS signals

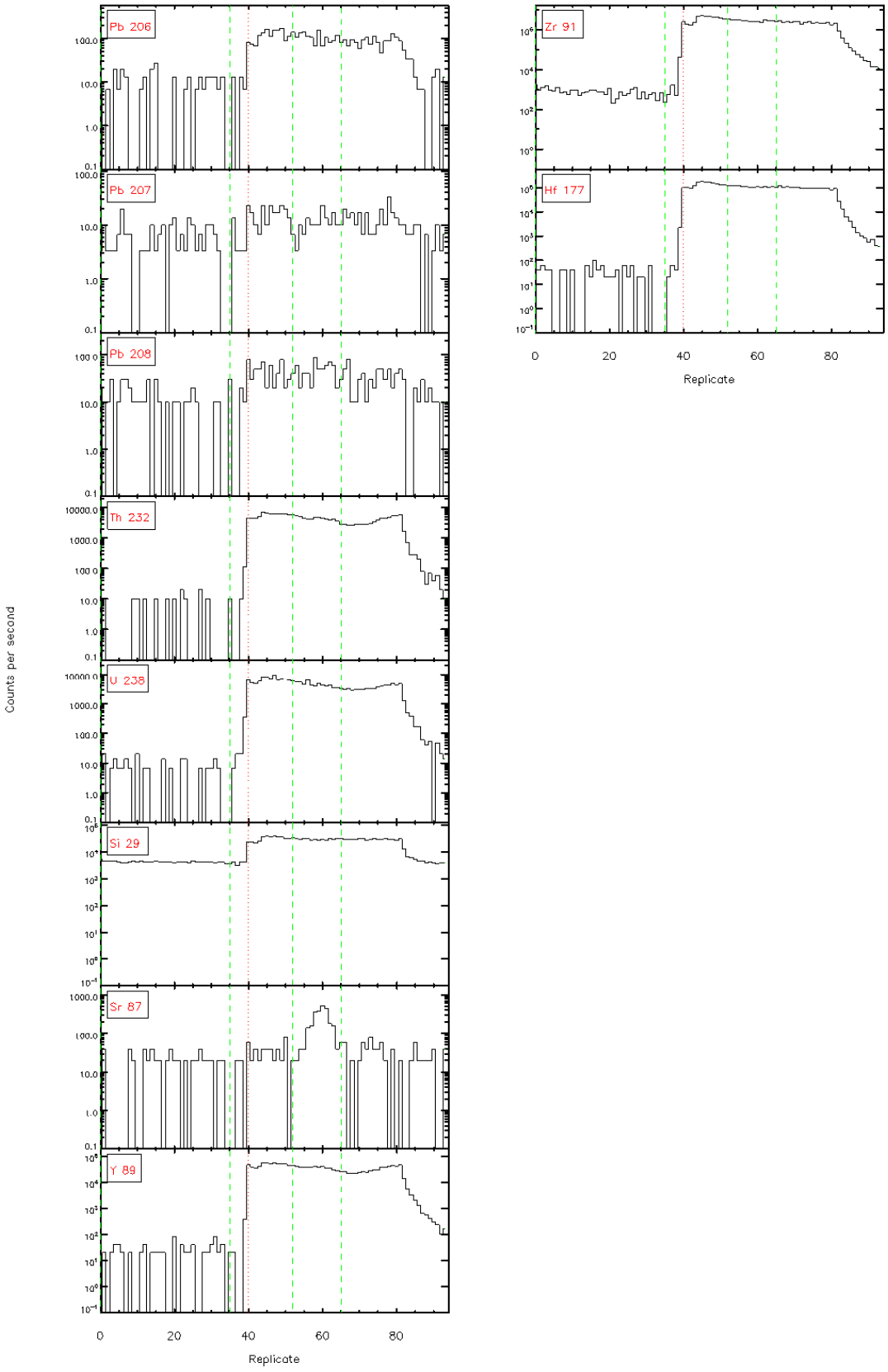
Pb 206
Pb 207
Pb 208
Th 232
U 238
Si 29
Sr 87
Y 89
Zr 91
Hf 177
Counts per second
Replicate
Glitter 4.4.1 - Time resolved LA-ICP/MS signals

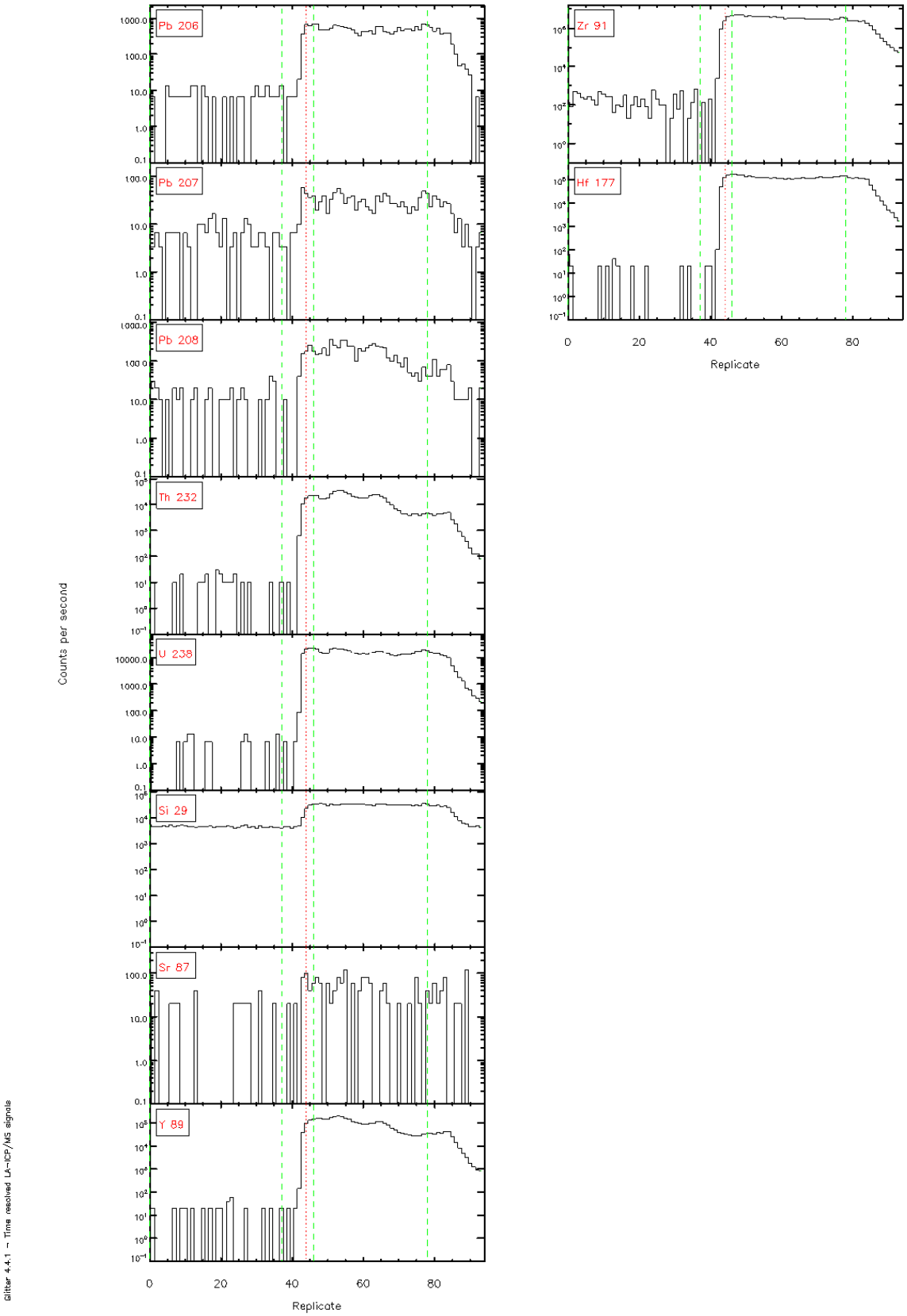
Pb 206
Pb 207
Pb 208
Th 232
U 238
Si 29
Sr 87
Y 89
Zr 91
Hf 177
Counts per second
Replicate
Glitter 4.4.1 - Time resolved LA-ICP/MS signals

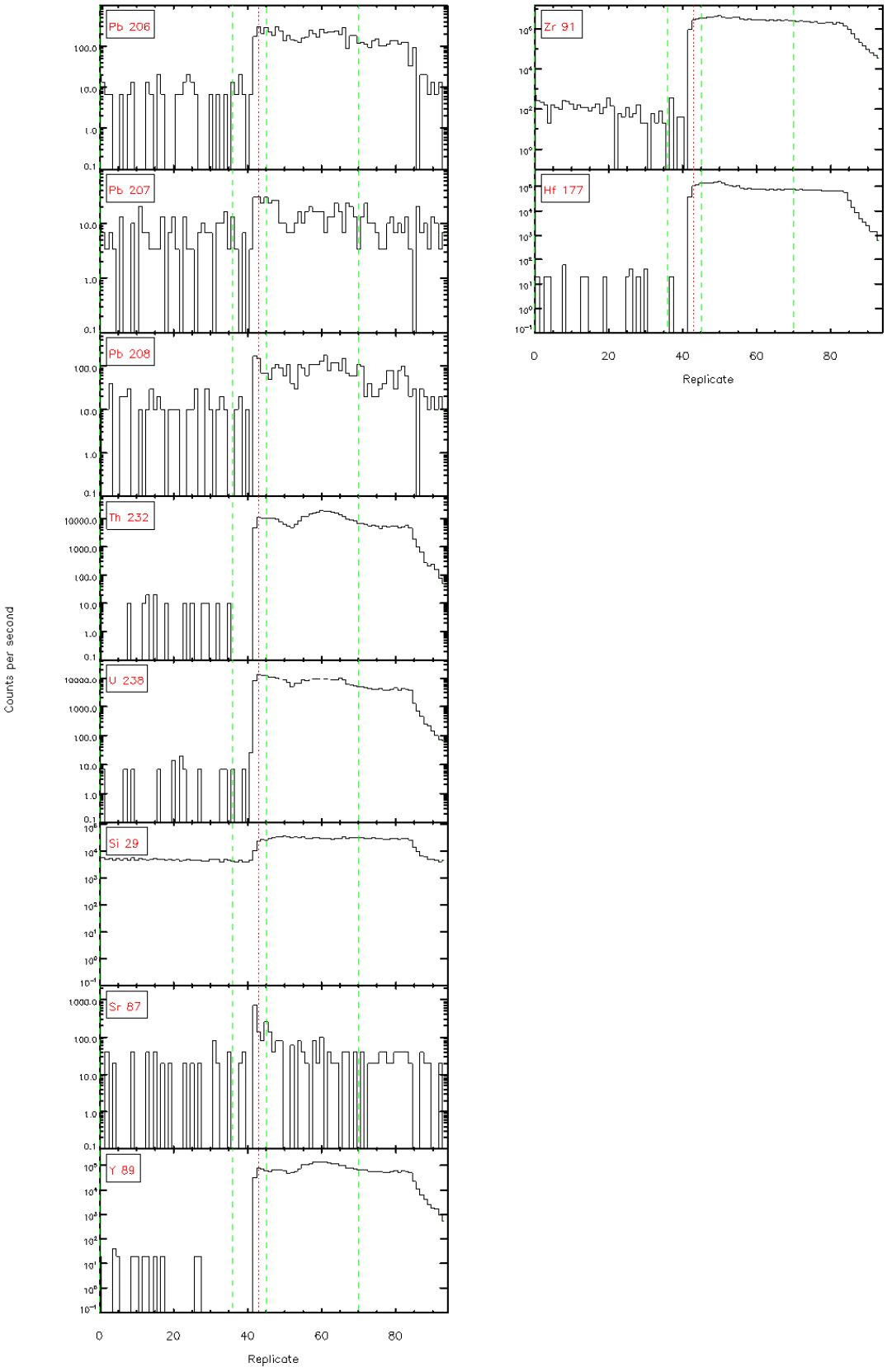
Pb 206
Pb 207
Pb 208
Th 232
U 238
Si 29
Sr 87
Y 89
Zr 91
Hf 177
Counts per second
Replicate
0
20
40
60
80
Glitter 4.4.1 – Time resolved LA-ICP/MS signals

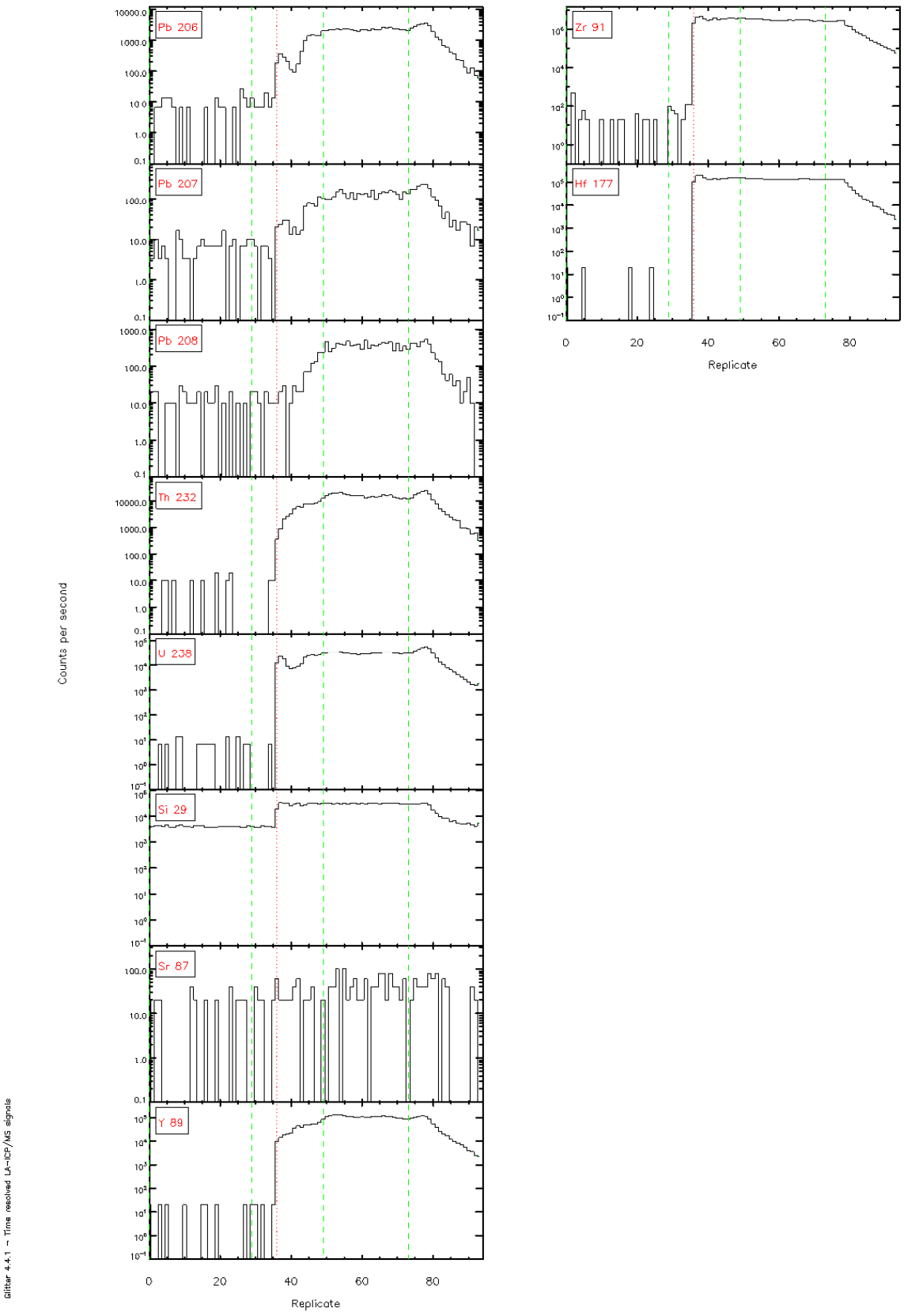
Pb 206
Pb 207
Pb 208
Th 232
U 238
Si 29
Sr 87
Y 89
Zr 91
Hf 177
Counts per second
Replicate
Glitter 4.4.1 - Time resolved LA-ICP/MS signals

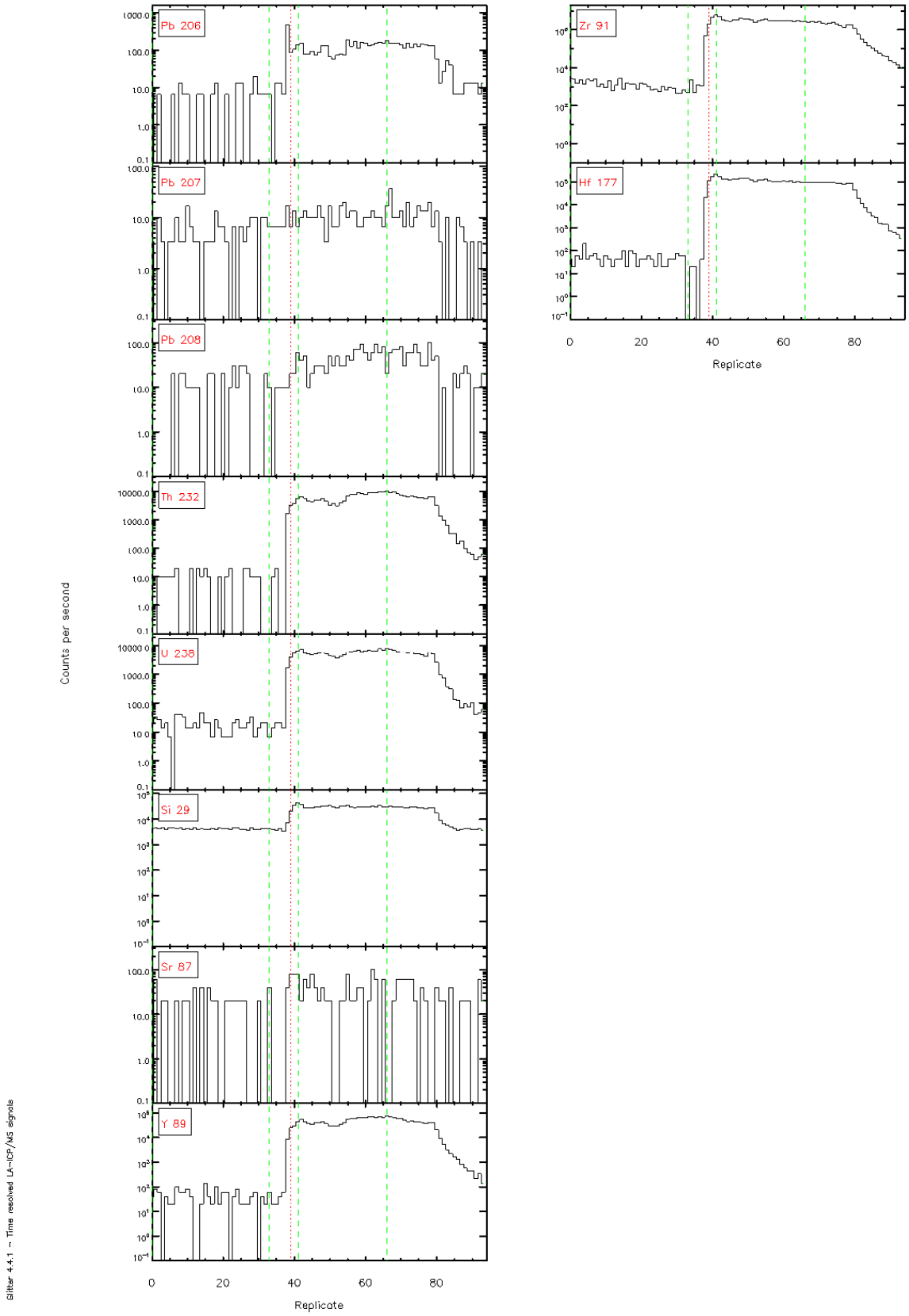
Pb 206
Pb 207
Pb 208
Th 232
U 238
Si 29
Sr 87
Y 89
Zr 91
Hf 177
Counts per second
Replicate
Glitter 4.4.1 - Time resolved LA-ICP/MS signals

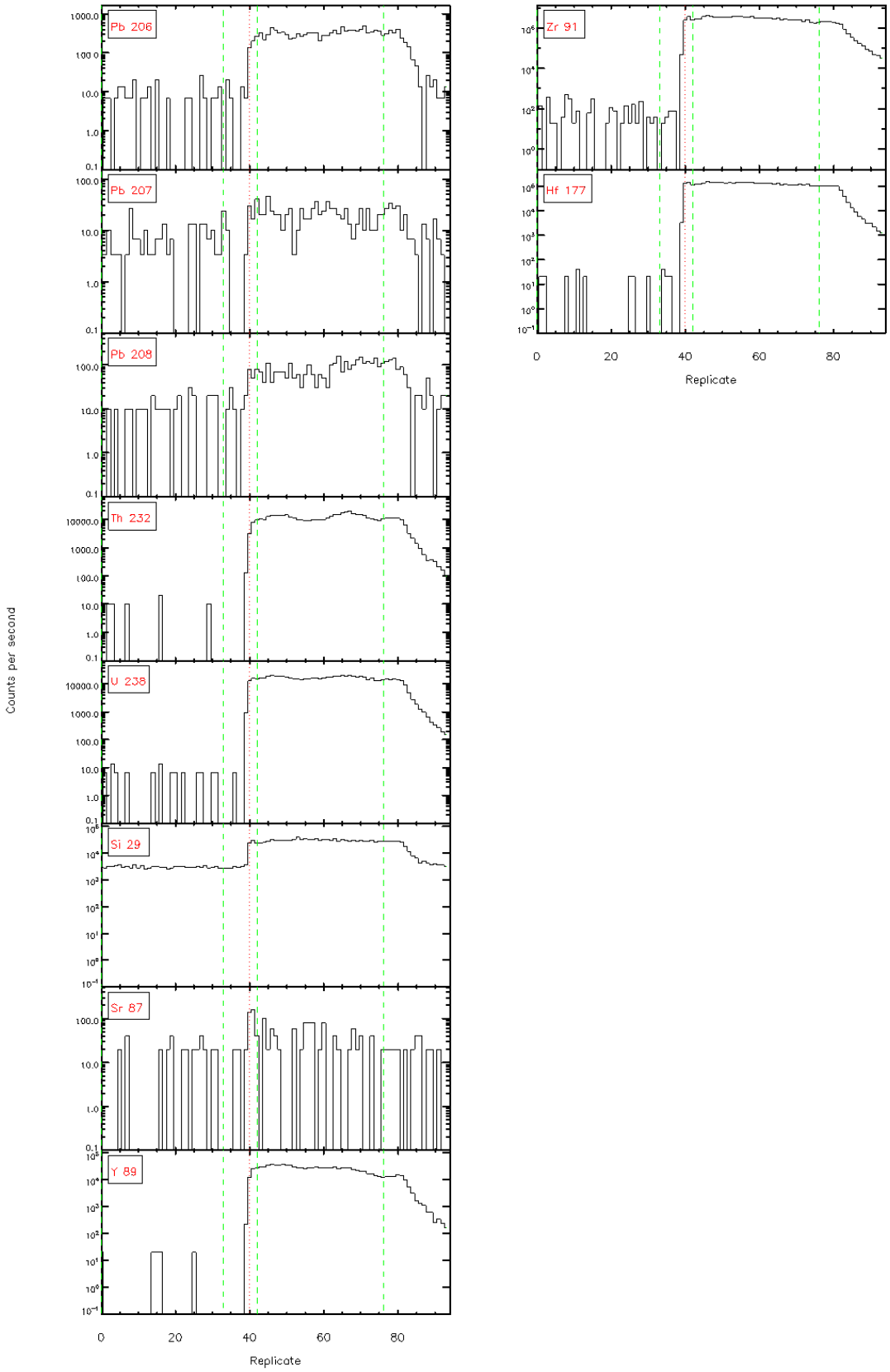
Pb 206
Pb 207
Pb 208
Th 232
U 238
Si 29
Sr 87
Y 89
Zr 91
Hf 177
Counts per second
Replicate
Glitter 4.4.1 - Time resolved LA-ICP/MS signals

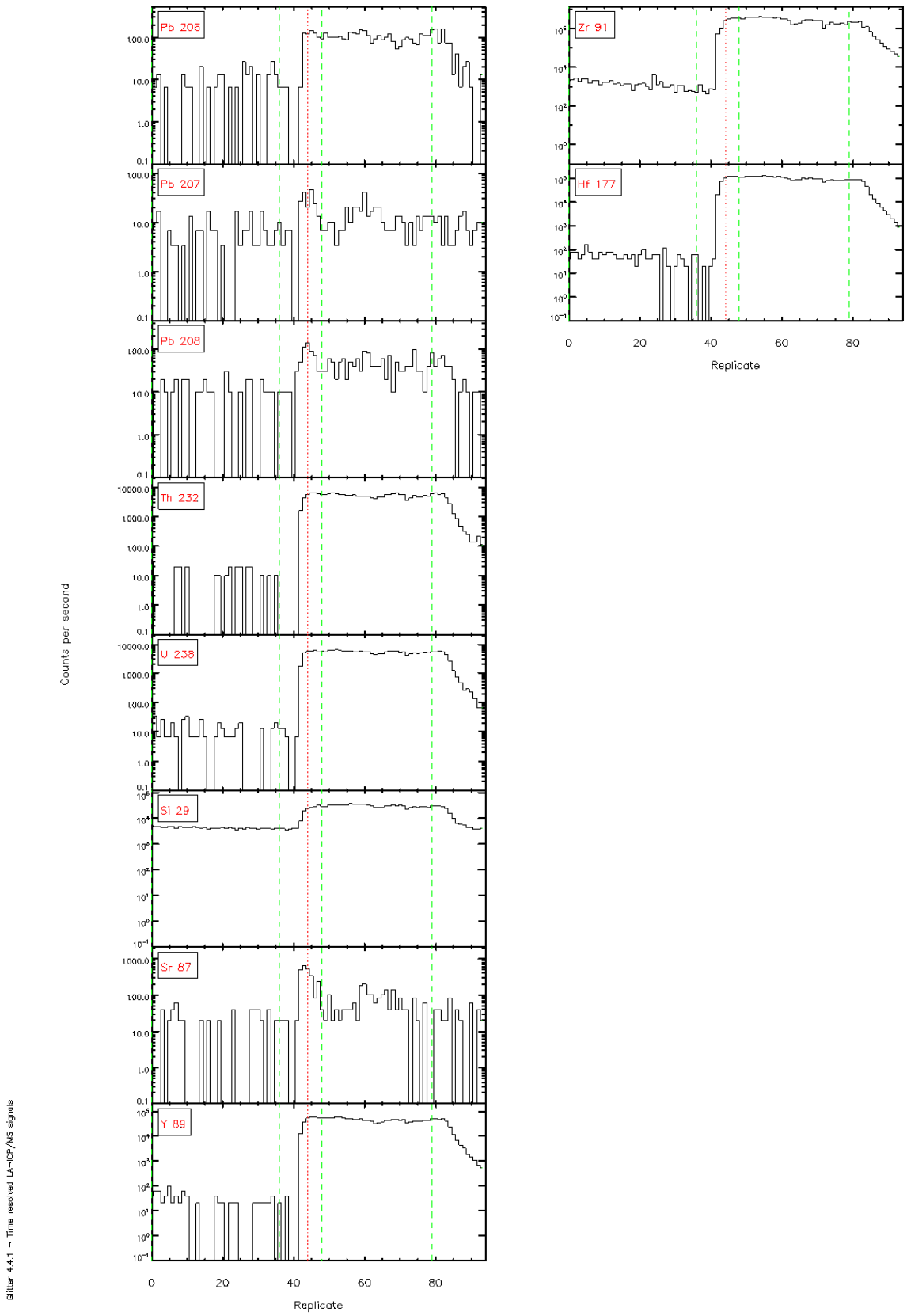
Pb 206
Pb 207
Pb 208
Th 232
U 238
Si 29
Sr 87
Y 89
Zr 91
Hf 177
Counts per second
Replicate
Glitter 4.4.1 - Time resolved LA-ICP/MS signals

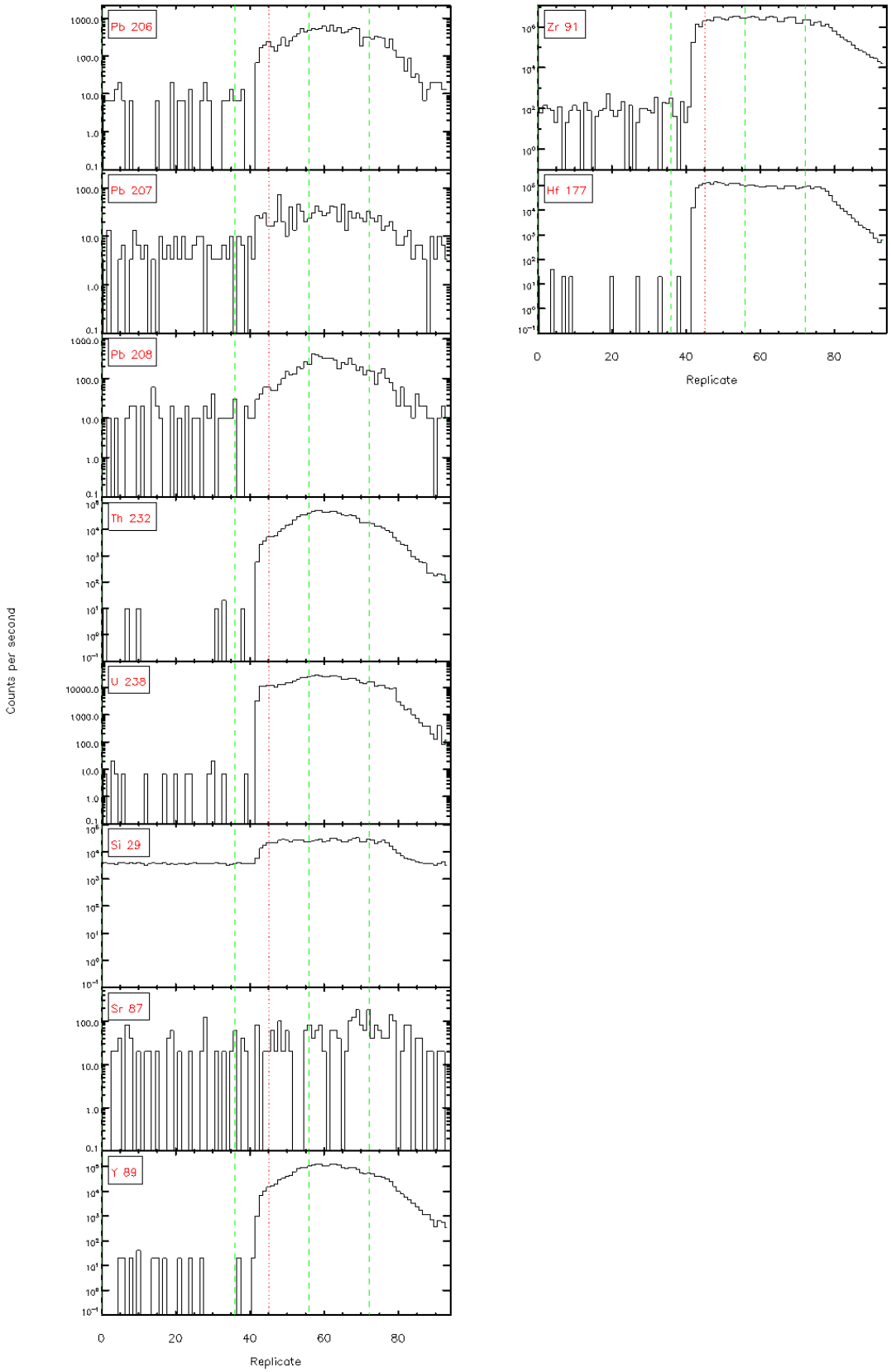
Pb 206
Pb 207
Pb 208
Th 232
U 238
Si 29
Sr 87
Y 89
Zr 91
Hf 177
Counts per second
Replicate
Glitter 4.4.1 - Time resolved LA-ICP/MS signals

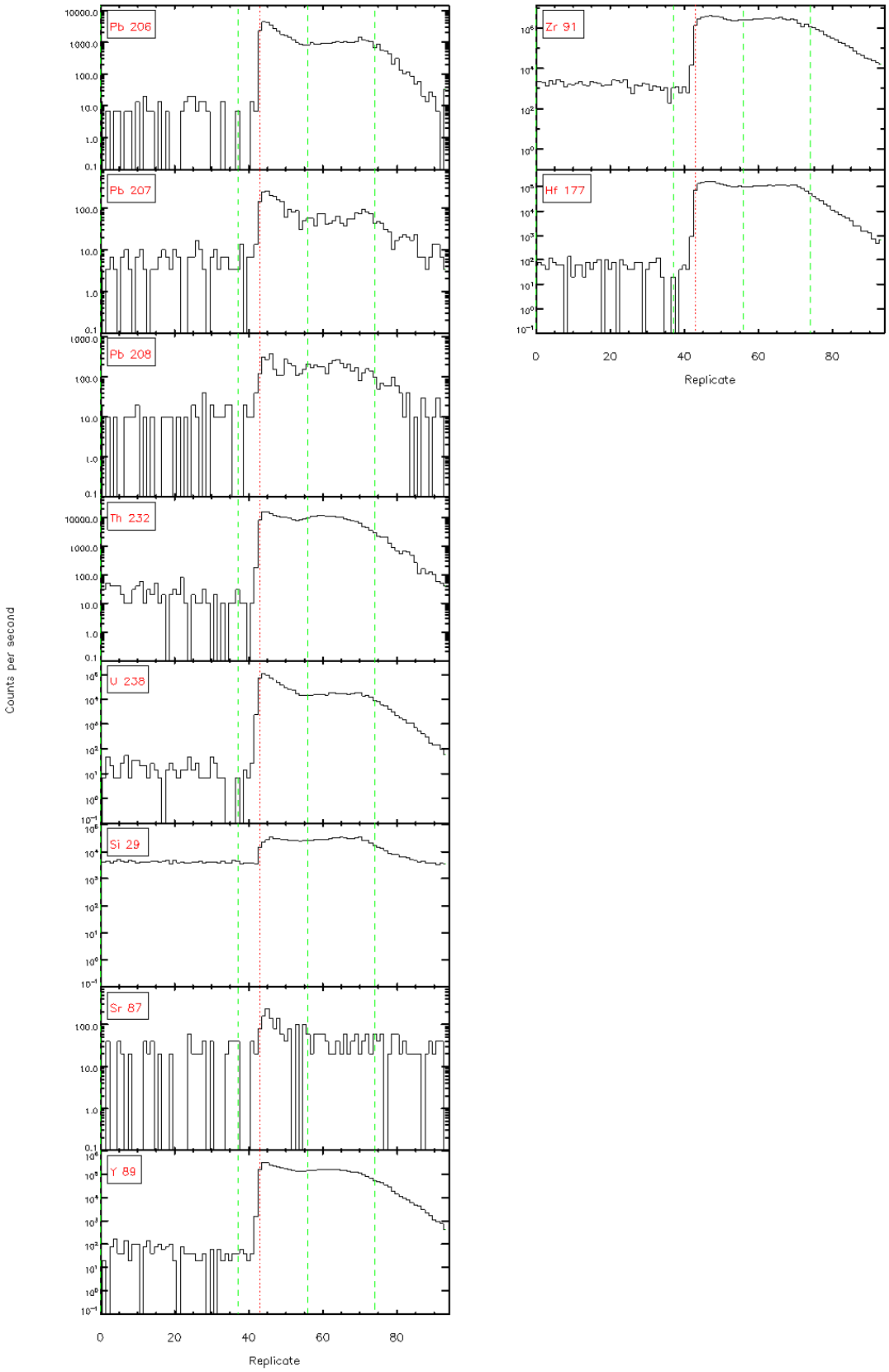
Pb 206
Pb 207
Pb 208
Th 232
U 238
Si 29
Sr 87
Y 89
Zr 91
Hf 177
Counts per second
Replicate
Glitter 4.4.1 - Time resolved LA-ICP/MS signals

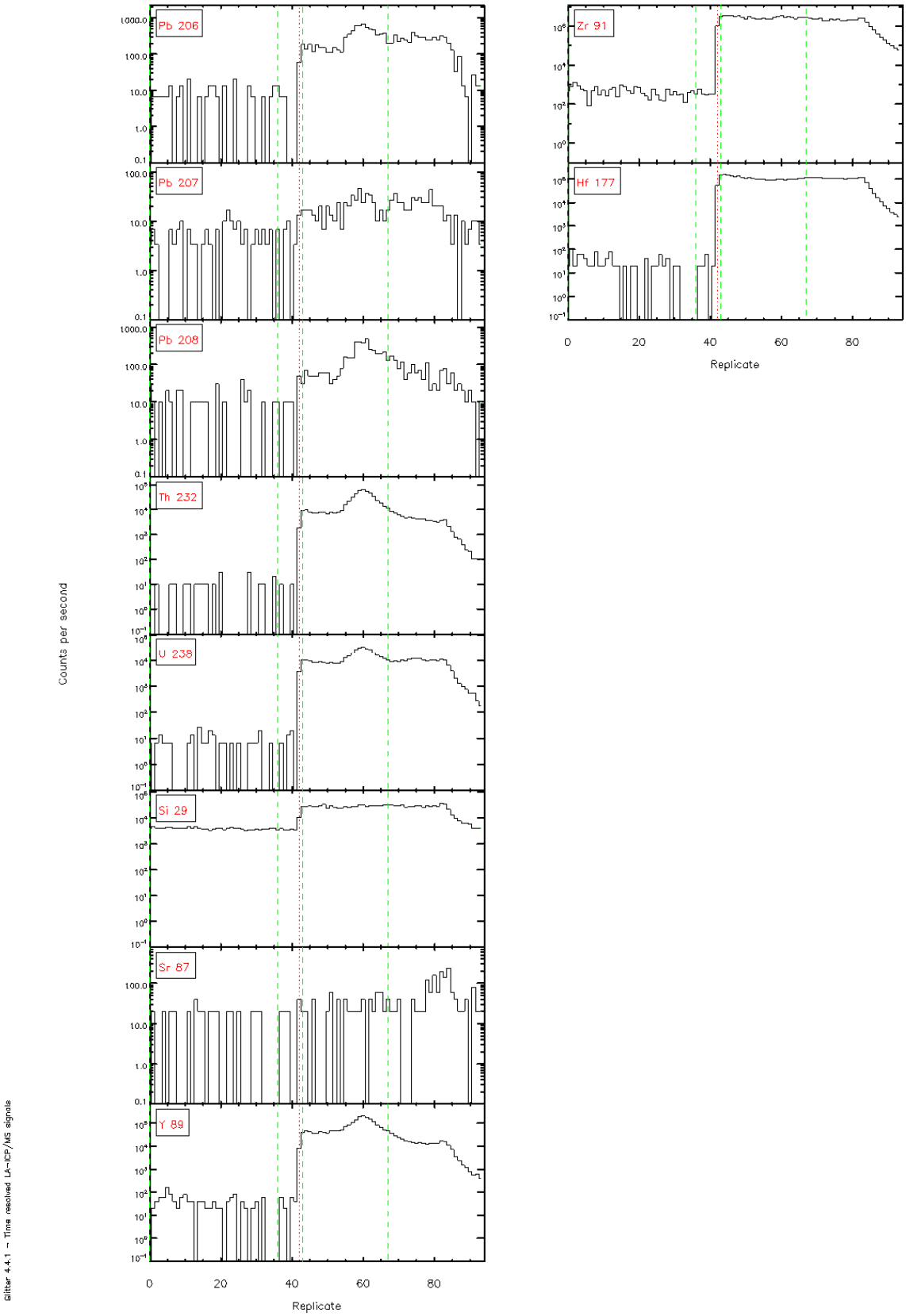
Pb 206
Pb 207
Pb 208
Th 232
U 238
Si 29
Sr 87
Y 89
Zr 91
Hf 177
Counts per second
Replicate
Glitter 4.4.1 - Time resolved LA-ICP/MS signals

6 – Hauturu Sandstone

7.

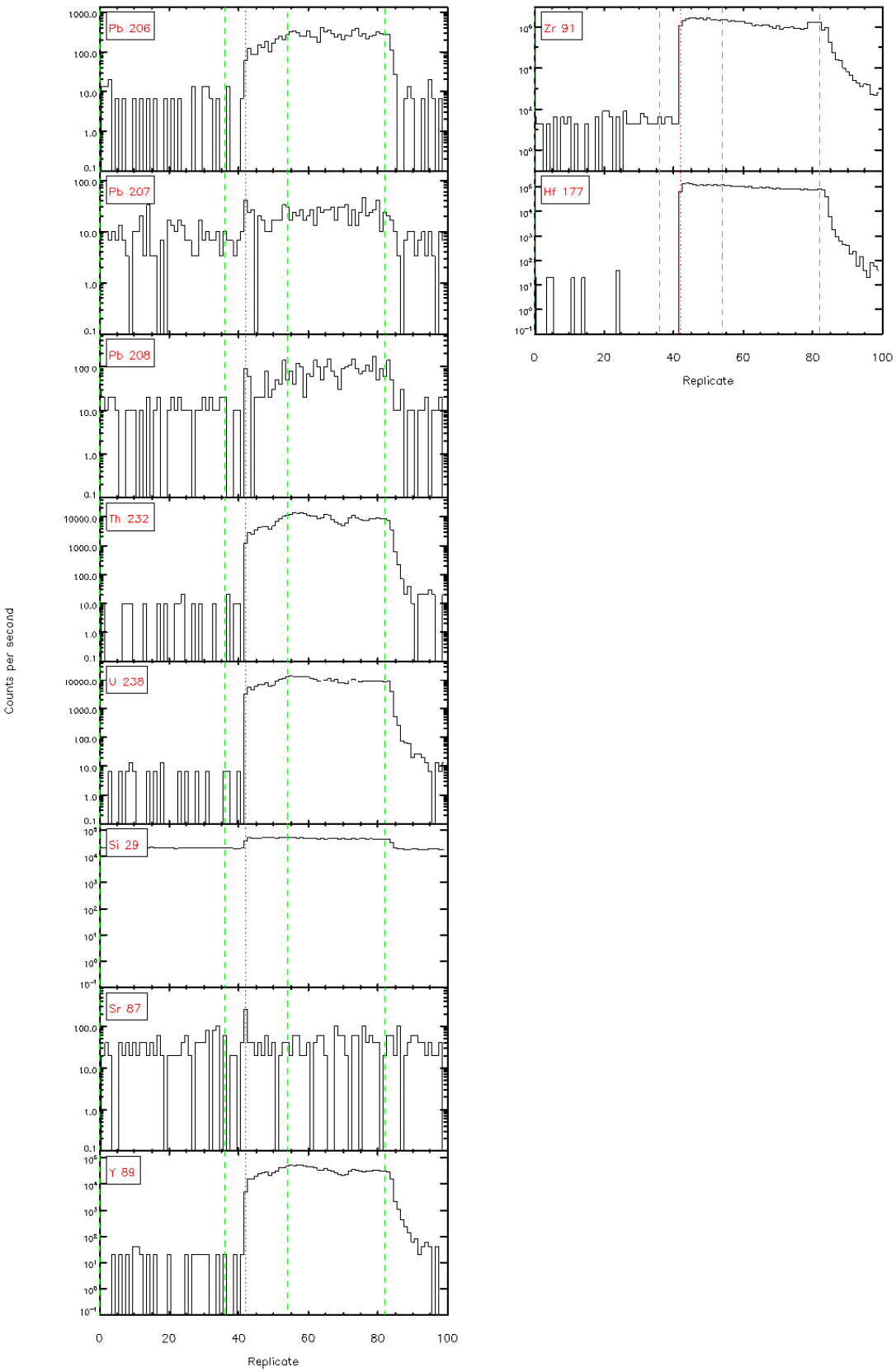

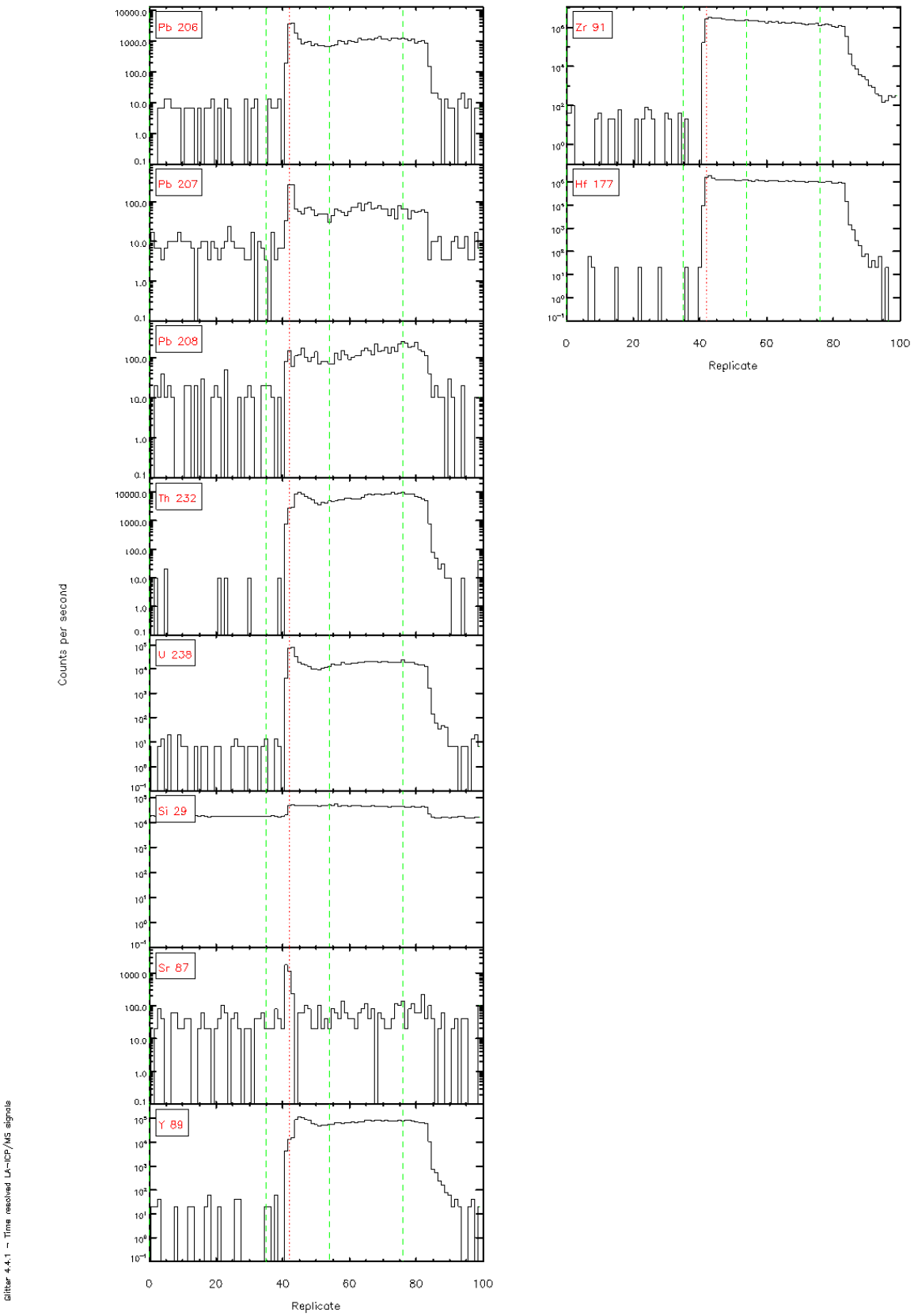
Pb 206
Pb 207
Pb 208
Th 232
U 238
Si 29
Sr 87
Y 89
Zr 91
Hf 177
Counts per second
Replicate
Glitter 4.4.1 - Time resolved LA-ICP/MS signals

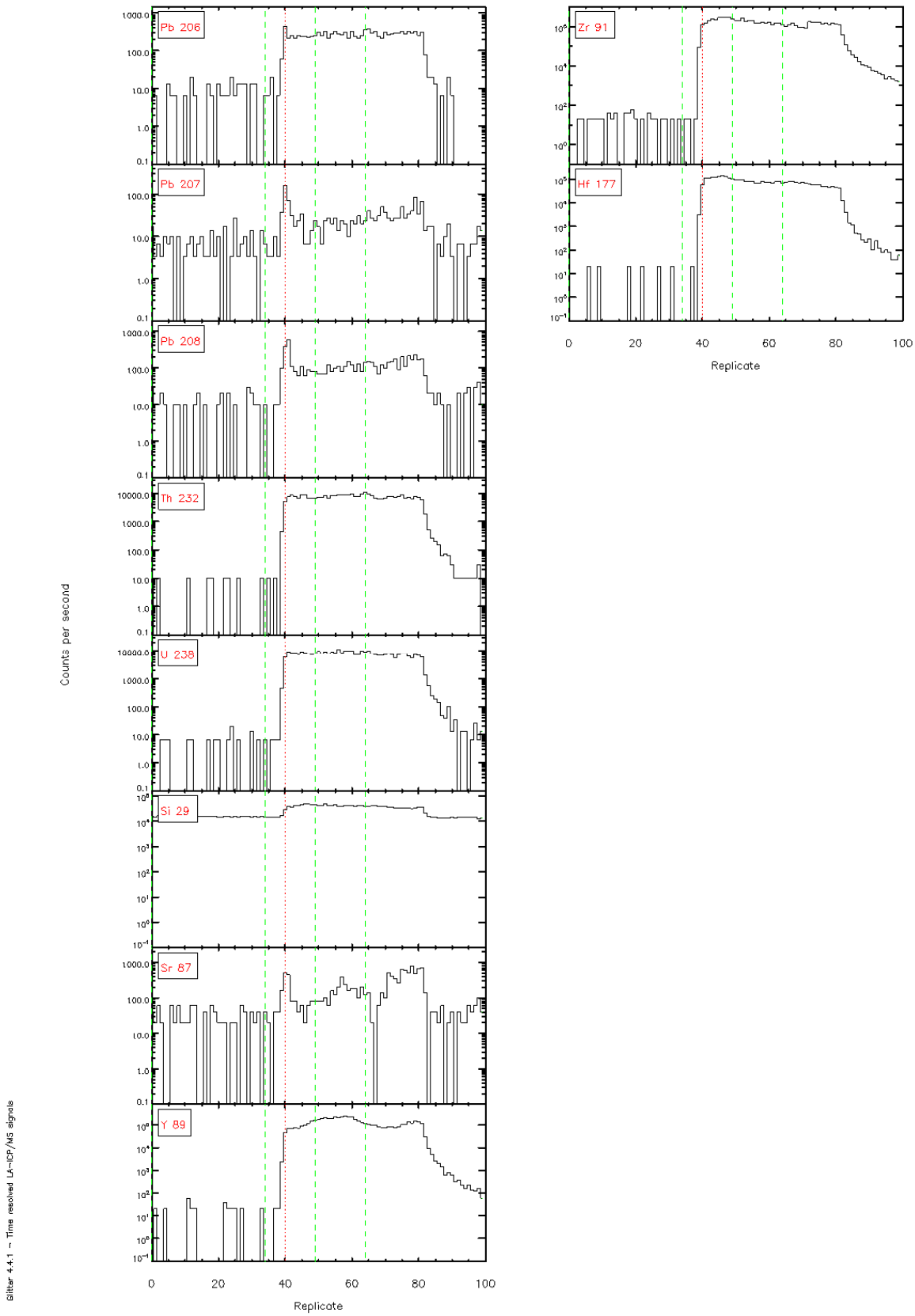
Pb 206
Pb 207
Pb 208
Th 232
U 238
Si 29
Sr 87
Y 89
Zr 91
Hf 177
Counts per second
Replicate
Glitter 4.4.1 ~ Time resolved LA-ICP/MS signals

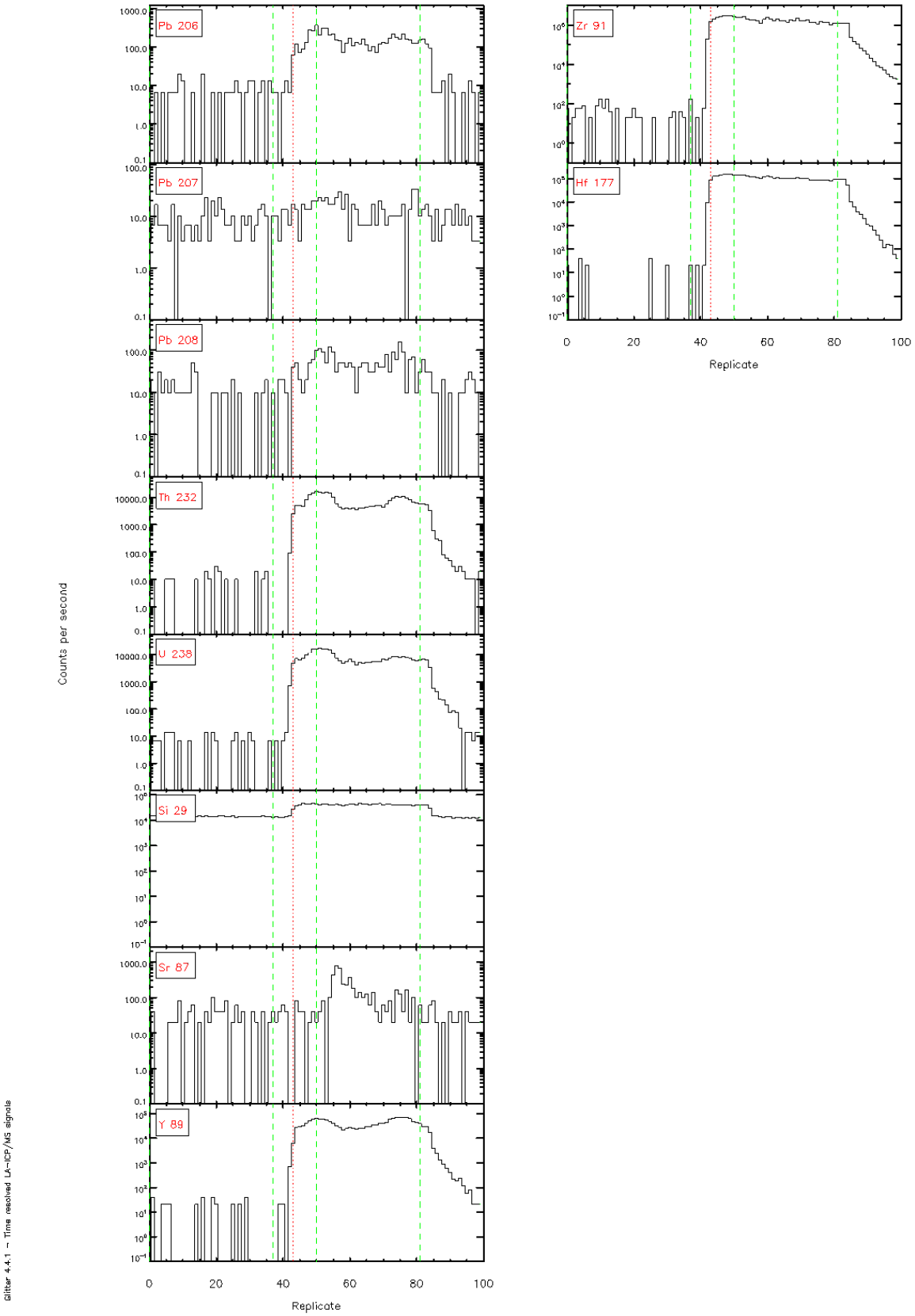
Pb 206
Pb 207
Pb 208
Th 232
U 238
Si 29
Sr 87
Y 89
Zr 91
Hf 177
Counts per second
Replicate
Glitter 4.4.1 - Time resolved LA-ICP/MS signals

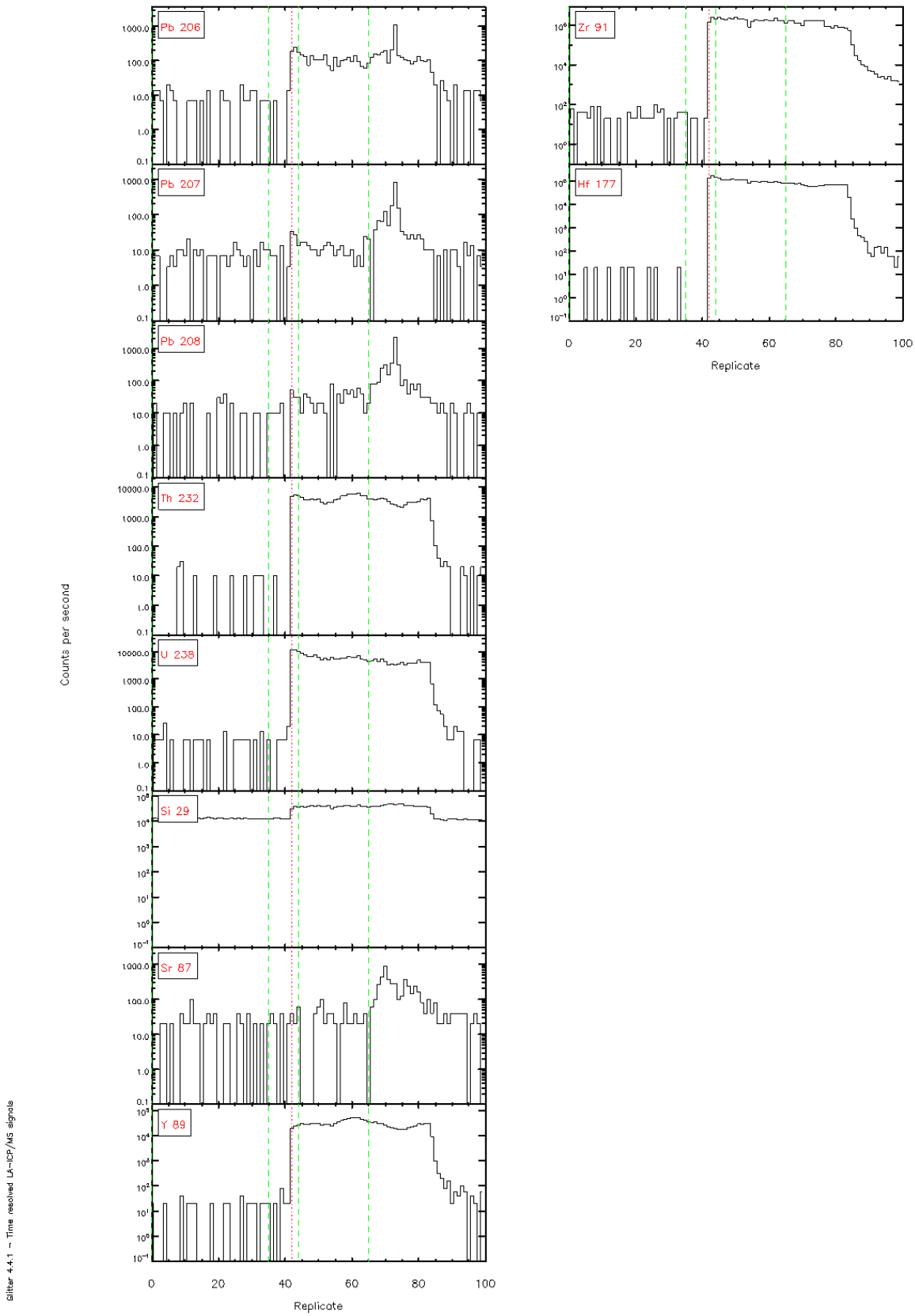
Pb 206
Pb 207
Pb 208
Th 232
U 238
Si 29
Sr 87
Y 89
Zr 91
Hf 177
Counts per second
Replicate
Glitter 4.4.1 ~ Time resolved LA-ICP/MS signals

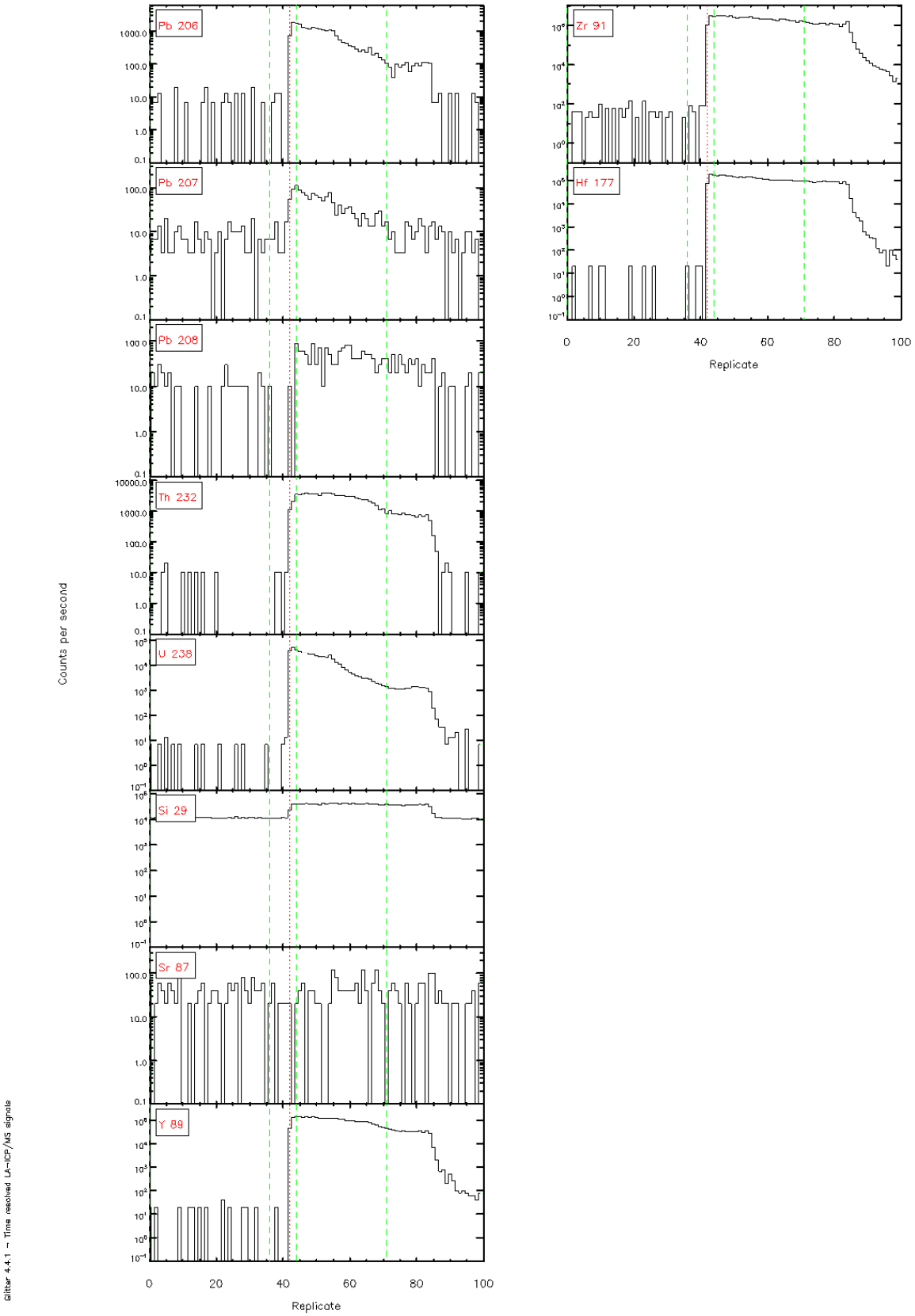
Pb 206
Pb 207
Pb 208
Th 232
U 238
Si 29
Sr 87
Y 89
Zr 91
Hf 177
Counts per second
Replicate
Glitter 4.4.1 - Time resolved LA-ICP/MS signals

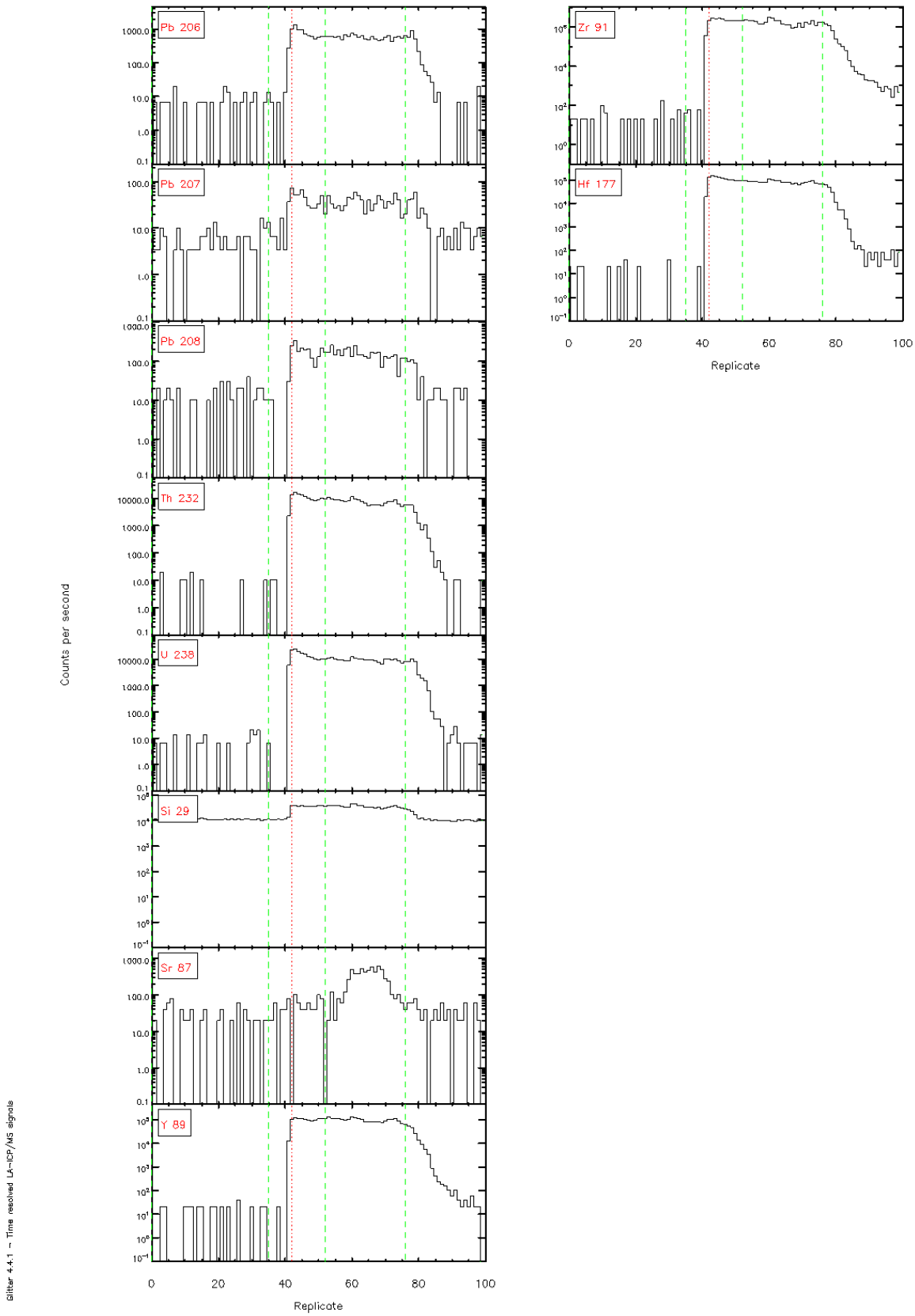
Pb 206
Pb 207
Pb 208
Th 232
U 238
Si 29
Sr 87
Y 89
Zr 91
Hf 177
Counts per second
Replicate
Glitter 4.4.1 ~ Time resolved LA-ICP/MS signals

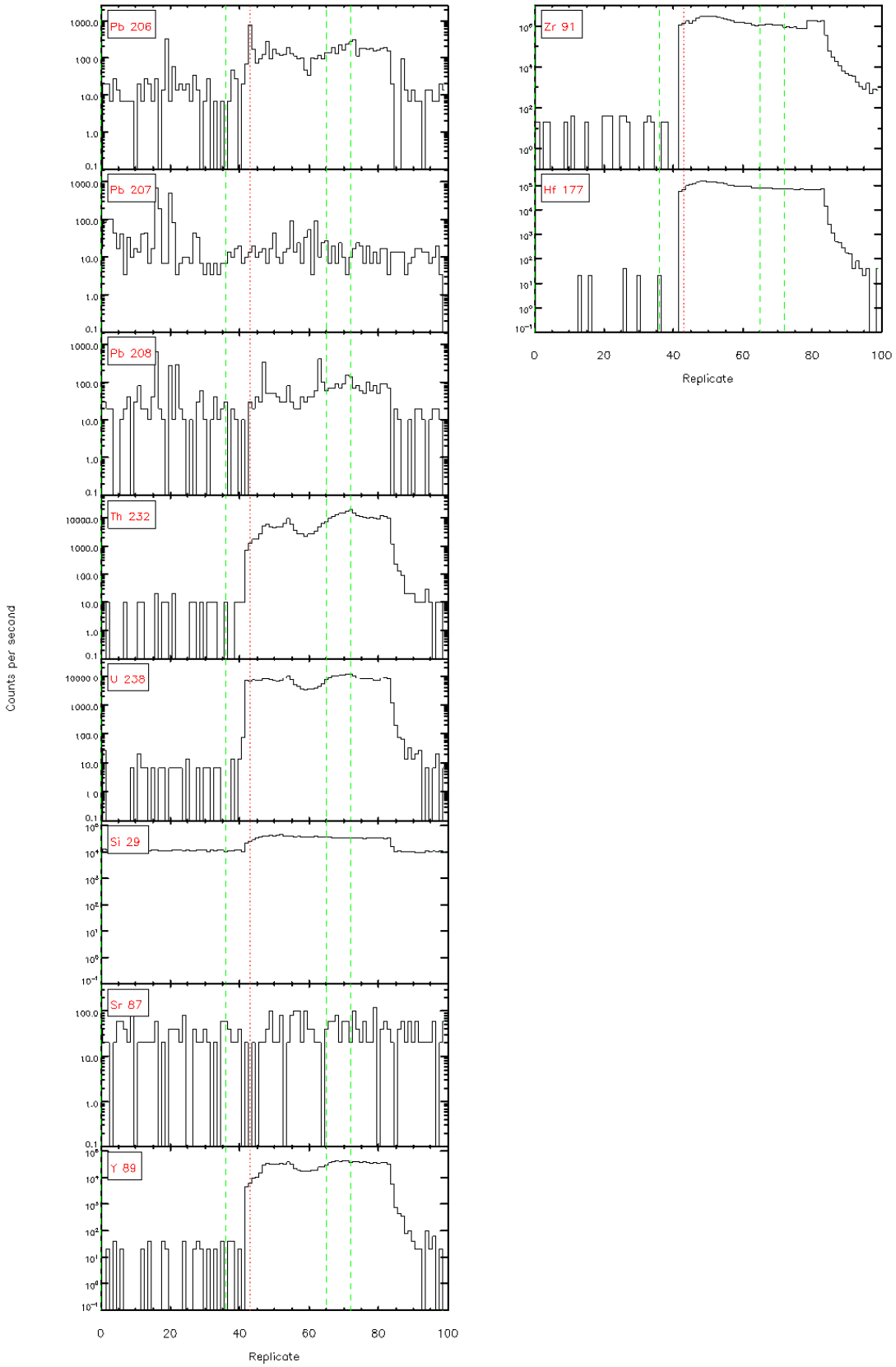
Pb 206
Pb 207
Pb 208
Th 232
U 238
Si 29
Sr 87
Y 89
Zr 91
Hf 177
Counts per second
Replicate
Glitter 4.4.1 - Time resolved LA-ICP/MS signals

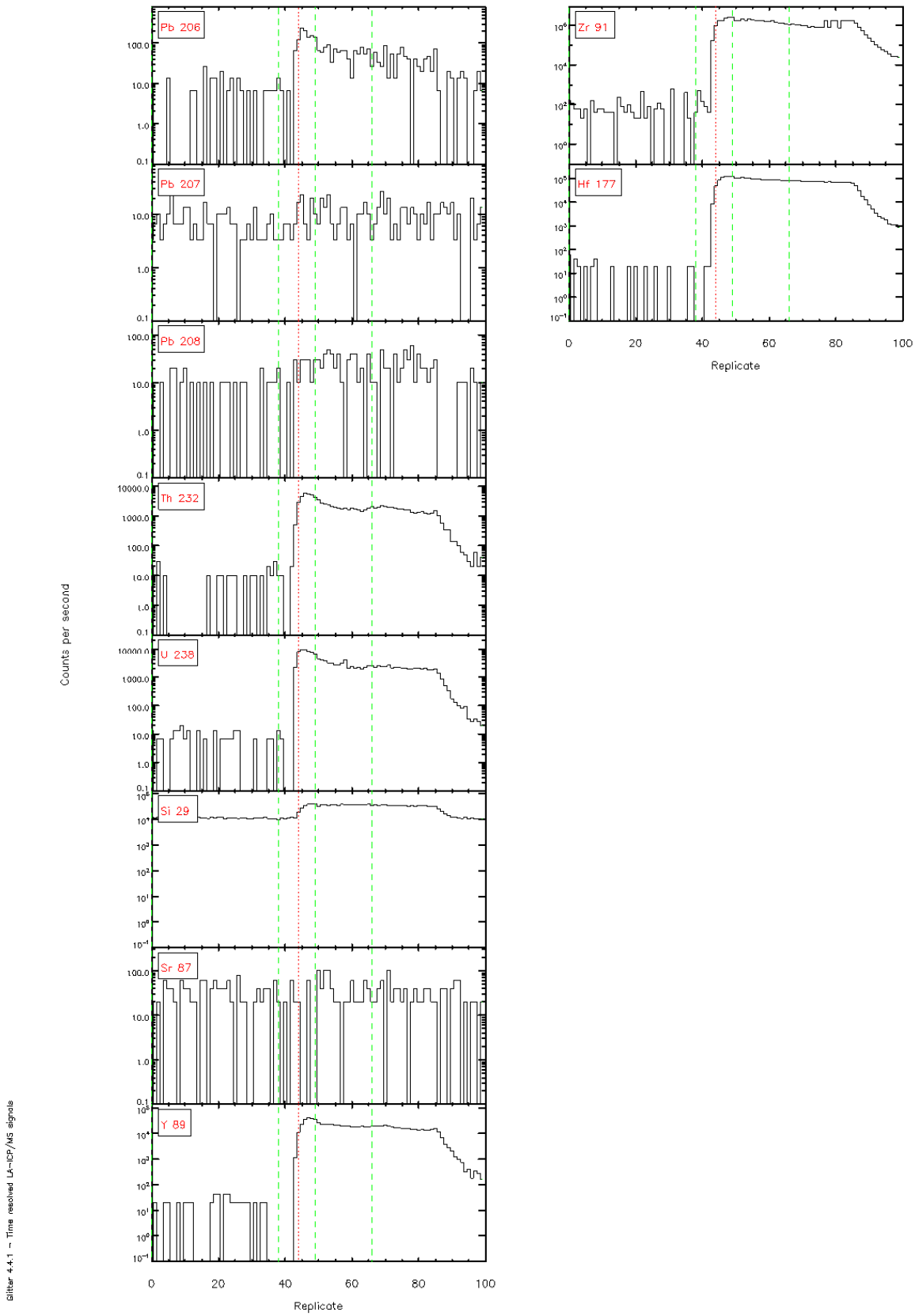
Pb 206
Pb 207
Pb 208
Th 232
U 238
Si 29
Sr 87
Y 89
Zr 91
Hf 177
Counts per second
Replicate
Glitter 4.4.1 ~ Time resolved LA-ICP/MS signals

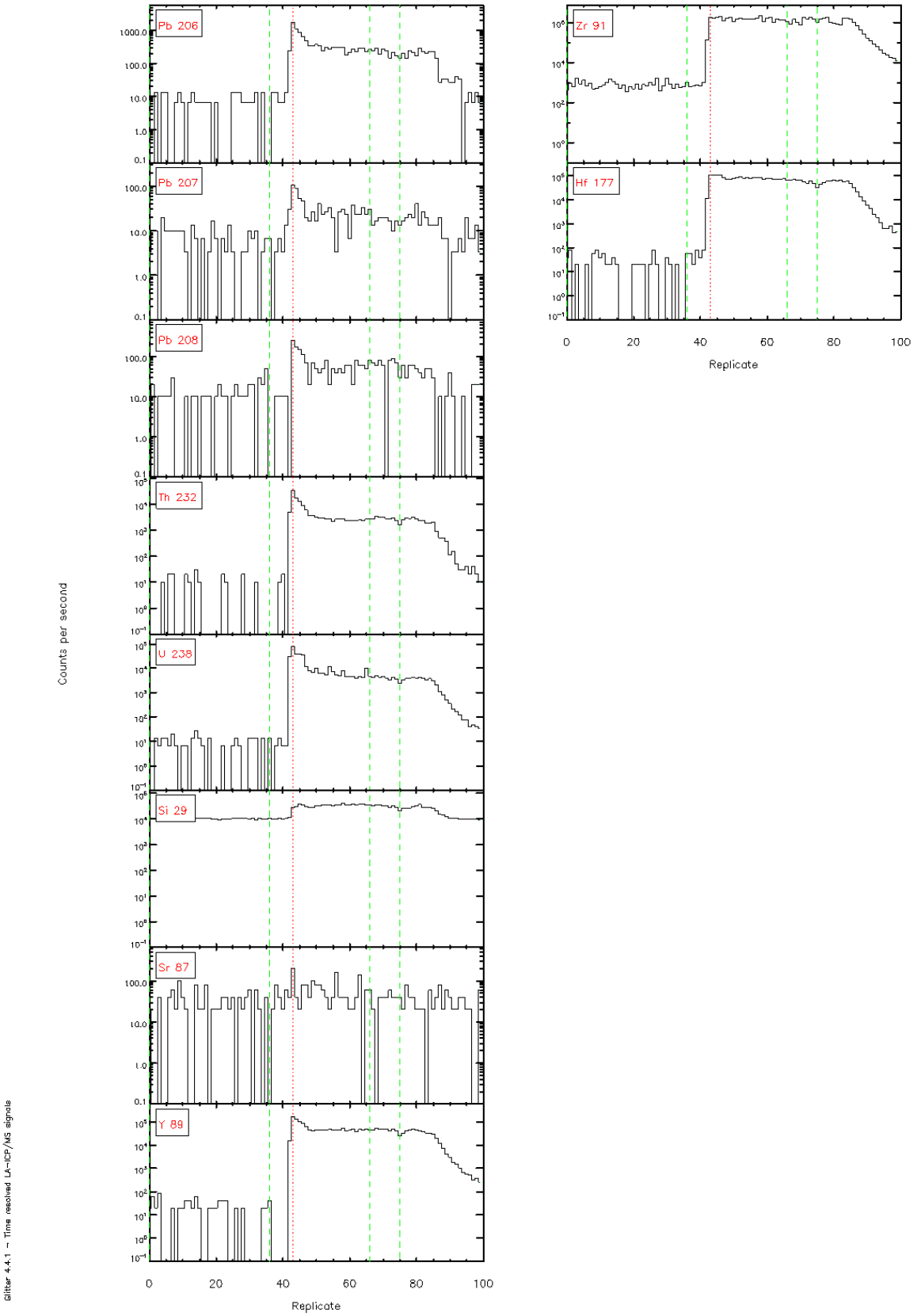
Pb 206
Pb 207
Pb 208
Th 232
U 238
Si 29
Sr 87
Y 89
Zr 91
Hf 177
Counts per second
Replicate
Glitter 4.4.1 - Time resolved LA-ICP/MS signals

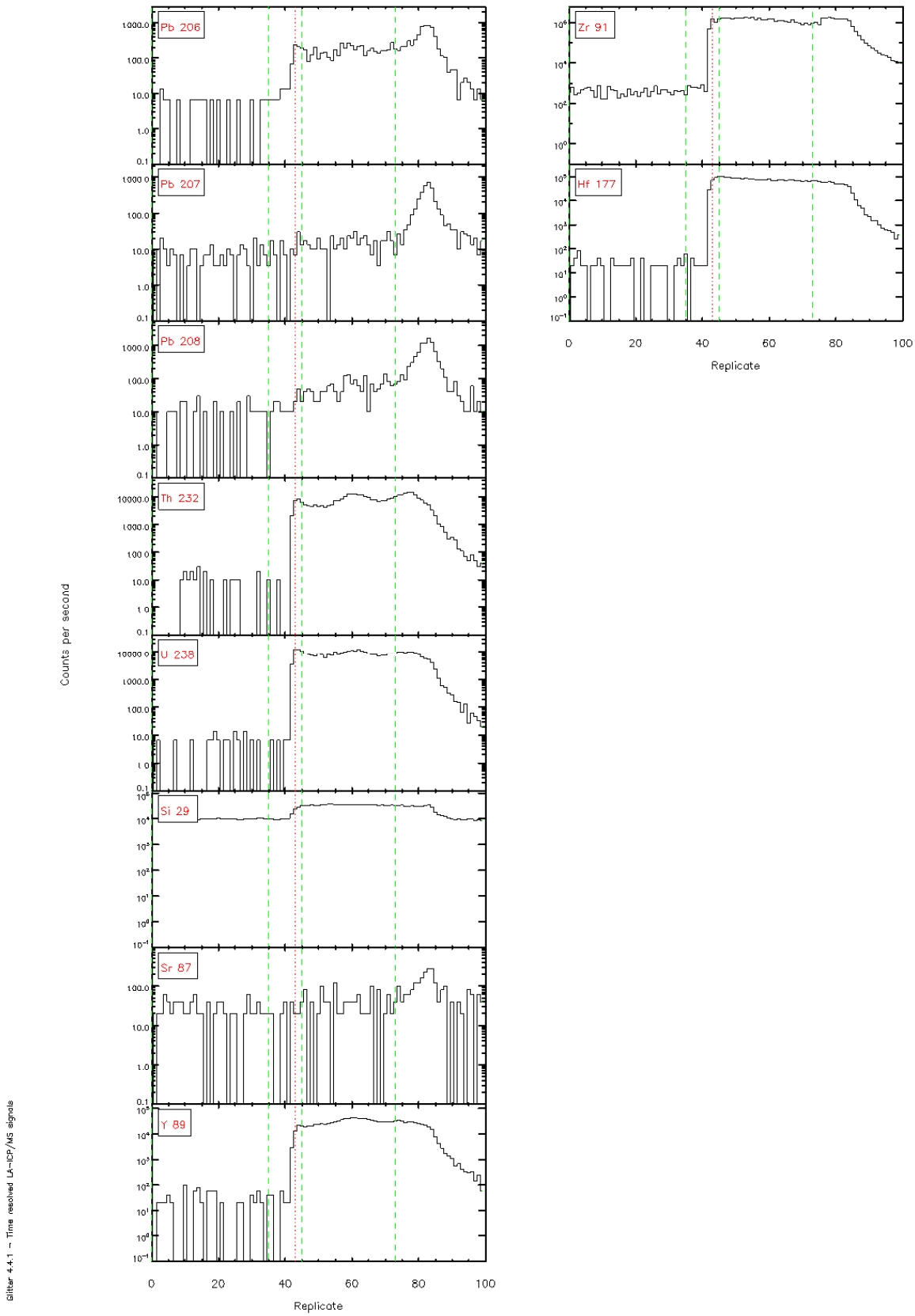
Pb 206
Pb 207
Pb 208
Th 232
U 238
Si 29
Sr 87
Y 89
Zr 91
Hf 177
Counts per second
Replicate
Glitter 4.4.1 ~ Time resolved LA-ICP/MS signals

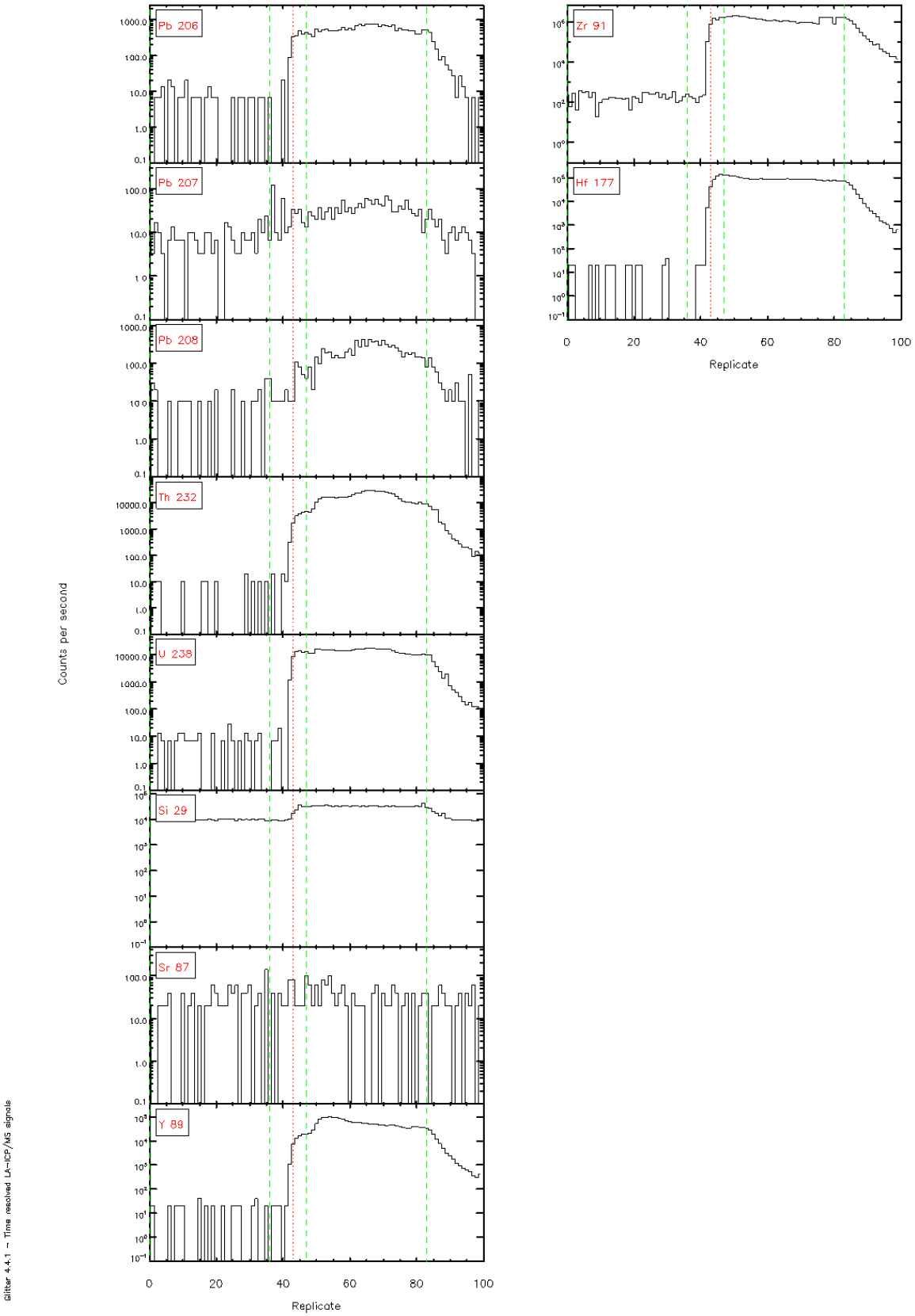
Pb 206
Pb 207
Pb 208
Th 232
U 238
Si 29
Sr 87
Y 89
Zr 91
Hf 177
Counts per second
Replicate
Glitter 4.4.1 - Time resolved LA-ICP/MS signals

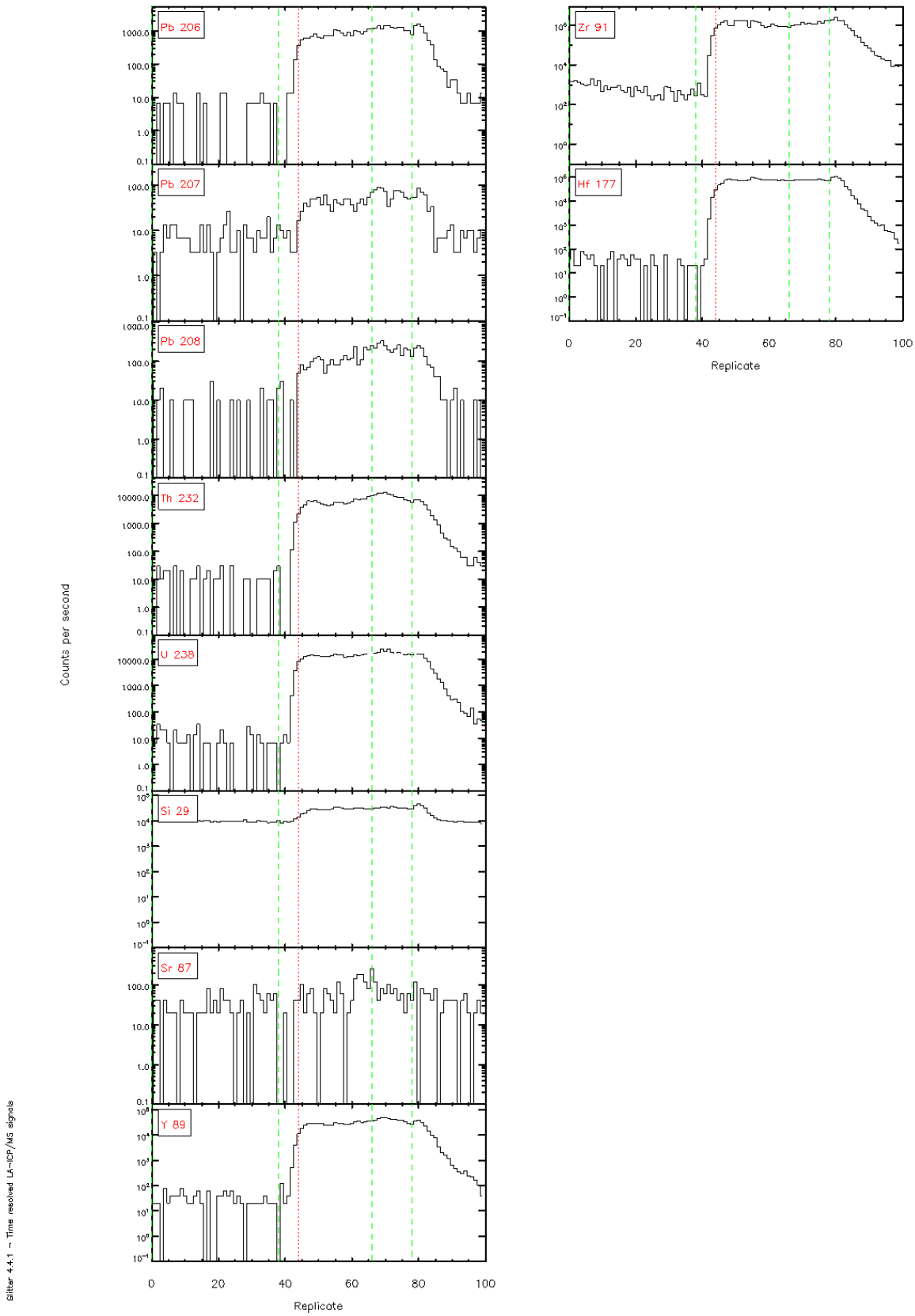
Pb 206
Pb 207
Pb 208
Th 232
U 238
Si 29
Sr 87
Y 89
Zr 91
Hf 177
Counts per second
Replicate
Glitter 4.4.1 ~ Time resolved LA-ICP/MS signals

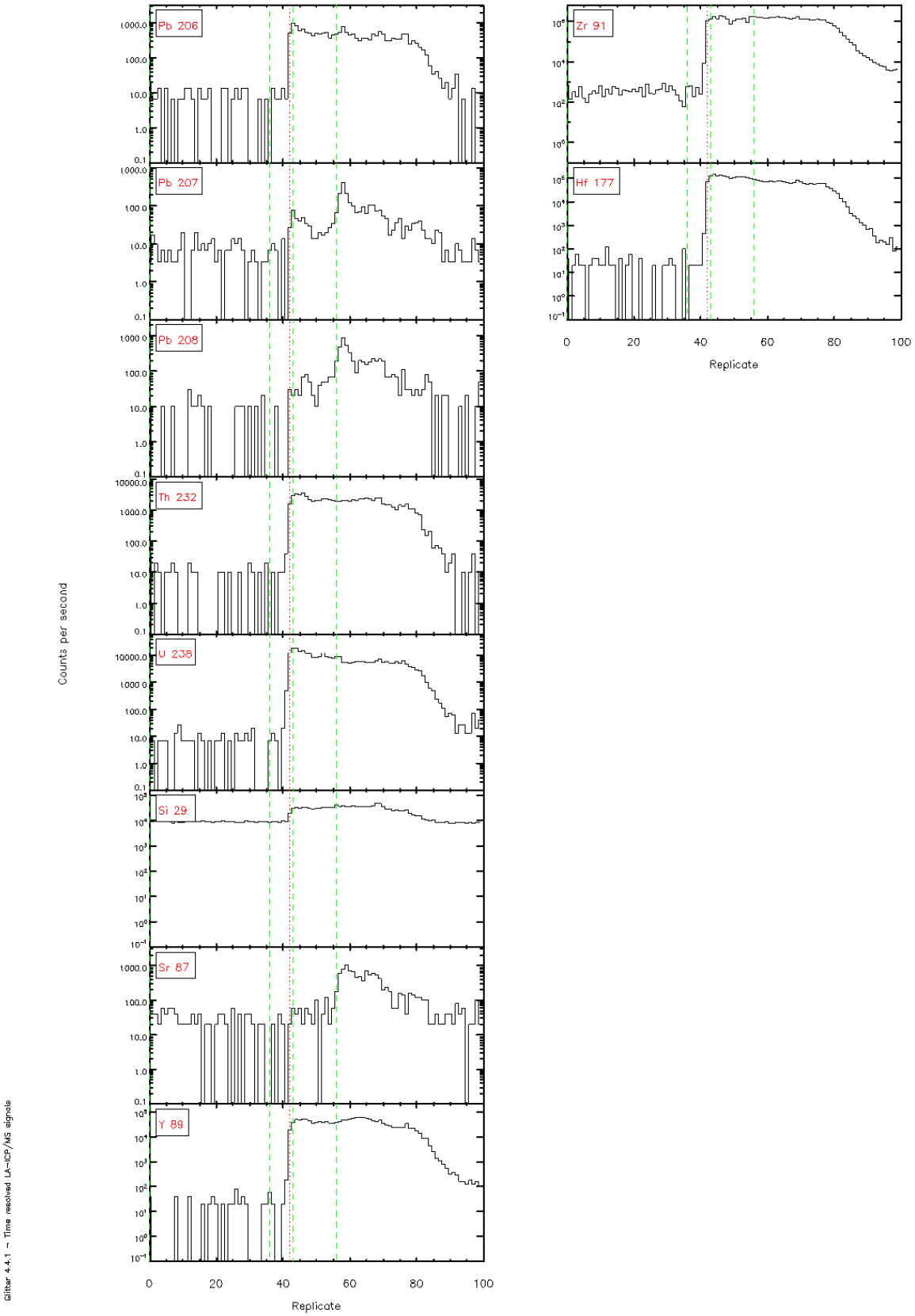
Pb 206
Pb 207
Pb 208
Th 232
U 238
Si 29
Sr 87
Y 89
Zr 91
Hf 177
Counts per second
Replicate
Glitter 4.4.1 - Time resolved LA-ICP/MS signals

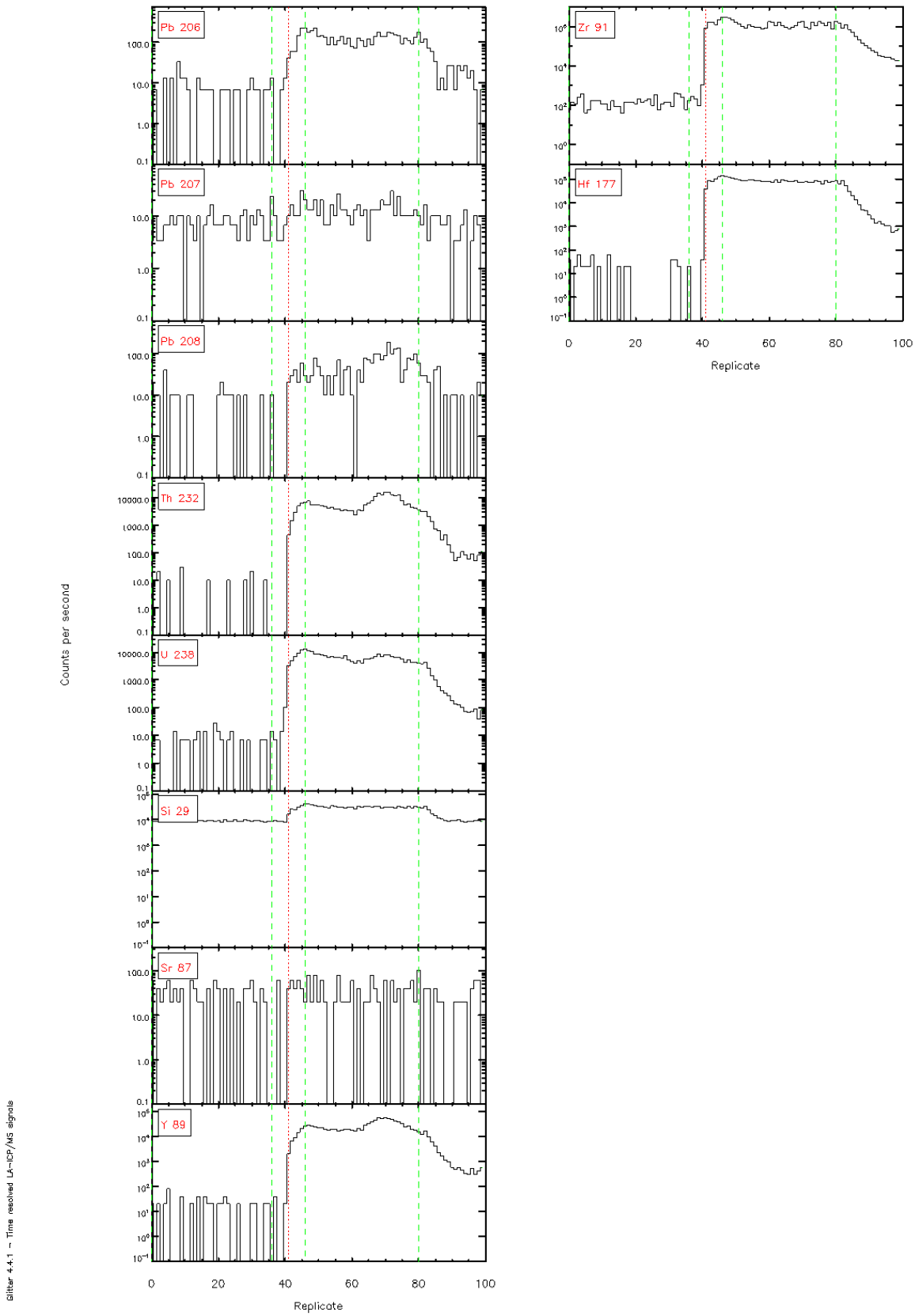
Pb 206
Pb 207
Pb 208
Th 232
U 238
Si 29
Sr 87
Y 89
Zr 91
Hf 177
Counts per second
Replicate
Glitter 4.4.1 - Time resolved LA-ICP/MS signals

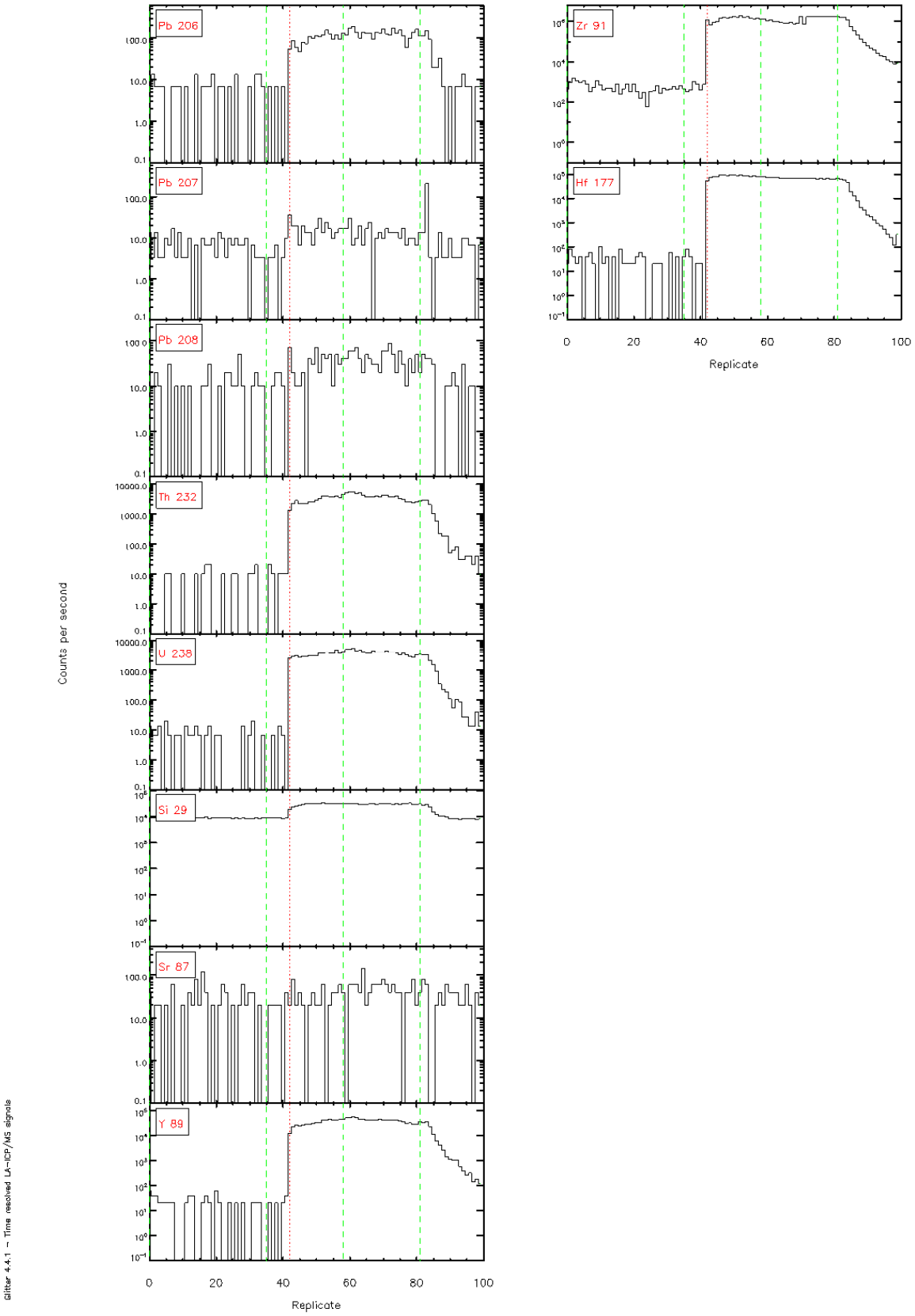
Pb 206
Pb 207
Pb 208
Th 232
U 238
Si 29
Sr 87
Y 89
Zr 91
Hf 177
Counts per second
Replicate
Glitter 4.4.1 - Time resolved LA-ICP/MS signals

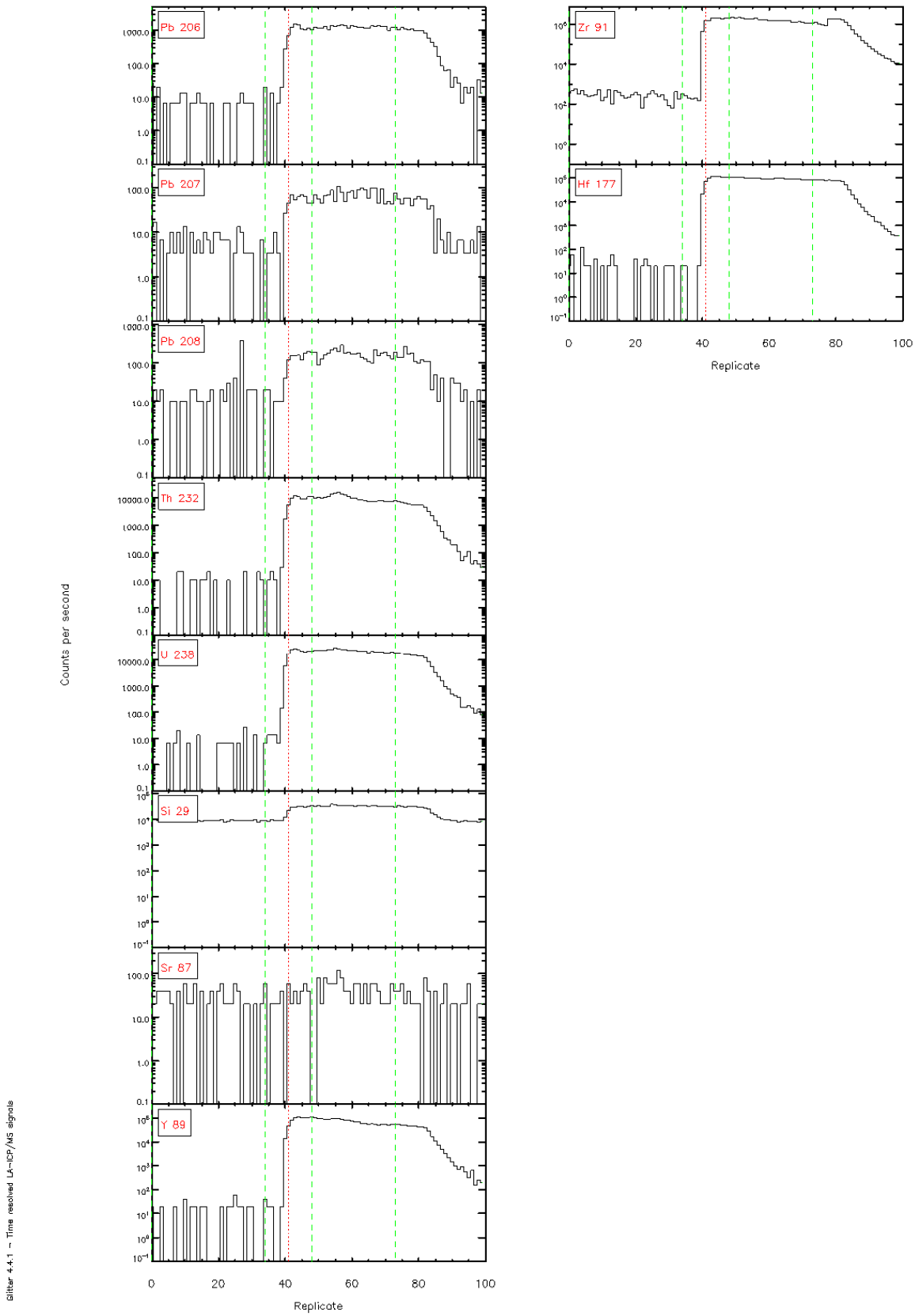
Pb 206
Pb 207
Pb 208
Th 232
U 238
Si 29
Sr 87
Y 89
Zr 91
Hf 177
Counts per second
Replicate
Glitter 4.4.1 - Time resolved LA-ICP/MS signals

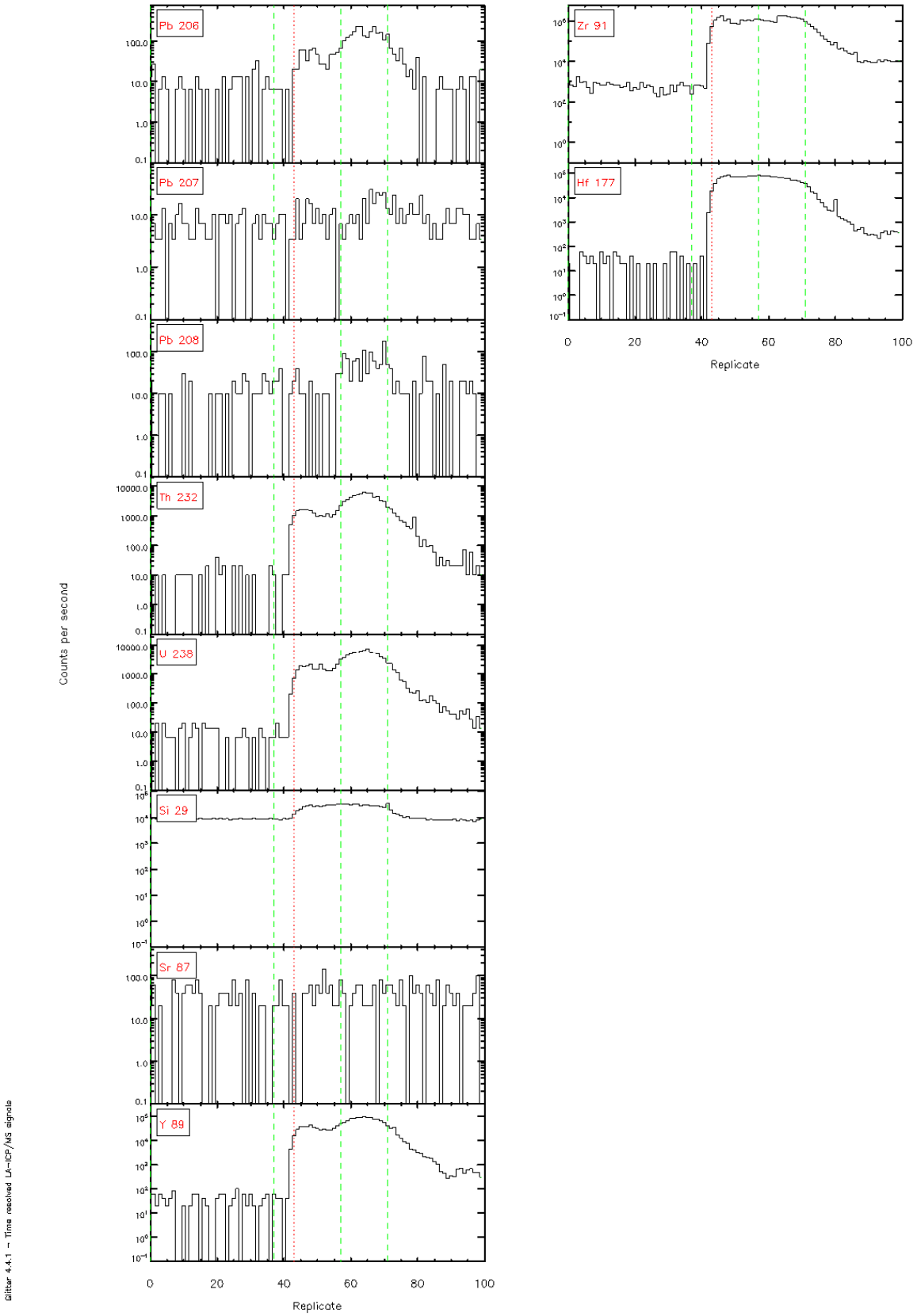
Pb 206
Pb 207
Pb 208
Th 232
U 238
Si 29
Sr 87
Y 89
Zr 91
Hf 177
Counts per second
Replicate
Glitter 4.4.1 - Time resolved LA-ICP/MS signals

APPENDIX VII

U-Pb GEOCHRONOLOGY DATA

VII.1 – U-Pb geochronology samples

Sample location	Formation/Member	Depth (m)	Sample number
Kihi Road	Aotea Formation (Hauturu Sandstone Member)	~	**5**
Hautapu Hill	Aotea Formation (Hauturu Sandstone Member)	~	**4**
Tariki-1	Otaraoa Formation (Tariki Sandstone Member)	2810 - 2860	**14**
Tariki-1	Otaraoa Formation (Tariki Sandstone Member)	2870 - 2920	**13**
Tariki-1	Otaraoa Formation (Tariki Sandstone Member)	2940 - 2990	**9**
Awamarino	Glen Massey Formation (Ahirau Sandstone Member)	~	**3**
Aotea Harbour	Glen Massey Formation (Ahirau Sandstone Member)	~	**2**
Port Waikato	Glen Massey Formation (Ahirau Sandstone Member)	~	**1**
Taumarunui	Taumarunui quartz sandstone	~	**7**
Ngatoro-1	Otaraoa Formation (Matapo Sandstone Member)	3550 - 3600	**10**
Otaihanga	Otaihanga Outlier	~	**15**
Pohokura-1	Turi Formation	3420 - 3470	**12**
Kaimiro-1	McKee Formation	3784 - 3740	**8**

VII.2 – Isotope ratio and age estimate data

The following tables summarise $^{207}Pb/^{235}U$ and $^{206}Pb/^{238}U$ isotope ratio and age estimate data for the 13 analysed samples.

Table legend

- Standards
- Concordant/near concordant zircons
- Discordant zircons

	ISOPTOPE RATIOS				AGE ESTIMATES (Ma)			
Sample No.	**Pb207/U235**	**1 σ error**	**Pb206/U238**	**1 σ error**	**Pb207/U235**	**1 σ error**	**Pb206/U238**	**1 σ error**
NIST610-1	20.27421	0.4442	0.17393	0.00205	-	-	-	-
NIST610-2	19.8354	0.47457	0.17807	0.00219	-	-	-	-
GJ-1	0.63867	0.06835	0.07979	0.00284	501.5	42.35	494.9	16.95
GJ-2	0.73514	0.04876	0.0833	0.00187	559.6	28.53	515.8	11.12
GJ-3	0.54115	0.04959	0.07974	0.00198	439.2	32.67	494.6	11.81
GJ-4	0.59779	0.04596	0.08405	0.00199	475.8	29.21	520.3	11.81
tem1-1	1.11748	0.14449	0.10638	0.00549	761.8	69.29	651.7	31.99
tem1-2	0.68252	0.13993	0.11134	0.0061	528.3	84.45	680.5	35.37
1	0.26624	0.02966	0.03921	0.00137	239.7	23.79	247.9	8.5
2	0.53931	0.06987	0.04754	0.00258	438	46.09	299.4	15.9
3	0.5127	0.06432	0.0707	0.00285	420.3	43.17	440.4	17.18
4	0.5359	0.0544	0.06986	0.00247	435.7	35.96	435.3	14.9
5	0.17204	0.08283	0.02528	0.00277	161.2	71.76	160.9	17.39
6	0.60847	0.06721	0.07233	0.00294	482.6	42.42	450.2	17.68
8	0.49241	0.05821	0.06494	0.00259	406.5	39.61	405.6	15.7
9	0.59868	0.03497	0.07741	0.00171	476.4	22.21	480.7	10.24
10	0.34236	0.01968	0.0475	0.00102	299	14.89	299.1	6.27
33	1.29996	0.08977	0.15561	0.00409	845.7	39.63	932.3	22.82
34	1.28905	3.9711	0.13766	0.08116	840.9	1761.51	831.4	459.86
GJ_5	1.13051	0.09206	0.14241	0.00445	768	43.88	858.3	25.12
GJ_6	1.08252	0.07213	0.13454	0.00346	744.9	35.17	813.7	19.64
GJ_7	1.04361	0.07621	0.14294	0.00381	725.7	37.87	861.2	21.51
35	2.76972	0.16915	0.27263	0.00734	1347.4	45.56	1554.2	37.16
11	0.29955	0.05051	0.04207	0.00201	266	39.47	265.7	12.45
12	0.20118	0.08677	0.03043	0.00297	186.1	73.35	193.2	18.6
13	0.3113	0.04248	0.02716	0.00151	275.2	32.89	172.7	9.47
14	0.1666	0.0313	0.02343	0.00128	156.5	27.24	149.3	8.09
15	0.19983	0.07162	0.02865	0.00257	185	60.61	182.1	16.13
18	0.18457	0.03301	0.02712	0.00149	172	28.29	172.5	9.34
19	0.36936	0.03758	0.04276	0.00159	319.2	27.87	269.9	9.82
20	0.16714	0.06342	0.02623	0.00216	156.9	55.17	166.9	13.57
TEM2_1	0.80018	0.19428	0.09061	0.00787	596.9	109.58	559.2	46.53
TEM2_2	0.72987	0.14394	0.08853	0.00592	556.5	84.49	546.8	35.07
22	0.22349	0.0548	0.02406	0.00204	204.8	45.48	153.2	12.86
24	0.94615	0.08879	0.1092	0.00378	676.1	46.33	668.1	21.97
25	0.59141	0.06484	0.07482	0.00285	471.8	41.37	465.1	17.06
26	0.36501	0.06974	0.04912	0.00287	315.9	51.88	309.1	17.63
27	0.23706	0.05502	0.03406	0.00208	216	45.16	215.9	12.98
28	0.68089	0.08359	0.0303	0.00211	527.3	50.49	192.4	13.22
29	0.21409	0.05563	0.03062	0.00221	197	46.53	194.5	13.8
30	0.32137	0.04338	0.02653	0.00144	283	33.33	168.8	9.02
31	0.21912	0.0997	0.03121	0.00307	201.2	83.04	198.1	19.21
gj-8	0.94147	0.07261	0.13857	0.00374	673.7	37.97	836.6	21.18
gj-9	1.02703	0.06727	0.14073	0.00344	717.4	33.69	848.8	19.46
gj-10	1.03484	0.07016	0.13769	0.00343	721.3	35.01	831.6	19.44
gj-11	1.12325	0.07868	0.14104	0.0038	764.5	37.62	850.5	21.45
NIST610-3	32.13441	0.74013	0.28831	0.00366	-	-	-	-
NIST610-4	34.82732	0.74247	0.31471	0.00405	-	-	-	-

	ISOPTOPE RATIOS				AGE ESTIMATES (Ma)			
Sample No.	Pb207/U235	1 σ error	Pb206/U238	1 σ error	Pb207/U235	1 σ error	Pb206/U238	1 σ error
NIST610-1	27.81509	1.03714	0.21732	0.00334	-	-	-	-
NIST610-2	27.59157	1.16557	0.21208	0.00342	-	-	-	-
gj1	0.8191	0.06554	0.09776	0.00229	607.5	36.58	601.3	13.45
gj2	0.90688	0.06705	0.10053	0.00233	655.4	35.7	617.5	13.64
gj3	0.71705	0.06083	0.09647	0.00226	548.9	35.97	593.7	13.26
gj4	0.78708	0.06408	0.09566	0.00227	589.5	36.41	588.9	13.34
tem1_1	0.489	0.06566	0.06414	0.00217	404.2	44.78	400.8	13.13
tem1_2	0.51811	0.12911	0.06845	0.00307	423.9	86.35	426.8	18.49
1	0.52114	0.10823	0.02825	0.00204	425.9	72.25	179.6	12.82
4	-0.02814	0.04441	0.01803	0.00092	-29	46.39	115.2	5.83
5	0.10831	0.02413	0.01594	0.00063	104.4	22.11	102	3.98
6	0.22708	0.01938	0.03215	0.00075	207.8	16.03	204	4.67
7	0.25082	0.12903	0.03661	0.00242	227.2	104.75	231.8	15.02
8	0.22974	0.0817	0.01955	0.00135	210	67.46	124.8	8.53
9	0.28074	0.05678	0.02387	0.00115	251.2	45.02	152.1	7.21
10	0.13948	0.04795	0.02064	0.00106	132.6	42.73	131.7	6.68
11	0.21101	0.05309	0.03224	0.00154	194.4	44.51	204.6	9.6
12	0.209	0.05275	0.03085	0.00155	192.7	44.3	195.9	9.67
tem2_1	0.52612	0.08216	0.06775	0.00233	429.2	54.66	422.6	14.06
tem2_2	0.38823	0.09517	0.06552	0.0025	333.1	69.61	409.1	15.16
gj5	0.80415	0.0694	0.09726	0.00253	599.2	39.06	598.3	14.88
gj6	0.92104	0.0788	0.09856	0.00268	662.9	41.65	606	15.71
13	0.18385	0.03447	0.02904	0.00125	171.4	29.56	184.5	7.85
14	0.37482	0.0677	0.04595	0.00206	323.2	50	289.6	12.67
15	236.04591	95.68575	2.01837	0.85068	5552.4	409.87	7121.5	1816.81
19	0.38736	0.05914	0.05618	0.00229	332.4	43.28	352.4	13.97
20	18.93382	3.62722	0.13668	0.0331	3038.5	184.76	825.9	187.7
21	0.774	0.05162	0.09279	0.00213	582.1	29.54	572	12.59
22	0.1712	0.02488	0.02545	0.00087	160.5	21.57	162	5.46
23	0.16419	0.06632	0.02527	0.00176	154.4	57.85	160.9	11.06
gj_7	0.90265	0.08208	0.10143	0.00287	653.1	43.8	622.8	16.81
gj_8	0.82285	0.07284	0.09765	0.00268	609.6	40.57	600.6	15.76
gj_9	0.87193	0.09507	0.09798	0.00329	636.6	51.57	602.6	19.33
gj_10	0.62257	0.07836	0.09628	0.00333	491.5	49.03	592.6	19.6
NIST610-3	27.07022	1.80743	0.21833	0.00479	-	-	-	-
NIST610-4	26.16027	1.75248	0.20973	0.00457	-	-	-	-

15 – Otaihanga Outlier

	ISOPTOPE RATIOS				AGE ESTIMATES (Ma)			
Sample No.	Pb207/U235	1 σ error	Pb206/U238	1 σ error	Pb207/U235	1 σ error	Pb206/U238	1 σ error
nist610-1	24.67769	0.40543	0.22168	0.00264	-	-	-	-
nist610-2	24.4864	0.39823	0.22048	0.00262	-	-	-	-
gj-1	1.97181	0.05641	0.10286	0.00179	1105.9	19.27	631.1	10.48
gj-2	1.43744	0.04708	0.10433	0.00182	904.7	19.61	639.7	10.63
gj-3	0.66776	0.03038	0.09767	0.00171	519.4	18.5	600.7	10.02
gj-4	0.71433	0.03351	0.09948	0.00179	547.3	19.85	611.3	10.47
1	0.66356	0.0542	0.08269	0.00184	516.8	33.08	512.2	10.99
2	0.30128	0.05537	0.04017	0.00173	267.4	43.2	253.9	10.74
3	0.66107	0.03329	0.08526	0.00162	515.3	20.35	527.5	9.61
4	1.97024	0.10401	0.18669	0.00419	1105.4	35.56	1103.4	22.74
6	0.3209	0.02746	0.03932	0.00115	282.6	21.11	248.6	7.11
8	0.252	0.02212	0.03937	0.00093	228.2	17.94	248.9	5.76
10	0.3169	0.03596	0.04486	0.00132	279.5	27.73	282.9	8.14
12	0.25734	0.0249	0.03812	0.00099	232.5	20.11	241.2	6.13
14	0.33116	0.05705	0.03969	0.00201	290.5	43.52	250.9	12.48
tem1-1	0.44481	0.03348	0.06336	0.00153	373.6	23.53	396	9.3
tem1-2	0.44559	0.05228	0.06525	0.00235	374.2	36.72	407.4	14.24
16	1.39209	0.04756	0.14747	0.00248	885.6	20.19	886.8	13.93
18	0.24217	0.01758	0.03774	0.0008	220.2	14.37	238.8	4.99
19	0.24705	0.08898	0.03979	0.0024	224.2	72.45	251.6	14.88
20	0.70701	0.092	0.08906	0.00344	543	54.73	550	20.37
21	0.31556	0.04763	0.04043	0.00147	278.5	36.76	255.5	9.14
22	0.26847	0.06877	0.04052	0.00221	241.5	55.05	256.1	13.7
23	0.75959	0.05089	0.09278	0.00227	573.8	29.37	571.9	13.37
24	0.22196	0.02046	0.03358	0.00087	203.5	17	212.9	5.44
gj-5	0.70626	0.03605	0.1007	0.00194	542.5	21.46	618.5	11.36
gj-6	0.73154	0.03531	0.09832	0.00187	557.5	20.71	604.6	10.95
tem1-3	0.45601	0.03912	0.06355	0.0018	381.5	27.28	397.2	10.92
tem1-4	0.442	0.03634	0.05963	0.00155	371.7	25.59	373.4	9.41
25	0.26675	0.02034	0.03911	0.00102	240.1	16.3	247.3	6.34
26	0.245	0.02916	0.04083	0.00122	222.5	23.78	257.9	7.53
27	0.75967	0.06031	0.07709	0.00226	573.8	34.8	478.7	13.54
28	0.24137	0.01787	0.03496	0.00085	219.5	14.62	221.5	5.3
31	0.25711	0.0386	0.03864	0.00145	232.3	31.18	244.4	9
33	0.28159	0.04202	0.04092	0.00161	251.9	33.29	258.5	9.98
34	0.27653	0.05253	0.04053	0.00174	247.9	41.78	256.1	10.75
36	0.2945	0.02828	0.04241	0.00123	262.1	22.18	267.8	7.61
37	0.26139	0.03449	0.03531	0.00129	235.8	27.77	223.7	8.03
Tem2-1	0.42923	0.05888	0.05926	0.00231	362.6	41.83	371.1	14.05
Tem2-2	0.48844	0.05625	0.06656	0.00216	403.8	38.37	415.4	13.08
gj-7	0.66696	0.03437	0.09521	0.00187	518.9	20.94	586.3	11.02
gj-8	0.67704	0.05169	0.08257	0.00231	525	31.3	511.4	13.77
gj-9	0.78309	0.06001	0.09375	0.00255	587.2	34.17	577.7	15.04
gj-10	0.73476	0.04729	0.0935	0.00219	559.3	27.68	576.2	12.93

	ISOPTOPE RATIOS				AGE ESTIMATES (Ma)			
Sample No.	Pb207/U235	1 σ error	Pb206/U238	1 σ error	Pb207/U235	1 σ error	Pb206/U238	1 σ error
NIST610-1	31.85206	0.76419	0.25394	0.00392	-	-	-	-
NIST610-2	27.24928	0.69776	0.21193	0.00293	-	-	-	-
gj_4	0.81912	0.0553	0.10207	0.0022	607.6	30.87	626.5	12.88
gj_5	0.84582	0.05638	0.0973	0.00213	622.4	31.01	598.5	12.5
gj_6	0.75767	0.06292	0.09982	0.0024	572.7	36.35	613.3	14.06
gj_7	0.74983	0.05424	0.09342	0.00218	568.1	31.47	575.7	12.88
tem1-1	0.51966	0.11543	0.06662	0.00284	424.9	77.13	415.8	17.19
tem1-2	0.51757	0.14794	0.06438	0.0044	423.5	98.98	402.2	26.66
1	0.23513	0.04818	0.03246	0.00166	214.4	39.61	205.9	10.34
2	0.34659	0.06152	0.04684	0.002	302.2	46.39	295.1	12.29
3	0.57866	0.25076	0.02643	0.00426	463.6	161.28	168.1	26.78
4	0.21106	0.08934	0.0295	0.0025	194.4	74.91	187.4	15.66
5	0.21395	0.03009	0.03058	0.00104	196.9	25.17	194.2	6.48
6	0.16843	0.05902	0.02603	0.00181	158.1	51.29	165.7	11.36
7	0.25475	0.02683	0.03753	0.00107	230.4	21.71	237.5	6.62
8	0.32644	0.08181	0.05009	0.00277	286.8	62.63	315.1	17
9	0.31962	0.03593	0.04106	0.00131	281.6	27.64	259.4	8.11
10	0.28516	0.03134	0.03575	0.00116	254.7	24.76	226.4	7.25
11	0.26699	0.06777	0.04441	0.00277	240.3	54.31	280.1	17.09
12	0.12889	0.06443	0.01913	0.00147	123.1	57.95	122.1	9.3
13	0.43105	0.02344	0.06015	0.00124	363.9	16.63	376.5	7.53
14	0.34635	0.05411	0.03977	0.00196	302	40.81	251.4	12.15
15	0.1262	0.06834	0.01982	0.00147	120.7	61.62	126.5	9.28
16	0.22758	0.05645	0.03699	0.00227	208.2	46.69	234.2	14.14
tem2_1	0.49321	0.04159	0.06525	0.00182	407.1	28.28	407.5	11.02
tem2_2	0.4978	0.06489	0.06448	0.0021	410.2	43.99	402.8	12.69
gj_8	0.88276	0.07376	0.10599	0.00299	642.5	39.78	649.4	17.42
gj_9	0.83643	0.07673	0.09882	0.00302	617.2	42.43	607.5	17.71
gj_10	0.74511	0.07594	0.09528	0.00303	565.4	44.19	586.7	17.82
gj_11	0.81754	0.08009	0.09943	0.00316	606.7	44.74	611	18.53
17	0.48788	0.06722	0.05137	0.00225	403.5	45.87	322.9	13.79
18	0.34223	0.04014	0.04469	0.00171	298.9	30.36	281.9	10.58
19	0.12438	0.10166	0.01809	0.00251	119	91.81	115.5	15.88
20	0.45678	0.04025	0.05302	0.00167	382	28.05	333.1	10.24
21	0.49601	0.03526	0.06158	0.00168	409	23.93	385.3	10.2
22	0.15053	0.04679	0.02373	0.00142	142.4	41.29	151.2	8.93
23	0.27107	0.02692	0.03841	0.0011	243.6	21.5	243	6.85
24	0.15103	0.06258	0.022	0.00164	142.8	55.21	140.3	10.32
25	0.15112	0.05036	0.02332	0.00119	142.9	44.43	148.6	7.49
26	21.24452	2.73147	0.17959	0.02851	3149.8	124.68	1064.7	155.83
27	0.49749	0.0756	0.06349	0.00292	410	51.26	396.8	17.67
28	0.36704	0.01763	0.04989	0.00094	317.5	13.1	313.8	5.8
29	0.15642	0.07151	0.02227	0.00172	147.6	62.79	142	10.86
30	0.23536	0.32796	0.02885	0.00628	214.6	269.56	183.3	39.37
31	0.21673	0.12392	0.03044	0.00291	199.2	103.42	193.3	18.19
33	-0.23461	0.04689	0.03829	0.00127	-271.5	62.21	242.2	7.89
GJ_12	0.96995	0.08544	0.09845	0.00315	688.4	44.04	605.3	18.46
GJ_13	0.76303	0.07355	0.10189	0.00307	575.8	42.36	625.5	17.95
GJ_14	0.79953	0.07599	0.10041	0.00307	596.6	42.88	616.8	18
GJ_15	0.72935	0.07285	0.09813	0.003	556.2	42.77	603.4	17.62
NIST610_3	28.43325	0.68629	0.22415	0.0033	-	-	-	-
NIST610_4	29.86375	0.76411	0.23267	0.00354	-	-	-	-

7 – Taumarunui quartz sandstone

	ISOPTOPE RATIOS				AGE ESTIMATES (Ma)			
Sample No.	Pb207/U235	1 σ error	Pb206/U238	1 σ error	Pb207/U235	1 σ error	Pb206/U238	1 σ error
NIST610-5	27.7413	0.57735	0.21558	0.00283	-	-	-	-
NIST610-6	27.44328	0.57082	0.21306	0.00279	-	-	-	-
gj1-1	0.74261	0.04378	0.0931	0.00194	563.9	25.51	573.8	11.42
gj1-2	0.79349	0.04835	0.09856	0.0021	593.1	27.37	606	12.33
gj1-3	0.81362	0.04968	0.09839	0.00211	604.5	27.81	605	12.38
gj1-4	0.89216	0.05453	0.10223	0.00225	647.5	29.26	627.5	13.17
Tem2-1	0.51633	0.07063	0.05758	0.00226	422.7	47.3	360.9	13.76
Tem2-2	0.45078	0.05276	0.06145	0.00188	377.8	36.92	384.4	11.44
6	0.33509	0.02889	0.0426	0.00115	293.4	21.97	268.9	7.14
7	1.43556	0.05298	0.14269	0.00233	903.9	22.09	859.8	13.17
8	0.38322	0.04167	0.05445	0.00163	329.4	30.59	341.8	9.99
tem2_3	0.4533	0.10427	0.06841	0.00306	379.6	72.85	426.6	18.46
tem2_4	0.4835	0.0868	0.06439	0.00282	400.5	59.41	402.2	17.07
9	0.18122	0.02355	0.02812	0.00081	169.1	20.25	178.8	5.05
10	0.18338	0.08404	0.02475	0.00191	171	72.11	157.6	12.04
11	0.28707	0.03899	0.04153	0.0014	256.3	30.76	262.3	8.64
12	0.37755	0.04252	0.02672	0.00105	325.2	31.34	170	6.57
13	0.2661	0.12945	0.03847	0.00247	239.6	103.82	243.4	15.3
14	0.15351	0.0967	0.02503	0.00194	145	85.12	159.3	12.21
15	0.20659	0.11314	0.0285	0.00218	190.7	95.21	181.2	13.67
16	0.36274	0.11186	0.02895	0.00241	314.3	83.35	184	15.07
gj1_5	0.84838	0.05439	0.09328	0.00207	623.8	29.88	574.9	12.22
gj1_5	0.84526	0.06551	0.09726	0.00247	622	36.05	598.3	14.51
gj1_7	0.76615	0.06101	0.10072	0.0025	577.6	35.08	618.6	14.62
gj1_8	0.79829	0.06086	0.09915	0.00243	595.9	34.36	609.4	14.23
gj1-9	0.79452	0.04836	0.09464	0.00208	593.7	27.36	582.9	12.25
gj1-10	0.71082	0.04725	0.09558	0.00211	545.2	28.05	588.5	12.41
gj1-11	0.81006	0.049	0.10027	0.00217	602.5	27.49	616	12.72
gj1-12	0.8707	0.05178	0.09908	0.00219	635.9	28.1	609	12.84
Tem2_5	0.41375	0.06083	0.06258	0.00211	351.6	43.69	391.3	12.8
Tem2_6	0.48625	0.05769	0.06285	0.00208	402.3	39.41	392.9	12.61
17	0.17928	0.0205	0.02702	0.00077	167.4	17.65	171.9	4.85
18	0.16497	0.01126	0.02289	0.0005	155	9.81	145.9	3.17
19	0.24683	0.01768	0.02634	0.00065	224	14.4	167.6	4.09
20	*********	*********	11.02824	18.27953	7318.9	1677.12	******	9796.73
21	0.20899	0.04162	0.03256	0.00133	192.7	34.96	206.5	8.33
22	0.30484	0.04486	0.03986	0.00152	270.2	34.91	251.9	9.43
23	0.26158	0.03252	0.02892	0.00108	235.9	26.18	183.8	6.77
24	0.20385	0.01773	0.0273	0.00073	188.4	14.96	173.6	4.6
Tem2_7	0.48437	0.03388	0.06503	0.00151	401.1	23.18	406.2	9.13
Tem2_8	0.55114	0.03966	0.06764	0.00166	445.7	25.96	421.9	10.02
26	0.34661	0.01668	0.04587	0.00085	302.2	12.58	289.1	5.21
27	0.20547	0.01521	0.02881	0.00068	189.7	12.82	183.1	4.29
28	0.29836	0.03398	0.03382	0.00117	265.1	26.57	214.4	7.27
29	0.43305	0.02323	0.05917	0.00115	365.3	16.46	370.6	7.01
30	0.20292	0.01492	0.02967	0.00069	187.6	12.59	188.5	4.32
31	0.26079	0.01848	0.02535	0.00066	235.3	14.89	161.4	4.15
32	0.21557	0.02611	0.03207	0.00101	198.2	21.81	203.5	6.32
33	0.3098	0.06893	0.03346	0.00186	274	53.44	212.2	11.59
TEM2-9	0.54114	0.03282	0.06747	0.00148	439.2	21.62	420.9	8.93
TEM2-10	0.66278	0.03553	0.07549	0.00156	516.3	21.7	469.1	9.34
gj_13	0.85785	0.04289	0.10296	0.00204	628.9	23.44	631.8	11.9
gj_14	0.79943	0.04278	0.0967	0.00197	596.5	24.14	595	11.57
34	0.44896	0.06336	0.0423	0.00181	376.6	44.4	267.1	11.2
35	0.41618	0.03066	0.05311	0.0013	353.3	21.98	333.6	7.95
36	0.4202	0.02738	0.05126	0.00118	356.2	19.57	322.3	7.22
37	0.33112	0.02658	0.03707	0.00101	290.4	20.27	234.7	6.29
38	0.76756	0.0486	0.08407	0.00198	578.4	27.92	520.3	11.79
39	1.49389	0.04764	0.09472	0.00161	927.9	19.39	583.4	9.47
gj_15	0.77066	0.04455	0.09539	0.00202	580.1	25.54	587.4	11.87
gj_16	0.83262	0.04544	0.09637	0.00203	615.1	25.17	593.1	11.96
gj_17	0.88068	0.04872	0.10016	0.00214	641.4	26.31	615.3	12.51
gj_18	0.77408	0.04335	0.09519	0.002	582.1	24.81	586.1	11.78
NIST610-7	27.72549	0.57473	0.21514	0.00278	-	-	-	-
NIST610-8	27.97542	0.58096	0.22054	0.00287	-	-	-	-

1 – Ahirau Sandstone

	ISOPTOPE RATIOS				AGE ESTIMATES (Ma)			
Sample No.	Pb207/U235	1 σ error	Pb206/U238	1 σ error	Pb207/U235	1 σ error	Pb206/U238	1 σ error
nist610-1	24.57221	0.41178	0.20687	0.00266	-	-	-	-
nist610-2	29.34963	0.51897	0.23057	0.00304	-	-	-	-
gj_1	0.71474	0.02603	0.08664	0.00143	547.6	15.42	535.6	8.51
gj_2	0.95302	0.04073	0.10329	0.00185	679.7	21.17	633.7	10.83
gj_3	0.86672	0.03638	0.10668	0.00191	633.8	19.79	653.4	11.14
gj_4	0.94166	0.03676	0.10295	0.00184	673.8	19.22	631.7	10.78
tem1-1	0.52921	0.04519	0.06928	0.00192	431.3	30	431.8	11.58
tem1-2	0.47533	0.02978	0.06682	0.00145	394.9	20.5	417	8.76
1	0.32286	0.03613	0.04992	0.00178	284.1	27.73	314	10.92
2	0.21951	0.11497	0.0299	0.00379	201.5	95.73	189.9	23.72
3	0.27554	0.03753	0.03952	0.00162	247.1	29.87	249.8	10.03
4	0.17048	0.01556	0.0215	0.00066	159.8	13.5	137.1	4.19
6	0.17541	0.0214	0.0279	0.00099	164.1	18.48	177.4	6.21
7	0.28065	0.01388	0.03982	0.00075	251.2	11.01	251.7	4.67
10	0.18742	0.02418	0.02682	0.00105	174.4	20.68	170.6	6.61
11	0.33341	0.02156	0.04437	0.00105	292.2	16.42	279.8	6.47
12	0.19066	0.01328	0.02906	0.00067	177.2	11.32	184.7	4.2
Tem1-3	0.52598	0.0307	0.06925	0.00147	429.1	20.43	431.6	8.86
Tem1-4	0.54853	0.04173	0.06716	0.00186	444	27.36	419	11.23
13	0.11134	0.01397	0.02248	0.00064	107.2	12.76	143.3	4.01
14	0.18033	0.02493	0.039	0.00099	168.3	21.45	246.6	6.15
16	0.23726	0.02213	0.02471	0.00083	216.2	18.16	157.4	5.23
17	0.2435	0.01585	0.03615	0.00083	221.3	12.94	229	5.15
20	0.52722	0.10372	0.06954	0.00393	430	68.96	433.4	23.67
21	0.15173	0.01464	0.01637	0.00053	143.4	12.91	104.7	3.38
22	0.19174	0.0229	0.02783	0.001	178.1	19.51	176.9	6.26
23	0.10852	0.01441	0.01648	0.00055	104.6	13.2	105.4	3.48
24	0.31149	0.04048	0.04309	0.00174	275.3	31.34	272	10.78
25	0.25939	0.0534	0.03564	0.00201	234.2	43.06	225.7	12.52
GJ_5	0.76965	0.03045	0.10181	0.00175	579.6	17.47	625	10.26
GJ_6	0.72243	0.02768	0.0952	0.00158	552.1	16.32	586.2	9.29
30	0.129	0.01928	0.01731	0.00069	123.2	17.34	110.6	4.4
32	0.13148	0.02375	0.02148	0.00091	125.4	21.32	137	5.72
33	0.4553	0.02158	0.0568	0.0011	381	15.05	356.1	6.71
34	0.24249	0.02473	0.03466	0.0011	220.5	20.21	219.7	6.84
36	0.24247	0.02593	0.0332	0.00107	220.4	21.19	210.5	6.69
37	0.14543	0.01927	0.02096	0.00077	137.9	17.08	133.7	4.88
GJ_7	0.7539	0.03096	0.10241	0.0018	570.5	17.92	628.5	10.51
GJ_8	0.82046	0.03278	0.10168	0.00177	608.3	18.28	624.3	10.35
GJ_9	0.75881	0.03375	0.09667	0.0018	573.3	19.48	594.8	10.59
NIST610-3	24.96625	0.40937	0.21257	0.00267	-	-	-	-
NIST610-4	25.4689	0.42518	0.21619	0.00279	-	-	-	-

2 – Ahirau Sandstone

	ISOPTOPE RATIOS				AGE ESTIMATES (Ma)			
Sample No.	Pb207/U235	1 σ error	Pb206/U238	1 σ error	Pb207/U235	1 σ error	Pb206/U238	1 σ error
std610-1	22.17056	0.38176	0.1988	0.00237	-	-	-	-
std610-2rep	25.39312	1.18848	0.2187	0.00485	-	-	-	-
gj_1	0.58645	0.09735	0.09207	0.00468	468.6	62.31	567.8	27.62
gj_2	0.89586	0.12505	0.09012	0.00476	649.5	66.97	556.2	28.17
gj_3	0.82025	0.12015	0.08362	0.00457	608.2	67.02	517.7	27.2
gj_4	0.75208	0.10987	0.07907	0.00427	569.4	63.67	490.6	25.5
tem1-1	0.4565	0.02557	0.06255	0.00132	381.8	17.83	391.1	7.99
tem1-2	0.45693	0.02256	0.06208	0.00111	382.1	15.72	388.3	6.76
1	-0.17182	0.02244	0.0221	0.0008	-191.4	27.51	140.9	5.03
2	0.16755	0.01519	0.02247	0.00072	157.3	13.21	143.2	4.53
3	0.1802	0.03788	0.02421	0.00154	168.2	32.59	154.2	9.71
6	0.1843	0.01655	0.0252	0.00073	171.8	14.19	160.4	4.6
12	0.28466	0.02698	0.04044	0.00132	254.3	21.33	255.6	8.19
13	0.21412	0.02132	0.03245	0.00105	197	17.83	205.9	6.54
14	0.16737	0.03332	0.02397	0.00143	157.1	28.98	152.7	9.02
15	0.38499	0.03936	0.05095	0.0018	330.7	28.86	320.3	11.01
16	0.17315	0.02239	0.02545	0.00102	162.1	19.38	162	6.44
18	0.41854	0.03232	0.06202	0.0017	355	23.14	387.9	10.3
tem1-3	0.59697	0.03915	0.07663	0.00181	475.3	24.89	476	10.83
tem1-4	0.54615	0.07175	0.0731	0.00316	442.5	47.12	454.8	18.96
19	0.54525	0.04762	0.07058	0.00222	441.9	31.29	439.6	13.37
20	0.14082	0.01096	0.02082	0.00057	133.8	9.76	132.8	3.61
21	0.20721	0.03639	0.02842	0.00162	191.2	30.6	180.7	10.15
23	0.20593	0.01834	0.03126	0.0009	190.1	15.44	198.4	5.63
24	0.44927	0.06201	0.0559	0.00269	376.8	43.44	350.6	16.4
25	1.83525	0.07817	0.17999	0.00352	1058.2	28	1066.9	19.22
26	0.1829	0.04282	0.02567	0.00193	170.6	36.75	163.4	12.1
27	0.50069	0.03706	0.06838	0.00187	412.2	25.07	426.4	11.27
28	0.15844	0.08278	0.02296	0.00285	149.3	72.56	146.3	17.99
29	0.23997	0.02679	0.03711	0.0014	218.4	21.94	234.9	8.72
GJ_5	0.78133	0.03569	0.10803	0.00199	586.2	20.34	661.3	11.6
GJ_6	0.80589	0.03733	0.10398	0.00199	600.1	20.99	637.7	11.64
TEM2_2	0.61521	0.06446	0.08023	0.00289	486.8	40.52	497.5	17.24
TEM2_3	0.59332	0.0772	0.07633	0.00326	473	49.2	474.2	19.52
31	0.34373	0.04228	0.04683	0.0019	300	31.95	295	11.73
33	0.13668	0.02681	0.02506	0.00131	130.1	23.95	159.6	8.25
39	0.19309	0.02305	0.02739	0.00117	179.3	19.61	174.2	7.33
42	0.23271	0.02608	0.03545	0.00131	212.4	21.48	224.6	8.19
43	0.16871	0.01467	0.02466	0.00074	158.3	12.74	157	4.65
44	0.14889	0.02788	0.02354	0.00126	140.9	24.64	150	7.93
45	0.17639	0.03466	0.02671	0.00143	165	29.92	169.9	8.98
46	0.48676	0.05243	0.06374	0.00239	402.7	35.81	398.3	14.51
GJ_7	0.86686	0.04752	0.10955	0.00237	633.9	25.85	670.2	13.74
GJ_8	0.7935	0.0444	0.10904	0.00233	593.2	25.14	667.2	13.57
GJ_9	0.73537	0.03449	0.10561	0.00198	559.7	20.18	647.2	11.54
std610-3	25.69598	0.42465	0.22962	0.00264	-	-	-	-
std610-4	25.87499	0.4277	0.23212	0.00267	-	-	-	-

	ISOPTOPE RATIOS				AGE ESTIMATES (Ma)			
Sample No.	**Pb207/U235**	**1 σ error**	**Pb206/U238**	**1 σ error**	**Pb207/U235**	**1 σ error**	**Pb206/U238**	**1 σ error**
nist610-1	30.8763	0.99423	0.26218	0.00444	-	-	-	-
nist610-2	31.74903	1.02409	0.26514	0.00454	-	-	-	-
nist610-3	30.4248	0.98249	0.25925	0.00446	-	-	-	-
gj1-1	0.8364	0.0847	0.09777	0.00358	617.2	46.83	601.3	21.03
gj1-2	0.90014	0.08568	0.09591	0.00349	651.8	45.78	590.4	20.5
gj1-3	0.71605	0.07356	0.09492	0.00326	548.3	43.53	584.6	19.17
gj1-4	0.7333	0.06494	0.09628	0.00304	558.5	38.04	592.6	17.88
tem-1	0.53627	0.09769	0.0652	0.0033	436	64.56	407.2	19.97
tem-2	0.40726	0.05863	0.06398	0.00219	346.9	42.3	399.8	13.26
2	0.4602	0.02995	0.05406	0.00129	384.4	20.83	339.4	7.87
4	0.23037	0.03891	0.03334	0.0015	210.5	32.11	211.4	9.37
6	0.38797	0.0216	0.05695	0.00114	332.9	15.8	357.1	6.98
7	0.24017	0.03102	0.03585	0.0013	218.6	25.4	227	8.1
10	0.26277	0.03443	0.03861	0.00139	236.9	27.68	244.2	8.6
12	0.27493	0.04439	0.03556	0.00159	246.6	35.35	225.2	9.9
14	-0.01149	0.08458	0.06342	0.00333	-11.7	86.88	396.4	20.18
16	0.36533	0.02416	0.04306	0.00106	316.2	17.97	271.8	6.55
tem1-3	0.56472	0.06387	0.07222	0.00214	454.6	41.45	449.5	12.89
tem1-4	0.23126	0.03916	0.05947	0.0014	211.2	32.29	372.4	8.53
18	*********	310.4157	0.21982	0.12858	-NaN	*******	1280.9	679.52
19	0.17455	0.04105	0.01887	0.0013	163.4	35.49	120.5	8.2
20	0.42957	0.02135	0.05651	0.00109	362.9	15.16	354.4	6.63
21	0.30619	0.07734	0.03684	0.00225	271.2	60.12	233.2	14
22	0.22437	0.02077	0.0301	0.00097	205.5	17.23	191.2	6.06
24	0.30406	0.02669	0.03781	0.00109	269.6	20.78	239.3	6.77
25	0.26802	0.10923	0.0375	0.00287	241.1	87.47	237.3	17.85
26	0.15132	0.01808	0.02232	0.00065	143.1	15.94	142.3	4.1
Tem2-5	0.47084	0.03911	0.06158	0.0015	391.8	27	385.3	9.11
Tem2-6	0.49428	0.02176	0.06411	0.00107	407.8	14.79	400.6	6.49
Gj1-5	0.73055	0.07732	0.10561	0.00369	556.9	45.37	647.2	21.49
Gj1-6	0.76191	0.06919	0.09194	0.00306	575.1	39.87	567	18.06
27	0.15904	0.02044	0.02117	0.0007	149.9	17.91	135	4.4
28	191.00916	225.4815	-0.85802	1.56308	5338.4	1192.39	******	*******
29	0.25157	0.01754	0.03019	0.00069	227.8	14.23	191.7	4.31
30	0.27376	0.01771	0.03857	0.00084	245.7	14.12	244	5.19
32	216.98811	158.9164	3.15526	2.2288	5467.3	740.23	9182.1	3457.72
34	0.27481	0.02963	0.03793	0.00117	246.5	23.6	240	7.25
36	0.13364	0.05052	0.02223	0.00184	127.4	45.25	141.8	11.62
42	0.55937	0.04323	0.05602	0.00162	451.1	28.15	351.4	9.87
Tem2-7	0.49862	0.04517	0.06505	0.00182	410.8	30.6	406.2	10.99
Tem2-8	0.48314	0.02047	0.0643	0.00113	400.2	14.02	401.7	6.86
45	0.14769	0.01996	0.02052	0.00073	139.9	17.66	130.9	4.61
46	0.26378	0.04781	0.03157	0.00148	237.7	38.41	200.3	9.25
48	0.29299	0.03561	0.03483	0.00126	260.9	27.97	220.7	7.82
50	0.16691	0.01895	0.023	0.00072	156.7	16.49	146.6	4.56
51	0.4877	0.02545	0.05966	0.0012	403.3	17.37	373.5	7.3
52	0.28105	0.02709	0.03322	0.00096	251.5	21.47	210.7	6.01
55	0.26697	0.03401	0.04012	0.00136	240.3	27.26	253.6	8.45
Gj1-7	0.88533	0.04162	0.09865	0.00183	643.9	22.42	606.5	10.74
Gj1-8	0.77238	0.04225	0.10102	0.00195	581.1	24.21	620.4	11.44
Gj1-9	0.77547	0.05666	0.09398	0.0024	582.9	32.4	579	14.14
Gj1-10	0.91008	0.05123	0.0984	0.00213	657.1	27.24	605.1	12.51
nist610-3	26.58705	0.4719	0.20877	0.00241	-	-	-	-
nist610-4	27.10157	0.50664	0.21211	0.00253	-	-	-	-

	ISOPTOPE RATIOS				AGE ESTIMATES (Ma)			
Sample No.	Pb207/U235	1 σ error	Pb206/U238	1 σ error	Pb207/U235	1 σ error	Pb206/U238	1 σ error
NIST610-1	27.59842	0.59425	0.20905	0.00271	-	-	-	-
NIST610-2	27.68714	0.6234	0.21214	0.00276	-	-	-	-
gj1	0.79256	0.05334	0.09679	0.0022	592.6	30.21	595.6	12.92
gj2	0.80761	0.05315	0.09578	0.00222	601.1	29.86	589.6	13.05
gj3	0.80029	0.05236	0.09531	0.00216	597	29.53	586.9	12.69
gj4	0.82586	0.05143	0.09565	0.00211	611.3	28.6	588.9	12.39
Tem1_1	0.49336	0.0421	0.06425	0.0018	407.2	28.63	401.4	10.91
Tem1_2	0.53363	0.0693	0.06797	0.00235	434.2	45.89	423.9	14.18
1	0.26049	0.0477	0.02038	0.0012	235.1	38.43	130.1	7.59
2	0.14524	0.04071	0.0182	0.00123	137.7	36.1	116.3	7.76
3	0.07224	0.05357	0.01889	0.00135	70.8	50.73	120.7	8.55
4	0.22175	0.04173	0.03297	0.00154	203.4	34.69	209.1	9.59
5	0.14521	0.15398	0.02212	0.00304	137.7	136.53	141.1	19.19
6	0.1332	0.03709	0.01896	0.00116	127	33.23	121.1	7.32
7	0.45308	0.05107	0.06032	0.00185	379.4	35.69	377.6	11.23
8	0.1331	0.09197	0.02069	0.00218	126.9	82.42	132	13.79
9	0.22803	0.03354	0.03425	0.00129	208.6	27.73	217.1	8.03
10	-12.62329	11.30208	-0.31236	0.19124	-NaN	-987.32	******	1792.8
11	0.20554	0.049	0.01855	0.00124	189.8	41.27	118.5	7.85
12	0.1533	0.06371	0.02141	0.0016	144.8	56.09	136.5	10.07
13	0.2924	0.09521	0.04115	0.00237	260.4	74.8	260	14.7
14	1.58782	0.22602	0.03513	0.00326	965.4	88.68	222.6	20.32
15	0.44787	0.04766	0.05974	0.00193	375.8	33.42	374	11.71
tem2_1	0.56708	0.03914	0.07061	0.00155	456.1	25.36	439.8	9.35
tem2_2	0.52736	0.03036	0.06835	0.00142	430.1	20.19	426.2	8.59
gj_5	0.79956	0.05669	0.09695	0.00238	596.6	31.99	596.5	13.96
gj_6	0.84756	0.06395	0.1016	0.00264	623.3	35.14	623.8	15.46
16	0.26963	0.02769	0.039	0.00109	242.4	22.15	246.6	6.75
17	0.59781	0.03237	0.04616	0.00112	475.8	20.57	290.9	6.93
18	0.19368	0.02535	0.02075	0.00087	179.8	21.56	132.4	5.52
19	0.37384	0.02979	0.05105	0.00124	322.5	22.01	321	7.58
20	0.42841	0.0564	0.04039	0.00181	362	40.09	255.3	11.22
21	0.12302	0.07965	0.0192	0.0017	117.8	72.02	122.6	10.75
22	0.17881	0.02728	0.01918	0.00092	167	23.5	122.5	5.84
23	0.12676	0.04364	0.01776	0.0013	121.2	39.33	113.5	8.26
26	0.17616	0.03012	0.01892	0.00096	164.7	26	120.8	6.04
27	0.13615	0.07023	0.01755	0.00152	129.6	62.76	112.2	9.63
28	0.36471	0.047	0.04717	0.00188	315.7	34.97	297.2	11.56
29	0.14871	0.03474	0.02141	0.00126	140.8	30.71	136.5	7.93
30	0.28872	0.03686	0.03642	0.00128	257.6	29.04	230.6	7.94
31	0.14312	0.07892	0.02098	0.00148	135.8	70.1	133.8	9.35
32	0.25459	0.05328	0.03537	0.00155	230.3	43.12	224.1	9.63
gj_7	0.74225	0.04962	0.09782	0.00217	563.7	28.92	601.6	12.72
gj_8	0.80758	0.05274	0.10012	0.00226	601.1	29.63	615.1	13.26
gj_9	0.80609	0.05257	0.09619	0.00222	600.3	29.56	592	13.04
gj_10	0.91653	0.05681	0.10204	0.00232	660.5	30.1	626.3	13.55
NIST610-3	27.85942	0.57495	0.21522	0.00285	-	-	-	-
NIST610-4	27.39947	0.5916	0.2104	0.00276	-	-	-	-

	ISOPTOPE RATIOS				AGE ESTIMATES (Ma)			
Sample No.	Pb207/U235	1 σ error	Pb206/U238	1 σ error	Pb207/U235	1 σ error	Pb206/U238	1 σ error
NIST610-1	28.0542	0.57055	0.22342	0.00299	-	-	-	-
NIST610-2	28.67475	0.59213	0.23061	0.00311	-	-	-	-
gj1	0.73851	0.05284	0.10068	0.00223	561.5	30.86	618.4	13.04
gj2	0.81525	0.05304	0.09733	0.00211	605.4	29.67	598.8	12.41
gj3	0.83864	0.04395	0.09154	0.00177	618.4	24.27	564.6	10.47
gj4	0.8036	0.0426	0.09255	0.00178	598.9	23.98	570.6	10.49
tem1_1	0.49159	0.12668	0.063	0.00348	406	86.24	393.9	21.08
tem1_2	0.59462	0.1404	0.0708	0.00298	473.8	89.4	441	17.95
1	0.3052	0.06908	0.02026	0.00149	270.5	53.74	129.3	9.44
2	0.45518	0.04326	0.0577	0.00173	380.9	30.18	361.6	10.56
3	0.1303	0.01403	0.0178	0.00059	124.4	12.61	113.7	3.72
4	0.15072	0.016	0.02116	0.00058	142.5	14.12	135	3.67
5	0.14297	0.08616	0.01963	0.00177	135.7	76.54	125.3	11.19
6	0.41101	0.09055	0.02577	0.00211	349.6	65.16	164	13.27
7	0.32598	0.05125	0.03705	0.00139	286.5	39.24	234.5	8.62
8	0.1391	0.02244	0.01951	0.00064	132.2	20.01	124.6	4.03
9	0.14688	0.0752	0.01918	0.00203	139.2	66.58	122.4	12.83
10	0.19869	0.06675	0.02883	0.00142	184	56.54	183.2	8.9
11	0.14058	0.28885	0.01931	0.00429	133.6	257.14	123.3	27.16
GJ_5	0.79523	0.04576	0.10074	0.00199	594.1	25.88	618.8	11.64
GJ_6	0.81941	0.04643	0.09993	0.00199	607.7	25.91	614	11.65
12	0.15474	0.10457	0.0193	0.00224	146.1	91.95	123.2	14.18
13	0.28139	0.05881	0.03798	0.00154	251.8	46.6	240.3	9.58
14	0.4196	0.03961	0.05379	0.00153	355.8	28.33	337.8	9.38
15	0.33941	0.10398	0.04383	0.00272	296.7	78.82	276.5	16.77
16	0.13897	0.0197	0.01934	0.00072	132.1	17.56	123.5	4.58
17	0.11688	0.07026	0.01761	0.00198	112.2	63.87	112.5	12.56
18	0.13595	0.01393	0.01964	0.00059	129.4	12.45	125.4	3.74
19	0.29729	0.04561	0.03882	0.00158	264.3	35.7	245.5	9.81
20	0.12718	0.0566	0.01724	0.00125	121.6	50.99	110.2	7.92
21	0.12512	0.08796	0.01994	0.00215	119.7	79.38	127.3	13.57
22	0.14441	0.01829	0.01721	0.00066	137	16.23	110	4.21
TEM2_1	0.54929	0.04972	0.07639	0.00206	444.5	32.58	474.6	12.32
TEM2_2	0.56549	0.04201	0.07059	0.00169	455.1	27.25	439.7	10.15
23	0.4361	0.02858	0.05605	0.00134	367.5	20.21	351.6	8.18
24	0.16993	0.03169	0.03086	0.00114	159.4	27.5	195.9	7.12
gj_7	0.76502	0.04631	0.10033	0.00211	576.9	26.64	616.3	12.38
gj_8	0.83028	0.04703	0.10133	0.00212	613.8	26.09	622.2	12.41
25	0.25593	0.07566	0.03964	0.00236	231.4	61.17	250.6	14.61
26	0.15347	0.01347	0.01739	0.00048	145	11.85	111.2	3.06
27	0.46292	0.01808	0.05807	0.001	386.3	12.55	363.9	6.08
28	0.38844	0.03136	0.05289	0.00128	333.2	22.94	332.2	7.87
29	0.14753	0.05466	0.02117	0.00172	139.7	48.37	135	10.86
30	0.17923	0.03515	0.02625	0.00105	167.4	30.27	167	6.59
31	0.18195	0.04689	0.02476	0.00135	169.7	40.28	157.7	8.49
GJ_9	0.83126	0.04666	0.10145	0.00205	614.3	25.87	622.9	12.02
GJ_10	0.78347	0.04604	0.09795	0.00208	587.5	26.21	602.4	12.2
GJ_11	0.89021	0.04926	0.09629	0.00206	646.5	26.46	592.6	12.12
GJ_12	0.79769	0.04863	0.09569	0.00211	595.5	27.47	589.1	12.39
NIST610_3	27.61048	0.5404	0.22212	0.00283	-	-	-	-
NIST610_4	31.3361	0.56394	0.25928	0.00328	-	-	-	-

	ISOPTOPE RATIOS				AGE ESTIMATES (Ma)			
Sample No.	Pb207/U235	1 σ error	Pb206/U238	1 σ error	Pb207/U235	1 σ error	Pb206/U238	1 σ error
NIST610-1	29.19339	0.92527	0.22606	0.00351	-	-	-	-
Nist610-2	31.214	0.92456	0.23663	0.00363	-	-	-	-
gj_1	0.76876	0.07702	0.09817	0.00256	579.1	44.21	603.7	15.03
gj_2	0.86153	0.07845	0.09989	0.00263	631	42.79	613.8	15.41
gj_3	0.79942	0.07817	0.09443	0.0025	596.5	44.11	581.7	14.71
gj_4	0.67659	0.07101	0.09584	0.00248	524.7	43.01	590	14.56
TEM1_1	0.58495	0.15702	0.06669	0.00373	467.6	100.59	416.2	22.54
TEM1_2	-0.39498	0.18739	0.06482	0.00457	-510.2	314.49	404.9	27.65
1	0.33658	0.0217	0.04622	0.00099	294.6	16.48	291.3	6.08
2	0.38509	0.34536	0.05312	0.00576	330.8	253.18	333.7	35.29
3	0.96485	0.28814	0.02277	0.00359	685.8	148.9	145.1	22.6
4	0.31324	0.10768	0.03702	0.0023	276.7	83.25	234.4	14.3
5	0.06012	0.1386	0.02369	0.00184	59.3	132.76	150.9	11.61
6	0.11627	0.12265	0.01795	0.00154	111.7	111.56	114.7	9.74
7	0.17289	0.14312	0.01854	0.00187	161.9	123.9	118.4	11.86
8	2.51491	0.18953	0.03392	0.00206	1276.3	54.75	215	12.86
9	0.53831	0.10654	0.01811	0.00172	437.3	70.33	115.7	10.88
10	0.62222	0.12015	0.05983	0.00358	491.2	75.2	374.6	21.76
11	0.25797	0.28288	0.03942	0.00522	233	228.33	249.3	32.36
GJ_5	0.87802	0.06841	0.09623	0.00214	639.9	36.99	592.3	12.6
GJ_6	0.71166	0.06145	0.09755	0.00212	545.7	36.45	600	12.45
12	0.24636	0.28531	0.01859	0.00342	223.6	232.43	118.7	21.67
15	0.37277	0.08444	0.04901	0.0022	321.7	62.46	308.4	13.5
16	0.2298	0.08917	0.03305	0.0017	210	73.62	209.6	10.6
17	0.27608	0.17373	0.03899	0.00298	247.5	138.24	246.6	18.49
18	1.46407	0.17694	0.0551	0.00319	915.7	72.91	345.8	19.48
20	0.28341	0.09787	0.04017	0.00175	253.4	77.43	253.9	10.83
21	1.88095	0.13711	0.06651	0.00239	1074.4	48.32	415.1	14.43
22	0.60754	0.10964	0.05154	0.00274	482	69.25	324	16.79
gj_7	0.78186	0.06748	0.09505	0.00217	586.5	38.45	585.3	12.79
gj_8	0.7816	0.06336	0.09459	0.0021	586.4	36.11	582.6	12.36
tem2_1	0.4621	0.12619	0.06999	0.00263	385.7	87.64	436.1	15.86
tem2_2	2.03414	0.42942	0.07362	0.00626	1127	143.71	457.9	37.59
23	0.21027	0.14262	0.02201	0.00189	193.8	119.66	140.4	11.92
24	0.14612	0.11437	0.02106	0.00188	138.5	101.33	134.4	11.84
25	0.29468	0.04515	0.0383	0.00143	262.2	35.41	242.3	8.85
26	1.01892	0.13844	0.03003	0.00216	713.4	69.62	190.7	13.49
27	0.1454	0.13971	0.02116	0.00203	137.8	123.85	135	12.84
28	0.08896	0.07455	0.01829	0.00114	86.5	69.51	116.8	7.21
29	0.42405	0.04682	0.05742	0.0016	358.9	33.38	359.9	9.78
30	0.38621	0.05479	0.03232	0.00153	331.6	40.13	205.1	9.54
31	0.31263	0.09329	0.0211	0.00136	276.2	72.17	134.6	8.58
32	0.26544	0.1323	0.03837	0.00267	239	106.15	242.7	16.6
gj_9	0.82283	0.06264	0.09682	0.00214	609.6	34.89	595.7	12.57
gj_10	0.96168	0.06872	0.09959	0.0022	684.2	35.57	612	12.89
gj_11	0.78354	0.06545	0.10109	0.00225	587.5	37.26	620.8	13.15
gj_12	0.82976	0.06532	0.09756	0.00215	613.5	36.25	600.1	12.65
NIST610-3	28.52846	0.72376	0.22198	0.00297	-	-	-	-
NIST610-4	28.07689	0.71546	0.21772	0.00291	-	-	-	-

	ISOPTOPE RATIOS				AGE ESTIMATES (Ma)			
Sample No.	Pb207/U235	1 σ error	Pb206/U238	1 σ error	Pb207/U235	1 σ error	Pb206/U238	1 σ error
nist610-1	25.31001	0.40702	0.20797	0.00238	-	-	-	-
nist610-2	28.45439	0.45821	0.22322	0.00256	-	-	-	-
gj-1	0.7436	0.02721	0.09466	0.00139	564.5	15.85	583	8.2
gj-2	1.05725	0.04196	0.10137	0.00178	732.5	20.71	622.4	10.42
gj-3	0.79032	0.03529	0.10008	0.00174	591.4	20.02	614.9	10.2
gj-4	0.74793	0.03259	0.09473	0.00163	567	18.93	583.5	9.58
1	0.16101	0.02279	0.02191	0.00073	151.6	19.93	139.7	4.57
2	0.15003	0.02603	0.02321	0.00075	141.9	22.98	147.9	4.74
8	0.13893	0.01134	0.01888	0.00043	132.1	10.11	120.5	2.74
9	0.38719	0.01493	0.05252	0.00083	332.3	10.93	329.9	5.06
12	0.12034	0.03313	0.01968	0.00099	115.4	30.03	125.7	6.24
13	0.19748	0.03964	0.02867	0.00112	183	33.61	182.2	7.04
15	0.21233	0.02903	0.02152	0.00078	195.5	24.31	137.3	4.93
16	0.10305	0.04145	0.01572	0.00113	99.6	38.15	100.6	7.2
17	0.12939	0.03723	0.01979	0.00093	123.5	33.47	126.3	5.86
TEM1-1	0.54333	0.07623	0.06956	0.00274	440.6	50.15	433.5	16.54
TEM1-2	0.51716	0.03972	0.06378	0.00153	423.3	26.58	398.6	9.27
18	0.12968	0.03405	0.01939	0.00097	123.8	30.61	123.8	6.16
19	0.44479	0.02046	0.05084	0.00091	373.6	14.38	319.7	5.57
20	0.10545	0.01409	0.01883	0.00053	101.8	12.94	120.3	3.36
22	0.10672	0.01601	0.01778	0.00055	103	14.69	113.6	3.5
24	0.10281	0.03009	0.01875	0.00085	99.4	27.71	119.7	5.39
26	0.16347	0.05655	0.0187	0.00119	153.7	49.35	119.4	7.51
28	0.1521	0.03448	0.02459	0.00103	143.8	30.39	156.6	6.48
29	0.81732	0.02816	0.09843	0.00152	606.6	15.73	605.2	8.91
GJ-5	0.76496	0.03464	0.09419	0.00171	576.9	19.93	580.3	10.07
GJ-6	0.81667	0.03825	0.10076	0.00186	606.2	21.38	618.8	10.9
30	0.1219	0.058	0.01725	0.00148	116.8	52.49	110.2	9.36
32	0.3389	0.01416	0.04885	0.00077	296.3	10.74	307.4	4.75
33	21.50205	1.57883	0.17896	0.0167	3161.5	71.24	1061.3	91.32
35	0.13392	0.04006	0.01926	0.00125	127.6	35.87	123	7.88
37	0.13357	0.04614	0.02162	0.00154	127.3	41.33	137.9	9.75
40	0.45933	0.03634	0.05735	0.0014	383.8	25.29	359.5	8.51
42	0.16489	0.05617	0.0226	0.00167	155	48.96	144.1	10.55
44	0.22224	0.01672	0.03018	0.0007	203.8	13.89	191.7	4.41
46	0.16323	0.02881	0.02413	0.00096	153.5	25.15	153.7	6.03
gj-7	0.81267	0.03956	0.1032	0.00194	603.9	22.16	633.2	11.35
gj-8	0.81124	0.03715	0.09942	0.00183	603.2	20.83	611	10.74
tem1-3	0.51282	0.03012	0.06616	0.00132	420.3	20.22	413	7.99
tem1-4	0.53226	0.04346	0.07039	0.00181	433.3	28.8	438.5	10.88
48	0.52972	0.02006	0.06925	0.00107	431.6	13.32	431.6	6.43
50	0.1425	0.03529	0.02116	0.00106	135.3	31.36	135	6.7
51	0.11649	0.01332	0.01871	0.00051	111.9	12.12	119.5	3.21
52	0.17282	0.0361	0.01829	0.00094	161.9	31.26	116.8	5.94
53	0.15105	0.01528	0.02008	0.00063	142.8	13.48	128.2	3.98
55	0.49096	0.03117	0.06443	0.00144	405.6	21.23	402.5	8.73
56	0.15377	0.01804	0.02128	0.0007	145.2	15.88	135.7	4.43
Gj-9	0.86153	0.03992	0.09733	0.00181	631	21.78	598.7	10.64
Gj-10	0.80016	0.03556	0.09641	0.00172	596.9	20.06	593.3	10.12
Gj-11	0.80327	0.03819	0.09944	0.00183	598.7	21.5	611.1	10.72
gj-12	0.84507	0.03586	0.10051	0.00171	621.9	19.73	617.4	10.03
nist610-3	27.69988	0.42388	0.22268	0.00247	-	-	-	-

6 – Hauturu Sandstone

	ISOPTOPE RATIOS				AGE ESTIMATES (Ma)			
Sample No.	Pb207/U235	1 σ error	Pb206/U238	1 σ error	Pb207/U235	1 σ error	Pb206/U238	1 σ error
nist610-1	25.94948	0.6315	0.20871	0.00243	-	-	-	-
nist610-2	26.99044	0.60365	0.2179	0.00252	-	-	-	-
gj1-1	0.76597	0.05413	0.09466	0.00182	577.4	31.13	583.1	10.74
gj1-2	0.73386	0.06228	0.09719	0.00198	558.8	36.47	597.9	11.62
gj1-3	0.90151	0.06643	0.09492	0.00197	652.5	35.47	584.6	11.59
gj1-4	0.71441	0.05878	0.0906	0.00183	547.4	34.81	559.1	10.84
gj1-5	-0.07227	0.07884	0.1015	0.00257	-76.2	86.29	623.2	15.07
gj1-6	0.81825	0.04658	0.09754	0.00196	607.1	26.01	599.9	11.5
7	0.19493	0.02401	0.02439	0.00076	180.8	20.4	155.3	4.8
8	0.40972	0.02512	0.05436	0.00111	348.7	18.09	341.2	6.78
9	0.21025	0.03537	0.02973	0.00126	193.8	29.68	188.9	7.87
12	0.10604	0.02496	0.01775	0.00071	102.3	22.91	113.4	4.47
13	0.11008	0.03755	0.01721	0.00102	106	34.35	110	6.49
14	0.35487	0.02514	0.05084	0.00111	308.4	18.84	319.7	6.83
15	0.42845	0.0339	0.05765	0.00144	362.1	24.09	361.3	8.77
16	-0.5551	0.0443	0.01384	0.00108	-822.4	101.09	88.6	6.86
19	0.12957	0.07423	0.01976	0.0017	123.7	66.72	126.1	10.75
20	0.35151	0.08022	0.04804	0.00286	305.9	60.27	302.5	17.62
21	0.13599	0.02439	0.01882	0.00075	129.5	21.8	120.2	4.75
25	0.25161	0.01855	0.036	0.00076	227.9	15.05	228	4.76
27	0.38844	0.02985	0.05588	0.00137	333.2	21.83	350.5	8.36
29	0.35395	0.03906	0.05112	0.00169	307.7	29.29	321.4	10.35
40	0.12456	0.02927	0.01844	0.00078	119.2	26.43	117.8	4.94
45	0.19834	0.04951	0.02846	0.00143	183.7	41.95	180.9	8.93
51	0.38865	0.02037	0.0524	0.00097	333.4	14.9	329.2	5.93
59	0.2033	0.05294	0.02785	0.00165	187.9	44.67	177.1	10.32
gj1-7	0.80304	0.06019	0.10418	0.00261	598.5	33.9	638.8	15.21
gj1-8	0.85853	0.06855	0.098	0.00279	629.3	37.45	602.7	16.37
gj1-9	0.80071	0.05051	0.10296	0.00224	597.2	28.48	631.7	13.11
gj1-10	0.82466	0.05466	0.10014	0.00233	610.6	30.42	615.2	13.68
nist610-3	26.95192	0.5651	0.21769	0.00246	-	-	-	-
nist610-4	27.14679	0.5693	0.21786	0.00247	-	-	-	-